

*KINEMATICS, DYNAMICS, AND  
DESIGN OF MACHINERY*



SECOND EDITION

---

# *KINEMATICS, DYNAMICS, AND DESIGN OF MACHINERY*

**K. J. WALDRON**

*Stanford University*

**G. L. KINZEL**

*The Ohio State University*



WILEY

**JOHN WILEY & SONS, INC.**

Acquisitions Editor *Joseph Hayton*  
Associate Director of Marketing *Ilse Wolfe*  
Senior Production Editor *Valerie A. Vargas*  
Senior Designer *Madelyn Lesure*

This book was set in 10/12 Times Roman by Argosy and printed and bound by Hamilton Printing. The cover was printed by Lehigh Press.

This book is printed on acid-free paper.



Copyright © 2004 John Wiley & Sons, Inc. All rights reserved.

No part of this publication may be reproduced, stored in a retrieval system or transmitted in any form or by any means, electronic, mechanical, photocopying, recording, scanning or otherwise, except as permitted under Sections 107 or 108 of the 1976 United States Copyright Act, without either the prior written permission of the Publisher, or authorization through payment of the appropriate per-copy fee to the Copyright Clearance Center, Inc. 222 Rosewood Drive, Danvers, MA 01923, (078)750-8400, fax (978)750-4470. Requests to the Publisher for permission should be addressed to the Permissions Department, John Wiley & Sons, Inc., 111 River Street, Hoboken, NJ 07030, (201)748-6011, fax (201)748-6008, E-Mail: PERMREQ@WILEY.COM. To order books or for customer service please call 1-800-CALL WILEY (225-5945).

***Library of Congress Cataloging-in-Publication Data***

Waldron, Kenneth J.

Kinematics, dynamics, and design of machinery / by K.J. Waldron and G.L. Kinzel.—2nd ed.

p. cm.

Includes bibliographical references.

ISBN 0-471-24417-1 (cloth)

1. Machinery, Kinematics of. 2. Machinery, Dynamics of. 3. Machine design. I. Kinzel, Gary L., 1944— II.

Title.

TJ175.W35 2003

621.8'1—dc21

2003050053

ISBN 0-471-24417-1

ISBN 0-471-42917-1 (WIE)

Printed in the United States of America

10 9 8 7 6 5 4 3 2 1

# PREFACE

The second edition of a textbook always provides the opportunity to improve those parts of the material that have been found in the classroom to fall short of the authors' original intent. So it is with this edition. Our intent of providing a teaching tool that features a straightforward presentation of basic principles while having the depth and rigor to serve as a basis for more advanced work has not changed. However, we have been listening to the voices of those who have used this work as students and as teachers. In this new edition we have attempted to address their main themes.

One major change is structural. We have separated the "superchapter" that was Chapter 2 in the first edition into three new chapters with some added explanatory material. This change is intended to ease the student's progress into the more mathematical part of the material. We have also removed the superscript notation for identifying reference frames in situations where it is superfluous because multiple frames are not needed. This means, for example, that the superscript notation is not used in the introductory chapter on graphical analysis techniques that is the new Chapter 2. The superscript notation is retained for those situations in which it is necessary to keep track of multiple moving reference frames, but it is introduced later after students should have gained some confidence in their basic techniques.

The introduction to algebraic solution techniques, which now forms Chapter 5, has been somewhat reorganized to provide a smoother progression into the topic. Once again, the superscript notation for reference frames has been removed whenever it is not needed.

We have added a significant number of new problems and new worked examples in selected locations in the text. The added problems include some open-ended design problems.

Chapter 1 now contains sections on bearings and actuation that provide a stronger link to practical engineering in which mechanisms must not only have the right dimensions, but must move freely over long service lives, and must be driven.

We have expanded the design chapter (Chapter 6) to include two-position double-rocker designs. Both graphical and analytical approaches are given. The section on path generation has also been expanded to include the design of eight-link mechanisms that guide a coupler along a path in curvilinear motion. In addition, the section on crank-rocker designs has been expanded.

We have upgraded the software provided on the CD that accompanies the book. The CD includes a new set of programs based on Matlab's graphical user interface (GUI). These programs are easier to use than the original programs. In the rigid-body guidance programs, we have also included a rectification feature that identifies solutions that have a branch problem. This greatly improves the usability of the programs for design problems. The cam design program also has been greatly improved. It is now possible to optimize cam motion and to create displacement profiles that are made up of several different standard mathematical functions. As is the case with other GUI-based programs, the entire process is interactive.

Although the new programs are easier to use, writing them is beyond the scope of what would normally be expected for students in an introductory level kinematics class. Therefore, the original programs are also included on the CD. These programs are simpler and could be written by many students at the junior and senior levels in mechanical engineering. These can be used directly or modified by the students. We have included comments so that an interested programmer can understand the flow of the programs.

The CD also contains animations of selected mechanisms generated using a solid modeling program (SolidEdge). These illustrate most of the common single-loop mechanisms. In addition, a set of PowerPoint slides is included as a supplement for the lectures. Some of these include step-by-step procedures for several of the figures given in the book. While these do not cover all aspects of the book, they cover most of the topics that would be included in an entry-level class. These can be easily tailored by the user for specific lectures.

These are only the more visible changes. There are lesser improvements throughout.

The book is intended for courses ranging from an introduction to planar linkage kinematics to more advanced courses that include spatial mechanisms. For example, an introductory course might cover Chapters 1, 2, 4, 5, 6, 8, and 13. The gear chapters could also be covered to some extent. A more advanced course might cover Chapters 1, 3, 4, 7, 8, 9, 14, and 15. Again, the gear chapters could be covered or omitted. In most instances, there are programs on the CD to augment the lecture material included in the book.

Although the book is intended mainly as a textbook, we have written it so that it can serve also as a reference book for mechanism kinematics. For example, where appropriate, we have summarized the equations developed in tables for easy access.

We trust that those who have used the work as a teaching tool will find that this new edition better serves their needs and that they will continue to tell us about the strengths and weaknesses they find in it. This is a topic of fundamental importance to mechanical engineering, as it has been since the time of James Watt. We hope that we have contributed positively to the training of students and hence to the practice of this important and rewarding field.

We would like to express our sincere thanks to the colleagues and students who have contributed to the success of the second edition of this book. We especially acknowledge Necip Berme for several of the examples and exercise problems in the book. A number of these are based on class assignments that he has made during the years. We also thank Yueh-Shao Chen, Sung-Lyul Park, and Michael Stevens who wrote the GUI-based programs that are included with this book. And finally, we would like to thank Edward Kinzel who contributed to the new section on design for path generation.

*Kenneth J. Waldron  
Gary L. Kinzel  
April 2003*

# CONTENTS

## CHAPTER 1 INTRODUCTION 1

- 1.1 Historic Perspective 1
- 1.2 Kinematics 2
- 1.3 Design: Analysis and Synthesis 2
- 1.4 Mechanisms 3
- 1.5 Planar Linkages 7
- 1.6 Visualization 9
- 1.7 Constraint Analysis 11
- 1.8 Constraint Analysis of Spatial Linkages 18
- 1.9 Idle Degrees of Freedom 23
- 1.10 Overconstrained Linkages 25
- 1.11 Uses of the Mobility Criterion 29
- 1.12 Inversion 30
- 1.13 Reference Frames 31
- 1.14 Motion Limits 31
- 1.15 Actuation 32
- 1.16 Coupler-Driven Linkages 37
- 1.17 Motion Limits for Slider-Crank Mechanism 38
- 1.18 Interference 40
- 1.19 Practical Design Considerations 44
  - 1.19.1 Revolute Joints 44
  - 1.19.2 Prismatic Joints 46
  - 1.19.3 Higher Pairs 47
  - 1.19.4 Cams vs. Linkages 47
  - 1.19.5 Actuation 48
- Problems 54

## CHAPTER 2 GRAPHICAL POSITION, VELOCITY, AND ACCELERATION ANALYSIS FOR MECHANISMS WITH REVOLUTE JOINTS OR FIXED SLIDES 60

- 2.1 Introduction 60
- 2.2 Graphical Position Analysis 61
- 2.3 Planar Velocity Polygons 62
- 2.4 Graphical Acceleration Analysis 65
- 2.5 Graphical Analysis of a Four-Bar Mechanism 67
- 2.6 Graphical Analysis of a Slider-Crank Mechanism 74
- 2.7 The Velocity Image Theorem 76
- 2.8 The Acceleration Image Theorem 79
- 2.9 Solution by Inversion 84
- Problems 89

## CHAPTER 3 LINKAGES WITH ROLLING AND SLIDING CONTACTS AND JOINTS ON MOVING SLIDERS 96

- 3.1 Introduction 96
- 3.2 Reference Frames 96
- 3.3 General Velocity and Acceleration Equations 98
  - 3.3.1 Velocity Equations 98
  - 3.3.2 Acceleration Equations 101
  - 3.3.3 Chain Rule for Positions, Velocities, and Accelerations 101
- 3.4 Special Cases for the Velocity and Acceleration Equations 104
  - 3.4.1 Points  $P$  and  $Q$  Fixed to  $B$  104
  - 3.4.2  $P$  and  $Q$  Are Coincident 105
  - 3.4.3  $P$  and  $Q$  Are Coincident and in Rolling Contact 105
- 3.5 Linkages with Rotating Sliding Joints 106
- 3.6 Rolling Contact 111
  - 3.6.1 Basic Kinematic Relationships for Rolling Contact 112
  - 3.6.2 Modeling Rolling Contact Using a Virtual Linkage 118
- 3.7 Cam Contact 121
  - 3.7.1 Direct Approach to the Analysis of Cam Contact 121
  - 3.7.2 Analysis of Cam Contact Using Equivalent Linkages 124
- 3.8 General Coincident Points 128
  - 3.8.1 Velocity Analyses Involving General Coincident Points 130
  - 3.8.2 Acceleration Analyses Involving General Coincident Points 130
- Problems 136

## CHAPTER 4 INSTANT CENTERS OF VELOCITY 145

- 4.1 Introduction 145
- 4.2 Definition 145
- 4.3 Existence Proof 146
- 4.4 Location of an Instant Center from the Directions of Two Velocities 147
- 4.5 Instant Center at a Revolute Joint 148
- 4.6 Instant Center of a Curved Slider 148

- 4.7 Instant Center of a Prismatic Joint **148**
- 4.8 Instant Center of a Rolling Contact Pair **149**
- 4.9 Instant Center of a General Cam-Pair Contact **149**
- 4.10 Centroides **150**
- 4.11 The Kennedy–Aronholdt Theorem **153**
- 4.12 Circle Diagram as a Strategy for Finding Instant Centers **155**
- 4.13 Using Instant Centers: The Rotating-Radius Method **156**
- 4.14 Finding Instant Centers Using Drafting Programs **164**
- Problems **165**

---

**CHAPTER 5 ANALYTICAL LINKAGE ANALYSIS 171**


---

- 5.1 Introduction **171**
- 5.2 Position, Velocity, and Acceleration Representations **172**
  - 5.2.1 Position Representation **172**
  - 5.2.2 Velocity Representation **172**
  - 5.2.3 Acceleration Representation **174**
  - 5.2.4 Special Cases **175**
  - 5.2.5 Mechanisms to Be Considered **175**
- 5.3 Analytical Closure Equations for Four-Bar Linkages **175**
  - 5.3.1 Solution of Closure Equations for Four-Bar Linkages When Link 2 Is the Driver **176**
  - 5.3.2 Analysis When the Coupler (Link 3) Is the Driving Link **179**
  - 5.3.3 Velocity Equations for Four-Bar Linkages **179**
  - 5.3.4 Acceleration Equations for Four-Bar Linkages **181**
- 5.4 Analytical Equations for a Rigid Body after the Kinematic Properties of Two Points Are Known **184**
- 5.5 Analytical Equations for Slider-Crank Mechanisms **187**
  - 5.5.1 Solution to Position Equations When  $\theta_2$  Is Input **190**
  - 5.5.2 Solution to Position Equations When  $r_1$  Is Input **192**
  - 5.5.3 Solution to Position Equations When  $\theta_3$  Is Input **193**
  - 5.5.4 Velocity Equations for Slider-Crank Mechanism **194**
  - 5.5.5 Acceleration Equations for Slider-Crank Mechanism **195**
- 5.6 Analytical Equations for the Slider-Crank Inversion **200**
  - 5.6.1 Solution to Position Equations When  $\theta_2$  Is Input **202**
  - 5.6.2 Solution to Position Equations When  $\theta_3$  Is Input **204**
  - 5.6.3 Solution to Position Equations When  $r_3$  Is Input **204**
  - 5.6.4 Velocity Equations for the Slider-Crank Inversion **205**
  - 5.6.5 Acceleration Equations for the Slider-Crank Inversion **207**
- 5.7 Analytical Equations for an RPRP Mechanism **211**
  - 5.7.1 Solution of Closure Equations When  $\theta_2$  Is Known **212**
  - 5.7.2 Solution of Closure Equations When  $r_4$  Is Known **213**
  - 5.7.3 Solution of Closure Equations When  $r_3$  Is Known **215**
  - 5.7.4 Velocity and Acceleration Equations for an RPRP Mechanism **216**
- 5.8 Analytical Equations for an RRPP Mechanism **218**
  - 5.8.1 Solution When  $\theta_2$  Is Known **219**
  - 5.8.2 Solution When  $r_1$  Is Known **220**
  - 5.8.3 Solution When  $r_3$  Is Known **221**
- 5.9 Analytical Equations for Elliptic Trammel **223**
  - 5.9.1 Analysis When  $\theta_3$  Is Known **224**
  - 5.9.2 Analysis When  $r_1$  Is Known **225**
- 5.10 Analytical Equations for the Oldham Mechanism **228**
  - 5.10.1 Analysis When  $\theta_2$  Is Known **229**
  - 5.10.2 Analysis When  $r_2$  Is Known **230**
- 5.11 Closure or Loop-Equation Approach for Compound Mechanisms **233**
  - 5.11.1 Handling Points Not on the Vector Loops **236**
  - 5.11.2 Solving the Position Equations **237**
- 5.12 Closure Equations for Mechanisms with Higher Pairs **243**
- 5.13 Notational Differences: Vectors and Complex Numbers **248**
- Problems **251**

---

**CHAPTER 6 PLANAR LINKAGE DESIGN 257**


---

- 6.1 Introduction **257**
- 6.2 Two-Position Double-Rocker Design **260**
  - 6.2.1 Graphical Solution Procedure **260**
  - 6.2.2 Analytical Solution Procedure **261**



6.3	Motion Generation	263	7.1.3	Exact Straight-Line Mechanisms	332
6.3.1	Introduction	263	7.1.4	Pantographs	333
6.3.2	Two Positions	263	7.2	Spherical Linkages	340
6.3.3	Three Positions with Selected Moving Pivots	266	7.2.1	Introduction	340
6.3.4	Synthesis of a Crank with Chosen Fixed Pivots	266	7.2.2	Gimbals	343
6.3.5	Design of Slider-Cranks and Elliptic Trammels	268	7.2.3	Universal Joints	343
6.3.6	Order Problem and Change of Branch	270	7.3	Constant-Velocity Couplings	347
6.3.7	Analytical Approach to Rigid-Body Guidance	276	7.3.1	Geometric Requirements of Constant-Velocity Couplings	347
6.4	Function Generation	283	7.3.2	Practical Constant-Velocity Couplings	347
6.4.1	Function Generation Using a Four-Bar Linkage	285	7.4	Automotive Steering and Suspension Mechanisms	349
6.4.2	Design Procedure When $y = y(x)$ Is to Be Generated	287	7.4.1	Introduction	349
6.4.3	Selection of Design Positions	288	7.4.2	Steering Mechanisms	349
6.4.4	Summary of Solution Procedure for Four-Bar Linkage and Three Precision Points	289	7.4.3	Suspension Mechanisms	353
6.4.5	Graphical Approach to Function Generation	293	7.5	Indexing Mechanisms	354
6.5	Synthesis of Crank-Rocker Linkages for Specified Rocker Amplitude	294	7.5.1	Geneva Mechanisms	354
6.5.1	Extreme Rocker Positions and Simple Analytical Solution	294	References	359	
6.5.2	The Rocker Amplitude Problem: Graphical Approach	295	Problems	360	
6.5.3	Transmission Angle	300	<b>CHAPTER 8 PROFILE CAM DESIGN 362</b>		
6.5.4	Alternative Graphical Design Procedure Based on Specification of $O_2-O_4$	301	8.1	Introduction	362
6.5.5	Analytical Design Procedure Based on Specification of $O_2-O_4$	304	8.2	Cam-Follower Systems	363
6.5.6	Use of Analytical Design Procedure for Optimization	307	8.3	Synthesis of Motion Programs	364
6.6	Path Synthesis	308	8.4	Analysis of Different Types of Follower Displacement Functions	366
6.6.1	Design of Six-Bar Linkages Using Coupler Curves	309	8.5	Uniform Motion	367
6.6.2	Motion Generation for Parallel Motion Using Coupler Curves	315	8.6	Parabolic Motion	368
6.6.3	Four-Bar Cognate Linkages	318	8.7	Harmonic Follower-Displacement Programs	373
References	320		8.8	Cycloidal Follower-Displacement Programs	375
Problems	321		8.9	General Polynomial Follower-Displacement Programs	376
<b>CHAPTER 7 SPECIAL MECHANISMS 329</b>			8.10	Determining the Cam Profile	381
7.1	Special Planar Mechanisms	329	8.10.1	Graphical Cam Profile Layout	381
7.1.1	Introduction	329	8.10.2	Analytical Determination of Cam Profile	391
7.1.2	Approximate Straight-Line Mechanisms	329	References	417	
			Problems	417	
			<b>CHAPTER 9 SPATIAL LINKAGE ANALYSIS 421</b>		
			9.1	Spatial Mechanisms	421
			9.1.1	Introduction	421
			9.1.2	Velocity and Acceleration Relationships	422
			9.2	Robotic Mechanisms	428

**X CONTENTS**

9.3 Direct Position Kinematics of Serial Chains **429**  
9.3.1 Introduction **429**  
9.3.2 Concatenation of Transformations **431**  
9.3.3 Homogeneous Transformations **435**  
9.4 Inverse Position Kinematics **438**  
9.5 Direct and Inverse Velocity Problems **438**  
9.5.1 Introduction **438**  
9.5.2 Direct Rate Kinematics **439**  
9.5.3 Inverse Velocity Problem **444**  
9.6 Closed-Loop Linkages **445**  
9.7 Lower Pair Joints **448**  
9.8 Motion Platforms **452**  
9.8.1 Mechanisms Actuated in Parallel **452**  
9.8.2 The Stewart Platform **452**  
9.8.3 The 3-2-1 Platform **454**  
References **454**  
Problems **454**

**CHAPTER 10 SPUR GEARS 458**

---

10.1 Introduction **458**  
10.2 Spur Gears **459**  
10.3 Condition for Constant-Velocity Ratio **460**  
10.4 Involutives **461**  
10.5 Gear Terminology and Standards **464**  
10.5.1 Terminology **464**  
10.5.2 Standards **465**  
10.6 Contact Ratio **467**  
10.7 Involutometry **471**  
10.8 Internal Gears **474**  
10.9 Gear Manufacturing **475**  
10.10 Interference and Undercutting **479**  
10.11 Nonstandard Gearing **482**  
10.12 Cartesian Coordinates of an Involute Tooth Generated with a Rack **487**  
10.12.1 Coordinate Systems **487**  
10.12.2 Gear Equations **491**  
References **494**  
Problems **494**

**CHAPTER 11 HELICAL, BEVEL, AND WORM GEARS 496**

---

11.1 Helical Gears **496**  
11.1.1 Helical Gear Terminology **497**  
11.1.2 Helical Gear Manufacturing **501**  
11.1.3 Minimum Tooth Number to Avoid Undercutting **501**

11.1.4 Helical Gears with Parallel Shafts **503**  
11.1.5 Crossed Helical Gears **509**  
11.2 Worm Gears **513**  
11.2.1 Worm Gear Nomenclature **514**  
11.3 Involute Bevel Gears **517**  
11.3.1 Tredgold's Approximation for Bevel Gears **519**  
11.3.2 Additional Nomenclature for Bevel Gears **520**  
11.3.3 Crown Bevel Gears and Face Gears **521**  
11.3.4 Miter Gears **523**  
11.3.5 Angular Bevel Gears **524**  
11.3.6 Zerol Bevel Gears **524**  
11.3.7 Spiral Bevel Gears **525**  
11.3.8 Hypoid Gears **526**  
References **528**  
Problems **528**

**CHAPTER 12 GEAR TRAINS 530**

---

12.1 Gear Trains **530**  
12.2 Direction of Rotation **530**  
12.3 Simple Gear Trains **531**  
12.3.1 Simple Reversing Mechanism **533**  
12.4 Compound Gear Trains **534**  
12.4.1 Concentric Gear Trains **537**  
12.5 Planetary Gear Trains **540**  
12.5.1 Planetary Gear Nomenclature **542**  
12.5.2 Analysis of Planetary Gear Trains Using Equations **544**  
12.5.3 Analysis of Planetary Gear Trains Using the Tabular Method **550**  
References **554**  
Problems **554**

**CHAPTER 13 STATIC FORCE ANALYSIS OF MECHANISMS 559**

---

13.1 Introduction **559**  
13.2 Forces, Moments, and Couples **560**  
13.3 Static Equilibrium **562**  
13.4 Free-Body Diagrams **562**  
13.5 Graphical Force Analysis **565**  
13.6 Analytical Approach to Force Analysis **573**  
13.6.1 Transmission Angle in a Four-Bar Linkage **575**  
13.7 Friction Considerations **578**  
13.7.1 Friction in Cam Contact **579**  
13.7.2 Friction in Slider Joints **579**  
13.7.3 Friction in Revolute Joints **581**

13.8	In-Plane and Out-of-Plane Force Systems	<b>586</b>
13.9	Conservation of Energy and Power	<b>590</b>
13.10	Virtual Work	<b>595</b>
13.11	Gear Loads	<b>597</b>
13.11.1	Spur Gears	<b>597</b>
13.11.2	Helical Gears	<b>599</b>
13.11.3	Worm Gears	<b>601</b>
13.11.4	Straight Bevel Gears	<b>603</b>
	Problems	<b>604</b>

---

**CHAPTER 14 DYNAMIC FORCE ANALYSIS 608**


---

14.1	Introduction	<b>608</b>
14.2	Problems Soluble via Particle Kinetics	<b>610</b>
14.2.1	Dynamic Equilibrium of Systems of Particles	<b>610</b>
14.2.2	Conservation of Energy	<b>615</b>
14.2.3	Conservation of Momentum	<b>615</b>
14.3	Dynamic Equilibrium of Systems of Rigid Bodies	<b>618</b>
14.4	Flywheels	<b>624</b>
	Problems	<b>646</b>

---

**CHAPTER 15 SHAKING FORCES AND BALANCING 629**


---

15.1	Introduction	<b>629</b>
15.2	Single-Plane (Static) Balancing	<b>630</b>
15.3	Multipane (Dynamic) Balancing	<b>633</b>
15.4	Balancing Reciprocating Masses	<b>639</b>
15.4.1	Expression for Lumped Mass Distribution	<b>640</b>
15.4.2	Analytical Approach to Balancing a Slider-Crank Mechanism	<b>643</b>
15.5	Expressions for Inertial Forces	<b>646</b>
15.6	Balancing Multicylinder Machines	<b>649</b>
15.6.1	Balancing a Three-Cylinder In-Line Engine	<b>653</b>
15.6.2	Balancing an Eight-Cylinder V Engine	<b>655</b>
	References	<b>657</b>
	Problems	<b>657</b>

---

**INDEX 662**


---



---

# INTRODUCTION

---

## 1.1 HISTORIC PERSPECTIVE

---

A mechanism is a machine composed of rigid members that are jointed together. The members interact with one another by virtue of the joints. The joints are formed by portions of the surfaces of the members joined that contact one another. The geometries of the contacting surface segments determine the properties of each joint.

Mechanisms may be simple or complex. Figure 1.1 shows a walking machine that is composed of dozens of mechanisms that must be coordinated through complex control systems. Other machines may involve only a single mechanism.

The design of mechanisms is a technical area that is unique to mechanical engineering. Its history stretches back to prehistoric times. Artisans such as blacksmiths and carpenters also functioned as the designers of mechanisms. One of the original functions of engineers was the design of mechanisms both for warfare and for peaceful uses. In Renaissance times, we find Leonardo da Vinci depicting a sophisticated variety of mechanisms, mostly for military purposes. Sometime thereafter the distinction between civil engineering and military engineering appeared. The modern era in mechanism design, along with the



**FIGURE 1.1** The Adaptive Suspension Vehicle. Each leg is a planar pantograph mechanism hinged to the body about an axis parallel to the longitudinal axis of the vehicle.

history of mechanical engineering as a distinct discipline, can be viewed as starting with James Watt.

That is not to say that the subject has remained static. In fact, there have been dramatic changes in the practice of mechanism design in recent years. Traditionally, machines have been designed to be powered by a single “prime mover,” with all functions mechanically coordinated. That tradition certainly predates Watt. Recent developments in computer technology, coupled with improvements in electric motors and other actuators, have made it possible to use a different approach. This is an approach in which machines are powered by multiple actuators coordinated electronically. The resulting machines are simpler, less expensive, more easily maintained, and more reliable. Another major change is in the techniques used in mechanism design. The use of interactive computer graphics has had a dramatic impact on design practice. One of our motivations in producing this book, even when a number of excellent texts are already available in mechanism kinematics, is to provide a treatment that reflects these changes in practice.

## **1.2 KINEMATICS**

---

Kinematics is the study of position and its time derivatives. Specifically, we are concerned with the positions, velocities, and accelerations of points and with the angular positions, angular velocities, and angular accelerations of solid bodies. Together these entities are sufficient to describe the motions of solid bodies. The position of a body can be defined by the position of a nominated point of that body combined with the angular position of the body. In some circumstances we are also interested in the higher time derivatives of position and angular position.

The subject of kinematics is a study of the geometry of motion. This is an accurate title because kinematics is geometry with the element of time added. The bulk of the subject matter of this book is often referred to as the kinematics of mechanisms. Our objective is to present techniques that can be used to design mechanisms to meet specific motion requirements. That is why the subject matter is approached from a mechanical designer’s perspective.

## **1.3 DESIGN: ANALYSIS AND SYNTHESIS**

---

The material in this book falls into two classifications. The first consists of techniques to determine the positions, velocities, and accelerations of points in the members of mechanisms and the angular positions, velocities, and accelerations of those members. These are kinematic analysis techniques. The second type of material comprises methods for mathematically determining the geometry of a mechanism to produce a desired set of positions and/or velocities or accelerations. These are rational synthesis techniques.

The activity that distinguishes engineering from science is design. Science is the study of what is; engineering is the creation of what is to be. This creative activity is design or, more formally, synthesis. The rational synthesis techniques developed by kinematicians offer a rather direct route to mechanism design that lends itself well to automation using computer graphics workstations. However, these techniques do not represent the only way to design mechanisms and they are relatively restrictive: Rational synthesis techniques exist only for specific types of mechanism design problems, and many practical mechanism design problems do not fit within the available class of solutions. An alternative is to use

informal synthesis. This is a methodology used by engineers to solve design problems in many technical areas, not just in mechanism design. The basic procedure is to “guess” a set of dimensions and then use analysis to check the resulting performance. The dimensions are then adjusted to attempt to match more closely the performance specifications, and the mechanism is analyzed again. The process is repeated until an acceptably close match to the specifications is achieved. Thus, a primary use of the analysis material is also in mechanism design.

From an engineering point of view, it is not possible to treat mechanism design solely in terms of kinematics. The motivation for performing an acceleration analysis is often to enable inertia forces on the links to be calculated, allowing, in turn, computation of the forces transferred between links and the internal forces, or stresses, within the links. Mechanisms must usually drive loads, as well as generate motions. Of course, as soon as we introduce the concept of force, we leave the domain of pure kinematics and enter that of kinetics. Insofar as the largest forces in many mechanisms are inertia forces created by motion, it is convenient to study them within the general framework of kinematic techniques. There is also an important symmetry between the geometry of the force distribution and that of the velocity distribution that is particularly useful when working with spatial mechanisms. Thus, it is entirely appropriate to treat mechanism statics or kinetics within the general geometry of motion framework constructed to study mechanism kinematics. Such a treatment is presented in the later chapters of this book.

## 1.4 MECHANISMS

---

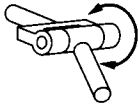


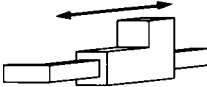
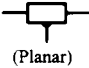

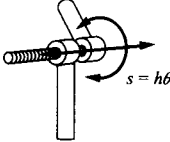
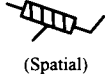
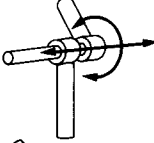
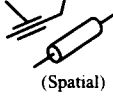
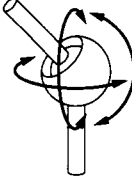
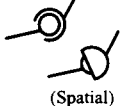
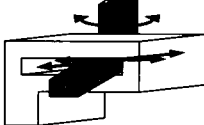

Mechanisms are assemblages of rigid members connected together by joints. Mechanisms transfer motion and mechanical work from one or more actuators to one or more “output” members. For the purposes of kinematic design, we idealize a mechanism to a kinematic linkage in which all the members are assumed to be perfectly rigid and are connected by kinematic joints. A kinematic joint is formed by direct contact between the surfaces of two members. One of the earliest codifications of mechanism kinematics was that of Reuleaux (1876),<sup>1</sup> and some of the basic terminology we use originated with him. He called a kinematic joint a “pair.” He further divided joints into “lower pairs” and “higher pairs.” A lower pair joint is one in which contact between two rigid members occurs at every point of one or more surface segments. A higher pair is one in which contact occurs only at isolated points or along line segments. All other things being equal, a higher pair will produce higher contact stresses than will a lower pair.

Joints are the most important aspect of a mechanism to examine during an analysis. They permit relative motion in some directions while constraining motion in others. The types of motion permitted are related to the number of degrees of freedom (dof) of the joint. The number of degrees of freedom of the joint is equal to the number of independent coordinates needed to specify uniquely the position of one link relative to the other constrained by the joint.

Lower pair joints are necessarily restricted to a relatively small number of geometric types, because the requirement that surface contact be maintained constrains the geometry of the contacting surfaces. It can be shown that there are only six fundamentally different types of lower pair joints, classified by the types of relative motion that they permit. There is, in contrast, an infinite number of possible higher pair geometries. The lower pair joint types are shown in Table 1.1. Some important examples of higher pair joints are shown in Table 1.2.

<sup>1</sup> Reuleaux, F., *The Kinematics of Machinery* (Translated and edited by A. B. W. Kennedy), Dover Publications, Inc., New York, 1963.

TABLE 1.1 Lower Pair Joints

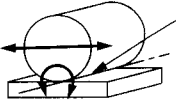
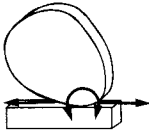

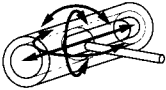
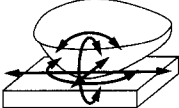
Connectivity (Number of degrees of freedom)	Names	Letter symbol	Typical form	Sketch symbol
1	Revolute Hinge Turning pair	R		  (Planar) (Spatial)
1	Prismatic joint Slider Sliding pair	P		  (Planar) (Spatial)
1	Screw joint Helical joint Helical pair	H		 (Spatial)
2	Cylindrical joint Cylindrical pair	C		 (Spatial)
3	Spherical joint Ball joint Spherical pair	S		 (Spatial)
3	Planar joint Planar pair	P <sub>L</sub>		 (Spatial)

Lower pair joints are frequently used in mechanism design practice. They give good service because wear is spread out over the contact surface and because the narrow clearance between the surfaces provides good conditions for lubrication and a tight constraint on the motion. Changes in the geometric properties of the joint with wear occur slowly for a lower pair. At least as important are the simple geometries of the relative motions that these joints permit.

Higher pair joints that involve pure rolling contact, or that approximate that condition, are also used frequently. In pure rolling contact, the points in one of the two joint surfaces that are actually in contact with the other surface at any instant are at rest relative to that surface. Hence there is no relative sliding of the surfaces and joint friction and wear are minimized. Physically, the limitation of this kind of joint is the stress intensity that the material of the contacting bodies can support. Stresses are necessarily high because of the very small



TABLE 1.2 Some Higher Pair Joints

Connectivity (Number of degrees of freedom)	Names	Typical form	Comments
1	Cylindrical roller		Roller rotates about this line at this instant in its motion. Roller does not slip on the surface on which it rolls.
2	Cam pair		Cam rolls and slides on follower.
3	Rolling ball		Ball rolls without slipping.
4	Ball in cylinder		Ball can rotate about any axis through its center and slide along cylinder axis.
5	Spatial point contact		Body can rotate about any axis through the contact point and slide in any direction in the tangent plane.

contact areas. If the bodies were perfectly rigid, contact would occur only at discrete points or along a line, the contact area would be zero, and the stresses would be locally infinite!

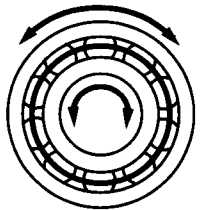
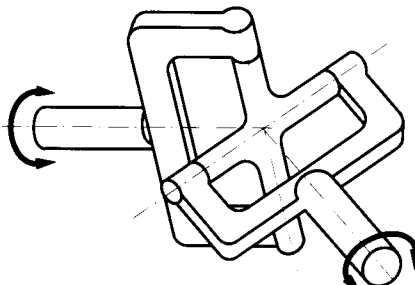
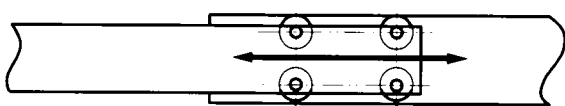
Lower pair joints such as revolute joints and cylindrical joints are also often simulated by systems such as ball or roller bearings in which there are actually many elements acting in parallel. The actual contact joints in a ball bearing are rolling contacts, which are higher pairs. In this way, the low-friction properties of rolling contacts are exploited to obtain a joint with lower friction and higher load and relative speed capabilities than would be possible with a plain revolute joint. At the same time, the simple overall relative motion geometry of the revolute joint is retained. This is one example of a compound joint in which the joint is actually a complex mechanism but is regarded as kinematically equivalent to a simple revolute. Several examples of compound joints are shown in Table 1.3.

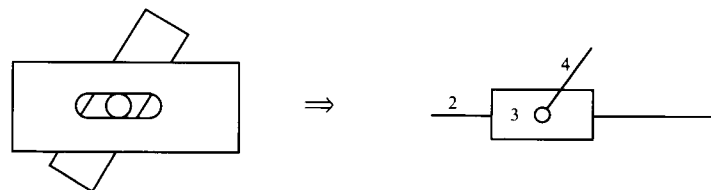
Conversely, higher pairs are sometimes replaced by equivalent lower pair joints (Fig. 1.2). For example, a pin-in-a-slot joint becomes a combination of a revolute joint and a prismatic joint. Note that this involves adding extra members to the mechanism. In both the case in which a lower pair is replaced by a rolling contact bearing, or compound joint, and this case, the two mechanisms are said to be *kinematically equivalent*. This means that the relative motions that are permitted between the bodies in the two cases are the same, even though the joint is physically quite different.

The number of degrees of freedom of a joint is the minimum number of independent parameters required to define the positions of all points in one of the bodies it connects relative to a reference frame fixed to the other. The term *connectivity* is used to denote this

freedom of the body, even though the “joint” may be something very elaborate such as the antifriction bearing shown in Table 1.3 and Fig. 1.3. If motion is restricted to a plane, the maximum number of degrees of freedom is three. In general spatial motion, the maximum number is six. The connectivity or number of degrees of freedom for each joint is listed in Tables 1.1, 1.2, and 1.3 in the first column.

**TABLE 1.3 Some Examples of Compound Joints**

Connectivity	Name	Form
1	Ball bearing Antifriction bearing Rolling contact friction	
2	Universal joint Hooke joint Cardan joint	
1	Roller slide Roller glide	



**FIGURE 1.2** Replacement of a higher pair joint by a kinematically equivalent combination of lower pair joints.

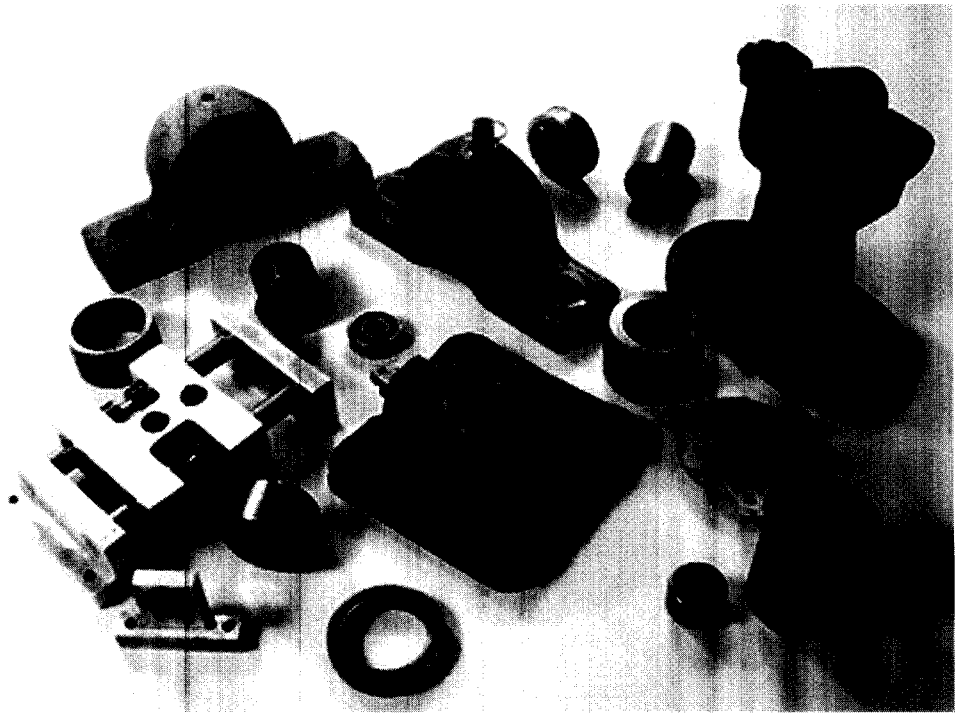


FIGURE 1.3 Various rolling-element and plain bearings.

## 1.5 PLANAR LINKAGES

---

A planar linkage is one in which the velocities of all points in all members are directed parallel to a plane, called the plane of motion. The only lower pair joints that are properly compatible with planar motion are revolute and prismatic joints. The axes of rotation of all revolute joints must be normal to the plane of motion because points would not move in parallel planes otherwise. The directions of sliding of all prismatic joints must be parallel to the plane of motion, since all points in a member connected to another by a prismatic joint move on lines parallel to the sliding direction relative to the second member. Occasionally other lower pair joints will appear in what is otherwise a planar linkage; however, they then function only as revolute or prismatic joints. For example, a spherical joint may be substituted for a revolute joint, but if the linkage is functionally planar, that spherical joint will operate as a revolute joint with rotation occurring only about the axis normal to the plane of motion. This type of situation will be discussed in more detail in the context of degrees of freedom and mobility.

A common schematic method of representing planar linkages is to represent revolute joints by small circles, as shown in Table 1.1. Binary links—those that have two joints mounted on them—are represented as lines joining those joints. Ternary links—those that have three joints mounted on them—are represented as triangles with the joints at the vertices, and so on. Examples of the resulting representations are shown in Figs. 1.4–1.6. The link geometries may then be easily reproduced, giving an accurate view of the linkage in a specified position. Alternatively, the schematic may be used conceptually without accurate

geometric data to indicate the topology of the linkage. Topology is the branch of geometry that deals with issues of connectedness without regard to shape. Links with three or more joints should be shaded or crosshatched. Otherwise, the schematic for a quaternary link, one with four joints, cannot be distinguished from the schematic for a four-bar linkage loop.

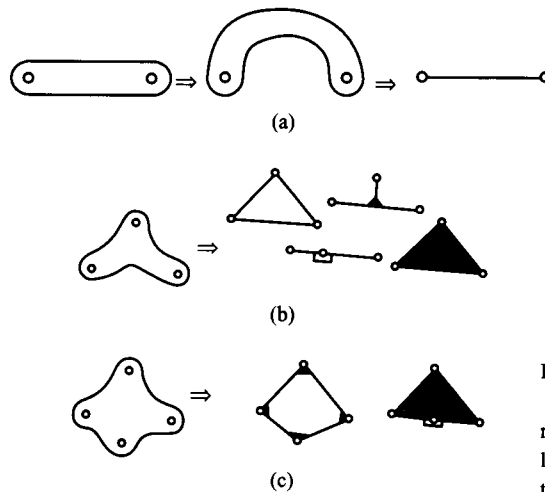
A kinematic chain is any assemblage of rigid links connected by kinematic joints. A closed chain is one in which the links and joints form one or more closed circuits. Each closed circuit is a loop in which each link is attached to at least two other links.

Prismatic joints are represented by means of a line in the direction of sliding, representing a slide, with a rectangular block placed on it. This produces linkage representations such as those shown in Fig. 1.6.

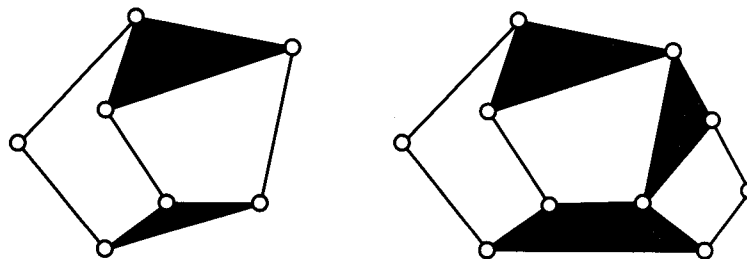
A *frame* or base member is a link that is fixed. That is, it has zero degrees of freedom relative to the fixed coordinate system. A *linkage* is a closed kinematic chain with one link selected as the frame.

In cases in which it is necessary to distinguish the base member of a linkage, it is customary not to show the base as a link in the normal manner but to indicate joints to base by “mounts,” as shown in Figs. 1.7 and 1.8.

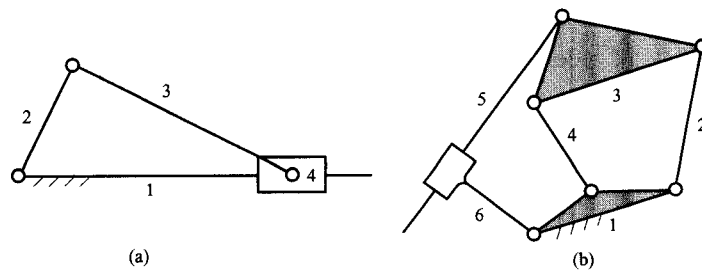
The term *mechanism* is somewhat interchangeable with *linkage*. In normal usage, mechanism is a somewhat more generic term encompassing systems with higher pairs, or



**FIGURE 1.4** Representations of links.  
 (a) Binary links: those to which two joints are mounted. (b) Ternary links and (c) Quaternary links; these have three and four joints, respectively.



**FIGURE 1.5** Conventional representations of planar linkages. Revolute joints are indicated by circles. Binary links, those with two joints mounted on them, are represented by line segments. Ternary links, with three joints, are represented by triangles, and so on.



**FIGURE 1.6** Representations of planar linkages with prismatic joints. (a) A four-bar slider-crank mechanism. Note that the sliding “block” is a binary member of the mechanism with a revolute joint and a prismatic joint providing the connections to adjacent members in the loop. The fillets connecting the block to a binary member represented by a line in (b) represent a rigid connection. Thus, the combination is, in this case, a binary member of the linkage.

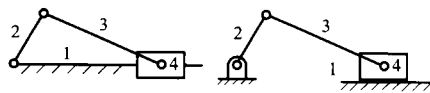
combinations of lower and higher pair joints, whereas the term linkage tends to be restricted to systems that have only lower pair joints. Mechanisms or linkages are generally represented by their links and joints. The links are numbered with the frame link usually taken as link 1.

Simple, single-loop linkages are given a symbolic designation by a sequence of letters denoting joint types written in clockwise order beginning and ending with the joints mounted to the frame link as shown in Fig. 1.9. The letter designations for the different joints are given in Table 1.1.

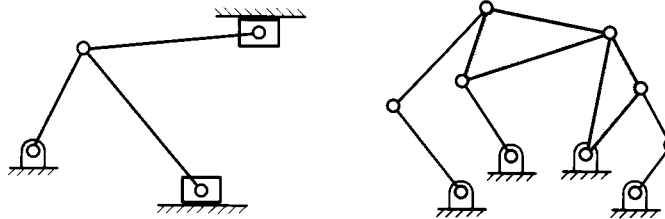
The profiles of the contacting surfaces of higher pairs, such as cams and followers, are drawn in planar linkages producing representations such as that shown in Fig. 1.10. Those surfaces must be general (not necessarily circular) cylinders whose straight-line generators are normal to the plane of motion. The profile drawn is, therefore, the generating curve of the cylinder shown in Fig. 1.11. The cylinder is generated by translating that curve along a straight line in the direction normal to its plane. The familiar cylinder with a circular generating curve is called a right circular cylinder.

## 1.6 VISUALIZATION

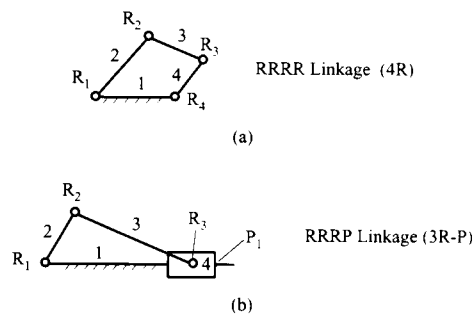
Because linkage motion is inextricably intertwined with geometry, it is always important to the designer to visualize the motion. In this respect, planar linkages are relatively easy to work with because their geometry and loci representing their motion can be drawn on a two-dimensional surface. Nevertheless, it can be very difficult to visualize successive positions of the links of a planar linkage from only a drawing of that linkage in a representative position. Yet this succession of positions and the relative locations of all the links in each of the positions are very important when trying to predict effects such as interference with each other and with other machine parts. Mechanism designers have traditionally solved this problem by constructing simple physical models with the links cut from cardboard and revolute joints formed by pins or grommets. Cards cut from a manila folder with thumbtacks for revolute joints provide an acceptable material for quick visualization models. Prototyping kits (Fig. 1.12) or even children’s construction toys (Fig. 1.13) provide an alternative that requires more construction time but gives a more functional model.



**FIGURE 1.7** Selection of a frame member converts the chain of Fig. 1.6a into a linkage. This linkage is known as a slider-crank linkage.



**FIGURE 1.8** Representations of planar linkages with the base link not shown in the same form as the other links. The page can be thought of as representing the base link. The joints to the base link are indicated by hatched “mounts.”

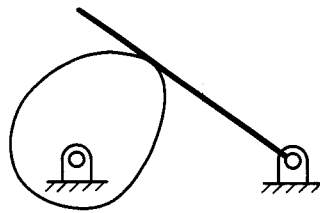


**FIGURE 1.9** Designation of single-loop linkages by means of their joints. The joints are taken in clockwise order around the loop, starting and finishing with a joint to frame.

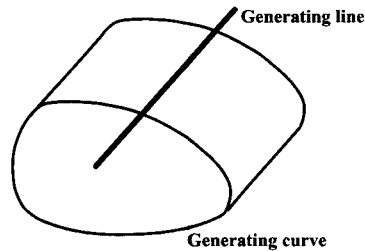
When mechanisms are designed using computer graphics systems, animation on a computer is often used to visualize the motion of the mechanism, rather than construction of a physical model. Animation should be used with caution, however. As will be seen in section 1.18 of this chapter, there are important interference effects that do not lend themselves to planar representation but which, if present, are immediately apparent in a physical model.

Furthermore, adding realistic boundary profiles to the representations of links on computer graphic systems is often time consuming and simply not worth the effort when trying a variety of different alternative linkage configurations. Instead, quick physical visualization models may be a more efficient alternative. The reader is urged to get into the habit of constructing simple models to visualize the motions of linkages that are being designed or analyzed, and to make use of computer animation when it is available.

Three-dimensional systems are much more difficult than planar systems to visualize because the depths of the positions for points on the links are no longer constant. Construction of an adequate physical model is often a major effort requiring machining to shape three-dimensional parts. In this case the most efficient solution is to use one of the solid



**FIGURE 1.10** Representation of a plate cam with a rocker follower. The face of the follower is a plane, so it is represented by a line. The cam is represented by its profile curve.



**FIGURE 1.11** General cylinder. The generating curve is a plane curve. Its plane is normal to the generating line. The surface may be considered to be generated by moving the generating curve so that a point on it moves along the generating line. Alternatively, it may be generated by moving the generating line so that a point on it traverses the generating curve.

modeling software packages that support linkage joint representations and animation of the linkage. Construction of the model involves a considerable effort since each link must be described as a three-dimensional solid. Nevertheless, the effort is usually much less than would be required for the construction of a physical model. Usually it is possible to change the viewpoint from which the representation is projected. This allows the motion to be viewed from several different directions. It also allows areas of interference to be identified and corrected.

## 1.7 CONSTRAINT ANALYSIS

---

The number of degrees of freedom of a body is the number of independent coordinates needed to specify uniquely the position of that body relative to a given reference frame. Similarly, we call the minimum number of coordinates needed to specify uniquely the positions of all of the members of a system of rigid bodies the number of degrees of freedom of that system. In fact, we will use the concept of the number of degrees of freedom in three distinct but closely related ways. The first is the number of degrees of freedom of a body relative to a specified reference frame, which is the definition just given. The second is the number of degrees of freedom of a kinematic joint. The third is the number of degrees of freedom of a linkage or mechanism.

Both because “number of degrees of freedom” is such a mouthful and because we are using a distinct concept, we will refer to the number of degrees of freedom of a joint as its *connectivity*. In addition, the term will apply to the number of relative freedoms between two bodies. Likewise, we will refer to the number of degrees of freedom of a linkage as the *mobility* of that linkage. These terms may be formally defined as follows:

If a kinematic joint is formed between two rigid bodies that are not otherwise connected, the *connectivity* of that joint is the number of degrees of freedom of motion of (either) one of the two bodies joined relative to the other.

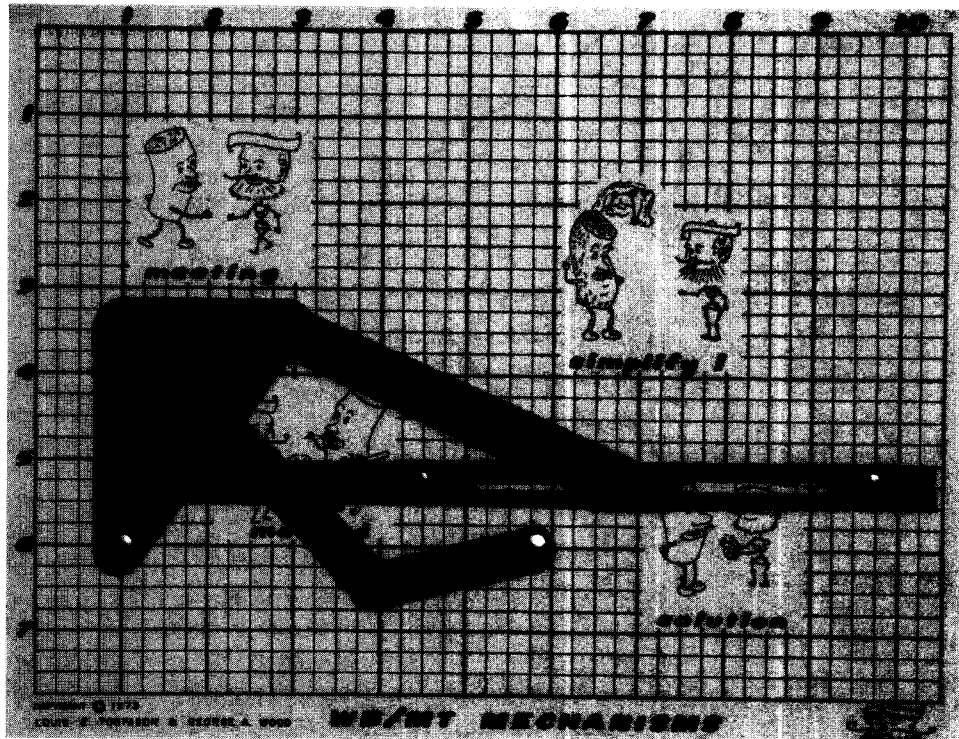


FIGURE 1.12 J. Woody Blockhead model.<sup>2</sup>

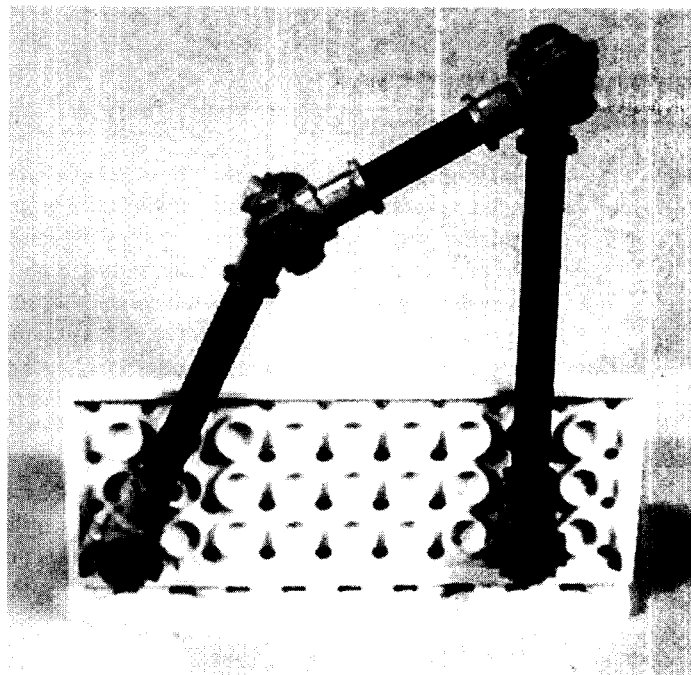


FIGURE 1.13 Model made with LEGOS Technics.<sup>3</sup>

<sup>2</sup> Wood, G. A., and Torfason, L. E., *Mechanism Modeling*. Wood & Torfason, Lincoln, MA, 1975.

<sup>3</sup> LEGO Systems, Inc., 555 Taylor Road, Enfield, CT.



The *mobility* of a mechanism is the minimum number of coordinates needed to specify the positions of all members of the mechanism relative to a particular member chosen as the base or frame.

The mobility, or number of degrees of freedom of a linkage, is used to determine how many pair variables must be specified before the positions of all of the points on all of the members of the linkage can be located as a function of time. A linkage has a mobility of one or more. Traditionally, almost all linkages had one degree of freedom. However, in modern design practice, linkages with two or more degrees of freedom are becoming more common. If the mobility is zero or negative, as determined by the constraint equations developed in the following, the assemblage is a structure. If the mobility is zero, the structure is statically determinate. If the mobility is negative, the structure is statically indeterminate.

To compute the mobility, let us consider the planar case first and then extend the results to the spatial case. As indicated in Fig. 1.14, in the plane, a body moving freely has three degrees of freedom. Suppose that in a given linkage there are  $n$  links. If they are all free to move independently, the system has mobility  $3n$ . If one link is chosen as the frame link, it is fixed to the base reference frame and loses all of its degrees of freedom. Therefore the total mobility of the system is  $3(n - 1)$  with no joints formed between the members.

If a joint with connectivity  $f_i$  ( $f_i$  degrees of freedom) is formed between two bodies, the mobility of the system is diminished since those two bodies originally had three degrees of freedom of motion relative to one another. After formation of the joint, they have only  $f_i$  degrees of freedom of relative motion. Hence the reduction in the system mobility is  $3 - f_i$ . If joints continue to be formed until there are  $j$  joints, the loss of system mobility is

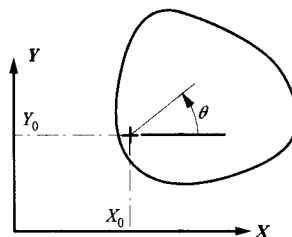
$$(3 - f_1) + (3 - f_2) + \dots + (3 - f_j) = \sum_{i=1}^j (3 - f_i) = 3j - \sum_{i=1}^j f_i$$

Then the total mobility of the linkage will be

$$M = 3(n - 1) - \left( 3j - \sum_{i=1}^j f_i \right) = 3(n - j - 1) + \sum_{i=1}^j f_i \quad (1.1)$$

Equation (1.1) is called a constraint criterion. There are many different-appearing versions of this relationship to be found in the literature. They all, in fact, are equivalent to one another, except that some are restricted to a subset of the cases covered by Eq. (1.1).

A problem arises in some cases in which more than two members are apparently connected by the same joint. Typically, three or more members are pinned together by the same shaft and are free to rotate relative to one another about the same revolute axis. This difficulty is readily resolved if we recall that a kinematic joint is formed by contact between the surfaces of *two* rigid bodies. This is the reason for Reuleaux's name "pair" for what we here call a "joint." Considering the present case, we see that there is not one joint but several between the bodies. In fact, if  $p$  members are connected by a "common" joint, the connection is equivalent to  $p - 1$  joints all of the same type. Inclusion of this number in  $j$ , and using  $(p - 1)f_i$  in the connectivity sum of Eq. (1.1) will ensure correct results. This is illustrated in a later example (see Example 1.3).

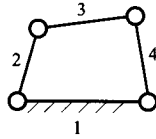


**FIGURE 1.14** One set of three coordinates that can be used to describe planar motion. The number of degrees of freedom of a body is the number of independent coordinates needed to specify its position. Therefore, a body moving freely in a plane has three degrees of freedom.

**EXAMPLE 1.1**  
**Degrees of Freedom in a Simple Four-Bar Linkage**

Determine the mobility of the planar four-bar linkage shown in Fig. 1.15.

**Solution**



$$n = j = 4$$

$$\sum_{i=1}^j f_i = j \times 1 = 4$$

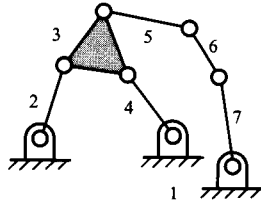
$$M = 3(4 - 4 - 1) + 4 = 1$$

**FIGURE 1.15** Mobility analysis of a planar four-bar linkage.

**EXAMPLE 1.2**  
**Degrees of Freedom in a Complex Mechanism**

Determine the mobility of the linkage shown in Fig. 1.16. The linkage is planar and all joints have connectivity one.

**Solution**



$$n = 7, j = 8$$

$$\sum_{i=1}^j f_i = j \times 1 = 8$$

$$M = 3(7 - 8 - 1) + 8 = 2$$

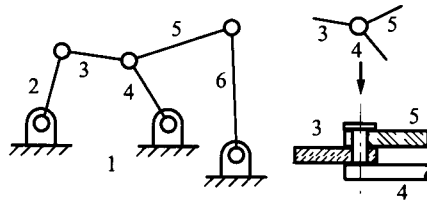
**FIGURE 1.16** Mobility analysis of a two-loop planar linkage.

Notice that the base member must always be counted even when it is not shown in the same way as the other members but just by a set of “bearing mounts.”

**EXAMPLE 1.3**  
**Degrees of Freedom When Joints Are Coincident**

Determine the mobility of the linkage shown in Fig. 1.17. The linkage is planar and all joints have connectivity one. Links 3, 4, and 5 are connected at the same revolute joint axis.

**Solution**



**FIGURE 1.17** Mobility analysis of a linkage when more than two members come together at a single point location.

$$n = 6, j = 7$$

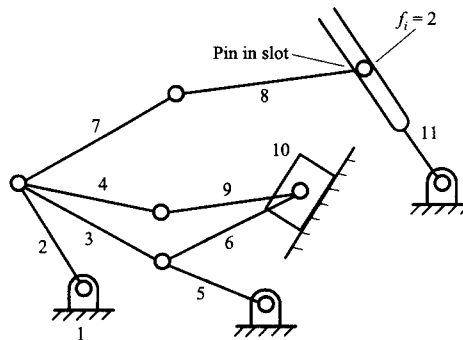
$$\sum_{i=1}^j f_i = j \times 1 = 7$$

$$M = 3(n - j - 1) + \sum_{i=1}^j f_i = 3(6 - 7 - 1) + 7 = 1$$

As indicated previously, when  $p$  members are connected at the same joint axis, then  $p - 1$  joints are associated with the same axis. Hence the location where links 3, 4, and 5 come together counts as two revolute joints. As indicated in the figure, members 3 and 5 can be thought of as being connected to link 4 by two separate revolute joints that have the same axis of rotation.

**EXAMPLE 1.4**  
**Degrees of Freedom for a Mechanism Containing a Higher Pair**

Determine the mobility of the linkage shown in Fig. 1.18. The linkage is planar and not all of the joints have connectivity one.



**FIGURE 1.18** Mobility analysis of a linkage with various types of joints.

**Solution**

In this mechanism, there are three places where more than two links come together at the same revolute joint location. In addition, there is a pin-in-a-slot joint that permits two degrees of freedom (connectivity equals two). Therefore, the joints must be counted carefully. When this is done, we find  $n$  and  $j$  to be

$$n = 11, j = 14$$

and

$$\sum_{i=1}^j f_i = 13 \times 1 + 1 \times 2 = 15$$

Then,

$$M = 3(n - j - 1) + \sum_{i=1}^j f_i = 3(11 - 14 - 1) + 15 = 3$$

A special case that deserves attention occurs when the mobility in Eq. (1.1) is set to one and all joints have connectivity one ( $f_i = 1$ ). Then, Eq. (1.1) gives

$$1 = 3(n - j - 1) + j$$

or

$$4 = 3n - 2j \tag{1.2}$$

Because  $n$  and  $j$  are integers,  $n$  must be even because 4 and  $2j$  are both even numbers. This is an example of a Diophantine equation. That is one that admits only integral solutions. Written as an expression for  $j$  in terms of  $n$ , the equation becomes

$$j = 3n/2 - 2$$

Some of the possible solutions are listed in Table 1.4. In each case, the joints may be either revolute or prismatic joints, since they are the only lower pair joints that can properly be included in planar linkages.

Solution 1 gives the rather trivial case of two bodies connected by a single revolute or slider joint. This is shown in Fig. 1.19a. Actually, this mechanism is very common. For example, a door, its hinges, and the door frame form an open kinematic chain and a mechanism of this type.

Solution 2 gives a single, closed loop of four members with four joints. Two forms are shown in Figs. 1.19b and 1.19c. The one in Fig. 1.19b is the planar four-bar linkage that forms a major element in planar linkage theory. The one in Fig. 1.19c is the slider-crank linkage, which is also extensively studied.

Solution 3 presents two new features. First members with more than two joints mounted on them appear. Second, even when only revolute joints are included, there are two possible, topologically distinct, configurations of six members with seven joints. These are respectively named the Watt and Stephenson six-bar chains and are shown in Fig. 1.20.

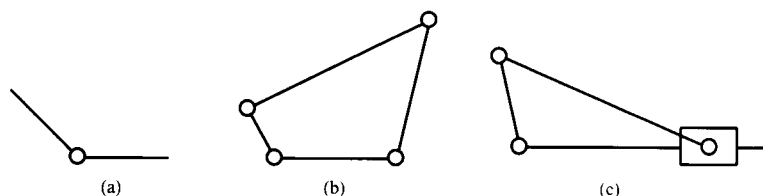
Solution 4 gives 16 possible different topological configurations, shown in Fig. 1.21, and solution 5 gives 230. The number increases very rapidly with larger numbers of members. For example, solution 6 gives 6856 configurations (Hunt, 1978).<sup>4</sup>

From this discussion, it should be apparent why we spend so much effort on the design of four-link mechanisms. The four-link arrangement is the simplest possible non-trivial linkage. It turns out that most design requirements can be met by four- or six-link mechanisms.

Note that, in this discussion, the type of the joints was not specified. All that was specified was that the joints have connectivity one and that the linkage is planar and has mobility one. Although the joints pictured in Figs. 1.19–1.21 are all revolute, rolling contact joints could be substituted for any of the joints, and prismatic joints could be substituted

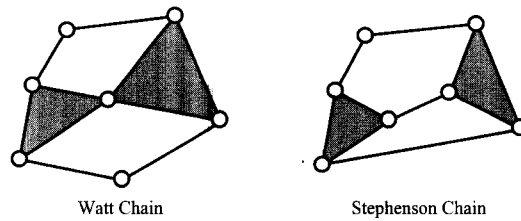
**TABLE 1.4** Different Integer Solutions to Eq. (1.2) for Mobility of One

Solution number	$n$	$j$	Number of configurations
1	2	1	1
2	4	4	1
3	6	7	2
4	8	10	16
5	10	13	230
6	12	16	6856

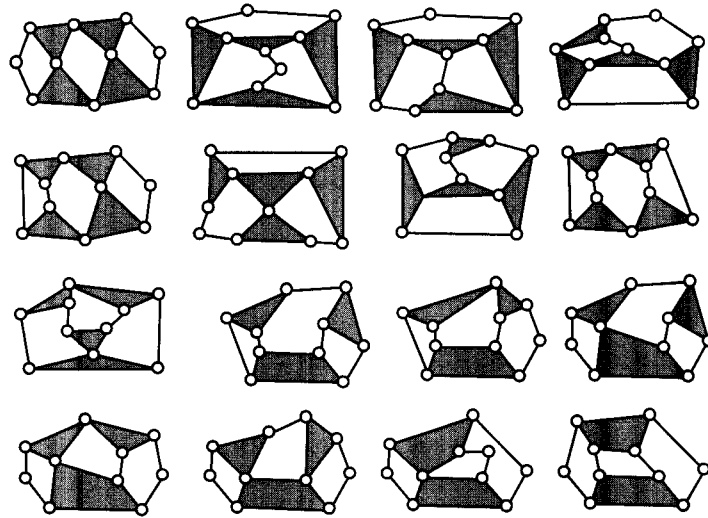


**FIGURE 1.19** Solutions of the planar mobility equation for  $M = 1$  when  $n = 2$  and  $n = 4$ .

<sup>4</sup>Hunt, K. H., *Kinematic Geometry of Mechanisms*, Oxford University Press, Oxford, UK, p. 40, 1978.



**FIGURE 1.20** The two solutions of the planar mobility equation for seven revolute joints.  $M = 1$  and each kinematic chain has six members.

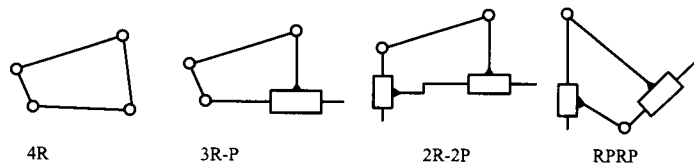


**FIGURE 1.21** The 16 solutions of the planar mobility equation for 10 revolute joints.  $M = 1$  and each kinematic chain has eight members.

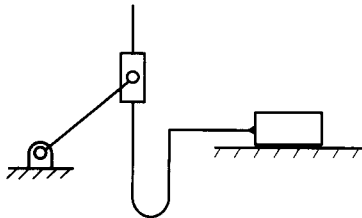
for some of them. Thus, even if the joints are confined to lower pairs, the four-link, four-joint solution represents the four different chains shown in Fig. 1.22. The Scotch yoke, based on the 2R-2P chain, is shown in Fig. 1.23.

Further, as discussed later in this chapter, the important concept of inversion generates several different linkages from any mechanism based on the 3R-P and 2R-2P chains. An inversion is a different mechanism derived from a given mechanism or linkage by changing the base member. “Different” means that the motion relative to the frame that can be produced by the inversion is different from that provided in the original mechanism, that is, the inversion produces a different general form for the paths of points on the different links or a different input–output function.

A different inversion is produced for each choice of frame link. As a result, the 3R-P chain produces four different mechanisms. In the basic slider-crank mechanism, the frame member has one revolute and one prismatic joint mounted on it. We can also make the slider the frame. The other two inversions are turning block linkages in which the base has two revolutes mounted on it. The 2R-2P chain can produce three different mechanisms: The Scotch yoke has one revolute and one prismatic joint mounted on the frame, the double slider has two prismatic joints on the frame, and the third mechanism, the Oldham coupling, has both revolutes mounted on the frame.



**FIGURE 1.22** Four different forms of four-bar chains with combinations of revolute and prismatic joints.



**FIGURE 1.23** The 2R-2P chain as a Scotch yoke mechanism.

## 1.8 CONSTRAINT ANALYSIS OF SPATIAL LINKAGES

In spatial motion, each body that moves freely has six degrees of freedom rather than three. Using exactly the same reasoning as was used in the planar case, the constraint criterion equation becomes

$$M = 6(n - j - 1) + \sum_{i=1}^j f_i \quad (1.3)$$

This is called the Kutzbach criterion. If only lower pair joints are involved, each with connectivity one, the equations become

$$M = 6(n - j - 1) + j = 6n - 5j - 6$$

If the linkage is required to have mobility one, this gives

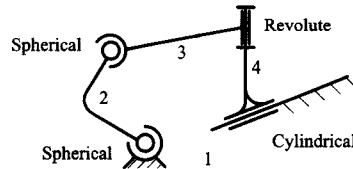
$$6n = 7 + 5j \quad (1.4)$$

Equation (1.4) corresponds to Eq. (1.2) derived in the case of planar motion. Like that equation, it is a Diophantine equation that admits only integral values of the variables. Evidently,  $j$  must be odd because  $5j$  must be odd to combine with the odd number 7 to produce the even number  $6n$ . The sum  $7 + 5j$  must also be divisible by 3. Solutions to Eq. (1.4) are a little harder to generate than those of Eq. (1.2). The simplest solution is given by  $j = 1$  and  $n = 2$ . This is exactly the same as the simplest solution in the planar case depicted in Fig. 1.19a. The next allowable solution is  $j = 7$  and  $n = 7$ . This is a single, closed loop with seven members and seven joints. It bears the same relationship to general spatial linkage topologies that the planar four-bar linkage does to planar ones. The next order solution is  $j = 13$ ,  $n = 12$ . There are three distinct topological forms in this case. For spatial mechanisms, the complexity increases with the number of members and joints even more rapidly than it does for planar joints.

**EXAMPLE 1.5**  
**Degrees of Freedom in a Spatial Mechanism**

Determine the mobility of the linkage shown in Fig. 1.24. The linkage is spatial. The joints are lower pairs of the types labeled.

Note how the three-dimensional joints are drawn. There is no formalism that is more or less universally recognized for representing spatial mechanisms as there is for planar linkages; however, we will follow the symbols shown in Table 1.1.



**FIGURE 1.24** A four-member, single-loop, spatial linkage.

**Solution**

$$n = j = 4$$

$$\sum_{i=1}^j f_i = 2 \times 3 + 1 \times 1 + 1 \times 2 = 9$$

$$M = 6(n - j - 1) + \sum_{i=1}^j f_i = 6(4 - 4 - 1) + 9 = 3$$

Another way of looking at the constraint criterion is in terms of closures. Imagine building up the linkage by starting with the base link and successively adding members and joints. If a joint connects an additional member to the system, the number of degrees of freedom is increased by  $f_j$  if  $f_i$  is the connectivity of that joint, and the numbers of members and joints are both increased by one. If a joint is made between two members that are already part of the linkage, the total number of degrees of freedom is decreased by the number of constraints imposed by that joint. The number of constraints imposed by a joint is the number of degrees of freedom lost by the system when that joint is formed. For a spatial mechanism, it is  $6 - f_i$  since two bodies have six degrees of freedom of motion relative to one another when they are free of each other and only  $f_i$  degrees of freedom of relative motion after the joint is formed. Also, in this case, the formation of the joint results in the formation of a closed loop of members and joints within the linkage. This is called a closure. Proceeding in this manner, we can express the mobility of the linkage as

$$M = \sum_{i=1}^j f_i - 6c$$

where  $c$  is the number of closures. Now, when a closure is formed, the number of members does not increase, whereas the number of joints increases by one. If there are no closures (open kinematic chains), the number of link members is given by

$$n = j + 1$$

the additional member being the base member. Therefore, if there are  $c$  closures in the linkage

$$c = j + 1 - n$$

Thus, substitution for  $c$  in the expression for the mobility leads to Eq. (1.4). The relationship among  $c, j$ , and  $n$  is illustrated in Fig. 1.25.

The reason for looking at the constraint criterion from this viewpoint is that it relates to the position analysis of a spatial linkage. When a closure is formed, a set of six algebraic equations called closure equations can be written. The formulation of these equations will be briefly treated in Chapter 9, although their study lies largely beyond the scope of this book. The quantity  $6c = 6(j + 1 - n)$  is therefore the number of equations available for position analysis of the mechanism. The variables in those equations are the joint parameters, the variables needed to fix the relative positions of the bodies connected by each joint. There are  $f_i$  of these joint parameters for joint  $i$ . Therefore the total number of variables in the linkage is

$$c = \sum_{i=1}^j f_i$$

In this way, it may be seen that Eq. (1.4) expresses the mobility of the linkage as the number of variables less the number of equations for the system.

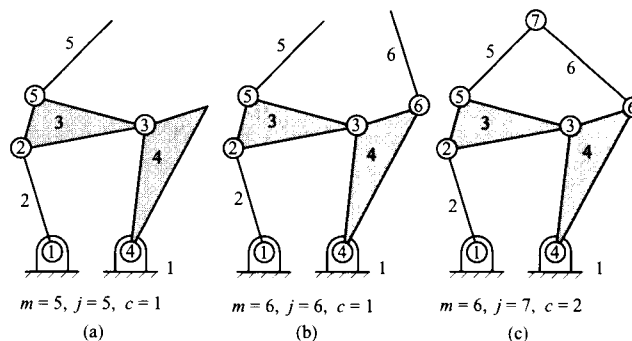
Yet another viewpoint on the constraint criterion that it is productive to pursue is that of static force analysis. Free body diagrams can be drawn for all members except the base. Six static equilibrium equations can be written for each free body. Hence there are  $6(n - 1)$  equations describing the system. At each joint there is a number of reaction force and torque components that is equal to the number of constraints of that joint. These force components are the variables in a static force analysis. Since the number of constraints at joint  $i$  is  $6 - f_i$ , the number of variables is

$$\sum_{i=1}^j (6 - f_i) = 6j - \sum_{i=1}^j f_i$$

Therefore, the difference between the number of variables and the number of equations is

$$6j - \sum_{i=1}^j f_i - 6(n - 1) = -M$$

Thus, the mobility is meaningful from the point of view of static force analysis also. If  $M = 0$ , the linkage is not movable and is a structure. The position problem can be solved to obtain the joint positions that cannot vary. The static equilibrium problem can be solved for all of the reaction force and torque components. The structure is statically determinate since there is a unique solution to the static equilibrium problem.



**FIGURE 1.25** The effect of adding a member to a linkage together with a joint (b) and of adding a joint without an additional member (c). Adding a joint without a member always closes a loop within the linkage.



If the mobility is  $-1$ , the number of equations for the position problem exceeds the number of variables. Therefore, in general there is no solution to the position problem. For a solution to exist it is necessary for the equations to be dependent. This means that the geometry of the mechanism must satisfy the conditions needed for the equations to be dependent. Physically, this means that, in general, it is not possible to assemble the linkage. One or more of the closures cannot be made. However, if the link geometry is changed to bring the surfaces for the closing joint into alignment, the linkage may be assembled.

From the viewpoint of force analysis, the mobility is the number of static equilibrium equations less the number of force variables: the converse of the situation for position analysis. Thus, if  $M = -1$  there is one more force variable than the number of force equations. Therefore, in this case solutions of the system exist, but there is no unique solution. The force problem cannot be solved without additional information relating the forces in the system. The linkage is a statically indeterminate structure. If the links are modeled as elastic rather than rigid solids, compatibility of their deflections under load provides the necessary additional relationship.

Conversely, if the mobility is one or more, the number of position variables is greater than the number of position equations. Solutions to the system exist, but there is no unique solution. The number of force equations is greater than the number of force variables, so, in general, no solution to the static force problem exists. In practice, application of an arbitrary set of loads to the linkage would lead to rapid, uncontrolled acceleration, and the system behavior could not be described without writing dynamic equations. However, this invalidates the assumption of a static model.

Specification of the value of a joint parameter is equivalent to fixing that joint. Physically, it might be done by putting an actuator on that joint that would hold it in position. The joint can now support a force, or torque. The effect is to increase the number of unknown force variables by one. If a linkage has mobility one, fixing the position of a joint with connectivity one converts it into a structure. It also converts the static force problem from one in which there is one more equation than there are variables to one in which the number of variables is the same as the number of equations. That is, it is statically determinate.

Fixing the torque applied about a revolute joint, or the force applied by an actuator at a prismatic joint, has a quite different effect. It does not change the number of variables or the number of equations in either the position or the force problem. This is because having a passive joint is already equivalent to fixing the force or torque variable about that joint. The torque applied at a passive revolute joint is fixed to zero. Changing it to any other value does not affect the number of unknown variables. Of course, it does affect the values of the unknown force variables.

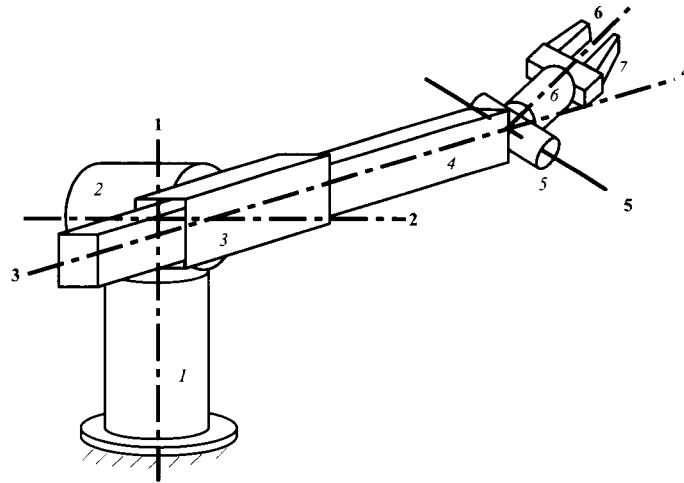
This effect is quite important in practical applications of multiply actuated mechanisms. Consider the manipulator arm shown in Fig. 1.26. It has seven members (*italic numbers*) and six joints. The heavy dashed lines with bold numbers indicate the joint axes. Joints 1, 2, 4, 5, and 6 are revolute joints. Joint 3 is a prismatic joint. The axes of joints 3 and 4 are the same. Member 1 is the base member.

Applying the constraint criterion to this mechanism, we have  $n = 7$ ,  $j = 6$ , and  $\sum f_i = 6$ , so

$$M = 6(n - j - 1) + \sum_{i=1}^j f_i = 6(7 - 6 - 1) + 6 = 6$$

If we actuate all of the joints so that we can specify their positions, the position of the mechanism is uniquely specified.

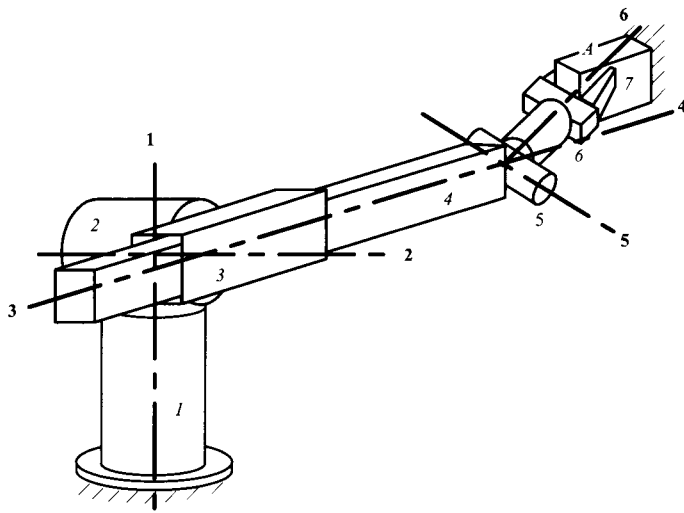
Consider now what happens if the manipulator grips an object that is fixed relative to the base member, as is shown in Fig. 1.27. It is assumed that the gripper grasps the object



**FIGURE 1.26** A robotic manipulator that is used to produce general spatial motions of its gripper. The mechanism has seven members, indicated by the italic numbers, and six joints. Joints 1, 2, 4, 5, and 6 are revolute. Joint 3 is a prismatic joint. The heavy dashed lines indicate the joint axes. The axes of joints 3 and 4 are coincident.

tightly so that no relative motion is possible. The effect is to make link 7 a part of link 1. Therefore, application of the constraint criterion gives  $n = 6$ ,  $j = 6$ , and  $\sum f_i = 6$ , so

$$M = 6(n - j - 1) + \sum_{i=1}^j f_i = 6(6 - 6 - 1) + 6 = 0$$



**FIGURE 1.27** The robotic manipulator of Fig. 1.26 gripping a fixed object. If the gripper grasps the object so that no relative motion is possible, the gripper becomes fixed to member one. This reduces the number of members in the system to six and closes a loop.

The mechanism is now a structure, and we do not have the liberty of setting the joint variables to any value we wish. Attempting to control the mechanism by commanding joint positions, as is done when the manipulator is moving freely, is not effective in this case. Since most manipulator structures are very stiff, a small position error results in very large forces on the actuators. The usual result is that the actuator controllers become unstable, producing violent vibratory behavior. However, commanding the actuators to produce specified forces or torques eliminates the problem. The actuator torques and forces can be set to any desired set of values. In this way it is possible to apply a specified force system to the fixed object  $A$  by means of the manipulator. Notice that commanding forces and torques all the time is not a solution. If actuator forces are commanded when the manipulator is moving freely, the number of static equilibrium equations exceeds the number of variables by six and the manipulator will perform rapid uncontrolled movements, violating the assumption of static stability.

## 1.9 IDLE DEGREES OF FREEDOM

---

Equation (1.4) sometimes gives misleading results. There are several reasons for this. One is the phenomenon of idle degrees of freedom. Consider the linkage shown in Fig. 1.28. This linkage has four members and four joints. Two of the joints are revolute. The other two are spherical joints. This mechanism is quite often used in situations such as the steering mechanisms of automobiles. Applying the constraint criterion, we have  $n = 4$ ,  $j = 4$ , and  $\sum f_i = 2 \times 1 + 2 \times 3 = 8$ . Therefore

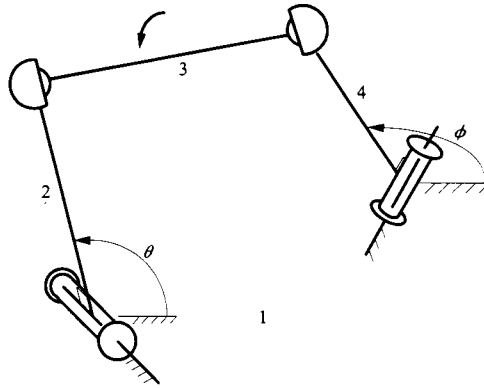
$$M = 6(n - j - 1) + \sum_{i=1}^j f_i = 6(4 - 4 - 1) + 8 = 2$$

Nevertheless, practical experience with this mechanism shows that there is a unique value of the output joint angle,  $\phi$ , for any given value of the input angle,  $\theta$ . How can this be explained?

Examination of the mechanism reveals that the coupler member is free to spin about the line through the centers of the two spherical joints. This motion—termed an idle degree of freedom—can take place in any position of the linkage without affecting the values of the input and output joint angles. That is, an idle degree of freedom is one that does not affect the input–output relationship of the linkage.

The real problem here is that usually we are not really interested in the mobility of the entire linkage, that is, of all of its links. Rather, we are interested in the connectivity that the linkage provides as a joint between two of its members. This is a new use of the term connectivity. Previously we applied it only to simple joints at which the members contact each other directly. However, a mechanism constrains the number of degrees of freedom of relative motion of any two of its members. Therefore it can be regarded as forming a kinematic joint between any two of its members. We can define its connectivity as a joint between those members and as the number of degrees of freedom of relative motion that it permits between the members.

In the example of Fig. 1.28, the connectivity of the linkage as a joint between the input and output members is one, even though the mobility of the linkage is two, and the connectivity between links 3 and 1 is two. The mobility places an upper bound on the connectivity of the mechanism as a joint between any two of its members. There is no simple method of directly determining connectivity, so the mobility equation is used. If the mobility is one and

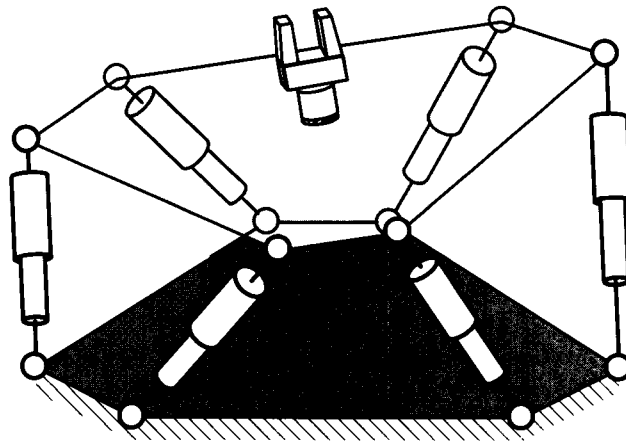


**FIGURE 1.28** A spatial four-member, four-joint linkage. Two of the joints are revolute. The other two are spherical joints.  $\theta$  is the input-joint angle, and  $\phi$  is the output-joint angle. The linkage has an idle degree of freedom since member 3 can spin about the line joining the centers of the spherical joints without affecting the relationship between  $\theta$  and  $\phi$ .

the linkage is not overconstrained in some local region, there is no problem. The connectivity of the linkage as a joint between any two of its members is also one. If the mobility is greater than one, strictly speaking, all that can be said is that the connectivity between any given pair of members may be equal to the mobility or may be less than that number. Fortunately, idle degrees of freedom usually can be identified by inspection.

Another example is shown in Fig. 1.29. This is one form of the so-called Stewart platform mechanism. This mechanism is commonly used to produce general spatial motions in aircraft simulators for training pilots. The output member is connected to the base by six "limbs," each of which has an actuated prismatic joint in the middle and two spherical joints at either end. There are 14 members: 2 in each of the limbs plus the base and output members. There are 18 joints: 6 prismatic joints and 12 spherical joints. Hence  $\sum f_i = 6 \times 1 + 12 \times 3 = 42$ . Therefore

$$M = 6(n - j - 1) + \sum_{i=1}^j f_i = 6(14 - 18 - 1) + 42 = 12$$



**FIGURE 1.29** Stewart platform.

However, it is easily seen that each limb is free to spin about the line joining the centers of its spherical joints without affecting the position of the output member relative to the base. Therefore, the mechanism has six idle degrees of freedom, and its connectivity as a joint between base and output member is

$$C = M - 6 = 6$$

Therefore, by appropriately positioning the actuated prismatic joints, the output member can be placed in any position within its working volume.

Although idle degrees of freedom are most common in spatial linkages, they can also occur in planar linkages. Typically, this occurs when cam roller followers are involved. For example, if the mobility of the linkage in Fig. 1.30 is computed, it will be found to be one if there is rolling contact between the roller (link 5) and the cam (link 6) at point  $C$ . However, if there is cam contact at  $C$ , the mobility will be two. The extra degree of freedom is associated with the free rotation of link 5 relative to the frame. Usually, this rotation will be of no interest because the motion of all of the other links in the mechanism will be unaffected by this rotation.

To locate the idle degrees of freedom, it is first necessary to identify the input link and output link. Then one must check to determine if a single link or a combination of connected links can move without altering the relative position of the input and output links. Idle degrees of freedom are dependent both on geometry and on the choice of the input and output. In some cases, idle degrees of freedom can exist for one choice of input and output but not for a different choice.

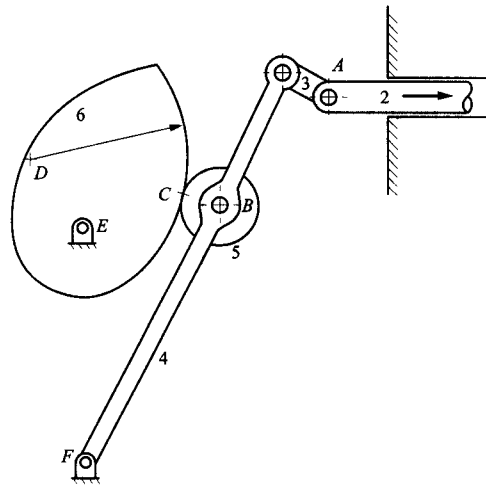
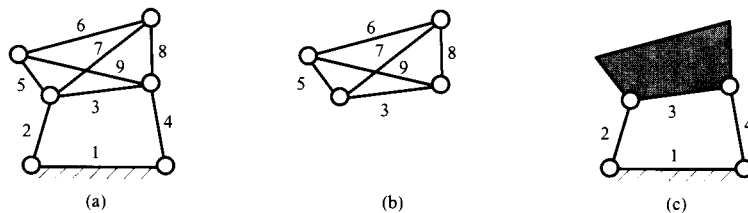


FIGURE 1.30 Planar mechanism with an idle degree of freedom.

## 1.10 OVERCONSTRAINED LINKAGES

A second reason why the constraint criteria [Eqs. (1.1) and (1.4)] sometimes give misleading results is the phenomenon of overconstraint. A mechanism can be overconstrained either locally or generally. If the mechanism is overconstrained locally, a portion of the system may be a structure, but the entire mechanism can move. When this happens, we must replace that portion of the linkage with a single rigid body and recompute the mobility of the mechanism. An example is shown in the planar system of Fig. 1.31a.



**FIGURE 1.31** (a) A planar mechanism in which part of the mechanism is a structure, leading to a misleading value of mobility. All joints are revolute. (b) The part of the mechanism that is a statically indeterminate structure. (c) A modified model of the linkage that gives the correct mobility value.

Here  $n = 9$ ,  $j = 2 \times 1 + 2 \times 2 + 2 \times 3 = 12$ . Note that there are two joints at which three members are connected and two at which four members are connected.  $\sum f_i = j - 12$ . Hence

$$M = 3(n - j - 1) + \sum_{i=1}^j f_i = 3(9 - 12 - 1) + 12 = 0$$

However, it can be observed that the portion of the linkage consisting of members 3, 5, 6, 7, 8, and 9 is a statically indeterminate structure. This portion is shown in Fig. 1.31b. Here  $n = 6$ , and because three members are connected at each joint location,  $j = 4 \times 2 = 8$ . Also,  $\sum f_i = j = 8$ . Therefore,

$$M = 3(n - j - 1) + \sum_{i=1}^j f_i = 3(6 - 8 - 1) + 8 = -1$$

revealing the statically indeterminate nature of the structure and the source of the error in the mobility value. A portion of the linkage that is a statically determinate structure does not cause an error in calculating mobility.

To compute a correct value of mobility, the linkage is remodeled as shown in Fig. 1.31c with the portion that is a structure replaced by a single, rigid member. The linkage is now revealed to be a planar four-bar linkage for which the mobility is one.

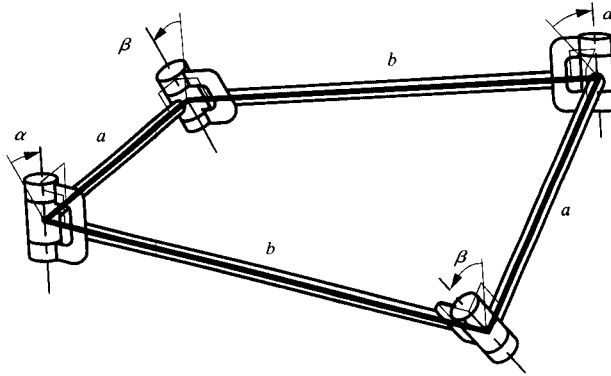
Mechanisms, especially spatial mechanisms, can also be generally overconstrained. Figure 1.32 shows a spatial linkage with four members and four revolute joints. It has a special geometry. The opposite members are identical, and the normals to the pairs of axes in the links intersect at the joint axes. The lengths of those normals ( $a$  and  $b$ ) are related to the angles between successive axes ( $\alpha$  and  $\beta$ ) by the relationship

$$a \sin \beta = b \sin \alpha$$

As was demonstrated approximately one hundred years ago by Bennett, this linkage has mobility one. However, if we apply the constraint criterion with  $n = j = 4$  and  $\sum f_i = 4$ , the result is

$$M = 6(n - j - 1) + \sum_{i=1}^j f_i = 6(4 - 4 - 1) + 4 = -2$$

In this case, because of the special geometry, the position equations of the linkage turn out to be dependent in all positions. For this reason, the effective number of equations is only three, rather than the six that would be expected for a single closed loop. Because the constraint criterion calculates the difference between the number of position variables and the number of available equations, it miscounts the mobility by three degrees of freedom. It

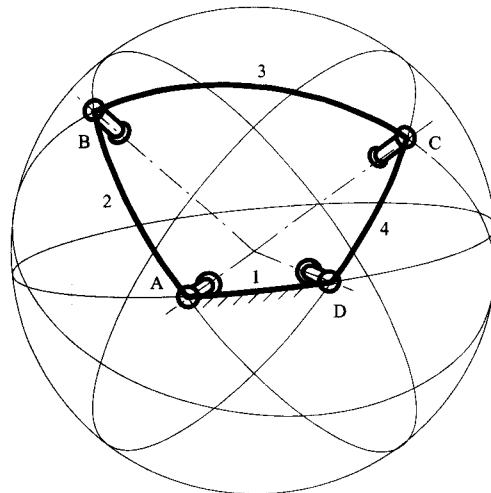


**FIGURE 1.32** The Bennett mechanism. The side lengths and twist angles obey the relationship  $a \sin \beta = b \sin \alpha$ .

turns out that rather a large number of linkages have anomalous mobility like the Bennett mechanism. They are called overconstrained linkages. Many of these are largely curiosities. However, there are several very important families of overconstrained linkages that are exceedingly common in engineering practice.

The most common example of overconstraint is the family of planar linkages. There is no *a priori* reason why planar linkages should not obey the general spatial mobility criterion. Nevertheless, they do not. Equation (1.3) gives a value for  $M$  that is always  $3c$  less than the correct value, where  $c$  is the number of independent closure equations for the linkage. The fact that planar linkages obey Eq. (1.1), which has the same form as Eq. (1.3) but with the coefficient 6 replaced by 3, indicates that only three of the six equations produced by any closure are independent for a planar linkage.

Another common family of overconstrained linkages is the family of spherical linkages. These are linkages whose joints are all revolute. The axes of those joints all pass through a single point. Figure 1.33 shows a spherical four-bar linkage.



**FIGURE 1.33** Spherical four-bar linkage.

Spherical linkages obey the same form of constraint criterion as planar linkages and the Bennett linkage. Thus, three of the equations resulting from each closure in a spherical linkage are always dependent.

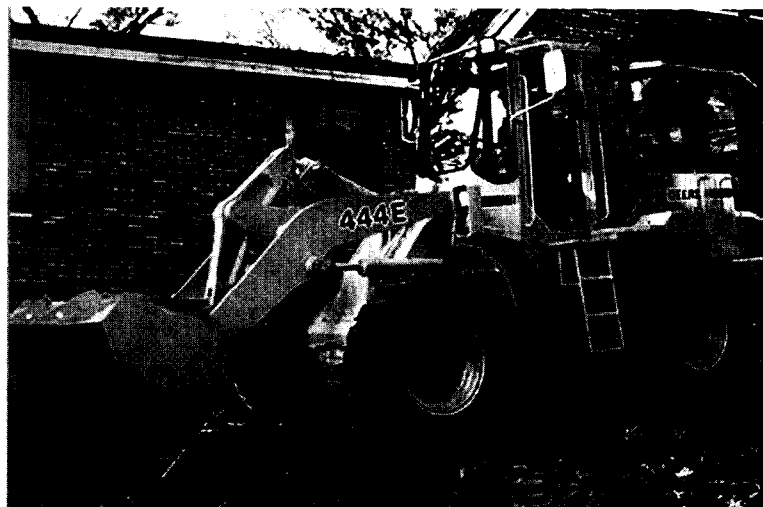
Compared with properly constrained linkages [those that obey Eq. (1.3)], overconstrained linkages have properties that are different in important and practical ways. They tend to be much stiffer and stronger in supporting loads, particularly those orthogonal to the direction of motion at the point of application. However, they are sensitive to dimensional accuracy in their members. This requires manufacture to relatively tight tolerances, which can increase cost. Conversely, properly constrained linkages are completely insensitive to link geometry, as far as mobility is concerned. This means that, in lightly loaded situations, they can absorb abuse that deforms links and still function, at least after a fashion. This is an important property in situations such as the control linkages of agricultural machinery. In heavily loaded situations, the design engineer will often deliberately increase the degree of overconstraint to improve stiffness and strength. An example is the bucket support linkage of a front-end loader. A photograph of the loader is shown in Fig. 1.34, and one of the bucket support linkages is identified in Fig. 1.35.

In principle, only one of the two planar inverted, slider-crank linkages is needed to lift or support the bucket. In this case, we would have  $n = j = \sum f_i = 4$  and

$$M = 6(n - j - 1) + \sum_{i=1}^j f_i = 6(4 - 4 - 1) + 4 = -2$$

Since the true mobility is 1, the degree of overconstraint is  $1 - (-2) = 3$ . However, the linkage is doubled up with identical linkages supporting each end of the bucket. This gives  $n = 6$  and  $j = \sum f_i = 8$ . Thus

$$M = 6(n - j - 1) + \sum_{i=1}^j f_i = 6(6 - 8 - 1) + 8 = -10$$



**FIGURE 1.34** Front-end loader. If analyzed using the planar mobility equations, the mechanism will be found to have fewer than one degree of freedom. Parallel actuators are used on both sides of the machine to balance the load and increase stiffness. The loader part of the machine has two degrees of freedom. (Courtesy of Deere & Company, Moline, Illinois.)



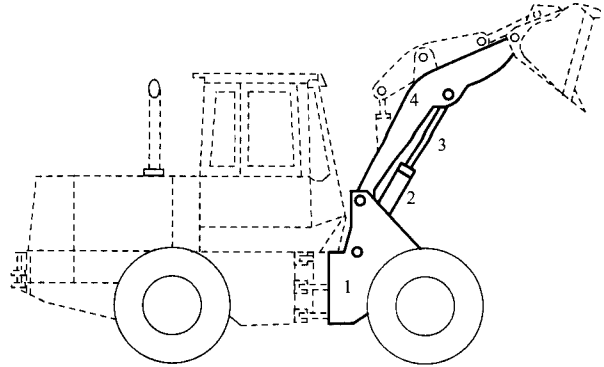


FIGURE 1.35 Schematic of the right-side bucket support linkage for the front-end loader in Fig. 1.34.

Therefore, for the doubled linkage the degree of overconstraint is  $1 - (-10) = 11$ . The result is a much stronger mechanism since the individual planar loops do not have to support the large out-of-plane moments that a single linkage would have to support. The cost is that the axes of the corresponding joints on either side must be collinear to a high degree of accuracy, requiring careful manufacturing.

## 1.11 USES OF THE MOBILITY CRITERION

The mobility criterion is most useful to the engineer when an unfamiliar mechanical system is examined. It allows a quick check to determine whether the links, joints, and actuators identified are consistent with system function. Inconsistency may indicate that some elements have been misidentified or that passive degrees of freedom are present. Of course, as already discussed, overconstraint may also need to be considered. In particular, if the linkage is planar or spherical, the appropriate form of the constraint equation should be used in place of the general form.

It is possible to formulate expressions for the mobility that accommodate overconstrained closures of arbitrary type. These expressions are equivalent to the form

$$M = \sum_{k=1}^c b_k + \sum_{i=1}^j f_i \quad (1.5)$$

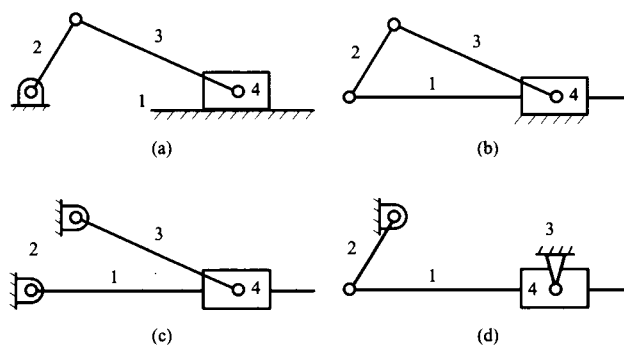
where  $c = n - j - 1$  is the number of closures of the linkage, and  $b_k$  is the loop closure rank. That is, it is the number of independent closure equations for that loop.

Unfortunately, unless the values of  $b_k$  associated with the different closures can be identified by inspection, such expressions have no value because the mobility equation gives a quick check of the number of position variables and independent equations without the need to develop those equations. However, the only way to verify an overconstrained closure of a type not identifiable by inspection is to develop the closure equations and analyze them for dependency. Therefore the quick-check advantage of the mobility equation disappears, and there is no way to derive information about the linkage without performing a complete position analysis.

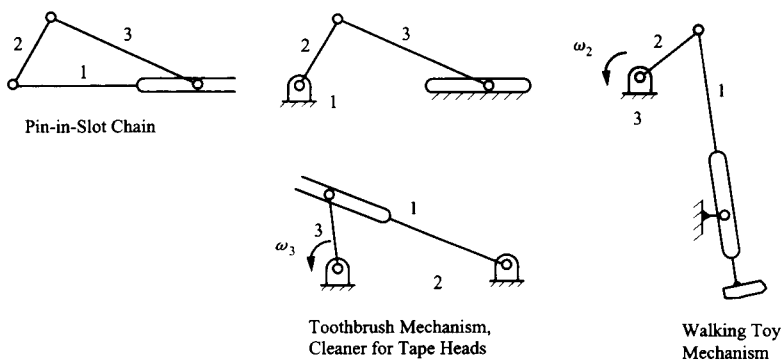
## 1.12 INVERSION

A commonly used tactic in studying mechanism kinematics is inversion. This is a change of the fixed reference frame from one link to another that causes different characteristics of the motion relative to the frame. For example, Fig. 1.36 shows the different inversions of a slider-crank linkage, and Fig. 1.37 shows the inversions of a pin-in-a-slot mechanism. The pin-in-a-slot inversions are often used as inexpensive substitutes for the slider-crank inversions. The motion characteristics of the coupler links for each of the mechanisms are all very different. Nevertheless, the linkage topology and the relative angular relationships among the links are the same in all cases. Therefore, useful information obtained from the study of the linkage in one inversion can be transferred to the study of other inversions. Note that in Fig. 1.36, the relative positions of all of the joints are the same for the position chosen. It is only when the mechanisms move that the different motion characteristics are revealed.

To determine the inversions of a mechanism, it is convenient to start with the chain from which the mechanism is formed. A different linkage results whenever a different link is selected as the frame.



**FIGURE 1.36** Inversions of the slider-crank linkage. The linkage in (a) is the original linkage and those in (b), (c), and (d) are the inversions.



**FIGURE 1.37** Uses of inversions of a pin-in-a-slot linkage.

## 1.13 REFERENCE FRAMES

---

It is necessary to be careful about reference frames when working with systems of many bodies. A reference frame can be attached to each body, and we can express positions, velocities, and accelerations relative to any or all of them.

As far as kinematics is concerned, there is no restriction on the use of reference frames. All frames are equally viable. We can invert from one frame to another without restriction.

It is only when we introduce forces and enter the realm of kinetics that a restriction appears. It is then that Newton's first and second laws, which relate motion properties to force, are true only if all motion properties are referred to a common reference frame. This common reference frame must be of a special type, called an inertial reference frame. For the purposes of mechanism design the inertial reference frame is almost always fixed to the earth. There are engineering problems, such as the design of mechanisms to be carried on spacecraft, for which the primary inertial reference frame must be used. The primary inertial reference frame is fixed relative to the "fixed" stars. A more complete discussion of inertial reference frames can be found in most texts on rigid-body dynamics. Einstein showed that in a space-time framework all reference frames are equally valid, thereby removing the Newtonian distinction between inertial reference frames and others. However, in the domain in which mechanical engineers usually operate, Newtonian mechanics provides a very accurate simplification of relativistic mechanics that is of great practical utility.

It is important to remember that position and motion properties can be expressed only relative to a reference frame. The habit of referring to a velocity or acceleration of a point relative to another point has been commonplace in this subject. This will be found to be convenient in some types of problems, particularly in graphical analysis, and there is no harm in using it provided that it is clearly understood that it is a shorthand expression for the velocity or acceleration of the first point relative to a reference frame in which the second point is fixed. The identity of that reference frame should always be kept in mind.

In many discussions in the following, it will be convenient to have a notation that explicitly states the reference frame in which a particular vector is expressed. A method that is often used is to indicate the reference frame by means of a superscript placed in front of the symbol for the vector. For example,  ${}^1v_A$  indicates the velocity of point  $A$  relative to reference frame 1, and  ${}^2\omega_3$  indicates the angular velocity of member 3 relative to reference frame 2.

Usually, we will associate one reference frame with each member of a linkage and will number it to agree with the number of the linkage. Reference frame 1 will usually refer to the fixed link. Unfortunately, the use of superscripts to indicate reference frames complicates expressions and makes them more difficult to read. For this reason, the superscripts will usually be dropped when all vectors are referred to reference frame 1.

## 1.14 MOTION LIMITS

---

A member of a linkage that is connected to the base by a revolute joint and that rotates completely as the linkage moves through its motion cycle is called a *crank*. Usually, there will also be members in the linkage that look exactly like cranks because they are connected to the base by a revolute, but these cannot rotate completely.

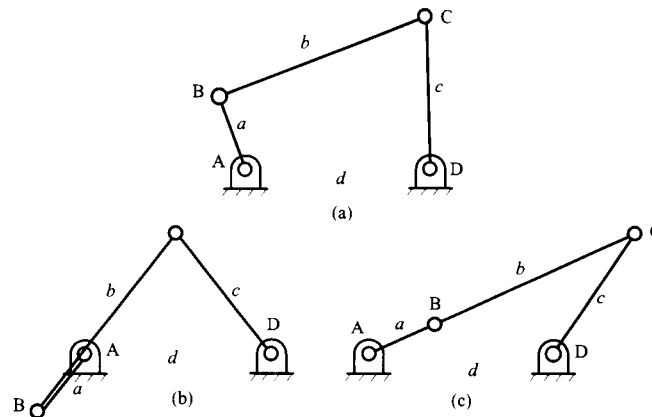


FIGURE 1.38 Limiting positions of joint  $C$  of a four-bar linkage.

Consider the four-bar linkage shown in Fig. 1.38a in which the link  $AB$  is a crank rotating fully about the revolute joint  $A$ . It will be assumed to rotate continuously in the counterclockwise direction. Complete revolution of this link requires that it pass through the positions shown in Figs. 1.38b and 1.38c. Now consider the motion of the revolute joint  $D$ . Prior to reaching the position of Fig. 1.38b link  $CD$  was rotating counterclockwise about joint  $D$ . In the position of Fig. 1.38b further rotation of  $CD$  about  $D$  in the counterclockwise direction is not possible.  $CD$  comes to rest and reverses its direction of motion. Similarly, before entering the position of Fig. 1.38c, the link  $CD$  is rotating clockwise about the joint  $D$ . In this position, further rotation in this direction is not possible and the link comes to rest and then reverses direction. The positions shown in Figs. 1.38b and 1.38c are called motion limit positions for the joint  $D$ . The link  $CD$  does not perform a full rotation but simply oscillates between these positions. That is, it is not a crank but a rocker.

## 1.15 ACTUATION

At this point it is necessary to introduce some terminology to describe the different members of a four-bar linkage. The fixed link, that is, the member to which the frame of reference is attached, is called the base or frame. The two members that are connected to the base by revolute joints are called turning links. The link that is jointed to both turning links and has no direct connection to the base is called the coupler. The turning links may be further distinguished by the terms crank, for a link capable of complete revolution relative to the base, and rocker, for a link that is only capable of oscillating between motion limits.

A linkage is actuated, or driven, by applying a force to one of its moving links or a torque to one of the axes. This may be done in a variety of ways, as is evident from the number of different types of commercial actuators (Fig. 1.39). It is frequently convenient for that powered link to be connected to the base by a revolute joint. The linkage may then be actuated by applying a torque to that link. In this case it is usually also preferable that the link be continuously rotatable since it may then be actuated by means of a continuously rotating motor. For this reason it is important to be able to identify four-bar linkages that have continuously rotatable joints and to locate those joints. This may be done by means of a simple set of rules called Grashof's rules.

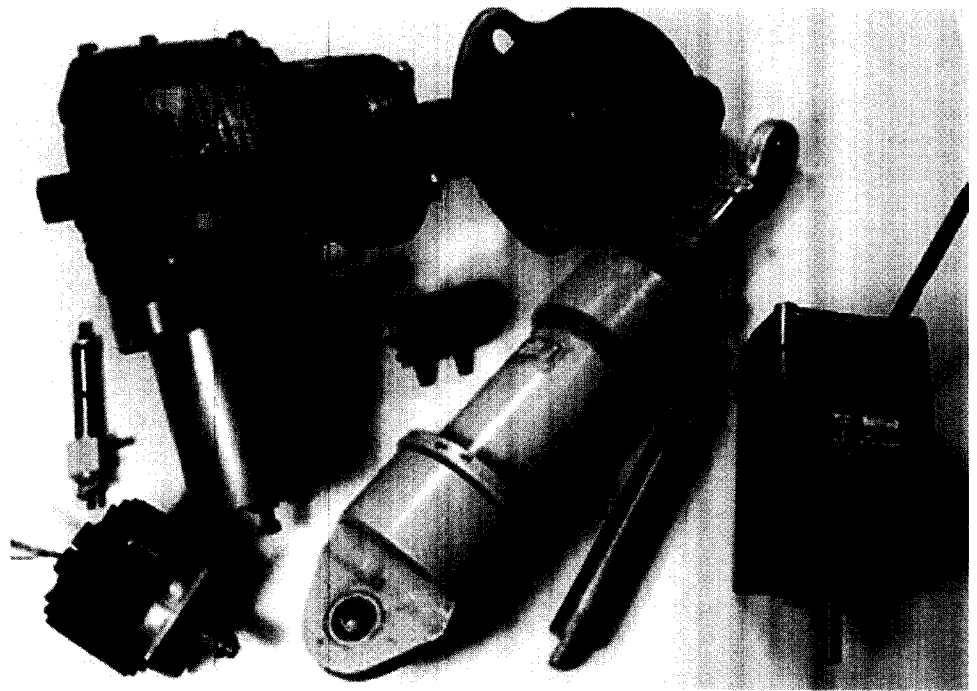


FIGURE 1.39 Photograph of a variety of actuators.

Grashof distinguished two fundamentally different types of four-bar linkage by means of the inequality

$$s + \ell < p + q \quad (1.6)$$

where, as shown in Fig. 1.40,  $s$  is the length of the shortest side,  $\ell$  is the length of the longest side, and  $p$  and  $q$  are the lengths of the other two sides. Linkages that obey this inequality (Grashof type 1 linkages) have two joints that perform complete rotations and two that oscillate between motion limits. The two fully rotatable joints are those on either end of the shortest link. Linkages that do not obey the inequality (Grashof type 2 linkages) have no fully rotatable joints. All four joints then oscillate between motion limits.

The behavior of a linkage that obeys the Grashof inequality is strongly dependent on the locations of the fully rotatable joints relative to the base link. That is, it is dependent on the inversion of the linkage. The following additional rules distinguish three subtypes that have different behaviors:

1. If the shortest link is jointed to the base, the linkage is a crank-rocker (Fig. 1.41). The joint between the shortest link and the base is fully rotatable. Hence that link is a crank.

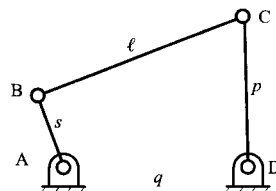
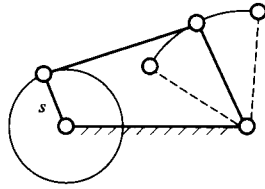


FIGURE 1.40 Nomenclature for Grashof's inequality.



**FIGURE 1.41** Crank-rocker subtype of Grashof type 1 linkage. This linkage type occurs when the shortest link is jointed to the base of the linkage.

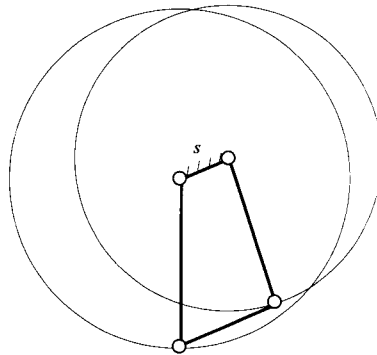
The other fully rotatable joint connects that crank to the coupler. Hence the other joint connected to the base is not fully rotatable, and the link it connects to base oscillates. It is the rocker. A crank-rocker can be conveniently driven by the joint connecting the crank to the base (or the joint connecting the crank to the coupler).

2. If the shortest link is the base, both joints at the base are fully rotatable, and so both links connected to the base are cranks (Fig. 1.42). The linkage is a double-crank, also known as a drag-link. It may be conveniently actuated at either of the base joints.
3. If the shortest link is the coupler, neither base joint is fully rotatable (Fig. 1.43). The linkage is a type 1 double-rocker. Its behavior is different from that of type 2 double-rockers, those that do not satisfy the inequality, because in the type 1 linkage the two floating joints can rotate completely. The result is that the coupler tumbles, performing a complete rotation relative to the base. Either joint attached to the coupler can be driven by a continuous rotation motor. This mechanism is often used in oscillating fans. The angular motion of the coupler of a type 2 double-rocker is an oscillation relative to the base.

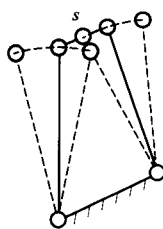
The Grashof inequality may be proved as follows:

Consider the linkage shown in Fig. 1.44a. To perform a complete rotation it must pass through the positions shown in Figs. 1.44b and 1.44c. Let  $a$  be the length  $AB$ ,  $b$  the length  $BC$ ,  $c$  the length  $CD$ , and  $d$  the length  $DA$ . It is assumed that

$$a < d$$



**FIGURE 1.42** Double-crank subtype of Grashof type 1 linkage. This linkage type is also called a drag-link. It occurs when the shortest link is the base.



**FIGURE 1.43** Type 1 double-rocker. This subtype occurs when the shortest link is the coupler.

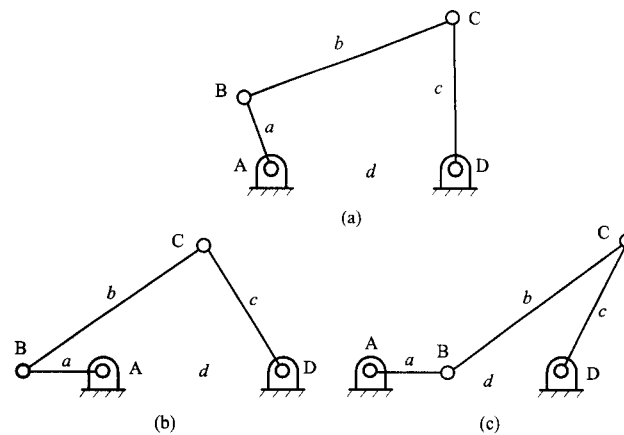


FIGURE 1.44 Extreme positions for a four-bar linkage.

The triangle inequality states that the sum of the lengths of any two sides of a triangle is greater than that of the third. This inequality may be applied three times to Fig. 1.44b to give

$$a + d < b + c \quad (\text{a})$$

$$b < c + a + d \quad (\text{b})$$

$$c < b + a + d \quad (\text{c})$$

It may also be applied three times to Fig. 1.44c to give

$$d - a < b + c \quad (\text{d})$$

$$b < c + d - a \quad (\text{e})$$

$$c < b + d - a \quad (\text{f})$$

Examination of these inequalities reveals that if (e) is true then (b) is certainly true, because the right-hand side of (b) is that of (e) plus  $2a$ . We say that Inequality (e) is stronger than Inequality (b). Hence Inequality (b) can be eliminated. Inequality (e) can be written in the form

$$a + b < c + d \quad (\text{e}')$$

by adding  $a$  to both sides of the inequality.

Similarly, Inequality (c) is certainly true if Inequality (f) is true. Once again, the right-hand side of Inequality (c) is larger by  $2a$ . Inequality (f) assumes the form

$$a + c < b + d \quad (\text{f}')$$

if  $a$  is added to both sides.

Inequality (d) is certainly true if Inequality (a) is true, since its left-hand side is less than that of Inequality (a) by  $2a$ . Hence, the six inequalities are reduced to three: (a), (e'), and (f'). Addition of both sides of Inequalities (a) and (e') gives

$$2a + b + d < 2c + b + d$$

so that

$$a < c$$

Likewise, addition of both sides of Inequalities (a) and (f') gives

$$2a + c + d < 2b + c + d$$

so that

$$a < b$$

Since  $a$  has also been assumed to be less than  $d$ , it follows that  $a$  is the shortest link length. Now, whichever of the inequalities (a), (e'), and (f') has the longest link length on the left added to  $a$  will be the strongest. That is, the left-hand side is largest and the right-hand side is smallest. Whichever one this is assumes the form

$$s + \ell < p + q$$

where  $s = a$  is the shortest link length,  $\ell$  is the longest link length, and  $p$  and  $q$  are the two remaining link lengths.

It must be remembered that we assumed that  $a$  was less than  $d$ . It is also necessary to deal with the case in which  $a$  is larger than  $d$ . This can be handled by inverting the linkage so that  $AB$  becomes the base link and  $DB$  becomes the link jointed to it by the continuously rotatable joint. Pursuing the application of the triangle inequality then results in  $d$  being the shortest link length, and the Grashof inequality again results.

What we have shown so far is that the Grashof inequality is a necessary condition for the presence of a fully rotatable joint, and that joint is always at one end of the shortest link. Now, there can never be just one fully rotatable joint in a four-bar linkage. There must always be at least two. If there were just one fully rotatable joint, a topological contradiction would result when the rotations of  $AB$  relative to the other links after one cycle were to be considered. If that link were to perform a complete rotation about joint  $A$ , and joints  $B$ ,  $C$ , and  $D$  were to oscillate back to their initial positions,  $AB$  would have performed a complete rotation relative to each of the other links. That is, it would have performed a complete revolution relative to  $BC$ . However, joint  $B$  has not performed a complete revolution but, rather, has performed zero net rotation. Hence there cannot be just one completely rotatable joint. Since we have shown that any completely rotatable joint must be at one end of the shortest link, it follows that there are two completely rotatable joints, and they are at either end of the shortest link. This completes the proof of Grashof's rules.

The shortest link of a type 1 linkage performs a complete revolution in each motion cycle relative to the other members. The net rotations of the fully rotatable joints on either end of that link cancel one another so that the net rotations of the remaining links relative to one another are zero for a complete motion cycle.

Of course, sometimes it is not necessary for the mechanism to perform a complete motion cycle. A restricted range of driving joint motion may be adequate. In that case linear actuators, such as hydraulic or pneumatic cylinders acting across the driving joint, may be used. However, it is still necessary that the driving joint not pass through a motion limit within the necessary range of motion. Grashof's rules are often useful in ensuring that this does not happen.

Occasionally it is necessary to drive a crank-rocker linkage by oscillating the rocker through a part of its motion range. In this case the linkage is usually referred to as a rocker-crank.

The reasons associated with the use of type 2 double-rocker linkages, or with the use of type 1 linkages driven by rockers rather than cranks, will be better understood after a dis-



cussion of linkage synthesis. Often, a linkage that is synthesized to produce a specific motion cannot be driven through that motion without the driving joint passing through a motion limit position. In that case, a solution might be to drive the other base joint.

A special case arises when

$$s + \ell = p + q$$

This is called a transition linkage or Grashof neutral linkage. In this case the linkage can assume a “flattened” configuration as shown in Fig. 1.45. When passing through this position, it can change from one to the other of the two configurations in which the linkage can be assembled with a given driving crank angle. In practice, this is often undesirable because it leads to unpredictable behavior and possibly large loads on the members and joints.

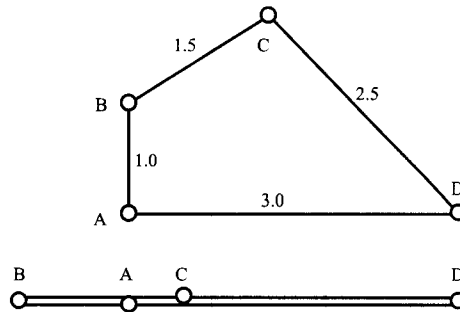


FIGURE 1.45 Grashof neutral linkage.

## 1.16 COUPLER-DRIVEN LINKAGES

In some applications linkages are actuated not by applying a force or torque to one of the links jointed to the base but rather by applying a force or torque to the coupler, the member that has no direct connection to the base. Everyday examples are not uncommon. Polycentric hinges for heavy doors or for automotive hood and trunk lids come to mind.

It is still important for a coupler-driven mechanism not to pass through a motion limit within the desired motion range. The motion limit positions for a coupler drive are quite different from those for a crank drive. They are the positions in which the two rotating links become parallel, as shown in Fig. 1.46. In these positions the angular motion of the coupler ceases and must reverse if motion is to continue. Elimination of these motion limits produces a linkage whose coupler performs a complete revolution relative to the base link. Because in a type 1 linkage the shortest link rotates completely relative to the remaining links, that link must be either the coupler or the base. It follows that the Grashof subtypes for which complete rotation of the coupler relative to the base is possible are the type 1 double-rocker and drag-link subtypes.

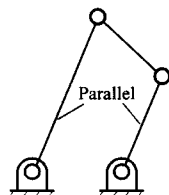


FIGURE 1.46 Motion limit for the coupler.

## 1.17 MOTION LIMITS FOR SLIDER-CRANK MECHANISM

The limits for a slider-crank mechanism can be determined by considering the combinations of link lengths that will cause the linkage to lock up. A typical slider-crank is shown in Fig. 1.47.

The limit positions of the rotating link  $a$  (Fig. 1.47) are determined when the coupler link is perpendicular to the direction of slider travel. The limiting assembly position occurs for one of the four geometries shown in Fig. 1.48.

From the four limit positions shown in Fig. 1.48, it is apparent that the following relationships must be maintained to allow the slider-crank to be driven through a full  $360^\circ$  rotation of the crank:

$$b > a$$

and

$$b - a > c$$

where

$a$  = length of the crank

$b$  = length of the coupler

$c$  = offset distance from crank-ground pivot to slider pin (measured positive upward)

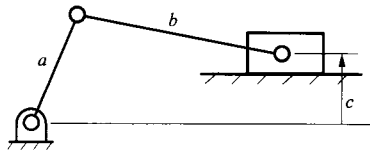


FIGURE 1.47 General slider-crank mechanism with offset dimension  $c$ .

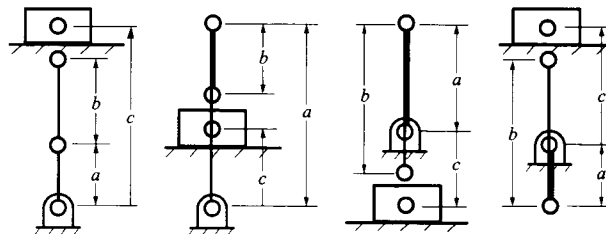


FIGURE 1.48 Positions for which the slider-crank mechanism cannot be assembled.

**EXAMPLE 1.6**  
**Using Grashof's**  
**Equation**

In the Watt six-bar linkage shown in Fig. 1.49, the joint between links 5 and 6 must be placed on the arc indicated. Using Grashof's rule, determine the region for joint  $E$  that will allow full rotation of link 6. The critical dimensions are

$$AB = 1.14 \text{ in}, BC = 2.26 \text{ in}, AD = 1.74 \text{ in}$$

$$AF = 2.00 \text{ in}, DE = 2.68 \text{ in}, c = 1.09 \text{ in}$$

**Solution**

Consider first the slider-crank mechanism ( $ABC$ ) even though the crank  $AB$  does not rotate  $360^\circ$ . Clearly, if the crank  $AB$  can rotate for  $360^\circ$ , it will not lock up in any intermediate position. Based on the dimensions given,

$$BC > AB$$

and  $BC - AB = 1.12$ . Therefore,

$$BC - AB > c$$

and the crank of the slider-crank mechanism can rotate a full  $360^\circ$ .

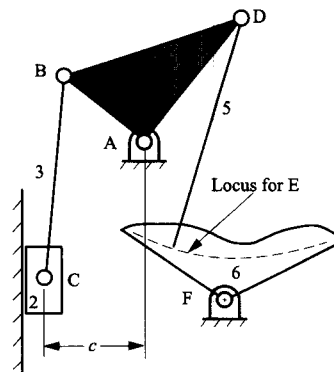


FIGURE 1.49 Mechanism for which point  $E$  is to be determined.

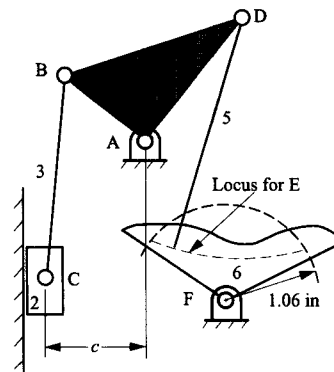


FIGURE 1.50 Allowable range for point  $E$ .

Next consider the crank–rocker mechanism ( $ADEF$ ). For a crank–rocker, link 6 must be the crank, which means that  $EF$  must be the shortest link. The longest link is  $DE$ . Therefore, based on Eq. (1.6), for  $ADEF$  to be a crank–rocker mechanism,

$$EF + DE < AF + AD$$

or

$$EF + 2.68 < 2.00 + 1.74$$

or

$$EF < 1.06 \text{ in}$$

The allowable range for  $E$  is shown in the Fig. 1.50.

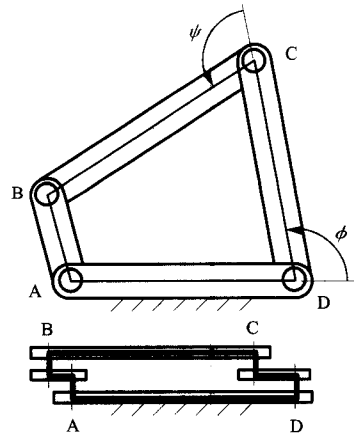
## 1.18 INTERFERENCE

This is a topic that is often ignored in courses and texts on mechanism design. That is unfortunate since a full-cycle-motion capability can be prevented by topological interference even when Grashof's rules indicate that it is possible. An understanding of topological interference is particularly important at the present time, when linkages are often designed using CAD systems and their functioning checked by animation rather than by construction of physical models. It is very difficult to represent topological interference adequately on a planar display. For this reason, the reader is urged to construct models using cardboard and thumbtacks, or whatever other appropriate materials are available, when reading this section. That is the best way to gain an understanding of the nature of topological interference. There is also a tendency to regard interference as a result of the physical shape of the links and as something that can be avoided if enough care is given to the design of the physical link geometry. That is not what we are talking about here. Topological interference is a fundamental property of a linkage configuration in the same way that Grashof type is. It cannot be avoided by simply reshaping the links.

Topological interference really affects only the capability of executing a complete motion cycle using a rotary input. If oscillatory motion over a partial cycle is all that is required, topological interference can usually be circumvented.

The topological and physical limitation that the links cannot pass through each other creates difficulties in arranging for input and output motion transfer to and from type 1 linkages. When a simple, type 1 four-bar linkage is viewed as a three-dimensional structure with revolute joint axes of finite length, there is only one way in which it can be assembled to avoid any of the links or joint axes having to pass through each other. This is shown in Fig. 1.51. The problem is the fully rotatable joints.

The oscillatory joints of a type 1 linkage never pass through positions in which their joint angles  $\phi$  and  $\psi$ , shown in Fig. 1.51, become either zero or  $\pi$ . If either one did so, the joint diagonally opposite it would be at a motion limit, preventing it from making a complete rotation. Consequently, the axes of these joints never cross the lines of the links  $BC$  and  $DA$ , so there is no interference. However, when joint  $A$  is fully rotated, the axis of joint  $B$  must cross the line  $DA$  and, since  $AB$  is the shortest link, it must cross between  $D$  and  $A$ . Likewise, when joint  $B$  is fully rotated, the axis of joint  $A$  will cross the line  $BC$  between  $B$  and  $C$ . Viewing the linkage from a direction normal to the joint axes, it can be seen that, if joint  $B$  is on one side of the link  $AB$ , the link  $DA$  must be on the other side, otherwise the link will cut the joint axis. Similarly, joint  $A$  must be on the opposite side of  $AB$  to link  $BC$ . It follows that, in the direction along the link axes,  $BC$  and  $DA$  are on either side of  $AB$  and

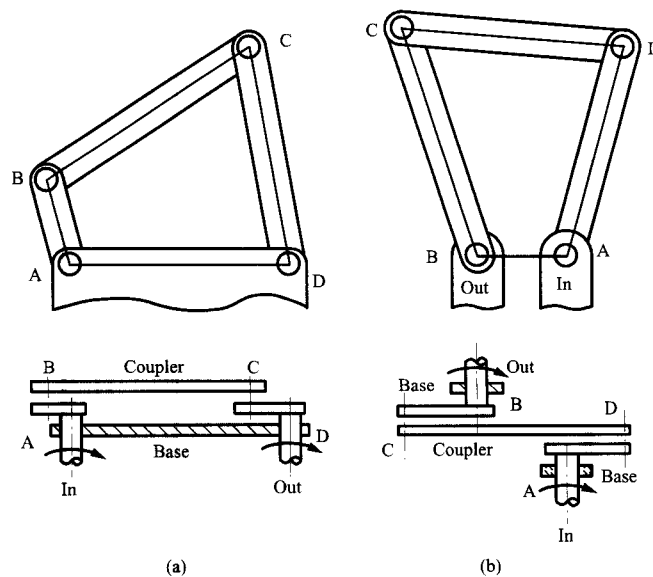


**FIGURE 1.51** Assembly of type 1 linkage needed to avoid interference.

*CD*. This may seem to be dependent on the physical realization of the links, but it is, in fact, a fundamental topological property of the loop.

The simplest situation for motion transfer is when both input and output motions are rotary. Motion can then be transferred into and out of the linkage by means of shafts attached to the turning links. Interference constrains the arrangement of the input and output shafts, as shown in Fig. 1.52. If the linkage is a *crank-rocker*, both shafts must enter from the same side to avoid interference between the shafts and the coupler link. Notice that the shafts must pass through the base link to get to the turning links, which are on the inside of the linkage in this inversion. Physically, the shafts are supported in bearings mounted in the base link.

If the linkage is a *drag-link*, the shafts may be attached directly to the turning links, one on either side, since those links are on the outside of the linkage in this inversion. However, if this is done, the fixed bearings may be moved to the outside, essentially turning the



**FIGURE 1.52** Shaft drive of (a) crank-rocker and (b) drag-link linkages.

base link inside out. The base link becomes a pair of fixed bearing mounts on either side of the linkage, as shown in Fig. 1.52b. A drag-link linkage must always be mounted in this manner to achieve full-cycle motion, regardless of the means of input or output, since otherwise the coupler must pass through the base.

The discussion of rotary input and output to *type 1 double-rocker* linkage will be left until later since it is not possible to achieve full-cycle motion with a crank drive in this type of linkage.

A more complex case is that in which the input is rotary and motion must be transferred from a point on the coupler link. This is easy enough to arrange in the crank-rocker case, as shown in Fig. 1.53, since the base and coupler are on the outside of the linkage.

Much more difficult is the case in which motion must be transferred from a point on a crank or on the coupler of a drag-link. Because the coupler moves between the cranks there is no way to avoid interference of a shaft coming off the coupler with those cranks in full-cycle motion. Furthermore, because the two parts of the base are outside the cranks, there is also a problem of interference with the base. This latter problem also affects the transfer of motion to or from points on the cranks.

It is possible to circumvent the interference problem for motion transfer from points on a crank by “doubling” the crank. This is shown in Fig. 1.54. The crank is essentially duplicated on the outside of the base bearing. A shaft rigidly fixed to both the crank and the duplicate passes through the bearing forming the base joint and ensures that both move together. This effectively makes points on the crank available outside the base, where additional links can be attached at motion transfer joints. In this way, multiloop linkages such as that shown in Fig. 1.55 can be built up and driven by the driving crank of the master drag-link loop.

If the transfer point is reasonably close to the base joint of the crank, the result in Fig. 1.54a can be achieved by using a bearing of sufficiently large diameter to encompass the transfer point. This is shown in Fig. 1.54b.

There is no simple way to transfer motion from a point on the coupler of the drag-link without preventing full-cycle mobility. It can be done by splitting one of the joints between the crank and coupler, allowing the linkage loop to pass through itself. This requires the addition of at least one auxiliary link, so the mechanism, strictly speaking, is no longer a four-bar one. The yoke shown in Fig. 1.55 carries the two bearings that replace the simple joint of the original linkage. It is undesirable to leave this link unconstrained, so it is usual to add a second link connecting it to base, as shown in the figure. This allows the coupler to

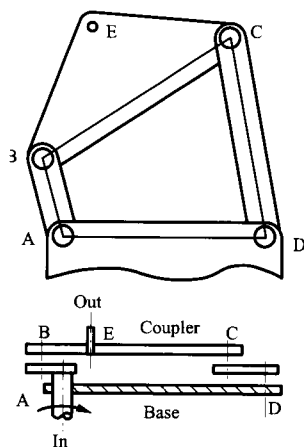


FIGURE 1.53 Transfer of motion from a point on the coupler of crank-rocker mechanism.

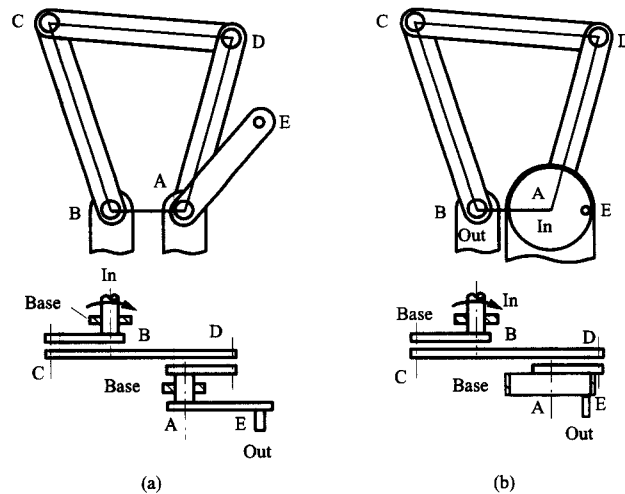


FIGURE 1.54 Motion transfer from a point on the crank of a drag-link.

be moved outside the crank. However, it is still not possible to transfer motion directly from a point on the coupler because of interference with the yoke. For this reason, the coupler is doubled in the same way that the crank was in Fig. 1.54, producing the six-bar arrangement shown. As can be seen, this is quite an extensive modification!

The situation for a coupler drive, in which the driving torque is applied to the coupler link and the output motion is taken off that same link, is quite similar. The two linkage types that can, in principle, perform complete motion cycles in the coupler drive mode are the *type 1 double-rocker* and *drag-link* types. Both present a problem because the base and coupler are inside the cranks in the basic loop. The type 1 double-rocker can be made to allow full-cycle motion, without interference, by doubling the coupler.

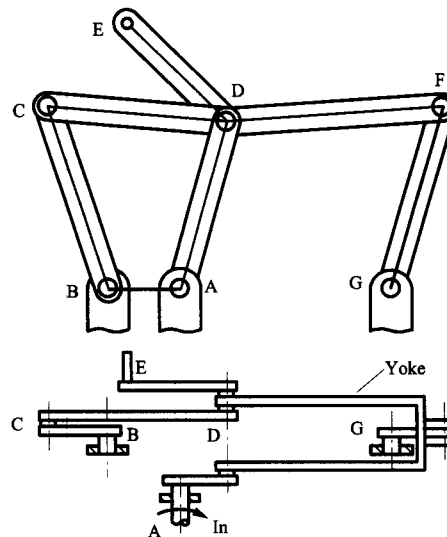


FIGURE 1.55 Six-bar modification to achieve motion transfer from the coupler of a drag-link linkage.

Once again, the drag-link presents additional problems because of the necessity of splitting the base resulting in the base being outside the cranks. Coupler-driven full-cycle motion of a simple drag-link is not possible because of interference. The six-bar arrangement of Fig. 1.55 can be used for full-cycle motion that is identical to that of the drag-link with coupler drive.

All of the foregoing discussion relates only to full-cycle motion, that is, to motion in which the driving link performs a complete rotation. If oscillation through a partial motion cycle is adequate for the application, interference can always be avoided by modifying the physical shapes of the links. This is true even for the drag-link type. Type 2 linkages can also be used in this mode. One only has to ensure that it is not necessary for such linkages to pass through motion limit positions of the driving link when traversing the desired segment of the motion cycle.

## 1.19 PRACTICAL DESIGN CONSIDERATIONS

---

### 1.19.1 Revolute Joints

A rubbing contact between two members, here called a kinematic joint, is also known as a bearing. Design of bearings to perform satisfactorily for long periods under load is the focus of the subject of tribology. Although an in-depth treatment of tribology is beyond the scope of this book, it is necessary for the mechanism designer to be aware of the limitations that may be placed on a design by the necessity of having bearings.

Revolute joints perform well under many conditions. As with all the lower pairs, the distribution of contact ideally over a surface distributes and normally slows wear. The closed geometry of the joint provides good conditions for trapping lubricant between the joint surfaces.

A revolute joint that is in continuous, unidirectional rotation at relatively high speeds can enter a regime called hydrodynamic lubrication in which the relative movement of the bearing elements acts to entrain lubricant and maintain a separation between the solid journal elements. The entrainment action creates an area of elevated pressure in the lubricant that supports the load on the bearing. The establishment of hydrodynamic action is often assisted by pumping lubricant into the bearing. In principal, once hydrodynamic action is established, there is no contact between the solid bearing elements, and hence there is no wear. The effective friction is solely due to viscous resistance in the lubricant and is, therefore, low. Typically wear occurs only when the machine is started up and shut down. The crankshaft support bearings and the bearings between the crankshaft and the connecting rods of an automotive engine are typical examples of hydrodynamic bearings.

Another type of bearing that has some of the characteristics of a hydrodynamic bearing, but is free of some of its limitations, is a hydrostatic bearing. Here the objective remains the same, to carry the bearing load by a pressure differential in the lubricant and to maintain separation between solid bearing journals at all times. However, in this case, the pressure to support the bearing load is provided by pumping the lubricant into the bearing on the loaded side at an elevated pressure. Hydrostatic bearings do not rely on continuous rotation to maintain bearing action. Therefore, they can be used when the rotation speeds are low, or when the direction of rotation reverses. They do tend to be expensive, because close tolerances are needed to minimize lubricant leakage out of the bearing and because of



the need for a relatively high-capacity lubricant pump. Hydrostatic bearings are usually used for the main rotor bearings on large turbogenerator sets.

When the speed of rotation is slow, or reverses, a greased bushing or a solid contact bearing may be used. These bearing types are geometrically similar and differ only in the use of a liquid lubricant. Usually that lubricant will be a viscous grease. The high viscosity both promotes some hydrodynamic action and diminishes leakage out the sides of the bearing. Frequent lubrication is, nevertheless, necessary for this type of bearing. The materials should also be chosen to provide adequate performance and wear resistance even in the absence of lubricant.

Solid contact bearings rely on the choice of contacting materials to provide both low friction and wear resistance. Teflon has a low coefficient of friction with most metals. It is also relatively hard and highly temperature resistant for a plastic material. Consequently, it is frequently chosen for one element of a bearing pair. Other plastic materials such as nylon and delrin are also used. Note that the same material should never be used for both journal members of a solid bearing pair because journals with similar materials can weld together at small asperities when driven under load, resulting in high friction and rapid wear. This is why bronze bushings are frequently partnered with steel journals for greased bearings. Generally harder materials wear better than softer ones. Hence steel is preferred to aluminum for bearing journals. One final caution is that some materials should never be lubricated with petroleum-based lubricants. Nylon tends to absorb oil and swell and fail. Solid lubricants such as graphite or molybdenum disulfide can be used when petroleum-based lubricants are not an option because of material or other constraints.

Yet another alternative for the support of rotary motion is provided by rolling element bearings. Here the load is transferred between the journals by hardened steel balls or rollers trapped between the journals. The contact between one of these rolling elements and the journal is, of course, a higher pair joint. However, the combined effect of all the balls or rollers rolling on the journals is kinematically equivalent to a revolute joint. Lubricants are used, but the way in which they work is somewhat different from that of lubricants in other types of joints. This kind of action is called boundary lubrication. The lubricant is squeezed to very high pressures between the rolling element and journal and plays a role in distributing the load over both elements. The contact between a ball and journal is a point, if both are perfectly rigid, and that between a roller and journal is a line. In either case the load is ideally locally infinite. Of course, elastic deformation of the elements acts to distribute the load over a local area. The boundary lubrication mechanism assists in this load distribution.

Because pure rolling contact does not involve sliding of one member over another, wear, of the type found in other bearings, is not an issue for rolling contact bearings. Also, the effective friction can be very low, and rolling element bearings work well with motion cycles that stop or reverse. However, the very high contact stresses in the elements require very hard, and very accurately manufactured, rolling elements and journals. Consequently, rolling element bearings can be relatively expensive. They are also relatively bulky and are not well suited to situations where space is limited. The principal failure mode of a rolling element bearing is fatigue owing to the high contact, or Hertzian, stresses in the rolling elements and journals. This leads to subsurface cracking and eventual spalling, or breaking out of pieces from the surface of a rolling element. Once this process starts, the bearing tends to fail quite rapidly. The nature of the failure mode is such that all rolling elements have finite life. Unfortunately that life is statistically distributed over a significant range, making it relatively difficult to predict failure and apply preventive maintenance procedures to change bearings before failure occurs.

### 1.19.2 Prismatic Joints

Compared to revolute joints, prismatic joints are much more problematic in their application. As will be shown, they are sensitive to the direction and manner of load application. Also, a prismatic joint cannot be infinite in length so all prismatic joints experience motion reversals, which precludes the use of fully established hydrodynamic lubrication.

If a sliding joint is loaded by a connecting rod, as in a slider-crank mechanism, the loading force is applied along the line through the bearing center, as shown in Fig. 1.56a. The friction force along the joint direction is proportional to the normal force. If the friction force exceeds the component of the applied force along the slide direction the joint will jam. That is, if the angle between the axis of the connecting rod and the normal to the joint direction is less than the friction angle

$$\phi = \tan^{-1} \mu$$

where  $\mu$  is the coefficient of friction, the joint will jam.

Figure 1.56b shows another effect that may lead to jamming of the slider. Applying a load offset from the slider surfaces results in an applied moment that must be resisted by a couple composed of normal forces, as shown in the figure. In a real prismatic joint, there must be a small clearance between the members. The application of the offset force,  $F$ , causes the block to angulate slightly relative to the shaft so that contact actually occurs only at the ends of the joint. Thus, the block is subject to normal and friction forces at the locations shown in the figure. The joint will jam if

$$F < \mu N$$

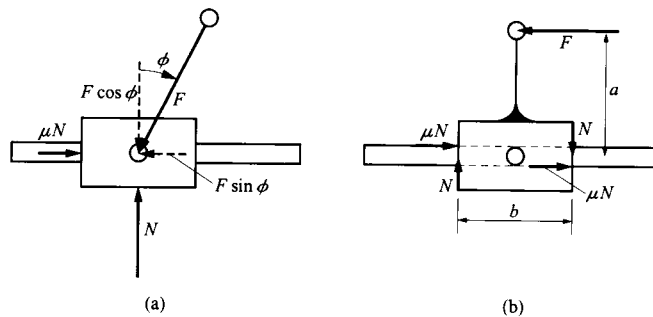
However, for horizontal force and moment equilibrium

$$2\mu N = F \text{ and } aF = bN$$

Therefore, the joint will jam if

$$b < 2\mu a$$

Offset loads and loading directions at large angles to the joint direction also combine to produce jamming.



**FIGURE 1.56** Jamming in sliding joints. In (a), the slide will jam if the angle between the applied force  $F$  and the direction of sliding becomes too great. The slider will jam when the angle  $\phi$  is less than  $\tan^{-1}\mu$ . In (b), the slider will jam because of the offset force if  $2\mu a < b$ .

Jamming is best avoided by shunning designs that have sliding joints with poor loading geometries. If such a geometry cannot be avoided, jamming caused by offset loading may be alleviated by increasing the length of the prismatic joint, if space allows. Increasing  $b$  until it is greater than any expected value of  $2\mu a$  should avoid the problem. Of course, reducing the effective coefficient of friction is effective in either case. That might be done by lubrication, or by choice of a low-friction material combination. Lubrication as a solution may be problematic if jamming is a catastrophic failure mode. Sooner or later, the joint is likely to have too little lubricant.

The best solution, in many cases, is to use a rolling contact joint to minimize the effective coefficient of friction. Roller on rail configurations that are kinematically equivalent to a prismatic joint are available. A ball bushing is a relatively inexpensive and compact device. It must roll on a smooth, hardened steel shaft. A ball bushing does not provide any restraint on twisting about the shaft axis. For this reason, when ball bushings are used, the bushings and shafts are usually configured in parallel pairs.

### 1.19.3 Higher Pairs

Pure rolling contact may not require any lubrication, or special attention, as is the case of the contact between a vehicle tire and the ground. Sliding contacts, however, can result in very rapid wear, jamming, and failure unless they are carefully designed and lubricated. Combined rolling and sliding, as in a gear mesh, also requires careful attention to lubrication at any but the lowest loads and speeds. Gears that carry significant loads and power flows are normally enclosed in gearboxes to allow lubricant to be actively splashed or pumped over them. The gearbox allows lubricant to run off the gears and collect in the bottom of the box, or sump, for recycling.

Cam and follower pairs are particularly demanding with respect to lubrication, especially if flat-faced followers are used. The valve timing cams in an automotive engine are housed in a sealed chamber so they can be bathed in lubricant. Oil is often pumped through the rocker shaft to ports in the faces of the followers to ensure lubrication and some hydrodynamic action over the rubbing surfaces.

### 1.19.4 Cams vs. Linkages

As will be seen, both cams and linkages are used to generate irregular motions. As solutions to design problems requiring irregular motions, they each have their strengths and weaknesses. Cams are usually easier to design geometrically but much harder to make work satisfactorily. The lubrication issues involved in rubbing contact have already been referred to. In low volumes, cams are expensive to manufacture. However, if the volume of parts needed is high enough to justify manufacture of a die and production of the cams by near net shape methods such as injection molding, die casting, forging, or powder metallurgy, cam mechanisms can be very economical. Cams are particularly convenient for timing mechanisms, such as valve lifters. They are easily designed to dwell in a set position for a set portion of the motion cycle.

Linkages are robust and inexpensive, particularly if only revolute joints are needed. They are economical to manufacture in either large or small volumes. Lubrication is, relatively speaking, very easy. However, linkages do not allow as much freedom to the designer as cams. It is quite difficult to design a high-quality dwell mechanism using only linkages. Also, linkages often consume more space than cam mechanisms.

Given an irregular motion generation problem, most experienced machine designers will seek a linkage solution first, unless the problem is clearly better suited to a cam.

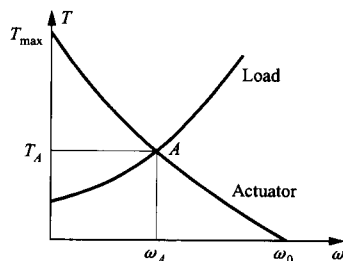
### 1.19.5 Actuation

**Introduction** Linkages and mechanisms are used to transfer mechanical work from a generating site to a site at which it produces a useful effect. An actuator is a motor or other device that generates mechanical work in a controlled manner. Traditionally, machines for complex operations involving many subfunctions, like printing or packaging, were powered by a single motor, referred to as the *prime mover*, with all of the subfunctions being performed by linkages of various types. The prime mover was sometimes a large electric motor, but it could equally be an internal combustion engine, a steam engine, or a water turbine. Once the system was tuned, timing was not an issue since everything was powered in lockstep off the same power train. This type of machine can achieve rapid cycle rates and hence high productivity. It is an appropriate design when motors are expensive and inflexible in their operation. It is still the best configuration for very high production rates such as when producing beverage cans or loading tissues into a package.

Improvements in actuator technologies have resulted in relatively compact and inexpensive devices that can be controlled with precision. Combining these with digital control technology has made it possible to replace mechanical coordination via linkages with digital coordination. This has several potential advantages. Production and other machines can be much more flexible in their operation. It is no longer necessary to design and build a machine especially to fill, cap, and label bottles of a particular shape. Rather, the same machine can be reprogrammed to fill a different type of bottle. The only mechanical changes needed are relatively minor tooling articles. Likewise, a production line can accommodate several different models of automobile, and many options on each, by use of digital reconfiguration for each model and option.

There is a large number of different actuator types available. We will review only the three most commonly used types: electric actuators, hydraulic actuators, and pneumatic actuators. In-depth discussion of these technologies is beyond the scope of this book.

**Operational Stability** A useful way of characterizing the behavior of an actuator is to plot force, for a linear actuator, or torque, for a rotary actuator, against speed. The shape of this characteristic curve and its relationship to the corresponding characteristic of the load have important implications for the behavior of the actuator under load. Consider the torque–speed curve shown on Fig. 1.57. The torque–speed demand curve of a typical load is also shown. In many applications, but not all, load increases with speed. Since the actuator torque is equal to the load at point *A*, the system will tend to settle into that operating point. If the speed increases above  $\omega_A$ , the load torque will exceed the actuator torque and the system will tend to decelerate back to speed  $\omega_A$ . Conversely, if the speed decreases below  $\omega_A$ , the actuator torque will exceed the load torque and the system will tend to accelerate back to point *A*. This is an example of stable operation. Note also that this actuator has



**FIGURE 1.57** Torque–speed characteristics of actuator and load for stable operation.

a finite maximum speed, which is the speed  $\omega_0$  at which the actuator torque drops to zero.  $\omega_0$  is called the *no-load speed*.

Consider now the situation depicted on Fig. 1.58. Here the actuator torque–speed characteristic increases in torque with increasing speed. The load torque does not increase as rapidly with speed. The operating point at which the actuator torque is equal to the load torque is point *B*. If the system is operating at point *B*, and the speed fluctuates even slightly higher than  $\omega_B$ , the actuator torque will exceed the load torque and the system will accelerate to even higher speed. Obviously the speed will continue to increase without bound and the system will *run away*, possibly resulting in catastrophic failure. Conversely, if the speed fluctuates even slightly below  $\omega_B$ , the load torque will exceed the actuator torque and the system will decelerate further. Very quickly the speed will drop to zero and the system will *stall*. It is not possible for the system to operate at point *B*. This is an example of an unstable operating point.

Many actuators display torque–speed curves that climb to a peak and then decline to zero with increasing speed. With a given load they may display both stable and unstable operating points. An internal combustion engine is a good example. A change gearbox is necessary in an automobile to keep the operating point on the declining side of the torque–speed curve. If the operating point shifts to the opposite side of the peak of the characteristic, the engine will stall. The torque  $T_S$  that the actuator produces at zero speed is called the *stall torque*.

**Electric Actuation** There are a truly bewildering variety of electrical actuators on the market today. The use of new technologies, such as solid-state power switching technologies, has allowed the introduction of new architectures and new uses for traditional architectures. New permanent magnet technologies have resulted in greatly improved performance for some classes of electrical actuator.

Electric motors work by virtue of the force experienced by a conductor carrying a current in the presence of a magnetic field. The magnetic field may be generated by a winding or by permanent magnets. The field interacts with the conductors in a second winding to produce torque. The mechanically fixed structure is called the *stator*. The rotating structure is called the *rotor*. If the rotor carries windings it is also called an *armature*. To produce a continuous torque, the electric field must typically rotate relative to the structure that generates it so that it maintains a fixed relationship to the magnetic field.

Electric machines actually produce a very modest torque or force in proportion to their weight. However, an electric motor may operate at very high speeds. These characteristics mean that, if reduction of weight or bulk is important, the output of the electric motor must be reduced in speed, and proportionately increased in torque, by means of a mechanical transmission. Alternatively, if motor size and weight are not a problem, a motor with a very large frame size and a large number of poles may be used. The speed of an electric

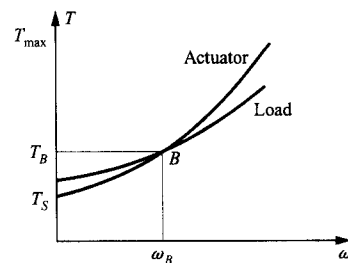


FIGURE 1.58 Torque–speed characteristics of actuator and load resulting in unstable operation.

motor is inversely proportional to the number of poles used in the field winding. It is easier to accommodate a large number of poles in a larger frame size. Consequently, smaller motors tend to have higher operating speeds.

**Commutated Motors** A commutator is a mechanical switch that is used to switch the current-carrying coils in the motor armature so that the torque produced is always in the same direction. The armature is the switched winding of the motor. Traditionally it was the winding on the rotor: the part of the motor mounted on the rotating shaft. In some modern motors the armature winding is in the stator: the part of the motor mounted to the fixed housing. A mechanical commutator is formed of a number of conducting segments mounted to form a cylindrical surface on the rotor, against which two or more “brushes” bear. The current is passed between the brush and whatever segment with which it is in contact. At one time the brushes consisted of bundles of fine brass wires (hence the name). Now they are solid blocks of conducting material, usually carbon.

Brushes eventually wear out and must be replaced. There may also be arcing between the brushes and the commutator segments producing radio interference and other problems. Commutation may also be done by solid-state electronic switching. Hall effect sensors are used to trigger the switches at the appropriate times. At the same time, the rotor and stator are reversed, with the field being on the rotor. Use of permanent magnets rather than field windings means that there is no need for any electrical connections to the rotor. The rotor magnets are commonly made from rare-earth materials that can maintain higher field strengths than traditional ferrous magnets. The result is a brushless direct current (DC) motor that works like a commutated motor, but it is mechanically simpler and more rugged and reliable.

All electric motors that run off direct current are commutated, whether by mechanical commutators or solid-state switches. Synchronous motors are an important class of motors that run off alternating current and are also commutated. The speed of a synchronous motor is locked to the frequency of the alternating current supply. This is useful in applications in which it is desired that the motor run at constant speed. Such applications range from electric clocks all the way up to large mill motors.

There are differences in the performance characteristics of mechanically commutated DC motors depending on the connectivity relationship between the field and armature windings. The field may be excited by an external source, in which case the motor is called externally excited. More often the field is excited by the same source as the current in the armature. If the field and armature windings are connected in parallel, the motor is called a *shunt wound* motor. If the torque produced by the motor is plotted against rotation speed, a shunt wound motor will have a characteristic performance curve like that shown in Fig. 1.59. It will have relatively constant torque over its typical operating range. The torque will eventually decline with speed, and there will be a finite maximum speed at which the torque becomes zero.

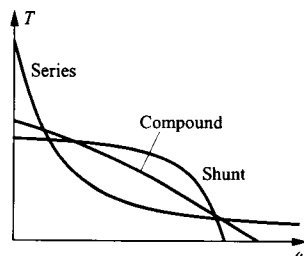


FIGURE 1.59 Torque–speed characteristics typical of DC motors of the shunt wound, series wound, and compound types.

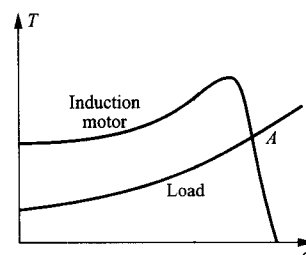
If the field windings are connected in series with the armature windings, the machine is called a *series wound* motor. This results in somewhat different performance characteristics, as shown in Fig. 1.59. The torque at stall or low speed is very high, with a sharp initial drop-off with increasing speed. Ideally the torque never drops to zero. The motor continues to produce some torque even at very high speed. Consequently, operation is unstable at no load. This can be very dangerous in practice if a series wound DC machine is allowed to run with no load. What then happens is the motor “runs away,” continuing to accelerate until the stresses produced by centrifugal forces reach the mechanical strength limits of the rotor components. At that point the rotor explodes, with very destructive consequences. Despite this risk, the characteristics of series wound motors are attractive for use as traction motors in electrically powered vehicles, with the motor being directly coupled mechanically to the load. In principle, a traction motor is never operated at no load.

What is often done, either to achieve series-machine-like behavior, but with a finite maximum speed, or to otherwise optimize the performance characteristics for a given application, is to use a hybrid configuration in which some of the field windings are in series with the armature and some are in parallel. The result is called a *compound wound* motor.

At this point it should also be pointed out that most electric motors cannot be run continuously at *stall*, which is zero speed, or at very low speed. This is because in those circumstances the motor is producing little, if any, mechanical power, and the current through the windings is limited only by their resistance. The power generated by passage of current through the windings is converted entirely into heat. The current is high, because there is no back emf to oppose its flow. The high current at stall is the reason for the high starting torque, since torque is proportional to armature current in these machines. However, the heat generated is the product of the square of the current and the winding resistance. If the motor is held at, or near, stall for an appreciable length of time, heat will typically build up until it damages the motor. This may happen by burning insulation, melting windings, or by heating permanent magnets beyond their Curie point. If heated beyond the Curie temperature, a permanent magnet loses its magnetism, and the motor ceases to function.

The ability of the motor to operate near stall may be seen to be a matter of heat transfer. If the motor is sufficiently well cooled to be able to dissipate the heat generated at stall without a damaging rise in temperature, it may be operated in that regime. That is important for some classes of machine, including industrial robots. Motors that can be operated at or near stall are called *torque motors*.

**Noncommutated Motors** There are also several types of electric motor that do not use commutators. The most commonly used type is the induction motor. In this type of alternating current (AC) motor, the armature has a simple “squirrel cage” configuration. The armature current necessary to produce torque is induced by the alternating current in the stator winding. Induction motors have torque–speed characteristics like that shown in Fig. 1.60. For stable operation it is necessary to operate the motor on the high-speed side of the



**FIGURE 1.60** Torque–speed characteristic of induction motors. With the load characteristic shown, the motor will be self-starting and will operate stably at point A.

hump in the torque–speed curve so that a decrease in speed produces an increase in torque. In contrast to the other types of electric motor we have discussed, the torque is typically not at its highest at stall. In some applications this may mean that the motor cannot be started under load but must be started with reduced load and brought up to a speed above that at which peak torque occurs before the load is applied. This may require use of a clutch to unload the motor. More typically the load torque is also low at start-up, as shown in Fig. 1.60, and the motor will start under load and reach a stable operating point. Induction motors are very popular in industrial applications because they are simple, rugged, and relatively inexpensive. They are best suited to situations in which constant speed need only be approximated. The steep slope of the torque–speed curve on the high-speed side of the hump means that speed will not change much, regardless of load fluctuations.

Another type of motor that does not use a commutator is commonly referred to as a stepping motor. In this type of motor, the torque is generated magnetically, rather than electromagnetically, as in other types of motor. The motor has a number of discrete, equally spaced stable positions. Feeding a voltage pulse to it causes it to rotate to the next stable position. Consequently, stepping motors are very useful for indexing. It is not necessary to provide a means of keeping track of position since the position of the motor is known simply by counting the number of pulses supplied to it.

**Solenoids** A solenoid is a simple, cylindrical winding that when energized by a direct current draws a ferromagnetic core into itself. Solenoids are used as simple, two-state, linear actuators.

Solenoids are not suited to providing variable force or stroke. Electric linear actuators for long or controllable stroke are compound devices using rotary motors in combination with power screws, racks and pinions, or similar mechanisms.

**Speed Control** The advent of solid-state power-switching devices has revolutionized electric actuator control. Pulse-width modulators and phase-controlled rectifiers make it possible to control DC motors without the energy losses inherent in earlier methods, which basically used potentiometer configurations. Variable frequency inverters that convert DC into AC, or AC into AC with different frequencies, allow synchronous and induction machines to be run as variable-speed devices.

DC devices typically respond to the *average* supply voltage. Pulse-width modulation controls that average by chopping a constant-voltage DC input into a train of pulses with controlled widths, thereby controlling the *average* voltage going to the motor. Phase-controlled rectifiers work similarly with an AC supply by switching off the supply at a designated phase on each transmitted half-cycle. This kind of device rectifies AC into DC with a controlled average voltage.

Inverters are devices that produce alternating current from direct current. Again, modern, solid-state power electronics has permitted the design of rugged, efficient, compact inverters that produce alternating current at variable, controlled frequencies. This allows AC motors to be used as servomotors. Induction motors powered by variable-frequency inverter drives are now used as traction drives in heavy mining machinery.

These developments have allowed controlled actuators, or servomotors, to be made much simpler, more compact, and more rugged than in the past. However, the cost and complexity have shifted to the control electronics from which the motor is supplied. When selecting electric actuators it is important to remember that the power control unit may cost as much, or more, than the motor.



**Hydraulic Actuation** An alternative to electric actuation is the use of a fluid power system. This term encompasses both hydraulic and pneumatic actuation systems.

In a hydraulic system energy is transmitted via a flowing liquid. Liquid at high pressure is provided by a pump, which might be driven by an electric motor, as is the case in the hydraulic actuation systems used on some industrial robots, or directly by the engine in the case of the hydraulic systems used in construction machinery.

Hydraulic actuators provide much higher force or torque per unit weight than electric actuators. For this reason they seldom require speed-reducing transmissions. Hydraulic actuation is often the system type of choice in heavy-duty applications, particularly when light weight and/or compactness are desired.

Hydraulic cylinders are widely used as linear actuators, particularly when loads are large and strokes are long. Just as the construction types of many electric motors are similar, if not identical to those of electric generators, hydraulic motors are very similar in construction to hydraulic pumps. That said, there is a considerable variety of different configurations available.

There are actually several different types of hydraulic power transmission systems in use. One common type uses a pressure-regulated supply pump to provide a near-constant supply pressure drop. The pressure to each of several actuators in the system is then tailored to that needed to support the load by means of a control valve.

Another type of hydraulic transmission is a hydrostatic system in which the flow of fluid to the actuator is controlled by means of a variable-displacement pump. This configuration requires use of a separate, variable-displacement pump for each actuator. It is a much more efficient type of system than the valve-controlled configuration, but it tends to be less compact. However, a hydrostatic system does not require a large reservoir for heat rejection like a valved system does.

**Pneumatic Actuation** The most common type of pneumatic actuator is a cylinder that is very similar in construction to a hydraulic cylinder. A pneumatic system is supplied by a compressor, rather than a pump. Some compressors are similar in construction to types of hydraulic pump, but others are quite different. Control valves for pneumatic systems also usually closely resemble their hydraulic counterparts.

Pneumatic actuation has been very popular for fixed automation equipment when high power levels are not required, for example in "light automation." The attraction is relatively low cost and easy maintenance. However, pneumatic systems do not lend themselves well to proportional control. The compressibility of air as a working fluid makes accurate control very problematic. Traditional pneumatic actuator arrangements required only two or a few discrete positions. This is acceptable for fixed automation in which the whole system is designed around a single product but does not work well for flexible automation in which the same machine or line may be reprogrammed to produce several different models or products.

Pneumatic systems share some of the shortcomings of electrical systems in the form of low force-to-weight ratios. This is because they are usually operated at supply pressures an order of magnitude lower than those of hydraulic systems. The low supply pressure is needed because the low viscosity of air compared to hydraulic oil makes it much harder to design seals to contain it at high pressure. Air motors perform much the same function in a pneumatic system that electric motors do in an electric system, providing a means of generating relatively high mechanical power by running a rotary device at high speed. As with electric motors, air motors usually have to be geared down to provide useful torque-speed characteristics. An air motor is basically a compressor running in reverse, so it is a much more complex device than a simple pneumatic cylinder.

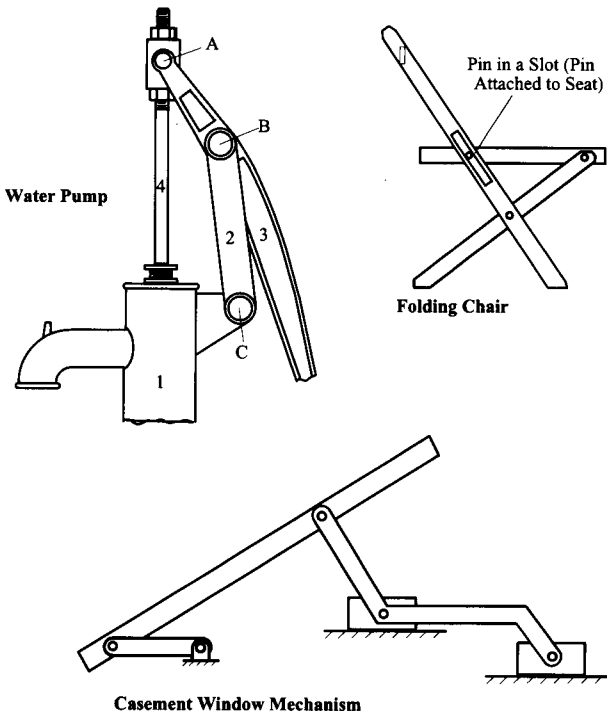
## PROBLEMS

### EXERCISE PROBLEMS ON LINKAGE STRUCTURE

1.1 Find a mechanism as an isolated device or in a machine and make a realistic sketch of the mechanism. Then make a freehand sketch of the kinematic schematics for the mechanism chosen.

1.2 Cabinet hinges use various types of linkages for the guiding mechanism. Identify three types of cabinet hinges employing more than a simple revolute joint and make a freehand sketch of the kinematic mechanism used.

1.3 The drawings shown are pictorial representations of real mechanisms that are commonly encountered. Make a freehand sketch of the kinematic schematic representation of each mechanism.



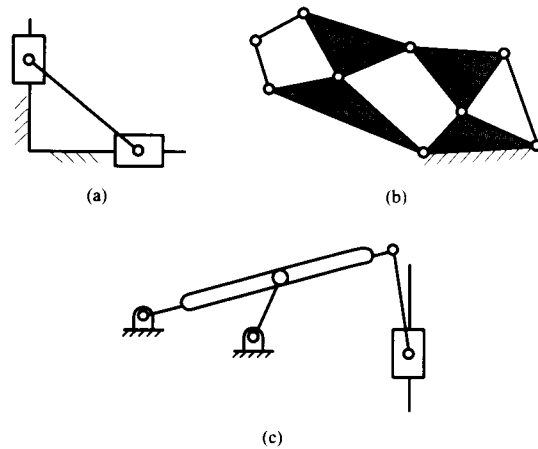
1.4 Linkages are often used to guide devices such as computer keyboards in and out of cabinets. Find three such devices, and make a freehand sketch of the kinematic mechanisms used for the devices.

1.5 Four-bar linkages are used in common devices found around the home and at businesses. Locate six such devices and make a freehand sketch of each device and describe its function.

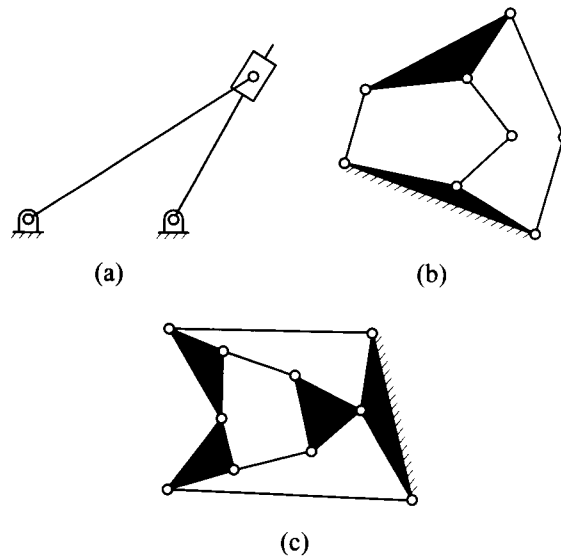
### EXERCISE PROBLEMS ON MECHANISM MOBILITY FOR PLANAR MECHANISMS

1.6 Calculate the mobility, or number of degrees of freedom, of each of the mechanisms in Problem 1.3.

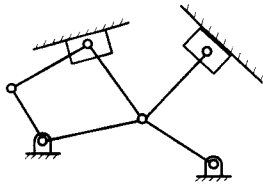
1.7 Determine the number of members, number of joints, and mobility of each of the planar linkages shown.



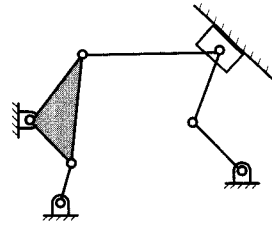
1.8 Determine the number of members, number of joints, and mobility of each of the planar linkages shown.



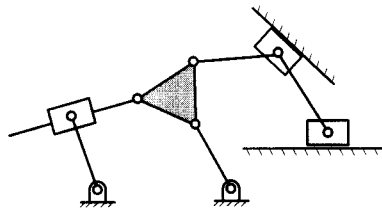
1.9 Determine the mobility and the number of idle degrees of freedom of each of the planar linkages shown. Show the equations used and identify the input and output links assumed when determining your answers.



(a)

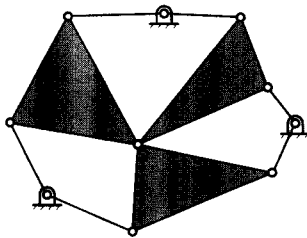


(b)

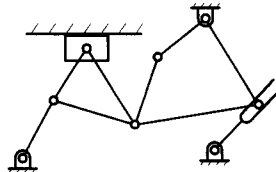


(c)

1.10 Determine the mobility and the number of idle degrees of freedom of the linkages shown. Show the equations used and identify any assumptions made when determining your answers.

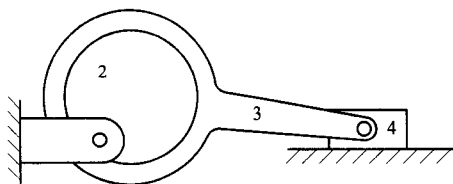


(a)

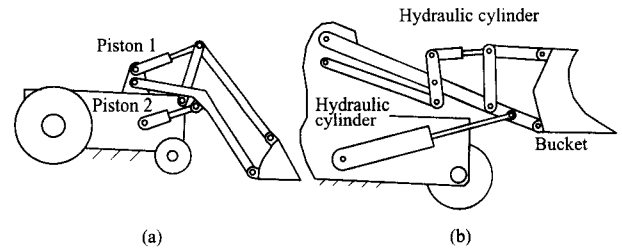


(b)

1.11 Determine the mobility and the number of idle degrees of freedom associated with the mechanism shown. Show the equations used and identify any assumptions made when determining your answers.



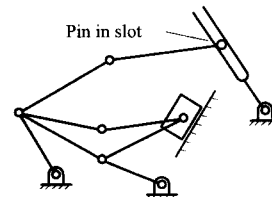
1.12 Determine the mobility of each of the planar linkages shown. Show the equations used to determine your answers.



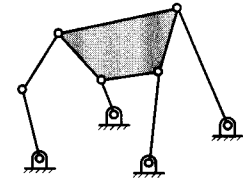
(a)

(b)

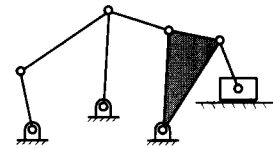
1.13 Determine the mobility and the number of idle degrees of freedom of each of the planar linkages shown. Show the equations used and identify any assumptions made when determining your answers.



(a)

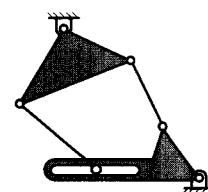


(b)

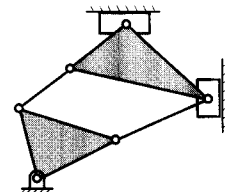


(c)

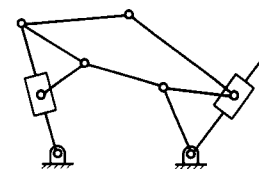
1.14 Determine the mobility and the number of idle degrees of freedom of each of the planar linkages shown. Show the equations used to determine your answers.



(a)

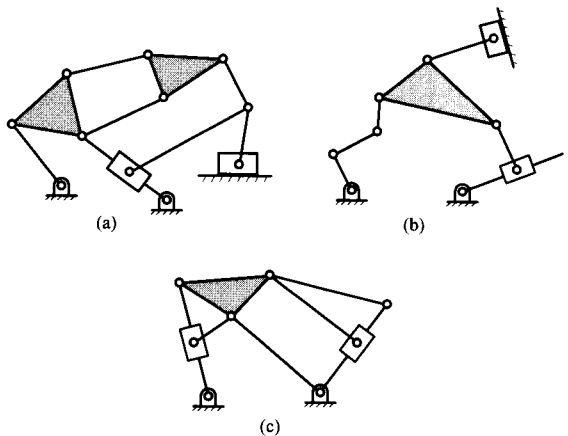


(b)

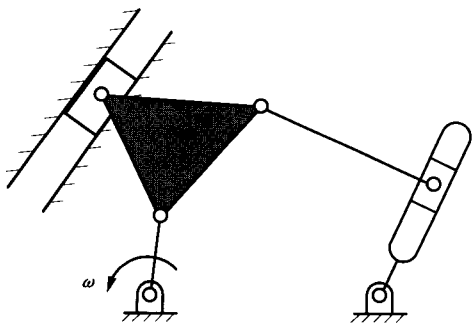


(c)

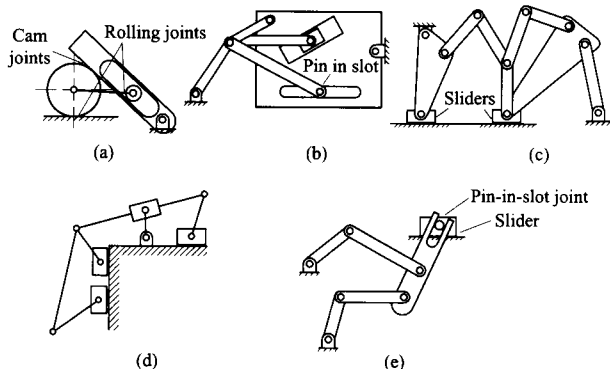
1.15 Determine the mobility and the number of idle degrees of freedom of each of the planar linkages shown. Show the equations used and identify any assumptions made when determining your answers.



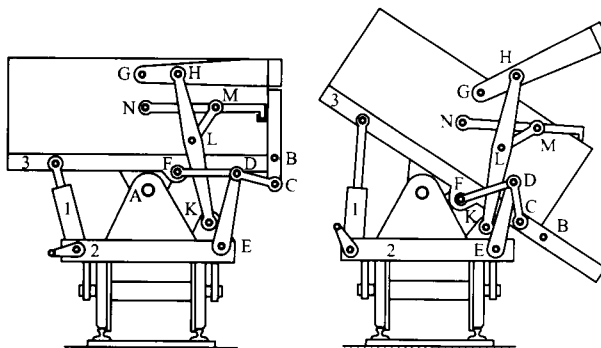
1.16 If position information is available for all points in the planar linkage shown, can all of the velocities be determined uniquely if the value of  $\omega$  is given? Explain your answer.



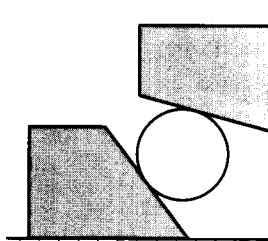
1.17 Determine the mobility and the number of idle degrees of freedom associated with each mechanism. Show the equations used and identify any assumptions made when determining your answers.



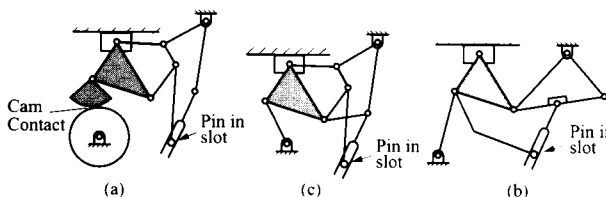
1.18<sup>5</sup> Determine the mobility and the number of idle degrees of freedom associated with the mechanism shown. The mechanism is a side-dumping car that consists of body 2 and truck 3 connected together by two six-bar linkages,  $ABCDEF$  and  $AGHKLMN$ . Link  $NM$  is designed as a latch on its free end (see left drawing). When jack 1 is operated, body 3 is lifted to the dumping position shown in the right-hand drawing. Simultaneously, the six-bar linkage  $AGHKLMN$  opens the latch on link  $NM$  and raises link  $GH$ . Linkage  $ABCDEF$  swings open side  $BC$  and the load can be dumped at some distance from the car (see right-hand drawing). Show the equations used to determine your answers.



1.19 Determine the mobility and the number of idle degrees of freedom associated with the mechanism shown. The round part rolls without slipping on the pieces in contact with it that slide on the fixed surfaces.

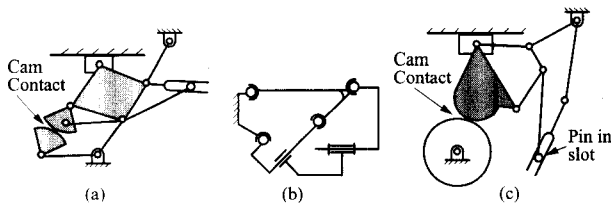


1.20 Determine the mobility and the number of idle degrees of freedom for each of the mechanisms shown. Show the equations used and identify any assumptions made when determining your answers.

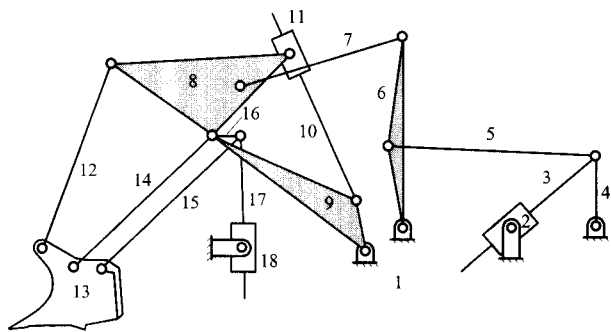


<sup>5</sup> Problem courtesy of Joseph Davidson, Arizona State University.

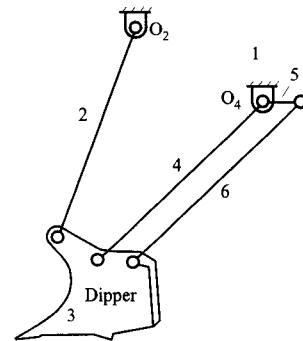
1.21 Determine the mobility and the number of idle degrees of freedom for each of the mechanisms shown. Show the equations used and identify any assumptions made when determining your answers.



1.22<sup>6</sup> Determine the mobility and the number of idle degrees of freedom associated with the mechanism shown. The figure is a schematic of the entire linkage for a large power shovel used in strip mining. It can cut into a bank 20-m high and can dump to a height of 14.5 m. Link 7 is connected to link 8 with a revolute joint. Show the equations used and identify any assumptions made when determining your answers.

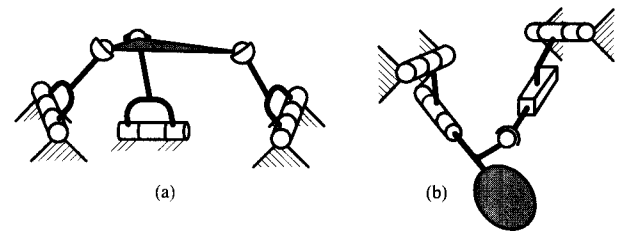


1.23 In the figure is a portion of the support mechanism for the dipper on a large earth-moving machine used in removing overburden in strip-mining operations. The fixed centers for the portion of the mechanism really move, but useful information can be obtained by observing the dipper motion relative to the "frame" as shown in the sketch. Both links 4 and 5 are mounted at  $O_4$ . Links 4 and 6 are parallel and of equal length. The dipper is moved by a hydraulic cylinder driving crank 5 about its  $O_4$ . Determine the mobility of the mechanism.

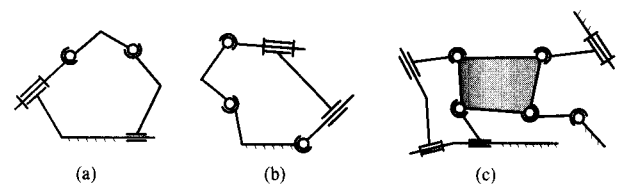


**EXERCISE PROBLEMS ON MECHANISM MOBILITY FOR SPATIAL MECHANISMS**

1.24 Determine the number of members, number of joints, mobility, and the number of idle degrees of freedom of each of the spatial linkages shown. For the idle degrees of freedom, identify the input and output links assumed.

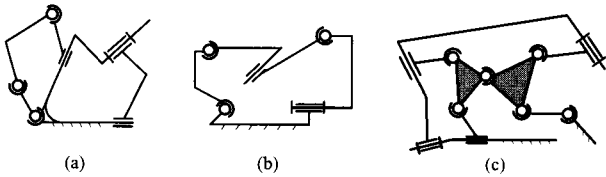


1.25 Determine the mobility and the number of idle degrees of freedom of the spatial linkages shown. Show the equations used to determine your answers. For the idle degrees of freedom, identify the input and output links assumed.

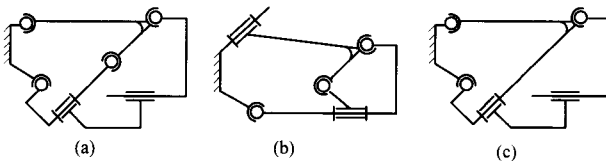


<sup>6</sup> Problem courtesy of Joseph Davidson, Arizona State University.

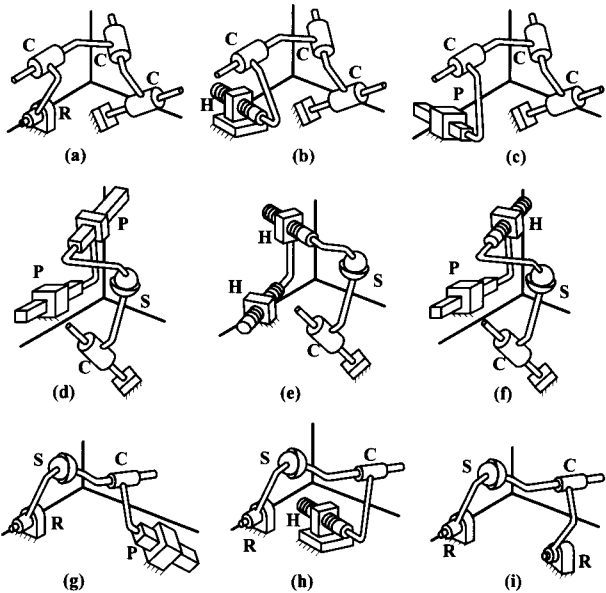
1.26 Determine the mobility and the number of idle degrees of freedom of the spatial linkages shown. Show the equations used to determine your answers. For the idle degrees of freedom, identify the input and output links assumed.



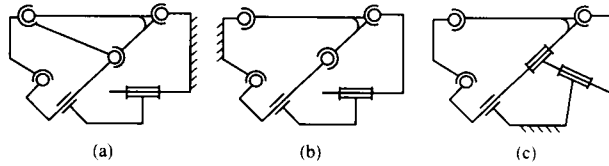
1.27 Determine the mobility and the number of idle degrees of freedom for each of the mechanisms shown. Show the equations used to determine your answers. For the idle degrees of freedom, identify the input and output links assumed.



1.28 Determine the mobility and the number of idle degrees of freedom associated with each mechanism.<sup>7</sup> Show the equations used to determine your answers.

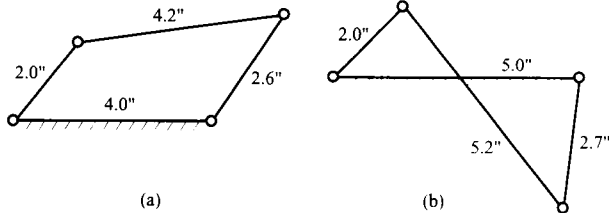


1.29 Determine the mobility and the number of idle degrees of freedom for each of the mechanisms shown. Show the equations used to determine your answers. For the idle degrees of freedom, identify the input and output links assumed.



**EXERCISE PROBLEMS ON FOUR-BAR LINKAGE TYPE (GRASHOF'S EQUATION)**

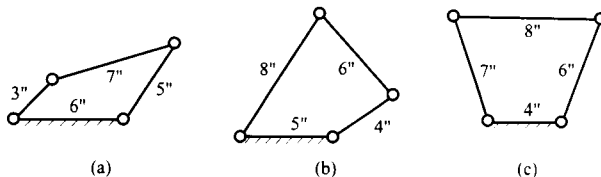
1.30 Determine which (if either) of the following linkages can be driven by a constant-velocity motor. For the linkage(s) that can be driven by the motor, indicate the driver link.



1.31 Assume that you have a set of links of the following lengths: 2 in, 4 in, 5 in, 6 in, and 9 in. Design a four-bar linkage that can be driven with a continuous-rotation electric motor. Justify your answer with appropriate equations, and make a scaled drawing of the linkage. Label the crank, frame, coupler, and rocker (follower).

1.32 Assume that you have a set of links of the following lengths: 20 mm, 30 mm, 45 mm, 56 mm, and 73 mm. Design a four-bar linkage that can be driven with a continuous-rotation electric motor. Justify your answer with appropriate equations, and make a freehand sketch (labeled) of the resulting linkage. Label the crank, frame, coupler, and rocker (follower).

1.33 For the four-bar linkages shown, indicate whether they are Grashof type 1 or 2 and whether they are crank-rocker, double-crank, or double-rocker mechanisms.



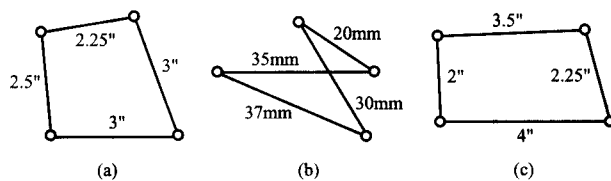
<sup>7</sup> Problem based on paper entitled "A Number Synthesis Survey of Three-Dimensional Mechanisms" by L. Harrisberger, *Trans. ASME, J. Eng. Ind.*, pp. 213-220, May 1965.

**1.34** You are given a set of three links with lengths 2.4 in, 7.2 in, and 3.4 in. Select the length of a fourth link and assemble a linkage that can be driven by a continuous-rotation motor. Is your linkage a Grashof type 1 or Grashof type 2 linkage? (Show your work.) Is it a crank-rocker, double-rocker, or double-crank linkage? Why?

**1.35** You have available a set of eight links from which you are to design a four-bar linkage. Choose the links such that the linkage can be driven by a continuous-rotation motor. Sketch the linkage and identify the type of four-bar mechanism resulting.

$L_1 = 2''$ ,  $L_2 = 3''$ ,  $L_3 = 4''$ ,  $L_4 = 6''$ ,  $L_5 = 7''$ ,  $L_6 = 9.5''$ ,  $L_7 = 13''$ , and  $L_8 = 9''$

**1.36** Determine the number of fully rotating cranks in the planar mechanisms shown. Show your calculations.



**1.37** If the link lengths of a four-bar linkage are  $L_1 = 1$  mm,  $L_2 = 3$  mm,  $L_3 = 4$  mm, and  $L_4 = 5$  mm and link 1 is fixed, what type of four-bar linkage is it? Also, is the linkage a Grashof type 1 or 2 linkage? Answer the same questions if  $L_1 = 2$  mm.

**1.38** You are given two sets of links. Select four links from each set such that the coupler can rotate fully with respect to the others. Sketch the linkage and identify the type of four-bar mechanism in each case.

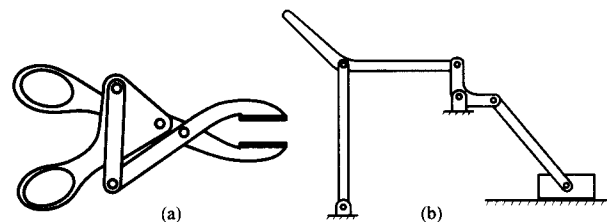
(a)  $L_1 = 5''$ ,  $L_2 = 8''$ ,  $L_3 = 15''$ ,  $L_4 = 19''$ , and  $L_5 = 28''$ .

(b)  $L_1 = 5''$ ,  $L_2 = 2''$ ,  $L_3 = 4''$ ,  $L_4 = 3.5''$ , and  $L_5 = 2.5''$ .

**1.39** The mechanisms shown are drawn to scale.

(a) Sketch kinematic schematics showing the relationships between the members and joints.

(b) Determine the Grashof type of the four-bar linkage in each mechanism.



---

# *GRAPHICAL POSITION, VELOCITY, AND ACCELERATION ANALYSIS FOR MECHANISMS WITH REVOLUTE JOINTS OR FIXED SLIDES*

---

## **2.1 INTRODUCTION**

---

Historically, planar linkage analysis problems were solved graphically using drafting equipment. In recent years computer techniques have offered a viable and attractive alternative. Some teachers of the subject now prefer to concentrate their time on analytical approaches. Nevertheless, there are still many situations in which graphical techniques offer the most efficient solution, and the insight into the problem obtained by an understanding of the graphical approach is, we feel, essential. For this reason we have chosen to present both approaches. In Chapters 2–4, we present the graphical approach, and in Chapter 5, we present the analytical approach.

We have separated the presentation of graphical analyses into three chapters. In this chapter, we present the analysis of mechanisms with only revolute joints or sliders on fixed slides. Such mechanisms constitute the majority of mechanisms found in the real world. These mechanisms can also be analyzed using relatively simple equations derived from basic physics. In Chapter 3, mechanisms involving higher pairs and moving slides will be addressed. The approach to analyzing these mechanisms is more involved than that required in Chapter 2 because moving coordinate systems must be considered directly.

In Chapter 4, we present a special graphical procedure based on instant centers of velocity. When two laminae are moving relative to one another there exists, at every instant, a point in one lamina that is at rest relative to the other, and vice versa. This is the instant center of relative motion of those laminae. The technique of velocity analysis based on instant centers presents advantages when solving certain types of problems. Therefore, it is advantageous for the engineer to be familiar with this technique, as well as the vector polygon technique. This is a very powerful procedure if only velocities are important, and the graphical approach gives considerable insight into the design of planar mechanisms.

A purely analytical approach to kinematic analysis based on vector loop equations is presented in Chapter 5. This procedure can be easily programmed, but, unless a program is readily available, it is typically much more time consuming than a graphical analysis when only one position of the mechanism is of interest.

There is a tendency to discard traditional graphical techniques in favor of numerical solutions based on the analytical formulations presented in Chapter 5. However, there are many situations in which graphical techniques are useful. For example, it is necessary to check and debug computer programs. This is done most effectively by comparing the



numerical solutions of sample problems with solutions to the same problems obtained using completely different techniques. Graphical techniques are ideal for providing these alternative solutions. At other times, a quick answer to a problem is needed, and no suitable program is available. Rather than writing and debugging a program specifically to solve the problem, one often finds it to be more efficient to use the graphical approach. Most important, insight into the kinematic geometry that governs all mechanism behavior is obtained by an understanding of the graphical approach.

## 2.2 GRAPHICAL POSITION ANALYSIS

---

Regardless of what procedure is used for a linkage analysis, it is *always* necessary to determine the angular positions of the links before a velocity analysis can be performed. Likewise, it is necessary to know the link angular velocities before an acceleration analysis can be performed. That is, the kinematic analysis of a linkage must *always* proceed in this sequence: position analysis, then velocity analysis, then acceleration analysis. If the linkage has one degree of freedom and the driver is a crank, the angular position, angular velocity, and angular acceleration of a driving link must all be specified for a solution to be possible. If the driving member is connected to the base by a prismatic joint, the linear position, velocity, and acceleration of any point in that link must be specified.

When working graphically, the position analysis consists of simply drawing the linkage to scale. Usually this is so straightforward that it tends to be forgotten as an important step in the solution process. The representation used is a geometric skeleton of the linkage: links with revolute joints are represented by the line, or lines, joining the joint axes. Prismatic joints are represented by lines in the direction of sliding. Revolute joints are usually represented only by the points that are the intersections of their axes with the plane of motion. The way the method works in the analysis of a simple linkage is illustrated in the examples. (See, for example, Fig. 2.8.) Note that this is different from the linkage skeleton representation used in Chapter 1. However, it is sometimes useful to indicate revolute joints by small circles centered on the joint axes and prismatic joints by sliding blocks. If this is done, the present representation becomes a geometrically accurate equivalent of the linkage skeleton.

As will be shown in Chapter 5, the position equations for mechanisms are inherently nonlinear. In many cases, the mechanism can be assembled (or drawn) in two possible configurations. It is necessary to know before the analysis is conducted which solution is desired. This will be illustrated in the examples that will be discussed after the equations for velocity and acceleration are developed.

We will begin the analysis of velocities and accelerations with a relatively simple case involving two points fixed to the same rigid link. The equations for this case are commonly developed in courses in mechanics using the procedure we shall use here. The equations developed will be directly applicable to mechanisms with revolute joints and/or sliders on fixed lines. We will illustrate the use of the procedure with several examples.

For more complex joints, a more rigorous and general approach will be used to develop the velocity and acceleration equations. This will entail identifying the coordinate systems relative to which each of the vectors is described and relative to that for which the time derivatives are desired. It will be shown that the velocity and acceleration equations developed for the case of two points on a rigid link are special cases of the more general equations. This procedure will be given in Chapter 3.

## 2.3 PLANAR VELOCITY POLYGONS

Velocity analysis is the determination of the angular velocities of different links in a mechanism and of the velocities of points on the links, given either the angular velocity of some member or the velocity of some point on the link designated as the input. The vector polygon technique will be used here to solve the velocity and acceleration equations. The method facilitates the solution of a large variety of velocity and acceleration problems and also has the advantage that the acceleration polygon solution has a strong similarity to that of the velocity polygon, which makes it relatively straightforward to learn and remember. Almost all practical problems can be solved by this approach.

In theory, however, the technique is not general. It is possible to formulate problems that cannot be solved by the methods presented here. Special techniques have been developed that allow treatment of some of the simpler cases that are not amenable to the vector polygon method; nonetheless, it is possible to formulate problems that cannot be solved by even these embellished techniques. The reader is referred to books by Hirschhorn,<sup>1</sup> Hall,<sup>2</sup> and Holowenko<sup>3</sup> for the auxiliary-point technique and other methods of handling more general mechanisms. It should be emphasized, however, that problems that cannot be solved by the methods presented in this chapter are rarely encountered in practice.

The key to the graphical velocity analysis of most linkages is the relationship between the velocities of any two points embedded in a rigid body. This relationship is

$$\mathbf{v}_B = \mathbf{v}_A + \boldsymbol{\omega} \times \mathbf{r}_{B/A} \quad 2.1$$

where  $A$  and  $B$  are points fixed in a moving lamina (rigid body) as shown in Fig. 2.1,  $\mathbf{v}_A$  and  $\mathbf{v}_B$  are the respective velocities relative to the frame of those points,  $\mathbf{r}$  is the vector  $\overline{AB}$ , and  $\boldsymbol{\omega}$  is the angular velocity of the lamina relative to the frame. Basically, if we draw a line on the lamina,  $\boldsymbol{\omega}$  is the time rate of change of the angular orientation of that line with respect to time.

For Eq. (2.1) to be valid, it is important that points  $A$  and  $B$  be fixed to the same rigid link. If one of the points is attached to a different link, the equation is incomplete. This case is covered in Chapter 3. In the examples, we will use subscripts on the point letters (e.g.,  $A_2$ ) to identify the link to which each point is attached to ensure that the proper points are being considered when using the equation. When developing the equations here, however, subscripts will not be used because only one link is being considered.

To prove this relationship, consider the two points  $A$  and  $B$  fixed in the lamina shown in Fig. 2.1. The lamina is moving with general planar motion. Let the position of point  $A$  relative to a fixed reference frame be  $\mathbf{r}_A$ , and let that of point  $B$  be  $\mathbf{r}_B$ . The vector  $\overline{AB}$  is  $\mathbf{r}_{B/A}$  and is pointed from  $A$  to  $B$ . Therefore

$$\mathbf{r}_B = \mathbf{r}_A + \mathbf{r}_{B/A} \quad 2.2$$

Differentiating Eq. (2.2) with respect to time gives

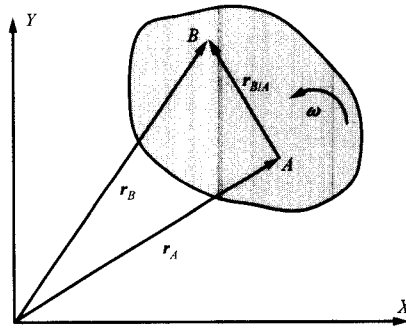
$$\mathbf{v}_B = \mathbf{v}_A + d\mathbf{r}_{B/A}/dt$$

Now, since points  $A$  and  $B$  are fixed in the moving lamina, vector  $\mathbf{r}_{B/A}$  is fixed in that lamina and moves with it. It has constant length, so only its direction changes. Let the change in

<sup>1</sup> Hirschhorn, J., *Kinematics and Dynamics of Plane Mechanisms*, McGraw-Hill Book Co., New York, 1962.

<sup>2</sup> Hall, A., *Kinematics and Linkage Design*, Balt Publishers, West Lafayette, IN, 1966.

<sup>3</sup> Holowenko, A. R., *Dynamics of Machinery*, John Wiley & Sons, Inc., New York, 1955.



**FIGURE 2.1** Position relationships of two points embedded in a moving lamina.

direction in a small time interval  $\delta t$  be  $\delta\theta$ , as shown in Fig. 2.2. The magnitude of the change in  $r_{B/A}$  is

$$\delta r = r_{B/A} \delta\theta$$

As  $\delta t$  and hence  $\delta\theta$  approach zero, the angle between the vectors  $\delta r_{B/A}$  and  $r_{B/A}$  approaches  $90^\circ$ . If  $\omega$  is the magnitude of the angular velocity of the lamina,

$$\delta\theta = \omega \delta t$$

Therefore

$$\delta r / \delta t = r_{B/A} \omega$$

so, in the limit as  $\delta t$  approaches zero,

$$\left| d\mathbf{r}_{B/A} / dt \right| = r_{B/A} \omega$$

If  $\omega$  is considered to be a vector normal to the plane of motion, clockwise (CW) if directed away from the observer and counterclockwise (CCW) if directed toward the observer, the direction of  $d\mathbf{r}_{B/A}/dt$  is normal to  $\omega$  and to  $r_{B/A}$  and obeys the right-hand screw rule with respect to those vectors. Therefore  $d\mathbf{r}_{B/A}/dt$  can be represented by the expression

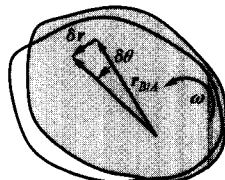
$$d\mathbf{r}_{B/A} / dt = \boldsymbol{\omega} \times \mathbf{r}_{B/A} \quad (2.3)$$

What we have actually derived here is a general expression for the derivative of a vector of constant magnitude ( $r_{B/A}$ ) embedded in a lamina in planar motion, for which  $\omega$  is the angular velocity relative to a fixed reference frame. We will make use of this expression in Chapter 3 and elsewhere.

Thus

$$\mathbf{v}_B = \mathbf{v}_A + \boldsymbol{\omega} \times \mathbf{r}_{B/A} \quad (2.1)$$

As will be shown in Chapter 3, this expression is actually valid for general spatial motion, although the derivation here applies only to planar motion.



**FIGURE 2.2** Successive positions of the lamina separated by a small time interval,  $\delta t$ .

It is convenient to write Eq. (2.1) in the form

$$\mathbf{v}_B = \mathbf{v}_A + \mathbf{v}_{B/A} \quad (2.4)$$

where

$$\mathbf{v}_{B/A} = \boldsymbol{\omega} \times \mathbf{r}_{B/A} \quad (2.5)$$

The vector  $\mathbf{v}_{B/A}$  is usually called the velocity of  $B$  relative to  $A$ , although, strictly speaking, it is meaningless to talk of a velocity relative to a point. Velocities are vectors and are measured relative to reference frames. Therefore,  $\mathbf{v}_{B/A}$  would be the velocity of point  $B$  relative to a reference frame that has its origin at point  $A$  and that moves so as to be always parallel to the fixed frame.

If only one letter is used as a subscript (e.g.,  $\mathbf{v}_B$ ), the resulting velocity is called an absolute velocity. This means that it is the derivative of a position vector that has its tail fixed to a point that has zero velocity. From Eq. (2.4) it is clear that  $\mathbf{v}_B = \mathbf{v}_{B/A}$  if  $\mathbf{v}_A = 0$ . Note that point  $A$  need not be absolutely fixed; it might have a velocity that is only momentarily zero.

The basic technique used in a graphical linkage analysis is to work from one or more points with known velocity to one of unknown velocity using the relationship in Eq. (2.1) between the velocities of two points fixed in the same lamina. The intersections of the axes of revolute joints with the plane of motion form transfer points because they are actually coincident points fixed in two different links. Thus, the velocity of a revolute joint can be obtained by considering it to be a point in one of the links it connects. That information can then be used by considering the point to be fixed in the other link.

Equation 2.4 can be represented graphically as the vector triangle shown in Fig. 2.3. This triangle can always be solved given the direction and magnitude of one of the three vectors and the directions of the remaining two. This is the normal situation in planar velocity analysis. Again, the way in which this works will be illustrated in several examples after all of the necessary equations have been developed.

Based on Eq. (2.5), to find the angular velocity  $\boldsymbol{\omega}$  for a given link, we must compute the relative velocity between two points on the link, and the velocity must be given relative to the desired reference frame. For example, the relative velocity relationship for points  $B$  and  $A$  can be written as

$$\mathbf{v}_{B/A} = \boldsymbol{\omega} \times \mathbf{r}_{B/A} \quad (2.6)$$

The vectors in Eq. (2.6) will be mutually orthogonal, as indicated schematically in Fig. 2.4. Because we will know the lines along which each of the vectors must lie, the main problem is to determine the directions along the lines and the magnitudes of each of the vectors. Given any two of the vector directions, we can find the direction of the third by observing the directions given by the right-hand screw rule. Two examples are shown in Fig. 2.4.

Notice that  $\mathbf{v}_{B/A}$  and  $\mathbf{r}_{B/A}$  are always perpendicular to each other. Also, visually, we can determine the direction of  $\mathbf{v}_{B/A}$  by rotating  $\mathbf{r}_{B/A}$   $90^\circ$  in the direction of  $\boldsymbol{\omega}$ . Similarly, if we

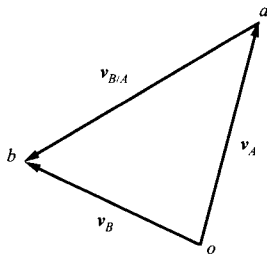


FIGURE 2.3 Velocities of two points embedded in a lamina.



**FIGURE 2.4** The direction relationship among the vectors  $\mathbf{v}_{B/A}$ ,  $\boldsymbol{\omega}$ , and  $\mathbf{r}_{B/A}$  for planar motion.

know the directions of  $\mathbf{r}_{B/A}$  and  $\mathbf{v}_{B/A}$ , we can determine the direction of  $\boldsymbol{\omega}$  by visualizing the direction in which we must rotate  $\mathbf{r}_{B/A}$  to obtain the direction of  $\mathbf{v}_{B/A}$ .

Because the three vectors in Eq. (2.5) are orthogonal, their magnitudes are related by

$$|\mathbf{v}_{B/A}| = |\boldsymbol{\omega}| |\mathbf{r}_{B/A}| \quad (2.7)$$

Given any two of the three magnitudes in Eq. (2.7), we can easily solve for the third magnitude.

## 2.4 GRAPHICAL ACCELERATION ANALYSIS

Just as was the case for velocity analysis, the key to most graphical acceleration analyses is the relationship between the accelerations of two points fixed in the same rigid lamina or link. This relationship can be derived by differentiating the velocity relationship with respect to time. Rewriting Eq. (2.1) we obtain

$$\mathbf{v}_B = \mathbf{v}_A + \boldsymbol{\omega} \times \mathbf{r}_{B/A} \quad (2.1)$$

Differentiating gives

$$\mathbf{a}_B = \mathbf{a}_A + (d\boldsymbol{\omega}/dt) \times \mathbf{r}_{B/A} + \boldsymbol{\omega} \times (d\mathbf{r}_{B/A}/dt)$$

As was shown in Section 2.3,

$$d\mathbf{r}_{B/A}/dt = \boldsymbol{\omega} \times \mathbf{r}_{B/A}$$

Also, angular acceleration  $\boldsymbol{\alpha}$  is defined to be  $d\boldsymbol{\omega}/dt$ . Hence

$$\mathbf{a}_B = \mathbf{a}_A + \boldsymbol{\alpha} \times \mathbf{r}_{B/A} + \boldsymbol{\omega} \times (\boldsymbol{\omega} \times \mathbf{r}_{B/A}) \quad (2.8)$$

As will be demonstrated in Chapter 3, this expression is generally valid for three-dimensional motion, although it has been derived here only in the planar motion context. For planar motion, it is possible to simplify the expression by noting that, in this case,  $\boldsymbol{\omega}$  and  $\mathbf{r}_{B/A}$  are orthogonal, as shown in Fig. 2.5. Also,  $\boldsymbol{\omega} \times \mathbf{r}_{B/A}$  has the magnitude  $\omega r_{B/A}$  and is normal to both  $\boldsymbol{\omega}$  and  $\mathbf{r}_{B/A}$  in the sense given by the right-hand screw rule. Then,  $\boldsymbol{\omega} \times (\boldsymbol{\omega} \times \mathbf{r}_{B/A})$  has the magnitude  $\omega^2 r_{B/A}$  and is orthogonal to both  $\boldsymbol{\omega}$  and  $\boldsymbol{\omega} \times \mathbf{r}_{B/A}$ . Applying the right-hand screw rule, it can be seen that this vector  $\boldsymbol{\omega} \times (\boldsymbol{\omega} \times \mathbf{r}_{B/A})$  is always in the negative  $\mathbf{r}_{B/A}$  direction. Therefore it can be written as  $-\omega^2 \mathbf{r}_{B/A}$ , and the relationship between the accelerations of points  $A$  and  $B$  is

$$\mathbf{a}_B = \mathbf{a}_A + \boldsymbol{\alpha} \times \mathbf{r}_{B/A} - \omega^2 \mathbf{r}_{B/A} \quad (2.9)$$

It is usual to write

$$\mathbf{a}_{B/A}^r = -\omega^2 \mathbf{r}_{B/A} \quad \text{and} \quad \mathbf{a}_{B/A}^t = \boldsymbol{\alpha} \times \mathbf{r}_{B/A} \quad (2.10)$$

with  $\mathbf{a}_{B/A}^r$  called the radial component of the acceleration of  $B$  relative to  $A$  and  $\mathbf{a}_{B/A}^t$  called the tangential component of the acceleration of  $B$  relative to  $A$ . As was noted in the case of

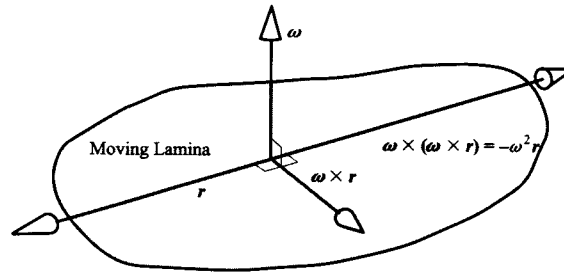


FIGURE 2.5 The derivation of the relationship  $\omega \times (\omega \times r) = -\omega^2 r$ , which is valid for planar motion.

velocities, it is not really proper to talk about the velocity or acceleration of one point relative to another point. The vector  $\mathbf{a}_{B/A}$  is really the acceleration of point  $B$  relative to a reference frame with origin at  $A$  and moves so that it is always parallel to the fixed frame.

The vector polygon corresponding to Eq. (2.8) is shown schematically in Fig. 2.6. If a velocity analysis of the linkage has been performed, the angular velocities of all the links are known, and so the radial component  $\mathbf{a}_{B/A}^r = -\omega^2 \mathbf{r}_{B/A}$  can always be calculated and plotted. Hence, if one of the other vectors is also known, and the directions of the remaining two are also known, the polygon can be solved in very much the same way as the vector triangle was used in the velocity analysis. This is the normal procedure for a graphical acceleration analysis.

The angular acceleration for a given link is obtained in the same manner as the angular velocity except that the *tangential* component of relative acceleration is used instead of the linear velocity. To find a value of  $\alpha$ , we must know the tangential component of the relative acceleration between any two points on the link. For example, the relative tangential acceleration relationship for points  $B$  and  $A$  can be written as

$$\mathbf{a}_{B/A}^t = \alpha \times \mathbf{r}_{B/A} \quad (2.11)$$

Because we will know the lines along which the vectors must lie, the main problem again is to determine the directions along the lines and the magnitude of each of the vectors. Given any two of the vector directions, we can find the direction of the third by observing the directions given by the right-hand screw rule. Two examples are shown schematically in Fig. 2.7.

Notice that these relationships are exactly the same as for the velocity expressions if  $\omega$  is replaced by  $\alpha$  and  $\mathbf{v}_{B/A}$  is replaced by  $\mathbf{a}_{B/A}^t$ . In particular, notice that  $\mathbf{a}_{B/A}^t$  and  $\mathbf{r}_{B/A}$  are always perpendicular to each other. Also, we can determine the direction of  $\mathbf{a}_{B/A}^t$  by visually rotating  $\mathbf{r}_{B/A}$   $90^\circ$  in the direction of  $\alpha$ . Similarly, if we know the directions of  $\mathbf{r}_{B/A}$  and  $\mathbf{a}_{B/A}^t$ , we can determine the direction of  $\alpha$  by visualizing the direction in which we must rotate  $\mathbf{r}_{B/A}$

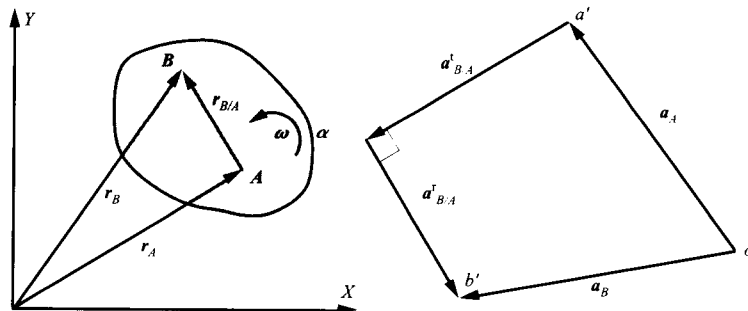


FIGURE 2.6 Accelerations of two points embedded in a moving lamina.

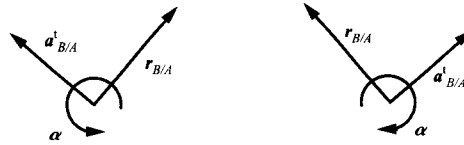


FIGURE 2.7 The direction relationship among the vectors  $a_{B/A}^t$ ,  $\alpha$ , and  $r_{B/A}$  for planar motion.

to obtain the direction of  $a_{B/A}^t$ .

Because the three vectors in Eq. (2.10) are orthogonal, their magnitudes are related by

$$|a_{B/A}^t| = |\alpha| |r_{B/A}| \quad (2.12)$$

Given any two of the three magnitudes in Eq. (2.12), we can easily solve for the third magnitude.

## 2.5 GRAPHICAL ANALYSIS OF A FOUR-BAR MECHANISM

Having derived the basic equations for relative velocities and accelerations between two points on a rigid link, we will illustrate the use of the equations for the graphical analysis of several mechanisms. The first example involves the position, velocity, and acceleration analysis of the four-bar mechanism given in Fig. 2.8. The analysis for this example will be conducted in detail, but in subsequent examples, less detail will be given. In all of the examples, subscripts will be used to identify the links to which the points are attached. This is necessary because *the equations derived in Sections 2.3 and 2.4 apply only when the points (A and B) are fixed to the same link or lamina.*

### EXAMPLE 2.1

#### Graphical Analysis of a Four-Bar Mechanism

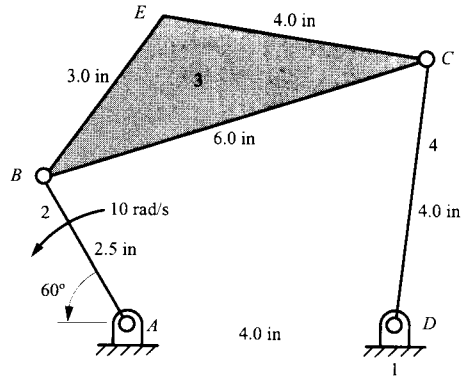
#### Solution

Determine the angular positions, angular velocities, and angular accelerations of all members of the linkage shown in Fig. 2.8 when link  $AB$  is at  $60^\circ$  to the horizontal. Also find the position, velocity, and acceleration of point  $E$  in the coupler member of the linkage. Link  $AB$  is driven at a constant angular velocity of 10 rad/s CCW.

#### (a) Position Analysis

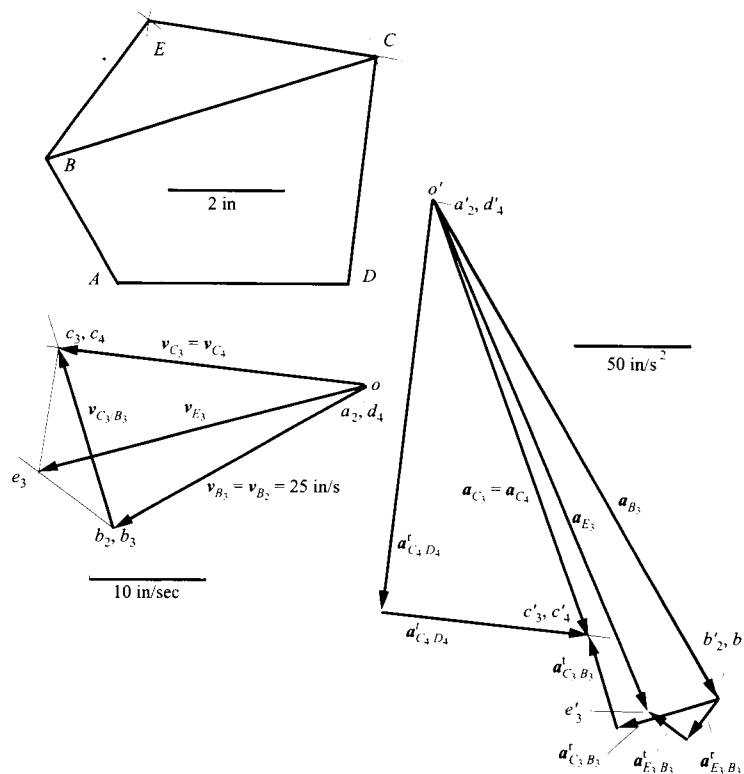
We will first address the graphical determination of the link positions. The first step is to choose a scale. The larger the scale, the more accurate the results. Therefore, it is best to use a drawing table with a drafting machine and B- or C-sized drawing paper if accurate results are desired. A CAD system that supports the construction of lines and arcs and locates intersections of lines and arcs may also be used. In the present case, we want to fit the figure onto a regular book page, so the construction will be described when it is drawn at half-scale (1 in on the drawing corresponds to 2 in on the actual mechanism). The reader is encouraged to draw the figures in this, and following examples, at full scale when working through them.

The construction is shown in the position diagram in Fig. 2.9. A horizontal line representing the base link is drawn first, and the two points bounding an interval of 2 in (half-scale) are marked to represent  $A$  and  $D$ . Next locate point  $B$ , which is where the driver link (link 2) is joined to the coupler (link 3). A line through point  $A$  at an angle of  $120^\circ$  to  $AD$  is drawn, and a point on that line at a distance of 1.25 in is marked to represent point  $B$ . Next locate point  $C$ , which is where the coupler is joined to the rocker (link 4).



**FIGURE 2.8** The four-bar linkage of Example 2.1. (Note that the figure has been reduced in size for printing.)

To locate point  $C$ , a compass is set to a radius of 3.0 in, and an arc is drawn with center point  $B$ . The compass is then reset to a 2.0-in radius, and a second arc is drawn with center  $D$ .  $C$  is at the intersection of the two arcs. Actually, there are two possible intersection points corresponding to the two assembly modes of the mechanism. This is a common situation with many mechanisms, and it is necessary for the designer to know which assembly mode is desired. In the present case, the correct one is easily located by referring to Fig. 2.8.



**FIGURE 2.9** Position, velocity, and acceleration polygons for the four-bar linkage of Fig. 2.8. Note that the position solution is necessary to draw the velocity polygon, and the velocity polygon is needed to draw the acceleration polygon. (Note also that the size of the figure has been reduced in the printing process.)



Point  $E$  can now be located in a similar manner to that used for  $C$  because we know the distance from point  $E$  to point  $B$  and to point  $C$ . The compass is set to a radius of 1.5 in (the scaled distance from  $E$  to  $B$ ), and an arc is drawn with center  $B$ . The compass is reset to a radius of 2.0 in (the scaled distance from  $E$  to  $C$ ), and an arc is drawn with center  $C$ .  $E$  is at an intersection of the two arcs. Once again two intersections are possible (one below  $BC$  and one above  $BC$ ), and the correct intersection can be identified by referring to Fig. 2.8.

This completes the construction of the scale drawing of the linkage and hence completes the solution of the position analysis problem. The resulting construction is shown in Fig. 2.9. The angular positions of the links may be measured from the drawing. Likewise, the position of point  $E$  can be measured and the coordinates can be multiplied by the scale factor of 2. In practice, if the position analysis is being performed solely as a preliminary step to a velocity analysis, the angular positions of the links and the position of point  $C$  would not need to be measured directly. Rather, the angular information would be directly transferred to the velocity diagram using a drawing machine or drafting triangles to construct normal or parallel lines. For the acceleration analysis, however, the linear distances would be required.

### (b) Velocity Analysis

In the velocity analysis, we will typically use the same points in the same order that we used for the position analysis. We will first compute the velocity of point  $B$ , then the velocity of  $C$ , and finally the velocity of  $E$ . Location  $B$  is the location of two points,  $B_2$  and  $B_3$ , and to be rigorous, we need to identify which of the points we are considering. Start with  $B_2$ , which is the point on driver link 2. We want to compute  $v_{B_2}$ , which is the absolute velocity of point  $B_2$ .

This absolute velocity can be expressed as the relative velocity between  $B_2$  and any point that has zero velocity. The point we shall use is  $A_2$ . It has zero velocity because it is always coincident with  $A_1$ , which is fixed to frame 1. All points in frame 1 have zero velocity. Then the velocity expression in Eq. (2.1) can be written as

$$v_{B_2} = v_{A_2} + v_{B_2/A_2} = \omega_2 \times r_{B/A}$$

because points  $A_2$  and  $B_2$  are both on the same link or lamina (link 2). Note that we do not need to identify the link associated with  $A$  and  $B$  in  $r_{B/A}$  because all of the  $A$ 's have the same coordinates, and all of the  $B$ 's also have the same coordinates.

Note also that we know the directions and magnitudes for both  $\omega_2$  and  $r_{B/A}$ , and we know that the two vectors are orthogonal to each other. Therefore, by the cross product, the velocity  $v_{B_2/A_2}$  will be orthogonal to  $\omega_2$  and  $r_{B/A}$ , and the direction will be given by the right-hand screw rule. The relationship among the three vectors is represented by a diagram similar to that shown in Fig. 2.5. We can compute the magnitude of the velocity of  $B_2$  from an equation similar to Eq. (2.6). The magnitude is given by

$$|v_{B_2/A_2}| = |\omega_2| |r_{B/A}| = (10 \text{ rad/s})(2.5 \text{ in}) = 25 \text{ in/s}$$

The direction for  $v_{B_2/A_2}$  is given by using the right-hand rule or by rotating  $r_{B/A}$   $90^\circ$  in the direction of  $\omega_2$ .

It is now necessary to select a scale to plot  $v_{B_2/A_2}$ . We used a scale of 10 in/s to 1 in in the velocity diagram shown in Fig. 2.9. This scale is based on the input velocity. We are assuming that all of the vectors will be of about the same order of magnitude. If the polygon began to move off of the page, we would need to select a new scale and redraw the vectors.

We must also select a starting point for drawing the velocity polygon. This starting point is labeled with a lower case  $o$  for origin. It is also called the velocity pole. Obviously, this starting point will also influence whether or not the velocity polygon will fit on the page. Therefore, the velocity pole and scale are selected together.

The direction of  $v_{B_2/A_2}$  may be obtained by placing one of the orthogonal edges of a triangle along  $\overline{AB}$ , and drawing a line along the other edge, since  $v_{B_2/A_2}$  is normal to  $r_{B/A}$  or  $\overline{AB}$ . Two points,  $o$  and  $b_2$ , separated by an interval of 2.5 in are marked as shown in Fig. 2.9. On the polygon,  $\overline{ob_2}$  may be labeled as the vector  $v_{B_2/A_2}$ . Here we are using the convention of labeling points on the velocity polygon with *lower case* letters and the corresponding points on the position polygon with *upper case* letters. Thus, the absolute velocity of point  $B_2$  given here by  $v_{B_2/A_2}$  would be represented on the velocity polygon by  $\overline{ob_2}$  or  $a_2b_2$ .

Next we want to compute the velocity of point  $C$ . We know that  $B_2$  and  $B_3$  are permanently pinned together so that

$$v_{B_3} = v_{B_2} = 25 \text{ in/s}$$

in the direction shown in Fig. 2.9. Similarly,  $C_3$  and  $C_4$  are permanently pinned together. Therefore,

$$v_{C_3} = v_{C_4}$$

Because  $B_3$  and  $C_3$  are both fixed to link 3, we can write a relative velocity equation similar to Eq. (2.1). That is,

$$v_{C_3} = v_{B_3} + v_{C_3/B_3} \quad (2.13)$$

In Eq. (2.13), the vector  $v_{B_3}$  is entirely known. Also, because  $B_3$  and  $C_3$  are on the same rigid link, we know that  $v_{C_3/B_3}$  is given by

$$v_{C_3/B_3} = \omega_3 \times r_{C/B}$$

Therefore, we know that the vector  $v_{C_3/B_3}$  is perpendicular to  $r_{C/B}$  or  $\overline{BC}$ . We can construct a line through point  $b_3$  on the velocity polygon in a direction perpendicular to  $\overline{BC}$  on the position diagram. This is easily done with the help of drafting triangles. This defines one locus of  $c_3$ . To find another locus for  $c_3$ , we need to find the direction of the vector  $v_{C_3}$ . We know that  $v_{C_3} = v_{C_4}$ , and we can identify the direction of the velocity of  $C_4$  by inspection ( $C$  can only move on a circle about point  $D$ , and therefore,  $v_{C_4}$  must be perpendicular to the line  $\overline{DC}$ ) or we can write a relative velocity equation for  $v_{C_4}$ . Again, the velocity  $v_{C_4}$  is an absolute velocity, and it can be expressed as the relative velocity between  $C_4$  and any point that has zero velocity. If we choose  $D_4$  as that point, the velocity equation becomes

$$v_{C_4} = v_{D_4} + v_{C_4/D_4} = v_{C_4/D_4} = \omega_4 \times r_{C/D} \quad (2.14)$$

Because of the cross product, it is clear that  $v_{C_4}$  must be perpendicular to  $r_{C/D}$  or the line  $\overline{DC}$ . To locate  $c_4$  on the velocity polygon, draw a line through the origin point  $o$  in a direction perpendicular to  $\overline{DC}$  on the position diagram. Once again, this is most easily done with drafting triangles. Because  $c_3$  and  $c_4$  are located at the same point, this gives a second locus for  $c_3$  that can be determined as shown in Fig. 2.9. The vectors  $v_{B_3}$ ,  $v_{C_4}$ , and  $v_{C_3/B_3}$  are as shown. The magnitude of  $\omega_3$  may be found from the expression for the relative velocity  $v_{C_3/B_3}$ . Then,

$$|v_{C_3/B_3}| = |\omega_3| |r_{C/B}|$$

or

$$|\omega_3| = |v_{C_3/B_3}| / |r_{C/B}|$$

To get  $v_{C_3/B_3}$ , measure the length of  $\overline{b_3c_3}$  on the velocity polygon and multiply by the scale factor. In the present case,<sup>4</sup>  $\overline{b_3c_3} = 1.65$  in, so  $v_{C_3/B_3} = 1.65 \times 10 = 16.5$  in/s. Then

$$|\omega_3| = |v_{C_3/B_3}| / |r_{C/B}| = 16.5 / 6.0 = 2.75 \text{ rad/s}$$

To get the direction, visualize the direction in which we would have to rotate  $r_{C/D}$  to obtain the direction of  $v_{C_3/B_3}$ . This is the CCW direction.

Next compute the angular velocity  $\omega_4$  from Eq. (2.14). The magnitude can be found from an expression for the relative velocity  $v_{C_4/D_4}$ . Then,

$$|v_{C_4/D_4}| = |\omega_4| |r_{C/D}|$$

<sup>4</sup> The distances identified refer to the original drawings developed for this book. Because the drawings were reduced when the book was printed, the distances reported here cannot be measured directly from the book pages. However, the results can be verified by making measurements from the drawings and using the small scales included with each of the drawings.

or

$$|\omega_4| = |v_{C_4/D_4}| / |r_{C/D}|$$

To obtain the velocity  $v_{C_4/D_4}$ , measure the distance  $c_4d_4$  on the velocity polygon and multiply by the scale factor. In the present case,  $c_4d_4 = 2.69$  in, so  $v_{C_4/D_4} = 2.69 \times 10 = 26.9$  in/s. Then

$$|\omega_4| = |v_{C_4/D_4}| / |r_{C/D}| = 26.9 / 4.0 = 6.73 \text{ rad/s}$$

To get the direction, visualize the direction in which we would have to rotate  $r_{C/D}$  to obtain the direction of  $v_{C_4/D_4}$ . The direction is CCW.

The velocity of point  $E_3$  may be obtained by considering first the point pair  $E_3$  and  $B_3$  and then the pair  $E_3$  and  $C_3$ . Both pairs are fixed to member 3. The relative velocity expressions are

$$v_{E_3} = v_{B_3} + v_{E_3/B_3} = v_{B_3} + \omega_3 \times r_{E/B} \quad (2.15)$$

and

$$v_{E_3} = v_{C_3} + v_{E_3/C_3} = v_{C_3} + \omega_3 \times r_{E/C} \quad (2.16)$$

The velocities  $v_{C_3}$  and  $v_{B_3}$  are known and have been plotted as  $\overline{ob_3}$  and  $\overline{oc_3}$  on the velocity polygon. We can compute  $|v_{E_3}|$  two different ways as implied by Eqs. (2.15) and (2.16). One way is to compute the cross product in Eq. (2.15) and add the resulting vector to  $|v_{B_3}|$ . We could make similar calculations using Eq. (2.16). A second way is to solve both equations simultaneously. Using Eq. (2.15), we know that  $|v_{E_3}|$  lies on a line through  $b_3$  on the velocity diagram and is perpendicular to  $\overline{EB}$  on the position diagram. Similarly,  $|v_{E_3}|$  lies on a line through  $c_3$  on the velocity diagram and is perpendicular to  $\overline{EC}$  on the position diagram. The point  $e_3$  lies on the intersection of the two lines, and  $|v_{E_3}|$  is the vector from  $o$  to the point  $e_3$ .

The magnitude of  $|v_{E_3}|$  can be obtained by measuring  $\overline{oe_3}$  and multiplying by the scale factor. The distance  $oe_3 = 2.93$  in, so  $|v_{E_3}| = 29.3$  in/s. Its direction may be measured from the diagram with a protractor. The direction is  $-164.9^\circ$  with the zero angle reference being horizontal and positive to the right. This completes the velocity analysis of the linkage.

### (c) Acceleration Analysis

The acceleration analysis can be conducted using the points that were used in the velocity analysis. In fact, usually the acceleration analysis can be conducted simply by differentiating the velocity equations. We will first compute the acceleration of point  $B_2$  (and  $B_3$ ), then the acceleration of  $C_3$  (and  $C_4$ ), and finally the acceleration of  $E_3$ . The acceleration of  $B_2$  can be expressed as the absolute acceleration between  $B_2$  and  $A_2$ . Because two points on the same rigid link are involved, an acceleration expression similar to Eq. (2.8) can be written as

$$a_{B_2} = a_{A_2} + a_{B_2/A_2} = \alpha_2 \times r_{B/A} + \omega_2 \times (\omega_2 \times r_{B/A}) = a_{B_2/A_2}^t + a_{B_2/A_2}^r$$

Note that we know the directions and magnitudes for  $\omega_2$ ,  $\alpha_2$ , and  $r_{B/A}$ , and therefore we can compute each of the vectors in the equation. Because of the cross product, the acceleration  $a_{B_2/A_2}^t$  will be orthogonal to  $\alpha_2$  and  $r_{B/A}$ , and the direction will be given by the right-hand screw rule. The direction of  $a_{B_2/A_2}^r$  will be opposite to the direction of  $r_{B/A}$ . We can compute the magnitude of  $a_{B_2/A_2}^t$  from an equation similar to Eq. (2.10). The magnitude is given by

$$|a_{B_2/A_2}^t| = |\alpha_2| |r_{B/A}| = (0)(2.5 \text{ in}) = 0$$

The magnitude of the radial component can be computed by using Eq. (2.8). Then,

$$a_{B_2/A_2}^r = \omega_2 \times (\omega_2 \times r_{B/A}) = |\omega_2|^2 |r_{B/A}| = 10^2 (2.5) = 250 \text{ in/s}^2$$

and the direction is opposite to that of  $r_{B/A}$ . The direction of  $a_{B_2/A_2}^r$  is therefore  $60^\circ$  below the horizontal (down and to the right). It is now necessary to choose a scale and starting point (acceleration pole) and plot the acceleration of point  $B_2$ . We will use a scale of  $50 \text{ in/s}^2$  to 1 in to ensure that the diagram will fit on a quarto-sized page. The acceleration  $a_{B_2/A_2} = a_{B_2/A_2}^r$  is plotted in Fig. 2.9 as  $\overline{ob'_2}$ . Here we

are using the convention that a lower case letter with a prime (') indicates the acceleration of the corresponding point on the position diagram. The most convenient way to plot a line parallel to  $\overline{AB}$  is to place a drafting triangle with one of the two orthogonal sides along  $\overline{ob_2}$  on the velocity diagram, and draw a line through  $o'$  along the other side of the triangle. Since  $\overline{ob_2}$  is normal to  $\overline{AB}$ , this results in a line parallel to  $\overline{AB}$ . Once again,  $\overline{o'b_2'}$  is directed down and to the right because it is in the minus  $\overline{AB}$  direction.

Next we want to compute the acceleration of point  $C$ . Recall that  $B_2$  and  $B_3$  are permanently pinned together. Therefore,

$$\mathbf{a}_{B_2} = \mathbf{a}_{B_3} = 250 \text{ in/s}^2$$

in the direction shown in Fig. 2.9. Similarly,  $C_3$  and  $C_4$  are permanently pinned together. Therefore,

$$\mathbf{a}_{C_3} = \mathbf{a}_{C_4}$$

Because  $B_3$  and  $C_4$  are both fixed to link 3, we can write the following relative acceleration equation:

$$\mathbf{a}_{C_3} = \mathbf{a}_{B_3} + \mathbf{a}_{C_3/B_3} = \mathbf{a}_{B_3} + \mathbf{a}_{C_3/B_3}^r + \mathbf{a}_{C_3/B_3}^t \quad (2.17)$$

In Eq. (2.17), the vector  $\mathbf{a}_{B_3}$  is entirely known. Also, the radial component of the acceleration that is a function of position and velocity only can be computed directly from the following:

$$\mathbf{a}_{C_3/B_3}^r = \boldsymbol{\omega}_3 \times (\boldsymbol{\omega}_3 \times \mathbf{r}_{C/B})$$

From the velocity analysis, we computed the magnitude of the angular velocity to be  $|\boldsymbol{\omega}_3| = 2.75 \text{ rad/s}$ . The radial acceleration is a vector from  $C$  to  $B$  on the position diagram (opposite  $\mathbf{r}_{C/B}$ ), and the magnitude is given by

$$\left| \mathbf{a}_{C_3/B_3}^r \right| = |\boldsymbol{\omega}_3|^2 |\mathbf{r}_{C/B}| = 2.75^2 (6) = 45.4 \text{ in/s}^2$$

A convenient way to draw a line parallel to  $\overline{BC}$  is, again, to place a triangle with one of the orthogonal sides along  $\overline{b_3c_3}$  on the velocity polygon and draw a line along the other orthogonal side through point  $b'_3$ . The direction is down and to the left because this component is in the minus  $\mathbf{r}_{C/B}$  direction.

The tangential component  $\mathbf{a}_{C_3/B_3}^t$  is given by

$$\mathbf{a}_{C_3/B_3}^t = \boldsymbol{\alpha}_3 \times \mathbf{r}_{C/B}$$

The magnitude of  $\mathbf{a}_{C_3/B_3}^t$  is unknown because  $\boldsymbol{\alpha}_3$  is unknown. However, this vector will be normal to  $\overline{BC}$ . Hence a line is drawn through the tip of the  $\mathbf{a}_{C_3/B_3}^r$  vector to represent this direction. This defines one locus of  $c'_3$ . To find another locus for  $c'_3$ , we need to find another equation for the vector  $\mathbf{a}_{C_3}$ . We know that  $\mathbf{a}_{C_3} = \mathbf{a}_{C_4}$ , and we can write an equation for the acceleration of  $C_4$ . Again, the acceleration  $\mathbf{a}_{C_4}$  is an absolute acceleration, and it can be expressed as the relative acceleration between  $C_4$  and any point that has zero acceleration. If we choose  $D_4$  as that point, the acceleration equation becomes

$$\mathbf{a}_{C_4} = \mathbf{a}_{C_4/D_4} = \mathbf{a}_{C_4/D_4}^r + \mathbf{a}_{C_4/D_4}^t$$

The radial component of the acceleration is a function of position and velocity only and can be computed directly from the following:

$$\mathbf{a}_{C_4/D_4}^r = \boldsymbol{\omega}_4 \times (\boldsymbol{\omega}_4 \times \mathbf{r}_{C/D})$$

From the velocity analysis, we computed the magnitude of the angular velocity to be  $|\boldsymbol{\omega}_4| = 6.73 \text{ rad/s}$ . The radial acceleration is a vector from  $C$  to  $D$  on the position diagram (opposite  $\mathbf{r}_{C/D}$ ), and the magnitude is given by

$$\left| \mathbf{a}_{C_4/D_4}^r \right| = |\boldsymbol{\omega}_4|^2 |\mathbf{r}_{C/D}| = 6.73^2 (4) = 181.2 \text{ in/s}^2$$

This vector is plotted from  $o'$  in Fig. 2.9.

The tangential component  $\mathbf{a}_{C_4/D_4}^t$  is given by

$$\mathbf{a}_{C_4/D_4}^t = \boldsymbol{\alpha}_4 \times \mathbf{r}_{C/D}$$

The magnitude of  $\mathbf{a}_{C_4/D_4}^t$  is unknown because  $\alpha_4$  is unknown. However, this vector will be normal to  $\overline{BD}$ . Hence a line is drawn through the tip of the  $\mathbf{a}_{C_4/D_4}^r$  vector to represent this direction. This defines a second locus for  $c'_3$  and  $c'_4$ . The points  $c'_3$  and  $c'_4$  are located where the two loci intersect as shown in Fig. 2.9. The vectors  $\mathbf{a}_{C_3/D_3}^t$ ,  $\mathbf{a}_{C_4/D_4}^t$ , and  $\mathbf{a}_{C_4/D_4}^r$  are as shown. The magnitude of  $\alpha_3$  may be found from the expression for the tangential component of the relative acceleration between  $C_3$  and  $B_3$ . Then,

$$\left| \mathbf{a}_{C_3/B_3}^t \right| = \left| \alpha_3 \right| \left| \mathbf{r}_{C/B} \right|$$

or

$$\left| \alpha_3 \right| = \left| \mathbf{a}_{C_3/B_3}^t \right| / \left| \mathbf{r}_{C/B} \right|$$

To get  $\left| \mathbf{a}_{C_3/B_3}^t \right|$ , measure the length of the vector on the acceleration polygon and multiply by the scale factor. On the acceleration polygon, the length of the line corresponding to  $\left| \mathbf{a}_{C_3/B_3}^t \right|$  is 0.847 in. Therefore,  $\left| \mathbf{a}_{C_3/B_3}^t \right| = 0.847 \times 50 = 42.2 \text{ in/s}^2$ . Then

$$\left| \alpha_3 \right| = \left| \mathbf{a}_{C_3/B_3}^t \right| / \left| \mathbf{r}_{C/B} \right| = 42.2 / 6.0 = 7.06 \text{ rad/s}^2$$

To get the direction, visualize the direction in which we would have to rotate  $\mathbf{r}_{C/B}$  to obtain the direction of  $\left| \mathbf{a}_{C_3/B_3}^t \right|$ . The direction is CCW.

Next compute the angular acceleration  $\alpha_4$ . The magnitude can be found from an expression for the tangential component of the relative acceleration  $\mathbf{a}_{C_4/D_4}^t$ . Then,

$$\left| \mathbf{a}_{C_4/D_4}^t \right| = \left| \alpha_4 \right| \left| \mathbf{r}_{C/D} \right|$$

or

$$\left| \alpha_4 \right| = \left| \mathbf{a}_{C_4/D_4}^t \right| / \left| \mathbf{r}_{C/D} \right|$$

To obtain the magnitude of the tangential component of acceleration, measure  $\left| \mathbf{a}_{C_4/D_4}^t \right|$  on the acceleration diagram and multiply by the scale factor. From Fig. 2.9,  $\left| \mathbf{a}_{C_4/D_4}^t \right| = 1.816 \times 50 = 90.8 \text{ in/s}^2$ . Then

$$\left| \alpha_4 \right| = \left| \mathbf{a}_{C_4/D_4}^t \right| / \left| \mathbf{r}_{C/D} \right| = 90.8 / 4.0 = 22.7 \text{ rad/s}^2$$

To get the direction, visualize the direction that we would have to rotate  $\mathbf{r}_{C/D}$  to obtain the direction of  $\left| \mathbf{a}_{C_4/D_4}^t \right|$ . The direction is CW.

The acceleration of point  $E_3$  may be obtained by considering first the point pair  $E_3$  and  $B_3$  and then the pair  $E_3$  and  $C_3$ . Both pairs are fixed to member 3. The relative acceleration expressions are

$$\mathbf{a}_{E_3} = \mathbf{a}_{B_3} + \mathbf{a}_{E_3/B_3} = \mathbf{a}_{B_3} + \mathbf{a}_{E_3/B_3}^r + \mathbf{a}_{E_3/B_3}^t = \mathbf{a}_{B_3} + \omega_3 \times (\omega_3 \times \mathbf{r}_{E/B}) + \alpha_3 \times \mathbf{r}_{E/B} \quad (2.18)$$

and

$$\mathbf{a}_{E_3} = \mathbf{a}_{C_3} + \mathbf{a}_{E_3/C_3} = \mathbf{a}_{C_3} + \mathbf{a}_{E_3/C_3}^r + \mathbf{a}_{E_3/C_3}^t = \mathbf{a}_{C_3} + \omega_3 \times (\omega_3 \times \mathbf{r}_{E/C}) + \alpha_4 \times \mathbf{r}_{E/C} \quad (2.19)$$

The accelerations  $\mathbf{a}_{B_3}$  and  $\mathbf{a}_{C_3}$  are known and have been plotted as  $\overline{o'b'_3}$  and  $\overline{o'c'_3}$  on the acceleration polygon. As in the corresponding case of velocities, we can compute  $\mathbf{a}_{E_3}$  two different ways as implied by Eqs. (2.18) and (2.19). One way is to compute the cross products in Eq. (2.18) and add the resulting vectors to  $\mathbf{a}_{B_3}$ . We could also make similar calculations using Eq. (2.19). A second way is to solve both equations simultaneously as was done in the velocity analysis. We will use the first procedure here. To determine  $\mathbf{a}_{E_3}$  using Eq. (2.18), we must compute  $\mathbf{a}_{E_3/B_3}^r$  and  $\mathbf{a}_{E_3/B_3}^t$ . The direction of the radial component is opposite to that of  $\mathbf{r}_{E/B}$ , and the magnitude is given by

$$\left| \mathbf{a}_{E_3/B_3}^r \right| = \left| \omega_3 \right|^2 \left| \mathbf{r}_{E/B} \right| = 2.75^2 (3) = 22.7 \text{ in/s}^2$$

This vector is added to  $\mathbf{a}_{B_3}$  in Fig. 2.9.

The direction of  $\mathbf{a}_{E_3/B_3}^t$  is found using the right-hand screw rule or by turning  $\mathbf{r}_{E/B}$   $90^\circ$  in the direction of  $\alpha_3$ . Recall that  $\alpha_3$  is CCW. The magnitude of  $\mathbf{a}_{E_3/B_3}^t$  is given by

$$\left| \mathbf{a}_{E_3/B_3}^t \right| = \left| \alpha_3 \right| \left| \mathbf{r}_{E/B} \right| = 7.06 (3) = 21.2 \text{ in/s}^2$$

This vector is plotted in Fig. 2.9. The point  $e'_3$  is located at the tip of  $a_{E_3/B_3}^t$ . The acceleration of  $E_3$  is located by the vector from  $o'$  to  $e'_3$  on the acceleration diagram. To determine the magnitude, measure  $\overline{o'e'_3}$  and multiply by the scale factor. The result is

$$|a_{E_3}| = 4.85 \times 50 = 2421.5 \text{ in/s}^2$$

The vector is pointed in a direction that is  $67^\circ$  below the horizontal and to the right. A much more efficient way to locate point  $e'_3$  will be presented later in this chapter.

## 2.6 GRAPHICAL ANALYSIS OF A SLIDER-CRANK MECHANISM

The analysis of a slider-crank mechanism depends on whether the crank or the slider is the driver. If the crank is the driver, we need to know the angular position, velocity, and acceleration of the crank. If the slider is the driver, we need to know the position, velocity, and acceleration of some point on the slider. Note that each point on the slider will have a unique position, but all points will have the same velocity and the same acceleration.

We will analyze the slider-crank mechanism shown in Fig. 2.10, where the crank is the driver. As was the case for the four-bar linkage, the key to the acceleration analysis of this mechanism is the relationship between the velocities and accelerations of two points on the same rigid body.

### EXAMPLE 2.2 Graphical Analysis of a Slider-Crank Mechanism

#### Solution

Find  $a_C$  and  $\omega_3$  for the slider-crank linkage in the position shown in Fig. 2.10. The crank  $AB$  (link 2) is driven at a constant angular velocity of  $10 \text{ rad/s}$  CCW.  $C$  is the axis of the revolute joint connecting the connecting rod, link 3, to the slider, link 4. In the position shown,  $AB$  is at  $45^\circ$  to  $AC$ , and the link lengths are shown on the drawing.

#### (a) Position Analysis

The linkage is first drawn to scale to establish the direction of member  $BC$ . To do this, first locate the horizontal line through  $A$  and on which  $C$  lies. Next, draw member  $AB$  to scale. Then draw an arc scaled to represent 8 in and centered at  $B$ . The arc intersects the horizontal line through  $A$  at two locations. The desired location is to the right of  $A$  as indicated in Fig. 2.10. The scaled drawing is shown in Fig. 2.11.

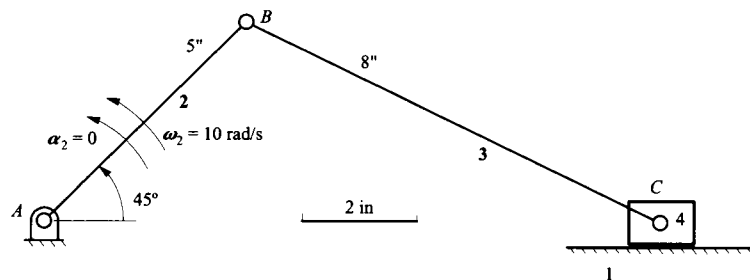


FIGURE 2.10 The slider-crank linkage to be analyzed in Example 2.2.

**(b) Velocity Polygon**

The basic equation to be solved is

$$\mathbf{v}_{C_3} = \mathbf{v}_{B_3} + \mathbf{v}_{C_3/B_3} = \mathbf{v}_{B_2} + \mathbf{v}_{C_3/B_3} = \mathbf{v}_{B_2/A_2} + \mathbf{v}_{C_3/B_3}$$

From the given data, we have

$$\mathbf{v}_{B_2} = \mathbf{v}_{B_2/A_2} = \boldsymbol{\omega}_2 \times \mathbf{r}_{B/A} = 10 \times 5 = 50 \text{ in/s (normal to } \mathbf{r}_{B/A} \text{)}$$

The direction for the velocity of  $C_3$  must be horizontal. This lets us solve the basic velocity equation as shown in Fig. 2.11. By measurement in Fig. 2.11, we obtain

$$|\mathbf{v}_{C_3/B_3}| = 1.98 \times 20 = 39.6 \text{ in/s}$$

Then

$$|\boldsymbol{\omega}_3| = |\mathbf{v}_{C_3/B_3}| / |\mathbf{r}_{C/B}| = 39.6 / 8 = 4.95 \text{ rad/s}$$

in the CW direction.

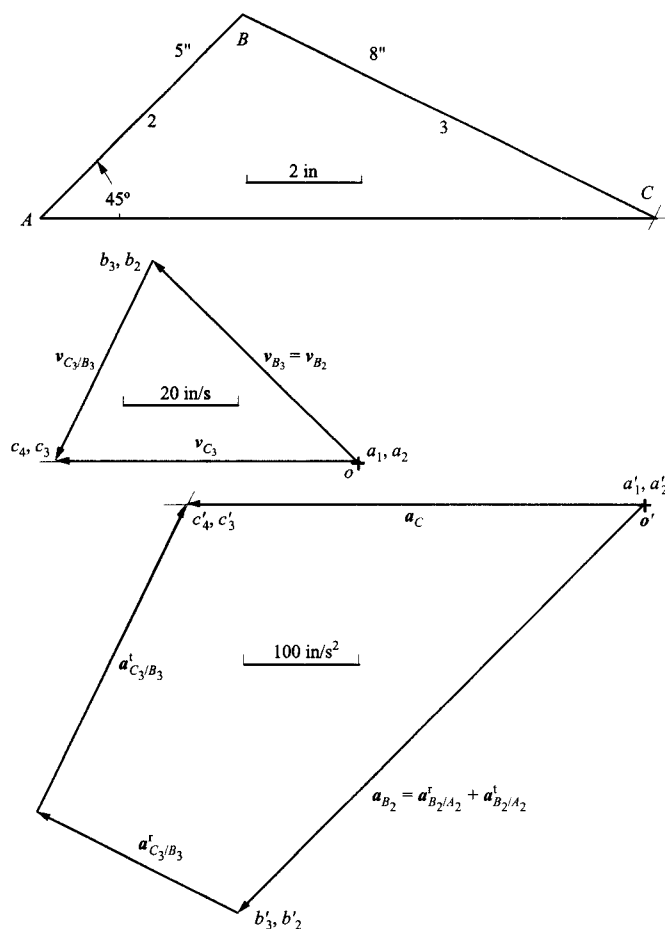


FIGURE 2.11 Velocity and acceleration polygons for Example 2.2.

**(c) Acceleration Polygon**

The basic acceleration equation to be solved is

$$\mathbf{a}_{C_3} = \mathbf{a}_{B_2/A_2} + \mathbf{a}_{C_3/B_3} = \mathbf{a}_{B_2/A_2}^r + \mathbf{a}_{B_2/A_2}^t + \mathbf{a}_{C_3/B_3}^r + \mathbf{a}_{C_3/B_3}^t$$

From the given data, we have

$$\left| \mathbf{a}_{B_2/A_2}^r \right| = \left| \omega_2 \right|^2 \left| \mathbf{r}_{B/A} \right| = 10^2 (5) = 500 \text{ in/s}^2$$

$$\left| \mathbf{a}_{B_2/A_2}^t \right| = \left| \alpha_2 \right| \left| \mathbf{r}_{B/A} \right| = 0(5) = 0$$

Using information from the velocity analysis, we obtain

$$\left| \mathbf{a}_{C_3/B_3}^r \right| = \left| \omega_3 \right|^2 \left| \mathbf{r}_{C/B} \right| = 4.95^2 (8) = 196 \text{ in/s}^2$$

The direction for the acceleration of  $C_3$  must be horizontal, and the basic acceleration equation can now be solved for the acceleration of  $C_3$ , as shown in Fig. 2.11. By measurement in Fig. 2.11, we get

$$\left| \mathbf{a}_{C_3} \right| = 3.98(100) = 398 \text{ in/s}^2$$

and

$$\left| \mathbf{a}_{C_3/B_3}^t \right| = 2.98 \times 100 = 298 \text{ in/s}^2$$

Then

$$\left| \alpha_3 \right| = \left| \mathbf{a}_{C_3/B_3}^t \right| / \left| \mathbf{r}_{C/B} \right| = \frac{298}{8} = 37.3 \text{ rad/s}^2$$

in the CCW direction.

The steps for the total analysis are summarized in the following, and the results are shown in Fig. 2.11.

1. Draw the linkage to scale.
2. Construct the velocity polygon and compute  $\omega_3$ .
3. Compute the magnitudes of  $\mathbf{a}_{B_2/A_2}^r$ ,  $\mathbf{a}_{B_2/A_2}^t$ , and  $\mathbf{a}_{C_3/B_3}^r$  and identify their directions.
4. Choose a suitable scale and plot  $\mathbf{a}_{B_2/A_2}^r$  opposite to  $\mathbf{r}_{B/A}$ . Put the tail of the vector at the acceleration pole,  $o'$ .
5. Plot  $\mathbf{a}_{B_2/A_2}^t$  (zero in this case) normal to  $\mathbf{r}_{B/A}$  and through the tip of  $\mathbf{a}_{B_2/A_2}^r$ . The tip of  $\mathbf{a}_{B_2/A_2}^t$  gives the point  $b'_2$ . Here, the direction for  $\mathbf{a}_{B_2/A_2}$  is in the direction of  $-\mathbf{r}_{B/A}$ .
6. Plot vector  $\mathbf{a}_{C_3/B_3}^r$  opposite to  $\mathbf{r}_{C/B}$  with its tail at point  $b'_2$ .
7. Draw a line through the tip of vector  $\mathbf{a}_{C_3/B_3}^r$  normal to line  $\overline{BC}$ .
8. Draw a line through  $o'$  parallel to line  $\overline{AC}$ . The intersection of the lines drawn in steps 7 and 8 gives point  $c'_3$ .
9. Measure the magnitude  $a_C$  as  $\overline{o'c'_3}$  and note its direction.
10. Measure  $\mathbf{a}_{C_3/B_3}^t$  and compute  $\alpha_3 = \left| \mathbf{a}_{C_3/B_3}^t \right| / \left| \mathbf{r}_{C/B} \right|$ . Note that the sense of  $\alpha_3$  is found by visualizing  $C$  rotating about  $B$  so that  $C$  moves in the  $\mathbf{a}_{C_3/B_3}^t$  direction.

## 2.7 THE VELOCITY IMAGE THEOREM

To conduct a graphical analysis of a linkage with more than one loop, it is necessary to obtain the velocities of additional points on a rigid link once the kinematic properties of the first two points are known. After the velocity and acceleration of two points are known, the angular



velocity of the body can be determined. Knowing the velocity of a point and the angular velocity of the body, the velocity of any other point on the rigid body can be computed using Eqs. (2.4) and (2.5). Similarly, if the velocity analysis has been conducted, and the acceleration of a point and the angular acceleration of the body are known, the acceleration of any other point on the body can be found using Eq. (2.9). An alternative method for determining the velocity and acceleration of a third point on a rigid body is to use the concept of velocity and acceleration image. The velocity image theorem will be discussed first.

**Notation** As indicated previously, a convenient means of labeling the velocity polygon is to use a lower case letter to identify the absolute velocity of each point on the position diagram. A vector from the velocity pole to the point will then represent the absolute velocity of the point. A vector between any two points will correspond to the relative velocity between the points. For example, in Fig. 2.12,  $v_{C/B} = \overrightarrow{bc}$ .

Consider the triangle  $PQR$  formed by three points ( $P$ ,  $Q$ , and  $R$ ) all fixed to the same rigid body. The velocity image theorem states that given the triangle  $PQR$  in a rigid body, the triangle  $pqr$  in the velocity diagram will be similar to triangle  $PQR$ , rotated from  $PQR$  by  $90^\circ$  in the positive  $\omega$  direction, and magnified by the factor  $\omega$ . This theorem, stated here for triangles, can be extended to apply to any polygon, because any polygon can be broken down into triangles, or indeed to any shape, since any shape can be approximated by a polygon to any desired degree of accuracy. Thus, the velocity image of any geometric shape is similar to that geometric shape, rotated relative to that shape through  $90^\circ$  in the positive  $\omega$  direction, and is magnified by a factor  $\omega$ .

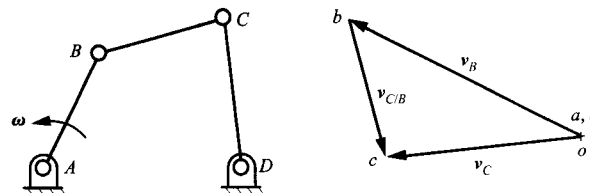
The proof of the theorem can be developed using Fig. 2.13. In that figure, the position diagram for the rigid link is  $PQR$  and the velocity diagram is  $pqr$ . Using  $v_{Q/P}$  as an example, we get

$$v_{P/Q} = \omega \times r_{P/Q}$$

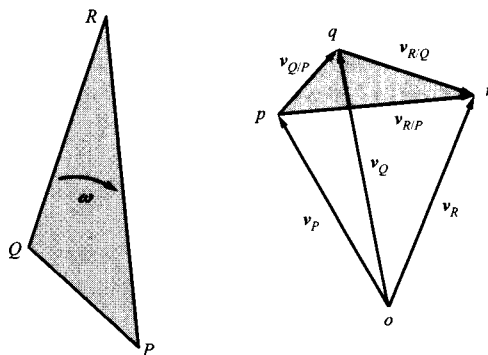
Therefore,  $v_{Q/P}$  is normal to  $\overrightarrow{PQ}$  and has the magnitude  $\omega PQ$ . Hence  $\overrightarrow{pq}$  has magnitude  $\omega PQ$  and is rotated  $90^\circ$  in the  $\omega$  direction. Similarly  $\overrightarrow{qr} = \omega RP$  and is rotated  $90^\circ$  in the  $\omega$  direction. Hence, triangle  $pqr$  is similar to triangle  $PQR$ , is rotated from triangle  $PQR$  through  $90^\circ$  in the  $\omega$  direction, and is magnified over triangle  $PQR$  by a factor  $\omega$ .

Note that the velocity image can be used to determine directly the velocity of any point in the rigid body given the position of the point and the velocity diagram. Conversely, the location of a point with a given velocity can be found by mapping points in the velocity diagram to points in the position diagram.

The manner in which the velocity image is used to analyze multiloop linkages is illustrated in Example 2.3 involving a six-bar linkage.



**FIGURE 2.12** Notation used on velocity polygon to facilitate velocity image. The lowercase letters on the velocity polygon correspond to the letters on the linkage.  $v_B = \overrightarrow{ob}$ ,  $v_C = \overrightarrow{oc}$ , and  $v_{B/A} = \overrightarrow{ab}$ . The point  $o$  corresponds to all fixed points. That is,  $A$  and  $D$  both map into point  $o$ .



**FIGURE 2.13** Link  $PQR$  and its velocity image in the velocity polygon. Triangle  $pqr$  is similar to triangle  $PQR$  and is rotated from it by  $90^\circ$  in the  $\omega$  direction.

**EXAMPLE 2.3**  
**Graphical Velocity**  
**Analysis of Six-Bar**  
**Linkage**

**Solution**

Develop a procedure for finding the angular velocities of links 3, 5, and 6 and the velocity of point  $B$  of the linkage shown in Fig. 2.14.

The polygons for the analysis are shown in Fig. 2.14. The velocity analysis starts with the slider–crank part of the mechanism. The equations involved and the order in which they are solved are given in the following:

$$\mathbf{v}_{B_3} = \mathbf{v}_{B_2} = \mathbf{v}_{B_2/A_2} = \boldsymbol{\omega}_2 \times \mathbf{r}_{A/B}$$

and

$$\mathbf{v}_{C_3} = \mathbf{v}_{B_3} + \mathbf{v}_{C_3/B_3}$$

Next we will find the velocity of point  $D_3$  by image. Then the dyad (links 5 and 6) can be analyzed using

$$\mathbf{v}_{E_5} = \mathbf{v}_{E_6}$$

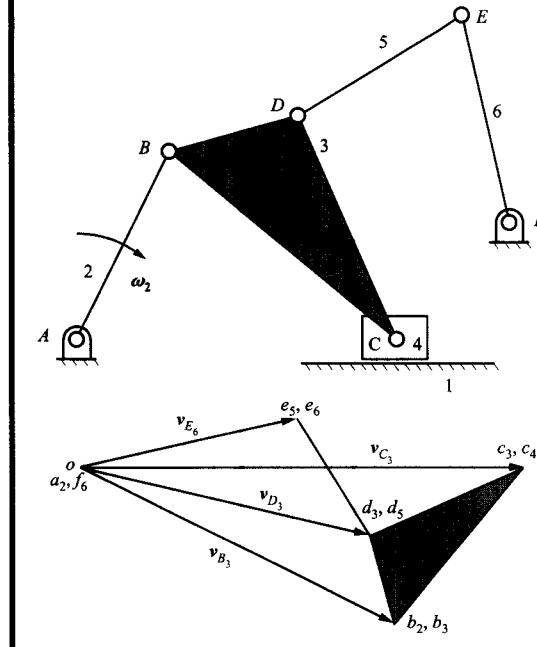
$$\mathbf{v}_{E_5} = \mathbf{v}_{D_5} + \mathbf{v}_{E_5/D_5} = \mathbf{v}_{D_5} + \boldsymbol{\omega}_5 \times \mathbf{r}_{E/D}$$

$$\mathbf{v}_{E_6} = \mathbf{v}_{F_6} + \mathbf{v}_{E_6/F_6} = \boldsymbol{\omega}_6 \times \mathbf{r}_{E/F}$$

**Steps**

1. Draw the linkage to scale in the position given.
2. Select a suitable scale and plot  $\mathbf{v}_{B_3} = \mathbf{v}_{B_2/A_2} = \overline{ob}$  normal to line  $\overline{AB}$ . Point  $o$  represents the points on the fixed frame and all other points with zero velocity. That is, all points with zero velocity in the linkage map into point  $o$ , and all points at  $o$  map to the linkage as points with zero velocity.
3. Draw a line through point  $o$  parallel to line  $\overline{AC}$ . The velocity of  $C_3$  must lie on this line.
4. Draw a line through point  $b_3$  normal to line  $\overline{BC}$ . The intersection of the lines drawn in steps 3 and 4 gives point  $c_3$ .
5. Now find the velocity image of  $D_3$ . Start by drawing a line through point  $b_3$  normal to line  $\overline{BD}$ .
6. Draw a line through point  $c_3$  normal to line  $\overline{CD}$ . The intersection of the lines drawn in steps 5 and 6 is point  $d_3$ .
7. Next locate  $e_5$  (and  $e_6$ ). Start by drawing a line through point  $d_3$  normal to line  $\overline{DE}$ .
8. Draw a line through point  $o$  normal to line  $\overline{EF}$ . The intersection of the lines drawn in steps 7 and 8 is point  $e_5$ .
9. Compute  $\omega_3$  from  $|\omega_3| = |\mathbf{v}_{C_3/B_3}|/|\mathbf{r}_{C/B}|$ . Note that the sense is CCW. This is inferred by noting that  $C_3$  must rotate CCW about  $B_3$  to move in the direction of  $\mathbf{v}_{C_3/B_3}$ .

10. Compute  $\omega_5$  from  $|\omega_5| = |v_{D_5/E_5}|/|r_{D/E}|$ . The sense is CCW, since  $D_5$  must rotate CCW about  $E_5$  to move in the direction of  $v_{D_5/E_5}$ .
11. Compute  $\omega_6$  from  $|\omega_6| = |v_{E_6/F_6}|/|r_{E/F}|$ . The sense is CW, since  $E_6$  must move CW about  $D_6$  to move in the direction of  $v_{E_6/F_6}$ .



**FIGURE 2.14** The linkage and velocity polygon of Example 2.3. The velocity image theorem is used to locate point  $d_3$ .

The velocity image theorem is very useful for finding the velocity of a point on the coupler of a linkage at which an additional joint is placed. It is important to notice that the *shape* of any velocity polygon (i.e., all angles within it) is determined only by the dimensions of the linkage. See, for instance, Fig. 2.14. Further, the speed at which the linkage is operated can affect only the *size*, or scale, of the polygon and not the shape. This property will play a pivotal role in later sections (e.g., Section 2.9).

## 2.8 THE ACCELERATION IMAGE THEOREM

As was the case in the velocity analysis, an acceleration image theorem provides an easy way to obtain accelerations of additional points on a rigid body when the accelerations of two points are already known. This is useful when multiple loops are involved in the linkage. In the acceleration diagram we will use primed lower case letters to indicate the absolute accelerations of various points. Thus  $\mathbf{a}_{Q/P} = \overrightarrow{p'q'}$ ,  $\mathbf{a}_{B/A} = \overrightarrow{a'b'}$ , etc. Once again,  $o'$  on the acceleration diagram corresponds to the pole where all points with zero acceleration map.

The acceleration image theorem states that, if  $PQR$  is a triangle fixed in a rigid link in motion relative to the fixed frame, then triangle  $p'q'r'$  is similar to triangle  $PQR$ .

Triangle  $p'q'r'$  is magnified by a factor that is a function of  $\alpha$  and  $\omega$  and is rotated from triangle  $PQR$  by an angle that is also a function of  $\alpha$  and  $\omega$ .

**Proof** To prove the acceleration image theorem, we will use Fig. 2.15. Then

$$\mathbf{a}_{Q/P} = \overrightarrow{p'q'} = -\omega^2 \mathbf{r}_{Q/P} + \alpha |\mathbf{r}_{Q/P}| \mathbf{n}'$$

where  $\mathbf{n}'$  is normal to  $\mathbf{r}_{Q/P}$ . Therefore the magnitude of the relative acceleration vector is given by

$$|\overrightarrow{p'q'}| = PQ \sqrt{\omega^4 + \alpha^2}$$

Similarly

$$|\overrightarrow{q'r'}| = QR \sqrt{\omega^4 + \alpha^2}$$

and

$$|\overrightarrow{r'p'}| = RP \sqrt{\omega^4 + \alpha^2}$$

Hence triangle  $p'q'r'$  is similar to triangle  $PQR$ . The magnification factor is  $|\overrightarrow{r'p'}|/RP = |\overrightarrow{q'r'}|/QR = |\overrightarrow{p'q'}|/PQ = \sqrt{\omega^4 + \alpha^2}$ . Referring to Fig. 2.15, we see that the angle of rotation is

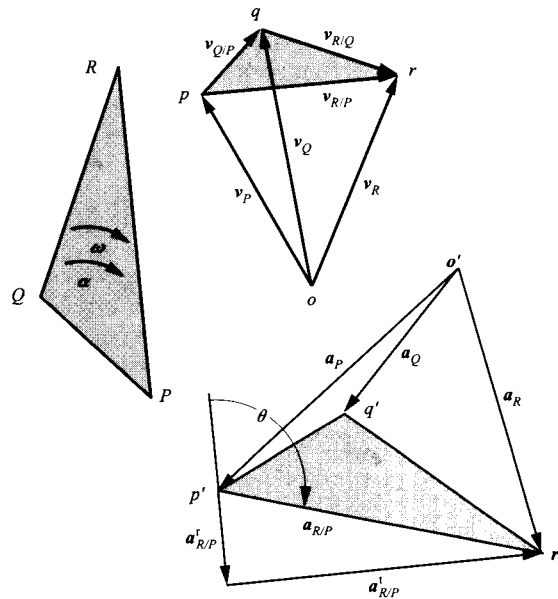
$$\theta = \pi - \tan^{-1} \left( \frac{a_{Q/P}^t}{a_{Q/P}^r} \right)$$

or

$$\theta = \pi - \tan^{-1} \left( \alpha / \omega^2 \right)$$

Once again, this result can be extended to cover members of any shape by noting that any polygon may be broken down into triangles, and any area bounded by a plane curve may be approximated by a polygon as closely as desired.

Because the angle of rotation in the acceleration image is not usually  $90^\circ$ , similar triangles must be constructed by making corresponding angles equal.



**FIGURE 2.15** The acceleration image theorem. The example used is the same as for the velocity image in Fig. 2.13. Triangle  $p'q'r'$  is similar to triangle  $PQR$  in the original lamina. Hence it is also similar to triangle  $pqr$ , which is the velocity image of  $PQR$ . If  $a_p$  is plotted, together with the radial and transverse components of the acceleration of  $R$  relative to  $P$  ( $a_{R/P}$ ) to locate points  $p'$  and  $r'$ ,  $q'$  can be located from the image to give  $a_Q$ .

**EXAMPLE 2.4**  
**Graphical**  
**Acceleration**  
**Analysis of a**  
**Six-Bar Linkage**

**Solution**

Given the dimensions of the linkage shown in Fig. 2.16, find  $a_C$  and  $\alpha_6$  if  $\omega_2 = 60$  rpm CW and  $\alpha_2 = 0$ .

The results of the analysis are shown in Fig. 2.17. The scales for position, velocity, and acceleration are shown with the polygons. The velocity analysis follows the procedure developed in Example 2.3. The initial equation to be solved is for the slider-crank mechanism. That is,

$$\mathbf{v}_{C_3} = \mathbf{v}_{B_3} + \mathbf{v}_{C_3/B_3}$$

where

$$\mathbf{v}_{B_3} = \mathbf{v}_{B_2} = \mathbf{v}_{B_2/A_2} = \boldsymbol{\omega}_2 \times \mathbf{r}_{B_2/A_2}$$

Next we will find the velocity of point  $D_3$  by image. Then the dyad (links 5 and 6) can be analyzed using

$$\mathbf{v}_{E_5} = \mathbf{v}_{D_5} + \mathbf{v}_{E_5/D_5} = \mathbf{v}_{E_6} = \mathbf{v}_{F_6} + \mathbf{v}_{E_6/F_6}$$

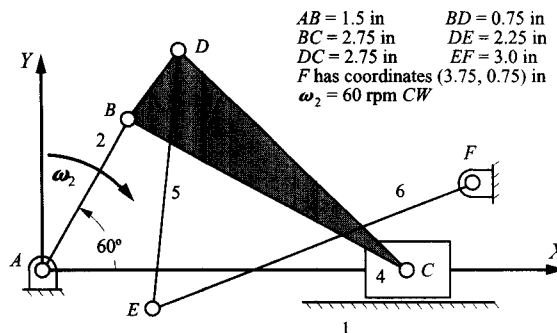
**Steps**

1. Draw the linkage to scale.
2. Compute the magnitude of  $\mathbf{v}_B = \mathbf{v}_{B_2/A_2}$  and identify its direction. Plot it as the vector  $\overrightarrow{ob}$ .

$$\omega_2 = 60 \times 2\pi / 60 = 6.283 \text{ rad/s}$$

$$v_B = 6.283 \times 1.5 = 9.42 \text{ in/s normal to } \overrightarrow{AB}$$

3. Draw a line through point  $b$  normal to line  $\overrightarrow{BC}$ .
4. Draw a line through  $o$  parallel to  $\overrightarrow{AC}$ . The intersection of this line with that plotted in step 3 gives point  $c_3$  (and  $c_4$ ).
5. Construct triangle  $bcd$  similar to triangle  $BCD$ , thereby locating point  $d_3$ . This step is a use of the velocity image theorem.
6. Draw a line through point  $d$  normal to line  $\overrightarrow{DE}$ .
7. Draw a line through point  $o$  normal to  $\overrightarrow{EF}$ . The intersection of this line with that drawn in step 6 gives point  $e_5$  (and  $e_6$ ).



**FIGURE 2.16** Problem statement for Example 2.4.

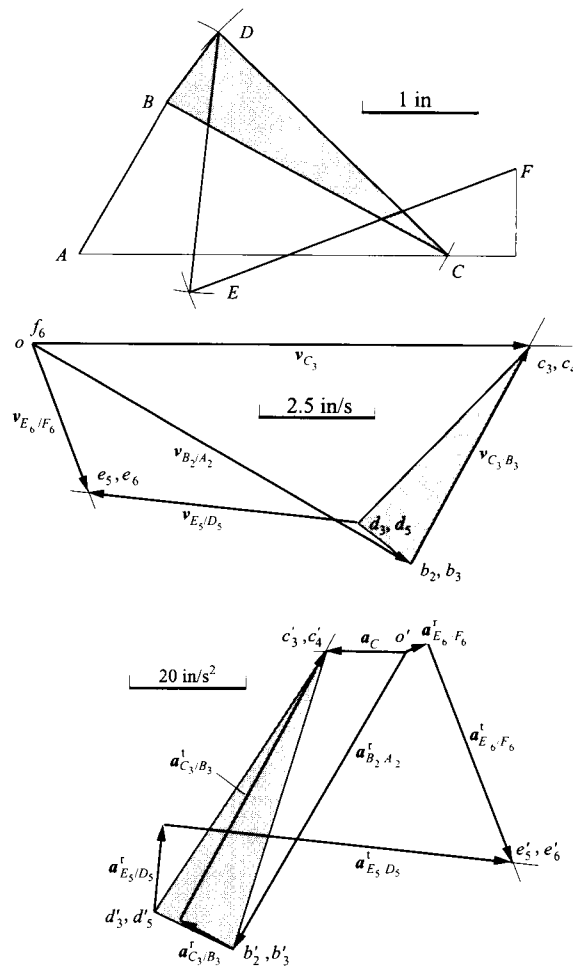


FIGURE 2.17 Position, velocity, and acceleration polygons for Example 2.4.

8. Measure the magnitudes of  $v_{C_3/B_3} = \overline{c_3 b_3}$ ,  $v_{E_5/D_5} = \overline{e_5 d_5}$ , and  $v_{E_6} = \overline{f_6 e_6}$ :

$$v_{C_3/B_3} = 5.34 \text{ in/s}, \quad v_{E_5/D_5} = 5.82 \text{ in/s}, \quad v_{E_6} = 3.41 \text{ in/s}$$

9. Compute  $|\omega_3| = |v_{C_3/B_3}|/|r_{C/B}|$ ,  $|\omega_5| = |v_{D_5/E_5}|/|r_{D/E}|$ , and  $|\omega_6| = |v_{E_6/F_6}|/|r_{E/F}|$ :

$$\omega_3 = 5.34/2.75 = 1.94 \text{ rad/s in the CCW direction}, \quad \omega_5 = 5.82/2.25 = 2.59 \text{ rad/s in the CW direction},$$

$$\omega_6 = 3.41/3.0 = 1.137 \text{ rad/s in the CCW direction}$$

This completes the velocity analysis of the linkage.

10. For the acceleration analysis, we must solve the equation

$$\mathbf{a}_{C_3} = \mathbf{a}_{B_2/A_2}^r + \mathbf{a}_{B_2/A_2}^t + \mathbf{a}_{C_3/B_3}^r + \mathbf{a}_{C_3/B_3}^t$$

Next we will find the acceleration of point  $D_3$  (and  $D_5$ ) by image. Then the dyad can be analyzed using

$$\mathbf{a}_{E_5} = \mathbf{a}_{D_3} + \mathbf{a}_{E_5/D_3}^r + \mathbf{a}_{E_5/D_3}^t = \mathbf{a}_{E_6} = \mathbf{a}_{F_6} + \mathbf{a}_{E_6/F_6}^r + \mathbf{a}_{E_6/F_6}^t$$

First compute  $\mathbf{a}_{B_2} = \mathbf{a}_{B_2/A_2}^r$  and plot as the vector  $\overrightarrow{o'b_2'}$ :

$$\mathbf{a}_{B_2} = 1.5 \times 6.283^2 = 59.2 \text{ in/s}^2 \text{ in the } \overrightarrow{BA} \text{ direction}$$

11. Compute the magnitudes of vectors  $\mathbf{a}_{C_3/B_3}^r$ ,  $\mathbf{a}_{E_5/D_5}^r$ ,  $\mathbf{a}_{E_6/F_6}^r$  and identify their directions:

$$\mathbf{a}_{C_3/B_3}^r = 2.75 \times 1.94^2 = 10.35 \text{ in/s}^2 \text{ in the } \overrightarrow{BC} \text{ direction}$$

$$\mathbf{a}_{E_5/D_5}^r = 2.25 \times 2.59^2 = 15.09 \text{ in/s}^2 \text{ in the } \overrightarrow{ED} \text{ direction}$$

$$\mathbf{a}_{E_6/F_6}^r = 3.0 \times 1.137^2 = 3.87 \text{ in/s}^2 \text{ in the } \overrightarrow{EF} \text{ direction}$$

12. Plot vector  $\mathbf{a}_{C_3/B_3}^r$  in the  $\overrightarrow{CB}$  direction with its tail at  $b'$ .
13. Draw a line normal to line  $\overrightarrow{CB}$  through the tip of vector  $\mathbf{a}_{C_3/B_3}^r$ .
14. Draw a line through  $o'$  parallel to line  $\overrightarrow{AC}$ . The intersection of this line with that drawn in step 13 gives point  $c'_3$ .
15. Construct triangle  $b'c'd'$  similar to triangle  $BCD$  to locate point  $d'_3$ . This step is a use of the acceleration image theorem.
16. Plot  $\mathbf{a}_{E_5/D_5}^r$  in the  $\overrightarrow{ED}$  direction with its tail at point  $d'$ .
17. Draw a line normal to  $\overrightarrow{ED}$  through the tip of vector  $\mathbf{a}_{E_5/D_5}^r$ .
18. Plot  $\mathbf{a}_{E_6/F_6}^r$  in the  $\overrightarrow{EF}$  direction with its tail at  $o'$ .
19. Draw a line normal to  $\overrightarrow{EF}$  through the tip of vector  $\mathbf{a}_{E_6/F_6}^r$ . The intersection of this line with that drawn in step 17 gives the point  $e'_5$  (and  $e'_6$ ).
20. Measure the magnitudes of  $\mathbf{a}_{C_4}$  and  $\mathbf{a}_{E_6/F_6}^t$ :
- $$|\mathbf{a}_{C_4}| = 13.9 \text{ in/s}^2, \quad |\mathbf{a}_{E_6/F_6}^t| = 40 \text{ in/s}^2$$
21. Compute  $\alpha_6 = |\mathbf{a}_{E_6/F_6}^t / r_{E/F}|$ :
- $$\alpha_6 = 40 / 3.0 = 13.3 \text{ rad/s}^2 \text{ in the CCW direction}$$
22. The sense of  $\alpha_6$  is obtained by visualizing  $E$  rotating about  $F$  so as to move in the  $\mathbf{a}_{E_6/F_6}^t$  direction.

### EXAMPLE 2.5 Using Velocity and Acceleration Images

The mechanism in Fig. 2.18 is drawn to scale. Also given is the velocity polygon for the slider–crank linkage, and the acceleration of point  $B$  on the round link is shown on the acceleration polygon. Use the image technique to determine the velocity and acceleration of point  $D_4$ . Then determine the velocity and acceleration images of link 4.

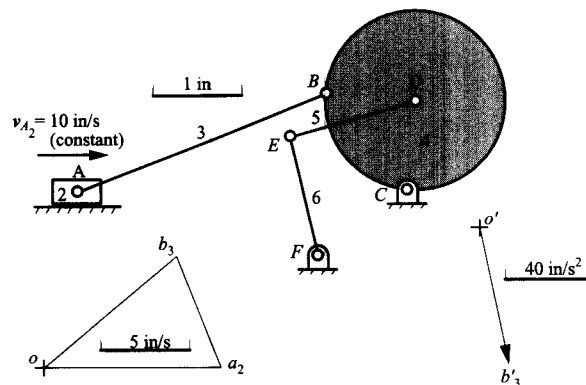
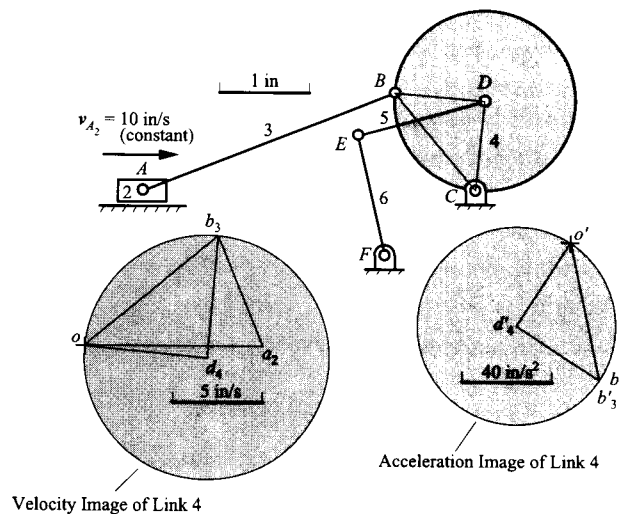


FIGURE 2.18 Figure for Example 2.5.

**Solution**

To solve the problem, we need only find the image of point  $D_4$  on both the velocity and acceleration diagrams. The images of link 4 will both be circles with centers at  $d$  and  $d'$ , respectively, and with radii of  $bd$  and  $b'd'$ , respectively. We find the velocity image of  $D_4$  by constructing triangle  $bdc$  similar to  $BDC$  to locate  $d$  and drawing the circle centered at  $d$  and with radius  $bd$ . Similarly, the acceleration image is found by constructing the triangle  $b'd'c'$  similar to  $BDC$  and drawing the circle centered at  $d'$  and with radius  $b'd'$ . The solution is shown in Fig. 2.19.



**FIGURE 2.19** Solution to Example 2.5.

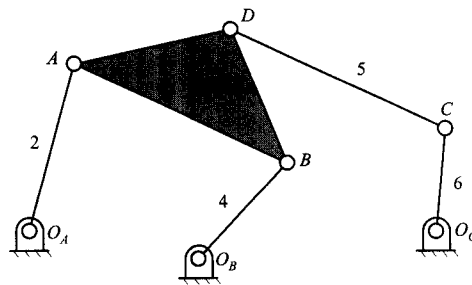
## 2.9 SOLUTION BY INVERSION

In general, if we have a linkage where the driver link is not part of a four-bar loop that contains the frame as one of the members, it is not possible to analyze the linkage directly using the vector polygon approach. The Stephenson six-bar linkage shown in Fig. 2.20 can be solved using the techniques in the previous sections *provided* the driving crank is  $O_A A$  or  $O_B B$ . However, if the linkage is driven by crank  $O_C C$ , the linkage cannot be analyzed using the techniques developed so far. This is because  $O_C C$  does not form a part of any four-bar loop in the linkage. Consequently, plotting the velocity, or acceleration, of point  $C$  does not provide enough information to close a velocity or acceleration polygon.

If the position of the linkage is known, however, a velocity solution can be achieved recognizing that all of the velocities in the linkage are linearly related to the velocity of the input member. Therefore, we can solve the velocity problem indirectly by first assuming the linkage to be driven by  $O_A A$ , rotating at 1 rad/s in a specified direction. The velocity polygon is completed and the angular velocity of  $O_C C$  is found. A scaling factor is then computed. It is the ratio of the actual angular velocity of  $O_C C$  to that calculated. It also carries a sign that is positive if both angular velocities are in the same direction and negative if they are opposed. All velocities and angular velocities are then multiplied by that scaling factor to complete the solution.

This solution technique is an example of *inversion*. The driving and driven cranks are interchanged to perform the solution. That is, the linkage is inverted by having the driver





**FIGURE 2.20** A simple linkage that can be analyzed using the techniques of the preceding sections if it is driven by crank  $O_A A$ , or by crank  $O_B B$ , but not by crank  $O_C C$ .

moved to a different location. This may seem different from inversion as described in Chapter 1, in which the base link is changed. However, it is closely related, as will be seen later when we deal with the case in which the mechanism is driven via a floating link. A detailed discussion of the issues involved in inversion is also given by Goodman.<sup>5</sup>

A serious situation arises in most problems requiring inversion. It was assumed earlier that the position of the linkage was known. Normally, that is not the case, and it is first necessary to determine the angular positions of all links by drawing the linkage to scale. Consideration of Fig. 2.20 reveals, however, that this is not straightforward when the position of crank  $O_C C$  is given. Again, the problem is that this crank does not form part of a four-bar loop but appears only in loops with five members. Therefore it is not possible to complete the loop when only the position of that crank is given.

One approach to the solution of this problem is to note that when the angular position of crank  $O_C C$  is specified, point  $D$  can lie anywhere on a circle with center point  $C$  and radius length  $CD$ . The position of point  $D$  is also constrained by the four-bar linkage  $O_A A B O_B$  to lie on a unique curve, called a coupler curve. If the coupler curve is plotted, its intersection with the circle gives the location of point  $D$ . Unfortunately, the coupler curve is a complicated planar curve of degree six. The only reasonably efficient way to plot it is to construct successive positions of the linkage  $O_A A B O_B$  as the angular position of the crank  $O_A A$  is incremented. Also, there may be as many as six intersections between the coupler curve and the circle, giving up to six different possible positions of the linkage with crank  $O_C C$  in the specified position. Each gives an acceptable assembly configuration for the linkage, so the designer must choose the proper one for a given application.

Another approach to the problem is to iterate for the location of the dyad made up of links  $D$  and  $C$ ; this technique works well when the linkage is drawn using a computer graphics package. For this approach, assume a position for link  $O_A A$ , draw the rest of the linkage, and note the position of link  $O_C C$ . If the position of link  $O_C C$  is not correct, select a different position for link  $O_A A$  and reconstruct the linkage again. Measure the position of link  $O_C C$  and continue changing  $O_A A$  and measuring the position of  $O_C C$  until  $O_C C$  is in the desired orientation. This may take a number of iterations; however, once the proper position for  $O_A A$  is bounded, the procedure will converge fairly rapidly.

If the entire range of motion for the linkage is of interest, then accurately locating the position of  $O_C C$  in specific positions is not necessarily an issue. Link  $O_A A$  can be located in

<sup>5</sup> Goodman, T.P., "An Indirect Method for Determining Accelerations in Complex Mechanisms." *Trans. ASME*, Nov., 1958, pp. 1676–1682.

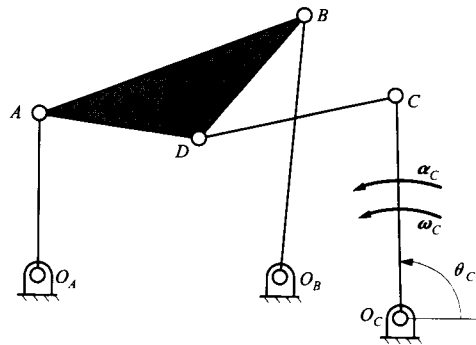
representative positions in its range of motion and the analysis can be conducted for each position. Smooth curves can then be drawn through the results.

A procedure for the solution of problems that can be approached by inversion is detailed in Example 2.6.

### EXAMPLE 2.6 Velocity Analysis by Inversion

#### Solution

The linkage shown in Fig. 2.21 is driven by crank  $O_C C$ . Find the angular velocities of all members of the linkage for the position in which  $\theta_C$  is  $135^\circ$ . The angular velocity of  $O_C C$  is 10 rad/s CCW.  $O_A A = 2$  in,  $AB = 3.5$  in,  $O_B B = 3.25$  in,  $CD = 2.5$  in,  $O_C C = 2.75$  in, and  $AD = BD = 2.0$  in. With origin at  $O_A$ ,  $O_B$  is the point (3.0, 0) and  $O_C$  is the point (4.5, -0.5).



**FIGURE 2.21** The linkage of Example 2.6. This is an example of a linkage that cannot be solved graphically without the use of inversion techniques.

We must conduct the analysis by starting with the position analysis.

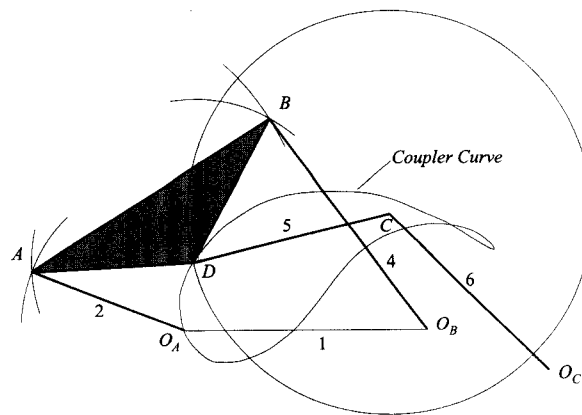
#### (a) Position

It is first necessary to construct the linkage in the specified position. The intersection of the coupler curve generated by point  $D$  with the circular locus of  $D$  centered on  $C$  is shown in Fig. 2.22. The coupler curve is plotted by constructing the four-bar  $O_A A B O_B$  in successive positions with equal increments of the angle of the crank  $O_A A$  and plotting the corresponding positions of point  $D$ . This process is not shown on the figure, but the basic steps are as follows:

1. Plot  $O_A$ ,  $O_B$ , and  $O_C$
2. Select the angle  $O_B O_A A$  and plot  $O_A A$ .
3. With center  $A$  and radius  $AB$ , draw an arc.
4. With center  $O_B$  and radius  $O_B B$  draw an arc. Its intersection with the arc from step 3 is point  $B$ .
5. Construct the triangle  $ABD$  on line  $AB$  to locate point  $D$ .
6. Increment angle  $O_B O_A A$  and repeat steps 1–5.
7. Plot the coupler curve, that is, the locus of the successive positions of point  $D$ . The comma-shaped curve shown in Fig. 2.22 is the resulting coupler curve.

The configuration of the linkage can now be constructed as follows:

8.  $O_C C$  is drawn at the specified angle and a circle is drawn with center  $C$  and radius  $CD$ . Its intersections with the coupler curve give possible positions of point  $D$  for the specified value of  $\theta_C$ . Notice that there are two possible positions for  $D$  in this case. (There may be as many as six.) We choose the position of  $D$  that gives the linkage configuration closest to that shown in Fig. 2.21.



**FIGURE 2.22** Position solution of the linkage of Example 2.6.

Once  $D$  is located, point  $A$  is located as follows:

9. Set radius  $O_A A$  and strike an arc centered on  $O_A$ .
10. Set radius  $\overline{DA}$  and strike an arc centered on  $D$ . The intersection with the arc of step 9 is point  $A$ .
11. Construct triangle  $ABD$  on  $\overline{DA}$  to locate point  $B$ . The linkage can now be drawn in the specified position.

#### (b) Velocities

The procedure for solving for the velocities is to draw the velocity polygon with the angular velocity of link 2 assumed to be  $\Omega_2 = 1$  rad/s. The value of the angular velocity of link 6,  $\Omega_6$ , is found for this assumption and a scaling factor is calculated to scale  $\Omega_6$  to the specified value of  $\omega_6 = 10$  rad/s. The same scaling factor is then applied to all other velocities and angular velocities to give their correct values when  $\omega_6 = 10$  rad/s. This is a solution by *inversion* because it is necessary first to solve the problem with link 2 assumed to be the driving crank rather than working directly with the actual driving crank, which is link 6. The solution with the assumed value of  $\omega_2$  is inverted to that with the required value of  $\omega_6$  by scaling it.

For the velocity analysis, the basic equations that we will solve are

$$\mathbf{v}_A = \mathbf{v}_{A/O_A} = \boldsymbol{\omega}_2 \times \mathbf{r}_{A/O_A}$$

$$\mathbf{v}_B = \mathbf{v}_A + \mathbf{v}_{B/A}$$

$$\mathbf{v}_D = \mathbf{v}_A + \mathbf{v}_{D/A} = \mathbf{v}_B + \mathbf{v}_{D/B}$$

$$\mathbf{v}_C = \mathbf{v}_D + \mathbf{v}_{C/D} = \mathbf{v}_{C/O_C}$$

The steps are as follows:

1. Compute the value of  $\mathbf{v}_A$  with the assumption that  $\Omega_2 = 1$  rad/s CCW, and plot  $\mathbf{v}_A$  (as  $\overline{oa}$ ) normal to  $\overline{O_A A}$  as shown in Fig. 2.23:

$$v_A = 2.0 \times 1 = 2 \text{ rad/s}$$

2. Draw a line through a normal to  $\overline{AB}$ .

3. Draw a line through  $o$  normal to  $\overrightarrow{O_B A}$ . The intersection of this line with that of step 2 gives point  $b$ .
4. Draw a line through  $a$  normal to  $\overrightarrow{AD}$ .
5. Draw a line through  $b$  normal to  $\overrightarrow{BD}$ . The intersection of this line with that from step 4 gives point  $d$  (velocity image).
6. Draw a line through  $d$  normal to  $\overrightarrow{CD}$ .
7. Draw a line through  $o$  normal to  $\overrightarrow{O_C C}$ . The intersection of this line with that from step 6 gives point  $c$ .
8. Measure  $v_C = \overline{oc}$  and compute  $\Omega_6$ :

$$v_C = 1.214 \text{ in/s}$$

$$\Omega_6 = v_C / O_C C = 1.214 / 2.75 = 0.441 \text{ rad/s}$$

9. Compute the scaling factor  $\sigma = \omega_6 / \Omega_6$ , where  $\omega_6$  is the specified angular velocity of link 6:

$$\sigma = 10 / 0.441 = 22.7$$

Since both the calculated and specified values of  $\omega_6$  are CCW,  $\sigma$  is positive. If they had been in opposite directions,  $\sigma$  would be negative.

10. Compute the angular velocities  $\Omega_2, \Omega_3, \Omega_4$ , and  $\Omega_5$  and scale the results:

$$\omega_2 = \sigma \times \Omega_2 = 1 \times 22.7 = 22.7 \text{ rad/s in the CCW direction}$$

$$\omega_3 = \sigma \times \Omega_3 = \sigma \times v_{BA} / AB = 22.7 \times 1.09 / 3.5 = 7.05 \text{ rad/s CCW}$$

$$\omega_4 = \sigma \times \Omega_4 = \sigma \times v_B / O_B B = 22.7 \times 1.62 / 3.25 = 11.32 \text{ rad/s CCW}$$

$$\omega_5 = \sigma \times \Omega_5 = \sigma \times v_{CD} / CD = 22.7 \times 0.42 / 2.5 = 3.73 \text{ rad/s CCW}$$

This completes the velocity analysis.

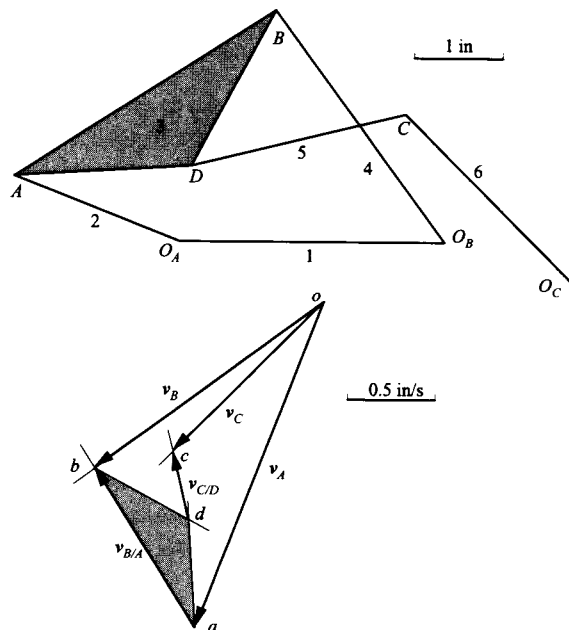


FIGURE 2.23 Velocity solution for Example 2.6.

## PROBLEMS

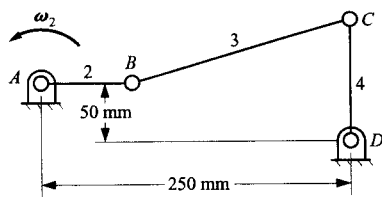
### EXERCISE PROBLEMS INVOLVING THE VELOCITY AND ACCELERATION ANALYSIS OF SINGLE-LOOP MECHANISMS

2.1 In the mechanism shown, link 2 is rotating CCW at the constant rate of 2 rad/s. In the position shown, link 2 is horizontal and link 4 is vertical. Write the appropriate vector equations, solve them using vector polygons, and

(a) determine  $v_{C_4}$ ,  $\omega_3$ , and  $\omega_4$ ;

(b) determine  $a_{C_4}$ ,  $\alpha_3$ , and  $\alpha_4$ .

Link lengths:  $AB = 75 \text{ mm}$ ,  $CD = 100 \text{ mm}$ .

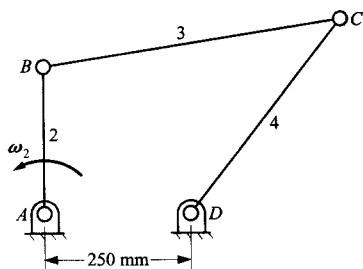


2.2 In the mechanism shown, link 2 is rotating CCW at the constant rate of 500 rad/s. In the position shown, link 2 is vertical. Write the appropriate vector equations, solve them using vector polygons, and

(a) determine  $v_{C_4}$ ,  $\omega_3$ , and  $\omega_4$ ;

(b) determine  $a_{C_4}$ ,  $\alpha_3$ , and  $\alpha_4$ .

Link lengths:  $AB = 1.2 \text{ in}$ ,  $BC = 2.42 \text{ in}$ ,  $CD = 2 \text{ in}$ .

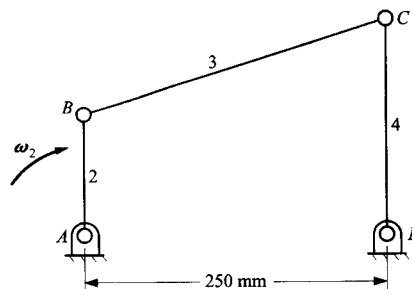


2.3 In the mechanism shown, link 2 is rotating CW at the constant rate of 10 rad/s. In the position shown, link 4 is vertical. Write the appropriate vector equations, solve them using vector polygons, and

(a) determine  $v_{C_4}$ ,  $\omega_3$ , and  $\omega_4$ ;

(b) determine  $a_{C_4}$ ,  $\alpha_3$ , and  $\alpha_4$ .

Link lengths:  $AB = 100 \text{ mm}$ ,  $BC = 260 \text{ mm}$ ,  $CD = 180 \text{ mm}$ .

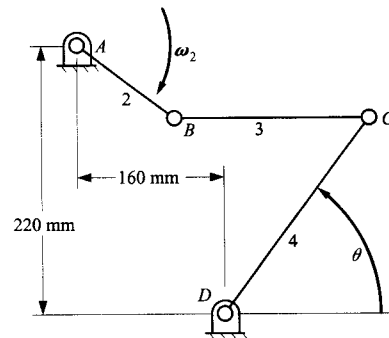


2.4 In the mechanism shown, link 2 is rotating CW at the constant rate of 4 rad/s. In the position shown,  $\theta = 53^\circ$ . Write the appropriate vector equations, solve them using vector polygons, and

(a) determine  $v_{C_4}$ ,  $\omega_3$ , and  $\omega_4$ ;

(b) determine  $a_{C_4}$ ,  $\alpha_3$ , and  $\alpha_4$ .

Link lengths:  $AB = 100 \text{ mm}$ ,  $BC = 160 \text{ mm}$ ,  $CD = 200 \text{ mm}$ .

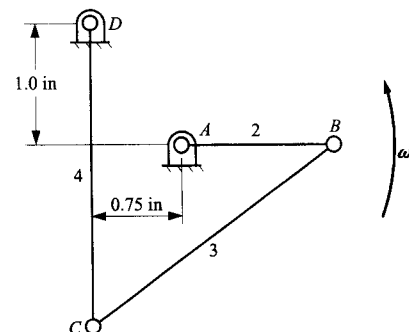


2.5 In the mechanism shown, link 2 is rotating CCW at the constant rate of 4 rad/s. In the position shown, link 2 is horizontal. Write the appropriate vector equations, solve them using vector polygons, and

(a) determine  $v_{C_4}$ ,  $\omega_3$ , and  $\omega_4$ ;

(b) determine  $a_{C_4}$ ,  $\alpha_3$ , and  $\alpha_4$ .

Link lengths:  $AB = 1.25 \text{ in}$ ,  $BC = 2.5 \text{ in}$ ,  $CD = 2.5 \text{ in}$ .

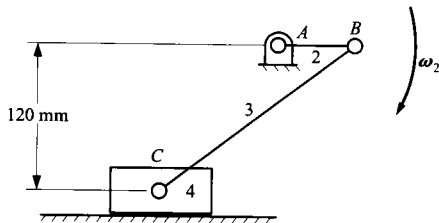


2.6 In the mechanism shown, link 2 is rotating CW at the constant rate of 100 rad/s. In the position shown, link 2 is horizontal. Write the appropriate vector equations, solve them using vector polygons, and

(a) determine  $v_{C_4}$ ,  $\omega_3$ ;

(b) determine  $a_{C_4}$ ,  $\alpha_3$ .

Link lengths:  $AB = 60$  mm,  $BC = 200$  mm.

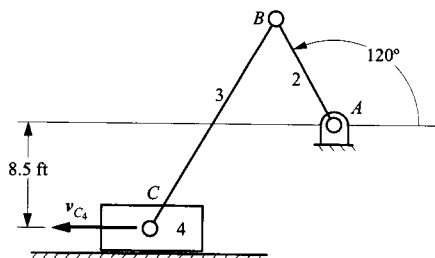


2.7 In the mechanism shown, link 4 is moving to the left at the constant rate of 4 ft/s. Write the appropriate vector equations, solve them using vector polygons, and

(a) determine  $\omega_3$  and  $\omega_4$ ;

(b) determine  $\alpha_3$  and  $\alpha_4$ .

Link lengths:  $AB = 10$  ft,  $BC = 20$  ft.

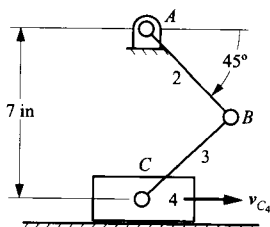


2.8 In the mechanism shown, link 4 is moving to the right at the constant rate of 20 in/s. Write the appropriate vector equations, solve them using vector polygons, and

(a) determine  $\omega_3$  and  $\omega_4$ ;

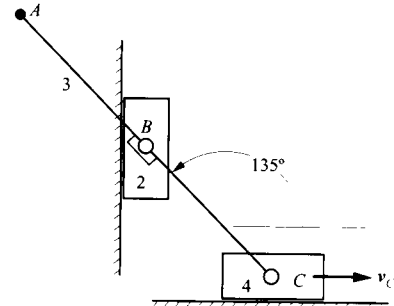
(b) determine  $\alpha_3$  and  $\alpha_4$ .

Link lengths:  $AB = 5$  in,  $BC = 5$  in.



2.9 In the mechanism shown, link 4 is moving to the left at the constant rate of 0.6 ft/s. Write the appropriate vector equations, solve them using vector polygons, and determine the velocity and acceleration of point  $A_3$ .

Link lengths:  $AB = 5$  in,  $BC = 5$  in.

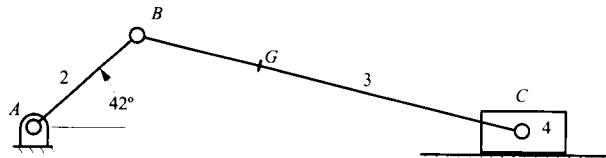


2.10 In the mechanism shown, link 4 moves to the right with a constant velocity of 75 ft/s. Write the appropriate vector equations, solve them using vector polygons, and

(a) determine  $v_{B_2}$ ,  $v_{G_3}$ ,  $\omega_2$ ,  $\omega_3$ ;

(b) determine  $a_{B_2}$ ,  $a_{G_3}$ ,  $\alpha_2$ , and  $\alpha_3$ .

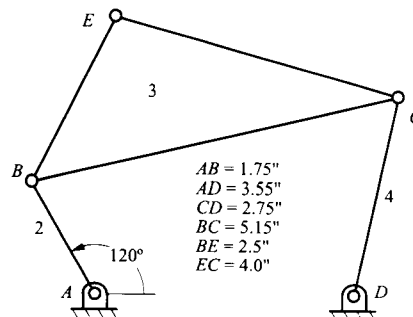
Link lengths:  $AB = 4.8$  in,  $BC = 16.0$  in,  $BG = 6.0$  in.



2.11 For the four-bar linkage, assume that  $\omega_2 = 50$  rad/s CW and  $\alpha_2 = 1600$  rad/s<sup>2</sup> CW. Write the appropriate vector equations, solve them using vector polygons, and

(a) determine  $v_{B_2}$ ,  $v_{C_3}$ ,  $v_{E_3}$ ,  $\omega_3$ , and  $\omega_4$ ;

(b) determine  $a_{B_2}$ ,  $a_{C_3}$ ,  $a_{E_3}$ ,  $\alpha_3$ , and  $\alpha_4$ .



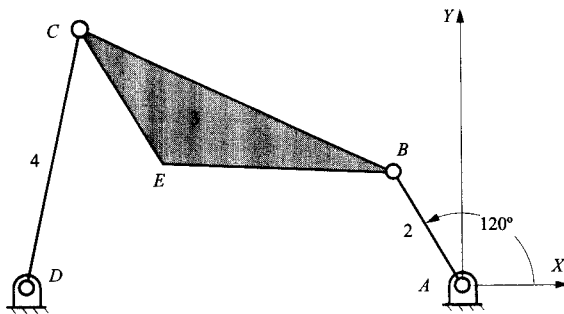
2.12 Re-solve Problem 2.11 if  $\omega_2 = 50 \text{ rad/s}$  CCW and  $\alpha_2 = 0$ .

2.13 In the mechanism shown, link 2 is rotating CW at the rate of  $180 \text{ rad/s}$ . Write the appropriate vector equations, solve them using vector polygons, and

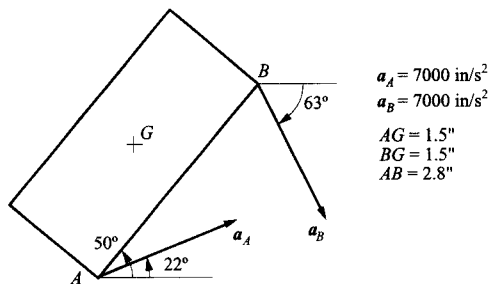
(a) determine  $v_{B_2}$ ,  $v_{C_3}$ ,  $v_{E_3}$ ,  $\omega_3$ , and  $\omega_4$ ;

(b) determine  $a_{B_2}$ ,  $a_{C_3}$ ,  $a_{E_3}$ ,  $\alpha_3$ , and  $\alpha_4$ .

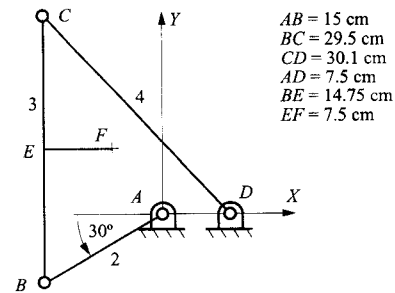
Link lengths:  $AB = 4.6 \text{ in}$ ,  $BC = 12.0 \text{ in}$ ,  $AD = 15.2 \text{ in}$ ,  $CD = 9.2 \text{ in}$ ,  $EB = 8.0 \text{ in}$ ,  $CE = 5.48 \text{ in}$ .



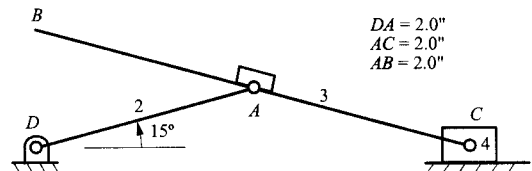
2.14 The accelerations of points  $A$  and  $B$  in the coupler shown are as given. Determine the acceleration of the center of mass  $G$  and the angular acceleration of the body. Draw the vector representing  $a_G$  from  $G$ .



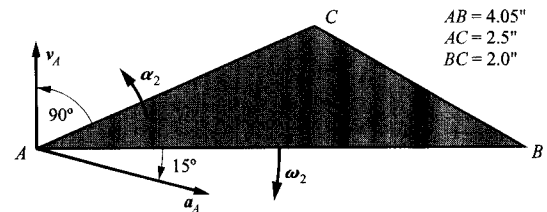
2.15 Crank 2 of the push-link mechanism shown in the figure is driven at a constant angular velocity  $\omega_2 = 60 \text{ rad/s}$  (CW). Find the velocity and acceleration of point  $F$  and the angular velocity and acceleration of links 3 and 4.



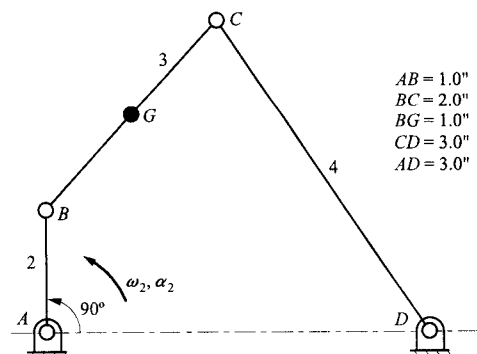
2.16 For the straight-line mechanism shown in the figure,  $\omega_2 = 20 \text{ rad/s}$  (CW) and  $\alpha_2 = 140 \text{ rad/s}^2$  (CW). Determine the velocity and acceleration of point  $B$  and the angular acceleration of link 3.



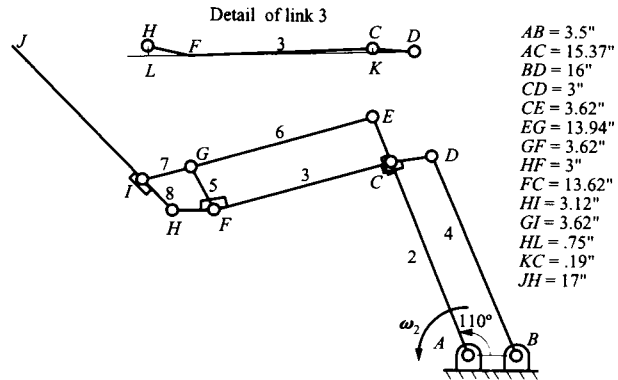
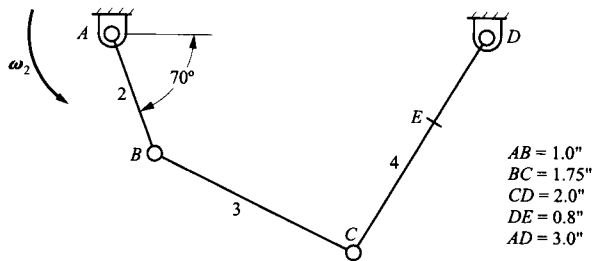
2.17 For the data given in the figure below, find the velocity and acceleration of points  $B$  and  $C$ . Assume  $v_A = 20 \text{ ft/s}$  and  $a_A = 400 \text{ ft/s}^2$  in the directions specified in the drawing.  $\omega_2 = 24 \text{ rad/s}$  (CW) and  $\alpha_2 = 160 \text{ rad/s}^2$  (CCW).



2.18 In the mechanism shown, link 2 is turning CCW at the constant rate of  $10 \text{ rad/s}$ . Draw the velocity and acceleration polygons for the mechanism, and determine  $a_{G_3}$  and  $\alpha_4$ .

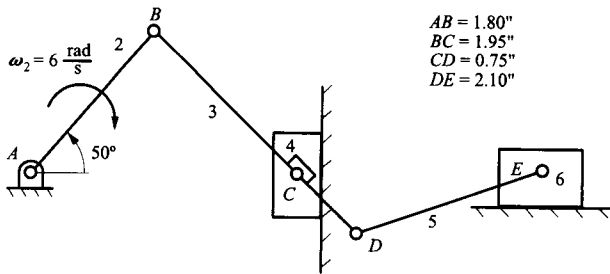


2.19 If  $\omega_2 = 100 \text{ rad/s}$  CCW (constant) find the velocity and acceleration of point  $E$ .

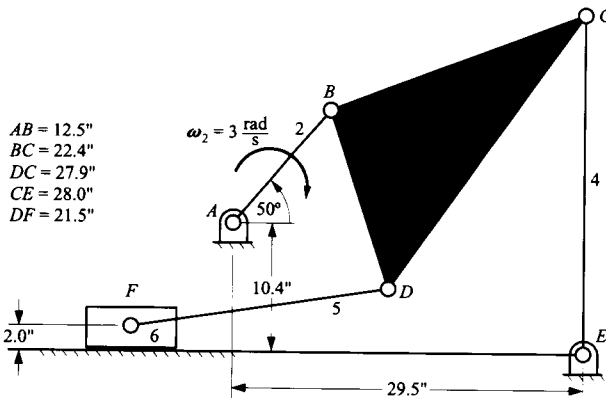


**EXERCISE PROBLEMS INVOLVING THE VELOCITY AND ACCELERATION ANALYSIS OF MULTILoop MECHANISMS**

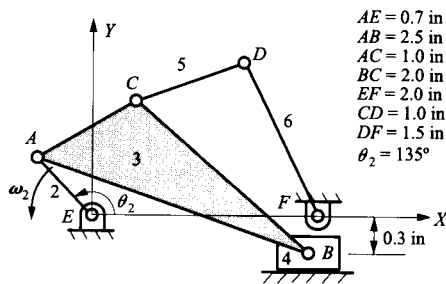
2.20 Draw the velocity polygon to determine the velocity of link 6. Points  $A$ ,  $C$ , and  $E$  have the same vertical coordinate.



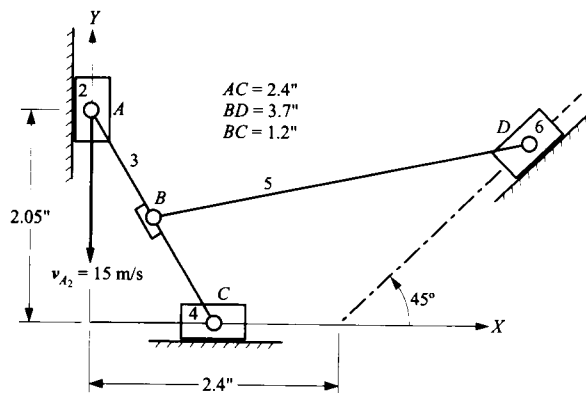
2.23 In the mechanism shown, determine the sliding velocity of link 6 and the angular velocities of links 3 and 5.



2.21 Link 2 of the linkage shown in the figure has an angular velocity of  $10 \text{ rad/s}$  CCW. Find the angular velocity of link 6 and the velocities of points  $B$ ,  $C$ , and  $D$ .



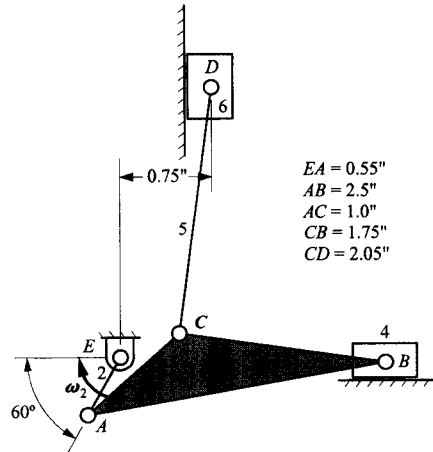
2.24 In the mechanism shown,  $v_{A_2} = 15 \text{ m/s}$  with direction downward. Draw the velocity polygon, and determine the velocity of point  $D$  on link 6 and the angular velocity of link 5.



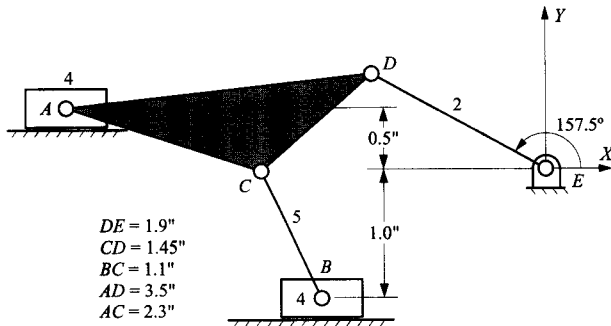
2.22 The linkage shown is used to raise the fabric roof on convertible automobiles. The dimensions are given as shown. Link 2 is driven by a DC motor through a gear reduction. If the angular velocity  $\omega_2 = 2 \text{ rad/s}$  CCW, determine the linear velocity of point  $J$ , which is the point where the linkage connects to the automobile near the windshield.



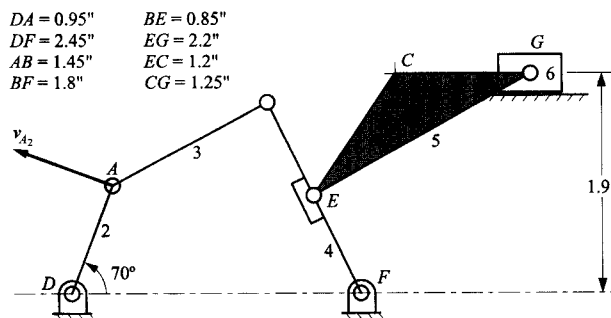
2.25 In the mechanism shown, points  $E$  and  $B$  have the same vertical coordinate. Find the velocities of points  $B$ ,  $C$ , and  $D$  of the double-slider mechanism shown in the figure if crank 2 rotates at  $42 \text{ rad/s}$  CCW.



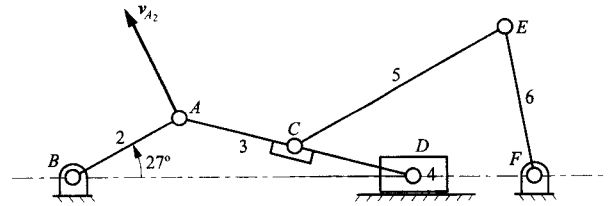
2.26 Given  $v_{A_4} = 1.0 \text{ ft/s}$  to the left, find  $v_{B_6}$ .



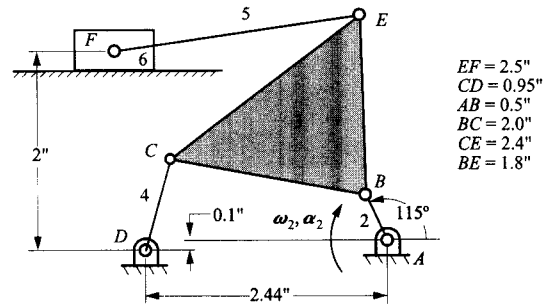
2.27 If  $v_{A_2} = 10 \text{ cm/s}$  as shown, find  $v_{C_5}$ .



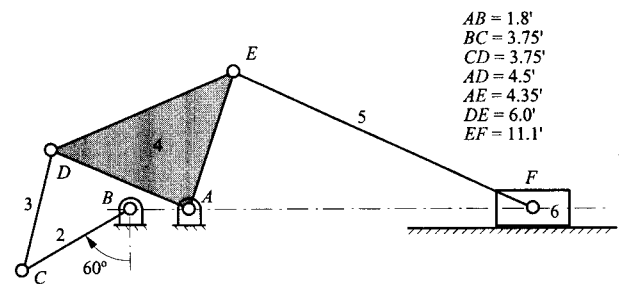
2.28 If  $v_{A_2} = 10 \text{ in/s}$  as shown, find the angular velocity of link 6.



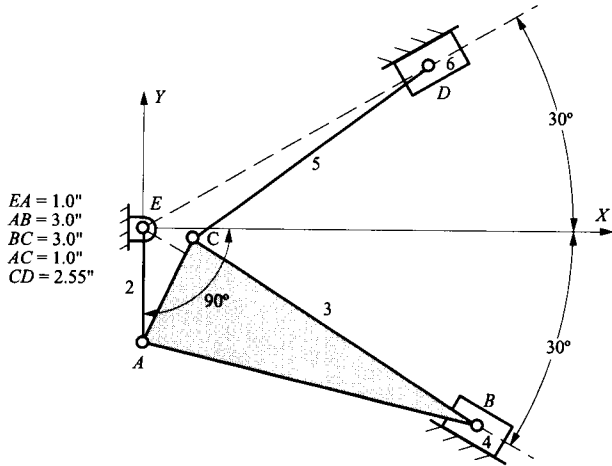
2.29 The angular velocity of link 2 of the mechanism shown is  $20 \text{ rad/s}$ , and the angular acceleration is  $100 \text{ rad/s}^2$  at the instant being considered. Determine the linear velocity and acceleration of point  $F_6$ .



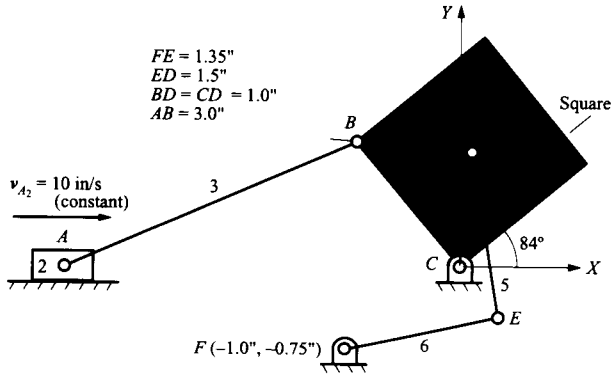
2.30 In the drag-link mechanism shown, link 2 is turning CW at the rate of  $130 \text{ rpm}$ . Construct the velocity and acceleration polygons and compute the following:  $a_{E_5}$ ,  $a_{F_6}$ , and the angular acceleration of link 5.



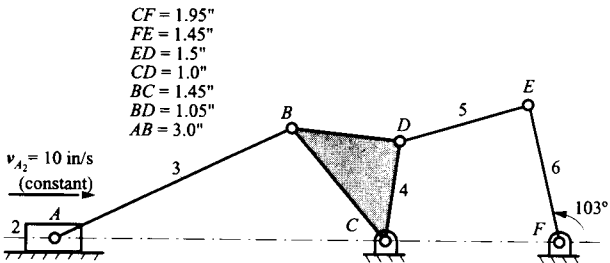
2.31 The figure shows the mechanism used in a two-cylinder 60-degree V-engine consisting, in part, of an articulated connecting rod. Crank 2 rotates at 2000 rpm CW. Find the velocities and acceleration of points B, C, and D and the angular acceleration of links 3 and 5.



Then determine the velocity and acceleration images of link 4. Draw the images on the velocity and acceleration polygons.



2.34 In the mechanism shown, the velocity of  $A_2$  is 10 in/s to the right and is constant. Draw the velocity and acceleration polygons for the mechanism, and record values for angular velocity and acceleration of link 6. Use the image technique to determine the velocity of points  $D_3$  and  $E_3$ , and locate the point in link 3 that has zero velocity.

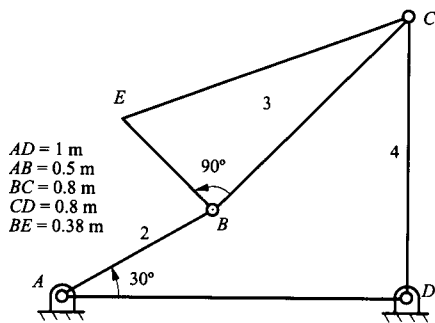


**EXERCISE PROBLEMS INVOLVING THE VELOCITY AND ACCELERATION IMAGE**

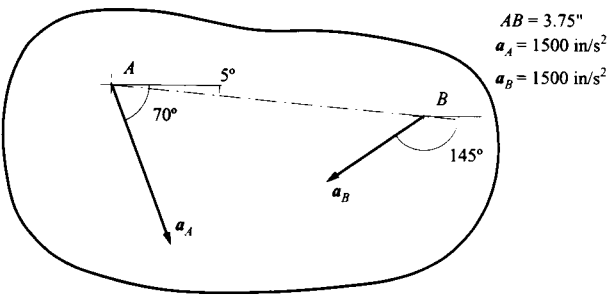
2.32 In the mechanism shown,  $\omega_2 = 4$  rad/s CCW (constant). Write the appropriate vector equations, solve them using vector polygons, and

- (a) determine  $v_{E_3}$ ,  $v_{E_4}$ ,  $\omega_3$ ;
- (b) determine  $a_{E_2}$ ,  $a_{E_4}$ ,  $\alpha_3$ .

Also find the point in link 3 that has zero acceleration for the position given.



2.35 The instant center of acceleration of a link can be defined as that point in the link that has zero acceleration. If the accelerations of points A and B are as given in the rigid body shown, find the point C in that link at which the acceleration is zero.

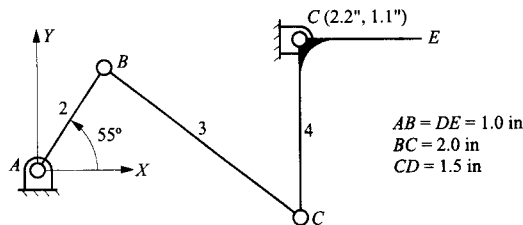


2.33 In the mechanism shown, point A lies on the X axis. Draw the basic velocity and acceleration polygons and use the image technique to determine the velocity and acceleration of point  $D_4$ .

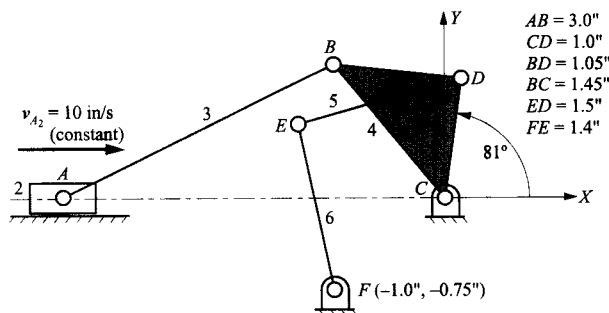
2.36 The following are given for the mechanism shown in the figure:

$$\omega_2 = 6.5 \text{ rad/s (CCW)}, \alpha_2 = 40 \text{ rad/s}^2 \text{ (CCW)}$$

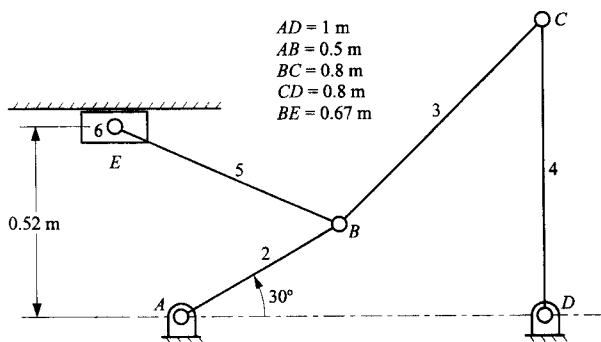
Draw the velocity polygon, and locate the velocity of point E using the image technique.



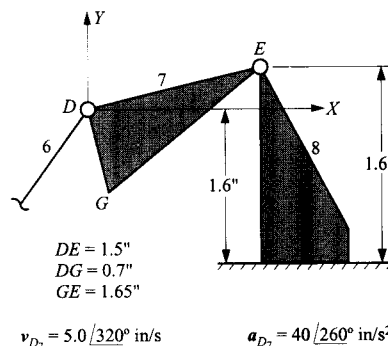
2.37 In the mechanism shown, find  $\omega_6$  and  $\alpha_3$ . Also, determine the acceleration of  $D_3$  by image.



2.38 In the mechanism shown,  $\omega_2 = 1 \text{ rad/s (CCW)}$  and  $\alpha_2 = 0 \text{ rad/s}^2$ . Find  $\omega_5$ ,  $\alpha_5$ ,  $v_{E_6}$ , and  $a_{E_6}$  for the position given. Also find the point in link 5 that has zero acceleration for the position given.



2.39 Part of an eight-link mechanism is shown in the figure. The velocity and acceleration of point  $D_7$  are given. Find  $\omega_7$  and  $\alpha_7$  for the position given. Also find the velocity of  $G_7$  by image.

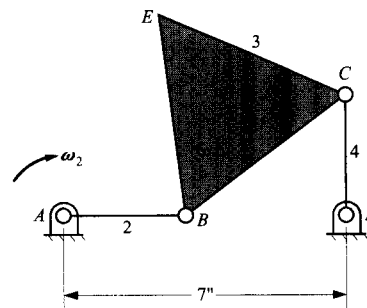


2.40 In the mechanism shown, link 2 is rotating CW at the constant rate of 3 rad/s. In the position shown, link 2 is horizontal. Write the appropriate vector equations, solve them using vector polygons, and

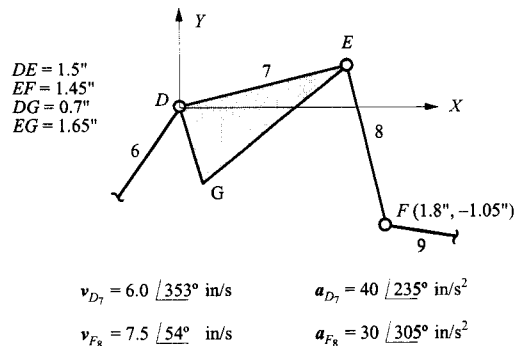
(a) determine  $v_{C_4}$ ,  $v_{E_4}$ ,  $\omega_3$ , and  $\omega_4$ ;

(b) determine  $a_{C_4}$ ,  $a_{E_4}$ ,  $\alpha_3$ , and  $\alpha_4$ .

Link lengths:  $AB = 3 \text{ in}$ ,  $BC = BE = CE = 5 \text{ in}$ ,  $CD = 3 \text{ in}$ .



2.41 Part of a 10-link mechanism is shown in the figure. The velocity and acceleration of points  $D_7$  and  $F_8$  are given. Find  $\omega_8$  and  $\alpha_7$  for the position given. Also find the velocity of  $G_7$  by image.



---

# *LINKAGES WITH ROLLING AND SLIDING CONTACTS AND JOINTS ON MOVING SLIDERS*

---

## **3.1 INTRODUCTION**

---

The methods introduced in Chapter 2 are straightforward and are perfectly adequate for analysis of linkages that have only revolute joints or sliding joints on fixed slides. However, to analyze linkages with other types of joints, including those with moving sliding joints, it is necessary to base the analysis on a more complex theory. The problem arises from differentiation of vector quantities that are referred to moving reference frames.

As was discussed in Chapter 1, a kinematic joint is formed by any contact between two bodies. The methods discussed in Chapter 2 apply only to linkages in which all the joints have the very specialized, surface-of-revolution geometry of revolute joints, or, in relatively few cases, the equally special generalized cylindrical surface geometry of prismatic joints. There are many other possible types of kinematic joints, a number of which are of great practical importance. In this chapter we provide the basic analysis tools needed to deal with linkages that include these more general joint types.

Many mechanisms include rolling contacts and contacts with irregularly shaped bodies. A cam mechanism will often include a cylindrical follower rolling on the irregularly shaped cam. Any wheeled vehicle makes use of rolling contact with the terrain over which it travels. When two bodies are in rolling contact the point in one body that contacts the other body is instantaneously at rest relative to that body. That is, its velocity relative to that body is zero. However, after an infinitesimally small time interval, that point will have separated from the body and will no longer be at rest relative to it. Thus, although the velocity of the contacting point relative to the body contacted is zero, its acceleration is not zero and is, in fact, directed along the contact normal away from the contacted body.

Other commonly used mechanisms have sliding joints that are not fixed relative to the base, but rotate. The Coriolis component of acceleration, which governs the direction of rotation of cyclonic weather systems, can also lead to significant internal loads in mechanisms. This is particularly relevant to mechanisms that have rotating sliding joints.

To address problems involving linkages of these types it is necessary first to think about what we mean by a reference frame and the implications of relative motion of two reference frames for velocity and acceleration analysis.

---

## **3.2 REFERENCE FRAMES**

---

If a linkage involves only revolute joints or sliders on fixed lines, the equations developed in Sections 2.3 and 2.4 are sufficient for conducting the kinematic analysis. However, for

other types of joints, the equations become more complex, and it is necessary to use more than one reference frame for the velocities and accelerations. In general, each link must be assumed to have a reference frame attached to it. In fact, when each link is manufactured, the machine tool that is used to form the link geometry will be guided relative to the local coordinate system or reference frame fixed to the link.

As is shown in Fig. 3.1, the position of a given point ( $Q$ ) can be quite different when it is measured relative to a different reference frame. Further, as will be demonstrated in the following, the velocity of a point relative to the fixed frame  $R$  depends not only on its velocity relative to a moving reference frame, such as frame  $M$ , but also on the velocity and angular velocity of frame  $M$  relative to frame  $R$ .

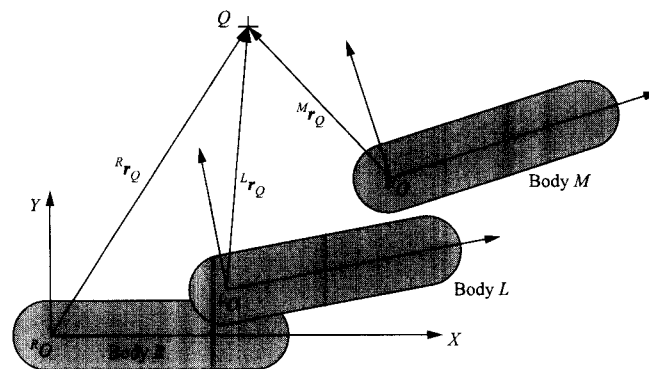
When it is important to distinguish the reference frames to which positions, velocities, and accelerations are referred, we will use a superscript before the vector symbol to identify the relevant reference frame. Typically, we will use the link number or letter as the reference frame for that link. That is the notation used on Fig. 3.1. Thus,  $^M O$  is the origin of the reference frame fixed to lamina  $M$ , and  $^M \mathbf{r}_Q$  is the position of point  $Q$  relative to frame  $M$ .

Typically, we will use the link number or letter as the reference frame for that link. Thus, if  $B$  is a general link that is moving relative to another link  $R$ ,  $^R \boldsymbol{\omega}_B$  is the angular velocity of the moving body  $B$ , relative to frame  $R$ . Then  $^B \boldsymbol{\omega}_R = -^R \boldsymbol{\omega}_B$  is the angular velocity of frame  $R$  relative to body  $B$ .  $^R \mathbf{v}_Q$  is the absolute velocity of point  $Q$  relative to frame  $R$ , and  $^B \mathbf{r}_Q$  is the position of point  $Q$  relative to the reference frame fixed to body  $B$ .  ${}^2\alpha_3$  is the angular acceleration of member 3 relative to the reference frame fixed in member 2.

The vector  $^R \mathbf{v}_{B/A}$  is usually called the velocity of  $B$  relative to  $A$  in reference frame  $R$ . However, as discussed earlier, this terminology is technically incorrect. Vectors must be measured relative to reference frames. Therefore,  $^R \mathbf{v}_{B/A}$  would be the velocity of point  $B$  relative to a reference frame  $R$  that has its origin at point  $A$  and moves so as always to be parallel to the fixed frame. Similarly, one would call  $^R \mathbf{r}_{Q/P}$  the position of  $Q$  relative to a reference frame, with origin at  $P$ , that remains at all times parallel to the frame  $R$ . The complexity of this statement explains the widespread use of the term "position of  $Q$  relative to  $P$ " for  $^R \mathbf{r}_{Q/P}$ .

Often, when all vectors are referred to the same reference frame  $R$ , we will drop the superscript  $R$  to simplify the notation. That is,  $\boldsymbol{\omega}_B = ^R \boldsymbol{\omega}_B$ . This was the case in Chapter 2 when the fixed frame (link 1) was understood to be the reference frame for all vectors.

The basis of the velocity analysis of planar linkages is the relationship between the velocities of two different points when something about the motion of the two points is known relative to a moving coordinate system. To derive this relationship in a form suitable for the formulation of a velocity polygon, let us consider the points  $P$  and  $Q$  shown in



**FIGURE 3.1** Position of a point relative to three different reference frames. The position of point  $Q$  relative to frame  $M$  is  $^M \mathbf{r}_Q$ . This vector is quite different from that of the position of point  $Q$  relative to the reference frame fixed to lamina  $L$ :  $^L \mathbf{r}_Q$  or from that to the position of the same point relative to lamina  $R$ :  $^R \mathbf{r}_Q$ .

Fig. 3.2. If  ${}^R r_P$  is the absolute position of point  $P$  relative to reference frame  $R$ ,  ${}^R r_Q$  is the absolute position of  $Q$  relative to reference frame  $R$ , and  ${}^B r_{Q/P}$  is the vector from point  $P$  to point  $Q$  defined relative to the moving reference system  $B$ , then we can write

$${}^R r_Q = {}^R r_P + {}^B r_{Q/P} \quad (3.1)$$

Note that Eq. (3.1) is the same as Eq. (2.2) with superscripts added to aid in keeping track of the reference frames. As indicated before, the vector  ${}^B r_{Q/P}$  is called the position of  $Q$  relative to  $P$  when the observer is fixed relative to reference system  $B$ .

Although  $P$  and  $Q$  may be fixed to body  $B$ , Eq. (3.1) is valid regardless of the link to which points  $P$  and  $Q$  are fixed (i.e.,  $P$  and  $Q$  may be fixed to link  $B$  or some other link). To obtain the velocities, we must differentiate Eq. (3.1) when the observer is in reference frame  $R$ .

Note that, in the position considered, the coordinate axes for systems  $B$  and  $R$  must be parallel. This condition will be assumed in all future developments requiring multiple coordinate systems. Otherwise we cannot add vector components as implied in Eq. (3.1). If the nominal coordinate systems attached to the two links are not parallel, we must use another set of coordinate systems that are momentarily parallel. The two coordinate systems fixed to a given link would be related by a simple coordinate transformation.

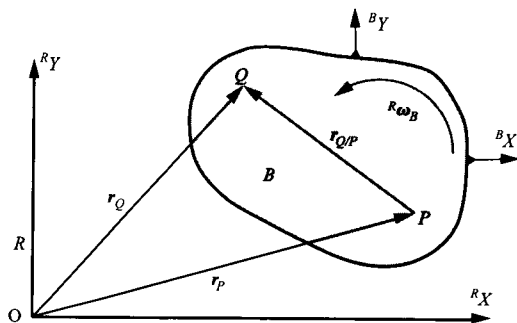
### 3.3 GENERAL VELOCITY AND ACCELERATION EQUATIONS

#### 3.3.1 Velocity Equations

When we differentiate Eq. (3.1) with the observer in the reference system  $R$ , we get

$$\frac{{}^R d}{{}^R dt} ({}^R r_Q) = \frac{{}^R d}{{}^R dt} ({}^R r_P) + \frac{{}^R d}{{}^R dt} ({}^B r_{Q/P}) \quad (3.2)$$

The derivatives of the position vectors defined relative to reference system  $R$  can be represented in a straightforward manner as velocities relative to reference system  $R$  because the reference axes relative to which the vectors are defined are fixed to  $R$  and do not move with time. Therefore, Eq. (3.1) becomes



**FIGURE 3.2** Positions of two points in the moving lamina,  $B$ .  $r_P$  and  $r_Q$  are the respective positions of points  $P$  and  $Q$  relative to the fixed reference frame  $R$ .  $\omega_B$  is the angular velocity of  $B$  relative to  $R$ . Note that this figure is similar to Fig. 2.1.

$${}^R\mathbf{v}_Q = {}^R\mathbf{v}_P + \frac{{}^R d}{dt} ({}^B\mathbf{r}_{Q/P}) \quad (3.3)$$

However, note that  ${}^B\mathbf{r}_{Q/P}$  is a vector defined relative to the coordinate system fixed to body  $B$ , and the reference axes of body  $B$  rotate relative to those of reference system  $R$  with an angular velocity  ${}^R\boldsymbol{\omega}_B$ . Therefore the derivative  $\frac{{}^R d}{dt}({}^B\mathbf{r}_{Q/P})$  must account for this rotation. In particular, the derivative involves two terms, one associated with the change in magnitude of the vector and one associated with the change in direction. This is apparent if we represent the vector  ${}^B\mathbf{r}_{Q/P}$  as a general three-dimensional vector in terms of its components and unit vectors. Then,

$${}^B\mathbf{r}_{Q/P} = x^B\mathbf{i} + y^B\mathbf{j} + z^B\mathbf{k}$$

and

$$\begin{aligned} \frac{{}^R d}{dt} ({}^B\mathbf{r}_{Q/P}) &= \frac{{}^R d}{dt} (x^B\mathbf{i} + y^B\mathbf{j} + z^B\mathbf{k}) \\ &= \left( \frac{{}^R dx}{dt} {}^B\mathbf{i} + \frac{{}^R dy}{dt} {}^B\mathbf{j} + \frac{{}^R dz}{dt} {}^B\mathbf{k} \right) + \left( x \frac{{}^R d{}^B\mathbf{i}}{dt} + y \frac{{}^R d{}^B\mathbf{j}}{dt} + z \frac{{}^R d{}^B\mathbf{k}}{dt} \right) \end{aligned} \quad (3.4)$$

In the first term, the derivatives of the components correspond to the change in the length of the vector, and this is defined relative to the coordinate system fixed to body  $B$ . Therefore, this is just the velocity defined relative to body  $B$ . The second term accounts for the rotation of the coordinate axes of  $B$  relative to the reference frame  $R$ .

Because  ${}^B\mathbf{i}$ ,  ${}^B\mathbf{j}$ , and  ${}^B\mathbf{k}$  are unit vectors, only their directions can change with time. We can determine how to evaluate the derivatives if we look at an infinitesimal angular displacement  $\delta\theta$  of body  $B$  relative to  $R$  during an infinitesimal time increment  $\delta t$ .

Because infinitesimal angular rotations are involved, we can treat  $\delta\theta$  as a vector with  $x$ ,  $y$ ,  $z$  components (i.e.,  $\delta\theta = \delta\theta_x {}^R\mathbf{i} = \delta\theta_y {}^R\mathbf{j} = \delta\theta_z {}^R\mathbf{k}$ ) and determine how each component changes the directions of the unit vectors. The angular velocity will be the change in the angular position during the infinitesimal time increment  $\delta t$ . That is,

$$\omega_x = \frac{{}^R\delta\theta_x}{\delta t}, \quad \omega_y = \frac{{}^R\delta\theta_y}{\delta t}, \quad \omega_z = \frac{{}^R\delta\theta_z}{\delta t}$$

and

$${}^R\boldsymbol{\omega}_B = \omega_x {}^R\mathbf{i} + \omega_y {}^R\mathbf{j} + \omega_z {}^R\mathbf{k} \quad (3.5)$$

To identify the trend, consider the effect of the angular components about the  $X$  axis. For the  $x$  direction (unit vector  ${}^B\mathbf{i}$ ), the change in the unit vector is represented in Fig. 3.3. From the figure,

$${}^R d ({}^B\mathbf{i}) = 1^R j d\theta_z - 1^R k d\theta_y \quad (3.6)$$

The change takes place during the time increment  $\delta t$ . Therefore, dividing Eq. (3.6) by  $\delta t$  we get

$$\frac{{}^R d}{dt} ({}^B\mathbf{i}) = {}^R\mathbf{j}\omega_z - {}^R\mathbf{k}\omega_y = {}^R\boldsymbol{\omega}_B \times {}^B\mathbf{i} = \begin{vmatrix} {}^R\mathbf{i} & {}^R\mathbf{j} & {}^R\mathbf{k} \\ \omega_x & \omega_y & \omega_z \\ 1 & 0 & 0 \end{vmatrix}$$

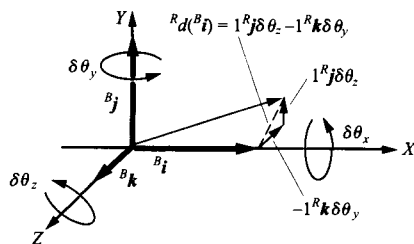


FIGURE 3.3 Change in  $i$  owing to a rotation about the  $X$ ,  $Y$ , and  $Z$  axes fixed to  $R$ .

Similarly,

$$\begin{aligned}\frac{R d}{dt}(Bj) &= {}^R \omega_B \times Bj \\ \frac{R d}{dt}(Bk) &= {}^R \omega_B \times Bk\end{aligned}$$

Therefore,

$$\begin{aligned}x \frac{R d B i}{dt} + y \frac{R d B j}{dt} + z \frac{R d B k}{dt} &= x {}^R \omega_B \times B i + y {}^R \omega_B \times B j + z {}^R \omega_B \times B k \\ &= {}^R \omega_B \times (x B i + y B j + z B k) = {}^R \omega_B \times B r_{Q/P}\end{aligned}$$

Then,

$$\begin{aligned}\frac{R d}{dt}(B r_{Q/P}) &= \left( \frac{R dx}{dt} B i + \frac{R dy}{dt} B j + \frac{R dz}{dt} B k \right) + \left( x \frac{R d B i}{dt} + y \frac{R d B j}{dt} + z \frac{R d B k}{dt} \right) \\ &= {}^B v_{Q/P} + {}^R \omega_B \times B r_{Q/P}\end{aligned}\quad (3.7)$$

Now, Eq. (3.3) can be written as

$${}^R v_Q = {}^R v_P + {}^B v_{Q/P} + {}^R \omega_B \times B r_{Q/P}\quad (3.8)$$

Before proceeding to the development of the acceleration equations, it is interesting to note that Eq. (3.7) is quite general. We could have derived a similar expression for the derivative of *any* vector that is defined relative to a moving coordinate system. For example, if  $s$  is any vector (e.g., position, velocity, or acceleration) and if  $U$  and  $W$  are any two different coordinate systems,

$$\frac{U d}{dt}(W s) = \frac{W d}{dt}(W s) + {}^U \omega_W \times W s\quad (3.9)$$

Note that angular velocity is a property of a body and linear velocity is a property of a point. In both cases, it is necessary to specify, or at least understand, which reference frame is used to define the quantity. Also note that if the vector is defined in the coordinate system in which the observer stands, the term involving the angular velocity will be zero. That is,

$${}^U \omega_U = 0$$



### 3.3.2 Acceleration Equations

The acceleration equations will involve the derivative of each angular velocity. In general, angular acceleration can be written as

$${}^R\boldsymbol{\alpha}_B = \frac{{}^R d}{dt} \left( {}^R\boldsymbol{\omega}_B \right)$$

where again  $B$  is the moving body and  $R$  is the reference system. As in the case of the angular velocity, the angular acceleration is a property of the entire body. It is a vector and has a magnitude and direction.

If a velocity vector is defined in the coordinate system in which the observer is located, the corresponding acceleration can be expressed simply. For example, if the velocity vector is given by  ${}^R\mathbf{v}_Q$ , then the acceleration is given by

$${}^R\mathbf{a}_Q = \frac{{}^R d}{dt} \left( {}^R\mathbf{v}_Q \right)$$

To obtain the linear acceleration relationship for the points  $P$  and  $Q$  in Fig. 3.2, we can differentiate Eq. (3.8). Differentiating term by term with the observer in reference system  $R$  gives

$${}^R\mathbf{a}_Q = \frac{{}^R d}{dt} \left( {}^R\mathbf{v}_Q \right) = \frac{{}^R d}{dt} \left( {}^R\mathbf{v}_P \right) + \frac{{}^R d}{dt} \left( {}^B\mathbf{v}_{Q/P} \right) + \frac{{}^R d}{dt} \left( {}^R\boldsymbol{\omega}_B \times {}^B\mathbf{r}_{Q/P} \right)$$

Considering each term and recognizing that vectors  ${}^B\mathbf{v}_{Q/P}$  and  ${}^B\mathbf{r}_{Q/P}$  are both defined relative to the moving coordinate system ( $B$ ), we get, after differentiation,

$${}^R\mathbf{a}_Q = {}^R\mathbf{a}_P + \frac{{}^B d}{dt} \left( {}^B\mathbf{v}_{Q/P} \right) + {}^R\boldsymbol{\omega}_B \times {}^B\mathbf{v}_{Q/P} + {}^R\boldsymbol{\alpha}_B \times {}^B\mathbf{r}_{Q/P} + {}^R\boldsymbol{\omega}_B \times \left( {}^B\mathbf{v}_{Q/P} + {}^R\boldsymbol{\omega}_B \times {}^B\mathbf{r}_{Q/P} \right)$$

and collecting terms gives

$${}^R\mathbf{a}_Q = {}^R\mathbf{a}_P + {}^B\mathbf{a}_{Q/P} + 2 {}^R\boldsymbol{\omega}_B \times {}^B\mathbf{v}_{Q/P} + {}^R\boldsymbol{\alpha}_B \times {}^B\mathbf{r}_{Q/P} + {}^R\boldsymbol{\omega}_B \times \left( {}^R\boldsymbol{\omega}_B \times {}^B\mathbf{r}_{Q/P} \right) \quad (3.10)$$

Note that in the last term, the operation  $({}^R\boldsymbol{\omega}_B \times {}^B\mathbf{r}_{Q/P})$  must be carried out before the operation  ${}^R\boldsymbol{\omega}_B \times ({}^R\boldsymbol{\omega}_B \times {}^B\mathbf{r}_{Q/P})$ . Obviously,  $(\boldsymbol{\omega} \times \boldsymbol{\omega}) \times \mathbf{r} \neq \boldsymbol{\omega} \times (\boldsymbol{\omega} \times \mathbf{r})$ .

The term  $2 {}^R\boldsymbol{\omega}_B \times {}^B\mathbf{v}_{Q/P}$  is called the Coriolis term and is a function of velocities only. The term  ${}^R\boldsymbol{\alpha}_B \times {}^B\mathbf{r}_{Q/P}$  is the transverse or tangential component of acceleration identified before. This component of acceleration is perpendicular to the radius vector. The term  ${}^R\boldsymbol{\omega}_B \times ({}^R\boldsymbol{\omega}_B \times {}^B\mathbf{r}_{Q/P})$  is the radial component of acceleration. In planar motion, but not in general, it points in the direction *opposite* to the radius vector. The term  ${}^B\mathbf{a}_{Q/P}$  is the acceleration of  $Q$  relative to  $P$  when the observer is in the moving body  $B$ .

### 3.3.3 Chain Rule for Positions, Velocities, and Accelerations

When dealing with mechanisms with a relatively large number of members, it is helpful to have relationships between the relative velocities and accelerations of several points and between the relative angular velocities and angular accelerations of several members. These relationships are particularly relevant to the spatial chain mechanisms discussed in Chapter 9.

**Positions, Velocities, and Accelerations of Points** Let  $A, B, C, D,$  and  $E$  be any arbitrary points moving with respect to the reference frame  $R$  as shown in Fig. 3.4. Then a position equation can be written as

$${}^R\mathbf{r}_{E/D} + {}^R\mathbf{r}_{D/C} + {}^R\mathbf{r}_{C/B} + {}^R\mathbf{r}_{B/A} = {}^R\mathbf{r}_{E/A} \quad (3.11)$$

This type of equation is just a simple expression of vector addition, and it applies regardless of the number of points involved. For velocities, we can differentiate Eq. (3.11) with the observer in system  $R$ . Then,

$${}^R\mathbf{v}_{E/D} + {}^R\mathbf{v}_{D/C} + {}^R\mathbf{v}_{C/B} + {}^R\mathbf{v}_{B/A} = {}^R\mathbf{v}_{E/A} \quad (3.12)$$

and the acceleration equation becomes

$${}^R\mathbf{a}_{E/D} + {}^R\mathbf{a}_{D/C} + {}^R\mathbf{a}_{C/B} + {}^R\mathbf{a}_{B/A} = {}^R\mathbf{a}_{E/A} \quad (3.13)$$

Equations (3.11) through (3.13) are applicable to any set of points, and they are especially useful when determining the kinematic information for points on mechanisms after the basic kinematic information associated with each link is known. They are also useful when analyzing manipulators and robots.

The relationship among three *arbitrary* points ( $A, B, C$ ) is

$${}^R\mathbf{r}_{C/A} = {}^R\mathbf{r}_{C/B} + {}^R\mathbf{r}_{B/A}$$

Then,

$${}^R\mathbf{r}_{C/B} = {}^R\mathbf{r}_{C/A} - {}^R\mathbf{r}_{B/A} \quad (3.14)$$

Because  $A$  is arbitrary, Eq. (3.14) indicates that we can find the relative position between two points by subtracting the relative position vectors between the two points and the same third point. Similarly, for velocities and accelerations,

$${}^R\mathbf{v}_{C/B} = {}^R\mathbf{v}_{C/A} - {}^R\mathbf{v}_{B/A} \quad (3.15)$$

and

$${}^R\mathbf{a}_{C/B} = {}^R\mathbf{a}_{C/A} - {}^R\mathbf{a}_{B/A} \quad (3.16)$$

Note the positions of  $A, B,$  and  $C$  in each of the expressions.

**Relative Angular Velocities** A chain rule for angular velocities works the same way as for linear velocities except that now reference systems are involved instead of points, as shown in Fig. 3.5. Consider three coordinate systems (1, 2, and 3) that are *momentarily parallel*. Then,

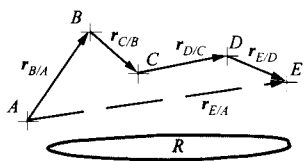


FIGURE 3.4 Relationship among the positions of a series of points.

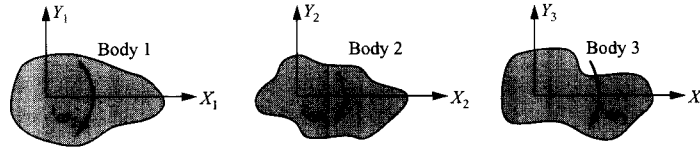


FIGURE 3.5 Relationship among the angular velocities for three links.

$${}^1\omega_3 = {}^1\omega_2 + {}^2\omega_3 \quad (3.17)$$

and

$${}^2\omega_3 = {}^1\omega_3 - {}^1\omega_2 = {}^1\omega_3 + {}^2\omega_1 \quad (3.18)$$

This means we can find the relative angular velocity between any two bodies by computing the angular velocity difference between each of the bodies and the same third body (in this case body 1).

For  $n$  bodies, the relative angular velocities are related by

$${}^n\omega_1 = {}^2\omega_1 + {}^3\omega_2 + {}^4\omega_3 + \cdots + {}^{n-1}\omega_{n-2} + {}^n\omega_{n-1}$$

**Relative Angular Accelerations** For relative accelerations, we can differentiate the relative velocity equation, Eq. (3.17):

$$\frac{{}^1d}{{}^1dt}({}^1\omega_3) = \frac{{}^1d}{{}^1dt}({}^1\omega_2) + \frac{{}^1d}{{}^1dt}({}^2\omega_3) \quad (3.19)$$

The first two terms are straightforward because the derivatives are both taken with respect to the reference system in which each vector is defined. That is,

$$\frac{{}^1d}{{}^1dt}({}^1\omega_3) = {}^1\alpha_3, \quad \frac{{}^1d}{{}^1dt}({}^1\omega_2) = {}^1\alpha_2$$

The third term is a vector described in the second coordinate system (superscript 2). Therefore using Eq. (3.9), this term can be written as

$$\frac{{}^1d}{{}^1dt}({}^2\omega_3) = \frac{{}^2d}{{}^2dt}({}^2\omega_3) + {}^1\omega_2 \times {}^2\omega_3 = {}^2\alpha_3 + {}^1\omega_2 \times {}^2\omega_3$$

The relative angular acceleration expression in Eq. (3.19) can then be written as

$${}^1\alpha_3 = {}^1\alpha_2 + {}^2\alpha_3 + {}^1\omega_2 \times {}^2\omega_3$$

This expression can be extended to  $n$  bodies using

$${}^1\alpha_n = {}^1\alpha_{n-1} + {}^{n-1}\alpha_n + {}^1\omega_{n-1} \times {}^{n-1}\omega_n$$

Then,

$${}^1\alpha_n = {}^1\alpha_2 + {}^2\alpha_3 + {}^3\alpha_4 + \cdots + {}^{n-1}\alpha_n + {}^1\omega_2 \times {}^2\omega_3 + {}^1\omega_3 \times {}^3\omega_4 + {}^1\omega_4 \times {}^4\omega_5 + \cdots + {}^1\omega_{n-1} \times {}^{n-1}\omega_n$$

Note that, in the plane, all of the  $\omega$ 's will be parallel, making the cross products all zero. Thus in *planar* problems, the chain rule for angular accelerations reduces to:

$${}^1\alpha_n = {}^1\alpha_2 + {}^2\alpha_3 + {}^3\alpha_4 + \dots + {}^{n-1}\alpha_n \quad (\text{planar problems})$$

Note that this equation could be treated as a scalar equation if signs are applied to the magnitudes of the angular accelerations according to some rule (say + for CCW and – for CW).

### 3.4 SPECIAL CASES FOR THE VELOCITY AND ACCELERATION EQUATIONS

Equations (3.8) and (3.10) are the most general forms for the relative velocity and acceleration equations for points that we will encounter in the kinematic analysis of linkages. In most practical problems, some of the terms in the expressions are zero. Three special cases often occur, and these will be discussed separately in the following.

#### 3.4.1 Points *P* and *Q* fixed to *B*

This is the most common situation that exists in the analysis of mechanisms. If *P* and *Q* are both fixed to *B*, as shown in Fig. 3.6, we have

$${}^B\mathbf{v}_{Q/B/P} = {}^B\mathbf{a}_{Q/B/P} = 0 \tag{3.20}$$

because *P* and *Q* do not have any motion relative to an observer in the moving body *B*. When Eq. (3.20) is used to simplify Eqs. (3.8) and (3.10), the results are

$${}^R\mathbf{v}_Q = {}^R\mathbf{v}_P + {}^R\boldsymbol{\omega}_B \times \mathbf{r}_{Q/P} \tag{3.21}$$

which can be recognized as being the same as Eq. (2.1), and

$${}^R\mathbf{a}_Q = {}^R\mathbf{a}_P + {}^R\boldsymbol{\alpha}_B \times \mathbf{r}_{Q/P} + {}^R\boldsymbol{\omega}_B \times ({}^R\boldsymbol{\omega}_B \times \mathbf{r}_{Q/P}) \tag{3.22}$$

which is the same as Eq. (2.8).

Here we have dropped the superscript on  $\mathbf{r}_{Q/P}$  because all coordinate systems are assumed to be parallel, and  $\mathbf{r}_{Q/P}$  will have the same coordinates in all coordinate systems. Note also that we could have rewritten Eqs. (3.8) and (3.10) relative to any other link; however, only the choice of the link (*B*) to which *Q* and *P* are attached simplifies the equation. Using the radial and tangential notation, we can also rewrite Eq. (3.22) as

$${}^R\mathbf{a}_Q = {}^R\mathbf{a}_P + {}^R\mathbf{a}_{Q/P}^r + {}^R\mathbf{a}_{Q/P}^t$$

where

$${}^R\mathbf{a}_{Q/P}^t = {}^R\boldsymbol{\alpha}_B \times \mathbf{r}_{Q/P} \tag{3.23}$$

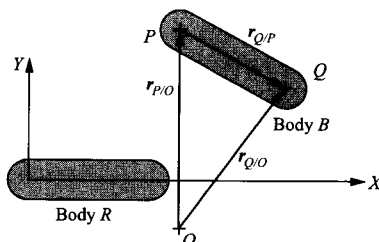


FIGURE 3.6 Two points fixed to the same link.

and

$${}^R \mathbf{a}_{Q/P}^r = {}^R \boldsymbol{\omega}_B \times ({}^R \boldsymbol{\omega}_B \times \mathbf{r}_{Q/P}) \quad (3.24)$$

We will use the radial and tangential notation extensively in mechanism analyses. For planar mechanisms,  ${}^R \mathbf{a}_{Q/P}^t$  and  ${}^R \mathbf{a}_{Q/P}^r$  will be orthogonal to each other because  ${}^R \boldsymbol{\omega}_B$  and  ${}^R \boldsymbol{\alpha}_B$  are both orthogonal to  $\mathbf{r}_{Q/P}$ . In spatial mechanisms, however, this will not always be the case.

### 3.4.2 $P$ and $Q$ Are Coincident

A second special case in kinematics is that in which  $P$  and  $Q$  belong to different bodies but are momentarily coincident. This case is shown in Fig. 3.7. Then,  $\mathbf{r}_{P/Q}$  is momentarily zero, and Eqs. (3.8) and (3.10) reduce to

$${}^R \mathbf{v}_Q = {}^R \mathbf{v}_P + {}^B \mathbf{v}_{Q/P} \quad (3.25)$$

If Eqs. (3.25) and (3.8) are considered carefully, it is apparent that the equation for the relative velocity remains the same regardless of the body chosen as the moving body. This means that the relative velocity term  ${}^B \mathbf{v}_{Q/P}$  is independent of the coordinate system chosen for the “moving” body. Therefore,

$${}^i \mathbf{v}_{Q/P} = {}^B \mathbf{v}_{Q/P} = {}^R \mathbf{v}_{Q/P}$$

where  $i$  and  $B$  are any systems.

The acceleration equation, Eq. (3.10), simplifies to

$${}^R \mathbf{a}_Q = {}^R \mathbf{a}_P + {}^B \mathbf{a}_{Q/P} + 2 {}^R \boldsymbol{\omega}_B \times {}^B \mathbf{v}_{Q/P} \quad (3.26)$$

Here, the Coriolis term is a function of velocities, so it can be computed as soon as the velocity analysis is completed. Only  ${}^B \mathbf{a}_{Q/P}$  involves new information not available from the velocity analysis.

### 3.4.3 $P$ and $Q$ Are Coincident and in Rolling Contact

If points  $P$  and  $Q$  are not only momentarily coincident but also in rolling contact, Eqs. (3.25) and (3.26) can be simplified still further. This condition is shown in Fig. 3.8. If two points are in rolling contact, they have the same velocity and their relative velocity must be zero. This means that

$$\begin{aligned} {}^B \mathbf{v}_{Q/P} &= 0 \\ {}^R \mathbf{v}_Q &= {}^R \mathbf{v}_P \end{aligned}$$

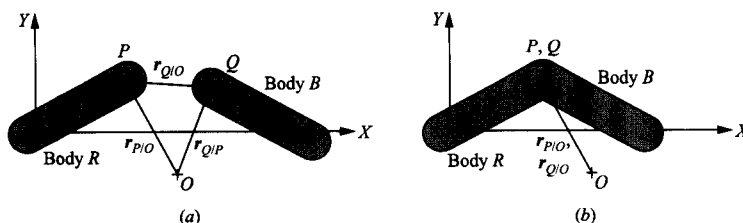


FIGURE 3.7 Condition when two separate points (a) become momentarily coincident (b).

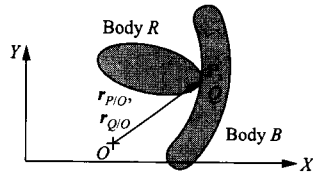


FIGURE 3.8 Condition for rolling contact.

and

$${}^R \mathbf{a}_Q = {}^R \mathbf{a}_P + {}^B \mathbf{a}_{Q/P}$$

Using logic similar to that used with Eq. (3.25), it is apparent that although the relative acceleration  ${}^B \mathbf{a}_{Q/P}$  is not usually zero, it is independent of whatever coordinate system is used for reference. This means that the relative acceleration will be the same when observed from any of the links in the mechanism.

We will examine examples of the special cases in the following. To simplify the equations and the nomenclature, we will use a superscript to identify the coordinate system only when the coordinate system is different from 1. Therefore, if no superscript is indicated as was done in Chapter 2, the frame coordinate system is automatically implied.

### 3.5 LINKAGES WITH ROTATING SLIDING JOINTS

Mechanisms in this class can have either a slider that slides on a line that is rotating or a pin-in-a-slot joint where the slot is straight and rotating. These cases are shown in Fig. 3.9, where the link numbers have been chosen arbitrarily.

Mechanisms with sliders that rotate are common in practice. Typical examples are door closers, the hydraulic cylinders on power shovels, and the power cylinders on some robots. The pin-in-slot joints, often with a free-spinning roller centered on the pin, are typically used as inexpensive substitutes for slider joints. They function where the transmitted loads are low. Examples where they appear are electric toothbrush mechanisms, audiotape cleaners, and walking-toy mechanisms.

The analysis of these mechanisms can be approached using the special case in section 3.4.2 for relative velocities and accelerations of coincident points. The resulting velocity and acceleration equations for two coincident points  $P$  and  $Q$  are given by Eqs. (3.25) and (3.26). Dropping the superscript  $R$  for the frame, we get

$$\mathbf{v}_Q = \mathbf{v}_P + {}^B \mathbf{v}_{Q/P}$$

$$\mathbf{a}_Q = \mathbf{a}_P + {}^B \mathbf{a}_{Q/P} + 2\boldsymbol{\omega}_B \times {}^B \mathbf{v}_{Q/P}$$

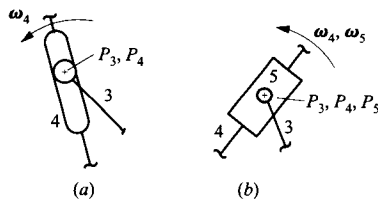


FIGURE 3.9 Joints that can be analyzed as rotating sliding joints. (a) Pin in straight slot, (b) rotating slider. The link numbers have been chosen arbitrarily.

When the points are coincident,  $P$  and  $Q$  will share the same coordinates, and they will usually be designated by the same letter with a subscript identifying the link to which they are attached. For example, if 3 and 4 are the links to which the coincident points are attached, if body  $B$  corresponds to link 5, and if the frame is 1, the velocity and acceleration equations can be written as

$$\mathbf{v}_{P_3} = \mathbf{v}_{P_4} + {}^5\mathbf{v}_{P_3/P_4} \quad (3.27)$$

and

$$\mathbf{a}_{P_3} = \mathbf{a}_{P_4} + {}^5\mathbf{a}_{P_3/P_4} + 2\boldsymbol{\omega}_5 \times {}^5\mathbf{v}_{P_3/P_4} \quad (3.28)$$

Once again,  ${}^5\mathbf{a}_{P_3/P_4}$  is called the acceleration of  $P_3$  relative to  $P_4$  when the observer is in system 5. The term  $2\boldsymbol{\omega}_5 \times {}^5\mathbf{v}_{P_3/P_4}$  is the Coriolis component of acceleration, and it can be written as  $\mathbf{a}_{P_3/P_4}^C$ . Eq. (3.28) can then be written as

$$\mathbf{a}_{P_3} = \mathbf{a}_{P_4} + {}^5\mathbf{a}_{P_3/P_4} + \mathbf{a}_{P_3/P_4}^C$$

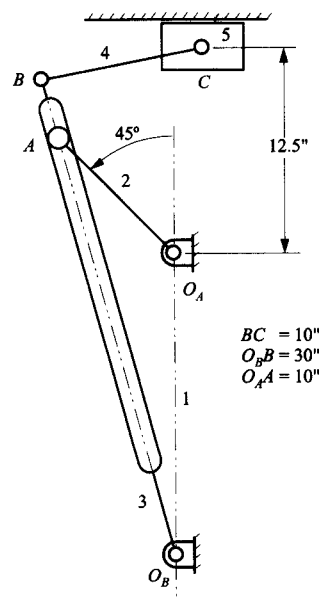
for graphical analyses.

In planar motion, the Coriolis component is normal to  ${}^5\mathbf{v}_{P_3/P_4}$  and has the magnitude  $2(\omega_5)|{}^5\mathbf{v}_{P_3/P_4}|$ . Its sense is obtained by imagining  ${}^5\mathbf{v}_{P_3/P_4}$  to be rotating about its tail in the  $\boldsymbol{\omega}_5$  direction. The direction of movement of the head of  ${}^5\mathbf{v}_{P_3/P_4}$  gives the sense. To illustrate the manner in which Eqs. (3.27) and (3.28) are used in graphical linkage analysis, consider the following example.

### EXAMPLE 3.1

**Velocity and Acceleration Analysis of a Quick-Return Mechanism**

Find the sliding velocities of the slide, the angular accelerations of links 3 and 4, and the acceleration of slide 5 for the quick-return mechanism of Fig. 3.10. The dimensions are as shown. Link 2 is driven with a constant angular velocity of 10 rpm CCW.



**FIGURE 3.10** The quick return linkage to be analyzed in Example 3.1.

**Solution**

Link 2 is the driver, so we will begin the analysis with point  $A_2$ . We must conduct the velocity analysis first. If that analysis is done carefully, we can proceed with the same points for the acceleration analysis. As in the previous examples, we will develop the basic equations first and then give the graphical procedure for solving them. The velocity of point  $A_2$  is given by

$$\mathbf{v}_{A_2} = \mathbf{v}_{A_2/O_4} = \boldsymbol{\omega}_2 \times \mathbf{r}_{A_2/O_4}$$

In the analysis of mechanisms of this type, it is important to identify the link in which the observer is located. Therefore, the left superscripts will be maintained when the coordinate system is different from 1. We must now use the coincident point  $A_3$  to be able to develop an equation relating a point on link 2 to a point on link 3. We can write the relative velocity equation in one of two ways:

$$\mathbf{v}_{A_2} = \mathbf{v}_{A_3} + \mathbf{v}_{A_2/A_3} = \mathbf{v}_{A_3} + {}^3\mathbf{v}_{A_2/A_3} \quad (3.29)$$

or

$$\mathbf{v}_{A_3} = \mathbf{v}_{A_2} + \mathbf{v}_{A_3/A_2} = \mathbf{v}_{A_2} + {}^2\mathbf{v}_{A_3/A_2} \quad (3.30)$$

To solve the problem, we must be able to recognize the direction of the relative velocity defined in the moving coordinate system. Referring to the mechanism in Fig. 3.10, we see that if the observer is fixed to link 2, it is not possible to identify directly the direction of the velocity  ${}^2\mathbf{v}_{A_3/A_2}$ ; however, if the observer is in link 3, it is possible to identify the direction of the velocity  ${}^3\mathbf{v}_{A_2/A_3}$  because the pin at  $A$  is constrained to move along the straight slot in link 3. Therefore, the direction of the velocity  ${}^3\mathbf{v}_{A_2/A_3}$  must be along the slot. Because we can determine the direction of  ${}^3\mathbf{v}_{A_2/A_3}$  by inspection, Eq. (3.29) is more useful than Eq. (3.30).

In problems such as this, it is important to identify clearly the links relative to which the velocity directions can be identified. The same links can be used for the subsequent acceleration analysis, and it is usually much easier to visualize velocities than it is to visualize accelerations.

After Eq. (3.29) is solved for the unknowns,  $\mathbf{v}_{A_3}$  will be known. Then  $\mathbf{v}_{B_3}$  can be found from the velocity image of link 3 using  $O_B$ ,  $A_3$ , and  $B_3$ . Knowing  $\mathbf{v}_{B_3}$ , which is the same as  $\mathbf{v}_{B_4}$  we can write the following equation for the velocity of  $C_4$ :

$$\mathbf{v}_{C_4} = \mathbf{v}_{B_4} + \mathbf{v}_{C_4/B_4} \quad (3.31)$$

Because the directions of  $\mathbf{v}_{C_4}$  and  $\mathbf{v}_{C_4/B_4}$  are known, we can solve Eq. (3.31) for the unknowns. After Eqs. (3.29) and (3.31) are solved, we can compute the angular velocities of links 3 and 4 from

$$\mathbf{v}_{B_3/O_B} = \boldsymbol{\omega}_3 \times \mathbf{r}_{B_3/O_B}$$

and

$$\mathbf{v}_{C_4/B_4} = \boldsymbol{\omega}_4 \times \mathbf{r}_{C_4/B_4}$$

For the acceleration analysis, we need only differentiate Eqs. (3.29) and (3.31). The results are

$$\mathbf{a}_{A_2} = \mathbf{a}_{A_3} + \mathbf{a}_{A_2/A_3}$$

and

$$\mathbf{a}_{C_4} = \mathbf{a}_{B_4} + \mathbf{a}_{C_4/B_4}$$

Expanding the equations in terms of vectors relative to moving coordinate systems, we obtain

$$\mathbf{a}_{A_2/O_4}^r + \mathbf{a}_{A_2/O_4}^t = \mathbf{a}_{A_3/O_B}^r + \mathbf{a}_{A_3/O_B}^t + {}^3\mathbf{a}_{A_2/A_3} + 2\left(\boldsymbol{\omega}_3 \times {}^3\mathbf{v}_{A_2/A_3}\right) \quad (3.32)$$



and

$$\mathbf{a}_{C_4} = \mathbf{a}_{B_3/O_B} + \mathbf{a}_{C_4/B_4}^r + \mathbf{a}_{C_4/B_4}^t \quad (3.33)$$

where

$$\mathbf{a}_{A_2/O_A}^r = r_{A_2/O_A} \omega_2^2 \text{ from } A \text{ to } O_A$$

$$\mathbf{a}_{A_2/O_A}^t = \alpha_2 \times r_{A_2/O_A} \text{ perpendicular to } \overrightarrow{AO_A}$$

$$\mathbf{a}_{A_3/O_B}^r = r_{A_3/O_B} \omega_2^2 \text{ from } A \text{ to } O_B$$

$$\mathbf{a}_{A_3/O_B}^t = \alpha_3 \times r_{A_3/O_B} \text{ (}\alpha_3 \text{ is unknown but the result is perpendicular to } \overrightarrow{AO_B}\text{)}$$

${}^3\mathbf{a}_{A_2/A_3}$  has a magnitude that is unknown but its direction is along the slot in link 3

$2(\boldsymbol{\omega}_3 \times {}^3\mathbf{v}_{A_2/A_3})$  is the Coriolis acceleration perpendicular to  ${}^3\mathbf{v}_{A_2/A_3}$

$\mathbf{a}_{C_4}$  is along the slider path of link 5

$\mathbf{a}_{B_3/O_B}$  is found by acceleration image of link 3

$$\mathbf{a}_{C_4/B_4}^r = r_{C_4/B_4} \omega_4^2 \text{ from } C \text{ to } B$$

$\mathbf{a}_{C_4/B_4}^t = \alpha_4 \times r_{C_4/B_4}$  has a magnitude that is unknown but a direction that is perpendicular to  $\overrightarrow{CB}$

Based on the position and velocity analyses, there will be only two unknown magnitudes in Eqs. (3.31) and (3.33). All of the directions will be known. Therefore, the equations can be solved.

### Steps

1. Draw linkage to scale as shown in Fig. 3.11.
2. Compute  $v_{A_2}$ , and plot  $v_{A_2}$  normal to  $\overrightarrow{O_A A}$  as  $\overrightarrow{oa_2}$ .  
 $\omega_2 = 10 \times 2\pi/60 = 1.0472 \text{ rad/s CCW}$   
 $v_{A_2} = \omega_2 \times r_{A_2/O_A} \times 10 = 10.472 \text{ in/s perpendicular to } AO_A \text{ in the direction shown in Fig. 3.11.}$
3. Draw a line through  $a_2$  parallel to  $\overrightarrow{O_B B}$ .
4. Draw a line through  $o$  normal to  $\overrightarrow{O_B A_3}$ . The intersection with the line from step 3 gives point  $a_3$ .
5. Locate  $b_3$  using the velocity image  $\frac{ob_3}{oa_3} = \frac{O_B B}{O_B A}$ .  
 $ob_3 = 7.26 \times (30/26.48) = 8.22 \text{ in/s}$
6. Draw a line through  $b_3$  normal to  $\overrightarrow{BC}$ .
7. Draw a line through  $o$  parallel to the slide. Its intersection with the line drawn in step 6 gives point  $c_4$ .
8. Measure  $v_{C_4} = oc_4$ ,  $v_{A_2/A_3} = \overrightarrow{a_2 a_3}$  and  $v_{C_4/B_4} = \overrightarrow{c_4 b_4}$ .  
 $v_{C_4} = 11.06 \text{ in/s}$ ,  $v_{A_2/A_3} = 5.09 \text{ in/s}$ ,  $v_{C_4/B_4} = 2.823 \text{ in/s}$
9. Compute  $\omega_3 = v_{A_3/O_B}/r_{A_3/O_B}$  and  $\omega_4 = v_{C_4/B_4}/r_{C_4/B_4}$ .  
 $\omega_3 = (9.07)/(26.37) = 0.344 \text{ rad/s CCW}$   
 $\omega_4 = 2.823/5 = 0.565 \text{ rad/s CCW}$

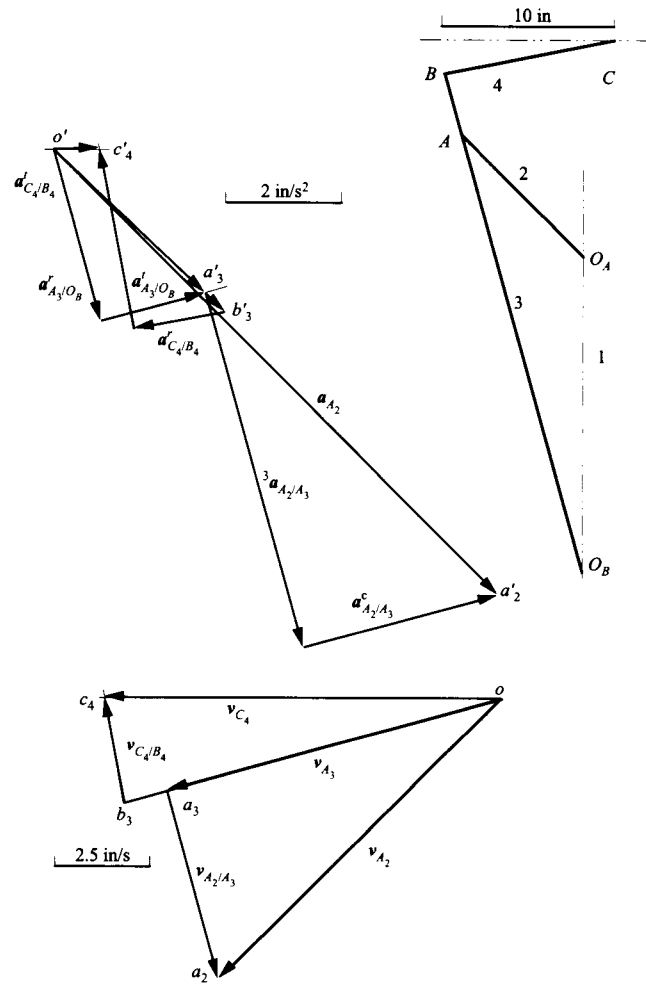


FIGURE 3.11 Solution for Example 3.1.

10. Get the senses of  $\omega_3$  and  $\omega_4$  by looking at the directions of rotation of  $r_{A_3/O_B}$  and  $r_{C_4/B_4}$  needed to get the respective relative velocity directions.
11. Compute  $a_{A_2}$  and plot it as  $\overline{o'a'}$ .

$$a_{A_2} = |r_{A_2/O_A}| |\omega_2|^2 = 10 \times 1.0472^2 = 10.97 \text{ in/s}^2$$

12. Compute  $a_{A_2/A_3}^C = 2(\omega_3)(v_{A_2/A_3})$  and get the sense of  $a_{A_2/A_3}^C$  by rotating  $(v_{A_2/A_3})$  90° in the  $\omega_3$  direction. Plot it with the tip at  $a'_2$ .

$$a_{A_2/A_3}^C = 2 \times 5.09 \times 0.344 = 3.50 \text{ in/s}^2$$

13. Draw a line normal to  $a_{A_2/A_3}^C$  and through the tail of  $a_{A_2/A_3}^C$ . This line corresponds to  ${}^3a_{A_2/A_3}$  that is along the slot.

14. Compute  $\mathbf{a}_{A_3/O_B}^r$  and plot it from  $o'$  in the  $\overline{A_3O_B}$  direction.

$$\mathbf{a}_{A_3/O_B}^r = \left| r_{A_3/O_B} \right| \left| \omega_3 \right|^2 = 26.37 \times 0.344^2 = 3.12 \text{ in/s}^2$$

15. Draw a line through the tip of  $\mathbf{a}_{A_3/O_B}^r$  normal to  $\overline{O_B A_3}$ . This vector corresponds to  $\mathbf{a}_{A_3/O_B}^t$ . Its intersection with the line drawn in step 13 gives point  $a'_3$ .

16. Locate point  $b'_3$  using the acceleration image  $\frac{o'b'_3}{o'a'_3} = \frac{O_B B}{O_B A}$ .

$$o'b'_3 = 3.62 \times (30/26.37) = 4.12 \text{ in/s}^2$$

17. Plot  $\mathbf{a}_{C_4/B_4}^r$  from point  $b'_3$  parallel to  $\overline{CB}$ .

$$\mathbf{a}_{C_4/B_4}^r = \left| r_{C_4/B_4} \right| \left| \omega_4 \right|^2 = 5 \times 0.608^2 = 1.85 \text{ in/s}^2$$

18. Draw a line through the tip of  $\mathbf{a}_{C_4/B_4}^r$  normal to  $\overline{CB}$ .

This vector corresponds to  $\mathbf{a}_{C_4/B_4}^t$ .

19. Draw a line through  $o'$  parallel to the slide. Its intersection with the line generated in step 18 gives point  $c'_4$ .

20. Measure  $\mathbf{a}_{A_3/O_B}^t$  and  $\mathbf{a}_{C_4/B_4}^t$ .

$$\mathbf{a}_{A_3/O_B}^t = 1.870 \text{ in/s}^2 \text{ and } \mathbf{a}_{C_4/B_4}^t = 3.197 \text{ in/s}^2$$

21. Compute  $\alpha_3 = \frac{\mathbf{a}_{A_3/O_B}^t}{r_{A_3/O_B}}$  and  $\alpha_4 = \frac{\mathbf{a}_{C_4/B_4}^t}{r_{C_4/B_4}}$  and get the senses of these angular accelerations by considering the directions of rotation needed to rotate the position vectors in the directions of  $\mathbf{a}_{A_3/O_B}^t$  and  $\mathbf{a}_{C_4/B_4}^t$ , respectively.

$$\alpha_3 = 1.870 / (26.37) = 0.071 \text{ rad/s}^2 \text{ CW}$$

$$\alpha_4 = 3.197 / 5 = 0.640 \text{ rad/s}^2 \text{ CCW}$$

22. Measure  $\mathbf{a}_{C_4}$ .

$$\mathbf{a}_{C_4} = 0.7986 \text{ in/s}^2 \text{ directed to the right}$$

One of the useful features of the quick-return linkage is a long range of motion with relatively uniform velocity on the forward stroke. The small value of  $\mathbf{a}_{C_4}$  is indicative of this property.

## 3.6 ROLLING CONTACT

Rolling contact is quite often used in practical linkages. In addition to the obvious case of a wheel rolling on a surface or a rail, rolling contact between a cam and a roller follower is a common example. Also, the pitch cylinders of spur and helical gear pairs and the pitch cones of bevel gear pairs can be considered to be in pure rolling contact. In that case, although the actual physical contact between the gear teeth is a general combination of rolling and sliding, the gear pair can be modeled as a pair of simple elements in pure rolling contact from the point of view of investigating gross kinematic properties.

Rolling contact can be approached in two different ways, depending on the level of detail desired. If the velocities and accelerations of the rolling elements themselves are immaterial, it is possible to solve for the velocities and accelerations of the other links in a

rolling-contact problem by replacing the actual linkage with a virtual linkage in which the rolling elements are replaced by a single link with length equal to the sum of their radii of curvature. If the velocities and accelerations of all the links are important, then one or more additional relative velocity (or angular velocity) relations are necessary to obtain the angular velocities of one or more rolling links. Both approaches will be discussed.

### 3.6.1 Basic Kinematic Relationships for Rolling Contact

Figure 3.12 shows two rigid bodies in rolling contact. The bodies are arbitrarily taken to be links 2 and 4. The contact location is  $B$ , and the centers of curvature of the two bodies corresponding to  $B_2$  and  $B_4$  are  $O_2$  and  $O_4$ , respectively. At the point of contact for two bodies rolling on each other, there is no relative sliding between the two points ( $B_2$  and  $B_4$ ) at the location of contact. Because  $B_2$  and  $B_4$  are not only momentarily coincident but also in rolling contact, they have the same velocity, and their relative velocity must be zero. This means that

$$\mathbf{v}_{B_2} = \mathbf{v}_{B_4}$$

and

$$\mathbf{v}_{B_2/B_4} = {}^4\mathbf{v}_{B_2/B_4} = {}^4\mathbf{v}_{B_2} = 0$$

Note that this is exactly the same velocity condition as that for a revolute joint. Therefore, for velocities *only*, the point of rolling contact can be treated as a revolute joint. However, this is not true for accelerations.

The relative acceleration  $\mathbf{a}_{B_2/B_4}$  is usually not zero, but it is independent of the coordinate system. Therefore,

$$\mathbf{a}_{B_2/B_4} = {}^4\mathbf{a}_{B_2/B_4} = {}^4\mathbf{a}_{B_2} \quad (3.34)$$

From Eq. (3.34), it is apparent that the direction of  ${}^1\mathbf{a}_{B_2/B_4}$  is the same as the direction of  ${}^4\mathbf{a}_{B_2}$ , which is the absolute acceleration of point  $B_2$  observed from link 4. Therefore, it is useful to determine the path that  $B_2$  traces on 4 (or  $B_4$  traces on 2) to determine the direction of the acceleration of  ${}^4\mathbf{a}_{B_2}$ . To do this, first imagine that link 2 is a circle and link 4 is a straight line.

From experience (for example, from looking at a bicycle tire reflector at night) we know that the path of  $B_2$  will look as shown in Fig. 3.13. That is, the path forms a cusp at the contact location. The cusp will approach the contact point in a direction that is tangent to the normal to the contacting surfaces at the contact point, and the cusp will also leave the contact point in a direction that is tangent to the common normal. This means that the accel-

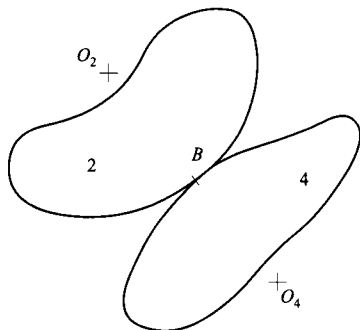
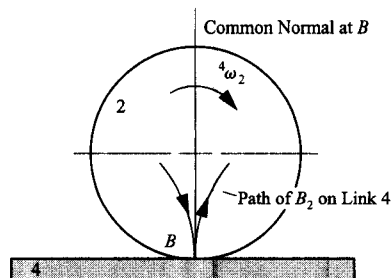


FIGURE 3.12 Two links in rolling contact.

FIGURE 3.13 Path of motion of  $B^2$  relative to link 4.

eration must be along the common normal at the point of contact. The same kind of relationship also applies for general bodies.

To conduct an acceleration analysis of mechanisms involving rolling contact, it is necessary to determine both the magnitude and direction of the relative acceleration between the two contact points. Because we know that the direction of the relative accelerations will be along the common normal at the point of contact, we need only determine the magnitude.

To do this, first consider a general rigid body  $R$ . If the contour of the rigid body is known at any given point on the contour, which must be the case for a kinematic analysis, the center of curvature,  $O_R$ , for that body can be found. If a circle of radius  $O_R B$  is drawn, that circle will be tangent to the contour at  $B$ , and it will share three points (separated by infinitesimal distances) with the curve  $R$ . This circle is called the osculating circle to the curve at point  $B$ , and the circle is a unique property of the curve for the point considered. An example is shown in Fig. 3.14.

If we consider two general links (2 and 4) in rolling contact, we can draw the osculating circle for each curve. As the two bodies roll together, the three points shared by the osculating circles will be in contact with each other. Therefore, for two differentially separated time periods, the curves could be replaced by their osculating circles. Because only two differentially separated time periods must be considered for accelerations, we can replace the original curves with their osculating circles, and the kinematic results for position, velocity, and acceleration will remain unchanged. If higher derivatives than accelerations are desired, however, we cannot replace the original surfaces with their osculating circles. Obviously, a different osculating circle may be required for each contact position if the surface of body  $R$  is general. However, for a kinematic analysis to be conducted, the geometry of the surface must be known, and therefore the osculating circle corresponding to each point on the periphery can be identified.

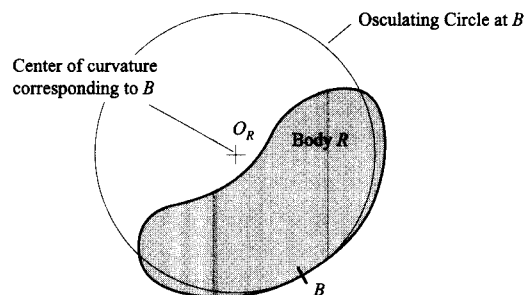


FIGURE 3.14 Osculating circle.

The replacement of the general surface with osculating circles is extremely useful in kinematics whenever higher pairs are involved. The special properties of circles make it relatively simple to analyze linkages with rolling and cam joints using this approach.

Because we can replace the two curves with their osculating circles, we can connect the two centers of curvature by a virtual link pinned to the two bodies at the centers of curvature, and the two bodies can still move relative to each other. This is precisely the condition existing when two gears in a standard transmission are meshed. For the sake of discussion, let the two bodies again be links 2 and 4 and let the virtual link be designated as  $x$ , as shown in Fig. 3.15. With this arrangement, we are now in a position to compute the relative acceleration  ${}^4a_{B_2/B_4}$ . To do this, we will use Eq. (3.34) and compute  $a_{B_2/B_4}$ , which is equal to  ${}^4a_{B_2/B_4}$ .

As with any planar vector, the acceleration  $a_{B_2/B_4}$  can be resolved into two orthogonal components. It is convenient to resolve the vector into one component along the common normal to the two curves at  $B$  and another along the common tangent. That is,

$$a_{B_2/B_4} = a_{B_2/B_4}^n + a_{B_2/B_4}^t$$

However, we know from our earlier discussion that the relative acceleration must lie along the common normal. Therefore, the tangential component must be zero, and the total relative acceleration between  $B_2$  and  $B_4$  can be represented as

$$a_{B_2/B_4} = a_{B_2/B_4}^n$$

We can compute the normal acceleration by writing the relative accelerations among the points  $B_2$ ,  $B_4$ ,  $O_2$ , and  $O_4$ . That is,

$$a_{B_2/B_4} = a_{B_2/O_2}^n + a_{(O_2)_x/(O_4)_x}^n + a_{O_4/B_4}^n$$

Now consider individually each term on the right-hand side of the equation. Each term will be a function of velocities and can be computed in a variety of ways. For example,

$$a_{B_2/O_2}^n = -\omega_2^2 r_{B/O_2} = \left| \omega_2 v_{B/O_2} \right| n = \frac{v_{B_2/O_2}^2}{r_{B/O_2}} n \quad (\text{from } B \text{ towards } O_2)$$

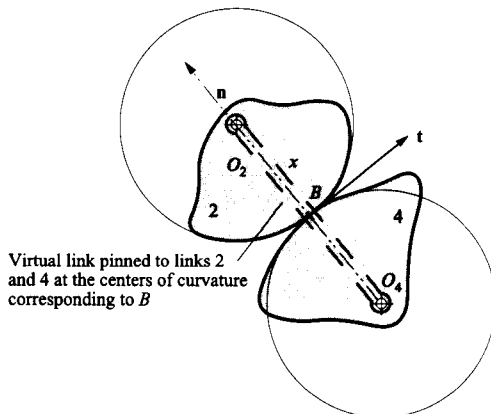


FIGURE 3.15 Virtual link pinned at the centers of curvature of the two bodies in rolling contact.

and

$$\mathbf{a}_{O_4/B_4}^n = -\omega_4^2 \mathbf{r}_{O_4/B_4} = \left| \omega_4 v_{O_4/B_4} \right| \mathbf{n} = \frac{v_{O_4/B_4}^2}{|\mathbf{r}_{O_4/B_4}|} \mathbf{n} \quad (\text{from } O_4 \text{ towards } B)$$

Similarly,

$$\mathbf{a}_{(O_2)_x/(O_4)_x}^n = -\omega_x^2 \mathbf{r}_{O_2/O_4} = -\left| \omega_x v_{O_2/O_4} \right| \mathbf{n} = -\frac{v_{O_2/O_4}^2}{|\mathbf{r}_{O_2/O_4}|} \mathbf{n} \quad (\text{from } O_2 \text{ towards } O_4) \quad (3.35)$$

To evaluate the first two expressions on the right-hand side of Eq. (3.35), we need to develop an expression for  $\omega_x$ . To do this, we can derive relative velocity expressions among  $B_2$ ,  $B_4$ ,  $O_2$ , and  $O_4$ . Considering links 2, 4, and  $x$ , we have

$$\begin{aligned} \mathbf{v}_{B_2} &= \mathbf{v}_{O_2} + \mathbf{v}_{B_2/O_2} = \mathbf{v}_{O_2} + \omega_2 \times \mathbf{r}_{B/O_2} \\ \mathbf{v}_{B_4} &= \mathbf{v}_{O_4} + \mathbf{v}_{B_4/O_4} = \mathbf{v}_{O_4} + \omega_4 \times \mathbf{r}_{B/O_4} \\ \mathbf{v}_{O_2} &= \mathbf{v}_{O_4} + \mathbf{v}_{O_2/O_4} = \mathbf{v}_{O_4} + \omega_x \times \mathbf{r}_{O_2/O_4} \end{aligned}$$

Combining these equations and recognizing that  $\mathbf{v}_{B_2} = \mathbf{v}_{B_4}$ , we get

$$\omega_x \times \mathbf{r}_{O_2/O_4} = \mathbf{v}_{O_2} - \mathbf{v}_{O_4} = \mathbf{v}_{O_2/O_4} = \omega_4 \times \mathbf{r}_{B/O_4} - \omega_2 \times \mathbf{r}_{B/O_2} \quad (3.36)$$

Recognizing that  $\mathbf{r}_{B/O_2} = -\mathbf{r}_{O_2/B}$ , we can also write Eq. (3.36) as

$$\omega_x \times \mathbf{r}_{O_2/O_4} = \omega_4 \times \mathbf{r}_{B/O_4} + \omega_2 \times \mathbf{r}_{O_2/B} \quad (3.37)$$

The magnitude of  $\omega_x$  is given by

$$\omega_x = \frac{|\omega_4 \times \mathbf{r}_{B/O_4} + \omega_2 \times \mathbf{r}_{O_2/B}|}{|\mathbf{r}_{O_2/O_4}|} = \frac{|\omega_2 \times \mathbf{r}_{O_2/B} + \omega_4 \times \mathbf{r}_{B/O_4}|}{|\mathbf{r}_{O_2/B} + \mathbf{r}_{B/O_4}|}$$

If the direction is of interest, it can be determined from the vectors in Eq. (3.37).

To summarize, in rolling contact problems, we know that the two contact points (e.g.,  $B_2$  and  $B_4$ ) have the same velocity. Also, given the acceleration of one of the points, say  $B_4$ , the acceleration of the other point can be computed from

$$\mathbf{a}_{B_2} = \mathbf{a}_{B_4} + \mathbf{a}_{B_2/B_4}^n$$

where  $\mathbf{a}_{B_2/B_4}^n$  can be computed using *any* of the following:

$$\mathbf{a}_{B_2/B_4}^n = \left( \frac{v_{B_2/O_2}^2}{|\mathbf{r}_{B_2/O_2}|} - \frac{v_{O_2/O_4}^2}{|\mathbf{r}_{O_2/O_4}|} + \frac{v_{O_4/B_4}^2}{|\mathbf{r}_{O_4/B_4}|} \right) \mathbf{n} \quad (3.38)$$

or

$$\mathbf{a}_{B_2/B_4}^n = \left( \omega_2^2 |\mathbf{r}_{B/O_2}| - \omega_x^2 |\mathbf{r}_{O_2/O_4}| + \omega_4^2 |\mathbf{r}_{O_4/B}| \right) \mathbf{n} \quad (3.39)$$

or

$$\mathbf{a}_{B_2/B_4}^n = \left( \left| \omega_2 v_{B/O_2} \right| - \left| \omega_x v_{O_2/O_4} \right| + \left| \omega_4 v_{O_4/B} \right| \right) \mathbf{n} \quad (3.40)$$

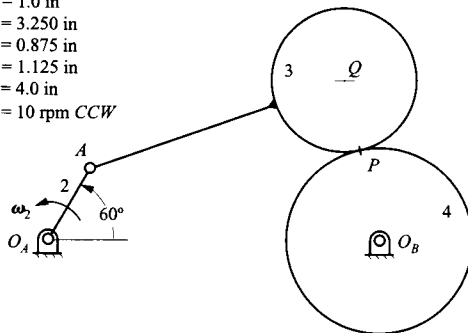
If one of the rolling surfaces is flat, the radius of curvature will approach infinity, and the corresponding acceleration term will become zero. For example, if the rolling surface for link 2 is flat, then  $O_2$  is at infinity, and the acceleration expressions reduce to

$$\mathbf{a}_{B_2/B_4}^n = \frac{v_{O_4/B_4}^2}{r_{O_4/B_4}} \mathbf{n} = \omega_4^2 r_{O_4/B} = \left| \omega_4 v_{O_4/B} \right| \mathbf{n} \quad (\text{from } O_4 \text{ towards } B)$$

**EXAMPLE 3.2**  
**Analysis of**  
**Linkage with a**  
**Rolling-Contact**  
**Joint**

In the linkage shown in Fig. 3.16, link 4 is a gear, pivoted at  $O_B$ . Link 3 is a gear meshing with 4 and has a lever fixed to it that is hinged to link 2 at  $A$ . Link 2 is driven at a constant angular velocity of 10 rad/s CCW. Find the angular acceleration of gear 4.

- $AO_A = 1.0$  in
- $AQ = 3.250$  in
- $PQ = 0.875$  in
- $O_B P = 1.125$  in
- $O_A O_B = 4.0$  in
- $\omega_2 = 10$  rpm CCW



**FIGURE 3.16** The linkage of Example 3.2. This is an example of a geared five-bar linkage. Geared five-bar and six-bar linkages are used quite frequently as alternatives to four-bar linkages. They allow more flexibility in synthesis than four-bar linkages because they have more dimensions that can be varied.

**Solution**

In this instance we cannot ignore the acceleration of either of the two contacting bodies. The angular acceleration of gear 3 is the same as that of arm  $AQ$  to which it is rigidly affixed. The angular acceleration of gear 4 is the quantity to be found.

For the velocity analysis, the equations to be solved are

$$\mathbf{v}_{A_2/O_A} = \boldsymbol{\omega}_2 \times \mathbf{r}_{A_2/O_A}$$

$$\mathbf{v}_{P_4/O_B} = \mathbf{v}_{A_3} + \mathbf{v}_{P_3/A_3}$$

For the acceleration analysis, the corresponding equations are

$$\mathbf{a}_{A_2/O_A} = \mathbf{a}_{A_2/O_A}^r + \mathbf{a}_{A_2/O_A}^t$$

$$\mathbf{a}_{P_4/O_B}^r + \mathbf{a}_{P_4/O_B}^t = \mathbf{a}_{A_2/O_A} + \mathbf{a}_{P_3/A_3}^r + \mathbf{a}_{P_3/A_3}^t + \mathbf{a}_{P_3/A_3}^n$$

Here the unknowns are the magnitudes of the two transverse components,  $\mathbf{a}_{P_3/A_3}^t$  and  $\mathbf{a}_{P_4/O_B}^t$ .

**Steps**

1. Draw the linkage to scale as shown in Fig. 3.17. To do this, first draw link 2 and locate point  $A$ . Next find the center  $Q$ , knowing that it is on a circle of radius  $AQ$  centered at  $A$  and also on a circle of radius  $QO_B$  centered at  $O_B$ . After locating  $Q$ , draw the line  $AQ$  and the circles corresponding to the pitch circles of the two gears.

2. Compute  $\mathbf{v}_{A_2}$  and plot as  $\overline{oa}$ .

$$\mathbf{v}_{A_2} = \boldsymbol{\omega}_2 \times \mathbf{r}_{A_2/O_2} = 10 \text{ in/s, } \mathbf{v}_{A_2} \text{ is normal to } \overline{O_A A}.$$



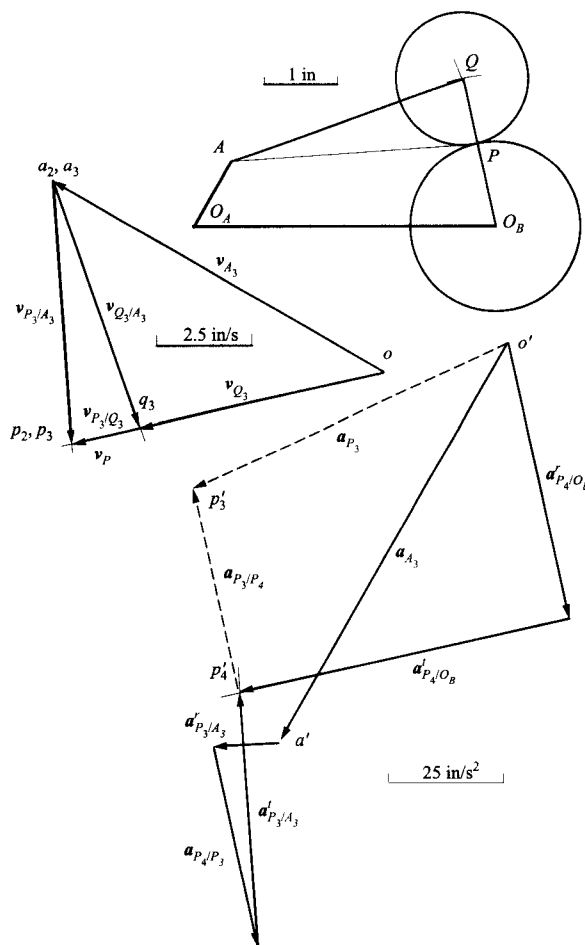


FIGURE 3.17 The graphical solution of Example 3.2.

3. Draw a line through  $o$  normal to  $\overline{O_B P}$ .
4. Draw line  $\overline{AP}$ .
5. Draw a line through  $a_2, a_3$  normal to  $\overline{AP}$ . The intersection of this line with the line generated in step 3 gives the point  $P$ . Notice that since the bar  $\overline{AQ}$  is rigidly fixed to gear 3, line  $\overline{AP}$  is fixed in member 3. Although at any instant, the point at  $P_3$  is fixed to member 3, a different  $P$  (and different point) is involved for each position of the linkage.
6. Draw a line through  $a_3$  normal to  $\overline{AQ}$ . The intersection of this line with the line generated in step 3 gives the point  $q_3$ . Point  $q_3$  could also have been located from points  $a_3$  and  $p_3$  by using the velocity image theorem.
7. Compute  $\omega_3 = v_{P_3/A_3}/r_{P_3/A_3}$  and  $\omega_4 = v_{P_4/O_B}/r_{O_B/P}$  and find the senses needed to give the directions of  $v_{P_3/A_3}$  and  $v_{P_4/O_B}$ . Because of the pure rolling condition of the pitch circles of the gears, the velocity of point  $P$  is the same regardless of whether it is considered to be in member 3 or member 4.

$$\omega_3 = 6.85/3.258 = 2.10 \text{ rad/s CW}$$

$$\omega_4 = 38.32/1.125 = 7.39 \text{ rad/s CCW}$$

8. Compute  $\mathbf{a}_{A_3} = \mathbf{a}_{A_3/O_4}^r$  and plot as  $\overline{o'a'}$ .

$$a_{A_3} = r_{A_2/O_2} \times \omega_2^2 = 1 \times 10^2 = 100 \text{ in/s}^2$$

9. Compute and plot  $\mathbf{a}_{P_3/A_3}^r$  in the  $\overline{PA}$  direction from point  $a'$ .

$$a_{P_3/A_3}^r = AP \times \omega_3^2 = 3.258 \times 2.10^2 = 14.39 \text{ in/s}^2$$

10. Compute  $\mathbf{a}_{P_4/P_3}$  using the equation form given in Eq. (3.54). Then,

$$a_{P_4/P_3}^n = \frac{|v_{P_4/O_B}|^2}{r_{P_4/O_B}} + \frac{|v_{O_B/Q_3}|^2}{r_{O_B/Q_3}} + \frac{|v_{Q_3/P_3}|^2}{r_{Q_3/P_3}} = \frac{|8.32|^2}{1.125} + \frac{|6.54|^2}{2} + \frac{|1.92|^2}{0.875}$$

$$(P \text{ to } O_B) \quad (O_B \text{ to } Q_3) \quad (Q_3 \text{ to } P_3) \quad (P \text{ to } O_B) \quad (O_B \text{ to } Q_3) \quad (Q_3 \text{ to } P_3)$$

By arbitrarily taking direction  $\overline{PO_B}$  as positive, the signs of the individual terms can be identified. Then,

$$a_{P_4/P_3} = 61.53 - 21.38 = 4.21 = 44.36 \text{ in/s}^2$$

Note also that  $\mathbf{a}_{P_4/P_3} = -\mathbf{a}_{P_3/P_4}$  and has the direction from the center of wheel 3 toward the center of wheel 4. Plot  $\mathbf{a}_{P_4/P_3}$  from the tip of  $\mathbf{a}_{P_3/A_3}^r$ .

11. Draw a line through the tip of vector  $\mathbf{a}_{P_4/P_3}$  normal to  $\overline{AP}$ .

12. Compute  $\mathbf{a}_{P_4/O_B}^r$  and plot  $\mathbf{a}_{P_4/O_B}^r$  from  $o'$  in the  $\overline{PO_B}$  direction.

$$a_{P_4/O_B}^r = r_{P_4/O_B} \times \omega_4^2 = 1.125 \times 7.39^2 = 61.4 \text{ in/s}^2$$

13. Draw a line through the tip of vector  $\mathbf{a}_{P_4/O_B}^r$  normal to  $\overline{O_B P}$ . The intersection of this line with that drawn in step 11 gives  $p'_4$ .

14. Compute  $\alpha_4 = a_{P_4/O_B}^b / r_{P_4/O_B}$  and find the sense needed to give the direction of  $\mathbf{a}_{P_4/O_B}^b$ .

$$\alpha_4 = 74.25 / 1.125 = 66.0 \text{ rad/s}^2 \text{ CCW}$$

Note that this construction, with the vectors in the order shown, gives the correct position for  $p'_4$  but not for  $p'_3$ . This does not matter for the present purpose. However, if the correct position of  $p'_3$  were required, either to get the absolute acceleration or to construct the acceleration image, it would be obtained by plotting  $\mathbf{a}_{P_3/P_4}$  from  $p'_4$  as shown in Fig. 3.17.

Although the acceleration of the contacting point in one body relative to that in the other has been worked out assuming circular contacting profiles, it can also be used if the profiles are not circular. The radius of the circular profile is simply replaced with the osculating circle of the profile at the point of contact.

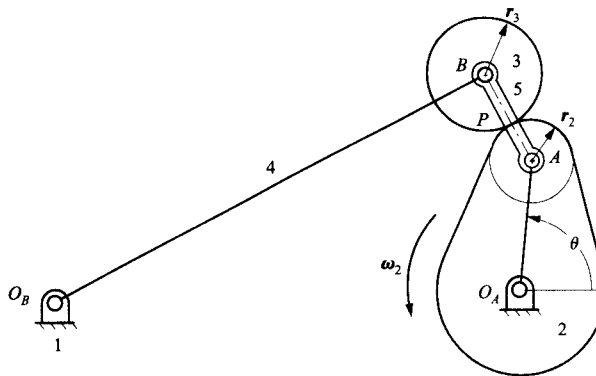
### 3.6.2 Modeling Rolling Contact Using a Virtual Linkage

As a second example of rolling contact, we will consider the plate cam with roller follower shown in Fig. 3.18. In this mechanism, we are given the angular velocity and acceleration of link 2, and we wish only to know the angular velocity and acceleration of link 4. We are not interested in the velocity and acceleration of link 3. When this is the case, we can model the linkage with a virtual link between the centers of curvature of links 2 and 3 corresponding to the contact point  $P$ . The cam-follower mechanism can then be analyzed as the virtual four-bar linkage  $O_A A B O_B$ . Line  $O_A A$  is fixed to link 2, so the angular velocity and acceleration of  $O_A A$  will be the angular velocity and acceleration for link 2.

**EXAMPLE 3.3**  
**Analysis of a**  
**G geared Linkage—**  
**Rolling**  
**Contact**

Find the angular velocity and angular acceleration of the arm (link 4) of the linkage in Fig. 3.18 for  $\theta = 90^\circ$  when the cam, 2, is rotated CCW with constant angular velocity 1000 rpm. The following basic dimensions are given for the mechanism:

$$O_A O_B = 4.0 \text{ in}, O_B B = 4.25 \text{ in}, r_2 = 0.5 \text{ in}, r_3 = 2.5 \text{ in}, O_A A = 1.153 \text{ in}, AB = 0.901 \text{ in}$$



**FIGURE 3.18** A plate cam with roller follower. For given angular velocity and acceleration of cam 2, the angular velocity and angular acceleration of the arm 4 can be found by replacing the linkage with the virtual four-bar linkage  $O_A A B O_B$ . Here point  $A$  is the center of curvature of the cam profile at the contact point  $P$ .

**Solution**

The steps to analyzing this mechanism are the same as those required for the four-bar linkage in Example 2.1. The velocity equations that must be solved graphically are

$$\mathbf{v}_{A_2/O_2} = \boldsymbol{\omega}_2 \times \mathbf{r}_{A_2/O_2}$$

$$\mathbf{v}_{B_4/O_B} = \mathbf{v}_{A_2/O_A} + \mathbf{v}_{B_5/A_5}$$

where the virtual link is designated as link 5. The acceleration equations that must be solved are

$$\mathbf{a}_{A_2/O_2} = \mathbf{a}_{A_2/O_2}^r + \mathbf{a}_{A_2/O_2}^t$$

$$\mathbf{a}_{B_4/O_B}^r + \mathbf{a}_{B_4/O_B}^t = \mathbf{a}_{A_2/O_A}^r + \mathbf{a}_{A_2/O_A}^t + \mathbf{a}_{B_5/A_5}^r + \mathbf{a}_{B_5/A_5}^t$$

**Steps**

1. Draw the mechanism to scale as shown in Fig. 3.19. Note that, for this analysis, we need draw only the virtual mechanism.

2. Compute  $\omega_2$ .

$$\omega_2 = 1000 \times 2\pi/60 = 104.75 \text{ rad/s}$$

3. Compute and plot  $\mathbf{v}_{A_2/O_A}$ .

$$\mathbf{v}_{A_2/O_A} = \boldsymbol{\omega}_2 \times \mathbf{r}_{A_2/O_A} = 104.72 \times 1.153 = 120.74 \text{ in/s normal to } \overrightarrow{O_A A}$$

4. Solve the velocity equation graphically and measure  $\mathbf{v}_{B_4/O_B}$  and  $\mathbf{v}_{B_5/A_5}$ .

$$\mathbf{v}_{B_4/O_B} = 38.95 \text{ in/s}; \mathbf{v}_{B_5/A_5} = 108.2 \text{ in/s}$$

5. Compute  $\omega_5$  and  $\omega_4$  and determine their senses.

$$\omega_5 = \mathbf{v}_{B_5/A_5} / r_{B_5/A_5} = 108.2/0.901 = 120.1 \text{ rad/s CW}$$

$$\omega_4 = \mathbf{v}_{B_4/O_B} / r_{B_4/O_B} = 38.95/4.25 = 9.16 \text{ rad/s CCW}$$

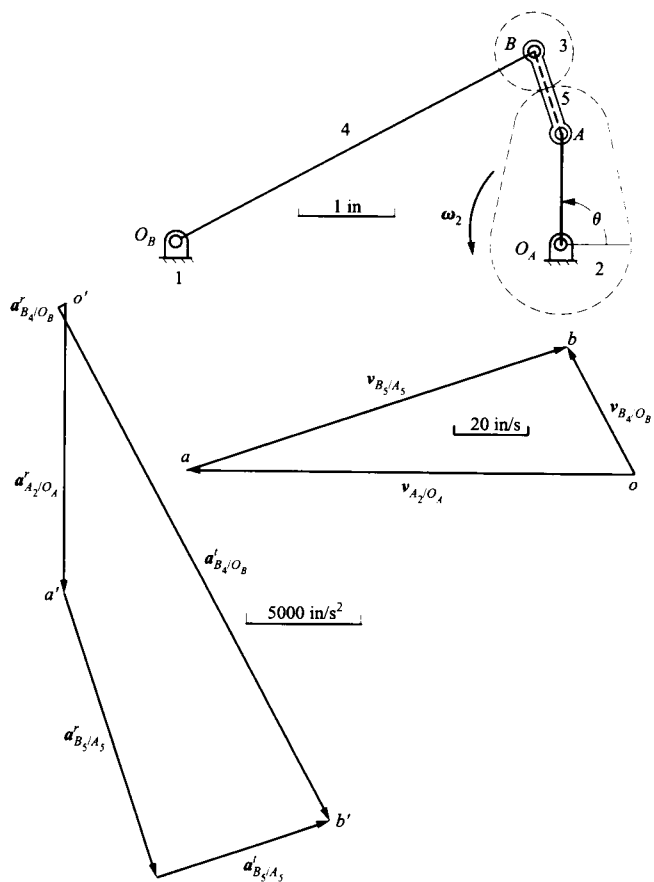


FIGURE 3.19 The velocity and acceleration polygons for Example 3.3.

Notice that  $\omega_5$  is the angular velocity of a *virtual* link containing the line  $AB$ .

6. Compute and plot  $\mathbf{a}_{A_2/O_A} = \mathbf{a}_{A_2/O_A}^r$ .

$$\mathbf{a}_{A_2/O_A}^r = r_{A_2/O_A} \times \omega_2^2 = 1.153 \times 104.7^2 = 12,640 \text{ in/s}^2 \text{ in the } \overrightarrow{AO_A} \text{ direction}$$

7. Compute and plot  $\mathbf{a}_{B_4/O_B}^r$  from point  $o'$  and  $\mathbf{a}_{B_3/A_5}^r$  from point  $a'$ .

$$\mathbf{a}_{B_4/O_B}^r = r_{B_4/O_B} \times \omega_4^2 = 4.25 \times 9.16^2 = 356.6 \text{ in/s}^2 \text{ in the } \overrightarrow{BO_B} \text{ direction}$$

$$\mathbf{a}_{B_3/A_5}^r = r_{B_3/A_5} \times \omega_5^2 = 0.901 \times 120.1^2 = 13,000 \text{ in/s}^2 \text{ in the } \overrightarrow{BA} \text{ direction}$$

8. Measure  $\mathbf{a}_{B_4/O_B}^t$ .

$$\mathbf{a}_{B_4/O_B}^t = 25,290 \text{ in/s}^2$$

9. Compute  $\alpha_4$  and determine its sense.

$$\alpha_4 = a_{B_4/O_B}^t / r_{B/O_B} = 25,290 / 4.25 = 4440 \text{ rad/s}^2 \text{ CW}$$

Notice that the reason this relatively simple approach can be used is that we are not interested in the angular acceleration of the roller, link 3. This is definitely not equal to the angular acceleration of the line  $AB$ , which, for convenience, was called the virtual link 5.

## 3.7 CAM CONTACT

The analysis of mechanisms with cam joints can be conducted either directly or through the use of equivalent linkages. We will look at the direct approach first.

### 3.7.1 Direct Approach to the Analysis of Cam Contact

In the general case of cam contact, there will be both rolling and sliding at the contact point, and this is probably the most typical type of higher pair contact between two bodies. If we look at two arbitrary bodies (e.g., 2 and 4 in Fig. 3.20) at the contact location  $B$ , we know  $B_2$  and  $B_4$  have the same coordinates:

$$\mathbf{r}_{B_2} = \mathbf{r}_{B_4}$$

However,

$$\mathbf{v}_{B_2} \neq \mathbf{v}_{B_4}$$

or

$$\mathbf{v}_{B_2/B_4} \neq 0$$

We can obtain some information on  $\mathbf{v}_{B_2/B_4}$  by recognizing that coincident points are involved and

$$\mathbf{v}_{B_2/B_4} = {}^4\mathbf{v}_{B_2/B_4} = {}^4\mathbf{v}_{B_2}$$

Therefore, to analyze the velocity of  $B_2$  relative to  $B_4$  or link 4, it is convenient to represent the velocity in terms of components in the tangential (t) and normal (n) directions relative to the tangent at the contact point as shown in Fig. 3.20. Then,

$$\mathbf{v}_{B_2/B_4} = {}^4\mathbf{v}_{B_2/B_4} = {}^4\mathbf{v}_{B_2}^n + {}^4\mathbf{v}_{B_2}^t$$

If the two bodies are rigid, there can be no component of velocity in the normal direction or the bodies would either penetrate each other or separate. Therefore, the normal component of the relative velocity must be zero, and the relative velocity direction must be along the common tangent to the two bodies at the point of contact. That is,

$${}^4\mathbf{v}_{B_2}^n = 0$$

and

$$\mathbf{v}_{B_2/B_4} = {}^4\mathbf{v}_{B_2}^t = \mathbf{v}_{B_2/B_4}^t$$

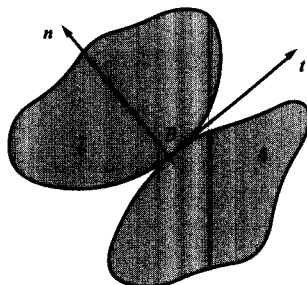


FIGURE 3.20 Cam contact.

We cannot determine anything more about  ${}^4v_{B_2/B_4}^t$ ; however, knowing the direction for the relative velocity usually provides sufficient information to conduct a velocity analysis.

We cannot determine anything about  $a_{B_2/B_4}$  directly; however, if we expand  $a_{B_2/B_4}$  into normal and tangential components, we can compute additional information about it. Then,

$$a_{B_2/B_4} = a_{B_2/B_4}^n + a_{B_2/B_4}^t$$

Note that there is no Coriolis term because the acceleration is defined in link 1 and not link 4. This is directly analogous to the case of rolling contact except that now the tangential component is not zero. However, by definition, we know the direction of the tangential component.

Using the same nomenclature as in the case of rolling contact (see Fig. 3.15), the normal component of relative acceleration is given by Eqs. (3.38), (3.39), or (3.40). For example,

$$a_{B_2/B_4}^n = \frac{|v_{B_2/O_2}|^2}{r_{B_2/O_2}} + \frac{|v_{O_2/O_4}|^2}{r_{O_2/O_4}} + \frac{|v_{O_4/B_4}|^2}{r_{O_4/B_4}}$$

(B to O<sub>2</sub>)    (O<sub>2</sub> to O<sub>4</sub>)    (O<sub>4</sub> to B)

If one of the rolling surfaces is flat, the relative position vector corresponding to the center of curvature will approach infinity, and the corresponding acceleration term will become zero. For example, if the surface for link 2 is flat, then O<sub>2</sub> is at infinity, and the expression for the normal component of acceleration reduces to

$$a_{B_2/B_4}^n = \frac{|v_{O_4/B_4}|^2}{r_{O_4/B_4}} \text{ from } O_4 \text{ to } B_4$$

**EXAMPLE 3.4**  
**Analysis of**  
**Mechanism with a**  
**Cam Joint**

Find the velocity and acceleration of the cam follower (link 3) given in Fig. 3.21 if the cam is rotating at a constant angular velocity of 100 rad/s CCW.

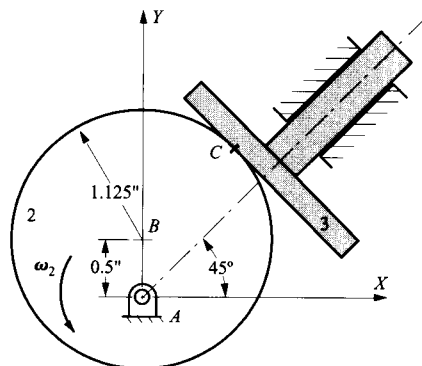


FIGURE 3.21 Cam and flat-faced follower.

**Solution**

To analyze the problem, we can determine the velocity and acceleration of any point on link 3 because *all* points on link 3 have the same velocity and the same acceleration. The point to choose is the contact point C<sub>3</sub>. To solve for the velocity and acceleration of C<sub>3</sub>, first find the velocity of point C<sub>2</sub>. Then

write the relative velocity expression between points  $C_2$  and  $C_3$  and solve for the velocity of  $C_3$ . The relevant equations are

$$v_{C_2} = v_{C_2/A_2} = \omega_2 \times r_{C/A}$$

and

$$v_{C_3} = v_{C_2} + v_{C_3/C_2}$$

Next solve for the velocity of  $B_2$  either directly or by image. This will be needed for the acceleration analysis. The acceleration equations that must be solved are

$$a_{C_2} = a_{C_2/A_2} = a_{C_2/A_2}^n + a_{C_2/A_2}^t$$

$$a_{C_3} = a_{C_2} + a_{C_3/C_2} = a_{C_2} + a_{C_3/C_2}^t + a_{C_3/C_2}^n$$

and

$$\left| a_{C_3/C_2}^n \right| = \left| a_{C_3/D_3}^n + a_{D_3/B_2}^n + a_{B_2/C_2}^n \right| = \frac{\left| v_{C_3/D_3} \right|^2}{\left| \infty \right|} + \frac{\left| v_{D_3/B_2} \right|^2}{\left| \infty \right|} + \frac{\left| v_{B_2/C_2} \right|^2}{\left| r_{B/C} \right|} = \frac{\left| v_{B_2/C_2} \right|^2}{\left| r_{B/C} \right|}$$

where  $D_3$  is the center of curvature of the cam follower surface and is located at infinity. The steps in solving the equations are given in the following.

#### Steps

1. Draw the mechanism to scale as shown in Fig. 3.22. To do this, draw the cam circle centered at  $B$ . Next locate point  $A$  at 0.5 in below  $B$ . Then construct a line through  $A$  at an angle of  $45^\circ$ . This locates the direction of travel of the flat-faced follower. Finally, draw a line perpendicular to the  $45^\circ$  line and tangent to the cam. This locates point  $C$ .

2. Compute  $v_{C_2} = \omega_2 \times r_{C/A}$ .

$$v_{C_2} = 100(1.52) = 152 \text{ in/s perpendicular to } AC \text{ and in the direction shown in Fig. 3.22.}$$

This will locate  $c_2$ .

3. Draw a line from  $o$  at an angle of  $45^\circ$  with the horizontal. Point  $c_3$  will be on this line.

4. Draw a line through the tip of  $c_2$  and perpendicular to the line at  $45^\circ$ . The intersection of this line with that drawn in step 3 locates  $c_3$ .

$$v_{C_3} = 35 \text{ in/s in the direction shown.}$$

5. Locate  $b_2$  by image.

6. Compute and plot  $a_{C_2/A_2} = a_{C_2/A_2}^t$ .

$$a_{C_2/A_2}^t = AC \times \omega_2^2 = 1.52 \times 100^2 = 15,200 \text{ in/s}^2 \text{ in the } CA \text{ direction}$$

7. Draw a line from  $o'$  at an angle of  $45^\circ$  with the horizontal. Point  $c'_3$  will be on this line.

8. Compute  $a_{C_3/C_2}^n$ , determine its direction, and plot the resulting vector through the tip of  $a_{C_2/A_2}^t$ .

$$a_{C_3/C_2}^n = \frac{\left| v_{B_2/C_2} \right|^2}{\left| r_{B/C} \right|} = \frac{\left| 112.9 \right|^2}{\left| 1.11 \right|} = 11,480 \text{ in/s}^2 \text{ from } B \text{ to } C$$

9. Draw a line through the tip of  $a_{C_3/C_2}^n$  and perpendicular to it. The intersection of this line with the line drawn in step 7 will be the point  $c'_3$ .

10. Measure  $a_{C_3}$ .

$$a_{C_3} = 3250 \text{ in/s}^2 \text{ in the direction shown}$$

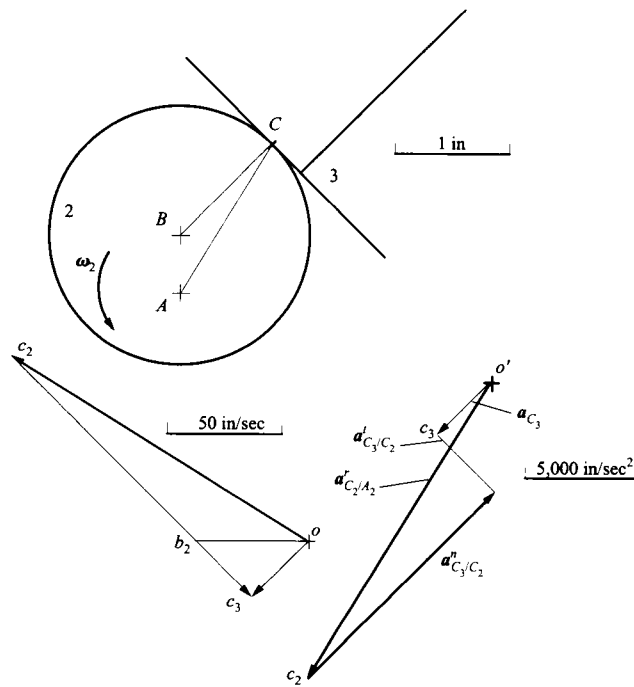


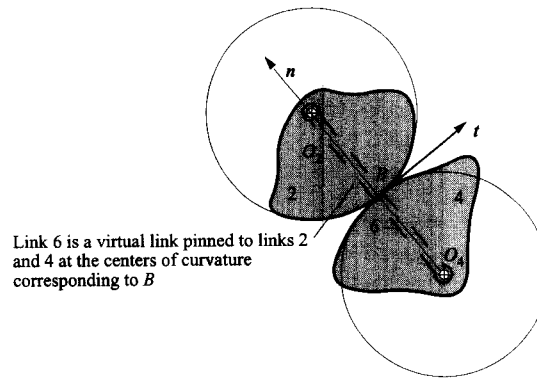
FIGURE 3.22 Position, velocity, and acceleration polygons for Example 3.4.

### 3.7.2 Analysis of Cam Contact Using Equivalent Linkages

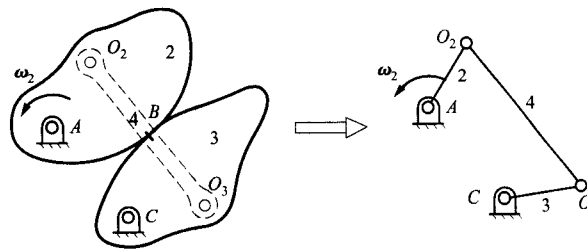
Another approach to determining the velocities and accelerations is to use the concept of equivalent linkages. For this we represent the two cam surfaces by their osculating circles and attach a binary link from one center of curvature to the other using revolute joints. As in the case of rolling contact, this technique can be used for velocities and accelerations, but it will not give correct results for higher derivatives. In Fig. 3.23, link 6 is a virtual link that usually changes length with each *finite* change in position. (It is constant for differential changes in position, however.)

The use of equivalent linkages usually simplifies the velocity and acceleration analyses because the equivalent linkages are usually standard four-bar linkages or one of the inversions of the common slider-crank mechanism. For example, a simple three-link cam mechanism becomes a four-bar linkage when replaced by its equivalent linkage as shown in Fig. 3.24. In the example in Fig. 3.24, the kinematic information for link 4 (virtual link) can be computed; however, this is usually of no interest. It is important to remember that the equivalent linkage is valid for one position only. The length of the virtual link usually changes with each position of interest.





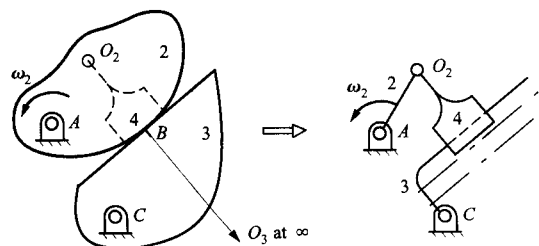
**FIGURE 3.23** Virtual link pinned at the centers of curvature of the two bodies in cam contact.



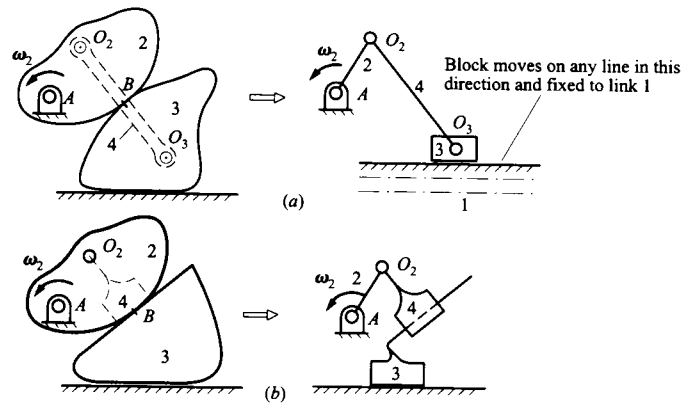
**FIGURE 3.24** Equivalent linkage for cam mechanism with curved cam surfaces and revolute joints between the cams and the frame.

If one of the surfaces is flat, the virtual link becomes infinitely long, and the movement of the virtual link can be represented by a slider. An example of this is shown in Fig. 3.25. The slider need not “slide” on the face of the flat cam surface through B. The only restriction is that it slide on a line that is parallel to the cam face.

The equivalent linkage is analyzed as any other linkage with pin and slider joints would be. The kinematic properties computed for links 2 and 3 will be the same for both the equivalent linkage and the actual linkage. The equivalent linkages for the other two types of three-bar cam linkages are given in Fig. 3.26.



**FIGURE 3.25** Equivalent linkage for cam mechanism with one flat-faced cam and revolute joints between the cams and the frame. The slider can slide on any line that is parallel to the cam face and fixed to link 3.



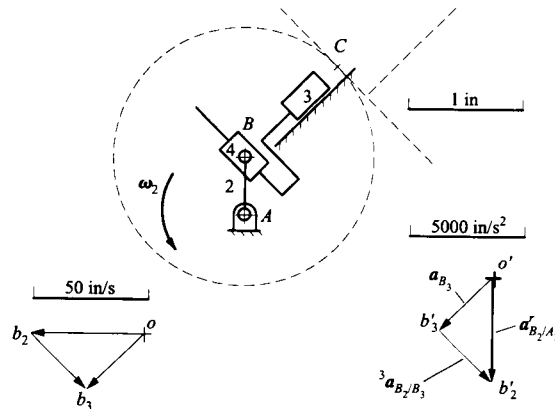
**FIGURE 3.26** Equivalent linkage for cam mechanism. (a) Sliding joint between link 3 and frame. (b) Sliding between links 2 and 3 and between link 3 and frame.

**EXAMPLE 3.5**  
**Mechanism**  
**Analysis Using**  
**an Equivalent**  
**Linkage**

**Solution**

Use equivalent linkages to compute the velocity and acceleration of the cam follower (link 3) in Fig. 3.21 if the cam is rotating at a constant angular velocity of 100 rad/s CCW.

The mechanism in Fig. 3.21 is of the type represented in Fig. 3.26b. Therefore, link 3, the follower, will have a sliding joint with the frame and with the virtual link (link 4). The resulting equivalent linkage is shown in Fig. 3.27. Notice that the location of the line on which link 4 must slide relative to link 3 is arbitrary as long as the line is fixed to link 3 and is parallel to the face of link 3. Therefore, the line that passes through  $B$  is chosen for simplicity. Similarly, the location of the line on which link 3 slides relative to the frame is arbitrary as long as the line is inclined at an angle of  $45^\circ$ .



**FIGURE 3.27** Position, velocity, and acceleration polygons for Example 3.5.

For the equivalent linkage, we need only find the velocity and acceleration of point  $B_2$ . The velocity and acceleration of  $B_3$  can then be found using the procedure given in Section 3.5. The velocity equations that must be solved are

$$\mathbf{v}_{B_2} = \mathbf{v}_{B_2/A_2} = \boldsymbol{\omega}_2 \times \mathbf{r}_{B/A}$$

and

$$\mathbf{v}_{B_2} = \mathbf{v}_{B_3} + \mathbf{v}_{B_2/B_3} \quad (3.41)$$

Here we have written the velocity equation in terms of the velocity of  $B_2$  relative to  $B_3$  rather than vice versa because we can easily identify the direction of the velocity of  $B_2$  relative to  $B_3$ . We also know the direction for the velocity and acceleration of  $B_3$ . The acceleration equations that must be solved are

$$\mathbf{a}_{B_2} = \mathbf{a}_{B_2/A_2} = \mathbf{a}_{B_2/A_2}^r + \mathbf{a}_{B_2/A_2}^t$$

$$\mathbf{a}_{B_2} = \mathbf{a}_{B_3} + \mathbf{a}_{B_2/B_3} = \mathbf{a}_{B_3} + \mathbf{a}_{B_2/B_3}^c + {}^3\mathbf{a}_{B_2/B_3}$$

and

$$\mathbf{a}_{B_2/B_3}^c = 2\boldsymbol{\omega}_3 \times {}^3\mathbf{v}_{B_2/B_3} = 0$$

The Coriolis term is a function of velocities only and can be computed; however, links 3 and 4 simply translate, making  $\boldsymbol{\omega}_3 = 0$ . Therefore, the acceleration expression becomes

$$\mathbf{a}_{B_2} = \mathbf{a}_{B_3} + {}^3\mathbf{a}_{B_2/B_3}$$

By geometry,  ${}^3\mathbf{a}_{B_2/B_3}$  must move in the direction parallel to the face of the cam follower. Therefore, the equation has only two unknowns (once  $\mathbf{a}_{B_2}$  is computed), and the equation can be solved for  $\mathbf{a}_{B_3}$  and  ${}^3\mathbf{a}_{B_2/B_3}$ .

#### Steps

1. Draw the mechanism to scale using the procedure given in Example 3.4. Then draw the equivalent mechanism.

2. Compute  $\mathbf{v}_{B_2} = \boldsymbol{\omega}_2 \times \mathbf{r}_{B/A}$ .

$\mathbf{v}_{B_2} = (\boldsymbol{\omega}_2)(\mathbf{r}_{B_2/A_2}) = 100(0.5) = 50$  in/s perpendicular to  $AB$  and pointed in the direction shown in Fig. 3.27.

This will locate  $b_2$ .

3. Draw a line from  $o$  at an angle of  $45^\circ$  with the horizontal. Point  $b_3$  will be on this line.

4. Draw a line through the tip of  $b_2$  and perpendicular to the line at  $45^\circ$ . The intersection of this line with that drawn in step 3 locates  $b_3$ .

$\mathbf{v}_{B_3} = 35$  in/s in the direction shown

5. Compute and plot  $\mathbf{a}_{B_2/A_2} = \mathbf{a}_{B_2/A_2}^r$ .

$\mathbf{a}_{B_2/A_2}^r = AB \times \boldsymbol{\omega}_2^2 = 0.5 \times 100^2 = 5000$  in/s<sup>2</sup>; in the  $\overrightarrow{BA}$  direction

6. Draw a line from  $o'$  at an angle of  $45^\circ$  with the horizontal. Point  $b'_3$  will be on this line.

7. Draw a line through the tip of  $\mathbf{a}_{B_2/A_2}^r$  and parallel to the face of the cam follower (link 3). This is the direction of  ${}^3\mathbf{a}_{B_2/B_3}$ . The intersection of this line with the line drawn in step 6 will be the point  $b'_3$ .

8. Measure  $\mathbf{a}_{B_3}$ .

$\mathbf{a}_{B_3} = 3250$  in/s<sup>2</sup> in the direction shown

This is the acceleration of link 3. Note that this is the same solution as obtained in Example 3.4. All points in link 3 have the same velocity and the same accelerations. Therefore, points  $B_3$  and  $C_3$  have the same velocity and the same acceleration. Also note that considerably less work is required to obtain the final result when equivalent linkages are used.

When equivalent linkages are used, no information is used about the relative motion at the contact point. If the relative motions between the coincident points at contact are of interest, these can be computed directly after the basic analysis is completed. This velocity might be of interest for lubrication considerations.

**EXAMPLE 3.6**  
**Analysis of Sliding**  
**Velocity in a Cam**  
**Mechanism**

**Solution**

Find the sliding velocity at the point of contact for the mechanism in Example 3.5.

The sliding velocity at the point of contact is the relative velocity between points  $C_2$  and  $C_3$ . This velocity can be computed from

$$\mathbf{v}_{C_3/C_2} = \mathbf{v}_{C_3} - \mathbf{v}_{C_2} \quad (3.42)$$

Because

$$\mathbf{v}_{C_3} = \mathbf{v}_{B_3}$$

we need only solve for  $\mathbf{v}_{C_2}$  to determine  $\mathbf{v}_{C_3/C_2}$  in Eq. (3.42). From Example 3.4,  $\mathbf{v}_{C_2} = \boldsymbol{\omega}_2 \times \mathbf{r}_{C_2/A}$ , and it is perpendicular to  $\overline{AC}$  as shown in Fig. 3.22. The vector  $\mathbf{v}_{C_3/C_2}$  is shown in Fig. 3.28. Measurement of the vector gives  $v_{C_3/C_2} = 148$  in/s, in the direction shown in the figure.

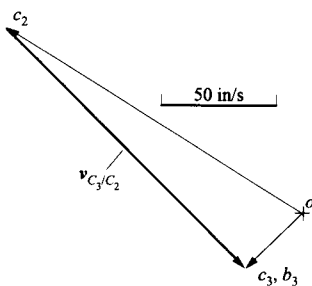


FIGURE 3.28 Calculation of the relative velocity  $\mathbf{v}_{C_3/C_2}$ .

### 3.8 GENERAL COINCIDENT POINTS

In mechanisms, pin-in-slot joints are common, and occasionally the slots will be curved paths. Also, occasionally, sliders will be used on circular paths that rotate. Mechanisms employing these types of joints can be analyzed using general coincident points. In general, we can use any coincident points to help in a kinematic analysis if we can recognize the path that one of the points traces on the other link. For this, we must “stand” in one link and watch the coincident point on the other link move.

For the analysis, we need the center of curvature of the path and the corresponding tangent to the path. The tangent is normal to the line from the coincident points to the center of curvature of the path. For illustration, assume that the two bodies in question are links 3 and 7, and the coincident points are located at  $P$  as shown in Fig. 3.29. Then for any coincident points,

$$\mathbf{v}_{P_3/P_7} = {}^7\mathbf{v}_{P_3/P_7} = -\mathbf{v}_{P_7/P_3} = -{}^3\mathbf{v}_{P_7/P_3}$$

Two paths will be traced, and these can be designated as path  $P_3/P_7$  and path  $P_7/P_3$ . The paths will share a common tangent vector, and the normal to the paths will contain the two coincident points and the two centers of curvature as shown in Fig. 3.29. The path that  $P_3$  traces on link 7 will be fixed to link 7, and the path  $P_7/P_3$  will be fixed to link 3.

To solve problems involving general coincident points, we must be able to recognize one of the relative paths by inspection. This means that we must be able to determine the center of curvature of the path. Sometimes, we can recognize one of the relative paths but not the other. This is still useful because of the relationships

$$\mathbf{v}_{P_7/P_3} = -{}^7\mathbf{v}_{P_3/P_7}$$

and

$$\mathbf{v}_{P_3/P_7} = -{}^3\mathbf{v}_{P_7/P_3}$$

This means that if we can recognize one of the paths, we can always rewrite the kinematic equations so that the information will appear in the correct form. Some examples of paths that are obvious are given in Fig. 3.30.

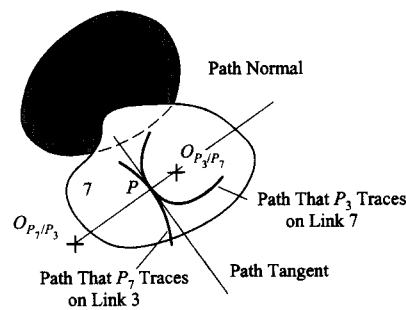


FIGURE 3.29 Geometric properties of relative paths traced by coincident points.

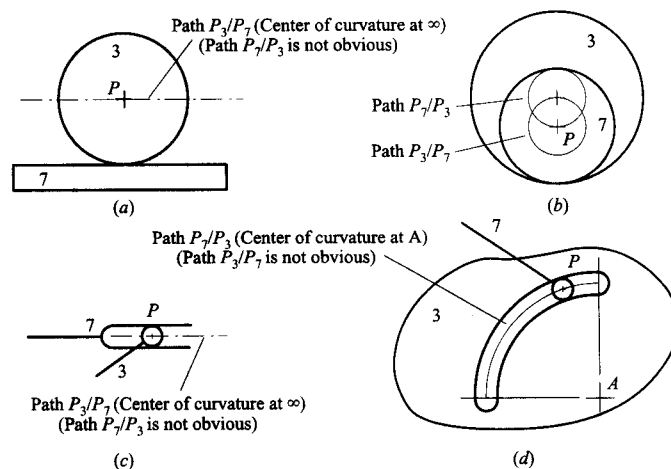


FIGURE 3.30 Obvious relative paths of general coincident points.

### 3.8.1 Velocity Analyses Involving General Coincident Points

The velocity analysis of mechanisms that involve general coincident points will generally require that the direction for the relative velocity vector ( $\mathbf{v}_{P_3/P_7}$  or  $\mathbf{v}_{P_x/P_7}$ ) be known. This direction can be determined by using the same technique as was used in the analyses using cam pairs. For this, we replace the path  $P_3/P_7$  by its osculating circle at  $P$ . Recall that we can do this without compromising the accuracy of the solution as long as we are interested in only velocities and accelerations. Next connect  $P_3$  to the center of curvature  $O$  of the path  $P_3/P_7$  by a virtual link  $x$ . The geometry is represented schematically in Fig. 3.31.

The motion of  $P_3$  relative to link 7 will be the same as for  $P_x$  relative to link 7 if the two points are considered to be pinned together. The relative velocity between  $P_3$  and  $P_7$  can then be written as

$$\mathbf{v}_{P_3/P_7} = {}^7\mathbf{v}_{P_3/P_7} = {}^7\mathbf{v}_{P_3/P_x} + {}^7\mathbf{v}_{P_x/O_x} + {}^7\mathbf{v}_{O_x/O_7} + {}^7\mathbf{v}_{O_7/P_7} \quad (3.43)$$

or because points  $P_3$  and  $P_x$  and  $O_x$  and  $O_7$  are considered to be pinned together, and the last term involves the motion of two points in system 7 as observed from system 7,

$$\mathbf{v}_{P_3/P_7} = {}^7\mathbf{v}_{P_3/P_7} = {}^7\mathbf{v}_{P_x/O_x} \quad (3.44)$$

Because two points on the same rigid link are involved, the term on the right-hand side of Eq. (3.44) can be written as

$$\mathbf{v}_{P_3/P_7} = {}^7\mathbf{v}_{P_3/P_7} = {}^7\boldsymbol{\omega}_x \times \mathbf{r}_{P_x/O_x}$$

This vector is perpendicular to the line from the point  $P$  to the center of curvature of the path  $P_3/P_7$ , and it is therefore along the direction of the tangent to the path. Therefore, when the direction for the relative velocity is required, we need only determine the center of curvature of the path  $P_3/P_7$  and draw a line perpendicular to it.

The magnitude of the angular velocity term will be required for the acceleration analysis, and it can be written as

$$|{}^7\boldsymbol{\omega}_x| = \frac{|\mathbf{v}_{P_3/P_7}|}{|\mathbf{r}_{P_x/O_x}|}$$

### 3.8.2 Acceleration Analyses Involving General Coincident Points

The acceleration analysis is slightly more complex than the velocity analysis when general coincident points are involved. For the relative acceleration, again assume that the path that  $P_3$  traces on link 7 is known. This means that the center of curvature of the path is also

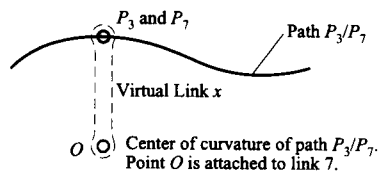


FIGURE 3.31 Connecting a virtual link from point  $P_3$  to center of curvature of path that  $P_3$  traces on link 7.

known. The development of the relative acceleration expression is similar to that used for the case of a rotating slider, and the relative acceleration expression can be written as

$$\mathbf{a}_{P_3/P_7} = {}^7\mathbf{a}_{P_3/P_7} + 2\boldsymbol{\omega}_7 \times {}^7\mathbf{v}_{P_3/P_7} + \boldsymbol{\omega}_7 \times (\boldsymbol{\omega}_7 \times \mathbf{r}_{P_3/P_7}) + \boldsymbol{\alpha}_7 \times \mathbf{r}_{P_3/P_7}$$

Because  $\mathbf{r}_{P_3/P_7} = 0$  at the moment considered,

$$\mathbf{a}_{P_3/P_7} = {}^7\mathbf{a}_{P_3/P_7} + 2\boldsymbol{\omega}_7 \times \mathbf{v}_{P_3/P_7} \quad (3.45)$$

The second term in the expression is the Coriolis term, which is a function of position and velocity only. Therefore, it can be computed as soon as the velocity analysis is completed. The direction of the Coriolis term is given by the cross product. Graphically, we can get the direction by rotating  ${}^7\mathbf{v}_{P_3/P_7}$  (which equals  $\mathbf{v}_{P_3/P_7}$ )  $90^\circ$  in the direction of  $\boldsymbol{\omega}_7$ .

The first term in Eq. (3.45) is simply the acceleration of  $P_3$  as observed from system 7. This term can be written as

$${}^7\mathbf{a}_{P_3/P_7} = {}^7\mathbf{a}_{P_3/\text{any point in system 7}} = {}^7\mathbf{a}_{P_3} \quad (3.46)$$

Unlike the case of the rotating slider, the direction for this acceleration component is not immediately obvious. However, by using the technique begun in the velocity analysis, we can determine a vector expression for this component that involves only one unknown.

To begin, replace the path  $P_3/P_7$  by its osculating circle at  $P$  and rewrite the acceleration expression in Eq. (3.46) in terms of the virtual link  $x$  and the center of curvature of the path of  $P_3/P_7$ . This is similar to what was done with velocities in Eq. (3.43). The relative acceleration between  $P_3$  and  $P_7$  can then be written as

$${}^7\mathbf{a}_{P_3} = {}^7\mathbf{a}_{P_3/P_7} = {}^7\mathbf{a}_{P_3/P_x} + {}^7\mathbf{a}_{P_x/O_x} + {}^7\mathbf{a}_{O_x/O_7} + {}^7\mathbf{a}_{O_7/P_7}$$

or because points  $P_3$  and  $P_x$  and  $O_x$  and  $O_7$  are pinned together, and the last term involves the motion of two points in system 7 as observed from system 7,

$${}^7\mathbf{a}_{P_3} = {}^7\mathbf{a}_{P_3/P_7} = {}^7\mathbf{a}_{P_x/O_x} \quad (3.47)$$

Because two points on the same rigid link are involved, the term on the right-hand side of Eq. (3.63) can be written as

$${}^7\mathbf{a}_{P_x/O_x} = {}^7\mathbf{a}_{P_x/O_x}^r + {}^7\mathbf{a}_{P_x/O_x}^t$$

The radial component is a function of velocities and position only and can be written as

$${}^7\mathbf{a}_{P_x/O_x}^r = {}^7\boldsymbol{\omega}_x \times {}^x\mathbf{v}_{P_x/O_x} = \frac{|\mathbf{v}_{P_x/O_x}|^2}{|\mathbf{r}_{P_x/O_x}|} = \frac{|\mathbf{v}_{P_3/P_7}|^2}{|\mathbf{r}_{P/O}|} \quad (\text{from } P \text{ to } O)$$

The magnitude of the vector  ${}^7\mathbf{a}_{P_x/O_x}^t$  cannot be computed directly; however, we know that the direction is perpendicular to the line from the point  $P$  to the center of curvature of the path  $P_3/P_7$ , and it is therefore along the direction of the tangent to the path. The total acceleration can now be represented as

$$\mathbf{a}_{P_3/P_7} = {}^7\mathbf{a}_{P_x/O_x}^t + {}^7\mathbf{a}_{P_x/O_x}^r + 2\boldsymbol{\omega}_7 \times {}^7\mathbf{v}_{P_3/P_7}$$

or in terms of the original subscripts,

$$\mathbf{a}_{P_3/P_7} = {}^7\mathbf{a}_{P_3/P_7}^t + {}^7\mathbf{a}_{P_3/P_7}^r + 2\boldsymbol{\omega}_7 \times {}^7\mathbf{v}_{P_3/P_7}$$

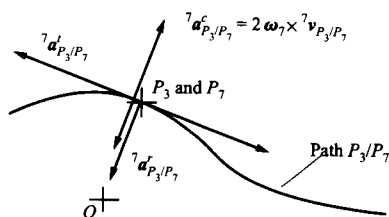


FIGURE 3.32 Acceleration components associated with the relative acceleration between  $P_3$  and  $P_7$ .

Of the three vectors on the right-hand side of the equation, only the magnitude of  $a_{P_3/P_7}^t$  will be unknown after the velocity analysis. The directions for the individual terms are summarized in Fig. 3.32. Note that the radial and Coriolis terms are both normal to the tangent of the path of  $P_3/P_7$ ; however, only the radial component always points from  $P$  to the center of curvature of the path of  $P_3/P_7$ . The direction of the Coriolis term will depend on the directions of both  $\omega_7$  and  $v_{P_3/P_7}$ .

**EXAMPLE 3.7**  
**Analysis of**  
**Mechanism with**  
**a Pin-in-Slot Joint**

In the mechanism shown in Fig. 3.33, point  $B_2$  moves on a curved slot in link 3. The radius of the slot is 3 m. Points  $C$ ,  $B$ , and  $D$  are collinear, and the other distances between points are as given in Fig. 3.33. Link 2 rotates with an angular velocity of 2 rad/s CCW and an angular acceleration of 3 rad/s<sup>2</sup> CCW. For the position shown, find the following:

1.  $\omega_3$ ,  $\alpha_3$ ,  $v_{D_3}$ , and  $a_{D_3}$ ;
2. The center of curvature of the path that  $B_3$  traces on link 2.

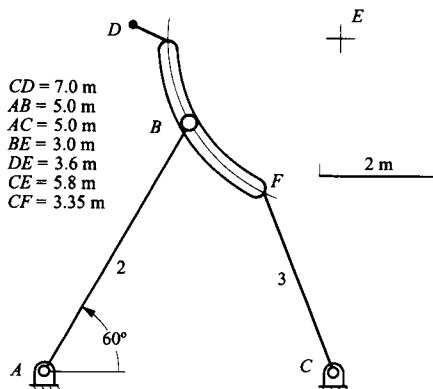


FIGURE 3.33 Mechanism for Example 3.7.

**Solution**

Once the position of the linkage is drawn, the following vector quantities can be measured:

$$\mathbf{r}_{B/A} = 5 \angle 60^\circ$$

$$\mathbf{r}_{B/C} = 5 \angle 120^\circ$$

$$\mathbf{r}_{D/C} = 7 \angle 120^\circ$$

For the velocity analysis, we can first compute the velocity of point  $B_2$ , which is

$$\mathbf{v}_{B_2} = \mathbf{v}_{B_2/A_2} = \boldsymbol{\omega}_2 \times \mathbf{r}_{B_2/A_2}$$



Next go to point  $B_3$  on link 3 to get

$$\mathbf{v}_{B_3} = \mathbf{v}_{B_3/C_3} = \boldsymbol{\omega}_3 \times {}^3\mathbf{r}_{B/C} \perp BC$$

Because  $\boldsymbol{\omega}_3$  is unknown, this term cannot be computed without another equation. Consider the two coincident points  $B_2$  and  $B_3$ . Then,

$$\mathbf{v}_{B_3} = \mathbf{v}_{B_2} + \mathbf{v}_{B_3/B_2}$$

This equation is technically correct; however, we cannot recognize the path that  $B_3$  traces on link 2. Consequently, the equation cannot be differentiated to help us in the acceleration analysis. Therefore, write the equation in terms of  $\mathbf{v}_{B_2}$ . Then,

$$\mathbf{v}_{B_2} = \mathbf{v}_{B_3} + \mathbf{v}_{B_2/B_3}$$

This equation is useful because we can pick out the path that  $B_2$  traces on link 3 by inspection. This equation can be solved, although there are two unknown directions on the right-hand side. This is handled by beginning one vector at the velocity pole and ending the other vector at the end of  $\mathbf{v}_{B_2}$ .

After the velocity polygon is drawn, we can measure  $\mathbf{v}_{B_3}$  and determine  $\mathbf{v}_{D_3}$  by image. We can also measure  $\mathbf{v}_{B_2/B_3}$ , which will be required for the acceleration analysis.

The velocity analysis uses two basic equations:

$$\mathbf{v}_{B_2} = \mathbf{v}_{B_2/A_2}$$

and

$$\mathbf{v}_{B_2} = \mathbf{v}_{B_3/C_3} + \mathbf{v}_{B_2/B_3}$$

and these two equations show the solution path for the accelerations. Again start at  $B_2$ . Then,

$$\mathbf{a}_{B_2} = \mathbf{a}_{B_2/A_2} = \mathbf{a}_{B_2/A_2}^t + \mathbf{a}_{B_2/A_2}^r = \boldsymbol{\alpha}_2 \times {}^2\mathbf{r}_{B/A} + \boldsymbol{\omega}_2 \times {}^2\mathbf{v}_{B/A}$$

Now differentiate the velocity expression involving  $B_3$  to get

$$\begin{aligned} \mathbf{a}_{B_2} &= \mathbf{a}_{B_3/C_3} + \mathbf{a}_{B_2/B_3} = \mathbf{a}_{B_3/C_3}^r = \mathbf{a}_{B_3/C_3}^t + {}^3\mathbf{a}_{B_2/B_3}^n + {}^3\mathbf{a}_{B_2/B_3}^t + 2\boldsymbol{\omega}_3 \times \mathbf{v}_{B_2/B_3} \\ &= \boldsymbol{\omega}_3 \times \mathbf{v}_{B_3/C_3} + \boldsymbol{\alpha}_3 \times {}^3\mathbf{r}_{B_3/C_3} + {}^3\mathbf{a}_{B_2/B_3}^n + {}^3\mathbf{a}_{B_2/B_3}^t + 2\boldsymbol{\omega}_3 \times \mathbf{v}_{B_2/B_3} \end{aligned} \quad (3.48)$$

This equation has only two unknowns and can be solved. We can compute the acceleration of  $D_3$  using the acceleration image.

To find the center of curvature of the path that  $B_3$  traces on link 2, we must find an expression that involves the radius of curvature of the path. This term is  ${}^2\mathbf{a}_{B_3/B_2}^n$ , and it can be evaluated from the following:

$$\mathbf{a}_{B_2/B_3} = -\mathbf{a}_{B_3/B_2}$$

Therefore,

$$\mathbf{a}_{B_2/B_3}^t = -\mathbf{a}_{B_3/B_2}^t$$

and

$$\mathbf{a}_{B_2/B_3}^n = -\mathbf{a}_{B_3/B_2}^n$$

Also,

$${}^3\mathbf{a}_{B_2/B_3}^n + 2\boldsymbol{\omega}_3 \times \mathbf{v}_{B_2/B_3} = -{}^2\mathbf{a}_{B_3/B_2}^n - 2\boldsymbol{\omega}_2 \times \mathbf{v}_{B_3/B_2}$$

and

$${}^2a_{B_3/B_2}^n = \frac{|v_{B_3/B_2}|^2}{|r_{B/G}|}$$

or

$$r_{B/G} = \frac{|v_{B_3/B_2}|^2}{{}^2a_{B_3/B_2}^n}$$

where  $G$  gives the location of the center of curvature of the path that  $B_3$  traces on link 2. The location of  $G$  on the proper side of  $B$  is found by the direction of  ${}^2a_{B_3/B_2}^n$ , because it points from  $B$  to the center of curvature of the path.

### Steps

1. Select a scale and draw link 2 at a scaled distance of 5 m at an angle of  $60^\circ$  to the horizontal. This will locate point  $B$  as shown in Fig. 3.34. Draw an arc of radius  $BE$  centered at  $B$ . Then draw a second arc centered at  $C$  of length  $CE$ . The intersection of this arc with the first will locate point  $E$ . Next draw the arc centered at  $E$  and of radius  $BE$ . Draw a line from point  $C$  through point  $B$  of length  $CD$ .

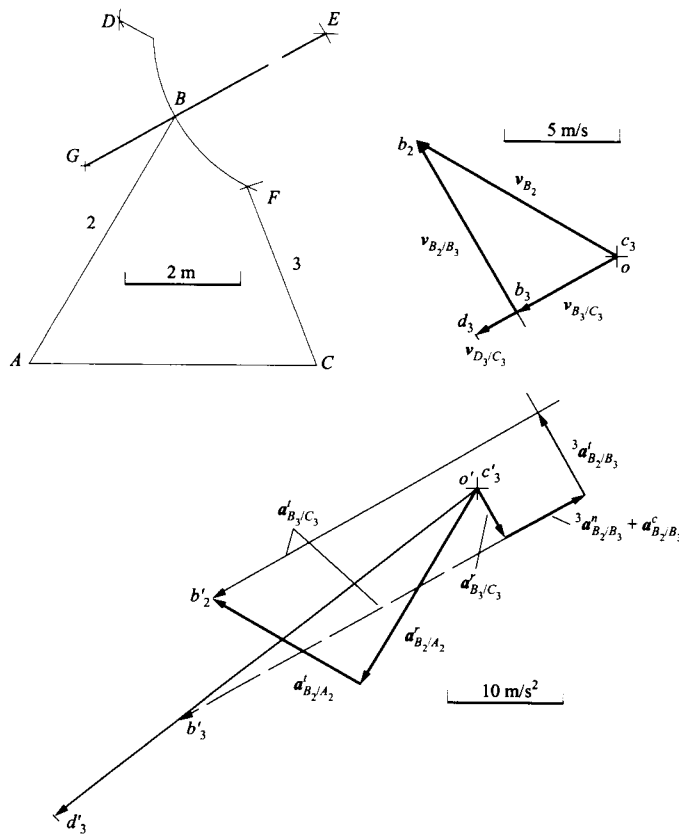


FIGURE 3.34 Solution to Example 3.7.

2. Compute  $\mathbf{v}_{B_2} = \mathbf{v}_{B_2/A_2} = \boldsymbol{\omega}_2 \times \mathbf{r}_{B_2/A_2}$  and draw the vector from  $o$  in the direction perpendicular to  $BA$ . The sense of  $\mathbf{v}_{B_2}$  is determined by rotation of  $\mathbf{r}_{B_2/A_2}$   $90^\circ$  in the direction of  $\boldsymbol{\omega}_2$ . This will locate  $b_2$ .

$$\mathbf{v}_{B_2/A_2} = \boldsymbol{\omega}_2 \times \mathbf{r}_{B_2/A_2} = (2)(5) \perp BA$$

3. Draw a line through  $o$  in the direction perpendicular to  $CB$ .
4. Draw a line through  $b_2$  in the direction tangent to the path that  $B_2$  traces on link 3 (perpendicular to the radius  $BE$ ). The intersection of this line with that drawn in step 3 will locate point  $b_3$ . Locate the arrowheads on the velocity polygon to conform with Eq. (3.48).
5. Locate point  $d_3$  by image.  
 $od_3 = \frac{CD}{CB} ob_3$ . Then we get  $\mathbf{v}_{D_3} = 7.0$  m/s at an angle of  $210^\circ$  to the horizontal.
6. Measure  $\mathbf{v}_{B_2/B_3} = 8.7$  m/s at an angle of  $120^\circ$  to the horizontal.
7. Measure  $\mathbf{v}_{B_3/C_3} = 5.0$  m/s at an angle of  $210^\circ$  to the horizontal and compute  $\boldsymbol{\omega}_3$ . Get the sense of  $\boldsymbol{\omega}_3$  by rotating  $\mathbf{r}_{B_3/C_3}$   $90^\circ$  in the direction of  $\boldsymbol{\omega}_3$  to the direction of  $\mathbf{v}_{B_3/C_3}$ .

$$\boldsymbol{\omega}_3 = \frac{|\mathbf{v}_{B_3/C_3}|}{|\mathbf{r}_{B_3/C_3}|} = \frac{5}{5} = 1 \text{ rad/s, } \boldsymbol{\omega}_3 \text{ is CCW}$$

8. Compute  $\mathbf{a}_{B_2/A_2}^t$  and  $\mathbf{a}_{B_2/A_2}^r$  and, starting from  $o'$ , draw the resulting vectors after scaling.

$$\mathbf{a}_{B_2/A_2}^r = \boldsymbol{\omega}_2 \times \mathbf{v}_{B/A} = 2(10) = 20 \text{ m/s}^2 \text{ opposite } \mathbf{r}_{B/A}$$

$$\mathbf{a}_{B_2/A_2}^t = \boldsymbol{\alpha}_2 \times \mathbf{r}_{B/A} = 3(5) = 15 \text{ m/s}^2 \text{ perpendicular to } \mathbf{r}_{B/A} \text{ in the direction given by rotating } \mathbf{r}_{B/A} \text{ } 90^\circ \text{ in the direction of } \boldsymbol{\alpha}_2.$$

This vector is added to  $\mathbf{a}_{B_2/A_2}^r$  as shown in Fig. 3.34.

9. Compute  $\mathbf{a}_{B_3/C_3}^r$ ,  ${}^3\mathbf{a}_{B_2/B_3}^n$ , and  $\mathbf{a}_{B_2/B_3}^c$ . All of these accelerations are functions of the velocity and position data.

$$\mathbf{a}_{B_3/C_3}^r = \boldsymbol{\omega}_3 \times \mathbf{v}_{B_3/C_3} = 1(5) = 5 \text{ m/s}^2 \text{ from } B \text{ to } C$$

$${}^3\mathbf{a}_{B_2/B_3}^n = \frac{|\mathbf{v}_{B_2/B_3}|^2}{|\mathbf{v}_{B_3/E_3}|} = \frac{(8.7)^2}{3} = 25.23 \text{ m/s}^2, \quad {}^3\mathbf{a}_{B_2/B_3}^n \text{ from } B \text{ to } E$$

$$\mathbf{a}_{B_2/B_3}^c = 2\boldsymbol{\omega}_3 \times \mathbf{v}_{B_2/B_3} = 2(1)(8.7) = 17.4 \text{ m/s}^2 \text{ from } E \text{ to } B$$

10. Note that  ${}^3\mathbf{a}_{B_2/B_3}^n$  and  $\mathbf{a}_{B_2/B_3}^c$  are in opposite directions. Therefore, determine the resultant before plotting.

$${}^3\mathbf{a}_{B_2/B_3}^n + \mathbf{a}_{B_2/B_3}^c = 25.23 - 17.4 = 7.83 \text{ m/s}^2 \text{ from } B \text{ to } E$$

11. Starting from  $o'$ , add the vectors  $\mathbf{a}_{B_3/C_3}^r$  and  ${}^3\mathbf{a}_{B_2/B_3}^n + \mathbf{a}_{B_2/B_3}^c$  as shown in Fig. 3.34.
12. Draw a line through the tip of  ${}^3\mathbf{a}_{B_2/B_3}^n + \mathbf{a}_{B_2/B_3}^c$  in the direction perpendicular to  ${}^3\mathbf{a}_{B_2/B_3}^n + \mathbf{a}_{B_2/B_3}^c$  and to  $\mathbf{r}_{B/E}$  (i.e., perpendicular to the tangent to the path that  $B_2$  traces on link 3).
13. Draw a line through the tip of  $\mathbf{a}_{B_2/A_2}^t$  in the direction perpendicular to  $\mathbf{r}_{C/B}$ . The intersection of this line with that from step 12 will give  ${}^3\mathbf{a}_{B_2/B_3}^t$  and  $\mathbf{a}_{B_3/C_3}^t$ . The locations of the arrowheads (directions) are given by Eq. (3.48).
14. Measure  $\mathbf{a}_{B_3/C_3}^t$  and compute the magnitude of the angular acceleration,  $\boldsymbol{\alpha}_3$ .

$$\boldsymbol{\alpha}_3 = \frac{|\mathbf{a}_{B_3/C_3}^t|}{|\mathbf{r}_{B_3/C_3}|} = \frac{32.2}{5} = 11.2 \text{ rad/s}^2$$

The sense is given by  $a_{B_3/C_3}^l$  and  $r_{B_3/C_3}$ . Namely, we rotate  $r_{B_3/C_3}$  90° in the direction of  $\alpha_3$  to get the direction of  $a_{B_3/C_3}^l$ . The direction is CCW.

15. Locate the acceleration of  $D_3$  by acceleration image. To do this, determine the absolute acceleration of  $B_3$ . This is done by adding  $a_{B_3/C_3}^l$  to  $a_{B_3/C_3}^r$  to locate  $b'_3$ . Then find  $d'_3$  using

$$o'd'_3 = \frac{CD}{CB} o'b'_3$$

This gives  $a_{D_3} = 45.9 \text{ m/s}^2$  in the direction shown in Fig. 3.34.

16. Compute  ${}^2a_{B_3/B_2}^n = -({}^3a_{B_2/B_3}^n + 2\omega_3 \times v_{B_3/B_2} + 2\omega_2 \times v_{B_3/B_2})$ . Arbitrarily select the direction  $r_{E/B}$  as positive. Then,

$${}^2a_{B_3/B_2}^n = -(25.23 - 17.4 + 34.8) = -42.63 \text{ m/s}^2$$

The minus sign means that the direction of the center of curvature of the path is opposite  $r_{E/B}$  or in the  $r_{B/E}$  direction.

17. Compute the radius of curvature by locating  $G_2$  using

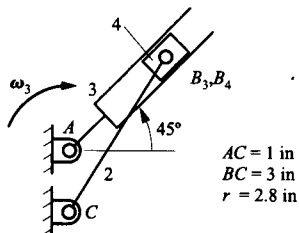
$$r_{B/G} = \frac{|v_{B_3/B_2}|^2}{|{}^2a_{B_3/B_2}^n|} = \frac{(8.7)^2}{42.63} = 1.78 \text{ m}$$

The center of curvature is shown in Fig. 3.34.

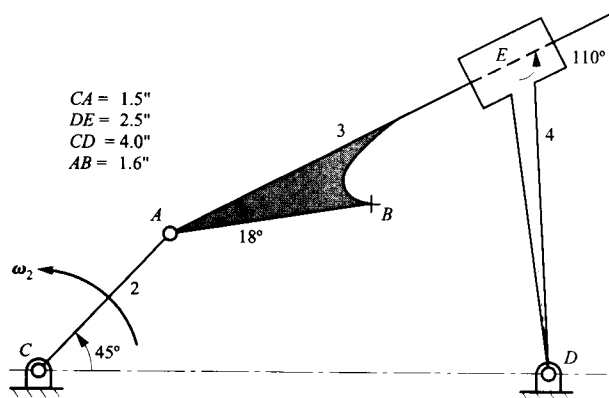
## PROBLEMS

### EXERCISE PROBLEMS INVOLVING ROTATING SLIDERS

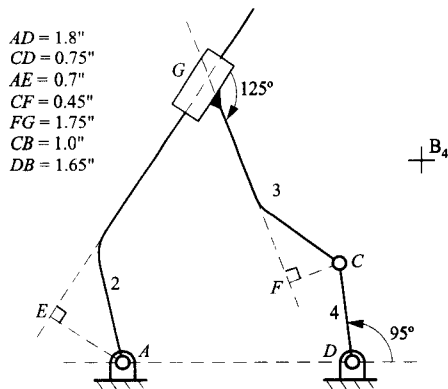
3.1 In the figure, points  $A$  and  $C$  have the same horizontal coordinate, and  $\omega_3 = 30 \text{ rad/s}$  in the direction shown. Draw and dimension the velocity polygon. Identify the sliding velocity between the block and the slide, and find the angular velocity of link 2.



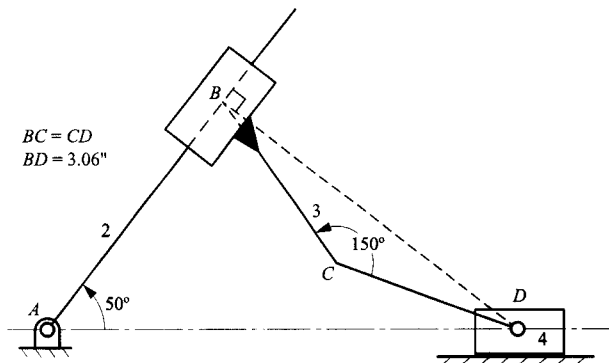
3.2 If  $\omega_2 = 10 \text{ rad/s}$  CCW, find the velocity of point  $B_3$ .



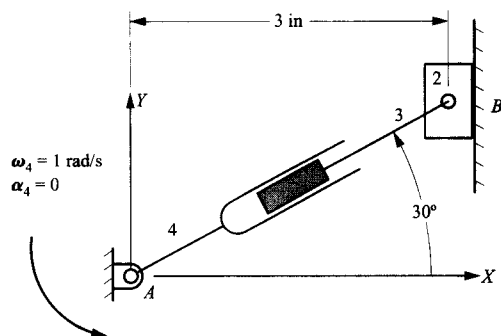
3.3 If  $\omega_2 = 100$  rad/s CCW, find  $v_{B_4}$ .



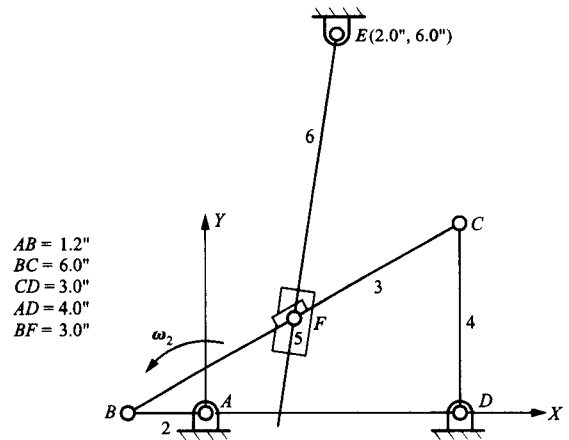
3.4 If  $\omega_2 = 50$  rad/s CCW, find  $v_{D_4}$ .



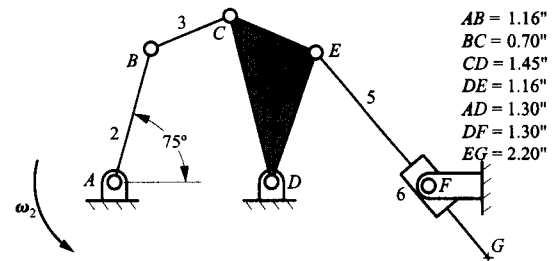
3.5 Determine the velocity and acceleration of point B on link 2.



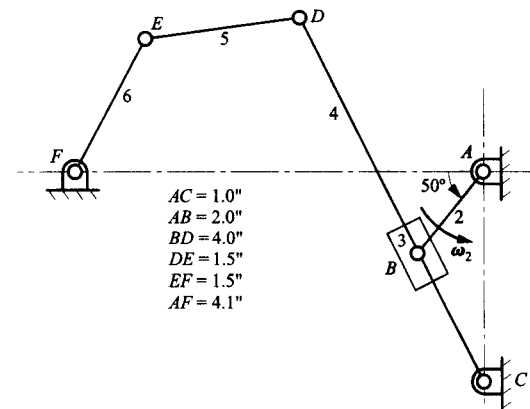
3.6 If  $\omega_2 = 100$  rad/s CCW, find  $\omega_6$ .



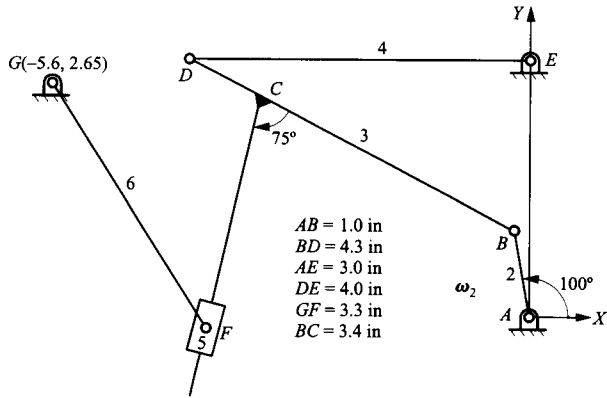
3.7 If  $\omega_2 = 50$  rad/s CCW, find the velocity of point  $G_5$ .



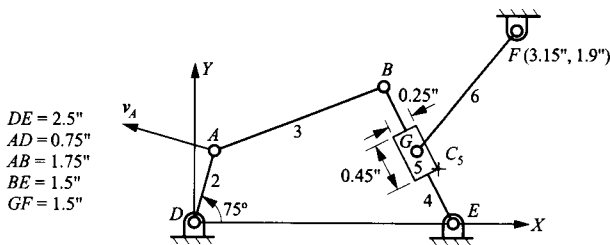
3.8 If  $\omega_2 = 5$  rad/s CCW, find  $\omega_6$ .



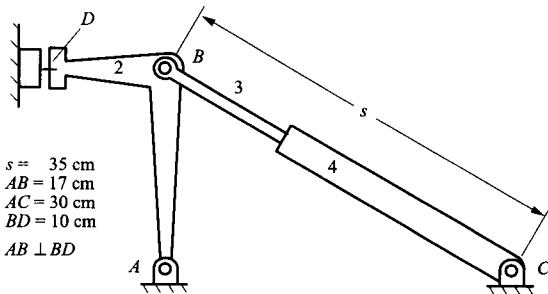
3.9 In the mechanism below,  $\omega_2 = 10 \text{ rad/s}$  CCW. Write the velocity equations and determine the following:  $v_{D_4}$ ,  $\omega_4$ ,  $v_{F_6}$ , and  $\omega_6$ .



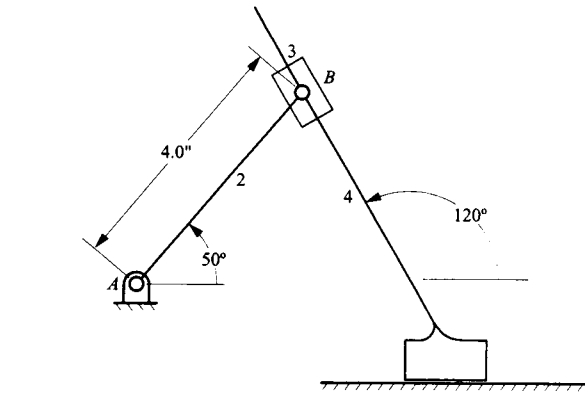
3.10 If the velocity of point A on link 2 is 10 in/s as shown, find the velocity of point C on link 5.



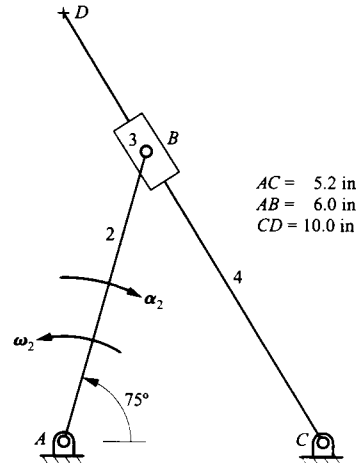
3.11 In the clamping device shown, links 3 and 4 are an air cylinder. If the opening rate of the air cylinder is 5 cm/s and the opening acceleration of the cylinder is 2 cm/s<sup>2</sup>, find the angular velocity and acceleration of link 2 and the linear velocity and acceleration of point D on link 2.



3.12 In the mechanism shown, link 4 moves to the left with a velocity of 8 in/s and the acceleration is 80 in/s<sup>2</sup> to the left. Draw the velocity and acceleration polygons and solve for the angular velocity and acceleration of link 2.

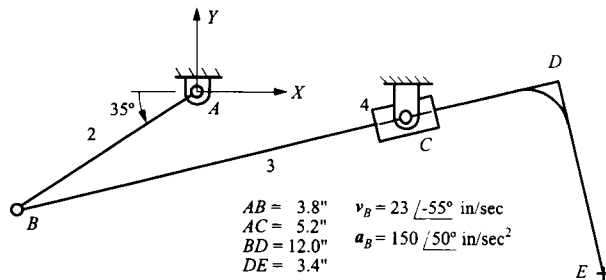


3.13 In the mechanism shown, the angular velocity of link 2 is 2 rad/s CCW and the angular acceleration is 5 rad/s<sup>2</sup> CW. Determine the following:  $v_{B_4}$ ,  $v_{D_4}$ ,  $\omega_4$ ,  $a_{B_4}$ ,  $a_{D_4}$ , and  $\alpha_4$ .

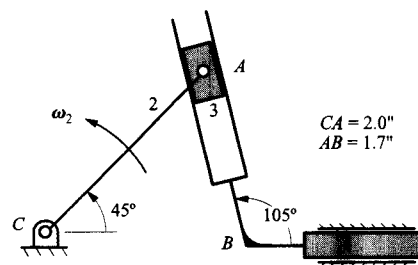
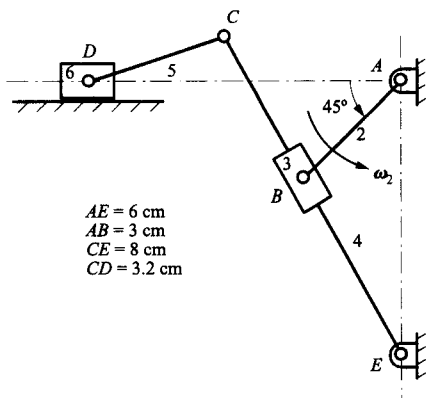


3.14 Re-solve Problem 3.13 if  $\omega_2 = 2 \text{ rad/s}$  CCW (constant).

3.15 In the mechanism shown, the velocity and acceleration of point B are given. Determine the angular velocity and acceleration of links 3 and 4. On the velocity and acceleration diagrams, locate the velocity and acceleration of point E on link 3.



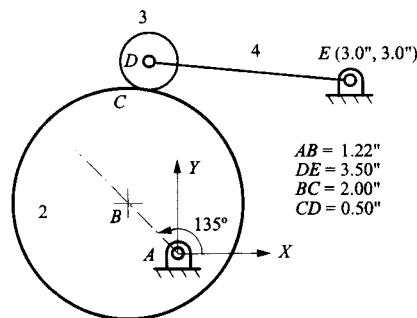
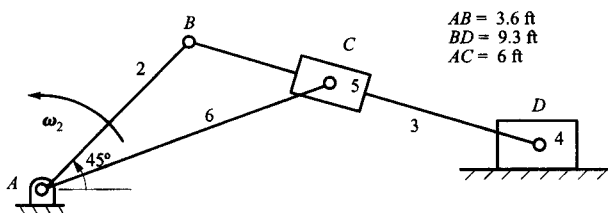
3.16 In the figure,  $\omega_2 = 500 \text{ rad/s}$  CCW (constant). Find  $\omega_4$ ,  ${}^2\omega_4$ ,  $\omega_3$ ,  ${}^6\omega_5$ ,  ${}^3\omega_5$ ,  $v_D$ ,  $\alpha_4$ ,  ${}^2\alpha_4$ ,  $\alpha_3$ ,  ${}^6\alpha_5$ , and  $a_D$ .



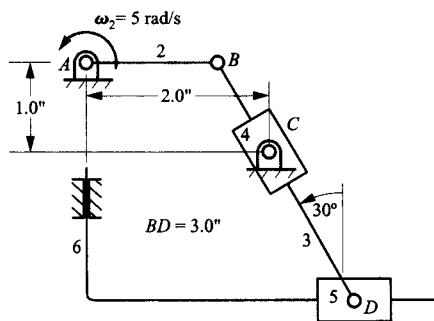
**EXERCISE PROBLEMS INVOLVING ROLLING CONTACT**

3.20 The circular cam shown is driven at an angular velocity  $\omega_2 = 15 \text{ rad/s}$  (CW) and  $\alpha_2 = 100 \text{ rad/s}^2$  (CW). There is rolling contact between the cam and the roller, link 3. Find the angular velocity and angular acceleration of the oscillating follower, link 4.

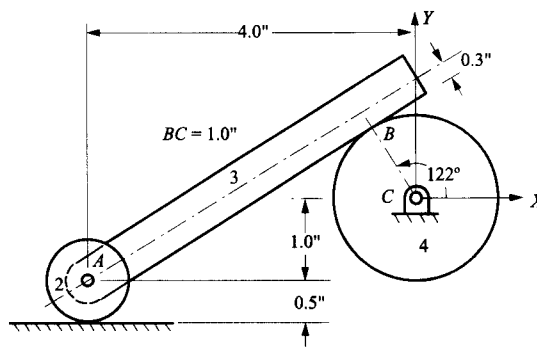
3.17 In the mechanism shown, the angular velocity of link 2 is 60 rpm CCW (constant). Determine the acceleration of point  $C_6$  and the angular velocity of link 6.



3.18 In the position shown  $AB$  is horizontal. Draw the velocity diagram to determine the sliding velocity of link 6. Determine a new position for point  $C$  (between  $B$  and  $D$ ) so that the velocity of link 6 would be equal and opposite to the one calculated for the original position of point  $C$ .

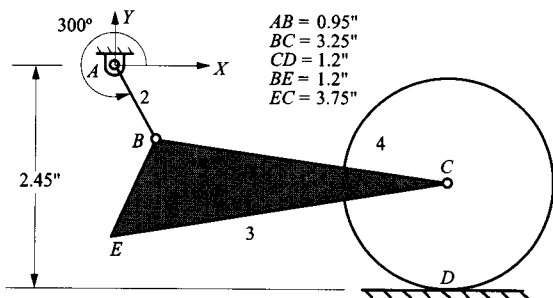


3.21 For the mechanism shown, assume that link 2 rolls on the frame (link 1) and link 4 rolls on Link 3. Assume that link 2 is rotating CW with a constant angular velocity of 100 rad/s. Determine the angular acceleration of link 3 and link 4.

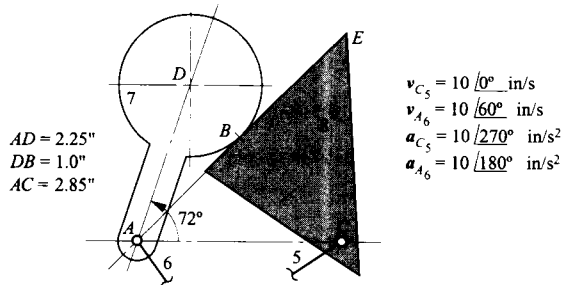


3.19 The scotch-yoke mechanism is driven by crank 2 at  $\omega_2 = 36 \text{ rad/s}$  (CCW). Link 4 slides horizontally. Find the velocity of point  $B$  on link 4.

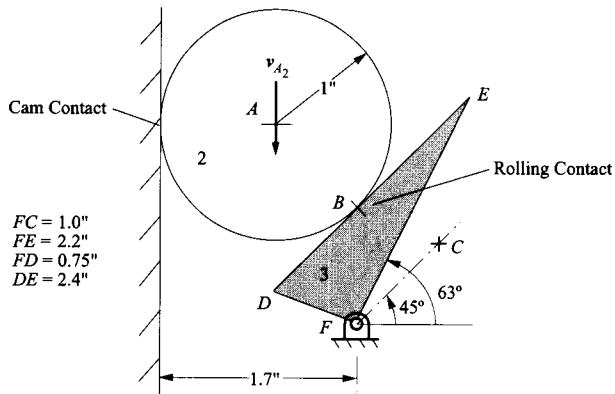
3.22 For the mechanism shown, assume that link 4 rolls on the frame (link 1). If link 2 is rotating CW with a constant angular velocity of 10 rad/s, determine the angular accelerations of links 3 and 4 and the acceleration of point E on link 3.



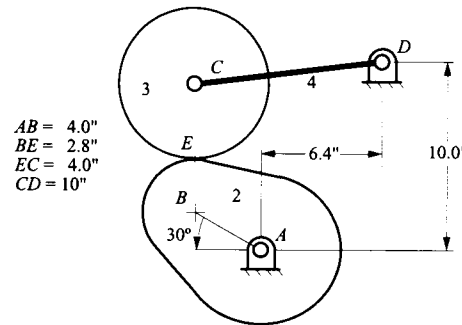
3.25 Part of an eight-link mechanism is shown in the figure. There is rolling contact at location B and the velocity and acceleration of points A<sub>6</sub> and C<sub>5</sub> are as shown. Find  $\omega_8$  and  $\alpha_7$  for the position given. Also find the velocity of E<sub>7</sub> by image.



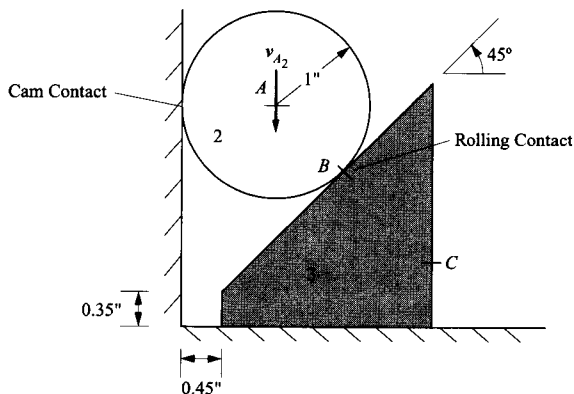
3.23 If  $v_{A_2} = 10$  in/s (constant) downward, find  $\omega_3$ ,  $\alpha_3$ ,  $v_{C_3}$ , and  $a_{C_3}$ .



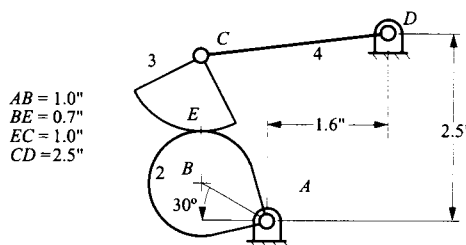
3.26 In the mechanism shown, link 2 is turning CW at the rate of 20 rad/s, and link 3 rolls on link 2. Draw the velocity and acceleration polygons for the mechanism, and determine  $a_{C_3}$  and  $\alpha_3$ .



3.24 In the figure shown, points A, B, and C are collinear. If  $v_{A_2} = 10$  in/s (constant) downward, find  $v_{C_3}$  and  $a_{C_3}$ .

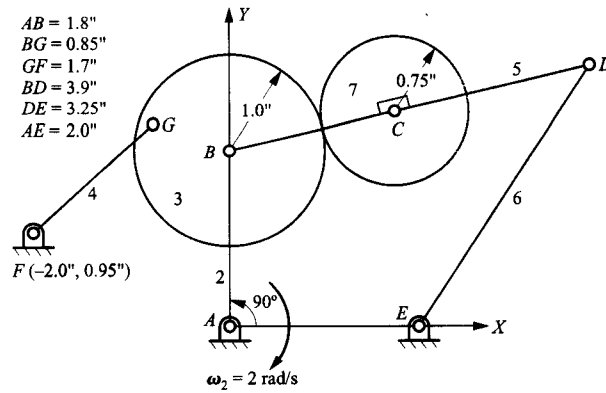


3.27 In the mechanism shown, link 2 is turning CW at the rate of 200 rpm. Draw the velocity polygon for the mechanism, and determine  $v_{C_3}$  and  $\omega_3$ .

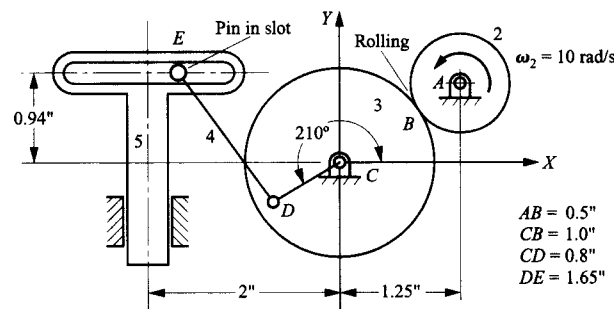




3.28 Assume that link 7 rolls on link 3 without slipping and find  $\omega_7$ .

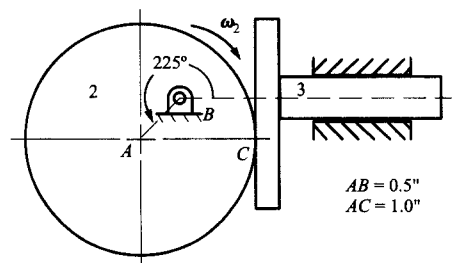


3.29 In the two-degree-of-freedom mechanism shown,  $\omega_2$  is given as 10 rad/s CCW. What should the linear velocity of link 6 be so that  $\omega_4 = 5 \text{ rad/s}$  CCW?



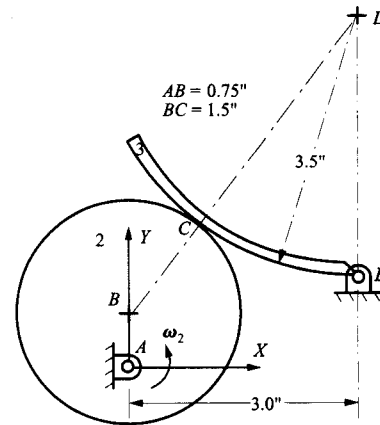
**EXERCISE PROBLEMS INVOLVING CAM CONTACT**

3.30 In the mechanism shown,  $\omega_2 = 10 \text{ rad/s}$  CW. Determine  $v_{C_3/C_2}$  and  $v_{C_3}$  using two approaches: (a) equivalent linkages and (b) coincident points at C.

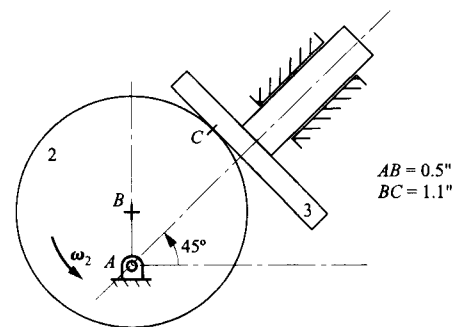


3.31 In the mechanism shown,  $\omega_2 = 20 \text{ rad/s}$  CCW. At the instant shown, point D, the center of curvature of link 3, lies directly above point E, and point B lies directly above point A.

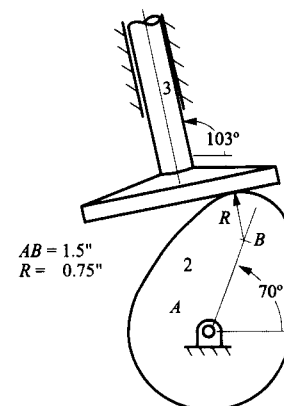
Determine  $v_{C_3/C_2}$  and  $\omega_3$  using: (a) equivalent linkages and (b) coincident points at C.



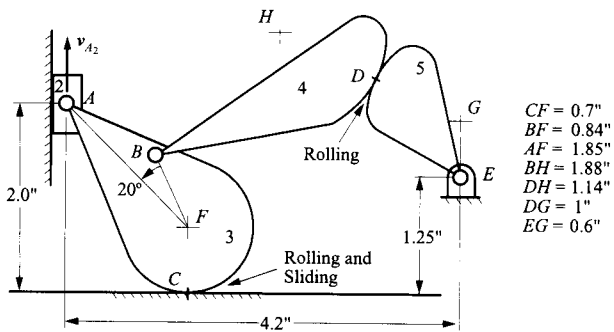
3.32 In the mechanism shown,  $\omega_2 = 100 \text{ rad/s}$  CCW and  $\alpha_2 = 20,000 \text{ rad/s}^2$  CCW. In the position shown, find the velocity and acceleration of link 3 using: (a) equivalent linkages and (b) coincident points at C.



3.33 Locate all of the instant centers in the mechanism shown. If the cam (link 2) is turning CW at the rate of 900 rpm, determine the linear velocity of the follower.

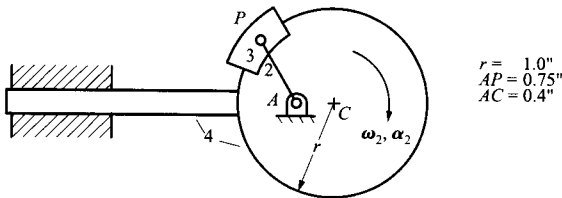


3.34 In the mechanism shown,  $v_{A_2} = 20$  in/s upward. Find  $\omega_5$  and  ${}^3\omega_4$ . Indicate on link 4 the point that has zero velocity. In the drawing,  $H$  and  $G$  are the centers of curvature of links 4 and 5, respectively, corresponding to location  $D$ .  $F$  is the center of curvature of link 3 corresponding to  $C$ . Also, point  $G$  lies exactly above point  $E$ .

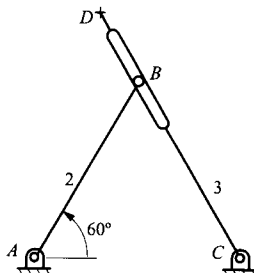


**EXERCISE PROBLEMS INVOLVING GENERAL COINCIDENT POINTS**

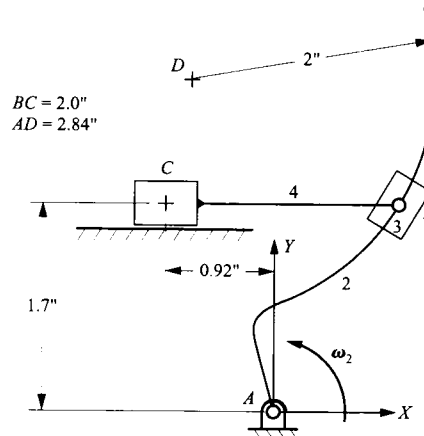
3.35 On the mechanism shown, link 4 slides on link 1, and link 3 slides on link 4 around the circle arc. Link 2 is pinned to links 1 and 3 as shown. Determine the location of the center of curvature of the path that point  $P_4$  traces on link 2. Assume  $\omega_2 = 10$  rad/s CW and  $\alpha_2 = 100$  rad/s<sup>2</sup> CW.



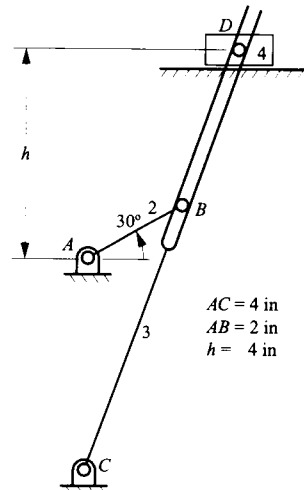
3.36 For the mechanism shown, find  $\omega_2$ ,  $\alpha_2$ ,  $v_{B_2}$ ,  $a_{B_2}$ ,  $v_{D_3}$ ,  $a_{D_3}$ , and the location of the center of curvature of the path that point  $B_3$  traces on link 2. Assume  $AB = AC = 10$  cm,  $CD = 14$  cm,  $\omega_3 = 1$  rad/s CCW, and  $\alpha_3 = 1$  rad/s<sup>2</sup> CW.



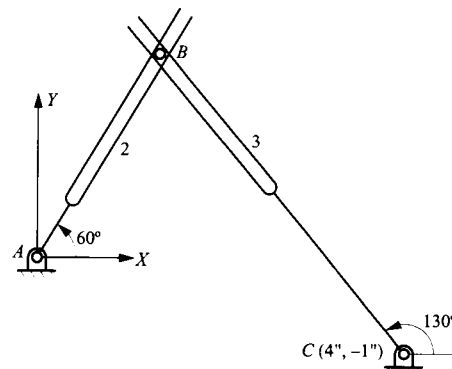
3.37 If  $\omega_2 = 10$  rad/s CCW (constant), find  $v_{B_2}$ ,  $v_{B_3}$ ,  $a_{B_3}$ , and  $a_{C_4}$ .



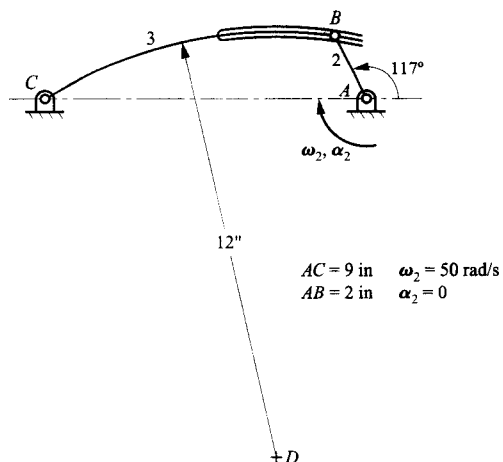
3.38 In the mechanism shown,  $\omega_2 = 10$  rad/s CW (constant). Determine the angular acceleration of link 3.



3.39 In the mechanism shown, slotted links 2 and 3 are independently driven at angular velocities of 30 and 20 rad/s CW and have angular accelerations of 900 and 400 rad/s<sup>2</sup> CW, respectively. Determine the acceleration of point  $B$ , the center of the pin carried at the intersection of the two slots.

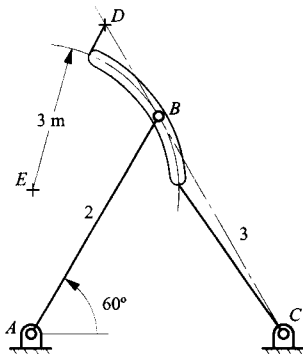


3.40 For the mechanism shown, find  $\omega_3$ ,  $\alpha_3$ ,  $a_{B_3}$ , and the location of the center of curvature of the path that point  $B_3$  traces on link 2.

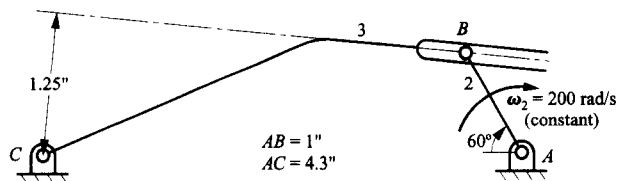


3.41 For the mechanism shown, points  $C$ ,  $B$ , and  $D$  are collinear. Point  $B_2$  moves in a curved slot on link 3. For the position given, find  $\omega_3$ ,  $\alpha_3$ ,  $v_{B_3}$ ,  $a_{B_3}$ ,  $v_{D_3}$ ,  $a_{D_3}$ , and the location of the center of curvature of the path that point  $B_3$  traces on Link 2. Assume

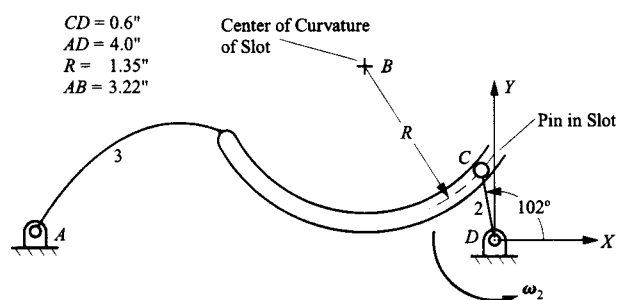
$AB = AC = 5 \text{ m}$ ,  $CD = 7 \text{ m}$ ,  $CE = 5.7 \text{ m}$   
 $\omega_2 = 2 \text{ rad/s}$  CCW,  $\alpha_2 = 3 \text{ rad/s}^2$  CCW



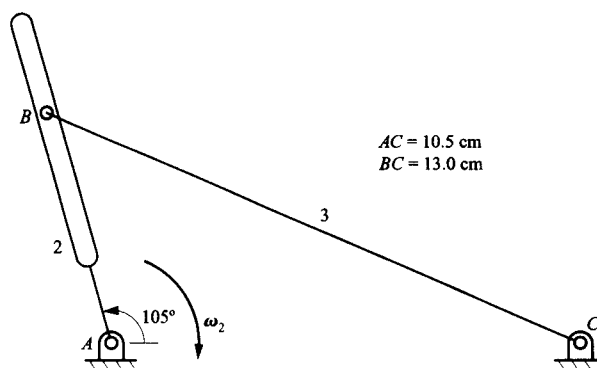
3.42 If the mechanism shown is drawn full scale, find  $\omega_3$ ,  $\alpha_3$ , and the location of the center of curvature of the path that point  $B_3$  traces on link 2. Assume that link 2 is driven at constant velocity.



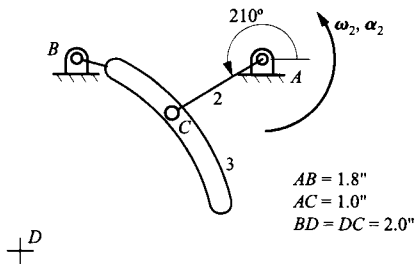
3.43 If  $\omega_2 = 20 \text{ rad/s}$  (constant) CCW, find  $\omega_3$ ,  $\alpha_3$ , and the center of curvature of the path that  $C_3$  traces on link 2.



3.44 If  $\omega_2 = 10 \text{ rad/s}$  CW (constant), find  $\alpha_3$ .

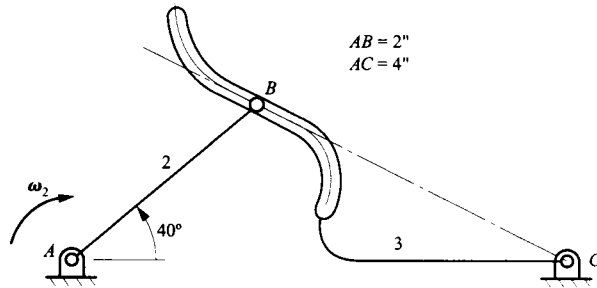


3.45 For the linkage shown,  $\omega_2 = 10 \text{ rad/s}$  CCW and  $\alpha_2 = 100 \text{ rad/s}^2$  CCW. Determine  $\omega_3$  and  $\alpha_3$ .



3.46 If  $\omega_2 = 10 \text{ rad/s}$  CW (constant), find

- $\omega_3$ ,
- the center of curvature of the path that  $B_2$  traces on link 3 (show on drawing),
- the center of curvature of the path that  $B_3$  traces on link 2 (show on drawing).



# CHAPTER 4

---

## INSTANT CENTERS OF VELOCITY

### 4.1 INTRODUCTION

---

At every instant during the motion of a rigid body in a plane, there exists a point that is instantaneously at rest. This point is called the instant center. The concept of an instant center of velocity for two bodies with planar motion was first discovered by Johann Bernoulli in 1742. This concept was later extended by Chasles in 1830 to include general spatial motion using the instantaneous screw axis concept.

The instant center technique for velocity analysis is particularly useful when only two or three velocities, or angular velocities, are of interest. It can be a very efficient technique, for example, for finding input-output velocity relationships of very complex mechanisms. When combined with virtual work, or conservation of energy (Chapter 13), it provides an efficient way to obtain input-output force or torque relationships. Instant centers are also very helpful when analyzing mechanisms with higher pairs, such as cam mechanisms, or gear trains. In principle, the instant center and velocity polygon techniques are *alternative* methods for solving the same set of problems. However, they are quite different techniques, and each is better suited to some situations than to others. Some experience is necessary to easily identify the most applicable technique for a particular problem.

It should be emphasized that instant centers of velocity are applicable to velocities only and are usually of little help if accelerations are ultimately of interest. If an acceleration analysis must be performed, then the velocity analysis should be conducted using one of the previously discussed traditional procedures based on vector methods.

Although the instant center of velocity has proved to be very useful in general mechanism velocity analysis, the corresponding instant center of acceleration has found little use. This is because, in general, more calculations are required to find the acceleration center than would be required to find the accelerations of interest using methods previously outlined. Therefore, only instant centers of velocity will be considered here.

### 4.2 DEFINITION

---

Given two bodies  $B$  and  $C$  moving with planar motion relative to each other in a reference frame  $R$ , there is, in general, only one location  $P$  in the plane of motion where the coincident points at a given instant have the same velocity with respect to the reference frame  $R$ . One coincident point is fixed to body  $B$  and the other is fixed to body  $C$ . This location is called the instant center of velocity for bodies  $B$  and  $C$  and is represented by  $I_{BC}$  or  $I_{CB}$ . If  $P$  is the instant center, then

$${}^R\mathbf{v}_{P_B} = {}^R\mathbf{v}_{P_C}$$

or

$${}^R\mathbf{v}_{P_B/P_C} = {}^R\mathbf{v}_{P_C/P_B} = 0$$

If the points are permanently attached to each other, they are called permanent instant centers. If the points are only momentarily coincident, the instant centers are called instantaneous instant centers.

### 4.3 EXISTENCE PROOF

The existence of an instant center between arbitrary links  $B$  and  $R$  may be inferred, and its location found, by the use of the relationship between the velocities of two points in body  $B$ . In the following, all velocities are defined in system  $R$ , so the left superscript designating the coordinate system will be omitted for simplicity. Then,

$$\mathbf{v}_{Q_B} = \mathbf{v}_{P_B} + \boldsymbol{\omega}_B \times \mathbf{r}_{Q/P}$$

Now, assume that  $Q$  is the instant center  $I_{RB}$ . Then,  $\mathbf{v}_{Q_B} = 0 = \mathbf{v}_{I_{RB}}$  and

$$-\mathbf{v}_{P_B} = \boldsymbol{\omega}_B \times \mathbf{r}_{Q/P} \quad (4.1)$$

From Section 2.4, we know that the radial component of the relative acceleration between two points  $P$  and  $Q$  on the same rigid link  $B$  is

$$\boldsymbol{\omega}_B \times (\boldsymbol{\omega}_B \times \mathbf{r}_{Q/P}) = -\omega_B^2 \mathbf{r}_{Q/P}$$

Therefore, cross multiplication of both sides of Eq. (4.1) by  $\boldsymbol{\omega}_B$  gives

$$\boldsymbol{\omega}_B \times (\boldsymbol{\omega}_B \times \mathbf{r}_{Q/P}) = -\boldsymbol{\omega}_B \times \mathbf{v}_{P_B} = -\omega_B^2 \mathbf{r}_{Q/P}$$

or

$$\mathbf{r}_{Q/P} = \frac{\boldsymbol{\omega}_B \times \mathbf{v}_{P_B}}{\omega_B^2}$$

In planar motion  $\boldsymbol{\omega}_B \times \mathbf{v}_{P_B}$  is normal to  $\mathbf{v}_{P_B}$  and may be written  $(\omega_B)(v_{P_B})\mathbf{n}$ , where  $\mathbf{n}$  is a unit vector normal to  $\mathbf{v}_{P_B}$  with the sense given by visualizing  $\mathbf{v}_{P_B}$  rotating about its tail in the  $\boldsymbol{\omega}_B$  direction. Hence

$$\mathbf{r}_{Q/P} = \frac{v_{P_B}}{\omega_B} \mathbf{n}$$

Thus, the distance,  $r_{P/Q}$ , in Fig. 4.1 from the instant center,  $I_{BR}$ , to point  $P$  is  $v_{P_B}/\omega_B$  and the line  $IP$  is normal to  $\mathbf{v}_{P_B}$ . Its sense is such that rotation of  $r_{P/Q}$  about  $I$  in the  $\boldsymbol{\omega}_B$  direction produces  $\mathbf{v}_{P_B}$ .

If more than one location in the plane of motion is found to be an instant center for two bodies, then those two bodies, for velocity analysis purposes, can be considered to be instantaneously fixed to each other. That is, if more than one location is an instant center, then all locations are instant centers.

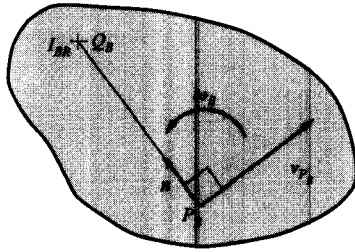


FIGURE 4.1 Proof of the existence of an instant center of velocity in planar motion.

However, if no finite location can be found that qualifies as an instant center of relative motion of two bodies, then the two bodies are translating with planar motion with respect to each other. In this case, the instant center can be considered to be located at infinity and reached by a line drawn perpendicular to the relative velocity vector between two arbitrary coincident points in the two bodies considered.

Instant centers are useful because they permit velocities to be computed easily. For example, if we know the velocity of point  $P_B$  by analysis, we know the velocity of  $P_R$  directly.

#### 4.4 LOCATION OF AN INSTANT CENTER FROM THE DIRECTIONS OF TWO VELOCITIES

Assume that we know the velocities of two points ( $P$  and  $Q$ ) in body  $C$  where the velocities are defined relative to the coordinate system in a second body  $B$ . This condition is shown in Fig. 4.2. We can then search for some point in  $C$  that has zero velocity relative to body  $B$ . The location of this point is the instant center designated by  $I_{BC}$  or, in the development here, it can be represented simply as  $I$ . To find the instant center location, let  $I_B$  be the point in body  $B$  and  $I_C$  be the coincident point in body  $C$ . We can write relative velocity expressions for points  $P$  and  $Q$  as follows:

$${}^B\mathbf{v}_{P_C} = {}^B\mathbf{v}_{P_C/I_B} = {}^B\mathbf{v}_{P_C/I_C} + {}^B\mathbf{v}_{I_C/I_B}$$

and

$${}^B\mathbf{v}_{Q_C} = {}^B\mathbf{v}_{Q_C/I_B} = {}^B\mathbf{v}_{Q_C/I_C} + {}^B\mathbf{v}_{I_C/I_B}$$

However, by definition of the instant center,

$${}^B\mathbf{v}_{I_C/I_B} = {}^B\mathbf{v}_{I_C} = 0$$

so that

$${}^B\mathbf{v}_{P_C/I_B} = {}^B\mathbf{v}_{P_C/I_C} = {}^B\boldsymbol{\omega}_C \times \mathbf{r}_{P_C/I_C}$$

and

$${}^B\mathbf{v}_{Q_C/I_B} = {}^B\mathbf{v}_{Q_C/I_C} = {}^B\boldsymbol{\omega}_C \times \mathbf{r}_{Q_C/I_C}$$

By definition of the cross product,  ${}^B\mathbf{v}_{P_C/I_C}$  must be perpendicular to  $\mathbf{r}_{P_C/I_C}$  and  ${}^B\mathbf{v}_{Q_C/I_C}$  must be perpendicular to  $\mathbf{r}_{Q_C/I_C}$ . The location of the instant center ( $I_{BC}$ ) is given by the intersection of the two perpendicular lines as shown in Fig. 4.2.

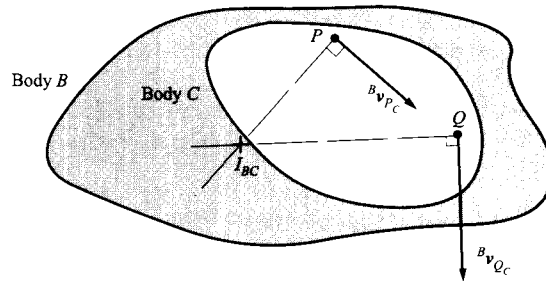


FIGURE 4.2 Location of the instant center given the directions of the velocities of two points.

### 4.5 INSTANT CENTER AT A REVOLUTE JOINT

The center of rotation at a revolute joint,  $I_{BC}$ , has the same velocity whether it is considered to be part of link  $B$  or link  $C$ . Therefore, it qualifies as a permanent instant center. This is indicated in Fig. 4.3.

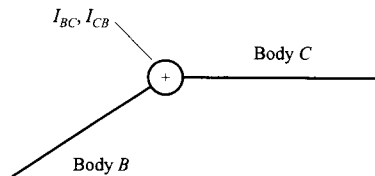


FIGURE 4.3 Permanent instant center.

### 4.6 INSTANT CENTER OF A CURVED SLIDER

If body  $B$  is a block moving on a circular arc on body  $C$  as shown in Fig. 4.4, then the center of the arc is a stationary location common to both bodies. Therefore, this location qualifies as a permanent instant center. If the curve is not circular at the location of interest, the curve can be replaced by its osculating circle (for velocities and accelerations) and the center of the osculating circle or center of curvature of the path at the given point would be the instant center. Actually, a circular slider is kinematically equivalent to a revolute joint. The center of the equivalent revolute is the center of curvature. That is, it is the instant center. A non-circular slide is realizable only as a higher pair, and the center of curvature is not a permanent instant center.

### 4.7 INSTANT CENTER OF A PRISMATIC JOINT

If the radius of curvature,  $\rho$ , in the case of the curved slider is allowed to become very large, the arc will approach a straight line. Also, the location of the instant center will tend toward infinity. However, the velocity of  $P$  relative to system  $B$  will still remain perpendicular to the line from  $P$  to the instant center. Therefore, if we know the direction of the velocity of *any* point  $P$  relative to system  $B$ , we can find one locus for the instant center; that is, it must lie on a line perpendicular to the velocity vector as shown in Fig. 4.5.



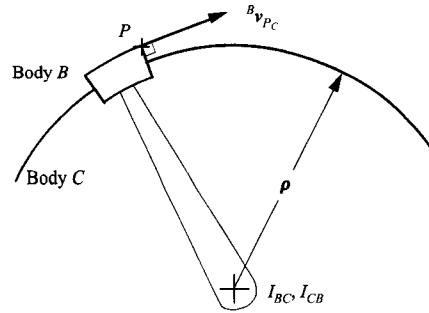


FIGURE 4.4 Instant center of a curved slide.

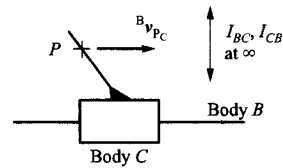


FIGURE 4.5 Instant center of a prismatic joint.

Note that the location of the line to infinity is unimportant; only the direction is defined by the velocity direction. This can be thought of as being the parallax phenomenon in which the direction to a distant object appears to remain the same, regardless of the motion of the observer.

## 4.8 INSTANT CENTER OF A ROLLING CONTACT PAIR

The instant center of pure rolling contact between two rigid bodies  $B$  and  $C$  is located at the point of contact of the two bodies as shown in Fig. 4.6. This is a direct consequence of the rolling condition that the two points in contact be at rest relative to one another. The instant center for the relative motion of involute spur gears is at the pitch point: the point of rolling contact between their pitch circles.

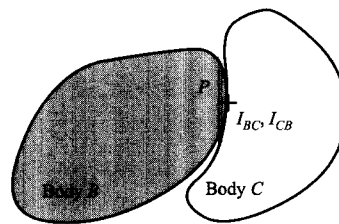


FIGURE 4.6 Instant center of a rolling contact.

## 4.9 INSTANT CENTER OF A GENERAL CAM-PAIR CONTACT

When two planar bodies ( $B$  and  $C$  in Fig. 4.7) are held in general cam contact, it is assumed that the bodies will neither penetrate each other nor separate. In general, the bodies both roll on each other and slide on each other. If sliding is involved, the direction of relative sliding must be along the common tangent of the profiles of the two bodies, as shown in Fig. 4.7.

If  $P$  is the contact point location, then the velocity of point  $P_C$ , relative to body  $B$  as well as the velocity of point  $P_B$  relative to body  $C$  will lie along the common tangent. Therefore, the instant center must be located on a line perpendicular to the common tangent at the contact point  $P$ . This means that the instant center must lie on a line through the centers of curvature ( $O_C$  and  $O_B$ ) corresponding to  $P$  in each of the two bodies.

To locate precisely the position of  $I_{BC}$ , some further information about the relative motion of bodies  $B$  and  $C$  is required. For example, assume that body  $B$  is link 2 and body  $C$  is link 3 and that links 2 and 3 are both connected to the frame by revolute joints as shown in Fig. 4.8.

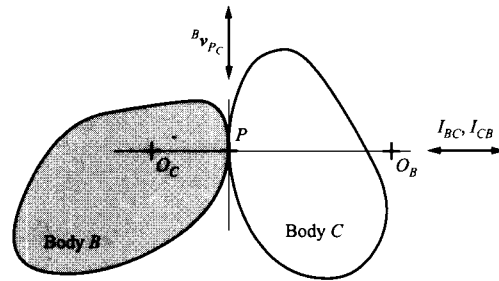


FIGURE 4.7 Relationship between instant centers and sliding velocity in cam contact.

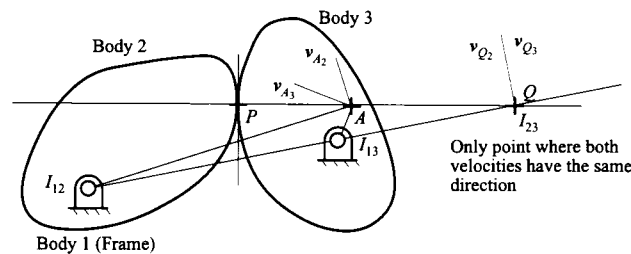


FIGURE 4.8 The instant center location between two frame-mounted cams.

If we arbitrarily pick the point  $A$  as a candidate for the instant center, we see that the velocities  $v_{A_2}$  and  $v_{A_3}$  cannot be equal because they are not in the same direction. The only location where they can be equal in direction is at the point  $Q$  on a line through the two pivots. Note that the two fixed pivots are the instant centers  $I_{12}$  and  $I_{13}$ .

## 4.10 CENTRODES

As two bodies,  $B$  and  $C$ , move relative to each other,  $I_{BC}$  traces a path on each of the bodies (path  $BC_B$  on body  $B$  and  $BC_C$  on body  $C$ ). These paths are the centrodes for the two bodies. At any instant, the two paths will be in contact with each other at the instant center where there is zero relative velocity between the two bodies and therefore between the two centrodes. That is, the instant center acts as a point of rolling contact between the two centrodes. This means that, as the two bodies move, the two centrodes will roll on each other. Conversely, the relative motion of the two bodies can be faithfully reproduced by rolling one

centrode on the other no matter how the original motion was produced. Therefore, the analysis of the relative motion of two bodies moving with planar motion can always be transformed to the study of two bodies rolling on each other. Note that as the two centrodes for links 2 and 3 roll on each other, the contact point ( $I_{23}$ ) and the instant centers  $I_{12}$  and  $I_{13}$  will be collinear, as illustrated in Fig. 4.8.

These concepts can be extended into spatial motion in which the instant center becomes an instantaneous screw axis (ISA), and the loci of the ISAs in the two bodies are ruled surfaces called axodes. These axodes roll on each other in a direction perpendicular to their generating instantaneous screw axes as well as sliding relative to each other along their instantaneous screw axes.

An example of the fixed and moving centrodes associated with the coupler of a four-bar linkage is shown in Fig. 4.9. This shows the centrodes generated by instant center  $I_{13}$ . The centrodes in Fig. 4.9 are very simple, but this is not the typical case. For crank-rocker mechanisms, the centrodes will extend to infinity (when the crank and rocker are parallel) in two directions, and for drag-link mechanisms, the centrodes can form multiple loops. Typical examples are shown in Figs. 4.10 and 4.11. These centrodes were generated with the MATLAB program *centrodes.m* included on the disk with this book.

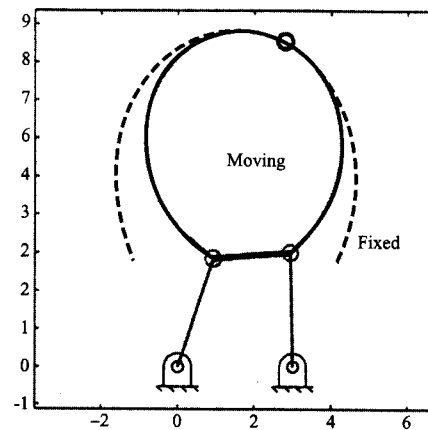


FIGURE 4.9 Centrodes associated with instant center  $I_{13}$  for a simple four-bar linkage.

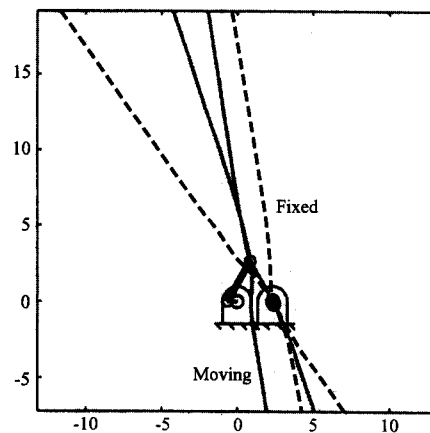
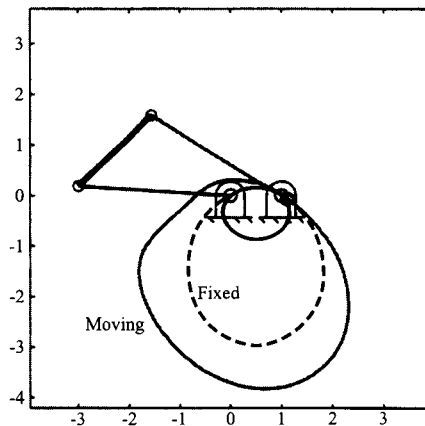
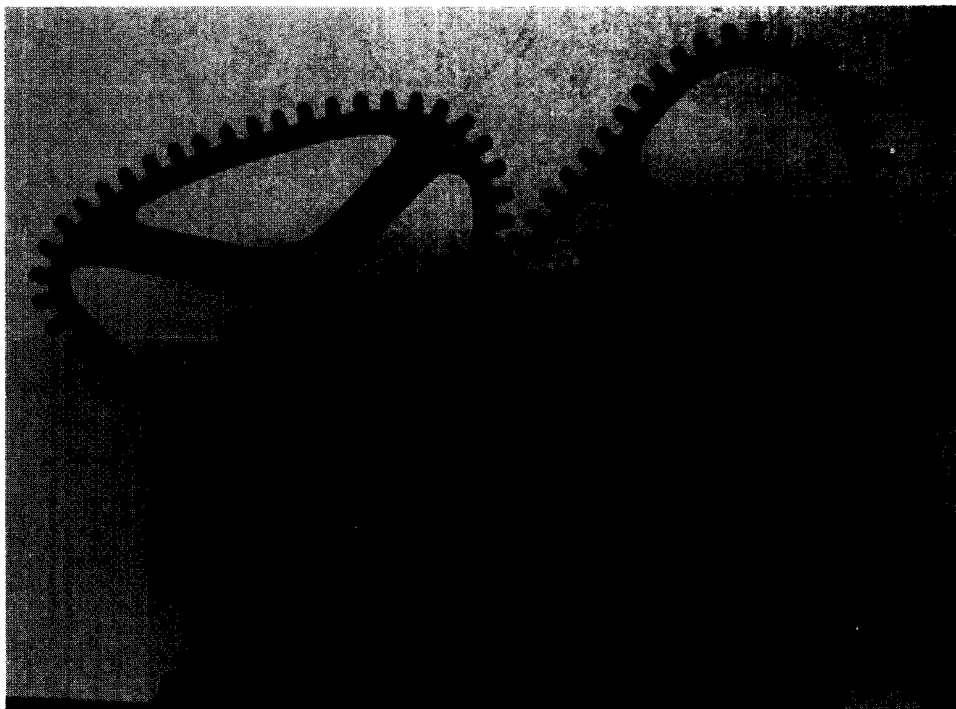


FIGURE 4.10 Centrodes associated with instant center  $I_{13}$  for a crank-rocker four-bar linkage.



**FIGURE 4.11** Centrodes associated with instant center  $I_{13}$  for a drag-link four-bar linkage.

Another example of centrodes is shown in the model in Fig. 4.12. The mechanism model is a six-bar linkage, and the noncircular gears attached to the two frame-mounted links correspond to the centrodes of relative motion of those links. The motion of the two links attached to the gears is the same relative to the frame and to each other whether the linkage is present without the gears or with the gears present but without the linkage.



**FIGURE 4.12** Six-bar linkage model with centrodes represented by noncircular gears. The gears roll on each other at the pitch points, and the pitch point is the instant center between the two frame-mounted cranks.

## 4.11 THE KENNEDY-ARONHOLDT THEOREM

If we have  $n$  bodies and we take them two at a time such that  $I_{AB} = I_{BA}$ , then the total number of instant centers is given by

$$N_{IC} = \frac{n(n-1)}{2}$$

Because of the large number of instant centers (ICs) occurring in a mechanism with a large number of links, it is desirable to develop a procedure that helps to identify the locations of the instant centers in a systematic manner. This can be done using the results of the Kennedy–Aronholdt theorem.

In the late 19th century, Kennedy (England) and Aronholdt (Germany) greatly extended the usefulness of instant centers by discovering independently the theorem of three centers. The theorem is stated as follows:

*If three bodies are in relative planar motion (or two bodies moving relative to each other and to the fixed reference frame), there are three instant centers pertaining to the relative motion of pairs of those bodies. Those three instant centers are collinear.*

Thus, in Fig. 4.13, given three bodies  $A$ ,  $B$ , and  $C$  moving with planar motion in reference frame  $R$ , the three instant centers  $I_{AB}$ ,  $I_{AC}$ , and  $I_{BC}$  all lie on the same straight line in the plane. To prove the theorem, it is necessary to recognize that the instant center is really two coincident points. One of these two points is embedded in each of the two laminae for which the instant center describes the relative motion. Hence, in Fig. 4.13:

$I_{AB}$  is two points common to  $A$  and  $B$ .

$I_{AC}$  is two points common to  $A$  and  $C$ .

$I_{BC}$  is two points common to  $B$  and  $C$ .

Also,

$${}^R\mathbf{v}_{(I_{AB})_A} = {}^R\mathbf{v}_{(I_{AB})_B}$$

$${}^R\mathbf{v}_{(I_{AC})_A} = {}^R\mathbf{v}_{(I_{AC})_C}$$

$${}^R\mathbf{v}_{(I_{BC})_B} = {}^R\mathbf{v}_{(I_{BC})_C}$$

Assume that we know the locations of  $I_{AB}$  and  $I_{AC}$  and we want to find  $I_{BC}$ . Relative to link  $A$ , we can first write

$${}^A\mathbf{v}_{(I_{BC})_B} = {}^A\mathbf{v}_{(I_{BC})_C}$$

or

$${}^A\mathbf{v}_{(I_{BC})_B} = {}^A\mathbf{v}_{(I_{BC})_B} / (I_{AB})_A = {}^A\mathbf{v}_{(I_{BC})_B} / (I_{AB})_B = {}^A\boldsymbol{\omega}_B \times \mathbf{r}_{(I_{BC})} / (I_{AB})$$

Also,

$${}^A\mathbf{v}_{(I_{BC})_C} = {}^A\mathbf{v}_{(I_{BC})_C} / (I_{AC})_A = {}^A\mathbf{v}_{(I_{BC})_C} / (I_{AC})_C = {}^A\boldsymbol{\omega}_C \times \mathbf{r}_{(I_{BC})} / (I_{AC})$$

or equating the two relationships, we get

$${}^A\omega_C \times \mathbf{r}_{I_{BC}/I_{AC}} = {}^A\omega_B \times \mathbf{r}_{I_{BC}/I_{AB}}$$

Since  ${}^B\omega_C$  is parallel to  ${}^A\omega_B$ , then the  $\mathbf{r}$ 's must also be parallel to make the cross products equal. Because both of the  $\mathbf{r}$ 's pass through  $I_{BC}$ , they must be collinear. This can happen only if  $I_{AB}$ ,  $I_{AC}$ , and  $I_{BC}$  all lie on the same line.

The Kennedy–Aronholdt theorem can be used in the following way to find instant centers. Assume that we have two groups of three links such that two links are common to both groups. For example, as shown in Fig. 4.14, if we have  $I_{45}$  and  $I_{47}$  and  $I_{35}$  and  $I_{37}$ , links 5 and 7 are common to both groups. We know that  $I_{57}$  must lie on a line through  $I_{45}$  and  $I_{47}$ , and it must also lie on the line through  $I_{35}$  and  $I_{37}$ . The location is defined by the intersection of the two lines.

Therefore, by selecting two pairs of appropriate instant centers, we can locate the instant center that is common to the two groups of links. A way in which the Kennedy–Aronholdt theorem can be used is illustrated by the following example.

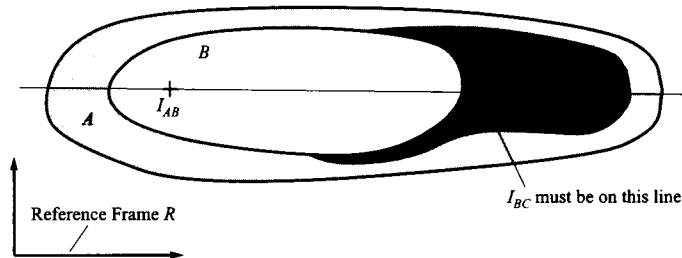


FIGURE 4.13 The Kennedy–Aronholdt theorem.

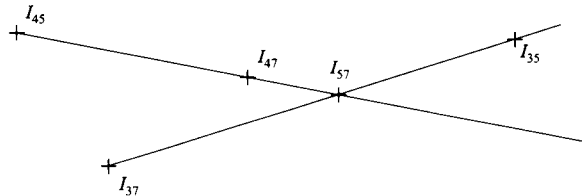


FIGURE 4.14 Triplets of instant centers.

**EXAMPLE 4.1**  
**Locating Instant Centers for a Four-Bar Linkage**

Locate all instant centers of the four-bar linkage in the position shown in Fig. 4.15.

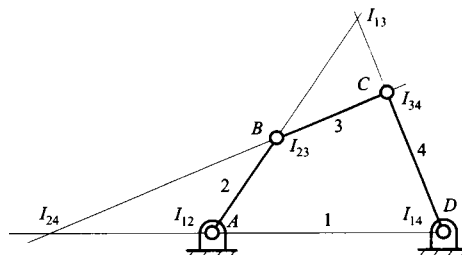


FIGURE 4.15 Application of the Kennedy–Aronholdt theorem to the location of all instant centers of a four-bar linkage.

**Solution**

By inspection,  $I_{12}$  is at  $A$ ,  $I_{23}$  at  $B$ ,  $I_{34}$  at  $C$ , and  $I_{14}$  at  $D$ . Thus, four of the six instant centers are already identified. To locate  $I_{13}$ , note that it is collinear with  $I_{12}$  and  $I_{23}$  and also with  $I_{14}$  and  $I_{34}$ . Thus it is at the intersection of  $BC$  and  $AD$ . Similarly, to locate  $I_{24}$ , note that it is collinear with  $I_{23}$  and  $I_{34}$  and also with  $I_{12}$  and  $I_{14}$ .

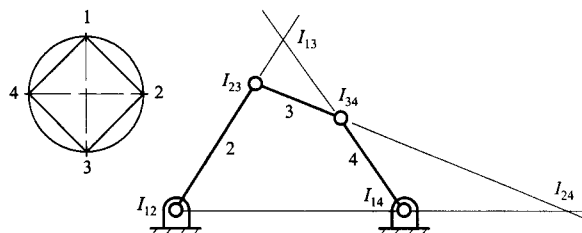
A set of three collinear instant centers always shares the same three subscripts, each subscript appearing on two instant centers. Given two instant centers with a common subscript, the third center, which completes the collinear set, has the two subscripts that are not common to the other two centers.

## 4.12 CIRCLE DIAGRAM AS A STRATEGY FOR FINDING INSTANT CENTERS

When the number of bodies is large, it is helpful to use some kind of bookkeeping method to help find all of the instant centers. One such method is the circle method, which is based directly on the Kennedy–Aronholdt theorem. The procedure is illustrated on the four-bar linkage in Fig. 4.16 as follows:

1. Draw the kinematic diagram for the mechanism to be analyzed.
2. Draw a circle of arbitrary radius and place tick marks representing all of the mechanism member symbols approximately equally spaced around the perimeter of the circle.
3. By inspection, determine as many instant centers as possible, and draw a straight line between the corresponding numbers on the circle. For example, if  $I_{12}$  is known, then a line is drawn between symbols 1 and 2.
4. If a line can be drawn between two points on the circle such that the line is the only unknown side of two triangles, the instant center represented by that line lies at the intersection of the two lines drawn through the instant center pairs that are identified by the two known sides of each triangle. Once the instant center is located, the appropriate two points on the circle diagram are connected.
5. Repeat the procedure in step 4 until all of the instant centers of interest are found.

As a second example, consider the slider-crank mechanism shown in Fig. 4.17. Again, the instant centers to be found are  $I_{24}$  and  $I_{13}$ . These can be found directly; however, it is necessary to note that  $I_{14}$  is located at infinity along a line perpendicular to the slider velocity direction given.



**FIGURE 4.16** Use of the circle diagram when locating instant centers.

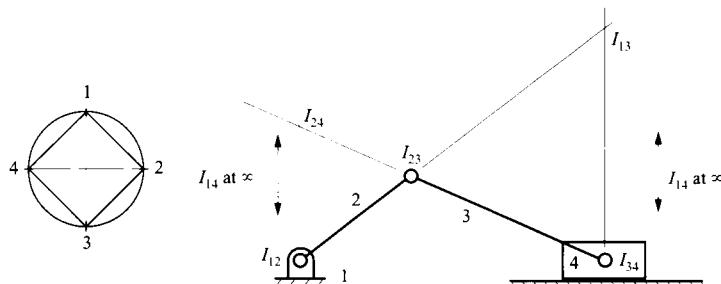


FIGURE 4.17 The instant centers of a slider-crank linkage.

### 4.13 USING INSTANT CENTERS: THE ROTATING-RADIUS METHOD

Once the proper instant centers are found, these can be used to find the velocities of selected points in a rigid body. This can be done analytically; however, graphical methods are generally much faster to use. An especially useful method for finding velocities is the rotating-radius method. To develop the method, assume we have an arbitrary link moving relative to the reference system. For the sake of illustration, assume that the link is 3 and the reference link is the frame (link 1). Let points  $P$  and  $Q$  be any points fixed to link 3 as shown in Fig. 4.18. Then, we can write

$$\mathbf{v}_{P_3/Q_3} = \boldsymbol{\omega}_3 \times \mathbf{r}_{P_3/Q_3} = \mathbf{v}_{P_3} - \mathbf{v}_{Q_3}$$

and this is perpendicular to the line from  $P$  to  $Q$ . If point  $Q_3$  has zero velocity relative to link 1, then

$$\mathbf{v}_{P_3/Q_3} = \mathbf{v}_{P_3}$$

However, the only point in link 3 that has zero velocity relative to the frame is  $I_{13}$ . Therefore,

$$\mathbf{v}_{P_3} = \boldsymbol{\omega}_3 \times \mathbf{r}_{P_3/I_{13}}$$

Because point  $P$  was *any* arbitrary point in link 3, this equation holds for *all* points in link 3. Therefore, if we know the angular velocity of the link and the instant center relative to the

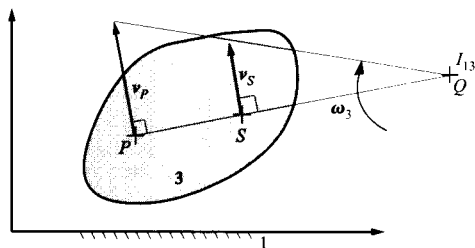


FIGURE 4.18 The rotating-radius method.



frame, we can compute the absolute velocity of any point in the body. Furthermore, the direction of the absolute velocity is perpendicular to the line from the point to the instant center.

For other points, only the vector  $\mathbf{r}_{P_3/I_{13}}$  will change as  $P$  changes. Considering the magnitude of the velocity, we have

$$|\mathbf{v}_{P_3}| = |\boldsymbol{\omega}_3| |\mathbf{r}_{P_3/I_{13}}|$$

Because  $\boldsymbol{\omega}_3$  is the same for all points in the link, the magnitude of the velocity for any other point  $S$  is given by

$$|\mathbf{v}_{S_3}| = |\boldsymbol{\omega}_3| |\mathbf{r}_{S_3/I_{13}}|$$

Therefore, dividing the two equations gives

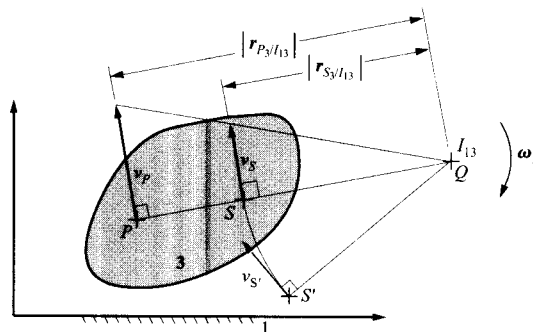
$$\frac{|\mathbf{v}_{P_3}|}{|\mathbf{v}_{S_3}|} = \frac{|\mathbf{r}_{P_3/I_{13}}|}{|\mathbf{r}_{S_3/I_{13}}|}$$

or

$$|\mathbf{v}_{S_3}| = |\mathbf{v}_{P_3}| \frac{|\mathbf{r}_{S_3/I_{13}}|}{|\mathbf{r}_{P_3/I_{13}}|}$$

This magnitude applies to any point that is the same distance from the instant center. The magnitude of the velocity is directly proportional to its distance from the instant center. Hence if two points in the rigid body have the same  $|\mathbf{r}_{S_3/I_{13}}|$ , they will have the same magnitude of velocity  $|\mathbf{v}_{S_3}|$ ; however, the directions of their velocities will differ because the velocity is perpendicular to the line from the point to the instant center. This is illustrated by  $S$  and  $S'$  in Fig. 4.19. The actual direction of the velocity is obtained by recognizing that all points will appear to rotate about the instant center relative to the frame.

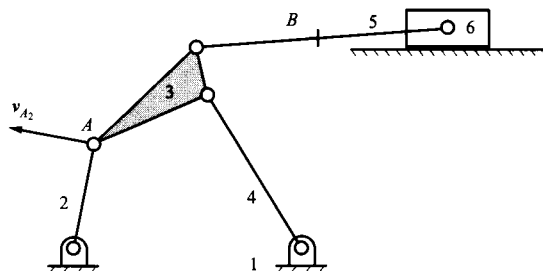
This theory is the basis for the rotating-radius method. The basic procedure is to find the magnitude of the velocity of one point in the rigid body and draw that velocity vector to scale on the link. The velocity of any other point on the body can then be found by recognizing that the magnitude of the velocity relative to the frame is proportional to the distance from the instant center. Proportional triangles can be drawn by using the line from the original point to the instant center as a baseline. Alternately, the line from the new point to the instant center can be used as a baseline.



**FIGURE 4.19** The rotating-radius method of obtaining the velocity of a point in a body relative to a reference frame (or another body) given the location of the instant center of the body and the velocity of some other point in the body relative to that frame.

**EXAMPLE 4.2**  
**Using the Rotating-Radius Method for Velocities**

Given the compound linkage shown in Fig. 4.20, the velocity of point  $A$  is given as shown. Find the velocity of point  $B$ .



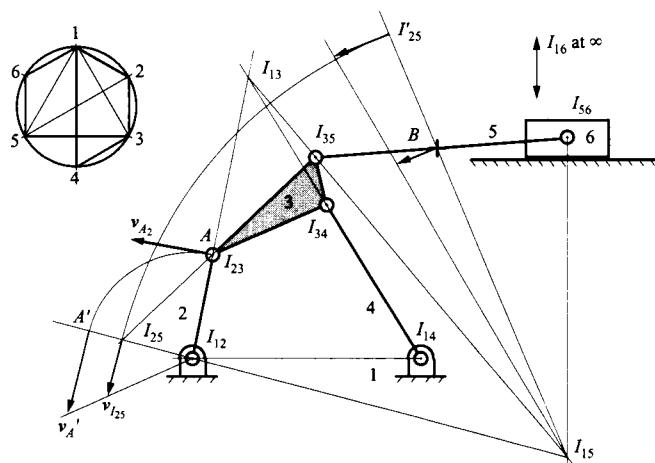
**FIGURE 4.20** Compound linkage for Example 4.2.

**Solution**

The first step in the procedure is to determine the instant centers that are needed. This can be done by rewriting the given and desired information in terms of the link numbers and frame number. That is, we are given the velocity  $v_{A_2}$  and we want to find  $v_{B_5}$ . Here we see that the reference system is 1 and the two links involved are 2 and 5. In this problem and in general problems using instant centers, we will need to locate three instant centers:

1.  $I_{12}$ , the instant center between the reference frame and the link where the input information is given,
2.  $I_{15}$ , the instant center between the reference frame and the link where the velocity is to be found, and
3.  $I_{25}$ , the instant center between the link where a velocity is specified and the link where the velocity is to be found.

When the linkage is analyzed, it is apparent that  $I_{12}$  can be found by inspection. Therefore, only  $I_{25}$  and  $I_{15}$  need to be constructed. This is done by first locating  $I_{13}$  using  $I_{12}$  and  $I_{23}$ , and  $I_{14}$  and  $I_{34}$ . Next,  $I_{15}$  is found using  $I_{13}$  and  $I_{35}$ , and  $I_{16}$  and  $I_{56}$ . Finally,  $I_{25}$  is found using  $I_{15}$  and  $I_{12}$  and  $I_{23}$  and  $I_{35}$ . The construction lines are shown in Fig. 4.21.

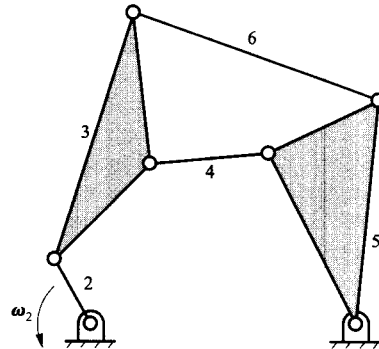


**FIGURE 4.21** Use of the rotating-radius method in a compound linkage.

After  $I_{25}$  is located, the velocity of  $I_{25}$  is found by rotating the triangle formed by the sides  $v_{A_2}$  and  $I_{12}A$  about  $I_{12}$  onto the baseline through  $I_{12}$  and  $I_{25}$ . The velocity of  $I_{25}$  is then found using proportional triangles. Next, the triangle defined by sides  $v_{I_{25}}$  and  $I_{15}I_{25}$  is rotated about  $I_{15}$  onto the baseline through  $I_{15}$  and  $B$ . The velocity of  $B$  is then determined using proportional triangles. Note that when the velocity of  $I_{25}$  is found, the instant center is treated as a point in link 2, that is,  $(I_{25})_2$ . However, when the velocity of  $B$  is to be found, the instant center is treated as a point in link 5. This illustrates the fact that the instant center location defines the location of two points, one in link 2 and the other in link 5; however, both points have the same velocity.

**EXAMPLE 4.3**  
Using Instant Centers to Analyze a Stephenson-II Six Bar Linkage

Consider the Stephenson-II six-bar linkage in Fig. 4.22. Assume that  $\omega_2$  is given and we want to find  $\omega_5$ . This linkage has the characteristics of those described in Section 2.9; that is, the driving link is not included in any four-link loop. The following solution method should be compared to the inversion method in Section 2.9.



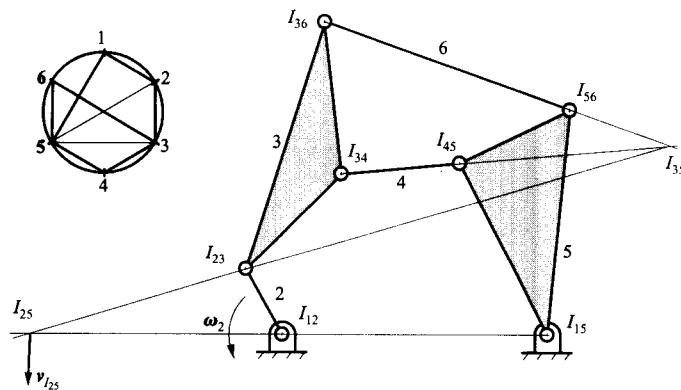
**FIGURE 4.22** Stephenson-II six-bar linkage for Example 4.3.

**Solution**

The use of instant centers to solve this problem is especially interesting because the linkage cannot be analyzed using the usual vector polygon approach described earlier.

Again, we need to determine which instant centers are required to solve the problem. Looking at the information that is given and that is to be found, we see that three links (1, 2, 5) are identified. Therefore, we need to find  $I_{12}$ ,  $I_{15}$ , and  $I_{25}$ . Of this set, only  $I_{25}$  cannot be determined by inspection. However, it can be found relatively easily from the instant centers that are available by inspection. First using  $I_{36}$  and  $I_{56}$  and  $I_{34}$  and  $I_{45}$ ,  $I_{35}$  can be located. Then using  $I_{35}$  and  $I_{23}$  and  $I_{12}$  and  $I_{15}$ ,  $I_{25}$  can be located. The resulting instant centers are shown in Fig. 4.23. The velocity of the coincident points at  $I_{25}$  is given by

$$v_{(I_{25})_2} = \omega_2 \times r_{I_{25}/I_{12}} = v_{(I_{25})_5} = \omega_5 \times r_{I_{25}/I_{15}}$$



**FIGURE 4.23** The instant center method applied to a Stephenson-II six-bar linkage.

Therefore, the magnitudes of the vectors are related by

$$\left| v_{(I_{25})_2} \right| = \left| \omega_2 \right| \left| r_{I_{25}/I_{12}} \right| = \left| v_{(I_{25})_5} \right| = \left| \omega_5 \right| \left| r_{I_{25}/I_{15}} \right|$$

and

$$\left| \omega_5 \right| = \left| \omega_2 \right| \frac{\left| r_{I_{25}/I_{12}} \right|}{\left| r_{I_{25}/I_{15}} \right|}$$

This gives the magnitude of  $\omega_5$ . We can get the direction by determining the sense of the velocity of  $v_{(I_{25})_5}$ . Because the vector is generally downward, the angular velocity must be CCW to satisfy the cross product sign convention.

#### EXAMPLE 4.4 Finding Instant Centers for a Quick-Return Mechanism

Find all the instant centers for the quick-return linkage shown in Fig. 4.24. The linkage is driven by the crank 2 rotating about the fixed revolute at point  $O_A$ . A pin fixed to link 2 at  $A$  slides in a slot in link 3. Link 3 rotates about a fixed revolute at point  $O_B$ . It is hinged at point  $B$  to the connecting link, 4. Link 4 connects to the horizontally sliding block, 5, via a revolute at point  $C$ . This type of linkage is used extensively in some machine tools (planers and shapers) because it generates a relatively slow and uniform forward, or cutting, stroke and a considerably quicker return stroke. The ratio of the durations of the two strokes can be determined by considering the angles through which the drive crank 2 rotates between the extreme positions of the rocker arm 3. The extreme positions are those in which  $O_A A$  is normal to  $O_B B$ .

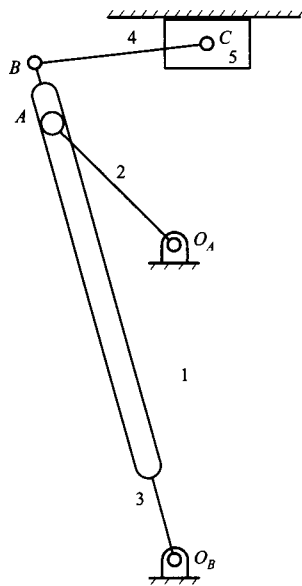


FIGURE 4.24 The linkage for Example 4.4.

#### Solution

The instant centers are shown in Fig. 4.25. In practice, it is seldom necessary to locate all instant centers. The great advantage of the instant center technique is its ease of use for complicated linkages, particularly when only the angular velocity of one member or the velocity of one point is to be found. For this problem only three instant centers are needed, although others may be needed in the process of locating them. The three instant centers needed are the set for the input link, output link, and base link. Here, the input link is the link whose angular velocity is given, or which contains a point whose velocity is given. The output link is the link whose angular velocity is sought, or which contains the point whose linear velocity is sought.

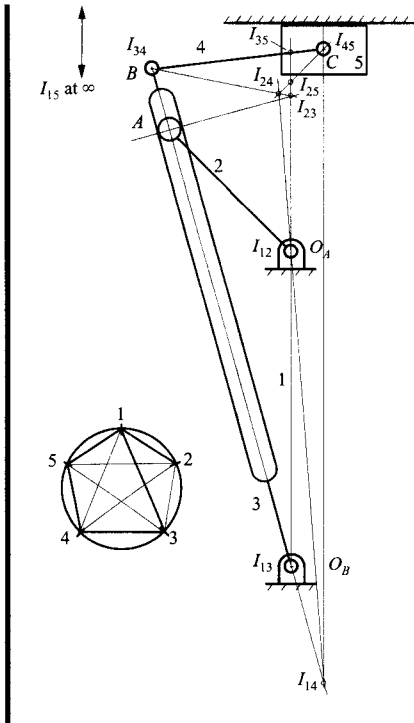


FIGURE 4.25 Location of instant centers for Example 4.4.

**EXAMPLE 4.5**  
**Finding Instant Centers of a Quick-Return Mechanism in a Singular Position**

Find all the instant centers of the quick-return linkage in Example 4.4 when point  $C$  is collinear with  $O_A$  and  $O_B$ . This is shown in Fig. 4.26.

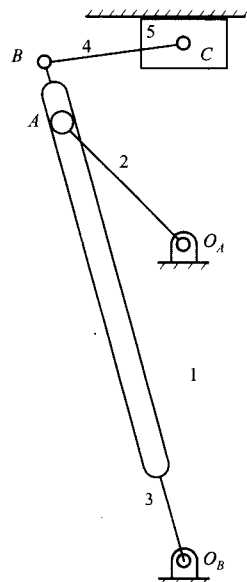


FIGURE 4.26 The linkage for Example 4.5.

**Solution**

If an attempt is made to find the instant centers with the procedure used in Example 4.4, it will be possible to find  $I_{23}$  and  $I_{35}$  directly, as shown in Fig. 4.27. However, it is not possible to find the locations of the remaining instant centers by simple construction because all of the remaining instant centers are located on the line defined by  $I_{12}$  and  $I_{13}$ . To determine the location of the remaining instant centers, let point  $C$  be moved slightly off of the line defined by  $I_{12}$  and  $I_{13}$  and locate the instant centers. The location of the instant centers in the true position can then be determined by visualizing their movement as  $C$  approaches its actual position. This is shown in Figs. 4.28 and 4.29. Note that as  $C$  moves toward the vertical position,  $I_{35}$  becomes coincident with  $I_{45}$ ,  $I_{14}$  becomes coincident with  $I_{13}$ , and  $I_{25}$  and  $I_{24}$  become coincident with  $I_{23}$ .

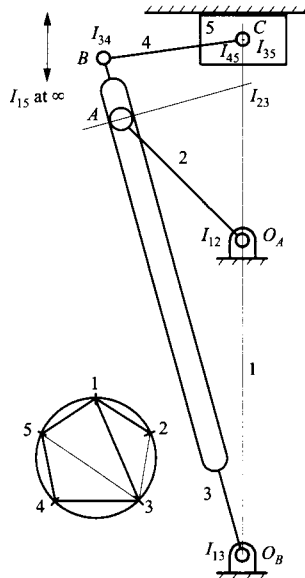


FIGURE 4.27 Location of  $I_{23}$  and  $I_{35}$  in Example 4.5.

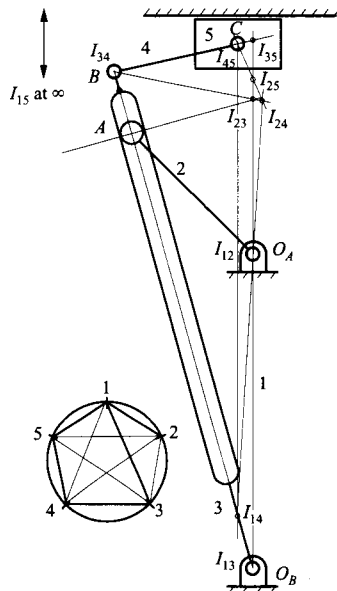
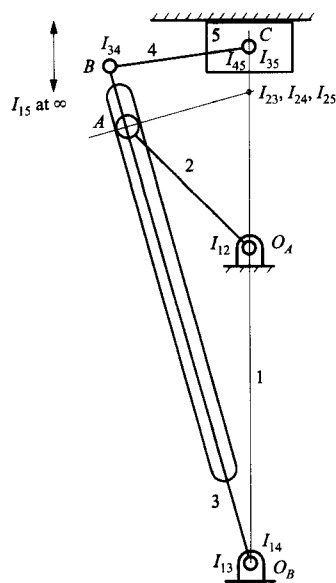


FIGURE 4.28 Instant centers when  $C$  is not in line with  $I_{35}$  in Example 4.5.

FIGURE 4.29 Actual location of  $I_{24}$ ,  $I_{25}$ , and  $I_{14}$  in Example 4.5.

**EXAMPLE 4.6**  
*Using Instant Centers to Analyze a Gear Mechanism*

Find the velocity of point  $C$  in Fig. 4.30 given that the angular velocity of gear 2 is 10 rad/s CW.  $B$  is a hinge connecting links 4 and 5 and does not connect to gear 3. Point  $A$  is a pin in link 3 that engages a slot in link 4.

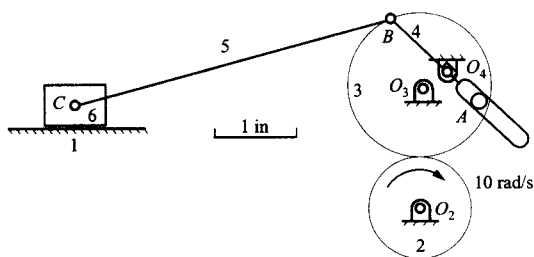


FIGURE 4.30 The linkage of Example 4.6.

**Solution**

To find the velocity of point  $C$ , considered as a point in link 5, from the angular velocity of link 2 relative to link 1, the instant centers  $I_{12}$ ,  $I_{15}$ , and  $I_{25}$  are needed. These may be located as shown in Fig. 4.31.

Then,

$$\omega_5 = \omega_2 \times (I_{12}I_{25}) / (I_{15}I_{25}) = 10 \times 0.940 / 7.261 = 1.29 \text{ rad/s CW}$$

$$v_{C_5} = \omega_5 \times (I_{15}C) = 1.29 \times 4.653 = 6.00 \text{ in/s to the left}$$

Notice that the instant center method is extremely efficient for simple input-output problems, such as this one, in which only two links are of interest.

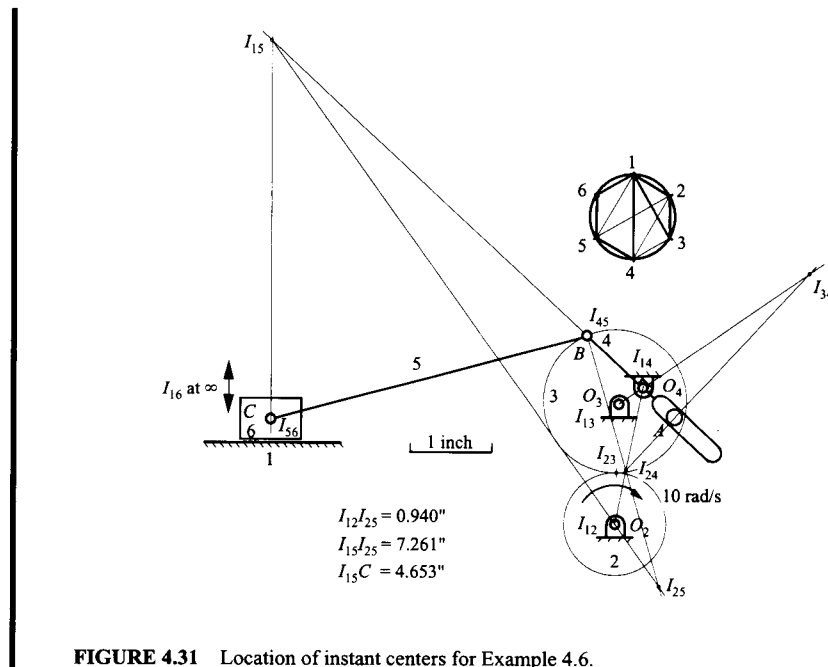


FIGURE 4.31 Location of instant centers for Example 4.6.

#### 4.14 FINDING INSTANT CENTERS USING DRAFTING PROGRAMS

In this chapter, we have implied that the instant-center approach to velocity analysis is a purely graphical method. However, this does not mean that the actual drawings must be done on a drawing board. A better approach is to use one of the many drafting programs available on computers. The drafting package can be used to

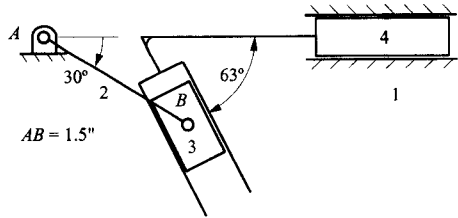
1. draw the basic linkage to scale,
2. find the instant centers,
3. find appropriate distances using available dimension routines, and
4. determine the desired velocities by using calculators available on computers.

This procedure is relatively fast and accurate, especially if the drafting package will allow the user to draw parallel and perpendicular lines accurately. The results can be easily imported into reports and other documents. This environment also allows the user to explore other design alternatives to obtain desired velocity results. From the examples in this chapter, it is clear that significant changes in the velocity can be made by small alterations in the link lengths or pivot locations.

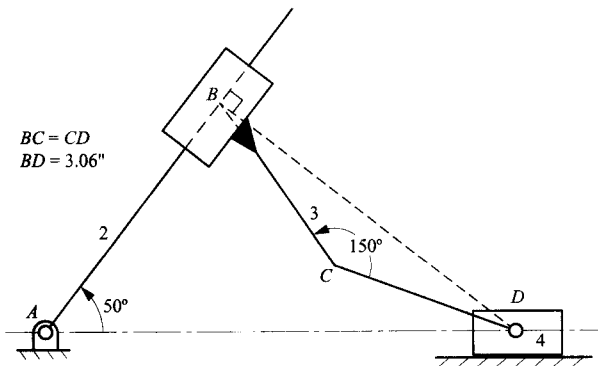


**PROBLEMS**

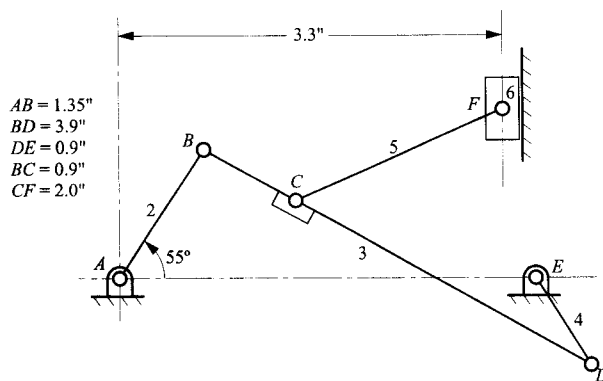
4.1 Locate all of the instant centers in the mechanism shown.



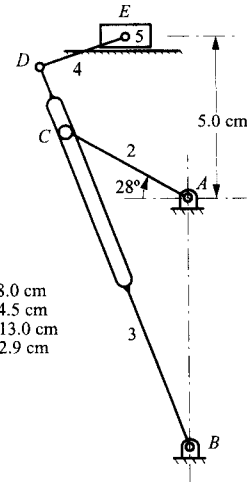
4.2 Find all of the instant centers of velocity for the mechanism shown.



4.3 In the linkage shown, locate all of the instant centers.

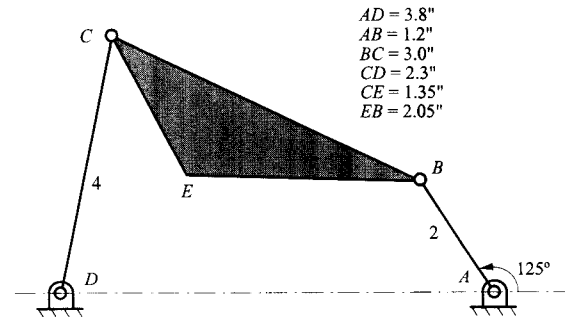


4.4 Find all of the instant centers of velocity for the mechanism shown.



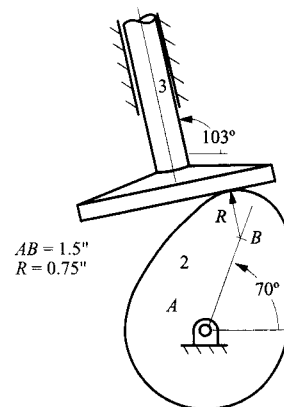
$AB = 8.0$  cm  
 $AC = 4.5$  cm  
 $BD = 13.0$  cm  
 $DE = 2.9$  cm

4.5 Locate all of the instant centers in the mechanism shown. If link 2 is turning CW at the rate of 60 rad/s, determine the linear velocity of points C and E using instant centers.

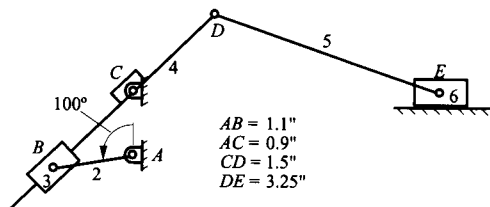


$AD = 3.8$ "  
 $AB = 1.2$ "  
 $BC = 3.0$ "  
 $CD = 2.3$ "  
 $CE = 1.35$ "  
 $EB = 2.05$ "

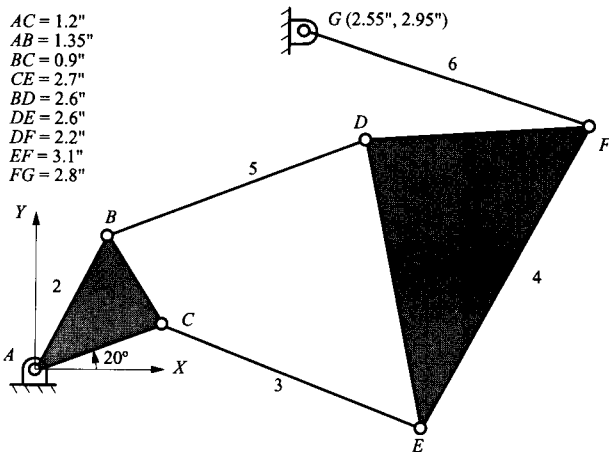
4.6 Locate all of the instant centers in the mechanism shown. If the cam (link 2) is turning CW at the rate of 900 rpm, determine the linear velocity of the follower using instant centers.



4.7 Locate all of the instant centers in the mechanism shown. If link 2 is turning CW at the rate of 36 rad/s, determine the linear velocity of point  $B_4$  by use of instant centers. Determine the angular velocity of link 4 in rad/s and indicate the direction. Points  $C$  and  $E$  have the same vertical coordinate, and points  $A$  and  $C$  have the same horizontal coordinate.

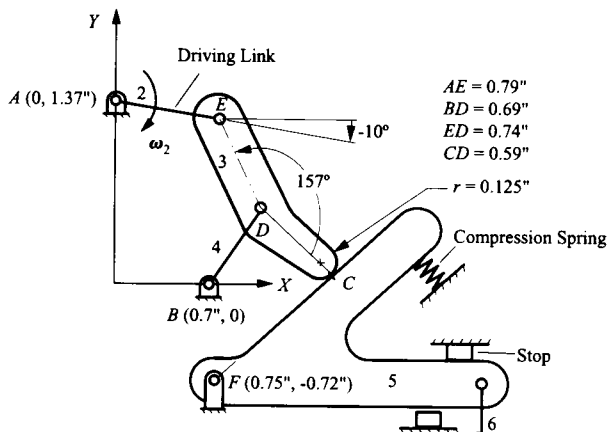


4.8 Using the instant-center method, find the angular velocity of link 6 if link 2 is rotating at 50 rpm CCW.

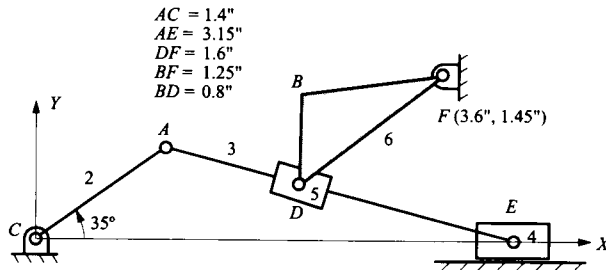


4.9 In the operation of this mechanism, link 3 strikes and trips link 5, which is initially at rest. High wear has been observed at the point of contact between links 3 and 5. As an engineer, you are asked to correct this situation. Therefore, you decide to do the following:

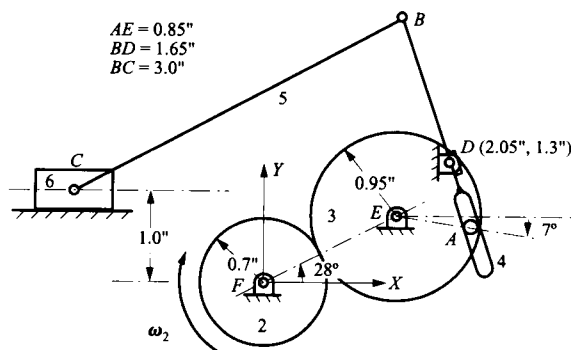
- Determine the direction of the velocity of point  $C$  on link 3 at the moment of contact.
- Relocate the ground pivot of link 4 to make the direction of the velocity of point  $C$  perpendicular to link 5 (hence less rubbing at the point of contact) when contact occurs.



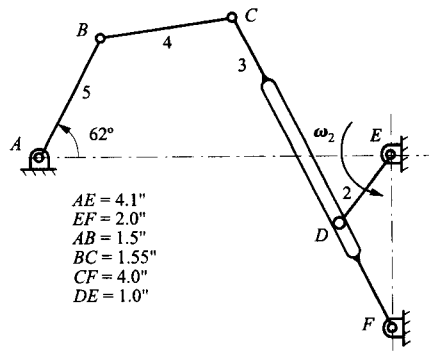
4.10 For the linkage given,  $\omega_2 = 1$  rad/s CCW. Find  $I_{26}$  using the circle-diagram method. Using  $v_{A_2}$  and  $I_{26}$ , determine the magnitude and direction of  $v_{B_6}$  using the rotating-radius method.



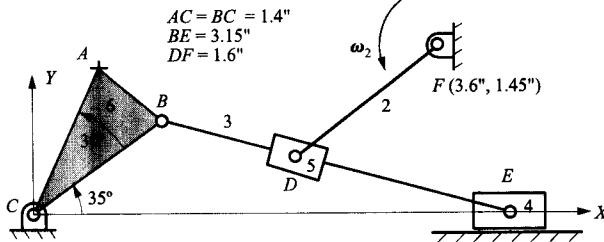
4.11 Find the velocity of point  $C$  given that the angular velocity of gear 2 is 10 rad/s CW.  $B$  is a pin joint connecting links 4 and 5. Point  $A$  is a pin in link 3 that engages a slot in link 4.



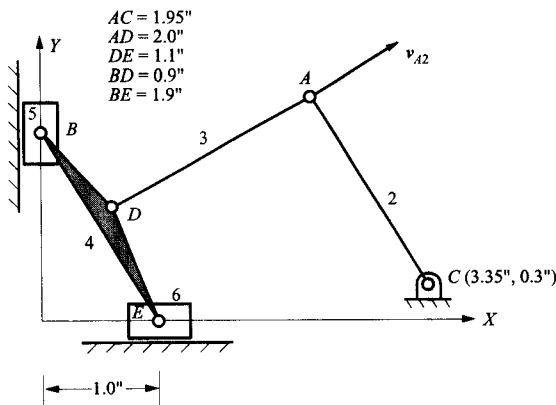
4.12 If  $\omega_2 = 5 \text{ rad/s}$  CCW, find  $\omega_5$  using instant centers.



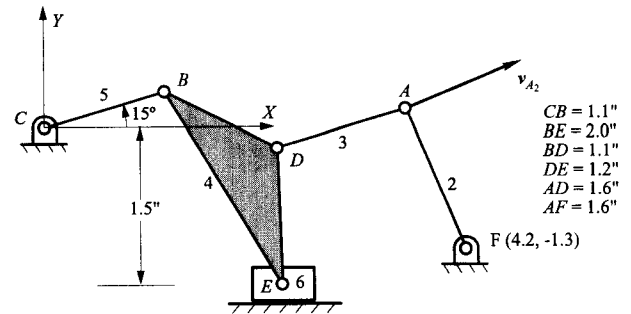
4.13 If  $\omega_2 = 1 \text{ rad/s}$  CCW, find the velocity of point A on link 6 using the instant-center method. Show  $v_{A_6}$  on the drawing.



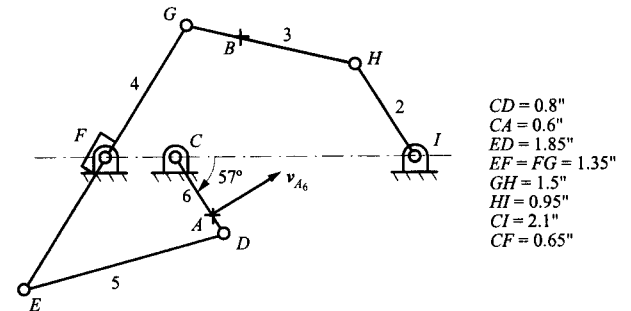
4.14 If  $v_{A_2} = 10 \text{ in/s}$  as shown, find  $v_{B_4}$  using the instant-center method.



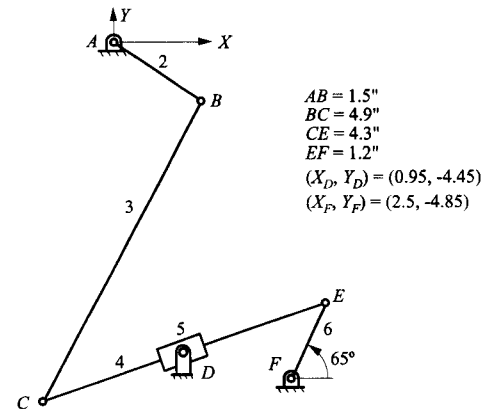
4.15 If  $v_{A_2} = 10 \text{ in/s}$  as shown, find  $v_{B_4}$  using the instant-center method.



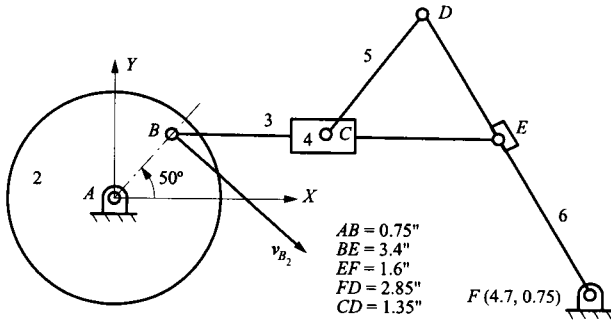
4.16 If  $v_{A_6} = 10 \text{ in/s}$  as shown, determine the velocity vector (direction and magnitude) for point B on link 3 using the instant-center method.



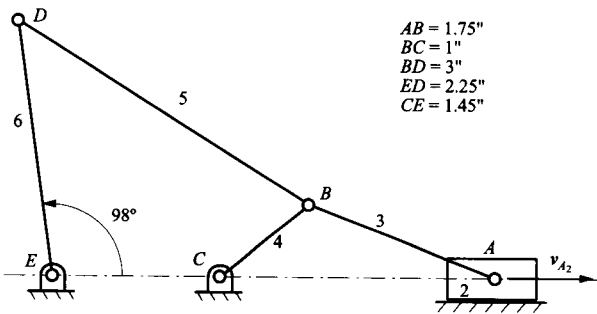
4.17 In the mechanism shown,  $\omega_2$  is 20 rad/s CCW. Find  $I_{26}$  and use it to find the angular velocity of link 6.



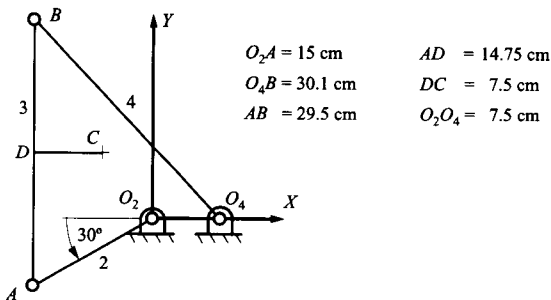
4.18 If  $v_{B_2} = 10$  in/s as shown, determine the velocity vector (direction and magnitude) of point  $C_4$  using the instant-center method.



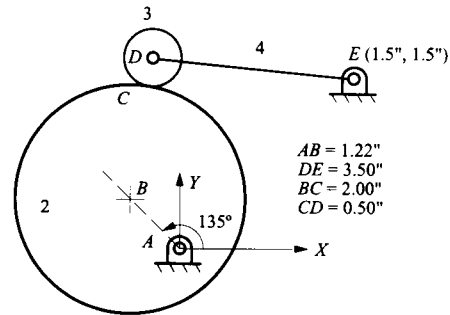
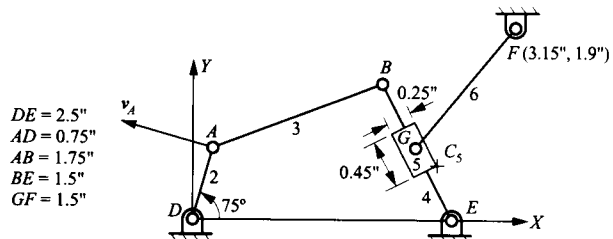
4.19 If the velocity of  $A_2$  is 10 in/s to the right, find  $\omega_6$  using instant centers.



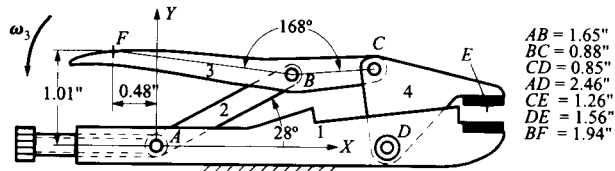
4.20 Crank 2 of the push-link mechanism shown in the figure is driven at  $\omega_2 = 60$  rad/s (CW). Find the velocity of points B and C and the angular velocity of links 3 and 4 using the instant-center method.



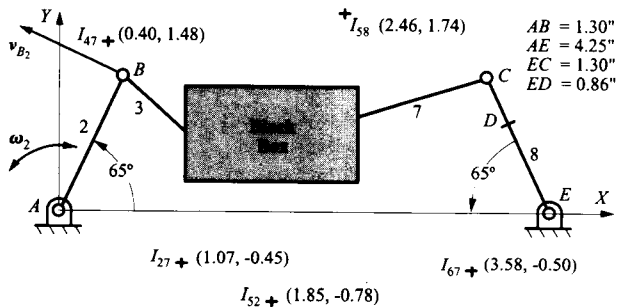
4.21 The circular cam shown is driven at an angular velocity  $\omega_2 = 15$  rad/s (CW). There is rolling contact between the cam and roller, link 3. Using the instant-center method, find the angular velocity of the oscillating follower, link 4.



4.22 If  $\omega_3 = 1$  rad/s CCW, find the velocity of points E and F using the instant-center method. Show the velocity vectors  $v_{F_3}$  and  $v_{E_4}$  on the figure.

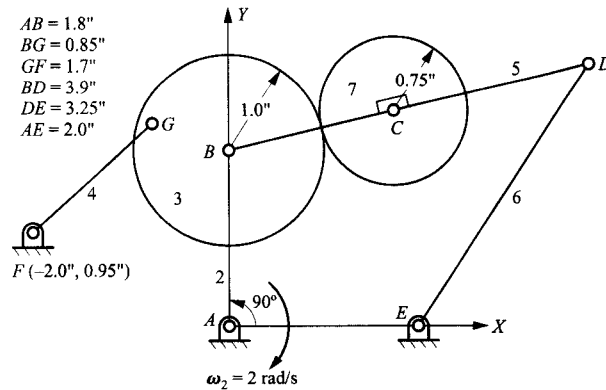


4.23 In the eight-link mechanism, most of the linkage is contained in the black box and some of the instant centers are located as shown. The velocity of point B is 100 in/s in the direction shown. Compute the velocity of point  $D_8$  and determine the angular velocity of link 2.

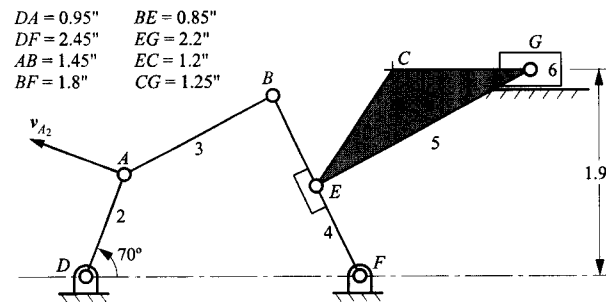


4.24 If the velocity of point A on link 2 is 10 in/s as shown, use the instant-center method to find the velocity of point C on link 5.

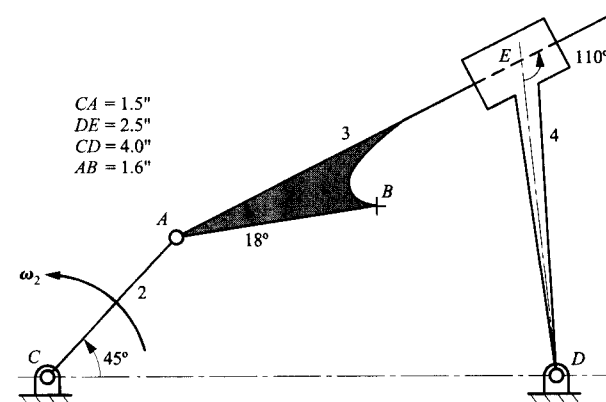
4.25 Assume that link 7 rolls on link 3 without slipping, and find the following instant centers:  $I_{13}$ ,  $I_{15}$ , and  $I_{27}$ . For the given value for  $\omega_2$ , find  $\omega_7$  using instant centers.



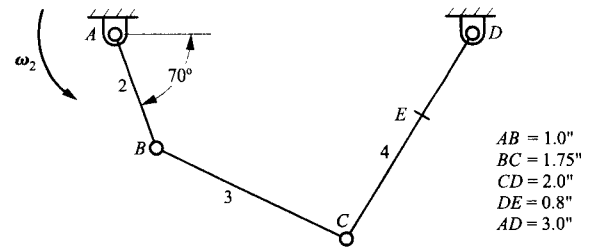
4.26 If  $v_{A_2} = 10 \text{ in/s}$  as shown, find  $v_{C_5}$  using the instant-center method.



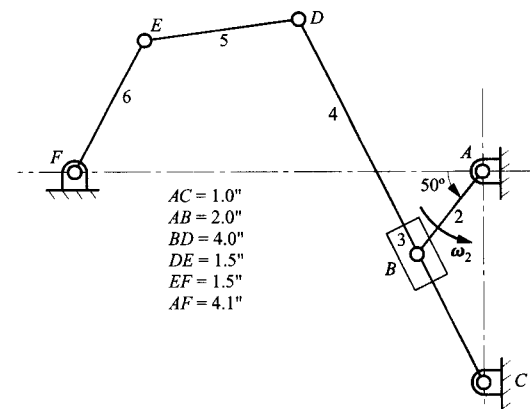
4.27 If  $\omega_2 = 10 \text{ rad/s}$  CCW, find the velocity of point  $B$  using the instant-center method. Show the velocity vector  $v_{B_3}$  on the figure.



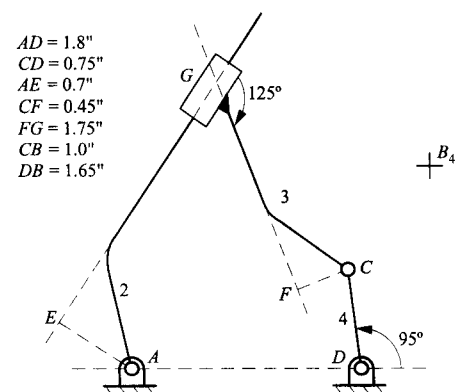
4.28 If  $\omega_2 = 100 \text{ rad/s}$  CCW, find the velocity of point  $E$  using the instant-center method. Show the velocity vector  $v_{E_4}$  on the figure.



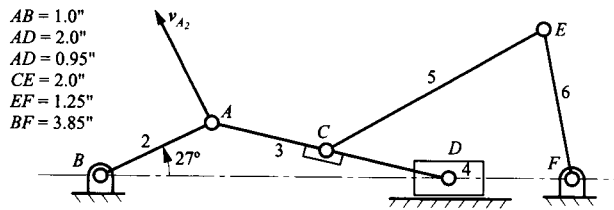
4.29 If  $\omega_2 = 5 \text{ rad/s}$  CCW, find  $\omega_6$  using instant centers.



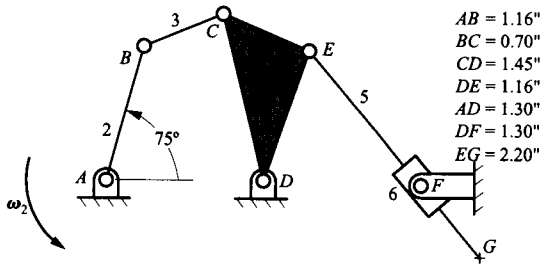
4.30 If  $\omega_2 = 100 \text{ rad/s}$  CCW, find  $v_{B_4}$  using instant centers and the rotating-radius method.



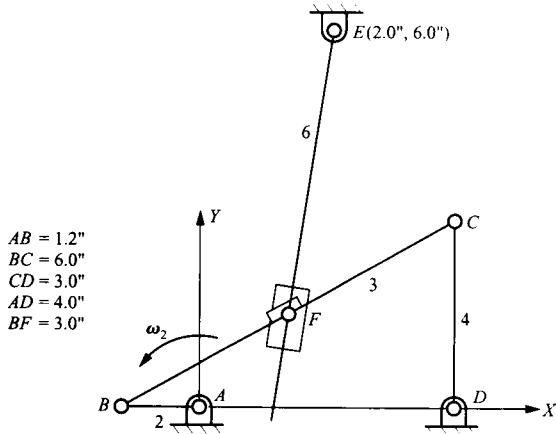
4.31 If  $v_{A_2} = 10$  in/s as shown, find the angular velocity ( $\omega_6$ ) of link 6 using the instant-center method.



4.32 If  $\omega_2 = 50$  rad/s CCW, find the velocity of point  $G$  using the instant-center method. Show the velocity vector  $v_{G_5}$  on the figure.



4.33 If  $\omega_2 = 100$  rad/s CCW, find  $\omega_6$ .



## 5.1 INTRODUCTION

In Chapters 2 and 3, graphical techniques for position, velocity, and acceleration analysis of linkages were presented. However, as was pointed out, there are circumstances in which it is preferable to use analytical solution techniques that can be conveniently programmed on a digital computer. In any circumstance in which repetitive or extensive analyses are required, the use of computer software is highly desirable. In the present chapter, the equations used to construct analysis software are developed in detail.

The geometric constraints associated with mechanisms can be formulated using vector displacement, velocity, and acceleration closure equations. The displacement closure equations are based on the observation that there are two different but equivalent paths connecting points on the same vector loop. For example, in the four-bar linkage shown in Fig. 5.1, one can reach point  $C$  from point  $A$  either by way of point  $B$  or point  $D$ .

It is convenient to represent the terms in the closure equations by vectors, and the procedures developed in this chapter work especially well for planar problems. It is also possible to apply the same general approach to spatial linkages. Another popular method for planar mechanisms, which involves slightly more computational work, is the complex number approach, in which the Cartesian vector components are expressed in terms of the real and imaginary parts of a complex number. The use of complex numbers is advantageous in some types of problem; however, the direct vector approach is preferred here. The complex number approach is outlined briefly at the end of this chapter.

There are also specialized techniques for forming closure equations for spatial mechanisms. The general trend is to work with coordinate transformation operators. For this a set of body-fixed coordinates is established at each joint, and the product of a series of joint-to-joint coordinate transformation operators is taken. When this product is continued around the entire mechanism loop, it must be equal to the identity operator. The resulting operator equation can then be manipulated, if required, and corresponding elements can be equated. The types of operators that have been used include dual complex number  $2 \times 2$  matrices, dual quaternions, real number  $4 \times 4$  matrices, and dual number  $3 \times 3$  matrices. A discussion of the mathematics of these operators is beyond the scope of this text. The description of spatial linkages using matrix transformations is discussed in Chapter 9.

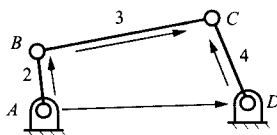


FIGURE 5.1 Closure of a four-bar linkage.

## 5.2 POSITION, VELOCITY, AND ACCELERATION REPRESENTATIONS

### 5.2.1 Position Representation

For the purpose of developing an analytical model, we can define the relative locations of a chain of points by a chain of vectors. The points will be associated with the links of a mechanism in some manner, but they do not have to be attached to specific links. An example is given in Fig. 5.2.

The position of point  $Q$  in the fixed reference frame is

$$r_Q = r_1 + r_2 + r_3 \quad (5.1)$$

Here, we will represent each vector by a length  $r_i$  and an angle  $\theta_i$ , as shown in Fig. 5.3. All angles are measured counterclockwise from a line that remains parallel to the fixed  $x$  axis attached to the reference frame.

With this notation, we can resolve each of the vectors in Eq. (5.1) into  $x$  and  $y$  components making use of the unit vectors  $i$  and  $j$  as follows:

$$\left. \begin{aligned} r_1 &= r_1(\cos\theta_1 i + \sin\theta_1 j) \\ r_2 &= r_2(\cos\theta_2 i + \sin\theta_2 j) \\ r_3 &= r_3(\cos\theta_3 i + \sin\theta_3 j) \end{aligned} \right\} \quad (5.2)$$

or

$$r_k = r_k(\cos\theta_k i + \sin\theta_k j), \quad k = 1, 2, 3 \quad (5.3)$$

### 5.2.2 Velocity Representation

To determine the velocity of point  $Q$ ,  $r_Q$  can be differentiated. Then,

$$v_Q = \dot{r}_Q = \dot{r}_1 + \dot{r}_2 + \dot{r}_3 \quad (5.4)$$

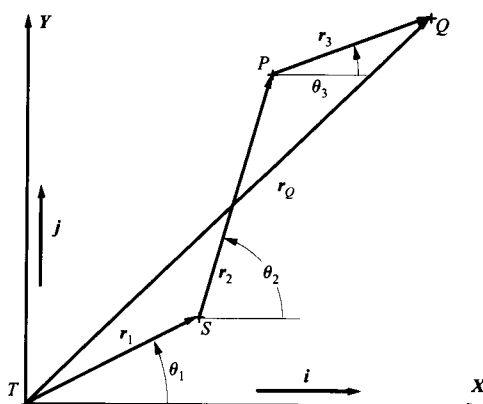


FIGURE 5.2 Representation of a chain of points by a set of vectors.



FIGURE 5.3 Notation used for vectors.



where

$$\dot{\mathbf{r}}_k = \frac{d\mathbf{r}_k}{dt} \quad (5.5)$$

Note that, in general, both the magnitude and direction of  $\mathbf{r}_k$  can change. When we differentiate Eq. (5.3) using the chain rule of calculus, we obtain

$$\dot{\mathbf{r}}_k = \dot{r}_k(\cos\theta_k\mathbf{i} + \sin\theta_k\mathbf{j}) + r_k(-\dot{\theta}_k\sin\theta_k\mathbf{i} + \dot{\theta}_k\cos\theta_k\mathbf{j}) \quad (5.6)$$

or

$$\dot{\mathbf{r}}_k = (\dot{r}_k\cos\theta_k - r_k\dot{\theta}_k\sin\theta_k)\mathbf{i} + (\dot{r}_k\sin\theta_k + r_k\dot{\theta}_k\cos\theta_k)\mathbf{j} \quad (5.7)$$

If we compare the vector components indicated in Eq. (5.6) with the equations developed in Section 3.3, we will notice a similarity between corresponding terms. In particular, if  $\mathbf{r}_k$  is the vector defining the relative position between two points  $P$  and  $Q$ , and body  $B$  is moving relative to the reference frame  $R$  as shown in Fig. 5.4, then

$$\dot{\mathbf{r}}_k(\cos\theta_k\mathbf{i} + \sin\theta_k\mathbf{j}) = {}^B\mathbf{v}_{Q/P} \quad (5.8)$$

and

$$r_k\dot{\theta}_k(-\sin\theta_k\mathbf{i} + \cos\theta_k\mathbf{j}) = \boldsymbol{\omega}_B \times \mathbf{r}_{Q/P} \quad (5.9)$$

Equation (5.8) can be verified by recognizing that it gives the component of the velocity associated with changing the magnitude of the vector between the two points. This component is clearly in the direction of the vector  $\mathbf{r}_k$ . The second term can be verified by computing the cross product. Recognizing that

$$\boldsymbol{\omega}_B = \dot{\theta}_k\mathbf{k}$$

and

$$\mathbf{r}_{Q/P} = \mathbf{r}_k = r_k(\cos\theta_k\mathbf{i} + \sin\theta_k\mathbf{j})$$

We then have,

$$\begin{aligned} \boldsymbol{\omega}_B \times \mathbf{r}_{Q/P} &= \dot{\theta}_k\mathbf{k} \times r_k(\cos\theta_k\mathbf{i} + \sin\theta_k\mathbf{j}) = \dot{\theta}_kr_k(\cos\theta_k\mathbf{k} \times \mathbf{i} + \sin\theta_k\mathbf{k} \times \mathbf{j}) \\ &= r_k\dot{\theta}_k(-\sin\theta_k\mathbf{i} + \cos\theta_k\mathbf{j}) \end{aligned}$$

Equation (5.4) can also be expressed as

$$\mathbf{v}_Q = \sum_{k=1}^3 \dot{r}_k(\cos\theta_k\mathbf{i} + \sin\theta_k\mathbf{j}) + r_k(-\dot{\theta}_k\sin\theta_k\mathbf{i} + \dot{\theta}_k\cos\theta_k\mathbf{j}) \quad (5.10)$$

or

$$\mathbf{v}_Q = \sum_{k=1}^3 (\dot{r}_k\cos\theta_k - r_k\dot{\theta}_k\sin\theta_k)\mathbf{i} + (\dot{r}_k\sin\theta_k + r_k\dot{\theta}_k\cos\theta_k)\mathbf{j} \quad (5.11)$$

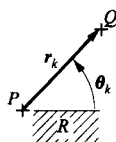


FIGURE 5.4 Position vector between two points.

### 5.2.3 Acceleration Representation

To obtain the acceleration expression, we need only to differentiate the velocity expression (Eq. 5.4). Symbolically, this is

$$\mathbf{a}_Q = \ddot{\mathbf{r}}_Q = \ddot{\mathbf{r}}_1 + \ddot{\mathbf{r}}_2 + \ddot{\mathbf{r}}_3 \quad (5.12)$$

where

$$\ddot{\mathbf{r}}_k = \frac{d^2 \mathbf{r}_k}{dt^2}$$

Because the vectors have been defined in a consistent manner (Fig. 5.3), the form for the derivatives for all of the vectors will be the same. Therefore, we can develop the expression with a general vector  $\mathbf{r}_k$ .

Note again that, in general, both the magnitude and direction of  $\mathbf{r}_k$  can change. When we differentiate Eq. (5.6) using the chain rule of calculus, we obtain

$$\begin{aligned} \ddot{\mathbf{r}}_k = & \ddot{r}_k (\cos \theta_k \mathbf{i} + \sin \theta_k \mathbf{j}) + r_k \ddot{\theta}_k (-\sin \theta_k \mathbf{i} + \cos \theta_k \mathbf{j}) - r_k \dot{\theta}_k^2 (\cos \theta_k \mathbf{i} + \sin \theta_k \mathbf{j}) \\ & + 2\dot{r}_k \dot{\theta}_k (-\sin \theta_k \mathbf{i} + \cos \theta_k \mathbf{j}) \end{aligned} \quad (5.13)$$

or

$$\begin{aligned} \ddot{\mathbf{r}}_k = & \left[ (\ddot{r}_k - r_k \dot{\theta}_k^2) \cos \theta_k - (r_k \ddot{\theta}_k + 2\dot{r}_k \dot{\theta}_k) \sin \theta_k \right] \mathbf{i} \\ & + \left[ (\ddot{r}_k - r_k \dot{\theta}_k^2) \sin \theta_k - (r_k \ddot{\theta}_k + 2\dot{r}_k \dot{\theta}_k) \cos \theta_k \right] \mathbf{j} \end{aligned} \quad (5.14)$$

As in the case of the velocity equations, we can compare the vector components indicated in Eq. (5.13) with the acceleration equations developed in Section 3.3. Using the same nomenclature as before (Fig. 5.4), we get

$$\ddot{r}_k (\cos \theta_k \mathbf{i} + \sin \theta_k \mathbf{j}) = {}^B \mathbf{a}_{Q/P} \quad (5.15)$$

$$r_k \ddot{\theta}_k (-\sin \theta_k \mathbf{i} + \cos \theta_k \mathbf{j}) = \boldsymbol{\alpha}_B \times \mathbf{r}_{Q/P} \quad (5.16)$$

$$-r_k \dot{\theta}_k^2 (\cos \theta_k \mathbf{i} + \sin \theta_k \mathbf{j}) = \boldsymbol{\omega}_B \times (\boldsymbol{\omega}_B \times \mathbf{r}_{Q/P}) \quad (5.17)$$

and

$$2\dot{r}_k \dot{\theta}_k (-\sin \theta_k \mathbf{i} + \cos \theta_k \mathbf{j}) = 2\boldsymbol{\omega}_B \times {}^B \mathbf{v}_{Q/P} \quad (5.18)$$

These can be verified by direct calculation.

If we add the individual components, we can obtain the acceleration of point  $Q$ . Then Eq. (5.12) can be expressed as

$$\mathbf{a}_Q = \sum_{k=1}^3 \left\{ \begin{array}{l} \ddot{r}_k (\cos \theta_k \mathbf{i} + \sin \theta_k \mathbf{j}) + r_k \ddot{\theta}_k (-\sin \theta_k \mathbf{i} + \cos \theta_k \mathbf{j}) \\ -r_k \dot{\theta}_k^2 (\cos \theta_k \mathbf{i} + \sin \theta_k \mathbf{j}) + 2\dot{r}_k \dot{\theta}_k (-\sin \theta_k \mathbf{i} + \cos \theta_k \mathbf{j}) \end{array} \right\} \quad (5.19)$$

or

$$a_Q = \sum_{k=1}^3 \left\{ \begin{aligned} & \left[ \left( \ddot{r}_k - r_k \dot{\theta}_k^2 \right) \cos \theta_k - \left( r_k \ddot{\theta}_k + 2 \dot{r}_k \dot{\theta}_k \right) \sin \theta_k \right] \mathbf{i} \\ & + \left[ \left( \ddot{r}_k - r_k \dot{\theta}_k^2 \right) \sin \theta_k + \left( r_k \ddot{\theta}_k + 2 \dot{r}_k \dot{\theta}_k \right) \cos \theta_k \right] \mathbf{j} \end{aligned} \right\} \quad (5.20)$$

### 5.2.4 Special Cases

Equations (5.6) and (5.13) or (5.7) and (5.14) are the most general forms of the velocity and acceleration equations. However, in most mechanisms usually some of the terms will be zero because of the special conditions associated with the way in which the vectors are defined. It is possible for any of the terms involved in the velocity and acceleration equations to be zero; however, a common case is to have the magnitude of a given position vector be constant. This is the case when the vector defines the relative positions of two points on a rigid link. When this happens,  $\dot{r}$  and  $\ddot{r}$  are zero. Then the velocity and acceleration expressions become

$$\dot{r}_k = r_k \dot{\theta}_k (-\sin \theta_k \mathbf{i} + \cos \theta_k \mathbf{j}) \quad (5.21)$$

$$\ddot{r}_k = r_k \ddot{\theta}_k (-\sin \theta_k \mathbf{i} + \cos \theta_k \mathbf{j}) - r_k \dot{\theta}_k^2 (\cos \theta_k \mathbf{i} + \sin \theta_k \mathbf{j}) \quad (5.22)$$

or

$$\ddot{r}_k = \left[ -r_k \dot{\theta}_k^2 \cos \theta_k - r_k \ddot{\theta}_k \sin \theta_k \right] \mathbf{i} + \left[ -r_k \dot{\theta}_k^2 \sin \theta_k + r_k \ddot{\theta}_k \cos \theta_k \right] \mathbf{j} \quad (5.23)$$

### 5.2.5 Mechanisms to Be Considered

There are six commonly used single-loop chains with revolute and slider joints. We will look at three of these in detail to illustrate how the equations can be developed in each case. Then we will present the results for the remaining three cases. We will then discuss more complex mechanisms that require several vector loops and mechanisms that contain higher pairs.

## 5.3 ANALYTICAL CLOSURE EQUATIONS FOR FOUR-BAR LINKAGES

We will first give an overview of the development of the equations for the four-bar linkage using the general nomenclature just discussed. The procedures used to solve the equations for the four-bar linkage are similar to the procedures required for solving the equations associated with most other simple mechanisms.

The closure condition simply expresses the condition that a loop of a linkage closes on itself. For the four-bar linkage shown in Fig. 5.5, the closure equations would be

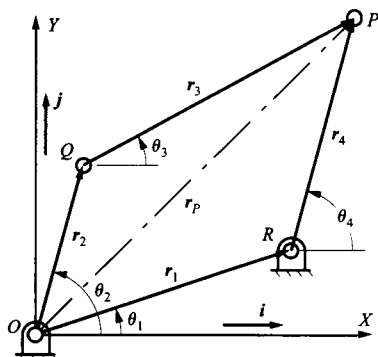
$$r_P = r_2 + r_3 = r_1 + r_4 \quad (5.24)$$

or

$$r_2 (\cos \theta_2 \mathbf{i} + \sin \theta_2 \mathbf{j}) + r_3 (\cos \theta_3 \mathbf{i} + \sin \theta_3 \mathbf{j}) = r_1 (\cos \theta_1 \mathbf{i} + \sin \theta_1 \mathbf{j}) + r_4 (\cos \theta_4 \mathbf{i} + \sin \theta_4 \mathbf{j}) \quad (5.25)$$

Rewriting Eq. (5.25) in its component equations, one gets

$$r_2 \cos \theta_2 + r_3 \cos \theta_3 = r_1 \cos \theta_1 + r_4 \cos \theta_4 \quad (5.26)$$



**FIGURE 5.5** Vector closure condition for a four-bar loop. The position of point  $P$  obtained by adding the vectors  $r_2$  and  $r_3$  must always be the same as that obtained by adding vectors  $r_1$  and  $r_4$ . Note that  $r_1$  is a constant vector that describes the base member of the linkage. Correspondingly,  $\theta_1$  is a constant angle

$$r_2 \sin \theta_2 + r_3 \sin \theta_3 = r_1 \sin \theta_1 + r_4 \sin \theta_4 \quad (5.27)$$

Equations (5.26) and (5.27) are the closure equations, and they must be satisfied throughout the motion of the linkage. The base vector will be constant, so  $r_1$  and  $\theta_1$  are constants. If  $\theta_2$  is given, that is, if crank  $OQ$  is a driving crank, it is necessary to solve Eqs. (5.26) and (5.27) for  $\theta_3$  and  $\theta_4$  in terms of  $\theta_2$ . Once these expressions are obtained  $\dot{\theta}_3$ ,  $\dot{\theta}_4$ ,  $\ddot{\theta}_3$ , and  $\ddot{\theta}_4$  can be obtained in terms of  $\theta_2$ ,  $\dot{\theta}_2$ , and  $\ddot{\theta}_2$  by differentiation. Velocities and accelerations of points in the mechanism can then be obtained from equations like Eqs. (5.11) and (5.19), recognizing that all of the vector magnitudes are constant ( $\dot{r} = \ddot{r} = 0$ ).

When  $\theta_3$  is given, the coupler is the driver, and we must solve Eqs. (5.26) and (5.27) for  $\theta_2$  and  $\theta_4$  in terms of  $\theta_3$ . The procedure for doing this is very similar to that used when  $\theta_2$  is the input. Therefore, we will first reconsider briefly the case in which  $\theta_2$  is the input.

### 5.3.1 Solution of Closure Equations for Four-Bar Linkages When Link 2 Is the Driver

The analytical solution procedure follows the same major steps as in the graphical solution. That is, a position analysis must first be performed, then a velocity analysis, and finally an acceleration analysis. The position analysis, for a closed-loop linkage, comprises the solution of the closure equations for the joint angles or link orientations. Once this solution is obtained, the velocity and acceleration states are quickly obtainable using the differentiated equations. It will be seen, however, that the position analysis, which is so easily performed graphically by construction of a drawing to scale, is a complex matter when performed analytically.

For all of the simple mechanisms that we will consider initially, the first step in solving the position equations is to identify the variable to be determined first. When the position equations involve two angles as unknowns, the solution procedure is to isolate the trigonometric function involving the angle to be eliminated on the left-hand side of the equation. To eliminate  $\theta_3$  in the linkage shown in Fig. 5.5, first isolate it on one side of Eqs. (5.26) and (5.27) as follows:

$$r_3 \cos \theta_3 = r_1 \cos \theta_1 + r_4 \cos \theta_4 - r_2 \cos \theta_2 \quad (5.28)$$

$$r_3 \sin \theta_3 = r_1 \sin \theta_1 + r_4 \sin \theta_4 - r_2 \sin \theta_2 \quad (5.29)$$

Notice that the angle  $\theta_1$  is a known constant. Now square both sides of both equations, add, and simplify the result using the trigonometric identity  $\sin^2 \theta + \cos^2 \theta = 1$ . This gives

$$r_3^2 = r_1^2 + r_2^2 + r_4^2 + 2r_1r_4(\cos\theta_1\cos\theta_4 + \sin\theta_1\sin\theta_4) - 2r_1r_2(\cos\theta_1\cos\theta_2 + \sin\theta_1\sin\theta_2) + 2r_2r_4(\cos\theta_2\cos\theta_4 + \sin\theta_2\sin\theta_4) \quad (5.30)$$

Equation (5.30) gives  $\theta_4$  in terms of the given angle  $\theta_2$  (and the constant angle  $\theta_1$ ) but not explicitly. To obtain an explicit expression, simplify Eq. (5.30) by combining the coefficients of  $\cos\theta_4$  and  $\sin\theta_4$  as follows:

$$A\cos\theta_4 + B\sin\theta_4 + C = 0 \quad (5.31)$$

where

$$\left. \begin{aligned} A &= 2r_1r_4\cos\theta_1 - 2r_2r_4\cos\theta_2 \\ B &= 2r_1r_4\sin\theta_1 - 2r_2r_4\sin\theta_2 \\ C &= r_1^2 + r_2^2 + r_4^2 - r_3^2 - 2r_1r_2(\cos\theta_1\cos\theta_2 + \sin\theta_1\sin\theta_2) \end{aligned} \right\} \quad (5.32)$$

To solve Eq. (5.31), use the standard trigonometric identities for half angles given in the following:

$$\sin\theta_4 = \frac{2\tan\left(\frac{\theta_4}{2}\right)}{1 + \tan^2\left(\frac{\theta_4}{2}\right)} \quad (5.33)$$

$$\cos\theta_4 = \frac{1 - \tan^2\left(\frac{\theta_4}{2}\right)}{1 + \tan^2\left(\frac{\theta_4}{2}\right)} \quad (5.34)$$

After substitution and simplification, we get

$$(C - A)t^2 + 2Bt + (A + C) = 0$$

where

$$t = \tan\left(\frac{\theta_4}{2}\right)$$

Solving for  $t$  gives

$$t = \frac{-2B + \sigma\sqrt{4B^2 - 4(C - A)(C + A)}}{2(C - A)} = \frac{-B + \sigma\sqrt{B^2 - C^2 + A^2}}{C - A} \quad (5.35)$$

and

$$\theta_4 = 2\tan^{-1}t \quad (5.36)$$

where  $\sigma = \pm 1$  is a sign variable identifying the assembly mode. Note that  $\tan^{-1}t$  has a valid range of  $-\pi/2 \leq \tan^{-1}t \leq \pi/2$ . Therefore,  $\theta_4$  will have the range  $-\pi \leq \theta_4 \leq \pi$ . Unless the linkage is a Grashof type II linkage in one of the extreme positions of its motion range, there are two solutions for  $\theta_4$  corresponding to the two values of  $\sigma$ , and they are both valid. These correspond to two assembly modes or branches for the linkage. Once we pick the value for  $\sigma$  corresponding to the desired mode, the sign normally stays the same for any value of  $\theta_2$ .

Because of the square root in Eq. (5.35), the variable  $t$  can be complex  $[(A^2 + B^2) < C^2]$ . If this happens, the mechanism cannot be assembled in the position specified. The assembly configurations would then appear as shown in Fig. 5.6.

After  $\theta_4$  is known, equations (5.28) and (5.29) can now be solved for  $\theta_3$ . Dividing Eq. (5.29) by Eq. (5.28) and solving for  $\theta_3$  gives

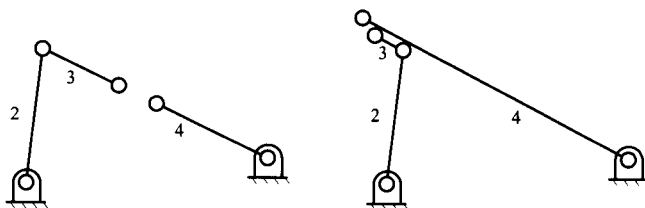
$$\theta_3 = \tan^{-1} \left[ \frac{r_1 \sin \theta_1 + r_4 \sin \theta_4 - r_2 \sin \theta_2}{r_1 \cos \theta_1 + r_4 \cos \theta_4 - r_2 \cos \theta_2} \right] \quad (5.37)$$

Note that in Eq. (5.37), it is essential that the sign of the numerator and denominator be maintained to determine the quadrant in which the angle  $\theta_3$  lies. This can be done directly in MATLAB by using the ATAN2 function. The form of this function is

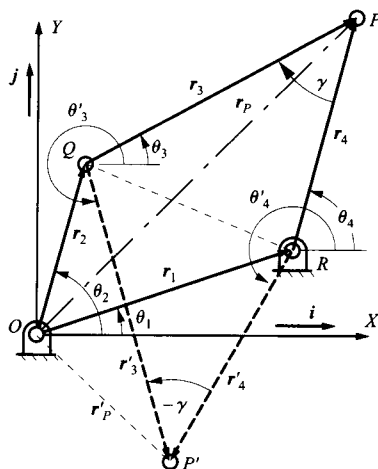
$$\text{ATAN2}(\sin \theta_3, \cos \theta_3) = \tan^{-1} \left[ \frac{\sin \theta_3}{\cos \theta_3} \right]. \quad (5.38)$$

Equations (5.35)–(5.37) give a complete and consistent solution to the position problem. As indicated before, for any value of  $\theta_2$ , there are typically two values of  $\theta_3$  and  $\theta_4$ , given by substituting  $\sigma = +1$  and  $-1$ , respectively, in Eq. (5.35). These two different solutions are shown in Fig. 5.7. The two solutions correspond to an assembly ambiguity that also appears in the graphical construction.

Note that the positions of  $r_3$  and  $r_4$  are symmetric about the line  $QR$ . Therefore, the angle  $\gamma = \theta_4 - \theta_3$  has the same magnitude, but opposite sign, in each of the two positions. The sign of  $\gamma$  provides a useful indicator as to which of the solution branches has been drawn, from the graphical point of view.



**FIGURE 5.6** Grashof type II linkages cannot be placed in positions that are transitions between solution branches. The variable  $t$  would be complex in these cases



**FIGURE 5.7** The two possible positions ( $P$  and  $P'$ ) of the point  $P$  for a given value of  $\theta_2$ . Note that  $QP'R$  is the mirror image of  $QPR$  about the line  $QR$ . Notice that there are two different possible values of  $\theta_3$  and two different values of  $\theta_4$  corresponding to the two possible positions of point  $P$ . The sign of the angle  $RPQ$  ( $\gamma$ ) is reversed in the second solution, although the magnitude of  $RP'Q$  is the same. The sign of  $\gamma$  is a useful graphical indicator of which solution is being examined (see Section 6.3.6).

Once all of the angular quantities are known, it is relatively straightforward to compute the coordinates of any point of the vector loops used in the closure equations. In particular, the coordinates of  $Q$ ,  $P$ , and  $R$  are given by

$$\mathbf{r}_Q = \mathbf{r}_2 = r_2(\cos\theta_2\mathbf{i} + \sin\theta_2\mathbf{j}) \quad (5.39)$$

$$\begin{aligned} \mathbf{r}_P &= \mathbf{r}_2 + \mathbf{r}_3 = r_2(\cos\theta_2\mathbf{i} + \sin\theta_2\mathbf{j}) + r_3(\cos\theta_3\mathbf{i} + \sin\theta_3\mathbf{j}) \\ &= \mathbf{r}_1 + \mathbf{r}_4 = r_1(\cos\theta_1\mathbf{i} + \sin\theta_1\mathbf{j}) + r_4(\cos\theta_4\mathbf{i} + \sin\theta_4\mathbf{j}) \end{aligned} \quad (5.40)$$

and

$$\mathbf{r}_R = \mathbf{r}_1 = r_1(\cos\theta_1\mathbf{i} + \sin\theta_1\mathbf{j}) \quad (5.41)$$

### 5.3.2 Analysis When the Coupler (Link 3) Is the Driving Link

The analytical procedure just given when one of the frame-mounted links (link 2) in Fig. 5.5 is the driver is very similar to the graphical procedure. However, if the coupler is the driver, it is difficult to analyze the linkage graphically. The analytical procedure, in contrast, is very straightforward and no more difficult to conduct than when one of the frame-mounted links is the driver. The details follow exactly the same procedure as that given in Section 5.3.1. Therefore, we will simply outline the procedure and tabulate the results.

In the procedure, we can assume that in Fig. 5.5 that  $\theta_1$ ,  $\theta_3$ ,  $\dot{\theta}_3$ , and  $\ddot{\theta}_3$  are known, and  $\theta_2$ ,  $\dot{\theta}_2$ ,  $\ddot{\theta}_2$ ,  $\theta_4$ ,  $\dot{\theta}_4$ , and  $\ddot{\theta}_4$  are to be found. All of the link lengths and  $\theta_1$  are constants. For the position analysis, again begin with Eqs. (5.26) and (5.27) and isolate the terms with either  $\theta_2$  or  $\theta_4$ . It is advantageous to select  $\theta_2$  for reasons that will become apparent. The resulting equations are

$$r_2 \cos\theta_2 = r_1 \cos\theta_1 + r_4 \cos\theta_4 - r_3 \cos\theta_3 \quad (5.42)$$

$$r_2 \sin\theta_2 = r_1 \sin\theta_1 + r_4 \sin\theta_4 - r_3 \sin\theta_3 \quad (5.43)$$

A comparison of Eqs. (5.42) and (5.43) with Eqs. (5.28) and (5.29) indicates that they are of exactly the same form except that the indices 2 and 3 are interchanged. Therefore, we can use directly the position solution derived in Section 5.3.1 if we interchange the indices 2 and 3.

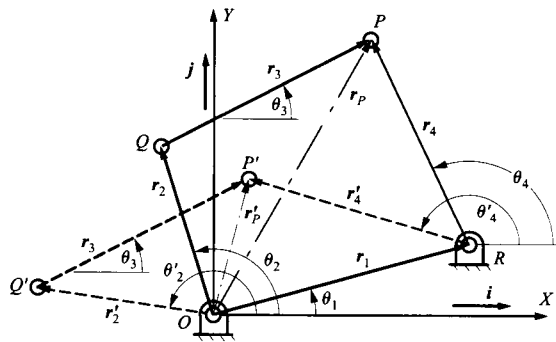
When the coupler is the driver, there is an assembly-mode ambiguity similar to that when link 2 is the driver. This is illustrated in Fig. 5.8. It is necessary to know the appropriate mode before the analysis is begun; however, once the assembly mode is selected, it is the same for any position of the input link unless the linkage is a type 2 linkage, and passes through a singular position.

The motion of the coupler in a coupler-driven four-bar linkage will be less than  $360^\circ$  unless the linkage is of type 1 with the coupler or base as the shortest link. When the linkage reaches its motion limits, links 2 and 4 will be parallel.

### 5.3.3 Velocity Equations for Four-Bar Linkages

The analytical form of the velocity equations for the four-bar linkage of Fig. 5.5 can be developed by differentiating Eq. (5.24). The result is

$$\dot{\mathbf{r}}_P = \dot{\mathbf{r}}_2 + \dot{\mathbf{r}}_3 = \dot{\mathbf{r}}_1 + \dot{\mathbf{r}}_4 \quad (5.44)$$



**FIGURE 5.8** The two possible positions ( $P$  and  $P'$ ) of the point  $P$  for a given value of  $\theta_3$ . There are two different possible values of  $\theta_2$  and two different values of  $\theta_4$  corresponding to the two possible positions of point  $P$ .

When this equation is written in component form, the result is the same as that of differentiating Eqs. (5.26) and (5.27). Recognizing that all of the link lengths are constant as is  $\theta_1$ , we have the resulting component equations

$$r_2 \dot{\theta}_2 \sin \theta_2 + r_3 \dot{\theta}_3 \sin \theta_3 = r_4 \dot{\theta}_4 \sin \theta_4 \quad (5.45)$$

$$r_2 \dot{\theta}_2 \cos \theta_2 + r_3 \dot{\theta}_3 \cos \theta_3 = r_4 \dot{\theta}_4 \cos \theta_4 \quad (5.46)$$

If  $\dot{\theta}_2$  is known, the only new unknowns are  $\dot{\theta}_3$  and  $\dot{\theta}_4$ , and if  $\dot{\theta}_3$  is known, the only new unknowns are  $\dot{\theta}_2$  and  $\dot{\theta}_4$ . In either case, the equations can be solved most easily using a linear equation solver. In matrix form, Eqs. (5.45) and (5.46) can be rearranged and rewritten as

$$\begin{bmatrix} -r_J \sin \theta_J & r_4 \sin \theta_4 \\ -r_J \cos \theta_J & r_4 \cos \theta_4 \end{bmatrix} \begin{Bmatrix} \dot{\theta}_J \\ \dot{\theta}_4 \end{Bmatrix} = \begin{Bmatrix} r_M \dot{\theta}_M \sin \theta_M \\ r_M \dot{\theta}_M \cos \theta_M \end{Bmatrix} \quad (5.47)$$

where  $M = 2$  and  $J = 3$  for  $\dot{\theta}_2$  as the input, and  $M = 3$  and  $J = 2$  for  $\dot{\theta}_3$  as the input. The terms in the matrix and vector on the right-hand side of the equation will be known. The equation can therefore be solved manually, on a programmable calculator, or with the matrix solvers in programs such as MATLAB.

Once the angular velocities are known, it is a simple matter to compute the linear velocities of any of the points on the vector loop. The velocities of points  $Q$  and  $P$  are given by

$$\dot{\mathbf{r}}_Q = \dot{\mathbf{r}}_2 = r_2 \dot{\theta}_2 (-\sin \theta_2 \mathbf{i} + \cos \theta_2 \mathbf{j}) \quad (5.48)$$

and

$$\begin{aligned} \dot{\mathbf{r}}_P &= \dot{\mathbf{r}}_2 + \dot{\mathbf{r}}_3 = (-r_2 \dot{\theta}_2 \sin \theta_2 - r_3 \dot{\theta}_3 \sin \theta_3) \mathbf{i} + (r_2 \dot{\theta}_2 \cos \theta_2 + r_3 \dot{\theta}_3 \cos \theta_3) \mathbf{j} \\ &= \dot{\mathbf{r}}_1 + \dot{\mathbf{r}}_4 = (-r_4 \dot{\theta}_4 \sin \theta_4) \mathbf{i} + (r_4 \dot{\theta}_4 \cos \theta_4) \mathbf{j} \end{aligned} \quad (5.49)$$



### 5.3.4 Acceleration Equations for Four-Bar Linkages

The analytical form of the acceleration equations for the linkage of Fig. 5.5 can be developed by differentiating Eq. (5.44). The result is

$$\ddot{\mathbf{r}}_P = \ddot{\mathbf{r}}_2 + \ddot{\mathbf{r}}_3 = \ddot{\mathbf{r}}_1 + \ddot{\mathbf{r}}_4 \quad (5.50)$$

When this equation is written in component form, the result is the same as differentiating Eqs. (5.45) and (5.46). The resulting component equations are

$$r_2\ddot{\theta}_2 \sin\theta_2 + r_2\dot{\theta}_2^2 \cos\theta_2 + r_3\ddot{\theta}_3 \sin\theta_3 + r_3\dot{\theta}_3^2 \cos\theta_3 = r_4\ddot{\theta}_4 \sin\theta_4 + r_4\dot{\theta}_4^2 \cos\theta_4 \quad (5.51)$$

$$r_2\ddot{\theta}_2 \cos\theta_2 - r_2\dot{\theta}_2^2 \sin\theta_2 + r_3\ddot{\theta}_3 \cos\theta_3 - r_3\dot{\theta}_3^2 \sin\theta_3 = r_4\ddot{\theta}_4 \cos\theta_4 + r_4\dot{\theta}_4^2 \sin\theta_4 \quad (5.52)$$

When  $\ddot{\theta}_2$  is known along with all of the position and velocity terms, the only new unknowns are  $\ddot{\theta}_3$  and  $\ddot{\theta}_4$ , and when  $\ddot{\theta}_3$  is known along with all of the position and velocity terms, the only new unknowns are  $\ddot{\theta}_2$  and  $\ddot{\theta}_4$ . Again, because a linear problem is involved, these can be solved for most easily using a linear equation solver. In matrix form, Eqs. (5.51) and (5.52) can be rearranged and rewritten as

$$\begin{bmatrix} -r_J \sin\theta_J & r_4 \sin\theta_4 \\ -r_J \cos\theta_J & r_4 \cos\theta_4 \end{bmatrix} \begin{Bmatrix} \ddot{\theta}_J \\ \ddot{\theta}_4 \end{Bmatrix} = \begin{Bmatrix} r_M \ddot{\theta}_M \sin\theta_M + r_M \dot{\theta}_M^2 \cos\theta_M + r_J \dot{\theta}_J^2 \cos\theta_J - r_4 \dot{\theta}_4^2 \cos\theta_4 \\ r_M \ddot{\theta}_M \cos\theta_M - r_M \dot{\theta}_M^2 \sin\theta_M - r_J \dot{\theta}_J^2 \sin\theta_J - r_4 \dot{\theta}_4^2 \sin\theta_4 \end{Bmatrix} \quad (5.53)$$

where  $M = 2$  and  $J = 3$  for  $\ddot{\theta}_2$  as the input, and  $M = 3$  and  $J = 2$  for  $\ddot{\theta}_3$  as the input. The terms in the matrix and vector on the right-hand side of the equation will be known. The equation can therefore be solved manually, on a programmable calculator, or with the matrix solvers in programs such as MATLAB. Notice that the coefficient matrix is the same for both the velocities (Eq. 5.47) and the accelerations (Eq. 5.53).

Once the angular accelerations are known, it is a simple matter to compute the linear accelerations of any of the points in the linkage. The accelerations of points  $Q$  and  $P$  are given by

$$\ddot{\mathbf{r}}_Q = \ddot{\mathbf{r}}_2 = \left(-r_2\ddot{\theta}_2 \sin\theta_2 - r_2\dot{\theta}_2^2 \cos\theta_2\right)\mathbf{i} + \left(r_2\ddot{\theta}_2 \cos\theta_2 - r_2\dot{\theta}_2^2 \sin\theta_2\right)\mathbf{j} \quad (5.54)$$

and

$$\begin{aligned} \ddot{\mathbf{r}}_P &= \ddot{\mathbf{r}}_2 + \ddot{\mathbf{r}}_3 = -\left(r_2\ddot{\theta}_2 \sin\theta_2 + r_2\dot{\theta}_2^2 \cos\theta_2 + r_3\ddot{\theta}_3 \sin\theta_3 + r_3\dot{\theta}_3^2 \cos\theta_3\right)\mathbf{i} \\ &\quad + \left(r_2\ddot{\theta}_2 \cos\theta_2 - r_2\dot{\theta}_2^2 \sin\theta_2 + r_3\ddot{\theta}_3 \cos\theta_3 - r_3\dot{\theta}_3^2 \sin\theta_3\right)\mathbf{j} \\ &= \ddot{\mathbf{r}}_1 + \ddot{\mathbf{r}}_4 = -\left(r_4\ddot{\theta}_4 \sin\theta_4 + r_4\dot{\theta}_4^2 \cos\theta_4\right)\mathbf{i} + \left(r_4\ddot{\theta}_4 \cos\theta_4 - r_4\dot{\theta}_4^2 \sin\theta_4\right)\mathbf{j} \end{aligned} \quad (5.55)$$

Now that the equations have been developed, it is relatively simple to write a computer program for the analysis of a four-bar linkage. To aid in this, the equations required are

summarized in Table 5.1. The authors have found that MATLAB is a very convenient language for solving simple kinematic equations, and this program runs on a variety of platforms. MATLAB routines for analyzing four-bar linkages are contained on the disk provided with this book.

**TABLE 5.1 Summary of Position, Velocity, and Acceleration Equations for a Four-Bar Linkage. Link 2 Is the Input Link When  $M = 2$  and  $J = 3$ . Link 3 Is the Input Link When  $M = 3$  and  $J = 2$ . Link 1 Is Assumed to Be the Frame. The Link Numbers and Points Are Defined in Fig. 5.5**

---

**Position**


---

$$A = 2r_1r_4 \cos \theta_1 - 2r_Mr_4 \cos \theta_M$$

$$B = 2r_1r_4 \sin \theta_1 - 2r_Mr_4 \sin \theta_M$$

$$C = r_1^2 + r_M^2 + r_4^2 - r_J^2 - 2r_1r_M(\cos \theta_1 \cos \theta_M + \sin \theta_1 \sin \theta_M)$$

$$\theta_4 = 2 \tan^{-1} \left[ \frac{-B + \sigma \sqrt{B^2 - C^2 + A^2}}{C - A} \right]; \quad \sigma = \pm 1$$

$$\theta_J = \tan^{-1} \left[ \frac{r_1 \sin \theta_1 + r_4 \sin \theta_4 - r_M \sin \theta_M}{r_1 \cos \theta_1 + r_4 \cos \theta_4 - r_M \cos \theta_M} \right]$$

$$\mathbf{r}_Q = \mathbf{r}_2 = r_2(\cos \theta_2 \mathbf{i} + \sin \theta_2 \mathbf{j})$$

$$\begin{aligned} \mathbf{r}_P &= \mathbf{r}_2 + \mathbf{r}_3 = r_2(\cos \theta_2 \mathbf{i} + \sin \theta_2 \mathbf{j}) + r_3(\cos \theta_3 \mathbf{i} + \sin \theta_3 \mathbf{j}) \\ &= \mathbf{r}_1 + \mathbf{r}_4 = r_1(\cos \theta_1 \mathbf{i} + \sin \theta_1 \mathbf{j}) + r_4(\cos \theta_4 \mathbf{i} + \sin \theta_4 \mathbf{j}) \end{aligned}$$

$$\mathbf{r}_R = \mathbf{r}_1 = r_1(\cos \theta_1 \mathbf{i} + \sin \theta_1 \mathbf{j})$$

---

**Velocity**


---

$$\begin{bmatrix} -r_J \sin \theta_J & r_4 \sin \theta_4 \\ -r_J \cos \theta_J & r_4 \cos \theta_4 \end{bmatrix} \begin{Bmatrix} \dot{\theta}_J \\ \dot{\theta}_4 \end{Bmatrix} = \begin{Bmatrix} r_M \dot{\theta}_M \sin \theta_M \\ r_M \dot{\theta}_M \cos \theta_M \end{Bmatrix}$$

$$\dot{\mathbf{r}}_Q = \dot{\mathbf{r}}_2 = r_2 \dot{\theta}_2 (-\sin \theta_2 \mathbf{i} + \cos \theta_2 \mathbf{j})$$

$$\dot{\mathbf{r}}_P = (-r_4 \dot{\theta}_4 \sin \theta_4) \mathbf{i} + (r_4 \dot{\theta}_4 \cos \theta_4) \mathbf{j}$$

---

**Acceleration**


---

$$\begin{bmatrix} -r_J \sin \theta_J & r_4 \sin \theta_4 \\ -r_J \cos \theta_J & r_4 \cos \theta_4 \end{bmatrix} \begin{Bmatrix} \ddot{\theta}_J \\ \ddot{\theta}_4 \end{Bmatrix} = \begin{Bmatrix} r_M \ddot{\theta}_M \sin \theta_M + r_M \dot{\theta}_M^2 \cos \theta_M + r_J \dot{\theta}_J^2 \cos \theta_J - r_4 \dot{\theta}_4^2 \cos \theta_4 \\ r_M \ddot{\theta}_M \cos \theta_M - r_M \dot{\theta}_M^2 \sin \theta_M - r_J \dot{\theta}_J^2 \sin \theta_J + r_4 \dot{\theta}_4^2 \sin \theta_4 \end{Bmatrix}$$

$$\ddot{\mathbf{r}}_Q = \ddot{\mathbf{r}}_2 = (-r_2 \ddot{\theta}_2 \sin \theta_2 - r_2 \dot{\theta}_2^2 \cos \theta_2) \mathbf{i} + (r_2 \ddot{\theta}_2 \cos \theta_2 - r_2 \dot{\theta}_2^2 \sin \theta_2) \mathbf{j}$$

$$\ddot{\mathbf{r}}_P = -(r_4 \ddot{\theta}_4 \sin \theta_4 + r_4 \dot{\theta}_4^2 \cos \theta_4) \mathbf{i} + (r_4 \ddot{\theta}_4 \cos \theta_4 - r_4 \dot{\theta}_4^2 \sin \theta_4) \mathbf{j}$$


---

**EXAMPLE 5.1**  
**Position Analysis**  
**of a Four-Bar**  
**Linkage**

For the linkage with  $r_1 = 1$ ,  $r_2 = 2$ ,  $r_3 = 3.5$ ,  $r_4 = 4$ , and  $\theta_1 = 0$  shown in Fig. 5.9, compute the corresponding values of  $\theta_3$  and  $\theta_4$  for each of the solution branches when the driving crank is in the positions  $\theta_2 = 0, \pi/2, \pi$ , and  $-\pi/2$ . Units for the lengths are not explicitly given in this example because the angular results are independent of the units for the lengths.

**Solution**

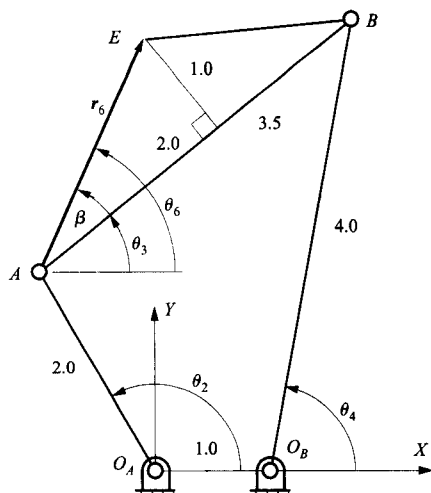


FIGURE 5.9 The linkage for Example 5.1, 5.2, and 5.3.

The solution procedure is to use the equations in Table 5.1. First compute  $A$ ,  $B$ , and  $C$  for each value of  $\theta_2$  and then select  $\sigma$ . Next compute  $\theta_4$  and then  $\theta_3$ . The calculations for  $\theta_2 = 0$  are as follows:

$$A = 2r_1r_4 \cos \theta_1 - 2r_2r_4 \cos \theta_2 = 2(1)(4) - 2(2)(4) = -8$$

$$B = 2r_1r_4 \sin \theta_1 - 2r_2r_4 \sin \theta_2 = 0$$

$$C = r_1^2 + r_2^2 + r_4^2 - r_3^2 - 2r_1r_2 (\cos \theta_1 \cos \theta_2 + \sin \theta_1 \sin \theta_2) = 1^2 + 2^2 + 4^2 - 3.5^2 - 2(1)(2) = 4.75$$

$$\begin{aligned} \theta_4 &= 2 \tan^{-1} \left[ \frac{-B + \sigma \sqrt{B^2 - C^2 + A^2}}{C - A} \right] \\ &= 2 \tan^{-1} \left[ \frac{-0 + \sqrt{0^2 - 4.75^2 + (-8)^2}}{4.75 + 8} \right] = 2 \tan^{-1} (0.5049) = 53.58^\circ \end{aligned}$$

$$\begin{aligned} \theta_3 &= \tan^{-1} \left[ \frac{r_1 \sin \theta_1 + r_4 \sin \theta_4 - r_2 \sin \theta_2}{r_1 \cos \theta_1 + r_4 \cos \theta_4 - r_2 \cos \theta_2} \right] \\ &= \tan^{-1} \left[ \frac{4 \sin(53.58^\circ)}{1 + 4 \cos(53.58^\circ) - 2} \right] = \tan^{-1} \left[ \frac{3.2187}{1.3748} \right] = \tan^{-1} (2.3412) = 66.87^\circ \end{aligned}$$

The remainder of the solution is summarized in Table 5.2.

TABLE 5.2 Summary of Results for Example 5.1

$\theta_2$	$\sigma$	$A$	$B$	$C$	$\theta_4$	$\theta_3$
0	1	-8	0	4.75	53.58°	66.87°
	-1				-53.58°	-66.87°
$\pi/2$	1	87	-16	8.75	177.28°	-143.85°
	-1				55.85°	21.98°
$\pi$	1	24	0	12.75	-122.09°	-75.52°
	-1				122.09°	75.52°
$-\pi/2$	1	8	16	8.75	-55.85°	-21.98°
	-1				-177.28°	148.85°

The arithmetic may also be checked by comparing  $\gamma = \theta_4 - \theta_3$  for  $\sigma = \pm 1$ . One value should be minus the other if both values are in the range  $-\pi < \gamma < \pi$ . It may be necessary to add or subtract  $2\pi$  to either value to bring  $\gamma$  into the range  $-\pi < \gamma < \pi$ .

**EXAMPLE 5.2**

**Velocity and  
Acceleration  
Analysis of a Four-  
Bar Linkage with  
Crank Input**

**Solution**

If, for the linkage in Example 5.1 (Fig. 5.9),  $\dot{\theta}_2 = 10$  rad/s and  $\ddot{\theta}_2 = 0$ , compute  $\dot{\theta}_3$ ,  $\dot{\theta}_4$ ,  $\ddot{\theta}_3$ ,  $\ddot{\theta}_4$  in the first of the four positions ( $\theta_2 = 0$ ).

Using the equations in Table 5.1, we write the velocity expression as

$$\begin{aligned} \begin{bmatrix} -r_3 \sin \theta_3 & r_4 \sin \theta_4 \\ -r_3 \cos \theta_3 & r_4 \cos \theta_4 \end{bmatrix} \begin{Bmatrix} \dot{\theta}_3 \\ \dot{\theta}_4 \end{Bmatrix} &= \begin{Bmatrix} r_2 \dot{\theta}_2 \sin \theta_2 \\ r_2 \dot{\theta}_2 \cos \theta_2 \end{Bmatrix} \\ &= \begin{bmatrix} -3.5 \sin(66.87^\circ) & 4 \sin(53.58^\circ) \\ -3.5 \cos(66.87^\circ) & 4 \cos(53.58^\circ) \end{bmatrix} \begin{Bmatrix} \dot{\theta}_3 \\ \dot{\theta}_4 \end{Bmatrix} = \begin{Bmatrix} 2(10) \sin(0^\circ) \\ 2(10) \cos(0^\circ) \end{Bmatrix} = \begin{bmatrix} -3.2187 & 3.2187 \\ -1.3749 & 2.3748 \end{bmatrix} \begin{Bmatrix} \dot{\theta}_3 \\ \dot{\theta}_4 \end{Bmatrix} = \begin{Bmatrix} 0 \\ 20 \end{Bmatrix} \end{aligned}$$

Solving the linear set of equations gives  $\dot{\theta}_3 = 20$  rad/s and  $\dot{\theta}_4 = 20.0$  rad/s. Both values are positive, so the corresponding angular velocities are counterclockwise. The acceleration expression is

$$\begin{aligned} \begin{bmatrix} -r_3 \sin \theta_3 & r_4 \sin \theta_4 \\ -r_3 \cos \theta_3 & r_4 \cos \theta_4 \end{bmatrix} \begin{Bmatrix} \ddot{\theta}_3 \\ \ddot{\theta}_4 \end{Bmatrix} &= \begin{Bmatrix} r_2 \ddot{\theta}_2 \sin \theta_2 + r_2 \dot{\theta}_2^2 \cos \theta_2 + r_3 \dot{\theta}_3^2 \cos \theta_3 - r_4 \dot{\theta}_4^2 \cos \theta_4 \\ r_2 \ddot{\theta}_2 \cos \theta_2 - r_2 \dot{\theta}_2^2 \sin \theta_2 - r_3 \dot{\theta}_3^2 \sin \theta_3 - r_4 \dot{\theta}_4^2 \sin \theta_4 \end{Bmatrix} \\ \begin{bmatrix} -3.2187 & 3.2187 \\ -1.3749 & 2.3748 \end{bmatrix} \begin{Bmatrix} \ddot{\theta}_3 \\ \ddot{\theta}_4 \end{Bmatrix} &= \begin{Bmatrix} 0 + 2(10)^2 + 3.5(20)^2 \cos(66.87^\circ) - 4(20)^2 \cos(53.58^\circ) \\ 0 - 0 - 3.5(20)^2 \sin(66.87^\circ) + 4(20)^2 \sin(53.58^\circ) \end{Bmatrix} = \begin{Bmatrix} -200.0265 \\ -0.0363 \end{Bmatrix} \end{aligned}$$

Solving the linear set of equations gives  $\ddot{\theta}_3 = 147.5634$  rad/s<sup>2</sup> and  $\ddot{\theta}_4 = 85.4150$  rad/s<sup>2</sup>. Again, both values are positive, so the corresponding angular accelerations are counterclockwise.

## 5.4 ANALYTICAL EQUATIONS FOR A RIGID BODY AFTER THE KINEMATIC PROPERTIES OF TWO POINTS ARE KNOWN

The equations presented so far will permit the kinematic properties of the points on the vector loop to be computed directly. However, often we need to compute the position, velocity, and acceleration of points that are not directly on the vector loops. In general, given the kinematic properties of *one* point on a rigid body and the angular position, angular velocity, and angular acceleration of the body, we can compute the position, velocity, and acceleration of *any* defined point on the rigid body.

Consider the rigid body represented in Fig. 5.10. Assume that *A* and *B* are two points attached to an arbitrary link, say link 5, and a third point is defined relative to the line between points *A* and *B* by the angle  $\beta$  and the distance  $r_{C/A}$ , which is represented in Fig. 5.10 as  $r_6$ . Then the linear position, velocity, and acceleration of point *C* can be computed directly if the following are known:  $r_A$ ,  $\dot{r}_A$ ,  $\ddot{r}_A$ ,  $\theta_5$ ,  $\dot{\theta}_5$ , and  $\ddot{\theta}_5$ .

The position of point *C* is given as

$$r_C = r_A + r_6$$

or

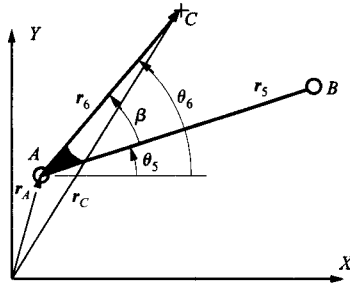


FIGURE 5.10 Calculation of the kinematic properties of a point on a link after the kinematic properties of one point and the angular velocity and acceleration of the link are known.

$$\mathbf{r}_C = \mathbf{r}_A + r_6(\cos \theta_6 \mathbf{i} + \sin \theta_6 \mathbf{j}) \quad (5.56)$$

where

$$\theta_6 = \beta + \theta_5 \quad (5.57)$$

Recognizing that  $\beta$  is a constant, we see that the velocity of point  $C$  is given by

$$\dot{\mathbf{r}}_C = \dot{\mathbf{r}}_A + r_6 \dot{\theta}_5 (-\sin \theta_6 \mathbf{i} + \cos \theta_6 \mathbf{j}) \quad (5.58)$$

and the acceleration is given by

$$\ddot{\mathbf{r}}_C = \ddot{\mathbf{r}}_A + r_6 \ddot{\theta}_5 (-\sin \theta_6 \mathbf{i} + \cos \theta_6 \mathbf{j}) - r_6 \dot{\theta}_5^2 (\cos \theta_6 \mathbf{i} + \sin \theta_6 \mathbf{j}) \quad (5.59)$$

Note that we have assumed here that  $\theta_5$ ,  $\dot{\theta}_5$ , and  $\ddot{\theta}_5$  are known. Often, we will know the kinematic information for two points on a rigid link instead of these angular quantities. If we know the position, velocity, and acceleration of two points (say  $A$  and  $B$ ), we can compute  $\theta_5$ ,  $\dot{\theta}_5$ , and  $\ddot{\theta}_5$  and proceed as before. The angle can be computed from the  $x$  and  $y$  components of the position vectors for  $A$  and  $B$  using

$$\theta_5 = \tan^{-1} \left[ \frac{r_{B_y} - r_{A_y}}{r_{B_x} - r_{A_x}} \right]$$

The angular velocity can be computed by rewriting Eq. (5.58) in terms of points  $A$  and  $B$ . That is,

$$\dot{\mathbf{r}}_B = \dot{\mathbf{r}}_A + r_5 \dot{\theta}_5 (-\sin \theta_5 \mathbf{i} + \cos \theta_5 \mathbf{j})$$

Therefore,

$$\dot{\theta}_5 = -\frac{\dot{r}_{B_x} - \dot{r}_{A_x}}{r_5 \sin \theta_5} = \frac{\dot{r}_{B_y} - \dot{r}_{A_y}}{r_5 \cos \theta_5}$$

Similarly, the angular acceleration can be computed by rewriting Eq. (5.59) in terms of  $A$  and  $B$ . That is,

$$\ddot{\mathbf{r}}_B = \ddot{\mathbf{r}}_A + r_5 \ddot{\theta}_5 (-\sin \theta_5 \mathbf{i} + \cos \theta_5 \mathbf{j}) - r_5 \dot{\theta}_5^2 (\cos \theta_5 \mathbf{i} + \sin \theta_5 \mathbf{j})$$

Therefore,

$$\ddot{\theta}_5 = -\frac{(\ddot{r}_{B_x} - \ddot{r}_{A_x}) + r_5 \dot{\theta}_5^2 \cos \theta_5}{r_5 \sin \theta_5} = \frac{(\ddot{r}_{B_y} - \ddot{r}_{A_y}) + r_5 \dot{\theta}_5^2 \sin \theta_5}{r_5 \cos \theta_5}$$

These equations are summarized in Table 5.3, and a MATLAB function routine for the calculations is included on the disk with this book.

**TABLE 5.3 Summary of Position, Velocity, and Acceleration Equations for an Arbitrary Point on a Rigid Body. The Vectors and Points Are Defined in Fig. 5.10**

If  $r_A$  and  $r_B$  are given instead of  $\theta_5$ ,  $\dot{\theta}_5$ , and  $\ddot{\theta}_5$ , first compute  $\theta_5$ ,  $\dot{\theta}_5$ , and  $\ddot{\theta}_5$  using the following:

$$\theta_5 = \tan^{-1} \left[ \frac{r_{B_y} - r_{A_y}}{r_{B_x} - r_{A_x}} \right],$$

$$\dot{\theta}_5 = -\frac{\dot{r}_{B_x} - \dot{r}_{A_x}}{r_5 \sin \theta_5} = \frac{\dot{r}_{B_y} - \dot{r}_{A_y}}{r_5 \cos \theta_5},$$

$$\ddot{\theta}_5 = -\frac{(\ddot{r}_{B_x} - \ddot{r}_{A_x}) + r_5 \dot{\theta}_5^2 \cos \theta_5}{r_5 \sin \theta_5} = \frac{(\ddot{r}_{B_y} - \ddot{r}_{A_y}) + r_5 \dot{\theta}_5^2 \sin \theta_5}{r_5 \cos \theta_5}$$

---

**Position**


---

$$r_C = r_A + r_6 (\cos \theta_6 i + \sin \theta_6 j)$$

$$\theta_6 = \beta + \theta_5$$

---

**Velocity**


---

$$\dot{r}_C = \dot{r}_A + r_6 \dot{\theta}_5 (-\sin \theta_6 i + \cos \theta_6 j)$$

---

**Acceleration**


---

$$\ddot{r}_C = \ddot{r}_A + r_6 \ddot{\theta}_5 (-\sin \theta_6 i + \cos \theta_6 j) - r_6 \dot{\theta}_5^2 (\cos \theta_6 i + \sin \theta_6 j)$$


---

**EXAMPLE 5.3**  
**Velocity and**  
**Acceleration**  
**Analysis of a**  
**Coupler Point**
**Solution**

For the linkage in Examples 5.1 and 5.2 shown in Fig. 5.9, compute the velocity and acceleration of point  $E_3$  when  $\theta_2 = 0$ ,  $\dot{\theta}_2 = 10$  rad/s,  $\ddot{\theta}_2 = 0$ , and  $\sigma = 1$ . Assume that the lengths are given in centimeters.

First compute the angle  $\beta$  between the line  $AB$  and the line  $AE$ . The angle is given by

$$\beta = \tan^{-1} \left( \frac{1}{2} \right) = 26.565^\circ$$

and the length  $AE$  is given by

$$r_6 = AE = 2.0 / \cos(26.565^\circ) = 2.236 \text{ cm}$$

Then the velocity of  $E_3$  is given by

$$\dot{r}_{E_3} = r_2 \dot{\theta}_2 (-\sin \theta_2 i + \cos \theta_2 j) + r_6 \dot{\theta}_3 (-\sin \theta_6 i + \cos \theta_6 j)$$

Substitution of  $\theta_2 = 0$ ,  $\theta_3 = 66.87^\circ$ ,  $\dot{\theta}_2 = 10.0$  rad/s, and  $\dot{\theta}_3 = 20.0$  rad/s from Example 5.2 gives

$$\theta_6 = \theta_3 + \beta = 66.87^\circ + 26.565^\circ = 93.435^\circ$$

and

$$\begin{aligned} \dot{r}_{E_3} &= 2(10)(0i + j) + 2.236(20.0)(-\sin(93.435^\circ)i + \cos(93.435^\circ)j) \\ &= 20j - 44.640i - 2.679j = -44.64i + 17.32j \text{ cm/s} \end{aligned}$$

The acceleration of  $E_3$  is given by

$$\begin{aligned}\ddot{\mathbf{r}}_{E_3} = & r_2 \ddot{\theta}_2 (-\sin \theta_2 \mathbf{i} + \cos \theta_2 \mathbf{j}) - r_2 \dot{\theta}_2^2 (\cos \theta_2 \mathbf{i} + \sin \theta_2 \mathbf{j}) \\ & + r_6 \ddot{\theta}_3 (-\sin \theta_6 \mathbf{i} + \cos \theta_6 \mathbf{j}) - r_6 \dot{\theta}_3^2 (\cos \theta_6 \mathbf{i} + \sin \theta_6 \mathbf{j})\end{aligned}$$

Substitution of  $\theta_2 = 0$ ,  $\theta_3 = 66.87^\circ$ ,  $\dot{\theta}_2 = 10.0$  rad/s,  $\ddot{\theta}_2 = 0$  rad/s<sup>2</sup>,  $\dot{\theta}_3 = 20.0$  rad/s, and  $\ddot{\theta}_3 = 147.56$  rad/s<sup>2</sup> gives

$$\begin{aligned}\ddot{\mathbf{r}}_{E_3} = & 0 - 2(10)^2 (\mathbf{i} + 0 \mathbf{j}) + 2.236(147.56) [-\sin(93.435^\circ) \mathbf{i} + \cos(93.435^\circ) \mathbf{j}] \\ & - 2.236(20.0)^2 [\cos(93.435^\circ) \mathbf{i} + \sin(93.435^\circ) \mathbf{j}] = -475.76 \mathbf{i} - 912.56 \mathbf{j} \text{ cm/s}^2\end{aligned}$$

## 5.5 ANALYTICAL EQUATIONS FOR SLIDER-CRANK MECHANISMS

Next to the four-bar linkage, the slider-crank is probably the most commonly used mechanism. It appears in all internal combustion engines (Fig. 5.11) and in numerous industrial (Fig. 5.12) and household devices (Fig. 5.13). A general slider-crank mechanism is represented in Fig. 5.14. To develop the closure equations, locate vectors  $\mathbf{r}_2$  and  $\mathbf{r}_3$  as was done in the regular four-bar linkage. To form the other part of the closure equation, draw two vectors, one in the direction of the slider velocity and one perpendicular to the velocity direction. The variables associated with the problem are then located as shown in Fig. 5.14. The loop closure equation is then the same as that for the regular four-bar linkage:

$$\mathbf{r}_p = \mathbf{r}_2 + \mathbf{r}_3 = \mathbf{r}_1 + \mathbf{r}_4 \quad (5.60)$$

or

$$r_2 (\cos \theta_2 \mathbf{i} + \sin \theta_2 \mathbf{j}) + r_3 (\cos \theta_3 \mathbf{i} + \sin \theta_3 \mathbf{j}) = r_1 (\cos \theta_1 \mathbf{i} + \sin \theta_1 \mathbf{j}) + r_4 (\cos \theta_4 \mathbf{i} + \sin \theta_4 \mathbf{j}) \quad (5.61)$$

where

$$\theta_4 = \theta_1 + \pi/2 \quad (5.62)$$

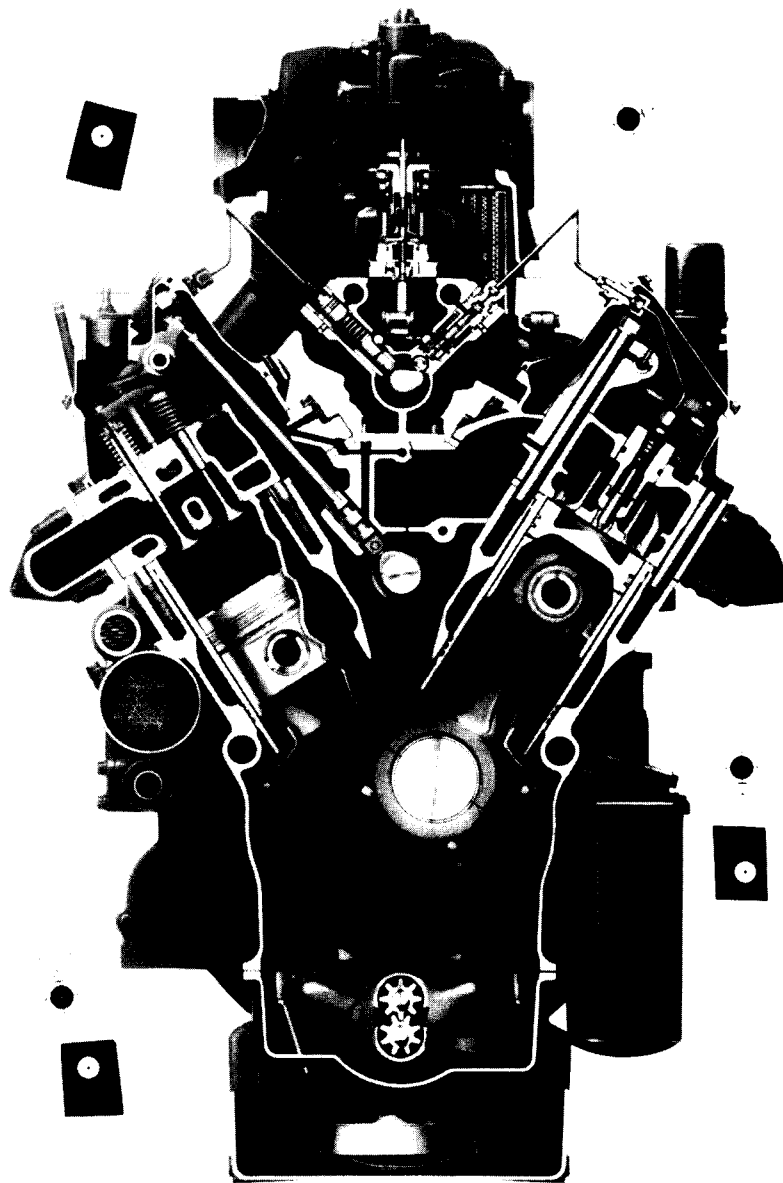
Because  $\theta_1$  is constant,  $\theta_4$  is also constant.

Rewriting Eq. (5.61) into its component equations gives

$$r_2 \cos \theta_2 + r_3 \cos \theta_3 = r_1 \cos \theta_1 + r_4 \cos \theta_4 \quad (5.63)$$

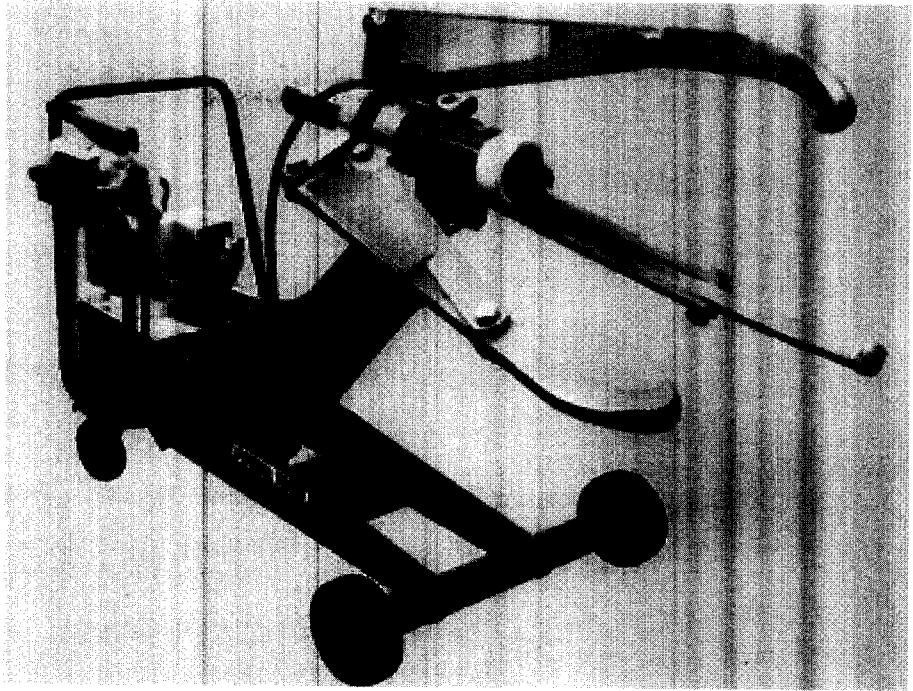
$$r_2 \sin \theta_2 + r_3 \sin \theta_3 = r_1 \sin \theta_1 + r_4 \sin \theta_4 \quad (5.64)$$

Equations (5.62)–(5.64) must be satisfied throughout the motion of the linkage. The base vector,  $\mathbf{r}_1$ , will vary in magnitude but be constant in direction. The vector  $\mathbf{r}_4$  will be constant. Therefore,  $r_2$ ,  $r_3$ ,  $r_4$ ,  $\theta_1$ , and  $\theta_4$  are constants. If  $\theta_2$  is given, it is necessary to solve Eqs. (5.63) and (5.64) for  $\theta_3$  and  $r_1$  in terms of  $\theta_2$ . If  $r_1$  is given, it is necessary to solve the same equations for  $\theta_2$  and  $\theta_3$ . And finally, if  $\theta_3$  is given, it is necessary to solve the equations for  $\theta_2$  and  $r_1$ . Once these expressions are obtained, the unknown velocities and accelerations can be computed in terms of the knowns by differentiation.

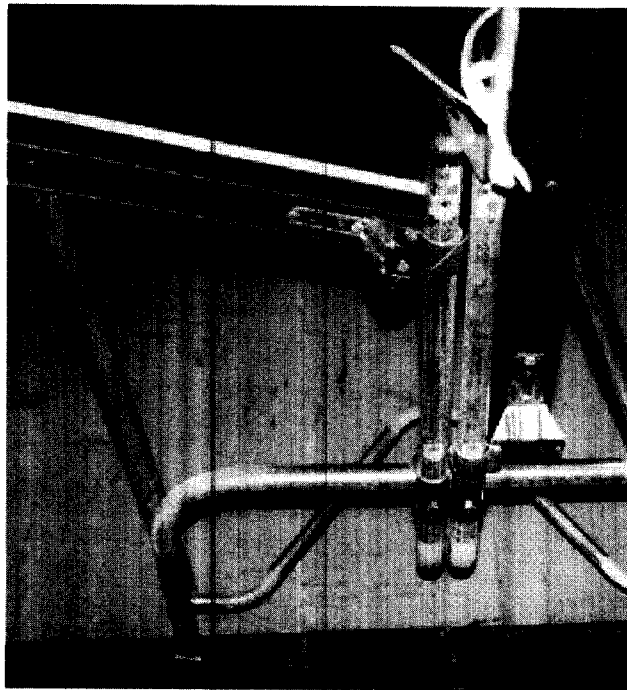


**FIGURE 5.11** Internal combustion engine. An example of a slider-crank mechanism where the crank is the output link. (Courtesy of Caterpillar, Inc., Peoria, Illinois.)





**FIGURE 5.12** Hydraulic shaft puller. An example of a slider-crank mechanism where the slider is the input link. (Courtesy of Power Team, Owatonna, Minnesota.)



**FIGURE 5.13** Ping-Pong table linkage. An example of a slider-crank mechanism where the coupler is the input link.

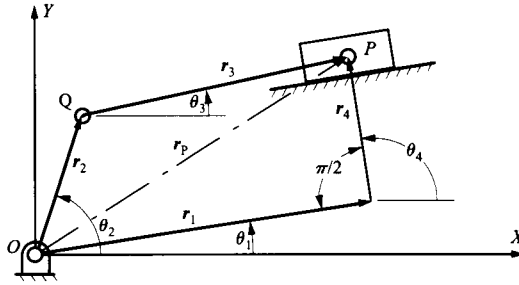


FIGURE 5.14 Vector closure condition for a slider-crank mechanism. The position of point  $P$  obtained by adding the vectors  $r_2$  and  $r_3$  is the same as that obtained by adding vectors  $r_1$  and  $r_4$ .

### 5.5.1 Solution to Position Equations When $\theta_2$ Is Input

The analytical solution procedure follows the same major steps as in the four-bar linkage case. To eliminate  $\theta_3$ , first isolate it in Eqs. (5.63) and (5.64) as follows:

$$r_3 \cos \theta_3 = r_1 \cos \theta_1 + r_4 \cos \theta_4 - r_2 \cos \theta_2 \quad (5.65)$$

$$r_3 \sin \theta_3 = r_1 \sin \theta_1 + r_4 \sin \theta_4 - r_2 \sin \theta_2 \quad (5.66)$$

Notice that in Fig. 5.14, the angles  $\theta_1$  and  $\theta_4$  are known constants, but  $r_1$  varies and is unknown. Now square both sides of both equations and add. This gives

$$r_3^2 (\cos^2 \theta_3 + \sin^2 \theta_3) = (r_1 \cos \theta_1 + r_4 \cos \theta_4 - r_2 \cos \theta_2)^2 + (r_1 \sin \theta_1 + r_4 \sin \theta_4 - r_2 \sin \theta_2)^2$$

Expansion and simplification using the trigonometric identity  $\sin^2 \theta + \cos^2 \theta = 1$  gives

$$\begin{aligned} r_3^2 = & r_1^2 + r_2^2 + r_4^2 + 2r_1r_4(\cos \theta_1 \cos \theta_4 + \sin \theta_1 \sin \theta_4) \\ & - 2r_1r_2(\cos \theta_1 \cos \theta_2 + \sin \theta_1 \sin \theta_2) - 2r_2r_4(\cos \theta_2 \cos \theta_4 + \sin \theta_2 \sin \theta_4) \end{aligned} \quad (5.67)$$

Equation (5.67) gives  $r_1$  in a quadratic expression involving  $\theta_2$  and the other known variables. To obtain a solution, collect together the coefficients of the different powers of  $r_1$  as follows:

$$r_1^2 + Ar_1 + B = 0 \quad (5.68)$$

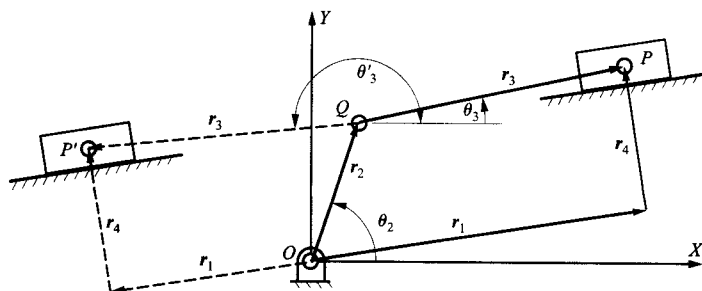
where

$$\begin{aligned} A = & 2r_4(\cos \theta_1 \cos \theta_4 + \sin \theta_1 \sin \theta_4) - 2r_2(\cos \theta_1 \cos \theta_2 + \sin \theta_1 \sin \theta_2) \\ B = & r_2^2 + r_4^2 - r_3^2 - 2r_2r_4(\cos \theta_2 \cos \theta_4 + \sin \theta_2 \sin \theta_4) \end{aligned} \quad (5.69)$$

Solving for  $r_1$  gives

$$r_1 = \frac{-A + \sigma \sqrt{A^2 - 4B}}{2} \quad (5.70)$$

where  $\sigma = \pm 1$  is a sign variable identifying the assembly mode. There are two assembly modes corresponding to the two configurations shown in Fig. 5.15.



**FIGURE 5.15** The two possible positions ( $P$  and  $P'$ ) of the point  $P$  for a given value of  $\theta_2$  in a slider-crank mechanism.

As in the case of the four-bar linkage, once we pick the value for  $\sigma$  corresponding to the desired mode, the sign in an actual linkage stays the same for any value of  $\theta_2$ .

Because of the square root in Eq. (5.70), the variable  $r_1$  can be complex ( $A^2 < 4B$ ). If this happens, the mechanism cannot be assembled in the position specified. The assembly would then appear as one of the configurations shown in Fig. 5.15.

Once a value for  $r_1$  is determined, Eqs. (5.65) and (5.66) can be solved for  $\theta_3$ . Dividing Eq. (5.66) by Eq. (5.65) and solving for  $\theta_3$  gives

$$\theta_3 = \tan^{-1} \left[ \frac{r_1 \sin \theta_1 + r_4 \sin \theta_4 - r_2 \sin \theta_2}{r_1 \cos \theta_1 + r_4 \cos \theta_4 - r_2 \cos \theta_2} \right] \quad (5.71)$$

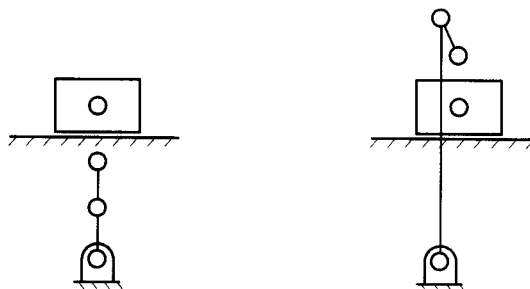
As in the case of the four-bar linkage, it is essential that the signs of the numerator and denominator in Eq. (5.71) be maintained to determine the quadrant in which the angle  $\theta_3$  lies.

Once all of the angular quantities are known, it is relatively straightforward to compute the coordinates of any point on the vector loops used in the closure equations. In particular, the coordinates of  $Q$  and  $P$  are given by

$$r_Q = r_2 = r_2 (\cos \theta_2 \mathbf{i} + \sin \theta_2 \mathbf{j}) \quad (5.72)$$

and

$$r_P = r_2 + r_3 = r_2 (\cos \theta_2 \mathbf{i} + \sin \theta_2 \mathbf{j}) + r_3 (\cos \theta_3 \mathbf{i} + \sin \theta_3 \mathbf{j}) \quad (5.73)$$



**FIGURE 5.16** Configurations giving complex solutions for slider-crank position problem.

### 5.5.2 Solution to Position Equations When $r_1$ Is Input

The analytical solution procedure follows the same major steps as in the previous case. Referring to Fig. 5.14, we again start by eliminating  $\theta_3$  from Eqs. (5.63) and (5.64) to get Eq. (5.67). Then we simplify Eq. (5.67) as follows:

$$A \cos \theta_2 + B \sin \theta_2 + C = 0 \quad (5.74)$$

where

$$\left. \begin{aligned} A &= -2r_1r_2 \cos \theta_1 - 2r_2r_4 \cos \theta_4 \\ B &= -2r_1r_2 \sin \theta_1 - 2r_2r_4 \sin \theta_4 \\ C &= r_1^2 + r_2^2 + r_4^2 - r_3^2 + 2r_1r_4(\cos \theta_1 \cos \theta_4 + \sin \theta_1 \sin \theta_4) \end{aligned} \right\} \quad (5.75)$$

To solve Eq. (5.74), the trigonometric half-angle identities given in Eqs. (5.33–5.34) can be used. Using these identities in Eq. (5.74) and simplifying gives

$$A(1-t^2) + B(2t) + C(1+t^2) = 0$$

where

$$t = \tan\left(\frac{\theta_2}{2}\right)$$

Further simplification gives

$$(C-A)t^2 + 2Bt + (A+C) = 0$$

Solving for  $t$  gives

$$t = \frac{-2B + \sigma \sqrt{4B^2 - 4(C-A)(C+A)}}{2(C-A)} = \frac{-B + \sigma \sqrt{B^2 - C^2 + A^2}}{C-A} \quad (5.76)$$

and

$$\theta_2 = 2 \tan^{-1} t \quad (5.77)$$

where  $\sigma = \pm 1$  is a sign variable identifying the assembly mode. Once again, because  $\tan^{-1} t$  has a valid range of values  $-\pi/2 \leq \tan^{-1} t < \pi/2$ ,  $\theta_2$  will have the range  $-\pi \leq \theta_2 \leq \pi$ . Typically, there are two solutions for  $\theta_2$  corresponding to the two values of  $\sigma$ , and they are both valid. These correspond to the two assembly modes shown in Fig. 5.17. Once we pick the

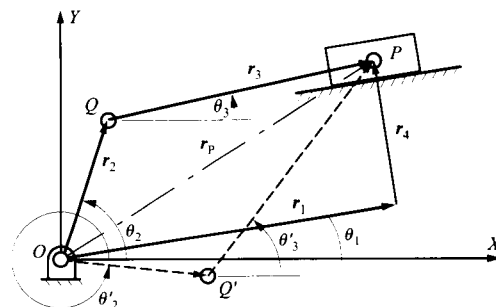


FIGURE 5.17 Two possible assembly modes when the position  $r_1$  of the slider is given as an input.

value for  $\sigma$  corresponding to the desired mode, the sign in an actual linkage stays the same for any value of  $r_1$ .

Because of the square root in Eq. (5.76), the variable  $t$  can be complex  $[(A^2 + B^2) < C^2]$ . If this happens, the mechanism cannot be assembled for the specified value of  $r_1$ . The assembly configurations would then appear as shown in Fig. 5.18.

Knowing  $r_1$ , equations (5.65) and (5.66) can now be solved for  $\theta_3$ . The resulting equation is Eq. (5.71). As in the previous cases, it is essential that the signs of the numerator and denominator in Eq. (5.71) be maintained to determine the quadrant in which the angle  $\theta_3$  lies. Note that the positions of  $r_2$  and  $r_3$  are symmetric about the line  $OP$ .

Once all of the angular quantities are known, it is relatively straightforward to compute the coordinates of any point on the vector loops used in the closure equations. The coordinates of  $Q$  and  $P$  are again given by Eqs. (5.72) and (5.73).

### 5.5.3 Solution to Position Equations When $\theta_3$ Is Input

When the coupler of the linkage in Fig. 5.14 is the input link, values for  $\theta_3$  and its derivatives will be known. The analytical procedure for solving the position equations follows the same major steps as when  $\theta_2$  is the input. Therefore, we will simply outline the procedure and tabulate the results.

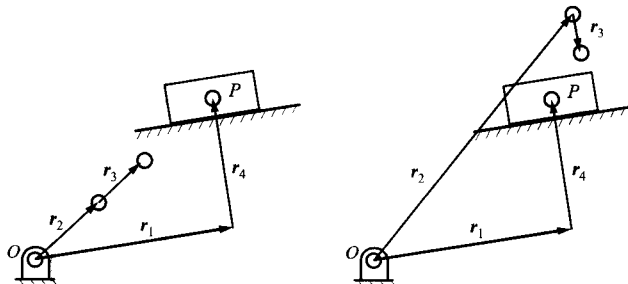
In the procedure, we can assume that  $\theta_1$ ,  $\theta_3$ ,  $\theta_4$ ,  $\dot{\theta}_3$ , and  $\ddot{\theta}_3$  are known and  $\theta_2$ ,  $\dot{\theta}_2$ ,  $\ddot{\theta}_2$ ,  $r_1$ ,  $\dot{r}_1$ , and  $\ddot{r}_1$  are to be found. The link lengths  $r_2$  and  $r_3$  and the angles  $\theta_1$  and  $\theta_4$  are constants. For the position analysis, again begin with Eqs. (5.63) and (5.64) and isolate the terms with either  $\theta_2$  or  $\theta_4$ . It is advantageous to select  $\theta_2$  because the resulting equations will be similar to those derived earlier. The resulting equations are

$$r_2 \cos \theta_2 = r_1 \cos \theta_1 + r_4 \cos \theta_4 - r_3 \cos \theta_3 \quad (5.78)$$

$$r_2 \sin \theta_2 = r_1 \sin \theta_1 + r_4 \sin \theta_4 - r_3 \sin \theta_3 \quad (5.79)$$

A comparison of Eqs. (5.78) and (5.79) with Eqs. (5.65) and (5.66) indicates that they are of the same form except that the indices 2 and 3 are interchanged. Therefore, we can use directly the position solution derived in Section 5.5.1 if we interchange the indices 2 and 3.

When the coupler is the driver, there is an assembly-mode ambiguity similar to that observed when link 2 is the driver. This is illustrated in Fig. 5.19. It is necessary to know the appropriate mode before the analysis can be completed; however, once the assembly mode is selected, it is the same for all positions of the input.



**FIGURE 5.18** Slider-crank mechanisms that cannot be assembled in the position chosen for  $r_1$ . The variable  $t$  would be complex in these cases.

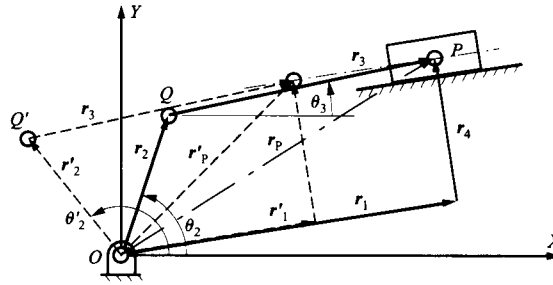


FIGURE 5.19 Two possible assembly modes when the coupler is the input link.

### 5.5.4 Velocity Equations for Slider-Crank Mechanism

The analytical form of the velocity equations for the linkage of Fig. 5.14 can be developed by differentiating Eq. (5.60). The result is

$$\dot{\mathbf{r}}_P = \dot{\mathbf{r}}_2 + \dot{\mathbf{r}}_3 = \dot{\mathbf{r}}_1 + \dot{\mathbf{r}}_4 \quad (5.80)$$

When this equation is written in component form, the result is the same as differentiating Eqs. (5.63) and (5.64). Recognizing that  $r_2$ ,  $r_3$ ,  $r_4$ ,  $\theta_1$ , and  $\theta_4$  are constants, we see the resulting component equations are

$$-r_2 \dot{\theta}_2 \sin \theta_2 - r_3 \dot{\theta}_3 \sin \theta_3 = \dot{r}_1 \cos \theta_1 \quad (5.81)$$

$$r_2 \dot{\theta}_2 \cos \theta_2 + r_3 \dot{\theta}_3 \cos \theta_3 = \dot{r}_1 \sin \theta_1 \quad (5.82)$$

The solution procedure depends on whether  $\dot{r}_1$ ,  $\dot{\theta}_2$ , or  $\dot{\theta}_3$  is known. If  $\dot{\theta}_2$  (or  $\dot{\theta}_3$ ) is input, then  $\dot{r}_1$  and  $\dot{\theta}_3$  (or  $\dot{\theta}_2$ ) will be unknown. Therefore, the matrix equation to be solved is

$$\begin{bmatrix} \cos \theta_1 & r_J \sin \theta_J \\ \sin \theta_1 & -r_J \cos \theta_J \end{bmatrix} \begin{Bmatrix} \dot{r}_1 \\ \dot{\theta}_J \end{Bmatrix} = \begin{Bmatrix} -r_M \dot{\theta}_M \sin \theta_M \\ r_M \dot{\theta}_M \cos \theta_M \end{Bmatrix} \quad (5.83)$$

where  $M = 2$  and  $J = 3$  for link 2 as the input, and  $M = 3$  and  $J = 2$  for link 3 as the input. If  $\dot{r}_1$  is input, then  $\dot{\theta}_2$  and  $\dot{\theta}_3$  will be unknown. The matrix equation to be solved then is

$$\begin{bmatrix} -r_2 \sin \theta_2 & -r_3 \sin \theta_3 \\ r_2 \cos \theta_2 & r_3 \cos \theta_3 \end{bmatrix} \begin{Bmatrix} \dot{\theta}_2 \\ \dot{\theta}_3 \end{Bmatrix} = \begin{Bmatrix} \dot{r}_1 \cos \theta_1 \\ \dot{r}_1 \sin \theta_1 \end{Bmatrix} \quad (5.84)$$

The terms in the matrix and in the vector on the right-hand sides of Eqs. (5.83) and (5.84) will be known. The equation can therefore be solved manually, on a programmable calculator, or numerically with the matrix solvers in programs such as MATLAB.

Once the angular velocities are known, it is a simple matter to compute the linear velocities of any of the points on the vector loop. The velocities of points  $Q$  and  $P$  are given by

$$\dot{\mathbf{r}}_Q = \dot{\mathbf{r}}_2 = r_2 \dot{\theta}_2 (-\sin \theta_2 \mathbf{i} + \cos \theta_2 \mathbf{j}) \quad (5.85)$$

and

$$\dot{\mathbf{r}}_P = \dot{\mathbf{r}}_2 + \dot{\mathbf{r}}_3 = (-r_2 \dot{\theta}_2 \sin \theta_2 - r_3 \dot{\theta}_3 \sin \theta_3) \mathbf{i} + (r_2 \dot{\theta}_2 \cos \theta_2 + r_3 \dot{\theta}_3 \cos \theta_3) \mathbf{j} \quad (5.86)$$

### 5.5.5 Acceleration Equations for Slider-Crank Mechanism

The analytical form of the acceleration equations for the linkage of Fig. 5.14 can be developed by differentiating Eq. (5.80). The result is

$$\ddot{\mathbf{r}}_P = \ddot{\mathbf{r}}_2 + \ddot{\mathbf{r}}_3 = \ddot{\mathbf{r}}_1 + \ddot{\mathbf{r}}_4$$

When this equation is written in component form, the result is the same as differentiating Eqs. (5.81) and (5.82). The resulting component equations are

$$-r_2\ddot{\theta}_2 \sin \theta_2 - r_2\dot{\theta}_2^2 \cos \theta_2 - r_3\ddot{\theta}_3 \sin \theta_3 - r_3\dot{\theta}_3^2 \cos \theta_3 = \ddot{r}_1 \cos \theta_1 \quad (5.87)$$

$$r_2\ddot{\theta}_2 \cos \theta_2 - r_2\dot{\theta}_2^2 \sin \theta_2 + r_3\ddot{\theta}_3 \cos \theta_3 - r_3\dot{\theta}_3^2 \sin \theta_3 = \ddot{r}_1 \sin \theta_1 \quad (5.88)$$

As was the case for velocities, the solution procedure depends on whether  $\ddot{\theta}_2$ ,  $\ddot{\theta}_3$ , or  $\ddot{r}_1$  is known. If  $\ddot{\theta}_2$  (or  $\ddot{\theta}_3$ ) is input, then  $\ddot{r}_1$  and  $\ddot{\theta}_3$  (or  $\ddot{\theta}_2$ ) will be unknown, and the matrix equation to be solved is

$$\begin{bmatrix} \cos \theta_1 & r_J \sin \theta_J \\ \sin \theta_1 & -r_J \cos \theta_J \end{bmatrix} \begin{Bmatrix} \ddot{r}_1 \\ \ddot{\theta}_J \end{Bmatrix} = \begin{Bmatrix} -r_M \ddot{\theta}_M \sin \theta_M - r_M \dot{\theta}_M^2 \cos \theta_M - r_J \dot{\theta}_J^2 \cos \theta_J \\ r_M \ddot{\theta}_M \cos \theta_M - r_M \dot{\theta}_M^2 \sin \theta_M - r_J \dot{\theta}_J^2 \sin \theta_J \end{Bmatrix} \quad (5.89)$$

If  $\ddot{r}_1$  is input, then  $\ddot{\theta}_2$  and  $\ddot{\theta}_3$  will be unknown, and the matrix equation to be solved then is

$$\begin{bmatrix} -r_2 \sin \theta_2 & -r_3 \sin \theta_3 \\ r_2 \cos \theta_2 & r_3 \cos \theta_3 \end{bmatrix} \begin{Bmatrix} \ddot{\theta}_2 \\ \ddot{\theta}_3 \end{Bmatrix} = \begin{Bmatrix} r_2 \dot{\theta}_2^2 \cos \theta_2 + r_3 \dot{\theta}_3^2 \cos \theta_3 + \ddot{r}_1 \cos \theta_1 \\ r_2 \dot{\theta}_2^2 \sin \theta_2 + r_3 \dot{\theta}_3^2 \sin \theta_3 + \ddot{r}_1 \sin \theta_1 \end{Bmatrix} \quad (5.90)$$

The terms in the matrix and in the vector on the right-hand sides of Eqs. (5.89) and (5.90) will be known. The equation can therefore be solved manually, on a programmable calculator, or with the matrix solvers in programs such as MATLAB. Notice again that the coefficient matrix is the same for both the velocities (Eqs. (5.83) and (5.84) and for the accelerations (Eqs. (5.89) and (5.90)).

Once the angular accelerations are known, it is a simple matter to compute the linear acceleration of any point on the vector loop. The accelerations of points  $Q$  and  $P$  are given by

$$\ddot{\mathbf{r}}_Q = \ddot{\mathbf{r}}_2 = (r_2\ddot{\theta}_2 \sin \theta_2 - r_2\dot{\theta}_2^2 \cos \theta_2)\mathbf{i} + (r_2\ddot{\theta}_2 \cos \theta_2 - r_2\dot{\theta}_2^2 \sin \theta_2)\mathbf{j} \quad (5.91)$$

and

$$\begin{aligned} \ddot{\mathbf{r}}_P = \ddot{\mathbf{r}}_2 + \ddot{\mathbf{r}}_3 = & -(r_2\ddot{\theta}_2 \sin \theta_2 + r_2\dot{\theta}_2^2 \cos \theta_2 + r_3\ddot{\theta}_3 \sin \theta_3 + r_3\dot{\theta}_3^2 \cos \theta_3)\mathbf{i} \\ & + (r_2\ddot{\theta}_2 \cos \theta_2 - r_2\dot{\theta}_2^2 \sin \theta_2 + r_3\ddot{\theta}_3 \cos \theta_3 - r_3\dot{\theta}_3^2 \sin \theta_3)\mathbf{j} \end{aligned} \quad (5.92)$$

Now that the equations have been developed, it is relatively simple to write a computer program for the analysis of a slider-crank linkage. To aid in this, the equations required are summarized in Tables 5.4 and 5.5. MATLAB programs for analyzing slider-crank linkages are included on the disk with this book.

**TABLE 5.4 Summary of Position, Velocity, and Acceleration Equations for a Slider-Crank Mechanism When Either the Crank or the Coupler is the Input. Link 2 Is the Input Link When  $M = 2$  and  $J = 3$ . Link 3 Is the Input Link When  $M = 3$  and  $J = 2$ . The Link Numbers and Points Are Defined in Fig. 5.14**

---

**Position**


---

$$A = 2r_4(\cos\theta_1 \cos\theta_4 + \sin\theta_1 \sin\theta_4) - 2r_M(\cos\theta_1 \cos\theta_M + \sin\theta_1 \sin\theta_M)$$

$$B = r_M^2 + r_4^2 - r_J^2 - 2r_M r_4(\cos\theta_M \cos\theta_4 + \sin\theta_M \sin\theta_4)$$

$$r_1 = \frac{-A + \sigma\sqrt{A^2 - 4B}}{2}; \quad \sigma = \pm 1$$

$$\theta_J = \tan^{-1} \left[ \frac{r_1 \sin\theta_1 + r_4 \sin\theta_4 - r_M \sin\theta_M}{r_1 \cos\theta_1 + r_4 \cos\theta_4 - r_M \cos\theta_M} \right]$$

$$\mathbf{r}_Q = r_2 = r_2(\cos\theta_2 \mathbf{i} + \sin\theta_2 \mathbf{j})$$

$$\mathbf{r}_P = r_2 + r_3 = r_2(\cos\theta_2 \mathbf{i} + \sin\theta_2 \mathbf{j}) + r_3(\cos\theta_3 \mathbf{i} + \sin\theta_3 \mathbf{j})$$

---

**Velocity**


---

$$\begin{bmatrix} \cos\theta_1 & r_J \sin\theta_J \\ \sin\theta_1 & -r_J \cos\theta_J \end{bmatrix} \begin{Bmatrix} \dot{r}_1 \\ \dot{\theta}_J \end{Bmatrix} = \begin{Bmatrix} -r_M \dot{\theta}_M \sin\theta_M \\ r_M \dot{\theta}_M \cos\theta_M \end{Bmatrix}$$

$$\dot{\mathbf{r}}_Q = r_2 \dot{\theta}_2 (-\sin\theta_2 \mathbf{i} + \cos\theta_2 \mathbf{j})$$

$$\dot{\mathbf{r}}_P = (-r_2 \dot{\theta}_2 \sin\theta_2 + r_3 \dot{\theta}_3 \sin\theta_3) \mathbf{i} + (r_2 \dot{\theta}_2 \cos\theta_2 + r_3 \dot{\theta}_3 \cos\theta_3) \mathbf{j}$$

---

**Acceleration**


---

$$\begin{bmatrix} \cos\theta_1 & r_J \sin\theta_J \\ \sin\theta_1 & -r_J \cos\theta_J \end{bmatrix} \begin{Bmatrix} \ddot{r}_1 \\ \ddot{\theta}_J \end{Bmatrix} = \begin{Bmatrix} -r_M \ddot{\theta}_M \sin\theta_M - r_M \dot{\theta}_M^2 \cos\theta_M - r_J \dot{\theta}_J^2 \cos\theta_J \\ r_M \ddot{\theta}_M \cos\theta_M - r_M \dot{\theta}_M^2 \sin\theta_M - r_J \dot{\theta}_J^2 \sin\theta_J \end{Bmatrix}$$

$$\ddot{\mathbf{r}}_Q = (r_2 \ddot{\theta}_2 \sin\theta_2 - r_2 \dot{\theta}_2^2 \cos\theta_2) \mathbf{i} + (r_2 \ddot{\theta}_2 \cos\theta_2 - r_2 \dot{\theta}_2^2 \sin\theta_2) \mathbf{j}$$

$$\begin{aligned} \ddot{\mathbf{r}}_P = & -(r_2 \ddot{\theta}_2 \sin\theta_2 + r_2 \dot{\theta}_2^2 \cos\theta_2 + r_3 \ddot{\theta}_3 \sin\theta_3 + r_3 \dot{\theta}_3^2 \cos\theta_3) \mathbf{i} \\ & + (r_2 \ddot{\theta}_2 \cos\theta_2 - r_2 \dot{\theta}_2^2 \sin\theta_2 + r_3 \ddot{\theta}_3 \cos\theta_3 - r_3 \dot{\theta}_3^2 \sin\theta_3) \mathbf{j} \end{aligned}$$


---



**TABLE 5.5 Summary of Position, Velocity, and Acceleration Equations for a Slider-Crank Mechanism When the Slider (Link 4) Is the Input Link. The Link Numbers and Points Are Defined in Fig. 5.14**

---

**Position**


---

$$A = 2r_1r_2 \cos \theta_1 - 2r_2r_4 \cos \theta_4$$

$$B = 2r_1r_2 \sin \theta_1 - 2r_2r_4 \sin \theta_4$$

$$C = r_1^2 + r_2^2 + r_4^2 - r_3^2 - 2r_1r_4(\cos \theta_1 \cos \theta_4 + \sin \theta_1 \sin \theta_4)$$

$$\theta_2 = 2 \tan^{-1} \left[ \frac{-B + \sigma \sqrt{B^2 - C^2 + A^2}}{C - A} \right]; \quad \sigma = \pm 1$$

$$\theta_3 = \tan^{-1} \left[ \frac{r_1 \sin \theta_1 + r_4 \sin \theta_4 - r_2 \sin \theta_2}{r_1 \cos \theta_1 + r_4 \cos \theta_4 - r_2 \cos \theta_2} \right]$$

$$\mathbf{r}_Q = r_2 = r_2(\cos \theta_2 \mathbf{i} + \sin \theta_2 \mathbf{j})$$

$$\mathbf{r}_P = r_2 + r_3 = r_2(\cos \theta_2 \mathbf{i} + \sin \theta_2 \mathbf{j}) + r_3(\cos \theta_3 \mathbf{i} + \sin \theta_3 \mathbf{j})$$

---

**Velocity**


---

$$\begin{bmatrix} -r_2 \sin \theta_2 & -r_3 \sin \theta_3 \\ r_2 \cos \theta_2 & r_3 \cos \theta_3 \end{bmatrix} \begin{Bmatrix} \dot{\theta}_2 \\ \dot{\theta}_3 \end{Bmatrix} = \begin{Bmatrix} \dot{r}_1 \cos \theta_1 \\ \dot{r}_1 \sin \theta_1 \end{Bmatrix}$$

$$\dot{\mathbf{r}}_Q = r_2 \dot{\theta}_2 (-\sin \theta_2 \mathbf{i} + \cos \theta_2 \mathbf{j})$$

$$\dot{\mathbf{r}}_P = (-r_2 \dot{\theta}_2 \sin \theta_2 - r_3 \dot{\theta}_3 \sin \theta_3) \mathbf{i} + (r_2 \dot{\theta}_2 \cos \theta_2 + r_3 \dot{\theta}_3 \cos \theta_3) \mathbf{j}$$

---

**Acceleration**


---

$$\begin{bmatrix} -r_2 \sin \theta_2 & -r_3 \sin \theta_3 \\ r_2 \cos \theta_2 & r_3 \cos \theta_3 \end{bmatrix} \begin{Bmatrix} \ddot{\theta}_2 \\ \ddot{\theta}_3 \end{Bmatrix} = \begin{Bmatrix} r_2 \dot{\theta}_2^2 \cos \theta_2 + r_3 \dot{\theta}_3^2 \cos \theta_3 + \ddot{r}_1 \cos \theta_1 \\ r_2 \dot{\theta}_2^2 \sin \theta_2 + r_3 \dot{\theta}_3^2 \sin \theta_3 + \ddot{r}_1 \sin \theta_1 \end{Bmatrix}$$

$$\ddot{\mathbf{r}}_Q = (-r_2 \ddot{\theta}_2 \sin \theta_2 - r_2 \dot{\theta}_2^2 \cos \theta_2) \mathbf{i} + (r_2 \ddot{\theta}_2 \cos \theta_2 - r_2 \dot{\theta}_2^2 \sin \theta_2) \mathbf{j}$$

$$\begin{aligned} \ddot{\mathbf{r}}_P = & -(r_2 \ddot{\theta}_2 \sin \theta_2 + r_2 \dot{\theta}_2^2 \cos \theta_2 + r_3 \ddot{\theta}_3 \sin \theta_3 + r_3 \dot{\theta}_3^2 \cos \theta_3) \mathbf{i} \\ & + (r_2 \ddot{\theta}_2 \cos \theta_2 - r_2 \dot{\theta}_2^2 \sin \theta_2 + r_3 \ddot{\theta}_3 \cos \theta_3 - r_3 \dot{\theta}_3^2 \sin \theta_3) \mathbf{j} \end{aligned}$$


---

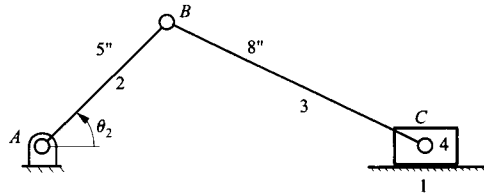
**EXAMPLE 5.4**  
**Kinematic**  
**Analysis of a Slider-**  
**Crank Mechanism**  
**with Crank Input**

**Solution**

In the slider-crank mechanism shown in Fig. 5.20,  $\theta_2 = 45^\circ$ ,  $\dot{\theta}_2 = 10 \text{ rad/s}$ , and  $\ddot{\theta}_2 = 0$ . The link lengths  $r_2$  and  $r_3$  are as shown, and the line of motion of point  $C_4$  is along the line  $AC$ . Find the position, velocity, and acceleration of  $C_4$  and the angular velocity and acceleration of link 3.

For this problem, the crank is the input, and the analysis can be conducted using the equations in Table 5.4 with  $M=2$  and  $J=3$ . The known input information is

$$\begin{aligned} \theta_1 &= 0^\circ, & \theta_2 &= 45^\circ, & \dot{\theta}_2 &= 10 \text{ rad/s}, & \ddot{\theta}_2 &= 0 \\ r_2 &= 5 \text{ in}, & r_3 &= 8 \text{ in}, & r_4 &= 0 \text{ in} \end{aligned}$$



**FIGURE 5.20** The slider-crank linkage to be analyzed in Example 5.4.

Start with the position analysis, and first compute the constants  $A$  and  $B$  from Eq. (5.69):

$$\begin{aligned} A &= 2r_4(\cos \theta_1 \cos \theta_4 + \sin \theta_1 \sin \theta_4) - 2r_2(\cos \theta_1 \cos \theta_2 + \sin \theta_1 \sin \theta_2) \\ &= -2(5)(\cos(0^\circ) \cos(45^\circ) + \sin(0^\circ) \sin(45^\circ)) = 7.70711 \\ B &= r_2^2 + r_4^2 - r_3^2 - 2r_2r_4(\cos \theta_2 \cos \theta_4 + \sin \theta_2 \sin \theta_4) \\ &= (5)^2 - (8)^2 = -39 \end{aligned}$$

The desired configuration of the linkage corresponds to the position of the slider with the larger  $x$  coordinate. Therefore,  $\sigma = +1$ . Then,

$$r_1 = \frac{-A + \sigma \sqrt{A^2 - 4B}}{2} = \frac{-(7.70711) + \sqrt{(7.70711)^2 - 4(-39)}}{2} = 10.712 \text{ in}$$

Then  $\theta_3$  is given by

$$\theta_3 = \tan^{-1} \left[ \frac{r_1 \sin \theta_1 + r_4 \sin \theta_4 - r_2 \sin \theta_2}{r_1 \cos \theta_1 + r_4 \cos \theta_4 - r_2 \cos \theta_2} \right] = \tan^{-1} \left[ \frac{-5 \sin(45^\circ)}{10.712 - 5 \cos(45^\circ)} \right] = -26.228^\circ$$

For the velocities, solve the linear set of velocity equations

$$\begin{bmatrix} \cos \theta_1 & r_3 \sin \theta_3 \\ \sin \theta_1 & -r_3 \cos \theta_3 \end{bmatrix} \begin{Bmatrix} \dot{r}_1 \\ \dot{\theta}_3 \end{Bmatrix} = \begin{Bmatrix} -r_2 \dot{\theta}_2 \sin \theta_2 \\ r_2 \dot{\theta}_2 \cos \theta_2 \end{Bmatrix} \quad \text{or} \quad \begin{bmatrix} 1 & 8 \sin(-26.228^\circ) \\ 0 & -8 \cos(-26.228^\circ) \end{bmatrix} \begin{Bmatrix} \dot{r}_1 \\ \dot{\theta}_3 \end{Bmatrix} = \begin{Bmatrix} -5(10) \sin(45^\circ) \\ 5(10) \cos(45^\circ) \end{Bmatrix}$$

Then

$$\begin{bmatrix} 1 & -3.5355 \\ 0 & -7.1764 \end{bmatrix} \begin{Bmatrix} \dot{r}_1 \\ \dot{\theta}_3 \end{Bmatrix} = \begin{Bmatrix} -35.3553 \\ 35.3553 \end{Bmatrix} \quad \text{or} \quad \begin{Bmatrix} \dot{r}_1 \\ \dot{\theta}_3 \end{Bmatrix} = \begin{Bmatrix} -52.774 \\ -4.927 \end{Bmatrix}$$

Therefore,  $\dot{r}_1 = 52.774 \text{ in/s}$  and  $\dot{\theta}_3 = -4.927 \text{ rad/s}$  CCW or  $4.927 \text{ rad/s}$  CW.

For the accelerations, solve the linear set of acceleration equations

$$\begin{bmatrix} \cos \theta_1 & r_3 \sin \theta_3 \\ \sin \theta_1 & -r_3 \cos \theta_3 \end{bmatrix} \begin{Bmatrix} \ddot{r}_1 \\ \ddot{\theta}_3 \end{Bmatrix} = \begin{Bmatrix} -r_2 \ddot{\theta}_2 \sin \theta_2 - r_2 \dot{\theta}_2^2 \cos \theta_2 - r_3 \dot{\theta}_3^2 \cos \theta_3 \\ r_2 \ddot{\theta}_2 \cos \theta_2 - r_2 \dot{\theta}_2^2 \sin \theta_2 - r_3 \dot{\theta}_3^2 \sin \theta_3 \end{Bmatrix}$$

or

$$\begin{bmatrix} 1 & -3.5355 \\ 0 & -7.1764 \end{bmatrix} \begin{Bmatrix} \ddot{r}_1 \\ \ddot{\theta}_3 \end{Bmatrix} = \begin{Bmatrix} -5(10)^2 \cos(45^\circ) - 8(-4.9266)^2 \cos(-26.228^\circ) \\ -5(10)^2 \sin(45^\circ) - 8(-4.9266)^2 \sin(-26.228^\circ) \end{Bmatrix} = \begin{Bmatrix} -527.7366 \\ -267.7395 \end{Bmatrix}$$

Then

$$\begin{Bmatrix} \ddot{r}_1 \\ \ddot{\theta}_3 \end{Bmatrix} = \begin{Bmatrix} -395.83 \\ 37.309 \end{Bmatrix}$$

Therefore,  $\ddot{r}_1 = -395.83 \text{ in/s}^2$  and  $\ddot{\theta}_3 = 37.30 \text{ rad/s}^2$  CCW. The results can be checked with the graphical analysis in Example 5.2.

**EXAMPLE 5.5**  
**Kinematic**  
**Analysis of a**  
**Slider-Crank**  
**Mechanism with a**  
**Slider Input**

**Solution**

Reanalyze the slider-crank mechanism shown in Fig. 5.20 when  $r_1 = 10.75 \text{ in}$ ,  $\dot{r}_1 = 50 \text{ in/s}$ , and  $\ddot{r}_1 = 400 \text{ in/s}^2$ . The link lengths  $r_2$  and  $r_3$  are the same as in Example 5.4, and again the line of action of point  $C_4$  is along the line  $AC$ . Find the position, angular velocity, and angular acceleration of link 2 and of link 3.

This is essentially the same problem as in Example 5.4 except that now the slider is the input link, and link 2 is the output. The analysis can be conducted using the equations in Table 5.5. The known input information is

$$\begin{aligned} \theta_1 &= 0^\circ, & r_1 &= 10.75 \text{ in}, & \dot{r}_1 &= 50 \text{ in/s}, & \ddot{r}_1 &= 400 \text{ in/s}^2 \\ r_2 &= 5 \text{ in}, & r_3 &= 8 \text{ in}, & r_4 &= 0 \text{ in} \end{aligned}$$

Start with the position analysis, and first compute constants  $A$ ,  $B$ , and  $C$ :

$$A = 2r_1r_2 \cos \theta_1 - 2r_2r_4 \cos \theta_4 = -2(10.75)(5) = -107.5$$

$$B = 2r_1r_2 \sin \theta_1 - 2r_2r_4 \sin \theta_4 = 0$$

$$C = r_1^2 + r_2^2 + r_4^2 - r_3^2 - 2r_1r_4(\cos \theta_1 \cos \theta_4 + \sin \theta_1 \sin \theta_4) = (10.75)^2 + (5)^2 - (8)^2 = 76.56$$

For the configuration in Fig. 5.20,  $\sigma = 1$ . Then,

$$\theta_2 = 2 \tan^{-1} \left[ \frac{-B + \sigma \sqrt{B^2 - C^2 + A^2}}{C - A} \right] = 2 \tan^{-1} \left[ \frac{+1 \sqrt{-(76.56)^2 + (-107.5)^2}}{76.56 - (-107.5)} \right] = 44.5850^\circ$$

and

$$\theta_3 = \tan^{-1} \left[ \frac{r_1 \sin \theta_1 + r_4 \sin \theta_4 - r_2 \sin \theta_2}{r_1 \cos \theta_1 + r_4 \cos \theta_4 - r_2 \cos \theta_2} \right] = \tan^{-1} \left[ \frac{-5 \sin(44.585^\circ)}{10.75 - 5 \cos(44.585^\circ)} \right] = -26.02^\circ$$

For the velocities, solve the linear set of velocity equations

$$\begin{bmatrix} -r_2 \sin \theta_2 & -r_3 \sin \theta_3 \\ r_2 \cos \theta_2 & r_3 \cos \theta_3 \end{bmatrix} \begin{Bmatrix} \dot{\theta}_2 \\ \dot{\theta}_3 \end{Bmatrix} = \begin{Bmatrix} \dot{r}_1 \cos \theta_1 \\ \dot{r}_1 \sin \theta_1 \end{Bmatrix} \quad \text{or} \quad \begin{bmatrix} -5 \sin(44.585^\circ) & -8 \sin(-26.02^\circ) \\ 5 \cos(44.585^\circ) & 8 \cos(-26.02^\circ) \end{bmatrix} \begin{Bmatrix} \dot{\theta}_2 \\ \dot{\theta}_3 \end{Bmatrix} = \begin{Bmatrix} 50 \\ 0 \end{Bmatrix}$$

Then

$$\begin{bmatrix} -3.5098 & 3.5098 \\ 3.5610 & 7.189 \end{bmatrix} \begin{Bmatrix} \dot{\theta}_2 \\ \dot{\theta}_3 \end{Bmatrix} = \begin{Bmatrix} 50 \\ 0 \end{Bmatrix} \quad \text{or} \quad \begin{Bmatrix} \dot{\theta}_2 \\ \dot{\theta}_3 \end{Bmatrix} = \begin{Bmatrix} -9.527 \\ 4.719 \end{Bmatrix}$$

Therefore,  $\dot{\theta}_2 = -9.527$  rad/s CCW or  $9.527$  rad/s CW and  $\dot{\theta}_3 = 4.719$  rad/s CCW. For the accelerations, solve the linear set of acceleration equations

$$\begin{bmatrix} -r_2 \sin \theta_2 & -r_3 \sin \theta_3 \\ r_2 \cos \theta_2 & r_3 \cos \theta_3 \end{bmatrix} \begin{Bmatrix} \ddot{\theta}_2 \\ \ddot{\theta}_3 \end{Bmatrix} = \begin{Bmatrix} r_2 \dot{\theta}_2^2 \cos \theta_2 + r_3 \dot{\theta}_3^2 \cos \theta_3 + \ddot{r}_1 \cos \theta_1 \\ r_2 \dot{\theta}_2^2 \sin \theta_2 + r_3 \dot{\theta}_3^2 \sin \theta_3 + \ddot{r}_1 \sin \theta_1 \end{Bmatrix}$$

or

$$\begin{bmatrix} -3.5098 & 3.5098 \\ 3.5610 & 7.189 \end{bmatrix} \begin{Bmatrix} \ddot{\theta}_2 \\ \ddot{\theta}_3 \end{Bmatrix} = \begin{Bmatrix} 5(9.527)^2 \cos(44.585^\circ) + 8(4.719)^2 \cos(-26.02^\circ) + 400 \\ 5(9.527)^2 \sin(44.585^\circ) + 8(4.719)^2 \sin(-26.02^\circ) \end{Bmatrix} = \begin{Bmatrix} 883.309 \\ 240.381 \end{Bmatrix}$$

Then

$$\begin{Bmatrix} \ddot{\theta}_2 \\ \ddot{\theta}_3 \end{Bmatrix} = \begin{Bmatrix} -145.933 \\ 105.726 \end{Bmatrix}$$

Therefore,  $\ddot{\theta}_2 = -145.933$  rad/s<sup>2</sup> CCW or  $145.933$  rad/s<sup>2</sup> CW and  $\ddot{\theta}_3 = 105.726$  rad/s<sup>2</sup> CCW.

## 5.6 ANALYTICAL EQUATIONS FOR THE SLIDER-CRANK INVERSION

The slider-crank inversion is a common mechanism when linear actuators are involved (e.g., Figs. 1.35 and 5.21). It is also used in various pump mechanisms. As discussed in Chapter 1, for low-load conditions, the slider is often replaced by a pin-in-a-slot joint. The resulting mechanisms can be analyzed using the equations developed in this section by modeling the pin-in-a-slot joint as a revolute joint and slider joint connected by a link. A



FIGURE 5.21 Backhoe. Each joint is actuated by an inversion of the slider-crank mechanism. (Courtesy of Deere & Co., Moline, Illinois.)

device that could be analyzed using this procedure is the walking toy shown in Fig. 5.22. To develop the closure equations, first locate vectors  $r_2$  and  $r_1$  as was done in the previous linkage. To form the other part of the closure equation, draw two vectors, one ( $r_3$ ) in the direction of the slider velocity from  $P$  to  $Q$  and one ( $r_4$ ) perpendicular to the velocity direction. The variables associated with the problem are then located as shown in Fig. 5.23, and the loop closure equation is given by

$$r_P = r_2 = r_1 + r_3 + r_4 \quad (5.93)$$

or

$$r_2(\cos\theta_2\mathbf{i} + \sin\theta_2\mathbf{j}) = r_1(\cos\theta_1\mathbf{i} + \sin\theta_1\mathbf{j}) + r_3(\cos\theta_3\mathbf{i} + \sin\theta_3\mathbf{j}) + r_4(\cos\theta_4\mathbf{i} + \sin\theta_4\mathbf{j}) \quad (5.94)$$

where

$$\theta_4 = \theta_3 - \pi/2 \quad (5.95)$$

Note that  $\theta_4$  is now a variable and that  $r_4$  can be negative.

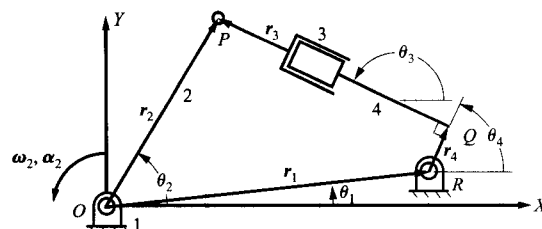
Rewriting Eq. (5.94) into its component equations gives

$$r_2 \cos\theta_2 = r_1 \cos\theta_1 + r_3 \cos\theta_3 + r_4 \cos\theta_4 \quad (5.96)$$

$$r_2 \sin\theta_2 = r_1 \sin\theta_1 + r_3 \sin\theta_3 + r_4 \sin\theta_4 \quad (5.97)$$



**FIGURE 5.22** Walking toy. The pin-in-a-slot joints can be modeled as a separate revolute and slider joint connected by a link. The resulting mechanism can be analyzed using the equations developed in this section.



**FIGURE 5.23** Vector closure condition for the slider-crank inversion. The position of point  $Q$  indicated by  $r_2 + r_3$  is the same as that obtained by adding vectors  $r_1 + r_4$ .

Equations (5.95)–(5.97) must be satisfied throughout the motion of the linkage. The base vector  $r_1$  will be constant in direction and magnitude. The vectors  $r_2$  and  $r_4$  will be constant in magnitude, and  $r_3$  will vary in both magnitude and direction. Therefore,  $r_1$ ,  $r_2$ ,  $r_4$ ,  $\theta_1$ , and  $\theta_4$  are constants.

If  $\theta_2$  is given, it is necessary to solve Eqs. (5.95)–(5.97) for  $\theta_2$  and  $r_3$  in terms of  $\theta_2$ , and if  $\theta_3$  is given, it is necessary to solve Eqs. (5.95)–(5.97) for  $\theta_2$  and  $r_3$  in terms of  $\theta_3$ . If  $r_3$  is given, it is necessary to solve the same equations for  $\theta_2$  and  $\theta_3$ . Once the position equations are solved, the equations for the unknown velocities and accelerations can be established in terms of the knowns by differentiation.

### 5.6.1 Solution to Position Equations When $\theta_2$ Is Input

The analytical solution procedure is slightly different from that used in the previous cases because  $\theta_4$  is a function of  $\theta_3$ . Therefore,  $\theta_3$  cannot be eliminated without first considering  $\theta_4$ . To proceed, first eliminate  $\theta_4$  from Eqs. (5.96) and (5.97) by using Eq. (5.95) and isolate the terms containing  $\theta_3$  on the right-hand side of the equations. Then,

$$r_2 \cos \theta_2 - r_1 \cos \theta_1 = r_3 \cos \theta_3 + r_4 \sin \theta_3 \quad (5.98)$$

$$r_2 \sin \theta_2 - r_1 \sin \theta_1 = r_3 \sin \theta_3 - r_4 \cos \theta_3 \quad (5.99)$$

Now square both sides of both equations and add. After simplifying using the trigonometric identity,  $\sin^2 \theta + \cos^2 \theta = 1$ , and solving for  $r_3$ , we get the resulting equation

$$r_3 = \sqrt{r_2^2 + r_1^2 - r_4^2 - 2r_1 r_2 (\cos \theta_1 \cos \theta_2 + \sin \theta_1 \sin \theta_2)} \quad (5.100)$$

To solve for  $\theta_3$ , replace  $\cos \theta_3$  and  $\sin \theta_3$  in Eq. (5.98) by using the trigonometric half-angle identities in Eqs. (5.33–5.34). Equation (5.98) then becomes

$$A(1+t^2) - r_3(1-t^2) - r_4(2t) = 0 \quad (5.101)$$

where

$$A = r_2 \cos \theta_2 - r_1 \cos \theta_1$$

and

$$t = \tan\left(\frac{\theta_3}{2}\right)$$

Collecting terms in Eqs. (5.101) gives

$$(A+r_3)t^2 - 2r_4t + (A-r_3) = 0$$

This equation will give two roots for  $t$ , but one root is extraneous in this problem. The roots are

$$t = \frac{r_4 + \beta \sqrt{r_4^2 - A^2 + r_3^2}}{(A+r_3)} \quad (5.102)$$

where  $\beta = \pm 1$ . To determine the correct value of  $\beta$  for the problem, we must first compute a value of  $\theta_3$  for each value of  $t$  using

$$\theta_3 = 2 \tan^{-1} t.$$

Next substitute both values of  $\theta_3$  into Eq. (5.99). The correct value of  $\beta$  will correspond to the value of  $\theta_3$  satisfying Eq. (5.99). The value of  $\beta$  must be computed for each value of  $\theta_2$  if more than one position is analyzed.

Because of the square root in Eq. (5.100), the value of  $r_3$  can be complex [ $r_2^2 + r_1^2 - r_4^2 - 2r_1r_2(\cos\theta_1\cos\theta_2 + \sin\theta_1\sin\theta_2) < 0$ ]. If this happens, the mechanism cannot be assembled for the value of  $\theta_2$  specified and for the given values of the link lengths. The results are summarized in Table 5.6.

**TABLE 5.6 Summary of Position, Velocity, and Acceleration Equations for an Inverted Slider-Crank Mechanism When  $\theta_2$  Is the Input Variable. The Link Numbers and Points Are Defined in Fig. 5.23**

---

**Position**

---

$$r_3 = \sqrt{r_2^2 + r_1^2 - r_4^2 - 2r_1r_2(\cos\theta_1\cos\theta_2 + \sin\theta_1\sin\theta_2)}$$

$$A = r_2 \cos\theta_2 - r_1 \cos\theta_1$$

$$\theta_3 = 2 \tan^{-1} \left[ \frac{r_4 + \beta \sqrt{r_4^2 - A^2 + r_3^2}}{(A + r_3)} \right]; \quad \beta = \pm 1$$

$$\theta_4 = \theta_3 - \pi/2$$

$$\mathbf{r}_P = \mathbf{r}_2 = r_2(\cos\theta_2\mathbf{i} + \sin\theta_2\mathbf{j})$$

$$\mathbf{r}_Q = \mathbf{r}_1 + \mathbf{r}_4 = r_1(\cos\theta_1\mathbf{i} + \sin\theta_1\mathbf{j}) + r_4(\cos\theta_4\mathbf{i} + \sin\theta_4\mathbf{j})$$

---

**Velocity**

---

$$\begin{bmatrix} \cos\theta_3 & -r_3 \sin\theta_3 - r_4 \sin\theta_4 \\ \sin\theta_3 & r_3 \cos\theta_3 + r_4 \cos\theta_4 \end{bmatrix} \begin{Bmatrix} \dot{r}_3 \\ \dot{\theta}_3 \end{Bmatrix} = \begin{Bmatrix} -r_2 \dot{\theta}_2 \sin\theta_2 \\ r_2 \dot{\theta}_2 \cos\theta_2 \end{Bmatrix}$$

$$\dot{\mathbf{r}}_P = \dot{\mathbf{r}}_2 = r_2 \dot{\theta}_2 (-\sin\theta_2\mathbf{i} + \cos\theta_2\mathbf{j})$$

$$\dot{\mathbf{r}}_Q = \dot{\mathbf{r}}_1 + \dot{\mathbf{r}}_4 = r_4 \dot{\theta}_3 (-\sin\theta_4\mathbf{i} + \cos\theta_4\mathbf{j})$$

---

**Acceleration**

---

$$\begin{bmatrix} \cos\theta_3 & -r_3 \sin\theta_3 - r_4 \sin\theta_4 \\ \sin\theta_3 & r_3 \cos\theta_3 + r_4 \cos\theta_4 \end{bmatrix} \begin{Bmatrix} \ddot{r}_3 \\ \ddot{\theta}_3 \end{Bmatrix} = \begin{Bmatrix} -r_2 \ddot{\theta}_2 \sin\theta_2 - r_2 \dot{\theta}_2^2 \cos\theta_2 + r_3 \dot{\theta}_3^2 \cos\theta_3 + 2\dot{r}_3 \dot{\theta}_3 \sin\theta_3 + r_4 \dot{\theta}_3^2 \cos\theta_4 \\ r_2 \ddot{\theta}_2 \cos\theta_2 - r_2 \dot{\theta}_2^2 \sin\theta_2 + r_3 \dot{\theta}_3^2 \sin\theta_3 - 2\dot{r}_3 \dot{\theta}_3 \cos\theta_3 + r_4 \dot{\theta}_3^2 \sin\theta_4 \end{Bmatrix}$$

$$\ddot{\mathbf{r}}_P = \ddot{\mathbf{r}}_2 = -(r_2 \ddot{\theta}_2 \sin\theta_2 + r_2 \dot{\theta}_2^2 \cos\theta_2)\mathbf{i} + (r_2 \ddot{\theta}_2 \cos\theta_2 - r_2 \dot{\theta}_2^2 \sin\theta_2)\mathbf{j}$$

$$\ddot{\mathbf{r}}_Q = \ddot{\mathbf{r}}_1 + \ddot{\mathbf{r}}_4 = -(r_4 \ddot{\theta}_3 \sin\theta_4 + r_4 \dot{\theta}_3^2 \cos\theta_4)\mathbf{i} + (r_4 \ddot{\theta}_3 \cos\theta_4 - r_4 \dot{\theta}_3^2 \sin\theta_4)\mathbf{j}$$


---

### 5.6.2 Solution to Position Equations When $\theta_3$ Is Input

When the coupler angle is the input variable for the linkage of Fig. 5.23, values for  $\theta_3$  and its derivatives will be known. The analytical procedure for solving the position equations follows the same steps as when  $\theta_2$  is the input, although the form of the equations is slightly different.

For the position analysis, again begin with Eqs. (5.63) and (5.64) and isolate the terms with  $\theta_2$ . The resulting equations are

$$r_2 \cos \theta_2 = r_1 \cos \theta_1 + r_3 \cos \theta_3 + r_4 \sin \theta_3 \quad (5.103)$$

$$r_2 \sin \theta_2 = r_1 \sin \theta_1 + r_3 \sin \theta_3 - r_4 \cos \theta_3 \quad (5.104)$$

These equations can be solved first for  $r_3$  and then for  $\theta_2$  using the procedures given in the previous sections. Two solutions are obtained corresponding to the two values of the sign variable  $\beta$ . The assembly positions are shown in Fig. 5.24. The results are summarized in Table 5.7.

### 5.6.3 Solution to Position Equations When $r_3$ Is Input

When  $r_3$  is input in Fig. 5.23, we can eliminate  $\theta_3$  from the component equations as was done previously to obtain Eq. (5.91). We can solve for  $\theta_2$  and then for  $\theta_3$ . Once again there are two possible solutions corresponding to the two values of the sign variable  $\beta$ . The assembly positions are shown in Fig. 5.25. The results are summarized in Table 5.8.

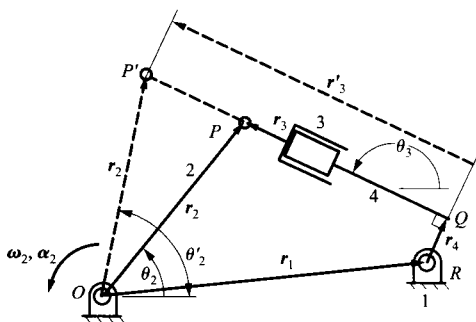


FIGURE 5.24 Two possible assembly modes for link 2 in Fig. 5.23 if  $\theta_3$  is given.

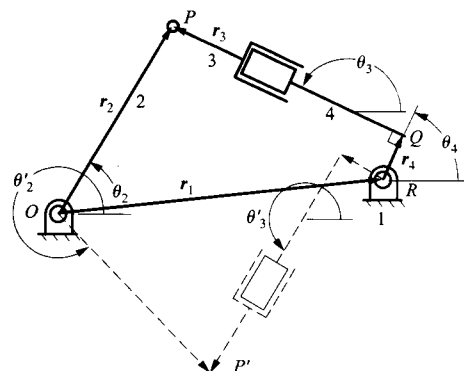


FIGURE 5.25 Two possible configurations for line  $PR$  in Fig. 5.23 if  $r_3$  is given.



**TABLE 5.7 Summary of Position, Velocity, and Acceleration Equations for an Inverted Slider-Crank Mechanism When  $\theta_3$  Is the Input Variable. The Link Numbers and Points Are Defined in Fig. 5.23**

---

**Position**


---

$$r_3 = \frac{1}{2} \left[ -B + \beta \sqrt{B^2 - 4C} \right]; \quad \beta = \pm 1$$

$$B = 2r_1 (\cos \theta_1 \cos \theta_3 + \sin \theta_1 \sin \theta_3)$$

$$C = r_1^2 - r_2^2 + r_4^2 = 2r_1 r_4 (\cos \theta_1 \sin \theta_3 - \sin \theta_1 \cos \theta_3)$$

$$\theta_2 = \tan^{-1} \left[ \frac{r_1 \sin \theta_1 + r_3 \sin \theta_3 - r_4 \cos \theta_3}{r_1 \cos \theta_1 + r_3 \cos \theta_3 + r_4 \sin \theta_3} \right]$$

$$\theta_4 = \theta_3 - \pi/2$$

$$\mathbf{r}_P = \mathbf{r}_2 = r_2 (\cos \theta_2 \mathbf{i} + \sin \theta_2 \mathbf{j})$$

$$\mathbf{r}_Q = \mathbf{r}_1 + \mathbf{r}_4 = r_1 (\cos \theta_1 \mathbf{i} + \sin \theta_1 \mathbf{j}) + r_4 (\cos \theta_4 \mathbf{i} + \sin \theta_4 \mathbf{j})$$

---

**Velocity**


---

$$\begin{bmatrix} -r_2 \sin \theta_2 & -\cos \theta_3 \\ r_2 \cos \theta_2 & -\sin \theta_3 \end{bmatrix} \begin{Bmatrix} \dot{\theta}_2 \\ \dot{\theta}_3 \end{Bmatrix} = \begin{Bmatrix} -r_3 \dot{\theta}_3 \sin \theta_3 - r_4 \dot{\theta}_3 \sin \theta_4 \\ r_3 \dot{\theta}_3 \cos \theta_3 + r_4 \dot{\theta}_3 \cos \theta_4 \end{Bmatrix}$$

$$\dot{\mathbf{r}}_P = \dot{\mathbf{r}}_2 = r_2 \dot{\theta}_2 (-\sin \theta_2 \mathbf{i} + \cos \theta_2 \mathbf{j})$$

$$\dot{\mathbf{r}}_Q = \dot{\mathbf{r}}_1 + \dot{\mathbf{r}}_4 = r_4 \dot{\theta}_3 (-\sin \theta_4 \mathbf{i} + \cos \theta_4 \mathbf{j})$$

---

**Acceleration**


---

$$\begin{bmatrix} -r_2 \sin \theta_2 & -\cos \theta_3 \\ r_2 \cos \theta_2 & -\sin \theta_3 \end{bmatrix} \begin{Bmatrix} \ddot{\theta}_2 \\ \ddot{\theta}_3 \end{Bmatrix} = \begin{Bmatrix} r_2 \dot{\theta}_2^2 \cos \theta_2 - r_3 \ddot{\theta}_3 \sin \theta_3 - r_3 \dot{\theta}_3^2 \cos \theta_3 - 2\dot{r}_3 \dot{\theta}_3 \sin \theta_3 - r_4 \ddot{\theta}_3 \sin \theta_4 - r_4 \dot{\theta}_3^2 \cos \theta_4 \\ r_2 \dot{\theta}_2^2 \sin \theta_2 + r_3 \ddot{\theta}_3 \cos \theta_3 - r_3 \dot{\theta}_3^2 \sin \theta_3 + 2\dot{r}_3 \dot{\theta}_3 \cos \theta_3 + r_4 \ddot{\theta}_3 \cos \theta_4 - r_4 \dot{\theta}_3^2 \sin \theta_4 \end{Bmatrix}$$

$$\ddot{\mathbf{r}}_P = \ddot{\mathbf{r}}_2 = -(r_2 \ddot{\theta}_2 \sin \theta_2 + r_2 \dot{\theta}_2^2 \cos \theta_2) \mathbf{i} + (r_2 \ddot{\theta}_2 \cos \theta_2 - r_2 \dot{\theta}_2^2 \sin \theta_2) \mathbf{j}$$

$$\ddot{\mathbf{r}}_Q = \ddot{\mathbf{r}}_1 + \ddot{\mathbf{r}}_4 = -(r_4 \ddot{\theta}_3 \sin \theta_4 + r_4 \dot{\theta}_3^2 \cos \theta_4) \mathbf{i} + (r_4 \ddot{\theta}_3 \cos \theta_4 - r_4 \dot{\theta}_3^2 \sin \theta_4) \mathbf{j}$$


---

### 5.6.4 Velocity Equations for the Slider-Crank Inversion

The analytical form of the velocity equations for the linkage of Fig. 5.23 can be developed by differentiating Eq. (5.93). The result is

$$\dot{\mathbf{r}}_P = \dot{\mathbf{r}}_2 = \dot{\mathbf{r}}_1 + \dot{\mathbf{r}}_4 + \dot{\mathbf{r}}_3 \quad (5.105)$$

**TABLE 5.8 Summary of Position, Velocity, and Acceleration Equations for Slider-Crank Inversion When  $r_3$  is the Input Variable. The Link Numbers and Points Are Defined in Fig. 5.23****Position**

$$\left. \begin{aligned} A &= -2r_1r_2 \cos \theta_1 \\ B &= -2r_1r_2 \sin \theta_1 \\ C &= r_2^2 + r_1^2 - r_4^2 - r_3^2 \end{aligned} \right\}$$

$$\theta_2 = 2 \tan^{-1} \left[ \frac{-B + \beta \sqrt{B^2 - C^2 + A^2}}{C - A} \right]; \quad \beta = \pm 1$$

$$A = r_2 \cos \theta_2 - r_1 \cos \theta_1$$

$$\theta_3 = 2 \tan^{-1} \left[ \frac{r_4 + \sigma \sqrt{r_4^2 - A^2 + r_3^2}}{(A + r_3)} \right]; \quad \sigma = \pm 1$$

$\sigma$  is constant for a given linkage and is determined by the sign of angle PQR.

$$\theta_4 = \theta_3 - \pi/2$$

$$\mathbf{r}_P = r_2 = r_2 (\cos \theta_2 \mathbf{i} + \sin \theta_2 \mathbf{j})$$

$$\mathbf{r}_Q = \mathbf{r}_1 + \mathbf{r}_4 = r_1 (\cos \theta_1 \mathbf{i} + \sin \theta_1 \mathbf{j}) + r_4 (\cos \theta_4 \mathbf{i} + \sin \theta_4 \mathbf{j})$$

**Velocity**

$$\begin{bmatrix} -r_2 \sin \theta_2 & r_3 \sin \theta_3 + r_4 \sin \theta_4 \\ r_2 \cos \theta_2 & -r_3 \cos \theta_3 - r_4 \cos \theta_4 \end{bmatrix} \begin{Bmatrix} \dot{\theta}_2 \\ \dot{\theta}_3 \end{Bmatrix} = \begin{Bmatrix} \dot{r}_3 \cos \theta_3 \\ \dot{r}_3 \sin \theta_3 \end{Bmatrix}$$

$$\dot{\mathbf{r}}_P = \dot{\mathbf{r}}_2 = r_2 \dot{\theta}_2 (-\sin \theta_2 \mathbf{i} + \cos \theta_2 \mathbf{j})$$

$$\dot{\mathbf{r}}_Q = \dot{\mathbf{r}}_1 + \dot{\mathbf{r}}_4 = r_4 \dot{\theta}_3 (-\sin \theta_4 \mathbf{i} + \cos \theta_4 \mathbf{j})$$

**Acceleration**

$$\begin{bmatrix} -r_2 \sin \theta_2 & r_3 \sin \theta_3 + r_4 \sin \theta_4 \\ r_2 \cos \theta_2 & -r_3 \cos \theta_3 - r_4 \cos \theta_4 \end{bmatrix} \begin{Bmatrix} \ddot{\theta}_2 \\ \ddot{\theta}_3 \end{Bmatrix} \\ = \begin{Bmatrix} r_2 \ddot{\theta}_2^2 \cos \theta_2 - r_3 \ddot{\theta}_3^2 \cos \theta_3 - 2\dot{r}_3 \dot{\theta}_3 \sin \theta_3 + \ddot{r}_3 \cos \theta_3 - r_4 \ddot{\theta}_3^2 \cos \theta_4 \\ r_2 \ddot{\theta}_2^2 \sin \theta_2 - r_3 \ddot{\theta}_3^2 \sin \theta_3 + 2\dot{r}_3 \dot{\theta}_3 \cos \theta_3 + \ddot{r}_3 \sin \theta_3 - r_4 \ddot{\theta}_3^2 \sin \theta_4 \end{Bmatrix}$$

$$\ddot{\mathbf{r}}_P = \ddot{\mathbf{r}}_2 = -(r_2 \ddot{\theta}_2 \sin \theta_2 + r_2 \dot{\theta}_2^2 \cos \theta_2) \mathbf{i} + (r_2 \ddot{\theta}_2 \cos \theta_2 - r_2 \dot{\theta}_2^2 \sin \theta_2) \mathbf{j}$$

$$\ddot{\mathbf{r}}_Q = \ddot{\mathbf{r}}_1 + \ddot{\mathbf{r}}_4 = -(r_4 \ddot{\theta}_3 \sin \theta_4 + r_4 \dot{\theta}_3^2 \cos \theta_4) \mathbf{i} + (r_4 \ddot{\theta}_3 \cos \theta_4 - r_4 \dot{\theta}_3^2 \sin \theta_4) \mathbf{j}$$

When this equation is written in component form, the result is the same as differentiating Eqs. (5.96) and (5.97). Recognizing that  $r_1$ ,  $r_2$ ,  $r_4$ , and  $\theta_1$  are constants, and that from Eq. (5.95)  $\dot{\theta}_3 = \dot{\theta}_4$ , we see that the resulting component equations are

$$-r_2\dot{\theta}_2 \sin \theta_2 = -r_3\dot{\theta}_3 \sin \theta_3 + \dot{r}_3 \cos \theta_3 + r_4\dot{\theta}_3 \sin \theta_4 \quad (5.106)$$

$$r_2\dot{\theta}_2 \cos \theta_2 = r_3\dot{\theta}_3 \cos \theta_3 + \dot{r}_3 \sin \theta_3 + r_4\dot{\theta}_3 \cos \theta_4 \quad (5.107)$$

The solution procedure depends on whether  $\dot{\theta}_2$ ,  $\dot{\theta}_3$ , or  $\dot{r}_3$  is known. If  $\dot{\theta}_2$  is input, then  $\dot{r}_3$  and  $\dot{\theta}_3$  will be unknown. Therefore, the matrix equation to be solved is

$$\begin{bmatrix} \cos \theta_3 & -r_3 \sin \theta_3 - r_4 \sin \theta_4 \\ \sin \theta_3 & r_3 \cos \theta_3 + r_4 \cos \theta_4 \end{bmatrix} \begin{Bmatrix} \dot{r}_3 \\ \dot{\theta}_3 \end{Bmatrix} = \begin{Bmatrix} -r_2\dot{\theta}_2 \sin \theta_2 \\ r_2\dot{\theta}_2 \cos \theta_2 \end{Bmatrix} \quad (5.108)$$

If  $\dot{\theta}_3$  is input, then  $\dot{r}_3$  and  $\dot{\theta}_2$  will be unknown, and the matrix equation to be solved is

$$\begin{bmatrix} -r_2 \sin \theta_2 & -\cos \theta_3 \\ r_2 \cos \theta_2 & -\sin \theta_3 \end{bmatrix} \begin{Bmatrix} \dot{\theta}_2 \\ \dot{r}_3 \end{Bmatrix} = \begin{Bmatrix} -r_3\dot{\theta}_3 \sin \theta_3 - r_4\dot{\theta}_3 \sin \theta_4 \\ r_3\dot{\theta}_3 \cos \theta_3 + r_4\dot{\theta}_3 \cos \theta_4 \end{Bmatrix} \quad (5.109)$$

If  $\dot{r}_3$  is input, then  $\dot{\theta}_2$  and  $\dot{\theta}_3$  will be unknown. The matrix equation to be solved then is

$$\begin{bmatrix} -r_2 \sin \theta_2 & r_3 \sin \theta_3 + r_4 \sin \theta_4 \\ r_2 \cos \theta_2 & -r_3 \cos \theta_3 - r_4 \cos \theta_4 \end{bmatrix} \begin{Bmatrix} \dot{\theta}_2 \\ \dot{\theta}_3 \end{Bmatrix} = \begin{Bmatrix} \dot{r}_3 \cos \theta_3 \\ \dot{r}_3 \sin \theta_3 \end{Bmatrix} \quad (5.110)$$

The terms in the matrix and vector on the right-hand sides of Eqs. (5.108)–(5.110) will be known. The equation can therefore be solved manually, on a programmable calculator, or with the matrix solvers in programs such as MATLAB.

Once the angular velocities are known, it is a simple matter to compute the linear velocities of any of the points on the vector loop. The velocities of points  $Q$  and  $P$  are given by

$$\dot{r}_P = \dot{r}_2 = r_2\dot{\theta}_2(-\sin \theta_2 \mathbf{i} + \cos \theta_2 \mathbf{j}) \quad (5.111)$$

and

$$\dot{r}_Q = \dot{r}_1 + \dot{r}_4 = r_4\dot{\theta}_3(-\sin \theta_4 \mathbf{i} + \cos \theta_4 \mathbf{j}) \quad (5.112)$$

### 5.6.5 Acceleration Equations for the Slider-Crank Inversion

The analytical form of the acceleration equations for the linkage of Fig. 5.23 can be developed by differentiating Eq. (5.105). The result is

$$\ddot{r}_P = \ddot{r}_2 = \ddot{r}_1 + \ddot{r}_3 + \ddot{r}_4 \quad (5.113)$$

When this equation is written in component form, the result is the same as differentiating Eqs. (5.106) and (5.107). The resulting component equations are

$$\begin{aligned} & -r_2\ddot{\theta}_2 \sin \theta_2 - r_2\dot{\theta}_2^2 \cos \theta_2 \\ & = -r_3\ddot{\theta}_3 \sin \theta_3 - r_3\dot{\theta}_3^2 \cos \theta_3 + \ddot{r}_3 \cos \theta_3 - 2\dot{r}_3\dot{\theta}_3 \sin \theta_3 - r_4\ddot{\theta}_3 \sin \theta_4 - r_4\dot{\theta}_3^2 \cos \theta_4 \end{aligned} \quad (5.114)$$

$$\begin{aligned} & -r_2\ddot{\theta}_2 \cos \theta_2 - r_2\dot{\theta}_2^2 \sin \theta_2 \\ & = -r_3\ddot{\theta}_3 \cos \theta_3 - r_3\dot{\theta}_3^2 \sin \theta_3 + \ddot{r}_3 \sin \theta_3 + 2\dot{r}_3\dot{\theta}_3 \cos \theta_3 + r_4\ddot{\theta}_3 \cos \theta_4 - r_4\dot{\theta}_3^2 \sin \theta_4 \end{aligned} \quad (5.115)$$

In a manner similar to that in the case of velocities, the solution procedure depends on whether  $\ddot{r}_3$  or  $\ddot{\theta}_2$  is known. If  $\ddot{\theta}_2$  is input, then  $\ddot{r}_3$  and  $\ddot{\theta}_3$  will be unknown. Therefore, the matrix equation to be solved is

$$\begin{aligned} & \begin{bmatrix} \cos \theta_3 & -r_3 \sin \theta_3 - r_4 \sin \theta_4 \\ \sin \theta_3 & r_3 \cos \theta_3 + r_4 \cos \theta_4 \end{bmatrix} \begin{Bmatrix} \ddot{r}_3 \\ \ddot{\theta}_3 \end{Bmatrix} \\ & = \begin{Bmatrix} -r_2 \ddot{\theta}_2 \sin \theta_2 - r_2 \dot{\theta}_2^2 \cos \theta_2 + r_3 \dot{\theta}_3^2 \cos \theta_3 + 2\dot{r}_3 \dot{\theta}_3 \sin \theta_3 + r_4 \dot{\theta}_3^2 \cos \theta_4 \\ r_2 \ddot{\theta}_2 \cos \theta_2 - r_2 \dot{\theta}_2^2 \sin \theta_2 + r_3 \dot{\theta}_3^2 \sin \theta_3 - 2\dot{r}_3 \dot{\theta}_3 \cos \theta_3 + r_4 \dot{\theta}_3^2 \sin \theta_4 \end{Bmatrix} \end{aligned} \quad (5.116)$$

If  $\ddot{\theta}_3$  is input, then  $\ddot{r}_3$  and  $\ddot{\theta}_2$  will be unknown, and the matrix equation to be solved is

$$\begin{aligned} & \begin{bmatrix} -r_2 \sin \theta_2 & -\cos \theta_3 \\ r_2 \cos \theta_2 & -\sin \theta_3 \end{bmatrix} \begin{Bmatrix} \ddot{\theta}_2 \\ \ddot{r}_3 \end{Bmatrix} \\ & = \begin{Bmatrix} r_2 \dot{\theta}_2^2 \cos \theta_2 - r_3 \ddot{\theta}_3 \sin \theta_3 - r_3 \dot{\theta}_3^2 \cos \theta_3 - 2\dot{r}_3 \dot{\theta}_3 \sin \theta_3 - r_4 \ddot{\theta}_3 \sin \theta_4 - r_4 \dot{\theta}_3^2 \cos \theta_4 \\ r_2 \dot{\theta}_2^2 \sin \theta_2 + r_3 \ddot{\theta}_3 \cos \theta_3 - r_3 \dot{\theta}_3^2 \sin \theta_3 + 2\dot{r}_3 \dot{\theta}_3 \cos \theta_3 + r_4 \ddot{\theta}_3 \cos \theta_4 - r_4 \dot{\theta}_3^2 \sin \theta_4 \end{Bmatrix} \end{aligned} \quad (5.117)$$

If  $\ddot{r}_3$  is input, then  $\ddot{\theta}_2$  and  $\ddot{\theta}_3$  will be unknown. The matrix equation to be solved is then

$$\begin{aligned} & \begin{bmatrix} -r_2 \sin \theta_2 & r_3 \sin \theta_3 + r_4 \sin \theta_4 \\ r_2 \cos \theta_2 & -r_3 \cos \theta_3 - r_4 \cos \theta_4 \end{bmatrix} \begin{Bmatrix} \ddot{\theta}_2 \\ \ddot{\theta}_3 \end{Bmatrix} \\ & = \begin{Bmatrix} r_2 \dot{\theta}_2^2 \cos \theta_2 - r_3 \dot{\theta}_3^2 \cos \theta_3 - 2\dot{r}_3 \dot{\theta}_3 \sin \theta_3 + \ddot{r}_3 \cos \theta_3 - r_4 \dot{\theta}_3^2 \cos \theta_4 \\ r_2 \dot{\theta}_2^2 \sin \theta_2 - r_3 \dot{\theta}_3^2 \sin \theta_3 + 2\dot{r}_3 \dot{\theta}_3 \cos \theta_3 + \ddot{r}_3 \sin \theta_3 - r_4 \dot{\theta}_3^2 \sin \theta_4 \end{Bmatrix} \end{aligned} \quad (5.118)$$

The terms in the matrix and vector on the right-hand sides of Eqs. (5.116–5.118) will be known. The equation can therefore be solved manually, numerically on a programmable calculator, or with the matrix solvers in programs such as MATLAB. Notice again that the coefficient matrix is the same for both the velocities (Eqs. (5.108) and (5.110) and for the accelerations (Eqs. (5.116)–(5.118)).

Once the angular accelerations are known, it is a simple matter to compute the linear accelerations of any of the points on the vector loop. The accelerations of points  $P$  and  $Q$  are given by

$$\ddot{\mathbf{r}}_P = \ddot{\mathbf{r}}_2 = -\left(r_2 \ddot{\theta}_2 \sin \theta_2 + r_2 \dot{\theta}_2^2 \cos \theta_2\right) \mathbf{i} + \left(r_2 \ddot{\theta}_2 \cos \theta_2 - r_2 \dot{\theta}_2^2 \sin \theta_2\right) \mathbf{j} \quad (5.119)$$

and

$$\ddot{\mathbf{r}}_Q = \ddot{\mathbf{r}}_1 + \ddot{\mathbf{r}}_4 = -\left(r_4 \ddot{\theta}_3 \sin \theta_4 + r_4 \dot{\theta}_3^2 \cos \theta_4\right) \mathbf{i} + \left(r_4 \ddot{\theta}_3 \cos \theta_4 - r_4 \dot{\theta}_3^2 \sin \theta_4\right) \mathbf{j} \quad (5.120)$$

Now that the equations have been developed, it is a relatively simple matter to write a computer program for the analysis of an inverted slider-crank linkage. To aid in this, the equations required are summarized in Tables 5.6, 5.7, and 5.8. A MATLAB program for analyzing an inverted slider-crank linkage is included on the disk that accompanies this book.

**EXAMPLE 5.6**  
**Kinematic**  
**Analysis of a**  
**Foot-Pump**  
**Mechanism**

The foot pump shown in Fig. 5.26 is to be analyzed in one position ( $\theta_2 = 60^\circ$ ) as an inverted slider-crank linkage. Dimensions for the mechanism are given in Fig. 5.27, and the vector diagram for the analysis is given in Fig. 5.28. Assume that the angular velocity of the driver (link 2) is constant at 2.5 rad/s CW. Conduct a position, velocity, and acceleration analysis to determine, respectively, the combined length of links 3 and 4, the angular velocity and acceleration of link 3 (or link 4), and the velocity and acceleration of point  $B$  observed from link 3. This information can be used to study the pumping action between links 3 and 4.

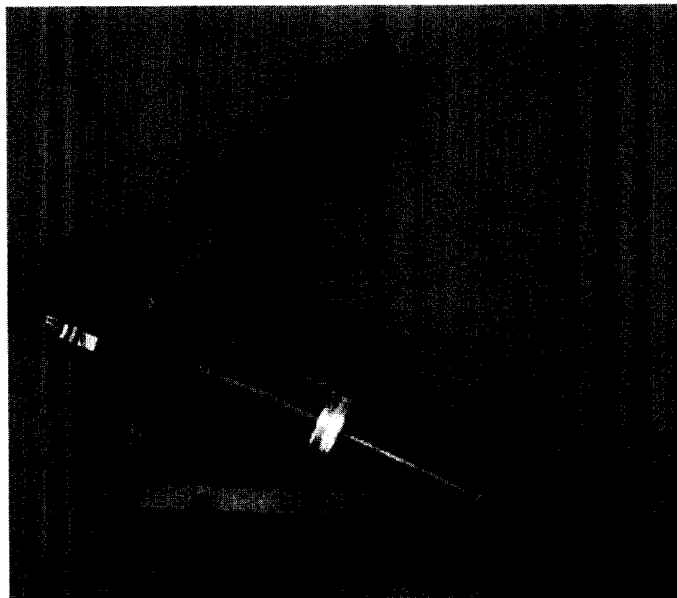


FIGURE 5.26 Foot-pump mechanism.

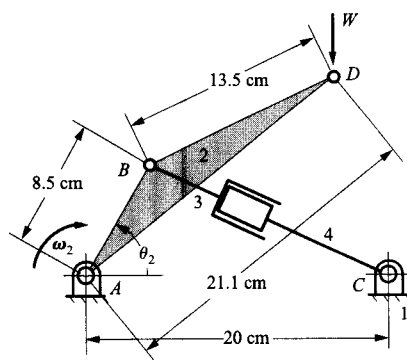


FIGURE 5.27 Kinematic model of foot-pump mechanism used in Example 5.6.

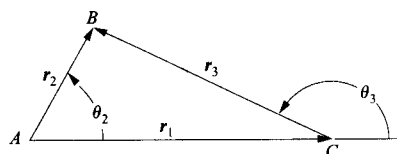


FIGURE 5.28 Position polygon for Example 5.6.

**Solution**

The analysis can be conducted using the equations in Table 5.6. The known input information is as follows:

$$\begin{aligned} r_1 &= 20 \text{ cm}, & \theta_1 &= 0 \\ r_2 &= 8.5 \text{ cm}, & \theta_2 &= 60^\circ, & \dot{\theta}_2 &= -2.5 \text{ rad/s}, & \ddot{\theta}_2 &= 0, \\ r_4 &= 0, & \theta_4 &= 60^\circ, & \dot{\theta}_4 &= 0, & \ddot{\theta}_4 &= 0, \end{aligned}$$

The unknown information is:  $r_3$ ,  $\theta_3$ ,  $\dot{\theta}_3$ , and  $\ddot{\theta}_3$ .

From Table 5.6,  $r_3$  is given by

$$\begin{aligned} r_3 &= \sqrt{r_2^2 + r_1^2 - r_4^2 - 2r_1r_2(\cos\theta_1\cos\theta_2 + \sin\theta_1\sin\theta_2)} \\ &= \sqrt{8.5^2 + 20^2 - 2(20)(8.5)\cos(60^\circ)} = \sqrt{302.2} = 17.38 \text{ cm} \end{aligned}$$

Next compute  $\theta_3$ . Start with the value of  $A$ :

$$A = r_2 \cos\theta_2 - r_1 \cos\theta_1 = 8.5 \cos(60^\circ) - 20 = -15.75 \text{ cm}$$

To determine  $\theta_3$ , we need to specify  $\beta$ . Often, we need to compute both values of  $\theta_3$  to determine the proper value for  $\beta$ . Thus

$$\begin{aligned} \theta_3 &= 2 \tan^{-1} \left[ \frac{r_4 + \beta \sqrt{r_4^2 - A^2 + r_3^2}}{(A + r_3)} \right] = 2 \tan^{-1} \left[ \frac{\beta \sqrt{-(-15.75)^2 + (17.38)^2}}{(-15.75 + 17.38)} \right] \\ &= 2 \tan^{-1} \left[ \frac{\beta(7.3486)}{(1.63)} \right] = \pm 154.98^\circ \end{aligned}$$

For this problem,  $\beta = +1$ .

For the velocity analysis, we can use Eq. (5.108). Then,

$$\begin{bmatrix} \cos\theta_3 & -r_3 \sin\theta_3 - r_4 \sin\theta_4 \\ \sin\theta_3 & r_3 \cos\theta_3 + r_4 \cos\theta_4 \end{bmatrix} \begin{Bmatrix} \dot{r}_3 \\ \dot{\theta}_3 \end{Bmatrix} = \begin{Bmatrix} -r_2 \dot{\theta}_2 \sin\theta_2 \\ r_2 \dot{\theta}_2 \cos\theta_2 \end{Bmatrix}$$

or

$$\begin{bmatrix} \cos(154.99) & -17.38 \sin(154.99) \\ \sin(154.99) & 17.38 \cos(154.99) \end{bmatrix} \begin{Bmatrix} \dot{r}_3 \\ \dot{\theta}_3 \end{Bmatrix} = \begin{Bmatrix} -8.5(-2.5) \sin(60^\circ) \\ 8.5(-2.5) \cos(60^\circ) \end{Bmatrix}$$

or

$$\begin{bmatrix} -0.9059 & -7.3612 \\ 0.4234 & -15.750 \end{bmatrix} \begin{Bmatrix} \dot{r}_3 \\ \dot{\theta}_3 \end{Bmatrix} = \begin{Bmatrix} 18.403 \\ -10.625 \end{Bmatrix} \Rightarrow \begin{Bmatrix} \dot{r}_3 \\ \dot{\theta}_3 \end{Bmatrix} = \begin{Bmatrix} -21.171 \text{ cm/s} \\ 0.1055 \text{ rad/s}^2 \end{Bmatrix}$$

For the acceleration analysis, we can use Eq. (5.117). Then,

$$\begin{bmatrix} \cos\theta_3 & -r_3 \sin\theta_3 - r_4 \sin\theta_4 \\ \sin\theta_3 & r_3 \cos\theta_3 + r_4 \cos\theta_4 \end{bmatrix} \begin{Bmatrix} \ddot{r}_3 \\ \ddot{\theta}_3 \end{Bmatrix} = \begin{Bmatrix} -r_2 \ddot{\theta}_2 \sin\theta_2 - r_2 \dot{\theta}_2^2 \cos\theta_2 + r_3 \dot{\theta}_3^2 \cos\theta_3 + 2\dot{r}_3 \dot{\theta}_3 \sin\theta_3 + r_4 \dot{\theta}_3^2 \cos\theta_4 \\ r_2 \ddot{\theta}_2 \cos\theta_2 - r_2 \dot{\theta}_2^2 \sin\theta_2 + r_3 \dot{\theta}_3^2 \sin\theta_3 - 2\dot{r}_3 \dot{\theta}_3 \cos\theta_3 + r_4 \dot{\theta}_3^2 \sin\theta_4 \end{Bmatrix}$$

or

$$\begin{aligned} & \begin{bmatrix} -0.9059 & -7.3612 \\ 0.4234 & -15.750 \end{bmatrix} \begin{Bmatrix} \ddot{\theta}_3 \\ \ddot{\theta}_3 \end{Bmatrix} \\ &= \begin{Bmatrix} -(8.5)(-2.5)^2 \cos(60^\circ) + 17.38(0.1055)^2 \cos(154.99^\circ) + 2(-21.171)(0.1055) \sin(154.99^\circ) \\ -(8.5)(-2.5)^2 \sin(60^\circ) + 17.38(0.1055)^2 \sin(154.99^\circ) + 2(-21.171)(0.1055) \cos(154.99^\circ) \end{Bmatrix} \\ &= \begin{Bmatrix} -25.1851 \\ -42.6038 \end{Bmatrix} \Rightarrow \begin{Bmatrix} \ddot{\theta}_3 \\ \ddot{\theta}_3 \end{Bmatrix} = \begin{Bmatrix} 4.777 \text{ cm/s}^2 \\ 2.833 \text{ rad/s}^2 \end{Bmatrix} \end{aligned}$$

The velocity and acceleration of point  $B$  when observed from link 4 are  $\dot{r}_3$  and  $\ddot{r}_3$ , respectively. Note that  $\dot{r}_3$  is negative when  $\dot{\theta}_2$  is CW.

## 5.7 ANALYTICAL EQUATIONS FOR AN RPRP MECHANISM

A schematic drawing of the RPRP mechanism is shown in Fig. 5.29. In the mechanism shown, link 2 is connected to the frame by a revolute joint and to the coupler by a prismatic joint. Link 4 is connected to the frame through a prismatic joint and to the coupler by a revolute joint. This is a less common mechanism than the various four-bar linkages and slider cranks; however, it does occur in industrial machinery. For example, one variation of it, the Rapson slide, is used in marine steering gear.

When there is a slider joint between two links, the actual location of the slider does not matter from a kinematic standpoint. Therefore, for simplicity, we can analyze the mechanism as if both sliders were at point  $P$ . The resulting mechanism then appears as shown in Fig. 5.30. In Fig. 5.30, the angles are not indicated for simplicity. The angles are again always measured counterclockwise from the horizontal as shown in Fig. 5.3. To develop the closure equations, locate vectors  $r_1$  through  $r_4$  as shown in Fig. 5.30. By locating point  $P$

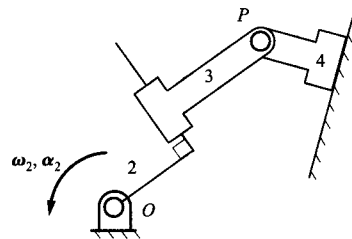


FIGURE 5.29 Schematic diagram of an RPRP mechanism.

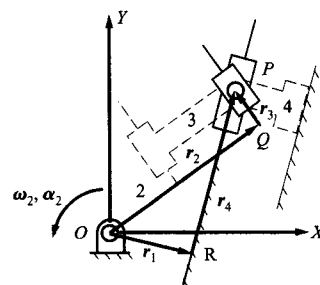


FIGURE 5.30 Vector closure condition for an RPRP mechanism. The position of point  $P$  obtained by the vectors  $r_2$  and  $r_3$  is the same as that obtained by adding vectors  $r_1$  and  $r_4$ .

using two different sets of vectors, the loop closure equation is then seen to be the same as that for the regular four-bar linkage. Namely,

$$\mathbf{r}_P = \mathbf{r}_2 + \mathbf{r}_3 = \mathbf{r}_1 + \mathbf{r}_4 \quad (5.121)$$

or

$$r_2(\cos\theta_2\mathbf{i} + \sin\theta_2\mathbf{j}) + r_3(\cos\theta_3\mathbf{i} + \sin\theta_3\mathbf{j}) = r_1(\cos\theta_1\mathbf{i} + \sin\theta_1\mathbf{j}) + r_4(\cos\theta_4\mathbf{i} + \sin\theta_4\mathbf{j}) \quad (5.122)$$

Rewriting Eq. (5.122) in its component equations gives

$$r_2 \cos\theta_2 + r_3 \cos\theta_3 = r_1 \cos\theta_1 + r_4 \cos\theta_4 \quad (5.123)$$

$$r_2 \sin\theta_2 + r_3 \sin\theta_3 = r_1 \sin\theta_1 + r_4 \sin\theta_4 \quad (5.124)$$

Before solving the equations, it is necessary to identify the magnitudes and directions that are constants. There are eight quantities to identify:  $r_1$  and  $\theta_1$ ,  $r_2$  and  $\theta_2$ ,  $r_3$  and  $\theta_3$ , and  $r_4$  and  $\theta_4$ . From the diagram in Fig. 5.30, the following are constants:  $r_1$ ,  $\theta_1$ ,  $r_2$ , and  $\theta_4$ . Furthermore, we know that

$$\theta_3 = \theta_2 + \pi/2 \quad (5.125)$$

and

$$\theta_4 = \theta_1 + \pi/2 \quad (5.126)$$

The variables are  $r_3$ ,  $\theta_2$ ,  $r_4$ , and  $\theta_3$ . For a one-degree-of-freedom mechanism, one of the variables must be an input (i.e., known) variable. Therefore, there are a total of three unknowns. Because we have three equations (5.123), (5.124), and (5.125) involving the unknowns, we can solve for them.

Once all of the position variables are obtained, the unknown velocities and accelerations can be obtained by differentiating Eqs. (5.123), (5.124), and (5.125) and solving the resulting set of linear equations for the unknowns.

Before solving the equations for the unknowns, it is necessary to select an input variable. Any of  $r_3$ ,  $\theta_2$ ,  $r_4$ , or  $\theta_3$  could be chosen. Because  $\theta_2$  and  $\theta_3$  are related by Eq. (5.125), there is no practical difference between specifying one or the other as the input. Therefore, the choices for inputs reduce to  $\theta_2$  (or  $\theta_3$ ) and  $r_4$  (or  $r_3$ ). The procedure for developing the equations is the same as that in Sections 5.4–5.6. Therefore, the detailed development of the equations will not be given here. Rather, an overview of each case will be given and the results will be summarized in a table.

### 5.7.1 Solution of Closure Equations When $\theta_2$ Is Known

The analytical solution procedure for the linkage of Fig. 5.30 follows the same major steps as in the previous cases. That is, a position analysis must be performed first, then a velocity analysis, and finally the acceleration analysis. The case in which  $\theta_2$  is an input is especially simple because  $\theta_3$  can be computed from Eq. (5.125), and Eqs. (5.123) and (5.124) then become linear in the unknowns  $r_3$  and  $r_4$ . The equations to be solved are

$$r_3 \cos\theta_3 - r_4 \cos\theta_4 = r_1 \cos\theta_1 - r_2 \cos\theta_2 \quad (5.127)$$

$$r_3 \sin\theta_3 - r_4 \sin\theta_4 = r_1 \sin\theta_1 - r_2 \sin\theta_2 \quad (5.128)$$

or in matrix form

$$\begin{bmatrix} \cos\theta_3 & -\cos\theta_4 \\ \sin\theta_3 & -\sin\theta_4 \end{bmatrix} \begin{Bmatrix} r_3 \\ r_4 \end{Bmatrix} = \begin{Bmatrix} r_1 \cos\theta_1 - r_2 \cos\theta_2 \\ r_1 \sin\theta_1 - r_2 \sin\theta_2 \end{Bmatrix} \quad (5.129)$$

The terms in the matrix and in the vector on the right-hand side of the equation will be known. The matrix equation can therefore be solved manually, on a programmable calculator, or with the matrix solvers in programs such as MATLAB.



Once the position equations are solved, the coordinates of points  $P$ ,  $Q$ , and  $R$  can be computed directly. The equations are given in Table 5.9.

### 5.7.2 Solution of Closure Equations When $r_4$ Is Known

When  $r_4$  is known for the linkage of Fig. 5.30, we must determine  $\theta_2$ ,  $\theta_3$ , and  $r_3$ . Of these unknowns,  $\theta_2$  and  $\theta_3$  are related in a trivial manner through Eq. (5.125). Therefore, the principal unknowns are  $\theta_2$  and  $r_3$ . The equations to be solved are Eqs. (5.123) and (5.124). In general, there are two solutions for  $r_3$ , and they are both valid. The two assembly modes are represented in Fig. 5.31. The equations from the position analysis are summarized as part of Table 5.10. The different assembly modes are identified by selecting values of  $\sigma$  in Table 5.10 as either +1 or -1.

**TABLE 5.9 Summary of Position, Velocity, and Acceleration Equations for an RPRP Mechanism When  $\theta_2$  Is the Input Variable. The Link Numbers and Points Are Defined in Fig. 5.30**

---

#### Position

---

$$\theta_3 = \theta_2 + \pi/2$$

$$\theta_4 = \theta_1 + \pi/2$$

$$\begin{bmatrix} \cos \theta_3 & -\cos \theta_4 \\ \sin \theta_3 & -\sin \theta_4 \end{bmatrix} \begin{Bmatrix} r_3 \\ r_4 \end{Bmatrix} = \begin{Bmatrix} r_1 \cos \theta_1 - r_2 \cos \theta_2 \\ r_1 \sin \theta_1 - r_2 \sin \theta_2 \end{Bmatrix}$$

$$\begin{aligned} r_P &= r_2 + r_3 = (r_2 \cos \theta_2 + r_3 \cos \theta_3)\mathbf{i} + (r_2 \sin \theta_2 + r_3 \sin \theta_3)\mathbf{j} \\ &= r_1 + r_4 = (r_1 \cos \theta_1 + r_4 \cos \theta_4)\mathbf{i} + (r_1 \sin \theta_1 + r_4 \sin \theta_4)\mathbf{j} \end{aligned}$$

$$r_Q = r_2 = (r_2 \cos \theta_2)\mathbf{i} + (r_2 \sin \theta_2)\mathbf{j}$$

$$r_R = r_1 = (r_1 \cos \theta_1)\mathbf{i} + (r_1 \sin \theta_1)\mathbf{j}$$

---

#### Velocity

---

$$\dot{\theta}_3 = \dot{\theta}_2$$

$$\begin{bmatrix} \cos \theta_3 & -\cos \theta_4 \\ \sin \theta_3 & -\sin \theta_4 \end{bmatrix} \begin{Bmatrix} \dot{r}_3 \\ \dot{r}_4 \end{Bmatrix} = \begin{Bmatrix} r_2 \dot{\theta}_2 \sin \theta_2 + r_3 \dot{\theta}_3 \sin \theta_3 \\ -r_2 \dot{\theta}_2 \cos \theta_2 - r_3 \dot{\theta}_3 \cos \theta_3 \end{Bmatrix}$$

$$\begin{aligned} \dot{r}_P &= \dot{r}_2 + \dot{r}_3 = (-r_2 \dot{\theta}_2 \sin \theta_2 - r_3 \dot{\theta}_3 \sin \theta_3 + \dot{r}_3 \cos \theta_3)\mathbf{i} + (r_2 \dot{\theta}_2 \cos \theta_2 + r_3 \dot{\theta}_3 \cos \theta_3 + \dot{r}_3 \sin \theta_3)\mathbf{j} \\ &= \dot{r}_4 = (\dot{r}_4 \cos \theta_4)\mathbf{i} + (\dot{r}_4 \sin \theta_4)\mathbf{j} \end{aligned}$$

$$\dot{r}_Q = \dot{r}_2 = (-r_2 \dot{\theta}_2 \sin \theta_2)\mathbf{i} + (r_2 \dot{\theta}_2 \cos \theta_2)\mathbf{j}$$

---

#### Acceleration

---

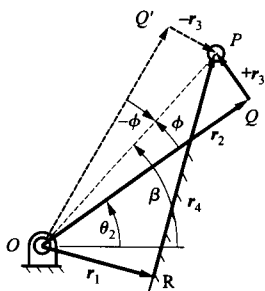
$$\ddot{\theta}_3 = \ddot{\theta}_2$$

$$\begin{bmatrix} \cos \theta_3 & -\cos \theta_4 \\ \sin \theta_3 & -\sin \theta_4 \end{bmatrix} \begin{Bmatrix} \ddot{r}_3 \\ \ddot{r}_4 \end{Bmatrix} = \begin{Bmatrix} r_2 \ddot{\theta}_2 \sin \theta_2 + r_2 \dot{\theta}_2^2 \cos \theta_2 + 2\dot{r}_3 \dot{\theta}_3 \sin \theta_3 + r_3 \ddot{\theta}_3 \sin \theta_3 + r_3 \dot{\theta}_3^2 \cos \theta_3 \\ -r_2 \ddot{\theta}_2 \cos \theta_2 + r_2 \dot{\theta}_2^2 \sin \theta_2 - 2\dot{r}_3 \dot{\theta}_3 \cos \theta_3 - r_3 \ddot{\theta}_3 \cos \theta_3 + r_3 \dot{\theta}_3^2 \sin \theta_3 \end{Bmatrix}$$

$$\ddot{r}_P = \ddot{r}_4 = (\ddot{r}_4 \cos \theta_4)\mathbf{i} + (\ddot{r}_4 \sin \theta_4)\mathbf{j}$$

$$\ddot{r}_Q = \ddot{r}_2 = (-r_2 \ddot{\theta}_2 \sin \theta_2 - r_2 \dot{\theta}_2^2 \cos \theta_2)\mathbf{i} + (r_2 \ddot{\theta}_2 \cos \theta_2 - r_2 \dot{\theta}_2^2 \sin \theta_2)\mathbf{j}$$


---


 FIGURE 5.31 Two assembly modes when  $r_4$  is input.

**TABLE 5.10 Summary of Position, Velocity, and Acceleration Equations for a RPRP Mechanism When  $r_4$  Is the Input Variable. The Link Numbers and Points Are Defined in Fig. 5.30**
**Position**

$$r_3 = \sigma \sqrt{r_4^2 + r_1^2 - r_2^2}; \quad \sigma = \pm 1$$

$$\phi = \tan^{-1} \left( \frac{r_3}{r_2} \right)$$

$$\beta = \tan^{-1} \left( \frac{r_1 \sin \theta_1 + r_4 \sin \theta_4}{r_1 \cos \theta_1 + r_4 \cos \theta_4} \right)$$

$$\theta_2 = \beta - \phi, \quad \theta_3 = \theta_2 + \pi/2, \quad \theta_4 = \theta_1 + \pi/2$$

$$\begin{aligned} \mathbf{r}_P &= \mathbf{r}_2 + \mathbf{r}_3 = (r_2 \cos \theta_2 + r_3 \cos \theta_3) \mathbf{i} + (r_2 \sin \theta_2 + r_3 \sin \theta_3) \mathbf{j} \\ &= \mathbf{r}_1 + \mathbf{r}_4 = (r_1 \cos \theta_1 + r_4 \cos \theta_4) \mathbf{i} + (r_1 \sin \theta_1 + r_4 \sin \theta_4) \mathbf{j} \end{aligned}$$

$$\mathbf{r}_Q = \mathbf{r}_2 = (r_2 \cos \theta_2) \mathbf{i} + (r_2 \sin \theta_2) \mathbf{j}$$

**Velocity**

$$\begin{bmatrix} \cos \theta_3 & -(r_3 \sin \theta_3 + r_2 \sin \theta_2) \\ \sin \theta_3 & (r_3 \cos \theta_3 + r_2 \cos \theta_2) \end{bmatrix} \begin{Bmatrix} \dot{r}_3 \\ \dot{\theta}_2 \end{Bmatrix} = \begin{Bmatrix} \dot{r}_4 \cos \theta_4 \\ \dot{r}_4 \sin \theta_4 \end{Bmatrix}$$

$$\dot{\theta}_3 = \dot{\theta}_2$$

$$\begin{aligned} \dot{\mathbf{r}}_P &= \dot{\mathbf{r}}_2 + \dot{\mathbf{r}}_3 = (-r_2 \dot{\theta}_2 \sin \theta_2 - r_3 \dot{\theta}_3 \sin \theta_3 + \dot{r}_3 \cos \theta_3) \mathbf{i} + (r_2 \dot{\theta}_2 \cos \theta_2 + r_3 \dot{\theta}_3 \cos \theta_3 + \dot{r}_3 \sin \theta_3) \mathbf{j} \\ &= \dot{\mathbf{r}}_4 = (\dot{r}_4 \cos \theta_4) \mathbf{i} + (\dot{r}_4 \sin \theta_4) \mathbf{j} \end{aligned}$$

$$\dot{\mathbf{r}}_Q = \dot{\mathbf{r}}_2 = (-r_2 \dot{\theta}_2 \sin \theta_2) \mathbf{i} + (r_2 \dot{\theta}_2 \cos \theta_2) \mathbf{j}$$

**Acceleration**

$$\begin{bmatrix} \cos \theta_3 & -(r_3 \sin \theta_3 + r_2 \sin \theta_2) \\ \sin \theta_3 & (r_3 \cos \theta_3 + r_2 \cos \theta_2) \end{bmatrix} \begin{Bmatrix} \ddot{r}_3 \\ \ddot{\theta}_2 \end{Bmatrix} = \begin{Bmatrix} \ddot{r}_4 \cos \theta_4 + r_2 \dot{\theta}_2^2 \cos \theta_2 + 2\dot{r}_3 \dot{\theta}_3 \sin \theta_3 + r_3 \dot{\theta}_3^2 \cos \theta_3 \\ \ddot{r}_4 \sin \theta_4 + r_2 \dot{\theta}_2^2 \sin \theta_2 - 2\dot{r}_3 \dot{\theta}_3 \cos \theta_3 + r_3 \dot{\theta}_3^2 \sin \theta_3 \end{Bmatrix}$$

$$\ddot{\theta}_3 = \ddot{\theta}_2$$

$$\ddot{\mathbf{r}}_P = \ddot{\mathbf{r}}_4 = (\ddot{r}_4 \cos \theta_4) \mathbf{i} + (\ddot{r}_4 \sin \theta_4) \mathbf{j}$$

$$\ddot{\mathbf{r}}_Q = \ddot{\mathbf{r}}_2 = (-r_2 \ddot{\theta}_2 \sin \theta_2 - r_2 \dot{\theta}_2^2 \cos \theta_2) \mathbf{i} + (r_2 \ddot{\theta}_2 \cos \theta_2 - r_2 \dot{\theta}_2^2 \sin \theta_2) \mathbf{j}$$

It is also possible to specify a value for  $r_4$  that will prevent the mechanism from being assembled. This is indicated when the argument of the square root in Table 5.10 is negative.

Once both  $r_3$  and  $r_4$  are known, we can find  $\theta_2$  (and  $\theta_3$ ) using simple geometry. First compute the angles  $\phi$  and  $\beta$  shown in Fig. 5.31 using

$$\phi = \tan^{-1}\left(\frac{r_3}{r_2}\right) \quad (5.130)$$

and

$$\beta = \tan^{-1}\left(\frac{r_{P_y}}{r_{P_x}}\right) = \tan^{-1}\left(\frac{r_1 \sin \theta_1 + r_4 \sin \theta_4}{r_1 \cos \theta_1 + r_4 \cos \theta_4}\right) \quad (5.131)$$

Then

$$\theta_2 = \beta - \phi \quad (5.132)$$

and

$$\theta_3 = \theta_2 + \pi/2 \quad (5.133)$$

Equation (5.132) is valid for both the plus and minus values for  $r_3$  because the sign of  $\phi$  will be positive when  $r_3$  is positive and negative when  $r_3$  is negative.

### 5.7.3 Solution of Closure Equations When $r_3$ Is Known

When  $r_3$  is known, we must determine  $\theta_2$ ,  $\theta_3$ , and  $r_4$ . Of these unknowns,  $\theta_2$  and  $\theta_3$  are related in a trivial manner through Eq. (5.125). Therefore, the principal unknowns are  $\theta_2$  and  $r_4$ . The procedure for solving the position equations is very similar to that when  $r_4$  was input. In general, there are two solutions for  $r_4$ , and they are both valid. The equations from the position analysis are summarized as part of Table 5.11. Note that it is possible to specify a value for  $r_3$  that will prevent the mechanism from being assembled. This is indicated when the argument of the square root in Table 5.11 is negative.

**TABLE 5.11 Summary of Position, Velocity, and Acceleration Equations for an RPRP Mechanism When  $r_3$  Is the Input Variable. The Link Numbers and Points Are Defined in Fig. 5.30**

#### Position

$$r_4 = \sigma \sqrt{r_3^2 - r_1^2 + r_2^2}; \quad \sigma = \pm 1$$

$$\phi = \tan^{-1}\left(\frac{r_3}{r_2}\right)$$

$$\beta = \tan^{-1}\left(\frac{r_1 \sin \theta_1 + r_4 \sin \theta_4}{r_1 \cos \theta_1 + r_4 \cos \theta_4}\right)$$

$$\theta_2 = \beta - \phi, \quad \theta_3 = \theta_2 + \pi/2, \quad \theta_4 = \theta_1 + \pi/2$$

$$\begin{aligned} r_P &= r_2 + r_3 = (r_2 \cos \theta_2 + r_3 \cos \theta_3)\mathbf{i} + (r_2 \sin \theta_2 + r_3 \sin \theta_3)\mathbf{j} \\ &= r_1 + r_4 = (r_1 \cos \theta_1 + r_4 \cos \theta_4)\mathbf{i} + (r_1 \sin \theta_1 + r_4 \sin \theta_4)\mathbf{j} \end{aligned}$$

$$r_Q = r_2 = (r_2 \cos \theta_2)\mathbf{i} + (r_2 \sin \theta_2)\mathbf{j}$$

(continued)

TABLE 5.11 continued

## Velocity

$$\begin{bmatrix} \cos \theta_4 & (r_3 \sin \theta_3 + r_2 \sin \theta_2) \\ \sin \theta_4 & -(r_3 \cos \theta_3 + r_2 \cos \theta_2) \end{bmatrix} \begin{Bmatrix} \dot{r}_4 \\ \dot{\theta}_2 \end{Bmatrix} = \begin{Bmatrix} \dot{r}_3 \cos \theta_3 \\ \dot{r}_3 \sin \theta_3 \end{Bmatrix}$$

$$\dot{\theta}_3 = \dot{\theta}_2$$

$$\begin{aligned} \dot{r}_P &= \dot{r}_2 + \dot{r}_3 = (-r_2 \dot{\theta}_2 \sin \theta_2 - r_3 \dot{\theta}_3 \sin \theta_3 + \dot{r}_3 \cos \theta_3) \mathbf{i} + (r_2 \dot{\theta}_2 \cos \theta_2 + r_3 \dot{\theta}_3 \cos \theta_3 + \dot{r}_3 \sin \theta_3) \mathbf{j} \\ &= \dot{r}_4 = (\dot{r}_4 \cos \theta_4) \mathbf{i} + (\dot{r}_4 \sin \theta_4) \mathbf{j} \end{aligned}$$

$$\dot{r}_Q = \dot{r}_2 = (-r_2 \dot{\theta}_2 \sin \theta_2) \mathbf{i} + (r_2 \dot{\theta}_2 \cos \theta_2) \mathbf{j}$$

## Acceleration

$$\begin{bmatrix} \cos \theta_4 & (r_3 \sin \theta_3 + r_2 \sin \theta_2) \\ \sin \theta_4 & -(r_3 \cos \theta_3 + r_2 \cos \theta_2) \end{bmatrix} \begin{Bmatrix} \ddot{r}_4 \\ \ddot{\theta}_2 \end{Bmatrix} = \begin{Bmatrix} -r_2 \ddot{\theta}_2^2 \cos \theta_2 - 2\dot{r}_3 \dot{\theta}_3 \sin \theta_3 - r_3 \dot{\theta}_3^2 \cos \theta_3 + \ddot{r}_3 \cos \theta_3 \\ -r_2 \ddot{\theta}_2^2 \sin \theta_2 + 2\dot{r}_3 \dot{\theta}_3 \cos \theta_3 - r_3 \dot{\theta}_3^2 \sin \theta_3 + \ddot{r}_3 \sin \theta_3 \end{Bmatrix}$$

$$\ddot{\theta}_3 = \ddot{\theta}_2$$

$$\ddot{r}_P = \ddot{r}_4 = (\ddot{r}_4 \cos \theta_4) \mathbf{i} + (\ddot{r}_4 \sin \theta_4) \mathbf{j}$$

$$\ddot{r}_Q = \ddot{r}_2 = (-r_2 \ddot{\theta}_2 \sin \theta_2 - r_2 \dot{\theta}_2^2 \cos \theta_2) \mathbf{i} + (r_2 \ddot{\theta}_2 \cos \theta_2 - r_2 \dot{\theta}_2^2 \sin \theta_2) \mathbf{j}$$

### 5.7.4 Velocity and Acceleration Equations for an RPRP Mechanism

The analytical form of the velocity equations can be developed by differentiating the position equations and solving the resulting linear set of equations for the unknowns as done in the previous examples. The acceleration equations are developed by differentiating the velocity equations. The acceleration equations are also linear and can easily be solved. The results for the RPRP mechanism are given in Tables 5.9, 5.10, and 5.11. These equations can easily be programmed, and MATLAB programs for solving the equations in the three tables are given on the disk with this book.

#### EXAMPLE 5.7 Kinematic Analysis of an RPRP Mechanism

##### Solution

In the mechanism shown in Fig. 5.32, link 3 slides on link 2, and link 4 is pinned to link 3; link 4 also slides on the frame (link 1). If  $\omega_2 = 10$  rad/s CCW and is constant, determine the velocity and acceleration of link 4 for the position defined by  $\theta_2 = 60^\circ$ .

Using the nomenclature developed earlier, the basic vector closure diagram is as shown in Fig. 5.33. Note that in this example,  $r_2 = 0$ . From Figs. 5.32 and 5.33, the following geometric quantities can be determined:

$$\begin{aligned} r_2 &= 0, & r_1 &= 10 \\ \theta_1 &= 90^\circ, & \theta_2 &= 60^\circ, & \theta_3 &= 60^\circ, & \theta_4 &= 180^\circ \end{aligned}$$

The geometric unknowns are  $r_3$  and  $r_4$ . Because  $\theta_2 = \theta_3$  is the input variable, we can compute the results using the equations in Table 5.9. To solve for  $r_3$  and  $r_4$ , solve

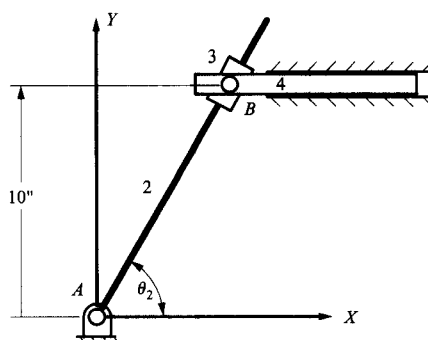


FIGURE 5.32 Mechanism for Example 5.7.

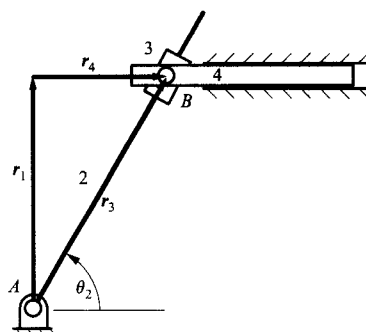


FIGURE 5.33 Vector closure diagram for Example 5.7.

$$\begin{bmatrix} \cos \theta_3 & -\cos \theta_4 \\ \sin \theta_3 & -\sin \theta_4 \end{bmatrix} \begin{Bmatrix} r_3 \\ r_4 \end{Bmatrix} = \begin{Bmatrix} r_1 \cos \theta_1 - r_2 \cos \theta_2 \\ r_1 \sin \theta_1 - r_2 \sin \theta_2 \end{Bmatrix}$$

or

$$\begin{bmatrix} \cos 60^\circ & -\cos 180^\circ \\ \sin 60^\circ & -\sin 180^\circ \end{bmatrix} \begin{Bmatrix} r_3 \\ r_4 \end{Bmatrix} = \begin{Bmatrix} 10 \cos 90^\circ - 0 \\ 10 \sin 90^\circ - 0 \end{Bmatrix}$$

Simplifying gives

$$\begin{bmatrix} 0.5 & 1 \\ 0.8660 & 0 \end{bmatrix} \begin{Bmatrix} r_3 \\ r_4 \end{Bmatrix} = \begin{Bmatrix} 0 \\ 10 \end{Bmatrix}$$

and solving then yields

$$\begin{Bmatrix} r_3 \\ r_4 \end{Bmatrix} = \begin{Bmatrix} 11.547 \\ -5.774 \end{Bmatrix}$$

The negative sign for  $r_4$  means that it is pointing in the opposite direction to that given by  $\theta_4 = 180^\circ$ . Clearly, the geometry in Fig. 5.33 could have been solved directly using geometry; however, the more general equations are used here to illustrate the procedure.

For the velocities, the unknowns are  $\dot{r}_3$  and  $\dot{r}_4$ . From the problem statement,  $\dot{\theta}_2 = \dot{\theta}_3 = 10$  rad/s CCW. Therefore, from Table 5.9,

$$\begin{bmatrix} \cos \theta_3 & -\cos \theta_4 \\ \sin \theta_3 & -\sin \theta_4 \end{bmatrix} \begin{Bmatrix} \dot{r}_3 \\ \dot{r}_4 \end{Bmatrix} = \begin{Bmatrix} r_2 \dot{\theta}_2 \sin \theta_2 + r_3 \dot{\theta}_3 \sin \theta_3 \\ -r_2 \dot{\theta}_2 \cos \theta_2 - r_3 \dot{\theta}_3 \cos \theta_3 \end{Bmatrix}$$

Note that the coefficient matrix on the left-hand side of the velocity equation is the same as the corresponding position matrix.

Substituting the known quantities into the matrix equation gives

$$\begin{bmatrix} 0.5 & 1 \\ 0.8660 & 0 \end{bmatrix} \begin{Bmatrix} \dot{r}_3 \\ \dot{r}_4 \end{Bmatrix} = \begin{Bmatrix} 0 + 11.547(10) \sin 60^\circ \\ 0 - 11.547(10) \cos 60^\circ \end{Bmatrix} = \begin{Bmatrix} 100 \\ -57.74 \end{Bmatrix}$$

or

$$\begin{Bmatrix} \dot{r}_3 \\ \dot{r}_4 \end{Bmatrix} = \begin{Bmatrix} -66.67 \\ 133.33 \end{Bmatrix}$$

Note that the positive value for  $\dot{r}_4$  means that  $r_4$  is increasing with time. Because  $r_4$  is negative when it points in the positive  $x$  direction ( $\theta_4 = 180^\circ$ ), a positive sign for  $\dot{r}_4$  means that  $r_4$  is increasing or becoming less negative with time. This means that link 4 is moving in the  $-x$  direction.

For the acceleration analysis, the unknowns are  $\ddot{r}_3$  and  $\ddot{r}_4$ . From the problem statement,  $\ddot{\theta}_2 = \ddot{\theta}_3 = 0$ , and from Table 5.9,

$$\begin{bmatrix} \cos \theta_3 & -\cos \theta_4 \\ \sin \theta_3 & -\sin \theta_4 \end{bmatrix} \begin{Bmatrix} \ddot{r}_3 \\ \ddot{r}_4 \end{Bmatrix} = \begin{Bmatrix} r_2 \ddot{\theta}_2 \sin \theta_2 + r_2 \dot{\theta}_2^2 \cos \theta_2 + 2\dot{r}_3 \dot{\theta}_3 \sin \theta_3 + r_3 \ddot{\theta}_3 \sin \theta_3 + r_3 \dot{\theta}_3^2 \cos \theta_3 \\ -r_2 \ddot{\theta}_2 \cos \theta_2 + r_2 \dot{\theta}_2^2 \sin \theta_2 - 2\dot{r}_3 \dot{\theta}_3 \cos \theta_3 - r_3 \ddot{\theta}_3 \cos \theta_3 + r_3 \dot{\theta}_3^2 \sin \theta_3 \end{Bmatrix}$$

Note again that the coefficient matrix on the left-hand side of the acceleration equation is the same as the corresponding position matrix. Substituting the known quantities into the matrix equation gives

$$\begin{bmatrix} 0.5 & 1 \\ 0.8660 & 0 \end{bmatrix} \begin{Bmatrix} \ddot{r}_3 \\ \ddot{r}_4 \end{Bmatrix} = \begin{Bmatrix} -577.4 \\ 1666.7 \end{Bmatrix}$$

or

$$\begin{Bmatrix} \ddot{r}_3 \\ \ddot{r}_4 \end{Bmatrix} = \begin{Bmatrix} 1924.5 \\ -1539.6 \end{Bmatrix}$$

Again, the positive value for  $\ddot{r}_4$  means the slider is accelerating in the positive  $r_4$  direction, that is, to the left.

## 5.8 ANALYTICAL EQUATIONS FOR AN RRPP MECHANISM

A schematic drawing of the RRPP mechanism is shown in Fig. 5.34. In the mechanism shown, link 2 is connected to the frame and to the coupler (link 3) by revolute joints. The coupler is connected to link 4 by a prismatic joint, and link 4 is connected to the frame through a prismatic joint. This mechanism occurs frequently in industrial machinery and household appliances. A common version of it is the Scotch yoke, which is a compact mechanism for converting rotary motion to reciprocating motion.

To analyze the mechanism using vector closure equations, we must align vectors in the directions of the slider motions as shown in Fig. 5.35. Only three vectors are required to model the motion. Vector  $r_1$  is fixed at an angle  $\theta_1$  and of variable length. This vector begins at point  $O$  and ends at point  $Q$ , where  $Q$  is the intersection of a line through  $O$  and in the direction of the velocity of link 4 relative to link 1 and a second line through  $P$  in the direction of the velocity of link 3 relative to link 4. The two lines intersect at an angle  $\beta$ . Vector  $r_2$  is the crank and of fixed length but variable orientation. Vector  $r_3$  is measured from point  $Q$  and gives the displacement of slider 3 relative to link 4.

To develop the closure equations, locate point  $P$  with vector  $r_2$  and with vectors  $r_1 + r_3$  as shown in Fig. 5.35. Then the vector closure equation is

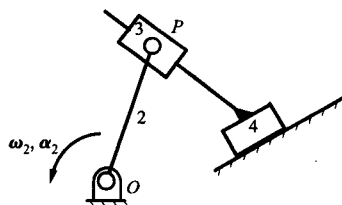


FIGURE 5.34 Schematic diagram of an RRPP mechanism.

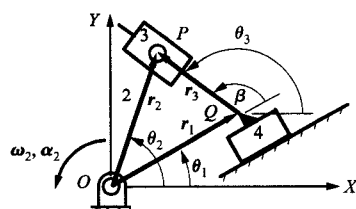


FIGURE 5.35 Vector closure diagram of an RRPP mechanism.

$$\mathbf{r}_P = \mathbf{r}_2 = \mathbf{r}_1 + \mathbf{r}_3 \quad (5.134)$$

or

$$r_2 (\cos \theta_2 \mathbf{i} + \sin \theta_2 \mathbf{j}) = r_1 (\cos \theta_1 \mathbf{i} + \sin \theta_1 \mathbf{j}) + r_3 (\cos \theta_3 \mathbf{i} + \sin \theta_3 \mathbf{j}) \quad (5.135)$$

Rewriting the components in Eq. (5.134) as separate equations gives

$$r_2 \cos \theta_2 = r_1 \cos \theta_1 + r_3 \cos \theta_3 \quad (5.136)$$

$$r_2 \sin \theta_2 = r_1 \sin \theta_1 + r_3 \sin \theta_3 \quad (5.137)$$

Equations (5.136) and (5.137) must be satisfied throughout the motion of the linkage. There are six quantities to identify:  $r_1$  and  $\theta_1$ ,  $r_2$  and  $\theta_2$ , and  $r_3$  and  $\theta_3$ . From the diagram in Fig. 5.35,  $\theta_1$ ,  $r_2$ , and  $\theta_3$  are constants. Furthermore, we know that

$$\theta_3 = \theta_1 + \beta \quad (5.138)$$

where  $\beta$  is a constant.

The variables are  $r_1$ ,  $\theta_2$ , and  $r_3$ . For a one-degree-of-freedom mechanism, one of the variables must be an input (i.e., a known) variable. Therefore, there are two unknowns, and we can solve for them using the two equations (5.136) and (5.137) involving the unknowns.

Once all of the position variables are obtained, the unknown velocities and accelerations can be obtained by differentiating Eqs. (5.136) and (5.137) and solving the resulting sets of linear equations for the unknowns.

Before solving the equations for the unknowns, it is necessary to select an input variable. Any of the variables  $r_1$ ,  $\theta_2$ , or  $r_3$  could be chosen, and the equations have been developed for each case. Again, we will not give a detailed development of the solution procedure because it is similar to the examples discussed before. An overview of each case is given in the following, and the results are summarized in tables.

### 5.8.1 Solution When $\theta_2$ Is Known

The case in which  $\theta_2$  is an input is especially simple because Eqs. (5.136) and (5.137) then become linear in the unknowns  $r_1$  and  $r_3$ . Only one assembly mode is possible, and if  $r_2$  is nonzero, there are no positions in which the mechanism cannot be assembled. The velocity and acceleration equations are obtained by differentiation. The solution for this case is given in Table 5.12, and a MATLAB program for solving the equations is given on the disk with this book.

**TABLE 5.12 Summary of Position, Velocity, and Acceleration Equations for an RRPP Mechanism When  $\theta_2$  Is the Input Variable. The Link Numbers and Points Are Defined in Fig. 5.34****Position**

$$\theta_3 = \theta_1 + \beta$$

$$\begin{bmatrix} \cos \theta_1 & \cos \theta_3 \\ \sin \theta_1 & \sin \theta_3 \end{bmatrix} \begin{Bmatrix} r_1 \\ r_3 \end{Bmatrix} = \begin{Bmatrix} r_2 \cos \theta_2 \\ r_2 \sin \theta_2 \end{Bmatrix}$$

$$\mathbf{r}_P = \mathbf{r}_2 = (r_2 \cos \theta_2)\mathbf{i} + (r_2 \sin \theta_2)\mathbf{j}$$

$$\mathbf{r}_Q = \mathbf{r}_1 = (r_1 \cos \theta_1)\mathbf{i} + (r_1 \sin \theta_1)\mathbf{j}$$

**Velocity**

$$\begin{bmatrix} \cos \theta_1 & \cos \theta_3 \\ \sin \theta_1 & \sin \theta_3 \end{bmatrix} \begin{Bmatrix} \dot{r}_1 \\ \dot{r}_3 \end{Bmatrix} = \begin{Bmatrix} -r_2 \dot{\theta}_2 \sin \theta_2 \\ r_2 \dot{\theta}_2 \cos \theta_2 \end{Bmatrix}$$

$$\dot{\mathbf{r}}_P = \dot{\mathbf{r}}_2 = (-r_2 \dot{\theta}_2 \sin \theta_2)\mathbf{i} + (r_2 \dot{\theta}_2 \cos \theta_2)\mathbf{j}$$

$$\dot{\mathbf{r}}_Q = \dot{\mathbf{r}}_1 = (\dot{r}_1 \cos \theta_1)\mathbf{i} + (\dot{r}_1 \sin \theta_1)\mathbf{j}$$

**Acceleration**

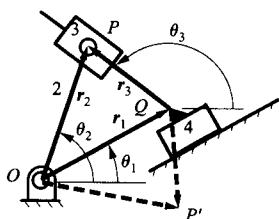
$$\begin{bmatrix} \cos \theta_1 & \cos \theta_3 \\ \sin \theta_1 & \sin \theta_3 \end{bmatrix} \begin{Bmatrix} \ddot{r}_1 \\ \ddot{r}_3 \end{Bmatrix} = \begin{Bmatrix} -r_2 \ddot{\theta}_2 \sin \theta_2 - r_2 \dot{\theta}_2^2 \cos \theta_2 \\ r_2 \ddot{\theta}_2 \cos \theta_2 - r_2 \dot{\theta}_2^2 \sin \theta_2 \end{Bmatrix}$$

$$\ddot{\mathbf{r}}_P = \ddot{\mathbf{r}}_2 = (-r_2 \ddot{\theta}_2 \sin \theta_2 - r_2 \dot{\theta}_2^2 \cos \theta_2)\mathbf{i} + (r_2 \ddot{\theta}_2 \cos \theta_2 - r_2 \dot{\theta}_2^2 \sin \theta_2)\mathbf{j}$$

$$\ddot{\mathbf{r}}_Q = \ddot{\mathbf{r}}_1 = (\ddot{r}_1 \cos \theta_1)\mathbf{i} + (\ddot{r}_1 \sin \theta_1)\mathbf{j}$$

**5.8.2 Solution When  $r_1$  Is Known**

When  $r_1$  is known, we must solve Eqs. (5.136) and (5.137) for  $\theta_2$  and  $r_3$ . The solution is similar to that for the slider-crank inversion. In general, there are two solutions for  $r_3$ , corresponding to the two assembly modes or branches for the linkage represented in Fig. 5.36. Also, it is possible to specify a value for  $r_1$  that will prevent the mechanism from being assembled. After the position equations are solved, the velocity and acceleration equations are obtained by differentiation. The results are summarized in Table 5.13 and a MATLAB program for solving the equations is given on the disk with this book.

**FIGURE 5.36** Two configurations possible when  $r_1$  is input.



**TABLE 5.13 Summary of Position, Velocity, and Acceleration Equations for an RRPP Mechanism When Either  $r_1$  or  $r_3$  is the input Variable. When  $r_1$  is the input,  $M = 1$  and  $J = 3$ . When  $r_3$  is the input,  $M = 3$  and  $J = 1$ . The Link Numbers and Points Are Defined in Fig. 5.34**

---

**Position**


---

$$\theta_3 = \theta_1 + \beta$$

$$B = r_M (\cos \theta_M \cos \theta_J + \sin \theta_M \sin \theta_J)$$

$$C = (r_M^2 - r_2^2)$$

$$r_J = -B + \sigma \sqrt{B^2 - C}; \quad \sigma = \pm 1$$

$$\theta_2 = \tan^{-1} \frac{r_1 \sin \theta_1 + r_3 \sin \theta_3}{r_1 \cos \theta_1 + r_3 \cos \theta_3}$$

$$r_P = r_2 = (r_2 \cos \theta_2) \mathbf{i} + (r_2 \sin \theta_2) \mathbf{j}$$

$$r_Q = r_1 = (r_1 \cos \theta_1) \mathbf{i} + (r_1 \sin \theta_1) \mathbf{j}$$

---

**Velocity**


---

$$\begin{bmatrix} -r_2 \sin \theta_2 & -\cos \theta_J \\ r_2 \cos \theta_2 & -\sin \theta_J \end{bmatrix} \begin{Bmatrix} \dot{\theta}_2 \\ \dot{r}_J \end{Bmatrix} = \begin{Bmatrix} \dot{r}_M \cos \theta_M \\ \dot{r}_M \sin \theta_M \end{Bmatrix}$$

$$\dot{r}_P = \dot{r}_2 = (-r_2 \dot{\theta}_2 \sin \theta_2) \mathbf{i} + (r_2 \dot{\theta}_2 \cos \theta_2) \mathbf{j}$$

$$\dot{r}_Q = \dot{r}_1 = (\dot{r}_1 \cos \theta_1) \mathbf{i} + (\dot{r}_1 \sin \theta_1) \mathbf{j}$$

---

**Acceleration**


---

$$\begin{bmatrix} -r_2 \sin \theta_2 & -\cos \theta_J \\ r_2 \cos \theta_2 & -\sin \theta_J \end{bmatrix} \begin{Bmatrix} \ddot{\theta}_2 \\ \ddot{r}_J \end{Bmatrix} = \begin{Bmatrix} \ddot{r}_M \cos \theta_M + r_2 \dot{\theta}_2^2 \cos \theta_2 \\ \ddot{r}_M \sin \theta_M + r_2 \dot{\theta}_2^2 \sin \theta_2 \end{Bmatrix}$$

$$\ddot{r}_P = \ddot{r}_2 = (-r_2 \ddot{\theta}_2 \sin \theta_2 - r_2 \dot{\theta}_2^2 \cos \theta_2) \mathbf{i} + (r_2 \ddot{\theta}_2 \cos \theta_2 - r_2 \dot{\theta}_2^2 \sin \theta_2) \mathbf{j}$$

$$\ddot{r}_Q = \ddot{r}_1 = (\ddot{r}_1 \cos \theta_1) \mathbf{i} + (\ddot{r}_1 \sin \theta_1) \mathbf{j}$$


---

### 5.8.3 Solution When $r_3$ Is Known

When  $r_3$  is known, we must solve Eqs. (5.136) and (5.137) for  $\theta_2$  and  $r_1$ . The solution is almost identical to that for the case in which  $r_1$  is known. We need only switch the indices for 1 and 3, and the results are otherwise the same. This is indicated in Table 5.13. This case is also included in a MATLAB routine on the disk with this book.

**EXAMPLE 5.8**  
**Kinematic**  
**Analysis of**  
**a Scotch Yoke**

**Solution**

In the Scotch yoke mechanism shown in Fig. 5.37, the angular velocity of link 2 relative to the frame is 1 rad/s CCW (constant) when the angle  $\theta_2$  is  $60^\circ$ . Also, the length  $OP = 2$  in. Determine the velocity and acceleration of link 4.

Using the nomenclature developed earlier, we can draw the basic vector closure diagram as shown in Fig. 3.38. From Figs. 5.37 and 5.38, the following geometry quantities can be determined:

$$\begin{aligned} r_2 &= 2 \\ \theta_1 &= 0^\circ, & \theta_2 &= 60^\circ, & \beta &= 90^\circ, & \theta_3 &= 90^\circ \\ \dot{\theta}_2 &= 1, & \ddot{\theta}_2 &= 0 \end{aligned}$$

Because the crank (link 2) is the driving link, we can use the equations in Table 5.12 to solve the problem. The geometric unknowns are  $r_1$  and  $r_3$ . To determine  $r_1$  and  $r_3$ , solve

$$\begin{bmatrix} \cos \theta_1 & \cos \theta_3 \\ \sin \theta_1 & \sin \theta_3 \end{bmatrix} \begin{Bmatrix} r_1 \\ r_3 \end{Bmatrix} = \begin{Bmatrix} r_2 \cos \theta_2 \\ r_2 \sin \theta_2 \end{Bmatrix}$$

or

$$\begin{bmatrix} 1 & 0 \\ 0 & 1 \end{bmatrix} \begin{Bmatrix} r_1 \\ r_3 \end{Bmatrix} = \begin{Bmatrix} r_2 \cos \theta_2 \\ r_2 \sin \theta_2 \end{Bmatrix}$$

Then

$$r_1 = r_2 \cos \theta_2$$

and

$$r_3 = r_2 \sin \theta_2$$

Notice that the motion of the slider is a sinusoidal function of the input rotation. This is one of the benefits of the Scotch yoke and is one of the reasons that it is used. For the given input values ( $r_2 = 2$  and  $\theta_2 = 60^\circ$ ) it is clear that  $r_1 = 1.0$  and  $r_3 = 1.732$ .

For the velocities, the unknowns are  $\dot{r}_1$  and  $\dot{r}_3$ . These can be determined from the matrix equation

$$\begin{bmatrix} \cos \theta_1 & \cos \theta_3 \\ \sin \theta_1 & \sin \theta_3 \end{bmatrix} \begin{Bmatrix} \dot{r}_1 \\ \dot{r}_3 \end{Bmatrix} = \begin{Bmatrix} -r_2 \dot{\theta}_2 \sin \theta_2 \\ r_2 \dot{\theta}_2 \cos \theta_2 \end{Bmatrix}$$

or

$$\begin{bmatrix} 1 & 0 \\ 0 & 1 \end{bmatrix} \begin{Bmatrix} \dot{r}_1 \\ \dot{r}_3 \end{Bmatrix} = \begin{Bmatrix} -2(1) \sin 60^\circ \\ 2(1) \cos 60^\circ \end{Bmatrix} = \begin{Bmatrix} -1.732 \\ 1 \end{Bmatrix}$$

or

$$\dot{r}_1 = -1.732 \text{ in/s}$$

and

$$\dot{r}_3 = 1 \text{ in/s}$$

The negative sign means that  $r_1$  is decreasing in length with increasing time.

For the accelerations, the unknowns are  $\ddot{r}_1$  and  $\ddot{r}_3$ . These can be determined by solving

$$\begin{bmatrix} \cos \theta_1 & \cos \theta_3 \\ \sin \theta_1 & \sin \theta_3 \end{bmatrix} \begin{Bmatrix} \ddot{r}_1 \\ \ddot{r}_3 \end{Bmatrix} = \begin{Bmatrix} -r_2 \ddot{\theta}_2 \sin \theta_2 - r_2 \dot{\theta}_2^2 \cos \theta_2 \\ r_2 \ddot{\theta}_2 \cos \theta_2 - r_2 \dot{\theta}_2^2 \sin \theta_2 \end{Bmatrix}$$

Substituting into the equation the known values, we get

$$\begin{bmatrix} 1 & 0 \\ 0 & 1 \end{bmatrix} \begin{Bmatrix} \ddot{r}_1 \\ \ddot{r}_3 \end{Bmatrix} = \begin{Bmatrix} 0 - 2(1)^2 \cos 60^\circ \\ 0 - 2(1)^2 \sin 60^\circ \end{Bmatrix} = \begin{Bmatrix} -1 \\ -1.732 \end{Bmatrix}$$

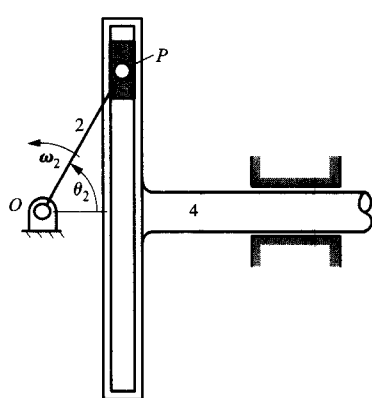


FIGURE 5.37 Scotch yoke mechanism.

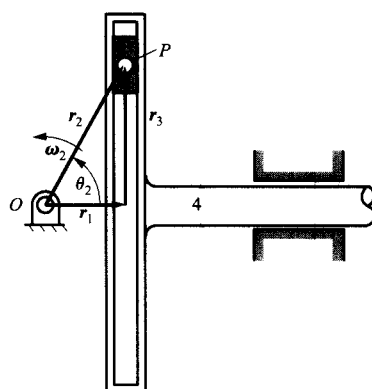


FIGURE 5.38 Vector diagram for Scotch yoke mechanism.

or

$$\ddot{r}_1 = -1 \text{ in/s}^2$$

and

$$\ddot{r}_3 = -1.732 \text{ in/s}^2$$

## 5.9 ANALYTICAL EQUATIONS FOR ELLIPTIC TRAMMEL

The elliptic trammel is an inversion of the RRPP mechanism, and a schematic drawing of this mechanism is shown in Fig. 5.39. In the mechanism, links 2 and 4 are connected to the frame by prismatic joints and to the coupler by revolute joints. A significant feature of this mechanism is that coupler points trace ellipses on the frame, and it is used in machine tools for this purpose.

To analyze the mechanism using vector closure equations, we must again align vectors in the directions of the slider motions as shown in Fig. 5.40. As in the case of the RRPP mechanism, only three vectors are required to model the motion. Vector  $r_1$  is fixed at an

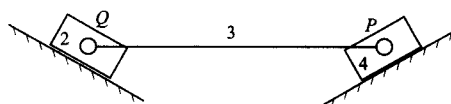


FIGURE 5.39 Schematic diagram of elliptic trammel.

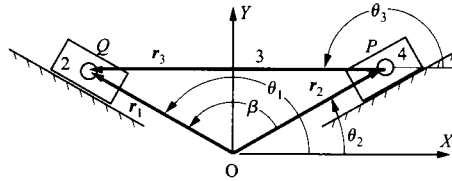


FIGURE 5.40 Vector closure diagram for elliptic trammel mechanism.

angle  $\theta_1$  and of variable length. This vector begins at point  $O$  and ends at point  $Q$ , where  $O$  is the intersection of a line through  $Q$  and in the direction of the velocity of link 2 relative to link 1 and a second line through  $P$  in the direction of the velocity of link 4 relative to link 1. Point  $O$  is the origin of the frame coordinate system. The two lines intersect at an angle  $\beta$ , measured from  $r_2$  to  $r_1$ . Vector  $r_2$  is fixed at an angle  $\theta_2$  and of variable length. Vector  $r_3$  is measured from point  $P$  to point  $Q$ .

As shown in Fig. 5.40, to develop the closure equations, locate point  $Q$  with vector  $r_1$  and with vectors  $r_2 + r_3$ . Then the vector closure equation is

$$r_Q = r_1 = r_2 + r_3 \quad (5.139)$$

or

$$r_1(\cos \theta_1 i + \sin \theta_1 j) = r_2(\cos \theta_2 i + \sin \theta_2 j) + r_3(\cos \theta_3 i + \sin \theta_3 j) \quad (5.140)$$

Rewriting the components in Eq. (5.139) as separate equations gives

$$r_1 \cos \theta_1 = r_2 \cos \theta_2 + r_3 \cos \theta_3 \quad (5.141)$$

$$r_1 \sin \theta_1 = r_2 \sin \theta_2 + r_3 \sin \theta_3 \quad (5.142)$$

Equations (5.141) and (5.142) must be satisfied throughout the motion of the linkage. As in the case of the RRPP mechanism, there are six quantities to identify:  $r_1$  and  $\theta_1$ ,  $r_2$  and  $\theta_2$ , and  $r_3$  and  $\theta_3$ . From the diagram in Fig. 5.40, the following are constants:  $\theta_1$ ,  $r_3$ , and  $\theta_2$ . Furthermore, we know that

$$\theta_1 = \theta_2 + \beta \quad (5.143)$$

where  $\beta$  is a constant.

The variables are  $r_1$ ,  $\theta_3$ , and  $r_2$ . For a one-degree-of-freedom mechanism, one of the variables must be an input (i.e., known) variable. Therefore, there are a total of two unknowns, and we can solve for them using the two equations (5.141) and (5.142) involving the unknowns. Once all of the position variables are obtained, the unknown velocities and accelerations can be found by differentiating Eqs. (5.141) and (5.142) and solving the resulting set of linear equations for the unknowns.

Before solving the equations for the unknowns it is necessary to select an input variable from  $r_1$ ,  $\theta_3$ , and  $r_2$ . Because of the symmetry of the mechanism, choosing  $r_1$  or  $r_2$  will give a similar set of equations. That is, if we establish the input-output relationships for  $r_1$  as the input, we can derive the relationships for  $r_2$  as the input by simply interchanging the subscripts 1 and 2 in the relationships derived for  $r_1$  as the driver. Therefore, we need to consider only the cases for  $\theta_3$  and  $r_1$  as input variables.

### 5.9.1 Analysis When $\theta_3$ Is Known

The analytical solution procedure follows the same major steps as were followed in the case of the RRPP mechanism. When  $\theta_3$  is an input, Eqs. (5.141) and (5.142) become linear in the unknowns  $r_1$  and  $r_2$ , and the equations for position, velocity, and acceleration can be solved easily. The resulting equations are summarized in Table 5.14.

**TABLE 5.14 Summary of Position, Velocity, and Acceleration Equations for an Elliptic Trammel Mechanism When  $\theta_3$  Is the Input Variable. The Link Numbers and Points Are Defined in Fig. 5.40**

---

**Position**


---

$$\theta_1 = \theta_2 + \beta$$

$$\begin{bmatrix} \cos \theta_1 & -\cos \theta_2 \\ \sin \theta_1 & -\sin \theta_2 \end{bmatrix} \begin{Bmatrix} r_1 \\ r_2 \end{Bmatrix} = \begin{Bmatrix} r_3 \cos \theta_3 \\ r_3 \sin \theta_3 \end{Bmatrix}$$

$$r_P = r_2 = (r_2 \cos \theta_2)\mathbf{i} + (r_2 \sin \theta_2)\mathbf{j}$$

$$r_Q = r_1 = (r_1 \cos \theta_1)\mathbf{i} + (r_1 \sin \theta_1)\mathbf{j}$$

---

**Velocity**


---

$$\begin{bmatrix} \cos \theta_1 & -\cos \theta_2 \\ \sin \theta_1 & -\sin \theta_2 \end{bmatrix} \begin{Bmatrix} \dot{r}_1 \\ \dot{r}_2 \end{Bmatrix} = \begin{Bmatrix} -r_3 \dot{\theta}_3 \sin \theta_3 \\ r_3 \dot{\theta}_3 \cos \theta_3 \end{Bmatrix}$$

$$\dot{r}_P = \dot{r}_2 = (\dot{r}_2 \cos \theta_2)\mathbf{i} + (\dot{r}_2 \sin \theta_2)\mathbf{j}$$

$$\dot{r}_Q = \dot{r}_1 = (\dot{r}_1 \cos \theta_1)\mathbf{i} + (\dot{r}_1 \sin \theta_1)\mathbf{j}$$

---

**Acceleration**


---

$$\begin{bmatrix} \cos \theta_1 & -\cos \theta_2 \\ \sin \theta_1 & -\sin \theta_2 \end{bmatrix} \begin{Bmatrix} \ddot{r}_1 \\ \ddot{r}_2 \end{Bmatrix} = \begin{Bmatrix} -r_3 \ddot{\theta}_3 \sin \theta_3 - r_3 \dot{\theta}_3^2 \cos \theta_3 \\ r_3 \ddot{\theta}_3 \cos \theta_3 - r_3 \dot{\theta}_3^2 \sin \theta_3 \end{Bmatrix}$$

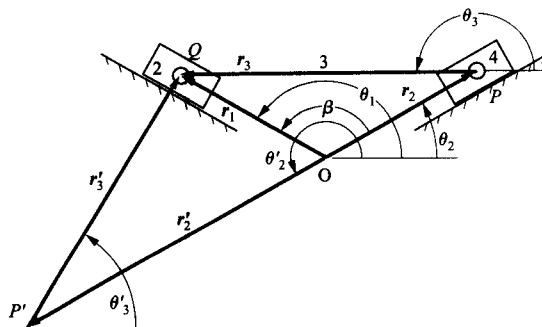
$$\ddot{r}_P = \ddot{r}_2 = (\ddot{r}_2 \cos \theta_2)\mathbf{i} + (\ddot{r}_2 \sin \theta_2)\mathbf{j}$$

$$\ddot{r}_Q = \ddot{r}_1 = (\ddot{r}_1 \cos \theta_1)\mathbf{i} + (\ddot{r}_1 \sin \theta_1)\mathbf{j}$$


---

### 5.9.2 Analysis When $r_1$ Is Known

When  $r_1$  is known, we must determine  $\theta_3$  and  $r_2$ . Two solutions result corresponding to the assembly modes shown in Fig. 5.41. It is also possible to specify values for  $r_1$  for which the mechanism cannot be assembled. The analytical form of the velocity and acceleration



**FIGURE 5.41** Two configurations possible for elliptic trammel when  $r_1$  is input.

equations can be developed by differentiating the position equations and solving the resulting linear equations for the unknowns. The results for  $r_1$  as the input are summarized in Table 5.15.

**TABLE 5.15 Summary of Position, Velocity, and Acceleration Equations for an Elliptic Trammel Mechanism When  $r_1$  Is the Input. The Link Numbers and Points Are Defined in Fig. 5.40**

---

**Position**

---

$$\theta_1 = \theta_2 + \beta$$

$$B = -r_1(\cos \theta_1 \cos \theta_2 + \sin \theta_1 \sin \theta_2)$$

$$C = (r_1^2 - r_3^2)$$

$$r_2 = -B + \sigma \sqrt{B^2 - C}$$

$$\theta_3 = \tan^{-1} \frac{r_1 \sin \theta_1 - r_2 \sin \theta_2}{r_1 \cos \theta_1 - r_2 \cos \theta_2}$$

$$\mathbf{r}_P = \mathbf{r}_2 = (r_2 \cos \theta_2)\mathbf{i} + (r_2 \sin \theta_2)\mathbf{j}$$

$$\mathbf{r}_Q = \mathbf{r}_1 = (r_1 \cos \theta_1)\mathbf{i} + (r_1 \sin \theta_1)\mathbf{j}$$

---

**Velocity**

---

$$\begin{bmatrix} \cos \theta_2 & -r_3 \sin \theta_3 \\ \sin \theta_2 & r_3 \cos \theta_3 \end{bmatrix} \begin{Bmatrix} \dot{r}_2 \\ \dot{\theta}_3 \end{Bmatrix} = \begin{Bmatrix} \dot{r}_1 \cos \theta_1 \\ \dot{r}_1 \sin \theta_1 \end{Bmatrix}$$

$$\dot{\mathbf{r}}_P = \dot{\mathbf{r}}_2 = (\dot{r}_2 \cos \theta_2)\mathbf{i} + (\dot{r}_2 \sin \theta_2)\mathbf{j}$$

$$\dot{\mathbf{r}}_Q = \dot{\mathbf{r}}_1 = (\dot{r}_1 \cos \theta_1)\mathbf{i} + (\dot{r}_1 \sin \theta_1)\mathbf{j}$$

---

**Acceleration**

---

$$\begin{bmatrix} \cos \theta_2 & -r_3 \sin \theta_3 \\ \sin \theta_2 & r_3 \cos \theta_3 \end{bmatrix} \begin{Bmatrix} \ddot{r}_2 \\ \ddot{\theta}_3 \end{Bmatrix} = \begin{Bmatrix} \ddot{r}_1 \cos \theta_1 + r_3 \dot{\theta}_3^2 \cos \theta_3 \\ \ddot{r}_1 \sin \theta_1 + r_3 \dot{\theta}_3^2 \sin \theta_3 \end{Bmatrix}$$

$$\ddot{\mathbf{r}}_P = \ddot{\mathbf{r}}_2 = (\ddot{r}_2 \cos \theta_2)\mathbf{i} + (\ddot{r}_2 \sin \theta_2)\mathbf{j}$$

$$\ddot{\mathbf{r}}_Q = \ddot{\mathbf{r}}_1 = (\ddot{r}_1 \cos \theta_1)\mathbf{i} + (\ddot{r}_1 \sin \theta_1)\mathbf{j}$$


---

**EXAMPLE 5.9**  
**Kinematic**  
**Analysis of an**  
**Elliptic Trammel**

**Solution**

In the elliptic trammel mechanism shown in Fig. 5.42a, the angular velocity of link 3 relative to the frame is 10 rad/s CCW (constant). Also, the length  $QP = 10$  cm and  $QR$  is 20 cm. Determine the position of point  $R$  and the velocity and acceleration of point  $P$  for a full rotation of the coupler.

Using the nomenclature developed earlier, the basic vector closure diagram for the linkage is as shown in Fig. 5.42a. From Figs. 5.41 and 5.42, the following geometric quantities can be determined:

$$\begin{aligned} r_3 &= 10 \\ \theta_1 &= 90^\circ, & \theta_2 &= 0^\circ, & \beta &= 90^\circ \\ \dot{\theta}_3 &= 10, & \ddot{\theta}_3 &= 0 \end{aligned}$$

Because we are interested in the behavior of the mechanism for its full range of motion, we must solve the position, velocity, and acceleration equations in terms of  $\theta_3$ . The vector diagram establishing the quantities involved is shown in Fig. 5.42b.

The position of  $R_3$  is given by

$$\mathbf{r}_{R_3} = \mathbf{r}_1 + \mathbf{r}_4$$

or, in component form,

$$\mathbf{r}_{R_3} = (r_1 \cos \theta_1 + r_4 \cos \theta_4)\mathbf{i} + (r_1 \sin \theta_1 + r_4 \sin \theta_4)\mathbf{j} \quad (5.144)$$

From Fig. 5.42b,  $\theta_4 = \theta_3 + \pi$ . Therefore, Eq. (5.144) becomes

$$\mathbf{r}_{R_3} = (r_1 \cos \theta_1 - r_4 \cos \theta_3)\mathbf{i} + (r_1 \sin \theta_1 - r_4 \sin \theta_3)\mathbf{j} \quad (5.145)$$

To solve for the position, velocity, and acceleration of  $P_3$ , we must determine the corresponding values for  $r_1$ . From Table 5.14, the equations to be solved are

$$\begin{bmatrix} 0 & -1 \\ 1 & 0 \end{bmatrix} \begin{Bmatrix} r_1 \\ r_2 \end{Bmatrix} = \begin{Bmatrix} r_3 \cos \theta_3 \\ r_3 \sin \theta_3 \end{Bmatrix} \quad (5.146)$$

$$\begin{bmatrix} 0 & -1 \\ 1 & 0 \end{bmatrix} \begin{Bmatrix} \dot{r}_1 \\ \dot{r}_2 \end{Bmatrix} = \begin{Bmatrix} -r_3 \dot{\theta}_3 \sin \theta_3 \\ r_3 \dot{\theta}_3 \cos \theta_3 \end{Bmatrix} \quad (5.147)$$

and

$$\begin{bmatrix} 0 & -1 \\ 1 & 0 \end{bmatrix} \begin{Bmatrix} \ddot{r}_1 \\ \ddot{r}_2 \end{Bmatrix} = \begin{Bmatrix} -r_3 \ddot{\theta}_3 \sin \theta_3 - r_3 \dot{\theta}_3^2 \cos \theta_3 \\ r_3 \ddot{\theta}_3 \cos \theta_3 - r_3 \dot{\theta}_3^2 \sin \theta_3 \end{Bmatrix} \quad (5.148)$$

From Eqs. (5.146)–(5.148),

$$r_1 = r_3 \sin \theta_3 \quad (5.149)$$

$$\dot{r}_1 = r_3 \dot{\theta}_3 \cos \theta_3 \quad (5.150)$$

and

$$\ddot{r}_1 = r_3 \ddot{\theta}_3 \cos \theta_3 - r_3 \dot{\theta}_3^2 \sin \theta_3 \quad (5.151)$$

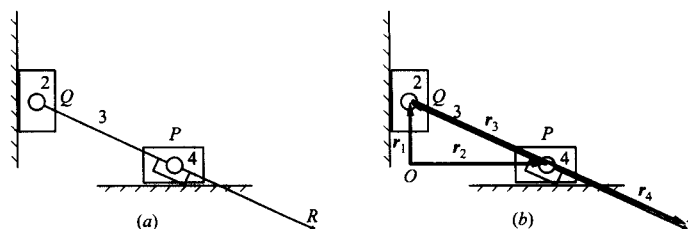


FIGURE 5.42 Elliptic trammel mechanism (a) and vector diagram (b) for Example 5.9.

Equations (5.149)–(5.151) can be combined with Eq. (5.145) to solve for the position of  $R_3$  and for the velocity and acceleration of  $P_3$  as a function of  $\theta_3$ . The equations can be computed easily, and the results are plotted in Fig. 5.43. The MATLAB program used to generate the curves is included on the disk with this book. Notice that the path of  $R_3$  is an ellipse.

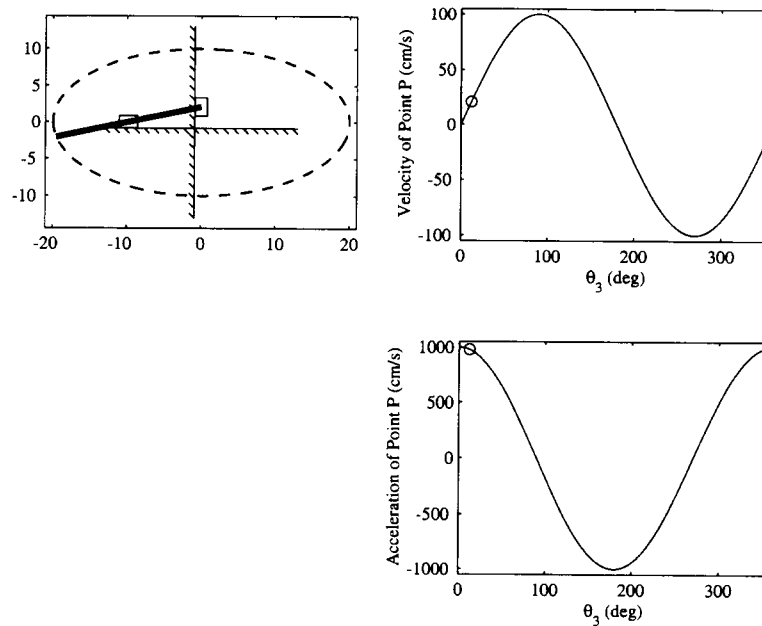


FIGURE 5.43 Results for Example 5.9.

## 5.10 ANALYTICAL EQUATIONS FOR THE OLDHAM MECHANISM

The Oldham (RPPR) mechanism is another inversion of the RRPP mechanism, and a schematic drawing of this mechanism is shown in Fig. 5.44. In the mechanism, links 2 and 4 are connected to the frame by revolute joints and to the coupler by prismatic joints. Therefore, the angle  $\beta$  between links 2 and 4 is fixed.

To analyze the mechanism using vector closure equations, we must again align vectors in the directions of the slider motions as shown in Fig. 5.45. As in the case of the elliptic trammel, only three vectors are required to model the motion. Vector  $r_1$  is fixed at an angle  $\theta_1$  and of constant length. Point  $O$  is the origin of the frame coordinate system. Links

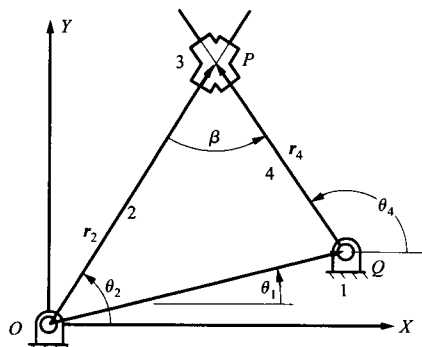


FIGURE 5.44 Schematic diagram of Oldham mechanism.



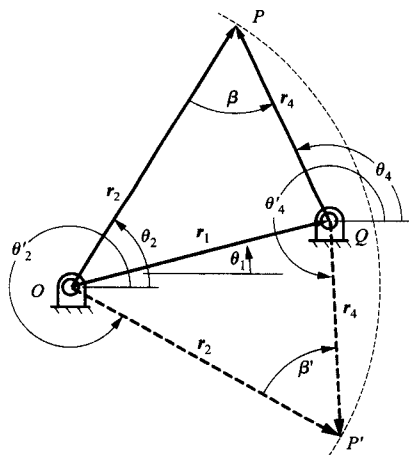


FIGURE 5.45 Two assembly modes for Oldham mechanism when  $r_2$  is the input variable.

2 and 4 intersect at an angle  $\beta$ , where  $\beta$  is measured from  $r_2$  to  $r_4$ . Vector  $r_2$  is at an angle  $\theta_2$  with respect to a horizontal line and is of variable length. Vector  $r_4$  is at an angle  $\theta_4$  with respect to a horizontal line and of variable length.

As shown in Fig. 5.44, to develop the closure equations, locate point  $P$  with vector  $r_2$  and with vectors  $r_1 + r_4$ . Then the vector closure equation is

$$\mathbf{r}_P = \mathbf{r}_2 = \mathbf{r}_1 + \mathbf{r}_4 \quad (5.152)$$

or

$$r_2 (\cos \theta_2 \mathbf{i} + \sin \theta_2 \mathbf{j}) = r_1 (\cos \theta_1 \mathbf{i} + \sin \theta_1 \mathbf{j}) + r_4 (\cos \theta_4 \mathbf{i} + \sin \theta_4 \mathbf{j}) \quad (5.153)$$

Rewriting the components in Eq. (5.153) as separate equations gives

$$r_2 \cos \theta_2 = r_1 \cos \theta_1 + r_4 \cos \theta_4 \quad (5.154)$$

$$r_2 \sin \theta_2 = r_1 \sin \theta_1 + r_4 \sin \theta_4 \quad (5.155)$$

As was the case for the other RRPP mechanisms, there are six quantities to identify:  $r_1$  and  $\theta_1$ ,  $r_2$  and  $\theta_2$ , and  $r_4$  and  $\theta_4$ . From Fig. 5.44,  $\theta_1$ , and  $r_1$  are constants. Furthermore, we know that

$$\theta_4 = \theta_2 + \beta \quad (5.156)$$

where  $\beta$  is a constant.

The variables are  $\theta_2$ ,  $\theta_4$ ,  $r_2$ , and  $r_4$ . For a one-degree-of-freedom mechanism, one of the variables must be an input (i.e., known) variable, and there are three unknowns. We can solve for them using the three equations (5.154)–(5.156) involving the unknowns. Once all of the position variables are obtained, the unknown velocities and accelerations can be found by differentiating Eqs. (5.154)–(5.156) and solving the resulting set of linear equations for the unknowns.

Before solving the equations for the unknowns, it is necessary to select an input variable from among  $r_2$ ,  $r_4$ ,  $\theta_2$ , and  $\theta_4$ . The equations will be similar when either  $r_2$  or  $r_4$  is selected, and when either  $\theta_2$  and  $\theta_4$  are selected. Therefore, we will consider only the two cases when  $r_2$  is a variable and when  $\theta_2$  is a variable.

### 5.10.1 Analysis When $\theta_2$ Is Known

When  $\theta_2$  is the input variable, Eqs. (5.154) and (5.155) become linear in the unknowns  $r_2$  and  $r_4$ , and the equations for position, velocity, and acceleration can be easily solved. The resulting equations are summarized in Table 5.16. The equations can be programmed easily,

**TABLE 5.16 Summary of Position, Velocity, and Acceleration Equations for an Oldham Mechanism When  $\theta_2$  Is the Input Variable. The Link Numbers and Points Are Defined in Fig. 5.44**

---

**Position**


---

$$\theta_4 = \theta_2 + \beta$$

$$\begin{bmatrix} \cos \theta_2 & -\cos \theta_4 \\ \sin \theta_2 & -\sin \theta_4 \end{bmatrix} \begin{Bmatrix} r_2 \\ r_4 \end{Bmatrix} = \begin{Bmatrix} r_1 \cos \theta_1 \\ r_1 \sin \theta_1 \end{Bmatrix}$$

$$\mathbf{r}_P = \mathbf{r}_2 = (r_2 \cos \theta_2)\mathbf{i} + (r_2 \sin \theta_2)\mathbf{j}$$

$$\mathbf{r}_Q = \mathbf{r}_1 = (r_1 \cos \theta_1)\mathbf{i} + (r_1 \sin \theta_1)\mathbf{j}$$

---

**Velocity**


---

$$\dot{\theta}_4 = \dot{\theta}_2$$

$$\begin{bmatrix} \cos \theta_2 & -\cos \theta_4 \\ \sin \theta_2 & -\sin \theta_4 \end{bmatrix} \begin{Bmatrix} \dot{r}_2 \\ \dot{r}_4 \end{Bmatrix} = \begin{Bmatrix} r_2 \dot{\theta}_2 \sin \theta_2 - r_4 \dot{\theta}_2 \sin \theta_4 \\ -r_2 \dot{\theta}_2 \cos \theta_2 + r_4 \dot{\theta}_2 \cos \theta_4 \end{Bmatrix}$$

$$\dot{\mathbf{r}}_{P_2} = (-r_2 \dot{\theta}_2 \sin \theta_2)\mathbf{i} + (r_2 \dot{\theta}_2 \cos \theta_2)\mathbf{j}$$

$$\dot{\mathbf{r}}_{P_3} = (\dot{r}_2 \cos \theta_2 - r_2 \dot{\theta}_2 \sin \theta_2)\mathbf{i} + (\dot{r}_2 \sin \theta_2 + r_2 \dot{\theta}_2 \cos \theta_2)\mathbf{j}$$

---

**Acceleration**


---

$$\ddot{\theta}_4 = \ddot{\theta}_2$$

$$\begin{bmatrix} \cos \theta_2 & -\cos \theta_4 \\ \sin \theta_2 & -\sin \theta_4 \end{bmatrix} \begin{Bmatrix} \ddot{r}_2 \\ \ddot{r}_4 \end{Bmatrix} = \begin{Bmatrix} (r_2 \ddot{\theta}_2 + 2\dot{r}_2 \dot{\theta}_2) \sin \theta_2 - (r_4 \ddot{\theta}_2 + 2\dot{r}_4 \dot{\theta}_2) \sin \theta_4 + r_2 \dot{\theta}_2^2 \cos \theta_2 - r_4 \dot{\theta}_2^2 \cos \theta_4 \\ -(r_2 \ddot{\theta}_2 + 2\dot{r}_2 \dot{\theta}_2) \cos \theta_2 + (r_4 \ddot{\theta}_2 + 2\dot{r}_4 \dot{\theta}_2) \cos \theta_4 + r_2 \dot{\theta}_2^2 \sin \theta_2 - r_4 \dot{\theta}_2^2 \sin \theta_4 \end{Bmatrix}$$

$$\ddot{\mathbf{r}}_{P_2} = (-r_2 \ddot{\theta}_2 \sin \theta_2 - r_2 \dot{\theta}_2^2 \cos \theta_2)\mathbf{i} + (r_2 \ddot{\theta}_2 \cos \theta_2 - r_2 \dot{\theta}_2^2 \sin \theta_2)\mathbf{j}$$

$$\begin{aligned} \ddot{\mathbf{r}}_{P_3} = & (\ddot{r}_2 \cos \theta_2 - 2\dot{r}_2 \dot{\theta}_2 \sin \theta_2 - r_2 \ddot{\theta}_2 \sin \theta_2 - r_2 \dot{\theta}_2^2 \cos \theta_2)\mathbf{i} \\ & + (\ddot{r}_2 \sin \theta_2 + 2\dot{r}_2 \dot{\theta}_2 \cos \theta_2 + r_2 \ddot{\theta}_2 \cos \theta_2 - r_2 \dot{\theta}_2^2 \sin \theta_2)\mathbf{j} \end{aligned}$$


---

and a MATLAB program for analyzing the mechanism when  $\theta_2$  is the driver is included on the disk with this book.

### 5.10.2 Analysis When $r_2$ Is Known

When  $r_2$  is known, we must determine  $\theta_2$ ,  $\theta_4$  and  $r_4$ , and the equations required for the analysis are given in Table 5.17. Two solutions corresponding to the assembly modes shown

**TABLE 5.17 Summary of Position, Velocity, and Acceleration Equations for an Oldham Mechanism When  $r_2$  is the Input Variable. The Link Numbers and Points Are Defined in Fig. 5.44**

---

**Position**


---

$$r_4 = r_2 \cos \beta + \sigma \sqrt{r_2^2 (\cos^2 \beta - 1) + r_1^2}; \quad \sigma = \pm 1$$

$$A = r_1 \sin \theta_1 - r_4 \sin \beta$$

$$B = -2(r_2 - r_4 \cos \beta)$$

$$C = r_4 \sin \beta + r_1 \sin \theta_1$$

$$\theta_2 = 2 \tan^{-1} \left[ \frac{-B + \gamma \sqrt{B^2 - C^2 + A^2}}{(C - A)} \right]; \quad \gamma = +1 \text{ or } -1; \text{ valid value satisfies Eq. (5.153)}$$

$$\theta_4 = \theta_2 + \beta$$

$$\mathbf{r}_P = r_2 = (r_2 \cos \theta_2)\mathbf{i} + (r_2 \sin \theta_2)\mathbf{j}$$

$$\mathbf{r}_Q = r_1 = (r_1 \cos \theta_1)\mathbf{i} + (r_1 \sin \theta_1)\mathbf{j}$$

---

**Velocity**


---

$$\dot{\theta}_4 = \dot{\theta}_2$$

$$\begin{bmatrix} -r_2 \sin \theta_2 + r_4 \sin \theta_4 & -\cos \theta_4 \\ r_2 \cos \theta_2 - r_4 \cos \theta_4 & -\sin \theta_4 \end{bmatrix} \begin{Bmatrix} \dot{\theta}_2 \\ \dot{r}_4 \end{Bmatrix} = \begin{Bmatrix} -\dot{r}_2 \cos \theta_2 \\ -\dot{r}_2 \sin \theta_2 \end{Bmatrix}$$

$$\dot{\mathbf{r}}_{P_2} = (-r_2 \dot{\theta}_2 \sin \theta_2)\mathbf{i} + (r_2 \dot{\theta}_2 \cos \theta_2)\mathbf{j}$$

$$\dot{\mathbf{r}}_{P_3} = (\dot{r}_2 \cos \theta_2 - r_2 \dot{\theta}_2 \sin \theta_2)\mathbf{i} + (\dot{r}_2 \sin \theta_2 + r_2 \dot{\theta}_2 \cos \theta_2)\mathbf{j}$$

---

**Acceleration**


---

$$\ddot{\theta}_4 = \ddot{\theta}_2$$

$$\begin{bmatrix} -r_2 \sin \theta_2 + r_4 \sin \theta_4 & -\cos \theta_4 \\ r_2 \cos \theta_2 - r_4 \cos \theta_4 & -\sin \theta_4 \end{bmatrix} \begin{Bmatrix} \ddot{\theta}_2 \\ \ddot{r}_4 \end{Bmatrix} = \begin{Bmatrix} 2\dot{r}_2 \dot{\theta}_2 \sin \theta_2 - 2\dot{r}_4 \dot{\theta}_2 \sin \theta_4 + r_2 \dot{\theta}_2^2 \cos \theta_2 - \ddot{r}_2 \cos \theta_2 - r_4 \dot{\theta}_2^2 \cos \theta_4 \\ -2\dot{r}_2 \dot{\theta}_2 \cos \theta_2 + 2\dot{r}_4 \dot{\theta}_2 \cos \theta_4 + r_2 \dot{\theta}_2^2 \sin \theta_2 - \ddot{r}_2 \sin \theta_2 - r_4 \dot{\theta}_2^2 \sin \theta_4 \end{Bmatrix}$$

$$\ddot{\mathbf{r}}_{P_2} = (-r_2 \ddot{\theta}_2 \sin \theta_2 - r_2 \dot{\theta}_2^2 \cos \theta_2)\mathbf{i} + (r_2 \ddot{\theta}_2 \cos \theta_2 + r_2 \dot{\theta}_2^2 \sin \theta_2)\mathbf{j}$$

$$\begin{aligned} \ddot{\mathbf{r}}_{P_3} = & (\ddot{r}_2 \cos \theta_2 - 2\dot{r}_2 \dot{\theta}_2 \sin \theta_2 - r_2 \ddot{\theta}_2 \sin \theta_2 - r_2 \dot{\theta}_2^2 \cos \theta_2)\mathbf{i} \\ & + (\ddot{r}_2 \sin \theta_2 + 2\dot{r}_2 \dot{\theta}_2 \cos \theta_2 + r_2 \ddot{\theta}_2 \cos \theta_2 - r_2 \dot{\theta}_2^2 \sin \theta_2)\mathbf{j} \end{aligned}$$


---

in Fig. 5.45 result. Note that in one assembly mode,  $\beta$  is positive, and in the other,  $\beta$  is negative. If the sign of  $\beta$  must be positive, the solution corresponding to a minus angle would be discarded. The value of  $\gamma$  that is valid is the one satisfying Eqs. (5.154) and (5.155). It is also possible to specify values for  $r_2$  for which the mechanism cannot be assembled. The analytical form of the velocity and acceleration equations can be developed by differentiating the position equations and solving the resulting linear equations for the unknowns. Again, the equations can be easily programmed, and a MATLAB program for analyzing the mechanism when  $r_2$  is the driver is included on the disk with this book.

**EXAMPLE 5.10**  
**Kinematic**  
**Analysis of**  
**the Oldham**  
**Mechanism**

**Solution**

In the Oldham mechanism shown in Fig. 5.46a, the angular velocity of link 2 relative to the frame is 10 rad/s CCW and the angular acceleration is 100 rad/s<sup>2</sup> CCW. Also, the length  $OQ = 10$  cm and the angle  $\beta$  is 45°. Determine the position of point  $P$  and the velocity and acceleration of points  $P_2$  and  $P_3$  in the position given.

Using the nomenclature developed earlier, we can draw the basic vector closure diagram for the linkage shown in Fig. 5.46b. From Fig. 5.46, the following geometry quantities can be determined:

$$\theta_1 = 0^\circ, \quad \theta_2 = 60^\circ, \quad \theta_4 = 105^\circ$$

$$r_1 = 10 \text{ cm}$$

To perform the analysis, we can use the equations in Table 5.16. For the position analysis, we need to solve

$$\begin{bmatrix} \cos \theta_2 & -\cos \theta_4 \\ \sin \theta_2 & -\sin \theta_4 \end{bmatrix} \begin{Bmatrix} r_2 \\ r_4 \end{Bmatrix} = \begin{Bmatrix} r_1 \cos \theta_1 \\ r_1 \sin \theta_1 \end{Bmatrix} \quad \text{or} \quad \begin{bmatrix} \cos(60^\circ) & -\cos(105^\circ) \\ \sin(60^\circ) & -\sin(105^\circ) \end{bmatrix} \begin{Bmatrix} r_2 \\ r_4 \end{Bmatrix} = \begin{Bmatrix} 10 \cos 0^\circ \\ 10 \sin 0^\circ \end{Bmatrix}$$

or

$$\begin{bmatrix} 0.500 & 0.2588 \\ 0.8660 & -0.9659 \end{bmatrix} \begin{Bmatrix} r_2 \\ r_4 \end{Bmatrix} = \begin{Bmatrix} 10 \\ 0 \end{Bmatrix} \Rightarrow \begin{Bmatrix} r_2 \\ r_4 \end{Bmatrix} = \begin{Bmatrix} 13.6603 \\ 12.2474 \end{Bmatrix}$$

The positions of  $P$  and  $Q$  are given by

$$\mathbf{r}_P = (r_2 \cos \theta_2)\mathbf{i} + (r_2 \sin \theta_2)\mathbf{j} = 6.8301\mathbf{i} + 11.8301\mathbf{j}$$

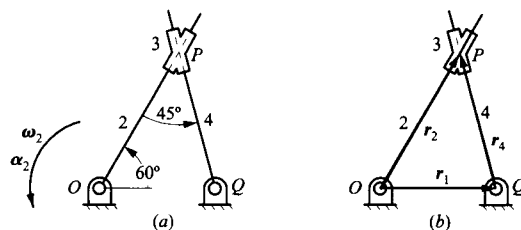
and

$$\mathbf{r}_Q = (r_1 \cos \theta_1)\mathbf{i} + (r_1 \sin \theta_1)\mathbf{j} = 10\mathbf{i}$$

For the velocity analysis, solve

$$\begin{bmatrix} \cos \theta_2 & -\cos \theta_4 \\ \sin \theta_2 & -\sin \theta_4 \end{bmatrix} \begin{Bmatrix} \dot{r}_2 \\ \dot{r}_4 \end{Bmatrix} = \begin{Bmatrix} r_2 \dot{\theta}_2 \sin \theta_2 - r_4 \dot{\theta}_2 \sin \theta_4 \\ -r_2 \dot{\theta}_2 \cos \theta_2 + r_4 \dot{\theta}_2 \cos \theta_4 \end{Bmatrix} \Rightarrow \begin{bmatrix} 0.500 & 0.2588 \\ 0.8660 & -0.9659 \end{bmatrix} \begin{Bmatrix} \dot{r}_2 \\ \dot{r}_4 \end{Bmatrix} = \begin{Bmatrix} 0 \\ -100 \end{Bmatrix}$$

or



**FIGURE 5.46** Oldham mechanism (a) and vector diagram (b) for Example 5.10.

$$\begin{Bmatrix} \dot{r}_2 \\ \dot{r}_4 \end{Bmatrix} = \begin{Bmatrix} -36.6025 \\ 70.7107 \end{Bmatrix}$$

The velocities of points  $P_2$  and  $P_3$  are

$$\dot{r}_{P_2} = (-r_2 \dot{\theta}_2 \sin \theta_2) \mathbf{i} + (r_2 \dot{\theta}_2 \cos \theta_2) \mathbf{j} = -118.3031 \mathbf{i} + 68.3013 \mathbf{j}$$

and

$$\dot{r}_{P_3} = (\dot{r}_2 \cos \theta_2 - r_2 \dot{\theta}_2 \sin \theta_2) \mathbf{i} + (\dot{r}_2 \sin \theta_2 + r_2 \dot{\theta}_2 \cos \theta_2) \mathbf{j} = -136.6025 \mathbf{i} + 36.6025 \mathbf{j}$$

For the acceleration analysis, solve

$$\begin{bmatrix} \cos \theta_2 & -\cos \theta_4 \\ \sin \theta_2 & -\sin \theta_4 \end{bmatrix} \begin{Bmatrix} \ddot{r}_2 \\ \ddot{r}_4 \end{Bmatrix} = \begin{Bmatrix} (r_2 \ddot{\theta}_2 + 2\dot{r}_2 \dot{\theta}_2) \sin \theta_2 - (r_4 \ddot{\theta}_2 + 2\dot{r}_4 \dot{\theta}_2) \sin \theta_4 + r_2 \dot{\theta}_2^2 \cos \theta_2 - r_4 \dot{\theta}_2^2 \cos \theta_4 \\ -(r_2 \ddot{\theta}_2 + 2\dot{r}_2 \dot{\theta}_2) \cos \theta_2 + (r_4 \ddot{\theta}_2 + 2\dot{r}_4 \dot{\theta}_2) \cos \theta_4 + r_2 \dot{\theta}_2^2 \sin \theta_2 - r_4 \dot{\theta}_2^2 \sin \theta_4 \end{Bmatrix}$$

or

$$\begin{bmatrix} 0.500 & 0.2588 \\ 0.8660 & -0.9659 \end{bmatrix} \begin{Bmatrix} \ddot{r}_2 \\ \ddot{r}_4 \end{Bmatrix} = \begin{Bmatrix} -1000 \\ -1000 \end{Bmatrix}$$

Then,

$$\begin{Bmatrix} \ddot{r}_2 \\ \ddot{r}_4 \end{Bmatrix} = \begin{Bmatrix} -1732.1 \\ -517.6 \end{Bmatrix}$$

Also,

$$\ddot{r}_{P_2} = (-r_2 \ddot{\theta}_2 \sin \theta_2 - r_2 \dot{\theta}_2^2 \cos \theta_2) \mathbf{i} + (r_2 \ddot{\theta}_2 \cos \theta_2 + r_2 \dot{\theta}_2^2 \sin \theta_2) \mathbf{j} = -1866 \mathbf{i} - 500 \mathbf{j}$$

and

$$\begin{aligned} \ddot{r}_{P_3} = & (\ddot{r}_2 \cos \theta_2 - 2\dot{r}_2 \dot{\theta}_2 \sin \theta_2 - r_2 \ddot{\theta}_2 \sin \theta_2 - r_2 \dot{\theta}_2^2 \cos \theta_2) \mathbf{i} \\ & + (\ddot{r}_2 \sin \theta_2 + 2\dot{r}_2 \dot{\theta}_2 \cos \theta_2 + r_2 \ddot{\theta}_2 \cos \theta_2 - r_2 \dot{\theta}_2^2 \sin \theta_2) \mathbf{j} = -2098.1 \mathbf{i} - 2366 \mathbf{j} \end{aligned}$$

## 5.11 CLOSURE OR LOOP-EQUATION APPROACH FOR COMPOUND MECHANISMS

As in the case of simple, single-loop mechanisms, each vector is represented by a length  $r_i$  and an angle  $\theta_i$ . All angles are measured counterclockwise from a fixed line parallel to the  $x$  axis attached to the frame as shown in Fig. 5.47.

To illustrate the method for compound mechanisms, consider the kinematic diagram of the mechanism given in Fig. 5.47. Each member is represented by a directed length and an angle. The formulation of the analytical procedure based on vector loops for compound mechanisms is straightforward, but it requires a system if results are to be meaningful. A procedure will be outlined in the following and illustrated on the mechanism in Fig. 5.47. It will be noted that the procedure presented is a generalization of that used for the single-loop mechanisms. In the mechanism shown, assume that  $\theta_2$ ,  $\omega_2$ , and  $\alpha_2$  are known values.

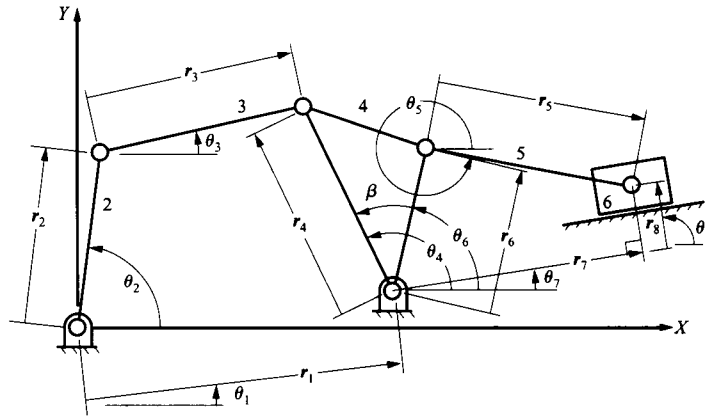


FIGURE 5.47 Example of formulation of solution procedure using vector loops.

### Procedure

1. Draw a kinematic sketch of the mechanism. The sketch need not be to scale; however, it must be sufficiently accurate that the assembly mode can be determined by inspection.
2. Establish a global coordinate system for the mechanism. This will establish the horizontal axis from which all angles will be measured and identify the system from which all global coordinates will be determined.
3. Represent the link between adjacent joints by a vector  $r_i$  defined by a directed line and an angle measured positive CCW from the  $x$  axis (or a line parallel to the  $x$  axis):

$$r_i = r_i \angle \theta_i$$

4. If sliders are involved, locate the slider by two vectors, one in the direction of the relative velocity between the slider and the slide and the second in a direction perpendicular to the direction of the velocity (see  $r_7$  and  $r_8$  in Fig. 5.47).
5. Note which lengths and angles are fixed and which are variable. In the mechanism above,  $r_7$  is the only *variable* length and  $\theta_1$ ,  $\theta_7$ ,  $\theta_8$ , and  $\beta$  are the only *fixed* angles.

If the vectors are properly defined, they will all be expressible as

$$r_i = r_i (\cos \theta_i i + \sin \theta_i j)$$

The cosine term will always go with  $i$  and the sine term will go with  $j$ . Some angles may be functions of others. For example,  $\theta_5 = \theta_4 - \beta$ .

6. Identify all of the joints on the linkage, and be sure that each one is located at the end of one of the vectors. Then identify all of the independent vector loops in the linkage, and write a vector equation for each loop. For the mechanism in Fig. 5.47, there are two obvious vector loops represented by the following equations:

$$r_1 + r_4 = r_2 + r_3 \quad (5.157)$$

$$r_5 + r_6 = r_7 + r_8 \quad (5.158)$$

7. Write the  $x, y$  scalar equations for each vector equation. Notice that the form of the equations is consistent, and once the basic vector equations are given (e.g., Eqs. (5.157) and (5.158)), it is not even necessary to look at the mechanism to be able to write the component equations.

$$x \Rightarrow r_1 \cos \theta_1 + r_4 \cos \theta_4 = r_2 \cos \theta_2 + r_3 \cos \theta_3 \quad (5.159)$$

$$y \Rightarrow r_1 \sin \theta_1 + r_4 \sin \theta_4 = r_2 \sin \theta_2 + r_3 \sin \theta_3 \quad (5.160)$$

$$x \Rightarrow r_5 \cos \theta_5 + r_6 \cos \theta_6 = r_7 \cos \theta_7 + r_8 \cos \theta_8 \quad (5.161)$$

$$y \Rightarrow r_5 \sin \theta_5 + r_6 \sin \theta_6 = r_7 \sin \theta_7 + r_8 \sin \theta_8 \quad (5.162)$$

8. Identify any constraints among the lengths or angles that are not identified by the vector loops. In the mechanism in Fig. 5.47,  $\theta_7$  is related to  $\theta_8$  by  $\pi/2$ , and  $\theta_6$  is related to  $\theta_4$  through  $\beta$ . Therefore, the extra constraint equations are

$$\theta_8 = \theta_7 + \pi/2 \quad (5.163)$$

and

$$\theta_6 = \theta_4 - \beta \quad (5.164)$$

9. Count the total number of variables in the component equations and the extra constraint equations. If  $n$  is the total number of equations and  $f$  is the number of degrees of freedom for the mechanism, the total number of unknowns should be  $n + f$ . If the number of unknowns is larger than this, it is necessary to identify additional constraints or to reformulate the loop closure equations. In the mechanism in Fig. 5.47, the total number of unknowns is seven ( $\theta_2, \theta_3, \theta_4, \theta_5, \theta_6, \theta_8$ , and  $r_7$ ), and the mechanism has only one degree of freedom. Therefore,  $n + f = 7$ , which indicates that the problem should be solvable. Note that the number of unknowns and the number of variables are not necessarily the same. In this mechanism,  $\theta_8$  is a constant but initially unknown. It must be computed using Eq. (5.163). Equations (5.159)–(5.164) are nonlinear in the unknowns ( $\theta_2, \theta_3, \theta_4, \theta_5, \theta_6$ , and  $r_7$ ), and most of the analysis difficulties are concentrated here.
10. For velocities, differentiate the position equations ( $x$  and  $y$  components) term by term. In the example case, the velocity equations are

$$\dot{r}_1 + \dot{r}_4 = \dot{r}_2 + \dot{r}_3 \quad (5.165)$$

$$\dot{r}_5 + \dot{r}_6 = \dot{r}_7 + \dot{r}_8 \quad (5.166)$$

and recognizing which terms are constants and which are variables, one gets

$$x \Rightarrow -r_4 \dot{\theta}_4 \sin \theta_4 = -r_2 \dot{\theta}_2 \sin \theta_2 - r_3 \dot{\theta}_3 \sin \theta_3 \quad (5.167)$$

$$y \Rightarrow r_4 \dot{\theta}_4 \cos \theta_4 = r_2 \dot{\theta}_2 \cos \theta_2 + r_3 \dot{\theta}_3 \cos \theta_3 \quad (5.168)$$

$$\dot{\theta}_6 = \dot{\theta}_4 \quad (5.169)$$

$$x \Rightarrow -r_5 \dot{\theta}_5 \sin \theta_5 - r_6 \dot{\theta}_6 \sin \theta_6 = \dot{r}_7 \cos \theta_7 \quad (5.170)$$

$$y \Rightarrow r_5 \dot{\theta}_5 \cos \theta_5 + r_6 \dot{\theta}_6 \cos \theta_6 = \dot{r}_7 \sin \theta_7 \quad (5.171)$$

Note that once we have solved the position equations, only the angle and length derivatives will be unknown. Hence the equations are linear in the unknowns and can be easily solved. There are five linear equations in five unknowns ( $\dot{\theta}_3, \dot{\theta}_4, \dot{\theta}_5, \dot{\theta}_6, \dot{r}_7$ ). These can be solved directly by Gaussian elimination, by using a programmable calculator, or by using a matrix solver such as MATLAB.

11. For accelerations, differentiate the velocity equations ( $x$  and  $y$  components) term by term. In the example case, the acceleration equations are

$$\ddot{r}_1 + \ddot{r}_4 = \ddot{r}_2 + \ddot{r}_3 \quad (5.172)$$

$$\ddot{\mathbf{r}}_5 + \ddot{\mathbf{r}}_6 = \ddot{\mathbf{r}}_7 + \ddot{\mathbf{r}}_8 \quad (5.173)$$

and, in terms of components,

$$x \Rightarrow -r_4 \ddot{\theta}_4 \sin \theta_4 - r_4 \dot{\theta}_4^2 \cos \theta_4 = -r_2 \ddot{\theta}_2 \sin \theta_2 - r_4 \dot{\theta}_2^2 \cos \theta_2 - r_3 \ddot{\theta}_3 \sin \theta_3 - r_3 \dot{\theta}_3^2 \cos \theta_3 \quad (5.174)$$

$$y \Rightarrow r_4 \ddot{\theta}_4 \cos \theta_4 - r_4 \dot{\theta}_4^2 \sin \theta_4 = r_2 \ddot{\theta}_2 \cos \theta_2 - r_4 \dot{\theta}_2^2 \sin \theta_2 + r_3 \ddot{\theta}_3 \cos \theta_3 - r_3 \dot{\theta}_3^2 \sin \theta_3 \quad (5.175)$$

$$\ddot{\theta}_6 = \ddot{\theta}_4 \quad (5.176)$$

$$x \Rightarrow -r_5 \ddot{\theta}_5 \sin \theta_5 - r_5 \dot{\theta}_5^2 \cos \theta_5 - r_6 \ddot{\theta}_6 \sin \theta_6 - r_6 \dot{\theta}_6^2 \cos \theta_6 = \ddot{r}_7 \cos \theta_7 \quad (5.177)$$

$$y \Rightarrow r_5 \ddot{\theta}_5 \cos \theta_5 - r_5 \dot{\theta}_5^2 \sin \theta_5 + r_6 \ddot{\theta}_6 \cos \theta_6 - r_6 \dot{\theta}_6^2 \sin \theta_6 = \ddot{r}_7 \sin \theta_7 \quad (5.178)$$

Note that once we have solved the position and velocity equations, only the derivatives of velocity will be unknown. Hence, the equations are linear in the unknowns and can be easily solved. There are five linear equations in five unknowns  $\ddot{\theta}_3$ ,  $\ddot{\theta}_4$ ,  $\ddot{\theta}_5$ ,  $\ddot{\theta}_6$ , and  $\ddot{r}_7$ . Once again, these can be solved directly by Gaussian elimination, by using a programmable calculator, or by using a matrix solver such as MATLAB.

### 5.11.1 Handling Points Not on the Vector Loops

The solution procedure outlined in the preceding section will give the position, velocity, and acceleration of each point at a vertex of a vector loop in addition to the angular velocity and acceleration of each link. The angular velocities and accelerations are the  $\dot{\theta}_i$  and  $\ddot{\theta}_i$  terms, respectively. In general,

$$\boldsymbol{\omega}_i = \dot{\theta}_i \mathbf{k}$$

and

$$\boldsymbol{\alpha}_i = \ddot{\theta}_i \mathbf{k}$$

Once the basic analysis is completed by solving the vector loop equations, we will be able to locate at least one point on each rigid body (link) as a function of time. We will also be able to determine the orientation of each rigid body as a function of time, that is,  $\theta_i$ ,  $\boldsymbol{\omega}_i$ , and  $\boldsymbol{\alpha}_i$  will be known or can be determined for each link.

Points that are not vertices of the vector loops must be associated with one of the rigid bodies in the mechanism. To determine the kinematic properties of a given point, we simply identify the point by a vector in terms of the known quantities, determine the  $x$ ,  $y$  components of the vector, and differentiate. For example, assume that we want to know the kinematic properties of a point  $Q$  on link 3 as shown in Fig. 5.48. Then,

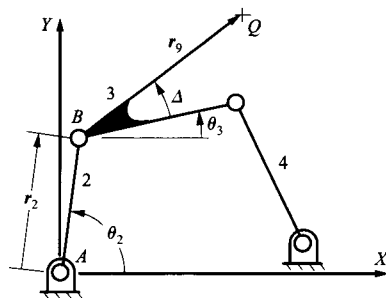


FIGURE 5.48 Determination of velocity and acceleration of a point  $Q$  that is not a vertex of a vector loop.



$$\mathbf{r}_{Q_3/A_2} = \mathbf{r}_2 + \mathbf{r}_9$$

or

$$\begin{aligned} \mathbf{r}_{Q_3/A_2} &= r_2 (\cos \theta_2 \mathbf{i} + \sin \theta_2 \mathbf{j}) + r_9 [\cos(\Delta + \theta_3) \mathbf{i} + \sin(\Delta + \theta_3) \mathbf{j}] \\ &= [r_2 \cos \theta_2 + r_9 \cos(\Delta + \theta_3)] \mathbf{i} + [r_2 \sin \theta_2 + r_9 \sin(\Delta + \theta_3)] \mathbf{j} \end{aligned} \quad (5.179)$$

All terms on the right-hand side of Eq. (5.179) will be known. Therefore, the position vector can be computed directly. The velocity is given by

$$\mathbf{v}_{Q_3/A_2} = \dot{\mathbf{r}}_2 + \dot{\mathbf{r}}_9$$

and

$$\begin{aligned} \mathbf{v}_{Q_3/A_2} &= r_2 \dot{\theta}_2 (-\sin \theta_2 \mathbf{i} + \cos \theta_2 \mathbf{j}) + r_9 \dot{\theta}_3 [-\sin(\Delta + \theta_3) \mathbf{i} + \cos(\Delta + \theta_3) \mathbf{j}] \\ &= -[r_2 \dot{\theta}_2 \sin \theta_2 + r_9 \dot{\theta}_3 \sin(\Delta + \theta_3)] \mathbf{i} + [r_2 \dot{\theta}_2 \cos \theta_2 + r_9 \dot{\theta}_3 \cos(\Delta + \theta_3)] \mathbf{j} \end{aligned} \quad (5.180)$$

Again, all quantities on the right-hand side of Eq. (5.180) are known, and so the velocity of point  $Q$  can be computed without difficulty. For the acceleration, differentiate the velocity expression. Then,

$$\mathbf{a}_{Q_3/A_2} = \ddot{\mathbf{r}}_2 + \ddot{\mathbf{r}}_9$$

and

$$\begin{aligned} \mathbf{a}_{Q_3/A_2} &= r_2 \ddot{\theta}_2 (-\sin \theta_2 \mathbf{i} + \cos \theta_2 \mathbf{j}) - r_2 (\dot{\theta}_2)^2 (\cos \theta_2 \mathbf{i} + \sin \theta_2 \mathbf{j}) \\ &\quad + r_9 \ddot{\theta}_3 [-\sin(\Delta + \theta_3) \mathbf{i} + \cos(\Delta + \theta_3) \mathbf{j}] - r_9 (\dot{\theta}_3)^2 [\cos(\Delta + \theta_3) \mathbf{i} + \sin(\Delta + \theta_3) \mathbf{j}] \\ &= \left[ -r_2 \ddot{\theta}_2 \sin \theta_2 - r_9 \ddot{\theta}_3 \sin(\Delta + \theta_3) - r_2 (\dot{\theta}_2)^2 \cos \theta_2 - r_9 (\dot{\theta}_3)^2 \cos(\Delta + \theta_3) \right] \mathbf{i} \\ &\quad + \left[ r_2 \ddot{\theta}_2 \cos \theta_2 + r_9 \ddot{\theta}_3 \cos(\Delta + \theta_3) - r_2 (\dot{\theta}_2)^2 \sin \theta_2 - r_9 (\dot{\theta}_3)^2 \sin(\Delta + \theta_3) \right] \mathbf{j} \end{aligned} \quad (5.181)$$

Again, all quantities on the right-hand side of Eq. (5.181) are known and so the acceleration of point  $Q$  can be computed without difficulty. Note that this procedure is simply a variation on the rigid-body analysis given in Section 5.4.

### 5.11.2 Solving the Position Equations

A review of the analysis just developed shows that only the position equations are nonlinear in the unknowns. Therefore specialized techniques are required to solve them. If a numerical solution is chosen, then an initial guess for the variables is required. This is best obtained by sketching the mechanism to scale. A numerical iteration method such as the Newton–Raphson method can be used to obtain refined values. If a series of input angles is to be investigated, then the final variable values for the previous input value can be used as the initial estimates of the variables for the next input value provided that the input angle increments are relatively small (i.e., within about  $10^\circ$  of each other).

Another numerical approach that is computationally more efficient than using Newton's method, but sometimes has convergence problems at end-of-travel positions, is to numerically integrate the velocity equations after a precise set of values for the variables is obtained by Newton's method. The input step size for this integration should not exceed  $2^\circ$ . This method is very convenient if a numerical integration is already needed for dynamic problems in which the equations of motion are required.

When it is possible, it is preferable to solve the displacement equations analytically. This method eliminates the numerical instability problems present in both Newton's method and numerical integration. In general, it is always possible to solve the equations analytically if the mechanism can be analyzed by hand using traditional graphical methods with vector polygons as presented in Chapters 2 and 3. When it is possible to do this, the position equations can be solved in sets of two equations in two unknowns as was done in Sections 5.3–5.10. If it is not possible to reduce the equations to a series of two equations in two unknowns, the equations must be solved iteratively using a numerical procedure such as Newton's method.

When it is possible to solve the position equations algebraically, one of two situations will usually occur. In the first situation, the compound mechanism can be treated as a series of simple mechanisms. In the second situation, the compound mechanism cannot be represented as a series of simple mechanisms; however, the equations can be partitioned into a sequential set of two equations in two unknowns. These two situations will be presented separately.

**Compound Linkage as a Series of Simple Mechanisms** When the compound linkage is a series of simple mechanisms, we can analyze each mechanism in sequence. The output for one mechanism is the input to the next mechanism. If we have computer routines to analyze the single-loop mechanisms, the routines can be concatenated to analyze the entire linkage. This is the case that exists in the mechanism of Fig. 5.47. When we examine the mechanism, we find that the first linkage is a four-bar linkage defined by vectors  $r_1$ ,  $r_2$ ,  $r_3$ , and  $r_4$ . This mechanism can be analyzed using the equations developed in Section 5.3. The four-bar loop drives link 4. Therefore, once the position, velocity, and acceleration for  $r_4$  are known, the corresponding values for  $r_6$  can be found using rigid-body conditions (Section 5.4). Link 4 is the input for the slider-crank mechanism defined by  $r_5$ ,  $r_6$ ,  $r_7$ , and  $r_8$ . This mechanism can be analyzed using the equations in Section 5.5 to determine the kinematic properties of the slider.

**EXAMPLE 5.11**  
**Kinematic**  
**Analysis of a**  
**Compound Linkage**  
**Mechanism**

**Solution**

Determine the angular position, velocity, and acceleration of link 6 in the mechanism in Fig. 5.49 if the slider is moving at 10 cm/s (constant) to the right. The following dimensions are known:

$$AB = 22.7 \text{ cm}, \quad CD = 7.5 \text{ cm}, \quad EF = 10.6 \text{ cm}$$

$$BC = 10.6 \text{ cm}, \quad CF = 14.6 \text{ cm}$$

$$AC = 28 \text{ cm}, \quad DE = 11.4 \text{ cm}$$

We will analyze the mechanism as three linkage systems in series. First we will analyze the slider-crank mechanism using the equations in Table 5.5. Next we will compute the position of  $CD$  from rigid-body conditions (Table 5.3). Last, the four-bar linkage ( $CDEF$ ) can be analyzed using Table 5.1. The actual numerical calculations can be made using the MATLAB routines included on the disk with this book.

To facilitate the analysis, the mechanism in Fig. 5.49 is represented by the vectors indicated in Fig. 5.50.

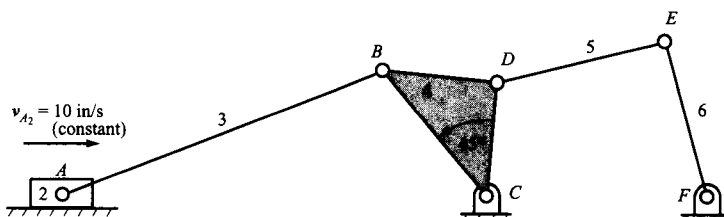


FIGURE 5.49 Mechanism for Example 5.11.

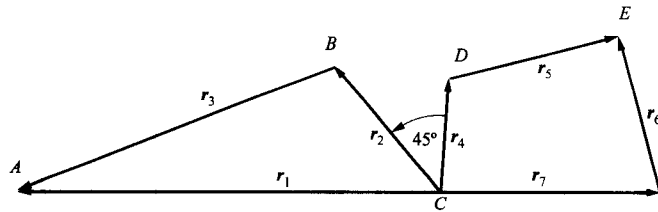


FIGURE 5.50 Vectors representing mechanism in Fig. 5.49.

For the slider-crank part of the mechanism, the following magnitudes and directions are known:

$$r_1 = 28, \quad \theta_1 = 180^\circ, \quad \dot{r}_1 = 10, \quad \ddot{r}_1 = 0$$

$$r_2 = 10.6$$

$$r_3 = 22.7$$

The unknowns are:  $\theta_2, \dot{\theta}_2, \ddot{\theta}_2, \theta_3, \dot{\theta}_3, \ddot{\theta}_3$ . For this set of values, the equations in Table 5.5 can be used. The value of  $\sigma$  is  $-1$  for the geometry given, and the results are

$$\theta_1 = 180^\circ, \quad \dot{\theta}_1 = 0 \text{ rad/s}, \quad \ddot{\theta}_1 = 0 \text{ rad/s}^2$$

$$\theta_2 = 129.94^\circ, \quad \dot{\theta}_2 = -0.9314 \text{ rad/s}, \quad \ddot{\theta}_2 = 0.5005 \text{ rad/s}^2$$

$$\theta_3 = -159.02^\circ, \quad \dot{\theta}_3 = 0.299 \text{ rad/s}, \quad \ddot{\theta}_3 = -0.459 \text{ rad/s}^2$$

The orientation of the vector  $r_4$  will be related to that of the vector  $r_2$  through the equation

$$\theta_4 = \theta_2 - 45^\circ$$

Therefore, the magnitudes and directions for the vectors defining the four-bar linkage are

$$r_4 = 7.5, \quad \theta_4 = 84.94^\circ, \quad \dot{\theta}_4 = -0.9314 \text{ rad/s}, \quad \ddot{\theta}_4 = 0.5005 \text{ rad/s}^2$$

$$r_5 = 11.4,$$

$$r_6 = 10.6,$$

$$r_7 = 14.6, \quad \theta_7 = 0^\circ$$

The unknowns are:  $\theta_5, \dot{\theta}_5, \ddot{\theta}_5, \theta_6, \dot{\theta}_6, \ddot{\theta}_6$ . For this set of values, the equations in Table 5.1 can be used. The value of  $\sigma$  is again  $-1$  for the geometry given, and the results are

$$\theta_4 = 84.94^\circ, \quad \dot{\theta}_4 = -0.9314 \text{ rad/s}, \quad \ddot{\theta}_4 = 0.5005 \text{ rad/s}^2$$

$$\theta_5 = 13.87^\circ, \quad \dot{\theta}_5 = 0.2175 \text{ rad/s}, \quad \ddot{\theta}_5 = 0.0536 \text{ rad/s}^2$$

$$\theta_6 = 105.7146^\circ, \quad \dot{\theta}_6 = -0.6237 \text{ rad/s}, \quad \ddot{\theta}_6 = 0.5978 \text{ rad/s}^2$$

$$\theta_7 = 0^\circ, \quad \dot{\theta}_7 = 0 \text{ rad/s}, \quad \ddot{\theta}_7 = 0 \text{ rad/s}^2$$

**General Cases In Which Two Equations in Two Unknowns Result** For simple lower pair mechanisms with one vector loop, the position analysis will reduce to two scalar equations in two unknowns, and it is relatively easy to develop closed-form equations for the unknown variables. However, when analyzing more complex lower pair mechanisms with  $n$  loop equations, the number of equations and the number of variable unknowns are both  $2n$ , and the solution can become much more complicated. However, not all the pair variables appear in each of the equations. Fortunately, it is often possible to group the equations into smaller sets that can be solved independently in a serial fashion.

If a given lower pair mechanism can be analyzed using the traditional vector-polygon approach, it is always possible to group the position equations in such a way that no more than two equations in two unknowns must be solved at any one time. For such mechanisms, the position equations can always be solved in closed form, and these types of mechanisms form the vast majority of the linkages that an engineer might design. For complex mechanisms that cannot be analyzed entirely using closed-form equations, it is often possible to analyze a part of the mechanism with closed-form equations after other parts are analyzed numerically.

For simplicity, the vector form of the loop closure equation for each loop will be represented in homogeneous form as

$$\sum_{i=1}^k \sigma_i r_i = 0$$

where  $\sigma_i = \pm 1$ . This equation can be divided into  $x$  and  $y$  components, and the corresponding component equations are

$$\sum_{i=1}^k \sigma_i r_i \cos \theta_i = 0 \quad (5.182)$$

$$\sum_{i=1}^k \sigma_i r_i \sin \theta_i = 0 \quad (5.183)$$

where  $r_i$  is the length of vector  $i$ ,  $\theta_i$  is the angle (measured CCW) between link  $i$  and a horizontal line, and  $k$  is the number of vectors in a given loop. Equations (5.182) and (5.183) are written for each closure loop of the mechanism, and for  $n$  loops there will be  $2n$  equations and  $2n$  unknowns. When the links contain more than two joints, there will also be auxiliary equations that relate joint angles. As shown in Fig. 5.51, these auxiliary equations can generally be written as

$$\theta_q = \theta_r - \Delta \quad (5.184)$$

where  $\Delta$  is a constant. When such equations are necessary, the equations can be written such that  $\theta_r$  is solved first so that it is a trivial matter to solve for  $\theta_q$ . Note that Eq. (5.184) is linear.

When all of the equations of the forms given by Eqs. (5.182)–(5.184) are considered as a set, it is usually possible to separate the  $2n$  nonlinear equations into smaller groups that can be solved serially, and in most cases the nonlinear equations can be grouped into sets of two equations and two unknowns of the following form:

$$\sigma_p r_p \cos \theta_p + \sigma_m r_m \cos \theta_m + \sum_{i=1}^{p-1} \sigma_i r_i \cos \theta_i + \sum_{i=p+1}^{m-1} \sigma_i r_i \cos \theta_i + \sum_{i=m+1}^k \sigma_i r_i \cos \theta_i = 0 \quad (5.185)$$

$$\sigma_p r_p \sin \theta_p + \sigma_m r_m \sin \theta_m + \sum_{i=1}^{p-1} \sigma_i r_i \sin \theta_i + \sum_{i=p+1}^{m-1} \sigma_i r_i \sin \theta_i + \sum_{i=m+1}^k \sigma_i r_i \sin \theta_i = 0 \quad (5.186)$$

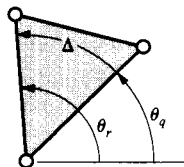


FIGURE 5.51 Geometry described by auxiliary equations.

where  $\sigma_p = \sigma_m$ , and all variables in the summation terms are known.

Then,

$$r_p \cos \theta_p + r_m \cos \theta_m = C_1 \quad (5.187)$$

$$r_p \sin \theta_p + r_m \sin \theta_m = C_2 \quad (5.188)$$

where

$$C_1 = -\frac{1}{\sigma_m} \left( \sum_{i=1}^{p-1} \sigma_i r_i \cos \theta_i + \sum_{i=p+1}^{m-1} \sigma_i r_i \cos \theta_i + \sum_{i=m+1}^k \sigma_i r_i \cos \theta_i \right)$$

and

$$C_2 = -\frac{1}{\sigma_m} \left( \sum_{i=1}^{p-1} \sigma_i r_i \sin \theta_i + \sum_{i=p+1}^{m-1} \sigma_i r_i \sin \theta_i + \sum_{i=m+1}^k \sigma_i r_i \sin \theta_i \right)$$

In Eqs. (5.187) and (5.188), two of the four variables  $r_p$ ,  $\theta_p$ ,  $r_m$ , and  $\theta_m$  can be unknown, resulting in six possible combinations; however, only four of these six combinations are unique. The four cases that must be considered are 1.  $r_p$  and  $\theta_p$  or  $r_m$  and  $\theta_m$  are the unknowns, 2.  $r_p$  and  $\theta_m$  or  $r_m$  and  $\theta_p$  are the unknowns, 3.  $r_p$  and  $r_m$  are the unknowns, and 4.  $\theta_p$  and  $\theta_m$  are the unknowns. The rest of the variables in the four cases are known for each position of the mechanism. When solving each of the cases, the three trigonometric identities discussed earlier for  $\sin \theta$ ,  $\cos \theta$ , and  $\tan \frac{\theta}{2}$  are used:

$$\cos^2 \theta + \sin^2 \theta = 1 \quad (5.189)$$

$$\cos \theta = \frac{1 - \tan^2 \left( \frac{\theta}{2} \right)}{1 + \tan^2 \left( \frac{\theta}{2} \right)} \quad (5.190)$$

and

$$\sin \theta = \frac{2 \tan \left( \frac{\theta}{2} \right)}{1 + \tan^2 \left( \frac{\theta}{2} \right)} \quad (5.191)$$

The equations for calculating the unknown variables in each of these cases are developed in the following:

**Case 1:  $r_p$  and  $\theta_p$  Unknown** To solve this case, the terms  $r_p \cos \theta_p$  and  $r_p \sin \theta_p$  are first isolated on the left-hand side of Eqs. (5.187) and (5.188).

$$r_p \cos \theta_p = C_1 - r_m \cos \theta_m \quad (5.192)$$

$$r_p \sin \theta_p = C_2 - r_m \sin \theta_m \quad (5.193)$$

Equation (5.193) is then divided by Eq. (5.192) to provide the solution for  $\theta_p$ . Next the two equations are squared, added together, and simplified using Eq. (5.189) to obtain a solution for  $r_p$ . The resulting expressions for  $r_p$  and  $\theta_p$  are

$$r_p = \sqrt{C_1^2 + C_2^2 + r_m^2 - 2C_1r_m \cos \theta_m - 2C_2r_m \sin \theta_m} \quad (5.194)$$

$$\theta_p = \tan^{-1} \left[ \frac{C_2 - r_m \sin \theta_m}{C_1 - r_m \cos \theta_m} \right] \quad (5.195)$$

**Case 2:  $r_p$  and  $\theta_m$  Unknown** To solve for the two unknown variables,  $r_p$  and  $\theta_m$ , the terms  $r_m \cos \theta_m$  and  $r_m \sin \theta_m$  are first isolated on the left-hand side of Eqs. (5.187) and (5.188).

$$r_m \cos \theta_m = C_1 - r_p \cos \theta_p \quad (5.196)$$

$$r_m \sin \theta_m = C_2 - r_p \sin \theta_p \quad (5.197)$$

Equations (5.196) and (5.197) are then squared, added together, and simplified using Eq. (5.189) to give a quadratic equation in the variable  $r_p$ . The solution to the resulting equation is

$$r_p = \frac{-b \pm \sqrt{b^2 - 4c}}{2} \quad (5.198)$$

where

$$b = -2C_1 \cos \theta_p - 2C_2 \sin \theta_p$$

and

$$c = C_1^2 + C_2^2 - r_m^2$$

The angle  $\theta_m$  is found by dividing Eq. (5.197) by Eq. (5.196) and solving for  $\theta_m$ :

$$\theta_m = \tan^{-1} \left[ \frac{-r_p \sin \theta_p + C_2}{-r_p \cos \theta_p + C_1} \right] \quad (5.199)$$

Equations (5.198) and (5.199) each have two solutions corresponding to the two assembly modes of this part of the linkage. The proper mode must be specified at the time of the analysis. This can be done directly or by providing an initial estimate of the position of the mechanism and determining which solution is closest to that indicated by the initial estimate. In practice, the initial estimate of the position of the mechanism could be provided by an approximate sketch drawn on a computer screen.

**Case 3:  $r_p$  and  $r_m$  Unknown** To solve for  $r_p$ , Eq. (5.187) is first multiplied by  $\sin \theta_m$  and the result is then simplified. Equation (5.188) is then multiplied by  $\cos \theta_m$  and the resulting equations from the two operations are subtracted. After simplification, the expression for  $r_p$  is

$$r_p = \frac{C_1 \sin \theta_m - C_2 \cos \theta_m}{\sin(\theta_m - \theta_p)} \quad (5.200)$$

After  $r_p$  is known, Eqs. (5.187) and (5.188) can be solved directly for  $r_m$ :

$$r_m = \frac{C_1 - r_p \cos \theta_p}{\cos \theta_m} = \frac{C_2 - r_p \sin \theta_p}{\sin \theta_m} \quad (5.201)$$

**Case 4:  $\theta_p$  and  $\theta_m$  Unknown** To solve for  $\theta_m$ , Eqs. (5.192) and (5.193) are squared, added together, and simplified with the aid of Eqs. (5.189)–(5.191) to give a quadratic equation in the variable  $\tan(\theta_m/2)$ . The resulting solution is

$$\theta_m = 2 \tan^{-1} \left( \frac{-C_4 \pm \sqrt{C_4^2 - 4C_3C_5}}{2C_3} \right) \quad (5.202)$$

where

$$C_3 = r_p^2 - C_1^2 - C_2^2 - r_m^2 - 2C_1r_m$$

$$C_4 = 4C_2r_m$$

and

$$C_5 = r_p^2 - C_1^2 - C_2^2 - r_m^2 + 2C_1r_m$$

Given  $\theta_m$ , an expression for  $\theta_p$  can be found by dividing Eq. (5.193) by Eq. (5.192) and simplifying,

$$\theta_p = \tan^{-1} \left( \frac{C_2 - r_m \sin \theta_m}{C_1 - r_m \cos \theta_m} \right) \quad (5.203)$$

Equations (5.202) and (5.203) each have two solutions, corresponding to the two assembly modes of this part of the linkage. As with case 2, the proper assembly mode must be identified before the analysis can be conducted.

## 5.12 CLOSURE EQUATIONS FOR MECHANISMS WITH HIGHER PAIRS

---

The closure equation approach can also be used for mechanisms with higher pairs if we use the centers of curvature of the contact surfaces corresponding to the contact points. This is exactly the approach employed when equivalent mechanisms are used, and, in fact, we could represent the higher pair mechanisms by their equivalent lower pair mechanism and determine the kinematic properties by analyzing the corresponding lower pair mechanism. By using the centers of curvature, however, we can also approach the problem without using equivalent mechanisms directly.

The approach using centers of curvature can be applied directly to mechanisms with cam joints and to mechanisms with rolling joints if the contact points (and the corresponding centers of curvature) are known. With rolling contact, locating the contact point as a function of the input motion requires that we know the initial contact point when the mechanism begins to move. Subsequent contact points are then located by enforcing the constraint that there is no slipping at the contacting surfaces. If circle arcs are involved, the resulting constraint equations are simple; however, if general surfaces are involved, the constraint equations require that the arc length on each contacting surface be determined by integration. For simplicity, we will limit the discussions here to cases in which the contact point either is known or can be determined simply.

For higher pair mechanisms, the vector closure diagrams are set up using the same procedure as would be used when the mechanism is drawn. In general, the same points and vectors will be used. The procedure will be illustrated with three examples.

**EXAMPLE 5.12**  
**Kinematic**  
**Analysis of**  
**a Mechanism with**  
**Cam Contact**

**Solution**

In the mechanism shown in Fig. 5.52,  $\omega_2 = 10$  rad/s CW and is constant. Determine  $v_{C_3/C_2}$ ,  $v_{C_3}$ ,  $a_{C_3/C_2}$  and  $a_{C_3}$  using vector closure equations.

To solve the problem, set up four vectors as shown in Fig. 5.53. The vector  $r_2$  is from point  $B$  to point  $A$ , the center of curvature of link 2 corresponding to the contact point at  $C$ . Vector  $r_1$  is from point  $A$  to point  $C$ , the contact location. The vector  $r_1$  is constant in both direction and magnitude. Vector  $r_3$  is from point  $B$  to the face of the cam follower. The direction of  $r_3$  is constant, but the magnitude varies. Because  $r_3$  is measured from a fixed point on the frame (point  $B$ ) to the face of the cam follower, the first and second derivatives of  $r_3$  correspond to the velocity and acceleration, respectively, of the cam follower. Vector  $r_4$  is measured from the contact point to a line through  $B$  and in the direction of travel of the cam.

The vector closure equation for the mechanism is

$$r_3 = r_2 + r_1 + r_4 \quad (5.204)$$

and the corresponding velocity and acceleration expressions are given by

$$\dot{r}_3 = \dot{r}_2 + \dot{r}_1 + \dot{r}_4 \quad (5.205)$$

and

$$\ddot{r}_3 = \ddot{r}_2 + \ddot{r}_1 + \ddot{r}_4 \quad (5.206)$$

Before actually solving the equations, we can summarize the variables that are known and unknown. These are

$$r_1 = 1.0 \text{ in.}, \quad \theta_1 = 0^\circ, \quad \dot{\theta}_1 = 0 \text{ rad/s}, \quad \ddot{\theta}_1 = 0$$

$$r_2 = 0.5 \text{ in.}, \quad \theta_2 = 225^\circ, \quad \dot{\theta}_2 = -10 \text{ rad/s}, \quad \ddot{\theta}_2 = 0$$

$$r_3 = ?, \quad \theta_3 = 0^\circ, \quad \dot{\theta}_3 = 0 \text{ rad/s}, \quad \ddot{\theta}_3 = 0$$

$$r_4 = ?, \quad \theta_4 = 90^\circ, \quad \dot{\theta}_4 = 0 \text{ rad/s}, \quad \ddot{\theta}_4 = 0$$

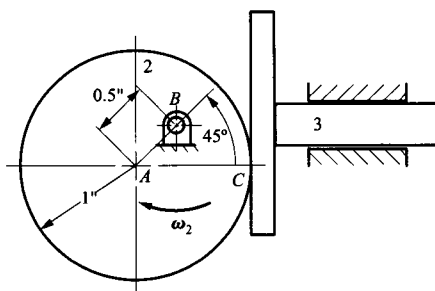


FIGURE 5.52 Figure for Example 5.12.

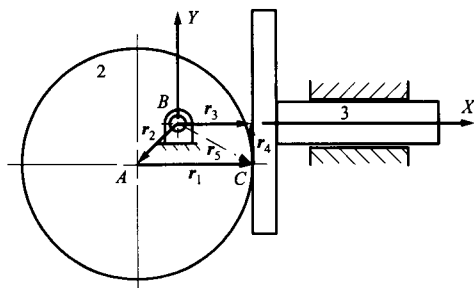


FIGURE 5.53 Vector closure for Example 5.12.



As in the cases of lower pair mechanisms, the position equation must be solved first. The resulting linear velocity and acceleration equations can then be solved easily. Rewriting the position closure equation in component form gives

$$\begin{aligned}r_3 \cos \theta_3 &= r_2 \cos \theta_2 + r_1 \cos \theta_1 + r_4 \cos \theta_4 \\r_3 \sin \theta_3 &= r_2 \sin \theta_2 + r_1 \sin \theta_1 + r_4 \sin \theta_4\end{aligned}$$

Simplifying based on the input values, we get

$$\begin{aligned}r_3 &= r_2 \cos \theta_2 + r_1 \\0 &= r_2 \sin \theta_2 + r_4\end{aligned}\tag{5.207}$$

Equations (5.207) are linear in the unknowns ( $r_3$  and  $r_4$ ) and can easily be solved. The results are

$$r_3 = r_2 \cos \theta_2 + r_1 = 0.5 \cos(225^\circ) + 1.0 = 0.646 \text{ in}$$

and

$$r_4 = -r_2 \sin \theta_2 = 0.354 \text{ in}$$

To conduct the velocity analysis, rewrite Eq. (5.205) in component form and simplify or differentiate Eqs. (5.207) and simplify. In either case, the results are

$$\begin{aligned}\dot{r}_3 &= -r_2 \dot{\theta}_2 \sin \theta_2 \\ \dot{r}_4 &= -r_2 \dot{\theta}_2 \cos \theta_2\end{aligned}\tag{5.208}$$

Substituting in the known values, we obtain

$$\begin{aligned}\dot{r}_3 &= -r_2 \dot{\theta}_2 \sin \theta_2 = -0.5(-10) \sin(225^\circ) = -3.535 \text{ in/s} \\ \dot{r}_4 &= -r_2 \dot{\theta}_2 \cos \theta_2 = -0.5(-10) \cos(225^\circ) = -3.535 \text{ in/s}\end{aligned}$$

The location of both  $C_2$  and  $C_3$  is given by  $r_5 = r_1 + r_2$  in Fig. 5.53. Both points momentarily have the same coordinates. However, the velocities of the corresponding points are different. To determine the velocities, we must carefully interpret the vectors. The velocity of all points on the follower is the same. Therefore, the velocity of  $C_3$  is given by  $\dot{r}_3$  if  $r_3$  remains horizontal. The velocity of  $C_2$  is given by the derivative of a vector fixed to link 2 and directed from point  $B$  to  $C$ . This is  $\dot{r}_5$  if we assume  $r_5$  is fixed to link 2. Then the velocity of  $C_2$  is given by  $\dot{r}_5 = \dot{r}_1 + \dot{r}_2$  if we assume that both  $r_1$  and  $r_2$  are fixed to (i.e., rotate with) link 2. Then the components of the velocity of  $C_2$  will be given by

$$v_{C_2} = \dot{r}_5 = \dot{r}_1 + \dot{r}_2 = (-r_1 \dot{\theta}_2 \sin \theta_1 - r_2 \dot{\theta}_2 \sin \theta_2) \mathbf{i} + (r_1 \dot{\theta}_2 \cos \theta_1 + r_2 \dot{\theta}_2 \cos \theta_2) \mathbf{j}$$

The relative velocity is given by

$$v_{C_3/C_2} = v_{C_3} - v_{C_2} = (\dot{r}_3 + r_1 \dot{\theta}_2 \sin \theta_1 + r_2 \dot{\theta}_2 \sin \theta_2) \mathbf{i} - (r_1 \dot{\theta}_2 \cos \theta_1 + r_2 \dot{\theta}_2 \cos \theta_2) \mathbf{j}$$

Substituting values for the variables gives

$$v_{C_3/C_2} = v_{C_3} - v_{C_2} = [0] \mathbf{i} - [1.0(-10) \cos(0^\circ) + 0.5(-10) \cos(225^\circ)] \mathbf{j} = 6.464 \mathbf{j} \text{ in/s}$$

For the acceleration analysis, differentiate Eqs. (5.208) and simplify. Then,

$$\begin{aligned}\ddot{r}_3 &= -r_2 \ddot{\theta}_2 \sin \theta_2 - r_2 \dot{\theta}_2^2 \cos \theta_2 \\ \ddot{r}_4 &= -r_2 \ddot{\theta}_2 \cos \theta_2 + r_2 \dot{\theta}_2^2 \sin \theta_2\end{aligned}\tag{5.209}$$

Substituting in the known values gives

$$\ddot{r}_3 = -r_2 \ddot{\theta}_2 \sin \theta_2 - r_2 \dot{\theta}_2^2 \cos \theta_2 = 0 - 0.5(-10)^2 \cos(225^\circ) = 35.35 \text{ in/s}^2$$

$$\ddot{r}_4 = -r_2 \ddot{\theta}_2 \cos \theta_2 + r_2 \dot{\theta}_2^2 \sin \theta_2 = 0 + 0.5(-10)^2 \sin(225^\circ) = -35.35 \text{ in/s}^2$$

Finally, we obtain

$$\begin{aligned} \mathbf{a}_{C_2} = \ddot{\mathbf{r}}_5 = \ddot{\mathbf{r}}_1 + \ddot{\mathbf{r}}_2 &= (-r_1 \ddot{\theta}_2 \sin \theta_1 - r_2 \ddot{\theta}_2 \sin \theta_2 - r_1 \dot{\theta}_2^2 \cos \theta_1 - r_2 \dot{\theta}_2^2 \cos \theta_2) \mathbf{i} \\ &\quad + (r_1 \ddot{\theta}_2 \cos \theta_1 + r_2 \ddot{\theta}_2 \cos \theta_2 - r_1 \dot{\theta}_2^2 \sin \theta_1 - r_2 \dot{\theta}_2^2 \sin \theta_2) \mathbf{j} \\ &= [0 - 0 - 1(-10)^2 - 0.5(-10)^2 \cos(225^\circ)] \mathbf{i} + [0 + 0 - 0 - 0.5(-10)^2 \sin(225^\circ)] \mathbf{j} \\ &= [-100 + 35.35] \mathbf{i} + [35.35] \mathbf{j} = -64.65 \mathbf{i} + 35.35 \mathbf{j} \end{aligned}$$

and

$$\mathbf{a}_{C_3/C_2} = \mathbf{a}_{C_3} - \mathbf{a}_{C_2} = [35.35 + 64.65] \mathbf{i} - 35.35 \mathbf{j} = 100 \mathbf{i} - 35.35 \mathbf{j} \text{ in/s}^2$$

**EXAMPLE 5.13**  
**Kinematic**  
**Analysis of a**  
**Mechanism with a**  
**Pin-in-a-Slot Joint**

**Solution**

For the mechanism shown in Fig. 5.54, find  $\omega_3$  and  $\alpha_3$  if  $\theta_2 = 100^\circ$  and  $\omega_2 = 50 \text{ rad/s}$  CCW and is constant.

To solve the problem, set up four vectors as shown in Fig. 5.55. The vector  $r_1$  is from point  $A$  to  $D$ , and  $r_2$  is from point  $A$  to  $B$ . The other two vectors involve the center of curvature,  $C$ , of the path that point  $B_2$  traces on link 3. Vector  $r_3$  is from point  $B$  to  $C$ , and  $r_4$  is from point  $D$  to  $C$ . Both points  $D$  and  $C$  are fixed to link 3; therefore,  $r_4$  is fixed to link 3. All of the vectors have constant lengths. The unknown

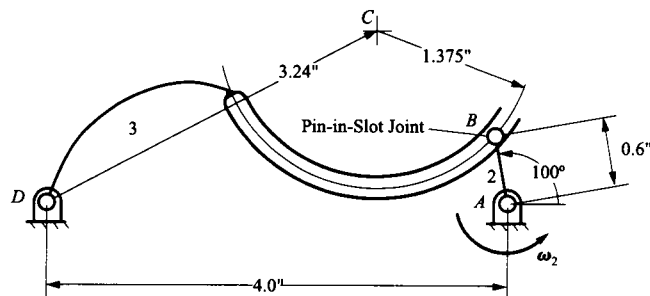


FIGURE 5.54 Mechanism for Example 5.13.

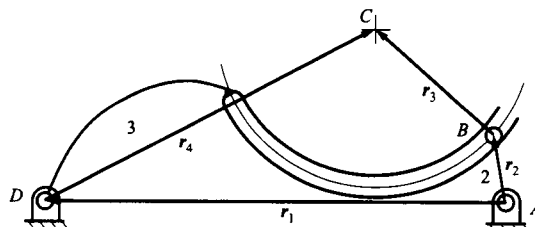


FIGURE 5.55 Vector loop for Example 5.13.

angles are  $\theta_3$  and  $\theta_4$  because  $\theta_1$  is fixed and  $\theta_2$  is the known input angle. The known and unknown information can be summarized as follows:

$$\begin{aligned} r_1 &= 4.0 \text{ in}, & \theta_1 &= 180^\circ, & \dot{\theta}_1 &= 0 \text{ rad/s}, & \ddot{\theta}_1 &= 0 \text{ rad/s}^2 \\ r_2 &= 0.6 \text{ in}, & \theta_2 &= 100^\circ, & \dot{\theta}_2 &= 50 \text{ rad/s}, & \ddot{\theta}_2 &= 0 \text{ rad/s}^2 \\ r_3 &= 1.375 \text{ in}, & \theta_3 &= ?, & \dot{\theta}_3 &= ?, & \ddot{\theta}_3 &= ? \\ r_4 &= 3.24 \text{ in}, & \theta_4 &= ?, & \dot{\theta}_4 &= ?, & \ddot{\theta}_4 &= ? \end{aligned}$$

Based on Fig. 5.55, the vector closure equation for this mechanism is

$$\mathbf{r}_2 + \mathbf{r}_3 = \mathbf{r}_1 + \mathbf{r}_4 \quad (5.210)$$

This equation is exactly the same as that for a four-bar linkage (Eq. 5.24). Therefore, the equations developed for a four-bar linkage and summarized in Table 5.1 can be applied directly to this example. The results are

$$\begin{aligned} \theta_3 &= 138.31^\circ, & \dot{\theta}_3 &= -22.21 \text{ rad/s}, & \ddot{\theta}_3 &= 73.77 \text{ rad/s}^2 \\ \theta_4 &= 27.69^\circ, & \dot{\theta}_4 &= 6.133 \text{ rad/s}, & \ddot{\theta}_4 &= -625.98 \text{ rad/s}^2 \end{aligned}$$

In the mechanism, vector  $\mathbf{r}_4$  is fixed to link 3. Therefore,

$$\begin{aligned} \omega_3 &= 6.133 \text{ rad/s CCW} \\ \alpha_3 &= -625.98 \text{ rad/s}^2 \text{ CW} \end{aligned}$$

**EXAMPLE 5.14**  
**Kinematic**  
**Analysis of a**  
**Mechanism with**  
**Rolling Contact**

**Solution**

In the mechanism shown in Fig. 5.56, link 2 is turning with a constant angular velocity of 200 rpm CCW. Determine the angular velocity and acceleration of link 4.

This mechanism involves rolling contact at point  $E$ . It is relatively straightforward to determine the angular quantities associated with link 4 if we locate the vectors for the closure equations using the centers of curvature of links 2 and 3 corresponding to the contact location  $E$ . This approach will not yield any angular information for link 3, however. In fact, the velocity and acceleration of link 4 are the same whether there is rolling or slipping at  $E$ .

The vector closure diagram is given in Fig. 5.57. The vector  $\mathbf{r}_1$  is from point  $A$  to  $D$ , and  $\mathbf{r}_2$  is from point  $A$  to  $B$ . The other two vectors involve the center of curvature,  $C$ , of the path that point  $B_2$  traces

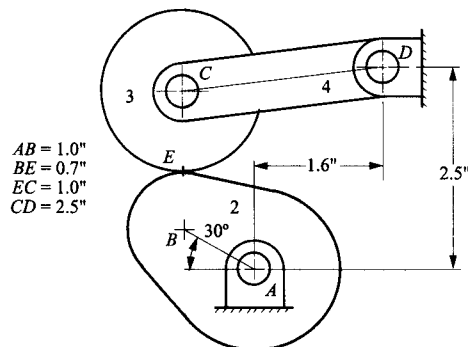


FIGURE 5.56 Mechanism for Example 5.14.

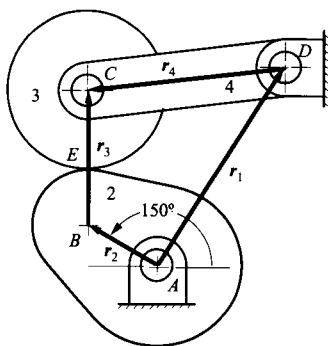


FIGURE 5.57 Vector loop for Example 5.14.

on link 3. Vector  $r_3$  is from point  $B$  to  $C$ , the centers of curvature corresponding to  $E_2$  and  $E_3$ , respectively, and  $r_4$  is from point  $D$  to  $C$ . Note that the points  $D$  and  $C$  of interest are those fixed to link 4. Therefore,  $r_4$  can be treated as a vector fixed to link 4.

All of the vectors have constant lengths. The unknown angles are  $\theta_3$  and  $\theta_4$  because  $\theta_1$  is fixed and  $\theta_2$  is the known input angle. The angle  $\theta_1$  can be computed from

$$\theta_1 = \tan^{-1} \left[ \frac{2.5}{1.6} \right] = 57.38^\circ$$

The known and unknown information can be summarized as follows:

$$\begin{aligned} r_1 &= \sqrt{2.5^2 + 1.6^2} = 2.968 \text{ in}, & \theta_1 &= 57.38^\circ, & \dot{\theta}_1 &= 0 \text{ rad/s}, & \ddot{\theta}_1 &= 0 \\ r_2 &= 1.0 \text{ in}, & \theta_2 &= 150^\circ, & \dot{\theta}_2 &= 200 \left( \frac{2\pi}{60} \right) = 20.94 \text{ rad/s}, & \ddot{\theta}_2 &= 0 \\ r_3 &= (0.7 + 1.0) = 1.7 \text{ in}, & \theta_3 &= ?, & \dot{\theta}_3 &= ?, & \ddot{\theta}_3 &= ? \\ r_4 &= 2.5 \text{ in}, & \theta_4 &= ?, & \dot{\theta}_4 &= ?, & \ddot{\theta}_4 &= ? \end{aligned}$$

Based on Fig. 5.57, the vector closure equation for this mechanism is

$$r_2 + r_3 = r_1 + r_4$$

This equation is again exactly the same as for a four-bar linkage (Eq. 5.24). Therefore, the equations developed for a four-bar linkage and summarized in Table 5.1 can again be applied directly to this example. The results are

$$\begin{aligned} \theta_3 &= 138.31^\circ, & \dot{\theta}_3 &= -22.21 \text{ rad/s}, & \ddot{\theta}_3 &= -73.77 \text{ rad/s}^2 \\ \theta_4 &= 27.69^\circ, & \dot{\theta}_4 &= 6.133 \text{ rad/s}, & \ddot{\theta}_4 &= -625.98 \text{ rad/s}^2 \end{aligned}$$

In the mechanism, vector  $r_4$  is fixed to link 4. Therefore,  $\omega_4 = 6.133 \text{ rad/s}$  CCW and  $\alpha_4 = 625.98 \text{ rad/s}^2$  CW.

### 5.13 NOTATIONAL DIFFERENCES: VECTORS AND COMPLEX NUMBERS

Several different notations are in widespread use for analytical solution of planar kinematic problems. The two principal notations are based on vectors and complex numbers. It is the purpose of this section to compare these two notations. In principle, they are completely

equivalent to one another, with every relationship written in one notation directly translatable to the other. Nevertheless, some relationships are more easily discerned when using one in preference to the other. Broadly speaking, the complex number notation tends to be most compatible with relationships that are most naturally expressed in polar coordinates. This includes most relationships describing the instantaneous motion state of a rigid body. These relationships are usually most compactly expressed in complex notation. Vector notation is, again broadly speaking, most compatible with relationships that are most naturally expressed in Cartesian coordinates. This is usually true whenever there is no single point that dominates the geometry of the system. In the opinion of the authors of this book, this includes the majority of situations to be studied. Also, planar vector notation is fully compatible with the corresponding techniques used for three-dimensional representation. Therefore, if only one notation is to be used, it should be the vector notation. For this reason, this text is based on the use of vector notation. Of course, advanced students of the subject should seek proficiency in both types of notation.

In complex number notation, planar vector quantities are represented by identifying the real and imaginary parts with orthogonal components. Normally, the  $x$  component is represented by the real part and the  $y$  component by the imaginary part. That is, the complex number

$$z = x + iy$$

represents the vector  $(x, y)$ . An important alternative form for  $z$  is

$$z = re^{i\theta} = r(\cos\theta + i\sin\theta) \quad (5.211)$$

where  $r$  is the length of the vector and  $\theta$  is its direction relative to the  $x$  axis. That is

$$r = \sqrt{x^2 + y^2}$$

and

$$\theta = \tan^{-1}(y/x)$$

It is this form that is effective in expressing polar relationships.

Referring to Fig. 5.58, we can write the basic closure equation for the four-bar linkage with the vectors  $a$ ,  $b$ ,  $c$ , and  $d$  interpreted as complex numbers. Then

$$b + c = a + d$$

Using the form of Eq. (5.211), this can be written

$$be^{i\theta} + ce^{i\psi} = a + de^{i\phi} \quad (5.212)$$

Decomposition of this expression into its real and imaginary parts, respectively, gives

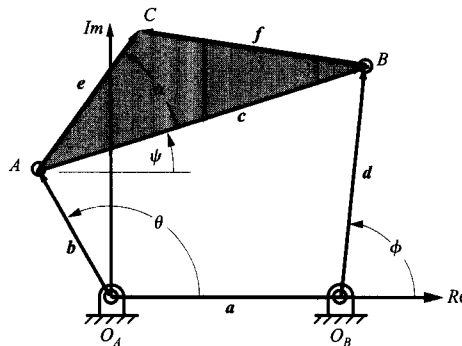


FIGURE 5.58 The real and imaginary axes used in setting up a complex number solution of the four-bar loop.

$$\begin{aligned} b \cos \theta + c \cos \psi &= a + d \cos \phi \\ b \sin \theta + c \sin \psi &= d \sin \phi \end{aligned}$$

which are identical to the component equations developed using the vector formulation. The development of a position solution and of the velocity and acceleration solutions of this chapter is then identical to that given earlier.

Alternatively, the elimination of one of the variables may be pursued in the complex variable form. Equation (5.212) may be written in the form

$$\mathbf{b} + \mathbf{c} - \mathbf{a} = \mathbf{d} \quad (5.213)$$

Now, the conjugates of  $\mathbf{b}$ ,  $\mathbf{c}$ , and  $\mathbf{d}$  are, respectively,

$$\tilde{\mathbf{b}} = b e^{-i\theta}, \quad \tilde{\mathbf{c}} = c e^{-i\psi}, \quad \text{and} \quad \tilde{\mathbf{d}} = d e^{-i\phi}$$

Also, the conjugate of  $\mathbf{a}$  is  $\mathbf{a} i$  since  $\mathbf{a}$  is a real number. The conjugate of Eq. (5.213)

$$\tilde{\mathbf{b}} + \tilde{\mathbf{c}} - \tilde{\mathbf{a}} = \tilde{\mathbf{d}}$$

is also true since the process of forming the conjugate simply changes the signs on all imaginary parts.

Multiplication of each side of Eq. (5.213) by its conjugate gives

$$(\mathbf{b} + \mathbf{c} - \mathbf{a})(\tilde{\mathbf{b}} + \tilde{\mathbf{c}} - \tilde{\mathbf{a}}) = \mathbf{d}\tilde{\mathbf{d}}$$

Now, referring to Eq. (5.212), we get

$$\mathbf{z}\tilde{\mathbf{z}} = r e^{i\theta} r e^{-i\theta} = r^2$$

Also

$$\mathbf{z} + \tilde{\mathbf{z}} = r e^{i\theta} + r e^{-i\theta} = r(\cos \theta + i \sin \theta) + r(\cos \theta - i \sin \theta) = 2r \cos \theta$$

Hence

$$\mathbf{b}\tilde{\mathbf{b}} = b^2, \quad \mathbf{c}\tilde{\mathbf{c}} = c^2, \quad \text{and} \quad \mathbf{d}\tilde{\mathbf{d}} = d^2$$

Thus, expansion of the foregoing expression gives

$$\mathbf{b}\tilde{\mathbf{b}} + \mathbf{c}\tilde{\mathbf{c}} + \mathbf{a}\tilde{\mathbf{a}} + \mathbf{b}\tilde{\mathbf{c}} + \tilde{\mathbf{b}}\mathbf{c} - \mathbf{b}\tilde{\mathbf{a}} - \tilde{\mathbf{b}}\mathbf{a} - \mathbf{c}\tilde{\mathbf{a}} - \tilde{\mathbf{c}}\mathbf{a} = \mathbf{d}\tilde{\mathbf{d}}$$

or

$$b^2 + c^2 + a^2 + b e^{i\theta} c e^{-i\psi} + b e^{-i\theta} c e^{i\psi} - a b e^{i\theta} - a b e^{-i\theta} - a c e^{i\psi} - a c e^{-i\psi} = d^2$$

or

$$b^2 + c^2 + a^2 + b c e^{i(\theta-\psi)} + b c e^{-i(\theta-\psi)} - a b e^{i\theta} - a b e^{-i\theta} - a c e^{i\psi} - a c e^{-i\psi} = d^2$$

or

$$b^2 + c^2 + a^2 + 2bc \cos(\theta - \psi) - 2ab \cos \theta - 2ac \cos \psi = d^2$$

which is the same as the form derived earlier.

Similarly, multiplying each side of the equation

$$\mathbf{b} - \mathbf{d} - \mathbf{a} = -\mathbf{c}$$

by its conjugate gives

$$\mathbf{b}\tilde{\mathbf{b}} + \mathbf{d}\tilde{\mathbf{d}} + \mathbf{a}\tilde{\mathbf{a}} - \mathbf{b}\tilde{\mathbf{d}} - \tilde{\mathbf{b}}\mathbf{d} - \mathbf{b}\tilde{\mathbf{a}} - \tilde{\mathbf{b}}\mathbf{a} + \mathbf{d}\tilde{\mathbf{a}} + \tilde{\mathbf{d}}\mathbf{a} = \mathbf{c}\tilde{\mathbf{c}}$$

or

$$b^2 + d^2 + a^2 - bde^{i(\theta-\phi)} - bde^{-i(\theta-\phi)} - abe^{i\theta} - abe^{-i\theta} + ade^{i\phi} + ade^{-i\phi} = c^2$$

giving

$$b^2 + d^2 + a^2 - 2bd \cos(\theta - \phi) - 2ab \cos \theta + 2ad \cos \phi = c^2$$

which is also the same as the form derived earlier

Equation (5.212) lends itself to development of velocity and acceleration expressions. Differentiation with respect to time gives

$$ib\dot{\theta}e^{i\theta} + ic\dot{\psi}e^{i\psi} = id\dot{\phi}e^{i\phi}$$

or, removing the common factor  $i$ , we get

$$b\dot{\theta}e^{i\theta} + c\dot{\psi}e^{i\psi} = d\dot{\phi}e^{i\phi} \tag{5.214}$$

Separation into the real and imaginary parts gives, respectively,

$$b\dot{\theta} \cos \theta + c\dot{\psi} \cos \psi = d\dot{\phi} \cos \phi$$

and

$$b\dot{\theta} \sin \theta + c\dot{\psi} \sin \psi = d\dot{\phi} \sin \phi$$

which may be recognized as the same form as given in Table 5.1.

Differentiation of Eq. (5.214) with respect to time gives

$$b\ddot{\theta}e^{i\theta} + ib\dot{\theta}^2e^{i\theta} + c\ddot{\psi}e^{i\psi} + ic\dot{\psi}^2e^{i\psi} = d\ddot{\phi}e^{i\phi} + id\dot{\phi}^2e^{i\phi}$$

Expansion of the  $e^{i\theta}$  terms gives

$$\begin{aligned} & b\ddot{\theta}(\cos \theta + i \sin \theta) + b\dot{\theta}^2(i \cos \theta - \sin \theta) + c\ddot{\psi}(\cos \psi + i \sin \psi) + c\dot{\psi}^2(i \cos \psi - \sin \psi) \\ & = d\ddot{\phi}(\cos \phi + i \sin \phi) + d\dot{\phi}^2(i \cos \phi - \sin \phi) \end{aligned}$$

Hence, separation into the real and imaginary parts gives

$$b\ddot{\theta} \cos \theta - b\dot{\theta}^2 \sin \theta + c\ddot{\psi} \cos \psi - c\dot{\psi}^2 \sin \psi = d\ddot{\phi} \cos \phi - d\dot{\phi}^2 \sin \phi$$

and

$$b\ddot{\theta} \sin \theta + b\dot{\theta}^2 \cos \theta + c\ddot{\psi} \sin \psi + c\dot{\psi}^2 \cos \psi = d\ddot{\phi} \sin \phi + d\dot{\phi}^2 \cos \phi$$

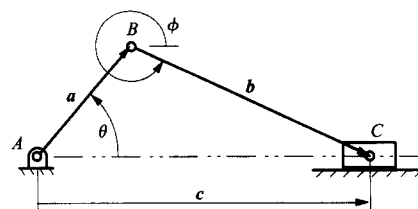
which can be recognized as the same form as those given in Table 5.1.

The foregoing illustrates the equivalence of the vector and complex number representations for simple planar mechanisms.

## PROBLEMS

5.1 For the mechanism shown, do the following:

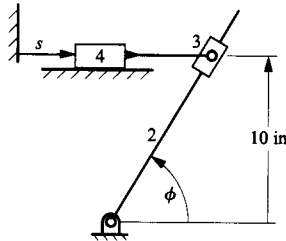
- Write the vector equation of the linkage shown.
- Write the  $x$  and  $y$  displacement equations.
- Find the velocity component equations.
- Find the acceleration component equations.



5.2 In the mechanism in Problem 5.1, determine  $\dot{\phi}$  analytically for the following values:

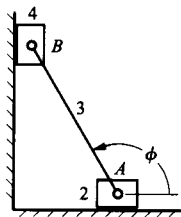
$$a = 1 \text{ cm}, \quad b = 4 \text{ cm}, \quad \theta = 60^\circ, \quad \dot{\theta} = 10 \text{ rad/s}$$

5.3 In the mechanism shown,  $\dot{s} = -10 \text{ in/s}$  and  $\ddot{s} = 0$  for the position corresponding to  $\phi = 60^\circ$ . Find  $\dot{\phi}$  and  $\ddot{\phi}$  for that position using the loop-equation approach.



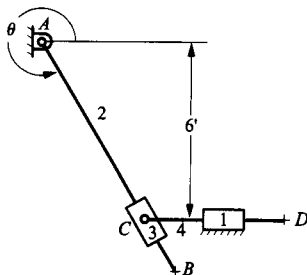
5.4 In the mechanism in Problem 5.3 assume that  $\dot{\phi}$  is 10 rad/s CCW. Use the loop-equation approach to determine the velocity of point  $B_4$  for the position defined by  $\phi = 60^\circ$ .

5.5 In the mechanism given, point  $A$  is moving to the right with a velocity of 10 cm/s. Use the loop-equation approach to determine the angular velocity of link 3. Link 3 is 10 cm long, and  $\phi$  is  $120^\circ$  in the position shown.

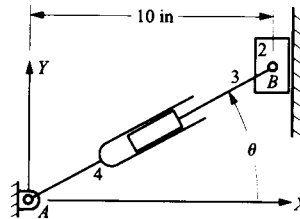


5.6 Re-solve Problem 5.5 if  $\phi$  is  $150^\circ$ .

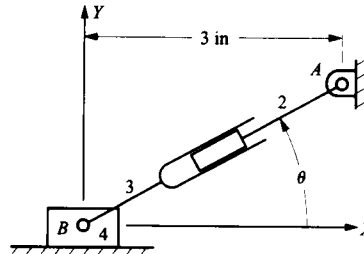
5.7 The mechanism shown is a marine steering gear called Rapson's slide.  $AB$  is the tiller, and  $CD$  is the actuating rod. If the velocity of rod  $CD$  is a constant 10 in/min to the right, and  $\theta = 300^\circ$ , use the loop-equation approach to determine the angular acceleration of the tiller.



5.8 Use loop equations to determine the velocity and acceleration of point  $B$  on link 2 when  $\theta = 30^\circ$ ,  $\omega_4 = 1 \text{ rad/s}$  CCW, and  $\alpha_4 = 0$ . Make point  $A$  the origin of your reference coordinate system.



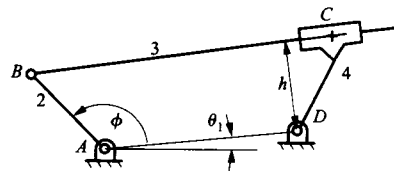
5.9 In the mechanism shown,  $\theta = 30^\circ$ ,  $\omega_2 = 1 \text{ rad/s}$  CCW, and  $\alpha_2 = 0$ . Use loop equations to determine the velocity and acceleration of point  $B$  on link 4.



5.10 In the mechanism for Problem 5.9, assume that  $v_{B_4}$  is a constant 10 in/s to the left and  $\theta$  is  $45^\circ$ . Use loop equations to determine the angular velocity and acceleration of link 3.

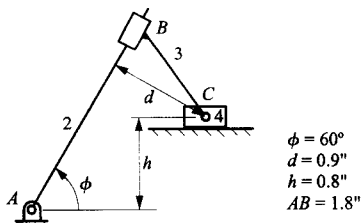
5.11 For the mechanism in the position shown, link 2 is the driver and rotates with a constant angular velocity of 100 rad/s CCW. Write vector loop equations for position, velocity, and acceleration, and solve for the velocity and acceleration of point  $C$  on link 4.

$$AB = 0.9", \quad AD = 1.7", \quad BC = 2.6", \quad h = 0.8", \quad \theta_1 = 6^\circ, \quad \phi = 120^\circ$$

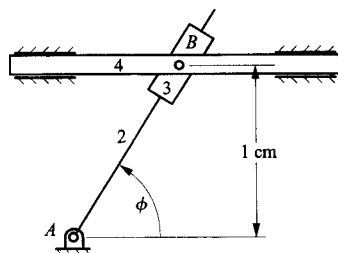




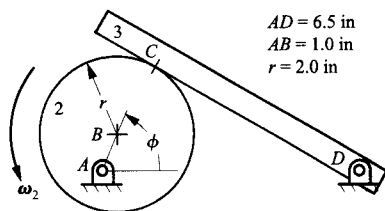
5.12 For the mechanism in the position shown, link 2 is the driver and rotates with a constant angular velocity of 50 rad/s CCW. Write vector loop equations for position, velocity, and acceleration, and solve for the velocity and acceleration of point C on link 3.



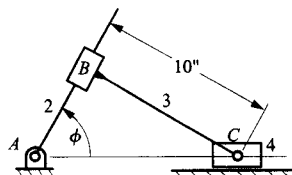
5.13 In the mechanism shown, link 3 slides on link 2, and link 4 is pinned to link 3 and slides on the frame. If  $\omega_2 = 10$  rad/s CCW (constant), use loop equations to find the acceleration of link 4 for the position defined by  $\phi = 90^\circ$ .



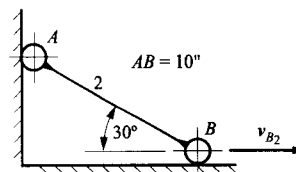
5.14 For the mechanism in the position shown, the cam (link 2) rotates with an angular velocity of 200 rad/s. Write the vector loop equations for position, velocity, and acceleration, and determine the angular velocity and acceleration of the follower (link 3). Use  $\phi = 60^\circ$  and neglect the follower thickness (i.e., assume that it is zero).



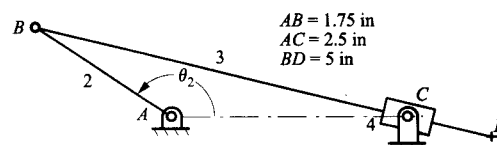
5.15 In the mechanism shown, link 3 is perpendicular to link 2. Write the vector loop equations for position and velocity. If the angular velocity of link 2 is 100 rad/s CCW, use the vector loop equations to solve for the velocity of point C<sub>4</sub> for the position corresponding to  $\phi = 60^\circ$ .



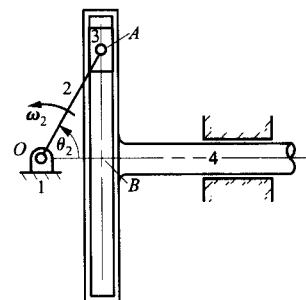
5.16 In the simple, two-link mechanism given,  $v_{B_2}$  is 10 in/s to the right. Use the loop-equation approach to determine  $v_{A_2}$  and  $\omega_2$ .



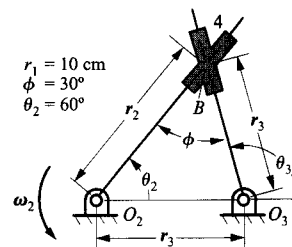
5.17 In the mechanism shown, the angular velocity of link 2 is 100 rad/s CCW and the dimensions of various links are given. Use loop equations to find the position and velocity of point D on link 3 when  $\theta_2$  is  $90^\circ$ .



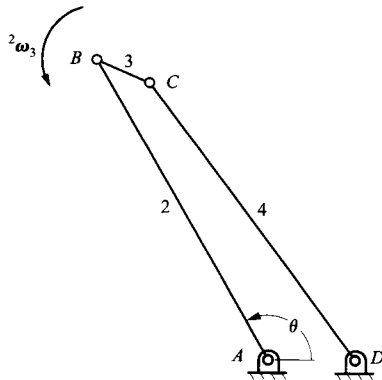
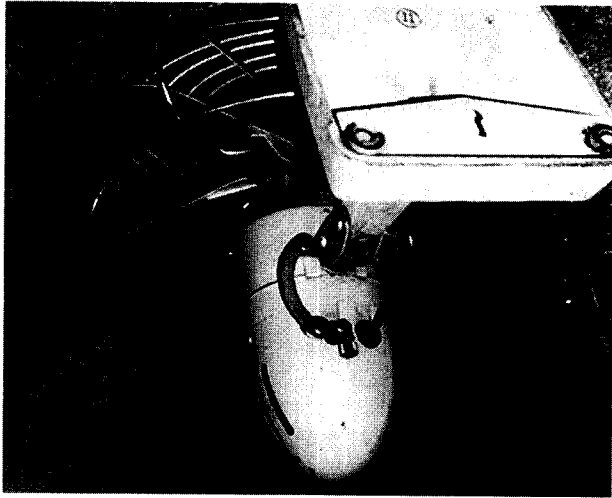
5.18 In the Scotch yoke mechanism shown,  $\omega_2 = 10$  rad/s,  $\alpha_2 = 100$  rad/s<sup>2</sup>, and  $\theta_2 = 60^\circ$ . Also, length  $OA = 20$  in. Determine  $v_{A_4}$  and  $a_{A_4}$  using loop equations.



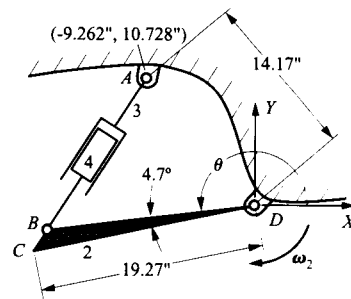
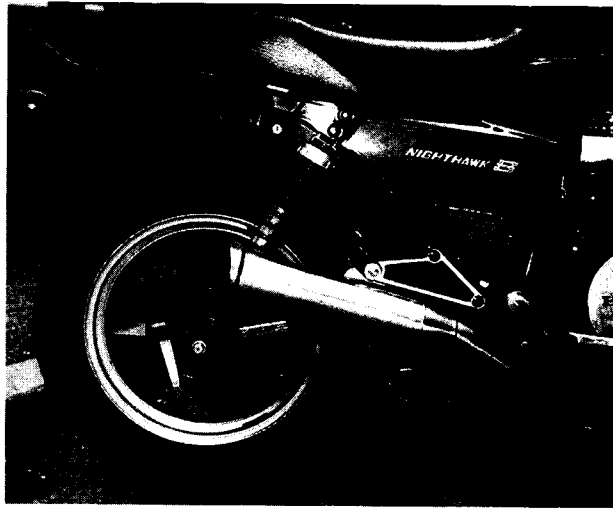
5.19 Use loop equations to determine the velocity and acceleration of point B on link 4. The angular velocity of link 2 is constant at 10 rad/s CCW.



5.20 The oscillating fan shown is to be analyzed as a double-rocker. The fan is link 2, the motor shaft is connected to link 3, and link 4 is connected from the coupler to the frame. The actual input of the mechanism is the coupler, and  ${}^2\omega_3$  is a constant 956 (rad/s) in the counterclockwise direction. Compute the angular velocity and angular acceleration of link 2 if  $\theta = 120^\circ$ ,  $AD = 0.75$  in,  $AB = DC = 3.0$  in, and  $BC = 0.50$  in.



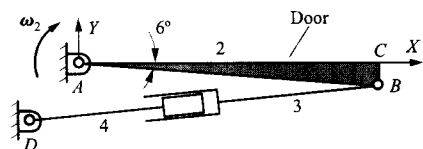
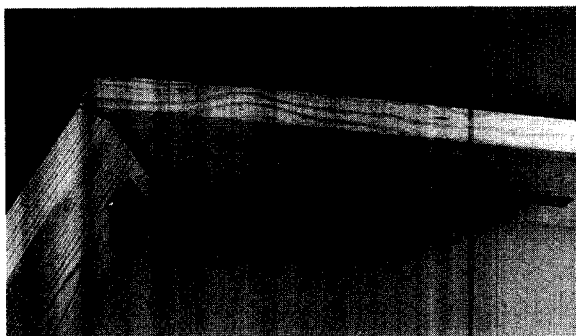
5.21 The rear suspension of a motorcycle can be analyzed as an inverted slider-crank mechanism. The frame of the motorcycle is link 1, and the tire assembly is attached to link 2 at point C. The shock absorber comprises links 3 and 4. As the motorcycle goes over a bump in the position shown, the angular velocity of link 2 relative to the frame,  $\omega_2$ , is 5 rad/s CW, and the angular acceleration,  $\alpha_2$ , is 45 rad/s<sup>2</sup> CW. Compute the angular velocity and angular acceleration of link 3 for the position defined by  $\theta = 187^\circ$ .



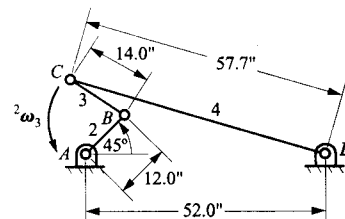
5.22 The door-closing linkage shown is to be analyzed as a slider-crank linkage. Link 2 is the door, and links 3 and 4 are the two links of the door closer. Assume that the angular velocity of the door (link 2) is a constant at 3.71 rad/s CW. Compute the angular velocity and angular acceleration of link 4 if the dimensions are as follows:

Coordinates of  $D$  ( $-2.5$ ",  $-3.0$ "")

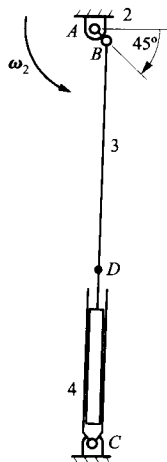
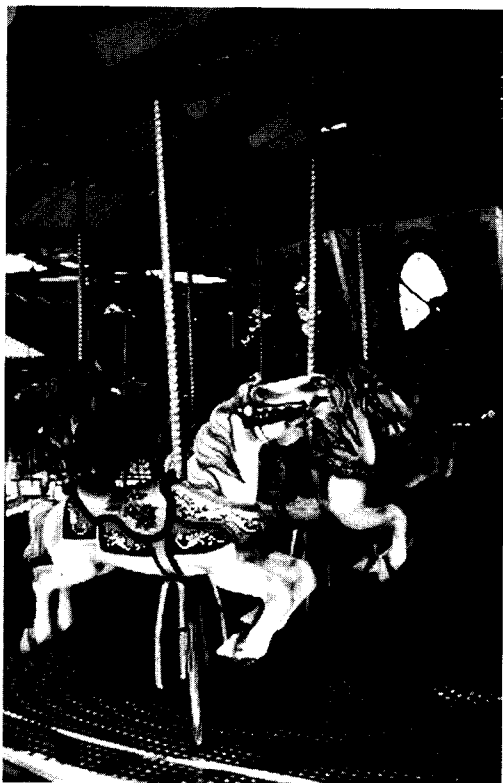
$$AB = 17.0"$$



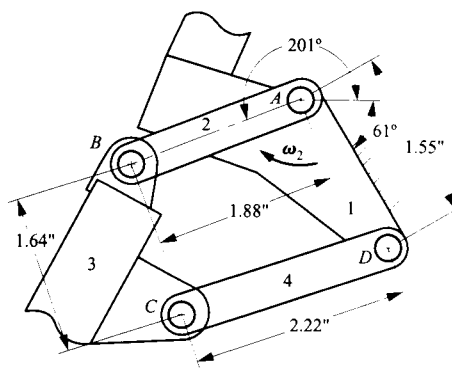
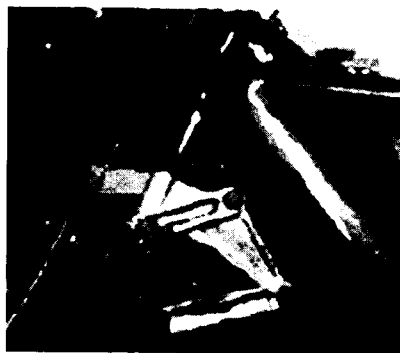
5.23 The general action of a person who is doing pushups can be modeled as a four-bar linkage as shown. The floor is the base link, and link 4 comprises the back and legs. Link 2 is the forearm, and link 3 is the upper arm. For the purposes of analysis, the motion that is controlled is the motion of link 3 relative to link 2 (elbow joint). Assume that  ${}^2\omega_3$  is a constant 6.0 rad/s CCW. Compute the angular velocity and angular acceleration of link 4 if link 2 is oriented at 45° to the horizontal.



5.24 A carousel mechanism can be modeled as an inverted slider-crank mechanism as shown. Point  $D$  is the location of the saddle on the horse. Assume that the angular velocity of the driver (link 2) is a constant  $2 \text{ rad/s}$  CCW. Compute the velocity and acceleration of  $D_3$  in the position shown if  $AB = 8.0 \text{ in}$ ,  $BC = 96.0 \text{ in}$ , and  $BD = 54 \text{ in}$ .



5.25 The shock-absorber mechanism on a mountain bicycle is a four-bar linkage as shown. The frame of the bike is link 1, the fork and tire assembly comprise link 3, and the connecting linkage comprises links 2 and 4. As the bicycle goes over a bump in the position shown, the angular velocity of link 2 relative to the frame,  $\omega_2$ , is  $205 \text{ rad/s}$  CW, and the angular acceleration,  $\alpha_2$ , is  $60 \text{ rad/s}^2$  CW. Compute the angular velocity and angular acceleration of link 3 for the position shown.



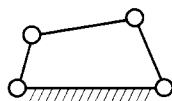
**6.1 INTRODUCTION**

The machine designer is often called upon to provide a means of generating an irregular motion. For our purposes, an irregular motion can be regarded as anything except either uniform rotation about a fixed axis or uniform rectilinear translation. There are two means of generating irregular motions by one-degree-of-freedom mechanisms: cams and linkages. As irregular motion generators, they each have advantages and disadvantages. In general, cams are easily designed but are relatively difficult, and therefore expensive, to manufacture. They are also relatively unreliable owing to wear problems. Linkages are difficult to design but are inexpensive to manufacture and relatively reliable. The subject of this chapter is linkage design.

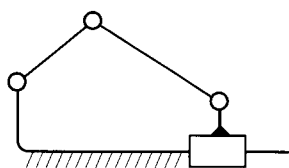
One naturally attempts to use the simplest mechanism capable of performing the desired function. For this reason, four-link mechanisms are by far the most widely used. The techniques used for the design of five- and six-bar mechanisms are basically extensions of those used for four-link mechanisms. Thus, the primary emphasis of this chapter will be on four-link mechanism synthesis.

The joints most commonly used in mechanisms are those in which the joint constraints are provided by two surfaces in contact, which, ideally, occurs over an area. This is as opposed to point or line contact as is used in cams and gears. Surface contact is desirable from the point of view of lubrication and wear resistance. The only surface contact, or lower pair, joints that are available for use in planar mechanisms are hinges and prismatic slides. There are, therefore, four possible basic types of four-link mechanisms with surface contact joints.

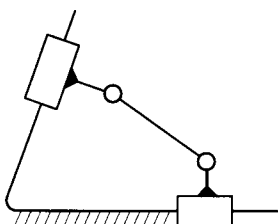
1. **The four-bar linkage.** In this linkage, all four joints are hinges as shown in Fig. 6.1. This is by far the most widely used linkage for irregular motion generation.
2. **The slider-crank (and its inversions).** The slider-crank chain is shown schematically in Fig. 6.2. Linkages based on this chain are very commonly used to convert linear to rotary motion and vice versa. It is little used when neither a linear input nor a linear output is needed.
3. **The elliptic trammel (and its inversions).** The chain for the elliptic trammel is shown in Fig. 6.3. Except for the Scotch yoke and Oldham inversions, the elliptic trammel is



**FIGURE 6.1** The four revolute four-bar linkage. This is one of four basic planar single-loop linkages. It is the most commonly used mechanism for generating irregular motions.



**FIGURE 6.2** The slider-crank linkage is obtained by replacing one revolute joint in a four-bar linkage with a prismatic joint. When inverted onto the crank, or the coupler, so that the slide rotates, the linkage becomes a turning block linkage.



**FIGURE 6.3** Elliptic trammel linkage. The paths of all points in the coupler are ellipses. When inverted onto one of the revolute-prismatic members, this becomes a Scotch yoke linkage. The Scotch yoke is sometimes used as a harmonic motion generator. The other possible inversion, onto the coupler, is used in practice as the Oldham coupling. This is a simple mechanism for accommodating misalignment between shafts.

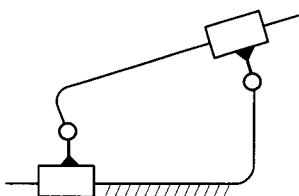
little used because of slip–stick friction problems in the two slides. Analysis equations for two inversions of this linkage are given in Sections 5.9 and 5.10.

4. **The Rapson slide.** A schematic diagram of the chain for the Rapson slide is shown in Fig. 6.4. There are two sliders that must be carefully designed if mechanisms based on the chain are to work properly. In practice, the Rapson slide is used much less frequently than the four-bar linkage or slider-crank because neither rotary joint can be made to rotate  $360^\circ$  and because of slip–stick friction in the two slides. The analysis equations for one inversion of this mechanism are given in Section 5.7.

The majority of the techniques discussed in this book are intended for four-bar linkage synthesis. This is primarily because of the large number of dimensions that can be varied, allowing more flexibility in design. Unfortunately, it also results in more complicated design techniques. When the techniques are applied to linkages having one or more slider joints, the results are somewhat simpler.

It is very rare for the desired motion to be exactly producible by a four-bar linkage. Thus, we can typically only approximate the desired motion. One approach is to select a number of positions (precision points) along the desired path and compel the linkage to move exactly through those positions. Using this method, one has no direct control over the behavior of the linkage between the design positions. One works in the (sometimes pious) hope that the linkage movement will not deviate too far from that desired between the design positions. It is, in fact, remarkable how accurate this method can be in favorable circumstances. It is possible to design a four-bar linkage for which the path of a point on the coupler deviates no more than  $\frac{1}{1000}$  of an inch from a straight line over a 10-in line length in this way.

The types of problems most usually tackled using the precision position approach permit a graphical solution. This is straightforward for problems with two and three design positions but becomes complex and laborious for four or five design positions. Most precision position problems do not admit more than five design positions. Computer packages,



**FIGURE 6.4** The Rapson slide linkage. Its inversions are also Rapson slide linkages.

such as KINSYN,<sup>1</sup> RECSYN,<sup>2</sup> and LINCAGES,<sup>3</sup> have been developed to automate the solution of precision position problems. Graphical techniques that are useful for small numbers of design positions will be described in this chapter. They form a basis for understanding the techniques of computer-aided synthesis required for more demanding problems.

The second basic approach is to select a rather large number of design positions and, instead of requiring the mechanism to pass through them exactly, minimize the sum of the squares of the deviations of the mechanism position from those positions. Thus, the linkage motion approaches the design positions but does not exactly pass through any of them. This method makes use of numerical optimization techniques to produce solution linkages. Consequently, the use of a computer is essential. Used directly, this type of approach requires the user to manipulate the mathematical constraints to obtain control over the type and properties of the solution linkage. Some packages, such as the automatic synthesis module of RECSYN, attempt to provide that control in a user-friendly form.

In a given problem, either of these approaches may yield good results. The choice is most often decided by the techniques with which the designer is most familiar and by what aids, such as synthesis programs, he or she has available.

The range of synthesis problems that arise is infinite. We will restrict our study to a few classes of problems that, because of a combination of practical importance and a well-developed theory, are most usually treated. They are as follows:

1. **The double-rocker problem.** This is one of the simplest linkage design problems. The problem is to design a four-bar linkage that will move its output link through an angle  $\phi$  while the input link moves through an angle  $\theta$ .
2. **The motion generation problem.** A linkage is to be synthesized whose coupler, as a whole, is to follow a desired trajectory. That is, the movement of the coupler as a whole is specified, not just that of a point or line lying on it.
3. **The function generation problem.** In this case the angles of the two cranks are to be coordinated. The name "function generation" originated in the days in which mechanical analog computers were used to perform complex mathematical calculations in such devices as naval gunsights. Linkages were used to generate angular relationships approximating logarithms, trigonometric functions, and so forth.
4. **The rocker amplitude problem.** In the rocker amplitude problem, the output link is to oscillate through a specified angular amplitude. Typically, the required linkage is a crank-rocker with continuously rotating driving crank. An oscillatory output motion of specified amplitude is required.
5. **The point path problem.** A single point on the coupler is to follow a nominated curve. In this form the problem does not admit a direct graphical solution. However, this class of problem is important from a practical point of view, and design methods will be presented. These are trial-and-error techniques starting with selection of an approximate coupler point path from an atlas of coupler curves or from curves generated with a computer program. Simple computer programs can be important aids in the trial-and-error process.

A modified type of point path problem in which the progression of the coupler point between design positions is coordinated with the corresponding angular displacements of the driving crank does permit direct graphical solution. This is referred to as the path-angle problem type. The techniques required for solution of this type of problem are beyond the scope of this book. KINSYN, RECSYN, and LINCAGES do provide the capability for its solution.

## 6.2 TWO-POSITION DOUBLE-ROCKER DESIGN

A common problem in kinematics is the design of a double-lever or double-rocker mechanism. The design situation is shown in Fig. 6.5a. The problem is to design a four-bar linkage such that the output link will rotate through an angle  $\phi$  when the input link rotates through an angle  $\theta$ . For the problem we will consider here, the distance between the fixed pivots  $O_2$  and  $O_4$  is given as is the length of the output link  $O_4B$ . To complete the design, we must determine the length of the input link  $O_2A$  and of the coupler  $AB$ .

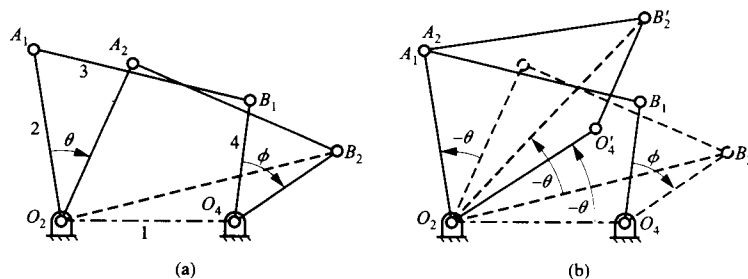
### 6.2.1 Graphical Solution Procedure

The basis for solving the problem is to invert the mechanism and visualize the motion of the mechanism when the observer is fixed to the input link. This apparent motion is shown in Fig. 6.5b. As observed from the ground or link 1, points  $A$  and  $B$  appear to move from position 1 to position 2 through their respective angles,  $\theta$  and  $\phi$ . However, if link 2 is the reference, then link 2 appears not to move and the other links, including the frame, appear to move relative to link 2 in the direction of  $-\theta$ . In a given position, the relative geometry is the same regardless of which link is the reference link. Therefore, the quadrilateral  $O_2A_2B_2O_4$  is the same whether link 1 is the reference or link 2 is the reference. To show the apparent position of the links relative to link 2, we need only rotate the quadrilateral  $O_2A_2B_2O_4$  through an angle of  $-\theta$  about pivot  $O_2$ . When this is done, note that lines  $O_2O_4$  and  $O_2B_2$  are both rotated by the angle  $-\theta$ . This observation is the basis for the design procedure given in the following.

The design procedure is illustrated in Fig. 6.6. We begin knowing the distance between the frame pivots  $O_2$  and  $O_4$  and the length of the output link,  $O_4B$ . First draw the line  $O_2B_2$  and rotate it by  $-\theta$  about the pivot  $O_2$ . This will locate  $B'_2$ , which is where  $B_2$  would appear to be if the observer were on link 2. Relative to the input link in position 1,  $B$  appears to rotate on a circular arc about  $A_1$  as  $B$  travels from  $B_1$  to  $B'_2$ . Therefore,  $A_1$  must lie on the perpendicular bisector of the line segment  $B_1B'_2$ . Also,  $A_1$  will lie on the designated line through  $O_2$  shown in Fig. 6.6a.

Once  $A_1$  is determined, the lengths of the input rocker and of the coupler will be known. The input rocker length is  $O_2A_1$  and the coupler length is  $A_1B_1$  (or  $A_1B'_2$ ).

Note that the solution to this problem makes use of inversion. We will use this concept of inversion again when we consider the design of linkages for motion generation or rigid-body guidance.



**FIGURE 6.5** Two positions of the rockers of a four-bar linkage. (a) shows the positions relative to the frame, and (b) shows the positions relative to the input rocker.



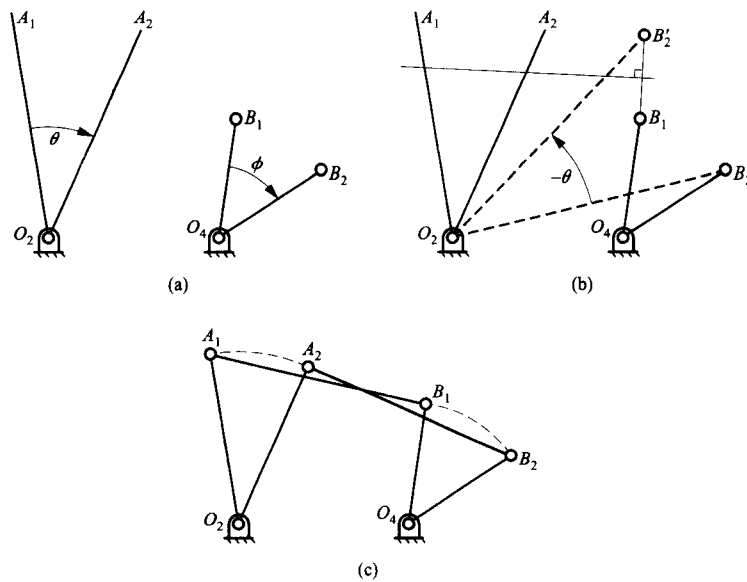


FIGURE 6.6 Locating point  $A_1$ , which in turn determines the length of the coupler and the input rocker.

### 6.2.2 Analytical Solution Procedure

The double-rocker problem can be solved analytically so that the design procedure can be easily programmed. To begin, locate the origin of the coordinate system at  $O_2$  and orient the  $x$  axis through  $O_4$  as shown in Fig. 6.7. Note that in Fig. 6.7, we have assumed that the direction of rotation is counterclockwise. This will allow us to use the standard positive sign convention for angles that was employed in Chapter 5. Using the variables represented in Fig. 6.7, we can compute the  $(x, y)$  coordinates of  $B_1$  and  $B_2$ .

For  $B_1$ ,

$$\begin{aligned} x_{B_1} &= r_1 + r_4 \cos \phi_1 \\ y_{B_1} &= r_4 \sin \phi_1 \end{aligned} \quad (6.1)$$

To simplify the resulting expression, let

$$\begin{aligned} \theta_2 &= \theta_1 + \theta \\ \phi_2 &= \phi_1 + \phi \end{aligned}$$

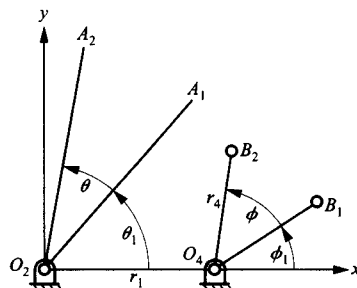


FIGURE 6.7 Parameters for analytical solution procedure.

Then for  $B_2$ ,

$$\begin{aligned}x_{B_2} &= r_1 + r_4 \cos \phi_2 \\y_{B_2} &= r_4 \sin \phi_2\end{aligned}\quad (6.2)$$

Similarly, the coordinates of  $A_1$  and  $A_2$  can be written in terms of the input crank  $r_2$ . For  $A_1$ ,

$$\begin{aligned}x_{A_1} &= r_2 \cos \theta_1 \\y_{A_1} &= r_2 \sin \theta_1\end{aligned}\quad (6.3)$$

and for  $A_2$ ,

$$\begin{aligned}x_{A_2} &= r_2 \cos \theta_2 \\y_{A_2} &= r_2 \sin \theta_2\end{aligned}\quad (6.4)$$

The distance between  $A$  and  $B$  is a constant ( $r_3$ ) for all positions of  $A$  and  $B$ . Therefore, we can write

$$r_3 = \sqrt{(x_{A_1} - x_{B_1})^2 + (y_{A_1} - y_{B_1})^2} = \sqrt{(x_{A_2} - x_{B_2})^2 + (y_{A_2} - y_{B_2})^2}\quad (6.5)$$

or

$$(x_{A_1} - x_{B_1})^2 + (y_{A_1} - y_{B_1})^2 = (x_{A_2} - x_{B_2})^2 + (y_{A_2} - y_{B_2})^2$$

Substituting values for the  $x$ 's and  $y$ 's in Eqs. (6.1–6.5), we get

$$\begin{aligned}&(r_2 \cos \theta_1 - r_1 - r_4 \cos \phi_1)^2 + (r_2 \sin \theta_1 - r_4 \sin \phi_1)^2 \\&= (r_2 \cos \theta_2 - r_1 - r_4 \cos \phi_2)^2 + (r_2 \sin \theta_2 - r_4 \sin \phi_2)^2\end{aligned}$$

Expanding and simplifying using  $\sin^2 \theta + \cos^2 \theta = 1$ , we get

$$\begin{aligned}&-r_1 r_2 \cos \theta_1 - r_2 r_4 \cos \theta_1 \cos \phi_1 + r_1 r_4 \cos \phi_1 - r_2 r_4 \sin \theta_1 \sin \phi_1 \\&= -r_1 r_2 \cos \theta_2 - r_2 r_4 \cos \theta_2 \cos \phi_2 + r_1 r_4 \cos \phi_2 - r_2 r_4 \sin \theta_2 \sin \phi_2\end{aligned}$$

In this equation, the only unknown is  $r_2$ . The equation is linear in the unknown and can be easily solved for  $r_2$ . Collecting terms, we obtain

$$\begin{aligned}&r_1 r_4 \cos \phi_2 - r_1 r_4 \cos \phi_1 \\&= r_2 [-r_1 \cos \theta_1 - r_4 \cos \theta_1 \cos \phi_1 - r_4 \sin \theta_1 \sin \phi_1 + r_1 \cos \theta_2 + r_4 \cos \theta_2 \cos \phi_2 + r_4 \sin \theta_2 \sin \phi_2]\end{aligned}$$

Then using the identity  $\cos(a + b) \equiv \cos a \cos b - \sin a \sin b$ , and solving for  $r_2$ , we get

$$r_2 = \frac{r_1 r_4 [\cos \phi_2 - \cos \phi_1]}{-r_4 [\cos(\theta_1 - \phi_1)] + r_1 [\cos \theta_2 - \cos \theta_1] + r_4 [\cos(\theta_2 - \phi_2)]}$$

Knowing  $r_2$ , we can compute  $r_3$  from Eq. (6.5); that is,

$$\begin{aligned}r_3 &= \sqrt{(r_2 \cos \theta_1 - r_1 - r_4 \cos \phi_1)^2 + (r_2 \sin \theta_1 - r_4 \sin \phi_1)^2} \\&= \sqrt{(r_2 \cos \theta_2 - r_1 - r_4 \cos \phi_2)^2 + (r_2 \sin \theta_2 - r_4 \sin \phi_2)^2}\end{aligned}$$

## 6.3 MOTION GENERATION

### 6.3.1 Introduction

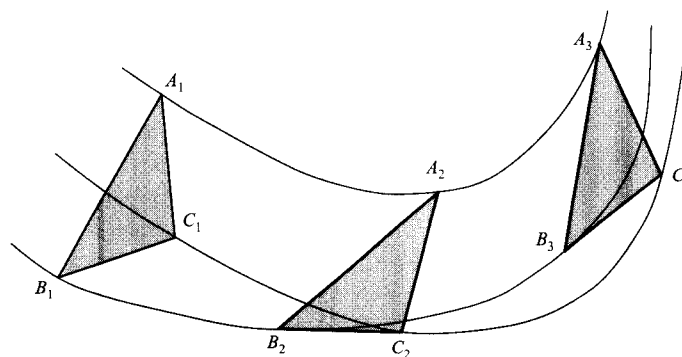
Figure 6.8 shows the path of a moving lamina as described by the paths of three points embedded in it:  $A$ ,  $B$ , and  $C$ . That is,  $A_1$  is the first position of point  $A$ ,  $A_2$  is its second position, and  $A_3$  is its third position, and similarly for points  $B$  and  $C$ . We will use this notation extensively in the following. As viewed in the moving lamina, there is only one point,  $A$ . As seen from the fixed reference frame, this point assumes three different positions,  $A_1$ ,  $A_2$ , and  $A_3$ , as the moving lamina moves through the three positions shown.

Actually, only the path of one point and the changes in the orientation of a line drawn on the lamina are needed to describe its motion. To synthesize a four-bar linkage whose coupler will approximate the given motion, we choose a number of positions on the trajectory, such as  $A_1B_1C_1$ ,  $A_2B_2C_2$ , and  $A_3B_3C_3$ , as design positions. This is shown in Fig. 6.8. The coupler will be made to pass through these positions precisely. Depending on the degree of accuracy required, a larger or smaller number of design positions should be chosen. Synthesis of the linkage is easier and the flexibility available to the designer is greater if fewer positions are used. Five is the upper limit to the number of design positions that can be used.

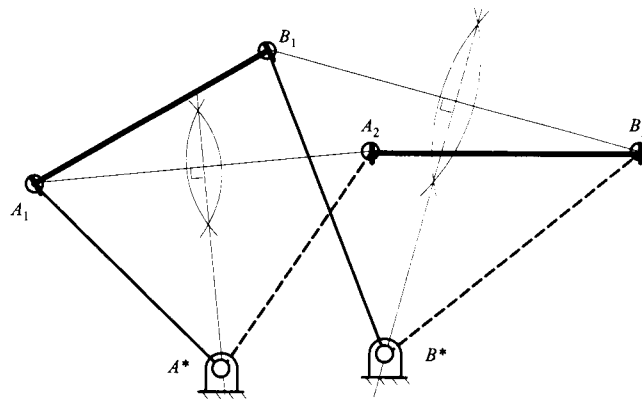
Geometrically, a crank has the effect of constraining the center of its moving pivot to move on a circle. The fixed pivot is at the center of that circle and is sometimes called a center point. Consequently, the problem of synthesizing a four-bar linkage to move its coupler through the design positions is basically the problem of locating two points in the moving lamina. Successive positions of each point all lie on the same circle. These points are sometimes called circle points. These points are taken as the locations of the moving pivots of the two cranks. The centers of the two circles on which their successive positions lie become the fixed pivots of the cranks.

### 6.3.2 Two Positions

Because an infinite number of circles can be drawn through any two points, any point in the moving lamina can be chosen as a moving pivot when two positions are of interest. In the example shown in Fig. 6.9, the two positions of the lamina are defined relative to the fixed frame by the line segments  $A_1B_1$  and  $A_2B_2$ , which are two positions of the line segment  $AB$



**FIGURE 6.8** Motion of a lamina along a continuous trajectory. Each point in the lamina moves along a continuous curve. The triangle  $ABC$  drawn on the lamina is shown in three different positions along the trajectory:  $A_1B_1C_1$ ,  $A_2B_2C_2$ , and  $A_3B_3C_3$ .



**FIGURE 6.9** Construction of a four-bar linkage that moves its coupler plane through the positions  $A_1B_1$  and  $A_2B_2$ .

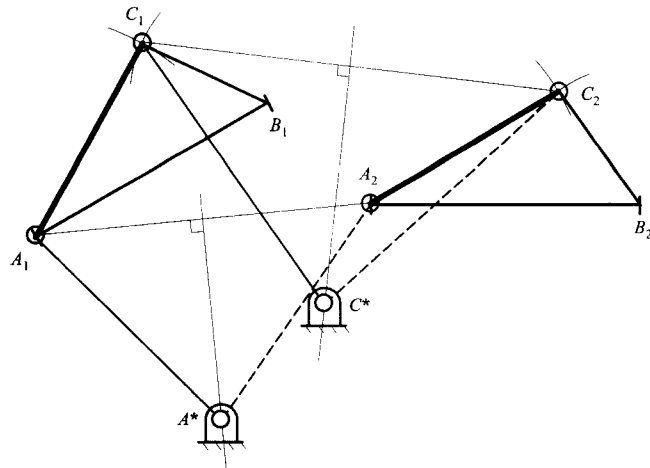
drawn on the moving lamina. Since any point in the lamina can be a moving pivot or circle point, we might as well choose  $A$  and  $B$ . In each case, we then have an infinite number of points that can be the fixed pivots or center points, namely all points on the perpendicular bisector of  $A_1A_2$  for the fixed pivot corresponding to  $A$  and all points on the perpendicular bisector of  $B_1B_2$  for the fixed pivot corresponding to  $B$ .

The perpendicular bisector of  $A_1A_2$  can be constructed by setting any convenient radius on a pair of compasses and drawing two arcs. The first arc is centered on  $A_1$ , and the second is centered on  $A_2$ . The perpendicular bisector is the line drawn through the two intersections of these two arcs. In practice, only small portions of the two arcs are drawn in the neighborhoods in which the intersections are expected, as shown in Fig. 6.9. This operation of constructing a perpendicular bisector will be used extensively in the following.

The four-bar linkage that results from this construction is, in its first position,  $A^*A_1B_1B^*$ . The base link is  $A^*B^*$ . The coupler is  $A_1B_1$ . That is, in this case, the coupler is simply the line segment used to define the positions of the moving lamina. This need not be so.

Any point in the moving lamina, not just  $A$  or  $B$ , can be chosen as a moving pivot. This is shown in Fig. 6.10, in which point  $C$  is chosen as the second moving pivot, rather than point  $B$ . The first step, in this case, is to locate the two positions  $C_1$  and  $C_2$  of this point. The convention for showing points on the moving plane that is used almost universally in the literature, and that is followed here, is that the moving lamina is drawn in its *first position*. Therefore, point  $C$  drawn on the moving lamina is identical to point  $C_1$ . To locate point  $C_2$ , we note that  $ABC$  is a triangle drawn on the rigid, moving lamina. It does not change shape, regardless of the motion. Therefore triangle  $A_2B_2C_2$  is congruent to triangle  $A_1B_1C_1$ . Consequently,  $C_2$  can be located by completing triangle  $A_2B_2C_2$ .

In practice, this is accomplished by setting radius  $A_1C_1$  on a pair of compasses and drawing an arc with center  $A_2$ . The compasses are then set to radius  $B_1C_1$ , and an arc is drawn with center  $B_2$ . The intersection of the two arcs is point  $C_2$ . It is important to note that there are actually two possible intersections of these two arcs. One gives triangle  $A_2B_2C_2$  congruent to triangle  $A_1B_1C_1$ , but the other gives the mirror image of that triangle. This



**FIGURE 6.10** Solution of the same two-position problem shown in Fig. 6.9 with a different point:  $C_1$  chosen as the second moving pivot.

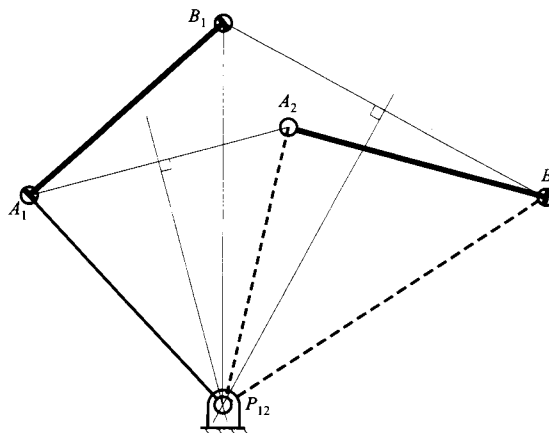
second possibility will give incorrect results. Care is necessary to ensure that the correct intersection is used. In some cases, the correct solution is not obvious. A simple check is to count off the vertices  $A_1, B_1, C_1$  when proceeding in a counterclockwise direction around the triangle. Counting off  $A_2, B_2, C_2$ , when proceeding around the triangle in its second position in the same direction, should give the same order. If the order is  $A_2C_2B_2$ , the triangle is the mirror image, and the solution is incorrect.

The problem can now be solved in exactly the same manner as it was before, except that  $C_1$  and  $C_2$  are used instead of  $B_1$  and  $B_2$ . That is, the perpendicular bisector of  $A_1A_2$  is constructed, and any point  $A^*$  is selected on that perpendicular bisector to be the fixed pivot corresponding to the moving pivot  $A$ . The perpendicular bisector of  $C_1C_2$  is then constructed, and any point  $C^*$  on that bisector is chosen to be the fixed pivot corresponding to the moving pivot  $C$ . The resulting four-bar linkage is, in its first position,  $A^*A_1C_1C^*$ . In its second position it is  $A^*A_2C_2C^*$ .

Actually, for two positions, it is possible to locate a unique point such that the moving lamina can be attached to a single, fixed pivot at that point and will rotate through the two design positions. This is shown in Fig. 6.11. This point,  $P_{12}$ , is called the displacement pole for the two positions. One position can be reached from the other by means of a pure rotation about the pole.

The construction for locating the pole is as shown in Fig. 6.11. Since  $P_{12}$  lies on the perpendicular bisector of  $A_1A_2$ , it is equidistant from  $A_1$  and  $A_2$ . Similarly, it is equidistant from  $B_1$  and  $B_2$ . Thus position 2 can be reached from position 1 by a pure rotation about  $P_{12}$ . Note that we can use the two positions of any two points on the moving body to locate the pole. For example, we could also have used points  $A$  and  $C$  or  $C$  and  $B$ .

If more than two positions are involved, as is the case in the next section, there will be a rotation pole for every two positions. For example, for three positions, there will be three poles  $P_{12}, P_{13}$ , and  $P_{23}$ . In each case, the poles will be located using the procedure shown in Fig. 6.11.



**FIGURE 6.11** Location of the pole,  $P_{12}$ , of displacement of the moving lamina from position 1 to position 2.  $P_{12}$  is located at the intersection of the perpendicular bisectors of  $A_1A_2$  and  $B_1B_2$ . The moving lamina can be displaced from position 1 to position 2 by a pure rotation about  $P_{12}$ .

### 6.3.3 Three Positions with Selected Moving Pivots

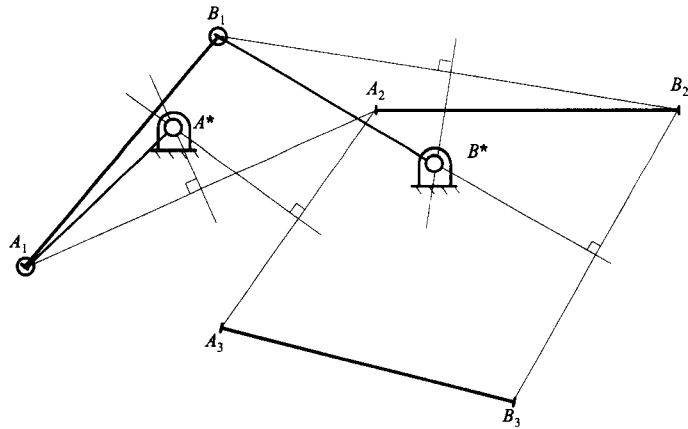
Because a circle can be drawn through any three points, any point on the moving lamina can be a moving pivot. The corresponding fixed pivot is at the center of the circle on which the three positions of the point lie. Taking  $A$  as one moving pivot, the corresponding fixed pivot  $A^*$  is located at the center of the circle upon which  $A_1$ ,  $A_2$ , and  $A_3$ , the three positions of point  $A$ , lie. Notice that  $A_1$ ,  $A_2$ , and  $A_3$  represent the three positions of a *single point*,  $A$ , in the moving plane. They are the positions of that point *as seen from the fixed plane*. The positions of points and lines in the moving plane are, by convention, drawn on the first position of the moving plane. Thus, points  $A$  and  $A_1$  can be regarded as being identical, as can  $B$  and  $B_1$ .

The center of the circle,  $A^*$ , can be found at the intersection of the perpendicular bisectors of  $A_1A_2$  and  $A_2A_3$ . Similarly,  $B^*$  is located at the center of the circle on which  $B_1$ ,  $B_2$ , and  $B_3$  lie. That is,  $B^*$  is at the intersection of the perpendicular bisectors of  $B_1B_2$  and  $B_2B_3$ . The solution linkage is then the four-bar  $A^*A_1B_1B^*$  as shown in position 1. This construction is shown in Fig. 6.12.

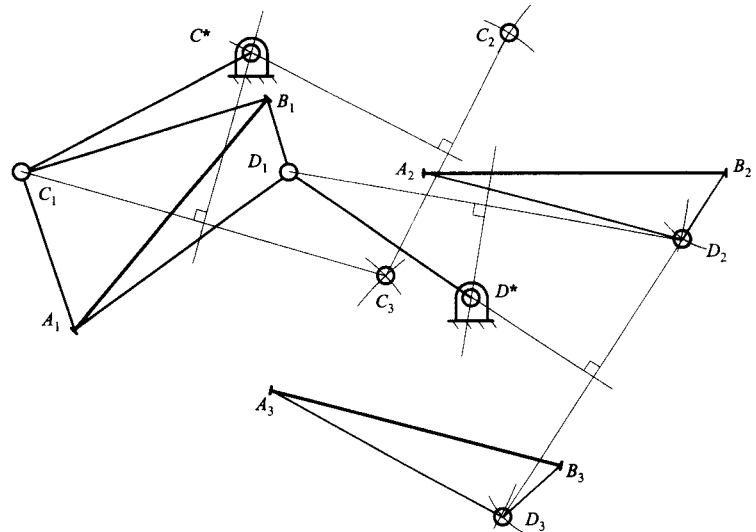
As pointed out in the two-position case, it is not necessary for  $A$  and  $B$  to be chosen as the moving pivots. If a third point,  $C$  ( $\equiv C_1$ ), is chosen as a moving pivot, its second and third positions may be found by constructing triangles  $A_2B_2C_2$  and  $A_3B_3C_3$  congruent to triangle  $A_1B_1C_1$ . Figure 6.13 shows the synthesis of a four-bar linkage that moves its coupler through the three positions in Fig. 6.12. The points  $C$  and  $D$  that do not lie on the line  $AB$  are chosen as the moving pivots. Points  $C_2$  and  $C_3$  are located by constructing congruent triangles. Likewise, points  $D_2$  and  $D_3$  are located by constructing triangles  $A_2B_2D_2$  and  $A_3B_3D_3$  congruent to triangle  $A_1B_1D_1$ . Notice that, although we represent the moving lamina by means of the line segment  $AB$ , the moving lamina is a *plane*, not a line, and we are at liberty to draw points and lines on it that do not lie on  $AB$ .

### 6.3.4 Synthesis of a Crank with Chosen Fixed Pivots

The procedure just given allows us to synthesize a crank with any chosen moving pivot. If we wish to choose the fixed pivot rather than the moving pivot, the linkage must be inverted



**FIGURE 6.12** Synthesis of a four-bar linkage that moves its coupler plane through three nominated positions. The line segment  $AB$  defines the three positions of the moving plane. The points  $A$  and  $B$  are also chosen as the moving pivots of the two cranks.  $A^*$  and  $B^*$  are the fixed pivots of those cranks.



**FIGURE 6.13** The same problem as that of Fig. 6.12 solved with points  $C$  and  $D$  selected as moving pivots, rather than  $A$  and  $B$ . Triangles  $A_2B_2D_2$  and  $A_3B_3D_3$  are congruent to  $A_1B_1D_1$ . The solution linkage, shown in its first position, is  $C^*C_1D_1D^*$ .

with the coupler becoming the reference frame. When this is done, the chosen fixed pivot is observed to move through three apparent positions as seen by the observer on the coupler. The resulting construction is shown in Fig. 6.14.

The three positions assumed by the chosen fixed pivot  $C^*$  relative to the moving lamina are plotted on the first position of that lamina. The apparent position of  $C^*$  when the lamina is in the first position is then its true position. Its apparent positions  $C^*_2$  and  $C^*_3$  when the lamina is in its second and third positions are obtained by constructing triangle  $A_1B_1C^*_2$  congruent to  $A_2B_2C^*$  and triangle  $A_1B_1C^*_3$  congruent to triangle  $A_3B_3C^*$ . The location,  $C_1$ , of the moving pivot in the first position is obtained as the center of the circle on which  $C^*$ ,  $C^*_2$ , and  $C^*_3$  lie. This defines the crank  $C^*C_1$  in its first position. If needed, the

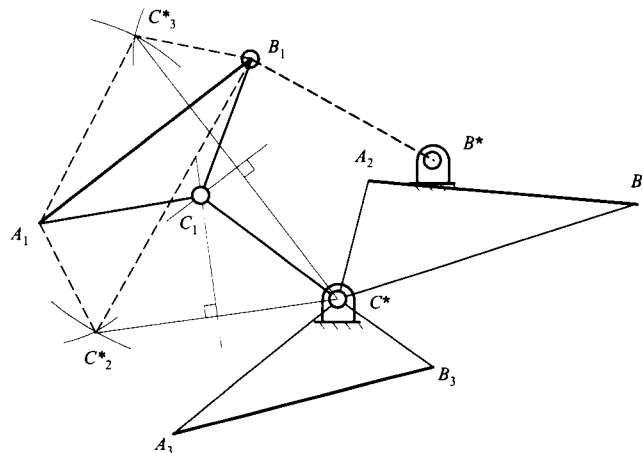
second and third positions ( $C_2, C_3$ ) of the moving pivot can be located by constructing triangle  $A_2B_2C_2$  congruent to triangle  $A_1B_1C_1$  and triangle  $A_3B_3C_3$  congruent to triangle  $A_1B_1C_1$ .

This technique gives, of course, only one crank. If both cranks are to have nominated fixed pivots, the construction must be repeated for the second crank. If the moving pivot of the second crank is to be chosen, then the earlier construction is used.

### 6.3.5 Design of Slider Cranks and Elliptic Trammels

To design a linkage that has a slider moving on a straight line, we must find a coupler point that has three positions on a straight line. This is shown in Fig. 6.15. The points having three positions on a straight line are those special circle points that move on a circle of infinite radius. Therefore, the points satisfying this condition are a select set of points. The procedure for finding these special points is described in the following:

1. Locate the poles  $P_{12}, P_{13}$ , and  $P_{23}$  for positions 1 and 2, 1 and 3, and 2 and 3, respectively.
2. Locate the point  $P'_{23}$  called an image pole by making triangle  $P_{12}P_{13}P'_{23}$  the mirror image of triangle  $P_{12}P_{13}P_{23}$  about the line through poles  $P_{12}$  and  $P_{13}$ . The image pole  $P'_{ij}$  is the point in the coupler about which the frame appears to pivot as the coupler moves from position  $i$  to position  $j$ . Poles  $P_{12}$  and  $P_{13}$  are both poles and image poles.
3. Locate the center of the circle circumscribing the image pole triangle  $P_{12}P_{13}P'_{23}$  by drawing the perpendicular bisectors of  $P_{12}P_{13}$  and  $P_{13}P'_{23}$  or  $P_{12}P'_{23}$ .
4. Draw the circle through  $P_{12}, P_{13}$ , and  $P'_{23}$ . This circle is fixed to the coupler and is called the circle of sliders. Any point on this circle has all three of its positions collinear. Hence, any point on this circle can be used as the moving pivot of a slider-hinge link.
5. Select a point on the circle of sliders and construct the three positions of that point (the moving pivot). These three positions will be collinear. The slide direction is parallel to the line on which all three positions lie. Actually, in this construction, one needs to construct only two of the three positions since any two positions will determine the slider line. Three positions of the coupler triangle ( $ABC$ ) are shown in Fig. 6.16. Note that the three triangles  $A_1B_1C_1, A_2B_2C_2$ , and  $A_3B_3C_3$  are congruent.



**FIGURE 6.14** Synthesis of a crank with a selected fixed pivot  $C^*$ .  $C^*_2$  and  $C^*_3$  are, respectively, the second and third positions of point  $C^*$  as seen from the moving lamina.  $C_1$  is the center of the circle passing through  $C^*, C^*_2$ , and  $C^*_3$ . After the crank  $C^*C_1$  has been synthesized, the linkage may be completed by designing a second crank by any method. The dashed crank is the result of choosing  $B_1$  as the moving pivot of the second



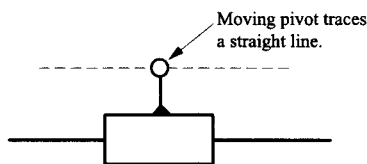


FIGURE 6.15 Geometric effect of replacing the fixed revolute of a crank by a prismatic joint.

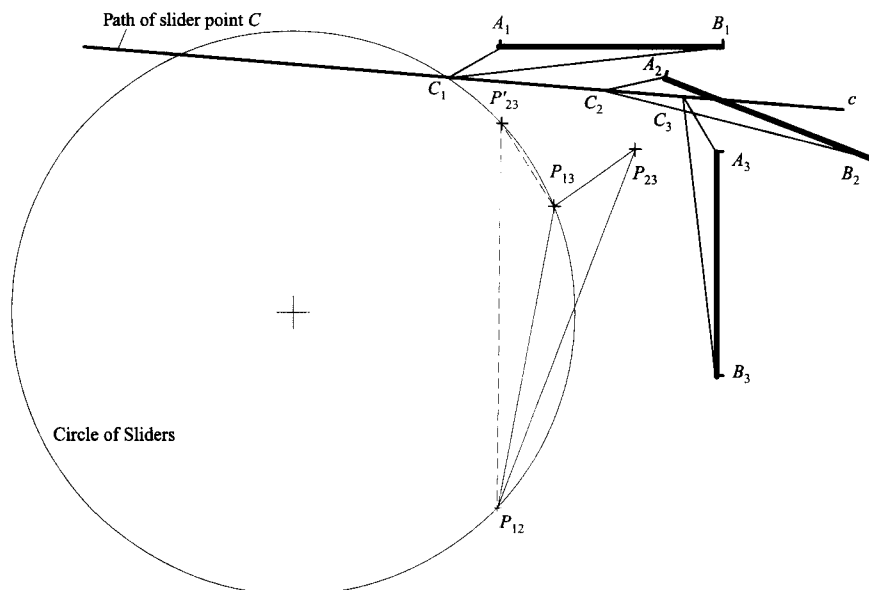


FIGURE 6.16 Construction of slider link and slider line. The three design positions are  $A_1B_1$ ,  $A_2B_2$ , and  $A_3B_3$ . The slider point,  $C_1$ , is chosen from the circle that passes through the points  $P_{12}$ ,  $P_{13}$ , and  $P_{23}'$ .  $C_2$  and  $C_3$  are the second and third positions of the slider point.  $c$  is the line in the direction of sliding.

That this construction will give slider points can be proved as follows (also, see Hall<sup>4</sup>):

1. The angle subtended at the pole  $P_{1i}$  by any crank is  $\theta_{1i}/2$ , where  $\theta_{1i}$  is the rotation of the moving plane between positions 1 and  $i$ . This is shown in Fig. 6.17. This follows because the circle point,  $X$ , being a point in the moving plane, rotates through angle  $\theta_{1i}$  about  $P_{1i}$  in moving from position 1 to position  $i$ . Since  $P_{1i}X^*$  is common for both positions, and  $X^*X_i = X^*X_1$ , and  $P_{1i}X_1 = P_{1i}X_i$ , it follows that triangle  $P_{1i}X^*X_i$  is the mirror image of  $P_{1i}X^*X_1$ . Therefore,  $\angle X_1P_{1i}X^* = \angle X^*P_{1i}X_i = \theta_{1i}/2$ .
2. A slider-hinge link can be thought of as a crank with its center point at infinity. If we draw a line from  $P_{1i}$  toward the center point at infinity, that line will be perpendicular to the slider line. From the result in item 1, the angle at the pole  $P_{1i}$  between the line joining  $P_{1i}$  to the circle point and a line normal to the slide is  $\theta_{1i}/2$ . Thus, given the direction  $c$  of the slide, the circle point  $C_1$  whose three positions lie on a line parallel to  $c$  is located by drawing normals from  $c$  to  $P_{12}$  and  $P_{13}$  as shown in Fig. 6.18, and constructing lines at angles  $\theta_{12}/2$  and  $\theta_{13}/2$ , respectively, to those normals. These lines intersect at the required point  $C_1$ , as shown in Fig. 6.18. The angle  $P_{12}C_1P_{13}$  is  $(\theta_{13}/2 - \theta_{12}/2)$ .

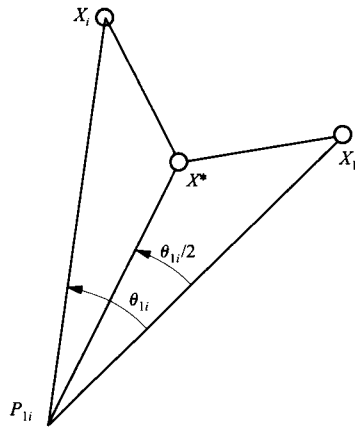


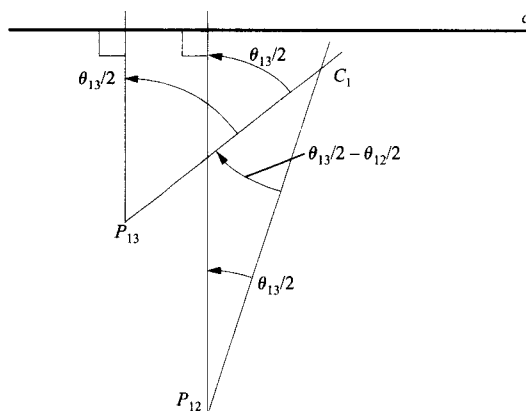
FIGURE 6.17 Relationship of angle subtended by a crank at a pole to the angular displacement about that pole.

3. The three poles,  $P_{12}$ ,  $P_{23}$ , and  $P_{13}$ , form a triangle called a pole triangle as shown in Fig. 6.19. From Fig. 6.18, the angle  $P_{12}C_1P_{13}$  is  $(\theta_{13}/2 - \theta_{12}/2)$ ; and from the pole triangle,  $(\theta_{13}/2 - \theta_{12}/2) = \theta_{23}/2$  (since the exterior angle of a triangle is equal to the sum of the opposite interior angles). Hence, the angle  $P_{12}C_1P_{13}$  is equal to  $\theta_{23}/2$  regardless of the direction of  $c$ , making the angle  $P_{12}C_1P_{13}$  independent of the direction of  $c$ , and the locus of all points having three positions collinear is the locus of all points  $C_1$  forming the angle  $(P_{12}C_1P_{13})/2$ . This is a circle passing through poles  $P_{12}$  and  $P_{13}$  with the central angle subtended by  $P_{12}P_{13}$  equal to  $\theta_{23}$ . The image pole,  $P'_{23}$ , also lies on this circle because it rotates with the body to  $P_{23}$  through the angle  $\theta_{13}$  about  $P_{13}$ . Thus, the angle  $P_{12}P'_{23}P_{13}$  is  $\theta_{23}/2$ . Hence, the required circle is the circle that circumscribes  $P_{12}P_{13}P'_{23}$ .

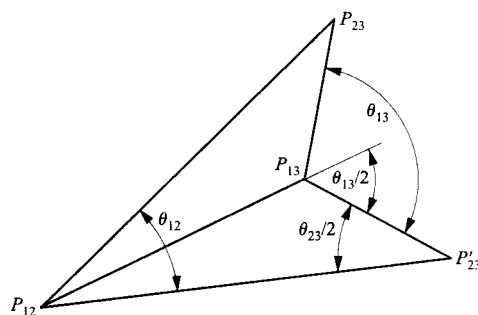
### 6.3.6 Order Problem and Change of Branch

Note that the preceding techniques really only guarantee that the mechanism can be assembled in the design positions; they do not guarantee that the mechanism will function correctly between different design positions. It is confusing, but it is quite possible for the simple graphical procedures developed here to produce spurious solutions. These are solutions that do not physically pass through the design positions or pass through the design positions in the wrong order. Thus, two problems can occur that may make the design unacceptable.

The first problem arises because there are two possible assembly modes for a four-bar linkage of given link lengths corresponding to a given value of the driving-crank angle. These are termed “assembly configurations” or “solution branches.” If the solution linkage for a motion generation problem is such that some of the design positions lie on one assembly configuration and others on the other assembly configuration, it may not be possible to move the linkage through all design positions without physically disconnecting it and reassembling it in the other assembly configuration. Fortunately, there is a simple graphical test to identify this problem.



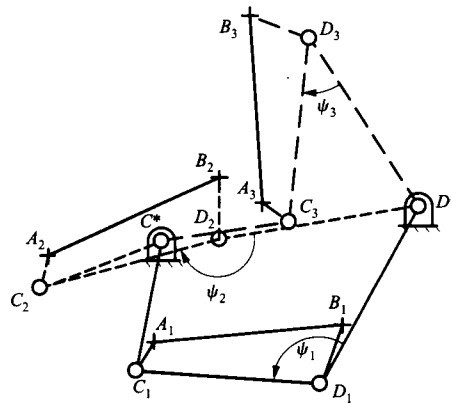
**FIGURE 6.18** Relationship of sliding direction  $c$  and slider point  $C_1$  to the poles  $P_{12}$  and  $P_{13}$ .



**FIGURE 6.19** Angular relationships of pole triangle and image pole triangle. The triangles are mirror images of each other.

To detect whether a mechanism must change branches to pass through all of the positions, it is necessary only to assemble the mechanism in one position and determine whether it can be moved through the other two positions. This can be done conveniently if the linkage can be animated on a computer screen. If one position is missed, then a change of branch is indicated.

Another way to determine whether a change of branch is indicated is to examine the angle  $\psi$  between the coupler and the output link. Because an extreme position of the driving joint corresponds to the angle  $\psi$  passing through an angle of either  $0$  or  $\pi$ , the key to determining the branch change is the sign of that angle. A convenient method is to construct the cranks and coupler in all design positions and inspect the angle  $\psi$  between the driven crank (the longer of the two cranks) and the coupler. A change in direction of this angle indicates a change of branch in a crank-rocker or drag-link type of mechanism and a drive failure in a double-rocker type of linkage. In either case, the solution linkage is not usable. An example of this condition is shown in Fig. 6.20. There the direction of the angle  $D^*D_1C_1$  is opposite to that of angles  $D^*D_2C_2$  and  $D^*D_3C_3$ . Hence the linkage passes through a position in which the driving joint  $C^*$  is at a motion limit.

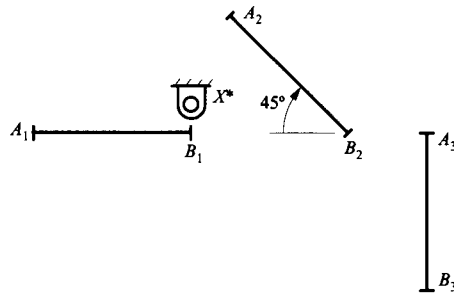


**FIGURE 6.20** An example in which the solution linkage is incapable of moving through the design positions without being disconnected and reassembled. The solution linkage is shown in all three design positions as  $C^*C_1D_1D^*$ ,  $C^*C_2D_2D^*$ , and  $C^*C_3D_3D^*$ , respectively. The angles between the driven (longer) crank and the coupler are examined in all three positions. These are the angles  $D^*D_1C_1 = \psi_1$ ,  $D^*D_2C_2 = \psi_2$ , and  $D^*D_3C_3 = \psi_3$ , respectively.  $\psi_1$  is counterclockwise, and  $\psi_2$  and  $\psi_3$  are clockwise. Thus the angle  $\psi$  changes sign, indicating a change of branch in the solution.

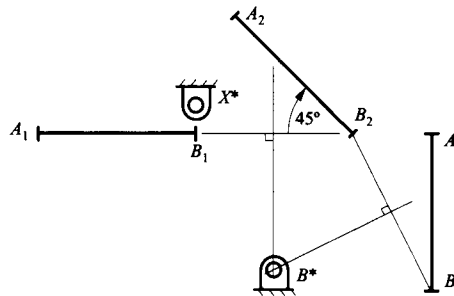
**EXAMPLE 6.1**  
**Position Synthesis**  
**of a Four-Bar**  
**Linkage**  
**Solution**

Design a four-bar linkage whose coupler moves through the three positions indicated by the line segment  $AB$  in Fig. 6.21. Point  $B$  is to be one moving pivot and point  $X^*$  is to be one fixed pivot.

1. The procedure for locating the fixed pivot  $B^*$  is shown in Fig. 6.22. The construction used is that of Fig. 6.12.

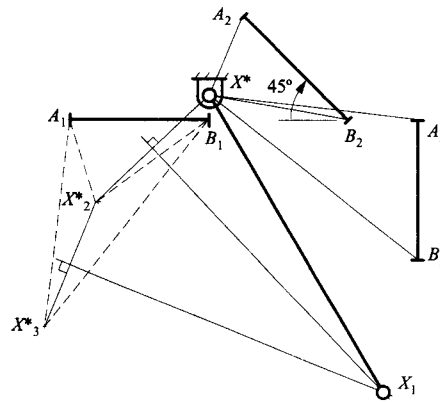


**FIGURE 6.21** The problem of Example 6.1.



**FIGURE 6.22** Location of the fixed pivot,  $B^*$ , given the moving pivot,  $B_1$ .

2. The procedure for the location of moving pivot  $X$  is shown in Fig. 6.23. The construction used is that of Fig. 6.14.



**FIGURE 6.23** Location of the moving pivot,  $X_1$ , given the location of the fixed pivot,  $X^*$ . Triangles  $A_1B_1X_2^*$  and  $A_2B_2X^*$  are congruent, as are triangles  $A_1B_1X_3^*$  and  $A_3B_3X^*$ .

Triangle  $A_1B_1X_2^*$  is congruent to triangle  $A_2B_2X^*$ , and triangle  $A_1B_1X_3^*$  is congruent to triangle  $A_3B_3X^*$ .

$X_1$  is located at the center of the circle  $X^*X_2^*X_3^*$ .

The other two positions of point  $X$  ( $X_2$  and  $X_3$ ) can then be located by constructing triangles  $A_2B_2X_2$  and  $A_3B_3X_3$  congruent to triangle  $A_1B_1X_1$ .

3. Check the solution.

We first check the Grashof type of the linkage:

$$X^*B^* = 2.41 = p$$

$$B_1X_1 = 4.28 = q$$

$$B^*B_1 = 2.06 = s$$

$$X^*X_1 = 4.62 = l$$

$$l + s = 6.68, \quad p - q = 6.69$$

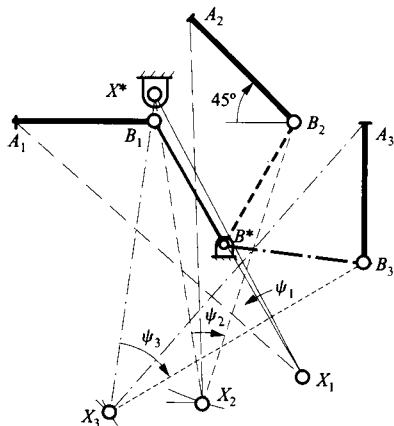
so

$$l + s < p + q \text{ (barely)}$$

The shortest link,  $s$ , is a crank, so the linkage is a crank-rocker.

To check for change of branch, we draw the linkage in all three of the design positions, as shown in Fig. 6.24. All of the information necessary to do this has already been generated in previous stages of the construction procedure.

Because  $X^*X_1$  is the longer of the two cranks, assume that it is the driven link, and  $B^*B_1$  is the driver link. We can then check the signs of the angles  $X^*X_1B_1$ ,  $X^*X_2B_2$ , and  $X^*X_3B_3$  to check for branching.  $\angle X^*X_1B_1$  is counterclockwise whereas  $\angle X^*X_2B_2$  and  $\angle X^*X_3B_3$  are clockwise. Hence a change of branch must occur.



**FIGURE 6.24** Construction of the solution linkage and verification that it satisfies the design positions without disconnection. In this case, the linkage fails the test because  $\psi_1 = \angle X^*X_1B_1$  is counterclockwise whereas  $\psi_2$  and  $\psi_3$  are clockwise. Hence, the linkage cannot be moved through the design positions by rotation of the crank  $B^*B$ .

**EXAMPLE 6.2**  
**Position Synthesis**  
**of a Slider-Crank**  
**Mechanism**

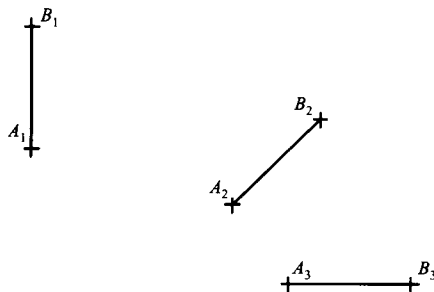
**Solution**

Design a slider-crank mechanism to move a coupler containing the line  $AB$  through the three positions shown in Fig. 6.25. Use point  $B$  as a circle point.

To design a slider-crank mechanism, it is necessary to identify a circle point and the corresponding center point (or vice versa) and a slider point. We must also identify the direction of the slider line. In this problem, point  $B$  has been identified as the circle point for the crank. Therefore, to locate the center point, we need only find the center of the circle on which the three positions of  $B$  lie. The construction for finding the center point ( $B^*$ ) and the crank in position 1 is shown in Fig. 6.26.

To locate the slider point, we must locate the poles, the image pole  $P'_{23}$ , and the circle of sliders in position 1. This circle is attached to the coupler. The construction of the poles is shown in Fig. 6.27, and the locations of the image pole and circle of sliders are shown in Fig. 6.28. We can select any point on the slider circle as a slider point. The point chosen is  $C$ . To complete the design, we need to locate the slider point in positions 2 and 3. The three positions,  $C_1$ ,  $C_2$ , and  $C_3$ , will be collinear on the slider line. The construction of the slider line is also shown in Fig. 6.28.

From the three positions of  $C$  shown in Fig. 6.28, it is clear that the linkage does go through the three positions in the correct order. However, in general it is necessary to check for both order and branch problems.



**FIGURE 6.25** Design positions for Example 6.2.

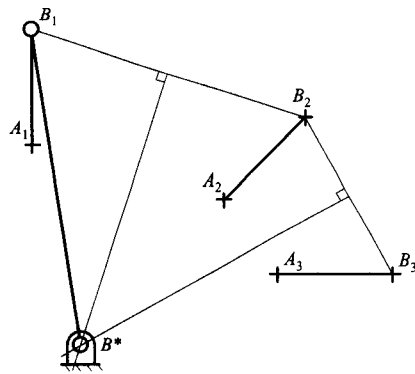


FIGURE 6.26 Construction of crank of slider-crank mechanism for Example 6.2.

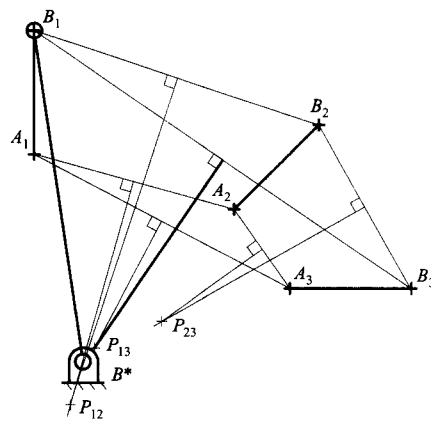


FIGURE 6.27 Construction of the poles for Example 6.2.

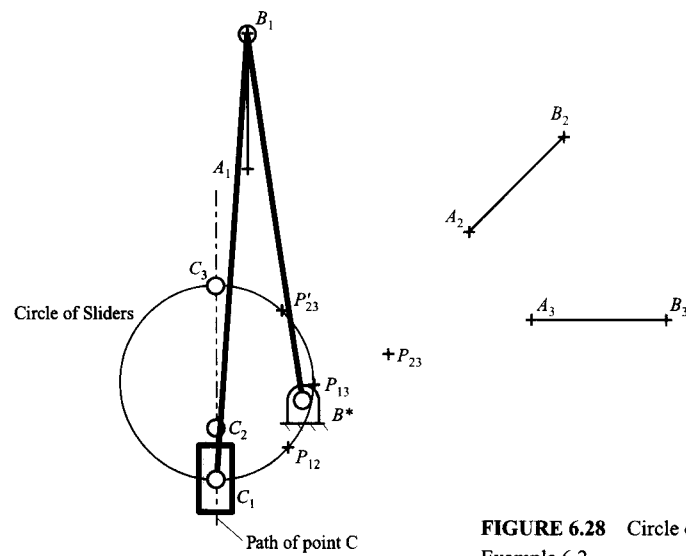


FIGURE 6.28 Circle of sliders and final linkage for Example 6.2.

### 6.3.7 Analytical Approach to Rigid-Body Guidance

Rigid-body guidance can be approached analytically in two ways. The first procedure requires coordinate transformations and is more general. It can be extended easily to four positions, and the different elements (such as the circle of sliders) developed in the graphical procedure arise naturally from the mathematics. However, for three positions, the first procedure is more involved than the second procedure, which is a mathematical representation of the graphical procedure. Therefore, only the second procedure will be presented here. Readers are referred to works by Sandor and Erdman,<sup>7</sup> Waldron,<sup>9</sup> or Suh and Radcliffe<sup>8</sup> for a more general analytical treatment.

The analytical approach to rigid-body guidance involves coordinate transformations when center points are selected. Therefore, before addressing the topic directly, let us develop the equations for the needed coordinate transformations between the coupler and frame coordinate systems.

**Coordinate Transformations** The general relationship between the coupler and frame systems is indicated in Fig. 6.29. From Fig. 6.29, we can write the vector equations as

$$\mathbf{r}_{P/O} = \mathbf{r}_{P/A} + \mathbf{r}_{A/O}$$

In this equation,  $\mathbf{r}_{P/O}$  and  $\mathbf{r}_{A/O}$  are defined in the frame coordinate system, and  $\mathbf{r}_{P/A}$  is defined in the coupler coordinate system. Therefore, only  $\mathbf{r}_{P/A}$  needs to be transformed to the frame coordinate system. This is shown in Fig. 6.30.

In matrix form, the coordinate transformation from the coupler to the frame system is

$$\begin{Bmatrix} x \\ y \end{Bmatrix} = [R] \begin{Bmatrix} X \\ Y \end{Bmatrix} + \begin{Bmatrix} a_x \\ a_y \end{Bmatrix} \quad (6.6)$$

In Eq. (6.6), the matrix  $R$  indicates the orientation (rotation) of the coupler coordinate system relative to the frame coordinate system. The vector  $\{a_x, a_y\}^T$  gives the origin of the coupler coordinate system relative to the frame system. We need to determine the rotation matrix  $[R]$  first. From Fig. 6.30, we have

$$x_{P/A} = X \cos \theta - Y \sin \theta$$

$$y_{P/A} = Y \cos \theta + X \sin \theta$$

or

$$\begin{Bmatrix} x_{P/A} \\ y_{P/A} \end{Bmatrix} = \begin{bmatrix} \cos \theta & -\sin \theta \\ \sin \theta & \cos \theta \end{bmatrix} \begin{Bmatrix} X \\ Y \end{Bmatrix}$$

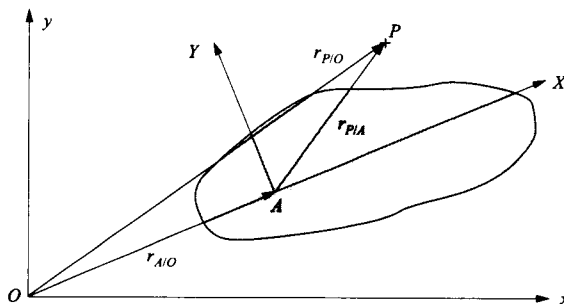
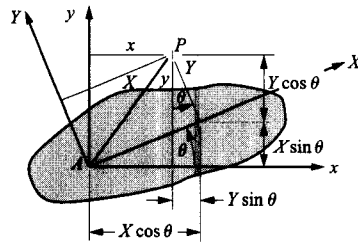


FIGURE 6.29 Relationship between coupler and frame coordinate systems.





**FIGURE 6.30** Transformation from coupler system  $XY$  to frame system  $xy$ .

For any general point with coordinates  $(X, Y)$  relative to the coupler, the coordinates  $(x, y)$  relative to the frame are given by Eq. (6.6) or

$$\begin{Bmatrix} x \\ y \end{Bmatrix} = \begin{bmatrix} \cos \theta & -\sin \theta \\ \sin \theta & \cos \theta \end{bmatrix} \begin{Bmatrix} X \\ Y \end{Bmatrix} + \begin{Bmatrix} a_x \\ a_y \end{Bmatrix} = [R] \begin{Bmatrix} X \\ Y \end{Bmatrix} + \begin{Bmatrix} a_x \\ a_y \end{Bmatrix}$$

Therefore,

$$[R] = \begin{bmatrix} \cos \theta & -\sin \theta \\ \sin \theta & \cos \theta \end{bmatrix} \quad (6.7)$$

We can also transform from the frame coordinate system to the coupler coordinate system. This is shown in Fig. 6.31. From that figure it is clear that

$$X_{P/A} = x_{P/A} \cos \theta + y_{P/A} \sin \theta$$

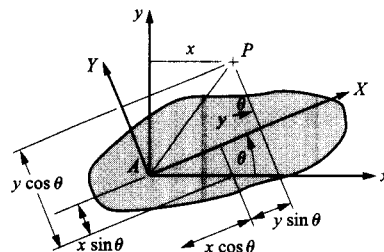
$$Y_{P/A} = y_{P/A} \cos \theta - x_{P/A} \sin \theta$$

or

$$\begin{Bmatrix} X_{P/A} \\ Y_{P/A} \end{Bmatrix} = \begin{bmatrix} \cos \theta & \sin \theta \\ -\sin \theta & \cos \theta \end{bmatrix} \begin{Bmatrix} x_{P/A} \\ y_{P/A} \end{Bmatrix} = [A] \begin{Bmatrix} x_{P/A} \\ y_{P/A} \end{Bmatrix} \quad (6.8)$$

where

$$[A] = \begin{bmatrix} \cos \theta & \sin \theta \\ -\sin \theta & \cos \theta \end{bmatrix} \quad (6.9)$$



**FIGURE 6.31** Transformation from frame system  $xy$  and coupler system  $XY$ .

When we compare Eqs. (6.8) and (6.9), it is clear that

$$\begin{bmatrix} \cos \theta & \sin \theta \\ -\sin \theta & \cos \theta \end{bmatrix} = \begin{bmatrix} \cos \theta & -\sin \theta \\ \sin \theta & \cos \theta \end{bmatrix}^T = \begin{bmatrix} \cos \theta & -\sin \theta \\ \sin \theta & \cos \theta \end{bmatrix}^{-1}$$

Therefore,

$$[A] = [R]^{-1} = [R]^T \quad (6.10)$$

Now assume that we have specified the position of the coupler coordinate system by the origin of the moving system  $(a_x, a_y)$  and the rotation angle  $\theta$  for the  $X$  axis. To transform from the coupler system  $(X, Y)$  to the frame coordinate system  $(x, y)$ , use

$$\begin{Bmatrix} x \\ y \end{Bmatrix} = \begin{bmatrix} \cos \theta & -\sin \theta \\ \sin \theta & \cos \theta \end{bmatrix} \begin{Bmatrix} X \\ Y \end{Bmatrix} + \begin{Bmatrix} a_x \\ a_y \end{Bmatrix} \quad (6.11)$$

To transform from the frame system to the coupler system, use

$$\begin{Bmatrix} X \\ Y \end{Bmatrix} = \begin{bmatrix} \cos \theta & \sin \theta \\ -\sin \theta & \cos \theta \end{bmatrix} \begin{Bmatrix} x - a_x \\ y - a_y \end{Bmatrix} = \begin{bmatrix} \cos \theta & \sin \theta \\ -\sin \theta & \cos \theta \end{bmatrix} \begin{Bmatrix} x \\ y \end{Bmatrix} - \begin{bmatrix} \cos \theta & \sin \theta \\ -\sin \theta & \cos \theta \end{bmatrix} \begin{Bmatrix} a_x \\ a_y \end{Bmatrix} \quad (6.12)$$

In the following, we will assume that each position of the coupler is given by the coordinates  $(a_x, a_y)$  of the origin of the coupler coordinate system relative to the frame and by the angle  $\theta$  for the  $X$  axis. If instead of the angle  $\theta$ , the coordinates  $(b_x, b_y)$  of a second point  $B$  in the coupler are given, we must first compute the angle  $\theta$  from the equation

$$\theta = \tan^{-1} \left[ \frac{b_y - a_y}{b_x - a_x} \right] \quad (6.13)$$

When a circle point is selected, the coordinates of that point are given relative to the coupler coordinate system  $(X, Y)$ . The coordinates of the three positions of that point relative to the frame coordinate system can be computed using Eq. (6.11). The corresponding center point is located by finding the center of the circle (analytically) on which the three positions of the circle point lie. The coordinates of the center of the circle will be defined in the frame coordinate system.

If a center point is given, the coordinates will be in the frame coordinate system  $(x, y)$ . To find the corresponding circle point, the three apparent positions of the center point relative to the coupler coordinate system must be found. This is done using Eq. (6.12). The corresponding circle point is located by finding the center of the circle (analytically) on which the three positions of the center point lie. The coordinates of the center of the circle will be defined in the coupler coordinate system. The coordinates of this point in any of the positions can be found relative to the frame using Eq. (6.11). The crank length can be determined by computing the distance between the circle and center points once both are defined relative to the same coordinate system.

Locating center points given circle points and vice versa requires that the center of the circle corresponding to three positions of a point be found. To find the circle of sliders, the locations of the poles and the image pole must be found. We will discuss an analytical procedure for finding poles first. After this is done, it will be apparent that the same procedure can be used to find the center of a circle given three positions of a point.

**Finding Poles** Let  $A_i$  and  $A_j$  and  $B_i$  and  $B_j$  be vectors defining the locations of two points in two positions. The  $x$  and  $y$  coordinates of each point are assumed to be known. As indicated in Fig. 6.11, the pole is the point that lets us move the rigid body from position  $i$  to position  $j$  by a simple rotation. To determine the location of the pole analytically, let  $r_A$  be the distance from the pole to point  $A$  and  $r_B$  be the distance from  $B$  to the pole  $P_{ij}$  as shown in Fig. 6.32a. The following geometric relationships then hold.

$$\begin{aligned} \left. \begin{aligned} (A_{x_i} - p_{ij_x})^2 + (A_{y_i} - p_{ij_y})^2 &= (r_A)^2 = (A_{x_j} - p_{ij_x})^2 + (A_{y_j} - p_{ij_y})^2 \\ (B_{x_i} - p_{ij_x})^2 + (B_{y_i} - p_{ij_y})^2 &= (r_B)^2 = (B_{x_j} - p_{ij_x})^2 + (B_{y_j} - p_{ij_y})^2 \end{aligned} \right\} \quad (6.14) \end{aligned}$$

Expanding Eqs. (6.14) gives

$$\begin{aligned} A_{x_i}^2 - 2A_{x_i}p_{ij_x} + p_{ij_x}^2 + A_{y_i}^2 - 2A_{y_i}p_{ij_y} + p_{ij_y}^2 &= A_{x_j}^2 - 2A_{x_j}p_{ij_x} + p_{ij_x}^2 + A_{y_j}^2 - 2A_{y_j}p_{ij_y} + p_{ij_y}^2 \\ B_{x_i}^2 - 2B_{x_i}p_{ij_x} + p_{ij_x}^2 + B_{y_i}^2 - 2B_{y_i}p_{ij_y} + p_{ij_y}^2 &= B_{x_j}^2 - 2B_{x_j}p_{ij_x} + p_{ij_x}^2 + B_{y_j}^2 - 2B_{y_j}p_{ij_y} + p_{ij_y}^2 \end{aligned}$$

These equations can be simplified to give

$$\begin{aligned} \left( A_{x_i}^2 + A_{y_i}^2 \right) - \left( A_{x_j}^2 + A_{y_j}^2 \right) &= 2(A_{x_i} - A_{x_j})p_{ij_x} + 2(A_{y_i} - A_{y_j})p_{ij_y} \\ \left( B_{x_i}^2 + B_{y_i}^2 \right) - \left( B_{x_j}^2 + B_{y_j}^2 \right) &= 2(B_{x_i} - B_{x_j})p_{ij_x} + 2(B_{y_i} - B_{y_j})p_{ij_y} \end{aligned} \quad (6.15)$$

These equations are linear in the unknown pole coordinates and can easily be solved. In matrix form, the equations become

$$\begin{bmatrix} 2(A_{x_i} - A_{x_j}) & 2(A_{y_i} - A_{y_j}) \\ 2(B_{x_i} - B_{x_j}) & 2(B_{y_i} - B_{y_j}) \end{bmatrix} \begin{Bmatrix} p_{ij_x} \\ p_{ij_y} \end{Bmatrix} = \begin{Bmatrix} (A_{x_i}^2 + A_{y_i}^2) - (A_{x_j}^2 + A_{y_j}^2) \\ (B_{x_i}^2 + B_{y_i}^2) - (B_{x_j}^2 + B_{y_j}^2) \end{Bmatrix} \quad (6.16)$$

Equations (6.16) can be solved using a calculator or a matrix equation solver such as MATLAB.

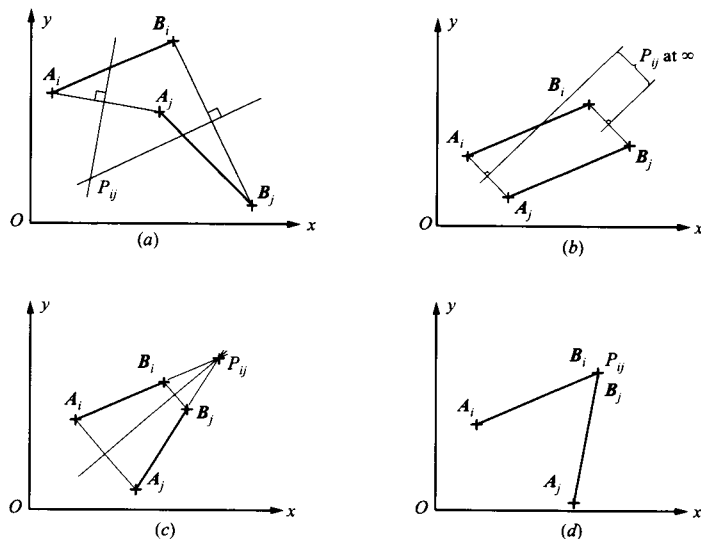
Equations (6.16) apply to most types of positions; however, there are three special cases that will make the matrix singular. These are shown in Fig. 6.32 and identified in the following:

1. Two positions of the coupler are parallel (Fig. 6.32b).
2. Lines linking the successive positions of two points are parallel (Fig. 6.32c).
3. Two successive positions of a point are coincident (Fig. 6.32d).

Each of these conditions can be handled separately.

**Two Parallel Positions** When two positions are parallel, the resulting pole is at infinity in the direction given by the angle  $\gamma$  where

$$\gamma = \frac{\pi}{2} + \tan^{-1} \left( \frac{A_{y_j} - A_{y_i}}{A_{x_j} - A_{x_i}} \right) = \frac{\pi}{2} + \tan^{-1} \left( \frac{B_{y_j} - B_{y_i}}{B_{x_j} - B_{x_i}} \right)$$



**FIGURE 6.32** Location of pole  $P_{ij}$ . (a) general case, (b) parallel positions, (c) symmetric positions, (d) intersecting positions at  $B$  (or  $A$ ).

**Lines  $A_iA_j$  and  $B_iB_j$  are Parallel** When this situation occurs, the pole is located at the intersection of the lines defined by  $A_iB_i$  and  $A_jB_j$ . The location of the pole is then given by solving the following simultaneous equations:

$$\left( \frac{p_{ijx} - A_{xi}}{B_{xi} - A_{xi}} \right) = \left( \frac{p_{ijy} - A_{yi}}{B_{yi} - A_{yi}} \right)$$

and

$$\left( \frac{p_{ijx} - A_{xj}}{B_{xj} - A_{xj}} \right) = \left( \frac{p_{ijy} - A_{yj}}{B_{yj} - A_{yj}} \right)$$

The equations can be simplified and rewritten as

$$\begin{aligned} p_{ijx}(B_{yi} - A_{yi}) - p_{ijy}(B_{xi} - A_{xi}) &= A_{xi}(B_{yi} - A_{yi}) - A_{yi}(B_{xi} - A_{xi}) \\ p_{ijx}(B_{yj} - A_{yj}) - p_{ijy}(B_{xj} - A_{xj}) &= A_{xj}(B_{yj} - A_{yj}) - A_{yj}(B_{xj} - A_{xj}) \end{aligned}$$

or in matrix form,

$$\begin{bmatrix} (B_{yi} - A_{yi}) & -(B_{xi} - A_{xi}) \\ (B_{yj} - A_{yj}) & -(B_{xj} - A_{xj}) \end{bmatrix} \begin{Bmatrix} p_{ijx} \\ p_{ijy} \end{Bmatrix} = \begin{Bmatrix} A_{xi}(B_{yi} - A_{yi}) - A_{yi}(B_{xi} - A_{xi}) \\ A_{xj}(B_{yj} - A_{yj}) - A_{yj}(B_{xj} - A_{xj}) \end{Bmatrix} \quad (6.17)$$

Equations (6.17) can be solved using a calculator or a matrix equation solver such as MATLAB.

**Two Successive Positions Coincident** When a point on the coupler does not move in successive coupler positions, that point is identical to the pole. Therefore, if  $A_i = A_j$  then both equal  $p_{ij}$  or if  $B_i = B_j$  then both equal  $p_{ij}$ .

**Finding the Center of a Circle on Which Three Points Lie** The procedure given for finding poles can be used to find the center of the circle that passes through three points. To do this, simply treat  $B_i$  and  $A_i$  as the same point. This is shown schematically in Fig. 6.33 to find  $A^*$  given three positions of  $A$ .

**Image Pole** The image pole is found by reflecting the pole about a line through the two other poles. To find the image pole  $P'_{23}$ , we reflect the pole  $P_{23}$  about the line through poles  $P_{12}$  and  $P_{13}$ . This is shown in Fig. 6.34. Given the coordinates of poles  $P_{12}$ ,  $P_{23}$ , and  $P_{13}$ , the coordinates of the image pole,  $P'_{23}$ , can be found as follows. First define

$$\mathbf{g} = (\mathbf{p}_{13} - \mathbf{p}_{12}) = (g_x, g_y)$$

and

$$\mathbf{h} = (\mathbf{p}_{23} - \mathbf{p}_{12}) = (h_x, h_y)$$

Then,

$$\beta = \tan^{-1} \left( \frac{h_y}{h_x} \right)$$

and

$$\theta = \tan^{-1} \left( \frac{g_y}{g_x} \right) - \beta$$

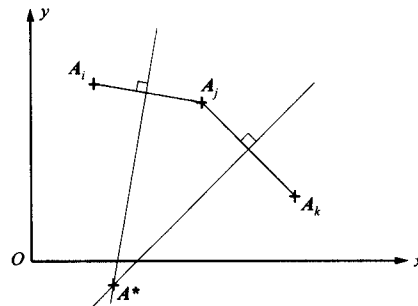
Let

$$r = \sqrt{h_x^2 + h_y^2}$$

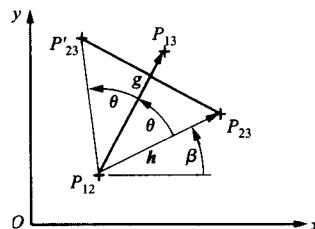
Then, the coordinates of the image pole are given by

$$\mathbf{p}'_{23} = \mathbf{p}_{12} + (r \cos(\beta + 2\theta)\mathbf{i} + r \sin(\beta + 2\theta)\mathbf{j})$$

MATLAB functions for the pole and image pole routines are given on the disk included with this book.



**FIGURE 6.33** Locating the center of a circle using the pole procedure. Compare this figure with Fig. 6.32a.



**FIGURE 6.34** Image pole location.

**Crank Design Given Circle Point** If the circle point is specified, the circle point coordinates  $(X, Y)$  will be given relative to the coupler coordinate system. The procedure for finding the corresponding center point and the resulting crank is given in the following.

1. Transform the coordinates of the circle point to the frame coordinate system using Eq. (6.11) for each position of the coupler. This will give three pairs of points,  $(x_1, y_1)$ ,  $(x_2, y_2)$ , and  $(x_3, y_3)$  relative to the frame coordinate system.
2. Set  $A_1 = (x_1, y_1)$ ;  $A_2 = (x_2, y_2)$ ; and  $A_3 = (x_3, y_3)$ . Then use the procedure in the subsection "Finding Poles" to find the location of the center point in the frame coordinate system. Call this point  $(x^*, y^*)$ .
3. The crank in position 1 is located by the line from  $(x^*, y^*)$  to  $(x_1, y_1)$ .
4. Locate the second crank using the same procedure and complete the linkage.

**Crank Design Given Center Point** If the center point is specified, the center point coordinates  $(x^*, y^*)$  will be given relative to the frame coordinate system. The procedure for finding the corresponding circle point relative to the coupler coordinate system and the subsequent crank is given in the following.

1. Transform the coordinates of the center point to the coupler coordinate system using Eq. (6.12) for each position of the coupler. This will give three pairs of points,  $(X_1^*, Y_1^*)$ ,  $(X_2^*, Y_2^*)$ , and  $(X_3^*, Y_3^*)$ , relative to the coupler coordinate system.
2. Set  $A_1 = (X_1^*, Y_1^*)$ ;  $A_2 = (X_2^*, Y_2^*)$ ; and  $A_3 = (X_3^*, Y_3^*)$ . Then use the procedure in subsection "Finding Poles" to find the location of the circle point relative to the coupler coordinate system. Call this point  $(X, Y)$ .
3. Identify the position  $i$  in which the linkage is to be displayed. Transform the coordinates of point  $(X, Y)$  to the frame coordinate system using Eq. (6.11) for position  $i$ . Call the transformed point  $(x_i, y_i)$ .
4. The crank in position  $i$  is located by the line from  $(x^*, y^*)$  to  $(x_i, y_i)$ .
5. Locate the second crank and complete the linkage.

**Design of a Slider** If a slider is to be used, we must find the circle of sliders and two of the three positions of the slider point. The procedure is given in the following.

1. Let two points in the coupler be given as  $A = (0, 0)$  and  $B = (1, 0)$  relative to the coupler coordinate system. Transform the coordinates of both points to the frame coordinate system using Eq. (6.11) for each position of the coupler. This will give three pairs of coordinates for  $A$  and three for  $B$  relative to the frame coordinate system. Call the point locations  $A_1, A_2, A_3, B_1, B_2,$  and  $B_3$ .
2. Compute the coordinates of the poles  $p_{12}, p_{13},$  and  $p_{23}$  using the coordinates of  $A$  and  $B$  and the procedure given in subsection "Finding Poles." The resulting coordinates will be in the frame coordinate system.
3. Compute the coordinates of the image pole  $p'_{23}$  using the procedure given in the subsection "Image Pole." The coordinates of  $P'_{23}$  will also be in the frame coordinate system.
4. Set  $C_i = p_{12}$ ;  $C_j = p_{13}$ ; and  $C_k = p'_{23}$ . Then use the procedure in subsection "Finding Poles" to find the location of the center  $(x_c, y_c)$  of the slider circle in the frame coordinate system. Compute the radius of the circle using

$$r_c = \sqrt{(C_{ix} - x_c)^2 + (C_{iy} - y_c)^2}$$

The center  $(x_c, y_c)$  and radius  $r_c$  will correspond to the circle of sliders in position 1.

5. Select the  $x$  coordinate of the slider point. Call this coordinate  $x_s$ . Solve for the coordinate  $y_s$  using

$$y_s = y_c \pm \sqrt{r_c^2 - (x_s - x_c)^2}$$

Notice that there will be two possible values for  $y_s$  for each value of  $x_s$ . It is necessary to select the specific point desired by identifying which sign (+ or -) gives the proper configuration for the linkage. The resulting point  $(x_s, y_s)_1$  will be the coordinates of the slider point in position 1 in the frame coordinate system.

6. Transform the point  $(x_s, y_s)_1$  to the coupler coordinate system using Eq. (6.12) and  $(a_x, a_y)_1$  and the rotation angle  $\theta_1$ . Call this point  $(X_s, Y_s)$ . It identifies the slider point relative to the coupler coordinate system.
7. Determine the coordinates of point  $(X_s, Y_s)$  in the frame coordinate system for positions 2 and 3 of the coupler. Call these positions  $(x_s, y_s)_2$  and  $(x_s, y_s)_3$ .
8. Define the slider line parametrically by

$$(x, y) = (x_s, y_s)_1 + \beta \left[ (x_s, y_s)_3 - (x_s, y_s)_1 \right] \quad (6.18)$$

where points along the slider line are a function of the single variable  $\beta$ . Note that  $\beta = 0$  at the first position  $(x_s, y_s)_1$  and  $\beta = 1$  at the third position  $(x_s, y_s)_3$ .

Compute  $\beta$  corresponding to the distance to the slider point in the second position using

$$\beta_2 = \frac{\left[ (x_s, y_s)_2 - (x_s, y_s)_1 \right]}{\left[ (x_s, y_s)_3 - (x_s, y_s)_1 \right]} \quad (6.19)$$

10. Check to ensure that the linkage goes through the positions in the correct order. For this to occur, position 2 must lie between positions 1 and 3 or  $0 < \beta_2 < 1$ .

**Implementing the Analytical Approach to Rigid-Body Guidance** The procedures given in the previous subsections can be used with a calculator to design four-bar linkages with revolute joints and sliders sliding on the frame. The procedures can also be programmed easily on a computer using any of the various languages. It is especially easy to program the procedure in MATLAB because of the ease with which matrix and vector manipulations may be carried out. A program that implements the procedure with limited graphical output is given on the disk included with this book.

## 6.4 FUNCTION GENERATION

---

The procedure developed here will use a four-bar linkage to generate the desired function; however, the general ideas presented can be used for any system for which a functional relationship can be derived between two variables. For example, assume that a "black box" is given such that the functional relationship between the two variables  $\alpha$  and  $\rho$  is

$$f(\alpha, \rho, a_1, a_2, a_3, a_4) = 0 \quad (6.20)$$

where  $a_1, a_2, a_3,$  and  $a_4$  are design variables defining the system. To design the system to approximate the function

$$g(\alpha, \rho) = 0 \quad (6.21)$$

we simply need to solve Eq. (6.21) four times to obtain four pairs of values for  $\alpha$  and  $\rho$ . We can designate these as  $(\alpha_1, \rho_1)$ ,  $(\alpha_2, \rho_2)$ ,  $(\alpha_3, \rho_3)$ , and  $(\alpha_4, \rho_4)$ . The points chosen where the approximate solution matches the exact solution are called precision points. Next rewrite Eq. (6.20) four times (corresponding to the number of design variables), one for each pair of  $(\alpha_i, \rho_i)$ , and solve the resulting set of equations for  $a_1$ ,  $a_2$ ,  $a_3$ , and  $a_4$ . Note that the equations may be nonlinear, requiring the use of numerical techniques.

**EXAMPLE 6.3**  
**Function**  
**Generation with a**  
**General Device**

**Solution**

A mechanical device characterized by the input–output relationship  $\phi = 2a_1 + a_2 \tan \theta$  is to be used to generate (approximately) the function  $\phi = 2\theta^3$  (with  $\theta$  and  $\phi$  both in radians) over the range  $0 \leq \theta \leq \pi/3$ .

- Determine the number of precision points required to complete the design of the system.
- Choose reasonable precision points and determine the values for the unknown design variables that will allow the device to approximate the function.

There are two unknowns ( $a_1$  and  $a_2$ ), so the number of precision points is two. We will determine a systematic way to locate the precision points later in this section, but for now, let us choose the two points to be at the quarter and three-quarter points of the range. Then

$$\theta_1 = \theta_{\min} + \frac{(\theta_{\max} - \theta_{\min})}{4} = 0 + \frac{(\pi/3 - 0)}{4} = 0 + \frac{\pi}{12} = 0.2618$$

and

$$\theta_2 = \theta_{\min} + \frac{3(\theta_{\max} - \theta_{\min})}{4} = 0 + \frac{3(\pi/3 - 0)}{4} = 0 + \frac{\pi}{4} = 0.7854$$

The corresponding values of  $\phi$  are

$$\phi_1 = 2\theta_1^3 = 2(0.2618)^3 = 0.03589, \quad \phi_2 = 2\theta_2^3 = 2(0.7854)^3 = 0.9689$$

We can now solve for  $a_1$  and  $a_2$  using the desired input–output relationship,

$$\phi = 2a_1 + a_2 \tan \theta$$

Substituting into the equation the values for  $\theta$  and  $\phi$  at the two precision points gives

$$0.03589 = 2a_1 + a_2 \tan(0.2618) = 2a_1 + 0.2679a_2$$

and

$$0.9689 = 2a_1 + a_2 \tan(0.7854) = 2a_1 + 1.0000a_2$$

Subtracting the two equations gives,

$$0.9330 = 0.7321a_2 \text{ resulting in } a_2 = 1.2746$$

Backsubstituting to determine  $a_1$  gives

$$2a_1 = 0.03589 - a_2 \tan(0.2618) = 0.03589 - 0.2679(1.2746) = -0.3055 \text{ resulting in } a_1 = -0.1528$$



The final equation for the device is

$$\phi = 2a_1 + a_2 \tan \theta = -0.3055 + 1.2746 \tan \theta$$

In the following example, the function  $f$  in Eq. (6.20) will be the governing position equation for a four-bar linkage. The function  $g$  will be an arbitrary function that is specified at the beginning of the analysis.

### 6.4.1 Function Generation Using a Four-Bar Linkage

Analytical function generation using a four-bar linkage was developed by Freudenstein,<sup>13</sup> and the basic equation relating the input and output variables for the four-bar linkage is called Freudenstein's equation.

Given three pairs of values for  $\theta$  and  $\phi$  in Fig. 6.35, the objective for the case considered here is to find  $r_2$ ,  $r_3$ , and  $r_4$  for the four-bar linkage. This is the linkage that will approximate the function implied by the three pairs of values for  $\theta$  and  $\phi$ . In the three-position function generation problem, the size of the linkage does not affect the functional relationship between  $\theta$  and  $\phi$ . Therefore, the frame link ( $r_1$ ) can be taken to initially have length 1, and the entire linkage can be scaled to any desired size after the basic design is established.

To develop the governing equation relating the input and output variables for the linkage, first determine expressions for the  $x$  and  $y$  components of the vectors corresponding to each link length. For the  $x$  direction,

$$r_2 \cos \theta + r_3 \cos \psi = 1 + r_4 \cos \phi \quad (6.22)$$

and for the  $y$  direction,

$$r_2 \sin \theta + r_3 \sin \psi = r_4 \sin \phi \quad (6.23)$$

We do not want  $\psi$  in the final equation. Therefore, isolate the terms involving  $\psi$  so that this angle can be eliminated. Then

$$\begin{aligned} r_3 \cos \psi &= 1 + r_4 \cos \phi - r_2 \cos \theta \\ r_3 \sin \psi &= r_4 \sin \phi - r_2 \sin \theta \end{aligned} \quad (6.24)$$

Square both equations and add to get

$$r_3^2 (\cos^2 \psi + \sin^2 \psi) = (1 + r_4 \cos \phi - r_2 \cos \theta)^2 + (r_4 \sin \phi - r_2 \sin \theta)^2$$

Expanding the equation and simplifying gives

$$r_3^2 = 1 + r_4^2 + r_2^2 + 2r_4 \cos \phi - 2r_2 \cos \theta - 2r_4 r_2 \cos(\theta - \phi)$$

Because we have three pairs of values for  $\theta$  and  $\phi$ , this equation can be written three times as

$$\begin{aligned} r_3^2 &= 1 + r_4^2 + r_2^2 + 2r_4 \cos \phi_1 - 2r_2 \cos \theta_1 - 2r_4 r_2 \cos(\theta_1 - \phi_1) \\ r_3^2 &= 1 + r_4^2 + r_2^2 + 2r_4 \cos \phi_2 - 2r_2 \cos \theta_2 - 2r_4 r_2 \cos(\theta_2 - \phi_2) \\ r_3^2 &= 1 + r_4^2 + r_2^2 + 2r_4 \cos \phi_3 - 2r_2 \cos \theta_3 - 2r_4 r_2 \cos(\theta_3 - \phi_3) \end{aligned} \quad (6.25)$$

Equations (6.25) can be solved for  $r_2$ ,  $r_3$ , and  $r_4$ . The procedure used to solve the equations depends on the tools that are available.

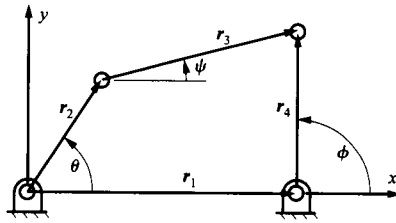


FIGURE 6.35 Four-bar linkage used for function generation.

**Solution by Matrices** The equations can be written simply in matrix form. To simplify the result, first rearrange the terms and divide each equation in Eqs. (6.25) by  $2r_2r_4$  and define the new unknowns as

$$z_1 = \frac{1 + r_2^2 + r_4^2 - r_3^2}{2r_2r_4} \quad (6.26)$$

$$z_2 = \frac{1}{r_2} \quad (6.27)$$

and

$$z_3 = \frac{1}{r_4} \quad (6.28)$$

We can then write the resulting equations as

$$\begin{aligned} z_1 + z_2 \cos \phi_1 - z_3 \cos \theta_1 &= \cos(\theta_1 - \phi_1) \\ z_1 + z_2 \cos \phi_2 - z_3 \cos \theta_2 &= \cos(\theta_2 - \phi_2) \\ z_1 + z_2 \cos \phi_3 - z_3 \cos \theta_3 &= \cos(\theta_3 - \phi_3) \end{aligned} \quad (6.29)$$

or in matrix form,

$$\begin{bmatrix} 1 & \cos \phi_1 & -\cos \theta_1 \\ 1 & \cos \phi_2 & -\cos \theta_2 \\ 1 & \cos \phi_3 & -\cos \theta_3 \end{bmatrix} \begin{Bmatrix} z_1 \\ z_2 \\ z_3 \end{Bmatrix} = \begin{Bmatrix} \cos(\theta_1 - \phi_1) \\ \cos(\theta_2 - \phi_2) \\ \cos(\theta_3 - \phi_3) \end{Bmatrix} \quad (6.30)$$

We can solve for  $z_1$ ,  $z_2$ , and  $z_3$  using MATLAB or some other matrix solver. Symbolically,

$$\begin{Bmatrix} z_1 \\ z_2 \\ z_3 \end{Bmatrix} = \begin{bmatrix} 1 & \cos \phi_1 & -\cos \theta_1 \\ 1 & \cos \phi_2 & -\cos \theta_2 \\ 1 & \cos \phi_3 & -\cos \theta_3 \end{bmatrix}^{-1} \begin{Bmatrix} \cos(\theta_1 - \phi_1) \\ \cos(\theta_2 - \phi_2) \\ \cos(\theta_3 - \phi_3) \end{Bmatrix} \quad (6.31)$$

Knowing  $z_1$ ,  $z_2$ , and  $z_3$ , we can solve for the unknown link lengths using Eqs. (6.26), (6.27), and (6.28). Then,

$$r_2 = \frac{1}{z_2} \quad (6.32)$$

$$r_4 = \frac{1}{z_3} \quad (6.33)$$

and

$$r_3 = \sqrt{1 + r_2^2 + r_4^2 - 2r_2r_4z_1} \quad (6.34)$$

Note that the square root used to compute  $r_3$  can be plus or minus. Only the plus sign has a physical meaning, however, since  $r_3$  is physically the distance from the end of link 2 to the end of link 4.

**Unscaling the Solution** In the previous derivation, it is assumed that the length of the base link ( $r_1$ ) is 1. This is not generally the case. However, to determine the true size of the links, it is necessary to know the size of just one of the links initially. Through a scaling factor, we can determine the size of the other links.

Assume that the actual link lengths are  $R_1$ ,  $R_2$ ,  $R_3$ , and  $R_4$ , where the  $R$ 's are related to the computed  $r$ 's through the following:

$$\left. \begin{aligned} R_1 &= Kr_1 \\ R_2 &= Kr_2 \\ R_3 &= Kr_3 \\ R_4 &= Kr_4 \end{aligned} \right\} \quad (6.35)$$

where  $K$  is the scale factor for the linkage. From Eq. (6.35), we have

$$K = R_1/r_1 = R_2/r_2 = R_3/r_3 = R_4/r_4 \quad (6.36)$$

After the design procedure is completed, we will know  $r_1$ ,  $r_2$ ,  $r_3$ , and  $r_4$ . Therefore, we need to specify only *one* of  $R_1$ ,  $R_2$ ,  $R_3$ , or  $R_4$  to find  $K$  using Eq. (6.36). Knowing  $K$ , we can compute the actual link lengths using Eq. (6.35).

### 6.4.2 Design Procedure When $y = y(x)$ Is to Be Generated

Generally, in function generation,  $\theta$  and  $\phi$  will not be given directly. Instead, the linkage will be designed to approximate a function  $y = y(x)$ , where  $y$  corresponds to  $\phi$  (the output) and  $x$  corresponds to  $\theta$  (the input). The angles  $\theta$  and  $\phi$  will be related to  $x$  and  $y$  such that, given  $\theta$  and  $\phi$ ,  $x$  and  $y$  can be computed. The functional relationships between  $\phi$  and  $y$  and  $\theta$  and  $x$  are somewhat arbitrary; however, the problem is most easily solved if linear relationships are used. The most common relationships are

$$\frac{x - x_0}{x_f - x_0} = \frac{\theta - \theta_0}{\theta_f - \theta_0}$$

and

$$\frac{y - y_0}{y_f - y_0} = \frac{\phi - \phi_0}{\phi_f - \phi_0}$$

or

$$x = \frac{x_f - x_0}{\theta_f - \theta_0} (\theta - \theta_0) + x_0 \quad (6.37)$$

$$y = \frac{y_f - y_0}{\phi_f - \phi_0} (\phi - \phi_0) + y_0 \quad (6.38)$$

and

$$\theta = \frac{\theta_f - \theta_0}{x_f - x_0} (x - x_0) + \theta_0 \quad (6.39)$$

$$\phi = \frac{\phi_f - \phi_0}{y_f - y_0} (y - y_0) + \phi_0 \quad (6.40)$$

When the design problem is formulated, we will know  $y = y(x)$  and the range for  $x$  ( $x_0 \leq x \leq x_f$ ). Given  $x_0$  and  $x_f$ , we can compute  $y_0$  and  $y_f$ . We must then pick  $\theta_0$  and  $\theta_f$  and  $\phi_0$  and  $\phi_f$ . Then, given three design positions for  $x$ , three values for  $y$ ,  $\theta$  and  $\phi$  can be computed, and given the three values for  $\theta$  and  $\phi$ , the link lengths can be computed using the procedure given here.

Often, instead of selecting  $\theta_0$ ,  $\theta_f$ ,  $\phi_0$ , and  $\phi_f$  directly,  $\theta_0$ ,  $\phi_0$ , and  $\Delta\theta = \theta_f - \theta_0$  and  $\Delta\phi = \phi_f - \phi_0$  are selected. Typically, choosing  $\Delta\theta$  and  $\Delta\phi$  to be between  $60^\circ$  and  $120^\circ$  usually works well. It is also usually better to avoid having either the driver or the output link pass below the line defined by the two fixed pivots (line of centers) in the range where the function is to be matched; that is, make  $0^\circ \leq \theta_0 \leq \theta \leq \theta_f \leq 180^\circ$  and  $0^\circ \leq \phi_0 \leq \phi \leq \phi_f \leq 180^\circ$ .

### 6.4.3 Selection of Design Positions

In general, the function generated by the linkage will match the actual function only at the precision points, and the error between the precision points will vary depending on where the precision points are placed in the range  $x_0 \leq x \leq x_f$ . Therefore, when trying to match the function  $y = y(x)$  over the range  $x_0 \leq x \leq x_f$ , the objective is to select the precision points so that the deviation of the function actually generated from that desired between the design positions is minimized. The difference between the actual function generated and the desired function is called the *structural error*  $e$ . If this error is plotted as a function of  $x$ , it can be shown that the maximum structural error ( $e^*$ ) is minimized when it takes the form shown in Fig. 6.36. Ideally, the maximum errors between the precision points are both equal in magnitude to the errors at the ends of the range.

It is usually difficult to locate the precision points so that this criterion for the error is met for an arbitrary function; however, a useful approximate solution is obtained by approximating the error function by a Chebyshev polynomial of order  $N$ , where  $N$  is equal to the number of precision points. If the approximation were exact, the optimum locations of the precision points are given by

$$x_i = \frac{x_f + x_0}{2} - \frac{x_f - x_0}{2} \cos\left(\frac{\pi i}{N} - \frac{\pi}{2N}\right) = \frac{x_f + x_0}{2} - \frac{x_f - x_0}{2} \cos\left\{\frac{\pi}{2N}(2i-1)\right\} \quad (6.41)$$

where  $i = 1, 2, \dots, N$ . These values for  $x_i$  are the roots of the Chebyshev polynomial of order  $N$ . As already noted, Eq. (6.41) approximates only the optimum locations of the precision points, but it is still a useful starting solution to use, especially when there is no other basis upon which to choose design positions.

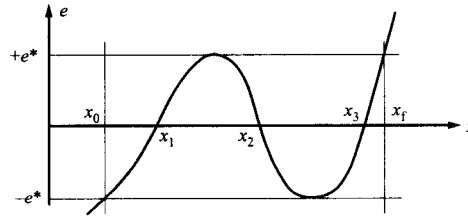


FIGURE 6.36 Optimum error distribution.

The roots of the Chebyshev polynomial can be given a geometric interpretation that makes it easy to derive Eq. (6.41) if the form of the equation is forgotten. For this, draw a circle of radius  $(x_f - x_0)/2$  with its center at  $(x_f + x_0)/2$ . Then divide the circle into a regular polygon with  $2N$  sides. The projection of the vertices of the polygon onto the  $x$  axis will give the locations of the precision points. This is shown in Fig. 6.37. When Chebyshev spacing is used, the center point,  $(x_f + x_0)/2$ , will be a precision point *only* when  $N$  is odd, and the extremes ( $x_f$  and  $x_0$ ) of the range will *never* be chosen as precision points.

#### 6.4.4 Summary of Solution Procedure for Four-Bar Linkage and Three Precision Points

Let  $y = y(x)$  be the function to be generated over the range  $x_0 \leq x \leq x_f$ . The design positions should be placed inside the range  $x_0 \leq x \leq x_f$ , and as a rule, for the three positions use

$$x_1 = \frac{x_f + x_0}{2} - \frac{x_f - x_0}{2} \cos 30^\circ$$

$$x_2 = \frac{x_f + x_0}{2}$$

$$x_3 = \frac{x_f + x_0}{2} - \frac{x_f - x_0}{2} \cos 150^\circ$$

Choose the angular range  $\Delta\theta$  of the input crank that is to correspond to the range  $x_0 \leq x \leq x_f$  for  $x$ . Also, choose the angle  $\theta_0$  corresponding to  $x_0$  from which this range is to start.

Choose the angular range  $\Delta\phi$  of the output crank that is to correspond to the range  $y_0 \leq y \leq y_f$  for  $y$  where  $y_0 = y(x_0)$  and  $y_f = y(x_f)$ . Also, choose the angle  $\phi_0$  corresponding to  $y_0$  from which the output range will start.

Compute the values of  $\theta$  and  $\phi$  that represent the precision points from the equations

$$\theta_i = \frac{\theta_f - \theta_0}{x_f - x_0} (x_i - x_0) + \theta_0 = \frac{x_i - x_0}{x_f - x_0} \Delta\theta + \theta_0$$

and

$$\phi_i = \frac{\phi_f - \phi_0}{y_f - y_0} (y_i - y_0) + \phi_0 = \frac{y_i - y_0}{y_f - y_0} \Delta\phi + \phi_0$$

where  $y_i = y(x_i)$ .

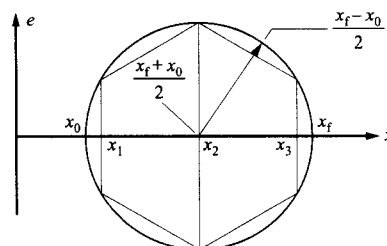


FIGURE 6.37 Chebyshev spacing for precision points.

Next let the base length be unity and calculate the lengths for the driver, coupler, and output links using Eqs. (6.31)–(6.34). To do this, solve

$$\begin{Bmatrix} z_1 \\ z_2 \\ z_3 \end{Bmatrix} = \begin{bmatrix} 1 & \cos \phi_1 & -\cos \theta_1 \\ 1 & \cos \phi_2 & -\cos \theta_2 \\ 1 & \cos \phi_3 & -\cos \theta_3 \end{bmatrix}^{-1} \begin{Bmatrix} \cos(\theta_1 - \phi_1) \\ \cos(\theta_2 - \phi_2) \\ \cos(\theta_3 - \phi_3) \end{Bmatrix}$$

for  $z_1$ ,  $z_2$ , and  $z_3$ . Then solve for  $r_1$ ,  $r_3$ , and  $r_4$  from

$$r_2 = \frac{1}{z_2}$$

$$r_4 = \frac{1}{z_3}$$

and

$$r_3 = \sqrt{1 + r_2^2 + r_4^2 - 2r_2r_4z_1}$$

Note that  $r_2$  and  $r_4$  can be negative. When  $r_2$  or  $r_4$  is negative, the direction for the vector representing the link length is reversed (see Fig. 6.38).

After the scaled link lengths are determined, determine the scale factor using

$$K = R_1/r_1 = R_2/r_2 = R_3/r_3 = R_4/r_4$$

and the true value of one of the link lengths. Then determine the true value for all of the link lengths using Eqs. (6.35).

Draw the linkage to scale, and check that a linkage with the calculated dimensions will pass through the design positions  $(\theta_1, \phi_1)$ ,  $(\theta_2, \phi_2)$ ,  $(\theta_3, \phi_3)$ . The procedure guarantees only that the linkage can be assembled in the design positions. It may not be able to move from one position to another without changing branches. It is also important to check the force and torque transmission characteristics of the linkage at each design position. As will be discussed when crank-rocker mechanisms are considered, the force transmission characteristics of a four-bar linkage can change greatly from position to position.

If for some reason the linkage is unacceptable, change either the range or starting point for either  $\theta$  or  $\phi$  and solve for another design.

Note that it is possible to choose different combinations of variables other than  $x_1$ ,  $x_2$ , and  $x_3$  when selecting the precision points. If we let

$$x_f - x_0 = \Delta x$$

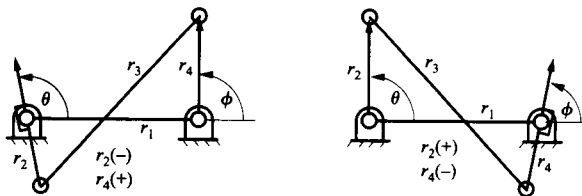


FIGURE 6.38 Interpretation of negative values for  $r_4$  and  $r_2$ .

then the basic equations for selecting the precision points can be written as

$$x_1 = \frac{x_f + x_0}{2} - \frac{\Delta x}{2} \cos 30^\circ$$

$$x_2 = \frac{x_f + x_0}{2}$$

$$x_3 = \frac{x_f + x_0}{2} + \frac{\Delta x}{2} \cos 30^\circ$$

From this it is clear that we can select any three from the list of variables,  $x_1$ ,  $x_2$ ,  $x_3$ ,  $x_f$ ,  $x_0$ , or  $\Delta x$  and solve for the other three.

The function generation equations have been programmed using MATLAB in the routine *funge.m* provided on the disk with this book. This routine can be easily modified to handle a relatively wide range of function generation problems involving a four-bar linkage.

**EXAMPLE 6.4**  
**Function**  
**Generation Using**  
**a Four-Bar Linkage**  
**Solution**

Design a linkage to generate the function  $y = \log_{10}x$  over the range  $1 \leq x \leq 2$ .

From the given information,

$$x_0 = 1 \quad \text{and} \quad x_f = 2$$

Using Chebyshev spacing for the precision points, we have

$$x_1 = \frac{x_f + x_0}{2} - \frac{x_f - x_0}{2} \cos 30^\circ = \frac{2+1}{2} - \frac{2-1}{2} \cos 30^\circ = 1.06699$$

Similarly,  $x_2 = 1.5$  and  $x_3 = 1.93301$ . Then, the corresponding values for  $y$  are

$$y_f = \log_{10} 2 = 0.30103$$

$$y_0 = \log_{10} 1 = 0$$

$$y_1 = \log_{10} x_1 = 0.028160$$

$$y_2 = \log_{10} x_2 = 0.176091$$

$$y_3 = \log_{10} x_3 = 0.28623$$

Note that a minimum of five decimal places is needed to ensure adequate solution accuracy. To identify the linkage angles, choose

$$\theta_0 = 45^\circ, \quad \Delta\theta = 60^\circ$$

and

$$\phi_0 = 0^\circ, \quad \Delta\phi = 60^\circ$$

Note that these values are somewhat arbitrary. If the resulting linkage is unacceptable, we can try other values. The precision points in terms of  $\theta$  are

$$\theta_1 = \frac{x_1 - x_0}{x_f - x_0} \Delta\theta + \theta_0 = \frac{1.06699 - 1}{1} 60^\circ + 45^\circ = 49.019^\circ$$

$$\theta_2 = \frac{x_2 - x_0}{x_f - x_0} \Delta\theta + \theta_0 = \frac{1.5 - 1}{1} 60^\circ + 45^\circ = 75.000^\circ$$

$$\theta_3 = \frac{x_3 - x_0}{x_f - x_0} \Delta\theta + \theta_0 = \frac{1.93301 - 1}{1} 60^\circ + 45^\circ = 100.981^\circ$$

Similarly,

$$\phi_1 = \frac{y_1 - y_0}{y_f - y_0} \Delta\phi + \phi_0 = \frac{0.028160 - 1}{0.30103} 60^\circ + 0^\circ = 5.612^\circ$$

$$\phi_2 = \frac{y_2 - y_0}{y_f - y_0} \Delta\phi + \phi_0 = \frac{0.176091 - 1}{0.30103} 60^\circ + 0^\circ = 35.098^\circ$$

$$\phi_3 = \frac{y_3 - y_0}{y_f - y_0} \Delta\phi + \phi_0 = \frac{0.28623 - 1}{0.30103} 60^\circ + 0^\circ = 57.050^\circ$$

Using the matrix solution procedure, we get

$$\begin{Bmatrix} z_1 \\ z_2 \\ z_3 \end{Bmatrix} = \begin{bmatrix} 1 & \cos\phi_1 & -\cos\theta_1 \\ 1 & \cos\phi_2 & -\cos\theta_2 \\ 1 & \cos\phi_3 & -\cos\theta_3 \end{bmatrix}^{-1} \begin{Bmatrix} \cos(\theta_1 - \phi_1) \\ \cos(\theta_2 - \phi_2) \\ \cos(\theta_3 - \phi_3) \end{Bmatrix} = \begin{bmatrix} 1 & 0.9952 & -0.6558 \\ 1 & 0.8182 & -0.2588 \\ 1 & 0.5439 & -0.1905 \end{bmatrix}^{-1} \begin{Bmatrix} 0.7265 \\ 0.7671 \\ 0.7202 \end{Bmatrix} = \begin{Bmatrix} 0.6383 \\ 0.2210 \\ 0.2008 \end{Bmatrix}$$

and

$$r_2 = \frac{1}{z_2} = \frac{1}{1.2574} = 0.7953$$

$$r_4 = \frac{1}{z_3} = \frac{1}{0.6631} = 1.5080$$

and

$$r_3 = \sqrt{1 + r_2^2 + r_4^2 - 2r_2r_4z_1} = \sqrt{1 + 0.7953^2 + 1.5080^2 - 2(0.7953)(1.5080)(-0.0900)} = 2.0304$$

For the overall size of the linkage, use a base link length of 2 in. Then the lengths of the other links become

$$R_1 = 1(2) = 2.0000 \text{ in}$$

$$R_2 = 0.7953(2) = 1.5905 \text{ in}$$

$$R_4 = 1.5080(2) = 3.0160 \text{ in}$$

$$R_3 = 2.0304(2) = 4.0608 \text{ in}$$

The linkage is drawn to scale in Fig. 6.39.



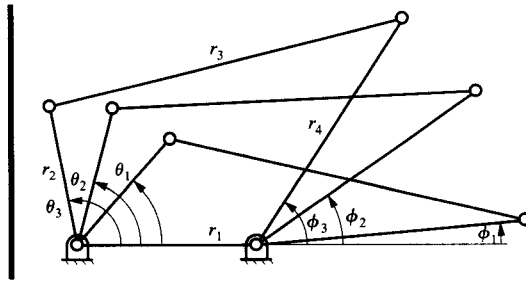


FIGURE 6.39 Final linkage for Example 6.4.

### 6.4.5 Graphical Approach to Function Generation

The function generation problem can be solved graphically if the linkage is inverted so that the crank becomes the temporary frame. We can choose any position of the crank to start the construction, but position 1 is the most common position to choose. To illustrate the procedure, the problem in Example 6.4 will be used again. That is, it will be assumed that three pairs of points,  $(\theta_1, \phi_1)$ ,  $(\theta_2, \phi_2)$ , and  $(\theta_3, \phi_3)$  are known. The input and output cranks in the three positions are shown in Fig. 6.40. Note that the base link ( $r_1$ ) has been chosen, but the lengths of the input and output links ( $r_2$  and  $r_4$ ) have not been specified.

The next step is to invert the linkage so that the driver ( $r_2$ ) becomes the frame. To do this, treat the group of links,  $r_1$ ,  $r_2$ , and  $r_4$ , as a rigid body in each position and rotate the group of links such that  $r_2$  is in the same location for each position. This is shown in Fig. 6.41. In the inverted linkage,  $r_2$  is the frame,  $r_3$ , the original coupler, is the output link, and  $r_4$ , the original output link, becomes the coupler. For the inverted linkage, one crank is known, so we need only establish the other crank ( $r_3$  for the original linkage), and the linkage geometry is established. The problem has therefore been converted to a rigid-body guidance problem where  $r_4$  is the coupler to be guided. One crank ( $r_1$ ) has already been established. To find the other crank, choose a point  $C$  on link 4. The center of the circle on which  $C_1$ ,  $C_2$ , and  $C_3$  lie is  $C^*$ . The synthesized linkage in position 1 is  $A$ ,  $B_1$ ,  $C_1$ ,  $C^*$  as shown in Fig. 6.42. When inverted back to the original base, we have the solution of the function generation problem. The final solution linkage is shown in Fig 6.43. Note that  $\theta_0$  and  $\theta_f$  are different in this solution compared with the analytical solution, but  $\Delta\theta$  is the same for both solutions. Here, we chose the position of  $C$  (that is, the length of  $r_4$ ) rather than  $\theta_0$ .

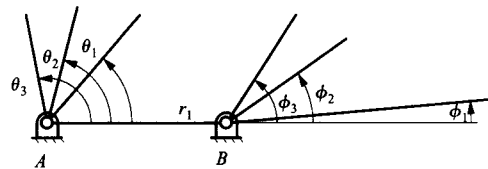


FIGURE 6.40 Three positions for input and output links for graphical synthesis.

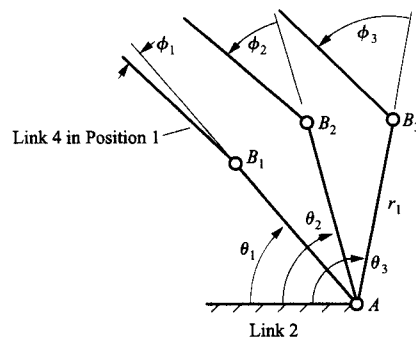


FIGURE 6.41 Inversion of linkage making  $r_2$  the frame. The original linkage is inverted onto its driving crank to convert the function generation problem into a motion generation problem.

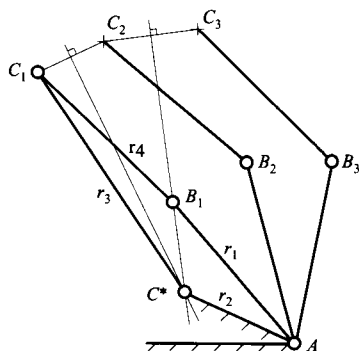


FIGURE 6.42 Construction of center point  $C^*$  given three positions of  $C$ .

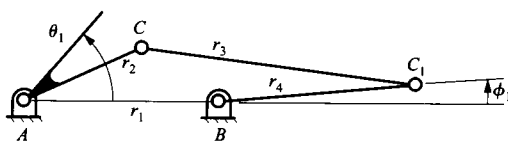


FIGURE 6.43 Final solution linkage.

## 6.5 SYNTHESIS OF CRANK-ROCKER LINKAGES FOR SPECIFIED ROCKER AMPLITUDE

In a crank-rocker mechanism, the crank rotates through  $360^\circ$ , and the rocker oscillates through an angle  $\theta$ . This mechanism is often used interchangeably with cam mechanisms for the same function; however, there are many cases in which a crank-rocker mechanism is superior to a cam-follower mechanism. Among the advantages over cam systems are the smaller contact forces involved, the elimination of the retaining spring, and the closer clearances achieved because of the use of revolute joints.

### 6.5.1 Extreme Rocker Positions and Simple Analytical Solution

The maximum and minimum rocker angles occur in the positions shown in Fig. 6.44. Using the cosine rule, we have

$$(r_2 + r_3)^2 = r_1^2 + r_4^2 - 2r_1r_4\cos\rho \quad (6.42)$$

and

$$(r_3 - r_2)^2 = r_1^2 + r_4^2 - 2r_1r_4\cos\beta \quad (6.43)$$

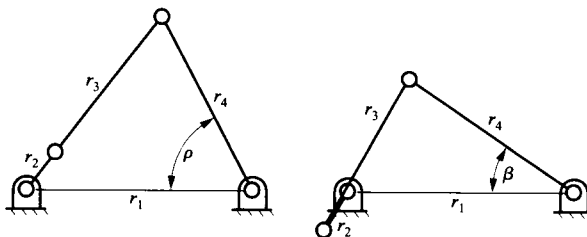


FIGURE 6.44 The positions of a crank-rocker linkage in which the rocker is at the extremes of its motion range.

Since we have two equations in six variables,  $r_1, r_2, r_3, r_4, \rho,$  and  $\beta,$  the values of four variables can be specified. As in the case of function generation, the angles in the triangles are independent of the size of the triangles. Therefore,  $r_1$  is usually taken as 1. Usually, the design problem requires only a specified value for the difference  $\beta - \rho.$  Nevertheless, the solution is much simpler if both  $\rho$  and  $\beta$  are specified. Since a crank-rocker linkage is sought, it is also helpful to specify  $r_2.$  Values in the range  $0.1 \leq r^2 \leq 0.4$  will usually give good results when  $r_1 = 1.$  Assuming  $\rho, \beta, r_1$  and  $r_2$  are specified, we can solve Eqs. (6.42) and (6.43) for  $r_3$  and  $r_4.$  Adding the equations and simplifying, we get

$$r_2^2 + r_3^2 = r_1^2 + r_4^2 - r_1 r_4 (\cos \rho + \cos \beta) \quad (6.44)$$

Subtracting Eq. (6.44) from (6.42), we get

$$2r_2 r_3 = r_1 r_4 (\cos \beta - \cos \rho) \quad (6.45)$$

Hence

$$r_3 = \frac{r_1 r_4 (\cos \beta - \cos \rho)}{2r_2} \quad (6.46)$$

Substitution into Eq. (6.44) gives, after some manipulation,

$$Pr_4^2 + Qr_4 + R = 0 \quad (6.47)$$

where

$$\begin{aligned} P &= 1 - \frac{r_1^2 (\cos \beta - \cos \rho)^2}{4r_2^2} \\ Q &= -r_1 (\cos \beta + \cos \rho) \\ R &= r_1^2 - r_2^2 \end{aligned} \quad (6.48)$$

The solution to the quadratic equation Eq. (6.47) gives a positive root and a negative root for  $r_4.$  The negative root can be discarded. If no real roots exist, it is necessary to choose a new value of  $\beta$  and try again. Once  $r_4$  is known,  $r_3$  can be found from Eq. (6.46). The formulation of the problem guarantees that the joint between  $r_2$  and  $r_3$  will rotate completely, but this still does not guarantee a crank-rocker solution (it could be a type 1 double-rocker). Thus, although it is a type 1 linkage, it is necessary to check that  $r_3 > r_2.$  The Grashof inequality can be used as a simple check on arithmetic.

The simplified procedure given here can be used if the oscillation amplitude ( $\rho - \beta$ ) is the only quantity of interest. The procedure gives no control over the time ratio of the forward oscillation to the reverse oscillation. This time ratio is often of interest, however, and the following procedure gives a means of incorporating it in the basic design procedure.

### 6.5.2 The Rocker Amplitude Problem: Graphical Approach

As the crank in a crank-rocker mechanism rotates through  $360^\circ,$  the output link or rocker will oscillate through an angle  $\theta.$  The limiting positions of the rocker occur when the crank and coupler are collinear as shown in Fig. 6.45. In general, the time required for the rocker oscillation in one direction will be different from the time required for the other direction. As previously indicated, the ratio of the times required for the forward and return motions

is called the time ratio. An expression for the time ratio can be developed by using the nomenclature defined in Fig. 6.45.

In the crank-rocker, the crank moves through the angle  $\psi$  while the rocker moves from  $B_1$  to  $B_2$  through the angle  $\theta$ . On the return stroke, the crank moves through the angle  $360^\circ - \psi$  and the rocker moves from  $B_2$  to  $B_1$  through the same angle  $\theta$ .

Assuming that the crank moves with constant angular velocity, the ratio of the times for the forward and reverse strokes of the follower can be related directly to the angles in Fig. 6.45. The crank angle for the forward stroke is  $\psi$  or  $180^\circ + \alpha$ . The crank angle for the return stroke is  $360^\circ - \psi$  or  $180^\circ - \alpha$ . Therefore, the time ratio,  $Q$ , can be written as

$$Q = \frac{180 + \alpha}{180 - \alpha} \quad (6.49)$$

where  $\alpha$  is given in degrees.

The most common problem associated with the synthesis of crank-rocker mechanisms is that of designing the linkage for a given oscillation angle and a given time ratio. For the discussion here, assume that the time ratio  $Q$  has been given. The first step in the synthesis is to compute the angle  $\alpha$ . This can be done by rewriting the basic equation for  $Q$ . Then,

$$\alpha = 180 \frac{(Q - 1)}{(Q + 1)} \quad (6.50)$$

Note that  $\alpha$  is positive when  $Q$  is greater than 1 and negative when  $Q$  is less than 1. Examples of positive and negative  $\alpha$  are shown in Fig. 6.46.

Once  $\alpha$  is known, there are a number of ways to proceed with the design. The simplest way is to choose a location for  $O_4$ , select a trial value for  $\phi$ , and draw the two positions of the rocker ( $r_4$ ) separated by the angle  $\theta$ . Draw any line  $x$  through the pivot at  $B_1$ , and construct a second line at an angle of  $\alpha$  to the line  $x$  and through the pivot at  $B_2$ . Call the second line  $y$ . The intersection of lines  $x$  and  $y$  defines the location of the second fixed pivot ( $O_2$ ).

Next compute the values of  $r_2$  and  $r_3$ . This is done by using the geometric relationships in Fig. 6.45. That is,

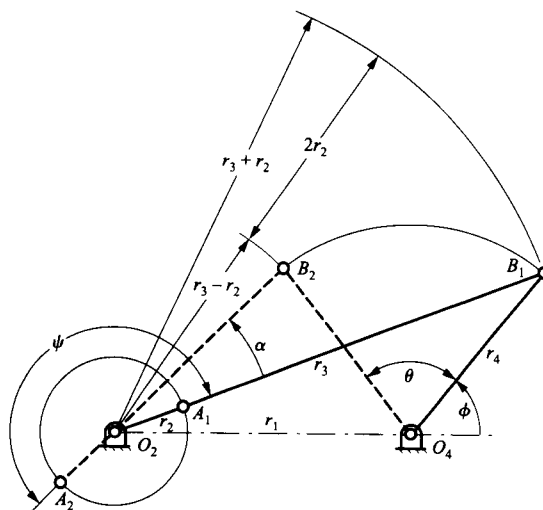


FIGURE 6.45 crank-rocker mechanism in extreme positions.

$$r_2 + r_3 = \overline{O_2 B_1}$$

and

$$r_3 - r_2 = \overline{O_2 B_2}$$

Therefore,

$$r_2 = \frac{\overline{O_2 B_1} - \overline{O_2 B_2}}{2} \quad (6.51)$$

and

$$r_3 = \frac{\overline{O_2 B_1} + \overline{O_2 B_2}}{2} \quad (6.52)$$

Note that during the design procedure, several choices were made. Among these were the starting angle  $\phi$  for the line  $O_4 B_1$  and the slope of the line  $x$ . There are an infinite number of choices for each, and each choice will give a different linkage.

Note also that not all solutions are valid. In particular, the pivots  $B_1$  and  $B_2$  may not extend below the line of centers defined by a line through the fixed pivots  $O_2$  and  $O_4$ . If this happens, the linkage must change branch to reach the two positions, and the desired oscillation angle will not be achieved. As indicated by Hall,<sup>4</sup> once  $\alpha$  and  $\theta$  are known, the locus of acceptable positions for  $O_2$  must lie on circle arcs represented by the heavy sections of the circles shown in Fig. 6.47. The locus of  $O_2$  must be on a circle arc because the triangle  $B_2 B_1 O_2$  has a fixed base and a constant apex angle ( $\alpha$ ). If  $O_2$  is chosen in the light part of the circles, the two positions of  $B$  will be on opposite sides of the line of centers.

In some instances, the length of one of the links must be a specific value. However, the procedure outlined here will permit only the length of the rocker to be specified directly. If the length of one of the other links is known, the lengths of the links in the linkage can be scaled using the procedure given in Section 6.4.1.

**Range for  $\alpha$**  A study of Fig. 6.47 will indicate the extreme values for the angle  $\alpha$ . When the time ratio is 1, then  $\alpha = 0$ . This case is shown in Fig. 6.48. When  $\alpha = 0$ , the limiting circles shown in Fig. 6.47 converge to a straight line through  $B_1$  and  $B_2$ . Any point outside the span between  $B_1$  and  $B_2$  may be chosen as the fixed pivot for the crank. Note that, for this case, the distance between  $B_1$  and  $B_2$  is equal to  $2r_2$ . [See Eq. (6.51).]

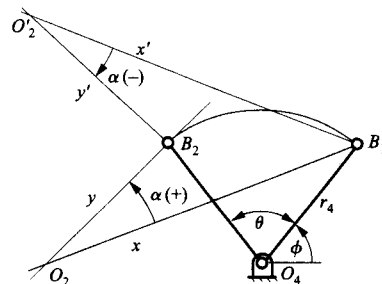


FIGURE 6.46 Locations of  $O_2$  given  $\theta$  and  $\pm \alpha$ .

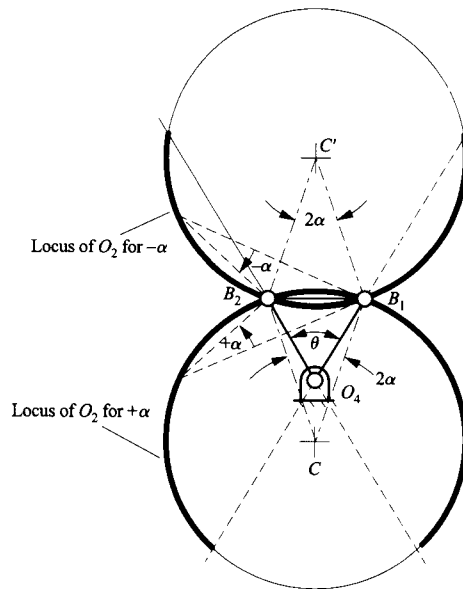


FIGURE 6.47 Possible locations for  $O_2$  given  $\theta$  and  $\alpha$ .

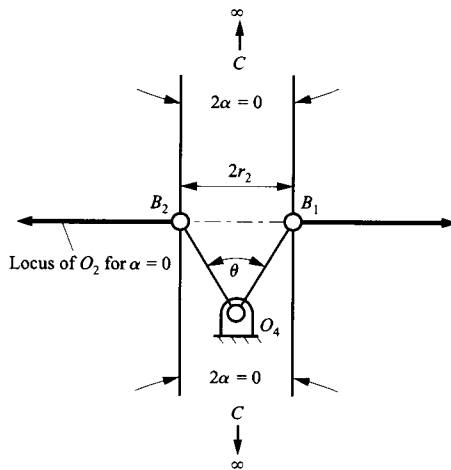
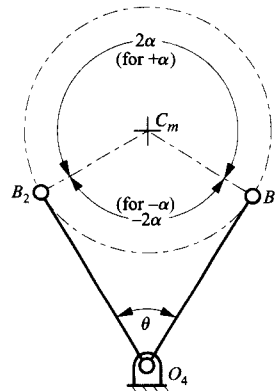


FIGURE 6.48 Limiting case when  $\alpha = 0$  or  $Q = 1$ .

As  $+\alpha$  increases from 0, the center  $C$  of the bottom circle in Fig. 6.47 will move from  $-\infty$  toward the pivot  $O_4$ . The highest location possible for the circle is when it is tangent to  $B_1$  and  $B_2$  at the two extreme locations of  $r_4$ . This is shown in Fig. 6.49. In this position, there are no solutions possible, but if  $C$  is only slightly lower than the location  $C_m$  shown in Fig. 6.49, solutions exist for  $O_2$  for positive  $\alpha$ . When  $C$  moves above the line between  $B_1$  and  $B_2$ , the angle  $2\alpha$  is the obtuse angle shown in Fig. 6.49. From the geometry shown in Fig. 6.49, the maximum value for  $\alpha$  will be  $\pi/2 + \theta/2$ .

As  $\alpha$  decreases from 0 (i.e.,  $\alpha$  becomes more negative), the center  $C'$  of the top circle in Fig. 6.47 will move from  $+\infty$  toward the pivot  $O_4$ . The lowest location possible for the circle is again when it is tangent to  $r_4$  at  $B_1$  and  $B_2$  for the two extreme locations of  $r_4$ . Again, in this position, no solutions are possible, but if  $C'$  is moved only slightly higher than the location  $C_m$  shown in Fig. 6.49, solutions will exist for  $O_2$ . When  $C'$  moves above  $C_m$ , the angle  $-2\alpha$  is the acute angle at  $C_m$  as shown. From the geometry shown in Fig. 6.49, the minimum value for  $\alpha$  shown in Fig. 6.47 will be  $-(\pi/2 - \theta/2)$ .



**FIGURE 6.49** Limiting values for  $\pm\alpha$ . The maximum value when  $\alpha$  is positive is  $\pi/2 + \theta/2$ . The minimum value when  $\alpha$  is negative is  $-(\pi/2 - \theta/2)$ .

**EXAMPLE 6.5**  
**Crank-rocker**  
**Design (Graphical)**

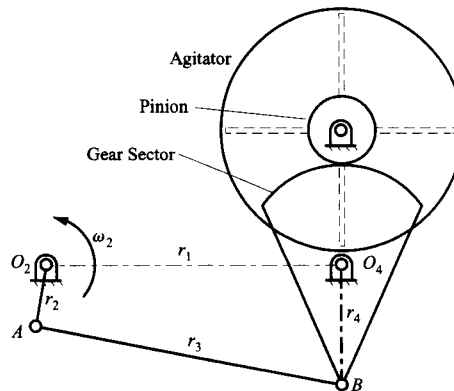
A crank-rocker is to be used in the transmission of an automatic washing machine to drive the agitator. The rocker link is attached to a gear sector, which drives a pinion gear attached to the agitator shaft. The radius of the sector gear is 3 in., and the pinion radius is 1 in. The pivot for the output link is at  $O_4$ . The sector gear is to oscillate  $90^\circ$ . The times for the forward and return stroke for the sector are the same. If the base link ( $r_1$ ) of the mechanism is to be 10-cm long, determine the lengths of the other links ( $r_2$ ,  $r_3$ , and  $r_4$ ).

**Solution**

A sketch of the mechanism is shown in Fig. 6.50. We must determine the four-bar linkage defined by  $O_2$ ,  $O_4$ ,  $A$ , and  $B$ . The sector gear is attached to the output link, which rotates through an angle  $\theta$  of  $90^\circ$ . The time ratio is 1 so

$$\alpha = 180^\circ \left[ \frac{Q-1}{Q+1} \right] = 180^\circ \left[ \frac{0}{2} \right] = 0$$

Therefore, the locus for  $O_2$  corresponds to that shown in Fig. 6.48. For the construction, let  $r_4$  be 1 in. Then a solution for the linkage can be constructed as shown in Fig. 6.51.



**FIGURE 6.50** Sketch of linkage for Example 6.5.

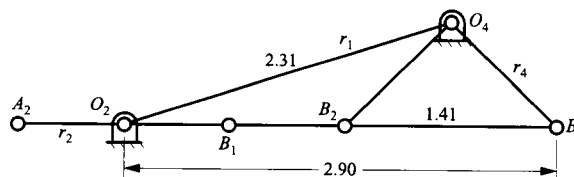


FIGURE 6.51 A solution to Example 6.5.

From Fig. 6.51, we have

$$r_4 = 1 \text{ in}$$

$$r_1 = 2.31 \text{ in}$$

$$r_2 + r_3 = O_2B_1$$

$$r_3 - r_2 = O_2B_2$$

or

$$r_2 = (O_2B_1 - O_2B_2)/2 = (2.90 - 1.49)/2 = 0.70 \text{ in}$$

$$r_3 = (O_2B_1 + O_2B_2)/2 = (2.90 + 1.49)/2 = 2.20 \text{ in}$$

Determining the scaling factor, we get

$$K = \frac{R_1}{r_1} = \frac{10}{3.31} = 3.021 = \frac{R_2}{r_2} = \frac{R_3}{r_3} = \frac{R_4}{r_4}$$

Using the unscaled lengths from the figure gives

$$R_2 = 3.021 r_2 = 3.021(0.70) = 2.11 \text{ cm}$$

$$R_3 = 3.021 r_3 = 3.021(2.20) = 6.65 \text{ cm}$$

$$R_4 = 3.021 r_4 = 3.021(1) = 3.02 \text{ cm}$$

The mechanism is drawn to scale in Fig. 6.52.

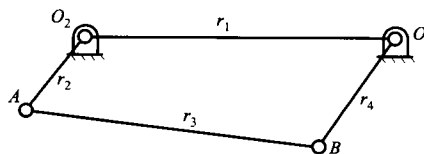


FIGURE 6.52 Final linkage for Example 6.5.

### 6.5.3 Transmission Angle

Ultimately, the design of the crank-rockers reduces to an optimization problem because a single design based on the construction discussed above will usually have poor transmission angle characteristics. The maximum ( $\eta_{\max}$ ) and minimum ( $\eta_{\min}$ ) transmission angles are shown in Fig. 6.53. Typically, a poor transmission angle corresponds to a large value of  $|(\pi/2 - \eta_{\max/\min})|$ . Note that the maximum and minimum values for the transmission angle



do not occur at the extreme positions of  $r_4$ , but  $\eta_{\max}$  and  $\eta_{\min}$  can be easily computed using the geometry in Fig. 6.53. The equations are

$$\eta'_{\max} = \cos^{-1} \left[ \frac{r_4^2 - (r_1 + r_2)^2 + r_3^2}{2r_4r_3} \right] \quad (6.53)$$

$$\eta'_{\min} = \cos^{-1} \left[ \frac{r_4^2 - (r_1 - r_2)^2 + r_3^2}{2r_4r_3} \right] \quad (6.54)$$

If  $\eta_{\max}$  is negative, then  $\eta_{\max} = \pi + \eta'_{\max}$ . Otherwise,  $\eta_{\max} = \eta'_{\max}$ . Similar conditions apply to  $\eta_{\min}$ .

### 6.5.4 Alternative Graphical Design Procedure Based on Specification of $O_2$ - $O_4$

The graphical procedure developed earlier could be programmed if desired. However, it has the undesirable characteristic of a variable length for the frame. An approach developed by Hall<sup>4</sup> is easier to program, and it will be discussed here. In this procedure, we will select the length of the frame link initially (instead of link 4). This approach reduces the design problem to a one-dimensional problem where well-defined limits are known for the design variable.

Assuming  $\theta$  and  $\alpha$  are known, the following procedure, represented in Fig. 6.54, provides a means for determining all of the linkages satisfying the design requirements. The approach is to determine the locus for all possible values of  $B_2$  relative to the frame. To construct the locus, do the following:

1. Pick the base link and locate the ground pivots  $O_2$  and  $O_4$ . The distance  $O_2O_4$  determines the scale for the linkage.
2. Draw the line  $O_2G$  at an angle  $\theta/2 - \alpha$  (positive clockwise) relative to  $O_2O_4$ .
3. Draw the line  $O_4G$  at an angle of  $\theta/2$  (positive counterclockwise) relative to  $O_2O_4$ .

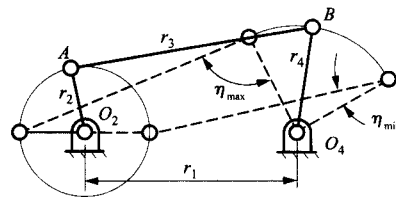


FIGURE 6.53 Maximum and minimum transmission angles.

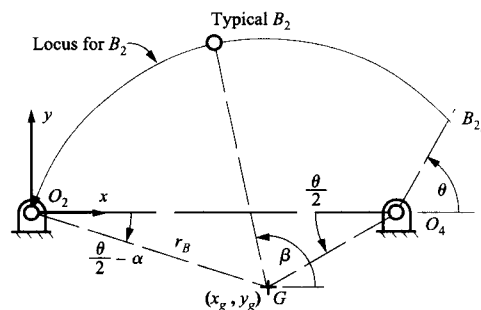


FIGURE 6.54 Construction of the circle giving the locus  $B_2$  and  $B_1$ .

4. Draw the circle of radius  $GO_2$  centered at  $G$ .
5. Draw a line ( $O_4B_{2m}$ ) through  $O_4$  at an angle of  $\theta$  (positive counterclockwise) relative to  $O_2O_4$ .
6. The circle arc starting at  $O_2$  and ending at the intersection with either  $O_4B_{2m}$  or  $O_2O_4$  (whichever occurs first) gives the locus of the point  $B$  in the second extreme position of the rocker. The point ( $B_1$ ) located at an angle  $\theta$  relative to the line  $O_4B_2$  is the other extreme position. The locus of  $B_1$  will be a second circle that has the same radius as the  $B_2$  circle, and the center for the  $B_1$  circle will be the reflection of point  $G$  about the  $O_2O_4$  axis. The length  $r_4$  is equal to  $O_4B$ .

After  $B_2$  is chosen and  $B_1$  is located, the remaining link lengths can then be computed by solving Eqs. (6.51) and (6.52). The transmission angle limits can be measured after drawing the linkage in the extreme positions shown in Fig. 6.53.

**EXAMPLE 6.6**  
**Crank-Rocker**  
**Design Using**  
**Alternate**  
**Graphical**  
**Procedure**  
**Solution**

A crank-rocker mechanism is to have an oscillation angle of  $80^\circ$  and a time ratio of 1.3. The base length is to be 2 in. Design a linkage that will satisfy these conditions.

The time ratio is 1.3 so

$$\alpha = 180^\circ \left[ \frac{Q-1}{Q+1} \right] = 180^\circ \left[ \frac{1.3-1}{1.3+1} \right] = 23.47^\circ$$

We will begin the design procedure by drawing the two fixed pivots, locating point  $G$ , and drawing the arc corresponding to the locus for  $B_2$ . The angles needed to locate  $G$  are

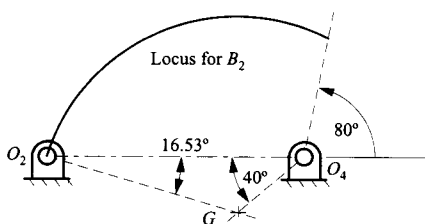
$$\frac{\theta}{2} = 40^\circ$$

and

$$\frac{\theta}{2} - \alpha = 40^\circ - 23.47 = 16.53^\circ$$

The construction is shown in Fig. 6.55.

Now we need to select any point on the locus for  $B_2$ . Once  $B_2$  is selected,  $B_1$  can be found. This is shown in Fig. 6.56. Given  $B_1$  and  $B_2$ , the link lengths can be found using Eqs. (6.51) and 6.52).



**FIGURE 6.55** Construction showing the locus of  $B_2$  for Example 6.6.

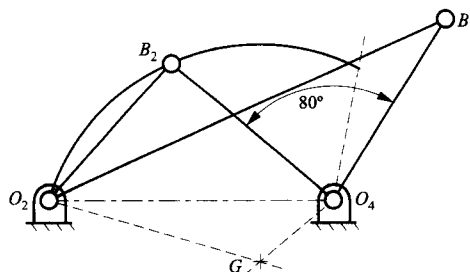


FIGURE 6.56 Construction of  $B_2$  and  $B_1$  for Example 6.6.

From Fig. 6.56, we have

$$r_4 = 1.51 \text{ in}$$

$$r_1 = 2 \text{ in}$$

$$r_2 + r_3 = O_2B_1$$

$$r_3 - r_2 = O_2B_2$$

$$r_2 = (O_2B_1 - O_2B_2)/2 = (3.09 - 1.29)/2 = 0.90 \text{ in}$$

$$r_3 = (O_2B_1 + O_2B_2)/2 = (3.06 + 1.29)/2 = 2.18 \text{ in}$$

The mechanism is drawn to scale in Fig. 6.57

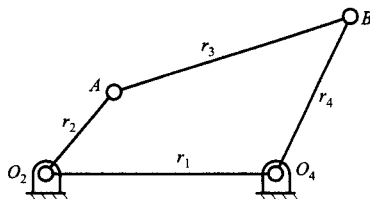


FIGURE 6.57 Final linkage for Example 6.6.

Reviewing the graphical procedure represented in Fig. 6.54, we see that once  $\theta$  and  $\alpha$  are known, the arc defining the loci for  $B_2$  is defined. Locating a point on the arc requires the specification of only one additional parameter ( $\beta$ ). Therefore, different designs can be developed by adjusting this single variable. Furthermore, because the locus for  $B_2$  is the circle arc between  $O_2$  and  $B_{2m}$ , the limits for  $\beta$  can be established at the beginning of the design procedure.

The geometry shown in Fig. 6.54 is the general geometry for the design procedure. However, depending on the values of  $\alpha$  and  $\theta$ , four cases need to be considered. These are represented in Figs. 6.48a–6.48d. The four cases are characterized by the following:

- a.  $0 < \alpha < \theta$  (the general case and the one represented in Figs. 6.54 and 6.58a),
- b.  $-(\pi/2 - \theta/2) < \alpha < 0$  (Fig. 6.58b),
- c.  $\alpha = \theta$  (Fig. 6.58c), and
- d.  $\pi/2 + \theta/2 > \alpha > \theta$  (Fig. 6.58d).

### 6.5.5 Analytical Design Procedure Based on Specification of $O_2-O_4$

**Case a ( $0 < \alpha < \theta$ )** To determine the analytical equations for the arc giving the locus of  $B_2$  in Fig. 6.58a, it is necessary only to find the coordinates of the circle center  $G$  and the limits  $\beta_1$  and  $\beta_2$ . Locating the  $x$  and  $y$  axes as shown in Fig. 6.54, we define the center  $(x_g, y_g)$  by the triangle  $O_2O_4G$ , which has one known side ( $O_2O_4$ ) and two known included angles ( $\theta/2 - \alpha$  and  $\theta/2$ ). By simple plane geometry, the coordinates of the center of the  $B_2$  circle are

$$x_g = O_2O_4 \left[ \frac{\tan(\theta/2)}{\tan(\theta/2) + \tan(\theta/2 - \alpha)} \right] \tag{6.55}$$

and

$$y_g = (O_2O_4 - x_g) \tan(\theta/2)$$

and the radius of the circle arc is

$$r_B = \sqrt{x_g^2 + y_g^2} \tag{6.56}$$

A given point on the  $B_2$  circle can be found using  $r_B$  and the angle  $\beta$ ; however, the allowable range for  $\beta$  must be determined first. The point  $B$  on the rocker cannot lie below the line defined by  $O_2O_4$ . Therefore, one extreme position of the locus for  $B_2$  is  $O_2$ .

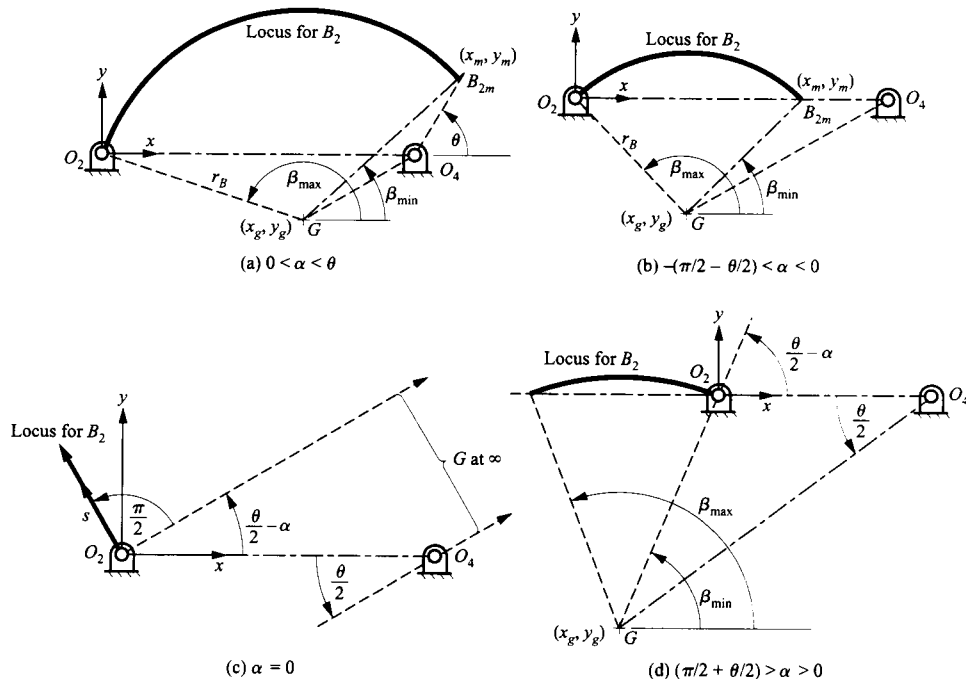


FIGURE 6.58 Different geometries based on relative values of  $\alpha$  and  $\theta$ .

In Fig. 6.58a, the other extreme position is found by noting that  $B_1$  cannot lie below the extension of  $O_2O_4$ . Therefore, the other extreme position of the  $B_2$  locus is at the intersection of the  $B_2$  circle and the line through  $O_4$  at an angle of  $\theta$  with the horizontal. The coordinates of this intersection point are found most easily if we first scale the linkage by setting  $O_2O_4 = 1$ . Then

$$r_B \cos(\beta_{\min}) = x_m - x_g \quad (6.57)$$

$$r_B \sin(\beta_{\min}) = y_m - y_g \quad (6.58)$$

and

$$\frac{y_m}{x_m - 1} = \tan \theta \quad (6.59)$$

If Eqs. (6.57) and (6.58) are squared and added and Eq. (6.59) is used to eliminate  $x_m$  from the result, the following quadratic equation results for  $y_m$ :

$$\left[ \frac{1}{\tan^2 \theta} + 1 \right] y_m^2 - 2 \left[ \frac{x_g - 1}{\tan \theta} + y_g \right] y_m + \left[ 1 + y_g^2 + x_g^2 - 2x_g - r_B^2 \right] = 0$$

or

$$y_m = \left[ -B \pm \sqrt{B^2 - 4AC} \right] / 2A \quad (6.60)$$

where

$$A = \frac{1}{\tan^2 \theta} + 1$$

$$B = -2 \left[ \frac{x_g - 1}{\tan \theta} + y_g \right]$$

$$C = \left[ 1 + y_g^2 + x_g^2 - 2x_g - r_B^2 \right]$$

Two values for  $y$  are mathematically possible, but there will be a maximum of one positive root. Only positive values for  $y_m$  are of interest. If both values of  $y$  are negative, the condition in Fig. 6.58b is indicated. If one  $y_m$  is positive, then  $x_m$  can be computed using Eq. (6.59) or

$$x_m = 1 + \frac{y_m}{\tan \theta} \quad (6.61)$$

Note that  $B^2 - 4AC$  must be positive for a valid solution to exist.

The minimum  $\beta$  is

$$\beta_{\min} = \tan^{-1} \left[ \frac{y_m - y_g}{x_m - x_g} \right] \quad (6.62)$$

and the maximum value for  $\beta$  is

$$\beta_{\max} = \pi + \alpha - \frac{\theta}{2} \quad (6.63)$$

For a valid design,  $\beta_{\min} \leq \beta \leq \beta_{\max}$ .

**Case b**  $[(\pi/2 - \theta/2) < \alpha < 0]$  For the case when  $\alpha$  is negative (Fig. 6.58b), the coordinates of  $G$  and the radius  $r_B$  are the same as in Case a. The coordinates at the extreme location  $B_{2m}$  are given by

$$y_m = 0 \quad (6.64)$$

and

$$x_m = 2r_B \cos\left(\frac{\theta}{2} - \alpha\right) \quad (6.65)$$

The equations for  $\beta_{\min}$  and  $\beta_{\max}$  and are given by Eqs (6.62) and (6.63).

**Case c** ( $\alpha = \theta$ ) When  $\alpha = \theta$ , the center  $G$  will be at infinity, as shown in Fig. 6.58c. This is indicated by Eq. (6.55) because the denominator in the expression for  $x_g$  becomes 0. Therefore, the locus for  $B_2$  is a straight line through  $O_2$  at an angle of  $\pi/2 + \theta/2 - \alpha$  to the horizontal.  $B_2$  can be located anywhere along the straight line, including at infinity. When  $B_2$  is located at infinity, the coupler becomes a slider and the mechanism becomes an inverted slider-crank mechanism (see Hall<sup>4</sup>). Computationally, this case can be best treated separately. Points on the locus for  $B_2$  are given by

$$x = s \cos(\theta/2 - \pi/2 + \alpha) \quad (6.66)$$

and

$$y = s \sin(\theta/2 - \pi/2 + \alpha) \quad (6.67)$$

where  $s$  is the distance measured from the pivot  $O_2$ . It is not necessary to compute  $\beta_{\min}$  and  $\beta_{\max}$ .

**Case d** ( $\pi/2 + \theta/2 > \alpha > \theta$ ) When  $\alpha > \theta$ , the center  $G$  will be located to the left of the pivot  $O_2$ , as shown in Fig. 6.58d. The center of the circle is given by the intersection of the line through  $O_4$  with the line through  $O_2$ . The coordinates of the center  $G$  are given by

$$x_g = O_2O_4 \left[ \frac{\tan(\theta/2)}{\tan(\theta/2) + \tan(\theta/2 - \alpha)} \right]$$

and

$$y_g = -(O_2O_4 - x_g) \tan(\theta/2)$$

and the radius is given by

$$r_B = \sqrt{x_g^2 + y_g^2}$$

Note that both  $x_g$  and  $y_g$  will be negative. The locus for  $B_2$  will begin at  $O_2$  and end at  $B_{2m}$ , where

$$y_m = 0$$

and

$$x_m = -2r_B \cos\left(\frac{\theta}{2} - \alpha\right)$$

The extreme values for  $\beta$  are given by

$$\beta_{\min} = \alpha - \frac{\theta}{2}$$

and

$$\beta_{\max} = \tan^{-1} \left[ \frac{y_m - y_g}{x_m - x_g} \right]$$

For Cases a, b, and d, we can locate  $B_2$  using any value of  $\beta$  between  $\beta_{\min}$  and  $\beta_{\max}$ . The link lengths are computed using Eqs. (6.51) and (6.52) together with the following:

$$\begin{aligned} x &= r_B \cos \beta + x_g \\ y &= r_B \sin \beta + y_g \\ r_4 &= \sqrt{(x-1)^2 + y^2} \end{aligned} \quad (6.68)$$

$$O_2B_2 = \sqrt{x^2 + y^2} \quad (6.69)$$

$$\phi = \tan^{-1} \left( \frac{y}{x-1} \right) \quad (6.70)$$

$$O_2B_1 = \sqrt{[1 + r_4 \cos(\phi - \theta)]^2 + [r_4 \sin(\phi - \theta)]^2} \quad (6.71)$$

In Eq. (6.70), it is important to preserve the signs of both the numerator and denominator since  $\phi$  may be greater than  $\pi/2$ .

For Case c, we can locate values of  $B_2$  by using the distance  $s$  from the pivot  $O_2$ . For a given value of  $s$ , we can compute the location  $(x, y)$  of  $B_2$  using Eqs. (6.66) and (6.67). Equations (6.68)–(6.71) can then be used to compute the remaining quantities needed to determine  $O_2B_2$  and  $O_2B_1$ .

The crank-rocker design equations are coded in MATLAB and included on the disk with this book.

### 6.5.6 Use of Analytical Design Procedure for Optimization

Using the procedure developed, any value of  $\beta$  satisfying  $\beta_{\min} \leq \beta \leq \beta_{\max}$  will produce a linkage that satisfies the basic design requirements for  $\theta$  and  $\alpha$  (or  $Q$ ). To choose the best linkage, we must select a criterion to optimize. If the output link of the linkage is subjected to a constant torque and we wish to design a linkage that can be driven with the smallest motor possible, it is reasonable to optimize the linkage based on the transmission angle. Therefore, we will use this as an example of the procedure that would be used for optimization. Referring to Fig. 6.53, we see that the maximum and minimum values for the transmission angle are given by Eqs. (6.53) and (6.54).

The basic objective function to be minimized during the optimization procedure is

$$U' = \max \left[ \left| \frac{\pi}{2} - \mu_{\max} \right|, \left| \frac{\pi}{2} - \mu_{\min} \right| \right]$$

However, if  $U'$  is used directly, the optimum linkage will occasionally be one where  $r_2$  is very small compared with one of the other link lengths. Therefore, it is convenient to

include the link length ratio as part of the objective function. Because  $r_2$  will be the shortest link, this function can be written as

$$F = \max \left[ \frac{r_1}{r_2}, \frac{r_3}{r_2}, \frac{r_4}{r_2} \right]$$

and

$$U'' = e^{(F-n)}$$

where  $n$  is an integer that represents the largest acceptable value for the link length ratio. Here, it is assumed that length ratios less than  $n$  are acceptable. A typical value for  $n$  is 5.

The combined objective function is

$$U = U' + WU''$$

where  $W$  is a weighting factor that can be chosen to adjust the relative importance of the length ratio. In many problems, the value chosen for  $W$  is not important because linkages that have good transmission angles often have good link length ratios. When  $n$  is 5, values between 1 and 5 for  $W$  will generally give good results.

Once  $\beta$  is selected, the crank-rocker linkage is completely defined, and a value for  $U$  can be computed. Therefore,  $U$  is a function of  $\beta$  only, and well-established limits for  $\beta$  are known. The optimization can then be easily accomplished by varying  $\beta$  and computing  $U$  until  $U$  is minimized. This can be done manually, interactively, or by using any one-dimensional (line search) optimization routine. Several such one-dimensional routines are described by Arora.<sup>6</sup>

## 6.6 PATH SYNTHESIS

---

The path synthesis problem is that of specifying the path taken by a single point fixed in some member of a mechanism. There may also be a requirement for faster or slower speeds along different portions of the path. Although many research papers have been written on the subject of path synthesis, designers usually use a trial-and-error approach in practice. The traditional tool for this purpose is the Hrones and Nelson coupler-curve atlas.<sup>10</sup> This is a large book containing plots of four-bar linkage coupler curves for a large variety of points located in the coupler plane and a large range of link length variations. The approach is to leaf through the coupler-curve atlas and pick out a curve that has more or less the right shape and then refine it by trial and error, testing the effect of small variations in the position of the coupler point or small variations in the link lengths. This gets quite laborious if done manually.

Use of either a simple program based on the theory presented in Chapter 5 or professionally written linkage analysis software can make this task much easier. Coupler-curve programs written in MATLAB for both four-bar linkages and slider-crank mechanisms are included on the disk provided with this book. These programs use the same nomenclature as the Hrones and Nelson atlas. Using these programs, it is possible to review quickly the coupler curves available and to determine the link lengths and coupler point that will generate the curve.



### 6.6.1 Design of Six-Bar Linkages Using Coupler Curves

Coupler curves from four-bar linkages and slider-crank mechanisms are used in two main ways. The first is to use the motion of the coupler in the area of the curve to perform some function. A common use for such points is in packaging and conveying equipment. Figure 6.59 shows a coupler mechanism design for packing hay in a round baler.<sup>11</sup> Figure 6.60 shows a mechanism that has been used to feed film in a motion picture projector.<sup>12</sup>

A second use for coupler curves is to facilitate the design of six- and eight-link mechanisms where the output link is to have a prescribed motion relative to the input link. A six-link mechanism is represented schematically in Fig. 6.61, where link 2 is the input and link 6 is the output. The output dyad (links 5 and 6) is driven by the coupler point ( $E$ ) of the four-bar linkage. By properly selecting the coupler curve, different functional relationships between  $\phi$  and  $\theta$  can be achieved. The design of six-link mechanisms using coupler curves is discussed extensively by Soni.<sup>5</sup> The design procedure is illustrated in the following two examples.

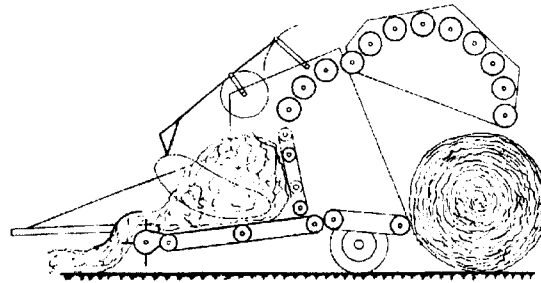


FIGURE 6.59 Coupler point used in packing mechanism in round baler.<sup>11</sup>

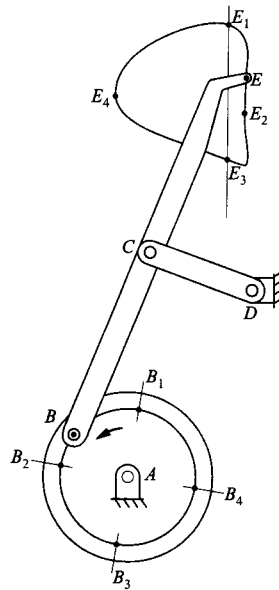
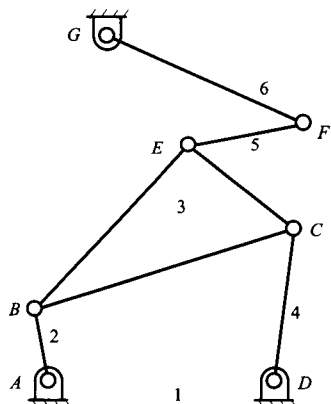


FIGURE 6.60 Coupler point used in film feed mechanism.<sup>18</sup>



**FIGURE 6.61** Six-link mechanism that can be designed using coupler curves.

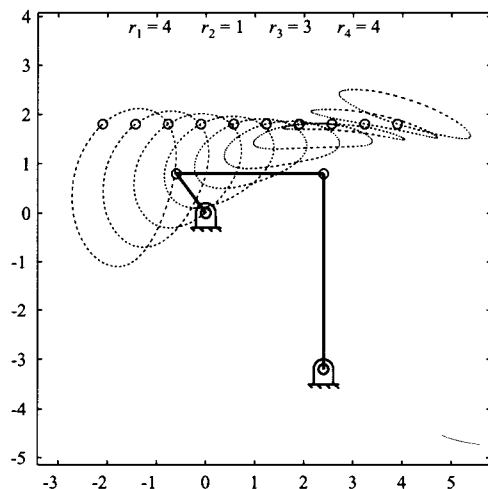
**EXAMPLE 6.7**  
**Design of a**  
**Six-Link Dwell**  
**Mechanism Using**  
**a Coupler Curve**

**Solution**

A mechanism of the type shown in Fig. 6.61 is to be designed such that link 6 is an oscillating lever and link 2 rotates a full  $360^\circ$ . The output link is to oscillate through a range of  $30^\circ$  during the first  $120^\circ$  of crank rotation. Link 6 is then to dwell for  $90^\circ$  of crank rotation and return during the remaining  $150^\circ$  of crank rotation.

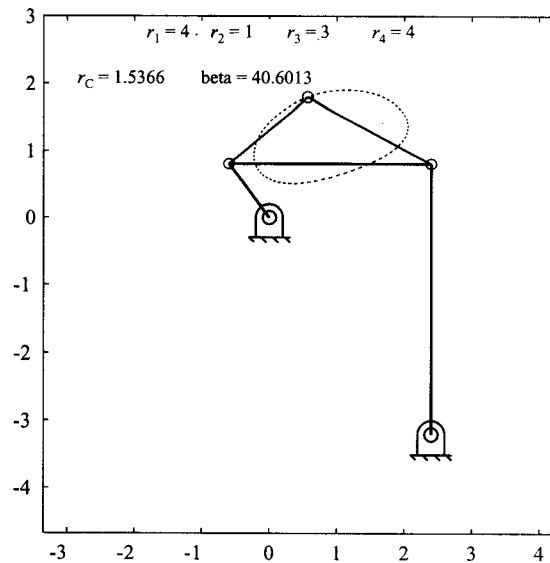
To solve this problem, it is necessary to have access to an atlas of coupler curves or to use a program that can generate the coupler curves. Regardless of the procedure used, we must be able to determine the geometry of the curve and the travel distance along the curve as a function of input rotation. In the Hrones and Nelson atlas and in the programs *hr\_crankrocker.m* and *hr\_slidercrank.m* provided on the disk with this book, a dashed line is used for each  $5^\circ$  of crank rotation. We will use the four-bar program *hr\_crankrocker.m* to generate candidate coupler curves. The first step is to visualize the shape of coupler curve that can be used to drive links 5 and 6. Several different geometries might be used, but the simplest is a curve of roughly elliptical shape. The coupler curves used are displayed in Figs. 6.62 and 6.63, and the design procedure is shown in Fig. 6.64. The procedure is described in the following.

1. Test different coupler curves to determine whether a portion of the curve in the vicinity of the minor axis is roughly circular in shape for the desired dwell period ( $90^\circ$  or 18 dashes). Fig. 6.62



**FIGURE 6.62** Coupler curves for Example 6.7. Note that each dash corresponds to  $5^\circ$  of crank rotation.

gives a set of curves generated with the program *hr\_crankrocker.m* when  $r_1 = 4$ ,  $r_2 = 1$ ,  $r_3 = 3$ , and  $r_4 = 4$ . From the curves displayed, we will select the curve shown in Fig. 6.63.



**FIGURE 6.63** Coupler curve chosen for design in Example 6.7.

2. After a coupler curve is identified, find the center of the circle that best fits the circular region identified in step 1. The radius of the circle will be the length of link 5. Identify explicitly the beginning and end of the circular portion of the curve. The center of the circle arc will be one extreme position for point  $F$ . This is shown in Fig. 6.64, where the mechanism has been redrawn so that the frame link ( $r_1$ ) is horizontal.
3. Point  $F'$  corresponds to the second extreme position of  $F$ . To locate  $F'$ , identify the point on the coupler curve corresponding to  $120^\circ$  (24 dashes) of crank rotation beyond the dwell. Locate a perpendicular line to the coupler point at this point, and locate  $F'$  on this line. Note that when link 5 is in an extreme position, it will be perpendicular to the coupler curve.
4. The pivot  $G$  must be located on the perpendicular bisector of the line  $FF'$ . Locate  $G$  such that the angle  $FGF'$  is  $30^\circ$ . The parameters corresponding to the solution are as follows:

$$r_1 = 4, \quad r_5 = 1.682, \quad BE = 1.537$$

$$r_2 = 1, \quad r_6 = 2.694, \quad \beta = 40.6^\circ$$

$$r_3 = 3, \quad G_x = 0.697, \quad \theta_1 = 0$$

$$r_4 = 4, \quad G_y = 3.740$$

5. Compute and plot the motion of link 6 relative to link 2 to evaluate the design. The resulting mechanism is simply a four-bar linkage with the addition of two more links (Watt's six-bar mechanism). The two additional links are called a dyad and can be easily analyzed using the procedures given previously. A MATLAB routine (*sixbar.m*) for a six-bar linkage analysis based on the four-bar and dyad routines is provided on the disk with this book. Part of the analysis from this program is given in Fig. 6.65. The results are close to the design specifications, and the basic design is acceptable. Note in Fig. 6.65 that the angular velocity of link 6 is approximately zero during the dwell. The input (crank) velocity was 1 rad/s.

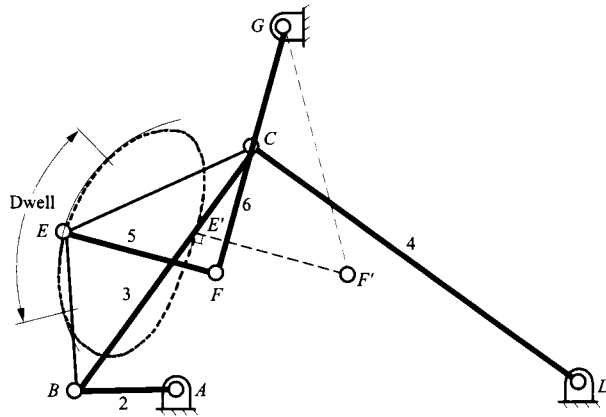


FIGURE 6.64 Design procedure for mechanism in Example 6.7.

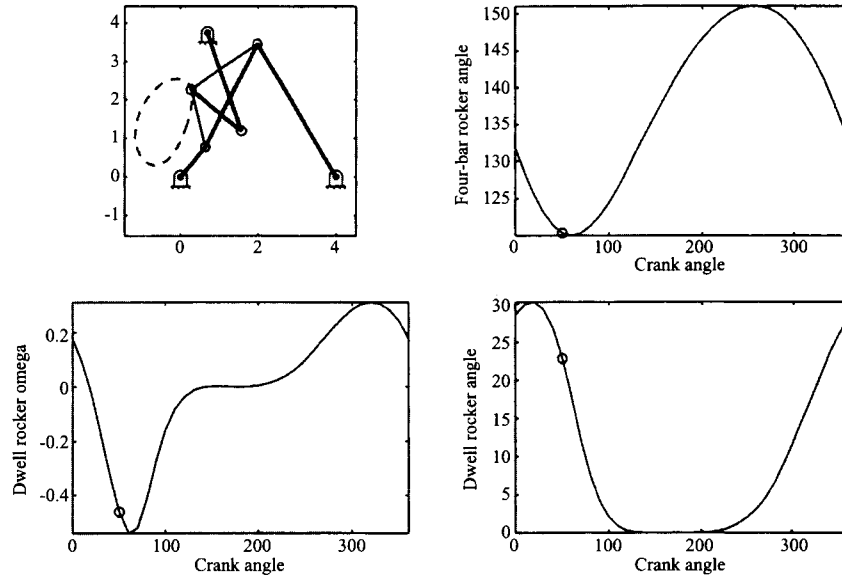


FIGURE 6.65 Analysis of linkage designed in Example 6.7. The velocity plot is based on a crank velocity of 1 rad/s.

This design procedure can yield a large number of candidate designs. The best design can be chosen by using an appropriate evaluation criterion. Typical criteria are linkage size, force transmission characteristics, and acceleration characteristics.

**EXAMPLE 6.8**  
**Design of a**  
**Six-Link**  
**Mechanism for a**  
**Double Oscillation**

**Solution**

A mechanism of the type shown in Fig. 6.61 is to be designed such that link 6 will make two complete  $30^\circ$  oscillations for each revolution of the driving link.

For this problem, no timing information is required. Therefore, we need only to ensure that the output link makes two complete oscillations for one oscillation of the input crank. Again, we will use the four-bar program *hr\_crankrocker.m* to generate candidate coupler curves. The first step is to visualize the shape of a coupler curve that can be used to drive links 5 and 6. One curve that will work for this

type of problem is a figure-eight curve. The design procedure is shown in Fig. 6.66 and described in the following:

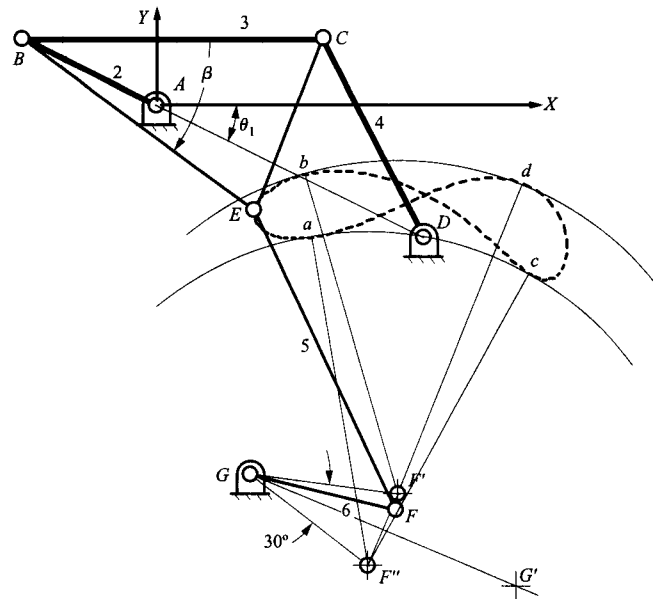


FIGURE 6.66 Procedure for designing linkage for Example 6.8.

1. Select a coupler curve that is a figure-eight curve with roughly equal lobes. The coupler curve selected is displayed in Fig. 6.67.
2. After the coupler curve is identified, select the length of link 5 and draw a circle or circle arc with a radius equal to the length of link 5 and tangent to the coupler curve at the two points  $b$  and  $d$ . The center,  $F'$ , of this circle is one extreme position of point  $F$ . Draw another circle or circle arc of the same radius tangent to the coupler curve at points  $a$  and  $c$ . The center,  $F''$ , of this circle is the second extreme position of  $F$ .
3. The pivot point,  $G$ , must be located on the perpendicular bisector of the line  $F'F''$ . Locate  $G$  such that the angle  $F'GF''$  is  $30^\circ$ . Link 6 is the link from  $F'$  to  $G$  (or from  $F''$  to  $G$ ). Note that there are two possible locations for point  $G$ . The location  $G$  is chosen in this example over  $G'$  because it will result in better transmission characteristics. If point  $G'$  is chosen, the linkage will lock up before it traverses its entire range of motion because the distance  $G'b$  is slightly larger than  $(EF + FG)$ . The parameters corresponding to the solution are as follows:

$$\begin{aligned} r_1 &= 2, & r_5 &= 2.212, & BE &= 1.927 \\ r_2 &= 1, & r_6 &= 1.000, & \beta &= -36.44^\circ \\ r_3 &= 2, & G_x &= 0.625, & \theta_1 &= -26.57^\circ \\ r_4 &= 1.5, & G_y &= -2.468 \end{aligned}$$

4. Compute and plot the motion of link 6 relative to link 2 to evaluate the design. This is done in Fig. 6.68 based on the program (*sixbar.m*) provided on the disk with this book. Again, the input (crank) velocity was chosen as 1 rad/s.

The results given in Fig. 6.68 are very close to the design specifications. If more accurate results are desired, the location of  $G$  or the lengths of  $r_5$  or  $r_6$  could be adjusted slightly. This can be done

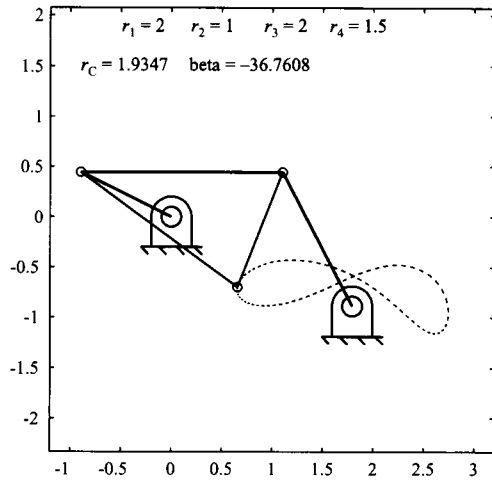


FIGURE 6.67 Curve that can be used for Example 6.8.

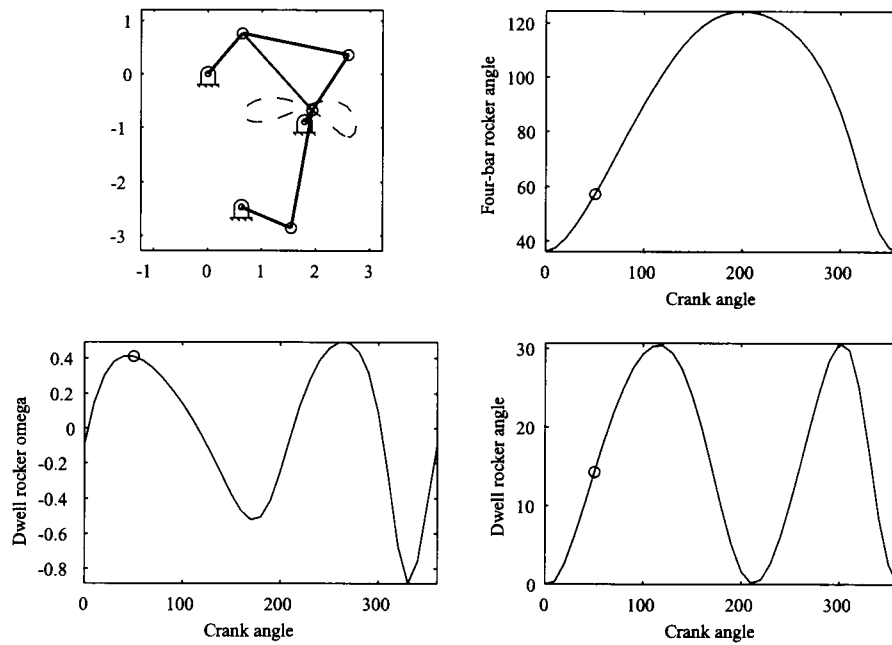


FIGURE 6.68 Analysis of mechanism designed for Example 6.8.

manually or by using an optimization program that minimizes the error created by the linkage. However, even if an optimization program is used, the graphical procedure, which is very simple and quick to apply, is a good means of generating an initial estimate of the optimum solution.

### 6.6.2 Motion Generation for Parallel Motion Using Coupler Curves

In industrial applications, it is sometimes necessary to move a rigid body along a curved path in such a way that the angular orientation of the rigid body does not change. This situation, shown in Fig. 6.69, is a special case of rigid-body guidance when all of the positions are parallel. If we attempt to use a four-bar linkage for this problem, only a parallelogram linkage can guide a linkage through more than two parallel positions in general,<sup>14</sup> and the design constraints for parallelogram linkages are severely restricted. Therefore, guiding a linkage in parallel motion along a complex path generally requires more than four links.

A relatively simple solution to parallel motion synthesis is to use a four-bar linkage and two parallelogram linkages in parallel to form an eight-link mechanism. The four-bar linkage defines a coupler path along which one point of the rigid body is guided, and the parallelogram linkages maintain the orientation of the rigid body relative to the ground. This configuration is shown in Fig. 6.70.

To design the eight-link mechanism, we need only find a four-bar linkage coupler curve that will approximate the curve that the output member must follow. This defines linkage  $ABCDE$  in Fig. 6.70. Next the parallelogram linkages are added to maintain the orientation of the rigid body. Referring to Fig. 6.70, we see that link  $FG$  is equal in length to  $CB$ , and link  $GH$  is equal in length to  $AB$ . Lengths  $HA$ ,  $BG$ , and  $CF$  are equal, but the actual length is arbitrary from the standpoint of kinematics. Note that the parallelograms could also have been used with lengths  $CD$  and  $DE$ . The side of the linkage used depends on the design constraints.

In practical situations, the parallelograms may not work for the full range of motion of the four-bar linkage either because of a need to change branch or because of a mechanical interference among the links. If a full range of motion is required, the parallelogram linkages can be replaced by two cable, belt, or chain drives. This is shown in Fig. 6.71. The motion of link 2 relative to link 4 is equivalent in both cases if the two pulley or sprocket diameters are equal. Any kind of belt, chain, or cable drive can be used as long as there is no slipping at the pulleys.

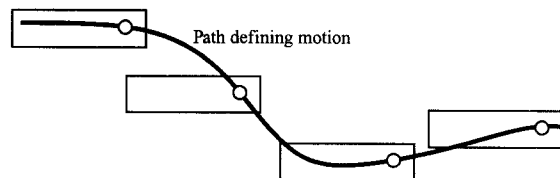


FIGURE 6.69 General parallel motion along a curved path.

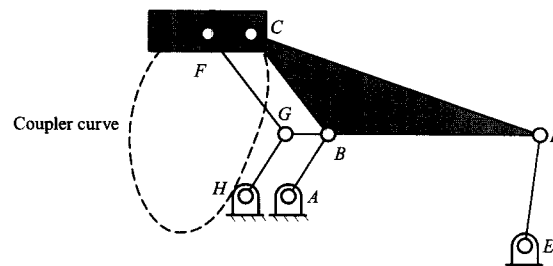
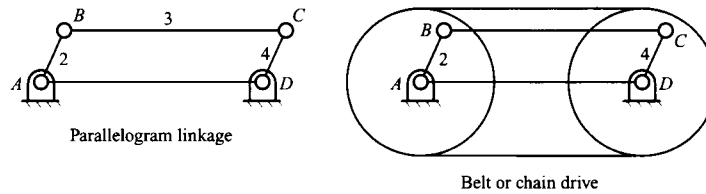
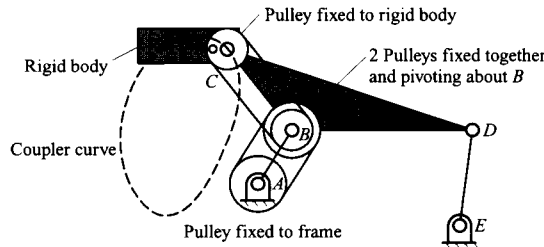


FIGURE 6.70 Eight-link mechanism to guide parallel motion along a curved path.



**FIGURE 6.71** The motion of a parallelogram linkage can be duplicated by a belt or chain drive if the pulleys are of equal diameter.

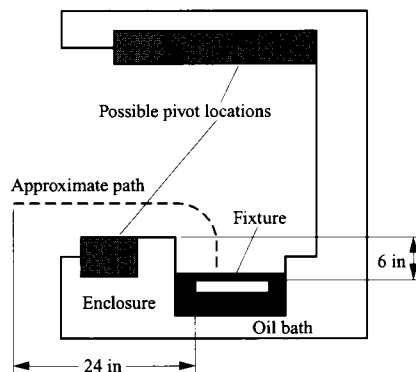
The equivalent system corresponding to Fig. 6.70 is shown in Fig. 6.72. Different pulley diameters are used for the two equivalent parallelogram-linkage drives to illustrate that the two drives are separate. However, the two pulleys pivoting about point *B* must be fixed together.



**FIGURE 6.72** Replacement of the parallelogram linkages in Fig. 6.70 by belt drives.

**EXAMPLE 6.9**  
**Design of an**  
**Eight-Link**  
**Mechanism for**  
**Parallel Motion**  
**Generation**

A test fixture must be removed from a hot hydraulic fluid bath. The fixture must be lifted vertically 6 in and then carried horizontally approximately 24 in along the approximate path shown in Fig. 6.73. The test fixture must remain parallel at all times. Design a linkage system that will move the fixture.



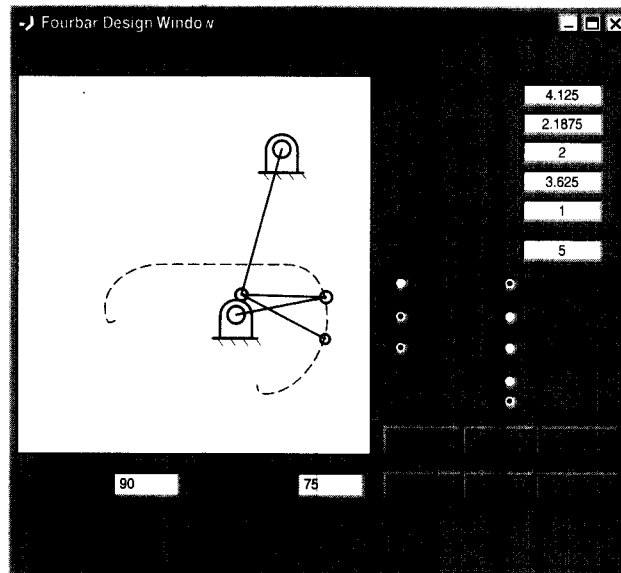
**FIGURE 6.73** General geometry for fixture and enclosure.

**Solution**

To solve the problem, it is necessary to identify a four-bar linkage coupler curve that will match approximately the curve represented in Fig. 6.73. The important features of the linkage are the pivot locations, the 6-in rise in the coupler curve, and the lateral motion of approximately 24 in.

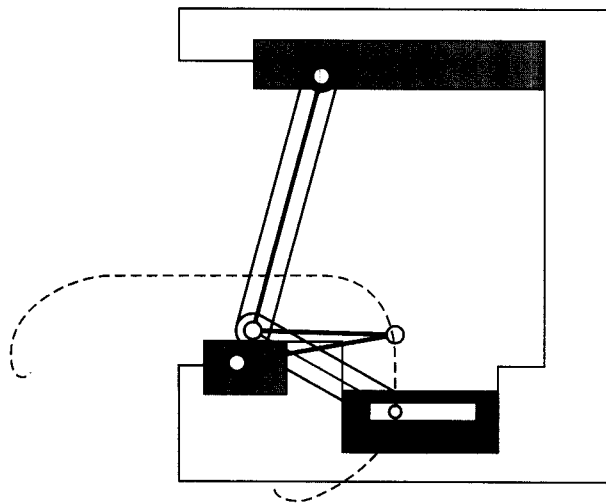


Two programs (*FourBarDesign* and *HRCrankRockerDesign*) for generating four-bar linkage coupler curves are available on the disk with this Book. The first program will generate coupler curves for both Grashof type I and type II linkages whereas the second program is limited to crank-rocker mechanisms. For this problem, a crank-rocker linkage is not necessary so the first program was used. The linkage was designed by trial and error, and the result is shown in Fig. 6.74.



**FIGURE 6.74** Screen capture from *FourBarDesign* program showing solution coupler curve.

The linkage is shown with the fixture in Fig. 6.75. Because of the range of motion required for the linkage, cable-driven pulleys are suggested for the final design rather than parallelogram linkages.



**FIGURE 6.75** The mechanism located in the chamber.

### 6.6.3 Four-Bar Cognate Linkages

A given four-bar linkage with coupler point  $C$  will generate a unique coupler curve. It is interesting to note that there are two other four-bar linkages that will generate exactly the same coupler curve. The three four-bar linkages that will generate the same coupler curve are called cognates. From a design standpoint, one of the linkages may have more desirable motion characteristics than the others. Therefore, to select the best one, it is useful to identify all three linkages once the coupler curve is defined. The existence of the three cognate linkages was originally discovered by Roberts.<sup>4,7</sup> A general discussion of cognate linkages and a proof for Roberts's theorem that identifies the geometric relationships among cognates are given in Chapter 7. In this chapter, we will limit our discussion to a procedure for finding cognates.

The geometry of the cognate linkages can be determined by considering extreme versions of the three linkages. The resulting diagram shown in Fig. 6.76 is called Roberts's linkage.<sup>4</sup> The mechanisms in this diagram will not move; however, the diagram shows the relationships that must exist among the three cognate linkages. These relationships are maintained when triangle  $MQO$  is shrunk while maintaining similarity, thereby permitting the linkages to move. In particular, triangles  $MQO$ ,  $ABC$ ,  $GCF$ , and  $CDE$  are similar. Also, figures  $MACG$ ,  $BQDC$ , and  $FCEO$  are parallelograms. The coupler point is  $C$ , and two cognate linkages share each of the pivots. Also, the couplers of each of the cognates are geometrically similar to each other and to the triangle formed by the pivots. If we identify the pivots as  $M$ ,  $Q$ , and  $O$ , we can identify the three four-bar linkages by their pivots. That is, one four-bar linkage is the  $MQ$  four-bar, one is the  $MO$  four-bar linkage, and the third is the  $QO$  four-bar linkage.

The geometric relationships among three general cognate linkages are shown in Fig. 6.77. When determining the cognate linkages, it is assumed that the  $MQ$  linkage is known along with the coupler point  $C$ . The cognate linkages can be identified with the aid of Roberts's linkage, which reveals the geometric relationships among the three linkages. Given the positions of  $M$  and  $Q$  and the lengths  $r_2$ ,  $r_3$ ,  $r_4$ ,  $r_5$ ,  $r_6$ , and  $r_7$ , the equations for the location of pivot  $O$  and the corresponding angles and lengths of the other cognate linkages are shown in Table 6.1. Note that the cognates will all be of the same Grashof type but may be different subtypes. When the location of the coupler point is specified, the coordinates of  $A$ ,  $B$ , and  $C$  must be given, or alternatively, the coordinates of  $A$  and  $B$  can be given along with the angle  $\beta$  and length  $r_5$ .

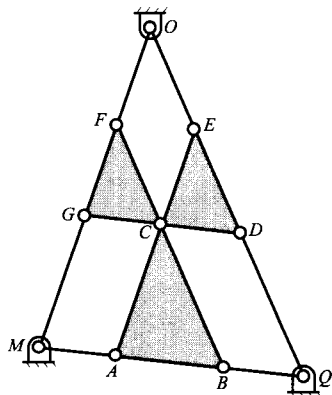


FIGURE 6.76 Roberts's linkage.

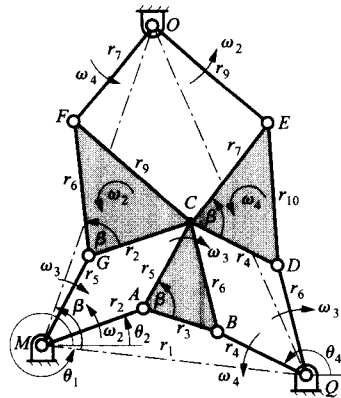


FIGURE 6.77 Three cognate linkages will generate the same coupler curve.

**TABLE 6.1 Angle and Link Relationships Permitting the Cognate Linkages to Be Determined. The Variables Refer to the Diagram in Fig. 6.77. The Coordinates  $(x_A, y_A)$ ,  $(x_B, y_B)$ , and  $(x_C, y_C)$  Are Assumed to Be Known from the Analysis of the MQ Linkage. Alternatively,  $\beta$ ,  $\phi$ , and  $\lambda$  Can Be Given Separately**

$$r_6 = r_2 \frac{r_5}{r_3} \quad r_7 = r_4 \frac{r_5}{r_3} \quad r_8 = r_1 \frac{r_5}{r_3}$$

$$\beta = \tan^{-1} \left[ \frac{y_C - y_A}{x_C - x_A} \right] - \tan^{-1} \left[ \frac{y_B - y_A}{x_B - x_A} \right]$$

$$x_O = x_M + r_8 \cos(\theta_1 + \beta) \quad y_O = y_M + r_8 \sin(\theta_1 + \beta)$$

$$x_G = x_M + (x_C - x_A) \quad y_G = y_M + (y_C - y_A)$$

$$x_D = x_Q + (x_C - x_B) \quad y_D = y_Q + (y_C - y_B)$$

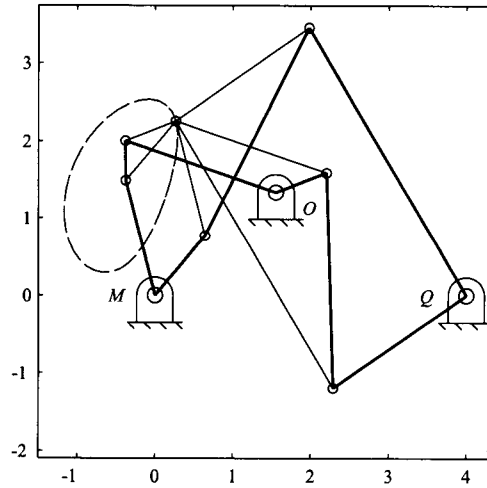
$$\phi = \tan^{-1} \left[ \frac{y_D - y_C}{x_D - x_C} \right] \quad \lambda = \tan^{-1} \left[ \frac{y_C - y_G}{x_C - x_G} \right]$$

$$x_E = x_D + r_1 \cos(\beta + \phi) \quad y_E = y_D + r_7 \sin(\beta + \phi)$$

$$x_F = x_G + r_6 \cos(\lambda + \beta) \quad y_F = y_G + r_6 \sin(\lambda + \beta)$$

$$r_9 = \sqrt{(x_E - x_O)^2 + (y_E - y_O)^2} \quad r_{10} = \sqrt{(x_E - x_D)^2 + (y_E - y_D)^2}$$

The equations in Table 6.1 can be easily programmed to determine the geometry of the cognate linkages, and this is done in a program (*cognates.m*) given on the disk with this book. Figure 6.78 shows the cognate linkages for the mechanism shown in Fig. 6.77.



**FIGURE 6.78** Three cognate linkages for the coupler curve in Fig. 6.63.

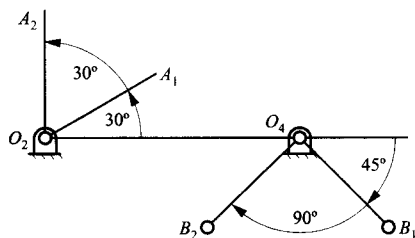
## 6.7 REFERENCES

- <sup>1</sup>Kaufman, R. E., "Mechanism Design by Computer," *Machine Design*, Vol. 50, pp. 94–100 (1978).
- <sup>2</sup>Waldron, K. J., "Improved Solutions of the Branch and Order Problems of Burmester Linkage Synthesis," *Journal of Mechanism and Machine Theory*, Vol. 13, pp. 199–207 (1978).
- <sup>3</sup>Erdman, A. G., and D. Riley, "Computer-Aided Linkage Design Using the LINCAGES Package," ASME Paper No. 81-DET-121 (1981).
- <sup>4</sup>Hall, A. S., *Kinematics and Linkage Design*. Balt Publishers, West Lafayette, IN (1961).
- <sup>5</sup>Soni, A. H., *Mechanism Synthesis and Analysis*, McGraw-Hill Book Co., New York (1974).
- <sup>6</sup>Arora, J. S., *Introduction to Optimal Design*, McGraw-Hill Book Co., New York (1989).
- <sup>7</sup>Sandor, G. N., and A. G. Erdman, *Advanced Mechanism Design: Analysis and Synthesis*, Prentice-Hall, Inc., Englewood Cliffs, NJ (1984).
- <sup>8</sup>Suh, C. H., and C. W. Radcliffe, *Kinematics and Mechanisms Design*, John Wiley & Sons, Inc., New York (1978).
- <sup>9</sup>Waldron, K. J., "The Order Problem of Burmester Linkage Synthesis," *ASME Journal of Engineering for Industry*, Vol. 97, pp. 1405–1406 (1975).
- <sup>10</sup>Hrones, J. A., and G. L. Nelson, *Analysis of the Four-Bar linkage*, The Technology Press of M.I.T., Cambridge, MA, and John Wiley & Sons, New York (1951).
- <sup>11</sup>Tooten, K., "Entwicklung und Konstruktion einer neuen Rundballenpresse," *Konstruktion*, Vol. 39, pp. 285–290 (1987).
- <sup>12</sup>Hartenberg, R. S., and J. Denavit, *Kinematic Synthesis of Linkages*, McGraw-Hill Book Co., New York (1964).
- <sup>13</sup>Freudenstein, F., "Approximate Synthesis of Four-Bar Linkages," *Transactions of ASME*, Vol. 77, pp. 853–861, (August 1959).
- <sup>14</sup>Song, S. M., *Theoretical and Numerical Improvements to Computer-Aided Linkage Design*, Ph.D. dissertation, The Ohio State University (1981).

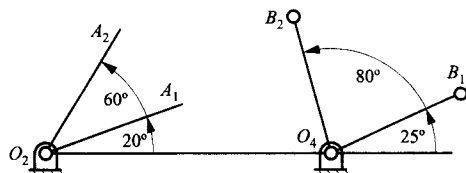
## PROBLEMS

### DOUBLE-ROCKER EXERCISE PROBLEMS

**6.1** Design a double-rocker, four-bar linkage so that the base link is 2-in long and the output rocker is 1-in long. The input link turns CCW  $60^\circ$  when the output link turns CW through  $90^\circ$ . The initial angle for the input link is  $30^\circ$  CCW from the horizontal, and the initial angle for the output link is  $-45^\circ$ . The geometry is indicated in the figure.



**6.2** Design a double rocker, four-bar linkage so that the base link is 4-in long and the output rocker is 2-in long. The input link turns CCW  $40^\circ$  when the output link turns CCW through  $80^\circ$ . The initial angle for the input link is  $20^\circ$  CCW from the horizontal, and the initial angle for the output link is  $25^\circ$ . The geometry is indicated in the figure.

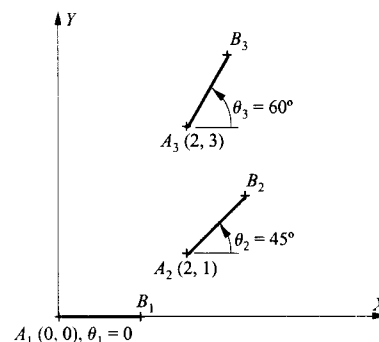


**6.3** In a back hoe, a four-bar linkage is added at the bucket in part to amplify the motion that can be achieved by the hydraulic cylinder attached to the link that rotates the bucket as shown in the figure. Design the link attached to the bucket and the coupler if the frame link is 13-in long and the input link is 12-in long. The input link driven by the hydraulic cylinder rotates through an angle of  $80^\circ$ , and the output link rotates through an angle of  $120^\circ$ . From the figure, determine reasonable angles for the starting angles ( $\theta_0$  and  $\phi_0$ ) for both of the rockers.

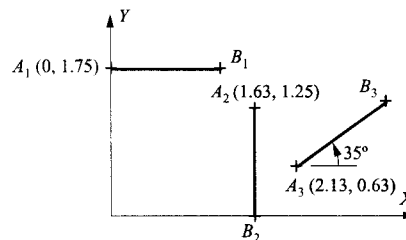


### RIGID-BODY GUIDANCE EXERCISE PROBLEMS

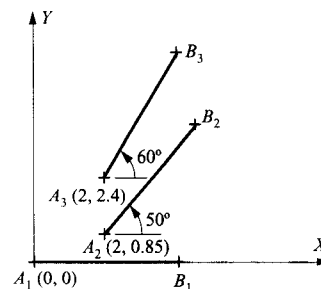
**6.4** In the drawing,  $AB = 1.25$  cm. Use  $A$  and  $B$  as circle points, and design a four-bar linkage to move its coupler through the three positions shown. Use Grashof's equation to identify the type of four-bar linkage designed.



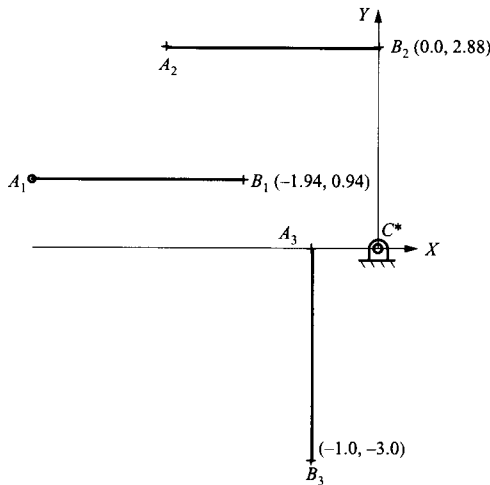
**6.5** Using points  $A$  and  $B$  as circle points, design a four-bar linkage that will position the body defined by  $AB$  in the three positions shown. Draw the linkage in position 1, and use Grashof's equation to identify the type of four-bar linkage designed. Position  $A_1B_1$  is horizontal, and position  $A_2B_2$  is vertical.  $AB = 1.25$  in.



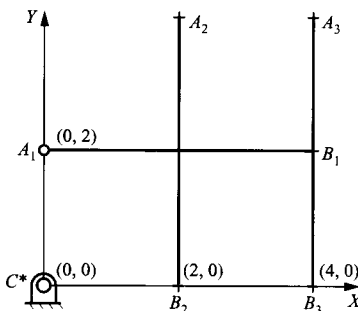
**6.6** Design a four-bar linkage to move its coupler through the three positions shown using points  $A$  and  $B$  as moving pivots.  $AB = 4$  cm. What is the Grashof type of the linkage generated?



6.7 A four-bar linkage is to be designed to move its coupler plane through the three positions shown. The moving pivot (circle point) of one crank is at  $A$  and the fixed pivot (center point) of the other crank is at  $C^*$ . Draw the linkage in position 1 and use Grashof's equation to identify the type of four-bar linkage designed. Also determine whether the linkage changes branch in traversing the design positions. Positions  $A_1B_1$  and  $A_2B_2$  are horizontal, and position  $A_3B_3$  is vertical.  $AB = 3$  in.

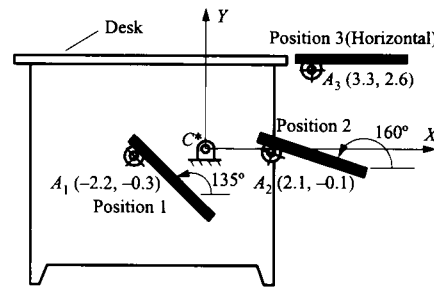


6.8 Design a four-bar linkage to move a coupler containing the line  $AB$  through the three positions shown. The moving pivot (circle point) of one crank is at  $A$ , and the fixed pivot (center point) of the other crank is at  $C^*$ . Draw the linkage in position 1, and use Grashof's equation to identify the type of four-bar linkage designed. Position  $A_1B_1$  is horizontal, and positions  $A_2B_2$  and  $A_3B_3$  are vertical.  $AB = 4$  in.

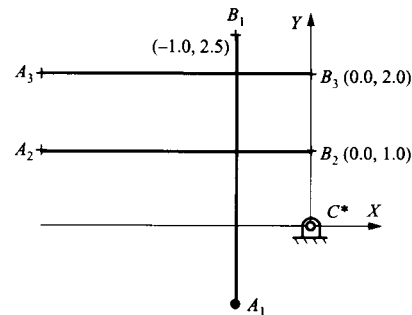


6.9 A mechanism must be designed to move a computer terminal from under a desk to its top. The system will be guided by a linkage, and the use of a four-bar linkage will be tried first. As a first attempt at the design, do the following:

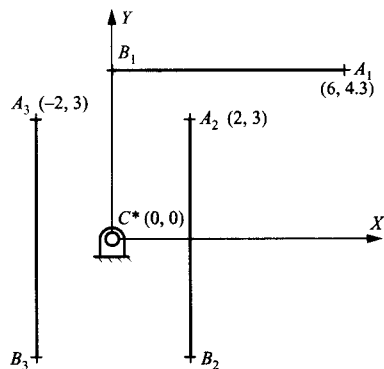
- Use  $C^*$  as a center point and find the corresponding circle point  $C$  in position 1.
- Use  $A$  as a circle point and find the corresponding center point  $A^*$ .
- Draw the linkage in position 1.
- Determine the type of linkage (crank-rocker, double-rocker, etc.) resulting.
- Evaluate the linkage to determine whether you would recommend that it be manufactured.



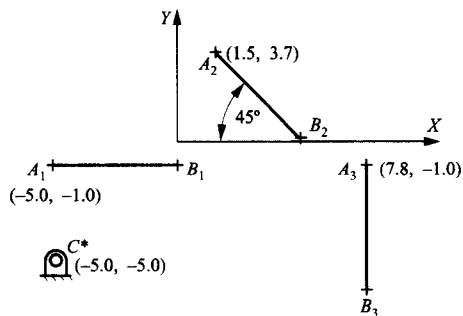
6.10 Design a four-bar linkage to move the coupler containing line segment  $AB$  through the three positions shown. The moving pivot for one crank is to be at  $A$ , and the fixed pivot for the other crank is to be at  $C^*$ . Draw the linkage in position 1 and determine the classification of the resulting linkage (e.g., crank-rocker, double-crank). Positions  $A_2B_2$  and  $A_3B_3$  are horizontal, and position  $A_1B_1$  is vertical.  $AB = 3.5$  in.



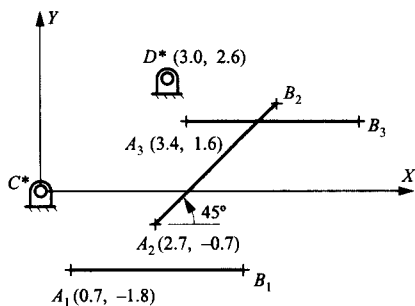
6.11 Design a four-bar linkage to move a coupler containing the line  $AB$  through the three positions shown. The moving pivot (circle point) of one crank is at  $A$  and the fixed pivot (center point) of the other crank is at  $C^*$ . Draw the linkage in position 1, and use Grashof's equation to identify the type of four-bar linkage designed. Position  $A_1B_1$  is horizontal, and positions  $A_2B_2$  and  $A_3B_3$  are vertical.  $AB = 6$  cm.



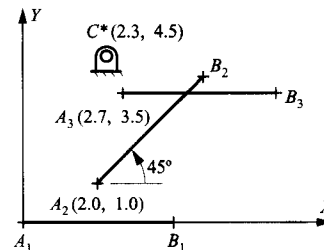
**6.12** Design a four-bar linkage to move the coupler containing line segment  $AB$  through the three positions shown. The moving pivot for one crank is to be at  $A$ , and the fixed pivot for the other crank is to be at  $C^*$ . Draw the linkage in position 1 and determine the classification of the resulting linkage (e.g., crank-rocker, double-crank). Also check to determine whether the linkage will change branch as it moves from one position to another. Position  $A_1B_1$  is horizontal, and position  $A_3B_3$  is vertical.  $AB = 5.1$  cm.



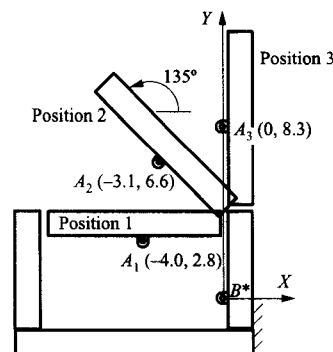
**6.13** Synthesize a four-bar mechanism in position 2 that moves its coupler through the three positions shown if points  $C^*$  and  $D^*$  are center points. Position  $A_1B_1$  and position  $A_3B_3$  are horizontal.  $AB = 4$  cm.



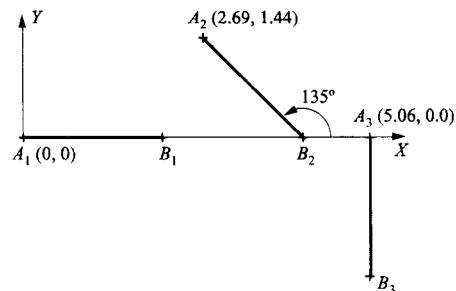
**6.14** Synthesize a four-bar mechanism in position 2 that moves its coupler through the three positions shown. Point  $A$  is a circle point, and point  $C^*$  is a center point. Position  $A_1B_1$  and position  $A_3B_3$  are horizontal.  $AB = 4$  cm.



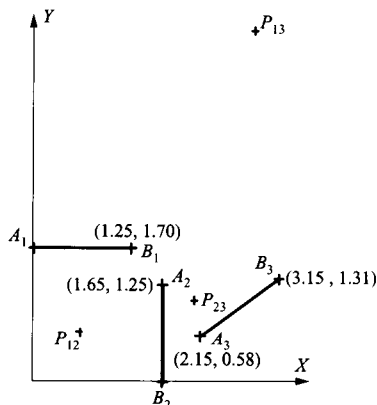
**6.15** A hardware designer wants to use a four-bar linkage to guide a door through the three positions shown. Position 1 is horizontal, and position 3 is vertical. As a tentative design, she selects point  $B^*$  as a center point and  $A$  as a circle point. For the three positions shown, determine the location of the circle point  $B$  corresponding to the center point  $B^*$  and the center point  $A^*$  corresponding to the circle point  $A$ . Draw the linkage in position 1 and determine the Grashof type for the linkage. Indicate whether you think that this linkage should be put into production.



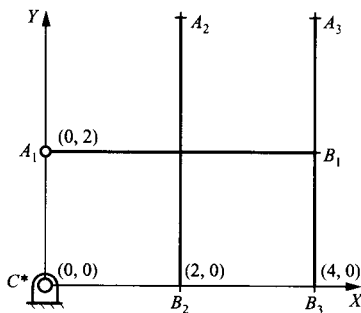
**6.16** Design a slider-crank mechanism to move the coupler containing line segment  $AB$  through the three positions shown. The moving pivot for the crank is to be at  $A$ . Determine the slider point, and draw the linkage in position 1. Also check to determine whether the linkage can be moved from one position to another without being disassembled. Position  $A_1B_1$  is horizontal, and position  $A_3B_3$  is vertical.  $AB = 2.0$  in.



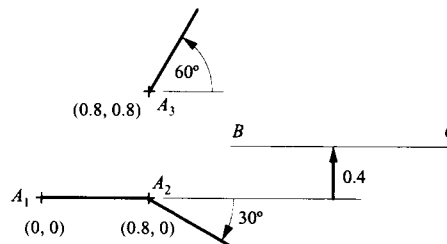
**6.17** Design a slider-crank mechanism to move a coupler containing the line  $AB$  through the three positions shown. The line  $AB$  is 1.25 in long. The moving pivot (circle point) of the crank is at  $A$ . The approximate locations of the three poles ( $P_{12}$ ,  $P_{13}$ ,  $P_{23}$ ) are shown, but these should be determined accurately after the positions are redrawn. Find  $A^*$ , the slider point that lies above  $B_1$  on a vertical line through  $B_1$ , and draw the linkage in position 1.



**6.18** Design a slider-crank linkage to move a coupler containing the line  $AB$  through the three positions shown. The fixed pivot (center point) of the crank is at  $C^*$ . Draw the linkage (including the slider line) in position 1. Position  $A_1B_1$  is horizontal, and positions  $A_2B_2$  and  $A_3B_3$  are vertical.  $AB = 4$  in.



**6.19** Design a slider-crank mechanism to move a coupler containing the line with  $A$  through the three positions shown. The moving pivot (circle point) of the crank is at  $A$ . Find the slider point that lies on line  $BC$  and draw the linkage (including the slider line) in position 1. Note that line  $BC$  is *not* the line on which the slider moves.



### FUNCTION-GENERATION EXERCISE PROBLEMS

**6.20** A device characterized by the input–output relationship  $\phi = a_1 + a_2 \cos \theta$  is to be used to generate (approximately) the function  $\phi = \theta^2$  (with  $\theta$  and  $\phi$  both in radians) over the range  $0 \leq \theta \leq \pi/4$ .

(a) Determine the number of precision points required to compute  $a_1$  and  $a_2$ .

(b) Choose the best precision point values for  $\theta$  from among 0, 0.17, 0.35, and 0.52, and determine the values of  $a_1$  and  $a_2$  that will allow the device to approximate the function.

(c) Find the error when  $\theta = \pi/8$ .

**6.21** A mechanical device characterized by the input–output relationship  $\phi = 2a_1 + 3a_2 \sin \theta + a_3^2$  is to be used to generate (approximately) the function  $\phi = 2\theta^2$  (with  $\theta$  and  $\phi$  both in radians) over the range  $0 \leq \theta \leq \pi/4$ . Exterior constraints on the design require that the parameter  $a_3 = 1$ .

(a) Determine the number of precision points required to complete the design of the system.

(b) Use Chebyshev spacing, and determine the values for the unknown design variables that will allow the device to approximate the function.

(c) Find the error when  $\theta = \pi/6$ .

**6.22** A mechanical device characterized by the input–output relationship  $\phi = 2a_1 + a_2 \tan \theta + a_3^2$  is to be used to generate (approximately) the function  $\phi = 3\theta^3$  (with  $\theta$  and  $\phi$  both in radians) over the range  $0 \leq \theta \leq \pi/3$ . Exterior constraints on the design require that the parameter  $a_3 = 1$ .

(a) Determine the number of precision points required to complete the design of the system.

(b) Use Chebyshev spacing, and determine the values for the unknown design variables that will allow the device to approximate the function.

(c) Find the error when  $\theta = \pi/6$ .

**6.23** A mechanical device characterized by the input–output relationship  $\phi = 2a_1 + a_2 \sin \theta$  is to be used to generate (approximately) the function  $y = 2x^2$  over the range  $0 \leq x \leq \pi/2$ , where  $x, y, \phi$ , and  $\theta$  are all in radians. Assume that the use of the device will be such that the starting point and range for  $x$  can be the same as those for  $\theta$ , and the range and starting point for  $y$  can be the same as those for  $\phi$ .



(a) Determine the number of precision points required to complete the design of the system.

(b) Use Chebyshev spacing, and determine the values for the unknown design variables that will allow the device to approximate the function.

(c) Compute the error generated by the device for  $x = \pi/4$ .

**6.24** Determine the link lengths and draw a four-bar linkage that will generate the function  $\phi = \theta^2$  (with  $\theta$  and  $\phi$  both in radians) for values of  $\theta$  between 0.5 and 1.0 radians. Use Chebyshev spacing with three precision points. The base length of the linkage must be 2 cm. Use the following angle information:

$$\theta_0 = 20^\circ, \Delta\theta = 60^\circ$$

$$\phi_0 = 45^\circ, \Delta\phi = 50^\circ$$

**6.25** Determine the link lengths and draw a four-bar linkage that will generate the function  $\phi = \sin\theta$  for values of  $\theta$  between  $0^\circ$  and  $90^\circ$ . Use Chebyshev spacing with three precision points. The base length of the linkage must be 2 cm. Use the following angle information:

$$\theta_0 = 30^\circ, \Delta\theta = 90^\circ$$

$$\phi_0 = 30^\circ, \Delta\phi = 60^\circ$$

**6.26** Design a four-bar linkage that generates the function  $y = (\sqrt{x} - x + 3)$  for values of  $x$  between 1 and 4. Use the Chebyshev spacing for three precision points. The base length of the linkage must be 2 in. Use the following angle information:

$$\theta_0 = 45^\circ, \Delta\theta = 50^\circ$$

$$\phi_0 = 30^\circ, \Delta\phi = 70^\circ$$

Compute the error at  $x = 2$ .

**6.27** Design a four-bar linkage to generate the function  $y = x^2 - 1$  for values of  $x$  between 1 and 5. Use Chebyshev spacing with three precision points. The base length of the linkage must be 2 cm. Use the following angle information:

$$\theta_0 = 30^\circ, \Delta\theta = 60^\circ$$

$$\phi_0 = 45^\circ, \Delta\phi = 90^\circ$$

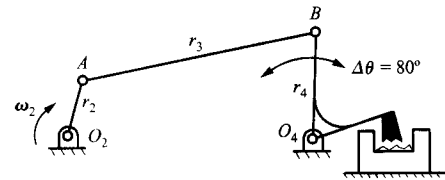
Compute the error at  $x = 3$ .

**CRANK-ROCKER EXERCISE PROBLEMS**

**6.28** The output arm of a lawn sprinkler is to rotate through an angle of  $90^\circ$ , and the ratio of the times for the forward and reverse rotations is to be 1 to 1. Design the crank-rocker mechanism for the sprinkler. If the crank is to be 1 in long, give the lengths of the other links.

**6.29** Design a crank-rocker mechanism such that with the crank turning at constant speed, the oscillating lever will have a time ratio of advance to return of 3:2. The lever is to oscillate through an angle of  $80^\circ$ , and the length of the base link is to be 2 in.

**6.30** A packing mechanism requires that the crank ( $r_2$ ) rotate at a constant velocity. The advance part of the cycle is to take twice as long as the return to give a quick-return mechanism. The distance between fixed pivots must be 0.5 m. Determine the lengths for  $r_2$ ,  $r_3$ , and  $r_4$ .



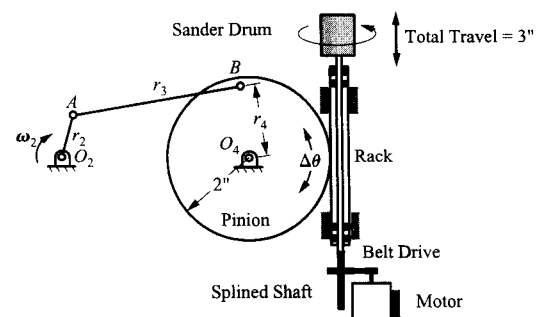
**6.31** The rocker  $O_4B$  of a crank-rocker linkage swings symmetrically about the vertical through a total angle of  $70^\circ$ . The return motion should take 0.75 times the time that the forward motion takes. Assuming that the two pivots are 2.5 in apart, find the length of each of the links.

**6.32** A crank-rocker is to be designed such that with the crank turning at a constant speed CCW, the rocker will have a time ratio of advance to return of 1.25. The rocking angle is to be  $40^\circ$ , and it rocks symmetrically about a vertical line through  $O_4$ . Assume that the two pivots are on the same horizontal line, 3 in apart.

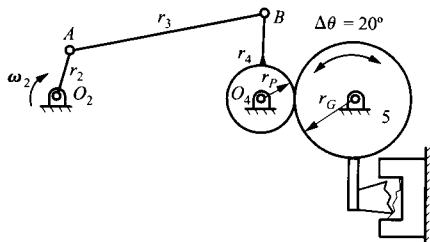
**6.33** Design a crank-rocker mechanism that has a base length of 2.0, a time ratio of 1.3, and a rocker oscillation angle of  $100^\circ$ . The oscillation is to be symmetric about a vertical line through  $O_4$ . Specify the length of each of the links.

**6.34** A crank-rocker mechanism with a time ratio of  $2\frac{1}{3}$  and a rocker oscillation angle of  $72^\circ$  is to be designed. The oscillation is to be symmetric about a vertical line through  $O_4$ . Draw the mechanism in any position. If the length of the base link is 2 in, give the lengths of the other three links. Also show the transmission angle in the position in which the linkage is drawn.

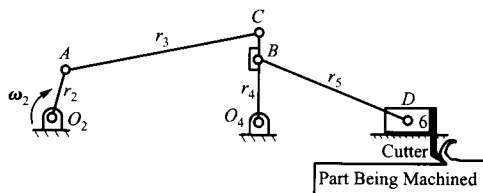
**6.35** The mechanism shown is used to drive an oscillating sander drum. The drum is rotated by a splined shaft that is cycled vertically. The vertical motion is driven by a four-bar linkage through a rack-and-pinion gear set (modeled as a rolling contact joint). The total vertical travel for the sander drum is 3 in, and the pinion has a 2-in radius. The sander mechanism requires that the crank ( $r_2$ ) rotate at a constant velocity, and the advance part of the cycle is to take the same amount of time as the return part. The distance between fixed pivots must be 4 in. Determine the lengths for  $r_2$ ,  $r_3$ , and  $r_4$ .



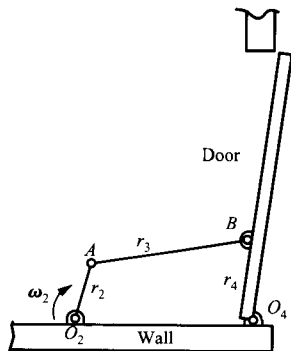
6.36 The mechanism shown is proposed for a rock crusher. The crusher hammer rotates through an angle of  $20^\circ$ , and the gear ratio  $R_G/R_P$  is 4:1, that is, the radius  $r_G$  is four times the radius  $r_P$ . Contact between the two gears can be treated as rolling contact. The crusher mechanism requires that the crank ( $r_2$ ) rotate at a constant velocity, and the advance part of the cycle is to take 1.5 times as long as the return part. The distance between fixed pivots  $O_2$  and  $O_4$  must be 4 ft. Determine the lengths for  $r_2$ ,  $r_3$ , and  $r_4$ .



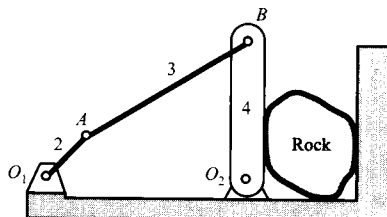
6.37 The mechanism shown is proposed for a shaper mechanism. The shaper cutter moves back and forth such that the forward (cutting) stroke takes twice as much time as the return stroke. The crank ( $r_2$ ) rotates at a constant velocity. The follower link ( $r_4$ ) is to be 4 in and to oscillate through an angle of  $80^\circ$ . Determine the lengths for  $r_1$ ,  $r_2$ , and  $r_3$ .



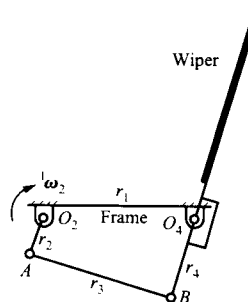
6.38 A crank-rocker is to be used in a door-closing mechanism. The door must open  $100^\circ$ . The crank motor is controlled by a timer mechanism such that it pauses when the door is fully open. Because of this, the mechanism can open and close the door in the same amount of time. If the crank ( $r_2$ ) of the mechanism is to be 10-cm long, determine the lengths of the other links ( $r_1$ ,  $r_3$ , and  $r_4$ ). Sketch the mechanism to scale.



6.39 A crank-rocker is to be used for the rock crusher mechanism shown. The oscillation angle for the rocker is to be  $80^\circ$ , and the time for the working (crushing) stroke for the rocker is to be 1.1 times the return stroke. If the frame link ( $r_1$ ) of the mechanism is to be 10-ft long, determine the lengths of the other links ( $r_2$ ,  $r_3$ , and  $r_4$ ). Sketch the mechanism to scale.



6.40 A crank-rocker is to be used in a windshield-wiping mechanism. The wiper must oscillate  $80^\circ$ . The times for the forward and return strokes for the wiper are the same. If the base link ( $r_1$ ) of the mechanism is to be 10-cm long, determine the lengths of the other links ( $r_2$ ,  $r_3$ , and  $r_4$ ). Sketch the mechanism to scale.



### PATH-GENERATION EXERCISE PROBLEMS

6.41 Design a six-bar linkage like that shown in Fig. 6.61 such that the output link will do the following for one complete revolution of the input crank:

(a) Rotate CW by  $30^\circ$  for a CW rotation of  $210^\circ$  of the input crank.

(b) Rotate CCW by  $30^\circ$  for a CW rotation of  $150^\circ$  of the input crank.

6.42 Design a six-bar linkage like that shown in Fig. 6.61 such that the output link will make two complete  $35^\circ$  oscillations for each revolution of the driving link. (Hint: Select a coupler curve that is shaped like a figure eight.)

6.43 Design a six-bar linkage like that shown in Fig. 6.61 such that the output link will do the following for one complete revolution of the input crank:

(a) Rotate CW by  $40^\circ$ .

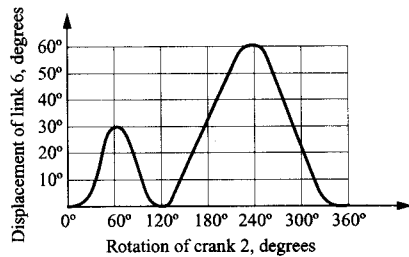
(b) Rotate CCW by  $35^\circ$ .

(c) Rotate CW by 30°.

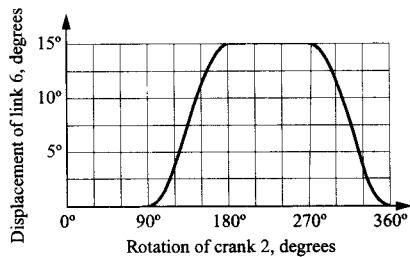
(d) Rotate CCW by 35°.

(Hint: Select a figure-eight- or kidney-bean-shaped coupler curve.)

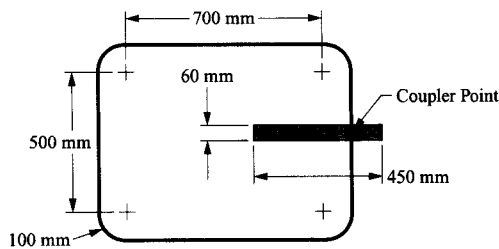
**6.44** Design a six-bar linkage like that shown in Fig. 6.61 such that the displacement of the output link (link 6) is the given function of the input link rotation. The output displacement reaches maximum values of 30° and 60° at input rotations of 60° and 240°, respectively. The rotation of the output link is zero when the input rotation angle is 0°, 120°, and 360°.



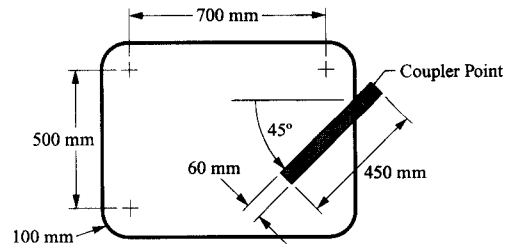
**6.45** Design a six-bar linkage like that shown in Fig. 6.61 such that the displacement of the output link (link 6) is the given function of the input link rotation. The output link dwells for 90° of input rotation starting at 0° and 180°. The maximum rotation angle for link 6 is 15°.



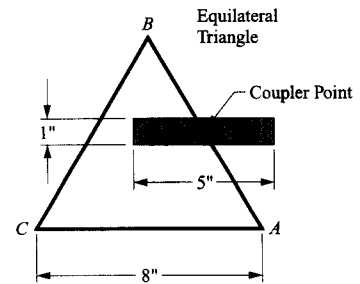
**6.46** Design an eight-bar linkage like that shown in Fig. 6.70 such that the coupler remains horizontal while the specified point on the coupler moves approximately along the path given.



**6.47** Re-solve Problem 6.46 if the coupler is inclined at an angle of 45°.

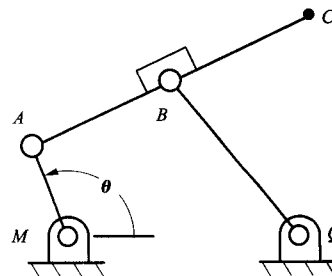


**6.48** Design an eight-bar linkage like that shown in Fig. 6.70 such that the coupler remains horizontal while the given point on the coupler moves approximately along the path from A to B to C. The coupler can return either by retracing the path from C to B to A or by going directly from C to A. This means that the basic four-bar linkage need not be a crank-rocker.

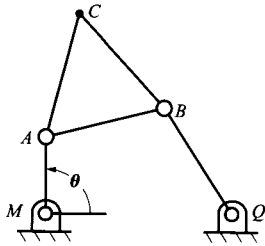


**COGNATE LINKAGE EXERCISE PROBLEMS**

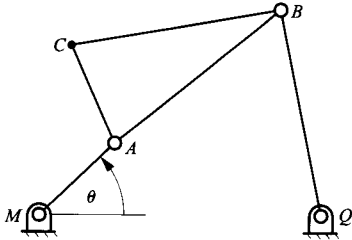
**6.49** Determine the two four-bar linkages cognate to the one shown. The dimensions are  $MA = 10$  cm,  $AB = 16$  cm,  $AC = 32$  cm,  $QB = 21$  cm, and  $MQ = 24$  cm. Draw the cognates in the position for  $\theta = 90^\circ$ .



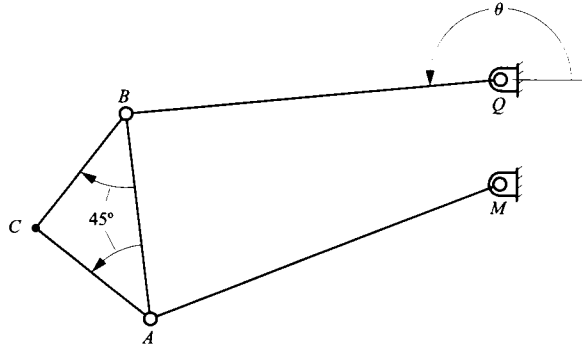
6.50 Determine the two four-bar linkages cognate to the one shown. The dimensions are  $MQ = 1.5$  in,  $AB = BC = BQ = AC = 1$  in, and  $AM = 0.5$  in. Draw the cognates in the position for  $\theta = 90^\circ$ .



6.51 Determine the two four-bar linkages cognate to the one shown. The dimensions are  $MQ = 2$  in,  $AB = BC = BQ = 1$  in, and  $AM = 1.5$  in.  $AC = 0.75$  in. Draw the cognates in the position for  $\theta = 45^\circ$ .



6.52 Determine the two four-bar linkages cognate for the drag-link mechanism shown. The dimensions are  $MQ = 1$  m,  $AM = BQ = 4$  m, and  $AB = 2$  m, and angles  $CAB$  and  $CBA$  both equal  $45^\circ$ . Notice that the cognates will also be drag-link mechanisms. Draw the cognates in the position in which  $\theta = 180^\circ$ .



---

**7.1 SPECIAL PLANAR MECHANISMS**

---

**7.1.1 Introduction**

Some mechanisms are unusual enough to require special attention. The classes of mechanisms discussed here meet a variety of common needs in mechanical engineering practice. For this reason they are important, but none requires such extensive treatment as to justify a chapter to themselves, as is the case with cam and gear mechanisms.

Generation of a straight line by a simple linkage mechanism is a recurring theme. Slides or roller ways are not always acceptable for implementation in real mechanism designs, and there continues to be a place for simple, four-bar linkages that can approximate a straight-line coupler point path with a high degree of accuracy. Likewise, linkages that can reproduce a path traced by one point at another tracing point with a change in scale find many uses ranging from machine tools for milling nonrotationally symmetric surfaces to remote actuation of robotic mechanisms.

Another recurring theme in mechanical engineering practice is the transfer of torque and motion between shafts that are not coaxial, particularly when the relative alignment of the shafts must change. Very common examples occur in the drive shafts of automobiles that must accommodate movements resulting in changes of shaft alignment caused by suspension movements and/or steering movements. There are also numerous examples of this situation in construction and manufacturing machinery.

Automotive steering and suspension mechanisms are among the most common linkage mechanisms in practical use. They are usually designed as decoupled, fundamentally planar linkages. However, misalignments are deliberately introduced to produce desirable effects such as a tendency for the steering to center itself. Thus, they become spatial linkages with complex interactions.

Yet another recurring need in practical linkage design is for indexing: intermittent, timed advancement of a drive in a constant direction. This technology had very numerous and visible applications in the days of mechanical punched-card readers and similar business machines. The problem is of continuing practical importance with many applications in manufacturing and packaging machinery.

**7.1.2 Approximate Straight-Line Mechanisms**

Approximate straight-line mechanisms occupy a very special place in the history of kinematics. These have been used in many practical devices from steam engines to stripchart recorders. The geometry of several linkages exhibiting approximate straight-line motions is discussed in the following.

**Watt's Straight-Line Mechanism** Toward the end of the 18th century, when James Watt and his contemporaries were developing the practical steam engines that powered the industrial revolution, there were no available means of machining long ways to a high degree of straightness or of achieving low-friction linear motion. This was needed both to guide the crosshead of the piston rod and for the valve gear that opened the valves in coordination with the piston motion. The solution used by Watt and his contemporaries was to devise a four-bar mechanism with an acceptably long coupler-point trajectory that approximated a straight line to an acceptable degree of accuracy.

Watt's straight-line mechanism continues to be of considerable practical importance.<sup>1</sup> The linkage is simple, and the configuration is very flexible, allowing great freedom to the designer. For example, the ratio of the lengths  $a$  and  $b$  shown in Fig. 7.1 is not very critical. The linkage will produce reasonably straight motion over a wide range of dimensional ratios  $b/a$ . It is not even essential that the two cranks have the same length. The essential feature is that the dimensions be such that the linkage is capable of assuming a position like that shown in Fig. 7.1 with the two cranks being parallel and opposed, with the coupler normal to both. If the cranks are of equal length the tracing point is the midpoint of the coupler, and the line of the coupler in the position shown is the straight line that is approximated.

Because of its simplicity and ability to provide low friction, approximately linear guidance, Watt's straight-line mechanism is useful anywhere exact conformance to linear motion is not essential. For example, it has been used in rear automotive suspensions of the live axle type to restrain lateral motion of the axle by constraining the center point of the axle to move along an approximate vertical straight line relative to the body.

The tracing point for the coupler curve shown in Fig. 7.1 is the midpoint of the coupler. The proportions of  $a$  and  $b$  are variable. In the case drawn,  $a = 3$  and  $b = 5$ . The form of the coupler curve is known as a lemniscate. As can be seen, the central limbs of the lemniscate are good approximations to straight lines over a considerable length.

**Chebyshev's Straight-Line Mechanism** The Chebyshev approximate straight-line mechanism is also a linkage that is both of historical importance and of continuing practical importance.<sup>1</sup> Like the Watt mechanism, it is simple. Its advantages are that it provides a very long segment of the path of the coupler midpoint that is approximately linear and that both fixed pivots are on the same side of the linear path, as compared with the Watt mechanism, in which they are on opposite sides. However, the dimensions are more critical in this case. Referring to Fig. 7.2, we see that the required proportions are  $a = 1$ ,  $b = 2.5$ , and  $c = 2$ . As already noted, the tracing point is the midpoint of the coupler. As can be seen, it approximates a straight line for a considerable distance. It might be noted that these proportions require that the linkage be a type 1 double-rocker. Since it is normally used for linear guidance of the tracing point, it is used in a coupler-driven mode.

**Roberts's Straight-Line Mechanism** Robert's approximate straight-line mechanism is also a symmetrical four-bar linkage, as shown in Fig. 7.3.<sup>1</sup> The coupler point indi-

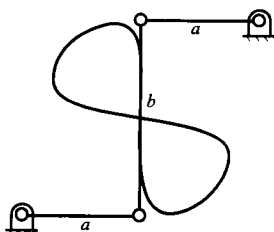


FIGURE 7.1 Watt's straight-line mechanism.

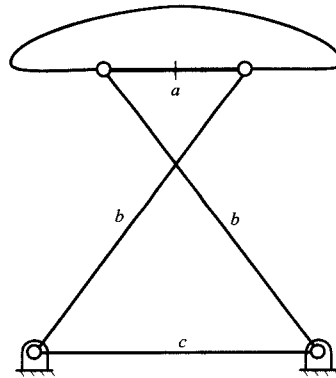


FIGURE 7.2 Chebyshev's approximate straight-line mechanism.

cated generates an approximate straight line for the motion between the fixed pivots. Referring to Fig. 7.3, we see that the required proportions are  $a = 1$ ,  $b = 1.2$ ,  $c = 2$ , and  $d = 1.09$ . These dimensions make the mechanism a type 2 double-rocker. It is normally used for linear guidance of the tracing point so that it is normally used in the coupler-driven mode.

**Other Approximate Straight-Line Mechanisms** There are many other four-bar linkage configurations that yield reasonable approximations to linear motion of a tracing point. Those used in level-luffing cranes and similar devices need to have the tracing point outside the interval between the coupler pivots. A good example is the level-luffing crane (Fig. 7.4) used on many docks to load and unload cargo. Here it is desirable that the path of the crane hook that carries the load be a horizontal straight line. This means that the load moves approximately in a horizontal plane when only turret and jib movements are used. Vertical motion is accomplished by the crane's winch hauling or lowering the cable. Horizontal motion of the load has two very significant advantages. First, little energy is used for turret or jib motions if the cranks are counterweighted to eliminate work done against gravity in moving the mechanism itself. The drives for those motions do not need to have large capacity. Second, it is relatively easy for the crane operator to visualize a horizontal trajectory of the load and determine whether that trajectory will interfere with fixed obstacles such as the side of the ship.

The jib of a typical level-luffing crane is arranged as a four-bar mechanism with a coupler point that approximately describes a horizontal straight line. The pulley at the end of the jib is placed at this point to produce the desired level-luffing action.

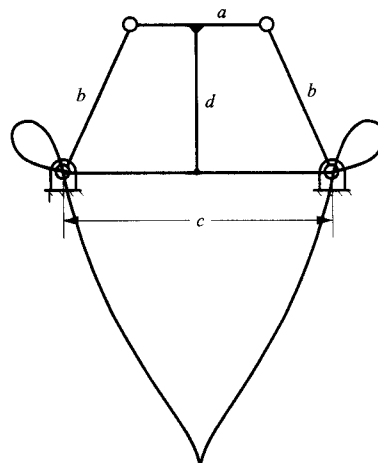
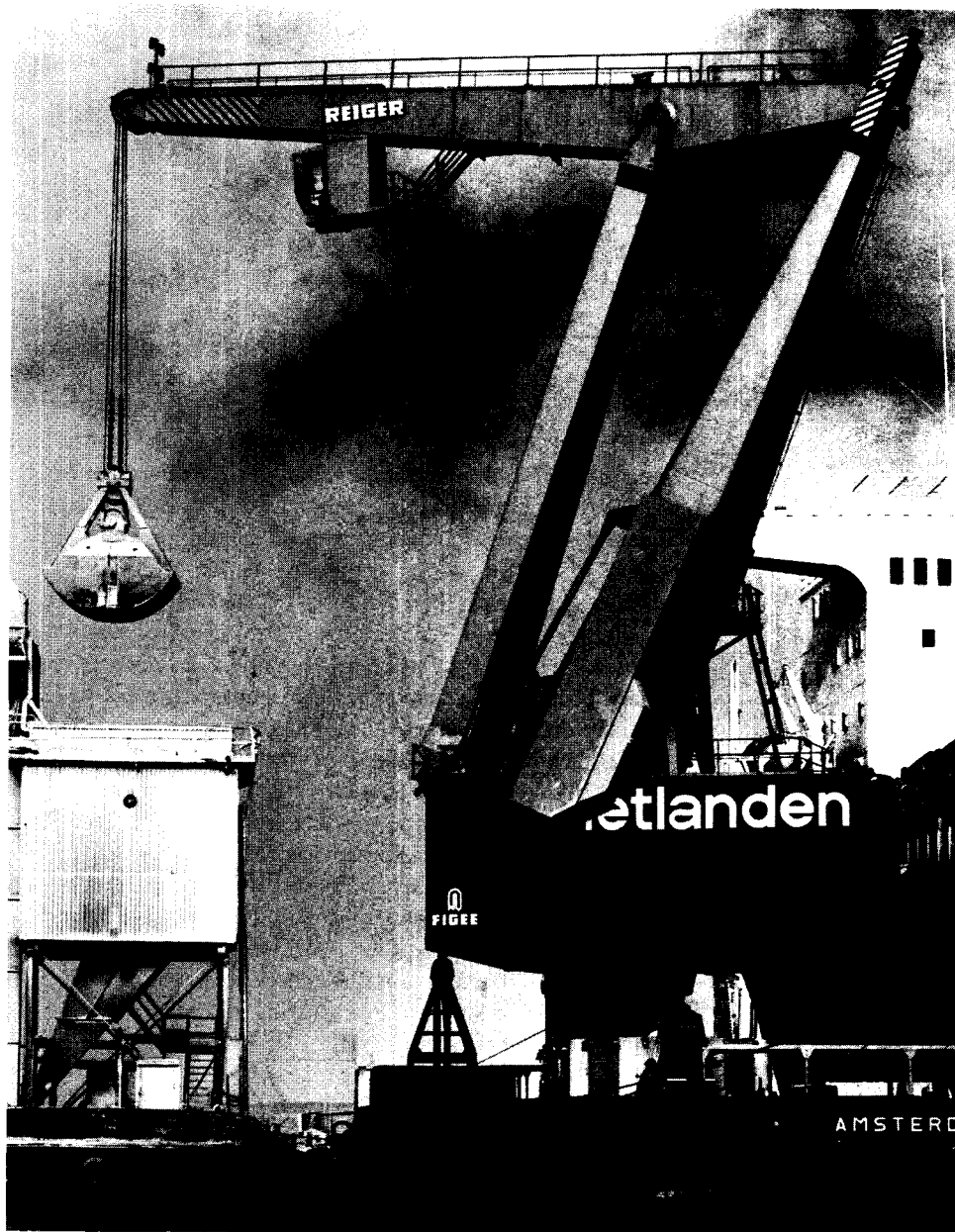


FIGURE 7.3 Roberts's approximate straight-line mechanism.



**FIGURE 7.4** A level-luffing crane. The jib of the crane is configured as a four-bar mechanism that generates an approximate horizontal straight line at the axis of the sheave over which the cable passes at the end of the jib. This means that the load moves approximately in a horizontal plane when only turret and jib movements are used.

### 7.1.3 Exact Straight-Line Mechanisms

It is also possible, in principle, to generate a perfectly straight line with a linkage mechanism, but generally only at the cost of a relatively complex mechanism if large motions are desired. The first such mechanism to be invented was that of Peaucellier.<sup>2</sup> Hart<sup>2</sup> devised a simpler mechanism that also generates an exact straight line, and several mechanisms based



on the slider-crank mechanism will generate a straight line for limited motion.<sup>3</sup> There are several other known exact straight-line generating linkages with revolute joints, but all are much more complex than the four-bar approximate straight-line generators discussed here.

A Peaucellier linkage is shown in Fig. 7.5. The linkage has a rhombic loop,  $ABCD$ , that forms a kite shape with the equal-length links  $PB$  and  $PD$ . The link  $OA$  is also equal in length to the base  $OP$ . Point  $C$  generates a true straight line normal to the base  $OP$ .

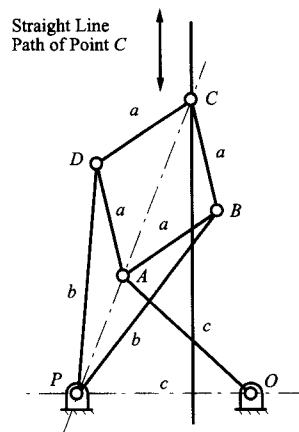
As may be seen, this is a much more complex linkage than the four-bar loops used previously to generate approximate straight lines. It has eight members and six joints, four of which are ternary joints.

If a slider is introduced, it is possible to generate an exact straight line using the slider-crank mechanism in Fig. 7.6. The range of motion is limited and a slider is required, but the basic mechanism is quite simple. Based on the geometry of the linkage, the output motion will be a simple sine function of the drive link (simple harmonic motion). As indicated in Fig. 7.6, the mechanism is made up of isosceles triangles.

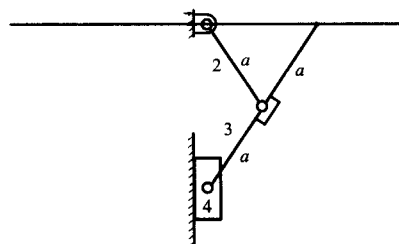
### 7.1.4 Pantographs

A plagiograph is a mechanism that exactly reproduces the path of a tracing point at a second tracer point, usually with a change of scale. The most common class of plagiographs is the family of pantograph mechanisms.

Pantographs have found many applications beyond that of plagiographs. These range from carrying contacts to overhead cables on electric trains and streetcars to legs of walking machines. As will be seen, pantographs are also of theoretical importance in that they lead to the theory of *cognate* linkages (Section 6.6.3). Cognate mechanisms, in turn, are of great usefulness in practical machine design.



**FIGURE 7.5** Peaucellier's exact straight-line mechanism. This was the first and most famous exact straight-line mechanism to be discovered. A number of others have since been discovered, including some that are a little simpler.  $ABCD$  is a rhombus, and links  $PB$  and  $PD$  have equal length. Link  $OA$  has the same length as the base  $OP$ . The path of point  $C$  is a true straight line normal to  $OP$ .



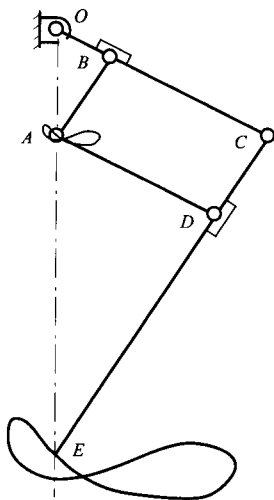
**FIGURE 7.6** Straight-line mechanism based on isosceles slider-crank mechanism. The entire range of the straight line can be reached if the mechanism is driven by the coupler.

**The Planar Collinear Pantograph** The special properties of the pantograph linkage have been used in a variety of applications. They also have important theoretical implications leading to the theory of cognate linkages, which will be discussed briefly later in this chapter.

A simple form of planar pantograph linkage is shown in Fig. 7.7. In Fig. 7.7, link  $AB$  has the length  $CD$ . Likewise, link  $AD$  has the length  $BC$ . Consequently,  $ABCD$  is a parallelogram, regardless of the position of the linkage. Further, the lengths  $OB$  and  $OC$  are in the ratio 1:4, as are the lengths  $CD$  and  $CE$ . It follows that triangle  $OBA$  is similar to triangle  $OCE$ , because  $OB/OC$  is equal to  $BA/CE$  and angle  $OBA$  is equal to angle  $OCE$ . Consequently, the ratio of the lengths  $OA$  and  $OE$  is always 1:4. If point  $A$  traces any path in the plane of the linkage, point  $E$  will trace a geometrically similar path that is magnified by a factor of 4 compared with the path of point  $A$ . This is best understood by considering the path of point  $A$  to be a curve described in polar coordinates with origin at  $O$ . The position of the corresponding point on the path of point  $E$  is also described in polar coordinates centered on  $O$ . The angular coordinate of that point is the same as that of the corresponding point on the path of point  $A$ . Its radial coordinate is four times that of the corresponding point on the path of point  $A$ . Hence the curve is the same. It is simply scaled up by a factor of 4.

Because of the tracing property, pantograph mechanisms have been used a great deal to copy and rescale text and other geometric figures. The magnification factor can be set to any desired value by varying the proportions of the links. In the form of the linkage that is shown in Fig. 7.7, it is always equal to the ratio of length  $OC$  to  $OB$ , which must also be equal to the ratio of  $CE$  to  $CD$ .

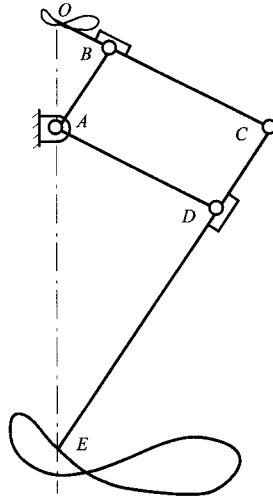
An example of the use of the pantograph mechanism to copy plane curves is a copy mill used to produce plate cams. The reader will find an in-depth discussion of cam geometry in Chapter 8. Most plate cams are bounded by mathematically complicated curves. To produce cams using a copy mill, a master cam is produced at an enlarged scale by hand. The profile of the master is traced by a roller with its central axis located at point  $E$  of Fig. 7.7. The axis of the milling cutter is at point  $A$ . The ratio of the roller diameter to the cutter diameter is the pantograph ratio. Consequently, the mill produces a cam that is geometrically similar to the master but is reduced in size by the pantograph ratio. The use of point  $E$ , rather than point  $A$ , to trace the master provides improved accuracy, because errors in the master profile are reduced by the pantograph ratio. The large size of the master also facilitates its accurate manufacture.



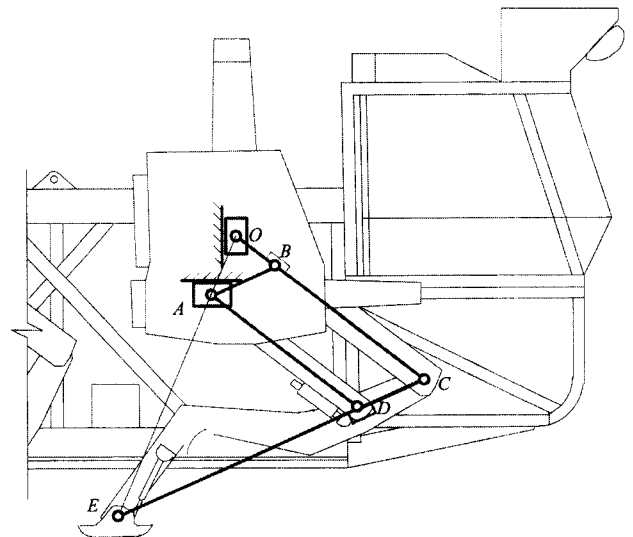
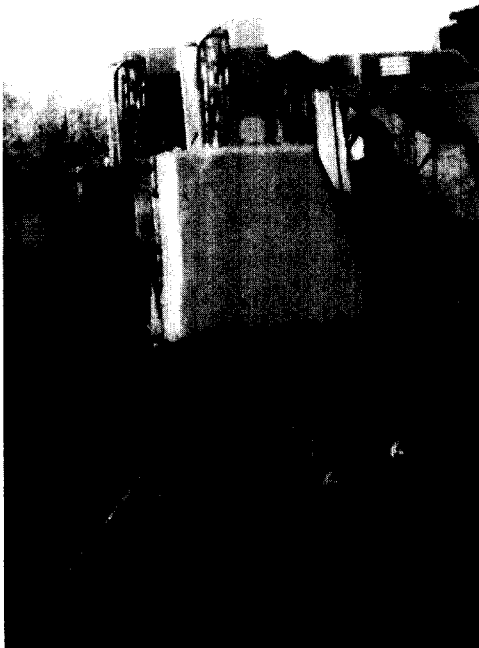
**FIGURE 7.7** A simple form of a planar pantograph linkage. Any path traced by point  $A$  is reproduced by point  $E$  at a magnification of 4:1.  $ABCD$  is a parallelogram. The ratios of lengths  $CD$  to  $CE$  and  $OB$  to  $OC$  are both 1:4. Link  $OC$  is connected to the base by a fixed revolute joint at  $O$ .

The application just described is an example of inversion of the linkage by interchanging the tracing points  $A$  and  $E$ . The pantograph can also be inverted by hinging it to the base with a fixed revolute coincident with  $A$ , rather than at point  $O$ . This is shown in Fig. 7.8. The path of point  $O$  is now copied by a geometrically similar path of point  $E$ . However, the magnification ratio is now 3:1 rather than 4:1. This is because, with these dimensions, the ratio of length  $AE$  to  $AO$  is 3:1.

There are other variations on the same theme. Figure 7.9 shows the pantograph linkage used in the legs of the Adaptive Suspension Vehicle that was shown in Fig. 1.1. Here there is no fixed pivot. Rather, point  $O$  is on a vertical slide and point  $A$  is on a horizontal



**FIGURE 7.8** The pantograph of Fig. 7.7 inverted by mounting with a fixed revolute at point  $A$ . The paths of points  $O$  and  $E$  are geometrically similar. The magnification factor is now 3:1.



**FIGURE 7.9** The leg mechanism of the Adaptive Suspension Vehicle. Point  $O$  moves on a slide that is vertical relative to the leg mounting structure to produce a corresponding vertical motion of the ankle point  $E$ . Point  $A$  moves on a slide that is horizontal relative to the vehicle body to drive point  $E$  along a horizontal path.

slide. Motion of point  $A$  alone, produced by a hydraulic cylinder, causes a horizontal rectilinear motion of the ankle point,  $E$ . Motion of point  $O$  alone, also produced by a hydraulic cylinder, causes a vertical rectilinear motion of point  $E$ . Simultaneous motion of points  $A$  and  $O$  results in motion of point  $E$  along a plane curve. This is what happens when the foot is picked up and the leg is swung back to its forward position. The magnification factor in this mechanism is 5:1 for the drive motion (point  $A$ ) and 4:1 for the lift motion (point  $B$ ).

**Skew Pantographs** A more general form of pantograph is the skew pantograph shown in Fig. 7.10.  $OLMN$  is a parallelogram, and triangle  $NMQ$  is similar to triangle  $LPM$ . As shown in the following, triangle  $OPQ$  is always similar to triangle  $LPM$ . Consequently, the path traced by point  $Q$  is similar to that traced by point  $P$ , is rotated through angle  $\alpha$  from the path of  $P$  about  $O$ , and is magnified by the ratio  $LM/LP$ .

These properties are proved as follows. Note that since  $OLMN$  is a parallelogram,  $\angle MLO = \angle ONM = \phi$ . Likewise,  $\angle LON = \angle NML = \pi - \phi$ .

Triangles  $PLO$  and  $ONQ$  are similar for the following reasons:

$$\angle PLO = \angle ONQ = \phi + \alpha.$$

Also

$$\frac{NQ}{NM} = \frac{ML}{PL}$$

because triangles  $NMQ$  and  $LPM$  are similar and these are corresponding pairs of sides. Now  $NM = OL$ , and  $ML = NO$  because  $OLMN$  is a parallelogram. Making these substitutions, we get

$$\frac{NQ}{OL} = \frac{NO}{PL} \text{ or } \frac{NQ}{NO} = \frac{OL}{PL}$$

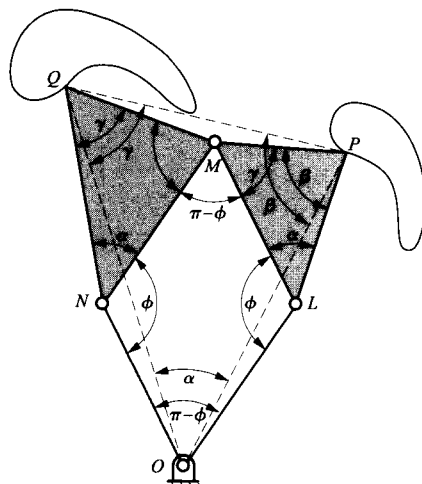
which establishes that triangles  $PLO$  and  $ONQ$  are similar since  $NQ$  and  $NO$ , and  $OL$  and  $PL$ , are corresponding side pairs and the equal angles  $\angle PLO$  and  $\angle ONQ$  are the included angles.

Also, triangle  $QMP$  is similar to  $PLO$  and  $ONQ$  for the following reasons:

$$\angle QMP = 2\pi - \beta - \gamma - (\pi - \phi) = \pi + \phi - \beta - \gamma$$

Also, because  $\alpha$ ,  $\beta$ , and  $\gamma$  are the vertex angles of triangle  $LPM$ ,

$$\alpha + \beta + \gamma = \pi$$



**FIGURE 7.10** A skew pantograph.  $OLMN$  is a parallelogram and triangles  $LPM$  and  $NMQ$  are similar. The triangle  $OPQ$  is always similar to triangles  $LPM$  and  $NMQ$ . Consequently, the path traced by point  $Q$  is similar to that traced by point  $P$ . The path traced by  $Q$  is rotated relative to that traced by  $P$  through angle  $\alpha$  and it is magnified by the ratio  $OQ/OP = LM/LP$ .

so

$$\angle QMP = \pi + \phi - (\pi - \alpha) = \phi + \alpha = \angle ONQ$$

Because triangles  $NMQ$  and  $LPM$  are similar

$$\frac{MQ}{NQ} = \frac{PM}{LM}$$

or

$$\frac{PM}{MQ} = \frac{LM}{NQ} = \frac{ON}{NQ}$$

noting that  $LM = ON$ .

Therefore triangles  $QMP$  and  $ONQ$  are similar because the corresponding sides  $PM$  and  $MQ$ , and  $ON$  and  $NQ$ , are in the same ratio and the included angles  $QMP$  and  $ONQ$  are equal. Triangles  $QMP$  and  $PLO$  are similar because both are similar to  $ONQ$ .

It follows that

$$\angle NQO = \angle MQP$$

and so

$$\angle OQP = \angle NQM = \gamma$$

Likewise

$$\angle QPM = \angle OPL$$

and so

$$\angle QPO = \angle MPL = \beta$$

Consequently,

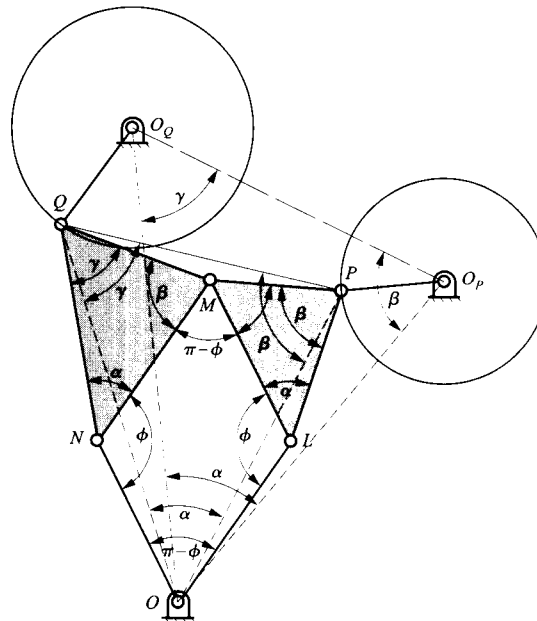
$$\angle POQ = \alpha$$

and triangle  $OPQ$  is similar to triangles  $LPM$  and  $NMQ$ .

The geometric similarity of the paths of points  $P$  and  $Q$  can be inferred from an argument similar to that employed in the case of the collinear pantograph. If the path of point  $P$  is considered to be a curve described in polar coordinates centered on  $O$ , the radial coordinate is  $OP$ . The path of  $Q$  is also described in polar coordinates centered on  $O$ . The radial coordinate is  $LM/LP$  times that of point  $P$ , and the angle reference is rotated through angle  $\alpha$  from that used for the path of point  $P$ .

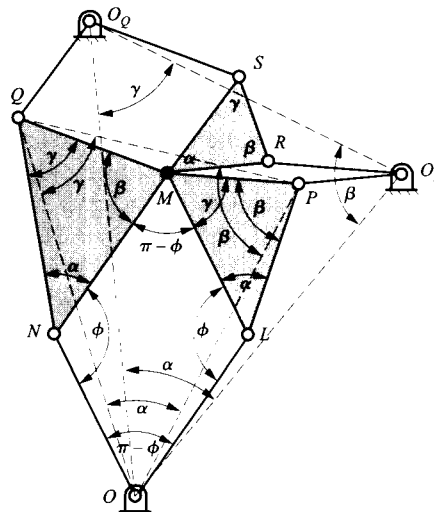
**Roberts's Theorem** If the path of point  $P$  of the skew pantograph of the preceding section is a circle, then that of point  $Q$  will also be a circle, as shown in Fig. 7.11. Thus, if  $P$  is constrained to move on a circle by a crank rotating about fixed pivot,  $O_p$ , then a crank can also be connected to point  $Q$  from a fixed pivot at the center of its path,  $O_q$ . Because the path of  $Q$  is similar to that of  $P$  and triangle  $OPQ$  is always similar to triangle  $LPM$ , it follows that triangle  $OO_pO_q$  is also similar to triangle  $LPM$ . This creates two planar four-bar linkages,  $OLPO_p$  and  $O_qQNO$ , for each of which  $M$  is a coupler point. Thus the path generated by point  $M$  as a coupler point of  $OLPO_p$  is identical to the path traced by  $M$  as a coupler point of  $O_qQNO$ . Thus we have generated two completely different four-bar mechanisms that generate identical coupler curves. Linkages that have this property are called *cognates*.<sup>4</sup> These are the same cognates that were briefly discussed in section 6.6.3.

We can go further. If points  $R$  and  $S$  are located by constructing the parallelograms  $O_pPMR$  and  $O_qQMS$ , it can be shown that triangle  $MRS$  is similar to triangle  $LPM$  and hence that the four-bar linkage  $O_pRSO_q$  is also cognate to  $OLPO_p$  and  $O_qQNO$ , again with  $M$  as the tracing point. The assemblage shown in Fig. 7.12 is known as Roberts's mechanism.



**FIGURE 7.11** A pair of cognate linkages. The path of point  $P$  in the skew pantograph of Fig. 7.10 is a circle centered on  $O_P$ . Therefore the path of point  $Q$  is also a circle, with center  $O_Q$ , where triangle  $OO_P O_Q$  is similar to triangle  $LPM$ . Therefore cranks  $O_P P$  and  $O_Q Q$  can be added, and the assemblage will be mobile.  $M$  is the common coupler point.

Roberts's theorem states that if a planar four-bar mechanism is constructed, a coupler point is selected, and the corresponding coupler curve is traced, then there are two other four-bar linkages that will generate the identical coupler curve. That is, there are two four-bar linkages that are cognate to the original four-bar. They may be obtained by constructing the Roberts's mechanism based on the original four-bar. In the case of Fig. 7.12, if we view  $OLPO_P$  as the original four-bar linkage, with  $M$  being the selected coupler point, then the



**FIGURE 7.12** A general Roberts mechanism. The three four-bar linkages  $OLPO_P$ ,  $O_P RSO_Q$ , and  $O_Q QNO$  are all cognates with  $M$  as the coupler point for each.

cognates are  $O_QQNO$  and  $O_PRSO_Q$  with  $M$  being the coupler point in both cases. Starting with points  $O, L, P, O_P,$  and  $M$ , we can construct the remainder of the figure by first completing the parallelograms  $OLMN$  and  $O_P RMP$  to locate points  $N$  and  $R$ . Triangles  $OO_P O_Q,$   $NMQ,$  and  $MRS$  may then be constructed similar to triangle  $LPM$  to complete the figure.

If the original four-bar linkage is of Grashof type 1, then the cognates will also be type 1. Likewise, if the original four-bar is type 2, then the cognates are also type 2. Further, if the original four-bar is type 1 and is a crank-rocker linkage, then one of the cognates will also be a crank-rocker linkage. The other will be a type 1 double-rocker. The cognates of a drag-link linkage are both also drag links. The cognates of a type 1 double-rocker are both crank-rockers.

As indicated in Chapter 6, cognate linkages can be very useful when a linkage has been found that generates a desired path but that solution linkage has undesirable properties such as interference with other components. Often one of the cognates will produce the desired path without the problems of the original linkage.

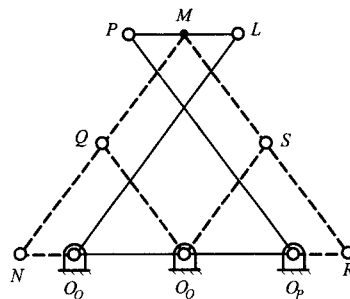
**EXAMPLE 7.1**  
**Using Roberts's**  
**Theorem to**  
**Generate**  
**Cognates of**  
**Chebyshev**  
**Mechanism**

**Solution**

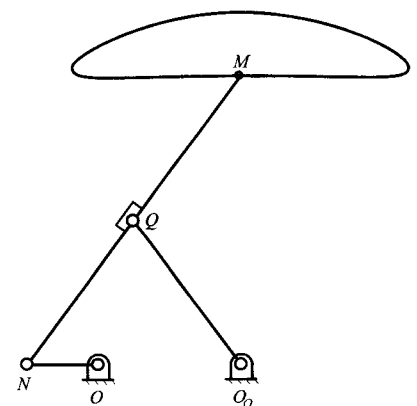
The Chebyshev linkage of Fig. 7.2 is a type 1 double-rocker. As was discussed in Section 1.18, it is difficult to transfer motion from the tracing point of this linkage owing to interference with the cranks since the coupler tumbles between the cranks. As just discussed, the cognates of a type 1 double-rocker are both crank-rockers and should be free of this problem. Construct the cognates and, hence, produce a crank-rocker linkage with the same approximate straight-line coupler curve segment as the Chebyshev linkage.

Examination of Fig. 7.2 indicates that the coupler point is the midpoint of the line between the coupler pivots. That is, the triangle  $LPM$  of Fig. 7.12 has collapsed into a line. Therefore triangle  $OO_P O_Q$  will also be collapsed to a line. Since  $O$  corresponds to  $L, O_P$  corresponds to  $P,$  and  $O_Q$  corresponds to  $M$  in these triangles (corresponding vertices have the same vertical angles), it follows that  $O_Q$  will be midway between  $O$  and  $O_P,$  as shown in Fig. 7.13. Similarly, triangles  $RMS$  and  $MNQ$  will collapse to line segments.

Parallelograms  $OLMN$  and  $O_P RMP$  are constructed as shown in Fig. 7.13 to locate points  $N$  and  $R$ . The line  $MQN$  is drawn. Note that in Fig. 7.12,  $N$  corresponds to  $L, M$  corresponds to  $P,$  and  $Q$  corresponds to  $M$  in the two similar triangles  $LPM$  and  $NMQ$ . Therefore  $Q$  will be at the midpoint of  $NM$  in



**FIGURE 7.13** Construction of the cognates of the Chebyshev linkage shown in Fig. 7.2.  $OLPO_P$  is the original Chebyshev four-bar mechanism, and  $M$  is the coupler point. The cognates are  $ONQO_Q$  and  $O_P RSO_Q$ . Their symmetry with one another is a result of the bilateral symmetry of the original linkage.



**FIGURE 7.14** The cognate  $ONQO_Q$  from Fig. 7.12 with its coupler curve plotted.

Fig. 7.13. Similarly, the line  $RSM$  is drawn to represent the coupler of the second cognate. The cranks  $O_QQ$  and  $O_QS$  are drawn to complete the two cognates shown by the dashed lines in Fig. 7.13.

The cognate  $ONQO_Q$  is drawn on its own in Fig. 7.14 with the path of point  $M$  plotted. Not only is it much easier to transfer motion from this linkage than from the original Chebyshev linkage, but the linkage can be driven by continuous rotation of the crank  $ON$ , if desired.

## 7.2 SPHERICAL LINKAGES

Although spatial linkages, in general, will be discussed in Chapter 9, there are other classes of mechanisms that are not general spatial linkages in the sense of satisfying the spatial Kutzbach criterion [Eq. (1.3)] and are certainly not planar mechanisms. One of the most extensive and practically important such groups is the class of spherical mechanisms, which includes not only linkages but also spherical cam mechanisms and gears, namely bevel gears, and rolling contact bearings, namely tapered roller bearings.

Although it is beyond the scope of this book, spherical mechanism theory is an important component of spatial mechanism theory. This is because the rotational equations defined for spatial mechanisms in Chapter 9 are identical for spherical mechanisms. However, the translation equations, also discussed in Chapter 9, are absent in the case of spherical mechanisms. This allows inferences to be made on the basis of a spherical analog, and these can be applied to spatial mechanisms. There is also a way of generating valid translation equations directly from the rotational equations.

### 7.2.1 Introduction

Spherical linkages form a family much like planar linkages. However, whereas in a planar linkage all the revolute joint axes are parallel, in a spherical linkage they all intersect at a common point, called the concurrency point. Actually, planar linkages can be thought of as spherical linkages for which the concurrency point is at infinity.

There are many similarities in the properties of spherical and planar linkages. For example, spherical linkages obey the same form of the Kutzbach criterion that planar linkages do (Section 1.7):

$$M = 3(m - j - 1) + \sum_{i=1}^j f_i \quad (1.1)$$

Consequently, the simplest nontrivial spherical linkage is a four-bar linkage, just as in the planar case.

Also, there is a form of the Grashof inequality governing rotatability of joints that works for spherical linkages:

$$\alpha_\ell + \alpha_s < \alpha_p + \alpha_q$$

Here, instead of dealing with the lengths of the links, as in the case of a planar linkage, we work with the angles between successive joint axes.  $\alpha_s$  is the smallest angle between two successive joints,  $\alpha_\ell$  is the largest such angle, and  $\alpha_p$  and  $\alpha_q$  are the other two angles.

As in the planar case, the inequality governs the presence of joints in a four-bar linkage that can be completely rotated. If the inequality is satisfied, there are two completely rotatable joints. They are the joints whose axes bound the angle  $\alpha_s$ . Depending on which link is chosen as the base, the linkage will have characteristics similar to those of a crank-rocker planar four-bar, or a drag-link, or a type 1 double-rocker. If the inequality is not satisfied, there is no completely rotatable joint, and the linkage behaves like a type 2 planar linkage.



There is one variation from the planar analog. Whereas there is no limit on the length of a link in a planar linkage—beyond the fact that it must be less than the sum of the lengths of the other three links for it to be possible to assemble the loop—no side angle of a spherical linkage can be greater than  $90^\circ$ . This is because there are, in fact, always two angles between two lines that are supplements of one another. Either the angle or its supplement can be viewed as the angle between two axes in a spherical four-bar linkage. If the angle is greater than  $90^\circ$ , its supplement is less than  $90^\circ$ , so side angles in a spherical linkage can be said to have an upper limit of  $90^\circ$ .

The closure equations for a spherical four-bar linkage, such as that shown schematically in Fig. 7.15, may, in principle, be developed using a procedure analogous to that used to derive the closure equations for a planar four-bar linkage in Chapter 5. However, this becomes very complex because the entities being dealt with are angles rather than lengths. A more convenient procedure is to use the loop matrix transformations defined in Chapter 9. Using either method, the relationship between angle  $\phi_1$ , considered to be the input angle, and  $\phi_2$ , considered to be the output angle, of the linkage of Fig. 7.15 can be expressed as follows:

$$\begin{aligned} \sin \phi_1 \sin \phi_2 \sin \alpha_2 \sin \alpha_4 - \cos \phi_1 \cos \phi_2 \cos \alpha_1 \sin \alpha_2 \sin \alpha_4 + \cos \phi_1 \sin \alpha_1 \cos \alpha_2 \sin \alpha_4 \\ + \cos \phi_2 \sin \alpha_1 \sin \alpha_2 \cos \alpha_4 + \cos \alpha_1 \cos \alpha_2 \cos \alpha_4 - \cos \alpha_3 = 0 \end{aligned} \quad (7.1)$$

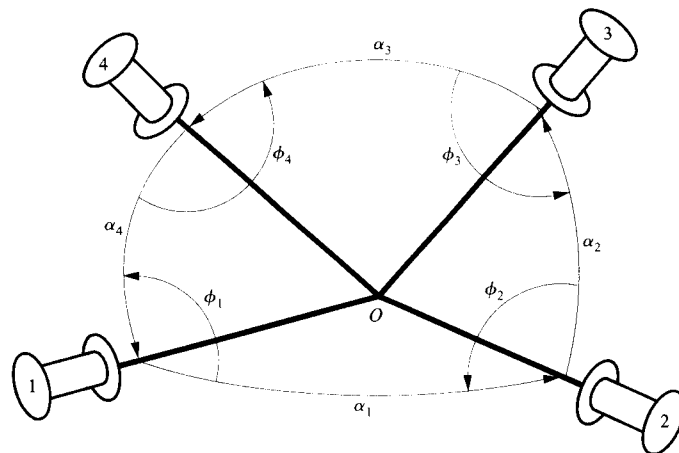
where  $\phi_1, \phi_2, \phi_3$ , and  $\phi_4$  are the joint angles and  $\alpha_1, \alpha_2, \alpha_3$ , and  $\alpha_4$  are the angles between the joint axes of the spherical four-bar loop as shown in Fig. 7.15.

If  $\phi_1$  is regarded as having a known value, this rather intimidating-looking equation has the form

$$P \cos \phi_2 + Q \sin \phi_2 + R = 0 \quad (7.2)$$

for which a solution was developed in Chapter 5. Here

$$\begin{aligned} P &= -\cos \phi_1 \cos \alpha_1 \sin \alpha_2 \sin \alpha_4 + \sin \alpha_1 \sin \alpha_2 \cos \alpha_4 \\ Q &= \sin \phi_1 \sin \alpha_2 \sin \alpha_4 \\ R &= \cos \phi_1 \sin \alpha_1 \cos \alpha_2 \sin \alpha_4 + \cos \alpha_1 \cos \alpha_2 \cos \alpha_4 - \cos \alpha_3 \end{aligned} \quad (7.3)$$



**FIGURE 7.15** A schematic representation of a spherical four-bar mechanism. The heavy lines represent the joint axes with concurrency point  $O$ .  $\alpha_1, \alpha_2, \alpha_3$ , and  $\alpha_4$  are the angles between the successive axes.  $\phi_1, \phi_2, \phi_3$ , and  $\phi_4$  are the joint angles.

Hence referring to Table 5.1, we can obtain values for  $\phi_2$ , given  $\phi_1$  from

$$t = \frac{-Q + \sigma \sqrt{P^2 + Q^2 - R^2}}{R - P} \quad (7.4)$$

where  $\sigma = \pm 1$  is a sign variable, and

$$\phi_2 = 2 \tan^{-1}(t). \quad (7.5)$$

We can also develop relationships between the angular velocities and accelerations about joints 1 and 2 by differentiation of Eq. (7.1). Differentiation of Eq. (7.1) with respect to time gives, after rearrangement,

$$\dot{\phi}_2 = -\dot{\phi}_1 \frac{\sin \alpha_4 (\cos \phi_1 \sin \phi_2 \sin \alpha_2 + \sin \phi_1 \cos \phi_2 \cos \alpha_1 \sin \alpha_2 - \sin \phi_1 \cos \alpha_1 \cos \alpha_2)}{\sin \alpha_2 (\sin \phi_1 \cos \phi_2 \sin \alpha_4 + \cos \phi_1 \sin \phi_2 \cos \alpha_1 \sin \alpha_4 - \sin \phi_2 \sin \alpha_1 \sin \alpha_4)} \quad (7.6)$$

Further differentiation gives

$$\ddot{\phi}_2 = \frac{\ddot{\phi}_1 \dot{\phi}_2}{\dot{\phi}_1} + \frac{B}{A} \dot{\phi}_1 \dot{\phi}_2 + \frac{C}{A} \dot{\phi}_1^2 + \frac{D}{A} \dot{\phi}_2^2 \quad (7.7)$$

where

$$\begin{aligned} A &= \sin \alpha_2 (\sin \phi_1 \cos \phi_2 \sin \alpha_4 + \cos \phi_1 \sin \phi_2 \cos \alpha_1 \sin \alpha_4 - \sin \phi_2 \sin \alpha_1 \cos \alpha_4) \\ B &= 2 \sin \alpha_2 \sin \alpha_4 (\sin \phi_1 \sin \phi_2 \cos \alpha_1 - \cos \phi_1 \cos \phi_2) \\ C &= \sin \alpha_4 (\sin \phi_1 \sin \phi_2 \sin \alpha_2 - \cos \phi_1 \cos \phi_2 \cos \alpha_1 \sin \alpha_2 + \cos \phi_1 \sin \alpha_1 \cos \alpha_2) \\ D &= \sin \alpha_2 (\sin \phi_1 \sin \phi_2 \sin \alpha_4 - \cos \phi_1 \cos \phi_2 \cos \alpha_1 \sin \alpha_4 + \cos \phi_2 \sin \alpha_1 \cos \alpha_4) \end{aligned} \quad (7.8)$$

### EXAMPLE 7.2 Analysis of a Spherical Four- Bar Mechanism

A spherical four-bar linkage is constructed with the angle between the axes of joints 1 and 2 ( $\alpha_1$ ) being  $120^\circ$ , the angle between axes 2 and 3 ( $\alpha_2$ )  $90^\circ$ , that between axes 3 and 4 ( $\alpha_3$ )  $75^\circ$ , and that between axes 1 and 4 ( $\alpha_4$ )  $30^\circ$ . Member 1 is the base and the mechanism is a spherical crank-rocker linkage. Find the output angle,  $\phi_2$ , when the driving joint angle,  $\phi_1$ , is  $90^\circ$ .

If the input crank is driven at a constant angular velocity of  $10 \text{ rad/s}$ , find the angular velocity,  $\dot{\phi}_2$ , of the driven crank, and its angular acceleration,  $\ddot{\phi}_2$ , in the same position.

#### Solution

Substitution of the values

$$\alpha_1 = 120^\circ, \alpha_2 = 90^\circ, \alpha_3 = 75^\circ, \alpha_4 = 30^\circ, \phi_1 = 90^\circ$$

into Eq. (7.3) gives

$$P = 0.75, Q = 0.5, R = -0.2588$$

Substitution of these values into Eq. (7.4) gives

$$t = -0.3603, \text{ or } t = 1.3515$$

Application of Eq. (7.5) gives

$$\phi_2 = -39.63^\circ, \text{ or } \phi_2 = 107.00^\circ$$

The two solutions correspond to the two solutions obtained in the solution of the position problem of a planar four-bar and have the same source in the reflection of the driven-crank and coupler about the plane of the moving joint axis of the driving crank and the fixed joint axis of the driven crank.

Substitution of these values plus  $\dot{\phi}_1 = 10 \text{ rad/s}$  into Eq. (7.6) gives the values  $\dot{\phi}_2 = 2.2302 \text{ rad/s}$  and  $\dot{\phi}_2 = 0.8467 \text{ rad/s}$ , respectively corresponding to the two solutions for  $\phi_2$  given here. Further substitution into Eq. (7.8) gives the following sets of values:

for  $\phi_2 = -39.63^\circ$ ,  $A = 0.8634$ ,  $B = 0.3189$ ,  $C = -0.3189$ ,  $D = 0.2588$

for  $\phi_2 = 107.00^\circ$ ,  $A = -0.8634$ ,  $B = -0.4781$ ,  $C = 0.4781$ ,  $D = 0.2588$

When substituted into Eq. (7.7) with  $\ddot{\phi}_1 = 0$  and the preceding values for  $\dot{\phi}_1$  and  $\dot{\phi}_2$ , we get the following two values for the acceleration of the driven crank:  $\ddot{\phi} = -27.20 \text{ rad/s}^2$  and  $\ddot{\phi} = 50.90 \text{ rad/s}^2$ , respectively. Once again, these correspond to the two possible solutions of the position problem.

### 7.2.2 Gimbals

A set of gimbals is a spherical serial chain that allows an axis through the concurrency point to be placed in any possible direction. Gimbals are often used in the mounts of directional instruments such as theodolites or telescopes. They are also used in gyroscopes to allow the rotor axis freedom to assume any direction relative to the base of the instrument.

### 7.2.3 Universal Joints

The simplest means of transferring motion between noncoaxial shafts is by means of one or two universal joints. For this reason this very simple spherical mechanism appears in an enormous variety of applications. They may be found as components of the Stewart platform and 3-2-1 platform parallel mechanisms discussed in Chapter 9 and in many other situations. (Universal joints are also known as Cardan joints in Europe and Hooke joints in Britain.)

**Properties of the Universal Joint** A common need in machinery is to transfer rotation between two shafts that are not parallel to one another and that may be free to move relative to one another. A universal joint is a simple spherical four-bar mechanism that transfers rotary motion between two shafts whose axes pass through the concurrency point. The joint itself consists of two revolute joints whose axes are orthogonal to one another. They are often configured in a cross-shaped member as shown in Fig. 7.16. One of these joints is arranged with its axis at  $90^\circ$  to that of the driving shaft, and the other has its axis at  $90^\circ$  to that of the driven shaft. In practice, the ends of the shafts are often configured as clevises to mate with the cruciform shafts of the intermediate member. Together with the bearings in which the two shafts turn, the universal joint forms a spherical four-bar linkage with three sides being  $90^\circ$  angles. The fourth side is, in general, not  $90^\circ$ . This may be better seen in Fig. 7.17, in which only one side of each of the crossed intermediate shafts is shown.

In general, the angular motion is not uniformly transferred from the driving shaft to the driven shaft. The relationship between the angles of the driving shaft,  $\theta_1$ , and the driven shaft,  $\theta_2$ , is

$$\cos \gamma = \tan \theta_1 \tan \theta_2 \quad (7.9)$$

where  $\gamma$  is the angular misalignment of the shafts. This relationship can be quickly derived from Eq. (7.1). As is indicated in Fig. 7.17,  $\alpha_2 = \alpha_3 = \alpha_4 = 90^\circ$ . Also,  $\alpha_1 = \gamma$  and  $\phi_1 = \theta_1$ ,

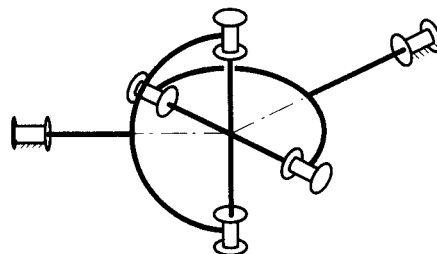
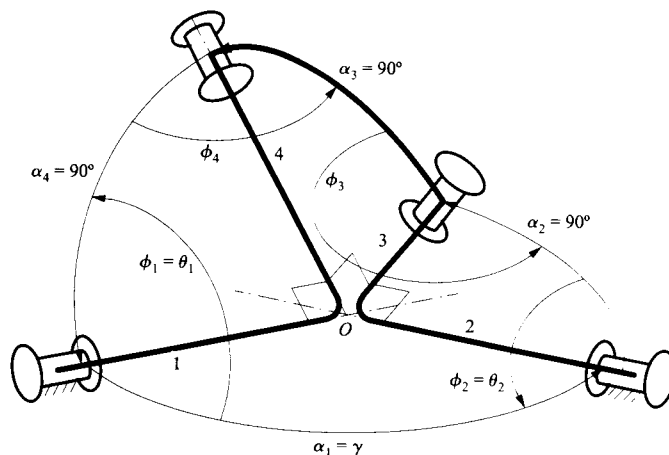


FIGURE 7.16 Universal, Cardan, or Hooke joint.



**FIGURE 7.17** Universal joint geometry:  $\gamma$  is the angular misalignment of the shafts;  $\theta_1$  is the angle of the input shaft;  $\theta_2$  is the angle of the output shaft.

$\phi_2 = \theta_2$  where  $\alpha_i$  and  $\phi_i$  ( $i = 1, 2, 3, 4$ ) are consistent with Eq. (7.1). Substituting these values into Eq. (7.1) reduces it to

$$\sin \theta_1 \sin \theta_2 - \cos \theta_1 \cos \theta_2 \cos \gamma = 0$$

which can be rearranged into Eq. (7.9).

If the driving shaft turns with a uniform angular velocity, the rotation of the driven shaft is not uniform but fluctuates. That is, a single universal joint is not a constant-velocity coupling like those that will be discussed in the next section. However, if the angle between the shaft axes is small, the fluctuation will also be small and is acceptable in many applications.

The angular velocity relationship can be obtained by differentiating Eq. (7.9) written in the form

$$\tan \theta_2 = \cos \gamma \cot \theta_1$$

Differentiation with respect to time gives

$$\dot{\theta}_2 \sec^2 \theta_2 = -\dot{\theta}_1 \csc^2 \theta_1 \cos \gamma$$

Hence the ratio of the magnitudes of the shaft velocities is

$$\frac{\omega_2}{\omega_1} = \frac{\dot{\theta}_2}{\dot{\theta}_1} = \frac{\cos^2 \theta_2 \cos \gamma}{\sin^2 \theta_1}$$

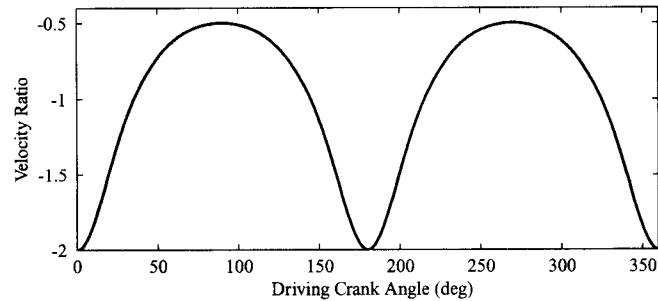
It is helpful to work in terms of the input angle,  $\theta_1$ , alone. First use  $\cos^2 \theta = 1/(1 + \tan^2 \theta)$  and then use the angle equation to eliminate  $\tan^2 \theta_2$ :

$$\frac{\omega_2}{\omega_1} = \frac{\cos \gamma}{\sin^2 \theta_1 (1 + \tan^2 \theta_2)} = \frac{\cos \gamma}{\sin^2 \theta_1 (1 + \cos^2 \gamma \cot^2 \theta_1)} = \frac{\cos \gamma}{\sin^2 \theta_1 + \cos^2 \gamma \cos^2 \theta_1}$$

This expression can be further simplified by replacing  $\sin^2 \theta_1$  by  $1 - \cos^2 \theta_1$  as follows:

$$\frac{\omega_2}{\omega_1} = \frac{\cos \gamma}{1 - \cos^2 \theta_1 + \cos^2 \gamma \cos^2 \theta_1} = \frac{\cos \gamma}{1 - \sin^2 \gamma \cos^2 \theta_1} \quad (7.10)$$

It may be seen that the velocity ratio is a function of  $\theta_1$  so that for constant input velocity the output velocity will fluctuate. The velocity ratio varies from  $1/\cos \gamma$  to  $\cos \gamma$  during the motion cycle. This relationship is plotted in Fig. 7.18.



**FIGURE 7.18** Velocity ratio fluctuation for a universal joint with  $\gamma = 120^\circ$ . The negative values of the velocity ratio are an artifact of the way these angles are defined in Fig. 7.17. Examination of that figure indicates that  $\theta_2$  decreases when  $\theta_1$  increases. Looking from the driving shaft toward the driven shaft, we see that both shafts are rotating in the same direction.

**EXAMPLE 7.3**  
**Analysis of a**  
**Universal Joint**  
**for a Front-**  
**Wheel-Driven Car**  
**Solution**

A simple automotive vehicle is driven via the front wheels. Universal joints are used in the shafts connecting the differential to the front wheels, as a low-cost alternative to the constant-velocity joints that are normally used to allow rotation of the front wheels about vertical axes for steering. At full steering lock, the inside front wheel is rotated  $30^\circ$  from the straight-ahead position. Calculate the percentage fluctuation in wheel velocity in this position.

If shaft 1 in Fig. 7.17 is viewed as the shaft from the engine and shaft 2 is viewed as the half-shaft driving the wheel, in the full lock position the angle between the axis of shaft 1 and the axis of shaft 2 will be  $30^\circ$ . That is,  $\gamma = 180^\circ - 30^\circ = 150^\circ$ . Applying Eq. (7.10) we get

$$\frac{\omega_4}{\omega_2} = \frac{-0.8660}{1 - 0.25 \cos^2 \theta_1}$$

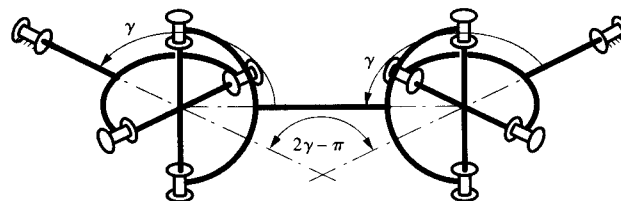
Thus, the maximum magnitude of the velocity ratio is  $0.8660/0.75 = 1.155$ , and the minimum magnitude is  $0.8660/1.25 = 0.693$ . Thus the maximum is 115% of the mean value of 1.0, and the minimum is 69% of the mean. The maximum percentage fluctuation is 31%.

**Dual Universal Joints** By using two universal joints in a symmetric combination, it is possible to have the second joint cancel out the fluctuation generated by the first. This combination then produces a constant-velocity action.<sup>5</sup> If the joints are aligned so that axis 3 of the first coupling is parallel to axis 2 of the second, as shown in Fig. 7.19, then  $\theta_1' = \theta_2$  where the prime (') is used to designate the angles of the second linkage. Hence, using Eq. (7.9), we have

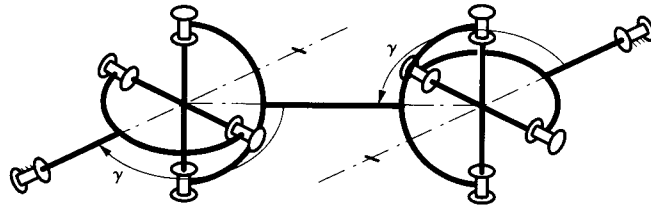
$$\begin{aligned} \cos \gamma &= \tan \theta_1 \tan \theta_2 \\ \cos \gamma &= \tan \theta_1' \tan \theta_2' \end{aligned} \quad (7.11)$$

and

$$\tan \theta_2' = \frac{\cos \gamma}{\tan \theta_1'} = \frac{\cos \gamma}{\tan \theta_2} = \frac{\cos \gamma \tan \theta_1}{\cos \gamma} = \tan \theta_1 \quad (7.12)$$



**FIGURE 7.19** Dual universal joints arranged symmetrically. The combination provides a true constant-velocity coupling, as described in the text.



**FIGURE 7.20** Dual universal joints on parallel, offset shafts. This arrangement also gives motion transfer between the input and output shafts at a constant velocity ratio.

Hence the output angle of the combined joint,  $\theta_2'$ , is always equal to the input angle  $\theta_1$ . The same relationship is true if the shafts are not angulated, as in Fig. 7.19, but are parallel and offset, as in Fig. 7.20. This is also a configuration of considerable practical importance. In fact, the drive shafts of almost all front-engine, rear-wheel-driven automobiles feature this arrangement.

**EXAMPLE 7.4**  
**Analysis of a**  
**Universal Joint of**  
**a Rear-Wheel-**  
**Driven Car**

A front-engine, rear-wheel-driven automobile employs a drive shaft with two universal joints in the alignment of Fig. 7.20 to transmit torque from the output shaft of the gearbox to the differential. The differential is mounted on the rear axle, and the suspension is of the live axle type (solid rear axle). The universal joints accommodate movement of the rear axle permitted by the suspension. The differential shaft is nominally parallel to the gearbox shaft. However, the suspension setup maintains this relationship only to a good approximation. Also, some fore-aft rocking of the differential housing occurs because of elastic deflection and backlash in suspension components. The angle  $\gamma$ , as defined in Fig. 7.20, varies from  $175^\circ$  to  $160^\circ$  between the suspension stops. The error in  $\gamma$  at the rear universal joint is estimated to be  $\pm 0.5^\circ$ . Estimate the maximum percentage fluctuation in the velocity ratio between the gearbox shaft and the differential shaft.

**Solution**

Because the error in  $\gamma$  is small, we should be able to use a small-angle approximation with acceptable accuracy.

Equations (7.11) become

$$\cos \gamma = \tan \theta_1 \tan \theta_2$$

and

$$\cos (\gamma + \delta \gamma) = \tan \theta_1' \tan \theta_2'$$

or

$$\cos \gamma - \delta \gamma \sin \gamma = \tan \theta_1' \tan \theta_2'$$

Noting that

$$\tan \theta_1' = \tan \theta_2 = \frac{\cos \gamma}{\tan \theta_1}$$

$$\cos \gamma - \delta \gamma \sin \gamma = \frac{\cos \gamma \tan \theta_2'}{\tan \theta_1}$$

or

$$\tan \theta_2' = \tan \theta_1 (1 - \delta \gamma \tan \gamma)$$

Differentiation of this expression with respect to time gives

$$\dot{\theta}_2' \sec^2 \theta_2' = \dot{\theta}_1 \sec^2 \theta_1 (1 - \delta \gamma \tan \gamma)$$

Using

$$\sec^2 \theta_2' = 1 + \tan^2 \theta_2' = 1 + \tan^2 \theta_1 (1 - \delta \gamma \tan \gamma)^2$$

gives the velocity ratio

$$\frac{\dot{\theta}'_2}{\dot{\theta}_1} = \frac{1 - \delta\gamma \tan \gamma}{\cos^2 \theta_1 \left\{ 1 + \tan^2 \theta_1 (1 - \delta\gamma \tan \gamma)^2 \right\}} = \frac{1 - \delta\gamma \tan \gamma}{1 - 2\delta\gamma \tan \gamma \sin^2 \theta_1}$$

Here the small-angle approximation has been used by dropping the  $\delta\gamma^2$  term in the expansion of the denominator. This expression may be further simplified by multiplying top and bottom by the factor  $1 + 2\delta\gamma \tan \gamma \sin^2 \theta_1$  and again applying the small-angle approximation. Then

$$\frac{\dot{\theta}'_2}{\dot{\theta}_1} = (1 + 2\delta\gamma \tan \gamma \sin^2 \theta_1)(1 - \delta\gamma \tan \gamma) = 1 - \delta\gamma \tan \gamma + 2\delta\gamma \tan \gamma \sin^2 \theta_1$$

or

$$\frac{\dot{\theta}'_2}{\dot{\theta}_1} = 1 - \delta\gamma \tan \gamma \cos 2\theta_1$$

It is clear from this expression that the maximum magnitude of the velocity ratio,  $R$ , is  $1 + \delta\gamma \tan \gamma$  and the minimum value is  $1 - \delta\gamma \tan \gamma$ . Applying the values given in this particular problem, we find that  $\tan \gamma$  will be at a maximum when  $\gamma = 160^\circ$  and  $\delta\gamma = 15^\circ$ . Then

$$\delta\gamma = 0.5 \times \pi / 180 = 0.00873 \text{ rad}$$

$$\tan \gamma = -0.364$$

so

$$R_{\max} = 1.0032 \text{ and } R_{\min} = 0.9968$$

The maximum percentage fluctuation of the velocity ratio is thus 0.32%.

## 7.3 CONSTANT-VELOCITY COUPLINGS

As can be seen in the preceding subsections, universal joints are not constant-velocity joints. Although paired universal joints can function as constant-velocity joints, the arrangement must satisfy special geometric conditions. There is a need for single joints that can provide true constant-velocity action and that can accommodate other changes of alignment such as plunging (movement in the direction of the shaft axis) of one shaft relative to the other.

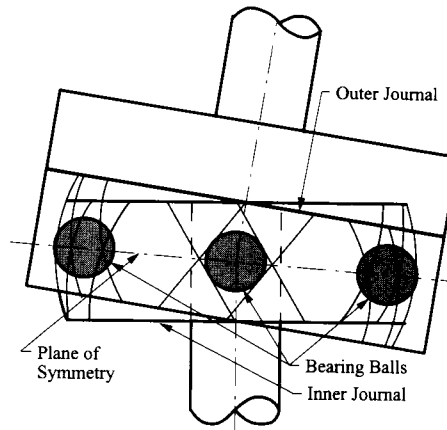
### 7.3.1 Geometric Requirements of Constant-Velocity Couplings

An essential requirement for constant-velocity transfer of rotation between nonaligned shafts is that the coupling mechanism be symmetric relative to the plane that bisects the spatial angle between the shaft axes. Examination of Fig. 7.19 indicates that this condition is satisfied by the double universal joint. However, in many situations, such as the drive trains of front-wheel-driven automobiles, a more compact joint is needed.

### 7.3.2 Practical Constant-Velocity Couplings

A common commercial constant-velocity coupling uses bearing balls moving in shaped races between inner and outer journals to transmit torque. The races are shaped so that the centers of the balls are always in the plane of symmetry. The arrangement is shown in Fig. 7.21.

Figure 7.21 shows a ball-type constant-velocity coupling with six balls, and Fig. 7.22 shows a photograph of the coupling. The inner journal has a spherical outer surface with six equally spaced races with semicircular cross sections cut into it. The centerline of each race



**FIGURE 7.21** Ball-type constant-velocity coupling. The balls, six in the configuration shown, roll in races cut in the inner and outer journals. The centerlines of the races are great circles with their planes inclined to the journal axes at the same angle. Alternate races are cut with opposing angles. The angles of the races in the inner and outer races are also opposite. In this way the center of each ball is always at the intersection of the centerlines of the races in the inner and outer journals, which lies in the plane of symmetry of the angulated joint. Because the ball centers always lie in a common plane of symmetry, the condition for constant-velocity action is satisfied.

is a great circle of a neutral sphere that is slightly larger than the surface of the journal. The planes of the great circles are inclined at equal angles to the journal axis, and alternate races are cut at opposing angles. The outer journal has a spherical inner surface slightly larger than the neutral sphere. Races are also cut into it with their centerlines being great circles in the neutral sphere.

They are cut at the same angle to the journal axis as the races in the inner journal, and successive races are again cut at opposing angles. The joint is assembled with each ball rolling in inner and outer races that are at opposing angles. Therefore, the ball center is always at the intersection of the race centerlines. This ensures that all ball centers lie in a common plane at all times. This plane bisects the angle between the two journal axes and is, therefore, a plane



**FIGURE 7.22** Ball-type constant-velocity coupling used in front-wheel-driven automobile.



of symmetry. Since the ball centers all lie in a common plane of symmetry at all times, the symmetry condition is satisfied and the joint transmits motion with constant velocity.

This type of joint can be made relatively compact and is commonly used in automotive drive shafts to allow smooth torque transmission despite the movements of the wheels permitted by the suspension.

## **7.4 AUTOMOTIVE STEERING AND SUSPENSION MECHANISMS**

---

### **7.4.1 Introduction**

Automotive steering and suspension mechanisms are primarily designed as separate, planar mechanisms acting in different planes. However, they are interconnected because they have common links. Also, both have modifications that make them spatial linkages. For example, the axis about which the wheel turns in response to movements of the steering linkage is not vertical. The inclination of the axis, called camber, creates a tendency for the steering to center itself at low speed, since it results in the vehicle body being raised slightly whenever the wheels are turned away from the straight-ahead position. Camber is not effective in providing centering at high speed. However, another modification, called caster, provides this action. The wheel steering axis is moved forward relative to the wheel a little way. The distance the wheel rotation axis trails the steering axis is the caster.

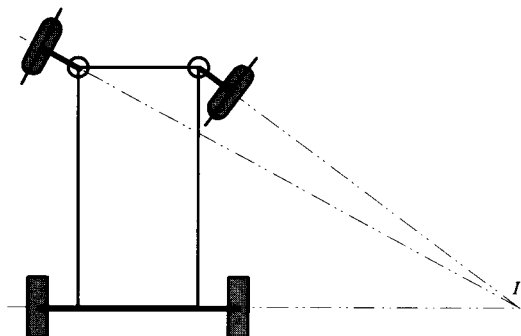
The interconnection, together with modifications such as camber that create a truly spatial character, can lead to undesirable dynamic interactions. It is very undesirable for suspension movements to be felt through the steering, or for the position of the steering linkage to influence suspension performance.

### **7.4.2 Steering Mechanisms**

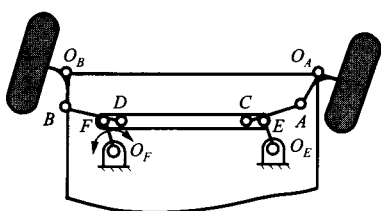
From a purely kinematic viewpoint, the essential geometry of an automotive steering linkage is that the axes of the front wheels should, at all times, be concurrent at the axis of the rear wheels. It is possible to synthesize a four-bar linkage that will constrain the front wheel axes to approximate this condition very closely. This is the basis of the Ackermann steering gear. As can be seen from Fig. 7.23, it is necessary that the front wheels be "toed out" to an increasing extent as the radius of curvature of the vehicle path is reduced.

However, a close approximation to Ackermann geometry is often not used on modern automobiles, particularly on high-performance vehicles and race cars. This is because, at high speed, steering becomes a dynamic problem. To change direction, it is necessary to develop lateral forces at the tire contacts with the road. The production of lateral force requires some slip between the wheel and the road. By using less toe-out than would be required by the Ackermann geometry, more lateral slip is generated at the outside front wheel, which also carries a greater share of the vehicle weight owing to dynamic load transfer and is, therefore, able to generate more lateral force. Some race car steering setups go so far as to reverse the kinematically ideal relationship by actually toeing the front wheels in by a small amount during turns. This very aggressive geometry produces very strong cornering action at the expense of tire wear, which is not, of course, such a concern in a race over a limited distance as it is in general automotive use.

Ackermann action, or any other desired relationship between the steering angles of the wheels, can be adequately approximated by an eight-bar steering linkage such as that shown in Fig. 7.24. Because the wheels move vertically with suspension travel, the joints at



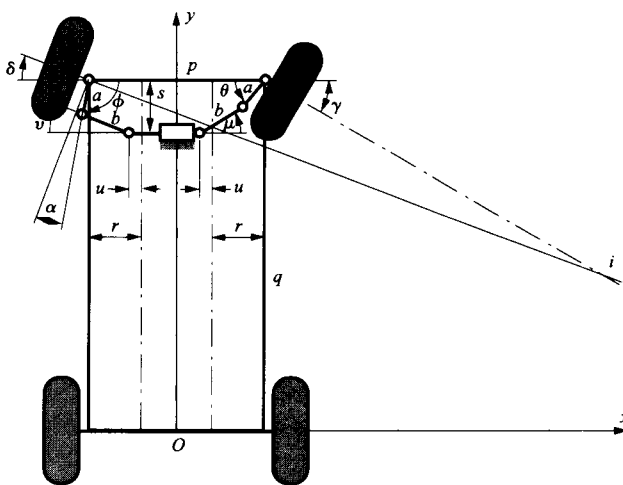
**FIGURE 7.23** The Ackermann steering condition. Since the axes of all four wheels meet at a common instantaneous center, the wheels can roll without any lateral scuffing action. This is the ideal steering geometry at low speeds.



**FIGURE 7.24** A typical steering gear arrangement. The Pitman arm,  $O_F F$ , is turned by the steering column. The four-bar loop  $O_E E F O_F$  is a parallelogram.  $O_E E$  is the idler arm, and  $EF$  is the relay rod.  $AC$  and  $BD$  are the tie rods, and  $O_A A$  and  $O_B B$ , which are fixed to the structures that carry the stub axles, are called the steering arms. The steering arms turn about the steering knuckles  $O_A$  and  $O_B$ . Note that the linkage is bilaterally symmetric about the centerline of the vehicle.

the ends of the tie rods must be spherical joints. Thus, the linkage becomes spatial, although still approximating the designed planar behavior.

In modern cars, it is more common to use a linear input to the steering linkage. This is typically produced by a rack-and-pinion type of steering box. This linear input is applied directly to the relay rod. This arrangement may be thought of as the limiting case of the mechanism in Fig. 7.24 as the arms  $O_E E$  and  $O_F F$  become infinitely long, producing the configuration of Fig. 7.25. It has the advantages of being simpler (using six members versus eight), more compact, and potentially lighter.



**FIGURE 7.25** The rack-and-pinion steering linkage geometry analyzed in Example 7.5. The position of the intersection of the front wheel axes as a function of the rack displacement,  $u$ , and the values of the wheel angles  $\gamma$  and  $\delta$  are tabulated in Table 7.1. The coordinates of  $i$  are plotted as a function of  $u$  in Fig. 7.26.

**EXAMPLE 7.5**  
**Analysis of a Rack-**  
**and-Pinion Type**  
**Steering Linkage**

A steering linkage for an automobile is shown in Fig. 7.25. The wheel base of the automobile (distance between front and rear wheel axes) is  $q = 100$  in. The distance between the steering knuckles is  $p = 50$  in. The length of the steering arm is  $a = 3$  in, and it is inclined at angle  $\alpha = 9^\circ$  to the plane of the wheel. The length of the tie rods is  $b = 10$  in. When the wheels are in the straight-ahead position shown in Fig. 7.25, the inner ends of the tie rods are a distance  $r = 10.08$  in from the steering knuckles in the lateral direction, and  $s = 7.72$  in in the longitudinal direction.

Plot the  $x$  and  $y$  coordinates of the intersection of the front wheel axes for increments of 0.1 in of the rack displacement,  $u$ , in the range  $0 < u < 1.5$  in, where the reference frame has its origin at the middle of the rear axle, as shown. The  $x$  coordinate can be interpreted as the radius of curvature of the path followed by the vehicle, and the  $y$  coordinate is the error from perfect Ackermann geometry. As indicated in Fig. 7.23, if the Ackermann condition were exactly met,  $y$  would be zero at all times. Also calculate the angles of the inner and outer front wheels relative to the straight-ahead position throughout this range.

**Solution**

The linkage can be analyzed as two slider-crank linkages acting in parallel with a common input,  $u$ , applied to the sliders. Resolving components in the  $x$  and  $y$  directions respectively, we have for the right side

$$a \cos \theta + b \cos \mu = r + u \quad (7.13)$$

$$a \sin \theta + b \sin \mu = s \quad (7.14)$$

where  $\mu$  is the tie rod angle as shown in Fig. 7.25.

Similarly, for the left side, we have

$$a \cos \phi + b \cos \nu = r - u \quad (7.15)$$

$$a \sin \phi + b \sin \nu = s \quad (7.16)$$

The angle  $\mu$  may be eliminated from Eqs. (7.13) and (7.14) by segregating the  $\mu$  terms on one side of each equation, squaring both sides of both equations, and adding to give

$$b^2 = (r + u - a \cos \theta)^2 + (s - a \sin \theta)^2$$

or

$$b^2 = r^2 + s^2 + a^2 + u^2 + 2ru - 2au \cos \theta - 2ar \cos \theta - 2as \sin \theta \quad (7.17)$$

This equation has the form

$$P \cos \theta + Q \sin \theta + R = 0 \quad (7.18)$$

where

$$P = 2a(u + r)$$

$$Q = 2as$$

$$R = b^2 - a^2 - r^2 - s^2 - u^2 - 2ru \quad (7.19)$$

Hence the standard solution of Table 5.1 may be applied to obtain values of  $\theta$  corresponding to given values of  $u$ . Two values of  $\theta$  are obtained for each value of  $u$ , one positive and one negative. Only the negative value is consistent with the configuration shown in Fig. 7.25, so the positive value is discarded.

Similarly, elimination of  $\nu$  from Eqs. (7.15) and (7.16) gives

$$b^2 = (r - u - a \cos \phi)^2 + (s - a \sin \phi)^2$$

or

$$b^2 = r^2 + s^2 + a^2 + u^2 - 2ru + 2au \cos \phi - 2ar \cos \phi - 2as \sin \phi \quad (7.20)$$

This equation has the form

$$P' \cos \phi + Q' \sin \phi + R' = 0 \quad (7.21)$$

where

$$\begin{aligned} P' &= 2a(r-u) \\ Q' &= 2as \\ R' &= b^2 - a^2 - r^2 - s^2 - u^2 + 2ru \end{aligned} \quad (7.22)$$

for which the solution is also given by Table 5.1. Values of  $\phi$  for incremental values of  $u$  throughout the specified range can be calculated. As was the case for  $\theta$ , two values of  $\phi$  are obtained for each value of  $u$ , one positive and one negative. Only the negative solution is consistent with the configuration drawn in Fig. 7.25, so the positive solution is discarded.

Now  $\gamma = \pi/2 - \theta - \alpha$ , and  $\delta = \phi + \alpha - \pi/2$ , where  $\gamma$  and  $\delta$  are the steering angles of the inner and outer front wheels, as shown in Fig. 7.25, and values of  $\gamma$  and  $\delta$  may now be calculated. The resulting values of  $\gamma$  and  $\delta$  throughout the range of values of  $u$  are listed in Table 7.1. Also,  $\gamma$  and  $\delta$  determine the location of the intersection,  $I$ , of the axes of the wheels:

$$\tan \gamma = \frac{q-y}{x-p/2}, \quad \tan \delta = \frac{q-y}{x+p/2} \quad (7.23)$$

Hence,

$$(x-p/2) \tan \gamma = (x+p/2) \tan \delta$$

which, when solved for  $x$ , gives

$$x = \frac{p}{2} \left( \frac{\tan \gamma + \tan \delta}{\tan \gamma - \tan \delta} \right) \quad (7.24)$$

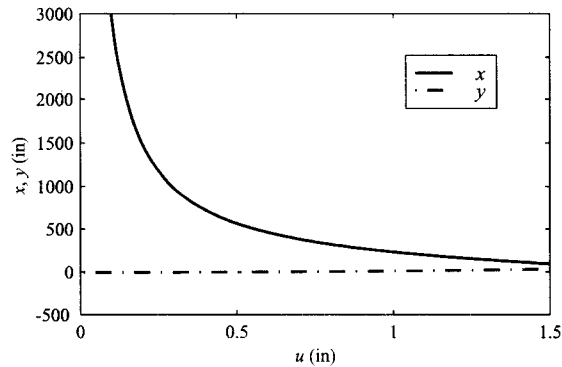
Substitution for  $x$  into either of Eqs. (7.23) allows a solution for  $y$  to be obtained:

$$y = q - p \left( \frac{\tan \gamma \tan \delta}{\tan \gamma - \tan \delta} \right)$$

The results are tabulated in Table 7.1 and are plotted in Fig. 7.26. It may be seen that the linkage gives a reasonable approximation to the Ackermann condition, except at very large wheel angles.

**TABLE 7.1 Numerical Values Obtained by Solution of Example 7.5**

$u$	$\gamma$	$\delta$	$x$	$y$
0.2	4.13	3.99	1475.17	-4.65
0.3	6.25	5.94	973.19	-3.91
0.4	8.43	7.87	718.74	-2.86
0.5	10.67	9.79	563.51	-1.50
0.6	12.99	11.68	457.89	0.17
0.7	15.38	13.56	380.59	2.18
0.8	17.88	15.43	320.98	4.52
0.9	20.50	17.29	273.11	7.23
1.0	23.28	19.13	233.42	10.34
1.1	26.25	20.98	199.57	13.90
1.2	29.50	22.81	169.98	17.99
1.3	33.13	24.65	143.39	22.74
1.4	37.38	26.48	118.66	28.44
1.5	42.87	28.31	94.09	35.86



**FIGURE 7.26** The coordinates of the intersection of the front wheel axes,  $i$ , plotted against the rack displacement,  $u$ .  $x$  approximates the radius of curvature of the vehicle's path, and  $y$  is the error in location of the intersection relative to the rear axle axis. That is,  $y$  is the deviation from the Ackermann condition. When  $u = 0$ ,  $x = \infty$  and  $y = 0$ . The values used in the plot are included in Table 7.1.

### 7.4.3 Suspension Mechanisms

An automotive suspension performs the function of a vibration filter, reducing the amplitudes of vibrations excited by geometric variations in the road surface. This is the function of the spring damper arrangements that are integral components of the suspension. Analysis of this vibration filtering action is normally covered in texts on mechanical vibrations and is beyond the scope of this book. Here we confine ourselves to the kinematic requirements of suspension mechanisms.

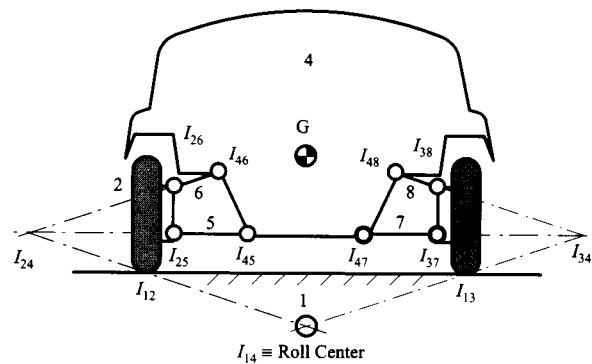
Automotive suspension mechanisms must allow controlled, single-degree-of-freedom motion of the wheel axis relative to the body of the vehicle. The travel allowed needs to be as close as possible to normal to the plane of the ground at the wheel contact. Also, it is necessary for the suspension mechanism to maintain the plane of the wheel as perpendicular as possible to the ground at all times. This is because automobile tires are designed to develop maximum lateral force when they are in the upright position, as opposed to motorcycle tires, which must function in inclined positions during hard cornering. Since the center of mass of an automotive vehicle is almost always higher than the wheel axes, there is a tendency for the body to roll toward the outside of a turn. Another objective of suspension design is to attempt to control this tendency to roll.

Automotive steering and suspension mechanisms are truly spatial mechanisms. However, their initial design generally rests on planar principles.

When viewed from the front, the instantaneous center of motion of the body of the vehicle relative to the ground is called the roll center. The location of the roll center for a typical independent suspension geometry is shown in Fig. 7.27. The center is located by using the Kennedy–Aronholdt theorem as described in Chapter 4.

Of course, the roll center moves as the position of the vehicle body moves. Whereas the roll center will be on the vehicle centerline for a road vehicle at rest on a level surface, it will shift off that line in the asymmetric positions that result from cornering. There is also a roll center for the rear suspension, so one can think of a roll axis, which is the line that passes through both roll centers.

The location of the roll center relative to the center of mass of the vehicle governs the effect of inertial forces caused by cornering on the system. Obviously, if the vertical distance between the roll center and the center of mass is large, the moment produced by lateral acceleration will be large. A suspension geometry that brings the roll center



**FIGURE 7.27** Roll center geometry for an automotive independent suspension system. The roll center is the instantaneous center of relative motion of the vehicle body and the ground.

progressively closer to the center of mass with increasing body roll might be attractive, because if the action of the suspension springs were linear, it would lead to increasing roll stiffness with increasing roll angle.

Suspension designers think of the roll center as the point of transfer of the inertial force between the sprung and unsprung masses of the vehicle. The unsprung mass comprises the wheels and suspension members directly attached to them whose position is directly determined by the road surface. The sprung mass is everything that moves when the springs are deflected.

## 7.5 INDEXING MECHANISMS

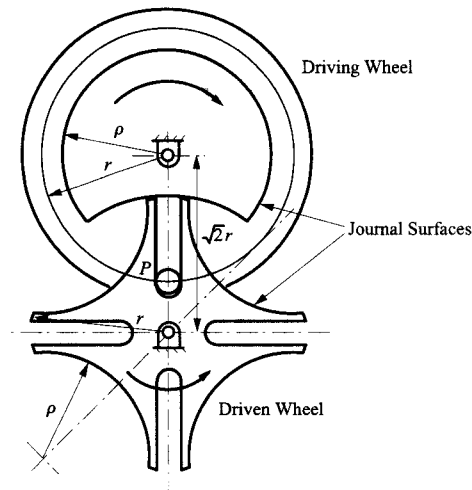
Indexing mechanisms are intermittent motion mechanisms that hold position alternately with a timed, unidirectional motion of the output member. This is distinct from other types of intermittent motion mechanisms such as dwell cams, which alternate forward and return motion with holding position. The output member of an indexing mechanism always advances in the same direction. Indexing mechanisms are of practical importance in applications such as weaving looms, advancing workpieces in repetitive manufacturing operations, and many instrument mechanisms.

### 7.5.1 Geneva Mechanisms

The most common type of indexing mechanism is a Geneva mechanism. Geneva mechanisms come in many varieties, both planar and spherical. When advancing, a Geneva mechanism is kinematically similar to an inverted slider-crank. When holding position, it functions as a simple journal bearing.

The name Geneva mechanism originated because these mechanisms were used in mechanical watch and clock movements in the days when mechanical movements were dominant, and Switzerland was the world center of the industry.

A simple example of a Geneva mechanism is shown in Fig. 7.28. The pin,  $P$ , on the driving wheel engages the slots in the star-shaped driven wheel to advance the driven wheel one-quarter turn for every rotation of the driving wheel. In between the advance movements, the eccentric cylindrical journal surfaces cut into the star wheel engage with the journal surface on the driving wheel to lock the star wheel in position, although the driving



**FIGURE 7.28** A four-station Geneva mechanism. The output member is the star wheel. The star wheel is advanced by the pin in the input wheel. The star wheel is advanced one-quarter revolution counter-clockwise for every revolution of the input wheel. The advance movement occurs during one-quarter of a cycle with the star wheel being locked by the journal surface on the input wheel for the other three-quarters of the cycle.

wheel continues to rotate. The centerline of the slot must be tangent to the circle, with radius  $r$ , described by the center of the pin at the position in which the pin enters or leaves the slot. If this condition is not satisfied, there will be infinite acceleration at the beginning of advancement and infinite deceleration at the end. This condition dictates that the center distance of the two wheels should be  $\sqrt{2}r$ . It also requires that the outer radius of the star wheel be  $r$ . The radius of the journal surfaces is flexible. The centers of the cylindrical cutouts on the star wheel lie on a circle with radius  $\sqrt{2}r$ .

During the advancing phase of the cycle, the mechanism is kinematically equivalent to an inverted slider-crank. One of its attractions is that it smoothly accelerates and then decelerates the star wheel.

The motion of the star wheel may be analyzed by reference to Fig. 7.29. Resolving the sides of the triangle whose vertices are the two shaft axes and the pin axis in the vertical and horizontal directions, we get

$$\begin{aligned} r \sin \theta &= x \sin \phi \\ r \cos \theta + x \cos \phi &= \sqrt{2}r \end{aligned} \quad (7.25)$$

Elimination of  $x$  by substitution from the first of these equations into the second gives

$$\cos \theta + \frac{\sin \theta}{\tan \phi} = \sqrt{2}$$

after canceling the common factor  $r$ . Rearrangement of this expression gives

$$\tan \phi = \frac{\sin \theta}{\sqrt{2} - \cos \theta} \quad (7.26)$$

or

$$\phi = \tan^{-1} \left( \frac{\sin \theta}{\sqrt{2} - \cos \theta} \right) \quad (7.27)$$

Differentiation of Eq. (7.26) with respect to time followed by simplification gives

$$\dot{\phi} (1 + \tan^2 \phi) = \dot{\theta} \frac{(\sqrt{2} \cos \theta - 1)}{(\sqrt{2} - \cos \theta)^2}$$

Substitution for  $\tan \phi$  from Eq. (7.26) gives, after rearrangement and simplification,

$$\dot{\phi} = \dot{\theta} \left( \frac{\sqrt{2} \cos \theta - 1}{3 - 2\sqrt{2} \cos \theta} \right) \quad (7.28)$$

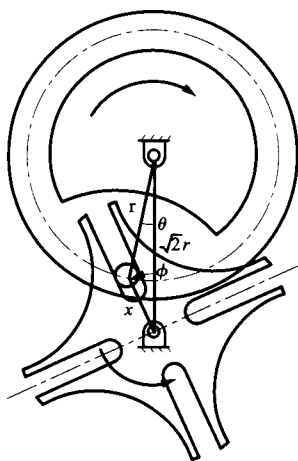
Differentiation again with respect to time gives, after simplification,

$$\ddot{\phi} = \ddot{\theta} \left( \frac{\sqrt{2} \cos \theta - 1}{3 - 2\sqrt{2} \cos \theta} \right) - \dot{\theta}^2 \frac{\sqrt{2} \sin \theta}{(3 - 2\sqrt{2} \cos \theta)^2}$$

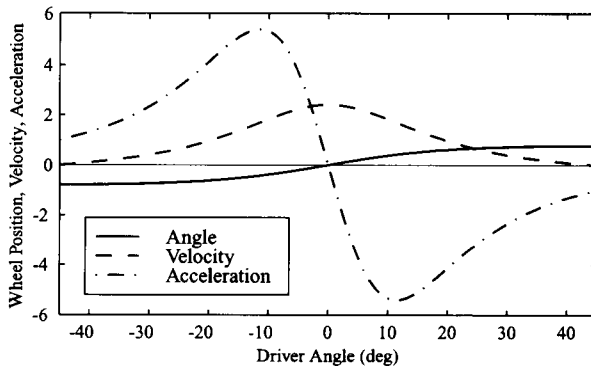
In the usual case in which the driving wheel is driven at constant angular velocity, the first term disappears and

$$\ddot{\phi} = -\dot{\theta}^2 \frac{\sqrt{2} \sin \theta}{(3 - 2\sqrt{2} \cos \theta)^2} \quad (7.29)$$

Equations (7.27), (7.28), and (7.29) are plotted versus  $\theta$  (in degrees) in Fig. 7.30.  $\phi$  is plotted in radians. Of course,  $\phi$  varies from  $-45^\circ$  to  $45^\circ$  during the advancement. The angular velocity curve is actually  $\dot{\phi}/\dot{\theta}$ , and the angular acceleration curve is  $\ddot{\phi}/\dot{\theta}^2$ .



**FIGURE 7.29** Kinematic modeling of the Geneva mechanism of Fig. 7.28.  $\theta$  is the angle of rotation of the driving wheel, measured from the line of centers.  $\phi$  is the angle of rotation of the star wheel.



**FIGURE 7.30** Position, velocity, and acceleration of the driven wheel of the Geneva mechanism shown in Figs. 7.28 and 7.29 during the advancement phase of the motion cycle. The angular position of the star wheel is in radians. The angular velocity and acceleration curves are respectively normalized to the driver angular velocity and driver angular velocity squared.



As can be seen from Fig. 7.30, the velocity and acceleration curves are smooth and well behaved, but the derivative of the acceleration (jerk) is infinite at the beginning and end of the advancement because the acceleration is discontinuous there. So far, we have considered only the simplest version of the Geneva mechanism: the four-station planar variety. The number of stations is the number of slots in the star wheel and may, in principle, be any number, although the geometric lower limit is three. There is also a practical upper limit at which the journal surfaces on the star wheel become too short to effectively lock the output between advancements. The number of pins on the driving wheel is usually one, but drivers with two or more are possible.

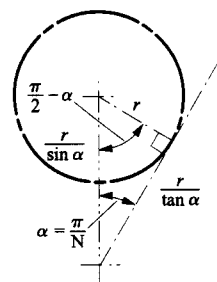
The essential geometry for relating the number of stations to the duration of the advancement is shown in Fig. 7.31. Here  $\alpha$  is the angle between the slot centerline and the line of centers of the two wheels at the moment of engagement or disengagement of the pin. That is,  $\alpha$  is half the angle between successive slots, or  $360^\circ/(2N)$ , where  $N$  is the number of stations. As already noted, the slot axis must be tangent to the circle traversed by the pin center at these positions to avoid infinite accelerations. This determines the relationship between  $N$  and the duration of the advancement, which is  $\pi - 2\alpha$  by inspection of the figure. Consequently, the duration of the advancement increases with the number of stations, approaching a limit of  $180^\circ$  as the number of stations becomes very large. This has the advantage of making the advancement motion more gentle but the possible disadvantage of decreasing the duration of the period for which the output is stationary. The trade-off between these effects and the desirability of avoiding gearing downstream of the indexing mechanism determine the choice of the number of stations. Gearing downstream of an indexing mechanism should be avoided because of the inaccuracy and uncertainty in position introduced by necessary backlash in the gear train. Gear backlash is not usually a problem if the gears are in uniform motion. However, the discontinuous motion output from an indexing mechanism and consequent reversals of acceleration result in slapping across the backlash interval. Hence, any speed reduction should be done upstream of the indexing mechanism.

The number of stations also determines the ratio of the center distance of the wheel axes to the pin radius and the outside diameter of the star wheel. By inspection of Fig. 7.31, the former ratio is  $1/\sin \alpha$  and the latter is  $1/\tan \alpha$ .

If we note that  $\alpha = \pi/N$ , Eqs. (7.27–7.29), respectively, become for this more general case

$$\phi = \tan^{-1} \left( \frac{\sin \alpha \sin \theta}{1 - \sin \alpha \cos \theta} \right) \quad (7.30)$$

$$\dot{\phi} = \dot{\theta} \sin \alpha \left( \frac{\cos \theta - \sin \alpha}{1 + \sin^2 \alpha - 2 \sin \alpha \cos \theta} \right) \quad (7.31)$$



**FIGURE 7.31** Critical geometry for a Geneva mechanism with  $N$  stations.  $\alpha$  is the angle between the slot centerline and the line of centers at the moment of engagement of the pin;  $\alpha$  is half the angle between successive slots on the star wheel.

$$\ddot{\phi} = -\dot{\theta}^2 \frac{\sin \alpha \cos^2 \alpha \sin \theta}{(1 + \sin^2 \alpha - 2 \sin \alpha \cos \theta)^2} \quad (7.32)$$

Spherical Geneva mechanisms allow indexed motion transfer between angulated shafts. More importantly, a large number of stations can be accommodated without losing positive locking action between advances.

**EXAMPLE 7.6**  
**Analysis of a**  
**Geneva Wheel**

An indexing drive is to be driven by a synchronous electric motor turning at 360 rpm. (The speed of a synchronous motor is locked to the alternating-current cycle frequency and so is essentially constant.) The single pin driver is to turn a six-station Geneva wheel. Compute the following:

- the number of advances per second,
- the angle through which the Geneva wheel advances during every revolution of the driving wheel,
- the duration in seconds of the dwell in the output motion,
- the peak angular velocity of the output shaft, and
- the peak angular acceleration of the output shaft.

**Solution**

- The number of advances per second is the number of revolutions of the driver per second, which is  $360/60 = 6$ .
- The angle advanced is  $2\alpha = 360^\circ/N = 60^\circ$ , with  $N$ , the number of stations, being 6 in this case. Hence  $\alpha = 30^\circ$ .
- The fraction of the cycle during which the output is locked (dwelling) is

$$\lambda = \frac{180 - 2\alpha}{360}$$

with  $\alpha$  in degrees, giving  $\lambda = 1/3$ . The duration of the complete cycle is  $T = 1/6$  s from part a. Hence the duration of the dwell is

$$\tau = \lambda T = 1/18 = 0.0555 \text{ s}$$

- Referring to Eq. (7.32), we see that  $\dot{\phi}$  is at its maximum value when  $\theta = 0$ . Also, for  $N = 6$ ,

$$\sin \alpha = 0.5$$

so, substituting this value and  $\theta = 0$  in Eq. (7.31) gives

$$\dot{\phi}_{\max} = \dot{\theta}$$

$\dot{\theta}$  is the angular velocity of the drive wheel, so

$$\dot{\theta} = 2\pi \times 6 = 37.70 \text{ rad/s}$$

Therefore,

$$\dot{\phi}_{\max} = 37.70 \text{ rad/s}$$

Note that  $\phi$  is positive in the CCW direction and  $\theta$  is positive in the CW direction (see Fig. 7.29). Therefore the positive values for both  $\phi$  and  $\theta$  indicate that the star wheel rotates in the opposite direction to the driver.

- It is necessary to determine the value of  $\theta$  that maximizes  $\dot{\phi}$ . A straightforward way to do this would be to plot Eq. (7.32) in the same way as in Fig. 7.30, but with  $\alpha = 30^\circ$ .  $\dot{\phi}$  and the angle  $\theta$  at which it occurs could then be read directly from the plot.

Alternatively, we can differentiate Eq. (7.32) to identify the extrema of  $\dot{\phi}$ . Noting that  $\dot{\theta}$  is constant, we have

$$\frac{d\ddot{\phi}}{dt} = \frac{-\dot{\theta}^3 \sin \alpha \cos^2 \alpha}{(1 + \sin^2 \alpha - 2 \sin \alpha \cos \theta)^3} \left[ (1 + \sin^2 \alpha - 2 \sin \alpha \cos \theta) \cos \theta - 4 \sin \alpha \sin^2 \theta \right]$$

and so

$$\frac{d\ddot{\phi}}{dt} = 0$$

when

$$(1 + \sin^2 \alpha) \cos \theta - 2 \sin \alpha \cos^2 \theta - 4 \sin \alpha \sin^2 \theta = 0$$

Replacement of  $\sin^2 \theta$  by  $1 - \cos^2 \theta$  and rearrangement of the equation give

$$\cos^2 \theta + \gamma \cos \theta - 2 = 0$$

where

$$\gamma = \frac{1 + \sin^2 \alpha}{2 \sin \alpha} \quad (7.33)$$

The preceding equation can be treated as a quadratic equation in the variable  $\cos \theta$ . Solving for  $\cos \theta$ , we get

$$\cos \theta = \frac{-\gamma \pm \sqrt{\gamma^2 + 8}}{2}$$

It is possible to show that only the positive value of the square root gives a value of  $\cos \theta$  with magnitude between 0 and 1 in the allowable range of  $0 < \alpha < 60^\circ$ , so only that solution is valid. Hence,  $\dot{\phi}$  is at a maximum when

$$\theta = \pm \cos^{-1} \left( \frac{-\gamma + \sqrt{\gamma^2 + 8}}{2} \right) \quad (7.34)$$

where the  $\pm$  sign now comes from inversion of the cosine, not from the quadratic solution. Equations (7.33) and (7.34) are of general validity for locating the maximal values of  $\dot{\phi}$ . In the present case, substituting  $\sin \alpha = 0.5$  in Eq. (7.33) gives

$$\gamma = 1.25$$

Hence Eq. (7.34) gives

$$\theta = \pm 22.90^\circ$$

Substitution of these values into Eq. (7.32) gives

$$\frac{\ddot{\phi}}{\dot{\theta}^2} = \pm 1.372$$

Hence, since  $\dot{\theta} = 6 \times 2\pi = 37.70$  rad/s, the peak angular acceleration is  $1950$  rad/s<sup>2</sup>.

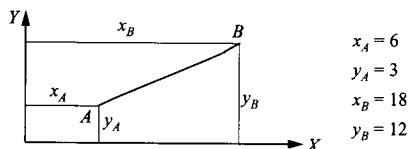
## REFERENCES

- <sup>1</sup>Hain, K., *Applied Kinematics*, McGraw-Hill Book Co., New York (1967).
- <sup>2</sup>Dijksman, E. A., *Motion Geometry of Mechanisms*, Cambridge University Press (1976).
- <sup>3</sup>Chironis, N. P., *Mechanisms, Linkages and Mechanical Controls*, McGraw-Hill Book Co., New York (1965).
- <sup>4</sup>Bottema, O. and Roth, B., *Theoretical Kinematics*, North-Holland Press, New York (1979).
- <sup>5</sup>Hunt, K. H., *Kinematic Geometry of Mechanisms*, Clarendon Press, Oxford (1978).

## PROBLEMS

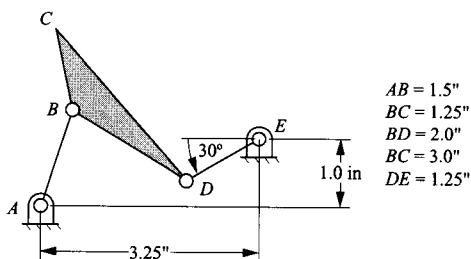
### Exercise Problems Involving Cognate Linkages

7.1 A coupler curve has the approximate straight-line section shown in the figure. Design a four-bar linkage that will generate the portion of the curve shown. Describe the linkage in sufficient detail that it can be manufactured.

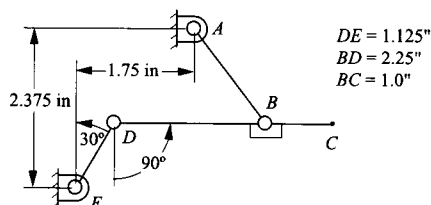


7.2 Re-solve Problem 7.1 if  $x_A = 3$ ,  $y_A = 3$ ,  $x_B = 20$ , and  $y_B = 25$ .

7.3 Determine the cognate linkages that will trace the same coupler curve as that traced by point  $C$  in the figure shown.

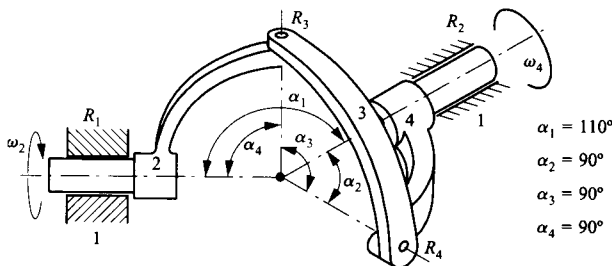


7.4 Determine the cognate linkages that will trace the same coupler curve as that traced by point  $C$  in the figure shown.



### Exercise Problems Involving Spherical Four-Bar Linkages

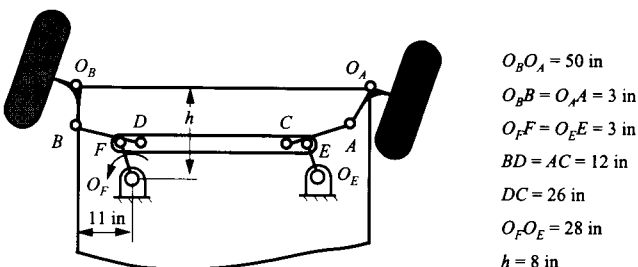
7.5 A spherical four-bar linkage is shown in the figure. If the angular velocity of link 2 is 100 rad/s (constant), find the angular velocity and angular acceleration of link 4 as a function of the rotation of link 2. Plot the angular velocity and angular acceleration of link 4 for a full rotation of link 2. Make the calculations for the assembly mode shown in the figure.



7.6 Re-solve Problem 7.5 if  $\alpha_1 = 150^\circ$  but all other data remain the same.

### Exercise Problems Involving Steering Linkages

7.7 The mechanism shown is used for a steering linkage for an automobile. The wheel base is 110 in, and link  $O_F F$  is driven by the steering column. The toe-in angle ( $\alpha$ ) is  $9^\circ$ . If the link dimensions are given as shown, determine the  $y$  error in the Ackermann steering condition (see Figs. 7.23 and 7.26) for a  $10^\circ$  CCW rotation of  $O_F F$ . Recall that the linkage  $O_E E F O_F$  is a parallelogram.



7.8 Write a computer program to analyze the steering linkage shown in Problem 7.7. If only  $h$  can change, determine the optimum value for  $h$  that will give the least error in  $y$  for the Ackermann steering condition for a  $\pm 15^\circ$  rotation of  $O_F F$ .

7.9 In the rack-and-pinion mechanism shown in Fig. 7.25, the wheel base is 125 in. If the link dimensions are

$$p = 55 \text{ in}, b = 12 \text{ in}$$

$$a = 3.5 \text{ in}, r = 11 \text{ in}$$

$$\alpha = 10^\circ, s = 6.0 \text{ in}$$

plot the  $y$  error in the Ackermann steering condition as a function of the displacement  $u$  (see Fig. 7.26) for a  $\pm 1.5$ -in displacement of  $u$ .

**7.10** A new subcompact automobile is being designed for rack-and-pinion steering. Assume that the wheel base is 90 in. Determine the other dimensions such that the error in the Ackermann steering condition is as small as possible for a  $\pm 1.5$ -in displacement of the rack.

### Exercise Problems Involving Geneva Mechanisms

**7.11** The center distance between the driver and follower of a Geneva mechanism is to be 3 in. The driver is to rotate five rev-

olutions for each rotation of the follower. The driving pin is to enter the slot tangentially so that there will be no impact load. Do the following:

(a) Design the Geneva mechanism and draw it.

(b) Determine the angular velocity and acceleration of the Geneva wheel for one fifth of a revolution if the angular velocity of the driver is 100 rpm CCW. Plot the results.

**7.12** Re-solve Problem 7.11 if the input link rotates three revolutions for each rotation of the follower. Conduct the velocity and acceleration analysis for one third of a rotation.

# PROFILE CAM DESIGN

## 8.1 INTRODUCTION

Cams are used for essentially the same purpose as linkages, that is, generation of irregular motion. Cams have an advantage over linkages because cams can be designed for much tighter motion specifications. In fact, in principle, any desired motion program can be exactly reproduced by a cam. Cam design is also, at least in principle, simpler than linkage design, although, in practice, it can be very laborious. Automation of cam design using interactive computing has not, at present, reached the same level of sophistication as that of linkage design.

The disadvantages of cams are manufacturing expense, poor wear resistance, and relatively poor high-speed capability. Although numerical control (NC) machining does cut the cost of cam manufacture in small lots, costs are still quite high in comparison with linkages. In large lots, molding or casting techniques cut cam costs, but not to the extent that stamping and so forth, can cut linkage costs for similar lot sizes.

Unless roller followers are used, cams wear quickly. However, roller followers are bulky and require larger cams, creating size and dynamic problems. In addition, the bearings in roller followers create their own reliability problems.

The worst problems with cams are, however, noise and follower bounce at high speeds. As a result, there is a preoccupation with dynamic optimization in cam design.

Cam design usually requires two steps (from a geometric point of view):

1. synthesis of the motion program for the follower and
2. generation of the cam profile.

If the motion program is fully specified throughout the motion cycle, as is the case, for example, with the stitch pattern cams in sewing machines, the first step is not needed. More usually, the motion program is specified only for portions of the cycle, allowing the synthesis of the remaining portions for optimal dynamic performance. An example is the cam controlling the valve opening in an automotive engine. Here the specification is that the valve should be fully closed for a specified interval and more or less fully open for another specified interval. For the portions of the cycle between those specified, a suitable program must be synthesized. This can be done, with varying levels of sophistication, to make the operation of the cam as smooth as possible. In general, the higher the level of dynamic performance required, the more difficult the synthesis process.

The second stage of the process, profile generation, is achieved by kinematic inversion. The cam is taken as the fixed link and a number of positions of the follower relative to the cam is constructed. A curve tangent to the various follower positions is drawn and becomes the cam profile. If the process is performed analytically, any level of accuracy can be achieved.

## 8.2 CAM-FOLLOWER SYSTEMS

A general cam-follower system consists of three elements as shown in Fig. 8.1. The first two are the cam and follower, and the third is a spring or other means of ensuring that the follower remains in contact with the cam. The function of the spring can be replaced by gravity or by constraining the follower between the two surfaces on the cam or constraining the cam between two surfaces on the follower. Both of these approaches are usually more expensive than using a spring and therefore are not commonly used.

A follower is characterized by its motion relative to the ground link and by the geometry of its face that contacts the cam. The cam-follower motion may be either rotational or translational, and translating followers may be either radial or offset. Examples of these are shown in Fig. 8.2. The follower surfaces may be either knife edged, flat, spherical (or cylindrical), or roller as shown in Fig. 8.3.

Actually, these geometries are all of the same class depending on the radius of curvature of the follower face. That is, the knife edge has a radius of curvature that is zero, the flat face has a radius of curvature that is infinite, and the general roller and cylindrical followers have a finite (but nonzero) radius of curvature. In this discussion, only planar cams will be considered, so no distinction between spherical and cylindrical follower faces will be made. Also, if only geometric information is of interest, no distinction needs to be made

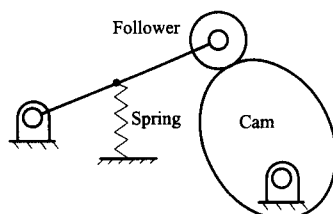


FIGURE 8.1 Elements of a cam-follower system.

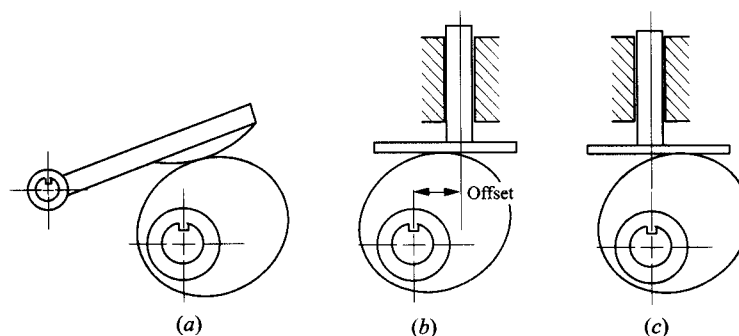


FIGURE 8.2 (a) Cylindrical-faced, oscillating follower. (b) Offset, flat-faced, translating follower. (c) Radial, flat-faced, translating follower.

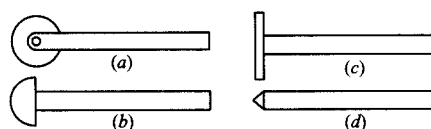
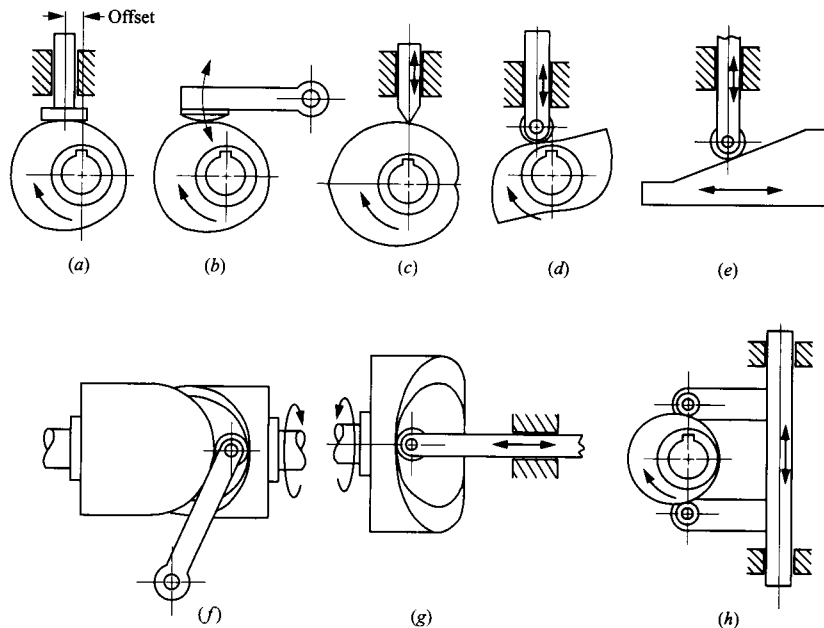


FIGURE 8.3 (a) Roller follower. (b) Cylindrical-faced follower. (c) Flat-faced follower. (d) Knife-edged follower.

between roller and rigid cylindrical-faced followers. Obviously, there is a significant difference from an overall design standpoint, however.

Although here we will consider only planar, rotating cams, in practice a large number of different cam geometries are found. Some of the different types of cams and follower systems are shown in Fig. 8.4.



**FIGURE 8.4** Some types of cams. (a) Radial cam and flat-faced, offset translating follower. (b) Radial cam and spherical-faced, oscillating follower (c) Radial (heart) cam and translating, knife-edged follower. (d) Radial two-lobe frog cam and translating, offset, roller follower. (e) Wedge cam and translating roller follower. (f) Cylindrical cam and oscillating roller follower. (g) End or face cam and translating roller follower. (h) Yoke cam and translating roller follower.

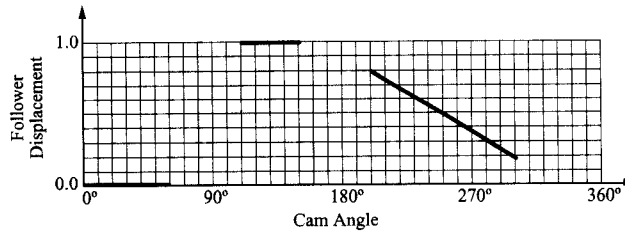
### 8.3 SYNTHESIS OF MOTION PROGRAMS

The problem of motion-program synthesis is the problem of filling in, in an optimal way, the portions of the motion cycle that are not completely specified. The characteristics of the problem may be demonstrated by consideration of a cam that is required to drive a follower that dwells at 0 for a cam rotation of  $60^\circ$ , dwells at 1.0 in for a cam rotation of  $110^\circ$  to  $150^\circ$ , and is required to move with constant velocity from a displacement of 0.8 to 0.2 in for  $200^\circ$  to  $300^\circ$  of cam rotation. The specified portions of the motion program are displayed in Fig. 8.5.

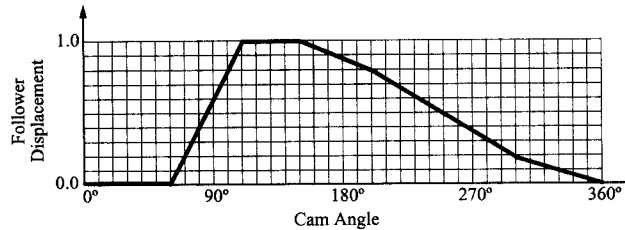
A simple solution to the problem of filling the gaps is simply to move the cam at constant velocity between the specified segments, giving a follower displacement diagram as shown in Fig. 8.6.

Notice, however, that if this is done, the velocity is discontinuous at cam angles  $60^\circ$ ,  $110^\circ$ ,  $150^\circ$ ,  $200^\circ$ ,  $300^\circ$ , and  $360^\circ$ , causing the acceleration to become infinite at these locations. Since the follower cannot follow an infinite acceleration, this leads to loss of contact and/or excessive local stresses and resultant noise and wear problems.





**FIGURE 8.5** The statement of the required displacements of a cam design problem in graphical form.



**FIGURE 8.6** A cam angle-follower displacement program that satisfies the displacement requirements specified in Fig. 8.5.

The preceding motion program matches only the *displacements* at the ends of the segments. The infinite acceleration problem can be removed by matching both displacement and velocity at the ends of segments of the program. One way to do this is to subdivide the synthesized segments into two parts with a constant acceleration on the first and constant deceleration on the second. On such a subsegment, if the acceleration is  $a$ , the velocity is given by

$$v = v_0 + at$$

where  $v_0$  is the velocity at the beginning of the segment. The displacement is given by

$$y = s_0 + v_0 t + \frac{a}{2} t^2$$

where  $s_0$  is the displacement at the beginning of the segment. Now, if the cam is driven at constant velocity,

$$\theta = \theta_0 + \omega t$$

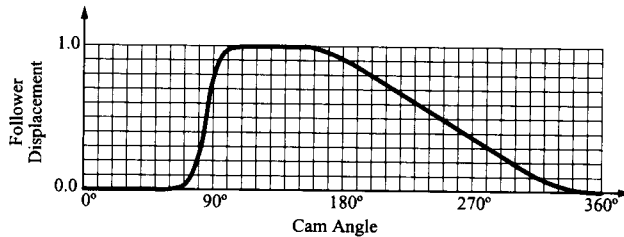
where  $\theta$  is the cam angle,  $\theta_0$  is the cam angle at the beginning of the segment, and  $\omega$  is the angular velocity. Hence

$$t = \frac{(\theta - \theta_0)}{\omega}$$

$$v = v_0 + a \frac{(\theta - \theta_0)}{\omega}$$

$$y = s_0 + v_0 \frac{(\theta - \theta_0)}{\omega} + a \frac{(\theta - \theta_0)^2}{2\omega^2}$$

Therefore, the relationship between  $s$  and  $\theta$ , as plotted on the follower-displacement diagram, is parabolic (see Fig. 8.7). Cam-follower displacement programs that use this type of transition are called parabolic. The cam profiles developed from them are also called



**FIGURE 8.7** A follower displacement program that satisfies the displacement requirements of Fig. 8.5 using parabolic transitions. This is called a *parabolic* follower-displacement program.

“parabolic.” It is important to understand that a so-called parabolic cam *does not* have a parabolic curve in its profile. Rather, the parabolas are in the transition curves used in the follower-displacement program.

## 8.4 ANALYSIS OF DIFFERENT TYPES OF FOLLOWER DISPLACEMENT FUNCTIONS

Several different standard functions can be used to connect the parts of the displacement diagram where a specific type of motion is required. These displacement profiles ultimately determine the shape of the cam. Many different types of motions have been used in practice, and some have been extensively studied. These include the following:

1. uniform motion,
2. parabolic motion,
3. simple harmonic motion,
4. cycloidal motion, and
5. general polynomial motion.

The first two types of program have already been introduced. The first four types of program can be generated graphically as well as analytically, but the fifth type is generated only analytically. Both graphical and analytical development will be considered here, where possible. Both methods assume that the angular velocity,  $\omega$ , of the cam is constant. If this is the case, then

$$y = y(\theta)$$

and

$$\theta = \theta_0 + \omega t$$

Here,  $y$  is used as a generic output variable. It may correspond to either a linear or angular displacement of the follower. Note that if the cam motion is given as a function of time, the motion can easily be represented as a function of the cam rotation in degrees using the preceding expressions.

The higher derivatives are given by

$$\dot{y} = \frac{dy(\theta)}{dt} = \frac{dy}{d\theta} \frac{d\theta}{dt} = y' \omega$$

and

$$\ddot{y} = \frac{d^2 y(\theta)}{dt^2} = \frac{d}{dt} \left( \frac{dy}{d\theta} \frac{d\theta}{dt} \right) = \frac{d^2 y}{d\theta^2} \left( \frac{d\theta}{dt} \right)^2 + \frac{dy}{d\theta} \frac{d^2 \theta}{dt^2} = \frac{d^2 y}{d\theta^2} \omega^2 + \frac{dy}{d\theta} \alpha$$

But because  $\omega$  is constant,  $\alpha = 0$  and

$$\ddot{y} = y'' \omega^2$$

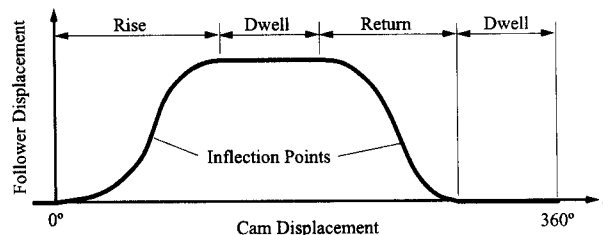
Therefore,  $\dot{y}$  is a simple constant times  $y'$ , and  $\ddot{y}$  is also a constant times  $y''$ . Consequently, even though we ultimately want to know the response to the time derivatives ( $\dot{y}$  and  $\ddot{y}$ ), we may work directly with the derivatives ( $y'$  and  $y''$ ) with respect to the cam displacement. If the cam velocity is not a constant, then the cam profile can be designed for only one operating situation if higher derivatives are important. In the following, a constant-velocity cam is assumed, and  $y$  is again used to represent either an angular or linear displacement of the follower. Similarly,  $\theta$  is used for the displacement of the cam, and it may be either an angular or a linear displacement.

The follower curves can be studied in terms of the simple diagram shown in Fig. 8.8. A general displacement diagram will be made up of three or more parts:

1. rises (1 or more),
2. returns (1 or more), and
3. dwells (0 or more).

Both the rise and return parts will contain one or more inflection points. These are points where a maximum slope is reached, and they correspond to points on the cam surface with maximum steepness. These points are identified by the locations where the curvature of the diagram changes sign. At the inflection points, the radius of curvature of the curve is infinite.

In each of the standard curve cases, we will look at mainly the rise part of the follower profile. The return part can be determined using the mirror images of the curves considered.



**FIGURE 8.8** Terminology used when discussing follower-displacement programs.

## 8.5 UNIFORM MOTION

Uniform motion is represented in Fig. 8.9. To derive the equations for the follower displacement, a general form for the mathematical expression corresponding to the type of motion is assumed. The general equation will have undetermined constants in it, and these constants can be determined by matching boundary conditions at the two ends of the curve. For uniform motion, the general form of the curve used is

$$y = C\theta$$

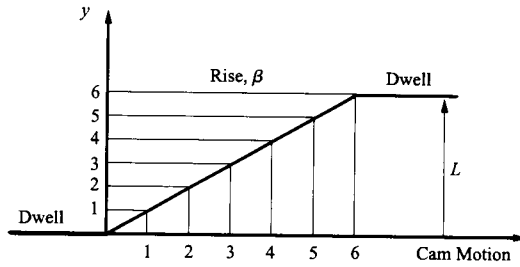


FIGURE 8.9 Uniform motion.

If  $L$  is the amount of the rise, and  $\beta$  is the cam rotation required for the rise, then the constant  $C$  must be  $L/\beta$  and  $y$  becomes

$$y = \frac{L}{\beta} \theta$$

During the rise, the velocity and acceleration are

$$\dot{y} = \frac{L}{\beta} \omega$$

and

$$\ddot{y} = 0$$

The displacement, velocity, and acceleration are plotted in Fig. 8.10. As noted earlier, the acceleration is infinite at the points where the uniform motion meets the dwells. Therefore, even for low speeds and elastic members, the forces transmitted will be very large. For very low speeds, however, this type of displacement diagram might be acceptable.

Graphically, the uniform motion–displacement diagram is characterized by a uniform change in  $y$  for a uniform change in the cam motion. This condition is shown in Fig. 8.9.

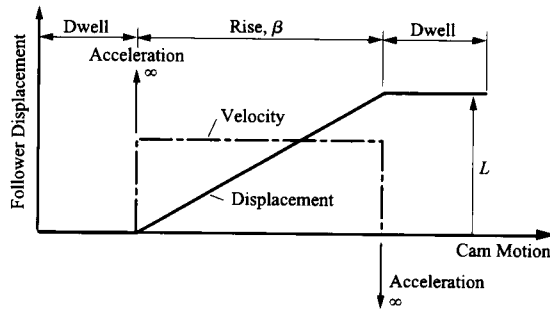


FIGURE 8.10 Displacement, velocity, and acceleration relations for uniform motion.

## 8.6 PARABOLIC MOTION

The equations for parabolic motion can be derived using the same procedure as described in Section 8.3. However, two parabolas must be used for each transition. The two parabolas meet at the point midway between the ends of the two dwell regions. The general form for both parabolas is

$$y = C_0 + C_1\theta + C_2\theta^2 \tag{8.1}$$

and

$$\begin{aligned}y' &= C_1 + 2C_2\theta \\y'' &= 2C_2\end{aligned}\tag{8.2}$$

If the cam displacement is taken as 0 at the beginning of the rise, then at  $\theta = 0$ ,  $y = y' = 0$ . Then,  $C_0 = C_1 = 0$ . Also, at  $\theta = \beta/2$ ,  $y = L/2$ . Therefore, the displacement and first and second derivatives with respect to  $\theta$  are

$$\begin{aligned}y &= 2L\left(\frac{\theta}{\beta}\right)^2 \\y' &= 4\frac{L}{\beta^2}\theta \\y'' &= 4\frac{L}{\beta^2}\end{aligned}\tag{8.3}$$

and the velocity and acceleration are

$$\begin{aligned}\dot{y} &= 4\frac{L\omega}{\beta^2}\theta \\ \ddot{y} &= 4\frac{L\omega^2}{\beta^2}\end{aligned}$$

At the point at which the curve meets the first dwell, the velocity and acceleration are continuous, but the third derivative, or jerk, is infinite. This derivative is proportional to the change in force and for high-speed cams is an important aspect of the motion. Although not so serious as having an infinite acceleration pulse, an infinite jerk can excite vibratory behavior in the system.

For the second half of the rise, the conditions to match are at  $\theta = \beta/2$ ,  $y = L/2$ , and at  $\theta = \beta$ ,  $y = L$ , and  $y' = 0$ . Then from Eqs. (8.61) and (8.62), we get

$$\begin{aligned}\frac{L}{2} &= C_0 + C_1\frac{\beta}{2} + C_2\left(\frac{\beta}{2}\right)^2 \\L &= C_0 + C_1\beta + C_2\beta^2 \\0 &= C_1 + 2C_2\beta\end{aligned}$$

The solution to this linear set of equations yields

$$\begin{aligned}C_0 &= -L \\C_1 &= \frac{4L}{\beta} \\C_2 &= -\frac{2L}{\beta^2}\end{aligned}$$

so that

$$y = L\left[1 - 2\left(1 - \frac{\theta}{\beta}\right)^2\right]\tag{8.4}$$

and

$$y' = \frac{4L}{\beta} \left( 1 - \frac{\theta}{\beta} \right)$$

$$y'' = -\frac{4L}{\beta^2}$$

Finally, the velocity, acceleration, and jerk are given by

$$\dot{y} = \frac{4L\omega}{\beta} \left( 1 - \frac{\theta}{\beta} \right)$$

$$\ddot{y} = -\frac{4L\omega^2}{\beta^2}$$

These equations apply to the segment of the program to the right of the inflection point shown in Fig. 8.11.

Graphically, the part of the curve up to the inflection point can be generated using the construction shown in Fig. 8.12. For the construction, the horizontal axis is divided into uniform increments, and the maximum rise is evenly divided into the same number of equal increments. The point at the origin is then connected to each of the points on the line of the maximum rise. Points on the displacement curve are given by the intersection of the diagonal lines with the corresponding vertical lines.

A cam return using parabolic motion is shown in Fig. 8.13. To determine the equations for the return from  $y = L$  to 0 during the angular displacement  $\beta$ , we can use Eq. (8.1) again but with different boundary conditions. To simplify the equations, we will shift the origin of the coordinate system to the end of the dwell at the beginning of the return. For the first part of the return,  $y = L$  and  $y' = 0$  at  $\theta = 0$  and  $y = L/2$  at  $\theta = \beta/2$ . For these conditions,  $C_0 = L$ ,  $C_1 = 0$ , and  $C_2 = \frac{-2L}{\beta^2}$

The displacement equation is

$$y = L \left[ 1 - 2 \left( \frac{\theta}{\beta} \right)^2 \right] \tag{8.5}$$

For the second half of the return, the conditions to match are at  $\theta = \beta/2$ ,  $y = L/2$ , and at  $\theta = \beta$ ,  $y = 0$ , and  $y' = 0$ . For these conditions,

$$y = 2L \left( 1 - \frac{\theta}{\beta} \right)^2 \tag{8.6}$$

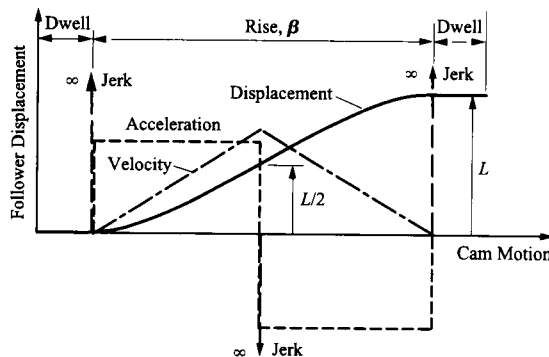


FIGURE 8.11 Displacement, velocity, acceleration, and jerk relations for parabolic motion during rise.

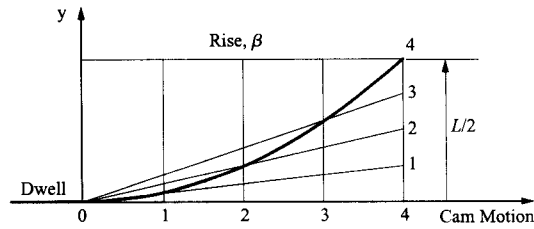


FIGURE 8.12 Construction of parabolic segment of follower-displacement program.

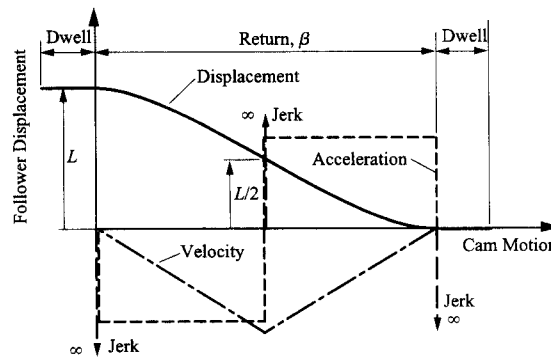


FIGURE 8.13 Displacement, velocity, acceleration, and jerk relations for parabolic motion during return.

In general, the rise and return will not always start at  $\theta = 0$ . However, in these cases, a simple coordinate transformation can be used. If the rise or return actually starts at  $\theta = \gamma$ , substitute  $(\theta - \gamma)$  wherever  $\theta$  appears in Eqs. (8.3)–(8.6).

**EXAMPLE 8.1**  
*Design for Parabolic Motion*

**Solution**

Design a parabolic cam–follower displacement program to provide a dwell at zero lift for the first  $120^\circ$  of the motion cycle and to dwell at 0.8 in lift for cam angles from  $180^\circ$  to  $210^\circ$ . The cam profile will be laid out using  $10^\circ$  plotting intervals. Assume that the cam rotates with constant angular velocity.

The motion specification is as shown in Fig. 8.14. For the first part of the rise ending at  $\phi = 150^\circ$  in the interval  $120^\circ$  to  $180^\circ$ , Eq. (8.3) applies if we use  $\theta = (\phi - 120^\circ)$  and  $0.8 = L$ . The resulting expression for the first part of the rise is

$$y = 2L \left( \frac{\theta}{\beta} \right)^2 = 1.6 \left( \frac{\phi - 120^\circ}{60^\circ} \right)^2 \tag{8.7}$$

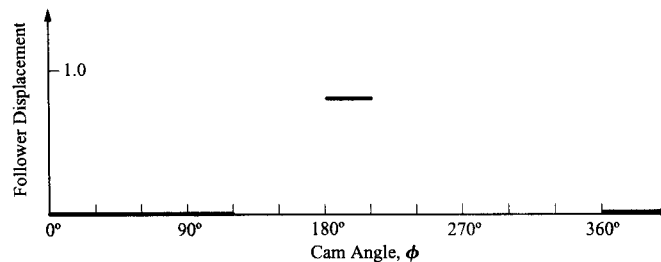


FIGURE 8.14 The motion specification for Example 8.1.

For the second part of the rise starting at  $\theta = 150^\circ$ , Eq. (8.4) applies if we use  $\theta = (\phi - 120^\circ)$  and  $0.8 = L$ . The resulting expression is

$$y = L \left[ 1 - 2 \left( 1 - \frac{\theta}{\beta} \right)^2 \right] = 0.8 \left[ 1 - 2 \left( 1 - \frac{(\phi - 120^\circ)}{60^\circ} \right)^2 \right] \tag{8.8}$$

Using Eqs. (8.7) and (8.8) produces the successive lifts given in Table 8.1. For the first part of the return ending at  $\theta = 285^\circ$  in the interval  $210^\circ$  to  $360^\circ$ , Eq. (8.5) applies if we use  $\theta = (\phi - 210^\circ)$  and  $0.8 = L$ . The resulting expression for the first part of the return is

$$y = L \left[ 1 - 2 \left( \frac{\theta}{\beta} \right)^2 \right] = 0.8 \left[ 1 - 2 \left( \frac{(\phi - 210^\circ)}{150^\circ} \right)^2 \right] \tag{8.9}$$

For the second part of the return starting at  $\theta = 285^\circ$ , Eq. (8.6) applies if we use  $\theta = (\phi - 210^\circ)$  and  $0.8 = L$ . The resulting expression is

$$y = 2L \left( 1 - \frac{\theta}{\beta} \right)^2 = 1.6 \left( 1 - \frac{\phi - 210^\circ}{150^\circ} \right)^2 \tag{8.10}$$

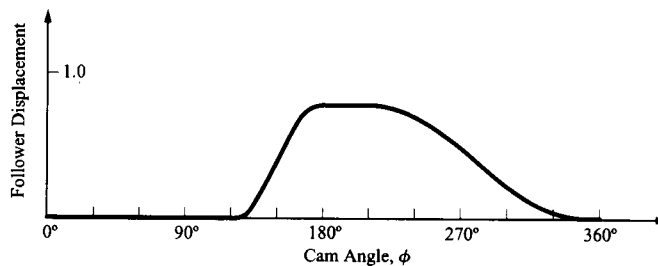
Using Eqs. (8.9) and (8.10) produces points on the return curve given in Table 8.2. The resulting transition curves are plotted in Fig. 8.15. Notice that the lift values are tabulated to four decimal places. Cam and follower systems normally use very rigid components and even small profile variations are important. For this reason, we normally work with at least four decimal places when doing cam calculations. Gears are another type of profile mechanism in which the components are very rigid and, consequently, even tiny profile variations can be important.

**TABLE 8.1 Cam-Follower Data for Rise in Example 8.1**

$\theta$	$120^\circ$	$130^\circ$	$140^\circ$	$150^\circ$	$160^\circ$	$170^\circ$	$180^\circ$
$y$	0.0000	0.0444	0.1778	0.4000	0.6222	0.7556	0.8000

**TABLE 8.2 Cam-Follower Data for Return in Example 8.1**

$\theta$	$210^\circ$	$220^\circ$	$230^\circ$	$240^\circ$	$250^\circ$	$260^\circ$	$270^\circ$	$280^\circ$
$y$	0.8000	0.7929	0.7716	0.7360	0.6862	0.6222	0.5440	0.4516
$\theta$	$290^\circ$	$300^\circ$	$310^\circ$	$320^\circ$	$330^\circ$	$340^\circ$	$350^\circ$	$360^\circ$
$y$	0.3484	0.2560	0.1778	0.1138	0.0640	0.0284	0.0071	0.0000



**FIGURE 8.15** The parabolic follower-displacement program generated in Example 8.1.



## 8.7 HARMONIC FOLLOWER-DISPLACEMENT PROGRAMS

Simple harmonic motion can be generated by an offset (eccentric) circular cam with a radial follower and is therefore a common form to use for a displacement diagram. Cams with this type of transition curve are commonly referred to as “harmonic cams.” The equations for simple harmonic motion are formed from the basic equation

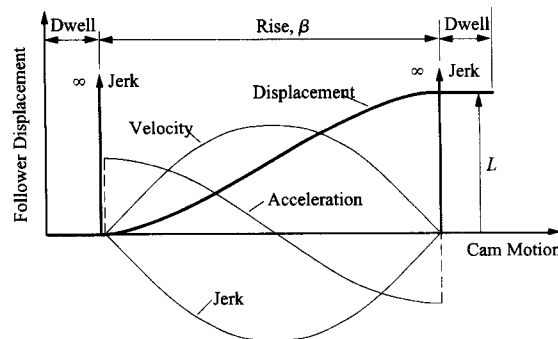
$$y = C_0 + C_1 \cos C_2 \theta = C_0 \left( 1 + \frac{C_1}{C_0} \cos C_2 \theta \right)$$

The displacement, velocity, acceleration, and jerk diagrams are shown in Fig. 8.16. Simple harmonic motion produces a sine velocity curve and a cosine acceleration curve. There is no discontinuity at the transition point, so that  $\theta$  is defined for all angles between zero and  $\beta$ . The equations for a rise starting from  $\theta = 0$  and ending at  $\theta = \beta$  and  $y = L$  are

$$\begin{aligned} y &= \frac{L}{2} \left( 1 - \cos \frac{\pi \theta}{\beta} \right) \\ y' &= \frac{\pi L}{2\beta} \sin \frac{\pi \theta}{\beta}, \quad \dot{y} = \frac{\pi L \omega}{2\beta} \sin \frac{\pi \theta}{\beta} \\ y'' &= \frac{L}{2} \left( \frac{\pi}{\beta} \right)^2 \cos \frac{\pi \theta}{\beta}, \quad \ddot{y} = \frac{L}{2} \left( \frac{\pi \omega}{\beta} \right)^2 \cos \frac{\pi \theta}{\beta} \\ y''' &= -\frac{L}{2} \left( \frac{\pi}{\beta} \right)^3 \sin \frac{\pi \theta}{\beta}, \quad \ddot{\dot{y}} = -\frac{L}{2} \left( \frac{\pi \omega}{\beta} \right)^3 \sin \frac{\pi \theta}{\beta} \end{aligned} \quad (8.11)$$

The equations for the return from  $\theta = 0, y = L$  to  $\theta = \beta, y = 0$  are

$$\begin{aligned} y &= \frac{L}{2} \left( 1 + \cos \frac{\pi \theta}{\beta} \right) \\ y' &= -\frac{\pi L}{2\beta} \sin \frac{\pi \theta}{\beta}, \quad \dot{y} = -\frac{\pi L \omega}{2\beta} \sin \frac{\pi \theta}{\beta} \end{aligned} \quad (8.12)$$



**FIGURE 8.16** Shape of the displacement, velocity, acceleration, and jerk curves for simple harmonic motion.

$$y'' = -\frac{L}{2} \left(\frac{\pi}{\beta}\right)^2 \cos \frac{\pi\theta}{\beta}, \quad \ddot{y} = -\frac{L}{2} \left(\frac{\pi\omega}{\beta}\right)^2 \cos \frac{\pi\theta}{\beta}$$

$$y''' = \frac{L}{2} \left(\frac{\pi}{\beta}\right)^3 \sin \frac{\pi\theta}{\beta}, \quad \ddot{\dot{y}} = \frac{L}{2} \left(\frac{\pi\omega}{\beta}\right)^3 \sin \frac{\pi\theta}{\beta}$$

A simple harmonic displacement diagram can be generated graphically by drawing a semicircle on the vertical axis and dividing it into an even number of segments. The cam motion axis is then divided into the same number of even increments, and horizontal lines are drawn from the points on the semicircle axis. The intersections of the horizontal lines with the corresponding vertical lines give the location of points on the simple harmonic curve. This construction is shown in Fig. 8.17. For the construction, note that

$$\frac{\Delta\alpha}{\Delta\theta} = \frac{180}{\beta}$$

where  $\beta$  is the cam rotation for the follower to move from lift 0 to  $L$ . With the advent of computers, the graphical procedure is typically used only for schematic representations of simple harmonic motion.

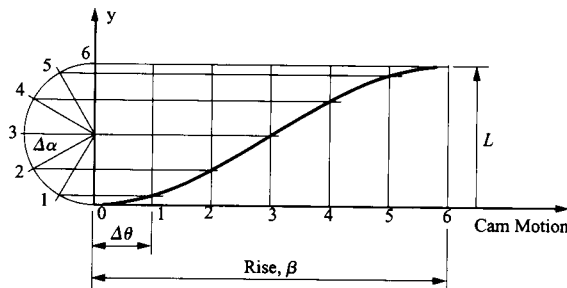


FIGURE 8.17 Graphical construction of displacement diagram for a simple harmonic rise.

**EXAMPLE 8.2**  
**Design for**  
**Harmonic Motion**

**Solution**

Design a harmonic cam to satisfy the same motion specifications as for Example 8.1. That is, the motion program is to provide a dwell at zero lift for the first  $120^\circ$  of the motion cycle and to dwell at 0.8 in lift for cam angles from  $180^\circ$  to  $210^\circ$ . The cam profile will be laid out using  $10^\circ$  plotting intervals.

The motion specification is as shown in Fig. 8.14 where  $\phi$  is the cam rotation angle.

The rise in the interval  $120^\circ$  to  $180^\circ$  can be computed using Eq. (8.11) if we use  $\theta = (\phi - 120^\circ)$  and  $0.8 = L$ . The resulting expression for the rise is

$$y = \frac{L}{2} \left(1 - \cos \frac{\pi\theta}{\beta}\right) = 0.4 \left(1 - \cos \frac{\pi(\phi - 120^\circ)}{60^\circ}\right) \tag{8.13}$$

The results are given in Table 8.3.

For the return in the interval  $210^\circ$  to  $360^\circ$ , Eq. (8.12) applies if we use  $\theta = (\phi - 210^\circ)$  and  $0.8 = L$ . The resulting expression for the return is

$$y = \frac{L}{2} \left(1 + \cos \frac{\pi\theta}{\beta}\right) = 0.4 \left(1 + \cos \frac{\pi(\phi - 210^\circ)}{150^\circ}\right) \tag{8.14}$$

Using this equation produces the successive values for  $y$  given in Table 8.4.

**TABLE 8.3 Cam-Follower Data for Rise Using Simple Harmonic Motion in Example 8.2**

$\theta$	120°	130°	140°	150°	160°	170°	180°
$y$	0.0000	0.0536	0.2000	0.4000	0.6000	0.7464	0.8000

**TABLE 8.4 Cam-follower Data for Return in Example 8.2**

$\theta$	210°	220°	230°	240°	250°	260°	270°	280°
$y$	0.8000	0.7913	0.7654	0.7236	0.6677	0.6000	0.5236	0.4418
$\theta$	290°	300°	310°	320°	330°	340°	350°	360°
$y$	0.3582	0.2764	0.2000	0.1323	0.0764	0.0346	0.0087	0.0000

The tabulated lift values may be compared with those of Example 8.1 to observe the differences between comparable parabolic and harmonic transition curves. If plotted, the follower-displacement program would be difficult to distinguish from Fig. 8.15. However, there will be important differences in the values for the derivatives.

## 8.8 CYCLOIDAL FOLLOWER-DISPLACEMENT PROGRAMS

All of the motions given so far have nonzero values of acceleration (and therefore infinite jerk) at the beginnings and ends of the motion and therefore are limited to relatively low speeds. Cycloidal motion has zero acceleration at the beginning and end of the motion and so is useful for relatively high speeds.

A cycloidal transition produces a sinusoidal acceleration curve. The equations for the rise are

$$y = L \left( \frac{\theta}{\beta} - \frac{1}{2\pi} \sin \frac{2\pi\theta}{\beta} \right)$$

$$y' = \frac{L}{\beta} \left( 1 - \cos \frac{2\pi\theta}{\beta} \right), \quad \dot{y} = \frac{L\omega}{\beta} \left( 1 - \cos \frac{2\pi\theta}{\beta} \right)$$

$$y'' = \frac{2L\pi}{\beta^2} \sin \frac{2\pi\theta}{\beta}, \quad \ddot{y} = 2L\pi \left( \frac{\omega}{\beta} \right)^2 \sin \frac{2\pi\theta}{\beta}$$

$$y''' = \frac{4L\pi^2}{\beta^3} \cos \frac{2\pi\theta}{\beta}, \quad \ddot{\dot{y}} = 4L\pi^2 \left( \frac{\omega}{\beta} \right)^3 \cos \frac{2\pi\theta}{\beta}$$

These curves are plotted in Fig. 8.18. There is no discontinuity at the inflection point, and therefore the equations are valid for values of  $\theta$  from zero to  $\beta$ . The curve is symmetric, and the return is given by  $\bar{y} = L - y$ . Therefore,  $\bar{y}' = -y'$ ,  $\bar{y}'' = -y''$ , and  $\bar{y}''' = -y'''$ .

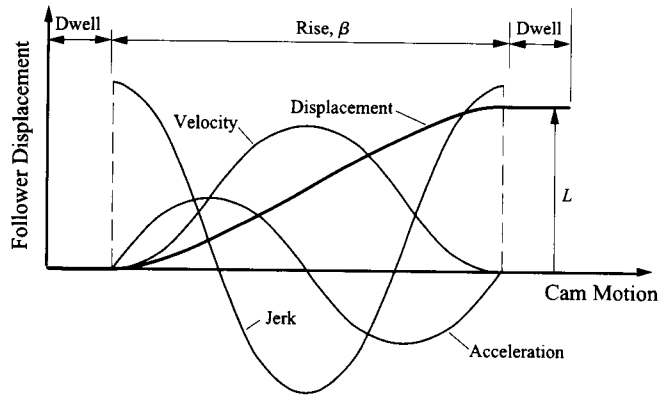


FIGURE 8.18 Shape of the displacement, velocity, acceleration, and jerk relations for cycloidal motion.

Cycloidal motion may be obtained by rolling a circle of radius  $L/2\pi$ , where  $L$  is the total rise, on the displacement axis as shown in Fig. 8.19. However, to construct the curve graphically, a more convenient, alternative way is shown in Fig. 8.19. First, a circle with diameter  $L/\pi$  and center at  $(\beta, L)$  is divided into an even number of increments, and the resulting points are projected onto the displacement axis. The cam motion axis is divided into the same number of increments. A series of lines parallel to the line from the origin to the point  $(\beta, L)$  is then drawn from the projected points on the circle diameter. The intersections of these lines with the corresponding vertical lines from the cam-motion axis give points on the cycloidal curve.

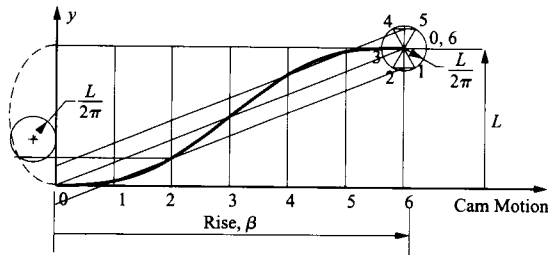


FIGURE 8.19 Graphical construction of displacement diagram for cycloidal motion.

## 8.9 GENERAL POLYNOMIAL FOLLOWER-DISPLACEMENT PROGRAMS

For high-speed machines, it is common to specify a general polynomial profile for a cam. Depending on the order of the polynomial chosen, it is theoretically possible to match almost any conditions posed by the designer. A polynomial curve is fitted to the rise or return. Only odd-order polynomials are appropriate for rises or returns between dwells if the same conditions are to be matched at both ends of the polynomial. A first-order polynomial gives constant velocity and infinite acceleration at the beginning and end of the transition. This is the uniform motion profile discussed previously. A third-order polynomial gives a parabolic velocity variation, linear acceleration, and infinite jerk at the beginning and end

of the transition. A fifth-order polynomial gives finite acceleration and jerk. The derivative of jerk is infinite at the ends of the transition. A fifth-order fit is the practical maximum unless great care is taken during manufacturing. Dynamic effects resulting from manufacturing errors tend to become more important than those from curve fitting at this stage.

For a general polynomial follower displacement, the displacement function is given by

$$y = f(\theta) = \sum_{i=0}^n A_i \theta^i$$

where  $\theta$  is the cam angle, and the  $A$ 's must be determined from the conditions to be matched. The equation permits us to match the same number of conditions as there are  $A$ 's, that is,  $n + 1$  conditions. When  $n$  is large and the angles are measured in degrees, the terms in the summation can vary greatly in size. For example, if  $\theta$  is  $100^\circ$  and  $n$  is 10, the coefficients of  $\theta^i$  in the equation can vary hugely, and round-off error will make it difficult to obtain an accurate solution. Therefore, it is convenient to rewrite the displacement equation in terms of the cam rotation angle  $\beta$ , which gives the range over which the equation is to be used. The resulting equation is

$$y = f(\theta) = \sum_{i=0}^n C_i \left(\frac{\theta}{\beta}\right)^i$$

Now the coefficients of the constants are always numbers between 0 and 1, and round-off error problems have been greatly reduced. The constants in the two equations are related by the simple expression

$$A_i = \frac{C_i}{\beta^i}$$

The conditions to be matched will typically involve at least the velocity and acceleration of the follower, and the required equations for these conditions can be written as

$$\dot{y} = \dot{f}(\theta) = \frac{1}{\beta} \frac{d\theta}{dt} \sum_{i=1}^n i C_i \left(\frac{\theta}{\beta}\right)^{(i-1)}$$

and

$$\ddot{y} = \ddot{f}(\theta) = \frac{1}{\beta} \frac{d^2\theta}{dt^2} \sum_{i=1}^n i C_i \left(\frac{\theta}{\beta}\right)^{(i-1)} + \frac{1}{\beta^2} \left(\frac{d\theta}{dt}\right)^2 \sum_{i=2}^n i(i-1) C_i \left(\frac{\theta}{\beta}\right)^{(i-2)}$$

Notice that the summation on the velocity term starts at 1 because  $C_0$  does not appear in the equation, and the summation on the acceleration term starts at 2 because neither  $C_0$  nor  $C_1$  appears in the acceleration equation.

Now if a constant-velocity cam is used,

$$\frac{d\theta}{dt} = \omega$$

and

$$\frac{d^2\theta}{dt^2} = 0$$

where  $\omega$  is the angular velocity of the cam. The follower equations may then be written as the following:

$$y = f(\theta) = \sum_{i=1}^n C_i \left( \frac{\theta}{\beta} \right)^i$$

$$\dot{y} = \dot{f}(\theta) = \frac{\omega}{\beta} \sum_{i=1}^n i C_i \left( \frac{\theta}{\beta} \right)^{(i-1)}$$

$$\ddot{y} = \ddot{f}(\theta) = \left( \frac{\omega}{\beta} \right)^2 \sum_{i=2}^n i(i-1) C_i \left( \frac{\theta}{\beta} \right)^{(i-2)}$$

$$\ddot{\ddot{y}} = \ddot{\ddot{f}}(\theta) = \left( \frac{\omega}{\beta} \right)^3 \sum_{i=3}^n i(i-1)(i-2) C_i \left( \frac{\theta}{\beta} \right)^{(i-3)}$$

As an example of the use of the polynomial profile, assume that we begin and end the follower displacement with a dwell as shown in Fig. 8.20 and assume that we want to match the position, velocity, and acceleration at both the beginning and end of the period being considered.

For points  $A$  and  $B$  in Fig. 8.20, the following conditions apply:

$$\theta = 0 \Rightarrow y = \dot{y} = \ddot{y} = 0$$

$$\theta = \beta \Rightarrow y = L$$

$$\dot{y} = \ddot{y} = 0$$

There are six conditions, so the position equation must have six constants. The resulting equations for position, velocity, and acceleration are

$$y = C_0 + C_1 \left( \frac{\theta}{\beta} \right) + C_2 \left( \frac{\theta}{\beta} \right)^2 + C_3 \left( \frac{\theta}{\beta} \right)^3 + C_4 \left( \frac{\theta}{\beta} \right)^4 + C_5 \left( \frac{\theta}{\beta} \right)^5$$

$$\dot{y} = \frac{\omega}{\beta} \left[ C_1 + 2C_2 \left( \frac{\theta}{\beta} \right) + 3C_3 \left( \frac{\theta}{\beta} \right)^2 + 4C_4 \left( \frac{\theta}{\beta} \right)^3 + 5C_5 \left( \frac{\theta}{\beta} \right)^4 \right]$$

$$\ddot{y} = \left( \frac{\omega}{\beta} \right)^2 \left[ 2C_2 + 6C_3 \left( \frac{\theta}{\beta} \right) + 12C_4 \left( \frac{\theta}{\beta} \right)^2 + 20C_5 \left( \frac{\theta}{\beta} \right)^3 \right]$$

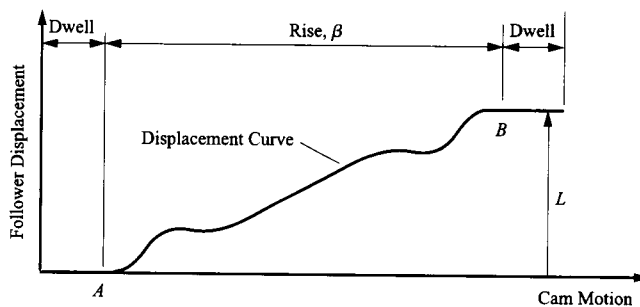


FIGURE 8.20 Initial information for polynomial profile example.

Evaluation of these equations at the beginning and end of the rise period gives the following six equations that must be solved:

$$0 = C_0$$

$$0 = \frac{\omega}{\beta} C_1$$

$$0 = \left(\frac{\omega}{\beta}\right)^2 2C_2$$

$$L = C_0 + C_1 + C_2 + C_3 + C_4 + C_5$$

$$0 = \frac{\omega}{\beta} [C_1 + 2C_2 + 3C_3 + 4C_4 + 5C_5]$$

$$0 = \left(\frac{\omega}{\beta}\right)^2 [2C_2 + 6C_3 + 12C_4 + 20C_5]$$

Solution for the unknown constants  $C_0$  through  $C_6$  gives

$$C_0 = C_1 = C_2 = 0$$

$$C_3 = 10L, \quad C_4 = -15L, \quad C_5 = 6L$$

The displacement equation can then be written in the form

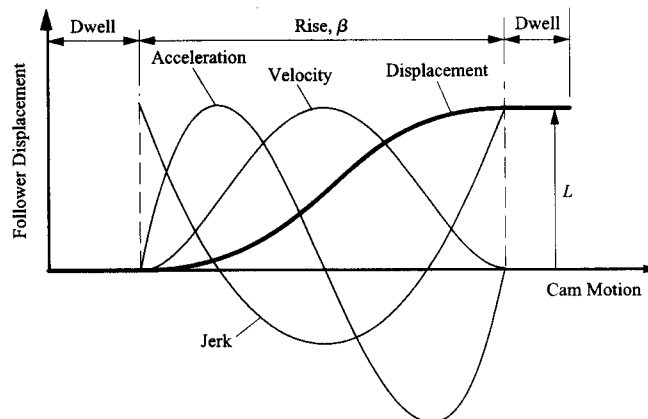
$$y = 10L \left(\frac{\theta}{\beta}\right)^3 - 15L \left(\frac{\theta}{\beta}\right)^4 + 6L \left(\frac{\theta}{\beta}\right)^5$$

This is called the 3-4-5 polynomial transition because of the powers of the terms that remain in the expression. The first three derivatives and the velocity, acceleration, and jerk are given by

$$y' = \frac{30L}{\beta} \left[ \left(\frac{\theta}{\beta}\right)^2 - 2\left(\frac{\theta}{\beta}\right)^3 + \left(\frac{\theta}{\beta}\right)^4 \right], \quad \dot{y} = \frac{30\omega L}{\beta} \left[ \left(\frac{\theta}{\beta}\right)^2 - 2\left(\frac{\theta}{\beta}\right)^3 + \left(\frac{\theta}{\beta}\right)^4 \right]$$

$$y'' = \frac{60L}{\beta^2} \left[ \left(\frac{\theta}{\beta}\right) - 3\left(\frac{\theta}{\beta}\right)^2 + 2\left(\frac{\theta}{\beta}\right)^3 \right], \quad \ddot{y} = 60L \left(\frac{\omega}{\beta}\right)^2 \left[ \left(\frac{\theta}{\beta}\right) - 3\left(\frac{\theta}{\beta}\right)^2 + 2\left(\frac{\theta}{\beta}\right)^3 \right]$$

$$y''' = \frac{60L}{\beta^3} \left[ 1 - 6\left(\frac{\theta}{\beta}\right) + 6\left(\frac{\theta}{\beta}\right)^2 \right], \quad \ddot{\dot{y}} = 60L \left(\frac{\omega}{\beta}\right)^3 \left[ 1 - 6\left(\frac{\theta}{\beta}\right) + 6\left(\frac{\theta}{\beta}\right)^2 \right]$$



**FIGURE 8.21** Shape of the displacement, velocity, acceleration, and jerk relations for the 3-4-5 polynomial motion.

These general relationships are plotted in Fig. 8.21. The displacement results are visually similar to the cycloidal curve, but the velocity, acceleration, and jerk are somewhat different. In general, this type of cam will begin and end its motion more slowly than the other types, and to produce such a cam, extreme machining accuracy is required, especially at the beginning and end of the motion. The machining is commonly done on a computer numerically controlled (CNC) milling machine.

**TABLE 8.5 Comparison of the Different Types of Cam-Follower Motion for  $\beta = L = 1$**

$\theta$	$y$ (linear)	$y$ (parabolic)	$y$ (harmonic)	$y$ (cycloidal)	$y$ (polynomial)
0.00	0.0000	0.0000	0.0000	0.0000	0.0000
0.05	0.0500	0.0050	0.0062	0.0008	0.0012
0.10	0.1000	0.0200	0.0245	0.0065	0.0086
0.15	0.1500	0.0450	0.0545	0.0212	0.0266
0.20	0.2000	0.0800	0.0955	0.0486	0.0579
0.25	0.2500	0.1250	0.1464	0.0908	0.1035
0.30	0.3000	0.1800	0.2061	0.1486	0.1631
0.35	0.3500	0.2450	0.2730	0.2212	0.2352
0.40	0.4000	0.3200	0.3455	0.3065	0.3174
0.45	0.4500	0.4050	0.4218	0.4008	0.4069
0.50	0.5000	0.5000	0.5000	0.5000	0.5000
0.55	0.5500	0.5950	0.5782	0.5992	0.5931
0.60	0.6000	0.6800	0.6545	0.6935	0.6826
0.65	0.6500	0.7550	0.7270	0.7788	0.7648
0.70	0.7000	0.8200	0.7939	0.8514	0.8369
0.75	0.7500	0.8750	0.8536	0.9092	0.8965
0.80	0.8000	0.9200	0.9045	0.9514	0.9421
0.85	0.8500	0.9550	0.9455	0.9788	0.9734
0.90	0.9000	0.9800	0.9755	0.9935	0.9914
0.95	0.9500	0.9950	0.9938	0.9992	0.9988
1.00	1.0000	1.0000	1.0000	1.0000	1.0000

To compare the profiles generated by the different follower-displacement programs, let  $\beta = L = 1$ , and vary  $\theta$  from 0 to  $\beta$ . We can then compute  $y$  as a function of  $\theta$  in increments of 0.05. The results are shown in Table 8.5. Notice that the variation among the different profiles is very small in most cases. This emphasizes that extreme accuracy must be achieved if the benefits of using the different follower-displacement programs are to be realized.

## 8.10 DETERMINING THE CAM PROFILE

Once the follower motion is determined as a function of the cam displacement, the cam surface can be found either graphically or analytically. For extremely accurate cams, the geometry must be determined analytically and the machining must be done using CNC milling machines. For low-speed cams, however, a graphical layout and manual machining are adequate.



In both the graphical and analytical approaches to determining the cam geometry, the cam mechanism must be inverted. That is, the cam is taken as the reference system, and the frame and follower are considered to move relative to the cam. To maintain the correct relative motion, the follower will move relative to the cam in a direction opposite to the motion of the cam relative to the follower.

If we restrict our discussions to planar, rotating cams, four general types of followers are possible: (a) a translating cylindrical-faced follower, (b) a translating flat-faced follower, (c) a rotating cylindrical-faced follower, and (d) a rotating flat-faced follower (Fig. 8.22).

Notice that the cam geometry is independent of the type of joint between the cylindrical-faced follower and the cam. The kinematic design procedure is exactly the same when a roller follower or a solid cylindrical-faced follower is involved. We will consider both graphical and analytical approaches to the design of the cam for each type of follower shown in Fig. 8.22.

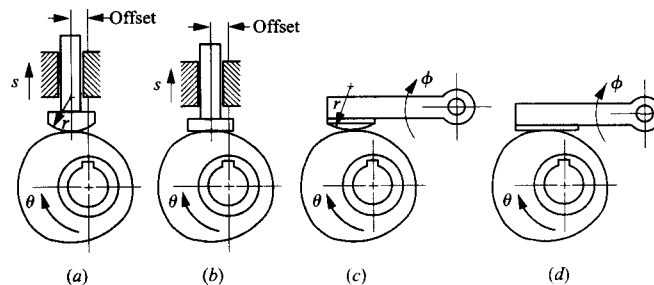
### 8.10.1 Graphical Cam Profile Layout

As already indicated, cam profiles are laid out graphically using inversion. That is, the cam is viewed as stationary, and the successive positions of the follower are located relative to it. This results in a polar plot of successive follower positions. The cam profile is then filled in as the envelope curve of the follower positions.

The first step in laying out the cam profile is to select a base circle radius. The base circle represents the position of the follower at zero lift. Successive lift values are plotted radially outward from the base circle.

Choosing a large base circle radius results in a large cam. However, if the base circle is too small the cam profile may have hollows of smaller radius than the follower. Since the follower will bridge across such a hollow, it will not follow the desired lift program. Obviously, this situation must be avoided, and it is therefore necessary to have a means of computing the radius of curvature of the cam at different locations.

The pressure angle of a cam is the angle between the contact normal and the velocity of the point on the follower at the contact location. Reducing the pressure angle reduces the contact loads and promotes smoother operation with less wear. Increasing the base circle radius decreases the maximum value of pressure angle. Thus, it is good practice to use the largest base circle that the design constraints will allow. As a general rule of thumb, the base circle radius should be two to three times the maximum lift value.



**FIGURE 8.22** Common follower configurations for planar, rotating cams. (a) Translating cylindrical-faced follower; (b) translating flat-faced follower; (c) rotating cylindrical-faced follower; (d) rotating flat-faced follower.

#### **EXAMPLE 8.3** **Layout of a Cam** **Profile for a Radial** **Roller Follower**

Lay out a cam profile using the harmonic follower displacement profile of Example 8.2. That is, the follower is to dwell at zero lift for the first  $120^\circ$  of the motion cycle and to dwell at 0.8 in lift for cam angles from  $180^\circ$  to  $210^\circ$ . The cam is to have a translating, roller follower with a 1-in roller diameter. The cam will rotate clockwise. Lay out the cam profile using  $10^\circ$  plotting intervals.

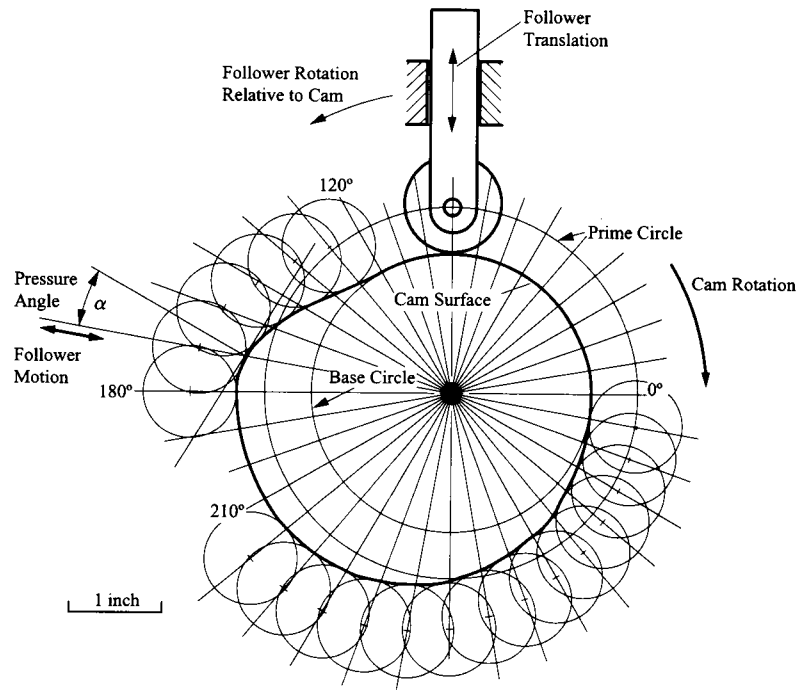
**Solution**

The basic motion specification is as shown in Fig. 8.15. Using the results of Example 8.2 produces the lift values to be plotted given in Table 8.6. Notice that the dwells correspond to locations on the cam where the radius is constant.

**TABLE 8.6 Follower Displacements for Example 8.3**

$\theta$	0, 360°	10°	20°	30°	40°	50°	60°	70°	80°
$y$	0.0000	0.0000	0.0000	0.0000	0.0000	0.0000	0.0000	0.0000	0.0000
$\theta$	90°	100°	110°	120°	130°	140° <td 150°	160°	170°	
$y$	0.0000	0.0000	0.0000	0.0000	0.0536	0.2000	0.4000	0.6000	0.7464
$\theta$	180°	190°	200°	210°	220°	230°	240°	250°	260°
$y$	0.8000	0.8000	0.8000	0.8000	0.7913	0.7654	0.7236	0.6677	0.6000
$\theta$	270°	280°	290°	300°	310°	320°	330°	340°	350°
$y$	0.5236	0.4418	0.3582	0.2764	0.2000	0.1323	0.0764	0.0346	0.0087

The layout of the cam is accomplished by drawing radial lines at 10° increments. Because the cam rotates clockwise, the radial lines are laid off and labeled in the counterclockwise direction, as shown in Fig. 8.23. Next, the base circle and the prime circle are drawn. The *base circle* is chosen to have a 1.5-in radius, and it is the largest circle that can be drawn inside the cam profile and be tangent to the cam profile. The radius of the *prime circle* is equal to  $r_b + r_0$  where  $r_b$  is the base circle radius and  $r_0$  is the radius of the roller follower. In this problem, the prime-circle radius is 2.0 in. The cam profile is initially laid off from the prime circle to give the pitch curve. The *pitch curve* is the curve traced by the center of the roller follower. Notice that the pitch curve will be the cam profile if  $r_0$  is zero. This corresponds to the case of a knife-edged follower.



**FIGURE 8.23** Layout of the cam profile for Example 8.3. The process of laying out a cam profile is one of inversion. That is, the cam is viewed as being stationary, and successive positions of the follower are plotted relative to it. In this case, a prime circle of 2.0-in radius was chosen. This represents the location of the follower center at zero lift. Positive lift values are plotted outward from the base circle. The successive positions of the follower are then drawn using the plotted points as centers. Finally, the profile is plotted as an envelope curve of the successive follower positions. Because of the inversion, if the cam is to rotate clockwise, the positions of the follower must be plotted in the opposite direction, that is, counterclockwise.

Once the radial lines and prime circle are established, the displacements can be laid off from the prime circle as shown in Fig. 8.23. The radius of the follower is drawn with its center located on the pitch curve at a series of locations. The cam can be defined by drawing a curve tangent to roller locations as shown in Fig. 8.23.

As indicated before, an important parameter for cam motion is the pressure angle. In the case of the translating, roller follower, this is the angle between the direction of the follower travel and the normal to the curve. For a given force on the follower roller, the force in the direction of travel of the follower will be proportional to the cosine of the pressure angle. The force normal to the travel of the follower is proportional to the sine of the pressure angle. Wear on the follower stem will increase with the normal force. Therefore, from design considerations, we want the pressure angle ( $\alpha$ ) to be as small as possible.

The maximum pressure angle will occur at the *pitch points*. These correspond to the inflection points on the follower displacement curves (see Fig. 8.8). If the torque on the cam is more or less constant, the pressure angles at the pitch points will correspond to the parts of the cycle where the maximum normal force occurs and hence the times when the follower stem wear will be greatest. It will also correspond to the parts of the cycle where the follower will tend to bind in the stem bearing. Because of problems with wear and binding, the pressure angle is usually limited to angles on the order of  $\pm 30^\circ$ . If the pressure angle becomes excessive, the base circle should be increased or the follower-displacement profile should be changed.

The problem statement indicated that a roller follower was to be designed. However, the construction would be *exactly* the same if a solid cylindrical-faced follower were involved. From the standpoint of the cam geometry, the important issues are the radius of the cylindrical face and the direction of translation relative to the cam.

**EXAMPLE 8.4**  
**Layout of a Cam**  
**Profile for a Radial**  
**Flat-Faced**  
**Follower**

**Solution**

Again, lay out a cam profile using the harmonic displacement profile of Examples 8.2 and 8.3. The cam is to have a translating flat-faced follower that is offset by 0.2 in. The cam will rotate clockwise. Lay out the cam profile using  $10^\circ$  plotting intervals.

The basic motion specification is the same as in Example 8.3 (Table 8.6). The layout of the cam is again accomplished by drawing radial lines at  $10^\circ$  increments. Because the cam rotates clockwise, the radial lines are laid off and labeled in the counterclockwise direction as was done in Fig. 8.23. Next the base circle is drawn. Because a flat-faced follower is being designed, there is no prime circle. However, selection of the base circle requires careful consideration.

A major restriction on the cam profile driving a flat-faced follower is that the profile must form a convex surface. This means that the vectors from every point on the cam to the corresponding center of curvature must point toward the interior of the cam. An alternative way to approach the convexity problem is to imagine an arbitrary line drawn across the face of the cam. If it is possible to select an arbitrary line that intersects the cam at more than two points, the cam profile is not convex. If the cam is not convex, the flat-faced follower cannot contact the cam at all points, and the desired motion will not be generated. This condition will be illustrated mathematically when an analytical approach to cam synthesis is discussed. Clearly, the cam generated in Fig. 8.23 does not satisfy the convexity condition; however, this is not necessarily an issue with roller followers. When the resulting cam is not convex for flat-faced followers, we must increase the size of the base circle or change the follower-displacement function. The effect of changing the base circle can be easily investigated by running one of the cam design programs supplied on the disk with this book.

To begin the construction, we can select a base circle somewhat arbitrarily. However, if the radius of curvature at some location on the resulting cam is too small, the base circle diameter must be increased.

The follower is offset, but this does not affect the geometry of the cam. All points on the follower have the same velocity because its motion is pure translation. Therefore, from a kinematic standpoint, the actual location of the follower stem is not important. From a machine design standpoint it is important, however, because the larger the offset, the higher the moment on the follower stem.

We can lay off the displacements in Table 8.6 from the base circle and along the radial lines. At each of these locations on the radial lines, draw a line perpendicular to each radial line. These perpendicular lines correspond to the face of the follower. This is illustrated in Fig. 8.24. The lines for different positions of the follower will form an envelope that defines the geometry of the cam surface. We construct the outline of the cam by drawing a curve that contacts the lines corresponding to the different positions of the follower face at the tangent points.

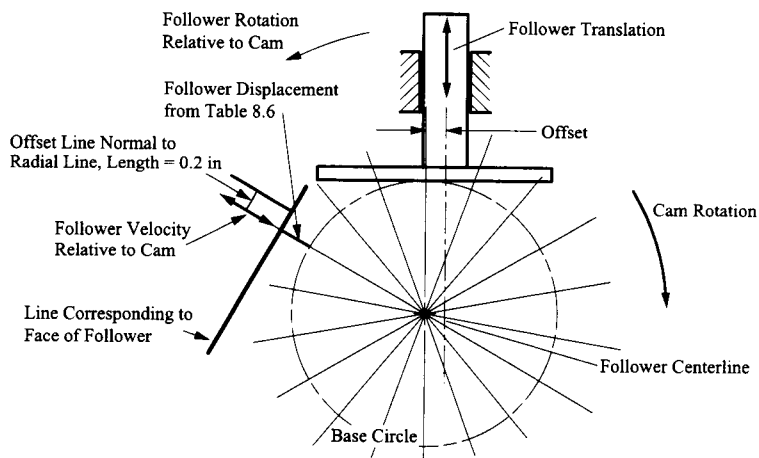


FIGURE 8.24 Basic construction lines for determining the cam profile for a flat-faced follower.

As the lines corresponding to the different positions of the follower face are drawn, successive lines will intersect. For the geometry to be valid, the angle increment for successive intersections must be positive. If an intersection requires a negative angle increment, it will not be possible to generate the cam, and a larger base circle must be used. This situation is illustrated in the current problem in Fig. 8.25 for the positions corresponding to rotation angles of  $150^\circ$ ,  $160^\circ$ ,  $170^\circ$ , and  $180^\circ$ . In Fig. 8.25, a base circle radius of 1.5 in was chosen. The angle increment for the intersection corresponding to  $160^\circ$  and  $170^\circ$  is positive, but the increment corresponding to  $170^\circ$  and  $180^\circ$  is negative. This situation makes the cam nonconvex and indicates that the base circle is too small and must be increased.

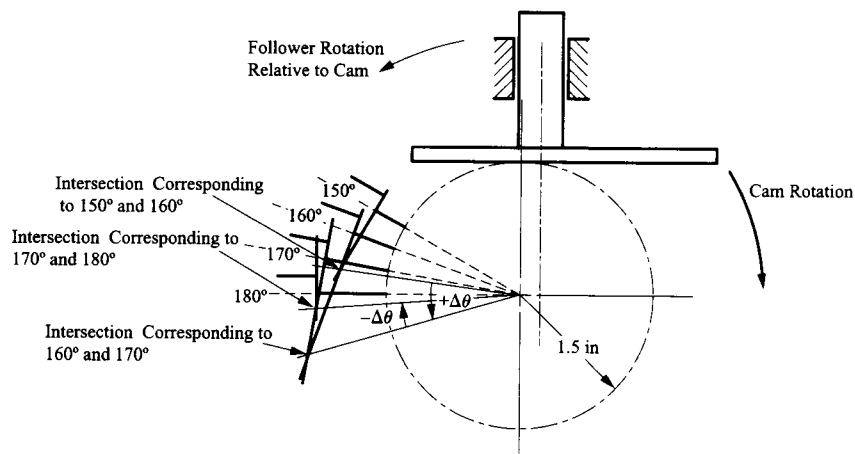
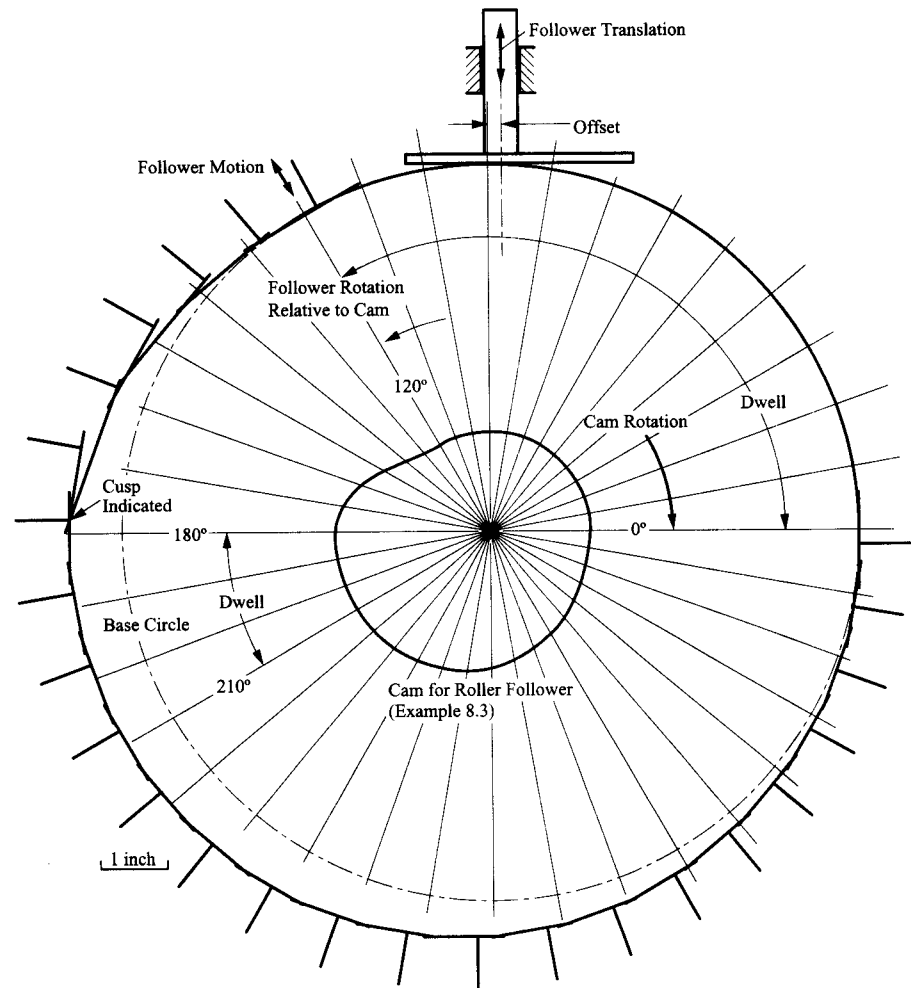


FIGURE 8.25 Condition when the base circle is too small to generate an acceptable cam for a flat-faced follower.

The smallest base circle is the one for which the angle increment corresponding to  $170^\circ$  and  $180^\circ$  is no longer negative, that is, when it is zero. This occurs when the follower-face lines corresponding to  $160^\circ$ ,  $170^\circ$ , and  $180^\circ$  intersect. This occurs for a base circle radius of approximately 5.5 in. For this base circle, the cam will have a point or cusp corresponding to the location where the face lines intersect. The envelope of the face lines and the resulting cam is shown in Fig. 8.26. The cam designed for the roller follower and for the same displacement profile is also shown in Fig. 8.26 for comparison. Based on the size of the cam required, a flat-faced follower would not be a good choice for this type of displacement profile.

After the follower-face locations are found, the stem locations can be shown by drawing parallel lines to the radial lines. These are also shown in Fig. 8.26.

As indicated before, an important parameter for cam motion is the pressure angle. When a flat-faced follower is used, the normal to the follower profile is always in the direction of the follower travel if the follower face is perpendicular to the stem. This makes the pressure angle always zero; however, there can be significant lateral loads on the follower bearings caused by the frictional force



**FIGURE 8.26** Envelope generated by drawing lines corresponding to the follower face for Example 8.4. The base circle is the minimum possible for the flat-faced follower to generate the profile indicated in Table 8.6. The cam generated for the roller follower in Example 8.3 is included for comparison.

at the cam–follower interface and by the moment generated by the normal force at the cam–follower interface and the offset line of action. The friction force can be reduced by lubrication but never completely eliminated, and the bearing couple that opposes the moment from the normal force must be addressed in the design of the cam and follower system. Depending on the lubrication and design, the lateral forces can be as high as or higher than the corresponding lateral force with a roller follower. Also, the cam may be so large that, to avoid the convexity condition, the roller follower would be preferred from size considerations.

Another important parameter that must be determined for the design of a cam for a flat-faced follower is the size (length) of the follower face. It is essential that the face be long enough on both sides to maintain contact with the cam on a tangent line. The minimum length of the follower face can be established by direct measurement. The actual length would be equal to the minimum length plus a small increment.

**EXAMPLE 8.5**  
**Layout of a Cam**  
**Profile for an**  
**Oscillating**  
**Cylindrical**  
**Follower**

**Solution**

Lay out a cam profile assuming that the follower starts from a dwell for 0° to 120° of cam rotation, and the cam rotates clockwise. The rise occurs during the cam rotation from 120° to 200°. The follower then dwells for 40° of cam rotation, and the return occurs for the cam rotation from 240° to 360°. The amplitude of the follower rotation is 30°, and the follower radius is 0.75 in. Lay out the cam profile using 20° plotting intervals. (This plotting interval is too coarse for the development of an accurate cam; however, it will be used to simplify the resulting drawing.)

The basic motion specification is visually similar to that shown in Fig. 8.15; however, the follower motion is a rotation instead of a translation. To begin the design, we must determine the follower rotation,  $\phi$ , as a function of the cam rotation,  $\theta$ . Assume parabolic motion for the follower. From section 8.6, the equations for each part of the motion are

$$0 < \theta \leq 120^\circ: \quad \phi = 0$$

$$120^\circ \leq \theta \leq 160^\circ: \quad \phi = 2L \left( \frac{\Delta\theta}{\beta} \right)^2 = 60 \left( \frac{\theta - 120^\circ}{80^\circ} \right)^2$$

$$160^\circ \leq \theta \leq 200^\circ: \quad \phi = L \left[ 1 - 2 \left( 1 - \frac{\Delta\theta}{\beta} \right)^2 \right] = 30 \left[ 1 - 2 \left( 1 - \frac{\theta - 120^\circ}{80^\circ} \right)^2 \right]$$

$$200^\circ \leq \theta \leq 240^\circ: \quad \phi = 30^\circ$$

$$240^\circ \leq \theta \leq 300^\circ: \quad \phi = L \left[ 1 - 2 \left( \frac{\Delta\theta}{\beta} \right)^2 \right] = 30 \left[ 1 - 2 \left( \frac{\theta - 240^\circ}{120^\circ} \right)^2 \right]$$

$$300^\circ \leq \theta \leq 360^\circ: \quad \phi = 2L \left( 1 - \frac{\Delta\theta}{\beta} \right)^2 = 60 \left( 1 - \frac{\theta - 240^\circ}{120^\circ} \right)^2$$

Here,  $L$  is treated as the generic amplitude of the follower motion. In this case,  $L$  is given as 30°.

Using these equations provides the lift values to be plotted given in Table 8.7. Notice that the dwells correspond to locations on the cam where the radius is constant.

**TABLE 8.7 Follower Displacements for Example 8.5**

$\theta$	0, 360°	20°	40°	60°	80°	100°	120°	140°	160°
$y$	0.0000	0.0000	0.0000	0.0000	0.0000	0.0000	0.0000	3.7500°	15.0000°
$\theta$	180°	200°	220°	240°	260°	280°	300°	320°	340°
$y$	26.2500°	30.0000°	30.0000°	30.0000°	28.3333°	23.3333°	15.0000°	6.6666°	1.6666°

The cam-follower system is similar to that shown in Fig. 8.27, and the points shown in Fig. 8.27 will be used to describe the layout of the cam. In particular,  $A$  is the location of the axis of rotation of the cam,  $B$  is the center of curvature of the follower, and  $C$  is the rotation axis of the follower.

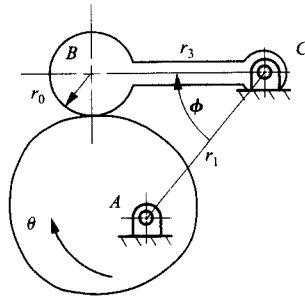


FIGURE 8.27 Cam-follower system to be designed in Example 8.5.

The first step in the cam layout is to draw the base circle and prime circle. The *base circle* is chosen to have a 1.25-in radius, and the radius of the *prime circle* is equal to  $r_b + r_0 = 1.25 + 0.75 = 2.0$  in. The base circle radius is the radius of the cam during the dwell for the first  $120^\circ$  of cam rotation.

The second step is to select the distance from the cam rotation axis to the pivot of the follower ( $AC$ ). The larger the value chosen, the smaller will be the pressure angle; however, this distance also directly affects the size of the cam-follower system. We will choose the distance between pivots to be 4 in. When we invert the motion, the follower pivot will appear to rotate around the cam. Therefore, we must draw a circle with a radius of 4 in about the cam for the follower pivot circle. The pivot circle is shown in Fig. 8.28.

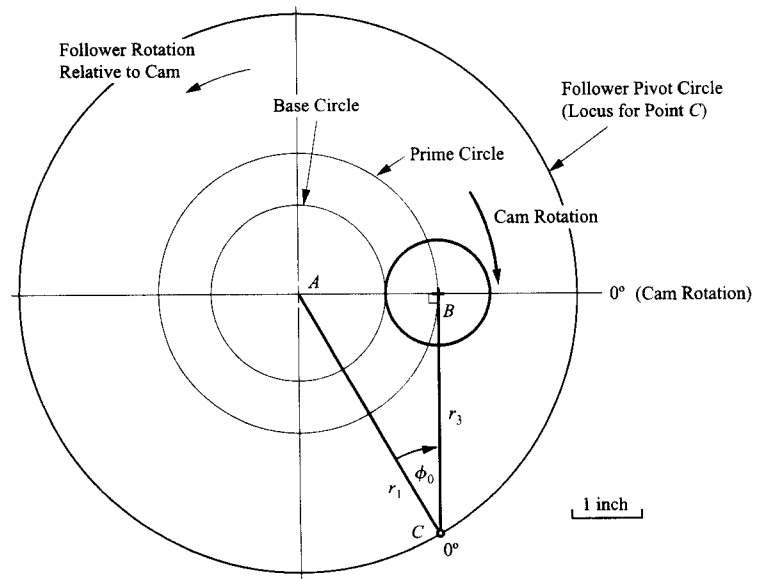


FIGURE 8.28 Location of the follower in the initial position. This determines the reference angle  $\phi_0$ .

The third step is to determine the length of the follower ( $BC = r_3$ ) and the reference angle  $\phi_0$  for  $\phi$ . We will locate the follower in the initial dwell position in such a way that the pressure angle is zero. This is done by drawing a line tangent to the prime circle through the ray corresponding to  $\theta = 0$ . The intersection of this tangent line with the follower pivot circle will give the location of the follower pivot for the initial position of the cam. Two intersections will be given. One will correspond to a CW rotation of the follower, and the second will correspond to a CCW rotation. Based on the problem statement, we will choose the intersection corresponding to the CW rotation as shown in Fig. 8.28. Because a right triangle is involved, the follower length is given by

$$r_3 = \sqrt{r_1^2 - (r_b + r_0)^2} = \sqrt{4^2 - 2^2} = 3.464$$

We also need to determine the base angle,  $\phi_0$ , because all subsequent displacements of the follower will be measured relative to this angle. If we let the distance between the cam and follower pivots be  $r_1$ , the angle  $\phi_0$  is given directly by

$$\phi_0 = \tan^{-1} \left( \frac{r_b + r_0}{r_3} \right) = \tan^{-1} \left( \frac{2}{3.464} \right) = 30.000^\circ$$

The location of pivot  $C$  for the follower when the cam angle is  $0^\circ$  gives the first position of the follower pivot. Subsequent positions of the pivot will be at angle increments of  $20^\circ$ . Therefore, the fourth step in the cam layout is to draw radial lines at  $20^\circ$  increments from the cam rotation axis to the follower pivot circle starting from the initial position of  $AC$  corresponding to the cam rotation angle of  $0^\circ$ . Label the radial lines corresponding to the beginning and end of dwells. These radial lines are shown in Fig. 8.29.

The fifth step is to draw a line tangent to the prime circle from the intersection of the radial lines and the follower pivot circle, as shown in Fig. 8.29. These lines give the position of the follower relative to the cam, if the cam is a simple cylinder. These lines will give the base lines from which to measure the  $\phi$  angles given in Table 8.7. Next lay off lines 3.464-in long at the angles indicated in Table 8.7 from the corresponding base lines. The ends of these lines will be the centers of the cylindrical cam follower in the different positions. Draw circles corresponding to the follower, and construct the cam surface tangent to the follower positions. The final cam is shown in Fig. 8.29.

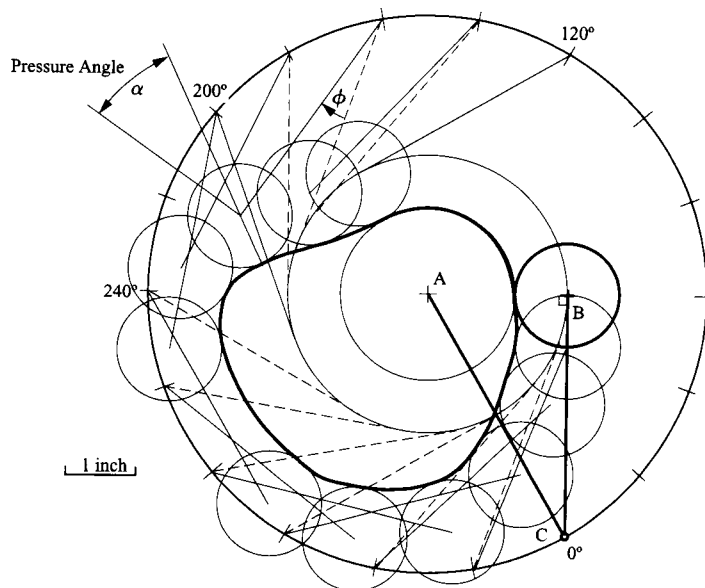


FIGURE 8.29 Final layout of the cam profile for Example 8.5.



As in the case of an axial roller follower, an important parameter for cam motion is the pressure angle. For the oscillating cylindrical follower, this is the angle between the velocity of the contact point on the follower (vector normal to line from contact point and point  $C$ ) and the normal to the cam at the contact point. To reduce wear on the follower pivot, we want the pressure angle to be as small as possible. In the design shown in Fig. 8.29, the pressure angle will become fairly high ( $\alpha > 30^\circ$ ) in the rise region. To improve the design, the diameter of the base circle should be increased.

The problem statement indicated that a cylindrical follower was to be designed. However, the construction would be *exactly* the same if a roller follower were involved. From the standpoint of the cam geometry, the important issues are the radius of the cylindrical face and the direction of motion relative to the cam.

**EXAMPLE 8.6**  
**Layout of the**  
**Cam Profile for**  
**an Oscillating,**  
**Flat-Faced**  
**Follower**

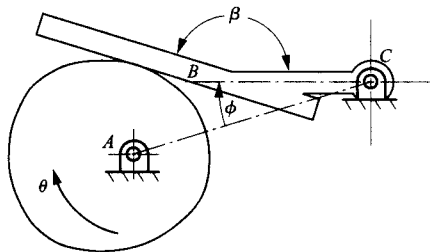
**Solution**

Lay out the rise portion of the cam profile for the follower motion indicated in Table 8.7. The cam will rotate *counterclockwise*. Assume that the follower face angle is  $170^\circ$ , and lay out the cam profile using  $20^\circ$  plotting intervals. Again, this plotting interval is too coarse for an accurate cam; however, it will be used to illustrate the procedure.

The cam–follower system is similar to that shown in Fig. 8.30, and the points shown in that figure will be used to describe the layout of the cam. Point  $A$  is the location of the axis of rotation of the cam,  $C$  is the rotation axis of the follower, and  $\beta$  is the follower face angle. Point  $B$  is the location of the intersection of the centerline of the follower stem with the face of the follower.

The first step in the cam layout is to select and draw the base circle. The base circle is chosen to be 2.0 in.

The second step is to select the distance from the cam rotation axis to the pivot of the follower ( $AC$ ). The value chosen will affect the size of the cam, and typically the smallest value possible is chosen. The pivot distance must be large enough that the cam does not contact the follower pivot. Also, the force between the cam and follower will increase as the distance decreases. Therefore, it may be necessary to increase the pivot distance from machine design considerations. We will choose the distance between pivots to be 4 in. When we invert the motion, the follower pivot will appear to rotate around the cam. Therefore, we must draw a circle with a radius of 4 in about the cam for the follower pivot circle, as shown in Fig. 8.31.



**FIGURE 8.30** Cam–follower system to be designed in Example 8.6.

The third step is to determine the reference angle  $\phi_0$  for  $\phi$ . The location of the follower to determine  $\phi_0$  will affect the length of the follower and therefore the cost of the system. For simplicity, we will locate the follower in the initial dwell position (cam angle  $\theta = 0$ ) in such a way that point  $B$  contacts the cam in that position. This is done by drawing a line tangent to the base circle at  $B$ . Then construct a line at an angle of  $170^\circ$  to the tangent line at  $B$ . The intersection of this line with the follower pivot circle will locate  $C$  in the initial position. This is shown in Fig. 8.31. The length  $BC$  can then be computed using the law of cosines. That is,

$$BC^2 + AB^2 = AC^2 + 2(BC)(AB) \cos 100^\circ$$

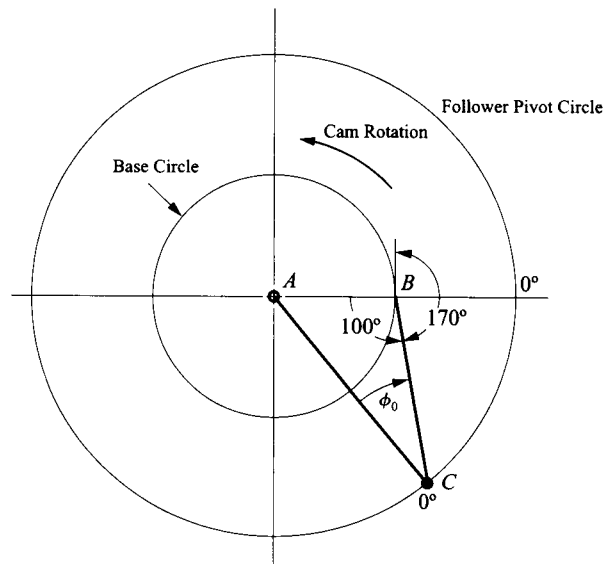


FIGURE 8.31 Determining the initial position of the follower.

or

$$BC^2 - 2(BC)(AB)\cos 100^\circ + (AB^2 - AC^2) = 0$$

and

$$BC = \frac{2(AB)\cos 100^\circ + \sqrt{[2(AB)\cos 100^\circ]^2 - 4(AB^2 - AC^2)}}{2} = \frac{-0.694 + \sqrt{48.482}}{2} = 3.134$$

The base angle,  $\phi_0$ , can be computed using the law of sines. That is,

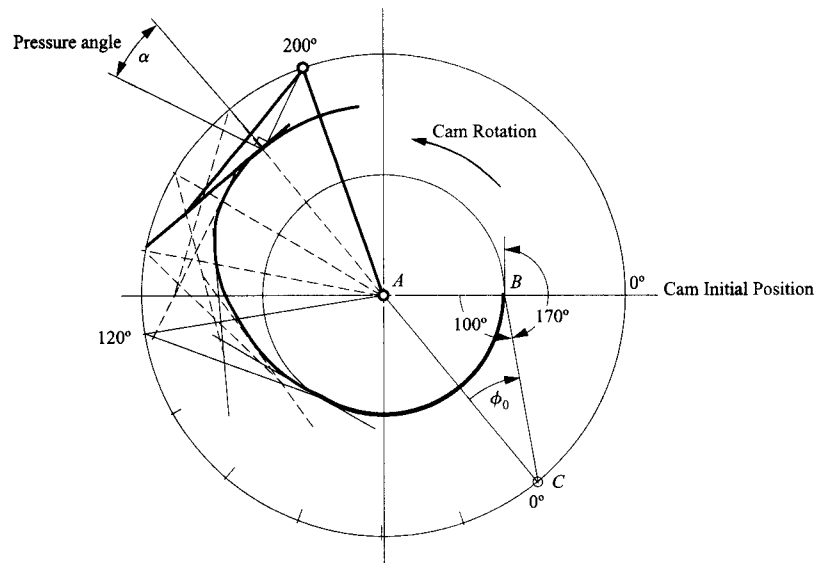
$$\phi_0 = \sin^{-1}\left[\frac{AB}{AC}\sin 100^\circ\right] = \sin^{-1}\left[\frac{2}{4}\sin 100^\circ\right] = 29.499^\circ$$

This angle is important because all subsequent displacements of the follower will be measured relative to this angle.

The location of pivot  $C$  for the follower when the cam angle is zero gives the first position of the follower pivot. Subsequent positions of the pivot will be at increments of  $20^\circ$  in the clockwise direction (opposite the cam rotation). Therefore, the fourth step in the cam layout is to draw radial lines at  $20^\circ$  increments from the cam rotation axis to the follower pivot circle starting from the initial position of  $AC$  corresponding to the cam rotation angle of  $0^\circ$ . These will be the positions of  $AC$  for each  $20^\circ$  rotation of the cam. Label the radial lines corresponding to the beginning and end of the first dwell and the second dwell. In the dwell regions, the cam will have a circular contour. These radial lines are shown in Fig. 8.32.

The fifth step is to draw the line  $CB$  relative to each position of  $AC$ , where the angle between  $CB$  and  $AC$  is  $(\phi_0 + \phi)$  measured in the clockwise direction about  $C$ . This will locate the successive positions of  $B$ . Next, draw a line through each position of  $B$  at an angle of  $170^\circ$  to  $BC$ . This will locate the successive positions of the face of the cam follower. Construct the cam surface tangent to the follower positions. The rise portion of the final cam is shown in Fig. 8.32.

Because of the follower face angle  $\beta$ , the pressure angle will not be constant as in the case of the axial flat-faced follower. The pressure angle will depend on the contact point as shown in Fig. 8.32



**FIGURE 8.32** Final layout of the rise portion of the cam profile for Example 8.6.

and will be equal to  $10^\circ \pm \zeta$ , where  $\zeta$  is the angle between a line from the contact point to  $C$  and the line  $BC$ . If the follower face angle is  $180^\circ$ , the pressure angle will be a constant, that is,  $0^\circ$ . Because of this, the angle  $\beta$  would be  $180^\circ$  unless specific design conditions dictated otherwise.

### 8.10.2 Analytical Determination of Cam Profile

Although the graphical approach works well for low-speed cams, for high speeds greater accuracy is required, making analytical techniques necessary. The analytical approach to determining the cam profiles also uses inversion. The general procedure is to establish a coordinate system on both the cam and the frame. To determine the location of the follower relative to the cam, it is necessary only to determine the location of the follower relative to the cam coordinate system. Successive positions of the follower will generate an envelope that will define the geometry of the cam profile.

The approach to the design of each of the four different follower systems considered is slightly different, and in each case the analytical approach will follow much the same procedure as was illustrated in the graphical approach.

#### **Analytical Determination of Cam Profile for an Offset, Radial Roller Follower**

Prior to determining the geometry of the cam, it is assumed that the basic motion specification for the follower is known in the form  $y = f(\theta)$ , where  $y$  is the displacement of the follower and  $\theta$  is the cam rotation angle. The base circle radius ( $r_b$ ), the follower radius ( $r_f$ ), and the offset  $\delta$  are also assumed to be known. The positive direction for  $\delta$  is defined by rotating  $R 90^\circ$  in the counterclockwise direction. The procedure is the same for both a roller follower and a cylindrical-faced follower. We will first locate successive positions of the roller center and then determine the envelope formed by the rollers.

Two positions of the follower relative to the cam are shown in Fig. 8.33. In the figure, it is assumed that the cam rotates clockwise, which means that the follower moves relative

to the cam in the counterclockwise direction. The radial position of the center of the follower from the origin of the coordinate system located at the center of the cam is given by

$$R = r_0 + r_b + f(\theta) \quad (8.15)$$

where  $f(\theta)$  is the function defining the follower displacement as a function of the cam rotation angle,  $\theta$ . Referring to Fig. 8.33, we have

$$x = R \cos \theta - \delta \sin \theta = [r_0 + r_b + f(\theta)] \cos \theta - \delta \sin \theta \quad (8.16)$$

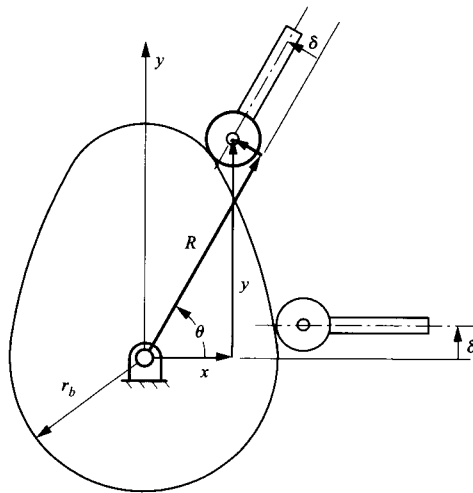
and

$$y = R \sin \theta + \delta \cos \theta = [r_0 + r_b + f(\theta)] \sin \theta + \delta \cos \theta \quad (8.17)$$

Given the follower displacement, the center of the roller can be easily computed as a function of the cam rotation angle  $\theta$ . These equations will also define the cam profile if a knife-edged follower is involved. Also, if the cutter radius is the same as the roller radius, the coordinates can be used to generate the cam profile directly. However, for other cases, we must determine the cam profile indirectly.

As the cam angle  $\theta$  is incremented, the roller follower can be represented in a series of positions as shown in Fig. 8.34. In any given position, the coordinates of all points on the roller follower can be defined relative to the cam. The cam surface is tangent to the successive positions of the rollers. Therefore, to determine the cam profile, we must locate points on a curve that is tangent to the series of circles.

The series of circles will form an envelope that will define the cam profile. Using envelope theory,<sup>1,2</sup> it is possible to define the profile exactly; however, envelope theory is somewhat complex except in the case of translating followers. Fortunately, if fine enough increments (less than  $1^\circ$ ) are used, the cam profile can be determined very accurately using numerical techniques, and this is the approach that we will use here. The numerical techniques are much simpler than envelope theory, and once the path of the center of the follower is known, the cam profile can be determined without knowledge of whether an oscillating or translating follower was used.



**FIGURE 8.33** Two positions of the roller follower relative to the cam.

Referring to Fig. 8.34, we can approximate the cam profile by a series of points defined in a variety of ways. Some of these are as follows:

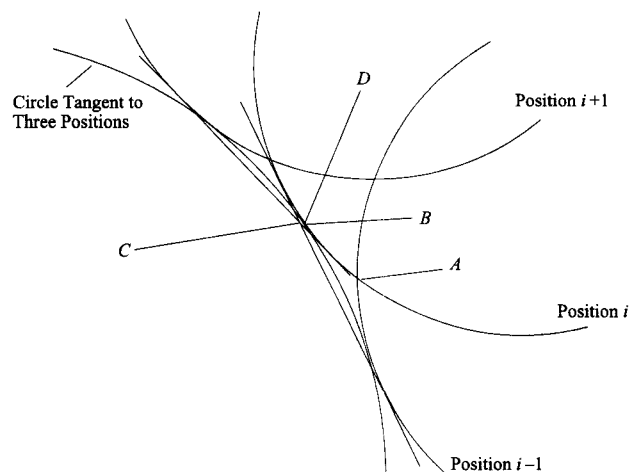
1. intersections of roller circles (*A*),
2. average tangent location formed by successive tangent lines (*B*),
3. intersections of successive tangent lines (*C*), and
4. tangent points formed by a circle tangent to three successive positions of the roller (*D*).

Other schemes based on fitting other curves to the circles could also be developed. However, it is apparent that each of the procedures will converge to the true tangent points defining the cam profile if the successive positions of the follower are close enough together.

Of the approximate methods available, procedures 2 and 4 will be the most accurate, and the simpler of these is procedure 4. It is also the procedure that is the more accurate of the two. Therefore, this is the procedure that will be developed here. This procedure is especially simple to program, and it can be made as accurate as desired by using increasingly smaller increments of the cam rotation angle. To begin the procedure, we will first determine an approximate location for the center of curvature of the cam as a function of  $\theta$ .

**Cam Radius of Curvature** The radius of curvature for a cam is important for several reasons. These include the following:

- If the cam is concave in a given area, the radius of curvature determines the minimum diameter of the cutter that can be used to machine the cam. The radius of curvature of the cam cannot be smaller than the cutter radius if the cam is concave in the area being machined.
- If the cam is concave in a given area, the radius of curvature defines the minimum diameter of the follower that can be used with the cam.



**FIGURE 8.34** Approximate procedures for locating a point on the cam profile given three successive positions of the roller follower. Point *A* is found by the simple intersection of two successive positions, point *B* is the average tangent location in position *i*, point *C* is the intersection of two successive tangents, and point *D* is the tangent location in position *i* of a circle tangent to positions *i* - 1, *i*, and *i* + 1.

- The contact stresses between the cam and the follower are a function of the cam radius of curvature.

If we have a parametric expression for the cam geometry in terms of  $x(\theta)$  and  $y(\theta)$ , an expression for the radius of curvature,  $\rho$ , in the  $x$ - $y$  plane is given from calculus as

$$\rho = \frac{\sqrt{\left[ \left( \frac{dx}{d\theta} \right)^2 + \left( \frac{dy}{d\theta} \right)^2 \right]^{3/2}}}{\left( \frac{dx}{d\theta} \right) \left( \frac{d^2 y}{d\theta^2} \right) - \left( \frac{dy}{d\theta} \right) \left( \frac{d^2 x}{d\theta^2} \right)} \quad (8.18)$$

To determine  $\rho$ , we need only differentiate the given expressions for  $x(\theta)$  and  $y(\theta)$ , and substitute the resulting expressions into Eq. (8.18).

The radius of curvature given in Eq. (8.18) will have a magnitude and direction, and both are important. When the cam profile is convex, the radius of curvature is positive, and when the cam is concave, the radius of curvature is negative. The radius can also be zero, which corresponds to a cusp. Technically, the cusp can be concave or convex, but from a practical standpoint, cusps are of interest only for convex surfaces. The transition between concave and convex areas of the cam results in the radius of curvature becoming infinite. The physical interpretations of the various signs of  $\rho$  are shown in Fig. 8.35.

Equation (8.18) applies to any cam profile regardless of the type of follower. However, to apply it directly, an analytical expression for  $x(\theta)$  and  $y(\theta)$  must be available. Except in the case of a translating flat-faced follower, simple expressions for  $x(\theta)$  and  $y(\theta)$  generally will not be available. Because of this, the purely analytical approach to determining the radius of curvature will not be addressed here except for this special case. Alternatively, a simpler numerical approach will be used.

If the points defining the cam profile are relatively close together, the radius of curvature can be determined numerically. This can be done by evaluating the derivatives in Eq. (8.18) numerically or by fitting circles to the points of the cam profile. Often an approximate value for the radius of curvature is sufficient because in most cases we do not wish to design cams that are close to the operating limits defined by the radii of curvature.

To determine the center of curvature of the cam profile, we will assume that for a given angle  $\theta$ , the center of curvature of the cam is the same as the center of curvature of the prime curve defined by the locations of the center of the cylindrical follower. We can approximate the center of curvature of the prime by fitting a circle through three successive positions of the center of the cylindrical follower. Designate these positions as  $p_{i-1} = (x_{i-1}, y_{i-1})$ ,  $p_i = (x_i, y_i)$ , and  $p_{i+1} = (x_{i+1}, y_{i+1})$ . Also, let the approximate location for the center of curvature be designated as  $p_c = (x_c, y_c)$ . We can now use Eq. (6.16) in Section 6.3

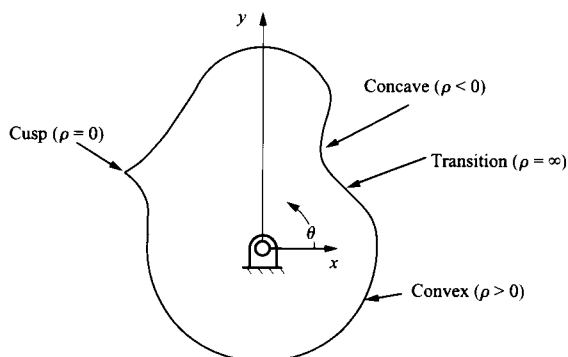


FIGURE 8.35 Interpretation of the sign of  $\rho$ .

to find the location of  $p_c$  because the procedure for finding  $p_c$  is the same as that required to find a pole or centerpoint. The result is

$$\begin{bmatrix} 2(x_{i+1} - x_i) & 2(y_{i+1} - y_i) \\ 2(x_{i-1} - x_i) & 2(y_{i-1} - y_i) \end{bmatrix} \begin{Bmatrix} x_c \\ y_c \end{Bmatrix} = \begin{Bmatrix} (x_{i+1}^2 - x_i^2) + (y_{i+1}^2 - y_i^2) \\ (x_{i-1}^2 - x_i^2) + (y_{i-1}^2 - y_i^2) \end{Bmatrix} \quad (8.19)$$

This linear matrix equation can be solved easily for  $(x_c, y_c)$ . The magnitude of the radius of curvature of the prime curve is given by

$$\rho = |r_{p_i/p_c}| = \sqrt{(x_i - x_c)^2 + (y_i - y_c)^2} \quad (8.20)$$

Once the center of curvature is known, the sign of the radius of curvature can be found by taking the cross product of the vector  $r_{p_i/p_{i-1}}$  with the vector  $r_{p_i+1/p_i}$ . The vectors are shown in Fig. 8.36, and the cross product is given by

$$r_{p_i/p_{i-1}} \times r_{p_{i+1}/p_i} = [(x_i - x_{i-1})(y_{i+1} - y_i) - (x_{i+1} - x_i)(y_i - y_{i-1})]k \quad (8.21)$$

If the cross product is in the positive  $k$  direction, the radius of curvature is positive, and the cam is convex at  $(x_p, y_p)$ . If the cross product is in the negative  $k$  direction, the cam is concave. If the determinant of the coefficient matrix in Eq. (8.19) is zero, then  $(x_c, y_c)$  is at infinity,  $r_{p_i/p_c}$  is infinite, and an inflection point is indicated. If  $(x_c, y_c) = (x_p, y_p)$ , the radius of curvature is zero and a cusp is indicated.

**Profile Approximation Using Center of Curvature** To locate points on the cam profile, we will approximate the center of curvature of three successive positions of the follower as shown in Fig. 8.37. From Eq. (8.19), the center of curvature is approximated as the intersection of lines through the midpoints of the line segments connecting successive follower centers and normal to these line segments as shown in Fig. 8.37.

The corresponding point on the cam profile lies on a line through this center of curvature and the center of the second roller circle. The location of this point  $(X_p, Y_p)$  is at the point where this line and the second roller circle intersect. Because there are two such points of intersection, care must be taken to find the right point. For the inner profile the desired point lies on the same side of the follower curve as the cam center.

To locate the line formed by the center of curvature and the second follower center, first calculate the slope orientation angle for the line using

$$\psi_i = \tan^{-1} \left( \frac{y_i - y_c}{x_i - x_c} \right) \quad (8.22)$$

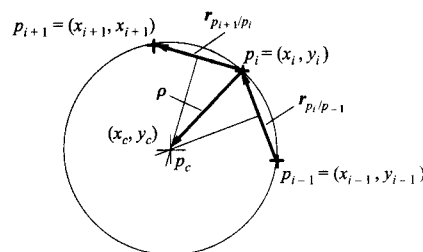


FIGURE 8.36 Use of vectors to determine the sign of  $\rho$ .

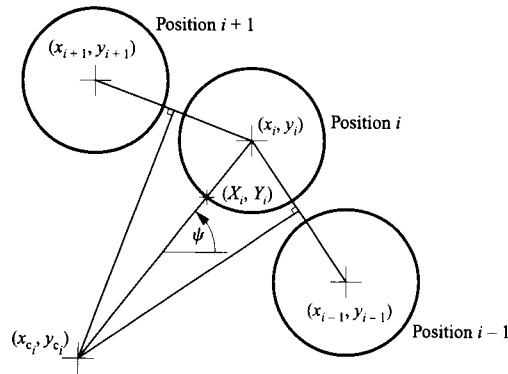


FIGURE 8.37 Approximate center of curvature of roller positions.

This angle is measured from the horizontal axis to the line from the center of curvature of the cam to the contact point. Note that the center of curvature, the contact point, and the center of the cam follower are all collinear. Equation (8.22) can be used directly when the cam is convex. Then the contact point will be located between the center of curvature and the center of the cylindrical follower. However, if the cam surface is concave, the follower center will be located between the center of curvature and the contact point.

The profile can be tested for concavity by solving Eq. (8.21). If the result is positive, the profile is convex and the coordinates on the cam profile are given by

$$\begin{aligned} X_i &= x_i - r_0 \cos \psi_i \\ Y_i &= y_i - r_0 \sin \psi_i \end{aligned} \tag{8.23}$$

If the result is negative, the profile is concave and the coordinates on the cam profile are given by

$$\begin{aligned} X_i &= x_i + r_0 \cos \psi_i \\ Y_i &= y_i + r_0 \sin \psi_i \end{aligned} \tag{8.24}$$

**Calculation of the Pressure Angle** As indicated previously, the pressure angle is the angle between the outward normal to the cam at the contact point and the direction of the velocity of the follower. The pressure angle is nominally the angle  $\phi_i = \psi_i - \theta$ , although to use this expression it is necessary to be careful with plus and minus angles. Another way to compute the pressure angle is to locate the center of curvature of the cam relative to the frame coordinate system and draw a line from the center of curvature to the center of the cylindrical follower. Because the cam is assumed to move horizontally, the inclination angle for the line connecting the cam center of curvature with the center of the cylindrical follower will be the pressure angle.

The equations necessary to determine points on the cam profile are summarized in Table 8.8. These can be easily programmed to determine the  $(X_i, Y_i)$  coordinates of points on the cam profile, and a MATLAB program for doing this is included on the disk with this book. Given the  $(X_i, Y_i)$  coordinates, the cam can be machined on a CNC milling machine. The accuracy of the profile will be determined in part by the angle increment chosen for the cam rotation angle  $\theta$ .



**TABLE 8.8 Summary of Equations for Determining the Cam Profile Coordinates and Pressure Angle for a Translating Cylindrical-Faced or Roller Follower. The Follower Displacement Is Assumed to Be Given by  $f(\theta)$ , the Radius of the Follower Is  $r_0$ , and the Base Circle Radius Is  $r_b$ . There Are Assumed to Be  $n$  Points on the Cam Profile.  $\delta$  Is the Follower Offset.**

---

**Radius of curvature**


---

$$\begin{Bmatrix} x_c \\ y_c \end{Bmatrix} = \begin{bmatrix} 2(X_{i+1} - X_i) & 2(Y_{i+1} - Y_i) \\ 2(X_{i-1} - X_i) & 2(Y_{i-1} - Y_i) \end{bmatrix}^{-1} \begin{Bmatrix} (X_{i+1}^2 - X_i^2) + (Y_{i+1}^2 - Y_i^2) \\ (X_{i-1}^2 - X_i^2) + (Y_{i-1}^2 - Y_i^2) \end{Bmatrix}$$

$$\rho = \frac{\left[ (X_i - X_{i-1})(Y_{i+1} - Y_i) - (X_{i+1} - X_i)(Y_i - Y_{i-1}) \right]}{\left[ (X_i - X_{i-1})(Y_{i+1} - Y_i) - (X_{i+1} - X_i)(Y_i - Y_{i-1}) \right]} \sqrt{(X_i - x_c)^2 + (Y_i - y_c)^2}$$

---

**Cam coordinates**


---

$$x_i = [r_0 + r_b + f(\theta_i)] \cos \theta_i - \delta \sin \theta_i$$

$$y_i = [r_0 + r_b + f(\theta_i)] \sin \theta_i + \delta \cos \theta_i$$

$$\psi_i = \tan^{-1} \left( \frac{y_i - y_c}{x_i - x_c} \right) \quad (i = 1, 2, 3, \dots, n)$$

$$X_i = x_i - r_0 \cos \psi_i \quad (\text{convex})$$

$$Y_i = y_i - r_0 \sin \psi_i$$

$$X_i = x_i + r_0 \cos \psi_i \quad (\text{concave})$$

$$Y_i = y_i + r_0 \sin \psi_i$$

---

**Pressure angle**


---

$$\phi_i = \psi_i - \theta$$


---

**EXAMPLE 8.7**  
**Cam Profile**  
**Coordinates for**  
**a Radial Roller**  
**Follower**

**Solution**

Determine the cam profile assuming that the follower starts from a dwell from  $0^\circ$  to  $90^\circ$  and rotates CW. The rise occurs with cycloidal motion during the cam rotation from  $90^\circ$  to  $180^\circ$ . The follower then dwells for  $60^\circ$  of cam rotation, and the return occurs with simple harmonic motion for the cam rotation from  $240^\circ$  to  $360^\circ$ . The amplitude of the follower translation is 2 cm, and the follower radius is 1 cm. The base circle radius is 4 cm, and the offset is 0.5 cm.

To solve the problem, we must identify the equations for the follower motion as a function of the cam rotation angle  $\theta$ , and then select an increment for  $\theta$ . From Sections 8.7 and 8.8, the equations (expressed in terms of radians) for each part of the motion are

$$\begin{aligned}
 0 \leq \theta \leq \pi/2: & \quad y = 0 \\
 \pi/2 \leq \theta \leq \pi: & \quad f(\theta) = \frac{2L}{\pi} \left( \left( \theta - \frac{\pi}{2} \right) - \frac{1}{4} \sin 4 \left( \theta - \frac{\pi}{2} \right) \right) \\
 \pi \leq \theta \leq 4\pi/3: & \quad f(\theta) = 2, \quad f'(\theta) = f''(\theta) = 0 \\
 4\pi/3 \leq \theta \leq 2\pi: & \quad f(\theta) = \frac{L}{2} \left( 1 + \cos \frac{3}{2} \left( \theta - \frac{4\pi}{3} \right) \right)
 \end{aligned}$$

These equations correspond to  $f(\theta)$  in Table 8.8, and using the equations in Table 8.8 we can compute the coordinates of the cam as accurately as we wish. For this problem, an angle increment of  $0.1^\circ$  was used. The problem was solved using the program included on the disk with this book. With this program, it is possible to evaluate quickly the cam profile for areas where the follower roller is too large. The cam, displacement diagram, radius of curvature, and pressure angle plots are shown in Fig. 8.38.

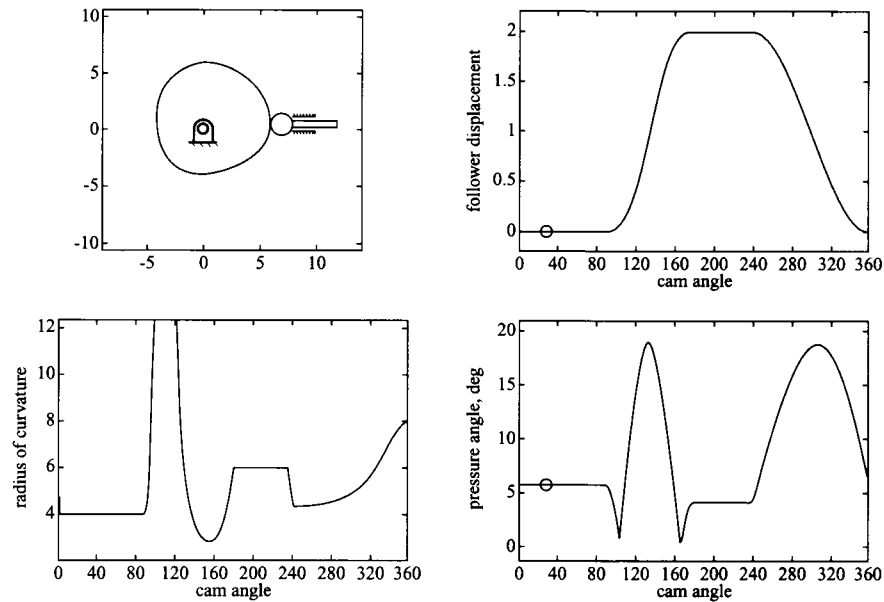


FIGURE 8.38 Cam profile, follower displacement, radius of curvature, and pressure angle for Example 8.7.

**Analytical Determination of the Cam Profile for a Radial Flat-Faced Follower** The development of the equations for a radial flat-faced follower can be accomplished using a procedure similar to that for a roller follower. Again, we must invert the mechanism so that the follower appears to rotate about the cam.

The radial displacement of the follower relative to the origin of the coordinate system located at the center of the cam is given by

$$R = r_b + f(\theta) \tag{8.25}$$

where  $f(\theta)$  is the function defining the follower displacement as a function of the cam rotation angle  $\theta$ . Referring to Fig. 8.39, we can write Eq. (8.25) as

$$R = y \sin \theta + x \cos \theta$$

If  $t$  is the distance from the follower axis to the point of contact,

$$t = y \cos \theta - x \sin \theta = \frac{dR}{d\theta} = f'(\theta)$$

The maximum and minimum values for  $t$  will give the minimum limits for the length of the follower face. Note that  $x$  and  $y$  are defined relative to the coordinate system fixed to the cam. Solving for  $x$  and  $y$  gives

$$x = R \cos \theta - t \sin \theta$$

$$y = R \sin \theta + t \cos \theta$$

and in terms of  $f(\theta)$ ,

$$\begin{aligned} x &= [r_b + f(\theta)] \cos \theta - f'(\theta) \sin \theta \\ y &= [r_b + f(\theta)] \sin \theta + f'(\theta) \cos \theta \end{aligned} \quad (8.26)$$

In general, we want to use the smallest base circle that will satisfy the geometric constraints. Normally, the base circle is determined in part by the pressure angle; however, for a radial, flat-faced follower, *the pressure angle is always zero*. Therefore, we must select another criterion for determining the base circle radius. The minimum base circle radius will be the one that avoids cusps in the cam profile.

For a given displacement profile, the cam becomes sharper and sharper as the base circle radius decreases. This is shown in Fig. 8.40. Eventually, the cam surface will generate a sharp point or cusp. This condition gives the limiting radius for the base circle.

To establish an equation for the base circle, we can use Eq. (8.18) directly because we have analytical expressions for  $x(\theta)$  and  $y(\theta)$ . For Eq. (8.18), we need the first and second derivatives of  $x(\theta)$  and  $y(\theta)$ . These are given in the following:

$$\frac{\partial x}{\partial \theta} = f'(\theta) \cos \theta - [r_b + f(\theta)] \sin \theta - f''(\theta) \sin \theta - f'(\theta) \cos \theta = -[r_b + f(\theta) + f''(\theta)] \sin \theta$$

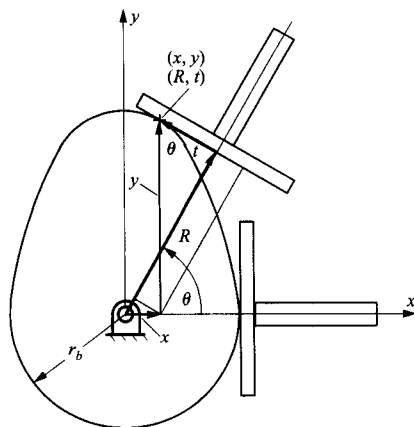


FIGURE 8.39 Radial, flat-faced follower.

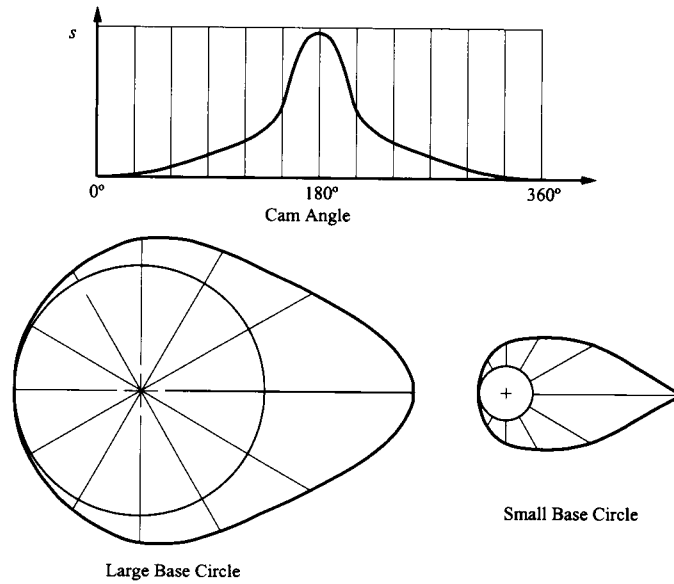


FIGURE 8.40 Formation of a cusp on the surface of the cam.

and

$$\frac{\partial^2 x}{\partial \theta^2} = -[f'(\theta) + f'''(\theta)] \sin \theta - [r_b + f'(\theta) + f'''(\theta)] \cos \theta$$

Also

$$\frac{\partial y}{\partial \theta} = f'(\theta) \sin \theta + [r_b + f(\theta)] \cos \theta + f''(\theta) \cos \theta - f'(\theta) \sin \theta = [r_b + f(\theta) + f''(\theta)] \cos \theta$$

and

$$\frac{\partial^2 y}{\partial \theta^2} = [f'(\theta) + f'''(\theta)] \cos \theta - [r_b + f(\theta) + f''(\theta)] \sin \theta$$

Substitution into Eq. (8.18) gives

$$\rho = \frac{\sqrt{[(dx/d\theta)^2 + (dy/d\theta)^2]^3}}{(dx/d\theta)(d^2y/d\theta^2) - (dy/d\theta)(d^2x/d\theta^2)} = [r_b + f(\theta) + f''(\theta)]$$

For there to be no cusp (and for the cam to be convex) at all locations

$$\rho \geq 0$$

or

$$[r_b + f(\theta) + f''(\theta)] \geq 0 \tag{8.27}$$

for all  $\theta$ . Both  $f(\theta)$  and  $f''(\theta)$  will be determined by the follower-displacement schedule. Therefore, only  $r_b$  can be externally controlled in Eq. (8.27); that is,

$$r_b \geq -f(\theta) - f''(\theta)$$

If  $-f(\theta) - f''(\theta)$  is negative, then any positive or zero value of the base circle radius will be acceptable from a cusp standpoint.

If the cam rotates counterclockwise, the equations developed must be modified slightly. In general, we will treat the follower displacement as a function of the angular displacement rather than the absolute angle. That is, the follower is assumed to translate a given distance regardless of the direction of rotation of the cam. The equations of Sections 8.3–8.9 were derived assuming that the cam angles were positive. When the cam rotates in the counterclockwise direction relative to the frame, the follower will rotate clockwise relative to the cam. This results in negative values for  $\theta$ . However, the expressions for  $f(\theta)$  must use the absolute values of  $\theta$ . The effect of this is that the correct sign of the derivative  $f'(\theta)$  is not preserved for counterclockwise rotation of the cam. The problem is re-solved by changing the sign of the derivative term in Eq. (8.26). That is, when a counterclockwise rotation of the cam is involved, the cam coordinates are given by

$$\begin{aligned} x &= [r_b + f(\theta)] \cos \theta + f'(\theta) \sin \theta \\ y &= [r_b + f(\theta)] \sin \theta - f'(\theta) \cos \theta \end{aligned}$$

The equations necessary to determine points on the cam profile and to determine the length of the follower face are summarized in Table 8.9. These can be programmed easily to determine the  $(x_i, y_i)$  coordinates of points on the cam profile relative to the cam coordinate system, and a MATLAB program for doing this is included on the disk with this book. Given the  $(x_i, y_i)$  coordinates, the cam can be machined on a CNC milling machine. The accuracy of the profile will be determined in part by the angle increment chosen for the cam rotation angle  $\theta$ .

**TABLE 8.9 Summary of Equations for Determining the Cam Profile Coordinates, Minimum Face Length, and Minimum Base Circle Radius for a Radial Flat-Faced Follower. The Follower Displacement Is Assumed to Be Given by  $f(\theta)$ , and the Base Circle Radius Is  $r_b$**

---

**Cam coordinates—clockwise rotation of cam**

---

$$\begin{aligned} x_i &= [r_b + f(\theta_i)] \cos \theta_i - f'(\theta_i) \sin \theta_i \\ y_i &= [r_b + f(\theta_i)] \sin \theta_i + f'(\theta_i) \cos \theta_i \end{aligned}$$

---

**Cam coordinates—counterclockwise rotation of cam**

---

$$\begin{aligned} x &= [r_b + f(\theta)] \cos \theta + f'(\theta) \sin \theta \\ y &= [r_b + f(\theta)] \sin \theta - f'(\theta) \cos \theta \end{aligned}$$

(continued)

TABLE 8.9 continued

## Minimum face length

$$t_{\max, \min} = f'(\theta_i) \Big|_{\max, \min}$$

## Radius of curvature

$$\rho = \left[ r_b + f(\theta) + f''(\theta) \right]$$

**EXAMPLE 8.8**  
**Cam Profile**  
**Coordinates for**  
**Radial Flat-Faced**  
**Follower**

**Solution**

Determine the cam profile for the follower motion given in Example 8.7. First find the minimum base circle radius based on avoiding cusps, and use that base circle to design the cam.

To solve the problem, we must determine the derivatives of the functions for the follower displacement. Because derivatives are involved, the angles in the displacement functions will be converted to radians. For the different intervals, the functions and derivatives are summarized in the following:

$$0 \leq \theta \leq \pi/2: f(\theta) = f'(\theta) = f''(\theta) = 0$$

$$\begin{aligned} \pi/2 \leq \theta \leq \pi: f(\theta) &= \frac{2L}{\pi} \left( \left( \theta - \frac{\pi}{2} \right) - \frac{1}{4} \sin 4 \left( \theta - \frac{\pi}{2} \right) \right), \quad f'(\theta) = \frac{2L}{\pi} \left( 1 - \cos 4 \left( \theta - \frac{\pi}{2} \right) \right), \\ f''(\theta) &= \frac{8L}{\pi} \left( \sin 4 \left( \theta - \frac{\pi}{2} \right) \right) \end{aligned}$$

$$\pi \leq \theta \leq 4\pi/3: f(\theta) = 2, \quad f'(\theta) = f''(\theta) = 0$$

$$\begin{aligned} 4\pi/3 \leq \theta \leq 2\pi: f(\theta) &= \frac{L}{2} \left( 1 + \cos \frac{3}{2} \left( \theta - \frac{4\pi}{3} \right) \right), \quad f'(\theta) = -\frac{3L}{4} \sin \frac{3}{2} \left( \theta - \frac{4\pi}{3} \right), \\ f''(\theta) &= -\frac{9L}{8} \cos \frac{3}{2} \left( \theta - \frac{4\pi}{3} \right) \end{aligned}$$

Given the equations for the follower displacement, we now need only to increment  $\theta$  and to evaluate the expressions in Table 8.9 to determine the minimum base circle radius and limiting values for the face length. We can then determine the cam coordinates. The values are computed for  $10^\circ$  increments of  $\theta$  in Table 8.10. From that table, it is clear that the base circle radius must be at least 3.147 cm and the follower face needs to be at least 2.47 cm above the centerline and 1.5 cm below it. Note that a negative value for  $t$  implies a distance below the stem centerline, and a positive value implies a distance above the centerline.

The cam will be designed with a base circle radius of 3.2 cm, and the follower face will be 2.6 cm above the stem centerline and 1.6 cm below it. The results obtained from the MATLAB program included on the disk with this book are shown in Fig. 8.41. To illustrate the effect of choosing a base circle radius less than the critical value, the program was rerun with the base circle radius of 1 cm. The results are shown in Fig. 8.42. The result is clearly a cam that cannot be manufactured.

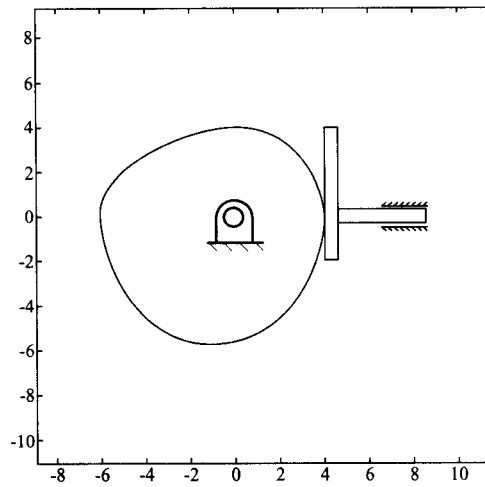


FIGURE 8.41 Cam designed for Example 8.8.

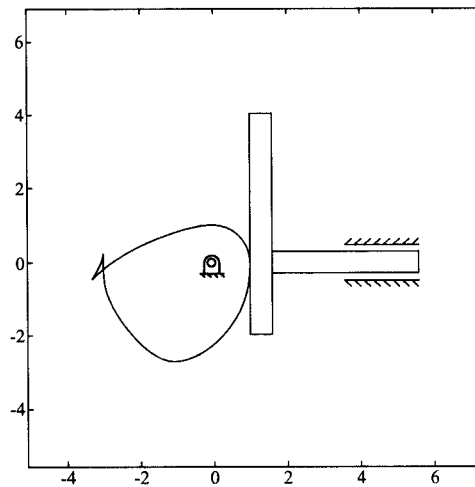


FIGURE 8.42 Results for Example 8.8 when a base circle radius of 1 cm is used. This cam cannot be manufactured. The smallest value for the base circle radius to avoid cusps is 3.147.

TABLE 8.10 Values for  $f(\theta)$  and Its Derivatives for Follower Displacement Specified for Example 8.8

$\theta$	$f(\theta)$ (cm)	$f'(\theta)$ (cm)	$f''(\theta)$ (cm)	$r_{bmin}$ (cm)	$t$ (cm)
$0^\circ$	0.000	0.000	0.000	0.000	0.000
			—dwell—		
$90^\circ$	0.000	0.000	0.000	0.000	0.000
$100^\circ$	0.018	0.298	3.274	-3.291	0.298
$110^\circ$	0.131	1.052	5.016	-5.147	1.052
$120^\circ$	0.391	1.910	4.411	-4.802	1.910
$130^\circ$	0.780	2.470	1.742	-2.522	2.470
$140^\circ$	1.220	2.470	-1.742	0.522	2.470
$150^\circ$	1.609	1.910	-4.411	2.802	1.910

(continued)

TABLE 8.10 continued

160°	1.869	1.052	-5.016	3.147	1.052
170°	1.982	0.298	-3.274	1.291	0.298
180°	2.000	0.000	0.000	-2.000	0.000
—dwell—					
240°	2.000	-0.000	-2.250	0.250	-0.000
250°	1.966	-0.388	-2.173	0.207	-0.388
260°	1.866	-0.750	-1.949	0.083	-0.750
270°	1.707	-1.061	-1.591	-0.116	-1.061
280°	1.500	-1.299	-1.125	-0.375	-1.299
290°	1.259	-1.449	-0.582	-0.676	-1.449
300°	1.000	-1.500	0.000	-1.000	-1.500
310°	0.741	-1.449	0.582	-1.324	-1.449
320°	0.500	-1.299	1.125	-1.625	-1.299
330°	0.293	-1.061	1.591	-1.884	-1.061
340°	0.134	-0.750	1.949	-2.083	-0.750
350°	0.034	-0.388	2.173	-2.207	-0.388

**Analytical Determination of a Cam Profile for an Oscillating, Cylindrical Follower**

The equations for an oscillating, cylindrical follower can be derived on the basis of the graphical procedure. Again, we must invert the mechanism so that the follower appears to rotate about the cam. To begin the procedure, we will assume that the cam base-circle radius  $r_b$ , the radius  $r_0$  of the cylindrical follower, the pivot distance  $r_1$ , and the distance  $r_3$  from the follower pivot to the center of the cylindrical contour are known.

In the procedure, the prime curve will be located first. This is the path traced by the center of curvature of the cylindrical follower. The cam profile can then be determined using the procedure developed in the first subsection of Section 8.10.2. The follower is assumed to begin in its lowest position when the follower contacts the base circle on the cam, as shown in Fig. 8.43. For this position, we need to determine the initial angles,  $\theta_0$  and  $\phi_0$ , where  $\theta_0$  gives the initial angle for the cam and  $\phi_0$  gives the initial angle for the follower. The motion of the cam and follower will be measured relative to these initial angles, respectively. From Fig. 8.43a, these angles can be computed using the law of cosines. That is,

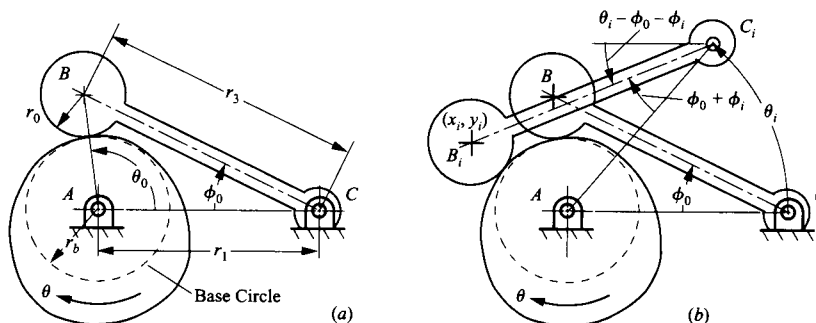


FIGURE 8.43 Oscillating, roller-faced follower. (a) Initial geometry. (b) Displaced geometry.



$$\phi_0 = \cos^{-1} \left[ \frac{r_1^2 + r_3^2 - (r_b + r_0)^2}{2r_1r_3} \right] \quad (8.28)$$

and

$$\theta_0 = \cos^{-1} \left[ \frac{r_1^2 + (r_b + r_0)^2 - r_3^2}{2r_1(r_b + r_0)} \right] \quad (8.29)$$

To compute the coordinates of the center of the follower ( $B$ ) relative to a coordinate system at point  $A$  on the cam, we will assume that the cam rotates clockwise so that the follower rotates *counterclockwise* relative to the cam.

Referring to Fig. 8.43b, for a given cam rotation angle  $\theta_i$ , we have that the coordinates of point  $B_i$  are given by

$$x_i = r_1 \cos \theta_i + r_3 \cos[\pi + \theta_i - \phi_i - \phi_0] \quad (8.30)$$

and

$$y_i = r_1 \sin \theta_i + r_3 \sin[\pi + \theta_i - \phi_i - \phi_0] \quad (8.31)$$

Given the coordinates of  $B_i$  for a series of cam rotation angles ( $\theta_i$ ), we can compute the coordinates of the corresponding contact points ( $X_p, Y_i$ ) on the cam face using the procedure in Section 8.10.2.

To compute the pressure angle at any given position, we must find the angle between a vector in the direction of the follower travel and a vector that is normal to the follower roller at each location, as shown in Fig. 8.44. The direction of travel of the follower pivot (point  $C$ ) relative to the cam is simply  $\theta$  the cam rotation angle (see Fig. 8.44); therefore, a vector in the direction of travel of point  $B$  relative to the cam is

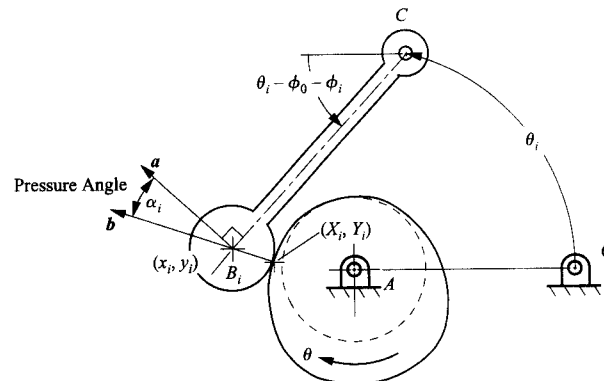
$$\mathbf{a} = 1 \angle \gamma_i$$

where

$$\gamma_i = \theta_i - \phi_i - \phi_0 + \pi/2$$

A vector in the direction normal to the roller is the line from ( $X_p, Y_i$ ) to ( $x_p, y_i$ ); therefore, the resulting vector is

$$\mathbf{b} = 1 \angle \lambda_i$$



**FIGURE 8.44** Pressure angle for oscillating, roller-faced follower.

where

$$\lambda_i = \tan^{-1} \left[ \frac{y_i - Y_i}{x_i - X_i} \right]$$

The resulting pressure angle is simply the angle between the vectors  $\mathbf{a}$  and  $\mathbf{b}$ . That is,

$$\alpha_i = \cos^{-1} \left[ \frac{\mathbf{a} \cdot \mathbf{b}}{\|\mathbf{a}\| \|\mathbf{b}\|} \right] = \cos^{-1} \left[ \cos \gamma_i \cos \lambda_i + \sin \gamma_i \sin \lambda_i \right] \quad (8.32)$$

The equations to determine points on the cam profile are summarized in Table 8.11. In Table 8.11, the equations for computing  $(X_i, Y_i)$  and for the radius of curvature of the cam are taken from Table 8.8. These can be programmed easily to determine the  $(X_i, Y_i)$  coordinates of points on the cam profile, and a MATLAB program for doing this is included on the disk with this book. Given the  $(X_i, Y_i)$  coordinates, the cam can be machined on a CNC milling machine. The accuracy of the profile will be determined in part by the increment chosen for the cam rotation angle  $\theta$ .

**TABLE 8.11 Summary of Equations for Determining the Cam Profile Coordinates and Pressure Angle for an Oscillating Cylindrical-Faced or Roller Follower. The Follower Oscillation  $\phi$  Is Assumed to Be Given by  $f(\theta)$ , the Radius of the Follower Is  $r_0$ , the Base Circle Radius Is  $r_b$ , the Distance Between the Cam and Follower Pivots Is  $r_1$ , and the Length of the Follower Is  $r_3$ . There Are Assumed to Be  $n$  Points on the Cam Profile**

---

**Radius of curvature**

---

$$\begin{aligned} \begin{Bmatrix} x_c \\ y_c \end{Bmatrix} &= \begin{bmatrix} 2(X_{i+1} - X_i) & 2(Y_{i+1} - Y_i) \\ 2(X_{i-1} - X_i) & 2(Y_{i-1} - Y_i) \end{bmatrix}^{-1} \begin{Bmatrix} (X_{i+1}^2 - X_i^2) + (Y_{i+1}^2 - Y_i^2) \\ (X_{i-1}^2 - X_i^2) + (Y_{i-1}^2 - Y_i^2) \end{Bmatrix} \\ \rho &= \frac{\left[ (X_i - X_{i-1})(Y_{i+1} - Y_i) - (X_{i+1} - X_i)(Y_i - Y_{i-1}) \right]}{\left| (X_i - X_{i-1})(Y_{i+1} - Y_i) - (X_{i+1} - X_i)(Y_i - Y_{i-1}) \right|} \sqrt{(X_i - x_c)^2 + (Y_i - y_c)^2} \end{aligned}$$

---

**Cam coordinates**

---

$$\phi_0 = \cos^{-1} \left[ \frac{r_1^2 + r_3^2 - (r_b + r_0)^2}{2r_1r_3} \right]$$

$$x_i = r_1 \cos \theta_i + r_3 \cos[\pi + \theta_i - \phi_i - \phi_0]; \quad y_i = r_1 \sin \theta_i + r_3 \sin[\pi + \theta_i - \phi_i - \phi_0]$$

$$\psi_i = \tan^{-1} \left( \frac{y_i - y_c}{x_i - x_c} \right) \quad (i = 1, 2, 3, \dots, n)$$

(continued)

TABLE 8.11 continued

$$X_i = x_i - r_0 \cos \psi_i \quad (\text{convex})$$

$$Y_i = y_i - r_0 \sin \psi_i$$

$$X_i = x_i + r_0 \cos \psi_i \quad (\text{concave})$$

$$Y_i = y_i + r_0 \sin \psi_i$$

**Pressure angle**

$$\gamma_i = \theta_i - \phi_i - \phi_0 + \pi/2$$

$$\lambda_i = \tan^{-1} \left( \frac{y_i - Y_i}{x_i - X_i} \right)$$

$$\alpha_i = \cos^{-1} [\cos \gamma_i \cos \lambda_i + \sin \gamma_i \sin \lambda_i]$$

**EXAMPLE 8.9**  
**Cam Profile**  
**Coordinates for a**  
**Roller Follower**  
**That Oscillates**

**Solution**

Determine the cam profile assuming that the follower dwells while the cam rotates *counterclockwise* from  $0^\circ$  to  $90^\circ$ . The rise occurs with 3-4-5 polynomial motion during the cam rotation from  $90^\circ$  to  $180^\circ$ . The follower then dwells for  $90^\circ$  of cam rotation, and the return occurs with simple harmonic motion for the cam rotation from  $270^\circ$  to  $360^\circ$ . The amplitude of the follower oscillation is  $30^\circ$ , and the follower radius is 1 in. The base circle radius is 2 in and the distance between pivots is 6 in. The length of the follower is to be determined such that the pressure angle starts out at zero.

To solve the problem, we must identify the equations for the follower motion as a function of the cam rotation angle  $\theta$  and then select an increment for  $\theta$ . Because the cam is rotating counterclockwise, the follower rotates clockwise relative to the cam. Mathematically, this is accomplished by using negative angles for the displacements starting from 0. However, the equations developed for the follower displacements give the follower position as a function of the cam position and do not depend on the direction of cam rotation. For a given angular displacement, the rise will be the same whether the cam is to be designed for clockwise or counterclockwise rotation. Therefore, we must use the magnitude of the cam angle from the start of the interval over which the function is defined. In the equations, we will let  $\bar{\theta}$  be the magnitude of  $\theta$ . Then from Sections 8.9 and 8.7, the equations (expressed in terms of radians) for each part of the motion become

$$0 < \bar{\theta} \leq \pi/2: \phi = 0$$

$$\begin{aligned} \pi/2 \leq \bar{\theta} \leq \pi \quad (\beta = \pi/2; L = \pi/6): \phi &= 10L \left( \frac{\bar{\theta} - \pi/2}{\beta} \right)^3 - 15L \left( \frac{\bar{\theta} - \pi/2}{\beta} \right)^4 + 6L \left( \frac{\bar{\theta} - \pi/2}{\beta} \right)^5 \\ &= \left( \frac{5\pi}{3} \right) \left( \frac{\bar{\theta} - \pi/2}{\pi/2} \right)^3 - \left( \frac{5\pi}{2} \right) \left( \frac{\bar{\theta} - \pi/2}{\pi/2} \right)^4 + \pi \left( \frac{\bar{\theta} - \pi/2}{\pi/2} \right)^5 \end{aligned}$$

$$\pi \leq \bar{\theta} \leq 3\pi/2: \phi = \frac{\pi}{6}$$

$$3\pi/2 \leq \bar{\theta} \leq 2\pi \quad (\beta = \pi/2; L = \pi/6): \phi = \frac{L}{2} \left( 1 + \cos \frac{\pi}{\beta} \left( \bar{\theta} - \frac{3\pi}{2} \right) \right) = \frac{\pi}{12} \left( 1 + \cos 2 \left( \bar{\theta} - \frac{3\pi}{2} \right) \right)$$

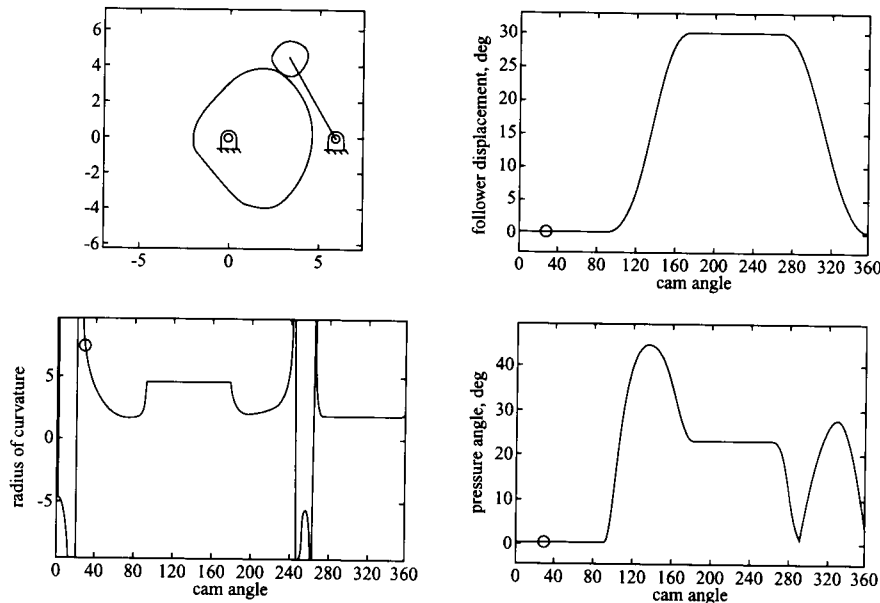
To determine the length,  $r_3$ , of the follower that will give zero pressure angle in the initial position, refer to Fig. 8.44. From that figure, the angle between the  $(r_0+r_b)$  and  $r_3$  must be  $90^\circ$  for the pressure angle to be zero during a dwell. Therefore,

$$r_3 = \sqrt{r_1^2 - (r_b + r_0)^2} = \sqrt{6^2 - (2+1)^2} = 5.196 \text{ in}$$

The equations for  $\phi$  and  $r_3$  can be used to determine  $\phi_0$  in Table 8.11, and using the equations in Table 8.11 we can compute the coordinates of the cam as accurately as we wish by using a small increment for the cam rotation angle  $\theta$ .

For the calculations, the angle  $\theta$  is incremented in the negative direction (the follower rotates CW relative to the cam). Therefore, the points corresponding to the center of the roller (prime curve points) will be generated and labeled initially in the CW direction. However, the equations in Table 8.11 were derived assuming that the points are ordered in the CCW direction. Therefore, after all of the prime points are generated, they must be reordered in the CCW direction. After the prime points are reordered in this way, the corresponding points on the cam surface can be computed directly as was done in Example 8.7.

For plotting purposes, we have used the program on the disk included with this book with an angle increment of  $1^\circ$ , which is adequate for visual purposes. If we want to machine the cam with high accuracy, a finer increment for  $\theta$  would be used. It should be noted, however, that when very fine increments are used, the errors of the computations using MATLAB can be significant. The cam, displacement diagram, radius of curvature, and pressure angle plots are shown in Fig. 8.45.



**FIGURE 8.45** Cam profile, follower displacement, radius of curvature, and pressure angle for Example 8.9.

### Analytical Determination of a Cam Profile for a Flat-Faced Follower That Oscillates

The cam-follower system is shown in Fig. 8.46, and the points shown in that figure will be used to describe the design of the cam. Point  $A$  is the location of the axis of rotation of the cam,  $C$  is the axis of rotation of the follower, and  $d$  is the follower offset. Point  $B$  is the location of the tangent point between the face of the follower and the cam surface, and  $D$  is located at the intersection of the follower face and a line from  $C$  perpendicular to the follower face. The distance  $R$  is the perpendicular distance from the follower face to the center of rotation of the cam.

The development of the equations for an oscillating flat-faced follower is similar to the graphical procedure in Example 8.6. As in the other cases, we must invert the mechanism so that the follower appears to rotate about the cam. To begin the procedure, we will assume that the cam base radius  $r_b$ , the pivot distance  $r_1$ , and the follower angle  $\beta$  are known.

In the procedure, we will locate the line representing the face of the cam first. We will then locate the points on the cam by locating successive circles that are tangent to three lines.

The first step is to determine the reference angle  $\phi_0$  that gives the orientation of the follower in the initial position. As shown in Fig. 8.46, in this position,

$$R = r_b = AB$$

From the geometry in Fig. 8.47, we have

$$AE = \frac{r_1}{1 + d/R} = \frac{r_1}{1 + d/r_b}$$

Then

$$BE = \sqrt{AE^2 - r_b^2}$$

and

$$\phi_0 = \tan^{-1} \frac{r_b}{BE}$$

For each position of the cam given by  $\theta$ , we will know  $\phi(\theta)$  from the follower-displacement equations. The orientation of the follower face relative to the cam is then given by the angle  $\phi + \phi_0$ .

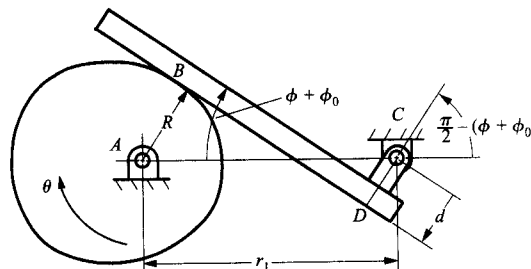


FIGURE 8.46 Geometry for oscillating, flat-faced follower.

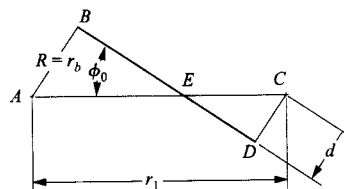


FIGURE 8.47 Geometry for finding  $\phi_0$ .

To locate the follower relative to the cam as the cam rotates, we can invert the motion relative to the cam. For simplicity, we will again assume that the cam rotates CW relative to the frame, which means that the frame rotates CCW relative to the cam. A typical position is shown in Fig. 8.48.

For a given rotation of the cam, the coordinates of point  $C$  relative to the cam are

$$x_C = r_1 \cos \theta$$

and

$$y_C = r_1 \sin \theta$$

Similarly, the coordinates of point  $D$  are

$$x_D = x_C + d \cos \left( \frac{3\pi}{2} - \phi - \phi_0 + \theta \right)$$

and

$$y_D = y_C + d \sin \left( \frac{3\pi}{2} - \phi - \phi_0 + \theta \right)$$

To locate the line defining the follower face, we need to locate a line oriented at an angle of  $\theta_i - \phi_i - \phi_0$  and passing through  $D_i$ . The equation of the line defining the follower face can be defined parametrically in terms of the distance  $\tau$  from  $D_i$  as shown in Fig. 8.49. The parametric equations are

$$x_f = x_D + \tau \cos \zeta \quad (8.33)$$

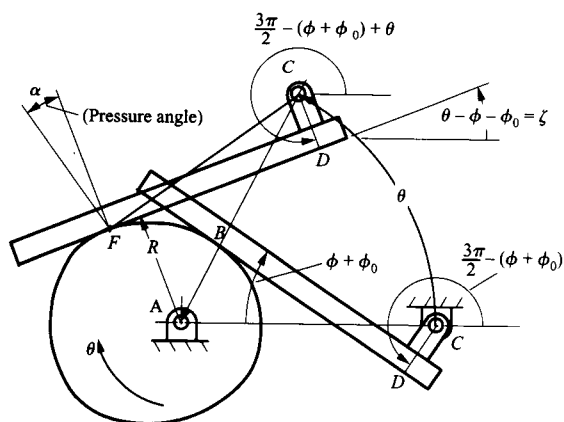
and

$$y_f = y_D + \tau \sin \zeta \quad (8.34)$$

where

$$\zeta = \theta - \phi - \phi_0$$

Using Eqs. (8.33) and (8.34), we can define a line corresponding to the follower face for each position chosen for the cam. To define the cam profile, we must locate a series of points that are tangent to the follower face in each position. The coordinates of the tangent points can be approximated using the geometry shown in Fig. 8.50. Assume that we have



**FIGURE 8.48** Motion of an oscillating, flat-faced follower relative to a cam.

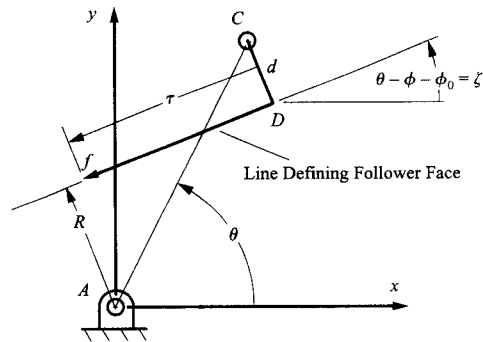


FIGURE 8.49 Parametric line defining a follower face. Here,  $\tau$  would be negative.

three positions ( $i-1$ ,  $i$ , and  $i+1$ ) of the follower relative to the cam. Each follower face line can be defined in terms of the coordinates of  $D$  and  $\tau$  and  $\zeta$ . To determine the location of the cam contact point on the centerline, approximate the cam by a circle that is tangent to each of the lines simultaneously. Referring to Fig. 8.50, we see that this can be done as follows:

1. Find the successive intersections ( $G_i$  and  $G_{i+1}$ ) of the face lines. To find  $G_i$ , use Eqs. (8.33) and (8.34), set  $x_{f_i} = x_{f_{i-1}}$  and  $y_{f_i} = y_{f_{i-1}}$ , and solve the resulting set of linear equations for  $\tau_{i-1}$  and  $\tau_i$ :

$$\begin{cases} x_{D_i} - x_{D_{i-1}} \\ y_{D_i} - y_{D_{i-1}} \end{cases} = \begin{bmatrix} -\cos \zeta_i & \cos \zeta_{i-1} \\ -\sin \zeta_i & \sin \zeta_{i-1} \end{bmatrix} \begin{cases} \tau_i \\ \tau_{i-1} \end{cases}$$

The location of  $G_i$  is then given by

$$x_{G_i} = x_{D_i} + \tau_i \cos \zeta_i$$

and

$$y_{G_i} = y_{D_i} + \tau_i \sin \zeta_i$$

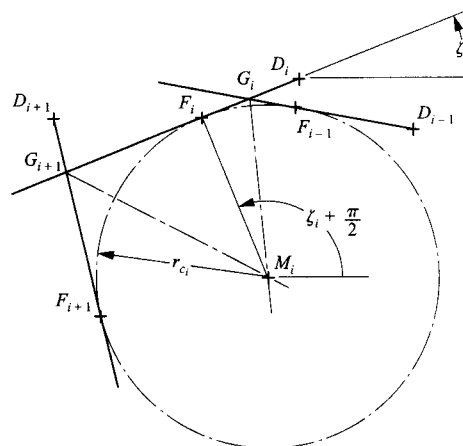


FIGURE 8.50 Locating a circle that is tangent to three successive positions of the follower face relative to the cam.

2. Find the equation of the line that bisects the angle between positions  $i$  and  $i - 1$  of the face line. This line passes through point  $G_i$  and is oriented at an angle of

$$\gamma_i = \frac{\zeta_i + \zeta_{i-1}}{2} + \frac{3\pi}{2}$$

The parametric equation of the line is then given by

$$x_{m_i} = x_{G_i} + v_i \cos \gamma_i$$

and

$$y_{m_i} = y_{G_i} + v_i \sin \gamma_i$$

where  $v_i$  is the distance from  $G_i$  in the positive  $\gamma_i$  direction.

3. Find the intersection of the lines bisecting the angles at  $G_i$  and  $G_{i+1}$ . For this, set  $x_{m_i} = x_{m_{i+1}}$  and  $y_{m_i} = y_{m_{i+1}}$  and solve the resulting set of linear equations for  $v_i$  and  $v_{i+1}$ .

$$\begin{cases} x_{G_i} - x_{G_{i+1}} \\ y_{G_i} - y_{G_{i+1}} \end{cases} = \begin{bmatrix} -\cos \gamma_i & \cos \gamma_{i+1} \\ -\sin \gamma_i & \sin \gamma_{i+1} \end{bmatrix} \begin{cases} v_i \\ v_{i+1} \end{cases}$$

The coordinates of the center of the circle tangent to the three positions of the face line are then given by

$$x_{M_i} = x_{G_i} + v_i \cos \gamma_i$$

and

$$y_{M_i} = y_{G_i} + v_i \sin \gamma_i$$

4. Find the radius of the tangent circle and coordinates of the tangent points. These are obtained by locating a line through  $M_i$  and perpendicular to each face line. The coordinates of the point  $F_i$  are given by

$$x_{F_i} = x_{M_i} + r_{c_i} \cos \left( \zeta_i + \frac{\pi}{2} \right) = x_{G_i} + \eta_i \cos \zeta_i$$

and

$$y_{F_i} = y_{M_i} + r_{c_i} \sin \left( \zeta_i + \frac{\pi}{2} \right) = y_{G_i} + \eta_i \sin \zeta_i$$

where  $\eta_i$  is the distance from  $G_i$  to the tangency point. Both  $r_{c_i}$  and  $\eta_i$  can be found by solving the resulting set of simultaneous linear equations:

$$\begin{cases} x_{M_i} - x_{G_i} \\ y_{M_i} - y_{G_i} \end{cases} = \begin{bmatrix} -\cos \left( \zeta_i + \frac{\pi}{2} \right) & \cos \zeta_i \\ -\sin \left( \zeta_i + \frac{\pi}{2} \right) & \sin \zeta_i \end{bmatrix} \begin{cases} r_{c_i} \\ \eta_i \end{cases}$$

(8.35)



The location of the tangent point is then given by

$$x_{F_i} = x_{G_i} + \eta_i \cos \zeta_i \quad (8.36)$$

and

$$y_{F_i} = y_{G_i} + \eta_i \sin \zeta_i \quad (8.37)$$

To find the tangency points on the other faces, substitute  $i - 1$  for  $i$  and then  $i + 1$  for  $i$  in Eqs. (8.36) and (8.37).

5. The cam coordinates can be approximated by the points  $F_i$  computed in step 4. To determine the minimum face length, we can compute the distance from  $F_i$  to  $D_i$  for each position of the cam.

To compute the pressure angle at any given position, we must find the angle between a vector in the direction of the follower travel and a vector that is normal to the follower face at each location as shown in Fig. 8.48. The direction of travel of the follower is given by a unit vector  $\mathbf{a}$  perpendicular to line  $F_i C_i$ . This vector is given by

$$\mathbf{a} = 1 \angle \psi_i$$

where

$$\psi_i = \tan^{-1} \left[ \frac{y_{F_i} - y_{C_i}}{x_{F_i} - x_{C_i}} \right] - \frac{\pi}{2}$$

We can approximate the direction that is perpendicular to the follower face by a unit vector  $\mathbf{b}$  from  $M_i$  to  $F_i$  or

$$\mathbf{b} = 1 \angle \lambda_i$$

where

$$\lambda_i = \tan^{-1} \left[ \frac{y_{F_i} - y_{M_i}}{x_{F_i} - x_{M_i}} \right] = \zeta_i + \frac{\pi}{2}$$

The resulting pressure angle is simply the angle between the vectors  $\mathbf{a}$  and  $\mathbf{b}$ . That is,

$$\alpha_i = \cos^{-1} \left[ \frac{\mathbf{a} \cdot \mathbf{b}}{|\mathbf{a}| |\mathbf{b}|} \right] = \cos^{-1} [\cos \psi_i \cos \lambda_i + \sin \psi_i \sin \lambda_i] \quad (8.38)$$

The equations necessary to determine points on the cam profile are summarized in Table 8.12, and the equations for the pressure angle and radius of curvature of the cam are summarized in Table 8.13. The equations for the radius of curvature are taken from Table 8.8. The equations in Table 8.12 can be easily programmed to determine the coordinates of points on the cam profile, and a MATLAB program for doing so is included on the disk with this book. Given the coordinates of a set of sequential points on the profile, the cam can be machined on a CNC milling machine. The accuracy of the profile will be determined in part by the increment chosen for the cam rotation angle  $\theta$ .

**TABLE 8.12 Summary of Equations for Determining the Cam Profile Coordinates for an Oscillating Flat-Faced Follower. The Follower Oscillation  $\phi$  Is Assumed to Be Given By  $f(\theta)$ , the Follower Offset Is  $d$ , the Base Circle Radius Is  $r_b$ , and the Distance between the Cam and Follower Pivots Is  $r_1$ . There Are Assumed to Be  $n$  Points on the Cam Profile**

Cam coordinates

$$AE = \frac{r_1}{1 + d/r_b}, \quad BE = \sqrt{AE^2 - r_b^2}$$

$$\phi_0 = \tan^{-1} \frac{r_b}{BE}$$

$$x_{C_i} = r_1 \cos \theta_i, \quad y_{C_i} = r_1 \sin \theta_i$$

$$x_{D_i} = x_{C_i} + d \cos \left( \frac{3\pi}{2} - \phi_i - \phi_0 + \theta_i \right), \quad y_{D_i} = y_{C_i} + d \sin \left( \frac{3\pi}{2} - \phi_i - \phi_0 + \theta_i \right)$$

$$\zeta_i = \theta_i - \phi_i - \phi_0$$

$$\begin{Bmatrix} x_{D_i} - x_{D_{i-1}} \\ y_{D_i} - y_{D_{i-1}} \end{Bmatrix} = \begin{bmatrix} -\cos \zeta_i & \cos \zeta_{i-1} \\ -\sin \zeta_i & \sin \zeta_{i-1} \end{bmatrix} \begin{Bmatrix} \tau_i \\ \tau_{i-1} \end{Bmatrix} \quad (i = 2, 3, \dots, n)$$

$$\begin{Bmatrix} x_{D_1} - x_{D_n} \\ y_{D_1} - y_{D_n} \end{Bmatrix} = \begin{bmatrix} -\cos \zeta_1 & \cos \zeta_n \\ -\sin \zeta_1 & \sin \zeta_n \end{bmatrix} \begin{Bmatrix} \tau_1 \\ \tau_n \end{Bmatrix}$$

$$x_{G_i} = x_{D_i} + \tau_i \cos \zeta_i, \quad y_{G_i} = y_{D_i} + \tau_i \sin \zeta_i$$

$$\gamma_i = \frac{\zeta_i + \zeta_{i-1}}{2} + \frac{3\pi}{2}$$

$$\begin{Bmatrix} x_{G_i} - x_{G_{i+1}} \\ y_{G_i} - y_{G_{i+1}} \end{Bmatrix} = \begin{bmatrix} -\cos \gamma_i & \cos \gamma_{i+1} \\ -\sin \gamma_i & \sin \gamma_{i+1} \end{bmatrix} \begin{Bmatrix} v_i \\ v_{i+1} \end{Bmatrix} \quad (i = 1, 2, \dots, n-1)$$

$$\begin{Bmatrix} x_{G_n} - x_{G_1} \\ y_{G_n} - y_{G_1} \end{Bmatrix} = \begin{bmatrix} -\cos \gamma_n & \cos \gamma_1 \\ -\sin \gamma_n & \sin \gamma_1 \end{bmatrix} \begin{Bmatrix} v_n \\ v_1 \end{Bmatrix}$$

$$x_{M_i} = x_{G_i} + v_i \cos \gamma_i, \quad y_{M_i} = y_{G_i} + v_i \sin \gamma_i$$

$$\begin{Bmatrix} x_{M_i} - x_{G_i} \\ y_{M_i} - y_{G_i} \end{Bmatrix} = \begin{bmatrix} -\cos(\zeta_i + \pi/2) & \cos \zeta_i \\ -\sin(\zeta_i + \pi/2) & \sin \zeta_i \end{bmatrix} \begin{Bmatrix} r_{c_i} \\ \eta_i \end{Bmatrix}$$

$$x_{F_i} = x_{G_i} + \eta_i \cos \zeta_i, \quad y_{F_i} = y_{G_i} + \eta_i \sin \zeta_i$$

**TABLE 8.13 Summary of Equations for Determining the Pressure Angle and Radius of Curvature for an Oscillating Flat-Faced Follower****Pressure angle**

$$\psi_i = \tan^{-1} \left[ \frac{y_{F_i} - y_{C_i}}{x_{F_i} - x_{C_i}} \right] - \frac{\pi}{2}$$

$$\lambda_i = \tan^{-1} \left[ \frac{y_{F_i} - y_{M_i}}{x_{F_i} - x_{M_i}} \right]$$

$$\alpha_i = \cos^{-1} \left[ \cos \psi_i \cos \lambda_i + \sin \psi_i \sin \lambda_i \right]$$

**Radius of curvature**

$$\begin{Bmatrix} x_c \\ y_c \end{Bmatrix} = \begin{bmatrix} 2(X_{i+1} - X_i) & 2(Y_{i+1} - Y_i) \\ 2(X_{i-1} - X_i) & 2(Y_{i-1} - Y_i) \end{bmatrix}^{-1} \begin{Bmatrix} (X_{i+1}^2 - X_i^2) + (Y_{i+1}^2 - Y_i^2) \\ (X_{i-1}^2 - X_i^2) + (Y_{i-1}^2 - Y_i^2) \end{Bmatrix}$$

$$\rho = \frac{\left[ (X_i - X_{i-1})(Y_{i+1} - Y_i) - (X_{i+1} - X_i)(Y_i - Y_{i-1}) \right]}{\left| (X_i - X_{i-1})(Y_{i+1} - Y_i) - (X_{i+1} - X_i)(Y_i - Y_{i-1}) \right|} \sqrt{(X_i - x_c)^2 + (Y_i - y_c)^2}$$

**EXAMPLE 8.10**  
**Cam Profile**  
**Coordinates for a**  
**Flat-Faced**  
**Follower That**  
**Oscillates**

**Solution**

Assume that the follower starts from a dwell from  $0^\circ$  to  $45^\circ$  and rotates CW. The rise occurs with simple harmonic motion during the cam rotation from  $45^\circ$  to  $180^\circ$ . The follower then dwells for  $90^\circ$  of cam rotation, and the return occurs with simple harmonic motion for the cam rotation from  $270^\circ$  to  $360^\circ$ . The amplitude of the follower oscillation is  $20^\circ$ , and the follower offset is 0.5 in. The base circle radius is 2 in, and the distance between pivots is 6 in.

To solve the problem, we must specify the length of the follower face, identify the equations for the follower motion as a function of the cam rotation angle  $\theta$ , and then select an increment for  $\theta$ . The length of the follower face is somewhat arbitrary as long as it is large enough to maintain contact with the cam. The minimum value can be calculated by computing the distance  $F_i$  to  $D_i$  for each position of the follower relative to the cam. However, in this example, we will select the length to be 9 in, which is large enough to ensure that the follower will maintain contact with the cam.

The second part of the displacement schedule is similar to that used in Example 8.9, and the equation for the rise portion can be obtained from Section 8.7. The resulting equations (expressed in terms of radians) are as follows:

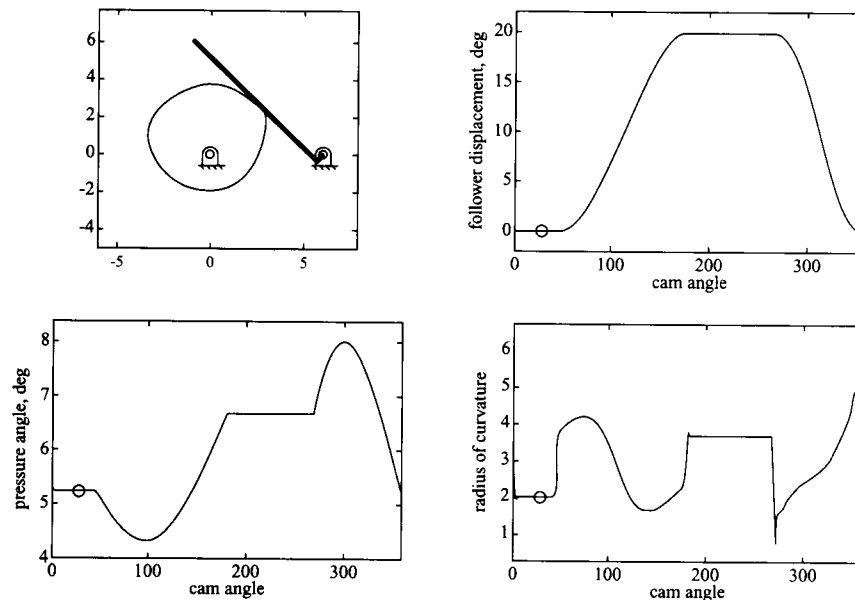
$$0 \leq \theta \leq \pi/2: \phi = 0$$

$$\pi/4 \leq \theta \leq \pi \left( \beta = 3\pi/4; L = \pi/9 \right): \phi = \frac{L}{2} \left( 1 - \cos \frac{\pi}{\beta} \left( \theta - \frac{\pi}{4} \right) \right) = \frac{\pi}{18} \left( 1 - \cos \frac{4}{3} \left( \theta - \frac{\pi}{4} \right) \right)$$

$$\pi \leq \theta \leq 3\pi/2: \phi = \frac{\pi}{6}$$

$$3\pi/2 \leq \theta \leq 2\pi \left( \beta = \pi/2; L = \pi/9 \right): \phi = \frac{L}{2} \left( 1 + \cos \frac{\pi}{\beta} \left( \theta - \frac{3\pi}{2} \right) \right) = \frac{\pi}{18} \left( 1 + \cos 2 \left( \theta - \frac{3\pi}{2} \right) \right)$$

Given the equations for the follower displacement, we now need only increment  $\theta$  and evaluate the expressions in Table 8.12 and 8.13 to determine the cam coordinates and pressure angle. The values were computed for  $2^\circ$  increments of  $\theta$ , and the results obtained from the MATLAB program included on the disk with this book are shown in Fig. 8.51.



**FIGURE 8.51** Cam profile, follower displacement, radius of curvature, and pressure angle for Example 8.10.

It is much more difficult to design a cam for an oscillating flat-faced follower than for the other types of followers. For example, if the amplitude of oscillation in Example 8.10 is changed to  $30^\circ$ , a cam will be developed that has a discontinuity and therefore cannot be manufactured. Changing the base circle radius may not always improve the situation, and the extent to which the base circle can be changed is limited by the distance between pivots. The problem can be improved by reducing the amplitude of oscillation, by changing the functions chosen for the rise and return, or by increasing the ranges chosen for the rise and return. However, in some cases, it may be necessary to choose another type of follower.

## REFERENCES

<sup>1</sup>Chen, F. Y., *Mechanics and Design of Cam Mechanisms*, Pergamon Press, New York (1982).

<sup>2</sup>Wilson, C. E., and Sadler, J. P. *Kinematics and Dynamics of Machinery*, Harper Collins, New York (1993).

## PROBLEMS

### EXERCISE PROBLEMS ON FOLLOWER-DISPLACEMENT SCHEDULES

**8.1** A cam that is designed for cycloidal motion drives a flat-faced follower. During the rise, the follower displaces 1 in for 180° of cam rotation. If the cam angular velocity is constant at 100 rpm, determine the displacement, velocity, and acceleration of the follower at a cam angle of 60°.

**8.2** A constant-velocity cam is designed for simple harmonic motion. If the flat-faced follower displaces 2 in for 180° of cam rotation and the cam angular velocity is 100 rpm, determine the displacement, velocity, and acceleration when the cam angle is 45°.

**8.3** A cam drives a radial, knife-edged follower through a 1.5-in rise in 180° of cycloidal motion. Give the displacement at 60° and 100°. If this cam is rotating at 200 rpm, what are the velocity ( $ds/dt$ ) and the acceleration ( $d^2s/dt^2$ ) at  $\theta = 60^\circ$ ?

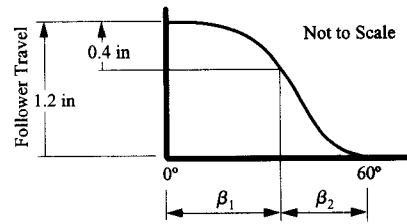
**8.4** Draw the displacement schedule for a follower that rises through a total displacement of 1.5 in with constant acceleration for 1/4 revolution, constant velocity for 1/8 revolution, and constant deceleration for 1/4 revolution of the cam. The cam then dwells for 1/8 revolution, and returns with simple harmonic motion in 1/4 revolution of the cam.

**8.5** Draw the displacement schedule for a follower that rises through a total displacement of 20 mm with constant acceleration for 1/8 revolution, constant velocity for 1/4 revolution, and constant deceleration for 1/8 revolution of the cam. The cam then dwells for 1/4 revolution and returns with simple harmonic motion in 1/4 revolution of the cam.

**8.6** Draw the displacement schedule for a follower that rises through a total displacement of 30 mm with constant acceleration for 90° of rotation and constant deceleration for 45° of cam rotation. The follower returns 15 mm with simple harmonic motion in 90° of cam rotation and dwells for 45° of cam rotation. It then returns the remaining 15 mm with simple harmonic motion during the remaining 90° of cam rotation.

**8.7** Draw the displacement schedule for a follower that rises through a total displacement of 3 in with cycloidal motion in 120° of cam rotation. The follower then dwells for 90° and returns to 0° with simple harmonic motion in 90° of cam rotation. The follower then dwells for 60° before repeating the cycle.

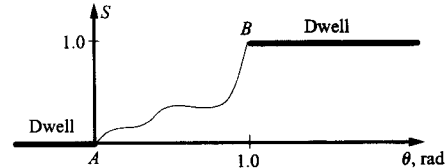
**8.8** A cam returns from a full lift of 1.2 in during its initial 60° rotation. The first 0.4 in of the return is half-cycloidal. This is followed by a half-harmonic return. Determine  $\beta_1$  and  $\beta_2$  so that the motion has continuous first and second derivatives. Draw a freehand sketch of  $y'$ ,  $y''$ , and  $y'''$  indicating any possible mismatch in the third derivative.



**8.9** Assume that  $s$  is the cam–follower displacement and  $\theta$  is the cam rotation. The rise is 1.0 cm after 1.0 rad of rotation, and the rise begins and ends at a dwell. The displacement equation for the follower during the rise period is

$$s = h \sum_{i=0}^n C_i \left( \frac{\theta}{\beta} \right)^i$$

If the position, velocity, and acceleration are continuous at  $\theta = 0$ , and the position and velocity are continuous at  $\theta = 1.0$  rad, determine the value of  $n$  required in the equation, and find the coefficients  $C_i$  if  $\dot{\theta} = 2$  rad/s. Note: Use the minimum possible number of terms.

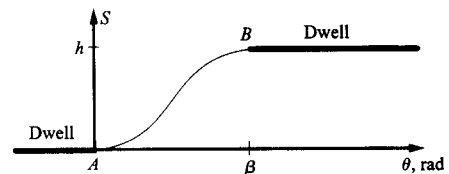


**8.10** Re-solve Problem 8.9 if  $\theta = 0.8$  rad and  $\dot{\theta} = 200$  rad/s.

**8.11** For the cam-displacement schedule given,  $h$  is the rise,  $\beta$  is the angle through which the rise takes place, and  $s$  is the displacement at any given angle  $\theta$ . The displacement equation for the follower during the rise period is

$$s = h \sum_{i=0}^5 a_i \left( \frac{\theta}{\beta} \right)^i$$

Determine the required values for  $a_0, \dots, a_5$  such that the displacement, velocity, and acceleration functions are continuous at the end points of the rise portion.



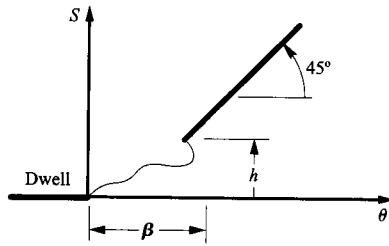
8.12 Re-solve Problem 8.11 if  $h = 20$  mm and  $\beta = 120^\circ$ .

8.13 Re-solve Problem 8.11 if  $h = 2$  in and  $\beta = 90^\circ$ .

8.14 Assume that  $s$  is the cam-follower displacement and  $\theta$  is the cam rotation. The rise is  $h$  after  $\beta$  degrees of rotation, and the rise begins at a dwell and ends with a constant velocity segment. The displacement equation for the follower during the rise period is

$$s = h \sum_{i=0}^n C_i \left( \frac{\theta}{\beta} \right)^i$$

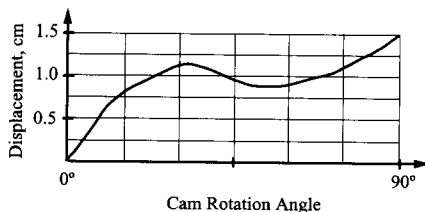
If the position, velocity, and acceleration are continuous at  $\theta = 0$  and the position and velocity are continuous at  $\theta = \beta$ , determine the  $n$  required in the equation, and find the coefficients  $C_i$  that will satisfy the requirements if  $s = h = 1.0$ .



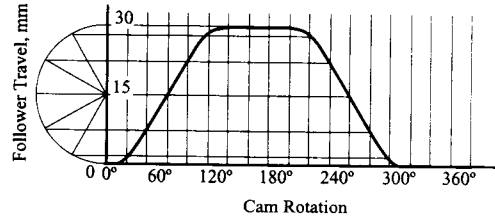
8.15 A follower moves with simple harmonic motion a distance of 20 mm in  $45^\circ$  of cam rotation. The follower then moves 20 mm more with cycloidal motion to complete its rise. The follower then dwells and returns 25 mm with cycloidal motion and then moves the remaining 15 mm with harmonic motion in  $45^\circ$ . Find the intervals of cam rotation for the cycloidal motions and dwell by matching velocities and accelerations, then determine the equations for the displacement ( $S$ ) as a function of  $\theta$  for the entire motion cycle.

**EXERCISE PROBLEMS ON GRAPHICAL CAM DESIGN**

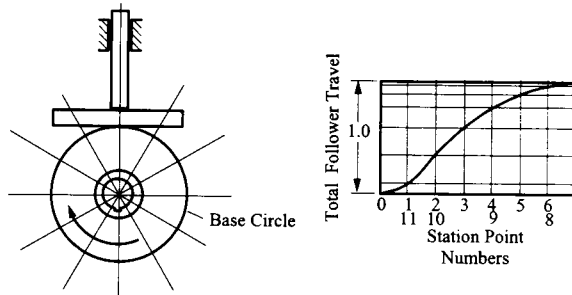
8.16 Construct the part of the profile of a disk cam that follows the displacement diagram shown. The cam has a 5-cm-diameter pitch circle and is rotating counterclockwise. The follower is a knife-edged, radial, translating follower. Use  $10^\circ$  increments for the construction.



8.17 Construct the profile of a disk cam that follows the displacement diagram shown. The follower is a radial roller and has a diameter of 10 mm. The base circle diameter of the cam is to be 40 mm and the cam rotates clockwise.



8.18 Accurately sketch one-half of the cam profile (stations 0–6) for the cam follower, base circle, and displacement diagram given. The base circle diameter is 1.2 in.



8.19 Lay out a cam profile using a harmonic follower displacement (both rise and return). Assume that the cam is to dwell at zero lift for the first  $100^\circ$  of the motion cycle and to dwell at a 1 in lift for cam angles from  $160^\circ$  to  $210^\circ$ . The cam is to have a translating, radial, roller follower with a 1 in roller diameter, and the base circle radius is to be 1.5 in. The cam will rotate clockwise. Lay out the cam profile using  $20^\circ$  plotting intervals.

8.20 Lay out a cam profile using a cycloidal follower displacement (both rise and return) if the cam is to dwell at zero lift for the first  $80^\circ$  of the motion cycle and to dwell at 2 in lift for cam angles from  $120^\circ$  to  $190^\circ$ . The cam is to have a translating, radial, roller follower with a roller diameter of 0.8 in. The cam will rotate counterclockwise, and the base circle diameter is 2 in. Lay out the cam profile using  $20^\circ$  plotting intervals.

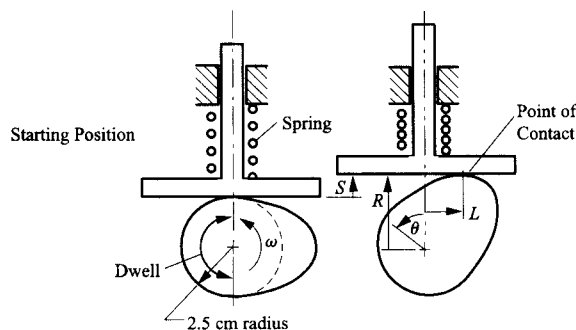
8.21 Lay out a cam profile assuming that an oscillating roller follower starts from a dwell for  $0^\circ$  to  $140^\circ$  of cam rotation, and the cam rotates clockwise. The rise occurs with parabolic motion during the cam rotation from  $140^\circ$  to  $220^\circ$ . The follower then dwells for  $40^\circ$  of cam rotation, and the return occurs with parabolic motion for the cam rotation from  $260^\circ$  to  $360^\circ$ . The amplitude of the follower rotation is  $35^\circ$ , and the follower radius is 1 in. The base circle radius is 2 in, and the distance between the cam axis and follower rotation axis is 4 in. Lay out the cam pro-

file using  $20^\circ$  plotting intervals such that the pressure angle is  $0^\circ$  when the follower is in the bottom dwell position.

**8.22** Lay out the rise portion of the cam profile if a flat-faced, translating, radial follower's motion is uniform. The total rise is 1.5 in, and the rise occurs over  $100^\circ$  of cam rotation. The follower dwells for  $90^\circ$  of cam rotation prior to the beginning of the rise and dwells for  $80^\circ$  of cam rotation at the end of the rise. The cam will rotate counterclockwise, and the base circle radius is 3 in.

### EXERCISE PROBLEMS ON ANALYTICAL CAM DESIGN

**8.23** In the sketch shown, the disk cam is used to position the radial, flat-faced follower in a computing mechanism. The cam profile is to be designed to give a follower displacement  $S$  for a CCW cam rotation  $\theta$  according to the function  $S = k\theta^2$  starting from dwell. For  $60^\circ$  of cam rotation from the starting position, the lift of the follower is 1.0 cm. By analytical methods, determine the distances  $R$  and  $L$  when the cam has been turned  $45^\circ$  from the starting position. Also calculate whether cusps in the cam profile would occur in the total rotation of  $60^\circ$ .



**8.24** Determine the cam profile assuming that the translating cylindrical-faced follower starts from a dwell from  $0^\circ$  to  $80^\circ$ , and the cam rotates clockwise. The rise occurs with cycloidal motion during the cam rotation from  $80^\circ$  to  $180^\circ$ . The follower then dwells for  $60^\circ$  of cam rotation, and the return occurs with simple harmonic motion for the cam rotation from  $240^\circ$  to  $360^\circ$ . The amplitude of the follower translation is 3 cm, and the follower radius is 0.75 cm. The base circle radius is 5 cm, and the offset is 0.5 cm.

**8.25** Re-solve Problem 8.24 if the amplitude of the follower translation is 4 cm, the follower radius is 1 cm, the base circle radius is 5 cm, and the offset is 1 cm.

**8.26** Re-solve Problem 8.24 if the cam rotates counterclockwise.

**8.27** Determine the cam profile assuming that the translating flat-faced follower starts from a dwell from  $0^\circ$  to  $80^\circ$  and rotates clockwise. The rise occurs with parabolic motion during the cam rotation from  $80^\circ$  to  $180^\circ$ . The follower then dwells for  $60^\circ$  of

cam rotation, and the return occurs with simple harmonic motion for the cam rotation from  $240^\circ$  to  $360^\circ$ . The amplitude of the follower translation is 3 cm. First find the minimum base circle radius based on avoiding cusps, and use that base circle to design the cam.

**8.28** Re-solve Problem 8.27 if the cam rotates counterclockwise.

**8.29** Determine the cam profile assuming that an oscillating cylindrical-faced follower dwells while the cam rotates counterclockwise from  $0^\circ$  to  $100^\circ$ . The rise occurs with 3-4-5 polynomial motion during the cam rotation from  $100^\circ$  to  $190^\circ$ . The follower then dwells for  $80^\circ$  of cam rotation, and the return occurs with simple harmonic motion for the cam rotation from  $270^\circ$  to  $360^\circ$ . The amplitude of the follower oscillation is  $25^\circ$ , and the follower radius is 0.75 in. The base circle radius is 2 in, and the distance between pivots is 6 in. The length of the follower is to be determined such that the pressure angle starts out at zero.

**8.30** Re-solve Problem 8.29 if the cam rotates clockwise.

**8.31** Design a cam and oscillating roller follower assuming that the follower starts from a dwell for  $0^\circ$  to  $80^\circ$  of cam rotation and the cam rotates clockwise. The rise occurs with cycloidal motion during the cam rotation from  $80^\circ$  to  $200^\circ$ . The follower then dwells for  $40^\circ$  of cam rotation, and the return occurs with cycloidal motion for the cam rotation from  $240^\circ$  to  $360^\circ$ . The amplitude of the follower rotation is  $45^\circ$ . Determine the cam base circle radius, distance between cam and follower pivots, the length of the follower, and the radius of the follower for acceptable performance.

**8.32** Determine the cam profile assuming that an oscillating flat-faced follower starts from a dwell from  $0^\circ$  to  $45^\circ$  and rotates counterclockwise. The rise occurs with simple harmonic motion during the cam rotation from  $45^\circ$  to  $180^\circ$ . The follower then dwells for  $90^\circ$  of cam rotation, and the return occurs with simple harmonic motion for the cam rotation from  $270^\circ$  to  $360^\circ$ . The amplitude of the follower oscillation is  $20^\circ$ , and the follower offset is 0.5 in. The base circle radius is 5 in, and the distance between pivots is 8 in.

**8.33** Re-solve Problem 8.32 if the cam rotates clockwise.

**8.34** Design a cam system assuming that an oscillating flat-faced follower starts from a dwell for  $0^\circ$  to  $100^\circ$  of cam rotation and the cam rotates counterclockwise. The rise occurs with uniform motion during the cam rotation from  $100^\circ$  to  $200^\circ$ . The follower then dwells for  $40^\circ$  of cam rotation, and the return occurs with parabolic motion for the cam rotation from  $240^\circ$  to  $360^\circ$ . The oscillation angle is  $20^\circ$ .

**8.35** Design a cam system assuming that an oscillating flat-faced follower starts from a dwell for  $0^\circ$  to  $50^\circ$  of cam rotation and the cam rotates clockwise. The rise occurs with cycloidal motion during the cam rotation from  $50^\circ$  to  $200^\circ$ . The follower then dwells for  $90^\circ$  of cam rotation, and the return occurs with harmonic motion for the cam rotation from  $290^\circ$  to  $360^\circ$ . The oscillation angle is  $25^\circ$ .

- 8.36** Determine the cam profile assuming that the translating knife-edged follower starts from a dwell from  $0^\circ$  to  $80^\circ$  and rotates clockwise. The rise occurs with cycloidal motion during the cam rotation from  $80^\circ$  to  $180^\circ$ . The follower then dwells for  $60^\circ$  of cam rotation, and the return occurs with simple harmonic motion for the cam rotation from  $240^\circ$  to  $360^\circ$ . The amplitude of the follower translation is 4 cm. The base circle radius is 5 cm, and the offset is 0.5 cm.
- 8.37** A radial flat-faced follower is to move through a total displacement of 20 mm with harmonic motion while the cam rotates through  $30^\circ$ . Find the minimum radius of the base circle that is necessary to avoid cusps.
- 8.38** A radial flat-faced follower is to move through a total displacement of 3 in with cycloidal motion while the cam rotates through  $90^\circ$ . Find the minimum radius of the base circle that is necessary to avoid cusps.
- 8.39** A radial roller follower is to move through a total displacement of  $L = 19$  mm with harmonic motion while the cam rotates  $60^\circ$ . The roller radius is 5 mm. Use the program supplied with the book and find the minimum radius necessary to avoid cusps during the interval indicated.
- 8.40** A radial roller follower is to move through a total displacement of  $L = 45$  mm with cycloidal motion. The roller radius is 5 mm, and the cam rotates  $90^\circ$  during the rise. Use the program supplied with the book and find the minimum radius necessary to avoid cusps during the interval.
- 8.41** Assume that a flat-faced translating follower is used with the displacement schedule in Problem 8.10. Determine if a cusp is present at  $\theta = 60^\circ$ .
- 8.42** Assume that a flat-faced translating follower is used with the displacement schedule in Problem 8.12. Determine if a cusp is present at  $\theta = 90^\circ$ .



---

# SPATIAL LINKAGE ANALYSIS

---

## 9.1 SPATIAL MECHANISMS

---

### 9.1.1 Introduction

There are many mechanisms that do not conform to planar, spherical, or other relatively simple motion domains. The landing gear of many aircraft involves a complex sequence of unfolding and rotation movements. The example of automotive suspension and steering linkages has already been discussed in Chapter 7. Control linkages used on farm and construction machinery are additional examples. Many problems involving spatial mechanisms can be attacked using the vector analysis techniques of courses in statics and dynamics. This is true if the information to be elicited is in the velocity or acceleration domain. Unfortunately, if the position of the linkage must be determined, such methods are likely to fall short in any but the simplest mechanism configurations. To develop systematic methods for handling position problems in spatial mechanism, it is necessary to develop new tools. This chapter provides a brief introduction to the most commonly used methods. More advanced texts specifically directed at kinematics and dynamics of spatial mechanisms or robotics may be consulted for more extensive treatment of these topics.

In this chapter we will develop methods for modeling simple spatial mechanisms. Among other applications, the material presented in this chapter is fundamental to the construction of coordination software for robotic mechanisms.

It is appropriate to consider, first of all, the behavior of serial chain mechanisms. A serial chain is simply a set of members connected in series. Each member has two joints connecting it to its neighbors, except for the end members, which have only one joint. This is actually a very important type of structure from a practical viewpoint, because it is the configuration of most industrial robots. We will start by developing the methods necessary for systematic position, velocity, and acceleration analysis of serial chains in which all joints are actively controlled and then introduce cases involving closed-loop structures and passive joints later in the chapter.

The study of spatial mechanisms is a large and complex subject. Even a very basic treatment would be much more extensive than we can supply in this one chapter. Consequently, this presentation is limited to an introduction to some of the more important fundamental concepts and the provision of some tools that can be employed to solve relatively simple spatial linkage problems.

### 9.1.2 Velocity and Acceleration Relationships

The relationship between the velocities of two points embedded in the same moving body that was derived for planar motion in Chapter 2 is actually perfectly general for three-dimensional motion:

$$\mathbf{v}_B = \mathbf{v}_A + \boldsymbol{\omega} \times \mathbf{r}_{B/A} \quad (2.1)$$

Similarly, the relationship between the accelerations of those two points

$$\mathbf{a}_B = \mathbf{a}_A + \boldsymbol{\alpha} \times \mathbf{r}_{B/A} + \boldsymbol{\omega} \times (\boldsymbol{\omega} \times \mathbf{r}_{B/A}) \quad (2.7)$$

was also shown to be valid for three-dimensional motion. These expressions, for which three-dimensional proofs were developed in Chapter 3, form the basis for velocity and acceleration analysis of simple spatial mechanisms.

In many cases these relationships can be applied directly. Examples are developed in the next two subsections. The limitations of this approach become evident only when the mechanism position is not known *a priori* and the configuration is sufficiently complex that the position cannot be determined by inspection. As pointed out for planar mechanisms in Chapters 2 and 3, analysis must proceed in the order position analysis, velocity analysis, and acceleration analysis. Spatial system geometry generally does not lend itself to graphical analysis because the essential geometry cannot be captured in a single two-dimensional representation. Consequently, any systematic approach to spatial linkage analysis must be analytically based. As was the case with planar mechanisms, in the analytical domain the position problem tends to be more complex than the velocity and acceleration problems. It is, therefore, advantageous to develop effective means of dealing with the position solution of spatial mechanisms and then to develop velocity and acceleration formulations that are fully compatible with the technique used for position modeling. This will be done in section 9.2 and subsequent sections of this chapter.

However, as noted already, simple vector analysis based on Eqs. (2.1) and (2.7) does work if the position of the mechanism is not an issue. It is, therefore, worthwhile to study some examples using this approach before moving to a more systematic and powerful approach.

Keeping track of the reference frame to which points in a given body are referred is even more important in spatial mechanism analysis than in planar mechanisms. Consequently, the notation used in Chapter 3, in which the reference frame to which a vector is referred is indicated by a superscript placed before the symbol, will be used again here.

#### EXAMPLE 9.1 Analysis of a Simple Spatial Linkage

Given that the disk shown in Fig. 9.1 is rotating about a horizontal axis at  $A$  with an angular velocity with magnitude  $\Omega$ , and the entire assembly is rotating about the  $Y$  axis with an angular velocity with magnitude  $\omega$ , determine the velocity of point  $q$  located on the perimeter of the disk at an angle of  $\beta$  from the  $y$  axis. The radius  $r$  of the disk is given.

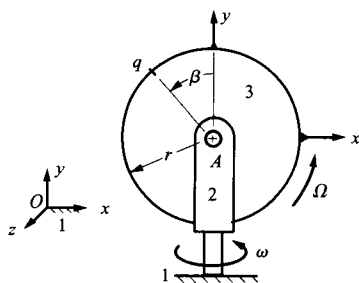


FIGURE 9.1 The mechanism analyzed in Example 9.1.

**Solution**

The problem may be restated in the following form: Given  ${}^1\omega_2 = \omega j$  and  ${}^2\omega_3 = \Omega k$ , together with the quantities  $r$  and  $\beta$ , find  $v_q = {}^1v_{q_3/O_1}$ .

We can use the chain rule developed in Section 3.3.3, but it is first necessary to recognize that location  $A$  gives the points that are easiest to use as a basis for the analysis. Thus

$${}^1v_{q_3/O_1} = {}^1v_{q_3/A_3} + {}^1v_{A_3/A_1} + {}^1v_{A_1/O_1}$$

Because  $A_3$  and  $A_1$  are permanently coincident and  ${}^1v_{A_1} = 0$ , and because  $A_1$  and  $O_1$  are both fixed to link 1, then

$${}^1v_{A_3/A_1} = {}^1v_{A_1/O_1} = 0$$

and

$${}^1v_{q_3/O_1} = {}^1v_{q_3/A_3} = {}^3v_{q_3/A_3} + {}^1\omega_3 \times {}^3r_{q_3/A_3}$$

Now,

$${}^3v_{q_3/A_3} = 0$$

and

$${}^1\omega_3 = \omega j + \Omega k = {}^1\omega_2 + {}^2\omega_3$$

Also

$${}^3r_{q_3/A_3} = -r \sin \beta i + r \cos \beta j$$

At this instant, the coordinate frames are all parallel. Therefore the original cross product can be written as

$${}^1\omega_3 \times {}^3r_{q_3/A_3} = \begin{vmatrix} i & j & k \\ 0 & \omega & \Omega \\ -r \sin \beta & r \cos \beta & 0 \end{vmatrix} = -(\Omega r \cos \beta)i - (\Omega r \sin \beta)j + (\omega r \sin \beta)k$$

and the solution is

$$v_q = {}^1v_{q_3/O_1} = -(\Omega r \cos \beta)i - (\Omega r \sin \beta)j + (\omega r \sin \beta)k$$

**EXAMPLE 9.2**  
**Velocity Analysis**  
**of Spatial**  
**Manipulator**

A simple, three-degree-of-freedom spatial manipulator arm is shown in Fig. 9.2. In this arm,  $AB = BC = CD = 2$  m, and  $AB$  is perpendicular to the  $y$  axis,  $CB$  is perpendicular to  $AB$ , and  $CD$  is perpendicular to  $BC$ . The pair variables associated with the three revolute joints are the angles  $\gamma$ ,  $\theta$ , and  $\phi$  defined as shown. At a given instant in time, rotary potentiometers and tachometers integral with each revolute joint servomotor ( $A$ ,  $B$ , and  $C$ ) indicate that  $\gamma = 30^\circ$ ,  $\theta = 30^\circ$ ,  $\phi = 75^\circ$ ,  $\dot{\gamma} = 20$  rpm,  $\dot{\theta} = -10$  rpm, and  $\dot{\phi} = 15$  rpm. (Positive angles and angular velocities are in the same directions as the angles shown in Fig. 9.2.) At this instant find the velocity of point  $D$  located on link 4 relative to the fixed reference frame.

**Solution**

In our nomenclature, we want to find

$$v_D = {}^1v_{D_4} = {}^1v_{D_4/A_1}$$

Using the chain rule, the velocity equation for point  $D$  is

$${}^1v_{D_4/A_1} = {}^1v_{D_4/C_4} + {}^1v_{C_3/B_3} + {}^1v_{B_2/A_2}$$

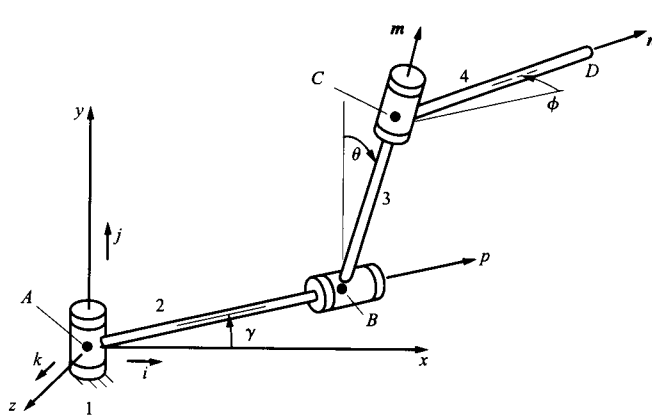


FIGURE 9.2 The three-degree-of-freedom manipulator analyzed in Example 9.2.

which can be expanded to give

$${}^1v_{D_4/A_1} = {}^1\omega_4 \times {}^4r_{D_4/C_4} + {}^1\omega_3 \times {}^3r_{C_3/B_3} + {}^1\omega_2 \times {}^2r_{B_2/A_2}$$

Let  $p$  and  $m$  be unit vectors along lines  $AB$  and  $BC$ , respectively. The components of  $p$  and  $m$  resolved in the fixed frame are

$$p = \cos \gamma i - \sin \gamma k$$

and referring to Fig. 9.3, we have

$$m = \cos \theta j + \sin \theta (\cos \gamma k + \sin \gamma i) = \sin \theta \sin \gamma i + \cos \theta j + \sin \theta \cos \gamma k$$

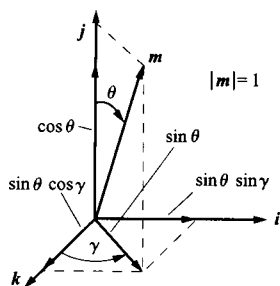
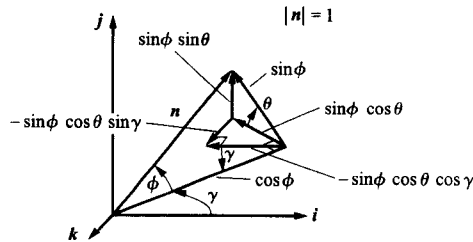


FIGURE 9.3 Decomposition of the vector  $m$  into components parallel to the axes of the fixed reference frame.

To decompose  $n$ , think of it being initially parallel to  $p$ . Then imagine that  $n$  moves in a plane inclined at an angle of  $\theta$  to the  $x$ - $z$  plane, as shown in Fig. 9.4. Then

$$\begin{aligned} n &= \cos \phi p + \sin \phi (\sin \theta j - \cos \theta [\cos \gamma k + \sin \gamma i]) \\ &= (\cos \phi \cos \gamma - \sin \phi \cos \theta \sin \gamma) i + (\sin \phi \sin \theta) j - (\cos \phi \sin \gamma + \sin \phi \cos \theta \cos \gamma) k \end{aligned}$$



**FIGURE 9.4** Decomposition of the vector  $n$  into components parallel to the axes of the fixed reference frame.

The relative angular velocity expressions that are given in the problem statement may now be expressed in the following forms:

$${}^1\omega_2 = \dot{\gamma}j = 20(2\pi)/60 j = 2.094 j \text{ rad/s}$$

$$\begin{aligned} {}^2\omega_3 &= \dot{\theta}p = -10(2\pi)/60 p = -1.047 p \text{ rad/s} \\ &= -1.047(\cos \gamma i - \sin \gamma k) = (-0.9069i + 0.5236k) \text{ rad/s} \end{aligned}$$

$$\begin{aligned} {}^3\omega_4 &= \dot{\phi}m = 15(2\pi)/60 m = 1.571 m \text{ rad/s} = 1.571(\sin \theta \sin \gamma i + \cos \theta j + \sin \theta \cos \gamma k) \\ &= (0.3927i + 1.360j + 0.6802k) \text{ rad/s} \end{aligned}$$

The angular velocities relative to the fixed reference frame necessary for evaluating the cross products are then found using the chain rule (Section 3.3.3). That is,

$${}^1\omega_3 = {}^1\omega_2 + {}^2\omega_3 = 2.094 j - 0.9609i + 0.5236k = (-0.9609i + 2.094j + 0.5236k) \text{ rad/s}$$

and

$$\begin{aligned} {}^1\omega_4 &= {}^1\omega_3 + {}^3\omega_4 = -0.9609i + 2.094j + 0.5236k + 0.3927i + 1.360j + 0.6802k \\ &= (-0.514i + 3.454j + 1.204k) \text{ rad/s} \end{aligned}$$

The required displacement vectors are

$${}^2r_{B_2/A_2} = 2p = 2(\cos \gamma i - \sin \gamma k) = (1.732i - k) \text{ m}$$

$${}^3r_{C_3/B_3} = 2m = 2(\sin \theta \sin \gamma i + \cos \theta j + \sin \theta \cos \gamma k) = (0.5i + 1.732j + 0.866k) \text{ m}$$

$$\begin{aligned} {}^4r_{D_4/C_4} &= 2n = 2[(\cos \phi \cos \gamma - \sin \phi \cos \theta \sin \gamma)i + (\sin \phi \sin \theta)j \\ &\quad - (\cos \phi \sin \gamma + \sin \phi \cos \theta \cos \gamma)k] = (-0.388i + 0.966j - 1.708k) \text{ m} \end{aligned}$$

The terms in the velocity equation can now be computed as follows:

$${}^1v_{B_2/A_2} = {}^1\omega_2 \times {}^2r_{B_2/A_2} = 2.094 j \times (1.732i - k) = (-2.094i - 3.627k) \text{ m/s}$$

$$\begin{aligned} {}^1v_{C_3/B_3} &= {}^1\omega_3 \times {}^3r_{C_3/B_3} = (-0.9069i + 2.094j + 0.5236k) \times (0.5i + 1.732j + 0.866k) \\ &= (0.906i + 1.047j - 2.618k) \text{ m/s} \end{aligned}$$

$$\begin{aligned} {}^1v_{D_4/C_4} &= {}^1\omega_4 \times {}^4r_{D_4/C_4} = (-0.514i + 3.454j + 1.204k) \times (-0.388i + 0.966j - 1.708k) \\ &= (-7.062i - 1.345j + 0.844k) \text{ m/s} \end{aligned}$$

Therefore, the velocity of point  $D$  relative to the fixed reference frame is

$$\begin{aligned} {}^1\mathbf{v}_{D_4/A_1} &= {}^1\mathbf{v}_{B_2/A_2} + {}^1\mathbf{v}_{C_3/B_3} + {}^1\mathbf{v}_{D_4/C_4} = (-2.094\mathbf{i} - 3.627\mathbf{k}) + (0.906\mathbf{i} + 1.047\mathbf{j} - 2.618\mathbf{k}) \\ &\quad + (-7.062\mathbf{i} - 1.345\mathbf{j} + 0.844\mathbf{k}) \\ &= (-8.250\mathbf{i} - 0.298\mathbf{j} - 5.401\mathbf{k}) \text{ m/s} = 9.865(-0.836\mathbf{i} - 0.030\mathbf{j} - 0.547\mathbf{k}) \text{ m/s} \end{aligned}$$

The final result has been expressed in the form of the magnitude of velocity multiplied by a unit vector having the direction of the velocity.

Note that the complexities of this example originated in the necessity of resolving position vectors into components in the axis directions of the fixed reference frame. This resolution can be difficult to visualize and is a potential source of error. Removing those difficulties is a primary motivation of the matrix transformation approach to solving the position problem that is presented in Section 9.3.

### EXAMPLE 9.3

**Acceleration  
Analysis of a  
Spatial  
Manipulator**

#### Solution

In the spatial manipulator arm shown in Fig. 9.2 and considered in Example 9.2, the acceleration readings at the instant examined are  $\ddot{\gamma} = 3 \text{ rad/s}^2$ ,  $\ddot{\theta} = 1 \text{ rad/s}^2$ , and  $\ddot{\phi} = -2 \text{ rad/s}^2$ . As in the previous example,  $AB = BC = CD = 2 \text{ m}$ , and  $AB$  is perpendicular to the  $y$  axis,  $CB$  is perpendicular to  $AB$ , and  $CD$  is perpendicular to  $BC$ . Also  $\gamma = 30^\circ$ ,  $\theta = 30^\circ$ ,  $\phi = 75^\circ$ ,  $\dot{\gamma} = 20 \text{ rpm}$ ,  $\dot{\theta} = 10 \text{ rpm}$ , and  $\dot{\phi} = 15 \text{ rpm}$ .

Find the acceleration of point  $D$  relative to the fixed reference frame.

We shall make use of the following results from Example 9.2:

$$\mathbf{p} = \cos \gamma \mathbf{i} - \sin \gamma \mathbf{k}$$

$$\mathbf{m} = \sin \theta \sin \gamma \mathbf{i} + \cos \theta \mathbf{j} + \sin \theta \cos \gamma \mathbf{k}$$

$$\mathbf{n} = (\cos \phi \cos \gamma - \sin \phi \cos \theta \sin \gamma) \mathbf{i} + (\sin \phi \sin \theta) \mathbf{j} - (\cos \phi \sin \gamma + \sin \phi \cos \theta \cos \gamma) \mathbf{k}$$

$${}^1\boldsymbol{\omega}_2 = 2.094 \mathbf{j} \text{ rad/s}$$

$${}^1\boldsymbol{\omega}_3 = (-0.9069\mathbf{i} + 2.094\mathbf{j} + 0.5236\mathbf{k}) \text{ rad/s}$$

$${}^1\boldsymbol{\omega}_4 = (-0.514\mathbf{i} + 3.454\mathbf{j} + 1.204\mathbf{k}) \text{ rad/s}$$

$${}^2\mathbf{r}_{B_2/A_2} = 2\mathbf{p} = (1.732\mathbf{i} - \mathbf{k}) \text{ m}$$

$${}^3\mathbf{r}_{C_3/B_3} = 2\mathbf{m} = (0.5\mathbf{i} + 1.732\mathbf{j} + 0.866\mathbf{k}) \text{ m}$$

$${}^4\mathbf{r}_{D_4/C_4} = 2\mathbf{n} = (-0.388\mathbf{i} + 0.966\mathbf{j} - 1.708\mathbf{k}) \text{ m}$$

$${}^1\mathbf{v}_{B_2/A_2} = {}^1\boldsymbol{\omega}_2 \times {}^2\mathbf{r}_{B_2/A_2} = (-2.094\mathbf{i} - 3.627\mathbf{k}) \text{ m/s}$$

$${}^1\mathbf{v}_{C_3/B_3} = {}^1\boldsymbol{\omega}_3 \times {}^3\mathbf{r}_{C_3/B_3} = (0.906\mathbf{i} + 1.047\mathbf{j} - 2.618\mathbf{k}) \text{ m/s}$$

$${}^1\mathbf{v}_{D_4/C_4} = {}^1\boldsymbol{\omega}_4 \times {}^4\mathbf{r}_{D_4/C_4} = (-7.062\mathbf{i} - 1.345\mathbf{j} + 0.844\mathbf{k}) \text{ m/s}$$

The fundamental equation that must be solved to obtain  ${}^1\mathbf{a}_{D_4/A_1}$  is

$${}^1\mathbf{a}_{D_4/A_1} = {}^1\mathbf{a}_{D_4/C_4} + {}^1\mathbf{a}_{C_3/B_3} + {}^1\mathbf{a}_{B_2/A_2}$$

The individual terms in this equation will be evaluated separately. However, it is first necessary to evaluate the angular accelerations relative to the fixed reference frame.

The relative angular acceleration expressions are

$$\begin{aligned} {}^1\alpha_2 &= \dot{\gamma}j = 3j \text{ rad/s}^2 \\ {}^2\alpha_3 &= \ddot{\theta}p = 1p = 1(\cos \gamma i - \sin \gamma k) = (0.866i - 0.500k) \text{ rad/s}^2 \\ {}^3\alpha_4 &= \ddot{\phi}m = -2m = -2(\sin \theta \sin \gamma i + \cos \theta j + \sin \theta \cos \gamma k) \\ &= (-0.500i - 1.732j - 0.866k) \text{ rad/s}^2 \end{aligned}$$

so the angular accelerations relative to the fixed reference frame are

$$\begin{aligned} {}^1\alpha_2 &= \dot{\gamma}j = 3j \text{ rad/s}^2 \\ {}^1\alpha_3 &= {}^1\alpha_2 + {}^2\alpha_3 + {}^1\omega_2 \times {}^2\omega_3 = 3j + 0.866i - 0.500k + 2.094j \times (-0.9069i + 0.5236k) \\ &= (1.962i + 3j + 1.399k) \text{ rad/s}^2 \\ {}^1\alpha_4 &= {}^1\alpha_3 + {}^3\alpha_4 + {}^1\omega_3 \times {}^3\omega_4 = 1.962i + 3j + 1.399k - 0.500i - 1.732j - 0.866k \\ &\quad + (-0.907i + 2.094j + 0.524k) \times (0.3927i + 1.360j + 0.6802k) \\ &= (2.174i + 2.091j - 1.523k) \text{ rad/s}^2 \end{aligned}$$

Now the individual acceleration terms are

$$\begin{aligned} {}^1a_{B_2/A_2}^r &= {}^1\omega_2 \times {}^1v_{B_2/A_2} = (2.094j) \times (-2.094i - 3.627k) = (-7.595i + 4.385k) \text{ m/s}^2 \\ {}^1a_{B_2/A_2}^t &= {}^1\alpha_2 \times {}^2r_{B_2/A_2} = (3j) \times (1.732i - k) = (3i - 5.196k) \text{ m/s}^2 \\ {}^1a_{C_3/B_3}^r &= {}^1\omega_3 \times {}^1v_{C_3/B_3} = (-0.9069i + 2.094j + 0.5236k) \times (0.906i + 1.047j - 2.618k) \\ &= (-6.031i - 1.900j - 2.847k) \text{ m/s}^2 \\ {}^1a_{C_3/B_3}^t &= {}^1\alpha_3 \times {}^3r_{C_3/B_3} = (1.962i + 3j + 1.399k) \times (0.5i + 1.732j + 0.866k) \\ &= (0.175i + -1.00j + 1.898k) \text{ m/s}^2 \\ {}^1a_{D_4/C_4}^r &= {}^1\omega_4 \times {}^1v_{D_4/C_4} = (-0.514i + 3.454j + 1.204k) \\ &\quad \times (-7.062i - 1.345j + 0.844k) = (4.535i - 8.069j + 25.083k) \text{ m/s}^2 \\ {}^1a_{D_4/C_4}^t &= {}^1\alpha_4 \times {}^4r_{D_4/C_4} = (2.174i + 2.091j - 1.523k) \times (-0.388i + 0.966j - 1.708k) \\ &= (-2.100i + 4.304j + 2.911k) \text{ m/s}^2 \end{aligned}$$

The total acceleration of point  $D$  is now given by

$$\begin{aligned} {}^1a_{D_4/A_1} &= (-7.595 - 3.000 - 6.031 + 0.175 + 4.535 - 2.100)i \\ &\quad + (-1.900 - 1.000 - 8.069 + 4.304)j \\ &\quad + (4.385 - 5.196 + 2.847 + 1.898 + 25.083 + 2.911)k \\ &= (-14.02i - 6.67j + 26.23k) \text{ m/s}^2 = 30.48(-0.460i - 0.219j + 0.861k) \text{ m/s}^2 \end{aligned}$$

The final form of the result is expressed as the magnitude of the acceleration times a unit vector in the direction of the acceleration. Problems of this type can be solved relatively quickly with the aid of a programmable hand calculator set up to solve three-dimensional cross products or with computer tools such as MATLAB. Less powerful calculators will require some repetitious mathematical manipulations by the user but still enable such problems to be solved in a reasonable time.

## 9.2 ROBOTIC MECHANISMS

---

Robotic mechanisms form a very important class of spatial mechanisms. They are distinct from most of the mechanisms discussed elsewhere in this book in that they have a large number of actuated degrees of freedom. Whereas many mechanisms have only one degree of freedom, actuated by a single drive, robotic mechanisms have four, five, six, or more with independent actuation of each degree of freedom. This leads to the problem of *coordination*, which may be stated as follows: Given the desired motion of the robot “hand,” what should the commanded values of the joint actuator variables be to achieve that motion? In a complex one-degree-of-freedom mechanism there may be a considerable number of output motions all driven by a single input. These motions are coordinated kinematically via the mechanism. In a robotic mechanism, in contrast, the coordination is done electronically by a computer integrated into the machine. The need for a theory for robotic coordination has led to the formulation of several important subproblems.

Two important types of problem in robotic coordination have come to be known as the *direct* and *inverse* kinematics problems. There are actually direct and inverse position, velocity, and acceleration problems. They may be stated for position as follows.

The direct kinematics problem for a serial chain such as that shown in Fig. 9.5 is

*Given the positions of all of the joints, find the position of the “hand” relative to the “base.”*

We will commonly refer to the free end member of a serial chain as the “hand,” following from the common application of this type of analysis to robotic systems. In robotics, the free end member is also often called the “end effector.” This term results from its function as being the tool with which a manipulator interacts with the workpiece. We use “hand” for convenience, although the end member may not resemble a human hand and need not be a tool. Likewise, it is convenient to refer to the other end member as the “base,” even though in some situations it may not be fixed relative to Earth.

A more precise and general statement of the direct kinematics problem is

*Given the values of a number of joint parameters equal to the mobility (number of degrees of freedom) of a mechanism, find the relative position of any two designated members.*

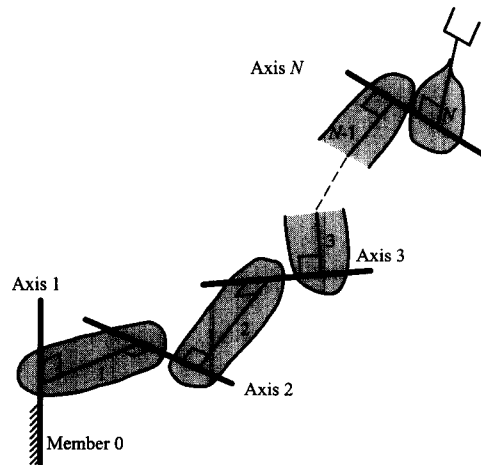
The inverse kinematics problem for the serial chain shown in Fig. 9.5 is

*Given the position of the hand relative to the base, find the positions of all of the joints.*

Once again, this is a simplified statement applying only to the serial chain. A more general statement is

*Given the relative positions of two members of a mechanism, find all of the joint parameters.*





**FIGURE 9.5** A general serial chain with axial joints. The chain has  $N$  joint axes, labeled as 1 to  $N$ , and  $N + 1$  members labeled as 0 to  $N$ . Member 0 is the fixed base member.

As will be seen later, it is necessary to qualify further the statements of the inverse kinematics problem. Those given thus far apply without qualification only to the case in which the mechanism has six degrees of freedom.

Analogs of the direct and inverse kinematics problems can be stated in terms of joint velocities and member velocities. These are also very important problems in the development of robotic software. They can be stated for the serial chain as follows.

The direct velocity problem for the serial chain is

*Given the positions of all members of the chain and the angular velocities about all joints, find the total velocity of the hand.*

Here the rate of motion about the joint is the angular velocity about a revolute joint or the translational velocity along a prismatic joint. The total velocity of a member is the velocity of the origin of the reference frame fixed to it, combined with its angular velocity. That is, the total velocity has six independent components and, therefore, completely represents the velocity field of the member.

The inverse velocity problem for a serial chain is

*Given the positions of all members of the chain and the total velocity of the hand, find the velocities about all joints.*

It is important to notice that these definitions include an assumption that the position of the mechanism is completely known. In many situations, this means that either the direct or inverse position kinematics problem must be solved before the direct or inverse velocity problem can be addressed.

## 9.3 DIRECT POSITION KINEMATICS OF SERIAL CHAINS

### 9.3.1 Introduction

The problem to be addressed here is that of finding the hand position of a serial chain when the joint positions are known. This is a very important problem from the point of view of

constructing manipulator coordination algorithms, because the joint positions are directly measured by sensors mounted on the joints. It is necessary to compute the positions of the joint axes relative to the fixed reference frame. This is done by means of the solution presented in the following.

The first problem in developing a mathematical model of a spatial mechanism, such as a robot, is that of algebraically describing the position of a body in space. There are many ways to do this. The approach we will use here is the most common one in which the position of a body is represented by the elements of a matrix coordinate transformation. This will be done by writing a position transformation between the two Cartesian coordinate frames in the moving and fixed bodies. The parameters that describe this transformation can then be said to describe the position of the moving body relative to the fixed frame.

Let  $[x,y,z]$  be a fixed reference frame and let  $[x',y',z']$  be a reference frame fixed in the moving body (Fig. 9.6). The coordinates of the point  $P$  in the fixed reference frame may be obtained from its coordinates in the moving reference frame by a transformation of the form

$$\mathbf{p} = \mathbf{Q}\mathbf{p}' + \mathbf{q}$$

$$\mathbf{p} = \begin{bmatrix} x \\ y \\ z \end{bmatrix}, \quad \mathbf{p}' = \begin{bmatrix} x' \\ y' \\ z' \end{bmatrix}$$
(9.1)

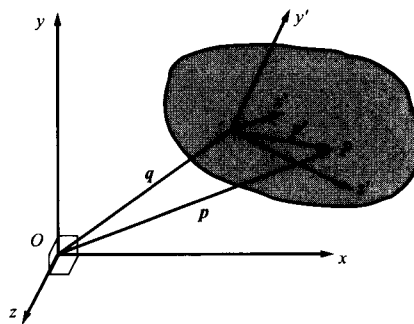
Here  $\mathbf{Q}$  is a  $3 \times 3$  matrix, and  $\mathbf{q}$  is the vector of components of the position of the origin of the moving reference frame relative to the fixed reference frame.

Now, if the geometry of the moving body is known in terms of the reference frame  $(x', y', z')$  fixed in it, the position of any point in that body with respect to the fixed frame is also known provided the matrix  $\mathbf{Q}$  and the vector  $\mathbf{q}$  are known. The transformation can be regarded as describing the position of the moving body in space.

The matrix  $\mathbf{Q}$  has a very special property: It is an orthogonal matrix. For an orthogonal matrix

$$\mathbf{Q}^T \mathbf{Q} = \mathbf{I} \quad \text{or} \quad \mathbf{Q}^T = \mathbf{Q}^{-1}$$
(9.2)

The property of orthogonality follows from the assumption that the body is rigid.



**FIGURE 9.6** Relationship between body reference frame  $[x',y',z']$  and fixed reference frame  $[x,y,z]$ .  $P$  is an arbitrary point,  $\mathbf{p}'$  is the position of  $P$  in the body fixed reference frame, and  $\mathbf{p}$  is the position of that point in the fixed reference frame.

An important feature of the description of the position of a body in space by coordinate transformation elements, that is, the elements of  $\mathbf{Q}$  and  $\mathbf{q}$ , is that there are 12 elements in these two entities, 9 in  $\mathbf{Q}$  and 3 in  $\mathbf{q}$ :

$$\mathbf{Q} = \begin{bmatrix} q_{11} & q_{12} & q_{13} \\ q_{21} & q_{22} & q_{23} \\ q_{31} & q_{32} & q_{33} \end{bmatrix}, \quad \mathbf{q} = \begin{bmatrix} q_1 \\ q_2 \\ q_3 \end{bmatrix}$$

Since only 6 coordinates are needed to fix the position of a body in space, these 12 quantities cannot be independent, but there must be at least six independent relationships among them. The orthogonality condition,  $\mathbf{Q}^T \mathbf{Q} = \mathbf{I}$ , provides these relationships.

$$\mathbf{Q}^T \mathbf{Q} = \begin{bmatrix} q_{11} & q_{21} & q_{31} \\ q_{12} & q_{22} & q_{32} \\ q_{13} & q_{23} & q_{33} \end{bmatrix} \begin{bmatrix} q_{11} & q_{12} & q_{13} \\ q_{21} & q_{22} & q_{23} \\ q_{31} & q_{32} & q_{33} \end{bmatrix} = \begin{bmatrix} 1 & 0 & 0 \\ 0 & 1 & 0 \\ 0 & 0 & 1 \end{bmatrix}$$

which gives

$$q_{11}^2 + q_{21}^2 + q_{31}^2 = 1 \quad (\text{i})$$

$$q_{11}q_{12} + q_{21}q_{22} + q_{31}q_{32} = 0 \quad (\text{ii})$$

$$q_{11}q_{13} + q_{21}q_{23} + q_{31}q_{33} = 0 \quad (\text{iii})$$

$$q_{12}q_{11} + q_{22}q_{21} + q_{32}q_{31} = 0$$

$$q_{12}^2 + q_{22}^2 + q_{32}^2 = 1 \quad (\text{iv})$$

$$q_{12}q_{13} + q_{22}q_{23} + q_{32}q_{33} = 0 \quad (\text{v})$$

$$q_{13}q_{11} + q_{23}q_{21} + q_{33}q_{31} = 0$$

$$q_{13}q_{12} + q_{23}q_{22} + q_{33}q_{32} = 0$$

$$q_{13}^2 + q_{23}^2 + q_{33}^2 = 1 \quad (\text{vi})$$

(9.3)

As can be seen, three of these equations are repeated, so only the six marked are distinct. Therefore, only three of the elements of  $\mathbf{Q}$  are independent. The rest can be generated from these three by means of Eqs. (i) to (vi). It follows that six variables are needed to specify the transformation in Eq. (9.1): three elements of  $\mathbf{Q}$  and the three elements of  $\mathbf{q}$ . That is, as expected, six coordinates are needed to describe the position of the body.

### 9.3.2 Concatenation of Transformations

In Section 9.3.1 the concept of representing the position of a body in space by means of a coordinate transformation was introduced. A reference frame is fixed to the body, and the transformation is written that converts the coordinates of points relative to that frame into their coordinates relative to the fixed frame. It has the form

$$\mathbf{p} = \mathbf{Q}\mathbf{p}' + \mathbf{q} \quad (9.1)$$

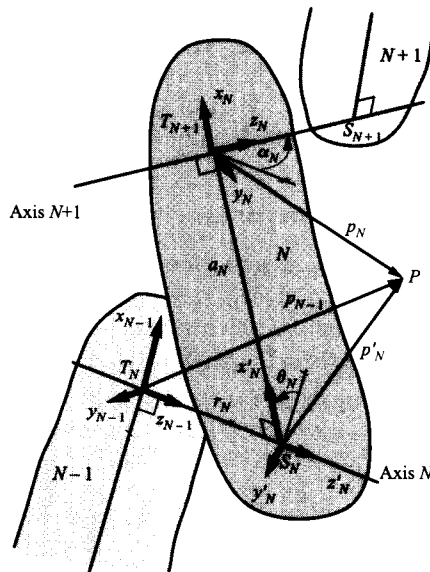
Here  $p'$  is the position of a point relative to the reference frame fixed in the body,  $p$  is the position of the same point referred to the fixed reference frame,  $Q$  is a  $3 \times 3$  matrix that rotates the body reference frame until it is parallel to the fixed frame, and  $q$  is the position of the origin of the body reference frame relative to that of the fixed frame.

We will now consider the application of this model to a serial chain in which  $N + 1$  members are connected by  $N$  joints with each member having two joints formed in it except for the two end members, which have only one joint each. Figure 9.5 shows a general serial chain.

The important feature here is to establish a convention that defines a consistent location for the reference frame in each member of the chain. The transformations representing the positions of the joints can then be applied successively to produce the transformation relating the end members of the chain.

Figure 9.7 shows the important geometric features of a binary link on which are mounted two axial joints. The term "axial joint" is used to define any joint that has a fixed axis of motion. Among lower pairs, revolute, screw, and cylindric joints are axial. A prismatic joint can also be regarded as axial with an axis in the direction of translation. The axis is, in this case, not unique and may be specified as lying along any convenient line parallel to the direction of translation. As will be seen, the restriction to axial joints allows simple expression of the transformation matrices. Because the overwhelming majority of kinematic joints in practical use are axial joints, this simplification is not unduly restrictive.

The two joints mounted on member  $N$  are named joints  $N$  and  $N + 1$ . The common normal to the two joint axes,  $S_N T_{N+1}$ , has length  $a_N$  and the distance  $T_N S_N$  along axis  $N$  between the foot of the common normal to joints  $N - 1$  and  $N$  and that to joints  $N$  and  $N + 1$  is the offset,  $r_N$ . The angle between those two normals is the joint angle,  $\theta_N$ . The positive direction of each normal for the purpose of defining this angle is directed from the lower numbered axis to the higher. The angle between axes  $N$  and  $N + 1$  is the twist angle,  $\alpha_N$ . The reference frame fixed to the  $N^{\text{th}}$  member has its origin located at  $T_{N+1}$ ; the foot of the common normal on axis  $N + 1$ . The  $x_N$  axis is aligned with the common normal, as shown, and the  $z_N$  axis lies along axis  $N + 1$ . Reference frame  $N - 1$  is located in the corresponding position on member  $N - 1$ . An intermediate reference frame  $N'$ ,  $[x', y', z']$  is also fixed to body  $N$ . Its origin is at  $S_N$ , the foot of the common normal on axis  $N$ . The  $x'_N$  axis lies along that normal, and the  $z'_N$  axis lies along axis  $N$ .



**FIGURE 9.7** The "skeleton" of a binary link. A binary link is one with two axial joints. The geometry of the link and the position of the joint on axis  $N$  are completely defined by the parameters  $a_N$ , the length of the common normal of the joint axes;  $r_N$ , the distance along axis  $N$  from the foot of the common normal of link  $N - 1$  to that of link  $N$ ;  $\alpha_N$ , the twist angle between axis  $N$  and axis  $N + 1$ ; and  $\theta_N$ , the angle between the normal of link  $N - 1$  and that of link  $N$ .

The joint axes together with the common normals on the links can be thought of as defining the “skeleton” of the linkage. The parameters  $a_N$ ,  $r_N$ ,  $\alpha_N$ , and  $\theta_N$  together completely define link  $N$  and the position of joint  $N$ .

Let us consider the transformation from reference frame  $N$  to frame  $N'$ . For the position of an arbitrary point  $P$  we have

$$\mathbf{p} = [x_N, y_N, z_N]^T \quad \text{and} \quad \mathbf{p}' = [x'_N, y'_N, z'_N]^T$$

where

$$\begin{aligned} x'_N &= x_N + a_N \\ y'_N &= y_N \cos \alpha_N - z_N \sin \alpha_N \\ z'_N &= y_N \sin \alpha_N + z_N \cos \alpha_N \end{aligned}$$

The last two equations are readily derived with the aid of Fig. 9.8, which shows a view of the system directed along the  $x_N x'_N$  axis. The preceding equations can be written in the form

$$\mathbf{p}'_N = \mathbf{V}_N \mathbf{p}_N + \mathbf{v}_N \quad (9.4)$$

where

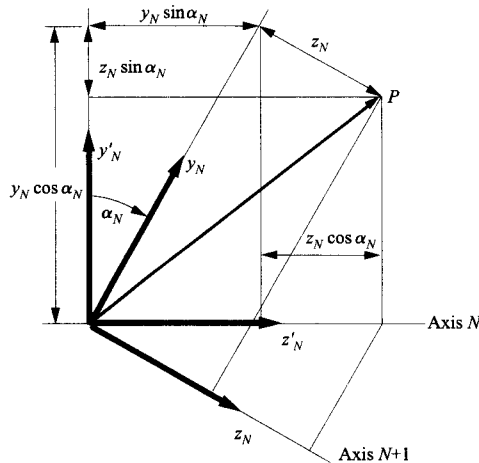
$$\mathbf{V}_N = \begin{bmatrix} 1 & 0 & 0 \\ 0 & \cos \alpha_N & -\sin \alpha_N \\ 0 & \sin \alpha_N & \cos \alpha_N \end{bmatrix} \quad \text{and} \quad \mathbf{v}_N = \begin{bmatrix} a_N \\ 0 \\ 0 \end{bmatrix}$$

The transformation from the  $N-1$  frame to the  $N'$  frame is obtained from

$$\mathbf{p}_{N-1} = [x_{N-1}, y_{N-1}, z_{N-1}]^T$$

where

$$\begin{aligned} x_{N-1} &= x'_N \cos \theta_N - y'_N \sin \theta_N \\ y_{N-1} &= x'_N \sin \theta_N + y'_N \cos \theta_N \\ z_{N-1} &= z'_N + r_N \end{aligned}$$



**FIGURE 9.8** View along the common normal of axes  $N$  and  $N+1$ . The coordinates of point  $P$  in the  $N$  and  $N'$  frames can be related by taking components as shown.

Figure 9.9 shows frames  $N-1$  and  $N'$  viewed along axis  $N$ . The equations can be written in the form

$$\mathbf{p}_{N-1} = \mathbf{U}_N \mathbf{p}'_N + \mathbf{u}_N \tag{9.5}$$

where

$$\mathbf{U}_N = \begin{bmatrix} \cos \theta_N & -\sin \theta_N & 0 \\ \sin \theta_N & \cos \theta_N & 0 \\ 0 & 0 & 1 \end{bmatrix} \quad \mathbf{u}_N = \begin{bmatrix} 0 \\ 0 \\ r_N \end{bmatrix}$$

Expanding Eq. (9.5), we get

$$\mathbf{p}_{N-1} = \mathbf{U}_N (\mathbf{V}_N \mathbf{p}_N + \mathbf{v}_N) + \mathbf{u}_N$$

which can be further rearranged to

$$\mathbf{p}_{N-1} = \mathbf{U}_N (\mathbf{V}_N \mathbf{p}_N + \mathbf{s}_N) \tag{9.6}$$

where

$$\mathbf{s}_N = \mathbf{v}_N + \mathbf{U}_N^T \mathbf{u}_N = [a_N, 0, r_N]^T$$

Equation (9.6) has the same form as Eq. (9.1) but is specialized for an axial joint.

Depending on which of the parameters of the transformation in Eq. (9.6) are allowed to vary, it can represent different types of axial joints. A revolute is obtained by allowing  $\theta_N$  to vary while keeping all other dimensions constant. A prismatic joint is obtained by allowing  $r_N$  to vary while  $\theta_N$  and all other dimensions remain constant.

It is now possible to write a transformation expressing the position of member  $N$  of a chain such as that shown in Fig. 9.5. The transformation is expressed in terms of the joint variables. For a chain containing only axial joints

$$\mathbf{p}_0 = \mathbf{U}_1 (\mathbf{V}_1 \mathbf{U}_2 (\mathbf{V}_2 \mathbf{U}_3 (\dots \mathbf{U}_N (\mathbf{V}_N \mathbf{p}_N + \mathbf{s}_N) + \dots) + \mathbf{s}_2) + \mathbf{s}_1) \tag{9.7}$$

This equation can be used to find the position in a fixed frame,  $\mathbf{p}_0$ , of any point given its position  $\mathbf{p}_N$ , relative to the end member, and the position coordinates of the joints in the chain. Alternatively, it may be used to derive equations between the joint position coordi-

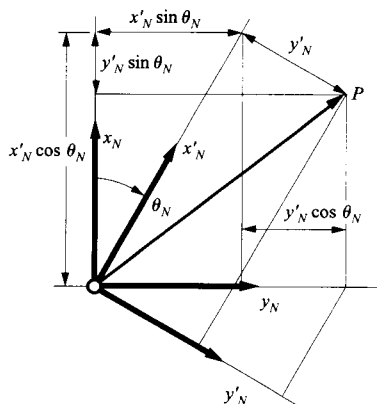


FIGURE 9.9 View along axis  $N$ . The coordinates of point  $P$  in the  $N-1$  and  $N'$  frames can be related by taking components as shown.

nates given the position of one end member relative to the other. In this latter case, the position of member  $n$  relative to member 0 is given by a known transformation

$$\mathbf{p}_0 = \mathbf{Q}\mathbf{p}_N + \mathbf{q} \quad (9.1)$$

Since this transformation and Eq. (9.7) must be identical, we have

$$\mathbf{Q} = \mathbf{U}_1\mathbf{V}_1\mathbf{U}_2\mathbf{V}_2\mathbf{U}_3 \dots \mathbf{U}_N\mathbf{V}_N \quad (9.8a)$$

The scalar component equations from Eq. (9.8a) are called the rotation equations. Also

$$\mathbf{q} = \mathbf{U}_1\mathbf{V}_1\mathbf{U}_2\mathbf{V}_2\mathbf{U}_3 \dots \mathbf{V}_{N-1}\mathbf{U}_N\mathbf{s}_N \dots + \mathbf{U}_1\mathbf{V}_1\mathbf{U}_2\mathbf{s}_2 + \mathbf{U}_1\mathbf{s}_1 \quad (9.8b)$$

The scalar component equations from Eq. (9.8b) are called the translation equations.

### 9.3.3 Homogeneous Transformations

The transformation

$$\mathbf{p}_{N-1} = \mathbf{U}_N(\mathbf{V}_N\mathbf{p}_N + \mathbf{s}_N) \quad (9.6)$$

that converts from the coordinate frame on link  $N$  to that on link  $N-1$  can be written as a single four-dimensional matrix-vector multiplication:

$$\mathbf{p}'_{N-1} = \mathbf{A}_N\mathbf{p}'_N \quad (9.9)$$

where

$$\mathbf{A}_N = \begin{bmatrix} \cos \theta_N & -\sin \theta_N \cos \alpha_N & \sin \theta_N \sin \alpha_N & a_N \cos \theta_N \\ \sin \theta_N & \cos \theta_N \cos \alpha_N & -\cos \theta_N \sin \alpha_N & a_N \sin \theta_N \\ 0 & \sin \alpha_N & \cos \alpha_N & r_N \\ 0 & 0 & 0 & 1 \end{bmatrix} \quad (9.10)$$

and

$$\mathbf{p}'_N = \begin{bmatrix} x_N \\ y_N \\ z_N \\ 1 \end{bmatrix} \quad (9.11)$$

The three-by-three submatrix in the top left-hand corner of  $\mathbf{A}_N$  can be recognized as  $\mathbf{U}_N\mathbf{V}_N$ , while the fourth column is  $\mathbf{U}_N\mathbf{s}_N$  with 1 added as the fourth element. The reader may verify that, when expanded, Eqs. (9.6) and (9.9) give the same three component equations. The fourth equation given by the latter is  $1 = 1$ . Note that, in this system, the "zero" vector is

$$\mathbf{O} = \begin{bmatrix} 0 \\ 0 \\ 0 \\ 1 \end{bmatrix}, \quad \text{not} \quad \begin{bmatrix} 0 \\ 0 \\ 0 \\ 0 \end{bmatrix}.$$

TABLE 9.1 Geometry Parameters for Example 9.4

$i$	$a_i$	$r_i$	$\alpha_i$	$\theta_i$
1	0	0	90°	60°
2	0	0	90°	120°
3	0	0	0°	135°
4	0	4.0	90°	0°
5	0	0	90°	-60°
6	0	1.0	0°	45°

Using this formulation, we find that Eqs. (9.8a) and (9.8b), which relate hand position to the joint variables, assume the form (for  $N = 6$ )

$$Q' = A_1 A_2 A_3 A_4 A_5 A_6 \quad (9.12)$$

where

$$Q' = \begin{bmatrix} q_{11} & q_{12} & q_{13} & q_1 \\ q_{21} & q_{22} & q_{23} & q_2 \\ q_{31} & q_{32} & q_{33} & q_3 \\ 0 & 0 & 0 & 1 \end{bmatrix} \quad (9.13)$$

This very compact formulation is attractive and variants of it have been extensively used in spatial mechanism theory, computer graphics, and robotics. It is particularly attractive when ease of programming is the most important consideration.

Equation (9.9) is called a homogeneous transformation because it has the form of a transformation of the homogeneous coordinates used in projective geometry.

#### EXAMPLE 9.4 Computation of Homogeneous Transformation

The fixed geometric parameters of the manipulator shown in Fig. 9.10 are shown in Table 9.1. If the joint variables have the values  $\theta_1 = 60^\circ$ ,  $\theta_2 = 120^\circ$ ,  $\theta_3 = 135^\circ$ ,  $r_4 = 4.0$ ,  $\theta_5 = -60^\circ$ , and  $\theta_6 = 45^\circ$ , find the homogeneous transformation  $Q'$  that specifies the position of the hand.

Notice that, because joint 4 is a prismatic joint, the joint variable is  $r_4$ , and  $\theta_4$  is a fixed geometric parameter. All of the other joints are revolute, so that  $\theta_i$  is the joint variable, and  $r_i$  is a fixed geometric parameter for all  $i$  except 4.

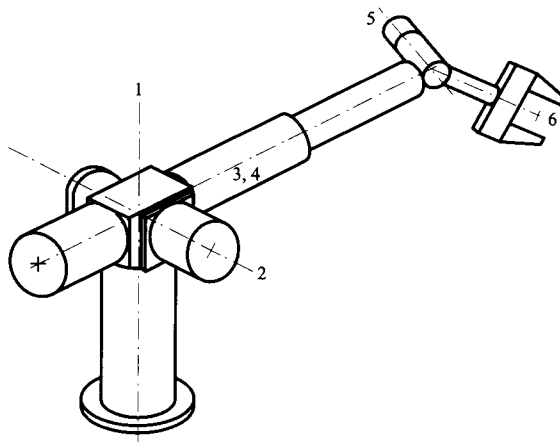


FIGURE 9.10 The manipulator of Example 9.4. The geometric parameters are summarized in Table 9.1.



**Solution**

Substitution of  $a_1$ ,  $\alpha_1$  and  $r_1$  from Table 9.1, together with the value of  $\theta_1$  in Eq. (9.10), gives

$$A_1 = \begin{bmatrix} 0.5 & 0 & 0.8660 & 0 \\ 0.8660 & 0 & -0.5 & 0 \\ 0 & 1 & 0 & 0 \\ 0 & 0 & 0 & 1 \end{bmatrix}$$

Similarly,

$$A_2 = \begin{bmatrix} -0.5 & 0 & 0.8660 & 0 \\ 0.8660 & 0 & 0.5 & 0 \\ 0 & 1 & 0 & 0 \\ 0 & 0 & 0 & 1 \end{bmatrix}, \quad A_3 = \begin{bmatrix} -0.7070 & -0.7070 & 0 & 0 \\ 0.7070 & -0.7070 & 0 & 0 \\ 0 & 0 & 1 & 0 \\ 0 & 0 & 0 & 1 \end{bmatrix}, \quad A_4 = \begin{bmatrix} 1 & 0 & 0 & 0 \\ 0 & 0 & -1 & 0 \\ 0 & 1 & 0 & 4 \\ 0 & 0 & 0 & 1 \end{bmatrix}$$

$$A_5 = \begin{bmatrix} 0.5 & 0 & -0.8660 & 0 \\ -0.8660 & 0 & -0.5 & 0 \\ 0 & 1 & 0 & 0 \\ 0 & 0 & 0 & 1 \end{bmatrix}, \quad A_6 = \begin{bmatrix} 0.7070 & -0.7070 & 0 & 0 \\ 0.7070 & 0.7070 & 0 & 0 \\ 0 & 0 & 1 & 1 \\ 0 & 0 & 0 & 1 \end{bmatrix}$$

Applying Eq. (9.12), we multiply these matrices together to get

$$Q' = A_1 A_2 A_3 A_4 A_5 A_6 = \begin{bmatrix} 0.3220 & 0.2945 & -0.8998 & 0.8323 \\ -0.9423 & 0.0096 & -0.3340 & 2.6660 \\ -0.0897 & 0.9555 & 0.2803 & 2.2803 \\ 0 & 0 & 0 & 1 \end{bmatrix}$$

Then  $Q'$  is the transformation matrix that describes the position of the hand.

An inconvenience of working with the  $A_N$  matrices, rather than the  $U_N$  and  $V_N$  matrices from which they are derived, is that, unlike  $U_N$  and  $V_N$ ,  $A_N$  is not an orthogonal matrix. That is,

$$A_N^{-1} \neq A_N^T$$

To derive an expression for  $A_N^{-1}$  it is most efficient to return to Eq. (9.6):

$$p_{N-1} = U_N (V_N p_N + s_N) \quad (9.6)$$

Premultiplication of both sides by  $U_N^T$  gives

$$U_N^T p_{N-1} = V_N p_N + s_N$$

Moving  $s_N$  to the other side of the equation and then premultiplying by  $V_N^T$  gives

$$p_N = V_N^T (U_N^T p_{N-1} - s_N) \quad (9.14)$$

In the same manner as Eq. (9.10), this expression can be written as a  $4 \times 4$  matrix expression:

$$p_{N'} = A_N^{-1} p_{N-1'} \quad (9.15)$$

where

$$A_N^{-1} = \begin{bmatrix} \cos \theta_N & \sin \theta_N & 0 & -a_N \\ -\sin \theta_N \cos \alpha_N & \cos \theta_N \cos \alpha_N & \sin \alpha_N & -r_N \sin \alpha_N \\ \sin \theta_N \sin \alpha_N & -\cos \theta_N \sin \alpha_N & \cos \alpha_N & -r_N \cos \alpha_N \\ 0 & 0 & 0 & 1 \end{bmatrix} \quad (9.16)$$

and

$$p_N' = \begin{bmatrix} x_N \\ y_N \\ z_N \\ 1 \end{bmatrix} \quad (9.11)$$

as before.

The reader may verify that the expressions for  $A_N$  and  $A_N^{-1}$  given by Eqs. (9.10) and (9.16) satisfy the relationship

$$A_N^{-1} A_N = I$$

## 9.4 INVERSE POSITION KINEMATICS

---

As stated earlier, the inverse kinematics problem for the serial chain shown in Fig. 9.5 is

*Given the position of the hand relative to the base, find the positions of all of the joints.*

This amounts to finding the joint parameters if the homogeneous matrix,  $Q'$ , of Eq. (9.12) is given. Solution requires expansion of Eq. (9.12) using the expression given by Eq. (9.10) for each of the matrices  $A_N$ . A total of  $N$  of the resulting set of scalar equations are selected to be solved for the variables  $\theta_i$ ,  $i = 1, \dots, N$ , describing the positions of revolute joints, or  $r_i$  describing the positions of prismatic joints. The resulting equations are nonlinear and are sometimes very difficult to solve, although the simple geometries commonly used are usually tractable.<sup>1</sup> Nevertheless, the solution of the inverse position equations is beyond the scope of this book. Fortunately, this problem is of less practical importance than the direct position kinematics and inverse velocity problems, which must be solved on-line many times per second in most manipulator coordination schemes.

## 9.5 DIRECT AND INVERSE VELOCITY PROBLEMS

---

### 9.5.1 Introduction

As was stated earlier, the direct rate velocity problem for the serial chain is

*Given the positions of all members of the chain and the rates of motion about all joints, find the total velocity of the hand.*

The rate of motion about the joint is the angular velocity of rotation about a revolute joint or the translational velocity of sliding along a prismatic joint. The total velocity of a

member is the velocity of the origin of the reference frame fixed to it combined with its angular velocity. That is, the total velocity has six independent components and therefore completely represents the velocity field of the member.

The inverse velocity problem for a serial chain is

*Given the positions of all members of the chain and the total velocity of the hand, find the rates of motion of all joints.*

Once again, it is important to notice that these definitions include an assumption that the position of the mechanism is completely known. In many situations, this means that either the direct or inverse position kinematics problem must be solved before the direct or inverse velocity problem can be addressed.

When controlling a movement of an industrial robot that operates in the point-to-point mode, it is not only necessary to compute the final joint positions needed to assume the desired final hand position. It is also necessary to generate a smooth trajectory for motion between the initial and final positions. There are, of course, infinitely many possible trajectories for this purpose. However, the most straightforward and successful approach employs algorithms based on the solution of the inverse rate kinematics problem. This technique originated in the work of Whitney<sup>2</sup> and of Pieper and Roth.<sup>3</sup>

### 9.5.2 Direct Rate Kinematics

According to the chain rule for angular velocities developed in Section 3.3.3, the angular velocity of the hand of a serial chain, such as that shown in Fig. 9.5, with  $N = 6$  joints (seven members including the base) is

$${}^0\boldsymbol{\omega}_6 = {}^0\boldsymbol{\omega}_1 + {}^1\boldsymbol{\omega}_2 + {}^2\boldsymbol{\omega}_3 + {}^3\boldsymbol{\omega}_4 + {}^4\boldsymbol{\omega}_5 + {}^5\boldsymbol{\omega}_6 \quad (9.17)$$

Here the base member to which the fixed reference frame is attached is referred to as member 0. This is the usual convention used for identifying members of robotic mechanisms.<sup>1</sup> Each member has a reference frame attached to it, and so  ${}^i\boldsymbol{\omega}_j$  is the angular velocity of member  $j$  relative to a reference frame fixed to member  $i$ . If  $i$  and  $j$  are consecutive members,  ${}^i\boldsymbol{\omega}_j$  becomes the angular velocity of one member relative to the other about the joint that connects them. That is,

$${}^{i-1}\boldsymbol{\omega}_i = \dot{\theta}_i {}^0\boldsymbol{w}_i \quad (9.18)$$

where  ${}^0\boldsymbol{w}_i$  is a unit vector having the direction of axis  $i$ .

Combining Eq. (9.18) with Eq. (9.17), we have that the angular velocity  ${}^0\boldsymbol{\omega}_N$  of the hand is related to the joint rates by

$${}^0\boldsymbol{\omega}_N = \sum_{k=1}^N \dot{\theta}_k {}^0\boldsymbol{w}_k \quad (9.19)$$

where  ${}^0\boldsymbol{w}_k$  is a unit vector having the direction of joint axis  $k$ .

The velocity of the origin,  $O_N$ , of the reference frame fixed to the hand (frame 6) relative to the fixed frame (frame 0) can be obtained by summing the components of that velocity due to motion about the respective joints. The velocity of point  $O_N$  relative to frame 0 produced by motion about joint  $i$  is

$${}^0\boldsymbol{v}_{O_N,i} = {}^{i-1}\boldsymbol{\omega}_i \times {}^0\boldsymbol{r}_i \quad (9.20)$$

where  ${}^0\mathbf{r}_i$  is the vector from any point on axis  $i$  to point  $O_N$ . Following the convention of Fig. 9.7, we set the origin,  $O_{i-1}$  of frame  $i-1$  on axis  $i$ . Hence  ${}^0\mathbf{r}_i$  can be interpreted as the vector from  $O_{i-1}$  to  $O_N$  referred to the fixed reference frame. That is, when  $N=6$ ,

$${}^0\mathbf{v}_{O_6} = {}^0\mathbf{v}_{O_6,1} + {}^0\mathbf{v}_{O_6,2} + {}^0\mathbf{v}_{O_6,3} + {}^0\mathbf{v}_{O_6,4} + {}^0\mathbf{v}_{O_6,5} + {}^0\mathbf{v}_{O_6,6}$$

More generally,

$${}^0\mathbf{v}_{O_N} = \sum_{i=1}^N {}^{i-1}\boldsymbol{\omega}_i \times {}^0\mathbf{r}_i = \sum_{i=1}^N \dot{\theta}_i {}^0\boldsymbol{\omega}_i \times {}^0\mathbf{r}_i$$

Now, if  ${}^0\boldsymbol{\rho}_i$  is the position, relative to the fixed reference frame, of the origin of reference frame  $i-1$  on joint axis  $i$ , then

$${}^0\mathbf{r}_i = {}^0\boldsymbol{\rho}_{N+1} - {}^0\boldsymbol{\rho}_i$$

Here the position of  $O_6$  is indicated by  ${}^0\boldsymbol{\rho}_{N+1}$ . In general, reference frame 6 is not placed with its origin on a joint axis, since there is no axis  $N+1$ . However, for consistency, it is convenient to use the same notation for the location of the origin of frame  $N$  as for the other reference frames.

Therefore

$$\begin{aligned} {}^0\mathbf{v}_{O_N} &= \sum_{i=1}^N \dot{\theta}_i {}^0\boldsymbol{\omega}_i \times ({}^0\boldsymbol{\rho}_{N+1} - {}^0\boldsymbol{\rho}_i) \\ {}^0\mathbf{v}_{O_N} &= {}^0\boldsymbol{\omega}_N \times {}^0\boldsymbol{\rho}_{N+1} - \sum_{i=1}^N \dot{\theta}_i {}^0\boldsymbol{\omega}_i \times {}^0\boldsymbol{\rho}_i \end{aligned} \quad (9.21)$$

To make use of Eqs. (9.19) and (9.21) it is necessary to be able to calculate  $\boldsymbol{\omega}_i$  and  $\boldsymbol{\rho}_i$  for each joint axis. This is actually a problem of direct position kinematics.

The notation used is that of Fig. 9.7. Joint axes  $k$  and  $k+1$  are fixed in member  $k$ . The reference frame on member  $k$  is placed with its  $z$  axis along joint axis  $k+1$  and with its  $x$  axis in the direction of the common normal from joint axis  $k$  to  $k+1$ . The members and joints are numbered serially outward, the fixed frame being 0 and the hand 6.

In reference frame  $k$ ,  $\boldsymbol{\omega}_{k+1} = \mathbf{k} = [0, 0, 1, 0]^T$ . A convenient point on axis  $k+1$  to use is the origin of frame  $k$ . Hence, in frame  $k$ ,  $\boldsymbol{\rho}_{k+1} = \mathbf{0} = [0, 0, 0, 1]^T$ .

Notice that in the  $4 \times 4$  representation, the fourth element of a unit vector, such as  $\mathbf{k}$ , is zero. This is because a unit vector expresses only a direction, and hence the position information in the fourth column of the  $A_k$  matrix has no relevance. If the fourth element of the unit vector  $\boldsymbol{\omega}$  were not zero,  $|\boldsymbol{\omega}|$  would no longer be one, and would change with the transformation by the  $A_k$  matrices. With zero as the fourth element, the magnitude of a unit vector is one and remains one when the vector is multiplied by  $A_k$ .

Using Eq. (9.9) gives the relationship between position vectors of a point  ${}^k\boldsymbol{\rho}_k$  in frame  $k$  and the same point  ${}^{k-1}\boldsymbol{\rho}_k$  in frame  $k-1$ :

$${}^{k-1}\boldsymbol{\rho}_k = A_k^k \boldsymbol{\rho}_k \quad (9.22)$$

where

$$A_k = \begin{bmatrix} \cos \theta_k & -\sin \theta_k \cos \alpha_k & \sin \theta_k \sin \alpha_k & a_k \cos \theta_k \\ \sin \theta_k & \cos \theta_k \cos \alpha_k & -\cos \theta_k \sin \alpha_k & a_k \sin \theta_k \\ 0 & \sin \alpha_k & \cos \alpha_k & r_k \\ 0 & 0 & 0 & 1 \end{bmatrix} \quad (9.10)$$

As indicated on Fig. 9.7,  $\alpha_k$  is the angle between axes  $k$  and  $k + 1$ ,  $a_k$  is the length of the common normal between those axes, and  $r_k$  is the distance along axis  $k$  from the origin of frame  $k - 1$  to the foot of that common normal. A unit vector  ${}^k \mathbf{u}_k$  in frame  $k$  is related to the same vector,  ${}^{k-1} \mathbf{u}_k$ , in frame  $k - 1$  by

$${}^{k-1} \mathbf{u}_k = A_k^k \mathbf{u}_k \quad (9.23)$$

Equations (9.20) and (9.21) can now be used recursively to obtain the vectors  $\boldsymbol{\rho}_k$  and  $\mathbf{w}_k$  referred to frame 0.

**EXAMPLE 9.5**  
**Direct Velocity**  
**Kinematics of a**  
**Three-Axis**  
**Manipulator**

The inner three joint axes of a manipulator are shown in Fig. 9.11. The geometric parameters of the links, the joint positions, and the joint rates are tabulated in Table 9.2. Calculate the angular velocity of member 3 and the velocity of the wrist concurrency point,  $P$ , relative to the fixed reference frame.

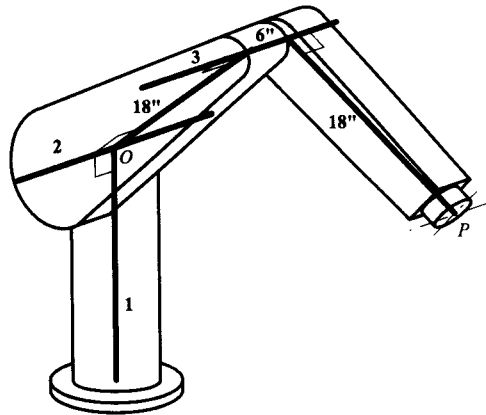


FIGURE 9.11 The three-axis manipulator analyzed in Example 9.5.

TABLE 9.2 Parameters for Robot in Fig. 9.11

$i$	$a_i$ (in)	$r_i$ (in)	$\alpha_i$	$\theta_i$	$\dot{\theta}_i$ (rad/s)
1	0	0	90°	45°	1
2	18	0	0°	30°	-0.75
3	18	6	0°	-60°	0.5

**Solution**

Since there are only three joint axes, we substitute  $N = 3$  in Eqs. (9.19) and (9.21) to get

$${}^0\boldsymbol{\omega}_3 = \sum_{k=1}^3 \dot{\theta}_k {}^0\boldsymbol{w}_k \quad (\text{a})$$

$${}^0\boldsymbol{v}_{O_3} = {}^0\boldsymbol{\omega}_3 \times {}^0\boldsymbol{\rho}_3 - \sum_{i=1}^3 \dot{\theta}_i {}^0\boldsymbol{w}_i \times {}^0\boldsymbol{\rho}_i \quad (\text{b})$$

$$\boldsymbol{\rho}_1 = \mathbf{0}$$

$${}^0\boldsymbol{w}_1 = k$$

so

$${}^0\boldsymbol{\omega}_1 = 1k = k \text{ rad/s}$$

Applying Eq. (9.22) gives

$$\boldsymbol{\rho}_2 = A_1 \mathbf{0} = \begin{bmatrix} \cos(45^\circ) & 0 & \sin(45^\circ) & 0 \\ \sin(45^\circ) & 0 & -\cos(45^\circ) & 0 \\ 0 & 1 & 0 & 0 \\ 0 & 0 & 0 & 1 \end{bmatrix} \begin{bmatrix} 0 \\ 0 \\ 0 \\ 1 \end{bmatrix} = \mathbf{0}$$

and from Eq. (9.23) we get

$${}^0\boldsymbol{w}_2 = A_1 k = \begin{bmatrix} \cos(45^\circ) & 0 & \sin(45^\circ) & 0 \\ \sin(45^\circ) & 0 & -\cos(45^\circ) & 0 \\ 0 & 1 & 0 & 0 \\ 0 & 0 & 0 & 1 \end{bmatrix} \begin{bmatrix} 0 \\ 0 \\ 1 \\ 0 \end{bmatrix} = \begin{bmatrix} \sin(45^\circ) \\ -\cos(45^\circ) \\ 0 \\ 0 \end{bmatrix} = \begin{bmatrix} 0.7071 \\ -0.7071 \\ 0 \\ 0 \end{bmatrix} = 0.707(i - j)$$

Therefore

$${}^1\boldsymbol{\omega}_2 = -0.75 \times 0.7071(i - j) = 0.5303(j - i) \text{ rad/s}$$

Similarly, applying Eq. (9.22) twice to transform from frame 2 to frame 0 we get

$$\begin{aligned} \boldsymbol{\rho}_3 = A_1 A_2 \mathbf{0} &= \begin{bmatrix} \cos(45^\circ) & 0 & \sin(45^\circ) & 0 \\ \sin(45^\circ) & 0 & -\cos(45^\circ) & 0 \\ 0 & 1 & 0 & 0 \\ 0 & 0 & 0 & 1 \end{bmatrix} \begin{bmatrix} \cos(30^\circ) & -\sin(30^\circ) & 0 & 18 \cos(30^\circ) \\ \sin(30^\circ) & \cos(30^\circ) & 0 & 18 \sin(30^\circ) \\ 0 & 0 & 1 & 0 \\ 0 & 0 & 0 & 1 \end{bmatrix} \begin{bmatrix} 0 \\ 0 \\ 0 \\ 1 \end{bmatrix} \\ &= \begin{bmatrix} 11.023 \\ 11.023 \\ 9.000 \\ 1 \end{bmatrix} = 11.023i + 11.023j + 9.000k \end{aligned}$$

and applying Eq. (9.23) twice we get

$$\begin{aligned}
 {}^0\omega_3 &= A_1 A_2 k \\
 &= \begin{bmatrix} \cos(45^\circ) & 0 & \sin(45^\circ) & 0 \\ \sin(45^\circ) & 0 & -\cos(45^\circ) & 0 \\ 0 & 1 & 0 & 0 \\ 0 & 0 & 0 & 1 \end{bmatrix} \begin{bmatrix} \cos(30^\circ) & -\sin(30^\circ) & 0 & 18 \cos(30^\circ) \\ \sin(30^\circ) & \cos(30^\circ) & 0 & 18 \sin(30^\circ) \\ 0 & 0 & 1 & 0 \\ 0 & 0 & 0 & 1 \end{bmatrix} \begin{bmatrix} 0 \\ 0 \\ 1 \\ 0 \end{bmatrix} \\
 &= \begin{bmatrix} \sin(45^\circ) \\ -\cos(45^\circ) \\ 0 \\ 0 \end{bmatrix} = \begin{bmatrix} 0.7071 \\ -0.7071 \\ 0 \\ 0 \end{bmatrix} = 0.7071(i - j) = \omega
 \end{aligned}$$

Since joint axes 2 and 3 are parallel,  ${}^0\omega_3$  should be equal to  ${}^0\omega_2$ . Hence

$${}^2\omega_3 = 0.5 \times 0.7071(i - j) = 0.3536(i - j) \text{ rad/s}$$

Finally, we need the location of point  $P$ . Point  $P$  is the origin of reference frame 3, that is, point  $\rho_4$ .

$$\begin{aligned}
 \rho_4 &= A_1 A_2 A_3 0 \\
 &= \begin{bmatrix} \cos(45^\circ) & 0 & \sin(45^\circ) & 0 \\ \sin(45^\circ) & 0 & -\cos(45^\circ) & 0 \\ 0 & 1 & 0 & 0 \\ 0 & 0 & 0 & 1 \end{bmatrix} \begin{bmatrix} \cos(30^\circ) & -\sin(30^\circ) & 0 & 18 \cos(30^\circ) \\ \sin(30^\circ) & \cos(30^\circ) & 0 & 18 \sin(30^\circ) \\ 0 & 0 & 1 & 0 \\ 0 & 0 & 0 & 1 \end{bmatrix} \\
 &\quad \times \begin{bmatrix} \cos(60^\circ) & \sin(60^\circ) & 0 & 18 \cos(60^\circ) \\ -\sin(60^\circ) & \cos(60^\circ) & 0 & -18 \sin(60^\circ) \\ 0 & 0 & 1 & 6 \\ 0 & 0 & 0 & 1 \end{bmatrix} \begin{bmatrix} 0 \\ 0 \\ 0 \\ 1 \end{bmatrix} \\
 &= \begin{bmatrix} 0.6123 & -0.3536 & 0.7071 & 11.022 \\ 0.6123 & -0.3536 & -0.7071 & 11.022 \\ 0.5000 & 0.8660 & 0 & 9.000 \\ 0 & 0 & 0 & 1 \end{bmatrix} \begin{bmatrix} 9.000 \\ -15.588 \\ 6 \\ 1 \end{bmatrix} = \begin{bmatrix} 26.288 \\ 17.803 \\ 0.001 \\ 1 \end{bmatrix} = 26.288i + 17.803j + 0.001k
 \end{aligned}$$

Now, using Eq. (a) gives

$${}^0\omega_3 = k + 0.5303(j - i) + 0.3536(i - j) = -0.1767i + 0.1767j + k \text{ rad/s}$$

and using Eq. (b) gives

$$\begin{aligned}
 {}^0v_{O_3} &= {}^0\omega_3 \times {}^0\rho_4 - \sum_{i=1}^3 \dot{\theta}_i {}^0\omega_i \times {}^0\rho_i \\
 &= {}^0\omega_3 \times {}^0\rho_4 - {}^0\omega_1 \times {}^0\rho_1 - {}^0\omega_2 \times {}^0\rho_2 - {}^0\omega_3 \times {}^0\rho_3
 \end{aligned}$$

or

$$\begin{aligned}
 {}^0v_{O_3} &= (-0.1767i + 0.1767j + k) \times (26.288i + 17.803j + 0.001k) \\
 &\quad - 0.3536(i - j) \times (11.023i + 11.023j + 9.000k) \\
 &= -14.62i + 29.47j - 15.59k
 \end{aligned}$$

### 9.5.3 Inverse Velocity Problem

As shown above, the position of the hand relative to the fixed frame can be described by means of a set of six independent algebraic equations containing the joint position variables  $\theta_1, \dots, \theta_N$ . Differentiation with respect to time of the direct position kinematics equations yields a set of equations of the form

$$\mathbf{v} = \mathbf{\Gamma} \dot{\boldsymbol{\theta}} \quad (9.24)$$

where  $\mathbf{v}$  is a six-component velocity vector,  $\dot{\boldsymbol{\theta}} = [\dot{\theta}_1, \dot{\theta}_2, \dots, \dot{\theta}_N^T]$  is an  $N$ -dimensional vector composed of the joint rates (velocities), and  $\mathbf{\Gamma}$  is a  $6 \times N$  matrix whose elements are, in general, nonlinear functions of  $\theta_1, \dots, \theta_N$ .  $\mathbf{\Gamma}$  is called the Jacobian matrix of this algebraic system. If the joint positions  $\theta_1, \dots, \theta_N$  are known, Eq. (9.24) yields six linear algebraic equations in the joint rates  $\dot{\theta}_1, \dots, \dot{\theta}_N$ . If the joint rates are given, solution of Eq. (9.24) for  $\mathbf{v}$  is a solution of the direct velocity problem. Notice that  $\mathbf{\Gamma}$  can be regarded as a known matrix for this purpose provided all the joint positions are known.

Solution of Eq. (9.24) for the joint rates is possible if  $N = 6$ . In the remainder of this chapter discussion will be limited to this case. A mode of control for  $N > 6$  compatible with the work presented here makes use of pseudoinversion of the Jacobian matrix to eliminate the ambiguity caused by the additional degrees of freedom.<sup>4</sup> This is beyond the scope of this book.

The ease of computation of the elements of the Jacobian matrix from the joint positions, and of the inverse solution of Eq. (9.24), is very strongly dependent on the way in which this equation is formulated. Since these computations must be repeated at each time step in a real-time rate coordination algorithm, the formulation becomes critical to the efficiency of the software. A very elegant and efficient geometric relationship between the rates of motion about the joints of a linkage and the velocity states of the members is available in the form of screw system theory.<sup>5</sup> Therefore, to make use of geometric information to give an efficient formulation of Eq. (9.24) an algebraic formulation based on Eqs. (9.19) and (9.21) will be used.

The angular velocity  $\boldsymbol{\omega}$  of the hand of a six-axis serial manipulator is related to the joint rates by

$${}^0\boldsymbol{\omega}_6 = \sum_{k=1}^6 \dot{\theta}_k {}^0\mathbf{w}_k \quad (9.19)$$

where  $\mathbf{w}_k$  is a unit vector having the direction of joint axis  $k$ .

Using Eq. (9.21),

$${}^0\mathbf{v}_{O_6} = {}^0\boldsymbol{\omega}_6 \times {}^0\boldsymbol{\rho}_7 - \sum_{i=1}^6 \dot{\theta}_i {}^0\mathbf{w}_i \times {}^0\boldsymbol{\rho}_i \quad (9.21)$$

we see that it is convenient in this case to combine  ${}^0\boldsymbol{\omega}_6 \times {}^0\boldsymbol{\rho}_7$  with  ${}^0\mathbf{v}_{O_6}$  because, for inverse velocity kinematics, we may assume that  ${}^0\boldsymbol{\omega}_6$  will be known, and  ${}^0\boldsymbol{\rho}_7$  may be calculated from the readings of the joint position sensors. Let

$${}^0\boldsymbol{\mu} = {}^0\mathbf{v}_{O_6} - {}^0\boldsymbol{\omega}_6 \times {}^0\boldsymbol{\rho}_7 \quad (9.25)$$

Then

$${}^0\boldsymbol{\mu} = \sum_{i=1}^6 \dot{\theta}_i {}^0\boldsymbol{\rho}_i \times {}^0\mathbf{w}_i \quad (9.26)$$



The velocity  ${}^0\boldsymbol{\mu}$  can be thought of as that of the point in the hand, possibly extended, that is instantaneously coincident with the origin of frame 0.

Equation (9.26) can be written in the form

$${}^0\boldsymbol{\mu} = \sum_{k=1}^6 \dot{\theta}_k {}^0\boldsymbol{\lambda}_k \quad (9.27)$$

where  ${}^0\boldsymbol{\lambda}_k = {}^0\boldsymbol{\rho}_k \times {}^0\boldsymbol{\omega}_k$ . If joint  $k$  is a slider, the  $k$ th term is replaced by  $\dot{r}_k {}^0\boldsymbol{w}_k$ . Note that the joint rates for sliders do not appear in Eq. (9.19).

Equations (9.19) and (9.27) can now be combined to form a system of the form of Eq. (9.24) with:

$$\boldsymbol{v} = \begin{bmatrix} \boldsymbol{\omega} \\ \boldsymbol{\mu} \end{bmatrix}, \quad \boldsymbol{F} = \begin{bmatrix} \boldsymbol{w}_1, & \dots, & \boldsymbol{w}_6 \\ \boldsymbol{\lambda}_1, & \dots, & \boldsymbol{\lambda}_6 \end{bmatrix} \quad (9.28)$$

Again, if the  $k$ th joint is a slider, the  $k$ th column of  $\boldsymbol{F}$  is replaced by  $[\mathbf{0}, \boldsymbol{w}_k]^T$ .

To compute the elements of  $\boldsymbol{F}$ , it is necessary to have expressions for  $\boldsymbol{w}_k$  and  $\boldsymbol{\rho}_k$  in terms of the joint angles. These can be obtained in a recursive form convenient for computation by means of a direct position kinematics solution in the same way as was done in Example 9.5.

As already noted, the direct velocity problem is that of finding  $\boldsymbol{v} = [\boldsymbol{\omega}, \boldsymbol{\mu}]^T$  given the joint rates  $\dot{\theta}_1, \dots, \dot{\theta}_6$ . It is solved by direct substitution of the joint rates in Eq. (9.24) to give  $\boldsymbol{v}$  directly. The direct rate kinematics problem is important when doing acceleration analysis for the purpose of studying dynamics. The total velocities of the members are needed for the computation of Coriolis and centripetal acceleration components.

The important problem from the point of view of robotic coordination is the inverse rate kinematics problem. As will be outlined, it is the basis of all robot software that generates prescribed trajectories relative to the world or fixed coordinate frame.

To solve the linear system of equations in the joint rates obtained by decomposing Eq. (9.24) into its component equations when  $\boldsymbol{v}$  is known, it is necessary to invert the Jacobian matrix  $\boldsymbol{F}$ . The equation becomes

$$\dot{\boldsymbol{\theta}} = \boldsymbol{F}^{-1}\boldsymbol{v}$$

Since  $\boldsymbol{F}$  is a  $6 \times 6$  matrix, numerical inversion is not very attractive in real-time software that must run at computation cycle rates of the order of 100 Hz or faster. Worse, it is quite possible for  $\boldsymbol{F}$  to become singular ( $|\boldsymbol{F}| = 0$ ). The inverse does not then exist. Even when the Jacobian matrix does not become singular (and, in fact, singularity is a rare occurrence in practice), it may become ill-conditioned, leading to degraded performance in significant portions of the manipulator's working envelope.

Most industrial robot geometries are simple enough that the Jacobian matrix can be inverted analytically, leading to a set of explicit equations for the joint rates. This greatly reduces the number of computation operations needed compared with numerical inversion.

## 9.6 CLOSED-LOOP LINKAGES

As was the case for planar linkages, closing a loop in the linkage results in the generation of a set of closure equations. To find the positions of all joints, given the position of one joint chosen as the input joint, it is necessary to solve the closure equations. The mobility criterion

$$M = 6(m - j - 1) + \sum_{i=1}^j f_i \tag{1.3}$$

can be used to determine the connectivity sum of the joints in a single closed-loop spatial linkage that has mobility one. In a single closed loop,  $m = j$ , so Eq. (1.3) gives

$$1 = -6 + \sum f_i$$

or

$$\sum f_i = 7$$

If all joints have connectivity one, this implies that the linkage has seven joints and hence seven members.

The closure equations can be generated using the transformation Eq. (9.9):

$$p_{N-1} = A_N p_N \tag{9.9}$$

If this transformation is applied between successive pairs of members around the loop, one eventually returns to the original reference frame. Hence

$$I = A_1 A_2 A_3 A_4 A_5 A_6 A_7 \tag{9.29}$$

Expansion of Eq. (9.29) produces a set of equations in the seven joint variables. By selecting six of these equations and solving them, it is possible to find all joint variables given the value of one input variable. The problem is actually very similar to the inverse position problem of the open chain linkage and presents similar difficulties of solution.<sup>6</sup>

**EXAMPLE 9.6**  
**Derivation of the**  
**Input-Output**  
**Relationship of a**  
**Universal Joint**

Develop an equation [Eq. (7.10)] relating the input and output shaft angles of the universal joint discussed in Section 7.2.3.

**TABLE 9.3 Geometric Properties of Universal Joint in Example 9.6**

<i>i</i>	<i>a<sub>i</sub></i>	<i>r<sub>i</sub></i>	<i>α<sub>i</sub></i>	<i>θ<sub>i</sub></i>
1	0	0	<i>γ</i>	<i>θ<sub>1</sub></i>
2	0	0	90°	<i>θ<sub>2</sub></i>
3	0	0	90°	<i>θ<sub>3</sub></i>
4	0	0	90°	<i>θ<sub>4</sub></i>

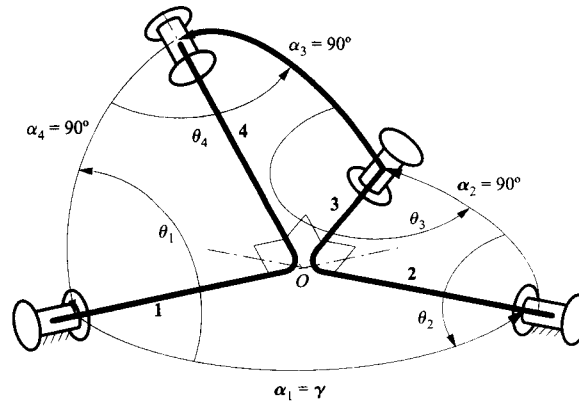
The mechanism is shown on Fig. 9.12, which is similar to Fig. 7.17. Its geometric parameters and kinematic variables are listed in Table 9.3. Here  $\theta_1$  and  $\theta_2$  are considered to be the input and output angles. The angle between shafts 1 and 2 is  $\alpha_1 = \gamma$ . All the other angles between successive joint angles ( $\alpha_2, \alpha_3,$  and  $\alpha_4$ ) are all 90°.

Applying Eq. (9.29) to the four-bar loop, we obtain

$$I = A_1 A_2 A_3 A_4 \tag{9.30}$$

There is great advantage to trying to simplify the equations as much as possible before expansion. In this case, we can separate the variables  $\theta_1$  and  $\theta_2$  from  $\theta_3$  and  $\theta_4$  by postmultiplying both sides of the equation first by  $A_4^{-1}$  and then by  $A_3^{-1}$  to get

$$A_1 A_2 = A_4^{-1} A_3^{-1} \tag{9.31}$$



**FIGURE 9.12** The geometric parameters and kinematic variables of the universal joint analyzed in Example 9.7. Note that this figure is similar to Fig. 7.17.

It is now time to expand into component equations by substituting from Eqs. (9.10) and (9.18):

$$\begin{bmatrix} \cos \theta_1 & -\sin \theta_1 \cos \gamma & \sin \theta_1 \sin \gamma & 0 \\ \sin \theta_1 & \cos \theta_1 \cos \gamma & -\cos \theta_1 \sin \gamma & 0 \\ 0 & \sin \gamma & \cos \gamma & 0 \\ 0 & 0 & 0 & 1 \end{bmatrix} \begin{bmatrix} \cos \theta_2 & 0 & \sin \theta_2 & 0 \\ \sin \theta_2 & 0 & -\cos \theta_2 & 0 \\ 0 & 1 & 0 & 0 \\ 0 & 0 & 0 & 1 \end{bmatrix} \\ = \begin{bmatrix} \cos \theta_4 & \sin \theta_4 & 0 & 0 \\ 0 & 0 & 1 & 0 \\ \sin \theta_4 & -\cos \theta_4 & 0 & 0 \\ 0 & 0 & 0 & 1 \end{bmatrix} \begin{bmatrix} \cos \theta_3 & \sin \theta_3 & 0 & 0 \\ 0 & 0 & 1 & 0 \\ \sin \theta_3 & -\cos \theta_3 & 0 & 0 \\ 0 & 0 & 0 & 1 \end{bmatrix}$$

Performing the matrix multiplications and equating corresponding elements, we get the following system of scalar equations:

$$\cos \theta_1 \cos \theta_2 - \sin \theta_1 \sin \theta_2 \cos \gamma = \cos \theta_3 \cos \theta_4 \quad (1,1)$$

$$\sin \theta_1 \sin \gamma = \sin \theta_3 \cos \theta_4 \quad (1,2)$$

$$\cos \theta_1 \sin \theta_2 + \sin \theta_1 \cos \theta_2 \cos \gamma = \sin \theta_4 \quad (1,3)$$

$$\sin \theta_1 \cos \theta_2 + \cos \theta_1 \sin \theta_2 \cos \gamma = \sin \theta_3 \quad (2,1)$$

$$-\cos \theta_1 \sin \gamma = -\cos \theta_3 \quad (2,2)$$

$$\sin \theta_1 \sin \theta_2 - \cos \theta_1 \cos \theta_2 \cos \gamma = 0 \quad (2,3)$$

$$\sin \theta_2 \sin \gamma = \cos \theta_3 \sin \theta_4 \quad (3,1)$$

$$\cos \gamma = \sin \theta_3 \sin \theta_4 \quad (3,2)$$

$$-\cos \theta_2 \sin \gamma = -\cos \theta_4 \quad (3,3)$$

Note that only the three-by-three submatrix in the top left-hand corner gives nontrivial equations. The remaining equations, which are  $0 = 0$  or  $1 = 1$ , have not been written out.

These are all valid relationships among the angle variables  $\theta_1$ ,  $\theta_2$ ,  $\theta_3$ , and  $\theta_4$ . They are not independent, since the corresponding elements on each side of the equation are related by Eq. (9.3). Inspection of these equations reveals that Eq. (2.3) contains only the two variables of interest,  $\theta_1$  and  $\theta_2$ . This equation can be readily manipulated into the form

$$\tan \theta_1 \tan \theta_2 = \cos \gamma \quad (7.9)$$

which was the result to be derived. As was shown in Section 7.2.3, this equation gives the input-output relationship of the shaft angles of the universal joint.

## 9.7 LOWER PAIR JOINTS

Linkages containing any combination of lower pair joints (see Table 1.1) can be analyzed by the methods presented in this chapter. For the *axial* joints, namely revolute, prismatic, screw, and cylindrical joints, a single transform is needed for each joint. Referring to Eq. (9.10),

$$A_N = \begin{bmatrix} \cos \theta_N & -\sin \theta_N \cos \alpha_N & \sin \theta_N \sin \alpha_N & a_N \cos \theta_N \\ \sin \theta_N & \cos \theta_N \cos \alpha_N & -\cos \theta_N \sin \alpha_N & a_N \sin \theta_N \\ 0 & \sin \alpha_N & \cos \alpha_N & r_N \\ 0 & 0 & 0 & 1 \end{bmatrix} \quad (9.10)$$

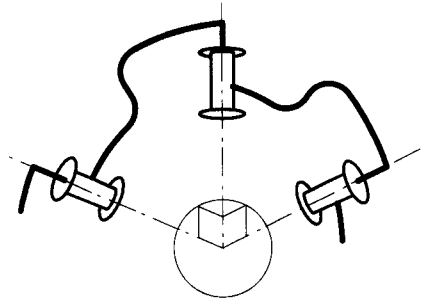
we see that this same transform works in all four cases. The only difference lies in which parameters are regarded as being variable. In the case of a revolute,  $\theta_N$  is the variable and  $r_N$  is a constant. For a prismatic joint,  $r_N$  is variable and  $\theta_N$  is a constant. In the case of a screw joint,  $\theta_N$  and  $r_N$  both vary, but they are not independent of one another, being related by the equation

$$r_N = R_N + h_N \theta_N \quad (9.32)$$

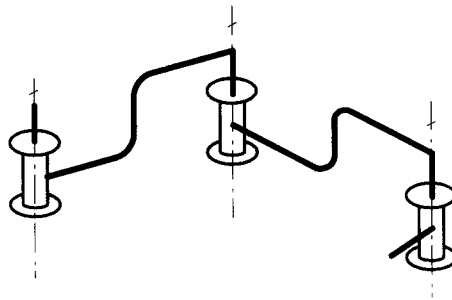
where  $R_N$  and  $h_N$  are constant. Here  $h_N$  is the pitch of the screw, and  $R_N$  is the constant value of the joint offset when  $\theta_N$  is zero. Finally, in the case of a cylindrical joint, both  $r_N$  and  $\theta_N$  are variable, and they may vary completely independently of one another.

The two remaining lower pair joint types, spherical and planar joints, may each be modeled by means of kinematically equivalent chains of three revolute joints. In the case of the spherical joint, the three revolute axes are concurrent at the center of the spherical joint being modeled, and the joint axes are successively orthogonal. That is, the middle joint axis is orthogonal to each of the other two. Those other two joint axes are not, in general, orthogonal to each other. In fact, the angle between them varies with motion about the middle joint. In the case of a planar joint, the three revolute axes are parallel and orthogonal to the plane of motion of the plane joint being modeled. These two equivalent chains are shown in Figs. 9.13 and 9.14, respectively.

The primary application of these equivalent mechanisms is in linkages that include closed loops. This is because spherical and plane joints are always passive joints that cannot be used in open-chain structures.



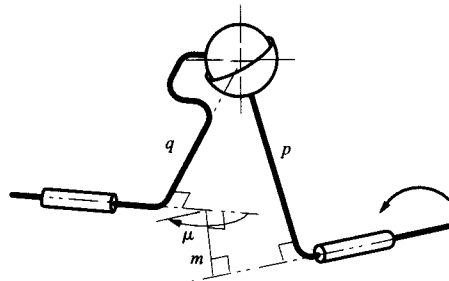
**FIGURE 9.13** Chain of three revolute joints that is kinematically equivalent to a spherical joint.



**FIGURE 9.14** Chain of three revolute joints that is kinematically equivalent to a planar joint.

**EXAMPLE 9.7**  
*Input–Output  
Relationship of a  
Simple Coupling*

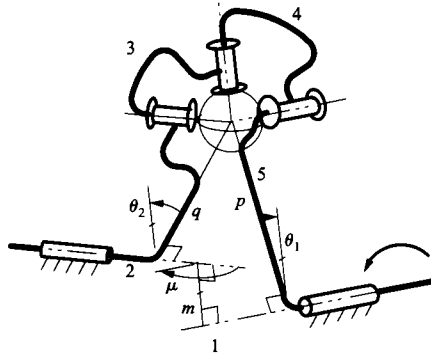
Two nonintersecting shafts turn in cylindric joints, as shown in Fig. 9.15. The shaft axes are at angle  $\mu$  to one another, and the length of their common normal is  $m$ . The two shafts are coupled by means of an offset spherical joint, as shown in the figure. The center of the spherical joint is a distance  $p$  and  $q$  from the two shafts as shown. Develop equations relating the angle of shaft 2 to that of shaft 1 and the axial displacements of both shafts to the angular displacement of shaft 1.



**FIGURE 9.15** The simple coupling between two skew shafts that is analyzed in Example 9.7. The linkage has only three members connected in a single loop via two cylindric joints and a spherical joint.

**Solution**

As indicated before, the spherical joint can be replaced by the kinematically equivalent combination of three successively orthogonal revolute joints, with concurrency point at the center of the sphere. This substitution is shown in Fig. 9.16. We are at liberty to arrange the directions of the axes of joints 3 and 5 relative to 2 and 1, respectively, for convenience. Hence we choose to make axis 3 parallel to 2 and axis 5 parallel to 1. The linkage geometric parameters and joint variables are then as shown in Table 9.4.



**FIGURE 9.16** The linkage of Fig. 9.15 with a chain of three successively orthogonal revolutes substituted for the spherical joint. The concurrency point of the revolute axes is at the center of the spherical joint that is replaced.

**TABLE 9.4** Parameters for the Linkage in Example 9.7

$i$	$a_i$	$r_i$	$\alpha_i$	$\theta_i$
1	$m$	$r_1$	$\mu$	$\theta_1$
2	$q$	$r_2$	0	$\theta_2$
3	0	0	$90^\circ$	$\theta_3$
4	0	0	$90^\circ$	$\theta_4$
5	$p$	0	0	$\theta_5$

In this case we have five joints, so the closure equation is

$$A_1 A_2 A_3 A_4 A_5 = I$$

As in the case of the previous example, it is advantageous to rearrange the equation to split up the variables before expanding. Postmultiplying in succession by  $A_5^{-1}$ ,  $A_4^{-1}$ ,  $A_3^{-1}$  gives the form

$$A_1 A_2 = A_5^{-1} A_4^{-1} A_3^{-1}$$

We now expand this equation, again referring to Eqs. (9.10) and (9.18). Hence

$$A_1 A_2 = \begin{bmatrix} \cos \theta_1 & -\sin \theta_1 \cos \mu & \sin \theta_1 \sin \mu & m \cos \theta_1 \\ \sin \theta_1 & \cos \theta_1 \cos \mu & -\cos \theta_1 \sin \mu & m \sin \theta_1 \\ 0 & \sin \mu & \cos \mu & r_1 \\ 0 & 0 & 0 & 1 \end{bmatrix} \begin{bmatrix} \cos \theta_2 & -\sin \theta_2 & 0 & q \cos \theta_2 \\ \sin \theta_2 & \cos \theta_2 & 0 & q \sin \theta_2 \\ 0 & 0 & 1 & r_2 \\ 0 & 0 & 0 & 1 \end{bmatrix}$$

and

$$A_5^{-1} A_4^{-1} A_3^{-1} = \begin{bmatrix} \cos \theta_5 & \sin \theta_5 & 0 & -p \\ -\sin \theta_5 & \cos \theta_5 & 0 & 0 \\ 0 & 0 & 1 & 0 \\ 0 & 0 & 0 & 1 \end{bmatrix} \begin{bmatrix} \cos \theta_4 & \sin \theta_4 & 0 & 0 \\ 0 & 0 & 1 & 0 \\ \sin \theta_4 & -\cos \theta_4 & 0 & 0 \\ 0 & 0 & 0 & 1 \end{bmatrix} \begin{bmatrix} \cos \theta_3 & \sin \theta_3 & 0 & 0 \\ 0 & 0 & 1 & 0 \\ \sin \theta_3 & -\cos \theta_3 & 0 & 0 \\ 0 & 0 & 0 & 1 \end{bmatrix}$$

Combining these expressions, performing the matrix multiplication, and equating corresponding elements of the matrices on either side give the following set of equations:

$$\cos \theta_1 \cos \theta_2 - \sin \theta_1 \sin \theta_2 \cos \mu = \cos \theta_3 \cos \theta_4 \cos \theta_5 + \sin \theta_3 \sin \theta_5 \quad (1,1)$$

$$-\cos \theta_1 \sin \theta_2 - \sin \theta_1 \cos \theta_2 \cos \mu = \sin \theta_3 \cos \theta_4 \cos \theta_5 - \cos \theta_3 \sin \theta_5 \quad (1,2)$$

$$\sin \theta_1 \sin \mu = \sin \theta_4 \cos \theta_5 \quad (1,3)$$

$$q(\cos \theta_1 \cos \theta_2 - \sin \theta_1 \sin \theta_2 \cos \mu) + r_2 \sin \theta_1 \sin \mu + m \cos \theta_1 = -p \quad (1,4)$$

$$\sin \theta_1 \cos \theta_2 + \cos \theta_1 \sin \theta_2 \cos \mu = -\cos \theta_3 \cos \theta_4 \sin \theta_5 + \sin \theta_3 \cos \theta_5 \quad (2,1)$$

$$-\sin \theta_1 \sin \theta_2 + \cos \theta_1 \cos \theta_2 \cos \mu = -\sin \theta_3 \cos \theta_4 \sin \theta_5 - \cos \theta_3 \cos \theta_5 \quad (2,2)$$

$$\cos \theta_1 \sin \mu = \sin \theta_4 \sin \theta_5 \quad (2,3)$$

$$q(\sin \theta_1 \cos \theta_2 + \cos \theta_1 \sin \theta_2 \cos \mu) - r_2 \cos \theta_1 \sin \mu + m \sin \theta_1 = 0 \quad (2,4)$$

$$\sin \theta_2 \sin \mu = \cos \theta_3 \sin \theta_4 \quad (3,1)$$

$$\cos \theta_2 \sin \mu = \sin \theta_3 \sin \theta_4 \quad (3,2)$$

$$\cos \mu = -\cos \theta_4 \quad (3,3)$$

$$q \sin \theta_2 \sin \mu + r_2 \cos \mu + r_1 = 0 \quad (3,4)$$

The equations corresponding to the fourth row of the matrices are trivial.

We have no interest in the angles of the “virtual” joints:  $\theta_3$ ,  $\theta_4$ , and  $\theta_5$ . The variables of interest are the independent variable  $\theta_1$  and the dependent variables  $\theta_2$ ,  $r_1$ , and  $r_2$ . Inspection of these equations reveals that the (1,4), (2,4), and (3,4) equations contain only these latter four variables. Therefore, it should be possible to solve these three equations to obtain expressions for  $\theta_2$ ,  $r_1$ , and  $r_2$  in terms of  $\theta_1$ .

If the (1,4) equation is multiplied by  $\cos \theta_1$  and added to the (2,4) equation multiplied by  $\sin \theta_1$ , the  $r_2$  terms cancel, and using  $\cos^2 \theta_1 + \sin^2 \theta_1 = 1$  reduces the resulting equation to

$$q \cos \theta_2 + m = -p \cos \theta_1$$

or

$$\theta_2 = \pm \cos^{-1} \left\{ \frac{m + p \cos \theta_1}{q} \right\}$$

Here the second solution corresponds to physically sliding the shaft out of cylindrical joint 2, turning member 2 through  $180^\circ$ , and sliding the shaft back into the bushing in the opposite direction, and then sliding along the joint axis until the spherical joint returns to its original position. This would not be physically possible without encountering interference unless the bushing and shaft are duplicated, in which case member 2 would be symmetric and the two solutions would be indistinguishable from one another. Therefore, nothing is lost by ignoring the second solution. Hence

$$\theta_2 = \cos^{-1} \left\{ \frac{m + p \cos \theta_1}{q} \right\}$$

(a)

Multiplying the (1,4) equation by  $\sin\theta_1$  and subtracting from it the (2,4) equation multiplied by  $\cos\theta_1$  gives, after similar simplification,

$$-q \sin \theta_2 \cos \mu + r_2 \sin \mu = -p \sin \theta_1$$

or

$$r_2 = \frac{q \sin \theta_2 \cos \mu - p \sin \theta_1}{\sin \mu} \quad (b)$$

Consequently, once  $\theta_2$  has been obtained from Eq. (a), this expression can be used to compute  $r_2$ .

Finally, after  $\theta_2$  and  $r_2$  have been computed, the (3,4) equation can be used to solve for  $r_1$ :

$$r_1 = \frac{p \sin \theta_1 \cos \mu - q \sin \theta_2}{\sin \mu} \quad (c)$$

Solution of Eqs. (a), (b), and (c) in sequence solves the problem of obtaining the values of  $\theta_2$ ,  $r_1$ , and  $r_2$  for any given value of  $\theta_1$ .

## 9.8 MOTION PLATFORMS

### 9.8.1 Mechanisms Actuated in Parallel

The mechanisms discussed in this section are spatial mechanisms and detailed analysis is complex and requires methods developed beyond those presented in earlier sections of this chapter and largely beyond the scope of this book. However, we will give a simple presentation here, since these are mechanisms that have considerable practical importance.

The mechanisms in this class provide multiple actuated degrees of freedom, typically three or six, in the same way that the serial chain mechanisms discussed earlier do. Compared with those serial mechanisms, parallel mechanisms are stronger and stiffer but are usually more restricted in the range of motion they provide.

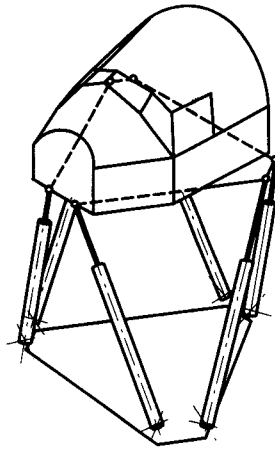
### 9.8.2 The Stewart Platform

Although it is far from the simplest parallel mechanism, we will discuss the Stewart platform first because of its practical and historic importance.<sup>7</sup> The Stewart platform has six limbs acting in parallel to connect the “platform” member to the base. Each limb has a linear actuator, such as a hydraulic cylinder or ball screw, that provides the kinematic equivalent of an actuated prismatic joint. Each limb is connected to the base and the platform by a spherical joint at one end and a universal joint at the other. In Fig. 9.17 the spherical joints are indicated as being at the upper ends of the limbs and the universal joints at the lower ends, but they may be reversed.

Stewart platforms have been very widely used as motion bases for aircraft simulators and similar devices. The great strength and stiffness of the mechanism, together with its ability to produce universally controlled spatial motion, make it ideal for this application. Its relatively restricted motion range is not usually a serious limitation in this instance.

Stewart platforms have mathematical properties that, in some respects, bear an inverse relationship to the corresponding properties of serial chains. The *inverse* position problem for a Stewart platform is very straightforward. Restating the problem, it is as follows: Given the transformation describing the position of the floating platform reference frame relative to the base reference frame, find the limb lengths.





**FIGURE 9.17** A Stewart platform used as the motion base of a flight simulator.

Referring to Fig. 9.18, we can restate the problem as follows:

Given the  $4 \times 4$  transformation

$$\mathbf{p} = \mathbf{Q}\mathbf{p}' \quad (9.33)$$

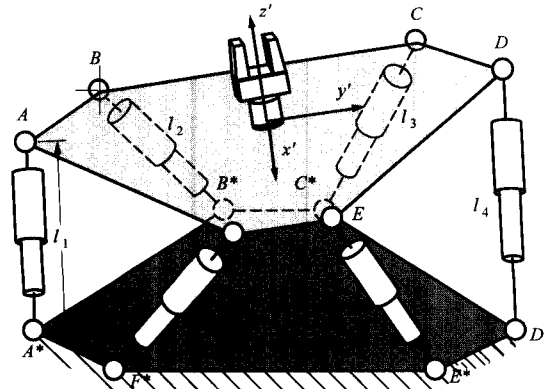
relating coordinates referred to the fixed and floating frames, respectively, find the lengths  $l_i$ ;  $i = 1, \dots, 6$ .

Because the positions of the points  $A, B, C, D, E$ , and  $F$  can be assumed to be known relative to the primed reference frame, Eq. (9.33) can be used to obtain their positions relative to the fixed frame. Similarly, the positions of the points  $A^*, B^*, C^*, D^*$ , and  $E^*$  can be assumed to be known relative to the fixed frame. Then Pythagoras' theorem can be used to find

$$l_i^2 = (\mathbf{p}_A - \mathbf{p}_{A^*})^2 \quad (9.34)$$

where  $\mathbf{p}_A$  is the position of  $A$  relative to the fixed frame, and  $\mathbf{p}_{A^*}$  is the position of  $A^*$  relative to that frame. Similarly, the lengths of the other limbs can be calculated.

In contrast, the *direct* position problem—namely, given  $l_i$ ,  $i = 1, \dots, 6$ , find the transformation matrix  $\mathbf{Q}$  in Eq. (9.33)—is quite difficult and has multiple solutions: 16 for the configuration shown in Fig. 9.18. This is in contrast to the serial chain as described earlier. There the direct problem was straightforward and single valued, and the *inverse* problem was demanding and multivalued.

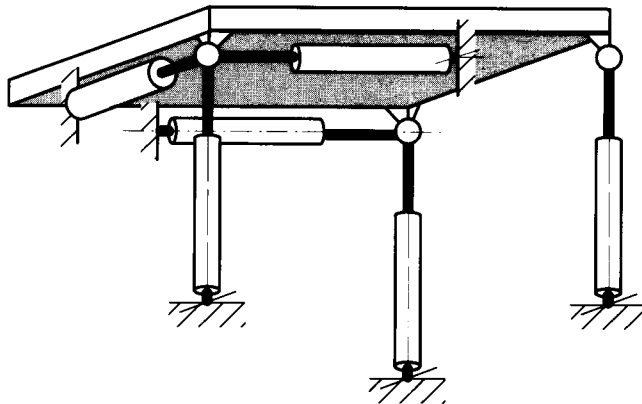


**FIGURE 9.18** The Stewart platform model used in describing its kinematic properties in the text.

The inverse symmetry is even more marked in the velocity domain. The *inverse* velocity kinematics may be solved directly. The *direct* velocity problem requires inversion of a  $6 \times 6$  matrix with structure closely related to the Jacobian matrix described in section 9.5.3.

### 9.8.3 The 3-2-1 Platform

The 3-2-1 platform (Fig. 9.19) is a special configuration that has some practical importance. It is arranged so that the motion and force equations decouple for small displacements. For this reason it has been used in three-dimensional vibration testing tables and for similar functions. The same configuration can be used as a six-component force sensor, with the actuators replaced by uniaxial load cells.



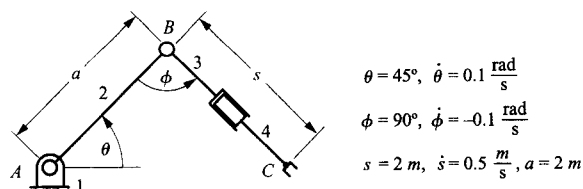
**FIGURE 9.19** A 3-2-1 motion platform. This is actually a variant of the Stewart platform. For small displacements the motion components are decoupled.

## REFERENCES

- <sup>1</sup>Craig, J. J., *Introduction to Robotics: Mechanics and Control*, 2nd ed., Addison-Wesley, MA. (1989).
- <sup>2</sup>Whitney, D. E., "The Mathematics of Coordinated Control of Prosthetic Arms and Manipulators," *J. Dyn. Syst. Meas. Control*, pp. 303–309 (1972).
- <sup>3</sup>Pieper, D. L., and Roth B., "The Kinematics of Manipulators under computer Control," *Proceedings of the Second International Conference on the Theory of Machines and Mechanisms*, Warsaw, Sept. 1969.
- <sup>4</sup>Strang, G., *Linear Algebra and its Applications*, 2nd ed., Academic Press, New York (1980).
- <sup>5</sup>Hunt, K. H., *Kinematic Geometry of Mechanisms*, Clarendon Press, Oxford (1978).
- <sup>6</sup>Duffy, J., *Analysis of Mechanisms and Robot Manipulators*, Edward Arnold, London (1980).
- <sup>7</sup>Tsai, L. W., *Robot Analysis*, Wiley Interscience, New York (1999).

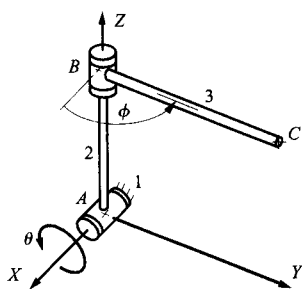
**PROBLEMS**

9.1 For the information given, find the velocity of point C. Show all equations used with terms properly labeled.

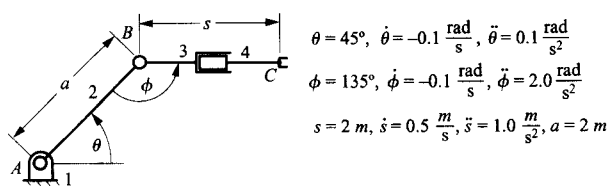


9.2 In the manipulator shown, the joint axes at A and B are oriented along the z and x axes, respectively, and link 3 is perpendicular to link 2. For the position shown, find the velocity of point C. Links 2 and 3 lie in the y-z plane.

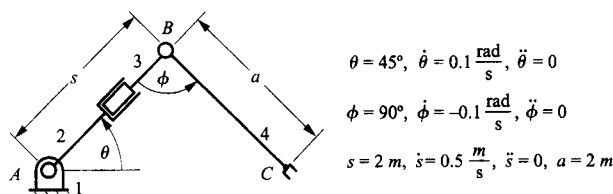
$\dot{\theta} = 100 \text{ rad/s}, \dot{\phi} = 10 \text{ rad/s}, \overline{AB} = \overline{BC} = 10 \text{ m}$



9.3 For the information given, find the velocity and acceleration of point C.

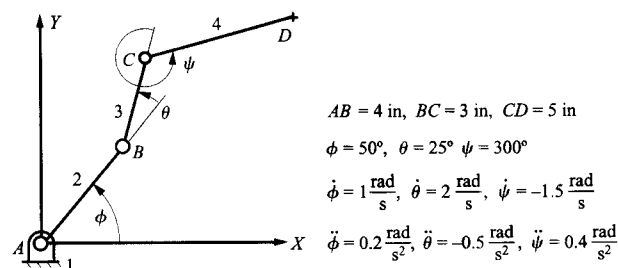


9.4 For the information given, find the velocity and acceleration of Point C.



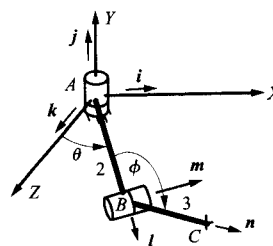
9.5 For the planar manipulator given, compute the following:

- (a)  $r_{B_2/A_2}, r_{C_3/B_3}, r_{D_4/C_4}, r_{D_4/A_1};$
- (b)  ${}^1\omega_2, {}^1\omega_3, {}^1\omega_4; v_{B_2/A_1}, v_{C_3/A_1}, v_{D_4/A_1};$
- (c)  ${}^1\alpha_2, {}^1\alpha_3, {}^1\alpha_4; a_{B_2/A_1}, a_{C_3/A_1}, a_{D_4/A_1}.$



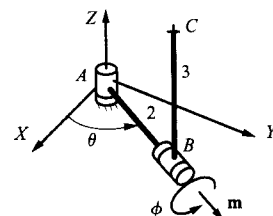
9.6 In the spatial manipulator, link 2, the unit vector  $l$ , and the unit vector  $m$  are all in the X-Z plane. The vector  $m$  is perpendicular to  $l$ , and the unit vector  $n$  is perpendicular to  $m$ . The angle  $\phi$  is measured positive CCW about the  $m$  axis. Compute the following:

- (a)  $r_{B_2/A_2}, r_{C_3/B_3}, r_{C_3/A_1};$
- (b)  ${}^1\omega_2, {}^1\omega_3; v_{B_2/A_1}, v_{C_3/A_1};$
- (c)  ${}^1\alpha_2, {}^1\alpha_3; a_{B_2/A_1}, a_{C_3/A_1}.$



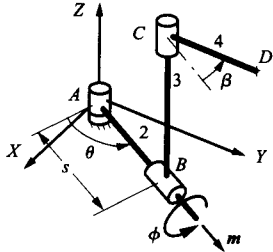
$\overline{AB} = \overline{BC} = 1 \text{ m},$   
 $\theta = 30^\circ, \dot{\theta} = 1 \frac{\text{rad}}{\text{s}}, \ddot{\theta} = 0$   
 $\phi = 120^\circ, \dot{\phi} = 2 \frac{\text{rad}}{\text{s}}, \dot{\phi} = 3 \frac{\text{rad}}{\text{s}^2}$

9.7 In the manipulator shown, the joint axes at A and B are oriented along the Z and m axes, respectively. Link 2 lies in the X-Y plane, and link 3 is perpendicular to link 2. For the position shown, link 3 is vertical (parallel to z). Determine  ${}^1v_{C_3/A_1}, {}^1v_{B_3/A_1},$  and  ${}^1\alpha_3.$



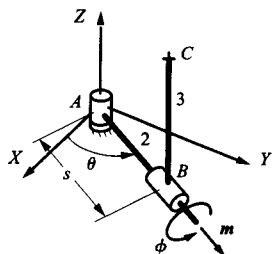
$\overline{AB} = 3 \text{ in}, \overline{BC} = 4 \text{ in}$   
 $\theta = 60^\circ, \dot{\theta} = 5 \frac{\text{rad}}{\text{s}}, \ddot{\theta} = 10 \frac{\text{rad}}{\text{s}^2}$   
 $\dot{\phi} = 5 \frac{\text{rad}}{\text{s}}, \ddot{\phi} = 0 \frac{\text{rad}}{\text{s}^2}$

9.8 In the manipulator shown, the joint axes at  $A$  and  $C$  are oriented along the  $Z$  axis, and the axis at  $B$  is oriented along the  $m$  axis. In the position to be analyzed, link 2 lies in a plane parallel to the  $X$ - $Y$  plane and points along a line parallel to the  $Y$  axis. Link 3 is perpendicular to link 2. Link 4 is perpendicular to link 3 and lies along a line parallel to the  $Y$  axis. For the position to be analyzed, link 3 is vertical (parallel to  $Z$ ). The joints between link 2 and the frame at  $A$  and between links 3 and 4 are revolute joints, and that at  $B$  is a cylindrical joint. From a previous analysis, we know that:  ${}^1v_{C_3/A_1} = 13i + j$ ,  ${}^1a_{B_3/A_1} = -4i$ , and  ${}^1\alpha_3 = k - 5i$ . Using this information, determine  ${}^1v_{D_4/A_1}$ ,  ${}^1a_{C_3/A_1}$ , and  ${}^1\alpha_4$ .



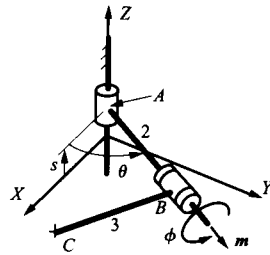
$$\begin{aligned} \theta &= 90^\circ, \dot{\theta} = 1 \frac{\text{rad}}{s}, \ddot{\theta} = 1 \frac{\text{rad}}{s^2} \\ \dot{\phi} &= 5 \frac{\text{rad}}{s}, \ddot{\phi} = 0 \frac{\text{rad}}{s^2}, \dot{s} = 1 \frac{\text{in}}{s}, \ddot{s} = 2 \frac{\text{in}}{s^2} \\ \dot{\beta} &= 1 \frac{\text{rad}}{s}, \ddot{\beta} = 1 \frac{\text{rad}}{s^2} \\ \overline{AB} &= 2 \text{ in}, \overline{BC} = 3 \text{ in}, \overline{CD} = 2 \text{ in} \end{aligned}$$

9.9 In the manipulator shown, the joint axes at  $A$  and  $B$  are oriented along the  $Z$  and  $m$  axes, respectively. In the position to be analyzed, link 2 lies in a plane parallel to the  $X$ - $Y$  plane and points along a line parallel to the  $Y$  axis, and link 3 is perpendicular to link 2. For the position to be analyzed, link 3 is vertical (parallel to  $Z$ ). The joint between link 2 and the frame at  $A$  is a revolute joint, and that at  $B$  is a cylindrical joint. Determine  ${}^1v_{C_3/A_1}$ ,  ${}^1a_{B_3/A_1}$ , and  ${}^1\alpha_3$ .



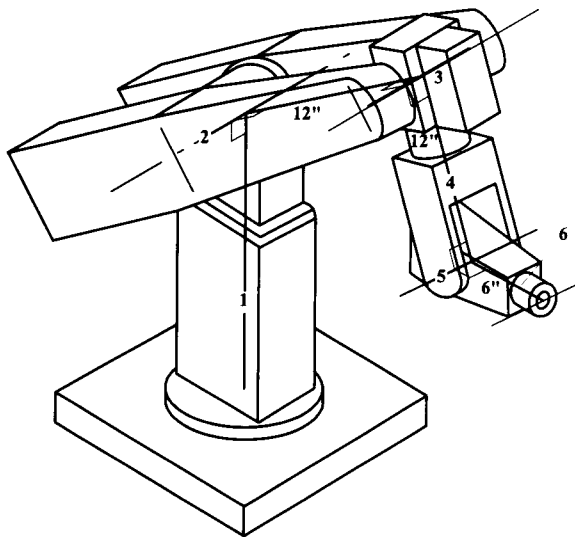
$$\begin{aligned} \theta &= 90^\circ, \dot{\theta} = 1 \frac{\text{rad}}{s}, \ddot{\theta} = 1 \frac{\text{rad}}{s^2} \\ \dot{\phi} &= 5 \frac{\text{rad}}{s}, \ddot{\phi} = 0 \frac{\text{rad}}{s^2} \\ \dot{s} &= 1 \frac{\text{in}}{s}, \ddot{s} = 2 \frac{\text{in}}{s^2} \\ \overline{AB} &= 2 \text{ in}, \overline{BC} = 3 \text{ in} \end{aligned}$$

9.10 In the manipulator shown, the joint axis at  $A$  is oriented along the  $Z$  axis. In the position to be analyzed, link 2 lies in a plane parallel to the  $Y$ - $Z$  plane and points along a line parallel to the  $Y$  axis. Link 3 is perpendicular to link 2 and lies parallel to the  $X$ - $Y$  plane. The joint between link 2 and the frame is a cylindrical joint, and the joint between links 2 and 3 is a revolute joint. Using the information given, determine  ${}^1v_{C_3/A_1}$ ,  ${}^1a_{C_3/A_1}$ , and  ${}^1\alpha_3$ .



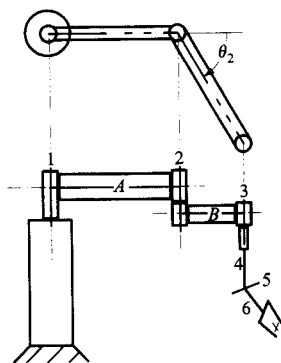
$$\begin{aligned} \theta &= 90^\circ, \dot{\theta} = 1 \frac{\text{rad}}{s}, \ddot{\theta} = 0 \frac{\text{rad}}{s^2} \\ \dot{\phi} &= 1 \frac{\text{rad}}{s}, \ddot{\phi} = 0 \frac{\text{rad}}{s^2}, \\ s &= 1 \text{ in}, \dot{s} = 0 \frac{\text{in}}{s}, \ddot{s} = 1 \frac{\text{in}}{s^2} \\ \overline{AB} &= 1 \text{ in}, \overline{BC} = 1 \text{ in} \end{aligned}$$

9.11 In the manipulator shown, all joints are revolute. The link parameters and joint angles are as tabulated. Find the  $4 \times 4$  matrix,  $Q'$ , that expresses the position of the mounting flange for the end effector in the position specified by the values of  $\theta_k$  given in the table.



$i$	$a_i$ (in)	$r_i$ (in)	$\alpha_i$	$\theta_i$
1	0	0	$90^\circ$	$30^\circ$
2	12	0	$0^\circ$	$45^\circ$
3	0	0	$90^\circ$	$-50^\circ$
4	0	12	$90^\circ$	$-20^\circ$
5	0	0	$90^\circ$	$40^\circ$
6	0	6	$0^\circ$	$30^\circ$

9.12 The SCARA robot geometry shown in the figure is often used for assembly robots because it is suited to moving and placing parts vertically over a relatively large horizontal area. All of its joint axes, except axis 4, are revolute. Axis 4 is a prismatic joint. Axes 1, 2, 3, and 4 are parallel, and axes 3 and 4 are coincident. (Note that this does not produce degeneracy, because 3 is a revolute joint and 4 is a prismatic joint.) For a given position of the manipulator, the linkage parameters are as tabulated. Find the matrix  $Q'$  that expresses the position of the end effector for the tabulated values of the joint variables.



$i$	$a_i$ (in)	$r_i$ (in)	$\alpha_i$	$\theta_i$
1	15	0	$0^\circ$	$60^\circ$
2	15	4	$0^\circ$	$45^\circ$
3	0	0	$0^\circ$	$-50^\circ$
4	0	9	$90^\circ$	$0^\circ$
5	0	0	$90^\circ$	$0^\circ$
6	0	6	$0^\circ$	$30^\circ$

9.13 For the manipulator of Example 9.4 (Fig. 9.10 and Table 9.1), find the  $4 \times 4$  matrix,  $Q'$ , that expresses the position of the gripper when the joint positions are as follows:  $\theta_1 = -30^\circ$ ,  $\theta_2 = 150^\circ$ ,  $\theta_3 = 30^\circ$ ,  $r_4 = 2.5$ ,  $\theta_5 = -45^\circ$ , and  $\theta_6 = 0$ .

9.14 For the three-axis manipulator of Example 9.5 (Fig. 9.11 and Table 9.2), find the angular velocity of member 3 and the velocity of the wrist concurrency point,  $P$ , relative to the fixed reference frame when the joint positions and rates are as follows:  $\theta_1 = -60^\circ$ ,  $\theta_2 = 45^\circ$ ,  $\theta_3 = -30^\circ$ ,  $\dot{\theta}_1 = -0.5$  rad/s,  $\dot{\theta}_2 = 0.5$  rad/s, and  $\dot{\theta}_3 = 1.0$  rad/s.

9.15 For a SCARA robot of basic geometry similar to that of Problem 9.12, the geometric parameters and joint variables in a general position are as tabulated below. The Jacobian matrix  $\Gamma$  that relates the velocity of the end effector to the joint velocities is also given.

(a) Find the angular velocity of the end effector when the joint positions and rates are as follows:

$$\theta_1 = 30^\circ, \theta_2 = 15^\circ, \theta_3 = -15^\circ, r_4 = 0.1, \theta_5 = 0^\circ, \theta_6 = 45^\circ$$

$$\dot{\theta}_1 = -0.2 \text{ rad/s}, \dot{\theta}_2 = 0.5 \text{ rad/s}, \dot{\theta}_3 = -0.2 \text{ rad/s},$$

$$\dot{r}_4 = 0.05 \text{ in/s}, \dot{\theta}_5 = 0, \dot{\theta}_6 = 0.1 \text{ rad/s}$$

(b) Verify that the system is singular whenever either  $\theta_2 = 0$  or  $\theta_5 = 0$ .

$i$	$a_i$ (in)	$r_i$ (in)	$\alpha_i$	$\theta_i$
1	0.5	0	$0^\circ$	$\theta_1$
2	0.4	0	$0^\circ$	$\theta_2$
3	0	0	$0^\circ$	$\theta_3$
4	0	$r_4$	$90^\circ$	$\theta_4$
5	0	0	$90^\circ$	$\theta_5$
6	0.1	0	$0^\circ$	$\theta_6$

$$\Gamma = \begin{bmatrix} 0 & 0 & 0 & 0 & 0 & \sin \theta_5 \\ 1 & 1 & 1 & 0 & 0 & -\cos \theta_5 \\ 0 & 0 & 0 & 0 & 1 & 0 \\ 0.4 \sin \theta_3 + 0.5 \sin(\theta_2 + \theta_3) & 0.4 \sin \theta_3 & 0 & 0 & 0 & 0 \\ 0 & 0 & 0 & 1 & 0 & 0 \\ -0.4 \cos \theta_3 - 0.5 \cos(\theta_2 + \theta_3) & -0.4 \cos \theta_3 & 0 & 0 & 0 & 0 \end{bmatrix}$$

## 10.1 INTRODUCTION

The mechanisms discussed in previous chapters are used primarily as nonuniform-motion or force transformers. In the case in which uniform motion (constant-velocity ratio) or force transmission is required, circular gears, friction drives, belt drives, and chain drives are preferred. In such devices, if the input shaft turns at a constant speed, then the output shaft will turn at a constant angular speed. In practice, however, there may be a small but undesirable oscillatory motion superposed on the output motion because of imperfections in the system.

When low power is to be transmitted, constant-velocity transfer can be achieved by friction drives, and a simplified version of such a drive is shown in Fig. 10.1. In the device shown, disk 2 is the driver and disk 3 is driven, and both disks are assumed to be perfect circular cylinders in contact at point  $P$ . Link 1 is fixed, and there is a spring that forces disk 3 against disk 2. The disks rotate about points  $A$  and  $B$ . Assuming that there is no slip at  $P$ , the two disks will roll on each other, and the condition for rolling can be written as

$$v_{P_2} = v_{P_3}$$

or

$$\omega_2 \times r_{P/A} = \omega_3 \times r_{P/B}$$

The vector form is needlessly cumbersome for simple friction drives, and only the magnitudes need to be considered. The directions can be determined easily by inspection, that is, the two disks in Fig. 10.1 rotate in opposite directions. Then,

$$\omega_2 r_2 = \omega_3 r_3$$

or

$$\frac{\omega_2}{\omega_3} = \frac{r_3}{r_2} \quad (10.1)$$

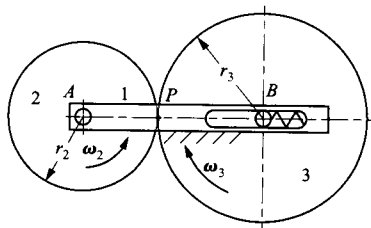


FIGURE 10.1 Friction disks.

where  $\omega_2 = |\omega_2|$ ,  $\omega_3 = |\omega_3|$ ,  $r_2$  is the radius of disk 2, and  $r_3$  is the radius of disk 3. Thus, the friction drive velocity ratio (the input angular velocity divided by the output angular velocity) is constant and inversely proportional to the ratio of the disk radii. Note that if a plus sign were assigned to one of the  $\omega$ 's, the other  $\omega$  would have a negative sign.

If an external disk drives an internal disk as shown in Fig. 10.2, the velocity ratio given by Eq. (10.1) would still apply; however, in that case, the two angular velocities would be in the same direction.

A friction drive can transmit torque only if the normal force at the contact point is sufficient to prevent slippage. If large torques are involved, large Hertzian contact stresses<sup>1</sup> will be created at the contact point and subsequent pitting and galling of the contact surfaces are inevitable. The wear can be lessened by using very hard contact surfaces. In addition, special lubricants have been developed that prevent actual molecular contact of the frictional surfaces but have a sufficiently high shear strength in very thin sections to provide a usable coefficient of friction.

Friction drives are used for their quietness and smoothness of operation relative to gear and chain drives. In addition, they are easily adaptable to situations in which a variable-speed transmission is required. One major disadvantage of friction drives is their relatively low power capacities. Another is that for maximum efficiency and life, they must be operated in extremely clean environments because particles can cause rapid wear rates and accelerated failure.

In the rugged environments in which most industrial machinery must operate, the use of friction drives is not practical. Instead, gear systems are often used. In gears, slip between disks is prevented by the gear teeth of mating gears. The gears contact each other like cammed surfaces; however, for smooth, low-maintenance operation, the gear teeth have a special geometry that permits constant-velocity transfer. If designed properly, two meshing gears will behave very much the same as two friction disks, which is why gears are usually modeled grossly as two disks rolling on each other.

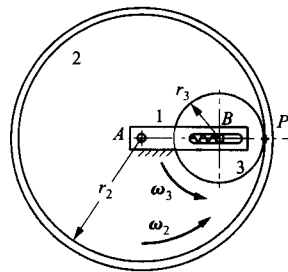


FIGURE 10.2 Internal friction drive.

## 10.2 SPUR GEARS

Gears are used to transmit power from one shaft to another, and the power is usually transferred in such a way that the velocity ratio remains constant. If the velocity ratio is not constant, the driven gear will be continuously accelerated and decelerated when the driving gear rotates at constant velocity. This results in cyclic stresses, vibration, noise, and other problems. Profiles of meshing gear teeth that give constant-velocity ratio are termed conjugate. As discussed later in this chapter, given the geometry of any gear tooth profile, it is possible to construct a conjugate profile using graphical and analytical techniques similar to those used for finding cam profiles. However, there are relatively few profile types that are useful for most applications.

Spur gears are the simplest type of gear commonly used in industry. The characteristic of spur gears is that the gear rotation axes are all parallel and the gear teeth are parallel to the rotation axes. The gear may be equivalent to a rolling cylinder of any radius called the *pitch cylinder*. When the pitch cylinder radius becomes infinitely large, the teeth are located on a plane, and such a gear is called a *rack*. A simple pair of meshing gears is shown in Fig. 10.3. When two gears of unequal size are meshed, the smaller gear is referred to as the *pinion* and the larger gear as the “gear” or “wheel.” A pinion and rack are shown in Fig. 10.4.

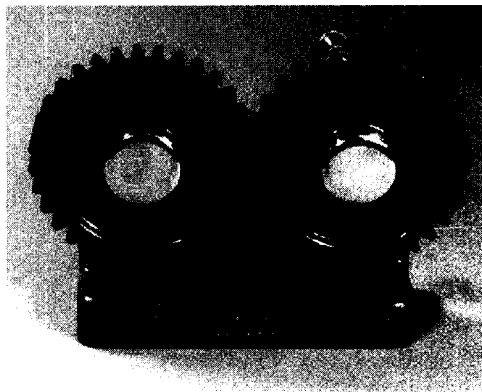


FIGURE 10.3 Meshing spur gears.

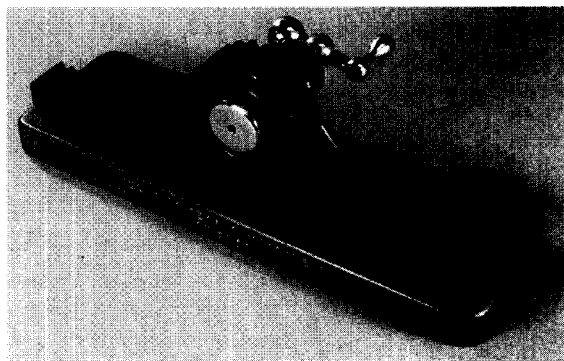


FIGURE 10.4 Pinion and rack.

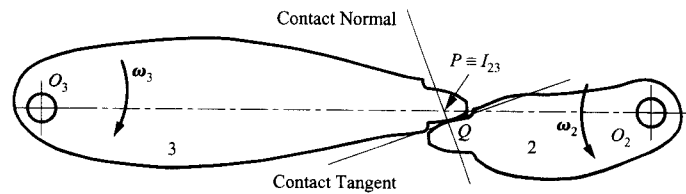
### 10.3 CONDITION FOR CONSTANT-VELOCITY RATIO

Figure 10.5 represents the teeth of two gears that rotate about  $O_1$  and  $O_2$ , respectively. The tooth profiles contact each other at point  $Q$ . The instantaneous center for the motion of gear 3 relative to gear 2 lies on the normal to the profiles at the point of contact. By the Kennedy-Aronholdt theorem, it also lies on the line joining the centers of rotation of gears 2 and 3 relative to the base. Thus, the instantaneous center of motion of gear 3 relative to gear 2 must be at point  $I_{23}$ , which is also known as the pitch point,  $P$ .

Hence

$$\omega_2 O_2 P = \omega_2 O_2 I_{23} = -\omega_3 O_3 I_{23} = -\omega_3 O_3 P$$





**FIGURE 10.5** The location of the instantaneous center of relative rotation of members 2 and 3, which respectively rotate relative to the base about  $O_2$  and  $O_3$ . The instantaneous center is  $P$  ( $I_{23}$ ). The point  $P$  is also called the pitch point. The angular velocities of members 2 and 3 relative to the base are, respectively,  $\omega_2$  and  $\omega_3$ . For the external gears shown, the senses of  $\omega_2$  and  $\omega_3$  are opposite.

or considering magnitudes only, we have

$$R = \frac{\omega_2}{\omega_3} = \frac{O_3P}{O_2P}$$

where  $R$  is the velocity ratio. Thus, a constant-velocity ratio implies that  $O_3P/O_2P$  is constant. That is,  $P$  is a fixed point on the line of centers between the two gears.

In summary, for conjugate profiles, the normal to the profiles at the point of contact always intersects the line of centers at the same point. This is the fundamental law of gearing. This point ( $P$ ) is called the pitch point. It is the instant center of the relative motion of the gears.

The velocity,  $v_s$ , with which the gear teeth slide over one another is important because the rate of wear of the gear teeth depends on it. The sliding velocity of point  $Q$  is the relative velocity between the coincident points at the contact location  $Q$ ; that is, it is the velocity  $v_{Q_2/Q_3}$ . From Chapter 3, the relative velocity between two coincident points can be written as

$$v_s = {}^1v_{Q_2/Q_3} = {}^3v_{Q_2/Q_3} = {}^3v_{Q_2/P_2} + {}^3v_{P_2/P_3} + {}^3v_{P_3/Q_3} = {}^3v_{Q_2/P_2} = {}^3\omega_2(r_{Q/P})$$

where “1” is used to designate the ground link. The relative angular velocity can be written as

$${}^3\omega_2 = {}^1\omega_2 - {}^1\omega_3$$

Dropping the superscripts that are associated with the ground link gives

$$v_s = (r_{Q/P})(\omega_2 - \omega_3)$$

or using the simpler nomenclature

$$v_s = PQ|\omega_2 - \omega_3| \quad (10.3)$$

The sliding velocity is proportional to the distance between the contact point  $Q$  and the pitch point  $P$ . When  $P$  and  $Q$  coincide, the sliding velocity becomes zero and the teeth are instantaneously rolling on one another.

## 10.4 INVOLUTES

Of the many shapes that are possible for tooth geometries, the involute and cycloid are the most common. Of these two forms, the involute is used in almost all cases except in

watches and clocks, in which the cycloidal form is still found. The involute form has several advantages, but two are most important. The first is that it is very easy to manufacture involute gears with simple tooling. The second is that the constant-velocity ratio is maintained even when the center distance between the two gears is changed. This is important in manufacturing, because it is never possible to mount the gears precisely at the designed center distance.

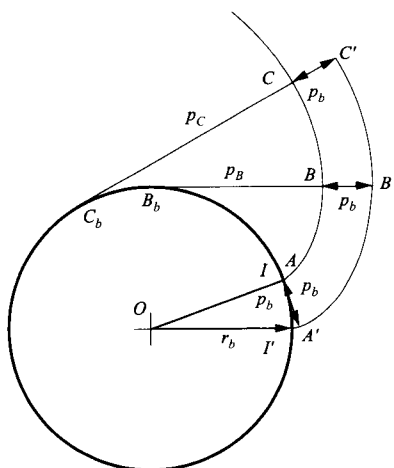
The involute profile is developed from a circle called a base circle. The involute of a given base circle is the curve traced by any fixed point on a taut string that is being unwound from the base circle as shown in Fig. 10.6. The involute curve has the following important properties:

1. A line that is normal to the involute at any point on the curve is also tangent to the base circle.
2. The length of the normal is equal to the corresponding arc of the base circle; that is,  $B_bB = \text{arc } B_bI$ ,  $C_bC = \text{arc } C_bI$ . Consequently, the normal distance between two involutes of the same base circle is equal to their base pitch; that is,  $AA' = BB' = CC' = \text{arc } II' = p_b$ .
3. The length of the normal is equal to the local radius of curvature of the involute; that is,  $B_bB' = \rho_B$ ,  $C_bC' = \rho_C$ .
4. Any two involute profiles are mutually conjugate regardless of the base-circle diameters.
5. The path of contact between two involute profiles is rectilinear. Consequently, the pressure angle is constant.
6. A gear with involute tooth profiles can be generated by a straight-sided rack cutter.
7. Two involute profiles remain conjugate if their center distance is changed.

**Proofs:** Properties 1, 2, 3. These proofs are obtained by inspection of Fig. 10.6.

4. See Fig. 10.7. This figure shows two involute profiles in contact in an arbitrary position. The normal at the point of contact  $Q$  is tangent to both base circles. Clearly this normal remains the same regardless of the motion of the profiles. Hence, its intersection,  $P$ , with the line of centers is fixed and the velocity ratio is constant. The velocity ratio is

$$R = \frac{O_3P}{O_2P} = \frac{r_{p_3}}{r_{p_2}} \tag{10.4}$$



**FIGURE 10.6** Generation of an involute by a point on a stretched string unwound from a cylinder.  $IABC$  and  $I'A'B'C'$  are two involutes generated off the same base circle that has radius  $r_b$ . The string is originally wrapped around the base circle with its end at  $I'$ . When it has been unwrapped until it is tangent to the base circle at  $A$ , its end is at  $A'$ . Therefore line  $AA'$  has the same length as the curvilinear distance  $II'$ . ( $I \equiv A$ .) When it has been unwrapped so that its end is at point  $B'$ , it is tangent to the base circle at  $B_b$ . Similarly, when the end is at  $C'$ , the string is tangent to the base circle at  $C_b$ . Similarly, the point on the string that was initially at  $A$  is at  $B$  when the end of the string is at  $B'$ , and it is at  $C$  when the end is at  $C'$ . Hence the normal distance between the two involutes is constant.

where  $r_{p_2} = O_2P$  is the radius of the pitch circle of gear 2, and  $r_{p_3} = O_3P$  is the radius of the pitch circle of gear 3. The pitch circles are the dashed circles shown in Fig. 10.7. The radii of the pitch circles are related to those of the corresponding base circles by the equations

$$r_{p_2} = \frac{r_{b_2}}{\cos \phi} \quad (10.5)$$

and

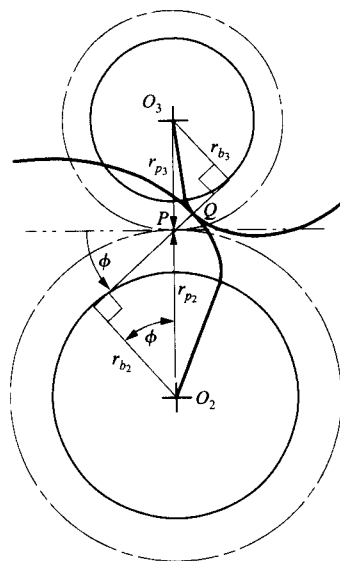
$$r_{p_3} = \frac{r_{b_3}}{\cos \phi}$$

These equations follow from the fact illustrated in Fig. 10.7 that  $r_{p_2}$  is the hypotenuse of a right-angled triangle, with  $r_{b_2}$  as another side of that triangle, and  $\phi$  as the angle included between them. The same condition holds for gear 3. Therefore,

$$R = \frac{r_{b_3}}{r_{b_2}} \quad (10.6)$$

where  $r_{b_2}$ ,  $r_{b_3}$  are the pitch circle radii. The constant angle  $\phi$  made by the contact normal with the tangent to the pitch circles at point  $P$  is called the pressure angle.

- 5, 6. Since the normal at the point of contact is always the same line, it follows that the point of contact simply moves backward and forward along this line. This profile is conjugate to a straight-sided rack. That is, if we have a linear profile inclined at angle  $\phi$  to the line  $OP$  that simply slides back and forth without rotating, the involute profile is conjugate to it. The normal at the point of contact is always normal to the linear profile as indicated in Fig. 10.8. Because it is also always tangent to the base circle, it is always the line shown. The point  $P$  is fixed. This implies that a gear with involute teeth can be cut by a cutter in the shape of a straight-sided rack that reciprocates in a direction parallel to the axis of the gear blank.
7. The proof of item 7 follows from the proof of item 4, because the involute profiles are arbitrary and their center distance is arbitrary.



**FIGURE 10.7** Two involutes in contact. The normal to both curves at the point of contact,  $Q$ , is tangent to both base circles. Hence it always passes through the fixed point  $P$ . Therefore two involutes are always conjugate.

## 10.5 GEAR TERMINOLOGY AND STANDARDS

### 10.5.1 Terminology

Several terms commonly used for describing gears can be defined with the aid of Fig. 10.9. The *pitch circle* is the circle centered on the gear axis passing through the *pitch point*. The pitch circles of meshing gears roll on one another, and the point of contact is the pitch point. The *pitch circle diameter* or *pitch diameter* will be designated as  $d_p$ .

Although a gear will be designed to have a particular pitch circle, the actual pitch circle will depend on the gear with which it meshes and the center distance.

The *circular pitch*,  $p_c$ , is the curvilinear distance measured on the pitch circle from a point on one tooth to the corresponding point on the next tooth.

The *base pitch*,  $p_b$ , is the curvilinear distance measured on the base circle from a point on one tooth to the corresponding point on the next tooth.

The *diametral pitch*,  $P_d$ , is the number of teeth on the gear per unit of pitch diameter. That is,

$$P_d = N/d_p \quad (10.7)$$

where  $N$  is the number of teeth on the gear. Also, from the definition of circular pitch

$$p_c = \pi d_p / N \quad (10.8)$$

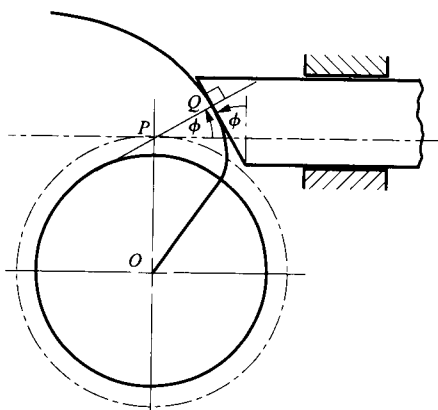


FIGURE 10.8 Conjugacy of involute to a straight-sided rack.

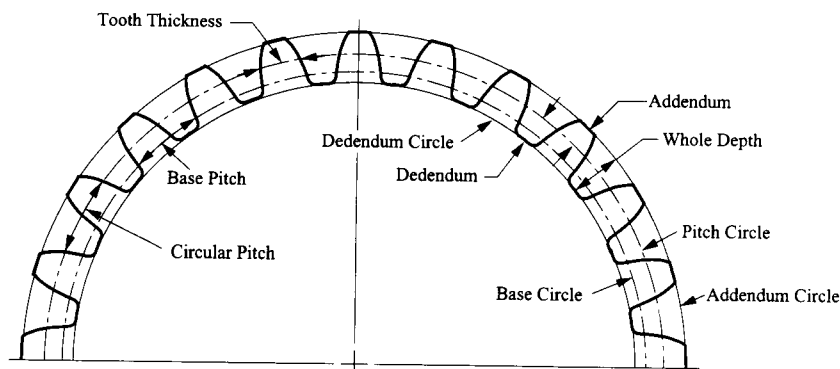


FIGURE 10.9 Gear tooth in-plane geometry terminology.

so

$$P_d = \pi / p_c \quad (10.9)$$

or

$$P_d p_c = \pi \quad (10.10)$$

The base pitch is given by

$$p_b = \pi d_b / N \quad (10.11)$$

From Eq. (10.5) the base circle diameter and the pitch circle diameter are related by

$$d_p = \frac{d_b}{\cos \phi}$$

Therefore, Eq. (10.8) can be rewritten as

$$p_c = \pi d_p / N = \frac{\pi d_b}{N \cos \phi} = \frac{p_b}{\cos \phi} \quad (10.12)$$

or

$$p_b = p_c \cos \phi \quad (10.13)$$

In the metric system, gears are specified by the ratio of the pitch diameter in millimeters to the number of teeth. This ratio, called the *module*, is expressed as follows:

$$m = \frac{d_p}{N} \quad (10.14)$$

From Eq. (10.8),

$$p_c = m\pi \quad (10.15)$$

The *addendum circle* passes through the tips of the gear teeth, and the *dedendum circle* passes through the base of the gear teeth. The *addendum* is the radial distance from the pitch circle to the top land (see Figs. 10.9 and 10.10) of the gear, and the *dedendum* is equal to the radial distance from the pitch circle to the bottom land of the tooth. The *whole depth* is the sum of addendum and dedendum.

With involute gears, the contact between the two gears occurs on the pressure line. This line then is called the *line of action*.

### 10.5.2 Standards

If two gears are to mesh, it is necessary that their pitches be the same. Since the base pitch, circular pitch, diametral pitch, and module are uniquely related, if any one of these pitch measures is the same for both gears, all will be.

Gears cut to standard dimensions (see Table 10.1) are interchangeable in the sense that any two standard gears can be meshed together. For this to be possible, the following conditions are required:

1. The pressure angles must be the same.
2. The diametral pitches must be the same.
3. The dedendum on a given gear must be greater than the addendum on the mating gear.
4. The tooth thicknesses must be equal to one-half the circular pitch.

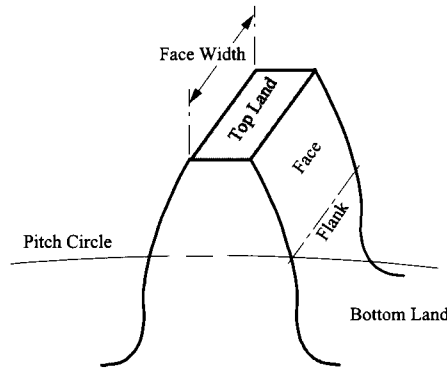


FIGURE 10.10 Gear tooth axial geometry terminology.

TABLE 10.1 Standard AGMA<sup>a</sup> and USASI<sup>b</sup> Tooth Systems for Involute Spur Gears<sup>2</sup>

System <sup>c</sup>	Coarse pitch (1P to 19.99P) full depth		Fine pitch (20P to 200P) full depth	Stub teeth
Pressure angle, $\phi$	20°	25°	25°	20°
Addendum, $a$	$1/P_d$	$1/P_d$	$1/P_d$	$0.8/P_d$
Dedendum, $b$	$1.25/P_d$	$1.25/P_d$	$1.20/P_d + 0.002$ in	$1/P_d$
Working depth, $h_k$	$2/P_d$	$2/P_d$	$2/P_d$	$1.6/P_d$
Whole depth, $h_t$ (min)	$2.25/P_d$	$2.25/P_d$	$2.25/P_d + 0.002$ in	$1.8/P_d$
Circular tooth thickness, $t$	$\pi/2P_d$	$\pi/2P_d$	$\pi/2P_d$	$\pi/2P_d$
Fillet radius of basic rack, $r_f$	$0.3/P_d$	$0.3/P_d$	Not standardized	
Basic clearance, $c$ (min)	$0.25/P_d$	$0.25/P_d$	$0.2/P_d + 0.002$ in	$0.2/P_d$
Clearance, $c$ (shaved or ground teeth)	$0.35/P_d$	$0.35/P_d$	$0.35/P_d + 0.002$ in	
Minimum width of top land, $t_o$	$0.25/P_d$	$0.25/P_d$	Not standardized	

<sup>a</sup>American Gear Manufacturers' Association.

<sup>b</sup>United States of America Standards Institute.

<sup>c</sup>The standard pitches in common use are as follows: 1 to 2 varying by  $\frac{1}{4}$  pitch, 2 to 4 varying by  $\frac{1}{2}$  pitch, 4 to 10 varying by 1 pitch, 10 to 20 varying by 2 pitch, and 20 to 200 varying by 4 pitch.

This is what permits vendors to offer off-the-shelf gears. It is also what makes possible applications such as the change gears used in a lathe to set up different cutting and feed rates. However, nonstandard gears are also used in many applications, for a variety of reasons, some of which will be discussed later in this chapter. In general, nonstandard gears have to be designed as a meshing pair, and neither member of the pair will mesh satisfactorily with a standard gear.

Table 10.1 shows the standard equations for the 20° and 25° pressure angles that are the most commonly used standard gears. A gear system that is now little used is the  $14\frac{1}{2}^\circ$  pressure angle system. This system was used extensively when gears were cast because the sine of  $14\frac{1}{2}^\circ$  is approximately  $\frac{1}{4}$ , which facilitated pattern layout. As will be shown later, the  $14\frac{1}{2}^\circ$  system is inferior to the systems with higher pressure angles because the gears must have more teeth to avoid interference than are required in the 20° and 25° systems. Therefore, for a relatively small number of teeth, gears in the  $14\frac{1}{2}^\circ$  system will have a lower beam strength and a lower load rating than corresponding gears in the 20° and 25° systems.

Although any diametral pitch is technically possible, the standard pitches in common use are 1 to 2 varying by  $\frac{1}{4}$  pitch, 2 to 4 varying by  $\frac{1}{2}$  pitch, 4 to 10 varying by 1 pitch, 10 to 20 varying by 2 pitch, and 20 to 200 varying by 4 pitch.

Based on the equations in Table 10.1, the physical size of the gear teeth decreases as the diametral pitch,  $P$ , increases. This is also shown in Fig. 10.11. In general, for a given set of pitch diameters, the load transfer will be smoother and undesirable affects such as noise will be lower if a large number of small teeth are used rather than a small number of larger teeth. This is because more teeth share the load when smaller teeth are used.

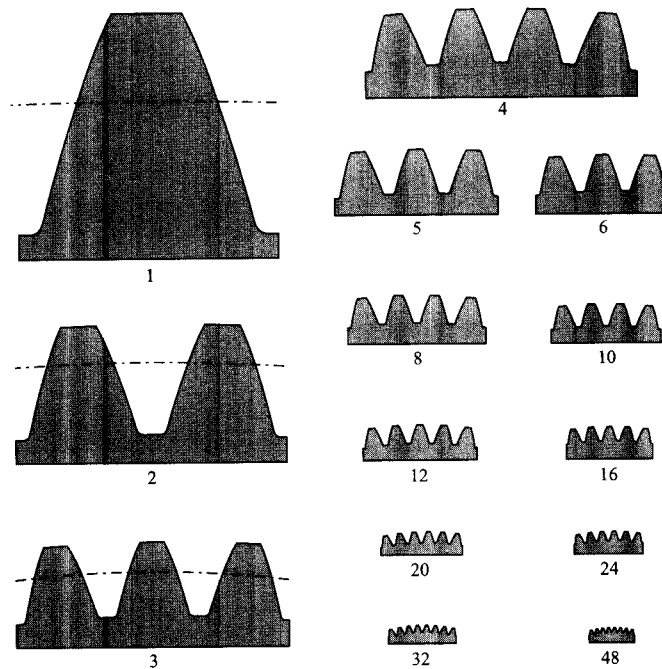


FIGURE 10.11 Actual relative sizes of gear teeth with diametral pitches shown.

## 10.6 CONTACT RATIO

An important feature of gear action is the *contact ratio*, which can be thought of as the *average* number of tooth pairs that are in contact through the gear cycle. Thus, a contact ratio of 1.2 indicates that one tooth pair is contacting 80% of the time and two pairs 20% of the time; this is generally considered to be the minimum contact ratio that should be used for typical designs. If the contact ratio is less than one, contact will be lost part of the time, and the gear pair cannot function properly. A larger contact ratio normally means smoother running gears and enhanced load-carrying capacity and stiffness, since the load is transferred in parallel between several tooth pairs. However, to take full advantage of a high contact ratio, very accurately cut tooth profiles are necessary.

Figure 10.12 shows a pair of mating teeth in the two positions in which they first come in contact and are at the point of losing contact. Between these two positions, the point of contact moves along the line of contact through the pitch point, as described in section 10.4. As can be seen from the figure, the locations of first and last contact are determined by the addenda of the teeth. Contact is initiated at point  $I$ , which is the intersection of

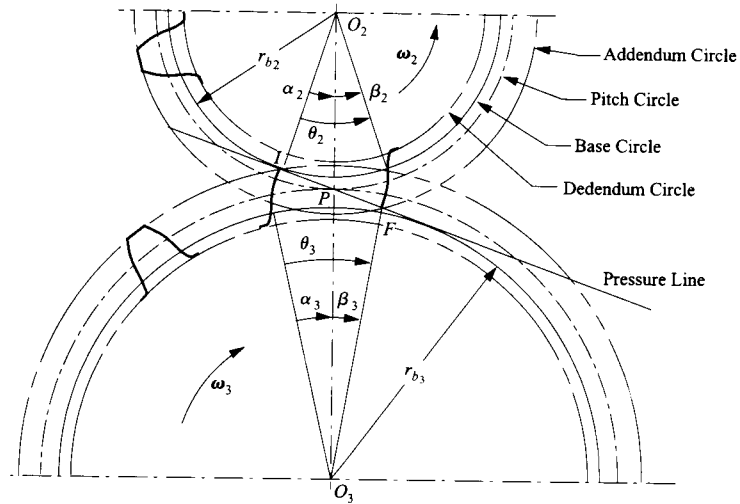


FIGURE 10.12 Contact angles: The contact angle of gear 2 is  $\theta_2$  and that of gear 3 is  $\theta_3$ .

the pressure line with the addendum circle of gear 3. Contact is terminated at point  $F$ , which is the intersection of the pressure line with the addendum circle of gear 2.

For gear 2, the angle of approach,  $\alpha_2$ , is the angle through which the gear rotates from the time of first contact between a pair of teeth and the time at which the contact point reaches the pitch point. Correspondingly, the angle of recess,  $\beta_2$ , is the angle through which the gear rotates from the time at which contact is at the pitch point to the time at which contact is lost. The angle  $\theta_2 = \alpha_2 + \beta_2$  is the angle of contact of gear 2 when in mesh with gear 3. Meshing gear 2 with another gear will change both  $\alpha_2$  and  $\beta_2$  if the size of the second gear changes.

Because the distance the contact point moves along the path of contact is equal to the curvilinear distance around the base circle, according to the relationship illustrated in Fig. 10.12,

$$\alpha_2 = IP/r_{b_2}$$

and

$$\beta_2 = PF/r_{b_2}$$

Hence

$$\theta_2 = IF/r_{b_2}$$

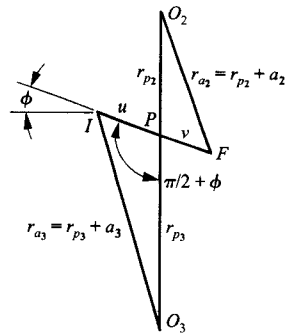
The distance  $IP$  from the point of initial contact to the pitch point can be computed from the geometry shown in Fig. 10.13, where  $r_{p_3}$  and  $r_{a_3}$  are, respectively, the pitch circle radius and addendum (tip) circle radius of the driven gear (gear 3). Here,  $\phi$  is the pressure angle, and  $u$  is the length  $IP$ . Application of the cosine rule to the triangle  $IPO_3$  gives

$$r_{a_3}^2 = u^2 + r_{p_3}^2 - 2ur_{p_3} \cos(\phi + \pi/2)$$

or

$$u^2 + r_{p_3}^2 + 2ur_{p_3} \sin \phi - r_{a_3}^2 = 0$$





**FIGURE 10.13** The geometry used in computing the length of the path of contact,  $IF$ . The points  $O_2$ ,  $O_3$ ,  $P$ ,  $I$ , and  $F$  are the same as those shown in Fig. 10.12.

Solving this quadratic equation for  $u$  and simplifying using  $\sin^2\phi + \cos^2\phi = 1$  gives

$$u = -r_{p_3} \sin \phi \pm \sqrt{r_{a_3}^2 - r_{p_3}^2 \cos^2 \phi}$$

Now  $r_{a_3} = r_{p_3} + a_3$ , where  $a_3$  is the addendum of gear 3. Therefore this equation can be written in the form

$$u = -r_{p_3} \sin \phi \pm \sqrt{a_3^2 + 2a_3r_{p_3} + r_{p_3}^2 \sin^2 \phi}$$

It can be seen that the square root term is always larger than  $r_{p_3} \sin \phi$ , so there will always be a positive root and a negative root. Only the positive root is consistent with the geometry presented. Therefore

$$u = -r_{p_3} \sin \phi + \sqrt{a_3^2 + 2a_3r_{p_3} + r_{p_3}^2 \sin^2 \phi} \quad (10.16)$$

Because of the symmetry between the triangles in Fig. 10.13, Eq. (10.16) may also be used to compute  $v = PF$  by replacing  $r_{p_3}$  with  $r_{p_2}$  and  $a_3$  with  $a_2$ . That is,

$$v = -r_{p_2} \sin \phi + \sqrt{a_2^2 + 2a_2r_{p_2} + r_{p_2}^2 \sin^2 \phi}$$

As shown in Fig. 10.14, the distance along the respective base circles between the involutes in the initial and final positions is

$$\lambda = IF = IP + PF = u + v$$

or

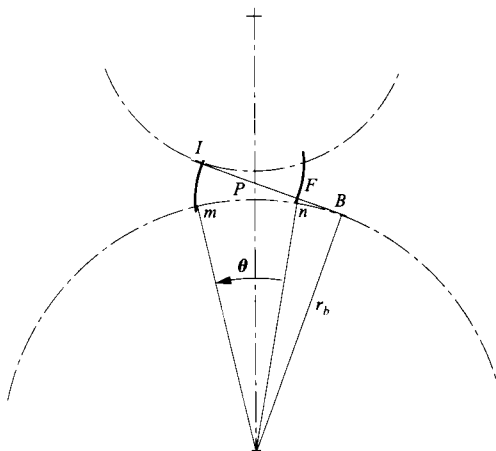
$$\lambda = -r_{p_2} \sin \phi + \sqrt{a_2^2 + 2a_2r_{p_2} + r_{p_2}^2 \sin^2 \phi} - r_{p_3} \sin \phi + \sqrt{a_3^2 + 2a_3r_{p_3} + r_{p_3}^2 \sin^2 \phi} \quad (10.17)$$

The angle of recess of the driving gear is, therefore,

$$\eta_2 = v/r_{b_2} = v/(r_{p_2} \cos \phi)$$

Similarly, the angle of approach of the driven gear is

$$\eta_3 = u/r_{b_3} = u/(r_{p_3} \cos \phi)$$



**FIGURE 10.14** Relationship of the length of the path of contact to the angle of contact. The length  $IF$  is equal to the curvilinear distance  $mn$  around the base circle. Hence the angle of contact is  $\theta = IF/r_b$ .

Using Eqs. (10.7)–(10.13) and (10.17), we can now compute the contact ratio as the ratio of the length of the path of contact to the base pitch. That is,

$$m_c = \frac{\lambda}{p_b} = \frac{\lambda}{p_c \cos \phi} = \frac{\lambda P_d}{\pi \cos \phi}$$

$$= \frac{P_d \left\{ -r_{p_2} \sin \phi + \sqrt{a_2^2 + 2a_2 r_{p_2} + r_{p_2}^2 \sin^2 \phi} - r_{p_3} \sin \phi + \sqrt{a_3^2 + 2a_3 r_{p_3} + r_{p_3}^2 \sin^2 \phi} \right\}}{\pi \cos \phi} \quad (10.18)$$

As previously stated, the significance of the contact ratio ( $m_c$ ) is that it determines the load sharing among the teeth. If the contact ratio is less than 1, there will be periods in which contact is completely lost and the gears cannot function. If the contact ratio is close to 1, variations caused by errors in mounting or wear may cause loss of contact. In practice, contact ratios less than 1.2 should be avoided.

**EXAMPLE 10.1**  
**Contact Ratio for**  
**Two 20° Pressure-**  
**Angle Gears**

**Solution**

Two gears are in mesh such that one gear (gear 2) has 20 teeth and the other (gear 3) has 30. The diametral pitch for each gear is 4, and the working pressure angle is 20°. Standard gears are involved in each case, and the addendum constant is 1. Determine the length of the contact line and the contact ratio.

To compute the contact ratio, we need to determine the base pitch and all of the terms in Eq. (10.17). From Table 10.1, the addendum for both gears is given by

$$a = \frac{1}{P_d} = \frac{1}{4} = 0.25 \text{ in} = a_2 = a_3$$

Similarly, the circular pitch for both gears is given by

$$p_c = \frac{\pi}{P_d} = \frac{\pi}{4} = 0.785 \text{ in}$$

and from Eq. (10.13), the base pitch is related to the circular pitch by

$$p_b = p_c \cos \phi = 0.785 \cos 20^\circ = 0.738 \text{ in}$$

From Eq. (10.7), the two pitch radii are given by

$$r_{p_2} = \frac{N_2}{2P_d} = \frac{20}{2(4)} = 2.5 \text{ in}$$

and

$$r_{p_3} = \frac{N_3}{2P_d} = \frac{30}{2(4)} = 3.75 \text{ in}$$

The length of the line of contact is given by Eq. (10.17) as

$$\begin{aligned} \lambda &= -r_{p_2} \sin \phi + \sqrt{a_2^2 + 2a_2r_{p_2} + r_{p_2}^2 \sin^2 \phi} - r_{p_3} \sin \phi + \sqrt{a_3^2 + 2a_3r_{p_3} + r_{p_3}^2 \sin^2 \phi} \\ &= -2.5 \sin 20^\circ + \sqrt{0.25^2 + 2(0.25)(2.5) + 2.5^2 \sin^2 20^\circ} \\ &\quad - 3.75 \sin 20^\circ + \sqrt{0.25^2 + 2(0.25)(3.75) + 3.75^2 \sin^2 20^\circ} \\ &= 1.185 \text{ in} \end{aligned}$$

From Eq. (10.18), the contact ratio is

$$m_c = \frac{\lambda}{p_b} = \frac{1.185}{0.7380} = 1.6052$$

Therefore, on average, approximately 1.6 teeth are in contact as the gears mesh.

## 10.7 INVOLUTOMETRY

It is important, for the purpose of analyzing stress and deflection of gear teeth, to be able to compute the thickness of a tooth at any radius. From Fig. 10.15, the arc distance  $AB$  is equal to the linear distance  $BT$ . Therefore,

$$AB = BT = r_b \tan \xi$$

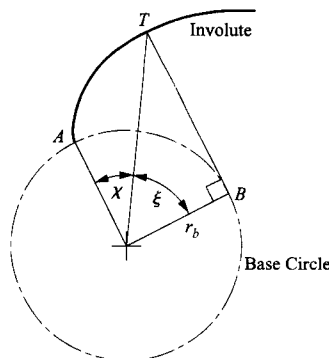
and

$$\chi = AB/r_b - \xi = \tan \xi - \xi$$

where  $\chi$  is called the involute function of  $\xi$  and is written

$$\text{inv}(\xi) = \tan \xi - \xi$$

Involute functions can be obtained from tables. They are also easily calculated on a calculator. The thickness of the tooth at any radius  $r$  can be computed using involute functions.



**FIGURE 10.15** The basic geometry for the definition of the involute function.

Referring to Fig. 10.16, we have

$$\frac{t_p}{2r_p} = \alpha - \text{inv}\phi$$

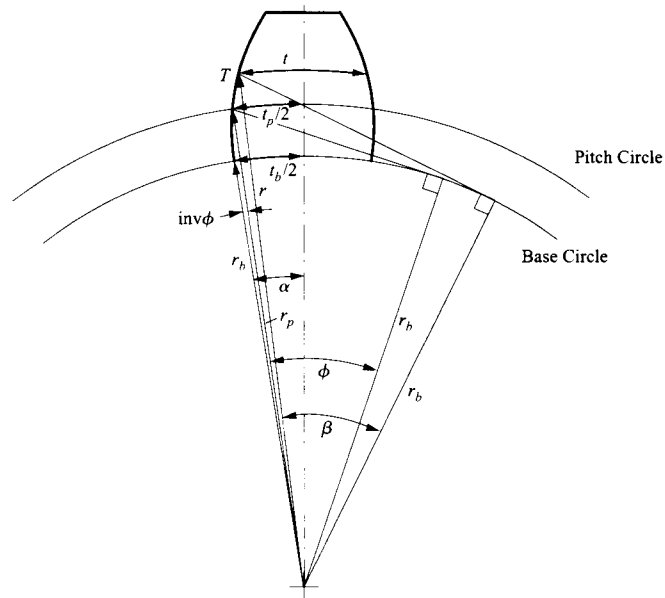
$$\frac{t}{2r} = \alpha - \text{inv}\beta$$

Hence

$$\frac{t}{2r} = \frac{t_p}{2r_p} + \text{inv}\phi - \text{inv}\beta \tag{10.20}$$

where

$$\cos\beta = \frac{r_b}{r} = \frac{r_p \cos\phi}{r} \tag{10.21}$$



**FIGURE 10.16** Computation of the tooth thickness,  $t$ , at any radius,  $r$ . Tooth thickness is computed as a *curvilinear* length along the circumference of the circle of radius  $r$  through point  $T$ .

**EXAMPLE 10.2**  
**Thickness of a Gear Tooth**

Find the thickness at the addendum and base circles of a tooth of diametral pitch 4 on a gear with 30 teeth cut with a  $20^\circ$  pressure angle, standard dimensions, and with the tooth thickness at the pitch circle equal to half the circular pitch.

**Solution**

First compute the radii at the three locations for which the tooth thickness is desired. The radius of the pitch circle is given by Eq. (10.7) as

$$r_p = \frac{N}{2P_d} = \frac{30}{2(4)} = 3.75 \text{ in}$$

Using Table 10.1 gives the addendum radius of

$$r_a = r_p + a = r_p + \frac{1}{P_d} = 3.75 + \frac{1}{4} = 4.0 \text{ in}$$

The base circle radius is given by Eq. (10.5) as

$$r_b = r_p \cos \phi = 3.75 \cos 20^\circ = 3.524 \text{ in}$$

From Table 10.1, the circular tooth thickness is

$$t_p = \frac{\pi}{2P_d} = \frac{\pi}{2(4)} = 0.393 \text{ in}$$

Next compute the angle  $\beta$  at the addendum circle. From Eq. (10.21), we have

$$\beta_a = \cos^{-1} \left[ \frac{r_p \cos \phi}{r_a} \right] = \cos^{-1} \left[ \frac{3.75 \cos 20^\circ}{4.0} \right] = 28.241^\circ$$

The value of  $\beta$  at the base circle is zero.

From Eq. (10.20), the equation for the tooth thickness at the addendum is

$$t_a = 2r_a \left( \frac{t_p}{2r_p} + \text{inv}\phi - \text{inv}\beta_a \right) = 2(4.0) \left( \frac{0.393}{2(3.75)} + \text{inv}20^\circ - \text{inv}28.241^\circ \right) = 0.184 \text{ in}$$

The value of  $\beta$  at the base circle is zero. Therefore, the tooth thickness at the base circle is

$$t_b = 2r_b \left( \frac{t_p}{2r_p} + \text{inv}\phi - \text{inv}\beta_b \right) = 2(3.524) \left( \frac{0.393}{2(3.75)} + \text{inv}20^\circ - 0 \right) = 0.474 \text{ in}$$

### EXAMPLE 10.3

#### Minimum Thickness of a Gear Tooth

#### Solution

From Example 10.2, it is clear that the gear tooth thickness becomes smaller as the radius increases from the base circle radius. In the limiting case, the tooth thickness is zero. For the gear in Example 10.2, determine the maximum radius that could be specified for the addendum circle if a nonstandard gear were used.

From Eq. (10.20) and Fig. 10.17, the gear tooth thickness becomes zero when

$$2r \left( \frac{t_p}{2r_p} + \text{inv}\phi - \text{inv}\beta \right) = 0 \quad (10.22)$$

Equation (10.22) is satisfied when

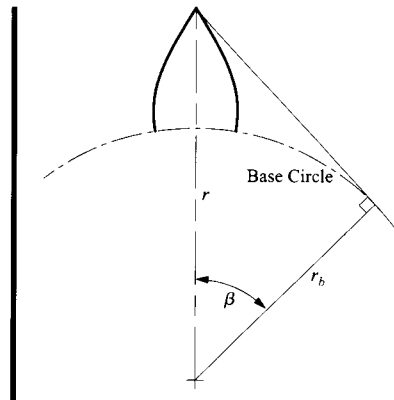
$$\text{inv}\beta = \frac{t_p}{2r_p} + \text{inv}\phi = \frac{0.393}{2(3.75)} + \text{inv}20^\circ = 0.0673$$

This equation can be solved for  $\beta$  by using a table of values for the involute function or by simply computing a series of values for  $\text{inv}\beta$  on a calculator or with a program such as MATLAB. The solution is  $\beta = 32.13^\circ$ . From Fig. 10.17, it is clear that  $\beta$  and  $r$  are related by

$$r = r_b / \cos \beta \quad (10.23)$$

Therefore,

$$r = r_b / \cos \beta = 3.524 / \cos 32.13^\circ = 4.161 \text{ in} \quad (10.24)$$

FIGURE 10.17 Limiting case for  $r$  (tooth thickness = 0).

## 10.8 INTERNAL GEARS

An internal or annular gear is a gear that has its center on the same side of the pitch circle as the pinion meshing with it, as shown in Fig. 10.18. The addendum circle for the internal gear is inside the pitch circle, and the teeth are concave rather than convex. Internal gears are commonly used in planetary gear systems and compact gear boxes. The primary advantage of an internal gear set is the compactness of the drive. Also, both the pinion and gear rotate in the same direction. Other advantages are the lower contact stresses because the surfaces conform better than external gear sets. There are also lower relative sliding between teeth and a greater length of contact possible between mating teeth since there is no limit to the involute profile on the flank of the internal gear.

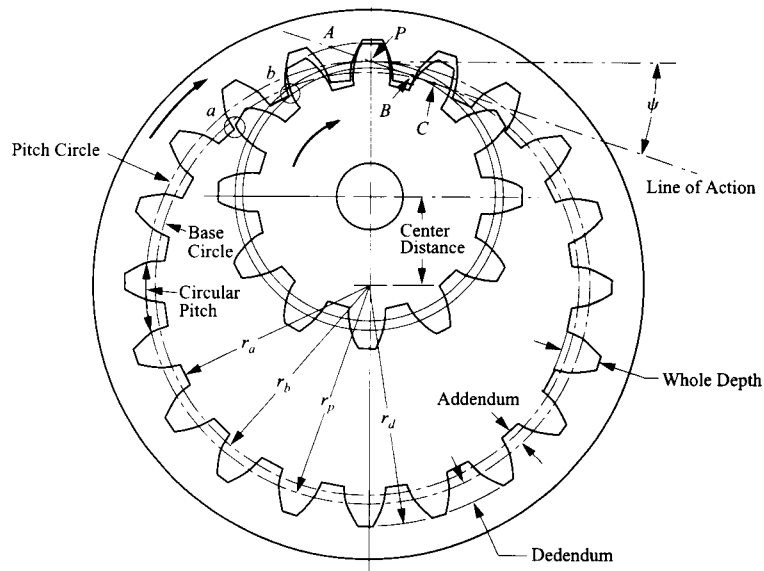


FIGURE 10.18 Internal gear and pinion.

Because of the tooth shape, the bending strength of the internal teeth is much greater than the strength of the teeth on the pinion. Therefore, the pinion is always the weaker member unless different materials are used for the two gears.

As in the case of external gears, the contact occurs along the line of action that is tangent to both base circles and passes through the pitch point or point of tangency between the two pitch circles. Referring to Fig. 10.18, we see that the line of action is tangent to the base circle of the internal gear at  $C$  and to the base circle of the pinion at  $B$ . If contact occurs between  $B$  and  $C$ , interference will result because the involute part of the pinion tooth does not cross the line of action until  $B$  is reached. Contact continues until point  $A$  is reached, where  $A$  is the intersection of the line of action with the addendum of the pinion. Therefore, the length of the line of action is  $AB$ , and the addendum of the gear should not extend beyond point  $B$ .

A different type of interference between the gear and pinion can also occur when the number of teeth on both gears varies only slightly. The interference is called *fouling*, and it occurs at inactive profiles when the teeth of the pinion withdraw from the space of the gear. Potential sites for fouling are locations  $a$  and  $b$  in Fig. 10.18. To remove the potential for fouling, internal gears are usually cut with a shaper cutter that has two teeth fewer than the internal gear being cut. This automatically relieves the tips of the internal gear and eliminates the potential for fouling for any pinion with fewer teeth than the cutter.<sup>3</sup>

Standard tooth proportions are not used for internal gears because the addendum of the gears must be shorter than those given in Table 10.1 to avoid interference. However, the basic equations for circular and diametral pitch apply, and the contact ratio and angles of action can be determined in the same manner as for external gears.

## 10.9 GEAR MANUFACTURING

---

Gear teeth can be formed in a variety of ways including various forms of casting: sand casting, investment casting, and die casting. They can be cut from flat stock using electron-discharge machining (EDM), CNC milling, and even precision sawing (and secondary machining or grinding). Gears made from polymers, aluminum, magnesium, and so on can be extruded and cut to width. Thin gears can be blanked from sheet stock.

Gears that must carry large loads relative to their overall size are usually made of high-strength materials such as steel. Some gears, such as bevel gears, can be forged; however, the vast majority of production gears are machined from blanks. Very small quantities can be machined using EDM, CNC milling, or horizontal milling with a formed cutter; however, when large volumes are involved, the machining is usually done with a generating cutter. In formed cutters, the tooth takes the exact shape of the cutter. Therefore, a separate cutter is technically required for each gear pitch and each number of teeth because the shape of the space between the teeth varies with both pitch and tooth number. In reality, the change in space is not significant in many cases. For a given pitch, only eight cutters are required to cut any gear in the range of 12 teeth to a rack with reasonable accuracy. However, such gears are usually not accurate enough for high speeds. A separate set of cutters is required for each pitch.<sup>4</sup> Figure 10.19 shows an example of milling using a formed cutter.

In a generating cutter, the tool has a shape different from the tooth profile, and the tool is moved relative to the gear blank to produce the desired gear shape.



**FIGURE 10.19** Milling gear teeth using a formed cutter. For a given gear pitch, eight cutters are required to form gears with from (approximately) 12 teeth to a rack. (Courtesy of Horsburgh and Scott Company, Cleveland, Ohio.)

When large volumes are involved, the fabrication of gears normally involves the following steps:

1. blank fabrication,
2. forming of teeth,
3. refining of teeth,
4. heat treatment,
5. grinding, deburring, and cleaning, and
6. finish coating.

Blank fabrication involves all of the general and special features of the gear blank. This includes forming the hub and keyways. Tooth generation includes machining the gear teeth using one of the processes discussed later in this section. The refining operations include shaving, grinding, burnishing, and lapping and are used to improve the accuracy of the gear teeth. These are necessary to remove machining marks and to improve the gear quality. The higher the gear quality, the greater the power rating and the lower the noise generated by meshing gear pairs. Heat treatment includes case hardening, which is necessary for high-performance gears to improve the resistance to surface pitting and tooth fracture. If heat treated, the gears must be reground if high accuracy is required. Deburring and cleaning are essential for all gears regardless of how they have been manufactured or the accuracy desired. Finish coatings include processes such as anodizing aluminum or depositing diamond films, but they may involve only grease or paint. The objective is to improve corrosion resistance, to reduce friction and wear, or simply to improve appearance.



Machining by shaping and hobbing are the most common methods of gear tooth generation. The objective is to slowly mesh a gear blank into a cutting tool that has teeth that will be conjugate with the teeth cut into the blank. The cutting action is always orthogonal to the side of the gear blank. In the shaping process, the cutter looks like a gear but is made of much harder material (see Figs. 10.20 and 10.21). When the gear is shaped, the reciprocating shaper cutter is moved radially into the blank until the pitch circle of the cutter and the gear blank are tangent. After each cutting stroke, the cutter is raised above the blank, and both the blank and the cutter rotate a very small amount on their pitch circles. The process continues until all of the teeth are cut. Shaping is the main method used to produce internal gears and gears integral with a shaft that has a shoulder next to the gear.

The shaping cutter can also be in the form of a rack. In this case, the pitch circle of the cutter is a straight line, and the cutter moves on a straight line tangent to the pitch circle of the gear. Relative to the gear, the pitch line of the rack appears to roll around the pitch circle of the gear. The gear teeth are formed by the envelope of the rack teeth, as shown in Fig. 10.22.

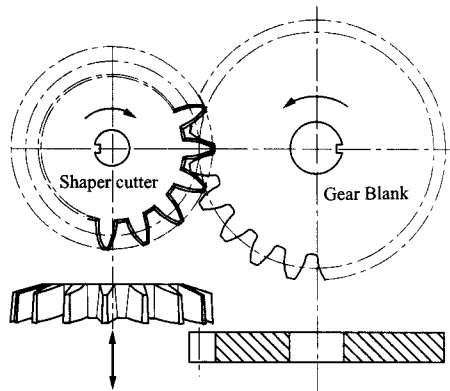


FIGURE 10.20 Forming gear teeth with shaper.

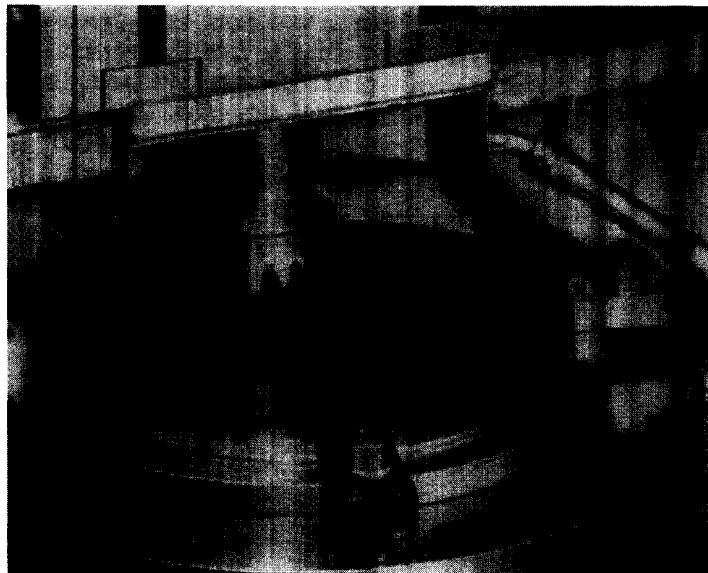
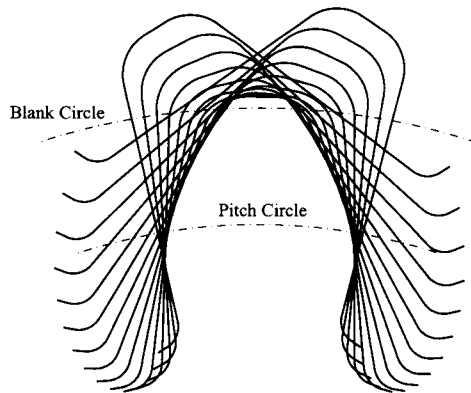
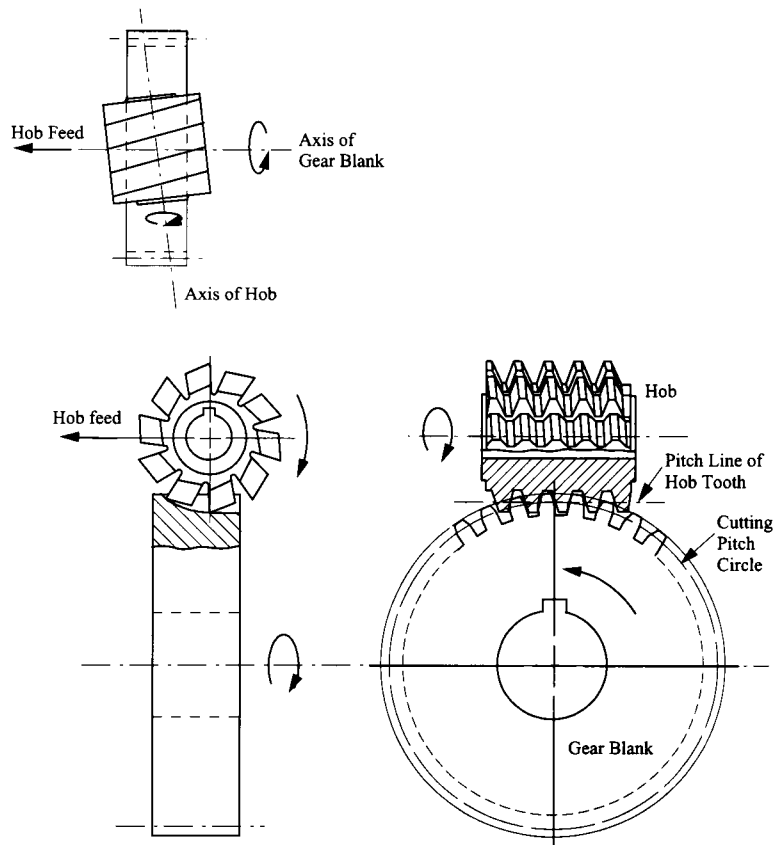


FIGURE 10.21 Shaping an internal gear. (Courtesy of Fellows Corporation, Springfield, Vermont.)



**FIGURE 10.22** Envelope of rack teeth relative to gear blank.

Hobbing is a method of generating gear teeth that is geometrically similar to generating the teeth with a rack cutter. The teeth of a hob are of the same shape as those on a rack cutter. However, the teeth are attached to a helical path on a cylindrical cutter. The hob looks like a worm gear with horizontal slices taken out of it. It is similar in appearance to a machine screw tap. The hob action is shown in Fig. 10.23, and a hobbing machine is shown



**FIGURE 10.23** Tooth generation with a hob.

in Fig. 10.24. In the hobbing machine, the hob teeth are aligned with the axis of the gear teeth. The hob and blank are rotated continuously at the proper angular velocity ratio, and the hob is fed slowly across the face of the width of the blank from one side to the other to form the teeth. The hobbing process is the most popular among the machining processes because it produces the most teeth in a given time and because the same tool can be used to cut helical as well as spur gear teeth. However, for internal gears, a gear shaper must be used.

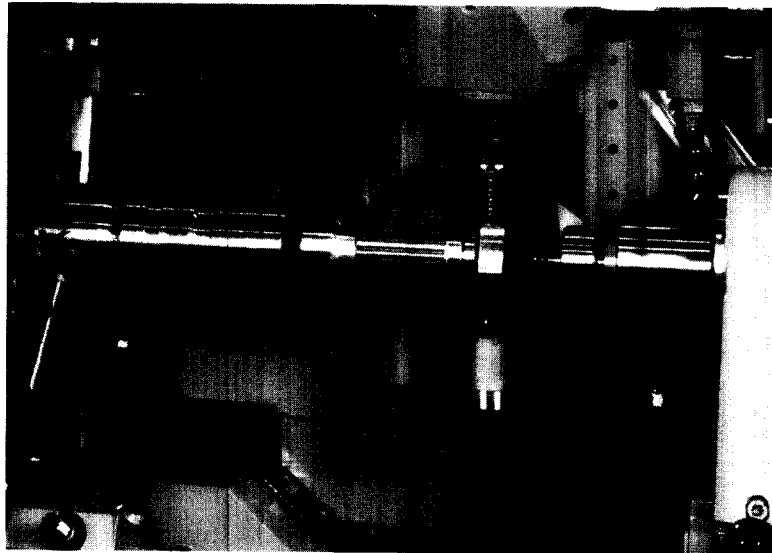


FIGURE 10.24 Hobbing spur gear teeth. (Courtesy of Bourn & Koch.)

## 10.10 INTERFERENCE AND UNDERCUTTING

If the path of contact extends beyond the point of tangency with the base circle of the pinion, called the interference point, the tips of the teeth on the gear come into contact with portions of the pinion tooth profile inside the base circle. Because the involute is not defined inside the base circle, conjugate action is lost, and, in fact, the tips of the gear teeth will interfere with the lower portion of the pinion tooth flank if the tooth is machined with a formed cutter. If the pinion is generated with a rack-type cutter or hob, the cutter teeth will undercut the pinion teeth and weaken them. This situation is shown in Fig. 10.25. Thus, it is very undesirable to have the path of contact extend past the interference point.

In Fig. 10.26, two gears are shown in mesh. The interference point on gear 2 is point *A* and that on gear 3 is point *D*. The addendum circle of gear 3 intersects the line of action at *B*, and the addendum circle of gear 2 intersects the line of action at *C*. If the addendum circle for gear 2 extends beyond point *D* or the addendum circle of gear 3 extends beyond point *A*, interference will occur. Actually, we need only investigate one of these conditions because, as indicated in Fig. 10.26, interference will always occur first on the smaller gear. Therefore, we need only check point *D*. In Fig. 10.26, if we visualize the pitch diameter of gear 2 becoming larger, point *C* will gradually move toward point *D*. Eventually, there will be a diameter that causes point *C* to move beyond point *D*, and interference will occur. If gear 2 is actually a shaper cutter, the material in the interference region will simply be

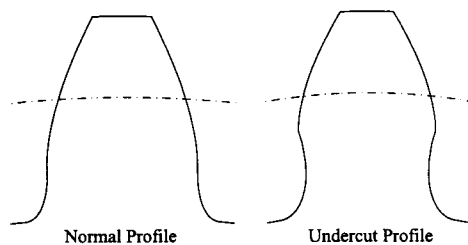


FIGURE 10.25 Normal and undercut gears.

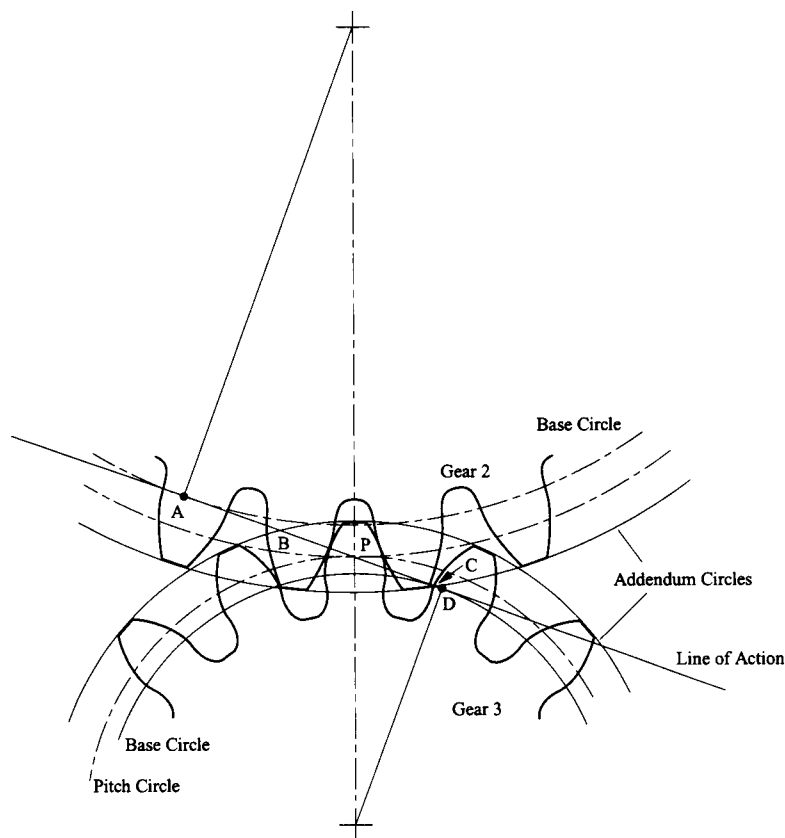
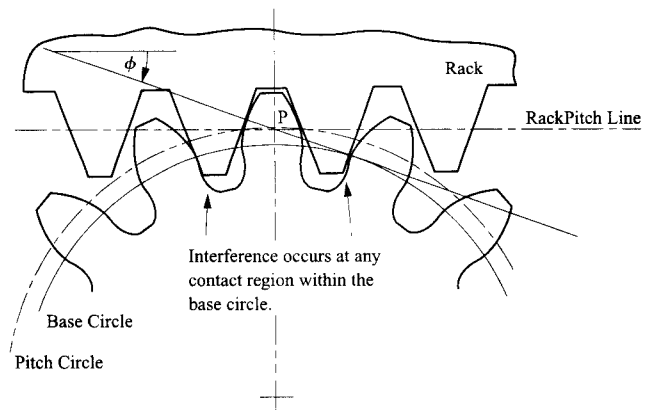


FIGURE 10.26 Meshing conditions for two gears.

removed. If, however, the teeth on gear 3 were formed by a smaller shaper cutter or cut directly, for example, by using a conforming milling cutter, then material might exist in the problem region. In that case, when gear 2 is meshed with gear 3, there will be volumetric interference, and the gear loads could be high enough to cause premature failure.

The worst case for interference or undercutting is when the pinion is meshed with a rack or generated with a rack cutter. This condition is shown in Fig. 10.27. Therefore, if we design the gear to avoid interference with a rack, the gear will mesh with all other standard gears satisfying the criteria in Section 10.5.2. Undercutting becomes more severe as the number of teeth on the gear is reduced because, for a given diametral pitch, the pitch diam-



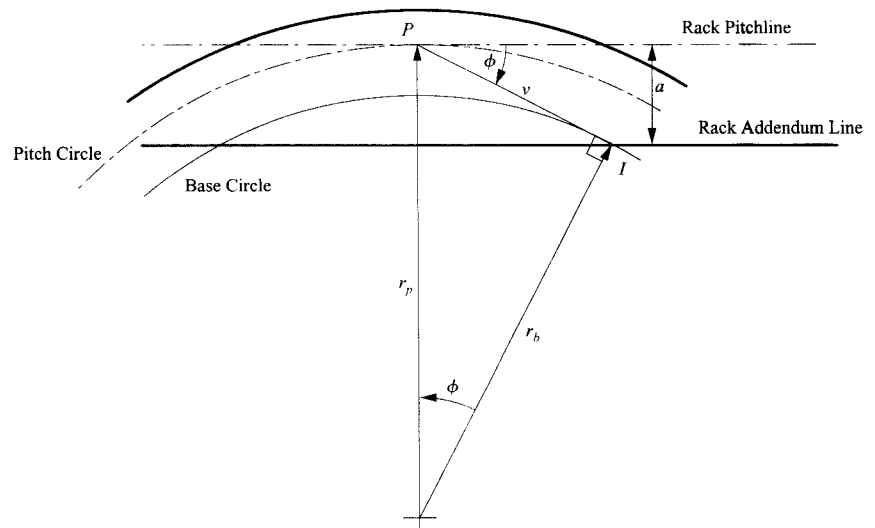
**FIGURE 10.27** Interference will occur at all contact locations within the base circle.

eter decreases when the number of teeth is reduced. Therefore, there will be a critical number of teeth on the gear to just avoid undercutting. The minimum number of teeth to avoid undercutting can be determined by identifying when the addendum circle of the rack cutter extends beyond the interference point on the gear. This can be done using the simplified geometry in Fig. 10.28. Using that figure, we get

$$v = \frac{a}{\sin \phi} = r_p \sin \phi$$

or

$$r_p = \frac{a}{\sin^2 \phi} \quad (10.25)$$



**FIGURE 10.28** Geometry for determining undercutting.

We may use  $k/P_d$  as the addendum for a standard gear, where  $k$  is a constant (1 for full-depth gears and 0.8 for stub tooth gears), and from Eq. (10.7) we have

$$2r_p = \frac{N}{P_d}$$

Substituting into Eq. (10.25) gives

$$N = \frac{2k}{\sin^2 \phi} \quad (10.26)$$

Results for some of the common pressure angles and systems are summarized in Table 10.2. Note that the number of teeth must be a whole number for a continuously rotating gear. Also notice that the minimum number of teeth varies inversely with the pressure angle. Therefore, the minimum number of teeth for a  $14\frac{1}{2}^\circ$  pressure angle is 32, whereas for a  $20^\circ$  pressure angle it is 18. This is one of the reasons why the  $14\frac{1}{2}^\circ$  system is rarely used in modern machinery.

**TABLE 10.2 Minimum Number of Teeth to Avoid Undercutting for Standard Gears**

System	Full depth	Full depth	Full depth	Stub
$\phi$	$14\frac{1}{2}^\circ$	$20^\circ$	$25^\circ$	$20^\circ$
$k$	1	1	1	0.8
$N$	31.9	17.10	11.20	13.68
$N_{\min}$	32	18	12	14

## 10.11 NONSTANDARD GEARING

Sometimes, for reasons of saving space, the aforementioned minima are violated. Interference can still be avoided by offsetting the cutting rack so that the addendum line of the rack passes through the interference point or outside it. This requires a larger blank for the pinion. The net effect is to increase the addendum of the pinion and decrease its dedendum. This is shown in Table 10.3. The removal of undercutting is accompanied by other beneficial effects: The tooth shape is stronger and the contact ratio is improved. However, a non-standard gear results.

Referring to Fig. 10.29, we see that the cutter can be offset a distance  $e$  to bring the addendum line through the pitch point. This offset distance can be computed from

$$e = a + r_b \cos \phi - r_p \quad (10.27)$$

where  $\phi$  is the cutting pressure angle and  $r_p$  is the cutting pitch radius. We can eliminate  $r_b$  from Eq. (10.27) using Eq. (10.5) and the expression  $\sin^2 \phi + \cos^2 \phi = 1$ . Then,

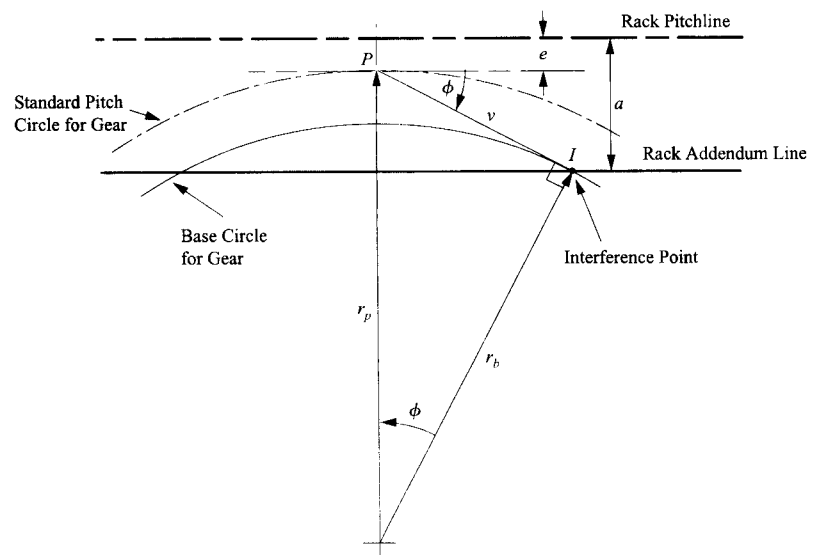
$$e = a + r_p \cos^2 \phi - r_p = a - r_p \sin^2 \phi$$

**TABLE 10.3 Minimum Values of Addendum for Unequal Addendum and Dedendum Gears to Avoid Undercut<sup>a</sup>**

Number of pinion teeth	AGMA 20° coarse-pitch system		Minimum number of gear teeth	AGMA 20° fine-pitch system		Minimum number of gear teeth
	$a_p$	$a_G$		$a_p$	$a_G$	
7	—	—	—	1.4143 <sup>b</sup>	0.4094	42
8	—	—	—	1.43669 <sup>b</sup>	0.4679	39
9	—	—	—	1.4190 <sup>b</sup>	0.5264	36
10	1.468	0.532	25	1.4151	0.5849	33
11	1.409	0.591	24	1.3566	0.6434	30
12	1.351	0.649	23	1.2982	0.7019	27
13	1.292	0.708	22	1.2397	0.7604	25
14	1.234	0.766	21	1.1812	0.8189	23
15	1.117	0.825	20	1.1227	0.8774	21
16	1.117	0.883	19	1.0642	0.9358	19
17	1.058	0.942	18	1.0057	0.9943	18
18	1.000	1.000	18	1.0000	1.0000	18

<sup>a</sup>The values in this table are for one diametral pitch; divide them by the desired diametral pitch to obtain the addendum.

<sup>b</sup>Not proportional to the increase in tooth thickness; a reasonable top land must be provided.



**FIGURE 10.29** Geometry for determining undercutting when the hob is withdrawn by an amount  $e$ .

The expression for the tooth thickness can be used to relate tooth thickness at any radius to the actual meshing pressure angle ( $\phi_m$ )

$$t_{m_2} = 2r_{m_2} \left( \frac{t_2}{2r_2} + \text{inv}\phi - \text{inv}\phi_m \right)$$

$$t_{m_3} = 2r_{m_3} \left( \frac{t_3}{2r_3} + \text{inv}\phi - \text{inv}\phi_m \right)$$

where  $t_{m_2}$  and  $t_{m_3}$  are the thicknesses at the meshing pitch circle, and  $r_{m_2}$  and  $r_{m_3}$  are the meshing pitch radii.

Now

$$t_{m_2} + t_{m_3} = \frac{2\pi r_{m_2}}{N_2}$$

and

$$\frac{r_{m_3}}{r_{m_2}} = \frac{r_3}{r_2} = \frac{N_3}{N_2}$$

Therefore,

$$t_{m_2} + t_{m_3} = 2r_{m_2} \left( \frac{t_2}{2r_2} + \text{inv}\phi - \text{inv}\phi_m \right) + 2r_{m_3} \left( \frac{t_3}{2r_3} + \text{inv}\phi - \text{inv}\phi_m \right)$$

gives

$$\frac{2\pi r_{m_2}}{N_2} = 2r_{m_2} \left( \frac{t_2}{2r_2} + \text{inv}\phi - \text{inv}\phi_m \right) + \frac{2N_3}{N_2} r_{m_2} \left( \frac{t_3}{2r_3} + \text{inv}\phi - \text{inv}\phi_m \right)$$

or

$$\frac{2\pi}{N_2} = \frac{t_2 + t_3}{r_2} + \frac{2(N_2 + N_3)}{N_2} (\text{inv}\phi - \text{inv}\phi_m)$$

giving

$$\text{inv}\phi_m = \text{inv}\phi - \frac{2\pi r_2 - N_2(t_2 + t_3)}{2r_2(N_2 + N_3)} \quad (10.28)$$

This equation permits computation of  $\phi_m$  given the cutting pitch radius,  $r_2$ , of the gear, the cutting pressure angle,  $\phi$ , the tooth numbers,  $N_2$  and  $N_3$ , the tooth thickness,  $t_2$ , at the cutting pitch circle of the gear, and the tooth thickness,  $t_3$ , of the pinion at the cutting pitch radius.

Referring to Fig. 10.30, we have

$$t_3 = t^* + 2e \tan \phi$$

and

$$t^* = \frac{P_c}{2} = \frac{\pi}{2P_d}$$



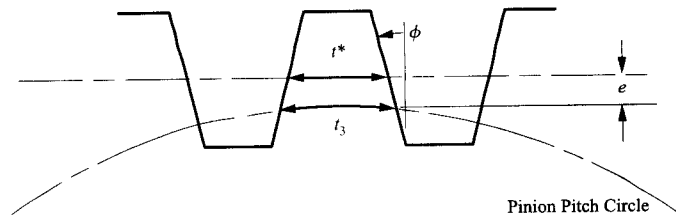


FIGURE 10.30 Cutting a nonstandard pinion.

Hence

$$t_3 = \frac{\pi}{2P_d} + 2e \tan \phi \quad (10.29)$$

but

$$e = a - r_3 \sin^2 \phi$$

or

$$e = \frac{1}{P_d} - \frac{N_3}{2P_d} \sin^2 \phi \quad (10.30)$$

The equations for spur tooth gearing are summarized in Table 10.4.

TABLE 10.4 Summary of Spur Gear Formulas

Quantity	Formula
Diametral pitch	$P_d = \frac{N}{d_p} = \frac{N}{2r_p} = \frac{\pi}{p_c}$
Circular pitch	$p_c = \frac{\pi}{P_d} = \frac{\pi d_p}{N} = \pi m = \frac{p_b}{\cos \phi} = \frac{\pi d_b}{N \cos \phi}$
Base pitch	$p_b = \frac{\pi d_b}{N} = p_c \cos \phi = \frac{\pi d_p \cos \phi}{N}$
Module	$m = \frac{d_p}{N} = \frac{1}{P_d} = \frac{p_c}{\pi}$
Tooth thickness at pitch circle	$t = \frac{p_c}{2} = \frac{\pi}{2P_d} = \frac{\pi d_p}{2N} = \frac{\pi m}{2} = \frac{p_b}{2 \cos \phi} = \frac{\pi d_b}{2N \cos \phi}$
Pitch diameter	$d_p = \frac{N}{P_d} = \frac{N p_c}{\pi} = Nm$
Outside diameter	$d_o = d_p + 2a$ (typically $a = k/P_d$ , where $k = 1$ or $0.8$ )

(continued)

TABLE 10.4 continued

Root diameter	$d_r = d_p - 2b$ (typically $b = q/P_d$ , where $q = 1.25, 1.2,$ or $1$ )
Base Circle Diameter	$d_b = d_p \cos \phi$
Center distance	$C = r_{p_2} + r_{p_3} = \frac{d_{p_2} + d_{p_3}}{2} = \frac{N_2 + N_3}{2P_d} = \frac{p_c(N_2 + N_3)}{2\pi}$
Length of line of contact	$\lambda = -r_{p_2} \sin \phi + \sqrt{a_2^2 + 2a_2r_{p_2} + r_{p_2}^2 \sin^2 \phi}$ $- r_{p_3} \sin \phi + \sqrt{a_3^2 + 2a_3r_{p_3} + r_{p_3}^2 \sin^2 \phi}$
Contact ratio	$m_c = \frac{\lambda}{p_b} = \frac{\lambda}{p_c \cos \phi} = \frac{\lambda P_d}{\pi \cos \phi}$
Velocity ratio	$R = \frac{\omega_2}{\omega_3} = \frac{r_{p_3}}{r_{p_2}} = \frac{d_{p_3}}{d_{p_2}} = \frac{N_3}{N_2}$
Tooth thickness at radius $r$	$t = 2r \left[ \frac{t_p}{2r_p} + \text{inv} \phi - \text{inv} \beta \right]; \cos \beta = \frac{r_b}{r} = \frac{r_p \cos \phi}{r}$
Involute function	$\text{inv} \phi = \tan \phi - \phi$
Number of teeth at undercutting	$N = \frac{2aP_d}{\sin^2 \phi}$
Hob withdrawal for no undercutting	$e = \frac{1}{P_d} - \frac{N_3}{2P_d} \sin^2 \phi$

**EXAMPLE 10.4**  
**Computing**  
**Nonstandard**  
**Gear Geometry**

**Solution**

A 13-tooth pinion with diametral pitch 6 and  $20^\circ$  cutting pressure angle is to mate with a 50-tooth gear. Find the center distance, and the meshing pressure angle if the pinion is cut with a standard cutter offset so that the addendum line passes through the interference point. (Compare with the corresponding values for a standard pinion.)

From Eq. (10.30),

$$e = \frac{1}{P_d} - \frac{N_3}{2P_d} \sin^2 \phi = \frac{1}{6} - \frac{13}{2 \times 6} \sin^2 20^\circ = 0.03994$$

From (10.29),

$$t_3 = \frac{\pi}{2P_d} + 2e \tan \phi = \frac{\pi}{2 \times 6} + 2 \times 0.03994 \tan 20^\circ = 0.29087$$

From Eq. (10.7),

$$r_2 = \frac{N_2}{2P_d} = \frac{50}{2 \times 6} = 4.1667$$

and from Table 10.1,

$$t_2 = \frac{2\pi r_2}{2N_2} = 0.26180$$

From Eq. (10.28)

$$\text{inv}\phi_m = \text{inv}20^\circ - \frac{2\pi \times 4.1667 - 50(0.29087 + 0.26180)}{2 \times 4.1667(50 + 13)} = 0.017673$$

To find the value for  $\phi_m$ , it is possible to use tables<sup>4</sup> or the value can be found using a simple program. A MATLAB function, *inverse\_inv(y)*, is given on the disk with this book for doing this. The result is

$$\phi_m = 21.127^\circ$$

Next use Eq. (10.5) to compute

$$r_{m_2} = \frac{r_{b_2}}{\cos\phi_m} = \frac{r_2 \cos\phi}{\cos\phi_m} = 4.1975$$

and

$$r_{m_3} = \frac{r_{b_3}}{\cos\phi_m} = \frac{r_3 \cos\phi}{\cos\phi_m} = \frac{N_3 \cos\phi}{2P_d \cos\phi_m} = \frac{13 \cos 20^\circ}{2 \times 6 \times \cos 21.127^\circ} = 1.0914 \text{ in}$$

The meshing center distance is

$$C_m = 4.1975 + 1.0914 = 5.2889 \text{ in}$$

The standard center distance

$$C_s = r_2 + r_3 = r_2 + \frac{N_3}{2P_d} = 4.1667 + \frac{13}{2 \times 6} = 5.2500 \text{ in}$$

## 10.12 CARTESIAN COORDINATES OF AN INVOLUTE TOOTH GENERATED WITH A RACK

It is often desirable to know the coordinates of the tooth profile for a given generating rack. This is of interest for drawing the gear or for machining the gear on a standard CNC milling machine without form cutters. If only the involute portion is required, it is relatively easy to compute the coordinates of points on the gear contact surface. However, if the entire profile is desired, the procedure is considerably more difficult. The problem can be approached directly if the geometry of the rack is known analytically<sup>5,6</sup>. However, an indirect approach developed by Vijayakar<sup>7</sup> is more general and applicable to a wide range of gear generators. This approach, which is relatively easy to program, is given here. The data required to generate the gear are a description of the rack, the number of teeth on the gear, and the outer diameter of the gear.

### 10.12.1 Coordinate Systems

Figure 10.31 shows a coordinate system attached to the rack that is assumed to be fixed. The origin of the system is at the intersection of the centerline of a rack tooth and the pitch line of the rack. The coordinates of any point  $P$  on the surface of the rack can be defined by  $(x_r, y_r)$  relative to the coordinate system fixed to the rack. Also, the outer normal to the rack

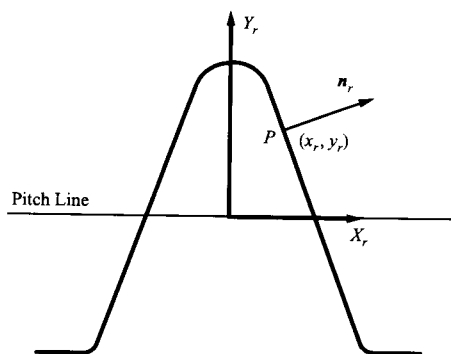


FIGURE 10.31 Rack and its attached coordinate system.

at this point can be represented by  $(n_x, n_y)$ . For any specified rack geometry, the coordinates and outer normal at any point on the rack profile are easily obtained.

Figure 10.32 shows a gear tooth with an attached coordinate system with its origin at the center of the gear. Let point  $P'$  be a point on the gear profile that corresponds to point  $P$  on the rack. As the gear pitch circle rolls on the rack pitch line, the point  $P$  on the rack makes sliding (cam) contact with the point  $P'$  on the gear.

Figure 10.33 shows the relative position of the gear and rack after the gear has rolled through the angle  $\theta$ . The pitch circle radius of the gear is  $r_p$ . For this arbitrary orientation of the gear, the transformation from the rack coordinate system to the gear coordinate system is defined by the matrix equation

$$\begin{Bmatrix} x_g \\ y_g \end{Bmatrix} = \begin{bmatrix} -\cos \theta & \sin \theta \\ -\sin \theta & -\cos \theta \end{bmatrix} \begin{Bmatrix} x_r - r_p \theta \\ y_r - r_p \end{Bmatrix} \quad (10.31)$$

As the gear rolls, the relative velocity of the point  $P'$  on the gear with respect to the rack (fixed system) is given by

$${}^r \mathbf{v}_P = {}^r \mathbf{v}_{B/C} + {}^r \mathbf{v}_{P/B}$$

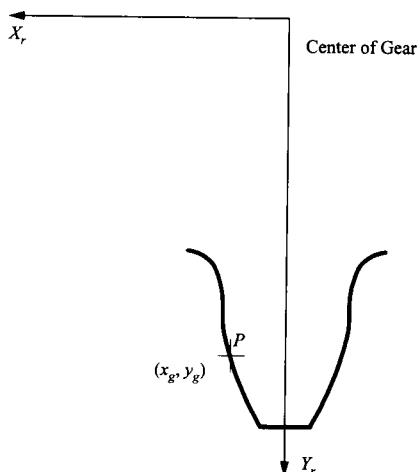
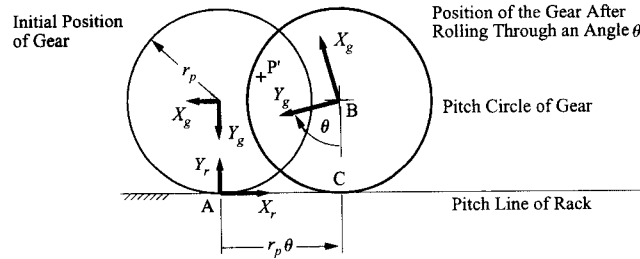


FIGURE 10.32 Gear and its attached coordinate system.



**FIGURE 10.33** Relative orientation of gear and rack coordinate systems during generation.

Recognizing that  $C$  is the instant center between the gear and the rack and that points  $P'$ ,  $A$ ,  $B$ , and  $C$  are all fixed to the gear, we have

$${}^r \mathbf{v}_P = {}^r \boldsymbol{\omega}_g \times \mathbf{r}_{B/C} + {}^r \boldsymbol{\omega}_g \times \mathbf{r}_{P/B} = {}^r \boldsymbol{\omega}_g \times (\mathbf{r}_{B/C} + \mathbf{r}_{P/B}) = {}^r \boldsymbol{\omega}_g \times \mathbf{r}_{P/C}$$

where  ${}^r \boldsymbol{\omega}_g$  is the angular velocity of the gear relative to the rack. In matrix form, this equation becomes

$${}^r \mathbf{v}_P = -{}^r \boldsymbol{\omega}_g \begin{Bmatrix} y_r \\ r_p \theta - x_r \end{Bmatrix}$$

Because cam contact is involved at the contact point (assumed to be  $P'$ ), the relative velocity of the point on the gear should have no component normal to the rack. Hence the dot product between the normal and  ${}^r \mathbf{v}_P$  must be zero. Then,

$${}^r \mathbf{v}_P \cdot \begin{Bmatrix} n_x \\ n_y \end{Bmatrix} = 0$$

or

$$-n_x y_r + (x_r - r_p \theta) n_y = 0$$

The roll angle for the gear at which the point  $P$  makes contact with a point on the gear is given by

$$\theta = \frac{n_y x_r - n_x y_r}{r_p n_y} \quad (10.32)$$

Given any point  $P$  on the rack, its coordinates, and its normal vector, the roll angle at which it makes contact with the gear can be computed using Eq. (10.32). The coordinates of the corresponding point  $P'$  on the gear can be obtained by substituting for  $\theta$  in Eq. (10.31). Therefore, a sequence of points on the gear profile can be found that corresponds to a sequence of points on the rack profile.

The procedure is to begin with points at the tip of the hob tooth and to sequence through the points until the corresponding points on the gear are located beyond the addendum circle. If  $r_o$  is the outer radius of the gear, the extreme points are reached when the coordinates given in Eq. (10.31) satisfy the following inequality:

$$\sqrt{x_g^2 + y_g^2} \geq r_o$$

Before drawing the gear tooth profile, it is necessary to check for undercutting. If undercutting occurs, the tooth profile generated using the foregoing procedure will look like that

shown in Fig. 10.34. The part  $B-C-D-B$  must be detected, and the parts associated with this region must be eliminated from the sequence of points used to define the gear profile.

Let  $r_i, i = 1, 2, \dots, n$  be a sequence of vectors corresponding to the points on the gear tooth profile. To detect the crossover point  $B$  shown in Fig. 10.34, we need to check whether there are integers  $i$  and  $j$  such that the line segment  $(i, i + 1)$  that joins  $r_i$  with  $r_{i+1}$  intersects the line segment  $(j, j + 1)$ . Figure 10.35 shows two line segments  $(a, b)$  and  $(c, d)$ . These line segments will intersect if and only if<sup>6</sup>

$$A(a, b, c) \cdot A(a, b, d) < 0$$

and

$$A(c, d, a) \cdot A(c, d, b) < 0$$

where

$$A(a, b, c) = (r_b - r_a) \times (r_c - r_a)$$

and

$$r_a = \begin{Bmatrix} x_a \\ y_a \\ 0 \end{Bmatrix}, \quad r_b = \begin{Bmatrix} x_b \\ y_b \\ 0 \end{Bmatrix}, \quad r_c = \begin{Bmatrix} x_c \\ y_c \\ 0 \end{Bmatrix}, \quad r_d = \begin{Bmatrix} x_d \\ y_d \\ 0 \end{Bmatrix}$$

The location of the point of intersection will be given by  $r_e$ , where

$$r_e = \alpha r_a + (1 - \alpha) r_b$$

where

$$\alpha = \frac{|A(c, d, b)|}{|A(c, d, a)| + |A(c, d, b)|}$$

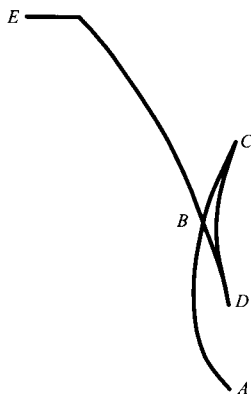


FIGURE 10.34 Gear profile with undercutting.

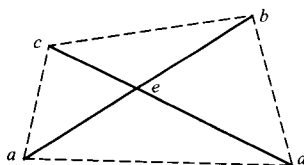


FIGURE 10.35 Determination of the point of intersection of two line segments.

Using this method, the whole profile can be searched for segments  $(i, i + 1), i = 1, 2, \dots, n - 2$  and  $(j, j + 1), j = i + 1, i + 2, \dots, n - 1$  that intersect. If such an  $i$  and  $j$  are found, then all points on the profile between  $i + 1$  and  $j + 1$  are discarded and replaced by the single point  $r_e$  at the point of intersection.

### 10.12.2 Gear Equations

Once the set of points is defined for the single tooth, this set of coordinates can be rotated in increments of  $2\pi/N$  to form the other tooth. If  $\theta$  is the rotation angle, the coordinates  $(X_i, Y_i)$  of successive teeth are related to the original coordinates  $(x_i, y_i)$  by

$$X_i = x_i \cos \theta - y_i \sin \theta$$

$$Y_i = x_i \sin \theta + y_i \cos \theta$$

The rotation angle is incremented for each tooth to be drawn. For example, for the first tooth,  $\theta = 0$ ; for the second tooth,  $\theta = 2\pi/N$ ; for the third tooth,  $\theta = 2(2\pi/N)$ ; and for the  $j$ th tooth,  $\theta = (j - 1)(2\pi/N)$ . A MATLAB routine for drawing the hob, gear tooth, and gear is given on the disk with this book.

#### EXAMPLE 10.5 Geometry of a Simple Rack

Half of the tooth for a standard rack is represented in Fig. 10.36. Determine the equations for each region and the equations for the corresponding normal vectors.

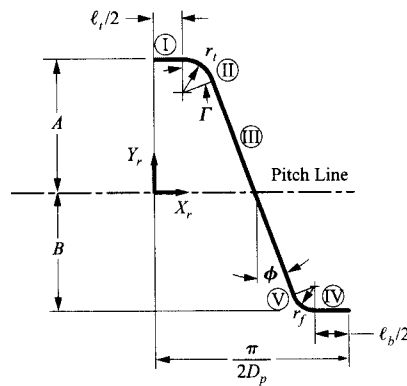


FIGURE 10.36 Geometry of a basic rack.

#### Solution

Before developing the equations for the different regions, define the following terms:

- $D_p$  = diametral pitch
- $A$  = addendum of rack
- $B$  = dedendum of rack
- $\phi$  = pressure angle
- $r_t$  = radius of tip of rack tooth
- $r_f$  = radius of fillet of rack tooth

Miscellaneous terms can be computed based on geometry to be

$$\Gamma = \frac{\pi}{2} - \phi$$

$$\ell_t = \frac{\pi}{2D_p} - 2A \tan \phi - 2r_t \tan\left(\frac{\Gamma}{2}\right)$$

$$\ell_b = \frac{\pi}{2D_p} - 2B \tan \phi - 2r_f \tan\left(\frac{\Gamma}{2}\right)$$

It is assumed that the maximum radius,  $r_t$ , at the tip of the hob is a full radius that occurs when  $\ell_t$  is zero. Then, the maximum tip radius is

$$r_t = \frac{\frac{\pi}{2D_p} - 2A \tan \phi}{2 \tan\left(\frac{\Gamma}{2}\right)}$$

Similarly, it is assumed that the maximum radius,  $r_b$ , at the fillet of the hob is a full radius that occurs when  $\ell_b$  is zero. Then, the maximum fillet radius is

$$r_f = \frac{\frac{\pi}{2D_p} - 2B \tan \phi}{2 \tan\left(\frac{\Gamma}{2}\right)}$$

The coordinates of the points and normal vectors along the rack profile in each region are given by:

**Region I (top land)**

$$\begin{Bmatrix} x_r \\ y_r \end{Bmatrix} = \begin{Bmatrix} \beta \ell_t / 2 \\ A \end{Bmatrix}, \quad \begin{Bmatrix} n_x \\ n_y \end{Bmatrix} = \begin{Bmatrix} 0 \\ 1 \end{Bmatrix} \quad (0 < \beta \leq 1)$$

**Region II (tip radius)**

$$\begin{Bmatrix} x_r \\ y_r \end{Bmatrix} = \begin{Bmatrix} \ell_t / 2 + r_t \sin(\beta \Gamma) \\ A - r_t [1 - \cos(\beta \Gamma)] \end{Bmatrix}, \quad \begin{Bmatrix} n_x \\ n_y \end{Bmatrix} = \begin{Bmatrix} \sin(\beta \Gamma) \\ \cos(\beta \Gamma) \end{Bmatrix} \quad (0 < \beta \leq 1)$$

**Region III (tooth flank)**

$$\begin{Bmatrix} x_r \\ y_r \end{Bmatrix} = \begin{Bmatrix} (1 - \beta) [\ell_t / 2 + r_t \sin(\Gamma)] + \beta [\pi / (2D_p) - \ell_b / 2 - r_f \sin \Gamma] \\ (1 - \beta) [A - r_t \{1 - \cos(\Gamma)\}] + \beta [-B + r_f (1 - \cos \Gamma)] \end{Bmatrix}, \quad \begin{Bmatrix} n_x \\ n_y \end{Bmatrix} = \begin{Bmatrix} \cos \phi \\ \sin \phi \end{Bmatrix} \quad (0 < \beta \leq 1)$$

**Region IV (root fillet)**

$$\begin{Bmatrix} x_r \\ y_r \end{Bmatrix} = \begin{Bmatrix} \pi / (2D_p) - \ell_b / 2 - r_f \sin[(1 - \beta)\Gamma] \\ -B + r_f \{1 - \cos[(1 - \beta)\Gamma]\} \end{Bmatrix}, \quad \begin{Bmatrix} n_x \\ n_y \end{Bmatrix} = \begin{Bmatrix} \sin[(1 - \beta)\Gamma] \\ \cos[(1 - \beta)\Gamma] \end{Bmatrix} \quad (0 < \beta \leq 1)$$



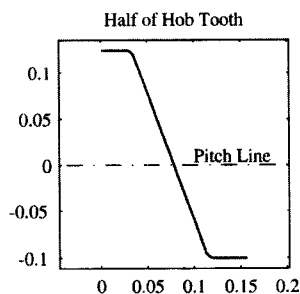
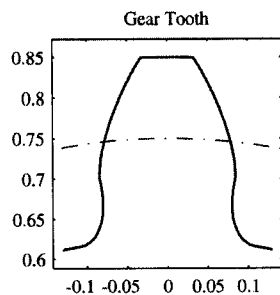
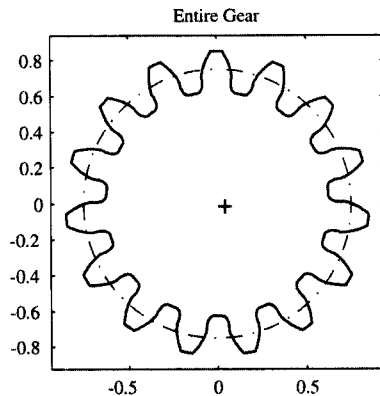
**Region V (bottom land)**

$$\begin{Bmatrix} x_r \\ y_r \end{Bmatrix} = \begin{Bmatrix} \pi/(2D_p) - \ell_b/2(1-\beta) \\ -B \end{Bmatrix}, \quad \begin{Bmatrix} n_x \\ n_y \end{Bmatrix} = \begin{Bmatrix} 0 \\ 1 \end{Bmatrix} \quad (0 < \beta \leq 1)$$

**EXAMPLE 10.6**  
**Generation**  
**of a Gear****Solution**

Assume that the rack in Example 10.5 is used to generate a gear. The pressure angle is  $20^\circ$  with a diametral pitch ( $D_p$ ) of 10 teeth per inch. The tip and root radii are both 0.01 in. The addendum constant for the rack is 1.25, and the dedendum constant is 1.1. There are 15 teeth on the gear, and the addendum constant for the gear is 1.0. Determine the shape of the gear tooth.

Because of the number of calculations required to solve the problem, it is efficient to program the equations given in Example 10.5. This was done using the program *geardr.m* given on the disk with this book. The hob profile (half of a tooth) is shown in Fig. 10.37, and the tooth and gear profiles are shown in Figs. 10.38 and 10.39. Notice that the gear is undercut.

**FIGURE 10.37** Profile of half of a hob tooth.**FIGURE 10.38** Generated gear tooth.**FIGURE 10.39** Profile of generated gear.

## REFERENCES

---

- <sup>1</sup>Dudley, D. W., *Handbook of Practical Gear Design*, McGraw-Hill, New York (1984).
- <sup>2</sup>American Gear Manufacturers' Association (AGMA), "Tooth Proportions for Coarse Pitch Involute Spur Gears," AGMA Publications 201.02 and 201.02A (1968).
- <sup>3</sup>Mabie, H. H. and F. W. Ocvirk, *Mechanisms and Dynamics of Machinery*, 3rd ed., John Wiley & Sons, New York (1975).
- <sup>4</sup>Shigley, J. E., *Kinematic Analysis of Mechanisms*, McGraw-Hill Book Co., New York (1975).
- <sup>5</sup>Kinzel, G. L., and D. M. Farley, "A Computer Approach to the Generation of Conjugate Tooth Forms," *Proceedings of the Sixth IFToMM Congress on Theory of Machines and Mechanisms*, New Delhi, December 15–20, pp. 778–782 (1983).
- <sup>6</sup>Mitchiner, R. G., and H. H. Mabie, "The Determination of the Lewis Form Factor and the AGMA Geometry Factor J for External Spur Gear Teeth," *Transactions of ASME*, Vol. 104, pp. 148–158 (January 1982).
- <sup>7</sup>Vijayakar, S., *Finite Element Methods for Quasi-Prismatic Bodies with Application to Gears*, Ph.D. dissertation, The Ohio State University (1987).

## PROBLEMS

---

- 10.1** Two spur gears have a diametral pitch of 6. Gear 2 has 24 teeth, and gear 3 has 48. The working pressure angle is  $20^\circ$ , and both gears are standard involutes. Determine the length of the contact line and the contact ratio.
- 10.2** For the gear pairs given below and meshing at their correct center-to-center distance, determine whether any interference is present and determine the contact ratio for each case. Assume that the addendum is  $1/P_d$  in each case, and if any interference is present, assume that the interference is removed by cutting off the ends of the gear teeth before determining the contact ratio.
- (a)  $14\frac{1}{2}^\circ$  involute gears having 30 and 45 teeth.
- (b)  $20^\circ$  involute gears having 20 teeth and a rack.
- (c)  $25^\circ$  involute gears having 30 and 60 teeth.
- 10.3** A  $20^\circ$  involute pinion having 30 teeth is meshing with a 60-tooth internal gear. The addendum of the pinion is  $1.25/P_d$ , and the addendum of the gear is  $1/P_d$ . Is there any interference? Determine the contact ratio. If there is interference, assume that the interfering portion is removed by cutting off the ends of the teeth.
- 10.4** What is the largest gear that will mesh with a  $20^\circ$  standard full-depth gear of 22 teeth with no interference?
- 10.5** What is the smallest gear that will mesh with a  $20^\circ$  standard full-depth gear of 22 teeth with no interference?
- 10.6** Assume a gear has a diametral pitch of 6. Determine the addendum, dedendum, and clearance if the pressure angle is  $20^\circ$  full depth,  $25^\circ$  full depth, and  $20^\circ$  with stub teeth.
- 10.7** Assume two meshing gears have a diametral pitch of 6 and a  $20^\circ$  pressure angle. The gear has 38 teeth, and the pinion has 24. Determine the design center distance. Now assume that the center distance is increased by 0.01 in. Determine the pressure angle for the new center distance.
- 10.8** Assume a standard full-depth rack has a diametral pitch of 2. Determine the smallest gear that will mesh with the rack without interference if the pressure angle is: (a)  $20^\circ$  or (b)  $25^\circ$ .
- 10.9** Assume two meshing gears have a diametral pitch of 8 and a  $25^\circ$  pressure angle. The gear has 60 teeth, and the pinion has 30. Determine the design center distance. Now assume that the center distance is increased by 0.012 in. Determine the pressure angle for the new center distance.
- 10.10** Two standard gears have a diametral pitch of 2 and a pressure angle of  $14\frac{1}{2}^\circ$ . The tooth numbers are 14 and 16. Determine whether interference occurs. If it does, compute the amount that the addendum(s) must be shortened to remove the interference and the new contact ratio.
- 10.11** Two standard gears have 18 and 32 teeth, respectively. The diametral pitch is 10, and the pinion rotates at 1000 rpm. Determine the following: (a) center distance, (b) pitch diameters, (c) circular pitch, (d) pitch line velocity, and (e) angular velocity of the gear.
- 10.12** Two standard gears have a diametral pitch of 10 and a velocity ratio of 2.5. The center distance is 3.5 in. Determine the number of teeth on each gear.
- 10.13** Is it possible to specify arbitrary values for the velocity ratio, center distance, and diametral pitch in a problem such as that given in Problem 10.12? Explain.
- 10.14** Two standard meshing gears are to have 9 and 36 teeth, respectively. They are to be cut with a  $20^\circ$  full-depth cutter with a diametral pitch of 3.
- (a) Determine the amount that the addendum of the gear is to be shortened to eliminate interference.
- (b) If the addendum of the pinion is increased the same amount, determine the new contact ratio.

**10.15** Two standard meshing gears are to have 13 and 20 teeth, respectively. They are to be cut with a  $20^\circ$  full-depth cutter with a diametral pitch of 2. To reduce interference, the center distance is increased by 0.1 in. Determine the following:

- (a) whether the interference is completely eliminated,
- (b) the pitch diameters of both gears,
- (c) the new pressure angle, and
- (d) the new contact ratio.

**10.16** Assume that you have a 13-tooth pinion and a 50-tooth gear. What is the smallest (nonstandard) pressure angle that can be used if interference is to be avoided? What is the smallest pressure angle that can be used if only standard pressure angles can be considered?

**10.17** A standard, full-depth spur gear has a pressure angle of  $25^\circ$  and an outside diameter of 225 mm. If the gear has 48 teeth, find the module and circular pitch.

**10.18** The pinion of a pair of spur gears has 16 teeth and a pressure angle of  $20^\circ$ . The velocity ratio is to be 3:2, and the module is 6.5 mm. Determine the initial center distance. If the center distance is increased by 3 mm, find the resulting pressure angle.

**10.19** Two standard, full-depth spur gears are to have 10 and 35 teeth, respectively. The cutter has a  $20^\circ$  pressure angle with a

module of 10 mm. Determine the amount by which the addendum of the gear must be reduced to avoid interference. Then determine the length of the new path of contact and the contact ratio.

**10.20** A standard, full-depth spur-gear tooth has been cut with a  $20^\circ$  hob and has a diametral pitch of 6. The tooth thickness at a radius of 2.1 in is 0.1860 in. Determine the thickness of the gear tooth at the base circle.

**10.21** A pair of standard, full-depth spur gears has been cut with a  $25^\circ$  hob. The pinion has 31 teeth and the gear 60 teeth. The diametral pitch is 4. Find the velocity ratio, the pitch circle radii, the outside diameters, the center distance, and the contact ratio.

**10.22** A pair of standard, full-depth spur gears has been cut with a  $25^\circ$  hob. The pinion has 14 teeth and the gear 51 teeth. The diametral pitch is 5. Find the velocity ratio, the pitch circle radii, the outside diameters, the center distance, and the contact ratio.

**10.23** A pair of standard, full-depth spur gears has been cut with a  $20^\circ$  hob. The pinion has 27 teeth and the gear 65 teeth. The diametral pitch is 2. Find the velocity ratio, the pitch circle radii, the outside diameters, the center distance, and the contact ratio.

---

# HELICAL, BEVEL, AND WORM GEARS

---

## 11.1 HELICAL GEARS

---

Helical gears have the same involute tooth form as spur gears but are cut with the teeth inclined to the gear axes so that the intersections of tooth faces with cylindrical surfaces about the gear axis are helices. This produces a progressive contact action with contact beginning at a point at one end of the tooth, enlarging progressively to an inclined line across the tooth face, and then diminishing progressively to a point at the other end of the tooth. This progressive action carries important benefits in reductions of gear noise and vibration. Because of the gradual load transfer and longer teeth, helical gears will also have a higher load rating for a given size gear than spur gears. Another advantage of helical gears is that the gear axes do not need to be parallel. Because of these advantages, helical gears are almost always used in high-speed transmissions where noise and high power are issues. Examples of helical gears are shown in Figs. 11.1–11.4.

The helical tooth geometry results in a reaction thrust component along the shaft axis, which therefore requires a thrust bearing. For this reason, gears are sometimes cut with two sets of helical teeth with opposite pitch. The resulting chevron-shaped teeth lead to the name “herringbone gears” for this type. Herringbone gears do not have an axial reaction thrust component.

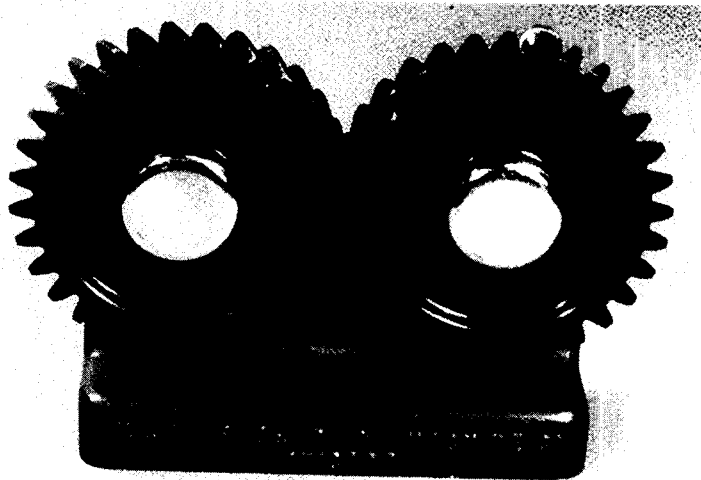
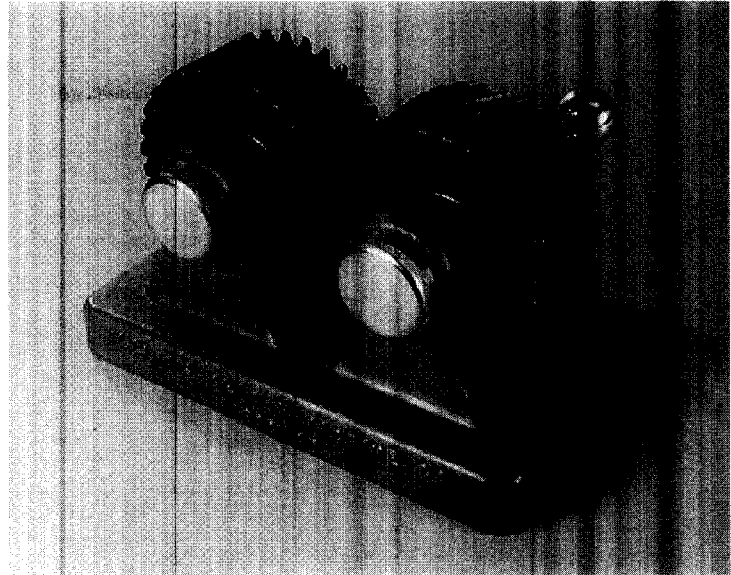
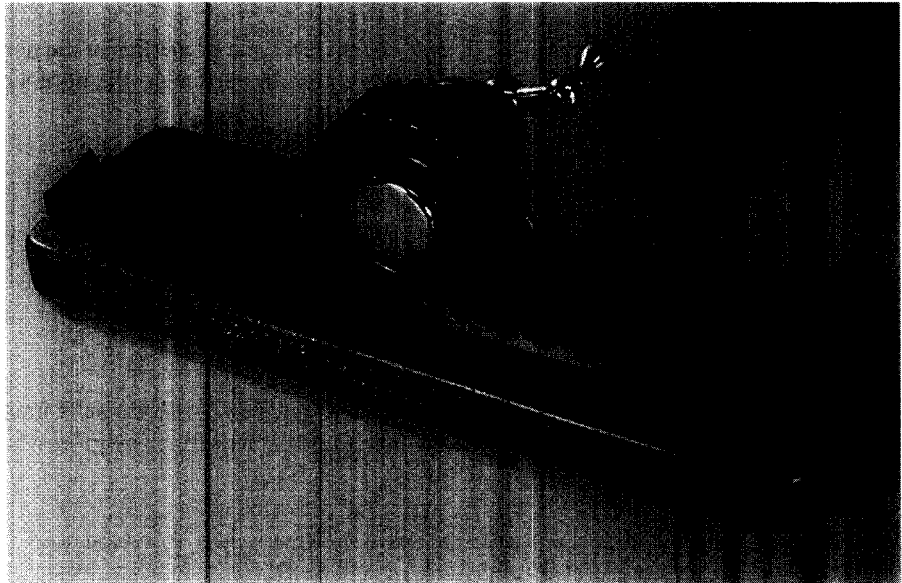


FIGURE 11.1 Helical gears.



**FIGURE 11.2** Herringbone gears.



**FIGURE 11.3** Helical rack and pinion.

### 11.1.1 Helical Gear Terminology

As indicated in Fig. 11.5, the terminology for helical gears is defined in two planes, the transverse plane and the normal plane. The transverse plane is viewed along the axis of the gear shaft, and the normal plane is viewed along the tooth of the gear. The rotation of the gear is in the transverse plane; however, the gear is manufactured by a cutting action along the normal plane.

Three pitches must be considered when evaluating the geometry of helical gears. These are the normal pitch, the transverse pitch, and the axial pitch.



FIGURE 11.4 Crossed helical gears.

When a helical gear is generated, the properties in the normal plane will correspond to those of the hob or shaper cutter. In particular, the normal pitch,  $p_n$ , is related to the normal diametral pitch,  $P_n$ , by

$$p_n = \frac{\pi}{P_n} \tag{11.1}$$

and both  $p_n$  and  $P_n$  are the same as those for the cutter if the gear is cut with a hob. The normal pitch is usually the one specified in gear catalogs.

Also, from Fig. 11.5,

$$p_n = p_t \cos \psi \tag{11.2}$$

where  $p_t$  is the transverse circular pitch and  $\psi$  is the helix angle. The transverse circular pitch is the distance from tooth to tooth on the pitch cylinder when observed from the trans-

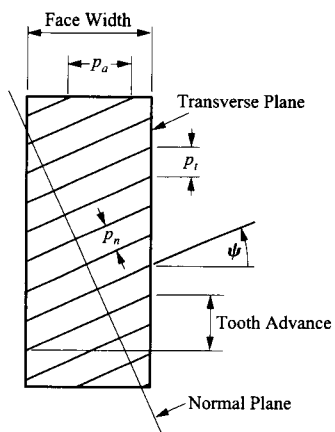


FIGURE 11.5 End view of helical gear showing normal and transverse planes.  $\psi$  is the helix angle, the angle at which the teeth are inclined to the axis of the gear;  $p_n$  is the circular pitch normal to the tooth face;  $p_t$  is the transverse circular pitch in a plane normal to the gear axis.

verse plane. The transverse circular pitch is related to the transverse diametral pitch through an equation similar to Eq. (11.1). That is,

$$p_t = \frac{\pi}{P_t} \quad (11.3)$$

and

$$P_t = \frac{N}{d_t} \quad (11.4)$$

where  $p_t$  is the transverse diametral pitch and  $d_t$  is the diameter of the pitch cylinder. From Eqs. (11.1)–(11.4),

$$\frac{\pi}{P_n} = \frac{\pi}{P_t} \cos \psi$$

or

$$P_t = P_n \cos \psi \quad (11.5)$$

The transverse diametral pitch has the traditional meaning of being the number of teeth per inch of pitch diameter in the transverse plane. However, the normal diametral pitch is less obvious. We can still think of  $P_n$  as the number of teeth per pitch diameter if the gear were a spur gear with a pitch diameter equal to the transverse pitch diameter. Obviously, the helical gear appears as an ellipse when viewed from the normal plane; however, the circular approximation is useful when considering the local geometry in the vicinity of an individual tooth.

In the metric system, the module,  $m_t$ , is used, and

$$m_t = \frac{d_t}{N} = \frac{m_n}{\cos \psi}$$

where  $m_n$  is the module for the hob. Comparing Eqs. (11.1)–(11.5), we see that the metric system and the conventional system used in the United States are related by

$$m_t = \frac{1}{P_t} \quad \text{and} \quad m_n = \frac{1}{P_n}$$

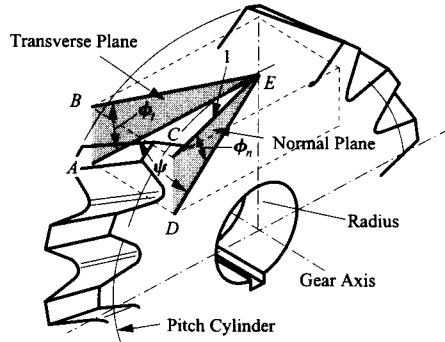
and

$$p_t = \pi m_t \quad \text{and} \quad p_n = \pi m_n$$

The third pitch is the axial pitch,  $p_a$ , which is analogous to the pitch of a screw. This is the distance from a point on one tooth to the corresponding point on an adjacent tooth measured at the pitch cylinder and in the direction of the rotation axis. The axial pitch is related to the other pitches by

$$p_a = \frac{p_t}{\tan \psi} = \frac{p_n}{\sin \psi} \quad (11.6)$$

There are two pressure angles for helical gears, one for each of the two principal planes, and the relationship among the pressure angles and the helix angle is shown in Fig. 11.6. The transverse pressure angle,  $\phi_t$ , is measured in the transverse plane, and the normal pressure angle,  $\phi_n$ , is measured in the normal plane.



**FIGURE 11.6** Relationship among normal and transverse pressure angles and helix angle.

Because helical gears are usually cut with the same hob cutters as spur gears, the normal diametral pitch and pressure angle usually have standard spur gear values, but the transverse diametral pitch and pressure angle do not. Since the transverse diametral pitch and pressure angle determine the kinematic characteristics of the gear pair, it is important to be able to obtain them from the corresponding normal values and the helix angle. Conversely, the tooth stiffness and strength are determined by the thickness in the normal plane. Thus, this is the plane used when analyzing tooth stresses.

The relationship among  $\phi_t$ ,  $\phi_n$ , and  $\psi$  can be determined by looking at the lines  $AE$ ,  $BE$ ,  $CE$ , and  $DE$  in Fig. 11.6. Assume that line  $CE$  is 1 unit long and normal to the gear tooth at the pitch cylinder. Triangle  $CED$  is in the normal plane,  $BEA$  is in the transverse plane,  $AED$  is in the plane tangent to the pitch circle at point  $E$ , and  $BACD$  is a rectangle.

Then  $DE$  is the projection of  $CE$  in the tangent plane,  $BE$  is the projection of  $CE$  in the transverse plane, and  $AE$  is the projection of  $BE$  in the tangent plane. From simple geometry,

$$AB = CD$$

Also,

$$DE = \cos \phi_n$$

$$CD = \sin \phi_n$$

$$AE = DE \cos \psi = \cos \phi_n \cos \psi$$

$$AB = AE \tan \phi_t = \cos \phi_n \cos \psi \tan \phi_t$$

And because  $AB=CD$ ,

$$\sin \phi_n = \cos \phi_n \cos \psi \tan \phi_t$$

or

$$\tan \phi_t = \frac{\tan \phi_n}{\cos \psi}$$

(11.7)



### 11.1.2 Helical Gear Manufacturing

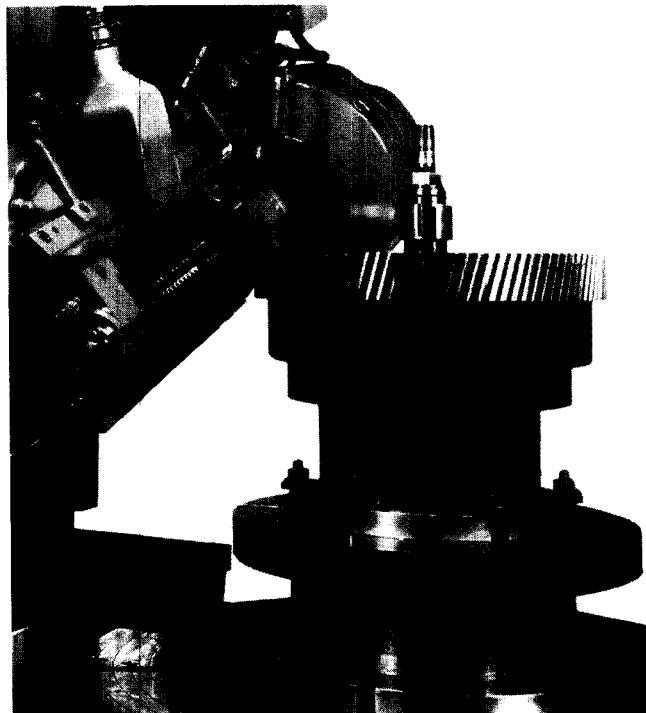
As was the case for spur gears, the vast majority of helical gears are manufactured by hobbing (Fig. 11.7) or shaping (Fig. 11.8). When gears are hobbled, the hob axis is inclined at an angle equal to the gear helix angle relative to the gear rotation axis. The hob properties correspond to the gear properties in the normal plane. Therefore, the normal diametral pitch ( $P_n$ ) of the gear is equal to the diametral pitch ( $P_d$ ) of the hob. The same hob can be used to cut both spur and helical gears.

If the gear is an internal gear, if it has a shoulder, or if it is a herringbone gear (Fig. 11.2), the gear cannot be hobbled. Such gears are normally fabricated by shaping. The shaper axis is parallel to the gear rotation axis. Therefore, the shaper properties correspond to the transverse plane. The transverse circular pitch of the gear is equal to the transverse circular pitch of the shaper cutter, so that Eqs. (11.3) and (11.4) apply to both the cutter and gear. When the gear is shaped, the same cutter cannot be used for both helical and spur gears.

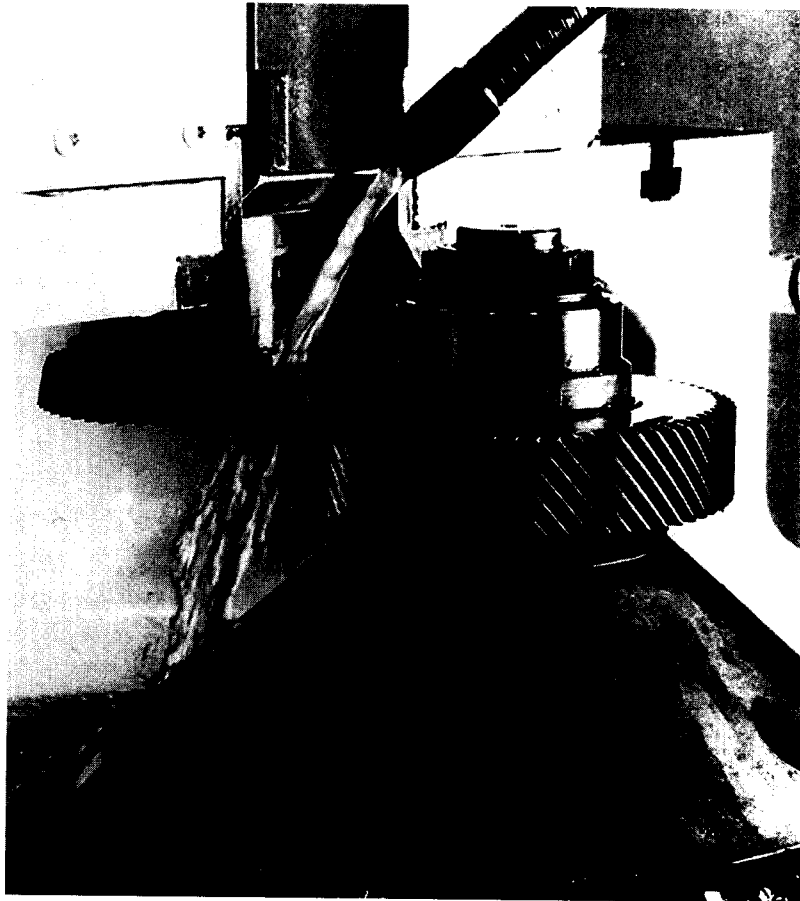
### 11.1.3 Minimum Tooth Number to Avoid Undercutting

One of the advantages of helical gears is that they can have fewer teeth on the pinion than can the corresponding spur gear and still avoid undercutting. The minimum number of teeth to avoid undercutting is given by using Fig. 10.28 and Eq. (10.25) in Chapter 10, where all quantities are for the transverse plane. Then,

$$r_p = \frac{a}{\sin^2 \phi_t} \quad (11.8)$$



**FIGURE 11.7** Hobbing a helical gear. (Courtesy of Bourns & Koch.)



**FIGURE 11.8** Shaping a helical gear. (Courtesy of Fellows Corp., Springfield, Vermont.)

where  $a$  is the addendum for the cutter used to form the gear. The cutter properties are associated with the *normal* plane. Therefore,

$$a = \frac{k}{P_n}$$

and Eq. (11.8) can be rewritten as

$$r_p = \frac{k}{P_n \sin^2 \phi_t}$$

The pitch radius ( $r_p$ ) is related to the number of teeth ( $N$ ) and transverse diametral pitch ( $P_t$ ) by

$$r_p = \frac{N}{2P_t} \quad (11.9)$$

Therefore,

$$\frac{N}{2P_t} = \frac{k}{P_n \sin^2 \phi_t}$$

Using Eq. (11.5) and simplifying gives the minimum number of teeth to avoid undercutting as

$$N = \frac{2kP_t}{P_n \sin^2 \phi_t} = \frac{2k \cos \psi}{\sin^2 \phi_t} \quad (11.10)$$

Values for  $N$  as a function of helix angle and *normal* pressure angle are given in Table 11.1 for standard full-depth ( $k = 1$ ) gears cut with a hob. The values were computed by first solving Eq. (11.7) for  $\phi_t$  for selected values of  $\psi$  and  $\phi_n$  and then substituting the results into Eq. (11.10). Notice that for very large helix angles, the number of teeth on the gear can be reduced to one. This is the case that exists with worm gears, which will be discussed later in this chapter. The helix angle for helical gears is usually limited to  $45^\circ$ .

Unlike spur gears, two helical gears can be meshed with either parallel shafts or crossed shafts. The properties in Eqs. (11.1)–(11.10) apply to individual helical gears regardless of the axis orientation of the meshing gear.

#### 11.1.4 Helical Gears with Parallel Shafts

Two parallel-shaft gears will mesh if the following conditions are satisfied:

1. Both gears have equal pitches.
2. Both gears have equal helix angles.
3. The helix angles on the two gears are opposite hand. This means that one helix is left handed and the other is right handed (see Fig. 11.9).

**TABLE 11.1 Minimum Tooth Numbers as a Function of the Helix Angle for Standard Values of the Normal Pitch**

$\psi$	$\phi_n$ (degrees)		
	$14\frac{1}{2}^\circ$	$20^\circ$	$25^\circ$
$0^\circ$ (spur gear)	32	18	12
$5^\circ$	32	17	12
$10^\circ$	31	17	11
$15^\circ$	29	16	11
$20^\circ$	27	15	10
$25^\circ$	25	14	9
$30^\circ$	22	12	8
$35^\circ$	19	10	7
$40^\circ$	15	9	6
$45^\circ$	12	7	5
$50^\circ$	10	6	4
$55^\circ$	7	4	3
$60^\circ$	5	3	3
$65^\circ$	4	2	2
$70^\circ$	2	2	2
$75^\circ$	2	1	1
$80^\circ$	1	1	1

**Velocity Ratio and Center Distance** The expressions for the angular velocity ratio and the center distance for two parallel-shaft helical gears are the same as the corresponding expressions for spur gears. The velocity ratio is given by

$$\frac{\omega_2}{\omega_3} = \frac{r_{p_3}}{r_{p_2}} = \frac{d_{t_3}}{d_{t_2}} = \frac{N_3/P_t}{N_2/P_t} = \frac{N_3}{N_2} \quad (11.11)$$

where  $\omega_2$ ,  $r_{p_2}$ ,  $d_{t_2}$ , and  $N_2$  are the angular velocity magnitude, pitch radius, pitch diameter, and number of teeth, respectively, on gear 2. The corresponding values are for gear 3. The center distance is given by

$$C = r_{p_2} + r_{p_3} = \frac{d_{t_2} + d_{t_3}}{2} \quad (11.12)$$

or in terms of the pitches,

$$C = \frac{N_2 + N_3}{2P_t} = \frac{N_2 + N_3}{2P_n \cos \psi} \quad (11.13)$$

**Minimum Face Width** The maximum face width of a pair of spur gears is limited by the accuracy of alignment; however, the minimum face width can be much smaller than the circular pitch. Helical gears are much more expensive to produce than spur gears, and therefore, from practical considerations, the face width must be large to achieve the stated benefits compared with spur gears. In general, the face width ( $F$ ) should be larger than the axial pitch ( $p_a$ ), and the AGMA<sup>1</sup> recommends that the face width be at least 15% larger than the axial pitch. Typically, the face width is at least two times the axial pitch.<sup>2</sup> The axial pitch is given by Eq. (11.6). Therefore the limiting condition for the face width is

$$F \geq \frac{1.15p_t}{\tan \psi} \quad (11.14)$$

or

$$F \geq \frac{1.15p_n}{\sin \psi} \quad (11.15)$$

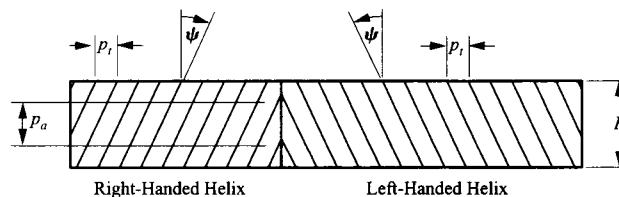


FIGURE 11.9 Conditions for two helical gears to mesh.

**Contact Ratio** Mating spur gears make contact on a line that is parallel to the axis of rotation, as shown in Fig. 11.10. Helical gear teeth make contact on a line that is diagonal across the gear teeth as shown in Fig 11.11. Contact between the two teeth begins at  $A$ , and as the gears mesh the contact moves diagonally across the gear tooth. When contact is being lost at  $B$  on one side of the tooth, it is just beginning at  $C$  on the other side. This gradual contact is one of the benefits of helical gears.

The contact ratio of helical gears is increased over that of equivalent spur gears by the axial overlap of the teeth. Therefore, the contact ratio ( $m_c$ ) is the sum of the transverse contact ( $m_{c_t}$ ) ratio and the axial or face contact ratio ( $m_{c_a}$ ). The transverse contact ratio is computed in the same manner as for spur gears. Therefore, the transverse contact ratio is given as

$$m_{c_t} = \frac{p_t \lambda}{\pi \cos \phi_t} \quad (11.16)$$

where

$$\lambda = \sum_{i=2}^3 \left\{ -r_{p_i} \sin \phi_t + \sqrt{a_i^2 + 2a_i r_{p_i} + r_{p_i}^2 \sin^2 \phi_t} \right\}$$

The axial contact ratio is the ratio of the face width of the gear to the axial pitch. This is

$$m_{c_a} = \frac{F}{p_a} = \frac{F \tan \psi}{p_t} \quad (11.17)$$

Notice that the transverse contact ratio is not defined for a single gear; however, the axial contact ratio depends on the properties of a single gear. The normal and tangential pitches will be the same for both gears. If the face widths are different, the face width of the narrower gear is used in Eq. (11.17).

The total contact ratio is

$$m_c = m_{c_t} + m_{c_a} \quad (11.18)$$

As in the case of spur gears,  $m_c$  gives the average number of teeth in contact during the gear action. The contact ratio for helical gears is always higher than for comparable spur gears.

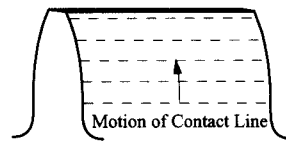


FIGURE 11.10 Contact lines for spur gear.

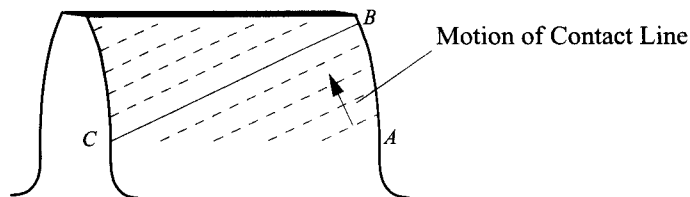


FIGURE 11.11 Contact lines for helical gear.

**EXAMPLE 11.1**
**Helical Gear  
Geometry**

A pair of helical gears with 19 and 34 teeth, respectively, and a 30° helix angle are cut with a standard spur gear hob that has a diametral pitch of 4 and a pressure angle of 20°. Find the transverse diametral pitch, the pitch cylinder radii, and the axial, transverse, and total contact ratios. The face width is 12 in.

**Solution**

The properties of the gears in the normal direction will be the same as those of the hob. The transverse diametral pitch ( $P_t$ ) for both gears is related to the normal diametral pitch by Eq. (11.5). Based on the diametral pitch of the hob,

$$P_t = P_n \cos \psi = 4 \cos 30^\circ = 3.464$$

The pitch cylinder diameters are related to the diametral pitch through Eq. (11.4). Therefore,

$$d_t = \frac{N_t}{P_t}$$

and

$$r_{t_2} = \frac{N_2}{2P_t} = \frac{19}{2(3.464)} = 2.742 \text{ in}$$

and

$$r_{t_3} = \frac{N_3}{2P_t} = \frac{34}{2(3.464)} = 4.908 \text{ in}$$

The transverse contact ratio is given by Eq. (11.16) as

$$m_{c_t} = \frac{p_t \lambda}{\pi \cos \phi_t}$$

where

$$\lambda = \sum_{i=2}^3 \left\{ -r_{p_i} \sin \phi_t + \sqrt{a_i^2 + 2a_i r_{p_i} + r_{p_i}^2 \sin^2 \phi_t} \right\}$$

The addenda are determined by the hob. Because a standard hob is used, both addenda are given by

$$a = \frac{1}{P_n} = \frac{1}{4} = 0.25 \text{ in}$$

The transverse circular pitch is given by Eq. (11.3) as

$$p_t = \frac{\pi}{P_t} = \frac{\pi}{3.464} = 0.907$$

and the transverse pressure angle is given by Eq. (11.7) as

$$\phi_t = \tan^{-1} \left( \frac{\tan \phi_n}{\cos \psi} \right) = \tan^{-1} \left( \frac{\tan 20^\circ}{\cos 30^\circ} \right) = 22.796^\circ$$

Now,

$$\begin{aligned} \lambda &= -r_{p_2} \sin \phi_t + \sqrt{a_2^2 + 2a_2 r_{p_2} + r_{p_2}^2 \sin^2 \phi_t} - r_{p_3} \sin \phi_t + \sqrt{a_3^2 + 2a_3 r_{p_3} + r_{p_3}^2 \sin^2 \phi_t} \\ &= -2.742 \sin 22.796^\circ + \sqrt{(0.25)^2 + 2(0.25)(2.742) + [2.742 \sin 22.796^\circ]^2} \\ &\quad - 4.908 \sin 22.796^\circ + \sqrt{(0.25)^2 + 2(0.25)(4.908) + [4.908 \sin 22.796^\circ]^2} = 1.1131 \end{aligned}$$

Therefore, the transverse contact ratio is

$$m_{c_t} = \frac{p_t \lambda}{\pi \cos \phi_t} = \frac{0.907(1.1131)}{\pi \cos 22.796^\circ} = 0.3486$$

The axial contact ratio is given by Eq. (11.17) as

$$m_{c_a} = \frac{F \tan \psi}{p_t} = \frac{12 \tan 30^\circ}{0.907} = 7.6394$$

The total contact ratio is

$$m_c = m_{c_t} + m_{c_a} = 0.3486 + 7.6394 = 7.99$$

Therefore, an average of approximately 8 teeth will be in contact as the gears mesh.

### EXAMPLE 11.2 Helical Gear Replacement of Spur Gears

#### Solution

Sometimes it is desirable to replace an existing set of spur gears to eliminate a noise problem or to increase the capacity of a gear box. Assume the original spur gears are 14 pitch, 20° full depth gears with 30 and 85 teeth. These are to be replaced by a set of helical gears without any major modifications to the gearbox. The size and angular velocity ratio are to remain the same. Determine the helix angle, outside diameters of the blanks, and the face width of the replacement gears. The new helical gears can be cut with the same hob as was used for the spur gears.

If there are to be no major modifications to the gearbox, the center distance must remain the same. The original pitch radii are given by

$$r_{p_2} = \frac{N_2}{2P_d} = \frac{30}{2(14)} = 1.071 \text{ in}$$

and

$$r_{p_3} = \frac{N_3}{2P_d} = \frac{85}{2(14)} = 3.036 \text{ in}$$

and the center distance is

$$C = r_{p_2} + r_{p_3} = \frac{N_2 + N_3}{2P_d} = \frac{30 + 85}{2(14)} = 4.286 \text{ in}$$

The velocity ratio is also to remain constant. The original velocity ratio was

$$\frac{\omega_2}{\omega_3} = \frac{N_3}{N_2} = \frac{85}{30} = \frac{17}{6} \quad (11.19)$$

For the helical gears, we need to determine the helix angle and the number of teeth on each gear. We will find the number of teeth and transverse diametral pitch first and then determine the helix angle. The velocity ratio is given by Eq. (11.11) as

$$\frac{\omega_2}{\omega_3} = \frac{r_{p_3}}{r_{p_2}} = \frac{d_{t_3}}{d_{t_2}} = \frac{N_3/P_t}{N_2/P_t} = \frac{N_3}{N_2}$$

and the center distance is given by Eq. (11.12) as

$$C = r_{p_2} + r_{p_3} = \frac{d_{t_2} + d_{t_3}}{2}$$

From these two equations, it is clear that the pitch radii for the helical gears must be the same as the corresponding radii for the spur gears. However, the tooth numbers can and will be different. The transverse diametral pitch is related to the normal diametral pitch by

$$P_t = P_n \cos \psi \tag{11.5}$$

and to the teeth numbers by

$$P_t = \frac{N_2}{2r_{p_2}} = \frac{N_3}{2r_{p_3}} \tag{11.20}$$

From Eq. (11.5), it is clear that  $P_t < P_n$ . Therefore, based on Eq. (11.20), the tooth numbers on the helical gears must be less than those on the spur gears. As a result, when we investigate tooth numbers that satisfy Eq. (11.19), we need only consider values that are lower than the corresponding values for the spur gears. A set of values is as follows:

$N_2$	$N_3 = \frac{17}{6} N_2$
30	85 (spur gear)
29	82.167
28	79.333
27	76.500
26	73.667
25	70.833
24	68

From the table, the first set of teeth numbers that are integers are  $N_2 = 24$  and  $N_3 = 68$ . For these numbers, the transverse pitch is given by Eq. (11.20) as

$$P_t = \frac{N_2}{2r_{p_2}} = \frac{N_3}{2r_{p_3}} = \frac{24}{2(1.071)} = \frac{68}{2(3.036)} = 11.199$$

From Eq. (11.5),

$$\psi = \cos^{-1} \left( \frac{P_t}{P_n} \right) = \cos^{-1} \left( \frac{11.199}{14} \right) = 36.877^\circ$$

Notice that this is the lowest helix angle possible (other than  $0^\circ$ ) if the center distance and velocity ratio are to be maintained. The blank diameters of the two gears are given by

$$D_{o_2} = 2r_{p_2} + 2a_2 = 2r_{p_2} + 2 \frac{k}{P_n} = 2(1.071) + 2 \frac{1}{14} = 2.286 \text{ in}$$

and

$$D_{o_3} = 2r_{p_3} + 2a_3 = 2r_{p_3} + 2 \frac{k}{P_n} = 2(3.036) + 2 \frac{1}{14} = 6.214 \text{ in}$$



The minimum face width is given by Eq. (11.14) as

$$F \geq \frac{1.15P_t}{\tan\psi} \quad \text{or} \quad F \geq \frac{1.15\pi}{P_t \tan\psi}$$

Therefore,

$$F \geq \frac{1.15\pi}{11.199 \tan 36.877^\circ} \quad \text{or} \quad F > 0.430$$

Use  $F = \frac{7}{16}$  in.

**Designing for Axial Force** When spur gears transmit power, the force between the gears lies entirely in the transverse plane. However, when helical gears mesh, there will be an axial force component because of the helix angle. This axial load must be considered when designing the shaft bearings. If the load is too large to be carried by the bearings, two helical gears of opposite hand can be used instead of a single gear. Alternatively, and more commonly, a herringbone gear (Fig. 11.2) can be used. A herringbone gear is in essence two helical gears of opposite hand cut on the same gear blank.

A summary of the equations specific to parallel-shaft helical gears is given in Table 11.2. Most of the equations in Table 10.4 apply to helical gears if the transverse plane is used. Therefore, most of the equations in Table 10.4 have not been repeated in Table 11.2.

### 11.1.5 Crossed Helical Gears

Helical gears need not be used on parallel shafts but can be used to transfer power between nonparallel, nonintersecting shafts (Fig. 11.4). When the shafts are not parallel, the gears are called crossed helical gears.

The only requirement for crossed helical gears to mesh properly is that they have the same normal pitch. The transverse pitches need not be the same, and the helix angles need not be the same. The helix angles can be of the same or opposite hand.

The velocity ratio for crossed helical gears can be developed from Eq. (11.11) as

$$R = \frac{\omega_2}{\omega_3} = \frac{N_3}{N_2} = \frac{d_{t_3} P_{t_3}}{d_{t_2} P_{t_2}} = \frac{d_{t_3} P_n \cos \psi_3}{d_{t_2} P_n \cos \psi_2} = \frac{d_{t_3} \cos \psi_3}{d_{t_2} \cos \psi_2} \quad (11.21)$$

**TABLE 11.2 Summary of Helical Gear Formulas (Parallel Shafts)**

Quantity	Formula
Transverse diametral pitch	$P_t = \frac{N}{d_t} = \frac{N}{2r_t} = \frac{\pi}{p_t} = P_n \cos \psi = \frac{1}{m_t} = \frac{\cos \psi}{m_n}$
Transverse circular pitch	$p_t = \frac{\pi}{P_t} = \frac{\pi d_t}{N} = \pi m_t = \frac{P_n}{\cos \psi} = p_a \tan \psi$
Normal diametral pitch	$P_n = \frac{P_t}{\cos \psi} = \frac{N}{2r_p \cos \psi} = \frac{\pi}{p_n} = \frac{1}{m_n} = \frac{1}{m_t \cos \psi}$

(continued)

TABLE 11.2 continued

Quantity	Formula
Normal circular pitch	$p_n = \frac{\pi}{P_n} = \pi m_n = p_t \cos \psi = p_a \sin \psi$
Axial pitch	$p_a = \frac{p_t}{\tan \psi} = \frac{p_n}{\sin \psi}$
Pitch cylinder diameter	$d_t = \frac{N}{P_t} = \frac{N}{P_n \cos \psi} = \frac{N p_t}{\pi} = \frac{N p_n}{\pi \cos \psi} = N m_t$
Center distance	$C = r_{p_2} + r_{p_3} = \frac{d_{t_2} + d_{t_3}}{2} = \frac{N_2 + N_3}{2 P_t}$ $= \frac{p_t (N_2 + N_3)}{2 \pi} = \frac{N_2 + N_3}{2 P_n \cos \psi}$
Velocity ratio	$R = \frac{\omega_2}{\omega_3} = \frac{r_{p_3}}{r_{p_2}} = \frac{d_{t_3}}{d_{t_2}} = \frac{N_3}{N_2}$
Minimum face width	$F \geq \frac{1.15 p_t}{\tan \psi} \quad \text{or} \quad F \geq \frac{1.15 \pi}{P_t \tan \psi}$
Number of teeth at undercutting	$N = \frac{2 a P_t}{\sin^2 \phi_t} = \frac{2 k P_t}{P_n \sin^2 \phi_t} = \frac{2 k \cos \psi}{\sin^2 \phi_t}$ $(k = 1 \text{ for full depth or } 0.8 \text{ for stub tooth})$
Length of line of contact	$\lambda = -r_{p_2} \sin \phi_t + \sqrt{a_2^2 + 2 a_2 r_{p_2} + r_{p_2}^2 \sin^2 \phi_t}$ $-r_{p_3} \sin \phi_t + \sqrt{a_3^2 + 2 a_3 r_{p_3} + r_{p_3}^2 \sin^2 \phi_t}$
Transverse contact ratio	$m_{c_t} = \frac{\lambda}{p_t \cos \phi_t} = \frac{\lambda P_t}{\pi \cos \phi_t}$
Axial contact ratio	$m_{c_a} = \frac{F}{p_a} = \frac{F \tan \psi}{p_t}$
Total contact ratio	$m_c = m_{c_t} + m_{c_a}$
Transverse pressure angle	$\tan \phi_t = \frac{\tan \phi_n}{\cos \psi}$

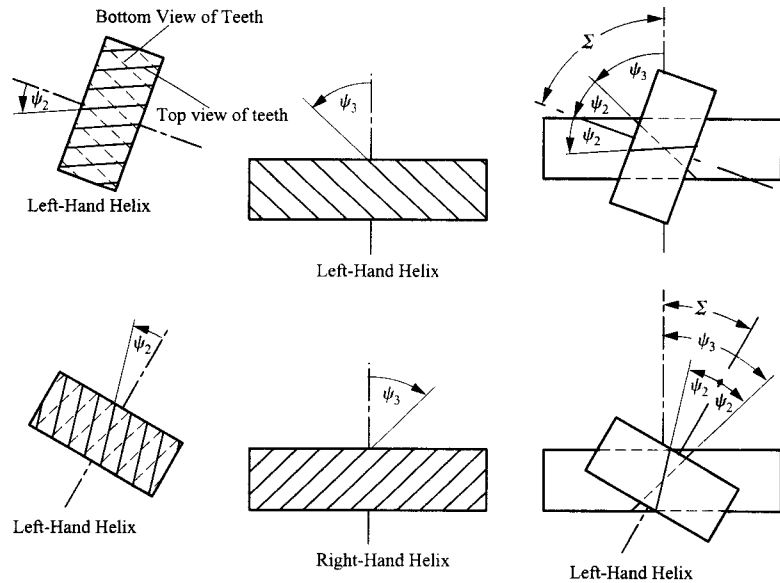


FIGURE 11.12 Relationship among shaft angle and helix angles for crossed helical gears.

If the angle between the shafts of the meshing crossed helical gears is  $\Sigma$  and the helix angles are  $\psi_2$  and  $\psi_3$ , the relationship among the three angles is

$$\Sigma = \psi_2 \pm \psi_3 \quad (11.22)$$

where the plus sign applies if the gears are of the same hand, and the minus sign applies if the gears are of the opposite hand. This is shown in Fig. 11.12.

The center distance in the U.S. system between crossed helical gears is given by

$$C = r_{p_2} + r_{p_3} = \frac{N_2}{2P_{t_2}} + \frac{N_3}{2P_{t_3}} = \frac{N_2}{2P_n \cos \psi_2} + \frac{N_3}{2P_n \cos \psi_3} = \frac{1}{2P_n} \left[ \frac{N_2}{\cos \psi_2} + \frac{N_3}{\cos \psi_3} \right] \quad (11.23)$$

and recalling that

$$m_n = \frac{1}{P_n}$$

we can write the center distance in the metric system as

$$C = r_{p_2} + r_{p_3} = \frac{N_2}{2P_{t_2}} + \frac{N_3}{2P_{t_3}} = \frac{N_2 m_n}{2 \cos \psi_2} + \frac{N_3 m_n}{2 \cos \psi_3} = \frac{m_n}{2} \left[ \frac{N_2}{\cos \psi_2} + \frac{N_3}{\cos \psi_3} \right] \quad (11.24)$$

This equation applies regardless of the hand of the gears.

Crossed helical gears are not used to transmit large amounts of power because the gears theoretically have only point contact where the teeth mesh. This is in contrast to parallel-shaft helical gears, which have line contact. For large power transfers between non-parallel shafts, bevel or hypoid gear sets are preferred. Worm gear sets can also be used when high velocity ratios are required.

**EXAMPLE 11.3****Crossed Helical Gear Geometry**

Assume that two crossed helical gears have a shaft angle of  $65^\circ$  and a velocity ratio of 2:1. The pinion (gear 2) has a normal diametral pitch of 10, a helix angle of  $30^\circ$ , and 70 teeth. Determine the helix angle, pitch diameter, and number of teeth on the meshing gears. Also find the center distance. Both gears are right handed, and both are cut with the same hob.

**Solution**

First find the pitch diameter for gear 2 using

$$d_{p_2} = \frac{N_2}{P_{t_2}} = \frac{N_2}{P_n \cos \psi_2} = \frac{70}{10 \cos 30^\circ} = 8.083 \text{ in}$$

From the expression for the velocity ratio, the number of teeth on gear 3 is

$$N_3 = N_2 \frac{\omega_2}{\omega_3} = 70 \frac{2}{1} = 140$$

Next find the helix angle of the second gear, using Eq. (11.22) with a plus sign. Then,

$$\Sigma = \psi_2 + \psi_3$$

where  $\Sigma = 65^\circ$  and  $\psi_2 = 30^\circ$ . Solving gives  $\psi_3 = 35^\circ$ .

The pitch diameter for gear 3 is then given by

$$d_{t_3} = \frac{N_3}{P_n \cos \psi_3} = \frac{140}{10 \cos 35^\circ} = 17.091 \text{ in}$$

The center distance is given by

$$C = \frac{d_{t_2} + d_{t_3}}{2} = \frac{8.083 + 17.091}{2} = 12.587 \text{ in}$$

A summary of the equations specific to crossed helical gears is given in Table 11.3.

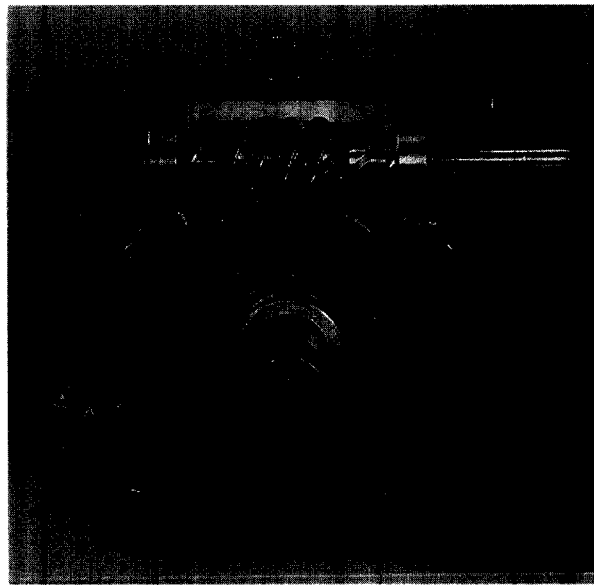
**TABLE 11.3 Summary of Crossed Helical Gear Formulas**

Quantity	Formula
Shaft angle	$\Sigma = \psi_2 \pm \psi_3$
Pitch cylinder diameter	$d_t = \frac{N}{P_t} = \frac{N}{P_n \cos \psi} = \frac{Np_t}{\pi} = \frac{Np_n}{\pi \cos \psi} = Nm_t$
Center distance	$C = \frac{d_{t_2} + d_{t_3}}{2} = \frac{N_2}{2P_{t_2}} + \frac{N_3}{2P_{t_3}} = \frac{1}{2P_n} \left[ \frac{N_2}{\cos \psi_2} + \frac{N_3}{\cos \psi_3} \right]$ $= \frac{m_n}{2} \left[ \frac{N_2}{\cos \psi_2} + \frac{N_3}{\cos \psi_3} \right]$
Velocity ratio	$R = \frac{\omega_2}{\omega_3} = \frac{N_3}{N_2} = \frac{d_{t_3} P_{t_3}}{d_{t_2} P_{t_2}} = \frac{d_{t_3} P_n \cos \psi_3}{d_{t_2} P_n \cos \psi_2} = \frac{d_{t_3} \cos \psi_3}{d_{t_2} \cos \psi_2}$

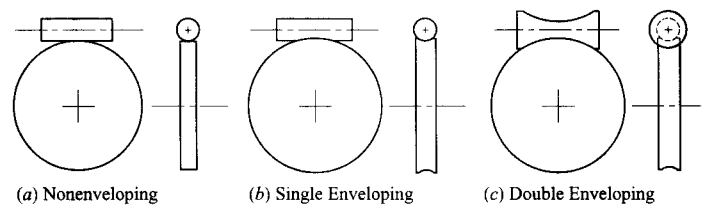
## 11.2 WORM GEARS

If the tooth of a helical gear makes a complete revolution on the pitch cylinder, the resulting gear is called a *worm*. This occurs when the helix angle and the gear face width are relatively large. In worms, the helix angle can exceed  $80^\circ$ . The mating gear is called a *worm gear* or *worm wheel*. Worm gear sets are used to connect nonintersecting shafts (usually at  $90^\circ$ ) when the desired velocity reduction is large. A worm gear set is shown in Fig. 11.13.

Involute worms can be meshed with either spur or helical gears; however, point contact occurs and only relatively small forces can be transmitted. Usually, the worm gear set is cut so that the gear partially envelops the worm. The design can be nonenveloping, single enveloping, or double enveloping. The three cases are illustrated schematically in Fig. 11.14. The worm and gear are nonenveloping (Fig. 11.14a) when the worm is meshed with a simple helical gear and point contact occurs. The worm and gear are single enveloping when the gear is cut to partially envelop the worm (Fig. 11.14b), and they are double enveloping when the pitch surface of the worm is cut in the shape of an hour glass and meshed with a gear that also envelops the worm partially (Fig. 11.14c). The single and



**FIGURE 11.13** Example of worm gear set.



**FIGURE 11.14** Types of worm gear sets.

double enveloping worm gear sets will have line contact and can transmit considerably more power than can nonenveloping worm gear sets.

Note that, in the cases of nonenveloping and single enveloping worm gear sets, the worm can drive the gear either by a rotation of the worm or by a translation of the worm along the axis tangent to the worm axis. Therefore, the alignment of the worm in the tangential direction is not critical. However, in double enveloping worm gear sets, the tangential alignment is critical. Both single and double enveloping worm gear sets must be accurately aligned in the axial and radial directions. Nonenveloping worm gears need to be accurately aligned in the radial direction. The shaft angles of all worm gear sets must be accurately aligned.

### 11.2.1 Worm Gear Nomenclature

A schematic drawing of a single enveloping worm gear set is shown in Fig. 11.15. The two gears have the same hand. The helix angle is defined in the same manner as was done for helical gears; however, as indicated in Fig. 11.15, the helix angle is usually quite large. The lead angle,  $\lambda$ , is the complement of the helix angle,  $\psi$ ; that is,

$$\lambda + \psi = \frac{\pi}{2} \quad (11.25)$$

The lead,  $L$ , is the amount that the worm will advance with one revolution of the worm gear. If there is only one tooth, the lead is equal to the axial pitch,  $p_a$ . In general, if  $N_2$  is the number of teeth on the worm,

$$L = N_2 p_a \quad (11.26)$$

If one tooth of the worm is unwrapped from the pitch cylinder, the lead of the worm is related to the lead angle,  $\lambda$ , as shown in Fig. 11.16. The relationship is

$$\tan \lambda = \frac{L}{\pi d_{t_2}} \quad (11.27)$$

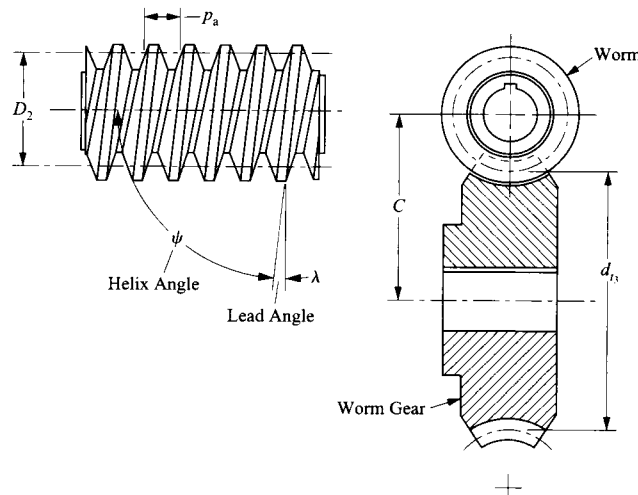


FIGURE 11.15 Worm gear nomenclature.

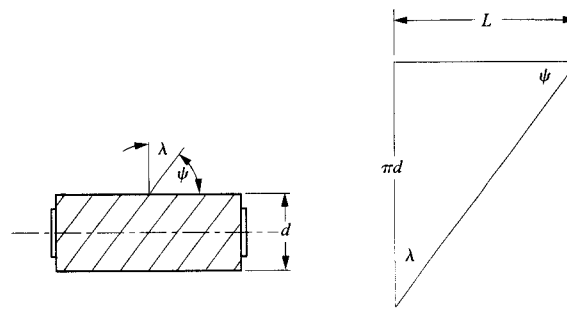


FIGURE 11.16 Representation of worm gear lead.

The pitch diameter of the worm gear is the same as that for helical gears; that is,

$$d_{t_3} = \frac{p_{t_3} N_3}{\pi}$$

where  $N_3$  is the number of teeth on the gear. The velocity ratio is given by Eq. (11.21) as

$$\frac{\omega_2}{\omega_3} = \frac{N_3}{N_2} = \frac{d_{t_3} \cos \psi_3}{d_{t_2} \cos \psi_2} \quad (11.28)$$

For a worm and worm gear to mesh properly with shafts at right angles, the following conditions must be satisfied:

1. The helix angle of the gear must equal the lead angle of the worm.
2. The transverse circular pitch of the gear must equal the axial pitch of the worm.

If the shafts of the worm and gear are at  $90^\circ$  to each other, then

$$\psi_2 + \psi_3 = \frac{\pi}{2} \quad (11.29)$$

and  $\psi_3 = \lambda$ . Equation (11.28) can then be written as

$$\frac{\omega_2}{\omega_3} = \frac{d_{t_3} \cos \psi_3}{d_{t_2} \cos \psi_2} = \frac{d_{t_3} \cos \psi_3}{d_{t_2} \cos(\pi/2 - \psi_3)} = \frac{d_{t_3} \cos \psi_3}{d_{t_2} \sin \psi_3} = \frac{d_{t_3}}{d_{t_2} \tan \psi_3} = \frac{d_{t_3}}{d_{t_2} \tan \lambda}$$

Therefore, from Eq. (11.27),

$$\frac{\omega_2}{\omega_3} = \frac{d_{t_3}}{d_{t_2}} \frac{\pi d_{t_2}}{L} = \frac{\pi d_{t_3}}{L} \quad (11.30)$$

Worm gear sets may or may not be driven from both the worm and gear. In some applications, it is necessary for the drive to be self-locking. In such cases, only the worm can be the driver. In other cases, it must be possible to drive the worm gear set from either the worm or gear. Worms usually have relatively few teeth (one to eight), and when the number of teeth is small, the worm must be the driver. If the lead angle of the worm is greater than the friction angle of the surfaces in contact, the drive will be reversible. The coefficient of friction,  $\mu$ , is related to the friction angle,  $\beta$ , by  $\mu = \tan \beta$ . Therefore, the worm gear set will be self-locking if the lead angle satisfies

$$\lambda < \tan^{-1} \mu \quad (11.31)$$

In general, a worm gear set cannot be back driven if the lead angle is less than  $5^\circ$  (helix angle  $> 85^\circ$ ).

A summary of the equations for worm gears is given in Table 11.4. A more complete list of equations is given by Townsend.<sup>6</sup>

**TABLE 11.4 Summary of Worm Gear Formulas (Gear 2 Is the Worm and 3 Is the Gear)**

Quantity	Formula
Axial pitch	$p_a = \frac{p_t}{\tan \psi} = \frac{p_n}{\sin \psi}$
Lead	$L = N_2 p_a = \pi d_{t_2} \tan \lambda$
Lead angle	$\tan \lambda = \frac{L}{\pi d_{t_2}} = \frac{N_2 p_a}{\pi d_{t_2}}$
Minimum length of worm <sup>6</sup>	$f = 2 \sqrt{\left(\frac{d_{t_3} + 2a}{2}\right)^2 - \left(\frac{d_{t_3} - 2a}{2}\right)^2}$
Normal circular pitch	$p_n = \frac{\pi}{P_n} = \pi m_n = p_t \cos \psi = p_a \sin \psi = p_a \cos \lambda$
Shaft angle	$\Sigma = \psi_2 \pm \psi_3$
Pitch cylinder diameter	$d_t = \frac{N}{P_t} = \frac{N}{P_n \cos \psi} = \frac{N p_t}{\pi} = \frac{N p_n}{\pi \cos \psi} = N m_t$
Effective face width of gear <sup>6</sup>	$F_e = \sqrt{(d_{t_2} + a + b)^2 - (d_{t_2})^2}$
Center distance	$C = \frac{d_{t_2} + d_{t_3}}{2} = \frac{N_2}{2P_{t_2}} + \frac{N_3}{2P_{t_3}} = \frac{1}{2P_n} \left[ \frac{N_2}{\cos \psi_2} + \frac{N_3}{\cos \psi_3} \right]$ $= \frac{m_n}{2} \left[ \frac{N_2}{\cos \psi_2} + \frac{N_3}{\cos \psi_3} \right]$
Velocity ratio	$R = \frac{\omega_2}{\omega_3} = \frac{N_3}{N_2} = \frac{d_{t_3} P_{t_3}}{d_{t_2} P_{t_2}} = \frac{d_{t_3} P_n \cos \psi_3}{d_{t_2} P_n \cos \psi_2}$ $= \frac{d_{t_3} \cos \psi_3}{d_{t_2} \cos \psi_2}$



**EXAMPLE 11.4**  
**Worm and Gear**  
**Geometry**

**Solution**

Assume that a worm has three teeth and is driving a gear with 60 teeth. The shaft angle is  $90^\circ$ , the gear transverse circular pitch is 1.25 in, and the pitch diameter of the worm is 3.8 in. Find the helix angle of the gear, the center distance, and the lead angle of the worm. If the coefficient of friction between the worm and gear is 0.1, estimate whether or not the worm gear set can be back driven.

The worm lead is given by Eq. (11.26) as

$$L = N_2 p_a = 3(1.25) = 3.75 \text{ in}$$

And from Eq. (11.30) the pitch diameter of the gear is

$$d_{t_3} = \frac{\omega_2 L}{\omega_3 \pi} = \frac{60}{3} \frac{3.75}{\pi} = 23.87 \text{ in}$$

The lead angle of the worm can be computed from Eq. (11.27) as

$$\lambda = \tan^{-1} \left( \frac{L}{\pi d_{t_2}} \right) = \tan^{-1} \left( \frac{3.75}{\pi 3.8} \right) = 17.44^\circ$$

Therefore, the helix angle of the gear is

$$\psi_3 = \lambda = 17.44^\circ$$

and the helix angle of the worm is given by Eq. (11.29) as

$$\psi_2 = 90^\circ - \psi_3 = 90^\circ - 17.44^\circ = 72.56^\circ$$

The center distance is given by

$$C = r_{p_2} + r_{p_3} = \frac{d_{t_2} + d_{t_3}}{2} = \frac{3.75 + 23.87}{2} = 13.81 \text{ in}$$

If the worm gear set is to be reversible,  $\lambda > \tan^{-1} \mu$ . For the conditions given,

$$\tan^{-1} \mu = \tan^{-1}(0.1) = 5.71^\circ$$

Therefore, the worm gear set is reversible.

## 11.3 INVOLUTE BEVEL GEARS

When power must be transferred between nonparallel intersecting shafts, bevel gears are usually used. In bevel gears, the pitch surfaces are cones. The shafts must have intersecting centerlines, but the intersection can be at any angle, although  $90^\circ$  (Fig. 11.17) is the most common angle.

The shafts have to be mounted so that the apexes of the pitch cones of the mating gears are coincident (Fig. 11.18). The cones roll on each other without slipping and have spherical motion. Each point on each gear remains at a constant distance from the common apex.

The pitch diameter for bevel gears is the pitch-cone diameter at the larger end (Fig. 11.19). The meshing bevel gears are contained within a sphere of radius  $r_o$ , as shown in Fig. 11.19, where the bases of the cones are contained on the surface of the sphere. The pitch cone angles,  $\gamma_i$ , determine the shaft angle,  $\Sigma$ , as shown in Fig. 11.19. These angles are related by

$$\Sigma = \gamma_2 + \gamma_3 \quad (11.32)$$



FIGURE 11.17 Bevel gears with 90° shaft angle.

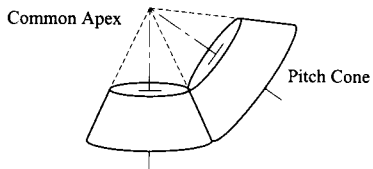


FIGURE 11.18 Pitch cones for bevel gears.

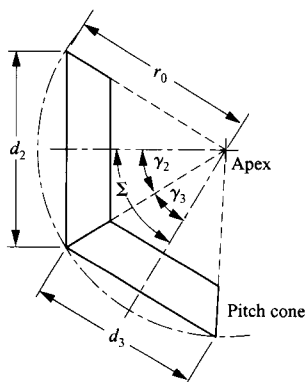


FIGURE 11.19 Relationship among pitch-cone angles.

The velocity ratio for bevel gears is similar to that for spur and helical gears; that is,

$$\frac{\omega_2}{\omega_3} = \frac{N_3}{N_2} = \frac{d_3}{d_2} = \frac{r_3}{r_2} \tag{11.33}$$

where  $N_2$  and  $N_3$  are the numbers of teeth on gears 2 and 3, respectively, and  $d_2$  and  $d_3$  are the diameters at the large end of the pitch cones of gears 2 and 3, respectively (see Fig. 11.19).  $r_2$  and  $r_3$  are the corresponding pitch radii.

The pitch diameters can be related to the cone angles by considering the geometry represented in Fig. 11.19. In particular,

$$\sin \gamma_2 = \frac{d_2}{2r_0} = \sin(\Sigma - \gamma_3) = \sin \Sigma \cos \gamma_3 - \cos \Sigma \sin \gamma_3$$

Dividing by  $\sin \Sigma \sin \gamma_3$  gives

$$\frac{\sin \gamma_2}{\sin \Sigma \sin \gamma_3} = \frac{\cos \gamma_3}{\sin \gamma_3} - \frac{\cos \Sigma}{\sin \Sigma}$$

or

$$\frac{1}{\sin \Sigma} \left[ \frac{\sin \gamma_2}{\sin \gamma_3} + \cos \Sigma \right] = \frac{1}{\tan \gamma_3} \quad (11.34)$$

From the geometry,

$$\frac{\sin \gamma_2}{\sin \gamma_3} = \frac{d_2}{d_3} \quad (11.35)$$

From Eqs.(11.34) and (11.35),

$$\tan \gamma_3 = \frac{\sin \Sigma}{\left[ d_2/d_3 + \cos \Sigma \right]} = \frac{\sin \Sigma}{\left[ N_2/N_3 + \cos \Sigma \right]} \quad (11.36)$$

Similarly,

$$\tan \gamma_2 = \frac{\sin \Sigma}{\left[ d_3/d_2 + \cos \Sigma \right]} = \frac{\sin \Sigma}{\left[ N_3/N_2 + \cos \Sigma \right]} \quad (11.37)$$

When the shaft angle is  $90^\circ$ , which is the most common case, Eqs. (11.36) and (11.37) reduce to

$$\tan \gamma_3 = \frac{d_3}{d_2} = \frac{N_3}{N_2} \quad (11.38)$$

and

$$\tan \gamma_2 = \frac{d_2}{d_3} = \frac{N_2}{N_3} \quad (11.39)$$

### 11.3.1 Tredgold's Approximation for Bevel Gears

Because of the spherical geometry of bevel gears, it is difficult to draw and evaluate bevel gear properties such as contact ratio. Tredgold's approximation lets us approximate the bevel gears as equivalent spur gears. This approximation is used extensively, and the terminology of bevel-gear teeth has evolved around it.<sup>2</sup> The approximation is accurate enough for most practical purposes as long as the gear has eight or more teeth.

Tredgold's approximation involves the concept of a back cone for both meshing gears, as shown in Fig. 11.20. The approximation recognizes that the action of the gear teeth in the vicinity of the contact location at the large end of the gear teeth is very similar to the action between two spur gears that have pitch radii  $r_{p_2}$  and  $r_{p_3}$  equal to the back cone radii,  $r_{e_2}$  and  $r_{e_3}$ .

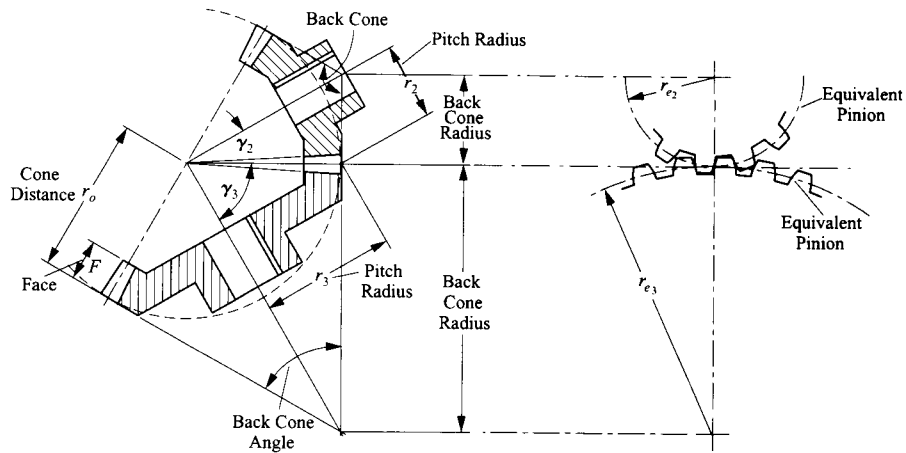


FIGURE 11.20 Approximation of bevel gears as equivalent spur gears (Tredgold's approximation).

Based on the geometry in Fig. 11.20, the pitch radii for the equivalent spur gears are given by

$$r_{e_2} = \frac{r_2}{\cos \gamma_2} \quad (11.40)$$

and

$$r_{e_3} = \frac{r_3}{\cos \gamma_3} \quad (11.41)$$

If  $p_c$  is the circular pitch at the large end of the bevel gears, the numbers of teeth on the equivalent spur gears are given by

$$N_{e_2} = \frac{2\pi r_{e_2}}{p_c} \quad (11.42)$$

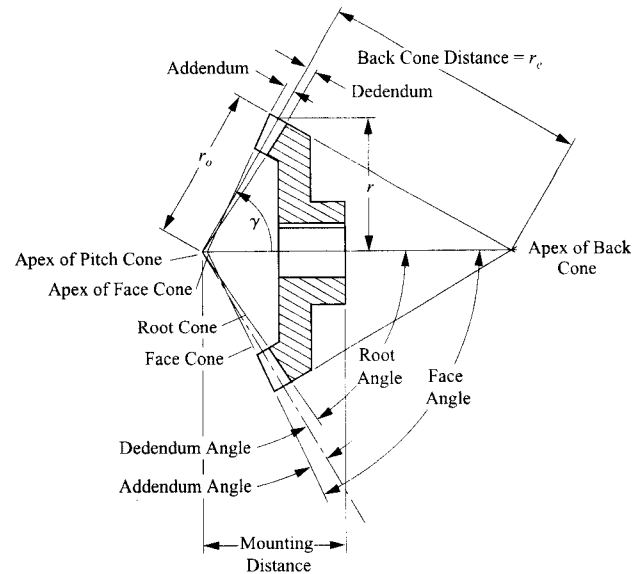
and

$$N_{e_3} = \frac{2\pi r_{e_3}}{p_c} \quad (11.43)$$

Note that  $N_{e_2}$  and  $N_{e_3}$  need not be integers in Eqs. (11.42) and (11.43).

### 11.3.2 Additional Nomenclature for Bevel Gears

Figure 11.21 shows some of the additional terms used with bevel gears. Notice that most of the information characteristic of teeth sizes is defined for the large end of the gear teeth. Also notice that the apex of the pitch cone is not coincident with the apex of the face cone. This is to ensure that there is a constant clearance between the addendum of the given gear and the dedendum of the meshing gear. This also allows a larger fillet at the small end of the tooth than would otherwise be possible.



**FIGURE 11.21** Nomenclature for bevel gears.

The AGMA<sup>4</sup> recommends a 20° pressure angle for bevel gears with 14 or more teeth and 25° for gears with 13 or fewer teeth. The minimum pressure angle is determined by undercutting on the pinion.

Bevel gears are usually mounted in a cantilever fashion. Because of this, the meshing gears will deflect away from each other, and the smaller end of the gears will carry even less load than they would without deflections. Because the large end of the gear tooth will carry most of the load, the face width of the teeth will be relatively small. Typical design practices are to limit the face width to

$$F < 0.3r_o \text{ or } \frac{10.0}{P_d} \text{ (or } 10.0 m) \quad (11.44)$$

whichever is smaller.<sup>3</sup> This guideline is beneficial from a manufacturing standpoint because simpler tooling can be used with a narrower face width.

In addition to the general type shown in Fig. 11.18, there are three special types of bevel gears:

1. crown bevel gears,
2. miter gears, and
3. angular bevel gears.

Each of these is discussed briefly in the following.

### 11.3.3 Crown Bevel Gears and Face Gears

Crown bevel gears are the bevel gear equivalent of a rack. A crown gear has a 90° pitch angle, and its teeth profiles are theoretically parts of great circles (the spherical equivalent

of a straight line in the plane). The pitch cone of a crown gear is a cylinder of infinite radius, and the resulting involute teeth have straight sides. The pitch surface is a plane. Crown gears are shown in Figs. 11.22 and 11.23.

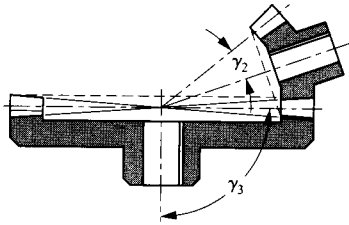


FIGURE 11.22 Crown gear geometry.

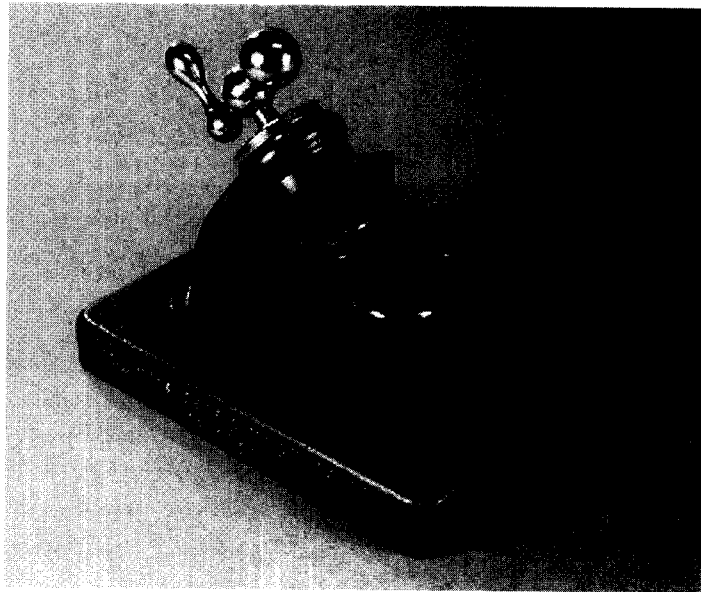


FIGURE 11.23 Crown gear model.

Face gears consist of a spur or helical pinion in combination with a conjugate gear of disk form. The face gear has the appearance of a crown gear except that the addendum and dedendum angles are zero. The gear is generated with a reciprocating pinion-shaped cutter that has the same diametral pitch and pressure angle as the mating pinion and is substantially the same size.<sup>5</sup> Face gears are shown in Figs. 11.24 and 11.25.

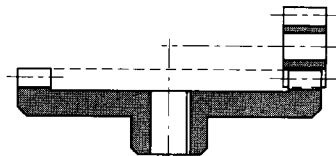
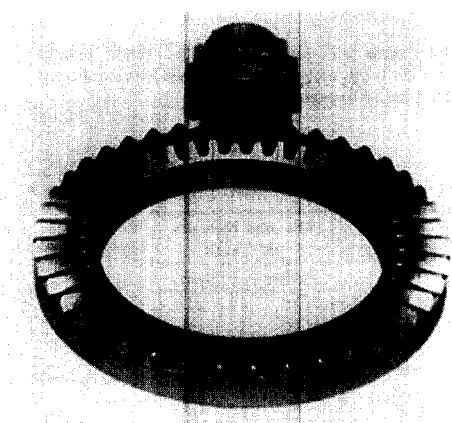


FIGURE 11.24 Face gear geometry.

FIGURE 11.25 Face gear and pinion.<sup>5</sup>

### 11.3.4 Miter Gears

Miter gears are mating bevel gears with equal numbers of teeth and with axes at right angles. These gears are used to transmit power around a 90° corner. Miter gears are shown in Figs. 11.26 and 11.27.

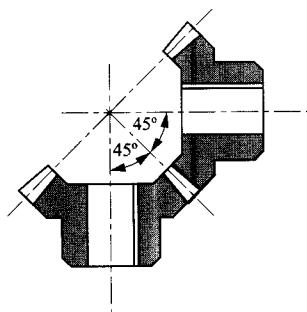


FIGURE 11.26 Miter gear geometry.



FIGURE 11.27 Miter gear model.

### 11.3.5 Angular Bevel Gears

Angular bevel gears have a shaft angle different from  $90^\circ$ . This is the most general type of bevel gear. Examples of angular bevel gears without a  $90^\circ$  shaft angle are shown in Figs. 11.28 and 11.29.

The AGMA<sup>4</sup> gives a standardized approach to determining bevel gear tooth proportions. Bevel gears in this system have unequal addendums for mating teeth. Tables are provided for  $20^\circ$  pressure angle gears with a  $45^\circ$  pitch angle. For angular bevel gears with a shaft angle different from  $90^\circ$ , a calculation procedure is given.

A summary of the equations for bevel gears is given in Table 11.5. A more complete list of equations is given by Townsend.<sup>6</sup>

### 11.3.6 Zerol Bevel Gears

The previous examples of bevel gears have straight teeth. In addition to these gears, there are two types of bevel gears that have curved teeth. Zerol gears are patented bevel gears that have curved teeth but zero spiral angle at the middle of the teeth. Zerol gears have the same general tooth actions as straight bevel gears, and they can be used to replace straight-toothed bevel gears. The primary advantage over straight-toothed bevel gears is that they can be cut in the same machines as are used for spiral bevel gears, and the teeth can be easily ground.

Most modern straight-toothed bevel gears are also slightly convex, so the contact occurs in the central section of the teeth. This avoids contact on the narrower (and weaker) part of the teeth and allows a slight amount of adjustment when the gears are installed.

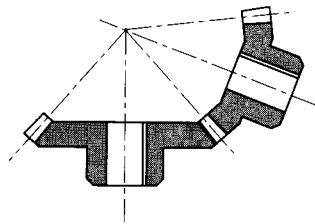


FIGURE 11.28 Angular bevel gear geometry.



FIGURE 11.29 Angular bevel gear model.



**TABLE 11.5 Summary of Straight Bevel Gear Formulas**

Quantity	Formula
Pitch diameter <sup>a</sup>	$d = \frac{N}{P} = \frac{Np}{\pi} = Nm$
Pitch angle of gear <sup>a</sup>	$\tan \gamma_2 = \frac{\sin \Sigma}{[d_3/d_2 + \cos \Sigma]} = \frac{\sin \Sigma}{[N_3/N_2 + \cos \Sigma]}$
Pitch angle of pinion <sup>a</sup>	$\tan \gamma_3 = \frac{\sin \Sigma}{[d_2/d_3 + \cos \Sigma]} = \frac{\sin \Sigma}{[N_2/N_3 + \cos \Sigma]}$
Circular pitch <sup>a</sup>	$p = \frac{\pi}{P} = \pi m$
Shaft angle	$\Sigma = \gamma_2 + \gamma_3$
Equivalent spur gear radius	$r_{e_i} = \frac{r_i}{\cos \gamma_i}, \quad i = 2, 3$
Number of teeth on equivalent spur gear	$N_{e_i} = \frac{2\pi r_{e_i}}{p_c}, \quad i = 2, 3$
Outer cone distance	$r_o = \frac{d_2}{2 \sin \gamma_2} = \frac{d_3}{2 \sin \gamma_3}$
Minimum face width	$F < 0.3r_o$ or $\frac{10.0}{P_d}$ (or 10.0 <i>m</i> )
Velocity ratio	$\frac{\omega_2}{\omega_3} = \frac{N_3}{N_2} = \frac{d_3}{d_2} = \frac{r_3}{r_2}$

<sup>a</sup>Pitch information is for the large end of the gear.

### 11.3.7 Spiral Bevel Gears

An example of spiral bevel miter gears is shown in Fig. 11.30. Spiral bevel gears have obliquely curved teeth. As in the case of straight-toothed bevel gears, the pitch cones of spiral bevel gears intersect and have a common apex. Spiral bevel gears are analogous to helical gears and are used for the same purpose. Spiral bevel gears have a gradual load transfer as the teeth engage, and they are much quieter and stronger than straight-toothed bevel gears. Therefore, spiral bevel gears are used for essentially all high-speed applications. The spiral angle (Fig. 11.31) is such that the tooth face advances as a result of the spiral exceeding the circular pitch. This provides a smooth transition of load from tooth to tooth and minimizes much of the tooth vibration that creates gear whine. This is in contrast to straight and Zerol bevel gears, with which the load is transferred from tooth to tooth immediately across the entire contact area. The geometries of Zerol and spiral bevel gears are compared in Fig. 11.32. The AGMA<sup>5</sup> gives standardized equations and graphs for determining spiral bevel tooth profiles.

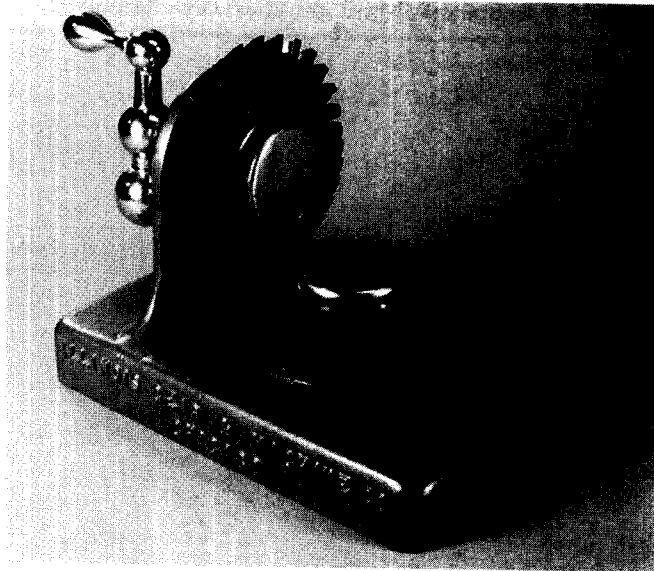


FIGURE 11.30 Spiral bevel miter gears.

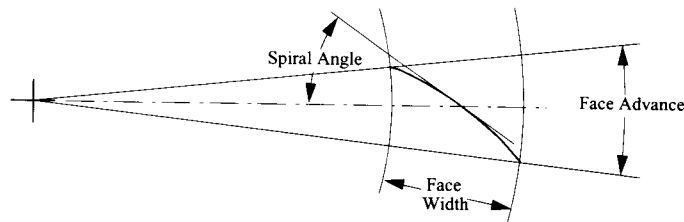


FIGURE 11.31 Geometry of one spiral gear tooth.

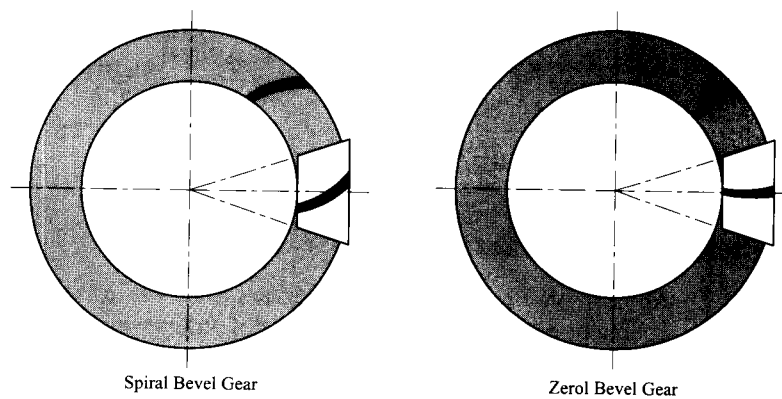
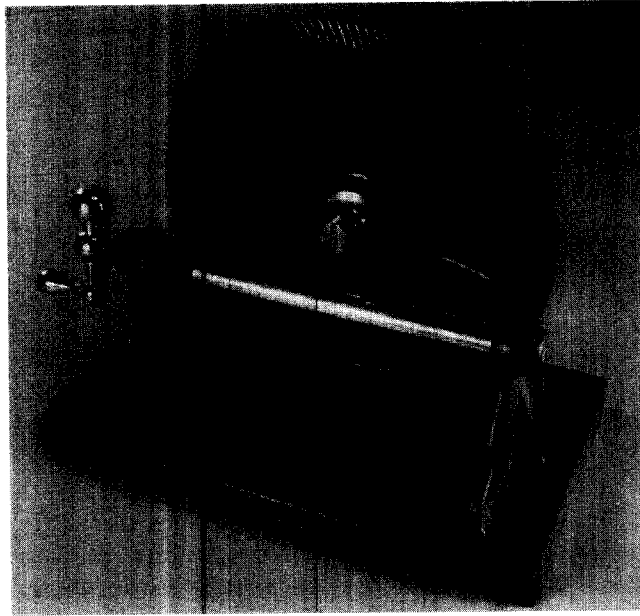


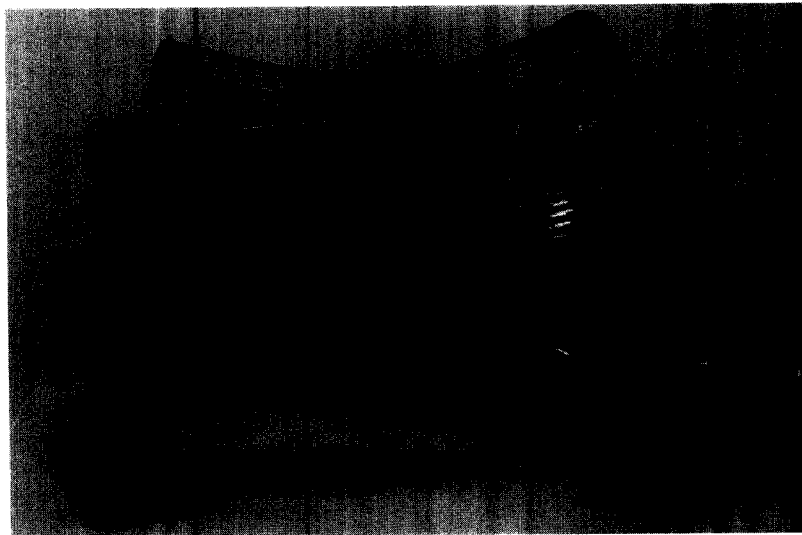
FIGURE 11.32 Comparison of spiral bevel gear and Zerol bevel gear.

### 11.3.8 Hypoid Gears

Hypoid gears are similar in appearance to spiral bevel gears; however, the shaft axes do not intersect (see Fig. 11.33). The pitch surfaces of hypoid gears are not cones as in the case of spiral bevel gears but are hyperboloids of revolution (see Fig. 11.34). This permits the teeth to maintain line contact.



**FIGURE 11.33** Hypoid gear set.



**FIGURE 11.34** The pitch surfaces of hypoid gears are hyperboloids of revolution.

Hypoid gears are used in the differentials of rear-wheel-driven automobiles because the geometry lowers the level of the drive shaft. This permits a lower body. Another advantage of hypoid gears over spiral bevel gears is that the hypoid pinion teeth are stronger. This is because the hypoid pinion can be designed so that the spiral angle of the pinion is larger than that of the gear. This results in a larger and stronger pinion tooth than that of a spiral bevel pinion. Because of the length of contact on each gear tooth, hypoid gears are quieter than spiral bevel gears. They can also be used with larger reduction ratios.

## REFERENCES

---

- <sup>1</sup>American Gear Manufacturers' Association (AGMA), "Tooth Proportions for Coarse Pitch Involute Spur Gears," AGMA Publications 201.02 and 201.02A (1968).
- <sup>2</sup>Shigley, J. E., *Kinematic Analysis of Mechanisms*, McGraw-Hill Book Co., New York (1975).
- <sup>3</sup>Mabie, H. H., and C. F. Reinholtz, *Mechanisms and Dynamics of Machinery*, 4th ed., John Wiley & Sons, New York (1987).
- <sup>4</sup>American Gear Manufacturers' Association (AGMA), "Design Manual for Bevel Gears," AGMA Publication 2005-B88 (May 1988).
- <sup>5</sup>American Gear Manufacturers' Association (AGMA), "Fine-Pitch On-Cutter Face Gears for 20-Degree Involute Spur Pinions," AGMA Publication 203.03 (May 1973).
- <sup>6</sup>Townsend, D. P., *Dudley's Gear Handbook*, McGraw-Hill Book Co., New York (1992).

## PROBLEMS

---

- 11.1** Two helical gears are cut with a spur gear hob that has a diametral pitch of 4 and a pressure angle of  $20^\circ$ . The pinion has 15 teeth, the gear has 35 teeth, and the helix angle is  $30^\circ$ . Determine the minimum recommended face width. Using the minimum face width, find the transverse diametral pitch, the pitch cylinder radii, and the axial, transverse, and total contact ratios.
- 11.2** Two helical gears are cut with the same tooth numbers and with the same cutter as given in Problem 11.1. The helix angle is  $30^\circ$ . Find the transverse pressure angle, the transverse diametral pitch, and the axial pitch.
- 11.3** Two parallel helical gears are cut with a  $20^\circ$  normal pressure angle and a  $45^\circ$  helix angle. They have a diametral pitch of 12 in the normal plane and have 10 and 41 teeth, respectively. Find the transverse pressure angle, transverse circular pitch, and transverse diametral pitch. Also determine the minimum face width, and using that face width, determine the total contact ratio.
- 11.4** A helical gear has 18 teeth and a transverse diametral pitch of 6. The face width is 1.5, and the helix angle is  $25^\circ$ . Determine the axial pitch, normal pitch, lead, transverse pitch diameter, and minimum face width.
- 11.5** Two helical gears have 20 and 34 teeth and a normal diametral pitch of 8. The left-handed pinion has a helix angle of  $40^\circ$  and a rotational speed of 1000 rpm. The gear is also left handed and has a helix angle of  $40^\circ$ . Determine the angular velocity of the gear, transverse diametral pitch of each gear, and pitch diameters.
- 11.6** Two standard spur gears have a diametral pitch of 10, a pressure angle of  $20^\circ$ , and a velocity ratio equal to 3.5:1. The center distance is 8.55 in. Two helical gears are to be used to replace the two spur gears such that the center distance and angular velocity ratio remain unchanged. The helical gears are also to be cut with the same hob as that used to cut the spur gears. Determine the helix angle, tooth numbers, and minimum face width for the new gears if the helix angle is kept to a minimum.
- 11.7** Two standard spur gears have a diametral pitch of 16 and a pressure angle of  $20^\circ$ . The tooth numbers are 36 and 100, and the gears were meshed at a standard center distance. After the gear reducer was designed and tested, the noise of the drive was found to be excessive. Therefore, the decision was made to replace the spur gears with helical gears. The helix angle chosen was  $22^\circ$ , and the tooth numbers were to remain unchanged. Determine the change in center distance required.
- 11.8** A spur gear transmission consists of a pinion that drives two gears. The pinion has 24 teeth and a diametral pitch of 12. The velocity ratio for the pinion and one gear is 3:2 and that for the pinion and the other gear is 5:2. To reduce the noise level, all three gears are to be replaced by helical gears such that the center distances and velocity ratios remain the same. The helical gears will be cut with a 16 pitch,  $20^\circ$  hob. If the helix angle is kept as low as possible, determine the number of teeth, face width, hand, helix angle, and outside diameter for each of the gears.
- 11.9** A pair of helical gears have a module in the normal plane of 3 mm, a normal pressure angle of  $20^\circ$ , and a helix angle of  $45^\circ$ . The gears mesh with parallel shafts and have 30 and 48 teeth. Determine the transverse module, the pitch diameters, the center distance, and the minimum face width.
- 11.10** Two  $20^\circ$  spur gears have 36 and 90 teeth and a module of 1.5. The spur gears are to be replaced by helical gears such that the center distance and velocity ratio are not changed. The maximum allowed face width is 12.7 mm, and the hob module is 1.5 mm. Design the helical gear pair that has the smallest helix angle possible. Determine the numbers of teeth, the face width, the helix angle, and the outside diameters of the gears.

- 11.11** Two helical gears are cut with a  $20^\circ$  hob with a module of 2. One gear is right handed, has a  $30^\circ$  helix angle, and has 36 teeth. The second gear is left handed, has a  $40^\circ$  helix angle, and has 72 teeth. Determine the shaft angle, the angular velocity ratio, and the center distance.
- 11.12** Two crossed shafts are connected by helical gears such that the velocity ratio is 3:1 and the shaft angle is  $60^\circ$ . The center distance is 10 in, and the normal diametral pitch is 8. The pinion has 35 teeth. Assume that the gears are the same hand and determine the helix angles, pitch diameters, and recommended face widths.
- 11.13** Two crossed shafts are connected by helical gears such that the velocity ratio is 3:2 and the shaft angle is  $90^\circ$ . The center distance is 5 in. Select a pair of gears that will satisfy the design constraints. What other information might be considered to reduce the number of arbitrary choices for the design?
- 11.14** A helical gear with a normal diametral pitch of 8 is to be used to drive a spur gear at a shaft angle of  $45^\circ$ . The helical gear has 21 teeth, and the velocity ratio is 2:1. Determine the helix angle for the helical gear and the pitch diameter of both gears.
- 11.15** Two crossed helical gears connect shafts making an angle of  $45^\circ$ . The pinion is right handed, has a helix angle of  $20^\circ$ , and contains 30 teeth. The gear is also right handed and contains 45 teeth. The transverse diametral pitch of the gear is 5. Determine the pitch diameter, the normal pitch, and the lead for each gear.
- 11.16** The worm of a worm gear set has 2 teeth, and the gear has 58 teeth. The worm axial pitch is 1.25 in, and the pitch diameter is 3 in. The shaft angle is  $90^\circ$ . Determine the center distance for the two gears, the helix angle, and the lead for the worm.
- 11.17** The shaft angle between two shafts is  $90^\circ$ , and the shafts are to be connected through a worm gear set. The center distance is 3 in, and the velocity ratio is 30:1. Determine a worm and gear that will satisfy the design requirements. Specify the number of teeth, lead angle, and pitch diameter for each gear. Also, determine the face width for the gear.
- 11.18** A worm with two teeth drives a gear with 50 teeth. The gear has a pitch diameter of 8 in and a helix angle of  $20^\circ$ . The shaft angle between the two shafts is  $80^\circ$ . Determine the lead and pitch diameter of the worm.
- 11.19** Two straight-toothed bevel gears mesh with a shaft angle of  $90^\circ$  and a diametral pitch of 5. The pinion has 20 teeth, and the gear ratio is 2:1. The addendum and dedendum are the same as for  $20^\circ$  stub teeth. For the gear, determine the pitch radius, cone angle, outside diameter, cone distance, and face width.
- 11.20** A pair of straight-toothed bevel gears mesh with a shaft angle of  $90^\circ$  and a diametral pitch of 6. The pinion has 18 teeth, and the gear ratio is 2:1. The addendum and dedendum are the same as for  $20^\circ$  full-depth spur-gear teeth. Determine the number of teeth on the gear and the pitch diameters of both the pinion and gear. Also, for the gear, determine the pitch-cone angle, outside diameter, cone distance, and face width.
- 11.21** A pair of straight-toothed bevel gears mesh with a shaft angle of  $80^\circ$  and a diametral pitch of 7. The pinion has 20 teeth and a pitch-cone angle of  $40^\circ$ . The gear ratio is 3:2. Determine the number of teeth on the gear and the pitch diameters of both the pinion and gear. Also, determine the equivalent spur gear radii for both the pinion and the gear.
- 11.22** A pair of straight-toothed bevel gears mesh with a shaft angle of  $45^\circ$  and a module of 5.08. The pinion has 16 teeth and a pitch-cone angle of  $20^\circ$ . The gear ratio is 3:2. Determine the number of teeth on the gear and the pitch diameters of both the pinion and gear. Also determine the back-cone distance and the back-cone angle for the gear.

# GEAR TRAINS

## 12.1 GEAR TRAINS

In Chapters 10 and 11, the characteristics of individual gears were discussed. However, in general, gears are of interest to designers only when they are used in pairs as motion and/or force transducers. These gear pairs can be combined in many ways to achieve desired input–output relationships. A combination of one or more gear pairs that are interrelated is called a *gear train*. All complex gear trains are combinations of the simple, compound, and planetary gear trains discussed in this chapter.

## 12.2 DIRECTION OF ROTATION

As discussed in Chapters 10 and 11, the velocity ratio for two meshing gears (2 and 3) is

$$R = \pm \frac{\omega_2}{\omega_3} = \pm \frac{r_3}{r_2} = \pm \frac{N_3}{N_2} \quad (12.1)$$

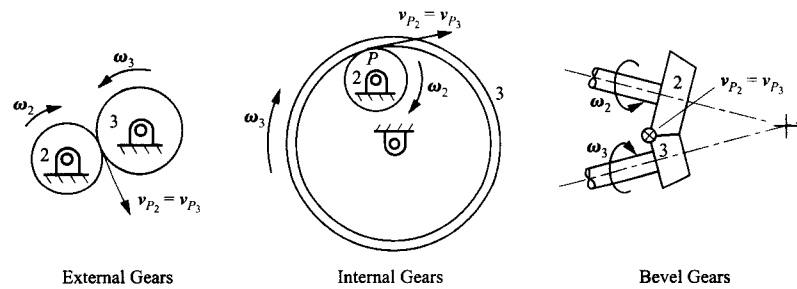
where  $r_i$  and  $N_i$  are the pitch radii and number of teeth on gear  $i$  ( $i = 2, 3$ ), the plus sign goes with an external gear meshing with an internal gear, and the minus sign goes with two external gears meshing.

When planar gears are involved, Eq. (12.1) can be used directly because all of the vectors are parallel. However, when bevel and crossed helical gears are involved, the angular velocities must be treated as vectors. For bevel gears, a relatively simple way to do this is to recognize that at the pitch point (the end of the tangent line to the pitch surfaces), rolling occurs, and the velocity at the pitch point on both gears is the same. From this, the direction of rotation can be inferred from the simple velocity relationship

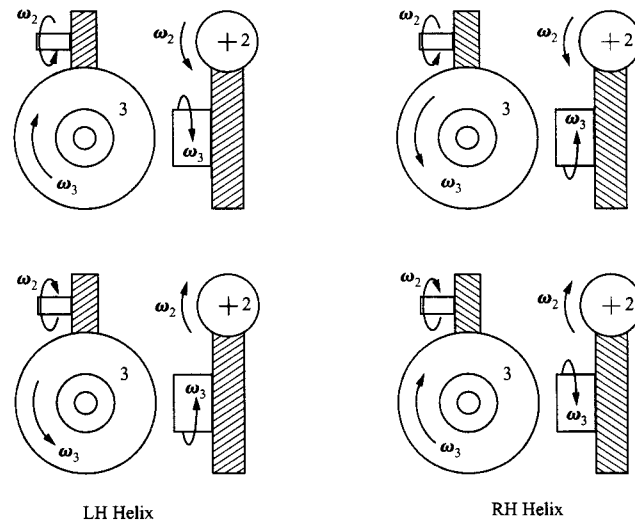
$$\mathbf{v}_{P_2} = \mathbf{v}_{P_3} = \boldsymbol{\omega}_2 \times \mathbf{r}_2 = \boldsymbol{\omega}_3 \times \mathbf{r}_3 \quad (12.2)$$

where the pitch radius vectors ( $r_2$  and  $r_3$ ) for gears 2 and 3, respectively, are directed from the rotation axis to the pitch point. For bevel gears, the large end of the gear is used for the measurement of the pitch radii. This is shown in Fig. 12.1.

When crossed helical gears are involved, the process becomes a little more complicated because the hand of the gears, that is, the direction of twist of the helical teeth, affects the direction of rotation of the driven gear, as shown in Fig. 12.2. To determine the direction of rotation of the pinion relative to the gear, treat the pinion as a screw and the gear as fixed. Observe the motion of the pinion relative to the gear as the pinion is rotated and the gear is viewed along the gear axis. If the pinion appears to advance toward the gear when the pinion is rotated, in reality the gear would rotate counterclockwise. If the pinion appears to withdraw from the gear when the pinion is rotated, the gear would rotate clockwise.



**FIGURE 12.1** The direction of the angular velocities of two meshing gears can be determined from the direction of the velocity of the pitch point.



**FIGURE 12.2** The direction of the angular velocities for crossed helical gears.

## 12.3 SIMPLE GEAR TRAINS

Simple gear trains can be divided into two types depending on whether idler gears are involved or not. Simple gear trains have only one gear on each shaft. These shafts rotate on bearings that are attached to the same frame. The gears may be of any type, for example, spur, bevel, hypoid, and worm. Figures 12.3–12.5 show various simple gear trains.

The idler gears in simple gear trains can serve two purposes in design. One is to change the direction of motion of the output gear, and the second is to provide a spacer when two gears cannot be directly meshed because of the shaft locations. This occurs when there is a limit to the sizes that two gears can be, but the shaft location is specified for reasons other than kinematics.

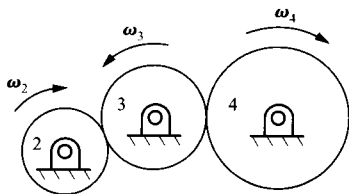


FIGURE 12.3 A simple gear train with all external gears and one idler (gear 3).

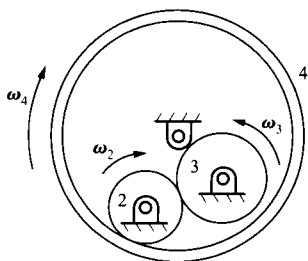


FIGURE 12.4 A simple gear train with internal gear and one idler (gear 3).

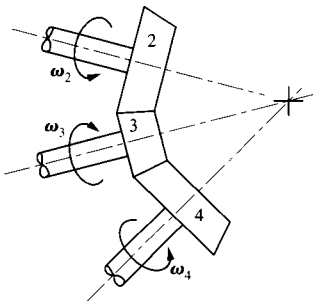


FIGURE 12.5 A simple gear train with external bevel gears and one idler (gear 3).

In gear trains, the overall gear reduction ratio for the gearbox is usually of interest. This can be determined by writing the velocity ratio in terms of the tooth numbers at each mesh. For example, in Fig. 12.3,

$$\frac{\omega_2}{\omega_3} = -\frac{N_3}{N_2} \quad (12.3)$$

and

$$\frac{\omega_3}{\omega_4} = -\frac{N_4}{N_3} \quad (12.4)$$

Multiplying Eq. (12.4) by Eq. (12.3) gives

$$\frac{\omega_2}{\omega_4} = \left(-\frac{N_3}{N_2}\right) \left(-\frac{N_4}{N_3}\right)$$

or

$$\frac{\omega_2}{\omega_4} = (-1)^2 \frac{N_4}{N_2} \quad (12.5)$$



If we analyze the gear train in Fig. 12.4, we will get

$$\frac{\omega_2}{\omega_4} = (-1)^1 \frac{N_4}{N_2} \quad (12.6)$$

The analysis of the gear train in Fig. 12.5 is more difficult because we must treat the angular velocities as vectors to determine the directions mathematically. However, if we trace the angular-velocity directions using the procedure indicated in Fig. 12.1, we can determine the direction and compute the magnitude of the angular velocities separately. If we do this, we will find that the magnitude of the overall velocity ratio is given by

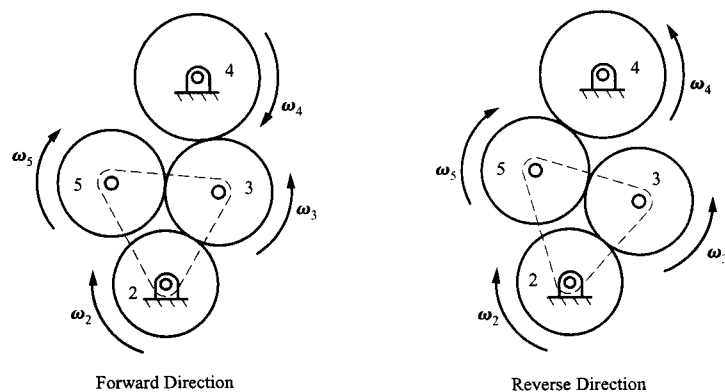
$$\frac{\omega_2}{\omega_4} = \frac{N_4}{N_2}$$

If we add more idler gears, the effect will be the same. Namely, the magnitude of the velocity ratio between the input and output shafts is a function of the numbers of teeth on the input and output gears only. The magnitude of the velocity ratio is independent of the size and number of idler gears. The sign of the train ratio for parallel-shaft gears, however, does depend on the number of idler gears. In particular, at each mesh between external gears, the velocity ratio changes sign. For internal gears, the velocity ratio remains the same sign. Therefore, if  $n$  is the number of meshes between *external* gears, the sign of the velocity ratio is given by  $(-1)^n$ . Note that each idler gear will have at least two mesh points.

A simple gear train can involve any number and types of gears. However, each gear in the gear train must be able to mesh with any other gear. Therefore, each gear must have the same normal pitch if the gears are to mesh properly.

### 12.3.1 Simple Reversing Mechanism

An idler gear can be used in a simple reversing mechanism shown in Fig. 12.6. This is a procedure commonly used to reverse the direction of rotation of the lead screw on small metal lathes. The procedure adds an extra idler to the simple gear train when the direction of rotation is to be reversed. The mechanism works well only when the gears are slowly moving or at rest, since there is no provision for ensuring that the gears will mesh easily when the direction change is made.



**FIGURE 12.6** A simple reversing mechanism using an extra idler gear.

## 12.4 COMPOUND GEAR TRAINS

For all types of gears, the velocity ratio is limited for each mesh by practical considerations. For example, in spur gears, the velocity ratio at any mesh should not exceed 1:5. For larger reductions, compound gear trains should be used. Compound gear trains are characterized by the presence of two or more gears attached to the same shaft. The shafts, however, still rotate on bearings that are fixed to the frame. Unlike simple gear trains, the gears in a compound gear train need not and generally will not be of the same type. This is evident in Fig. 12.7, which shows an example of a commercial gear reducer.

The velocity ratios attainable in a compound gear train can be any size, with ratios in the thousands being possible. There is no theoretical limit to the number of passes (gear meshes) that can be made; however, practical issues such as friction and the functional need restrict the number in most applications.

A compound gear train is shown in Fig. 12.8. The symbolism often used for gear trains is also illustrated in the figure. The velocity ratio for the gear mesh can be written as

$$\frac{\omega_2}{\omega_3} = -\frac{N_3}{N_2} \quad (12.7)$$

and

$$\frac{\omega_4}{\omega_5} = -\frac{N_5}{N_4} \quad (12.8)$$

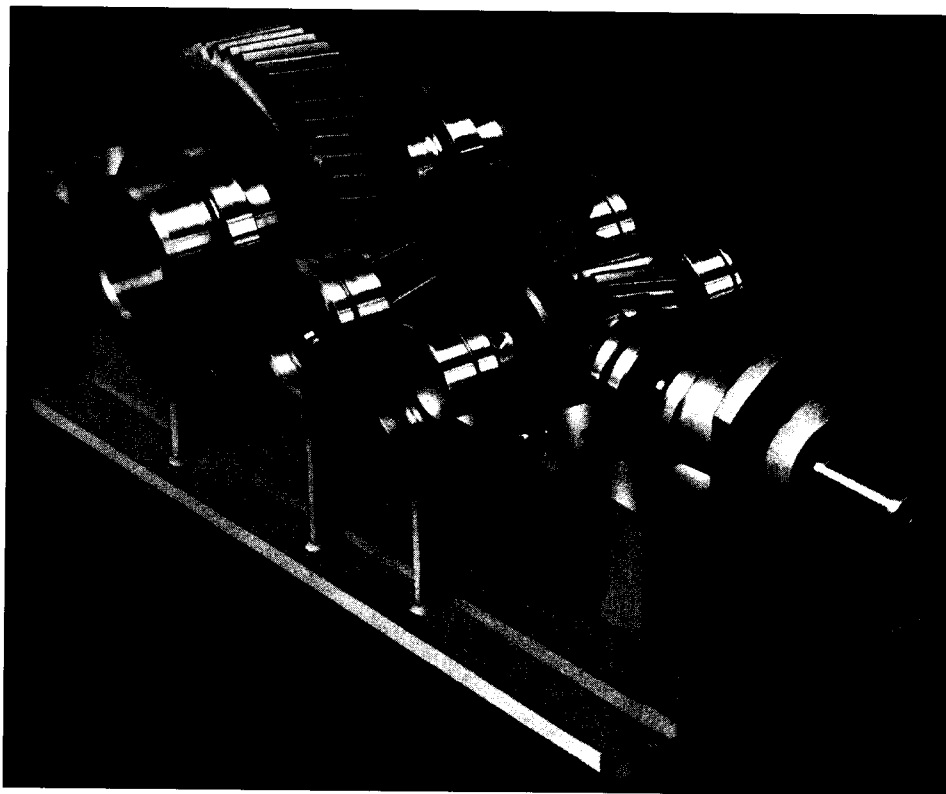


FIGURE 12.7 A compound gear train. (Courtesy of PT Components, Inc., Indianapolis, Indiana.)

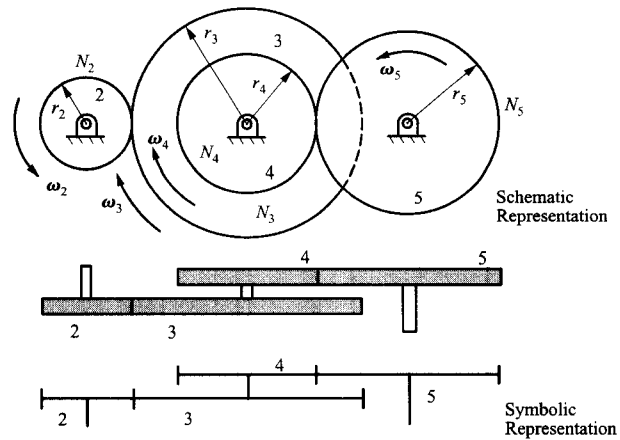


FIGURE 12.8 A compound gear train.

Because gears 3 and 4 are rigidly attached to the same shaft, we know that  $\omega_3 = \omega_4$ . The overall gear train velocity ratio is given by  $\omega_2/\omega_5$ .

If we solve Eq. (12.7) for  $\omega_2$  and Eq. (12.8) for  $\omega_5$  and use  $\omega_3 = \omega_4$ , the overall velocity ratio can be written as

$$\frac{\omega_2}{\omega_5} = \frac{-\omega_3 \left( \frac{N_3}{N_2} \right)}{-\omega_4 \left( \frac{N_4}{N_5} \right)} = \frac{\left( \frac{N_3}{N_2} \right)}{\left( \frac{N_4}{N_5} \right)} = \frac{N_3 N_5}{N_2 N_4} \quad (12.9)$$

or

$$\frac{\omega_2}{\omega_5} = \frac{\omega_2}{\omega_3} \frac{\omega_4}{\omega_5} = \frac{N_3 N_5}{N_2 N_4} \quad (12.10)$$

From Eq. (12.10), it is clear that we can compute the overall velocity ratio from the product of the velocity ratios at each mesh. We can do this either in terms of the velocities directly, or more beneficially, in terms of the tooth numbers. Notice that when parallel-shaft gearing is involved, we can also use the ratios of the pitch-circle radii, because these will be directly proportional to the tooth numbers. Equation (12.10) can then be extended to

$$\frac{\omega_2}{\omega_5} = \frac{\omega_2}{\omega_3} \frac{\omega_4}{\omega_5} = \frac{N_3 N_5}{N_2 N_4} = \frac{r_3 r_5}{r_2 r_4} \quad (12.11)$$

However, the most convenient parameter to use when computing velocity ratios is the tooth number on each gear. This is because the velocity ratios can be directly equated to the tooth ratios for all types of gearing, whereas the ratios of the pitch-cylinder radii alone are not valid for gears with nonparallel shafts.

If we start with gear 2 as the input gear, we can treat each mesh of the gear train as having an input side and an output side. For example, in Fig. 12.8, at the mesh between gears 2 and 3, gear 2 would be the driver and gear 3 would be the driven gear. At the mesh between gears 4 and 5, gear 4 would be the driver and gear 5 would be the driven gear. Therefore,  $N_3$  and  $N_5$  would be associated with driven gears, and  $N_2$  and  $N_4$  would be associated with driver gears. In Eq. (12.11), the velocity ratio can be represented as the product

of the driven gear tooth numbers divided by the product of the driver gear tooth numbers. This situation holds in general for compound gear trains. Mathematically, if  $n$  is the number of gear meshes (including idlers that each have two meshes), a general expression for the magnitude of the velocity ratio can be written as

$$\frac{\omega_{\text{input}}}{\omega_{\text{output}}} = \frac{\prod_{i=3}^n N_i}{\prod_{i=3}^n N_j} = \frac{\text{product of driven tooth numbers}}{\text{product of driver tooth numbers}} \quad (12.12)$$

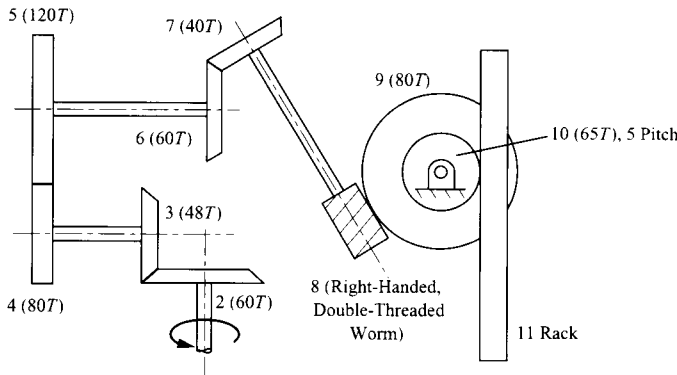
Assuming that the gears are numbered sequentially, in Eq. (12.12),  $i$  includes only the tooth numbers for the odd gear numbers, and  $j$  includes only the tooth numbers for the even gear numbers. The sign of the gear ratio depends on the type of gears. If all parallel-shaft gears are involved, we can use an extension of Eq. (12.4). Then,

$$\frac{\omega_{\text{input}}}{\omega_{\text{output}}} = (-1)^m \frac{\prod_{i=3}^n N_i}{\prod_{i=3}^n N_j} = (-1)^m \frac{\text{product of driven tooth numbers}}{\text{product of driver tooth numbers}}$$

where  $m$  is the number of meshes involving external gears.

**EXAMPLE 12.1**  
**Analysis of a Compound Gear Train**

Assume that the compound gear train in Fig. 12.9 has the tooth numbers given in parentheses. The angular velocity of gear 2 is 200 rpm in the direction shown. Find the magnitude and direction of the angular velocity of gear 10 and the velocity (magnitude and direction) of the rack that is gear 11.



**FIGURE 12.9** The gear train for Example 12.1.

**Solution**

The velocity ratio for the gear drive between gears 2 and 9 is given by

$$\frac{\omega_9}{\omega_2} = \frac{N_2 N_4 N_6 N_8}{N_3 N_5 N_7 N_9}$$

Therefore,

$$\omega_9 = \omega_{10} = \omega_2 \frac{N_2 N_4 N_6 N_8}{N_3 N_5 N_7 N_9}$$

and

$$\omega_9 = \omega_{10} = 200 \frac{60}{48} \frac{80}{120} \frac{60}{40} \frac{2}{80} = 6.25 \text{ rpm}$$

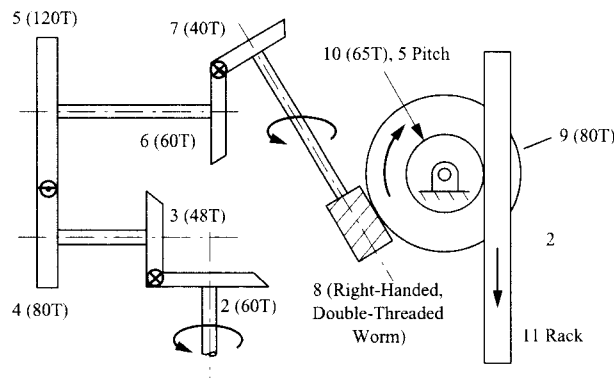
The velocity of the rack will be equal to the linear velocity of the pitch point on gear 10. The angular velocity of gear 10 is equal to the angular velocity of gear 9. The pitch diameter of gear 10 is given by

$$d_{10} = \frac{N_{10}}{P_{10}} = \frac{65}{5} = 13 \text{ in}$$

Therefore, the pitch velocity is given by

$$v = (\omega_{10})(d_{10}/2) = (6.25)(13/2)(2\pi/60) = 4.255 \text{ in/s}$$

However, we must now determine in which direction the rack moves (up or down). To do this, trace the pitch point velocities at each mesh. This is shown in Fig. 12.10. Gear 8 is a right-handed worm gear. Therefore, it will advance relative to gear 9 for a clockwise rotation. Consequently, gear 9 will rotate clockwise relative to the frame (link 1). If gear 9 and 10 rotate clockwise, then the rack will move down as shown.



**FIGURE 12.10** The directions of gear motion for Example 12.1.

### 12.4.1 Concentric Gear Trains

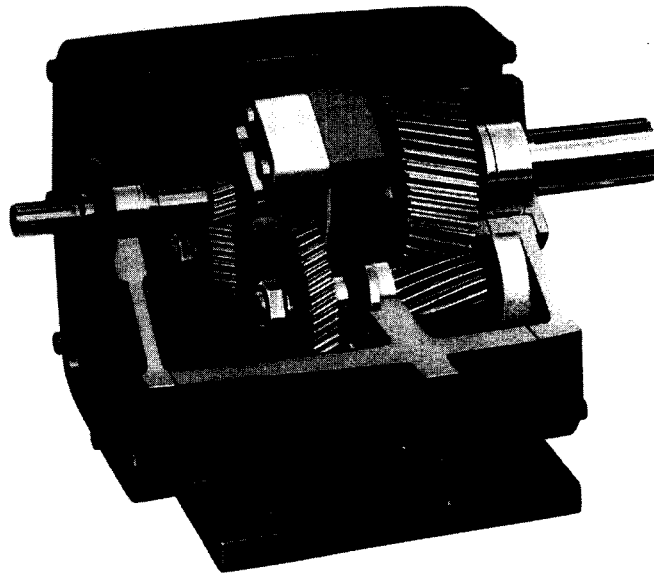
In a concentric gear train, the input and output shafts are collinear. An example of a concentric gear train is shown in Fig. 12.11. These gear trains are analyzed in much the same way as any compound gear train; however, the design is somewhat more complex. In the following, we will restrict the discussion to parallel-shaft gearing with a double reduction to illustrate a possible design procedure.

A concentric gear train with a two-stage reduction is shown in Fig. 12.12. A principal requirement for a concentric gear reducer is that

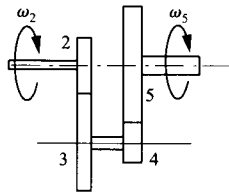
$$r_2 + r_3 = r_4 + r_5 \quad (12.13)$$

In addition, there may be a precise requirement for the overall reduction ratio. From before, the reduction ratio is given by

$$R = \frac{\omega_2}{\omega_5} = \frac{r_3}{r_2} \frac{r_5}{r_4} = \frac{N_3}{N_2} \frac{N_5}{N_4} \quad (12.14)$$



**FIGURE 12.11** A concentric gear reducer. (Courtesy of Rockwell Automation Dodge, Greenville, South Carolina.)



**FIGURE 12.12** A concentric gear reducer with a two-stage reduction.

To mesh properly, gears 2 and 3 must have the same normal pitch, and gears 4 and 5 must have the same normal pitch. If helical gears are involved, we must select the helix angles, and this will give us some latitude in the design. Then,

$$\begin{aligned} \frac{N_2}{2r_2} &= P_{n_2} \cos \psi_2 \\ \frac{N_3}{2r_3} &= P_{n_2} \cos \psi_2 \end{aligned} \tag{12.15}$$

and

$$\begin{aligned} \frac{N_4}{2r_4} &= P_{n_4} \cos \psi_4 \\ \frac{N_5}{2r_5} &= P_{n_4} \cos \psi_4 \end{aligned} \tag{12.16}$$

In Eqs. (12.13)–(12.16) there are 12 unknowns and 6 equations. In addition, there is the constraint that the tooth numbers must be integers. Therefore, we can select six of the variables to solve the equations subject to the constraint that the tooth numbers are integers.

One design approach is to select first the tooth numbers to satisfy Eq. (12.14), which is typically the most difficult equation to satisfy. This is equivalent to selecting three of the variables. It may not always be easy or even possible to select tooth numbers in a practical range to solve Eq. (12.14) exactly. If the values of  $R$  are formed by ratios of small whole numbers, for example  $1/2$ ,  $7/4$ , or  $4/9$ , many choices of whole numbers will satisfy the problem. In such cases, the best choice can be selected on the basis of criteria other than kinematics. However, other values of  $R$  are impossible to generate with simple gears. Examples are the square root of 2 and the ratio of two prime numbers (e.g., 503/2003). In such cases, it may only be possible to approximate the value for  $R$ .

When the machine function does not require an exact ratio, it is usual to select tooth numbers for a meshing gear pair that do not have common factors. This improves wear performance, because a defect on a gear tooth of one gear will make contact with all of the teeth on the mating gear equally rather than selectively making contact with a small number of teeth.

A number of elegant procedures are available for selecting the tooth numbers given  $R$  especially when  $R$  is given as a fraction where the numerator and denominator are whole numbers.<sup>1</sup> Such procedures may be aided by tables of factors. For example, if  $R = p/q$ , we would look for values of  $N_3$  and  $N_5$  such that  $N_3N_5 = p$  and values of  $N_2$  and  $N_4$  such that  $N_2N_4 = q$ . Alternatively, if the ranges for the tooth numbers are limited, we might simply conduct an exhaustive search for all possible combinations of tooth numbers that satisfy the condition for  $R$ . On modern computers, such a search is easy to program and takes very little time to conduct. A simple MATLAB program, *factor.m*, for finding factors of any integer is included on the disk with this book.

After the tooth numbers are established, we can select one of the normal diametral pitches, for example,  $P_{n_3}$ , and the corresponding helix angle ( $\psi_2$ ). Then solve for  $r_2$  and  $r_3$ . Given  $r_2$  and  $r_3$ , Eqs. (12.13) and (12.16) can be solved for  $r_4$ ,  $r_5$ , and  $P_{n_4} \cos \psi_4$ . Pick a standard value for  $P_{n_4}$ , and solve for the helix angle,  $\psi_4$ .

This discussion deals with kinematics alone. Obviously, other very important aspects of gear design are stress and wear considerations. The topic is properly treated in almost any book on machine design. Therefore, we will limit our discussion to kinematics with the assumption that sizing the teeth to carry the loading will be addressed elsewhere.

### EXAMPLE 12.2 Concentric Gearbox Design

#### Solution

Assume that a concentric gearbox is to be designed for a velocity ratio of  $R = 20:1$ . The first stage reduction is to have a helix angle of  $30^\circ$  and normal diametral pitch of 8. Both sets of gears will have a normal pressure angle of  $20^\circ$ . Find values for the tooth numbers, pitch cylinder radii for all of the gears, and the diametral pitch and helix angle for gears 4 and 5.

To avoid undercutting, we will limit the tooth numbers for  $N_2$  and  $N_3$  to 12 teeth (see Table 11.1). For the smallest possible gear box, assume that  $N_2$  is 12. Initially, select  $N_4$  to be 12 also. If the minimum helix angle for gears 4 and 5 is found to be less than  $30^\circ$ , we can specify it to be  $30^\circ$ , which will make 12 an acceptable tooth number. If the helix angle must be larger than  $30^\circ$ , the minimum value for  $N_4$  could be smaller than 12. The velocity ratio can be written as

$$R = \frac{20n}{n}$$

where  $n$  is any integer. From Eq. (12.14),  $n = N_2N_4$ . Therefore,  $n = 144$ , and  $20n$  is 2880.

To determine the factors for 2880, the MATLAB factor program was used. There are 42 factors for 2880. These are 1, 2, 3, 4, 5, 6, 8, 9, 10, 12, 15, 16, 18, 20, 24, 30, 32, 36, 40, 45, 48, 60, 64, 72, 80, 90, 96, 120, 144, 160, 180, 192, 240, 288, 320, 360, 480, 576, 720, 960, 1440, and 2880. When designing the two-stage gear reducer, it is generally desirable to make the two gear reductions about the same. This avoids making one gear significantly larger than the others. Of the factors, 48 and 60 will give gear reductions of 4 and 5 for the two stages. Let us select 60 for the first stage ( $N_3$ ) and 48

for the second stage ( $N_5$ ). This will permit larger teeth (lower  $P_n$ ) on the low-speed end of the gear reducer without making the gear diameters significantly larger than those for the high-end gears.

From Eqs. (12.15),

$$r_2 = \frac{N_2}{2P_{n_2} \cos \psi_2} = \frac{12}{2(8) \cos 30^\circ} = 0.866 \text{ in}$$

and

$$r_3 = \frac{N_3}{2P_{n_3} \cos \psi_3} = \frac{N_3}{2P_{n_2} \cos \psi_2} = \frac{60}{2(8) \cos 30^\circ} = 4.330 \text{ in}$$

From Eqs. (12.16),

$$\frac{N_4}{N_5} = \frac{r_4}{r_5} = \frac{12}{48} = \frac{1}{4}$$

Therefore,

$$r_5 = 4r_4$$

Substituting this expression into Eq. (12.13) gives

$$5r_4 = r_2 + r_3 = 0.866 + 4.330 = 5.196 \text{ in}$$

Therefore,

$$r_4 = \frac{5.196}{5} = 1.039 \text{ in}$$

and

$$r_5 = 4r_4 = 4(1.039) = 4.156 \text{ in}$$

The only unknowns are  $P_{n_4}$  and  $\psi_4$ . From Eqs. (12.16),

$$P_{n_4} \cos \psi_4 = \frac{N_4}{2r_4} = \frac{12}{2(1.039)} = 5.775$$

To illustrate the procedure, select a normal diametral pitch of 7. Then

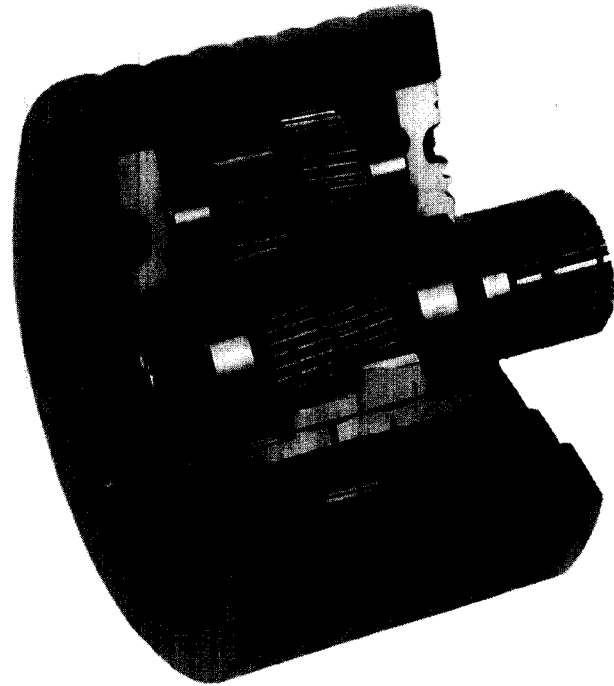
$$\psi_4 = \cos^{-1} \left( \frac{5.775}{7} \right) = \cos^{-1}(0.825) = 34.4^\circ$$

Note that in this example we have arbitrarily selected the diametral pitches. In an actual problem, these, along with the face widths, would be selected in part to accommodate the torque and speed requirements.

## 12.5 PLANETARY GEAR TRAINS

Both simple and compound gear trains have the restriction that their gear shafts must rotate in bearings fixed to the frame. However, this is a requirement that limits the versatility of the gear train. If one or more shafts rotate around another shaft as well as spinning about their own axes, the gear train is called a *planetary* or *epicyclic gear train*. Planetary gear trains are used extensively for compact gear reducers (Fig. 12.13). Also, because they are

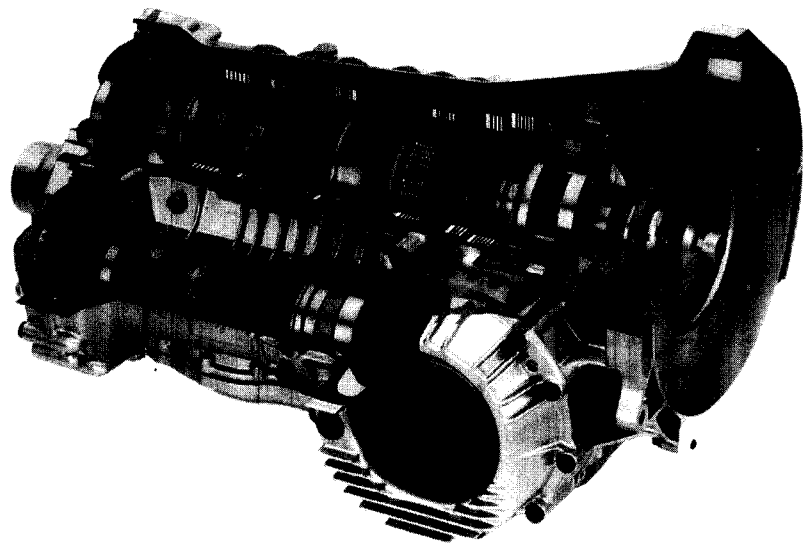




**FIGURE 12.13** A planetary gear reducer. (Courtesy of Andantex U.S.A., Wanamassa, New Jersey.)

basically devices with multiple degrees of freedom, they are used in automatic transmissions for automobiles and trucks (Fig. 12.14).

Determining the velocity ratio for planetary gear trains is more difficult than for plain simple and compound gear trains. The motion of the gears involves the motion of the moving shaft or carrier along with the motion of the gears with respect to the carrier.



**FIGURE 12.14** Planetary gears in an automatic transmission. (Courtesy of Zahnradfabrik Passau GmbH, Germany.)

### 12.5.1 Planetary Gear Nomenclature

A simple planetary drive is shown schematically in Fig. 12.15. Planetary gear trains are typically made up of the following:

1. a sun gear (which may or may not be fixed),
2. planet gears (one or more),
3. a planet carrier, and
4. an internal ring gear (not used in all planetary gear trains).

The symbolism used to represent planetary drives is also shown in Fig. 12.15. This symbolism allows the designer to represent the structure of the planetary drive simply.

In Fig. 12.15, note that the carrier, ring gear, and sun gear all rotate about concentric axes. Also, three axes are evident from the simple figure. As shown in the following, the planetary gear train has two degrees of freedom, and the angular motion of two of the axes must be specified before the angular motion of the third can be determined.

Very high velocity reductions can be achieved with compound planetary gear trains. These systems involve compound planetary gears as shown in Fig. 12.16a. This also permits the ring gear in Fig. 12.15 to be replaced by another sun gear. The carrier can involve several shafts containing four or more planetary gears as shown in Fig. 12.16b for still greater reductions. And finally, it is possible to connect planetary gears in series as shown in Fig. 12.16c. In Fig. 12.16, the bearings associated with the frame link are not shown. It is understood that frame bearings will be required for all of the shafts rotating with fixed axes.

In the planetary gear trains indicated in Fig. 12.16, two of the shafts are inputs and one is the output. Typically, the angular velocity of one of the bodies is zero, but this is not required.

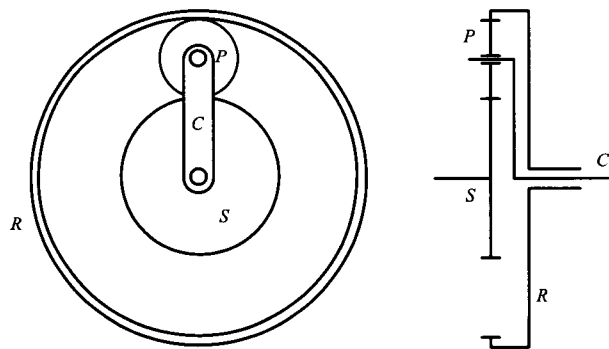


FIGURE 12.15 A simple planetary gear train.

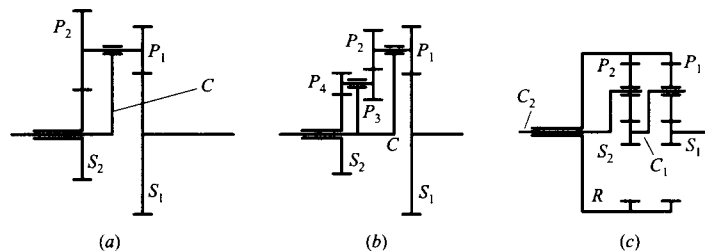
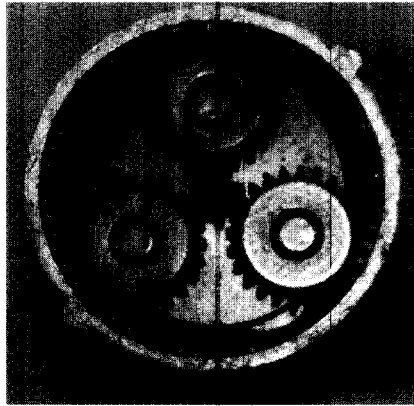


FIGURE 12.16 Complex planetary gear trains.

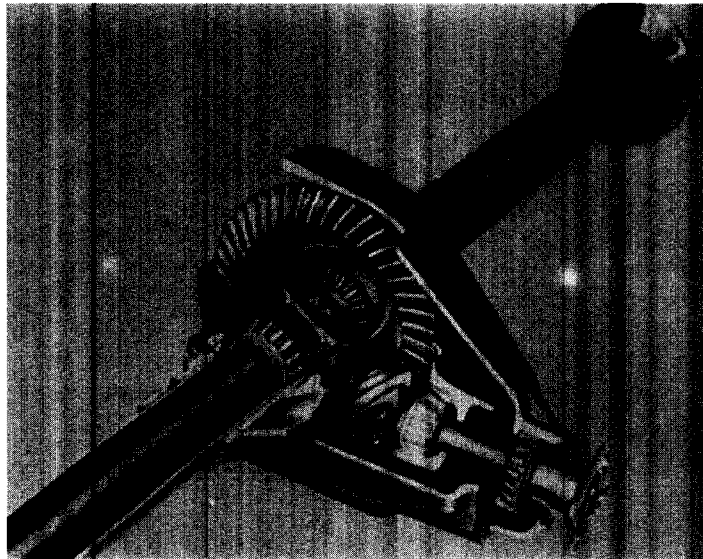
When planetary gear trains are connected in series, very high gear reductions are possible. Such gear reducers are common in small power tools. Figure 12.17 shows a small planetary gear reducer made up of two planetary systems in series used in a power screwdriver.

In Figs. 12.13–12.17, all of the gears in the planetary drives are parallel-shaft gears. However, this is not necessary. Perhaps the most common planetary drive is the differential (Fig. 12.18) in automobiles. This is a right-angle drive that involves a hypoid ring gear and pinion and bevel gear planets.

Planetary gear trains are commonly analyzed using either the equation method or the tabular method. We will look at each procedure separately by analyzing example gear trains.



**FIGURE 12.17** Planetary gear trains used in a power screwdriver.



**FIGURE 12.18** A planetary gear train used in the differential of a rear-wheel-driven vehicle. (Courtesy of The Gleason Works, Rochester, NY.)

### 12.5.2 Analysis of Planetary Gear Trains Using Equations

In the equation method, the procedure is to write relative angular velocity equations (relative to the frame) for each of the gears with fixed rotation axes. Also, write relative velocity equations for the same gears relative to the carrier. If the angular velocities of two of the shafts are given, this procedure will always yield enough equations to solve for the angular velocities of all of the members in the system.

**EXAMPLE 12.3**  
**Basic Procedure**  
**Using the**  
**Equation Method**

**Solution**

Assume that the gear train in Fig. 12.15 has the frame as member 1, the sun gear as member 2, the planet as member 3, and the ring gear as member 4. Gear 2 is the input and rotates CW with an angular velocity of  $\omega_2$ . Find an equation that involves the angular velocity of the carrier,  $\omega_c$ ,  $\omega_4$ , and the tooth numbers for the individual gears.

There are two gears (2 and 4) that rotate about fixed axes in the system, and we can write the following angular velocity relationships for these gears using the chain rule for angular velocities:

$$\omega_2 = {}^C\omega_2 + \omega_c \quad (12.17)$$

and

$$\omega_4 = {}^C\omega_4 + \omega_c \quad (12.18)$$

If we make the carrier the reference link, the gears will move as an ordinary gear train in which the planet gear acts as an idler. Therefore, we can compute the velocity ratio relative to the carrier as

$$\frac{{}^C\omega_2}{{}^C\omega_4} = -\frac{N_4}{N_2} \quad (12.19)$$

Next solve Eqs. (12.17) and (12.18) for  ${}^C\omega_2$  and  ${}^C\omega_4$ , respectively. Then

$${}^C\omega_2 = \omega_2 - \omega_c \quad (12.20)$$

and

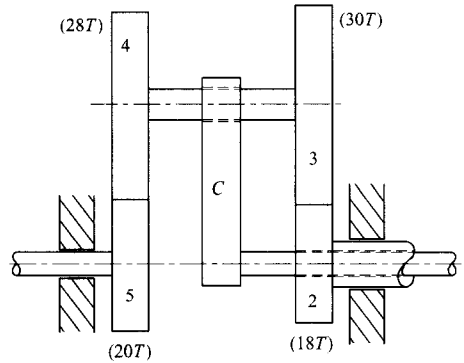
$${}^C\omega_4 = \omega_4 - \omega_c \quad (12.21)$$

Now divide Eq. (12.20) by (12.21) and equate the result to Eq. (12.19). The result is

$$\frac{\omega_2 - \omega_c}{\omega_4 - \omega_c} = -\frac{N_4}{N_2} \quad (12.22)$$

**EXAMPLE 12.4**  
**Analysis of a**  
**Planetary Gear**  
**Train Using the**  
**Equation Method**

Equation (12.22) gives the relationship for the velocities of the shafts coming from the gear train. Given any two of the angular velocities, the third can be determined. Note that it is important to identify the direction of the angular velocities with a plus or minus sign. Typically, we could select CCW as plus and CW as minus.



**FIGURE 12.19** The planetary gear train for Example 12.4.

### Solution

There are two gears (2 and 5) that rotate about fixed axes in the system. As in the case of the previous example, we can write the angular velocity relationships for these gears using the chain rule for angular velocities. The equations are

$$\omega_2 = {}^C\omega_2 + \omega_C \quad (12.23)$$

and

$$\omega_5 = {}^C\omega_5 + \omega_C \quad (12.24)$$

The angular velocity ratio of gears 2 and 5 relative to the carrier is

$$\frac{{}^C\omega_2}{{}^C\omega_5} = \frac{N_5 N_3}{N_4 N_2} \quad (12.25)$$

Notice that the velocity ratio is positive because both gears rotate in the same direction relative to the arm. Next solve Eqs. (12.23) and (12.24) for  ${}^C\omega_2$  and  ${}^C\omega_5$ , respectively. Then,

$${}^C\omega_2 = \omega_2 - \omega_C \quad (12.26)$$

and

$${}^C\omega_5 = \omega_5 - \omega_C \quad (12.27)$$

Now divide Eq. (12.26) by (12.27) and equate the result to Eq. (12.25). This gives

$$\frac{\omega_2 - \omega_C}{\omega_5 - \omega_C} = \frac{N_5 N_3}{N_4 N_2} \quad (12.28)$$

Assuming CCW as positive, from the problem statement,  $\omega_C = -150$  rpm and  $\omega_4 = -50$  rpm. The tooth numbers are given in Fig. 12.19. Substituting the known values into Eq. (12.28) gives

$$\frac{\omega_2 + 150}{-50 + 150} = \frac{20 \cdot 30}{28 \cdot 18}$$

or

$$\omega_2 + 150 = 119.04$$

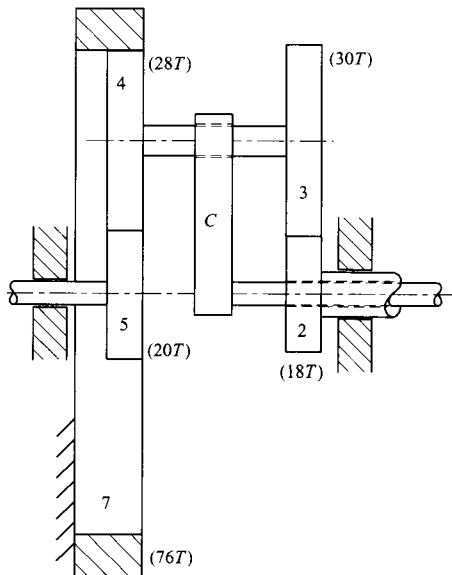
or

$$\omega_2 = -30.95 \text{ rpm}$$

Therefore, the velocity of gear 2 is 30.95 rpm in the CW direction.

**EXAMPLE 12.5**  
**Analysis of a**  
**Planetary Gear**  
**Train Using the**  
**Equation Method**

Assume that gear 2 in Fig. 12.20 is driven at a speed of 60 rpm in the CCW direction viewed from the right end. Gear 4 meshes with a fixed ring gear and with gear 5 as shown. Find the magnitude and direction of the angular velocity of gear 5.



**FIGURE 12.20** The planetary gear train for Example 12.5.

**Solution**

There are three gears (2, 5, and 7) that can rotate about fixed axes in the system. We include gear 7 in this list but ultimately will use the fact that its velocity is zero. As in Examples 12.3 and 12.4, we will solve the problem by writing relative velocity equations for all of the gears that have shafts that can rotate in fixed bearings. After rearranging, we have the resulting equations

$${}^C\omega_2 = \omega_2 - \omega_C \quad (12.29)$$

$${}^C\omega_5 = \omega_5 - \omega_C \quad (12.30)$$

and

$${}^C\omega_7 = \omega_7 - \omega_C \quad (12.31)$$

The angular velocity ratio of gears 2 and 5 relative to the carrier is

$$\frac{{}^C\omega_2}{{}^C\omega_5} = \frac{N_5 N_3}{N_4 N_2} \quad (12.32)$$

and that of gears 2 and 7 relative to the carrier is

$$\frac{{}^C\omega_2}{{}^C\omega_7} = -\frac{N_7 N_3}{N_4 N_2} \quad (12.33)$$

Now, divide Eq. (12.29) by Eq. (12.30) and equate the result with Eq. (12.32). This gives

$$\frac{\omega_2 - \omega_C}{\omega_5 - \omega_C} = \frac{N_5 N_3}{N_4 N_2} \quad (12.34)$$

Similarly, divide Eq. (12.29) by (12.31) and equate the result with Eq. (12.33) to get

$$\frac{\omega_2 - \omega_C}{\omega_7 - \omega_C} = -\frac{N_7 N_3}{N_4 N_2} \quad (12.35)$$

Equations (12.34) and (12.35) are the equations necessary for analyzing the planetary gear train. From the problem statement, we know that  $\omega_2 = 60$  rpm and  $\omega_7 = 0$ . With these known values, only  $\omega_C$  is unknown in Eq. (12.35). Substituting the known values into Eq. (12.35) gives

$$\frac{60 - \omega_C}{0 - \omega_C} = -\frac{76 \cdot 30}{28 \cdot 18} = -4.5238$$

Solving gives

$$\omega_C (1 + 4.5238) = 60 \Rightarrow \omega_C = 10.862 \text{ rpm}$$

Given  $\omega_C$  and  $\omega_2$ , we can solve Eq. (12.34) for  $\omega_5$ . Substituting the known values into Eq. (12.34) gives

$$\frac{60 - 10.862}{\omega_5 - 10.862} = \frac{20 \cdot 30}{28 \cdot 18} = 1.1905$$

Solving for  $\omega_5$  yields

$$\omega_5 - 10.862 = \frac{60 - 10.862}{1.1905} = 41.275 \Rightarrow \omega_5 = 52.137 \text{ rpm}$$

The value is positive, so  $\omega_5$  is rotating CCW when viewed from the right.

### EXAMPLE 12.6

**Analysis of  
Planetary Gear  
Trains in Series**

A two-stage planetary gear drive is represented in Fig. 12.21. Gear 2 is the input member, and carrier 7 is the output member. Gear 4 is a ring gear and is fixed. The carrier of the first stage is member 6, and it is rigidly connected to the gear that drives the second stage. Determine the velocity ratio of the gear drive.

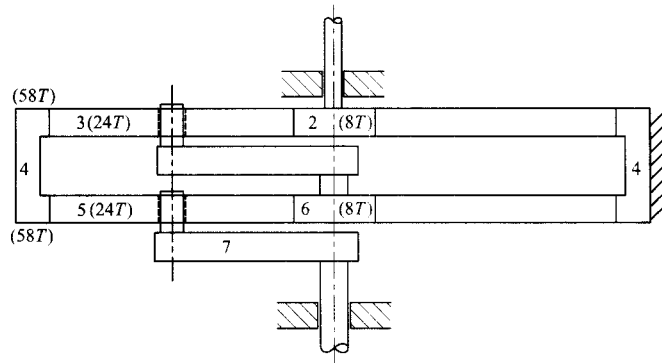


FIGURE 12.21 The planetary gear train for Example 12.6.

### Solution

There are three gears (2, 4, and 6) that can rotate about fixed axes in the system. Again, we will include the fixed ring gear in the equations and will set the velocity to zero once the equations are developed. As in the previous examples, we will solve the problem by writing relative velocity equations for all of the gears that have shafts that can rotate in fixed bearings. However, we must separate the two stages of the planetary drives when we write the equations. The first stage includes gears 2, 3, and 4 and the carrier is member 6. The second stage includes gears 6, 5, and 4 and carrier 7. The first stage can be analyzed independently of the second stage to determine the velocity of gear 6 in terms of the velocity of gear 2. The second stage can then be analyzed to determine the velocity of the

second carrier (7) in terms of the velocity of gear 6. By combining the results of both stages, the velocity of link 7 can be determined as a function of gear 2 to determine the overall velocity ratio of the gear train.

After being rearranged, the first-stage relative velocity equations are

$${}^6\omega_2 = \omega_2 - \omega_6 \quad (12.36)$$

$${}^6\omega_4 = \omega_4 - \omega_6 \quad (12.37)$$

The angular velocity ratio of gears 2 and 4 relative to the carrier (member 6) is

$$\frac{{}^6\omega_2}{{}^6\omega_4} = -\frac{N_4}{N_2} \quad (12.38)$$

Now, divide Eq. (12.36) by Eq. (12.37) and equate the result with Eq. (12.38). This gives

$$\frac{\omega_2 - \omega_6}{\omega_4 - \omega_6} = -\frac{N_4}{N_2} \quad (12.39)$$

Because  $\omega_4 = 0$ , this equation can be rewritten for  $\omega_6$  as a function of  $\omega_2$ . The result is

$$\omega_6 = \frac{\omega_2}{1 + N_4/N_2} \quad (12.40)$$

We can now analyze the second stage in exactly the same manner as the first stage except that now the gears are 6, 5, and 4, and the carrier is 7. After being rearranged, the second-stage relative velocity equations are

$${}^7\omega_6 = \omega_6 - \omega_7 \quad (12.41)$$

$${}^7\omega_4 = \omega_4 - \omega_7 \quad (12.42)$$

The angular velocity ratio of gears 4 and 6 relative to the carrier (member 7) is

$$\frac{{}^7\omega_6}{{}^7\omega_4} = -\frac{N_4}{N_6} \quad (12.43)$$

Now, divide Eq. (12.41) by Eq. (12.42) and equate the result with Eq. (12.43). This gives

$$\frac{\omega_6 - \omega_7}{\omega_4 - \omega_7} = -\frac{N_4}{N_6} \quad (12.44)$$

Because  $\omega_4 = 0$ , this equation can be rewritten for  $\omega_7$  as a function of  $\omega_6$ . The result is

$$\omega_7 = \frac{\omega_6}{1 + N_4/N_6} \quad (12.45)$$

Combining Eqs. (12.45) and (12.40) and substituting the known tooth numbers gives

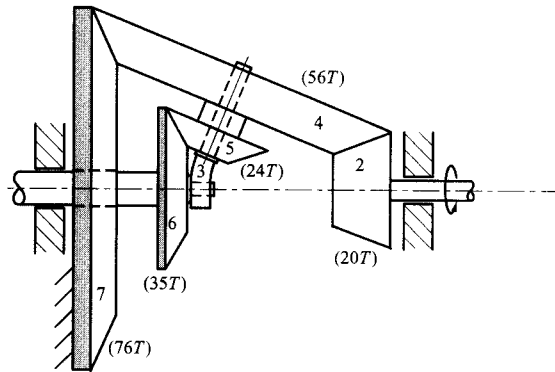
$$\frac{\omega_2}{\omega_7} = \left(1 + \frac{N_4}{N_2}\right) \left(1 + \frac{N_4}{N_6}\right) = \left(1 + \frac{58}{8}\right) \left(1 + \frac{58}{8}\right) = 68.06$$

Notice that, in this example, the size of the planet gears does not affect the velocity ratio. They will have an impact on the size of the gearbox, however. Also notice that members 2 and 7 both rotate in the same direction.



**EXAMPLE 12.7**  
**Analysis of a**  
**Planetary Gear**  
**Train with Bevel**  
**Gears**

All of the planetary gear trains considered in the previous examples involved only parallel-shaft gears. In this example, we will analyze a gear train with bevel gears. The gear train is shown in Fig. 12.22. The input to the gear train is gear 2 and the output is gear 6. The carrier is member 3, which rotates freely about the shaft on gear 6. Also, the compound planet gears (4 and 5) rotate about the axis of the carrier. Gear 7 is fixed to the frame. Assume that gear 2 rotates with an angular velocity of 100 rpm in the CCW direction viewed from the right. Find the angular velocity of gear 6.



**FIGURE 12.22** The planetary gear train for Example 12.7.

**Solution**

Even though bevel gears are involved, we can approach the analysis in exactly the same way that was used for the parallel-shaft gears. There are three gears (2, 6, and 7) that can rotate about fixed axes in the system. Again, we will include gear 7 in this list but ultimately will use the fact that its velocity is zero. As in the previous examples, we will solve the problem by writing relative velocity equations for all of the gears that have shafts that can rotate in fixed bearings. After being rearranged, the resulting equations are

$${}^3\omega_2 = \omega_2 - \omega_3 \quad (12.46)$$

$${}^3\omega_6 = \omega_6 - \omega_3 \quad (12.47)$$

and

$${}^3\omega_7 = \omega_7 - \omega_3 \quad (12.48)$$

The angular velocity ratio of gears 2 and 6 relative to the carrier (3) is

$$\frac{{}^3\omega_2}{{}^3\omega_6} = -\frac{N_4 N_6}{N_2 N_5} \quad (12.49)$$

In Eq. (12.49) we must determine the direction by inspection. This will show that if the carrier is fixed and the motion is inverted so that all of the other links and gears (including 4) can move relative to the carrier, gears 2 and 6 will move in opposite directions. Similarly, the motion of gears 2 and 7 relative to the carrier is

$$\frac{{}^3\omega_2}{{}^3\omega_7} = -\frac{N_7}{N_2} \quad (12.50)$$

Again, relative to the carrier, gears 2 and 7 are seen to move in opposite directions. Now, divide Eq. (12.46) by Eq. (12.48) and equate the result with Eq. (12.50). This gives

$$\frac{\omega_2 - \omega_3}{\omega_6 - \omega_3} = -\frac{N_4 N_6}{N_2 N_5} \quad (12.51)$$

Also divide Eq. (12.46) by Eq. (12.47) and equate the result to Eq. (12.49). This gives

$$\frac{\omega_2 - \omega_3}{\omega_7 - \omega_3} = -\frac{N_7}{N_2} \quad (12.52)$$

Equations (12.51) and (12.52) are the equations necessary for analyzing the planetary gear train. From the problem statement, we know that  $\omega_2 = 100$  and  $\omega_7 = 0$ . With these known values, only  $\omega_3$  is unknown in Eq. (12.52). Substituting the known values into Eq. (12.52) gives

$$\frac{100 - \omega_3}{0 - \omega_3} = -\frac{76}{20} = -3.8$$

Solving gives

$$\omega_3(1 + 3.8) = 100 \Rightarrow \omega_3 = 20.833 \text{ rpm}$$

Given  $\omega_3$  and  $\omega_2$ , we can solve Eq. (12.51) for  $\omega_6$ . Substituting the known values into Eq. 12.51) gives

$$\frac{100 - 20.833}{\omega_6 - 20.833} = -\frac{56}{20} = -4.0833$$

Solving for  $\omega_6$  gives

$$\omega_6 = \frac{100 - 20.833}{-4.0833} + 20.833 = 1.444 \text{ rpm}$$

The value is positive, so  $\omega_6$  is rotating in the same direction as  $\omega_2$ . Therefore,  $\omega_6$  is rotating when viewed from the right. The overall velocity ratio for the gearbox is

$$\frac{\omega_2}{\omega_6} = \frac{100}{1.444} = 69.2$$

### 12.5.3 Analysis of Planetary Gear Trains Using the Tabular Method

**Overview** The tabulation method is based on the knowledge that a planetary gear train is a linear system. The absolute angular velocity of any gear  $x$  that rotates about an axis fixed to the frame can be written as

$$\omega_x = {}^C\omega_x + \omega_C \quad (12.53)$$

where  $\omega_C$  is the absolute angular velocity of the carrier and  ${}^C\omega_x$  is the angular velocity of the gear relative to the carrier. Also, because Eq. (12.53) is linear, we can multiply the input values by a constant, and the output value will be multiplied by the same constant. The tabular method is based on the idea of the linear relationship shown in Eq. (12.53) and superposition.

A simple planetary gear train is fundamentally a two-degree-of-freedom device. Therefore, we must specify two input velocities or displacements to compute the unknown velocity or displacement. For discussion, consider the planetary gear train shown in Fig. 12.23. There is a compound gear for the planets and two sun gears, and the members are each assigned a number. Assume that the carrier is one of the input members, gear 2 is the other input member, and the known velocities are  $\omega_2$  and  $\omega_5$ , respectively.

Now let us fix all of the gears to the carrier and rotate all of the gears by the velocity  $\omega_5$ . Then all of the gears, including gear 2, will have an initial angular velocity of  $\omega_5$ . To correct the angular velocity of gear 2 without changing the angular velocity of the carrier, let

us fix the angular velocity of the carrier and move all of the gears relative to the carrier such that angular velocity of gear 2 ends up with the correct value when added to the velocity ( $\omega_5$ ) from step 1. This will also change all of the angular velocities in the gear train. The vector sum of the angular velocities from steps 1 and 2 for each gear will give the correct values. The vector sum is simply an algebraic sum because all of the gears have parallel shafts. The procedure, shown schematically in Fig. 12.23, is formalized in the tabular method of analysis as follows.

**Procedure** The tabulation method begins with a table in which there is one column for each member in the gear train and a row for each of the following three steps.

1. Assume that all of the gears are locked to the carrier, and rotate the assembly with an angular velocity equal to the angular velocity of the carrier member. Tabulate this velocity under each member in the train.
2. Fix the arm, and rotate the second input member such that it ends up with the proper input velocity when steps 1 and 2 are added together. Tabulate the resulting velocity for each member in the train.
3. Add the results from steps 1 and 2 for each member in the train.

We will illustrate the procedure on three examples.

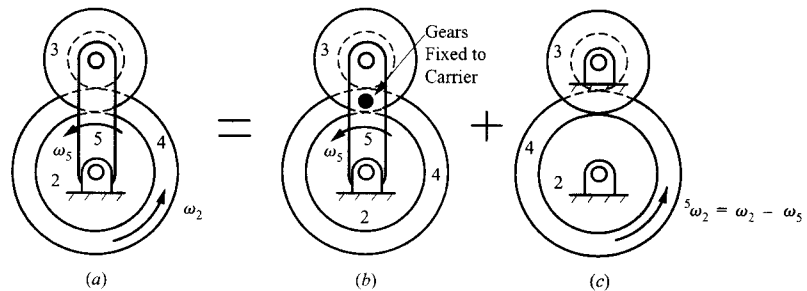


FIGURE 12.23 Analysis of a planetary drive using superposition.

**EXAMPLE 12.8**  
**Tabulation**  
**Method for a**  
**Simple Planetary**  
**Gear Train**

Assume that the planetary gear train in Fig. 12.24 has the frame as member 1, the sun gear as member 2, the planet gear as member 3, the ring gear as member 4, and the carrier as member 5. Gear 2 is the input and rotates CCW with an angular velocity of 100 rpm and the carrier rotates CCW with an angular velocity of 200 rpm. Find the angular velocities of gears 3 and 4.

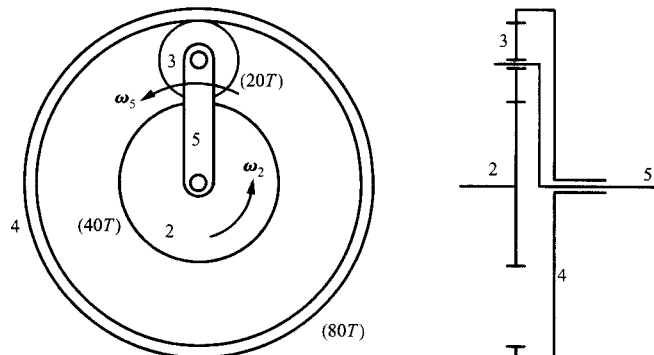


FIGURE 12.24 The planetary gear train for Example 12.8.

**Solution**

Following the aforementioned procedure, we can construct the solution table (Table 12.1). The four members of the system are associated with the columns, and the steps are associated with the rows. Step 1 of the procedure is to rotate the entire assembly by + 200 rpm, which is the velocity of the carrier. Next, we will fix the carrier and rotate gear 2 by the velocity required to make its total angular velocity 100 rpm. To do this, we need to rotate gear 2 by – 100 rpm relative to the arm.

**TABLE 12.1 Results for Example 12.8**

Step	Carrier 5 (rpm)	Gear 2 (rpm)	Gear 3 (rpm)	Gear 4 (rpm)
1. Gears locked	200	200	200	200
2. Carrier fixed	0	– 100	200	50
3. Total	200	100	400	250

When gear 2 rotates – 100 rpm relative to the carrier, gears 3 and 4 will also rotate. The angular velocity of gear 3 will be

$$\omega_3 = -\frac{N_2}{N_3}\omega_2 = -\frac{40}{20}(-100) = +200$$

and

$$\omega_4 = -\frac{N_2}{N_4}\omega_2 = -\frac{40}{80}(-100) = +50$$

These values are entered into Table 12.1. The results are obtained by adding the results from the first two steps. From this, it is apparent that gear 3 rotates 400 rpm and gear 4 rotates 250 rpm, both in the CCW (+) direction.

**EXAMPLE 12.9**

**Solution to  
Example 12.7  
Using the  
Tabulation  
Method**

**Solution**

Analyze the planetary gear train in Example 12.7 using the tabulation method.

The problem is to determine the velocity ratio for the gear train, where the velocity ratio is defined by  $\omega_2/\omega_6$ . If we set  $\omega_6 = 1$  and solve for the velocity of  $\omega_2$ , the velocity ratio will be given directly by the value for  $\omega_2$ . From the problem statement, we also know that  $\omega_7 = 0$ .

In the table, we will include only gears that rotate about axes that have bearings fixed to the frame. The planet gears rotate about the arm axis, which is skewed relative to the axis of the other gears. Therefore, the angular velocity of the planets is not obtained by a simple algebraic addition of the values from steps 1 and 2.

In the tabulation procedure, we assume that the velocity of the carrier is known. However, in this problem, the velocities of gears 6 and 7 are known. Therefore, we must treat the velocity of the carrier as unknown and solve for it. For step 1, assume that the gears are locked to the carrier and the assembly is turned by +  $x$  rpm. This is shown in Table 12.2. In step 2, we must rotate gear 7 such that when the results of the first two steps are added, the final velocity for gear 7 will be zero. Clearly, then, gear 7 must be rotated by –  $x$  rpm relative to the carrier. The remaining values in the second row of the table are determined by analyzing the gear train relative to the carrier.

**TABLE 12.2 Results for Example 12.9**

Step	Carrier 3(rpm)	Gear 2(rpm)	Gear 6(rpm)	Gear 7(rpm)
1. Gears locked	$x$	$x$	$x$	$x$
2. Carrier fixed	0	$x \frac{N_7}{N_2} = x \frac{76}{20}$	$-x \frac{N_7 N_5}{N_4 N_6}$ $= -x \frac{76 \cdot 24}{56 \cdot 35}$	$-x$
3. Total	$x$	$x \left[ 1 + \frac{76}{20} \right] = x(4.8)$	$x \left[ 1 - \frac{76 \cdot 24}{56 \cdot 35} \right]$ $= x(0.0694)$	0

Next sum the results from steps 1 and 2. From the problem statement, we know that  $\omega_6 = 1$ , and in the table, we can see that the velocity of gear 6 is also given by

$$\omega_6 = x(0.0694) = 1$$

Therefore,

$$x = 14.412$$

and

$$\omega_2 = x(4.8) = 14.412(4.8) = 69.2$$

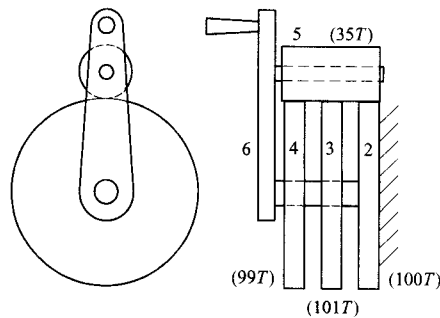
Therefore the velocity ratio for the planetary gear train is

$$\omega_2 / \omega_6 = 69.2$$

which is the same as that computed in Example 12.7.

**EXAMPLE 12.10**  
**Solution to**  
**Ferguson's**  
**Paradox Using the**  
**Tabulation**  
**Method**

An interesting application of planetary gearing is called the Ferguson's paradox.<sup>2</sup> The mechanism is shown in Fig. 12.25. Gear 2 is fixed to the frame, and gear 5 is a planet that rotates relative to the carrier, which is member 6. Gears 2, 3, and 4 have tooth numbers 99, 100, and 101, respectively. All of



**FIGURE 12.25** The planetary gear train for Example 12.10.

the gears are cut from the same blank so that they will all mesh with gear 5, which has 20 teeth. If the arm makes 100 revolutions CCW, determine the number of revolutions made by gears 3, 4, and 5.

**Solution**

Based on the problem statement, we know that the carrier moves 100 revolutions and gear 2 is fixed. As in the previous examples, the first step is to fix all of the gears to the arm and rotate the assembly by 100 turns. This is shown in Table 12.3. In step 2, we must rotate gear 2 such that when the results of the first two steps are added, the final velocity for gear 2 is zero. Therefore, gear 2 must be rotated by  $-100$  rpm relative to the carrier. The remaining values in the second row of the table are determined by analyzing the gear train relative to the carrier.

Next sum the results from steps 1 and 2. The number of turns made by each gear in the mechanism is shown in the third row of Table 12.3. Notice that gear 3 makes 1 revolution in the direction of the motion of the carrier while gear 4 makes 1 revolution in the opposite direction. Gear 2 is fixed by design. Therefore, as the carrier is turned, gear 3 will rotate very slowly in the direction of the carrier and gear 4 will rotate very slowly in the opposite direction.

**TABLE 12.3 Results for Example 12.10**

Step	Carrier 6 (revolution)	Gear 2 (revolutions)	Gear 3 (revolutions)	Gear 4 (revolutions)	Gear 5 (revolutions)
1. Gears locked	100	100	100	100	100
2. Carrier fixed	0	$-100$	$-100/1.01$	$-100/0.99$	$-100/35$
3. Total	100	0	1	$-1$	97.14

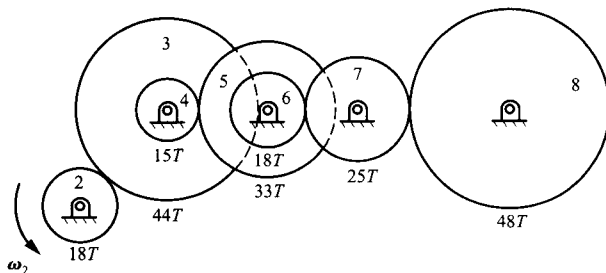
**REFERENCES**

<sup>1</sup>Merritt, H. E., *Gear Engineering*, John Wiley & Sons, New York (1971).

<sup>2</sup>Shigley, J. E., *Kinematic Analysis of Mechanisms*, McGraw-Hill Book Co., New York (1975).

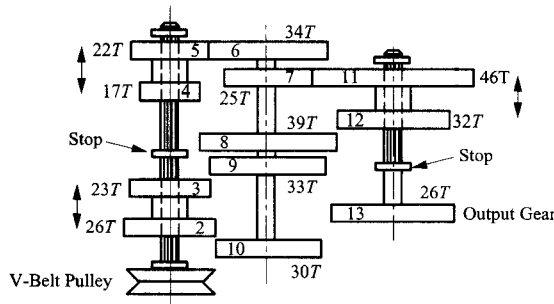
**PROBLEMS****EXERCISE PROBLEMS INVOLVING COMPOUND GEAR TRAINS**

**12.1** Find the angular velocity of gear 8 if the angular velocity of gear 2 is 800 rpm in the direction shown.

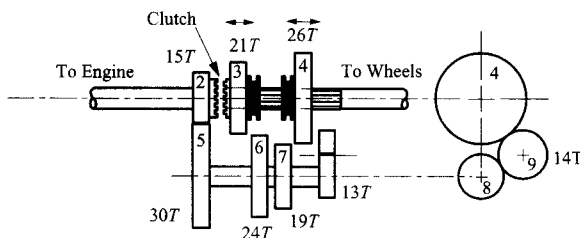


**12.2** Find the velocity of gear 8 in Problem 12.1 if the angular velocity of the driver (gear 2) is 300 rpm in the CW direction.

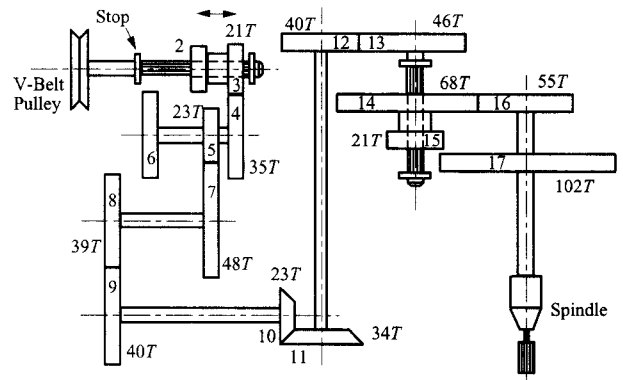
**12.3** The gear train given is for a machine tool. Power is input to the gearbox through the pulley indicated, and the output power to the machine table is through gear 13. Gears 2 and 3, 4 and 5, and 11 and 12 are compound gears that can move axially on splined shafts to mesh with various different gears so that various combinations of overall gear ratios ( $\omega_{13}/\omega_2$ ) can be produced. Determine the number of ratios possible and the overall gear ratio for each possibility.



**12.4** A simple three-speed transmission is shown. The power flow is as follows: (a) First gear: Gear 4 is shifted to mesh with gear 7; power flows through gears 2, 5, 7, and 4. (b) Second gear: Gear 3 is shifted to mesh with gear 6; power flows through gears 2, 5, 6, and 3. (c) Third gear: Gear 3 is shifted so that the clutch teeth on gear 3 mesh with those on gear 2; a direct drive results. (d) Reverse gear: Gear 4 is shifted to mesh with gear 9; power flows through gears 2, 5, 8, 9, and 4. An automobile with this transmission has a differential ratio of 3:1 and a tire outside diameter of 24 in. Determine the engine speed for the car under the following conditions: (i) first gear with the automobile traveling at 15 mph, (ii) third gear with the automobile traveling at 55 mph, and (iii) reverse gear with the automobile traveling at 3.5 mph.



**12.5** Part of the gear train for a machine tool is shown. Compound gears 2 and 3 slide on a splined shaft so that gear 3 can mesh with gear 4 or gear 2 can mesh with gear 6. Also, compound gears 14 and 15 slide on a splined shaft so that gear 14 can mesh with gear 16 or gear 15 can mesh with gear 17. (a) If gear 3 meshes with gear 4, what are the two possible spindle speeds for a motor speed of 1800 rpm? (b) Now assume that gear 14 meshes with gear 16, and gear 2 meshes with gear 6. Gears 2, 3, 4, and 6 are standard and have the same diametral pitch. What are the tooth numbers on gears 2 and 6 if the spindle speed is  $130 \pm 3$  rpm?



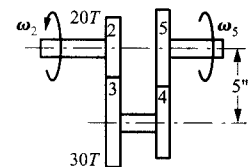
**12.6** An internal gear having 160 teeth and rotating CCW at 30 rpm is connected through a gear train to an external gear, which rotates at 120 rpm in the CCW direction. Using the minimum number of gears, select gears from the following list that will satisfy the design requirements. Tooth numbers for the available gears are 20, 22, 25, 30, 32, 34, 35, 40, 50, 55, 60, and 64. There is only one gear with each tooth number, and each gear has the same diametral pitch.

**12.7** Re-solve Problem 12.6 if the external gear is concentric with the internal gear (i.e., the rotation axis is the same for both gears) and the external gear rotates clockwise.

**12.8** Re-solve Problem 12.6 if the external gear is concentric with the internal gear and the external gear rotates counter-clockwise.

**12.9** Re-solve Problem 12.6 if the external gear rotates at 50 rpm.

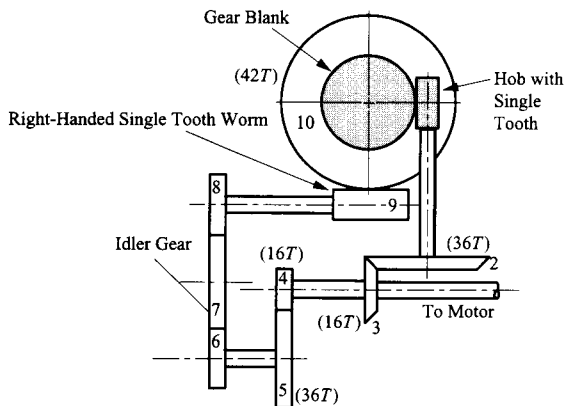
**12.10** A gear reducer is to be designed as shown in the figure. Determine the diametral pitch and number of teeth on gears 4 and 5 if the speed of gear 2 ( $\omega_2$ ) is to be 10 times the speed of gear 5 ( $\omega_5$ ). The pitches of the two gears should be as nearly equal as possible, and no gear should have fewer than 15 teeth.



**12.11** Re-solve Problem 12.10 if  $\omega_2$  is to be 8 times the speed of gear 5 ( $\omega_5$ ).

**12.12** Re-solve Problem 12.10 if  $\omega_2$  is to be 6.5 times the speed of gear 5 ( $\omega_5$ ).

**12.13** The gear train shown is a candidate for the spindle drive of a gear hobbing machine. The gear blank and the worm gear (gear 10) are mounted on the same shaft and rotate together. If the gear blank is to be driven clockwise, determine the hand of the hob. Also determine the velocity ratio ( $\omega_8/\omega_6$ ) to cut 72 teeth on the gear blank.



**12.14** Assume that the input shaft of a transmission rotates CW at 1800 rpm. The output shaft is driven at 160 rpm in the CCW direction. None of the gears in the transmission is to be an idler, and the gear ratio at any given mesh is not to exceed 3:1. Gears are available that have all tooth numbers between 13 and 85; however, only one gear is available with each tooth number. Select the appropriate gears for the transmission, and sketch the configuration designed. Label the gears and tooth numbers.

**12.15** Re-solve Problem 12.14 if the output shaft rotates at 210 rpm in the CCW direction.

**12.16** Re-solve Problem 12.14 if the output shaft rotates at 200 rpm in the CW direction.

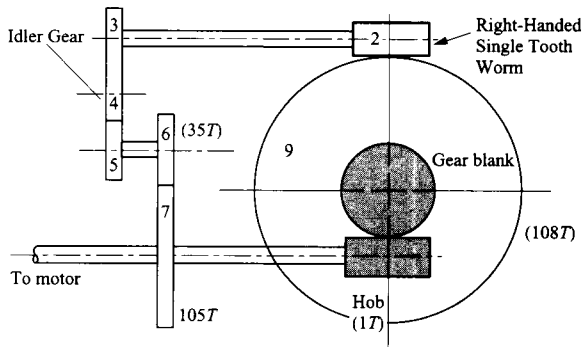
**12.17** A simple gear reduction is to be used to generate a gear ratio equal to  $\pi$ . Make up a table of possible gear ratios where the maximum number of teeth on either gear is 100. This can be conveniently done using a simple computer program. Identify the gear set that most closely approximates the desired ratio. What is the error?

**12.18** A simple gear reduction is to be used to generate the gear ratio 0.467927. Make up a table of possible gear ratios where the maximum number of teeth on either gear is 100. Identify the gear set that most closely approximates the desired ratio. What is the error?

**12.19** A simple gear reduction is to be used to generate a gear ratio equal to  $\sqrt{2}$ . Make up a table of possible gear ratios where the maximum number of teeth on either gear is 100. Identify the gear set that most closely approximates the desired ratio. What is the error?

**12.20** An alternative gear train is shown as a candidate for the spindle drive of a gear hobbing machine. The gear blank and the worm gear (gear 9) are mounted on the same shaft and rotate together. If the gear blank is to be driven clockwise, determine

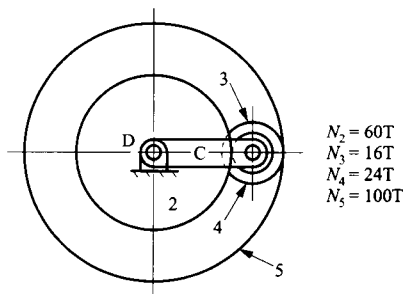
the hand of the hob. Next determine the velocity ratio ( $\omega_7/\omega_5$ ) to cut 75 teeth on the gear blank. Finally, select gears 3 and 5 that will satisfy the ratio. Gears are available that have all of the tooth numbers from 15 to 40.



**12.21** A simple gear reduction unit is to be used to generate the gear ratio 2.105399. Make up a table of possible gear ratios where the maximum number of teeth on all gears is 100. Identify the gear set that most closely approximates the desired ratio. Note that this can be done most easily with a computer program. What is the error?

**EXERCISE PROBLEMS INVOLVING PLANETARY GEAR TRAINS**

**12.22** In the gear train shown, gears 3 and 4 are integral. Gear 3 meshes with gear 2, and gear 4 meshes with gear 5. If gear 2 is fixed and  $\omega_5 = 100$  rpm CCW, determine the angular velocity of the carrier.

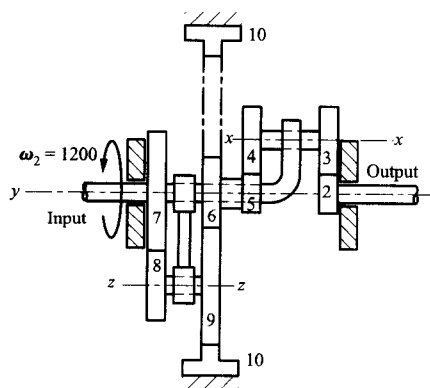


**12.23** Re-solve Problem 12.20 if gear 5 is fixed and  $\omega_5 = 100$  rpm CCW.

**12.24** Re-solve Problem 12.20 when  $N_2 = 70T$ ,  $N_3 = 35T$ ,  $N_4 = 15T$ , and  $N_5 = 12T$ .

**12.25** In the figure given, axis  $y-y$  is fixed whereas axes  $x-x$  and  $z-z$  move with the arm. Gear 7 is fixed to the carrier. Gears 3 and 4, 5 and 6, and 8 and 9 are fixed together, respectively. Gears 3 and 4 move with planetary motion. If the tooth numbers are  $N_2 = 16T$ ,  $N_3 = 20T$ ,  $N_4 = 22T$ ,  $N_5 = 14T$ ,  $N_6 = 15T$ ,  $N_7 = 36T$ ,  $N_8 = 20T$ ,  $N_9 = 41T$ , and  $N_{10} = 97T$ , determine the speed and direction of the output shaft.

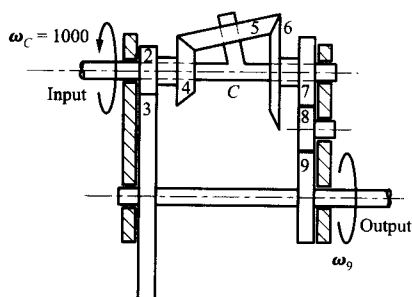




**12.26** Re-solve Problem 12.25 when  $N_2 = 16T$ ,  $N_3 = 20T$ ,  $N_4 = 16T$ ,  $N_5 = 20T$ ,  $N_6 = 15T$ ,  $N_7 = 40T$ ,  $N_8 = 15T$ ,  $N_9 = 40T$ , and  $N_{10} = 95T$ .

**12.27** Re-solve Problem 12.25 when  $N_2 = 14T$ ,  $N_3 = 30T$ ,  $N_4 = 14T$ ,  $N_5 = 30T$ ,  $N_6 = 15T$ ,  $N_7 = 60T$ ,  $N_8 = 15T$ ,  $N_9 = 60T$ , and  $N_{10} = 135T$ .

**12.28** In the gear train shown, gears 2 and 4, 6 and 7, and 3 and 9 are fixed together. If the angular velocity of the carrier is given, determine the angular velocity of gear 9.

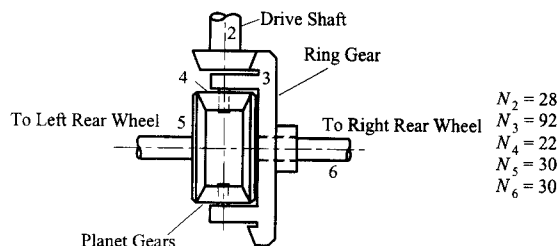


- $N_2 = 20$
- $N_3 = 90$
- $N_4 = 30$
- $N_5 = 90$
- $N_6 = 50$
- $N_7 = 30$
- $N_8 = 20$
- $N_9 = 40$

**12.29** Re-solve Problem 12.28 if  $N_2 = 10T$ ,  $N_3 = 100T$ ,  $N_7 = 20T$ ,  $N_8 = 10T$  and  $N_9 = 70T$ .

**12.30** Re-solve Problem 12.28 but assume that the shaft connecting gears 3 and 9 is the input shaft and the shaft of the carrier is the output shaft. Assume  $\omega_9 = 500$  rpm CCW and compute  $\omega_c$ .

**12.31** The differential for a rear-wheel-driven vehicle is shown schematically. If the drive shaft turns at 900 rpm, what is the speed of the vehicle if neither wheel slips and the outside diameter of the wheels is 24 in?

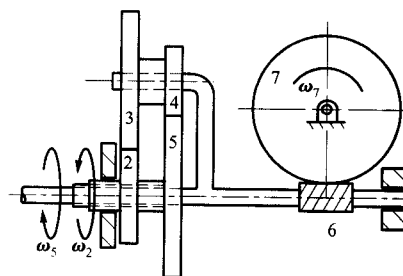


- $N_2 = 28$
- $N_3 = 92$
- $N_4 = 22$
- $N_5 = 30$
- $N_6 = 30$

**12.32** Assume that the vehicle in Problem 12.31 is stopped so that the right wheel sits on a small icy patch and can spin freely while the left wheel does not spin. Determine the angular velocity of the right wheel if the angular speed of the drive shaft is 500 rpm.

**12.33** Assume that the vehicle in Problem 12.31 is traveling at 35 mph and turns around a curve with a radius of 50 ft from the centerline of the vehicle. The center-to-center distance between the treads of the right and left wheels is 60 in. Compute the rotational speed of each rear wheel, the rotational speed of the ring gear, and the rotational speed of the drive shaft.

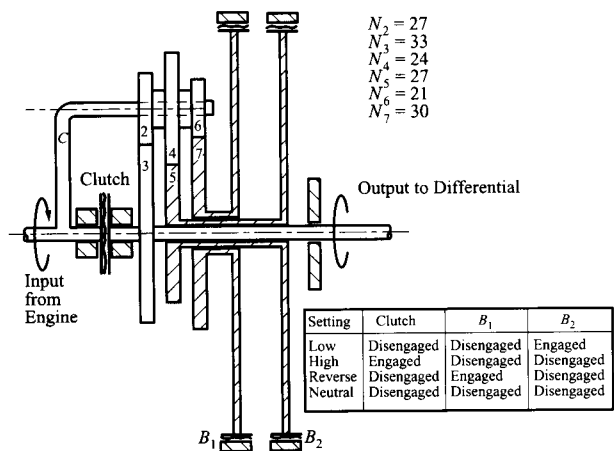
**12.34** In the mechanism shown, derive an expression for the angular velocity of gear 7 ( $\omega_7$ ) in terms of  $\omega_2$  and  $\omega_5$ , and the tooth numbers  $N_2, N_3, N_4, N_5, N_6$ , and  $N_7$ . Take counterclockwise viewing from the left as positive for the rotation of gears 2, 3, 4, 5, and 6. Viewed from the front of the page, take counterclockwise as the positive direction for gear 7.



**12.35** In Problem 12.34, assume that  $\omega_2 = 100$  rpm,  $\omega_5 = 60$  rpm,  $N_2 = 40T$ ,  $N_3 = 60T$ ,  $N_4 = 30T$ ,  $N_5 = 70T$ ,  $N_6 = 8T$ , and  $N_7 = 50T$ . Determine the angular velocity of both gears 6 and 7.

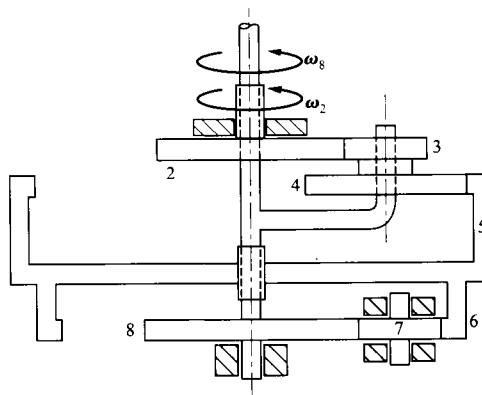
**12.36**<sup>1</sup> The figure on the next page shows a schematic diagram of a semiautomatic transmission from the Model-T automobile. This was the forerunner of today's automatic transmission. A plate clutch, two banded clutches, and a system of pedals and levers (used to engage and disengage these plate and band clutches) operated in the proper sequence are shown in the table. Determine the output/input speed ratio for each condition.

<sup>1</sup>Problem courtesy of Dr. Michael Stanisic, Notre Dame University.



12.37 In problem 12.36, if the engine rotates at 400 rpm determine the angular velocity of gear 5 when the transmission is in low gear.

12.38 In the mechanism shown, let the input be gear 2 and assume that all of the gear tooth numbers ( $N_2, N_3, N_4, N_5, N_6, N_7,$  and  $N_8$ ) are known. Derive an expression for the angular velocity of gear 8.



# STATIC FORCE ANALYSIS OF MECHANISMS

## 13.1 INTRODUCTION

Machines are used to apply mechanical force, energy, or power for useful purposes. So far, in this book, we have been concerned only with motion. However, mechanisms are used to transmit and apply force, as well as to generate desired motions. In many applications, the motion is per se unimportant. What is important is the application of force. The simplest, original “machines” transmitted force from an input location to an output location while magnifying or diminishing it. Examples are the first- and second-order levers, wedges, and pulley mechanisms. These are usually regarded as static machines. Many other forms of machine can be analyzed by the methods of statics because they function without motion, or because the velocities of their motions are small enough that dynamic effects can be neglected. Examples include many types of clamps and pliers, cutters jacks, winches, and other heavy lifting devices, and many kinds of latches and toggles. Further, many machines require structural supports such as brackets, beams, frames, and trusses.

The design analysis of these mechanisms and their associated structures depends on static force analysis. In many other cases, mechanisms must deliver forces of controlled magnitude while generating a specified motion. If the motion is sufficiently slow for inertial forces to be neglected in comparison with the applied loads, the techniques of static force analysis can be applied. Further, even when inertial forces must be included, in the common case in which the motion can be considered to be known, d’Alembert’s principle can be used to convert dynamic force analysis problems into the forms of static force analysis problems. This will be discussed in detail in Chapter 14.

The techniques used are fundamentally similar to those taught in introductory engineering mechanics courses. However, mechanisms and machines commonly have a relatively large number of members, some of which may have relatively complex geometries. Also, there are some techniques that lead to especially efficient solutions for some kinds of static machine problems. The basis of all static analysis is Newton’s third law, as embodied in the concept of static equilibrium. The material in this chapter is composed of systematic ways of applying static equilibrium so that correct solutions to relatively complex problems can be reliably generated.

A further powerful motivation for pursuing static or dynamic force analysis is that conversion of a kinematic design into a real physical mechanism design requires consideration of the loads on components and the stresses and deflections of those components. The loads on each member of a machine are usually of great interest to the machine designer because it is the engineer’s responsibility to select the material to be used and to size the component so that it can safely resist those loads. That is, computation of the complete set of loads acting on a member in any critical situation provides essential initial data for a

stress or deflection analysis of that member. Up to now in this book, we have usually indicated members by lines or simple polygons. It must always be remembered that this is a geometric convenience and that the lines and polygons represent physical objects with additional dimensions made of real engineering materials. Analysis of the worst-case stresses or deflections and application of a relevant failure theory allow selection of materials and dimensions with the assurance that the part will withstand that loading condition without failing.

## 13.2 FORCES, MOMENTS, AND COUPLES

A force is a vector that has a definite line of action on a given link of the mechanism but not necessarily a definite point of application. If  $i, j, k$  are unit vectors respectively parallel to the  $x, y,$  and  $z$  axes of a Cartesian reference frame, the components of  $F$  in the directions of those axes are given by the dot products

$$F_x = F \cdot i, \quad F_y = F \cdot j, \quad F_z = F \cdot k \quad (13.1)$$

and

$$F = F_x i + F_y j + F_z k$$

Forces may be internally applied forces such as a force due to a gas acting on a piston or body forces such as a weight or a magnetic force.

Two forces that have intersecting lines of action can be summed into a single, equivalent force, as shown in Fig. 13.1. The resultant force will act along a line that passes through the point of intersection and lies in the plane defined by the two force vectors.

If two forces are equal and opposite but not collinear, the two forces cannot be resolved into a single force. However, the vector sum of the two equal and opposite forces will be zero. The forces constitute a couple, as shown in Fig. 13.2. The moment of the couple is defined by

$$M = r \times F = \begin{vmatrix} i & j & k \\ r_x & r_y & r_z \\ F_x & F_y & F_z \end{vmatrix} = (r_y F_z - r_z F_y) i + (r_z F_x - r_x F_z) j + (r_x F_y - r_y F_x) k \quad (13.2)$$

where

$$r = r_x i + r_y j + r_z k$$

The moment of a couple is independent of the point of application. It is a free vector that can be assumed to be applied anywhere on the body of interest. Also, the magnitude and direction are independent of how  $r$  is chosen. Two couples are equal if their moments [ $M$  in Eq. (13.2)] are equal.

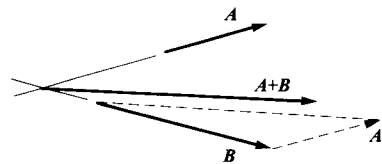


FIGURE 13.1 The resultant ( $A + B$ ) is equivalent to the forces  $A$  and  $B$  acting simultaneously.

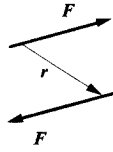


FIGURE 13.2 Two equal and opposite but noncollinear forces form a couple.

The moment generated by a single force about a point as shown in Fig. 13.3 is also given by Eq. (13.2). It is sometimes convenient to represent the moment in terms of the normal vector,  $r_n$ , from the point to the force. Then,

$$\mathbf{M} = \mathbf{r}_n \times \mathbf{F} \quad (13.3)$$

When this is done, we can compute the moment magnitude directly from the magnitudes of  $r_n$  and  $F$ . That is,  $M = r_n(F)$ . When this procedure is done, we must determine the direction of the moment by inspection.

The moment will be perpendicular to both  $F$  and  $r$  or  $r_n$ . In planar problems, the moment will be normal to the plane containing  $F$  and  $r$ . In this chapter, we will emphasize planar problems. Notice that the moment of a force about a point is very much dependent upon the location of the point.

If a force and a couple ( $F$  and  $M$ ) are applied to a rigid body, the system can be replaced by a single force such that the force will have the same effect on the system as the original force and couple. The new force vector will be equal to the original force vector but offset relative to the line of action of the original force vector by the normal distance  $h$ . Here  $h$  is computed in such a way that  $M = h \times F$ . Therefore,

$$|h| = \frac{|M|}{|F|} \quad (13.4)$$

The vector  $h$  can be drawn from either side of the line of action of  $F$ . However, the proper side of the line of action is the one that will make the sign of  $h \times F$  the same as the sign of  $M$ . An example is shown in Fig. 13.4. This procedure is used extensively when graphical analyses are conducted.

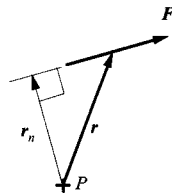


FIGURE 13.3 The moment of a force about a point.

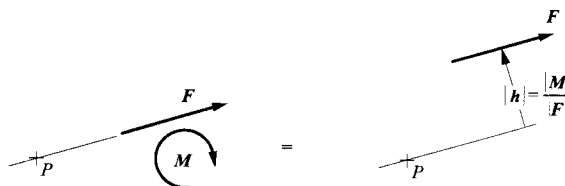


FIGURE 13.4 Replacing a force-moment system by a single force that is offset by the distance  $h$ .

### 13.3 STATIC EQUILIBRIUM

---

A direct consequence of Newton's first two laws of motion is that, if a body is at rest, the sum of all forces acting on the body must be zero. Further, the sum of the moments of those forces about any point must also be zero. Thus, for any member of a structure,

$$\sum F = 0 \quad (13.5)$$

$$\sum M_O = 0 \quad (13.6)$$

where  $\sum F$  is the vector sum of all forces acting on the body, and  $\sum M_O$  is the vector sum of the moments of those forces about any chosen point,  $O$ . Equations (13.5) and (13.6) are called the equations of *static equilibrium*.

The basis of the static force analysis of any structure is the algebraic solution of the static equilibrium equations written for every member in the system. Equations (13.5) and (13.6) are typically associated with free-body diagrams. When the equations are written, they include all of the forces and moments associated with a given free-body diagram.

### 13.4 FREE-BODY DIAGRAMS

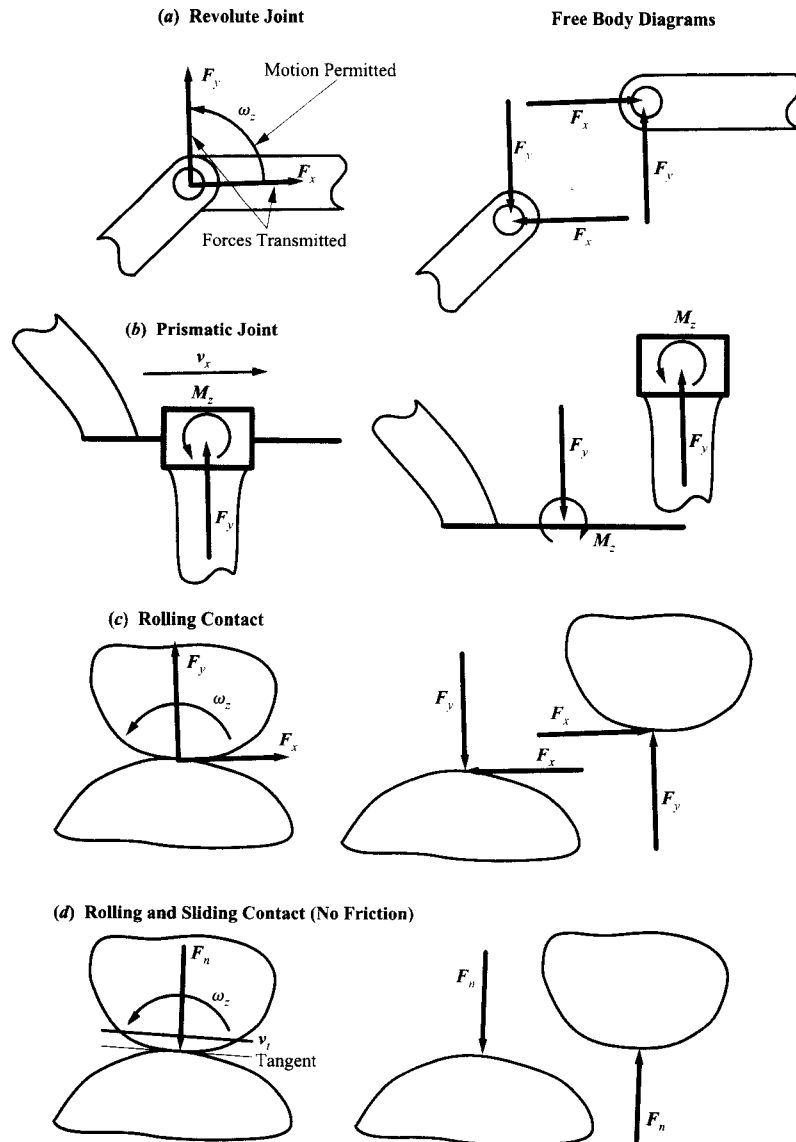
---

The first step in any static analysis of a mechanism is the construction or, more usually, sketching of a free-body diagram of each member of the mechanism. All forces acting on each member, including the forces of action and reaction between members, as well as externally applied loads, must be indicated on the free-body diagram.

A free-body diagram is a bookkeeping device to ensure that *all* relevant force components are included in the static equilibrium equations. The omission of *any* force component will lead to totally incorrect results. Experience has shown that disregard of the step of drawing free-body diagrams almost always results in incorrect equations and results. As a consequence, experienced machine designers never skip this step, although students often do!

The forces that can be transmitted across an ideal (frictionless) kinematic joint are related to the motions permitted by that joint. Basically, the work done by the transmitted forces in the directions of permitted motion must be zero. For example, a revolute joint permits rotation about its axis. Any force that is normal to that axis and whose line of action intersects it does no rotational work. Therefore, any force component in the plane of motion passing through the joint axis is transmitted. It is usually convenient to represent this set of possible forces by two components parallel to the  $x$  and  $y$  axis directions of the fixed reference frame, as shown in Figure 13.5a. In accordance with Newton's third law, the force components transmitted to one of the bodies joined from the other are equal and opposite to the force components received by the second body from the first. Therefore, when the free bodies are drawn these force components appear in equal and opposite pairs.

Similarly, a prismatic joint permits linear motion in one direction. A force normal to that direction does no work in the direction of motion. Also, a torque in the direction normal to the plane of motion will do no work in the direction of permitted motion. Therefore, these components will be transmitted by the prismatic joint, as indicated in Fig. 13.5b. Once again, the transmitted force and torque components will appear as equal and opposite pairs when the free bodies are drawn.



**FIGURE 13.5** Force components transmitted by different types of kinematic joints (with no friction) in planar linkages. (a) Revolute joint. (b) Prismatic joint. (c) Rolling contact. (d) Rolling and sliding contact. Free-body diagrams are shown on the right.

A rolling contact joint is similar to a revolute joint in permitting only pure rotation about the point of contact. The difference is that the axis of a revolute joint is fixed relative to each of the bodies that it joins, whereas the point of rolling contact migrates along the profiles of both bodies. The transmitted force system is also similar to that of a revolute joint, as indicated in Fig. 13.5c. A rolling and sliding contact permits both rotation in the direction normal to the plane of motion and sliding in the direction of the tangent at the point of contact. When friction is neglected, the only force component at the joint is a force

along the normal at the point of contact. Consequently, this is the only force component that can be transmitted by such a joint, as indicated in Fig. 13.5d.

As has been indicated, the forces transmitted by kinematic joints appear in equal and opposite pairs acting on the two members joined in the free-body diagrams. These are seldom the only forces acting in the system. Usually there will also be loads imposed on the system by external agencies. These external loads do not usually appear as equal and opposite pairs.

In addition to indicating all active force components on a set of free-body diagrams, it is good practice to include the dimensional information needed to locate the lines of action of the forces. This information will be needed when writing the static equilibrium equations.

### EXAMPLE 13.1

#### Drawing Free-Body Diagrams

Draw free-body diagrams of all members of the vice-grip pliers in the position shown in Fig. 13.6. The objective of the analysis will be to relate the forces,  $F_H$ , exerted by the user's hand to the gripping forces,  $F_G$ , exerted on the workpiece. The pliers mechanism can be regarded as being parallel to the horizontal plane, so there are no gravity loads in the plane of action.

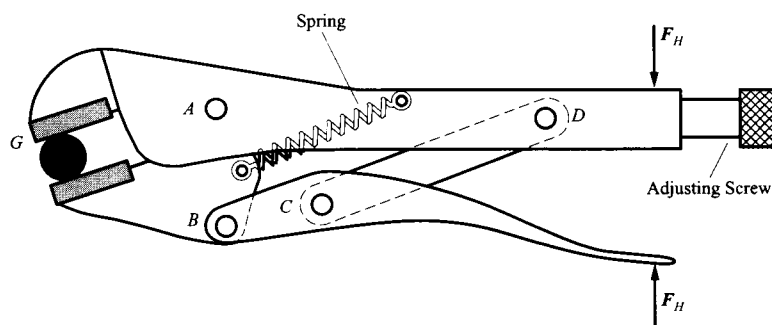


FIGURE 13.6 The vice-grip pliers of Example 13.1.

#### Solution

Free-body diagrams of the individual components in the pliers are shown in Fig. 13.7. The only external loads on the system are the equal and opposite forces  $F_H$  exerted on the handles by the user's hand. The system as a whole can be regarded as a single free body (Fig. 13.6) expressing the requirement that the system as a whole be in static equilibrium. That, in turn, implies that if there are only two external forces acting on the system, those forces must be equal and opposite and must act along the same line of action.

In Fig. 13.7, the force between links is represented by the letter  $F$  with a subscript including the numbers for the two links. The force  $F_{23}$  is interpreted as the force that link 2 exerts on link 3. Similarly,  $F_{32}$  is the force that link 3 exerts on link 2. Clearly,  $F_{23} = -F_{32}$ . If a force is not the internal force between two rigid bodies, the subscript will correspond to the location where the force is applied or to the type of force (e.g.,  $F_S$  or  $F_H$ ).

The forces,  $F_S$ , exerted on the system by the spring can also be treated as external forces for the purposes of the present analysis. Once again, these two forces are equal and opposite and act along the spring axis. The magnitude of  $F_S$  would be computed based on the current length of the spring, the free length, and the spring constant.

The two contacts between the workpiece and the jaws of the vice grip are modeled as rolling contacts. That is, they transmit only forces whose lines of action pass through the contact points. These contact forces are, in principle, unknown in both magnitude and direction. Therefore they are represented by two orthogonal force components  $F_{25N}$  and  $F_{25T}$  (or by  $F_{15N}$  and  $F_{15T}$ ). In fact, since there are only two forces acting on the workpiece, those two forces must be equal, opposite, and collinear. That is,  $F_{25T} = F_{15T} = 0$ .



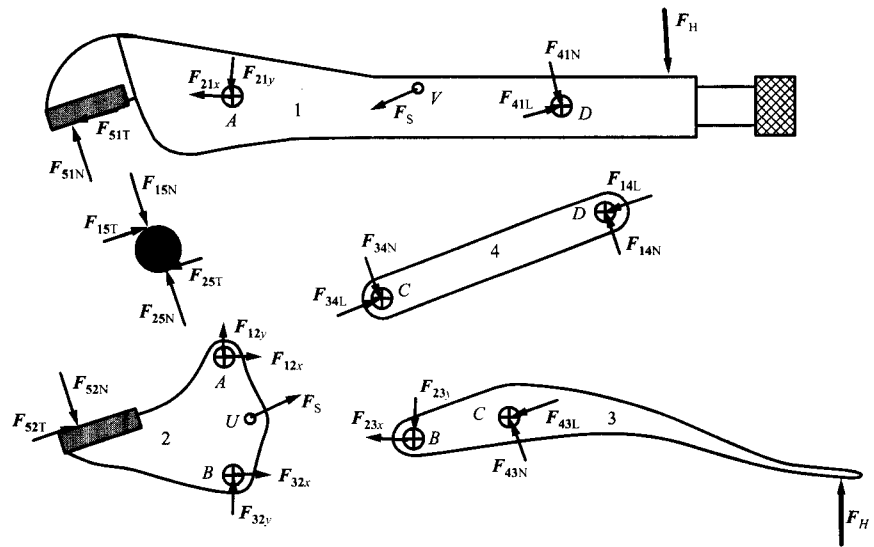


FIGURE 13.7 The free-body diagrams of Example 13.1.

The joints connecting the members of the mechanism are all revolute. That is, each of them transmits a force whose line of action passes through the revolute axis. These forces are initially unknown in both magnitude and direction. It is convenient to represent them by means of two components with specified directions but unknown magnitudes. In many cases those directions are arbitrarily assigned to be parallel to the  $x$  and  $y$  axes of the fixed reference frame, but it is not necessary that they have those directions. In the case of joints  $C$  and  $D$  the force components are taken to be along the line  $CD$  and normal to that line. This is helpful in this case because the link  $CD$  actually has only two forces acting on it, one at  $C$  and one at  $D$ , so equilibrium of that link requires that those forces be equal, opposite, and collinear. Therefore in link 4,  $F_{14N} = F_{34N} = 0$ , and  $F_{14L} = -F_{34L}$ . Note, however, that  $F_{14L}$  and  $F_{34L}$  may be either compressive or tensile.

Notice that every internal force component appears in two of the free-body diagrams and that the senses of the two equal components are opposed. It is convenient to label the two components of each pair identically rather than putting a negative sign on one of them. This is consistent if we regard the labels as representing their magnitudes and the vectors drawn as representing their directions, but it can be confusing because it seems different from the conventions used earlier in this book. It is, of course, necessary to use positive and negative signs on the components when writing equilibrium equations.

## 13.5 GRAPHICAL FORCE ANALYSIS

The force analysis of mechanisms can be conducted either graphically or analytically. The graphical approach is the easiest to perform if only one position is of interest. Also, in the design stage, the graphical procedure allows us to visualize the effect of the location of joints and force application points on the forces that are transmitted in the mechanism. However, for several positions, the graphical procedure is usually inefficient and analytical methods that can be computerized are preferred. Also, if extreme accuracy is required, the analytical procedure is necessary.

Static equilibrium of any free body requires that all forces acting on it sum to zero and that the moments of all those forces about any chosen point should also sum to zero. The force balance can be accomplished graphically by closing a force polygon. However, this does not ensure that the moment equation is satisfied. There are graphical methods for summing moments, but with an electronic calculator it is simpler to measure the normal distances to the lines of action of the forces from the point about which moments are being taken and to compute the moments.

Two special cases are very useful, regardless of whether graphical or analytical solution methods are used. They are shown in Fig. 13.8. The first of these is the case of a member with only two forces (and no couples or moments) acting on it. This case has already been referred to in Example 13.1. To satisfy the force equilibrium conditions, the two forces must be equal and opposite. However, a pair of equal and opposite forces constitutes a couple with moment about any point equal to the magnitude of one of the forces times the normal distance between them. This moment can be zero only if the two forces have the same line of action. Thus, if only two forces act on a member, the forces must be equal, opposite, and collinear.

The second case occurs when only three nonparallel forces act on a given member. In this case, their lines of action must intersect at a single point. This follows because the lines of action of any two nonparallel planar forces always intersect. If moments are taken about that point of intersection ( $O$  in Fig. 13.8), the moment of the system is the magnitude of the third force times the normal distance of its line of action from the point  $O$ . Therefore that moment can be zero only if the normal distance is zero; in other words, the system can be in equilibrium only if the lines of action of all three forces pass through a single point.

The result for a two-force member greatly simplifies the analysis because the line of action of the force pair of such a member is automatically the line joining the points of application of the forces. The result for a three-force member allows identification of the line of action of the third force if the lines of action of the other two are known.

The procedure used when graphically solving for the unknown forces in a mechanism is to first draw free-body diagrams of the members. The next step is to look for a solvable member. Since we have, effectively, three scalar equations for each member, a solvable member has three (or fewer) unknown force components. These might be a force that is unknown in both magnitude and direction, which is equivalent to two unknown components, plus a force with known direction but unknown magnitude, or a force unknown in both magnitude and direction plus an unknown torque. There may also be other known forces acting on the member.

It might seem that there are numerous possible combinations of three unknown force components. However, they all reduce to only two cases: (a) three forces on known lines of action with unknown magnitudes or (b) two forces on known lines of action with unknown

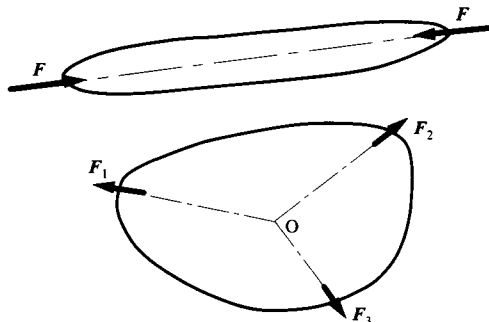


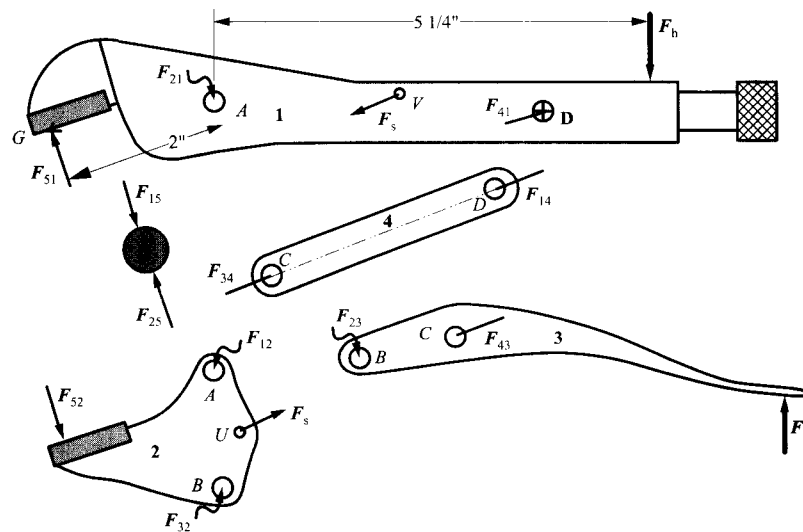
FIGURE 13.8 Two- and three-force members.

magnitudes plus an unknown torque. The first case cited in the previous paragraph—a force of unknown magnitude and direction applied at a known point plus a force with known line of action but unknown magnitude—is equivalent to case (a) stated here. If the force with unknown magnitude and direction is represented by two unknown components on lines of action passing through the point of application, the two cases become identical.

In both case (a) and case (b) the solution procedure can be started by taking moments about the point of intersection of two of the unknown forces. If two of those forces are components of a force with unknown magnitude and direction applied at a point, that point is the point of intersection and is a convenient point about which to take moments. Because the two forces whose lines of action intersect at the point about which moments are taken have zero moments about that point, the moment balance involves only one unknown force magnitude, or torque. This unknown can be solved for. A force polygon can then be drawn to solve for the remaining unknown force components. The procedure is illustrated in the following example.

**EXAMPLE 13.2**  
**Graphical Force**  
**Analysis of**  
**Vice-Grip Pliers**

Find the grip force  $F_G$  exerted on the workpiece by the vice-grip pliers of Example 13.1, shown in Fig. 13.7, if the forces  $F_H$  exerted by the user are 25 in-lb in the location shown in Fig. 13.9. The spring force  $F_S$  is 10 lb. Also find the forces transmitted by the revolute joints at  $A$ ,  $B$ , and  $C$ .



**FIGURE 13.9** The free-body diagrams of Examples 13.1 and 13.2 simplified by taking advantage of the fact that members 4 and 5 are two-force members.

**Solution**

This is an example of a mechanism that can be analyzed graphically without making any calculations beyond scaling and unscaling vectors drawn in polygons. The free-body diagrams of all members are shown in Fig. 13.7. However, those free-body diagrams can be simplified by taking advantage of the two-force members 4 and 5. The result is the set of free-body diagrams of Fig. 13.9. In Fig. 13.9 we have used the convention often used in graphical analyses of representing forces of unknown direction and magnitude by a wavy line. A force with a known direction but unknown magnitude is represented by a line without an arrowhead.

The first step in the analysis is to identify the free-body diagrams that have no more than three unknown quantities and that have at least one known vector (direction and magnitude). Member 3 is the only member satisfying this condition. Member 3 is a three-force member with the known force  $F_H$ , the force  $F_{43}$  whose line of action is known but whose magnitude is unknown, and the force  $F_{23}$

applied at point  $B$ , whose magnitude and direction are both unknown. Thus there are three unknown force magnitudes, two components of  $F_{23}$  and the magnitude of  $F_{43}$ .

Because member 3 is a three-force member with no applied couples, all of the lines of action of the forces must intersect at a point. We know the magnitude and direction of  $F_H$  and the direction of  $F_{43}$ . The lines of action of these two forces intersect at point  $O$  in Fig. 13.10. If we sum moments about point  $O$ , the only force contributing to the moment summation is  $F_{23}$ . Therefore, the line of action of  $F_{23}$  must pass through  $O$ . Now if we sum forces vectorially, we know that

$$\sum F = 0 = F_H + F_{23} + F_{43} \tag{13.7}$$

The force polygon corresponding to Eq. (13.7) is shown in Fig. 13.10. Note that the polygon is drawn so that the vectors add together in a head-to-tail fashion because all of the vectors in Eq. (13.7) are positive, and they sum to zero. From the polygon,

$$F_{23} = 709 \text{ lb and } F_{43} = 716 \text{ lb}$$

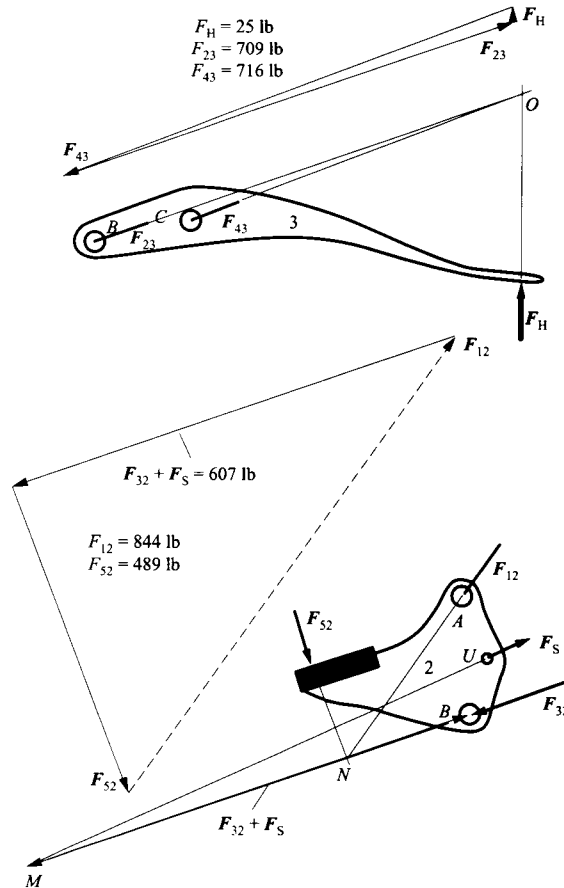


FIGURE 13.10 Force polygons for Example 13.2.

Next consider link 2. Initially, the free-body diagram associated with link 2 has five unknowns. However, we know the magnitude and direction for  $F_{32}$ . Also, there are no concentrated moments on link 2. Therefore, link 2 has a total of three unknowns, and these unknowns can be determined. When we begin, we have two known forces ( $F_{32}$  and  $F_S$ ) applied to link 2. The first operation is to replace these two forces by an equivalent force. The equivalent force will be the vector sum of  $F_{32}$  and  $F_S$  and will create the same moment about an arbitrary point. For this to be the case, the resultant of  $F_{32}$  and  $F_S$  must pass through point  $M$ , the intersection of  $F_{32}$  and  $F_S$ . The resultant of  $F_{32}$  and  $F_S$  is approximately equal to  $F_{32}$  because  $F_{32}$  is so much larger than  $F_S$ . The resultant ( $F_{32} + F_S$ ) is known in both direction and magnitude. Link 2 then reduces to another three-force member with one unknown magnitude ( $F_{52}$ ) and one unknown direction and magnitude ( $F_{12}$ ). The force  $F_{12}$  must pass through the intersection of the force  $F_{32} + F_S$  and  $F_{52}$ . This occurs at  $N$ . Knowing the direction of  $F_{12}$ , we can sum forces on the free-body diagram and get

$$\sum F = 0 = F_{32} + F_S + F_{12} + F_{52} \quad (13.8)$$

This equation can be solved using the force polygon in Fig. 13.10. Again, we add the vectors head to tail. This will give us both the magnitude and sense (i.e., the end that contains the arrowhead) of the unknown vectors. From the polygon,

$$F_{12} = 844 \text{ lb}$$

and

$$F_{52} = 489 \text{ lb}$$

Notice that free body 1 was not used. It might appear that 4 and 5 were also not used. However, these are two-force members. By identifying the lines of action of the respective force pairs, we have ensured their static equilibrium, so they have, in fact, been used. We would have needed to use free body 1 if we had not noted that the whole system is subject to only two external forces and required those two forces to be equal, opposite, and collinear. Because we effectively used the whole system as one free body, we could solve for the forces without considering one member as a free body. In general, if the linkage obeys the planar constraint criterion, the number of free bodies needed for complete solution is equal to the number of members in the linkage.

Notice also that this linkage converts the modest force of 25 lb applied to the handles by the user to a gripping force of 489 lb. That is, it magnifies the force by a factor of about 20. You may notice that  $BC$  is nearly aligned with  $CD$ . This is an example of a toggle linkage. As the linkage moves into the toggle position (with  $B$ ,  $C$ , and  $D$  collinear), the mechanism can generate a very large (theoretically infinite) force at  $G$ . Not only can toggle linkages like this be used to generate large forces but also they can be snapped over center into a statically stable position allowing the workpiece to be clamped indefinitely. This is, in fact, the way in which the vice-grip pliers are intended to be used.

This problem illustrates one of the reasons for conducting the force analysis graphically. By observing the force polygon associated with link 3, we can visualize how the forces increase as the linkage moves into the toggle position. Such visual feedback often provides valuable insight during the design stage of the product development into how a given linkage will behave.

### EXAMPLE 13.3

**Graphical Force  
Analysis of a  
Four-Bar Linkage**

For the linkage shown in Fig. 13.11, find the torque  $T_{12}$  required if  $P = 120$  in-lb the direction shown. The linkage dimensions are as follows:

$$AB = 6 \text{ in, } EC = 12 \text{ in, } AE = 8 \text{ in}$$

$$BC = 18 \text{ in, } ED = 5 \text{ in}$$

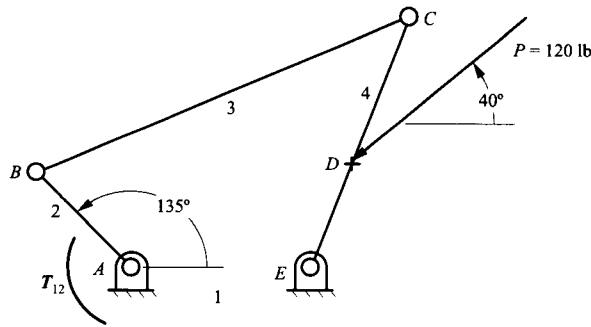


FIGURE 13.11 Mechanism for Example 13.3.

**Solution**

This mechanism can be analyzed graphically for most of the procedure; however, ultimately the unknown torque,  $T_{12}$ , must be computed. To begin the analysis, draw the general free-body diagrams for each link. We can simplify the free-body diagram for link 3 by noting that it is a two-force member. Therefore,  $F_{23}$  and  $F_{43}$  must be equal, opposite, and collinear as shown in Fig. 13.12. Knowing the direction of  $F_{23}$  (and therefore  $F_{32}$ ), it is apparent that link 2 has only two forces also. Therefore, because these two forces must sum to zero for static equilibrium, they are equal and opposite; however, they are *not* collinear because of the torque  $T_{12}$  applied to link 2. For the forces in a two-force member to be collinear, there must be no applied torques or moments.

Because the direction of  $F_{43}$  and therefore that of  $F_{34}$  are known, link 4 becomes a three-force member. The lines of action of the three forces must intersect as shown in Fig. 13.12, and this gives us the direction of  $F_{14}$ . Knowing the direction of  $F_{14}$  we can sum forces on link 4 and solve for the unknowns. That is,

$$\sum F = 0 = P + F_{14} + F_{34}$$

From the force polygon in Fig. 13.12,  $F_{34} = 33.6$  lb in the direction shown. From the free-body diagrams and force equilibrium considerations (see Fig. 13.12), we know that  $F_{34} = -F_{43} = F_{23} = -F_{32} = F_{12}$ . Knowing  $F_{32}$  and  $F_{12}$ , we can compute the torque  $T_{12}$ . Summing moments about point A gives

$$\sum M_A = T_{12} + h \times F_{32} = 0$$

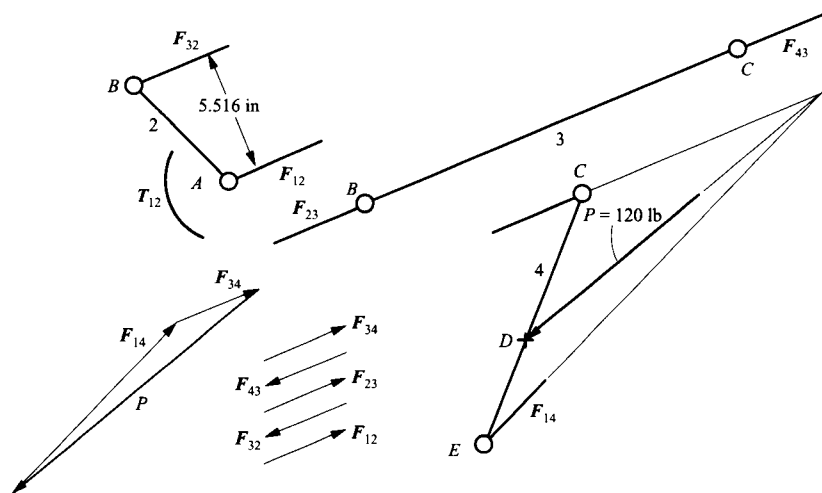


FIGURE 13.12 Free-body diagrams and force polygon for mechanism in Example 13.3.

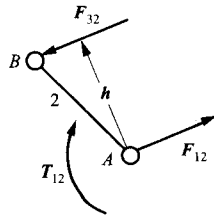


FIGURE 13.13 Free-body diagram for link 2.

For equilibrium, the torque  $T_{12}$  must be equal and opposite to  $h \times F_{32}$ . This is shown in Fig. 13.13. Because the cross product  $h \times F_{32}$  is counterclockwise, the torque must be clockwise. Therefore, we need to compute only the magnitude of the torque. This is given by

$$T_{12} = h(F_{32}) = 5.516(33.6) = 185.3 \text{ in-lb}$$

and therefore

$$T_{12} = 185.3 \text{ in-lb CW}$$

### EXAMPLE 13.4 Graphical Force Analysis of a Cam Mechanism

As an example of a mechanism with higher pairs, analyze the cam mechanism in Fig. 13.14 for the torque  $T_{12}$ . Assume that the kinetic coefficient of friction is 0.15 between the follower and cam and that the torque  $T_{13}$  on the follower is 60 in-lb CCW. The weight of the follower is 20 lb and the weight of the cam is 30 lb.

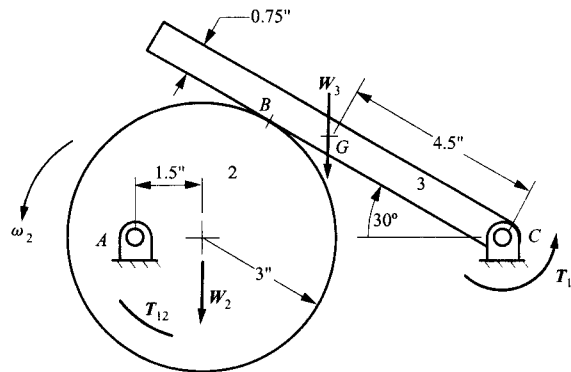


FIGURE 13.14 Cam mechanism for Example 13.4.

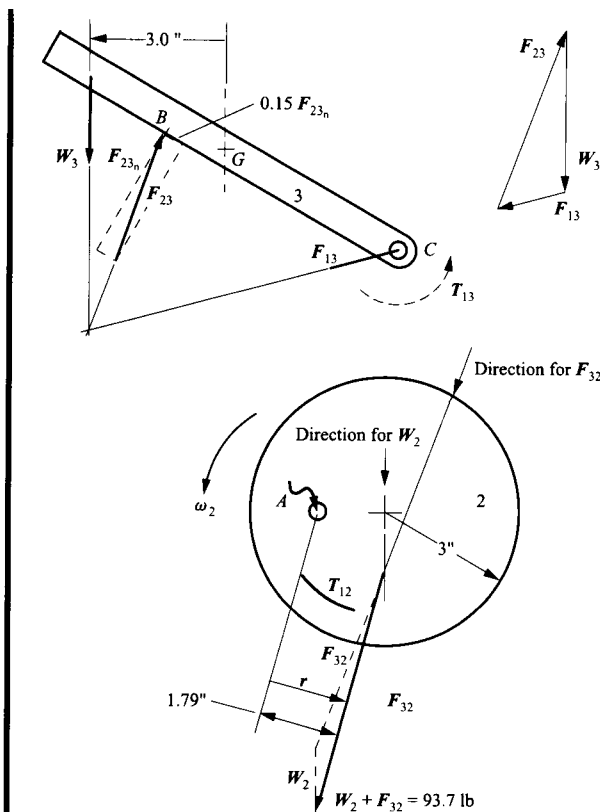
### Solution

The cam mechanism involves only two moving links, and therefore only two free-body diagrams are necessary. These are shown in Fig. 13.15. The force components will then be as shown in Fig. 13.15.

To begin the analysis, start with link 3, where the known forces are located. Initially, link 3 does not appear to be a three-force member that can be analyzed easily using graphical procedures because of the torque  $T_{13}$ . However, as discussed in Section 13.2, we can replace the force  $W_3$  and torque  $T_{13}$  with an equivalent system if we translate the force  $W_3$  by an amount  $h$ , where  $h$  is given by

$$h = \frac{|T_{13}|}{W_3} = \frac{60}{20} = 3 \text{ in}$$

Note that the force is translated so as to produce the torque  $T_{13}$ . Therefore, if we sum moments about any point, the force  $W_3$  alone will produce the same moment as the original set of  $T_{13}$  and  $W_3$ .



**FIGURE 13.15** Free-body diagrams and force polygon for mechanism for Example 13.4.

The next operation is to replace the normal force ( $F_{23_n}$ ) and friction force ( $0.15F_{23_n}$ ) at  $B$  with the total resultant force  $F_{23}$ . Before this is done, however, we must determine the direction for the friction force. Friction makes the mechanism analysis nonlinear, and we must know the correct sign for the friction force or we will not compute the correct answers. The friction force is in the direction of the relative motion or impending motion of the link contacting the body associated with the free-body diagram. In this problem, the cam rotates counterclockwise relative to the frame and the follower. Therefore, the motion of the cam relative to the follower at the point of contact is away from the follower pivot as shown in Fig. 13.14. After the direction of the friction force is known, we can determine the line of action of the resultant force  $F_{23}$  as shown in Fig. 13.15. The resultant force is applied at  $B$ .

We now have a three-force member that involves  $F_{23}$ ,  $F_{13}$ , and  $W_3$  (translated by the amount  $h$ ). The lines of action of these three forces must intersect at a point, as shown in Fig. 13.15. This identifies the line of action of force  $F_{13}$ , which was initially unknown. We can now sum forces on the free-body diagram using

$$\sum F = 0 = W_3 + F_{13} + F_{23}$$

The force polygon is shown in Fig. 13.15. The force  $F_{23}$  can be scaled from the force polygon to be 71.18 lb. We know that  $F_{23} = -F_{32}$ ; therefore, we can apply the known force to the free-body diagram for link 2. On link 2, there are two known forces and an unknown torque. We can proceed in several ways; however, an especially simple way is to find the resultant of  $W_2 + F_{32}$ . We will then have only one force other than  $F_{12}$  and a torque applied to link 2. If we sum moments about point  $A$ , only the resultant  $W_2 + F_{32}$  and  $T_{12}$  will enter into the calculations. The resulting equation is

$$\sum M_A = 0 = T_{12} + r \times (W_2 + F_{32})$$



This equation can be simplified because we can measure directly the perpendicular distance from point  $A$  to the line of action of the resultant  $W_2 + F_{32}$ . Then,

$$|T_{12}| = |r||W_2 + F_{32}| = 1.79(93.7) = 168 \text{ in-lb}$$

We can identify the direction of  $T_{12}$  by inspection or by actually performing the cross product as indicated in the moment-sum equation. The result is

$$T_{12} = 168 \text{ in-lb CCW}$$

## 13.6 ANALYTICAL APPROACH TO FORCE ANALYSIS

A body is in static equilibrium when the resultant (sum) of all the forces acting on it is zero and the resultant of all their moments about any point is zero.

If a system of rigid bodies, such as a mechanism, is in static equilibrium, then each individual body is in equilibrium under the action of all the forces acting on it, including those exerted on it by other members. A free-body diagram should be drawn for each member, and the appropriate force and moment equilibrium equations should then be written for each free body and solved for the unknown forces or moments.

For an analytical force analysis, we must know the coordinates of all points involved in the analysis. Therefore, before the force analysis is conducted, a position analysis must be conducted. As indicated in Chapters 2–5, the position equations will be nonlinear. After the position analysis is conducted, however, the force equations will be linear (unless friction is involved), and therefore they can be easily solved. We will illustrate the procedure in three examples.

### EXAMPLE 13.5 Analytical Force Analysis of a Four-Bar Linkage

#### Solution

Analyze the linkage in Example 13.3 analytically to find the torque  $T_{12}$  required if  $P = 120 \text{ lb}$  and the driver link 2 is at an angle of  $135^\circ$  with the horizontal axis.

Before the force analysis can be conducted, we must determine the coordinates of the points relative to the coordinate system shown in Fig. 13.16. This can be done using the procedures discussed in Chapter 5, and all vectors will be defined using the sign convention and nomenclature given in Chapter 5 (see Fig. 5.3). This will let us determine the angular orientation of each link and each force. After the position analysis, we can summarize the known position and force information as follows:

$$P = 120 \angle 220^\circ = -91i - 77.1j$$

$$F_{34} = F_{34} \angle 22.65^\circ = F_{34}(0.9228)i + F_{34}(0.3851)j$$

$$r_{B/A} = r_{B/A} \angle 135^\circ = 6 \angle 135^\circ = -4.243i + 4.243j$$

$$r_{C/B} = r_{C/B} \angle 22.65^\circ = 18 \angle 22.65^\circ = 16.61i + 6.93j$$

$$r_{C/E} = r_{C/E} \angle 68.65^\circ = 12 \angle 68.65^\circ = 4.368i + 11.18j$$

and

$$r_{D/E} = r_{D/E} \angle 68.65^\circ = 5 \angle 68.65^\circ = 1.820i + 4.657j$$

To begin the analysis, draw the general free-body diagrams for each link as shown in Fig. 13.17. Again, we can simplify the free-body diagram for link 3 by noting that it is a two-force member with no applied moments. However, in an analytical force analysis, it is usually inefficient to simplify

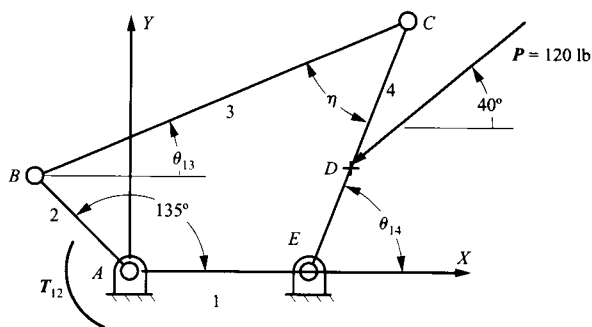


FIGURE 13.16 Coordinate axes for mechanism in Example 13.5.

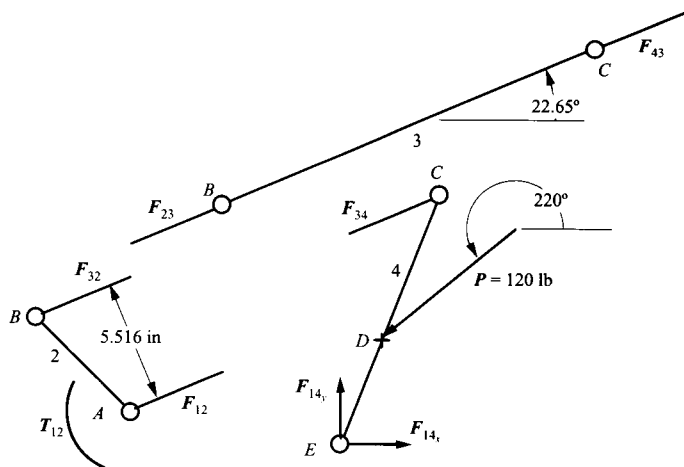


FIGURE 13.17 Free-body diagrams for analytical force analysis for Example 13.5.

three-force members as was done in the graphical analysis. Therefore, we will represent  $F_{14}$  by its  $x$  and  $y$  components. For the analysis, begin with link 4, because this is the only location where a force magnitude is known. There are only three unknowns associated with this link. These are the magnitude of  $F_{34}$  and the magnitude of the two components of  $F_{14}$ . We do not need to determine  $F_{14}$  to solve the problem. To compute  $F_{34}$ , sum moments about point  $E$  in the free-body diagram for link 4. Then,

$$\sum M_E = r_{C/E} \times F_{34} + r_{D/E} \times P = 0 \quad (13.9)$$

where

$$r_{C/E} \times F_{34} = \begin{vmatrix} i & j & k \\ 4.368 & 11.18 & 0 \\ 0.9228F_{34} & 0.3851F_{34} & 0 \end{vmatrix} = -8.635F_{34}k$$

and

$$r_{D/E} \times P = \begin{vmatrix} i & j & k \\ 1.820 & 4.657 & 0 \\ -91.9 & -77.1 & 0 \end{vmatrix} = 287.6k$$

Therefore,

$$F_{34} = 287.6/8.635 = 33.31 \text{ lb}$$

Because the force is positive,

$$F_{34} = 33.31 \angle 22.65^\circ$$

From the free-body diagrams,

$$F_{32} = -F_{23} = F_{43} = -F_{34}$$

Therefore,

$$F_{32} = -33.31 \angle 22.65^\circ = -30.74i - 12.83j$$

Now considering the free-body diagram for link 2, we can sum moments about point  $A$ . The result of this is

$$\sum M_A = r_{B/A} \times F_{32} + T_{12} = 0 \quad (13.10)$$

Here we are using the convention that a positive value for  $T_{12}$  corresponds to a counterclockwise torque. From Eq. (13.9),

$$T_{12} = -r_{B/A} \times F_{32} = - \begin{vmatrix} i & j & k \\ -4.243 & 4.243 & 0 \\ -30.74 & -12.83 & 0 \end{vmatrix} = -184.8k \text{ in-lb}$$

or

$$T_{12} = 184.8 \text{ in-lb CW}$$

Note that this result is very close to that computed in the graphical analysis. In general, some error must be expected in the graphical analysis because of the graphical constructions.

### 13.6.1 Transmission Angle in a Four-Bar Linkage

In Chapter 6, the transmission angle in a four-bar linkage was mentioned in conjunction with the design of optimal linkages for function generation. The transmission angle is the angle  $\eta$  in Fig. 13.16. If we reexamine Eq. (13.10) we find that

$$|T_{12}| = |r_{B/A} \times F_{32}| \quad (13.11)$$

For a given position of the linkage, the magnitude and orientation of  $r_{B/A}$  and  $F_{32}$  will be fixed, and the magnitude of the torque required for equilibrium will be directly proportional to the magnitude of  $F_{32}$ . Therefore, the torque required to maintain equilibrium will increase with the magnitude of  $F_{32}$ . Now examining Eq. (13.9) and using an alternative expression for the cross product gives

$$|r_{C/E} \times F_{34}| = |r_{C/E}| |F_{34}| \sin \eta = |r_{D/E} \times P|$$

or

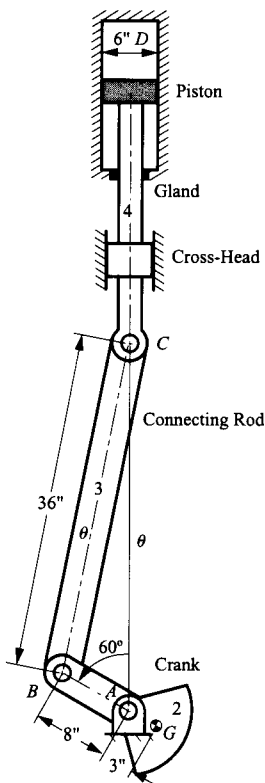
$$|F_{34}| = \frac{|r_{D/E} \times P|}{|r_{C/E}| \sin \eta} = |F_{32}| \quad (13.12)$$

From Eq. (13.12) it is clear that the magnitude of the force  $F_{32}$  increases rapidly in a non-linear fashion as the transmission angle  $\eta$  approaches 0 or  $\pi$ , and  $F_{32}$  reaches a minimum value for  $\pi/2$ . To reduce the torque required for equilibrium, we need to reduce the magnitude of  $F_{32}$ , which means we want to make the transmission angle as close to  $\pi/2$  as possible. This is consistent with the optimization procedure discussed in Chapter 6, where the objective was to minimize  $|\pi/2 - \eta|$ .

In general the transmission angle should be held between  $30^\circ$  and  $150^\circ$ . If the transmission angle approaches  $0^\circ$  or  $180^\circ$ , high bearing loads, excessive wear, and binding in the joints can be expected.

**EXAMPLE 13.6**  
**Analytical Force**  
**Analysis of a**  
**Drilling-Mud Pump**

A pump used for pumping drilling mud in oil-well drilling has two double-acting cylinders. The linkage of the piston to the crankshaft for each cylinder is arranged as shown in Fig. 13.18.



**FIGURE 13.18** The mechanism of an oil-drilling mud pump analyzed in Example 13.6.

On the upstroke, the gage pressure in the cylinder above the piston is 750 psi *above* atmospheric, and on the bottom side of the piston the pressure is 5 psi *below* atmospheric. The bore of the cylinder has a diameter of 6 in, and the piston rod has a diameter of 1.5 in. The weight of the connecting rod, which can be regarded as a uniform rod, is 50 lb. The weight of the piston, piston rod, and crosshead assembly is 30 lb. The crank weighs 45 lb and has its center of mass 3 in from the crankshaft axis as shown. The frictional resistance from the piston and gland seals and the cross head is estimated to total

12 lb. In the position shown, find the torque that must be applied to the crank by the motor, the axial loads in the connecting rod and piston rod, the loads on all three bearings, and the side thrust resisted by the crosshead.

### Solution

Before the force analysis can be conducted, we need to determine the orientation of the connecting rod and the force on the piston. The angle  $ACB$  can be calculated using the sine rule:

$$\frac{\sin \theta}{8} = \frac{\sin 60^\circ}{36}$$

or

$$\theta = 13.096^\circ$$

The area of the top face of the piston is

$$A_T = \pi \times 3^2 = 28.27 \text{ in}^2$$

Therefore the downward force on the top of the piston is

$$750 \times A_T = 21,210 \text{ lb}$$

The net area of the bottom face of the piston is

$$A_B = A_T - \pi \times 0.75^2 = 26.51 \text{ in}^2$$

Therefore the force on the bottom of the piston is

$$5 \times A_B = 130 \text{ lb}$$

This is also downward because the pressure is lower than atmospheric below the piston. The free-body diagrams for the pump members are shown in Fig. 13.19. Note that we have assumed the directions for the force components. If an assumed direction is wrong, the force component will be negative.

Applying static equilibrium to the piston (link 4), we get

$$\sum F_x = 0 = F_{34_x} - F_{14} \Rightarrow F_{34_x} = F_{14}$$

$$\sum F_y = 0 = F_{34_y} - 21,210 - 30 - 12 - 130 \Rightarrow F_{34_y} = 21,380 \text{ lb}$$

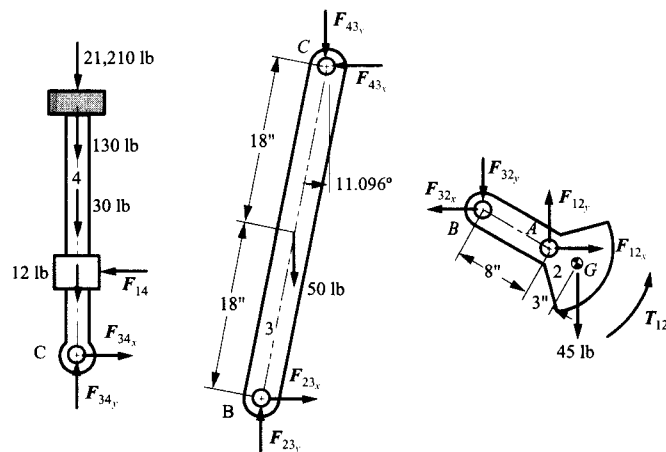


FIGURE 13.19 The free-body diagrams for the mechanism of Fig. 13.18 and Example 13.6.

Here we have rounded the result to four significant figures. Hence the piston rod axial load is 21,380 lb.

Applying static equilibrium to the connecting rod, we have

$$\sum F_x = 0 = F_{23_x} - F_{43_x} \Rightarrow F_{23_x} = F_{43_x} = F_{34_x} = F_{14}$$

Again note that we have assumed the direction for the force components and are dealing only with magnitudes. For the  $y$  components,

$$\sum F_y = 0 = F_{23_y} - 21,380 - 50 \Rightarrow F_{23_y} = 21,430$$

For the moment summation, we will use the forces and the normal distances from their lines of action to the point about which the summation of moments is made. For link 3, we will sum moments about point  $B$ ,

$$\sum M_B = \sum R_n(F) = F_{43_x}(36)(\cos 11.096^\circ) - 21,380(36)(\sin 11.096^\circ) - 50(18)(\sin 11.096^\circ)$$

giving

$$F_{43_x} = 4200 \text{ lb}$$

Hence the connecting rod load at  $C$  is  $\sqrt{21,430^2 + 4200^2} = 21,840$  lb. This is also the load on the bearing at  $C$ .

Applying static equilibrium to the crank and noting that  $F_{23_x} = F_{32_x}$  and  $F_{23_y} = F_{32_y}$ , we obtain

$$\sum F_x = 0 = F_{12_x} - 4200 \Rightarrow F_{12_x} = 4200 \text{ lb}$$

$$\sum F_y = 0 = F_{12_y} - 21,430 - 45 \Rightarrow F_{12_y} = 21,480 \text{ lb}$$

$$\sum M_A = 0 = T_{12} + 21,430(8)(\sin 60^\circ) + 4200(8)(\cos 60^\circ) - 45(3)(\sin 60^\circ)$$

So

$$T_{12} = -165,200 \text{ in-lb}$$

or

$$T_{12} = 13,800 \text{ ft-lb CW}$$

The bearing load at  $A$  is

$$F_{12} = \sqrt{21,480^2 + 4200^2} = 21,900 \text{ lb}$$

This completes the analysis.

## 13.7 FRICTION CONSIDERATIONS

In the previous examples, we have considered friction briefly. In this section, we will investigate the effect of friction more formally for various types of joints. Friction can be extremely important in the design of mechanisms. If not properly handled, friction can greatly reduce the efficiency of a mechanism and increase power requirements. Because of friction, mechanical work is converted to heat, and the resulting heat buildup can degrade the materials in the mechanism, especially when polymers are used. Friction also contributes to wear, and in extreme cases friction can cause a mechanism to seize up.

The friction force is perpendicular to the contact force at a joint, and assuming Coulomb friction, the friction force will be proportional to the normal contact force. The

direction of the friction force is determined by the direction of the relative motion or impending relative motion. Therefore, before a friction force analysis is conducted, it is important to conduct a velocity analysis in enough detail to determine the direction of the relative motion between different links. The magnitudes of the relative velocities are not required if Coulomb friction is assumed. The relative velocity magnitudes will be needed, however, if viscous friction is assumed. In the discussions here, only Coulomb friction will be considered. In the following, we will consider friction in cam joints, sliding or prismatic joints, and revolute joints.

### 13.7.1 Friction in Cam Contact

Two links (2 and 3) in cam contact are shown in Fig. 13.20. If we treat the problem as planar, the two links will have point contact at the cam joint, and the contact force can be resolved into two components, one normal to the common tangent and one along the common tangent. The component in the direction of the common tangent will be the friction force, and it can be related to the normal force by

$$F_{32_t} = \mu F_{32_n}$$

where  $\mu$  is the coefficient of friction. Note that when Coulomb friction is assumed, the friction force depends on  $\mu$  and  $F_{32_n}$  only; that is,  $F_{32_t}$  is independent of the area at the contact location. If the bodies have relative motion,  $\mu$  will be equal to the kinetic coefficient of friction. If the bodies are at rest but the motion is impending, then the effective value of  $\mu$  can range from 0 to  $\mu_s$ , the static coefficient of friction. The effective coefficient of friction is equal to  $\mu_s$  only when motion is about to occur.

To determine the direction of the friction force on link 2, we must determine the direction for the velocity  ${}^3\mathbf{v}_{P_2/P_3} = {}^3\mathbf{v}_{P_2}$ . This is the relative velocity of the contact point on link 2 relative to link 3. The friction force will be opposite to this relative velocity vector. Alternatively, we can determine the velocity of  $P_3$  relative to link 2 or  ${}^2\mathbf{v}_{P_3/P_2} = {}^2\mathbf{v}_{P_3}$ . This is the point on link 3 that is causing the force on link 2. The friction force on link 2 will be in the same direction as the velocity  ${}^2\mathbf{v}_{P_3/P_2} = {}^2\mathbf{v}_{P_3}$ . Simplistically, we can think of  $P_3$  dragging against link 2 to cause the friction force. In this case, the friction force will be in the direction of the dragging motion, that is, in the direction of  ${}^2\mathbf{v}_{P_3}$ .

### 13.7.2 Friction in Slider Joints

Two links (3 and 5) in sliding contact are shown in Fig. 13.21a. The slider (link 3) is assumed to have two loads  $\mathbf{P}$  and  $\mathbf{W}$  applied to it from links other than link 5. If we resolve the force from link 5 on link 3 into two components, the normal force will be perpendicular to the contact surface and the friction force will be tangent to it as shown in Fig. 13.21b.

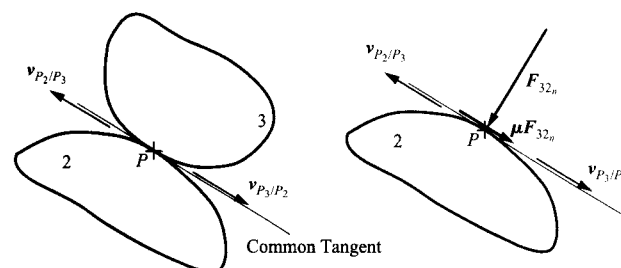


FIGURE 13.20 Friction forces in a cam joint.

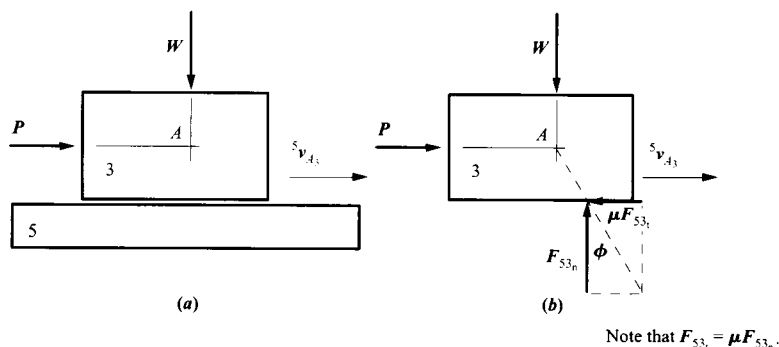


FIGURE 13.21 Friction forces in a slider joint.

The direction of the friction force will be opposite to the velocity of any point on the slider relative to link 5. In Fig. 13.21b, point  $A_3$  is chosen as a typical point.

The two components of the force  $F_{53}$  can be resolved into a single force if the friction angle  $\phi$  is known. This angle is given by

$$\phi = \tan^{-1} \left( \frac{\mu F_{53n}}{F_{53n}} \right) = \tan^{-1}(\mu) \quad (13.13)$$

Note that, from force equilibrium on link 3,  $W = F_{53n}$  and  $P = \mu F_{53n}$ . If both  $P$  and  $W$  are given and the block is in static equilibrium, then  $\mu$  cannot be specified. It will assume whatever value is required for equilibrium. However,  $\mu$  cannot be larger than the static coefficient of friction if the mechanism is not moving, or the kinetic coefficient of friction if the mechanism is moving. If  $\mu$  is given, then  $P$  can be computed if  $F_{53n}$  is known.

If the normal force and friction force are resolved into a single force oriented at an angle of  $\phi$  relative to the normal direction, link 3 becomes a three-force member. Therefore, the forces must intersect at a point, as shown in Fig. 13.21b. This will indicate the location where the total force  $F_{53}$  is applied to link 3. It is possible that the point of application of the force must be beyond the physical limits of the block. When this occurs, the block will tend to rotate, and if the block is not supported on both top and bottom, static equilibrium cannot be maintained. This condition is indicated in Fig. 13.22a. When designing a mechanism, we must provide for a support on both sides of the slider whenever there is a possibility that the friction force will become large enough to cause tipping.

If the location for contact from one side of the block is beyond the physical boundary of the block, the block will tip slightly and bring the opposite side into contact. There will then be a normal and friction force on both sides of the block. When this occurs, we must treat the force  $F_{53}$  as two components ( $F_{53}^{(1)}$  and  $F_{53}^{(2)}$ ), as shown in Fig. 13.22b. The two components will be oriented at an angle  $\pm \phi$  with respect to the normal direction; however, one component will be oriented at an angle of  $+\phi$ , and the other component will be oriented at an angle of  $-\phi$  as shown in Fig. 13.22b.

When the condition indicated in Fig. 13.22 is satisfied, we can analyze the problem directly using analytical techniques by summing forces and moments. For a graphical solution, the problem can be simplified by resolving  $F_{53}^{(1)}$  and  $F_{53}^{(2)}$  into a single force that acts through the intersection of the lines of action of the two components. This is shown in Fig. 13.23a. Initially, we will not know the direction for the resultant; however, we now have a three-force member, and the lines of action of all of the forces must intersect at a point. The directions of  $P$  and  $W$  are already known, and their lines of action intersect at  $A$ . Therefore,



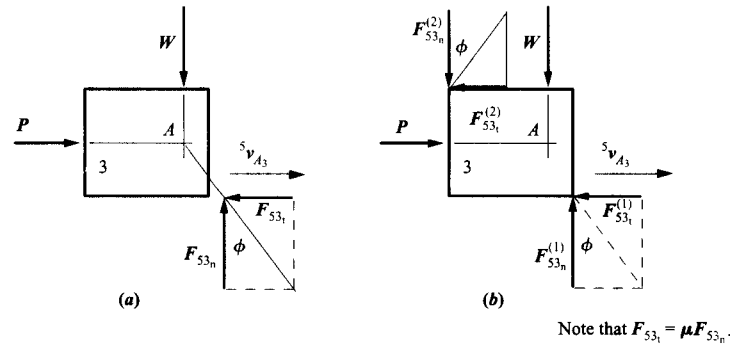


FIGURE 13.22 Condition indicating that the block must contact the slide at two locations.

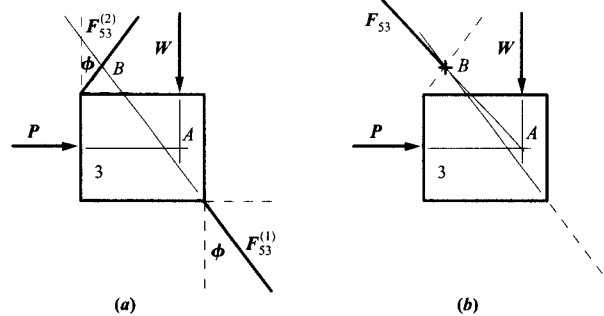


FIGURE 13.23 Resolving the two components of the slider force into a single component.

the line of action of the resultant  $F_{53}$  must be along the line through  $A$ , as shown in Fig. 13.23b. The individual components can then be determined by graphically summing forces.

The procedure indicated here can be used regardless of how the block is actually constrained; for example, it can be mounted over a rod or captured within a cylinder.

### 13.7.3 Friction in Revolute Joints

Although slider friction is probably the most significant problem area in mechanisms when friction is addressed, pin friction is also important, especially when transmission angles are poor.

Pin friction occurs in a revolute joint at the contact point between the pin and bearing. The effect is to create a torque called a friction torque in the joint. The magnitude of the torque can be determined by considering in detail how the forces are transmitted through the joint. A revolute joint between two arbitrary links (2 and 4) is represented in Fig. 13.24. In the figure, the clearance in the joint is greatly exaggerated. The nominal radius of the pin in the joint is  $R$ , and the friction coefficient is again taken as  $\mu$ .

Figure 13.24b shows the forces that act on the pin part of the joint. The friction force is again equal to  $\mu$  times the normal force, and the friction angle,  $\phi$ , is computed as was

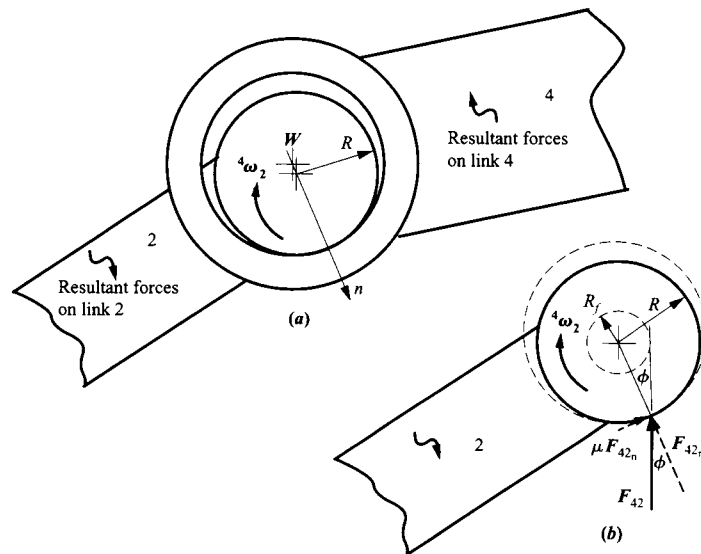


FIGURE 13.24 A revolute joint with friction.

done in Eq. (13.13). That is,  $\phi = \tan^{-1}(\mu)$ . Because of the friction force, a torque must be applied to link 2 for static equilibrium. The magnitude of the friction torque is equal to

$$T_f = \mu F_{42_n} R \tag{13.14}$$

The friction force opposes the motion of link 2 relative to link 4, and therefore the torque resulting from the friction force also opposes the relative motion. The total contact force is the resultant of the friction force and the normal force. As shown in Fig. 13.24b, the line of action of the resultant force  $F_{42}$  will be tangent to a circle called the friction circle, and the radius of the friction circle is given by

$$R_f = R \sin \phi \tag{13.15}$$

There will be a friction circle associated with each revolute joint, and in each case, the joint force will be tangent to the friction circle. The joint force must be located on the proper side of the friction circle to oppose the relative motion. The effect of the friction circles is to alter slightly the line of action of the joint forces. A binary link with a revolute joint at each end will still be a two-force member, but the line of action of the forces will not pass through the rotation axes. As shown in Fig. 13.25, there are four possible lines of action for the joint forces, depending on which side of the friction circles the joint forces are located.

To determine the proper side of the friction circles for the joint forces, it is necessary to know the general direction of the forces and the relative motion at the joints before the analysis is begun. This is usually done by conducting a frictionless analysis first and by conducting a velocity analysis. If the direction is chosen incorrectly, the wrong side of the friction circle will be indicated to oppose the relative motion in the joint. This in turn will slightly alter the exact direction of the joint force. Therefore, if any of the joint forces are negative (wrong direction assumed), the analysis must be redone using the proper directions.

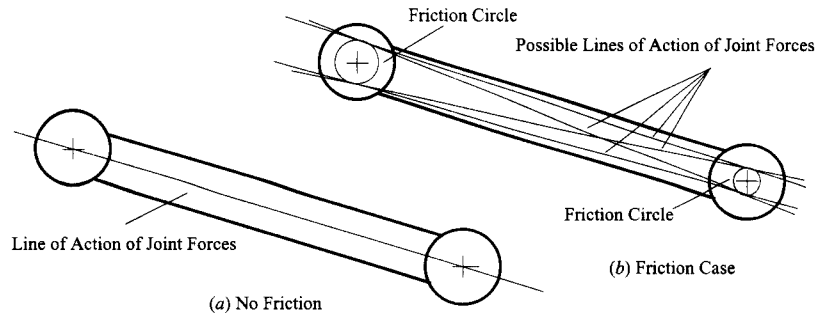


FIGURE 13.25 Possible lines of action of joint forces when pin friction is involved.

**EXAMPLE 13.7**  
**Analysis of a**  
**Slider-Crank**  
**Mechanism with**  
**Friction**

A slider-crank mechanism has a piston load of 200 in-lb in the direction shown in Fig. 13.26, and the crank angle ( $\theta_2$ ) is  $120^\circ$ . The coefficient of friction in each pin and between the slider and frame is 0.2, and the diameter of the pin at each revolute joint is 2 in. Find the torque  $T_{12}$  required for static equilibrium with and without friction.

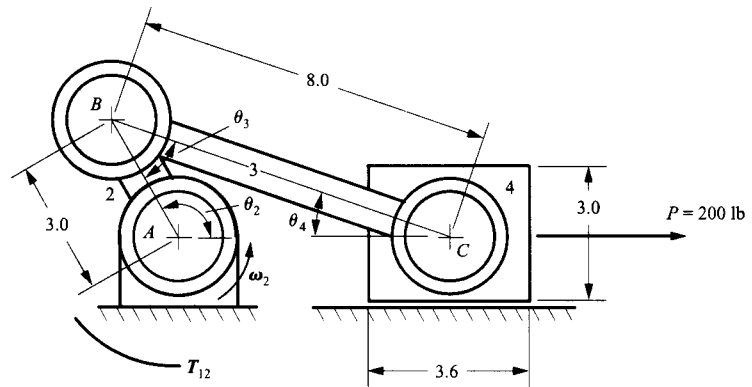


FIGURE 13.26 The mechanism for Example 13.7.

**Solution**

We will perform the analysis graphically. Before the friction analysis is conducted, we need to determine the relative motion at each joint and the general direction of the forces at each joint. We can determine the relative motion by inspection because we need only to identify whether individual angles are increasing or decreasing. For the direction of the crank rotation given,

$\theta_2$  is increasing,

$\theta_3$  is decreasing, and

$\theta_4$  is decreasing.

To determine the general directions of the joint forces, a zero-friction analysis can be conducted. For this analysis, the free-body diagrams and force polygons are shown in Fig. 13.27. To begin this analysis, we recognize that link 3 is a two-force member. Therefore, the line of action of the joint forces is along the line  $BC$ . Link 4 is then a three-force member, and the lines of action of the three

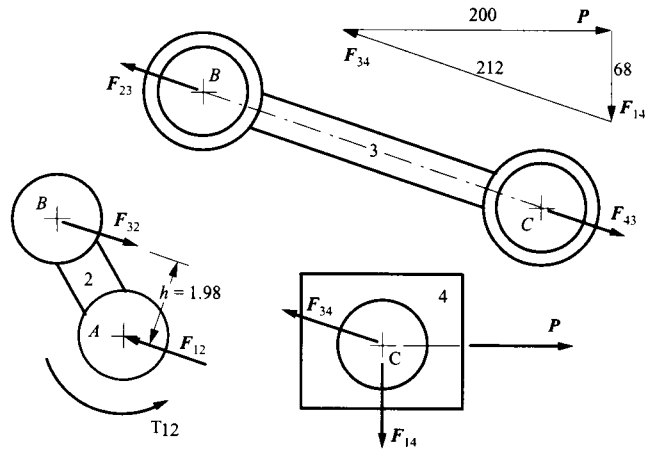


FIGURE 13.27 Free-body diagrams and force polygon for zero-friction case in Example 13.7.

forces intersect at point  $C$ . By summing forces vectorially on link 4, the magnitudes of all of the forces can be determined. The force summation equation is

$$\sum \mathbf{F} = 0 = \mathbf{F}_{14} + \mathbf{P} + \mathbf{F}_{34} \quad (13.16)$$

The force polygon gives the magnitude and direction for each of the vectors. From equilibrium considerations at each joint, we know

$$\mathbf{F}_{32} = -\mathbf{F}_{23} = \mathbf{F}_{43} = -\mathbf{F}_{34} \quad (13.17)$$

and

$$\mathbf{F}_{12} = -\mathbf{F}_{32} \quad (13.18)$$

This gives us the general direction of all forces at the joints. To determine the torque  $T_{12}$  for equilibrium in the nonfriction case, sum moments about point  $A$  of the free-body diagram for link 2. From this we get

$$T_{12} = hF_{32} = 212(1.98) = 420 \text{ in-lb}$$

By inspection, the torque must be counterclockwise. Therefore,

$$T_{12} = 420 \text{ in-lb CCW (no friction case)}$$

To analyze the system with friction, we need to compute the friction angle and friction circle radius for each joint. The friction angle is

$$\phi = \tan^{-1}(\mu) = \tan^{-1}(0.2) = 11.31^\circ$$

From Eq. (13.15), the friction circle radius at each joint is

$$R_f = R \sin \phi = 1 \sin 11.31^\circ = 0.20 \text{ in}$$

The friction circles are shown in Fig. 13.28. We must now determine at which side of the friction circles the forces are located. Considering joint  $C$  on link 3 first, the force  $F_{43}$  is tensile and link 3 is rotating CCW relative to link 4 ( $\theta_4$  is getting smaller). We must locate  $F_{43}$  tangent to the friction circle such that it opposes this CCW rotation. This means that  $F_{43}$  must be located on the upper side of the friction circle. Then,  $F_{34}$  will be located on the upper side of the corresponding friction circle on link 4.

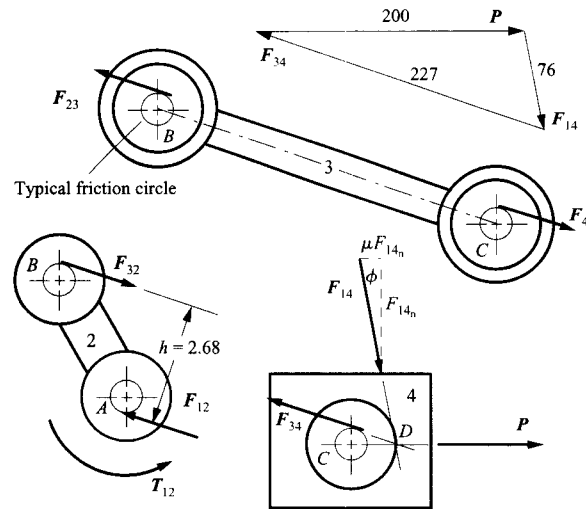


FIGURE 13.28 Free-body diagrams and force polygon for friction case in Example 13.7.

Next consider joint  $B$  on link 3. Force  $F_{43}$  is tensile, and link 3 rotates CW relative to link 2 ( $\theta_3$  is decreasing). We must locate  $F_{23}$  tangent to the friction circle such that it opposes this CW rotation. This means that  $F_{23}$  must be located on the upper side of the friction circle. Similarly,  $F_{32}$  will be located on the upper side of the corresponding friction circle on link 2.

Moving to joint  $A$  on link 2, we see that the force  $F_{12}$  is oriented approximately as shown in Fig. 13.27. Also, link 2 is rotating CCW relative to link 1. If  $F_{12}$  is to provide a torque that opposes this motion, it must be located on the lower part of the friction circle as shown in Fig. 13.28.

On link 4, we must orient the force  $F_{14}$  relative to the block. Because link 4 is a three-force member, all of the forces must intersect at a point. Because we know the lines of action of  $P$  and  $F_{34}$ , we know the location of the point of intersection ( $D$  in Fig. 13.28). We also know that the block is moving to the left relative to the frame so that the friction force must be directed toward the right. Therefore,  $F_{14}$  must be inclined as shown in Fig. 13.28, and its line of action must intersect the other two forces on link 4 at  $D$ . Note that  $F_{14}$  makes contact within the physical limits of the block, and therefore the block does not tip. If contact were indicated beyond the physical limits of the block, we would have to use the procedure indicated in Fig. 13.22.

Now the directions of the forces on link 4 are known. We can sum forces [Eq. (13.16)] and solve for the unknowns. The force polygon is shown in Fig. 13.28. From the force polygon and Eqs. (13.17) and (13.18), we can determine the forces on link 2. The torque  $T_{12}$  can then be computed. The magnitude of  $T_{12}$  is given by

$$T_{12} = hF_{32} = 227(2.38) = 540 \text{ in-lb}$$

By inspection, the torque must be counterclockwise. Therefore,

$$T_{12} = 540 \text{ in-lb CCW}$$

Because of friction, the torque needed for equilibrium has increased by almost 28%. The friction coefficients used in this example are high in order to illustrate the procedure. However, the torque

requirements to drive a mechanism can increase significantly when friction is involved. Therefore, the designer should reduce the effects of friction either by careful bearing design and lubrication or by altering the linkage geometry (when possible) to reduce the sensitivity of the mechanism to friction.

## 13.8 IN-PLANE AND OUT-OF-PLANE FORCE SYSTEMS

It is important to remember, when analyzing planar mechanisms, that although motion occurs only parallel to a single plane, it is possible to apply fully three-dimensional force systems to the mechanism. Only the components of force and moment that act in the plane of motion affect the action of the mechanism. These *in-plane* force components are the two components of force parallel to the plane of motion and the moment vector normal to that plane. If the force system is resolved into Cartesian components, the remaining three components—the force normal to the plane of motion and the two components of moment parallel to the plane of motion—do not affect the action of the mechanism. Nevertheless, they apply loads to the components and contribute to the stresses in those components. These *out-of-plane* force components act on the mechanism as a structure.

Deflections caused by out-of-plane forces are particularly important in planar mechanisms since an excessive deflection may result in significant deviations from parallelism of the joint axes, which can result in binding of the mechanism or generation of excessive internal stresses. For this reason, the deflection of members is often a concern even when strength is more than adequate.

Because in-plane and out-of-plane force systems affect a mechanism in quite different ways, it is convenient to decompose the force analysis of a planar mechanism into separate analyses of the in-plane and out-of-plane force systems. However, this must be done with some care, since an in-plane force may contribute to an out-of-plane moment and vice versa.

### EXAMPLE 13.8 Analysis of Out-of-Plane Forces

The SCARA robot shown in Fig. 13.29 has vertical revolute axes 1, 2, and 3. It carries a payload of 50 lb with center of mass on the axis of joint 3. In addition, the members *A* and *B* can be regarded as uniform beams with respective weights of 60 and 40 lb. Characterize all the loads on members *A* and *B* in the position shown.

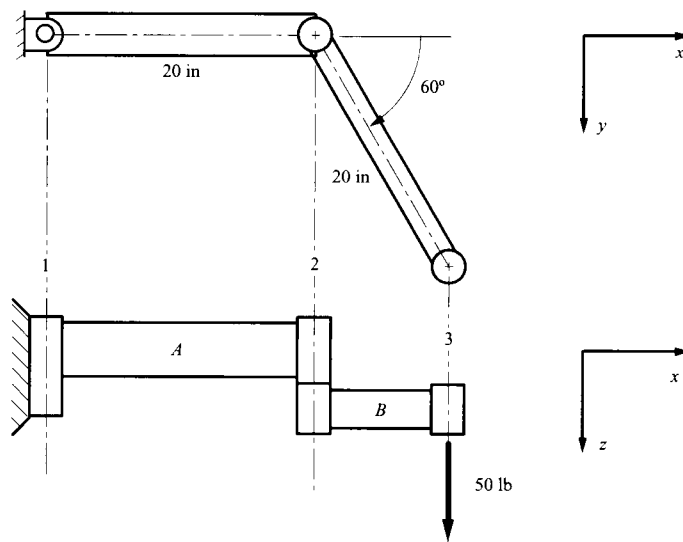
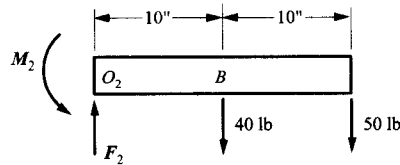


FIGURE 13.29 The SCARA robot considered in Example 13.8.

**Solution**

Here all the forces are out-of-plane forces. As far as a force analysis is concerned, the manipulator behaves as a cranked cantilever beam. To find the loads on the members *A* and *B* it is first necessary to draw free-body diagrams of each of them. A free-body diagram of member *B* in the *x-z* plane is shown in Fig. 13.30.



**FIGURE 13.30** The free-body diagram of member *B*.

As can be seen, member *B* is a simple cantilever beam considered to be embedded at joint 2. The shear force  $F_2$  and bending moment  $M_2$  at joint 2 can be found by writing the vertical force equilibrium equation and the moment equation about  $O_2$ :

$$\Sigma F_y = 0: \quad F_2 = 40 + 50 = 90 \text{ lb}$$

$$\Sigma M_2 = 0: \quad M_2 = 40 \times 10 + 50 \times 20 = 1400 \text{ in-lb}$$

The free-body diagram for member *A* is shown in Fig. 13.31.

The reaction force  $F_1$  and moments  $M_{1y}$  and  $M_{1x}$  at joint axis 1 can now be computed using vertical force equilibrium together with moment balances about the *y* and *x* directions.

In the plane of the beam,

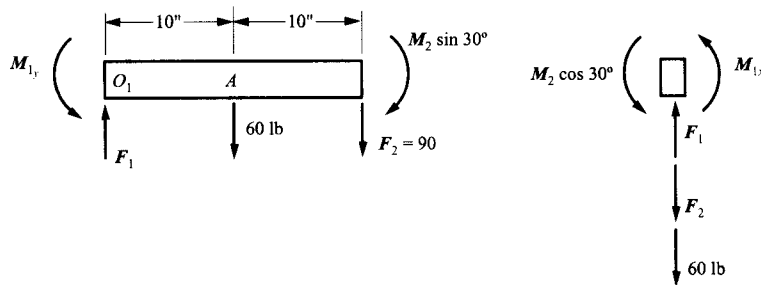
$$\Sigma F_y = 0: \quad F_1 = 60 + 90 = 150 \text{ lb}$$

$$\Sigma M_y = 0: M_{1y} = 1400 \sin 30^\circ + 90 \times 20 + 60 \times 10 = 3100 \text{ in-lb}$$

About the longitudinal axis of the beam:

$$\Sigma M_x = 0: \quad M_{1x} = -1400 \cos 30^\circ = -1212 \text{ in-lb}$$

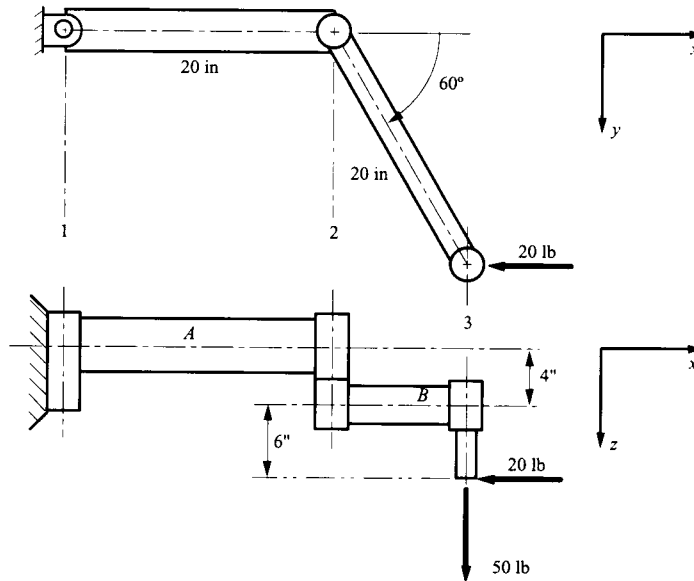
Notice that, although there are no forces in the plane of motion and no motion of the system, there are still significant forces acting on the members. It is always necessary to consider out-of-plane forces, as well as in-plane forces.



**FIGURE 13.31** The free-body diagram of member *A*. This figure shows the view of the member in its *x-y* plane together with an end view showing the torsional components. The bending moment  $M_2$  at joint 2 is applied, along with the shear force to member *A*. However, because of the  $60^\circ$  angle between the longitudinal axes of members *A* and *B*, it is necessary to resolve  $M_2$  into a component  $M_2 \sin 30^\circ$  in the plane of member *A*, along with a component  $M_2 \cos 30^\circ$ , which is a torsional moment about its longitudinal axis.

**EXAMPLE 13.9**  
**Three-Dimensional**  
**Force Analysis**  
**of a Robot**

The SCARA robot of Fig. 13.29 and Example 13.8 is required to exert a 20-lb horizontal tool force on the line of action shown in Fig. 13.32. Find the torques that must be exerted by the actuators at joints 1 and 2 and the reaction forces and moments at the joints. The weights of the members and end effector remain the same as in Example 13.8.



**FIGURE 13.32** A 20-lb horizontal tool load has been added to the weight load in Example 13.8. In this example we have both in-plane and out-of-plane force systems.

**Solution**

There are many different possible approaches to this problem. However, when dealing with fully three-dimensional systems like this, it is usually best to decide on three orthogonal coordinate axis directions and resolve all force and moment components into those directions. This may yield more equations than other choices of directions in which to resolve, but it has the advantage of being a very systematic procedure that reduces the chance of error.

It is first necessary to draw free-body diagrams of each of the two bodies in the system. Since the force system is three dimensional, in Fig. 13.33 we have resorted to three orthogonal views of each member to ensure that every force component is visible. In fact, each component should appear on at least two of these views.

We can now proceed to write the six static equilibrium equations for each member by referring to the free-body diagrams in Fig. 13.33.

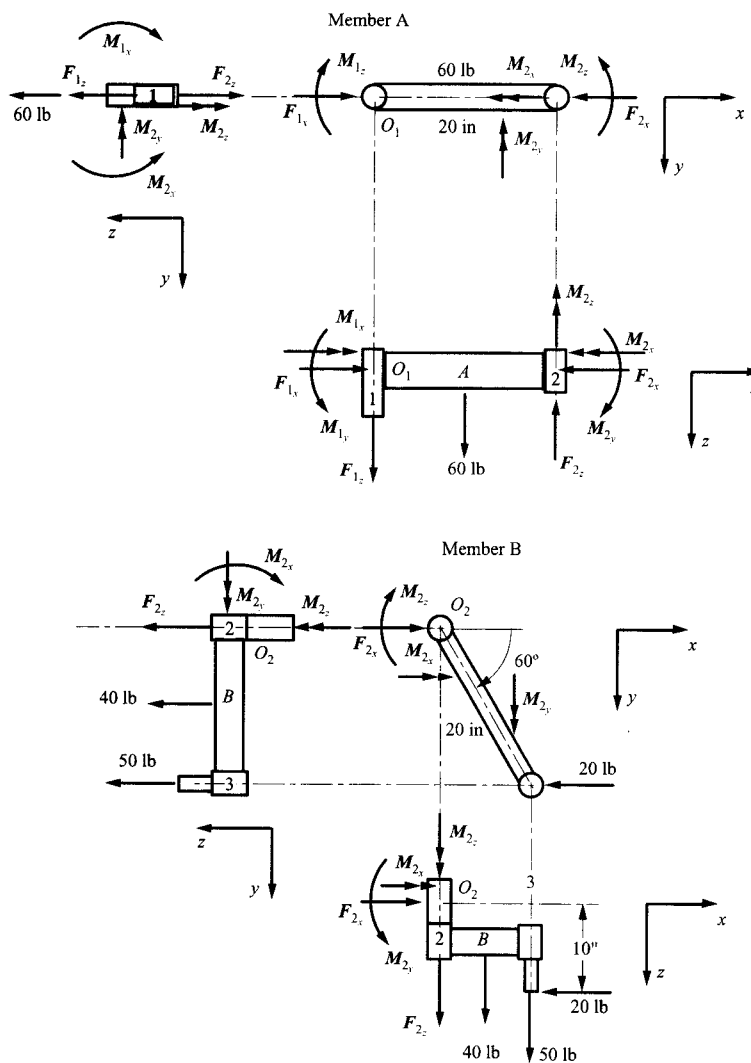
For member *B*,

$$\Sigma F_x = 0: F_{2x} = 20$$

$$\Sigma F_y = 0: 0 = 0$$

$$\Sigma F_z = 0: F_{2z} + 40 + 50 = 0$$





**FIGURE 13.33** Free-body diagrams for Example 13.9. Each free body is shown in three orthogonal views: projected on the  $x$ - $y$  plane, the  $x$ - $z$  plane and the  $y$ - $z$  plane, respectively.

Taking moments about point  $O_2$ , we have

$$\Sigma M_x = 0: M_{2_y} + 50 \times 20 \sin 60^\circ + 40 \times 10 \sin 60^\circ = 0$$

$$\Sigma M_y = 0: M_{2_x} = 10 \times 20 + 50 \times 20 \cos 60^\circ + 40 \times 10 \cos 60^\circ$$

$$\Sigma M_z = 0: M_{2_z} + 20 \times 20 \sin 60^\circ = 0$$

Solution of these equations gives

$$F_{2_x} = 20 \text{ lb}$$

$$F_{2_y} = -90 \text{ lb}$$

$$M_{2_x} = -1212 \text{ in-lb}$$

$$M_{2_y} = 900 \text{ in-lb}$$

$$M_{2_z} = -346 \text{ in-lb}$$

For member  $A$ ,

$$\Sigma F_x = 0: F_{1_x} = F_{2_x}$$

$$\Sigma F_y = 0: 0 = 0$$

$$\Sigma F_z = 0: F_{1_z} + 60 = F_{2_z}$$

Taking moments about point  $O_1$ , we have

$$\Sigma M_x = 0: M_{1_x} = M_{2_x}$$

$$\Sigma M_y = 0: M_{1_y} = M_{2_y} + 60 \times 10 - F_{2_z} \times 20$$

$$\Sigma M_z = 0: M_{1_z} = M_{2_z}$$

Substitution of the previously calculated values for  $F_{2_x}$ ,  $F_{2_y}$ ,  $M_{2_x}$ ,  $M_{2_y}$ , and  $M_{2_z}$  gives

$$F_{1_x} = 20 \text{ lb}$$

$$F_{1_z} = -150 \text{ lb}$$

$$M_{1_x} = -1212 \text{ in-lb}$$

$$M_{1_y} = 900 + 600 - (-90) \times 20 = 3300 \text{ in-lb}$$

$$M_{1_z} = -346 \text{ in-lb}$$

This completes the solution. The torques  $M_{1_x}$ ,  $F_{2_x}$  and  $M_{2_z}$  that must be produced by the actuators at joints 1 and 2, respectively, are both 346 in-lb in magnitude. The reaction forces and moments  $F_{1_x}$ ,  $F_{1_z}$ ,  $M_{1_x}$ ,  $M_{1_y}$ ,  $F_{2_x}$ ,  $F_{2_y}$ ,  $M_{2_x}$ , and  $M_{2_y}$  may be compared with the results of Example 13.8. As may be seen, the vertical forces  $F_{1_z}$  and  $F_{2_z}$  remain the same, as does  $M_{1_x}$ . The other forces and moments are changed by the presence of the horizontal tool load.

## 13.9 CONSERVATION OF ENERGY AND POWER

When a linkage is subjected to significant loads only on the input and output links and the system can be regarded as static, a quick and easy method of computing the ratio of input force/torque to output force/torque is available. This is particularly useful if a velocity analysis has already been performed for other reasons, because a velocity analysis is needed as part of the solution.

For a given mechanism, the input power equals the output power if the following are satisfied:

1. There are no energy losses in the mechanism. This means that there is no friction in the joints or no other form of energy dissipation.
2. There is no energy stored in the mechanism as it moves. This means that there are no springs in the system and that the energy associated with potential energy because of the weight of the links and the change in the centers of gravity of the links is negligible.
3. The velocities are small enough or the masses are small enough that changes in kinetic energy are negligible.

Thus, if the input and output loads are torques  $T_i$  and  $T_o$ , respectively, and the angular velocities of the input and output links are  $\omega_i$  and  $\omega_o$ , respectively, then

$$T_i \cdot \omega_i + T_o \cdot \omega_o = 0$$

The + sign in the equation implies that if  $T_i$  is in the same direction as  $\omega_i$ , as is often, but not necessarily, the case, then  $T_o$  will be in the opposite direction to  $\omega_o$ .

Similarly, if the input and output are forces  $F_i$  and  $F_o$ , and  $v_{pi}$  and  $v_{po}$  are the respective velocities of their points of application, then

$$F_i \cdot v_{pi} + F_o \cdot v_{po} = 0$$

Similarly, for a force input and torque output

$$F_i \cdot v_{pi} + T_o \cdot \omega_o = 0$$

and for a torque input and force output

$$T_i \cdot \omega_i + F_o \cdot v_{po} = 0$$

or, in general,

$$\sum_{k=1}^m T_k \cdot \omega_k + \sum_{j=1}^n F_j \cdot v_{pj} = 0 \quad (13.19)$$

where  $T_k$ ,  $k = 1, 2, \dots, m$  are all torques acting on members of the system and  $\omega_k$ ,  $k = 1, 2, \dots, m$ , are the angular velocities of the links to which they are respectively applied.  $F_j$ ,  $j = 1, 2, \dots, n$ , are all forces acting on the system, and  $v_{pj}$ ,  $j = 1, 2, \dots, n$ , are the respective velocities of their points of applications. Thus, more generally, if the necessary velocity information for the system is available, a static force analysis can be performed using power conservation as an alternative to static equilibrium. Depending on the system characteristics, this may or may not be more efficient than performing a force analysis using free-body diagrams and the equations for static equilibrium.

When computing the power, the dot product for the force–velocity expression is given by

$$F_j \cdot v_{pj} = F_j \cdot v_{pj} \cos \theta_j = F_x v_x + F_y v_y + F_z v_z$$

where the magnitudes of the force and torque can be both positive and negative, and  $\theta_j$  is the angle between  $F$ ,  $F_j$ , and  $v_{pj}$ . The dot product of the torque and angular velocity can be computed by multiplying the magnitudes of the two vectors, again realizing that the signs can be either positive or negative depending on whether the torque and angular velocity are in the same direction or opposite directions. Situations of positive and negative power are illustrated schematically in Fig. 13.34.

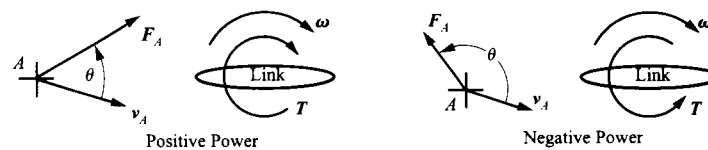


FIGURE 13.34 Situations for positive and negative power.

The velocity analysis can be conducted using any procedure that is convenient. Note, however, that only the velocities associated with the points and links associated with the application of external forces and torques are needed. Because only selected velocities are usually required in Eq. (13.19), force analyses using conservation of power are often done in conjunction with the use of instant centers for the velocity analysis. Of course, if the velocities are already known from some other type of analysis, these can be used directly.

Note that even though Eq. (13.19) involves the velocities, the results will not depend on the value chosen for the input velocity. This must be the case because we could also conduct the force analysis using free-body diagrams and the equations for force equilibrium, and these equations are a function of position and the applied forces only. Recall that the velocity problem is a linear problem. Therefore, if the input velocity is multiplied by a constant, then all of the velocities including the angular velocities will be multiplied by the same constant. Therefore, if we divide Eq. (13.19) by the magnitude of the input velocity, the force/torque results will be unchanged. Because of this, we need not know the actual value for the input velocity before conducting the force analysis. In fact, the mechanism need not be moving at all. Because of this, a common value to choose for the input velocity is 1.

**EXAMPLE 13.10**  
**Analysis of a**  
**Slider-Crank**  
**Mechanism Using**  
**Conservation of**  
**Power**  
**Solution**

Estimate the necessary driving torque for the mud pump of Example 13.6 using conservation of power.

To obtain a quick estimate of the forces, we will neglect the effect of the weight of the components. This is justifiable because those weights are much smaller than the piston load of  $P = 21,340$  lb (Example 13.6).

We will conduct the velocity analysis using instant centers because only two velocities are required. Since the piston load can be considered to act at point  $C$  on member 4 and the driving torque acts on member 2, we need  $I_{12}$ ,  $I_{14}$ , and  $I_{24}$  to develop the necessary relationship between the input and output velocity using the instantaneous center method.  $I_{24}$  is located as shown in Fig. 13.35. The distance  $I_{24}I_{12}$  can be scaled from the drawing or calculated. To calculate it, use angle  $ACB$  ( $11.096^\circ$  from Example 13.6) and first find

$$\phi = \angle BI_{24}A = 90^\circ - 11.096^\circ = 78.904^\circ$$

$$\beta = \angle BAI_{24} = 90^\circ - 60^\circ = 30^\circ$$

and

$$\gamma = \angle ABI_{24} = 180^\circ - \phi - \beta = 180^\circ - 78.904^\circ - 30^\circ = 71.096^\circ$$

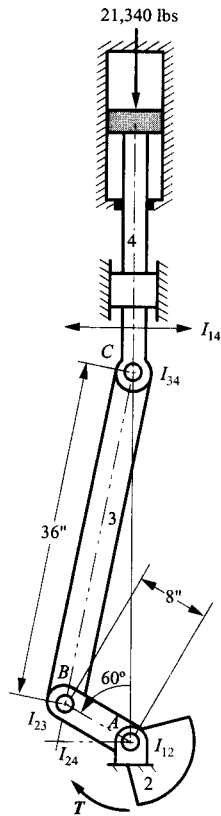


FIGURE 13.35 Location of instant centers for mud pump.

Now use the sine rule to find the length  $r = AI_{24}$ :

$$r = \sin \gamma \frac{AB}{\sin \phi} = \frac{8 \sin 71.096^\circ}{\sin 78.904^\circ} = 7.713 \text{ in}$$

The velocity of  $I_{24}$  is equal to the velocity of  $C_4$  where the force of 21,340 lb is applied. Also, if we consider  $I_{24}$  to be a point on link 2,

$$\mathbf{v}_{I_{24}} = \boldsymbol{\omega}_2 \times \mathbf{r}_{I_{24}/A}$$

and the magnitude is the velocity of  $I_{24}$ ,

$$v_{I_{24}} = \omega_2 (r_{I_{24}/A})$$

From conservation of power,

$$\mathbf{T} \cdot \boldsymbol{\omega}_2 + \mathbf{P} \cdot \mathbf{v}_{C_4} = 0 \quad (13.20)$$

Let us assume that link 2 is rotating clockwise. Then  $\mathbf{P}$  and  $\mathbf{v}_{C_4}$  are in opposite directions. Therefore, power is being taken out at the piston and put into the system at the crank. Consequently, the torque,  $\mathbf{T}$ , must be in the same direction as the angular velocity of link 2, or clockwise. Therefore, we need only use Eq. (13.20) to find the magnitude of  $\mathbf{T}$ . This gives

$$T = P \frac{v_{C_4}}{\omega_2} = P \frac{v_{I_{24}}}{\omega_2} = P \frac{\omega_2 (r_{I_{24}/A})}{\omega_2} = P (r_{I_{24}/A})$$

Therefore,

$$T = 21340(7.713) = 164,600 \text{ in-lb or } 13,700 \text{ ft-lb CW}$$

This may be compared with the value of  $T = 13,800 \text{ ft-lb}$  obtained from the full static equilibrium analysis. The difference between the values is accounted for by the fact that the weights of the linkage members were included in the former analysis.

**EXAMPLE 13.11**  
**Analysis of a**  
**Four-Bar Linkage**  
**Using**  
**Conservation**  
**of Power**

In the four-bar linkage represented in Fig. 13.36, a torque  $T_{12}$  is applied to link 2, and it is resisted by a torque  $T_{14}$  on link 4. Find a relationship for the mechanical advantage of the mechanism in terms of the mechanism geometry.

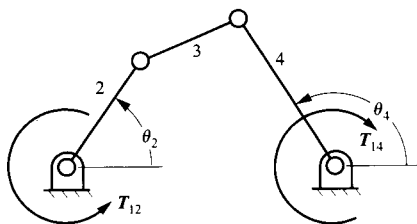


FIGURE 13.36 The linkage for Example 13.11.

**Solution**

The mechanical advantage ( $MA$ ) for the linkage is a function of position and is given by

$$MA = \frac{\text{output torque}}{\text{input torque}} = \frac{T_{14}}{T_{12}} \quad (13.21)$$

Therefore, we must find a geometric relationship equal to the ratio of the output torque divided by the input torque. We will use conservation of power for the analysis and conduct the velocity analysis using instant centers of velocity. To begin, the power expression is

$$T_{12} \cdot \omega_2 + T_{14} \cdot \omega_4 = 0 \quad (13.22)$$

From this expression, if  $T_{12}$  and  $\omega_2$  are in the same direction, then  $T_{14}$  and  $\omega_4$  must be in opposite directions. Therefore, if we know the signs of  $T_{12}$ ,  $\omega_2$ , and  $\omega_4$ , we can determine the sign of  $T_{14}$  by inspection after a kinematic analysis is conducted. Consequently, we can concentrate on the magnitude of  $T_{14}$ . We can compute the magnitude of  $T_{14}$  directly from Eq. (13.22). That is,

$$T_{14} = \frac{T_{12}\omega_2}{\omega_4} = T_{12} \frac{\omega_2}{\omega_4}$$

Therefore,

$$\frac{T_{14}}{T_{12}} = \frac{\omega_2}{\omega_4} \quad (13.23)$$

Based on our knowledge of instant centers, the ratio  $\omega_2/\omega_4$  will be a function of geometry only. To find the ratio of angular velocities, we need first to find the instant centers  $I_{12}$ ,  $I_{14}$ , and  $I_{24}$ . These are shown in Fig. 13.37. The velocity of the two points located at  $I_{24}$  is given by

$$\mathbf{v}_{I_{24}} = \boldsymbol{\omega}_2 \times \mathbf{r}_{I_{24}/I_{12}} = \boldsymbol{\omega}_4 \times \mathbf{r}_{I_{24}/I_{14}}$$

and

$$\omega_2 r_{I_{24}/I_{12}} = \omega_4 r_{I_{24}/I_{14}}$$

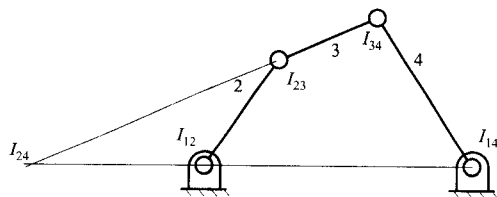


FIGURE 13.37 Instant center locations for the linkage in Fig. 13.36.

Therefore,

$$\frac{\omega_2}{\omega_4} = \frac{r_{I_{24}/I_{14}}}{r_{I_{24}/I_{12}}} \quad (13.24)$$

Equation (13.24) shows that the ratio of the angular velocities is clearly a function of position, that is, of the location of the instant centers.

Now combining Eqs. (13.21), (13.23), and (13.24) gives

$$MA = \frac{T_{14}}{T_{12}} = \frac{\omega_2}{\omega_4} = \frac{r_{I_{24}/I_{14}}}{r_{I_{24}/I_{12}}}$$

Note that the sign of either  $\omega_2$  or  $\omega_4$  can be negative. Therefore, mechanical advantage may be positive or negative, although in many instances only the magnitude is of interest. When  $MA$  is positive, the torques are in the same direction, and when it is negative they are in opposite directions. In this particular example,  $r_{I_{24}/I_{14}}$  and  $r_{I_{24}/I_{12}}$  (and therefore  $\omega_2$  and  $\omega_4$ ) will be in the same direction when  $I_{24}$  is outside of  $I_{12}$  and  $I_{14}$ . They will be in opposite directions when  $I_{24}$  is between  $I_{12}$  and  $I_{14}$ .

## 13.10 VIRTUAL WORK

It is possible to apply the conservation of energy method to obtain force relationships in truly static systems in which no real movement occurs. The technique is to imagine a small displacement of the point of application of the input force and compute the corresponding displacement of the point or points of application of the output force or forces. The sum of the work done by all external forces must be zero. This is the principle of *virtual work*. It is identical to conservation of power or conservation of energy except that the displacements are virtual or imaginary.

The problem of deriving a consistent set of displacements of the points of application of the external forces, which is the key to this technique, can be converted to a velocity analysis. If the velocity of each application point is multiplied by the same small time interval, the result is a set of consistent, small displacements. The time interval, being the same in all cases, will cancel from the energy equation so that it becomes, in fact, identical to Eq. (13.19). The way in which the method is used will be illustrated by the following example.

**EXAMPLE 13.12**  
**Analysis of a**  
**Vice Grip Using**  
**Virtual Work**

**Solution**

Find the grip force,  $F_G$ , when the force applied to the handles of the vice-grip pliers of Fig. 13.6 is 25 lb. The lines of action of the grip forces and hand forces are located as indicated in Fig. 13.7.

Although the system depicted in Fig. 13.6 is truly static, we can still imagine a small displacement such as might occur if the workpiece were compliant and deflected a little. When using virtual work, we must account for all of the work done during the virtual displacement. In Fig. 13.38, work will be done by the forces at  $G$  and  $H$  and by the spring force. However, the spring force is so much less than the other forces that the energy stored in the spring can be ignored.

To obtain consistent displacements efficiently, we can again use the instantaneous center method. The six instantaneous centers of the mechanism are located as shown in Fig. 13.38. If member 1 is treated as the base and the point of application of  $F_H$  on the lower handle is displaced, there will also be a displacement of the point of application of  $F_G$  on the lower jaw. Since the former is on member 3 and the latter is on member 2, we need  $I_{13}$ ,  $I_{12}$ , and  $I_{23}$  to obtain the necessary consistent pair of velocities (or displacements).

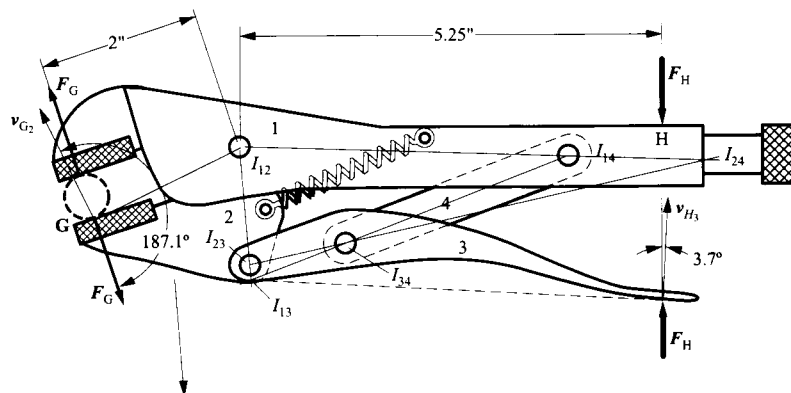


FIGURE 13.38 Locations of the instantaneous centers for the vice-grip pliers of Example 13.12.

Scaling from the drawing shown in Fig. 13.38 gives

$$\overrightarrow{I_{12}I_{23}} = 1.469 \text{ in, } \overrightarrow{I_{13}I_{23}} = 0.186 \text{ in}$$

Hence

$$\omega_2 / \omega_3 = 0.186 / 1.469$$

Also

$$\overrightarrow{HI_{13}} = 5.129 \text{ in and } \overrightarrow{GI_{12}} = 2.019 \text{ in}$$

Now

$$v_G / v_H = \left( \overrightarrow{GI_{12}} \times \omega_2 \right) / \left( \overrightarrow{HI_{13}} \times \omega_3 \right) = (2.019 \times 0.186) / (5.129 \times 1.469)$$

or

$$v_G = 0.0498v_H$$



Also, the angle between  $v_H$  and  $F_H$  is  $3.7^\circ$ , whereas that between  $v_G$  and  $F_G$  is  $187.1^\circ$ . Hence

$$F_H v_H \cos 3.7^\circ + F_G v_G \cos 187.1^\circ = 0$$

or

$$v_H \times 25 \times \cos 3.7^\circ + F_G \times v_H \times 0.0498 \times \cos 187.1^\circ = 0$$

Notice that the equation may be divided by  $v_H$ , indicating that the results are independent of the value chosen for  $v_H$ . The final result for  $F_G$  is

$$F_G = 505 \text{ lb}$$

This value may be compared with that obtained by a completely different method in Example 13.2. The small difference is due to graphical inaccuracies.

In the present instance we chose not to include the spring force because it proved to be negligible in Example 13.2. It could have been included, however, by finding the virtual velocity of its point of application on link 2 and including the scalar product of that velocity with the spring force in the conservation of energy equation (Eq. 13.19). The change in  $F_G$  would be insignificant, however.

## 13.11 GEAR LOADS

### 13.11.1 Spur Gears

In the analysis, we will assume that the spur gears have an involute profile. If friction is neglected, the force exerted by one of a pair of meshing gears on the other acts along the line normal to the teeth at the point of contact. That is, it acts along the line of action or pressure line shown in Fig. 13.39.

Free-body diagrams of the gear and pinion are shown in Fig. 13.40. The normal force  $W$  is tangent to the base circles of both the pinion and gear, and the magnitude of the torque on the pinion is

$$T_1 = W r_{b1} = W r_{p1} \cos \psi \quad (13.25)$$

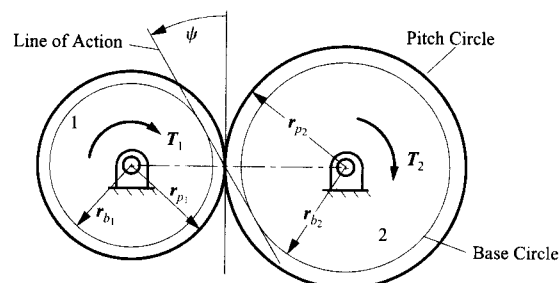


FIGURE 13.39 Torque transmitted through spur gears.

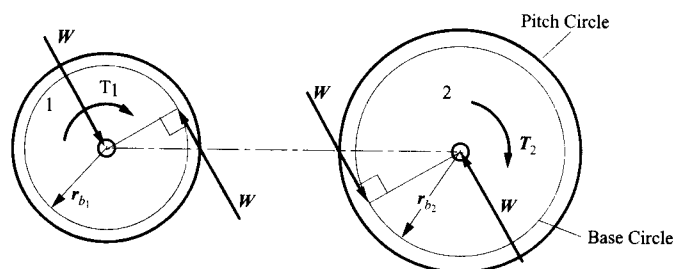


FIGURE 13.40 Free-body diagrams of spur gears.

The magnitude of the torque on the gear is

$$T_2 = Wr_{b_2} = Wr_{p_2} \cos \psi \quad (13.26)$$

Therefore

$$\frac{T_2}{T_1} = \frac{r_{p_2}}{r_{p_1}} = \frac{N_2}{N_1}$$

where  $N_1$  and  $N_2$  are the numbers of teeth on the pinion and gear, respectively.

Also, from Eqs. (13.25) and (13.26)

$$W = \frac{T_1}{r_{p_1} \cos \psi} = \frac{T_2}{r_{p_2} \cos \psi} \quad (13.27)$$

It can be seen that  $W$  is also the load on the bearings supporting the shafts of both the gear and the pinion.

If friction is considered, an additional force component of magnitude  $\mu W$ , where  $\mu$  is the coefficient of friction, appears tangent to the teeth at the point of contact. This is shown in Fig. 13.41. Because  $W$  is constant, the friction force is constant in magnitude, and the bearing reactions ( $F_B$ ) are also constant in magnitude and given by

$$F_B = \sqrt{W^2 + (\mu W)^2} = W\sqrt{1 + \mu^2}$$

The torque magnitudes are

$$T_1 = Wr_{b_1} - \mu Wx \quad (13.28)$$

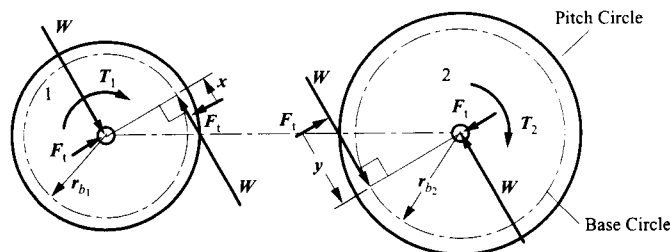
$$T_2 = Wr_{b_2} - \mu Wy \quad (13.29)$$

The distances  $x$  and  $y$  vary as the point of contact moves along the path of contact. However,

$$x + y = r_{b_1} \tan \psi + r_{b_2} \tan \psi = (r_{p_1} + r_{p_2}) \sin \psi = \frac{N_1 + N_2}{2P} \sin \psi \quad (13.30)$$

where  $P$  is the diametrical pitch. From Eqs. (13.28)–(13.30),

$$\frac{T_2}{T_1} = \frac{r_{b_2} - \mu y}{r_{b_1} - \mu x} = \frac{\frac{N_2}{2P} \cos \psi - \mu \left( \frac{N_1 + N_2}{2P} \sin \psi - x \right)}{\frac{N_1}{2P} \cos \psi - \mu x}$$



Note that  $F_f = \mu W$ .

FIGURE 13.41 Spur gears with friction.

or

$$\frac{T_2}{T_1} = \frac{N_2 \cos \psi - \mu(N_1 + N_2) \sin \psi + 2\mu Px}{N_1 \cos \psi - 2\mu Px}$$

Thus,  $T_2/T_1$  is no longer constant but is a function of the position  $x$  of the point of contact. This is a source of torsional vibration. The amount of variation is a function of the length of the path of contact. Note that  $T_2/T_1$  is always less than  $N_2/N_1$  when averaged over the contact cycle. The sharing of loads among two or more pairs of teeth in contact does not change the bearing loads, but it does affect the torque fluctuations and tends to diminish them. Since the load sharing depends on the tooth stiffnesses, modeling of this effect becomes complicated and is beyond the scope of this text.

### 13.11.2 Helical Gears

The teeth of an involute helical gear are similar in cross section to those of a spur gear. However, instead of being cut with their faces parallel to the gear axis, they are cut at an angle  $\alpha$  to that axis, where  $\alpha$  is the helix angle of the gear. It is similar to the lead angle of a screw, except that the teeth of the helical gear are straight. That is, a straight line tangent to the pitch cylinder of the gear at its midplane can be drawn on the face of each tooth. The set of such lines from all teeth form the generators of a hyperboloid of one sheet. If this line is moved parallel to itself along an involute curve with the pitch circle radius equal to that of the pitch cylinder, it will generate the tooth face.

If friction is neglected, the force transmitted between contacting teeth is normal to the gear teeth at the point of contact. That is, it lies in the normal plane. It is inclined at angle  $\psi_n$  to the cylinder tangent at the point of contact as shown in Fig. 13.42. Here,  $\psi_n$  is the pressure angle for the hob used to cut the gear. Resolving the contact force  $W$  into the plane normal to the gear tooth gives

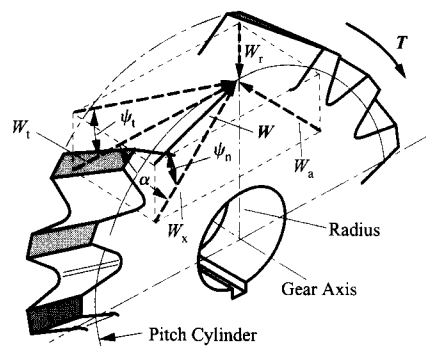
$$W_r = W \sin \psi_n$$

and

$$W_x = W \cos \psi_n$$

Resolving  $W_x$  in the plane tangent to the pitch cylinder gives

$$W_t = W_x \cos \alpha = W \cos \psi_n \cos \alpha$$



**FIGURE 13.42** Resolution of contact force on tooth of helical gear.  $W$  is the contact force acting along the pitch line.  $W_r$  is the radial component of  $W$ .  $W_x$  is the component of  $W$  that is orthogonal to  $W_r$ .  $W_x$  is tangent to the pitch cylinder of the gear.  $W$ ,  $W_r$ , and  $W_x$  lie in a plane normal to the gear tooth face at the point of contact.  $\alpha$  is the helix angle of the teeth.  $W_a$  is parallel to the gear axis of rotation, and  $W_t$  is the tangent to the pitch cylinder normal to  $W_a$  and passing through the pitch point.

and

$$W_a = W_x \sin \alpha = W \cos \psi_n \sin \alpha$$

Also, from Fig. 13.42,

$$W_r \tan \psi_n = W_t \tan \psi_t \cos \alpha$$

and

$$\tan \psi_t = \frac{\tan \psi_n}{\cos \alpha} \quad (13.31)$$

Hence

$$\frac{W_r}{W_t} = \frac{\sin \psi_n}{\cos \psi_n \cos \alpha} = \frac{\tan \psi_n}{\cos \alpha} = \tan \psi_t$$

or

$$\begin{aligned} W_r &= W_t \tan \psi_t \\ \frac{W_a}{W_t} &= \tan \alpha \end{aligned} \quad (13.32)$$

or

$$W_a = W_t \tan \alpha \quad (13.33)$$

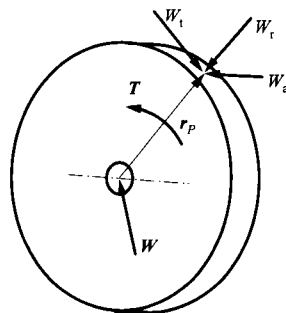
The torque acting on the gear is represented in the free-body diagram in Fig. 13.43. From the figure,

$$T = W_t r_p \quad (13.34)$$

where  $r_p$  is the radius of the pitch circle. Using these relationships, the components  $W_t$ ,  $W_a$ , and  $W_r$  can be computed in terms of the torque  $T$ .

Note that the axial thrust  $W_a$  also produces a couple tending to rotate the gear in the plane of the shaft axis. This produces an asymmetry in the bearing loads. The couple has magnitude

$$T_a = W_a r_p = W_t r_p \tan \alpha \quad (13.35)$$



**FIGURE 13.43** The free-body diagram of the gear. The only component of the contact force  $W$  that exerts a moment about the gear axis is  $W_t$ .

**EXAMPLE 13.13**  
**Analysis of**  
**Helical Gear**

**Solution**

A helical gear is cut with a standard  $25^\circ$  pressure angle, diametrical pitch 4 spur gear cutter at a helix angle of  $30^\circ$ . If the gear has 40 teeth and transmits 100 hp at a speed of 500 rpm, calculate the radial and thrust loads to be carried by the mounting bearings. Also compute the couple due to the axial component. If the shaft bearings are to be 6 in apart, compute the additional radial bearing load from this source.

To solve the problem, we must determine the tangential component,  $W_t$ , of the normal force, and from this we can determine the other components. Using Eq. (13.34), the relationship between  $W_t$ , the power  $P$ , and the angular velocity,  $\omega$ , of the gear is

$$W_t = \frac{T}{r_p} = \frac{P}{\omega r_p} \quad (13.36)$$

We can compute the pitch radius from the number of teeth and the diametrical pitch. That is,

$$r_p = \frac{N}{2P} = \frac{40}{2(4)} = 5 \text{ in}$$

Because the power is given in horsepower,  $r_p$  in inches, and  $\omega$  in revolutions per minute, Eq. (13.36) becomes

$$W_t = \frac{(100 \times 550)(12)(60)}{2\pi\omega r_p} = 2520 \text{ lb}$$

From Eqs. (13.31) and (13.32),

$$W_r = W_t \tan \psi_t = W_t \frac{\tan \psi_n}{\cos \alpha} = 2520 \frac{\tan 25^\circ}{\cos 30^\circ} = 1357 \text{ in}$$

And from Eq. (13.33),

$$W_a = W_t \tan \alpha = 2520 \tan 30^\circ = 1455 \text{ lb}$$

The couple due to the axial load is given by Eq. (13.35) as

$$T_a = W_a r_p = W_t r_p \tan \alpha = 2520(5) \tan 30^\circ = 7275 \text{ in-lb}$$

The shaft bearings must produce a couple that will react with this couple to place the shaft in static equilibrium. The magnitude of the couple produced by the bearings is  $6F$ , so the *increase* in the reaction forces to support the couple produced by the axial load is

$$F = \frac{7275}{6} = 1212 \text{ lb}$$

### 13.11.3 Worm Gears

Worm gears are a special case of crossed helical gears, and the forces on the worm from the gear are usually resolved as shown in Fig. 13.44. The force equations are similar to those for helical gears except that in the case of worm gears, the lead angle,  $\lambda$ , is usually used instead of the helix angle. With worm gears, the worm is almost always the driver because in most cases friction makes it impossible to drive the worm from the gear. Referring to Fig. 13.44, we can write the force component equations for the worm as

$$W_t = \frac{T}{r_p}$$

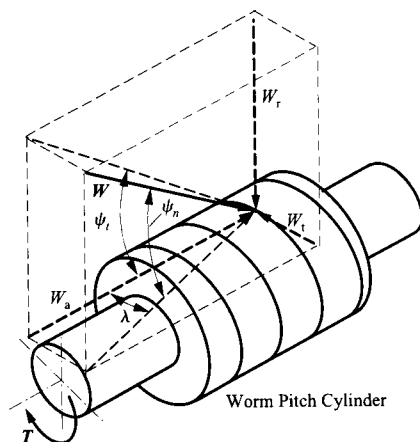


FIGURE 13.44 The forces on a worm gear.

where  $r_p$  is the pitch radius and  $T$  is the input torque on the worm,

$$W_a = \frac{W_t}{\tan \lambda}$$

$$W_r = W_t \frac{\tan \psi_t}{\tan \lambda}$$

and

$$W = \sqrt{W_a^2 + W_r^2 + W_t^2}$$

In most worm gear drives, the gear axis is at right angles to that of the worm. Because of this,  $W_a$  for the worm becomes  $W_t$  for the gear, and  $W_t$  for the worm becomes  $W_a$  for the gear. The radial component is the same for both the worm and the gear.

For typical values for  $\lambda$  and  $\psi_t$ , the magnitude of  $W$  is much larger than the magnitude  $W_t$ . This makes worm gears somewhat inefficient, because even small values of the coefficient of friction will produce large friction forces compared with  $W_t$ . This makes the equations in this section somewhat approximate for design purposes. For accurate designs, the contribution of friction must be included in the force calculations. If friction is not included in the analysis, the effect of friction must be accounted for through a safety factor for the gearbox.

It is also necessary to account for the frictional losses by providing a means for cooling the gearbox. This is commonly done by providing fins on the gearbox to improve convective heat transfer. In extreme cases, the oil is cooled separately. In general, the frictional losses will be converted to heat, and if the design does not properly account for this heat load, the oil temperature will rise and the gearbox will fail prematurely.

### 13.11.4 Straight Bevel Gears

In computing the tooth forces on bevel gears, it is necessary to estimate the point of application of the force. It is typical to assume that the contact force acts at the middle of the tooth face. In practice, it is probably somewhat farther toward the thick end of the tooth because the tooth is stiffer in that direction. However, the error in assuming that the force contacts the middle of the tooth is small, and this will generally give slightly conservative results. In the absence of friction, the contact force,  $W$ , will be normal to the tooth, and as indicated in Fig. 13.45, the force can be resolved into three components. The tangential component,  $W_t$ , is the component that generates the shaft torque, and it is given by

$$W_t = W \cos \psi$$

where  $\psi$  is the pressure angle. The force component in the plane of the gear shaft is

$$W_y = W \sin \psi$$

and this component can be used to compute the radial and axial components. These are

$$W_r = W_y \cos \gamma = W \sin \psi \cos \gamma$$

$$W_a = W_y \sin \gamma = W \sin \psi \sin \gamma$$

where  $\gamma$  is the cone angle for the gear. The magnitude of the torque,  $T$ , transmitted by the gear is given by

$$T = W_t r_{ave}$$

where  $r_{ave}$  is the average radius of the gear pitch cone. Note that as in the case of a helical gear, the force component  $W_a$  produces a time-varying couple on the shaft, and the couple must be resisted by the bearings.

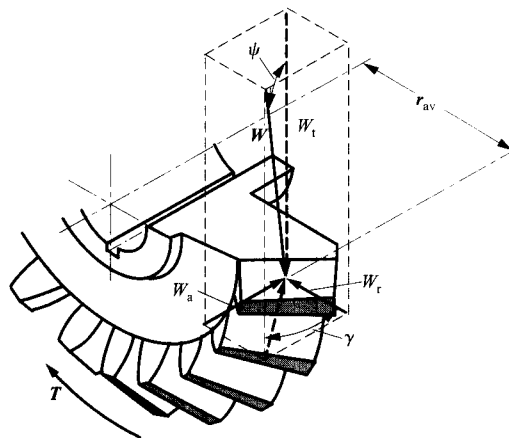
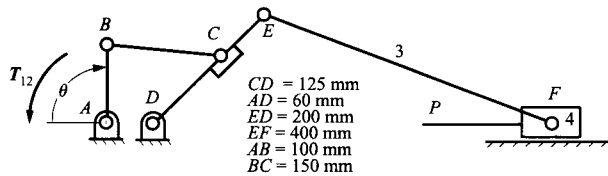


FIGURE 13.45 The force components for a straight-toothed bevel gear.

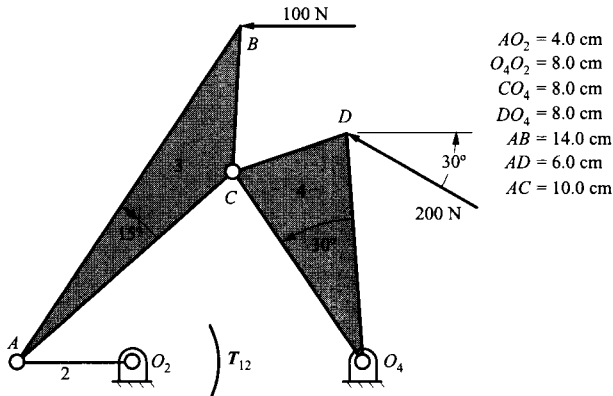
**PROBLEMS**

**EXERCISE PROBLEMS REQUIRING FREE-BODY DIAGRAMS**

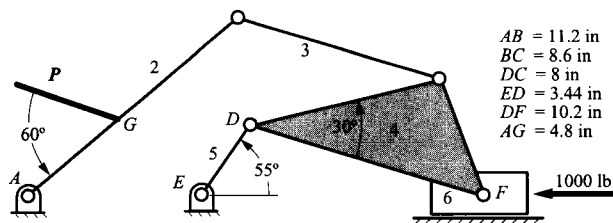
13.1 In the mechanism shown, sketch a free-body diagram of each link, and determine the force  $P$  that is necessary for equilibrium if  $T_{12} = 90 \text{ N}\cdot\text{m}$  and  $\theta = 90^\circ$ .



13.2 Draw a free-body diagram for each of the members of the mechanism shown, and find the magnitude and direction of all the forces and moments. Compute the torque applied to link 2 to maintain static equilibrium. Link 2 is horizontal.

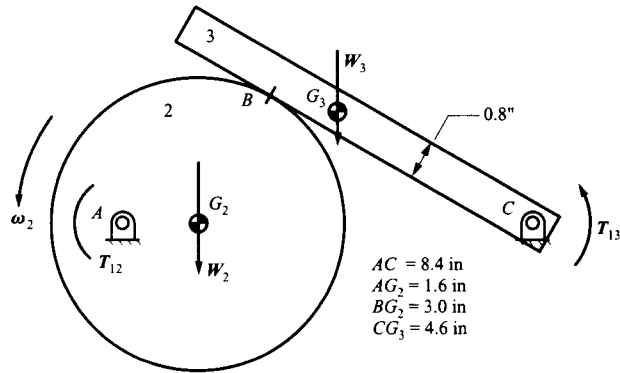


13.3 If a force of 1000 lb is applied to the slider as shown, determine the force  $P$  required for static equilibrium. Use free-body diagrams.



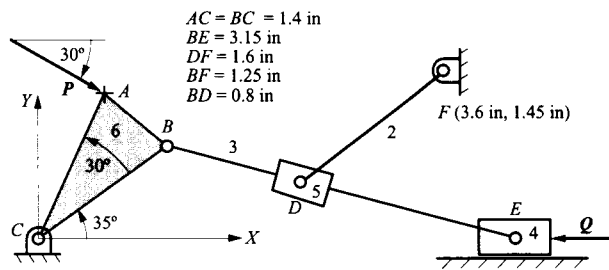
13.4 For the mechanism and data given, determine the cam torque,  $T_{12}$ , and the forces on the frame at points  $A$  and  $C$  ( $F_{21}$  and  $F_{31}$ ). Assume that there is friction between the cam and follower only. Use the following values:

$T_{14} = 50 \text{ in}\cdot\text{lb}$ ,  $W_2 = 16.1 \text{ lb}$   
 $\mu = 0.13$ ,  $W_3 = 32.2 \text{ lb}$

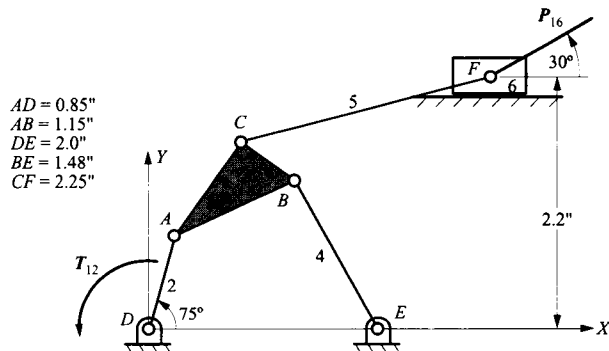


**EXERCISE PROBLEMS REQUIRING CONSERVATION OF POWER**

13.5 In the mechanism shown,  $P = 100 \text{ lb}$  in the direction shown. Find the value of the force  $Q$  on the block for equilibrium. Use conservation of power.

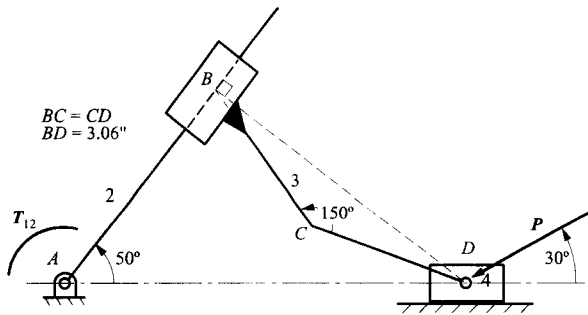


13.6 If  $T_{12}$  is 1 in-lb, find  $P_{16}$  using conservation of power.

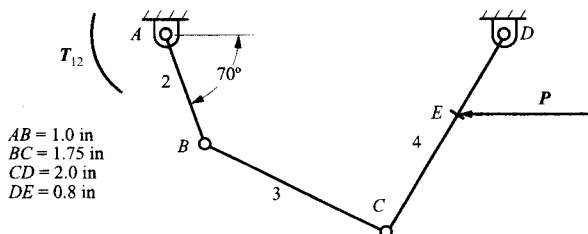


13.7 Assume that the force  $P$  is 10 lb in the direction shown. Find the torque  $T_{12}$  required for equilibrium.

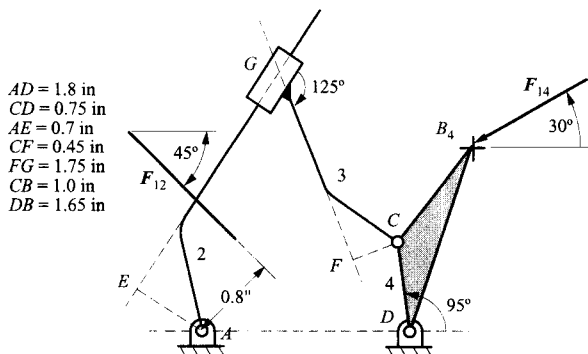




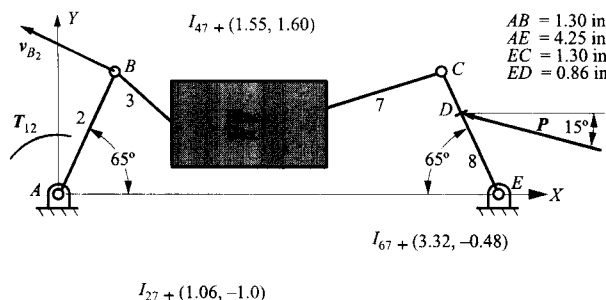
13.8 In the four-bar linkage shown, the force  $P$  is 100 lb in the direction shown. Find the torque  $T_{12}$  required for equilibrium.



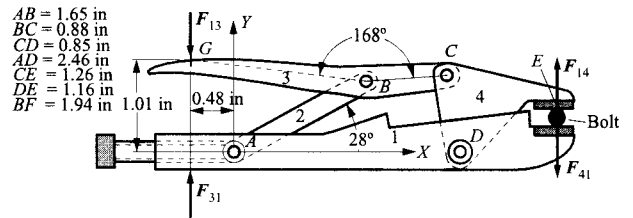
13.9 If  $F_{14}$  is 100 lb in the direction shown, find the force  $F_{12}$  required for static equilibrium.



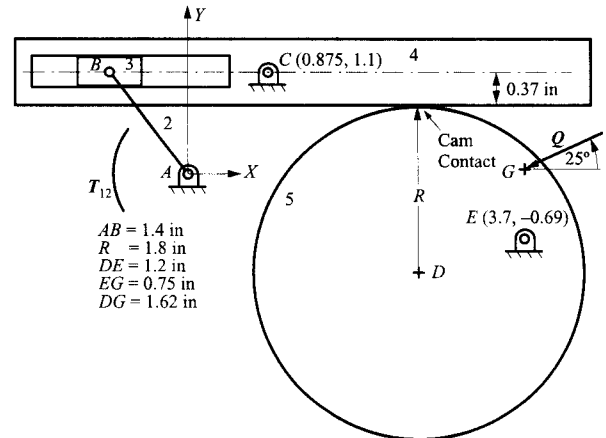
13.10 In the eight-link mechanism, most of the linkage is contained in the black box and some of the instant centers are located as shown. The force  $P$  is 100 lb and is applied to point  $D$  on link 8. If  ${}^1v_{B_2} = 100$  in/s in the direction shown, compute the velocity of point  $C_8$  and determine the torque  $T_{12}$  necessary for equilibrium.



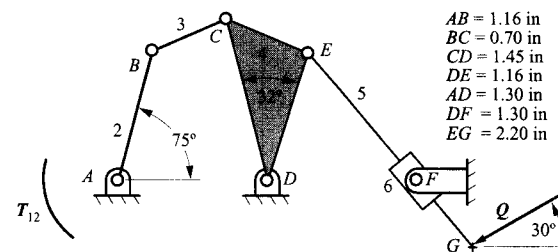
13.11 The mechanism shown is called a vice grip because a very high force at  $E$  can be generated with a relatively small force at  $G$  when points  $A$ ,  $B$ , and  $C$  are collinear (toggle position). In the position shown, determine the ratio  $F_{14}/F_{13}$ . Use conservation of power.



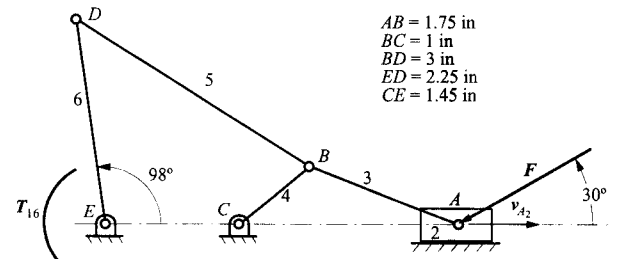
13.12 If  $Q$  is 100 in-lb in the direction shown, find the torque  $T_{12}$  required for equilibrium.



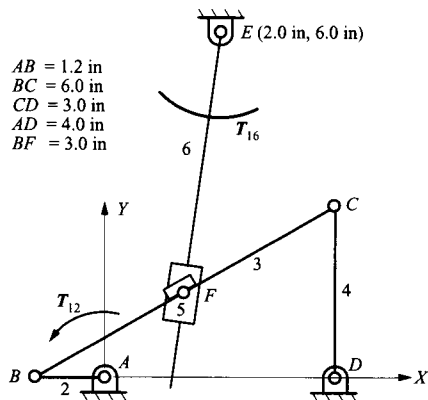
13.13 If  $Q$  is 100 in-lb in the direction shown, find  $T_{12}$ .



13.14 If the velocity of link 2 is 10 in/s, and the force on link 2 is 100 in-lb in the direction shown, find the torque on link 6 required to maintain equilibrium in the mechanism.

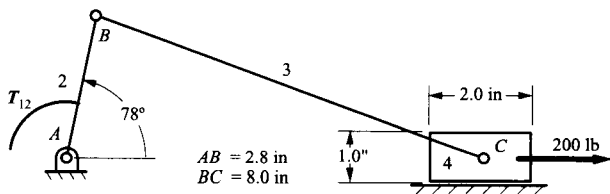


13.15 In the mechanism shown, point  $F$  is a swivel at the midpoint of link 3, which carries link 5. The motion of the four-bar linkage causes arm 6 to oscillate. If link 2 rotates CCW at 12 rad/s and is driven by a torque of 20 ft-lb, determine the resisting torque on link 6 required for equilibrium.

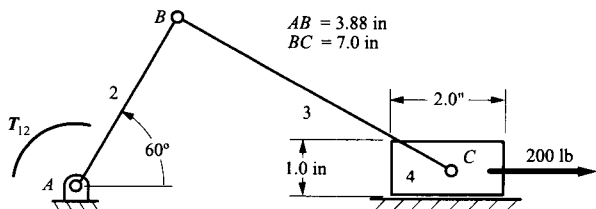


**EXERCISE PROBLEMS INVOLVING PIN FRICTION**

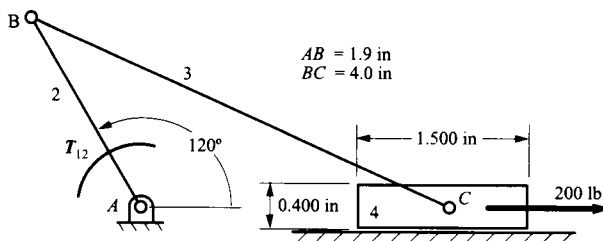
13.16 Find the torque  $T_{12}$  for a coefficient of friction  $\mu$  of 0.0 and 0.2. Assume that the radius of each pin is 1 in, and consider both pin and slider friction. Link 2 rotates CW.



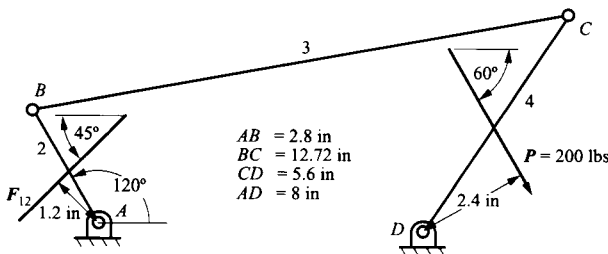
13.17 For the position given for the slider-crank mechanism, find the torque  $T_{12}$  required for equilibrium. The radius of each pin is 1 in, and the friction coefficient at the pin between links 3 and 4 and between the block and the frame is 0.3. Elsewhere, the coefficient of friction is 0. Link 2 rotates CCW.



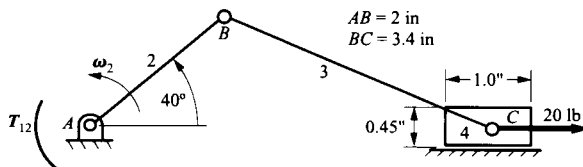
13.18 If the radius of each pin is 0.9 in and the coefficient of friction at all joints is 0.15, find the torque  $T_{12}$  required for equilibrium in the position shown. Link 2 rotates CCW.



13.19 If the coefficient of friction is 0.4 at each pin and each pin radius is 1 in, determine the force  $F$  required for equilibrium. Link 2 rotates CCW.



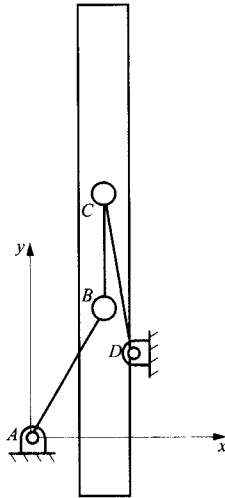
13.20 Find the torque  $T_{12}$  for a coefficients of friction  $\mu$  of 0.0 and 0.2. Consider friction at the slider only and neglect the masses of the links.



**EXERCISE PROBLEMS ON OUT-OF-PLANE FORCES**

13.21 The linkage shown is a type 1 double-rocker four-bar linkage in which the two coupler pivots,  $B$  and  $C$ , have been replaced by spherical joints. It moves in the horizontal plane and is used to guide and support a heavy door that is hung from the coupler. The vertical crankshafts are each supported on a tapered roller bearing that supports both radial and thrust loads. The centers of these bearings are 1.5 in below the horizontal plane in which the spherical joint centers lie. The crankshafts are also supported by ball bearings that support only radial loads. The central plane of the ball bearings is 2 in above the plane of the spherical joint centers. The door weighs 500 lb, including the weight of the coupler, and its center of mass is directly below the midpoint of the coupler. Each of the cranks  $AB$  and  $CD$  weighs 30 lb and can be modeled as a uniform rod. Find the radial loads carried by the ball bearings and the radial and thrust loads carried by the tapered roller bearings when the linkage is in the position shown.

$AB = CD = 18.0$  in,  $BC = 14.5$  in, and  $AD = 17.0$  in. The line  $AD$  is at  $45^\circ$  to the  $x$  axis.



**13.22** The robot of Example 13.8 is positioned so that the angle between members *A* and *B* is  $45^\circ$ ; the 30-lb payload is located on the axis of joint 3. Characterize the loads on members *A* and *B* in this position.

**EXERCISE PROBLEMS ON GEAR LOADS**

**13.23** A pair of spur gears with 31 and 57 teeth is cut to standard  $20^\circ$  pressure angle dimensions with diametral pitch 16. The wheel carries a load torque of 500 lb-ft. Find the reaction loads carried by the bearings on which the gears turn.

**13.24** A helical gear is cut with a standard  $25^\circ$  pressure angle, diametral pitch 8 spur gear cutter at a helix angle of  $30^\circ$ . The gear has 50 teeth and transmits 150 hp at a speed of 1500 rpm. Calculate the radial and thrust loads that must be carried by the mounting bearings. Also, compute the couple due to the axial component of the tooth loads. If the shaft bearings are to be 5 in apart, compute the additional radial bearing load from this source.

# DYNAMIC FORCE ANALYSIS

## 14.1 INTRODUCTION

In the subject of machine dynamics we bring together *kinematics*, the study of motion and geometry, with *kinetics*, the study of the relationship between force and motion, to derive information on the forces and torques active in moving machinery. This information is, in turn, essential to the computation of the stresses internal to the members of a machine and the elastic deflections of the members. Because two major failure modes of machine members are deformation or fracture caused by excessive stress, and vibration and interference caused by excessive elastic deflection, this information is obviously crucial for the purposes of machine design.

The computation of stresses and deflections in machine members is beyond the scope of this book. It is covered in texts on strength of materials, stress analysis, and design of machine elements. There are, of course, powerful computer tools such as finite-element analysis codes that can be used for this purpose. However, the input to such a program must include a complete description of the forces acting on the member. This includes both forces of reaction against the base or other members and active forces and torques produced by self-weight, by loads, including dynamic body forces such as centrifugal force, and by actuators or prime movers powering the machine.

The relationship between force and motion that is central to the study of kinetics is Newton's second law:

$$\mathbf{F} = m\mathbf{a} \quad (14.1)$$

where  $\mathbf{F}$  is the force acting on a particle,  $m$  is its mass, and  $\mathbf{a}$  is its acceleration.

Since this relationship refers to only a single particle and the machine members we want to deal with are bodies with distributed mass, it is necessary to derive appropriate equations relating force and torque for a rigid body with distributed mass from Newton's second law and the rigidity assumption. This results in the *Newton–Euler* equations describing the motion of a rigid body. The description of the motion of the *center of mass* of the body has exactly the same form as Eq. (14.1). That is, the center of mass moves as though the entire mass of the body were condensed into a particle at that point:

$$\Sigma \mathbf{F} = m\mathbf{a}_G \quad (14.2)$$

where  $\mathbf{a}_G$  is the acceleration of the center of mass.

Rotary motion of the body is described by Euler's equation:

$$\Sigma \mathbf{M}_G = I_G \boldsymbol{\alpha} \quad (14.3)$$

where  $\Sigma \mathbf{M}_G$  is the resultant moment of the force system acting on the body about the center of mass,  $\mathbf{I}_G$  is the inertia matrix based on fixed coordinate axes with origin at the center of mass, and  $\boldsymbol{\alpha}$  is the angular acceleration of the body relative to that same fixed frame. Alternatively, if the body is rotating about a fixed point,  $P$ , moments may be taken about that point and the inertia matrix can be expressed in the same fixed coordinate frame with origin at  $P$ . Euler's equation then becomes

$$\Sigma \mathbf{M}_P = \mathbf{I}_P \boldsymbol{\alpha} \quad (14.4)$$

It is important to note that this special case, rotation about a fixed point, is the only case in which the inertia matrix may be based on a point other than the center of mass.

In practice, for any case except rotation of a symmetric body about a fixed axis of symmetry, it is much more convenient to express the inertia matrix about a coordinate frame *fixed in the moving body*. There is always a set of three orthogonal axes, fixed in the body, for which the inertia matrix becomes a diagonal matrix. These axes are called the *principal axes of inertia* and constitute the *principal reference frame*. If the inertia matrix,  $\mathbf{I}_G$ , is expressed in the principal reference frame, and the angular velocity,  $\boldsymbol{\omega}$ , and angular acceleration,  $\boldsymbol{\alpha}$ , are expressed in the same frame, Eq. (14.3) becomes

$$\Sigma \mathbf{M}_G = \mathbf{I}_G \boldsymbol{\alpha} + \boldsymbol{\omega} \times \mathbf{I}_G \boldsymbol{\omega} \quad (14.5)$$

This is the form of Euler's equation most useful for spatial motion.

The methodology of dynamics problems is to use Eqs. (14.2)–(14.5) applied to each free body in the system in a manner exactly analogous to the use of static equilibrium equations in analyzing a structure. If the right-hand sides of Eqs. (14.2) and (14.3) are set to zero, they become identical to the static equilibrium equations. This is why Eqs. (14.2) and (14.3) are often called *dynamic equilibrium equations*.

Of course, the presence of the inertia terms on the right-hand sides of the dynamic equilibrium equations complicates their solution. Most dynamics problems in engineering fall into one of two classes. In the first of these, the motion of each body in the system is known. Therefore the acceleration of the center of mass and the angular acceleration of each member are known or can be computed by the use of kinematic techniques. Thus the right-hand sides of the dynamic equilibrium equations can be treated as known quantities, and the equations can be solved algebraically in a manner exactly analogous to the solution of the static equilibrium equations.

In the second class of dynamics problems, the motion of each body is not known *a priori*, and it is necessary to treat the accelerations on the right-hand sides of the equations as the second derivatives of position variables. The forces and moments acting on the member, which appear on the left-hand sides of the equations, must then also be related to the position variables to produce a set of differential equations in those position variables. These equations are called the *equations of motion* of the system. Description of the motion of the system then requires solution of the equations of motion.

In many machine design problems the motion of some input element is specified and dynamic analysis of these systems falls into the first of the two classes described here. These problems may be called *machine dynamics problems*. In this book we will confine ourselves to this class of dynamics problems.

Dynamics problems that must be solved by solution of the differential equations of motion are treated in courses and texts on vibrations or system dynamics. Another class of such problems is treated in the area of multibody system dynamics.

## 14.2 PROBLEMS SOLUBLE VIA PARTICLE KINETICS

Some machine design problems require only Eq. (14.1) or the energy and momentum relationships derived from it for solution. That is, it is not necessary to use rotary inertia. Effectively, the inertias can be modeled as particles with adequate accuracy.

### 14.2.1 Dynamic Equilibrium of Systems of Particles

First, it is necessary to relate the positions of the concentrated masses of the system kinematically to find their accelerations. In principle, this requires first relating their positions, then their velocities and accelerations. The way this works out is illustrated by the following examples.

#### EXAMPLE 14.1 Vehicle Acceleration and Braking

An automobile has a total weight of  $W = 4000$  lb. As shown in Fig. 14.1, its wheelbase (distance between the front and rear axle centers) is  $b + c = 90$  in, and its center of mass is  $b = 40$  in behind the front axle center. When it is parked on a level surface, the center of mass is  $h = 25$  in above the ground. The wheel radius is  $r = 14.5$  in, and on a good surface, the coefficient of friction between the tires and the road is  $\mu = 0.8$ . If the weights and moments of inertia of the wheels are neglected, estimate the ratio of the maximum acceleration that the vehicle can achieve to the gravitational acceleration,  $g$ , if it is driven by

1. the rear wheels or
2. the front wheels.

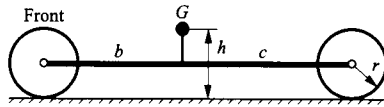


FIGURE 14.1 The vehicle model for Example 14.1.

Find the maximum deceleration that can be achieved if the braking effort is optimally apportioned between front and rear wheels. What is the percentage of the braking force at the front wheels?

#### Solution

In this instance, the kinematic part of the solution is trivial. Because the wheel inertia is neglected, it is not even necessary to develop expressions for the angular velocities and angular accelerations of the wheels. We will start with the case when the rear wheels are driving.

1. Since the wheel weight and inertia will not be considered separately, we start with a free-body diagram of the whole vehicle shown as Fig. 14.2.

There is no rotation of the vehicle mass, so the angular acceleration is zero. Therefore, the inertia torque term ( $I_G \alpha$ ) in Eq. (14.3) is zero.

The term  $ma_G$  in Eq. (14.2) can be computed and treated as a known force. If we move the term to the left-hand side of the equation, we can treat it as an applied force and solve the problem as a statics problem. As will be discussed in more detail later, when we treat the term  $ma_G$  in this way, it is called

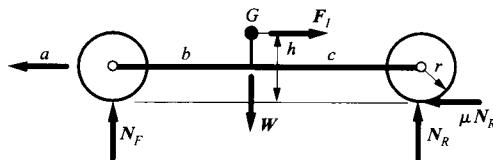


FIGURE 14.2 Free-body diagram when vehicle is driven via the rear wheels.

an inertia force,  $F_I$ , and it is in the direction opposite to that of the acceleration. The magnitude of  $F_I$  is given by

$$F_I = \frac{Wa}{g}$$

where  $a$  is the magnitude of the acceleration  $\mathbf{a}$ , which is positive in the forward direction, and  $W$  is the magnitude of the weight  $\mathbf{W}$ . That is, the mass of the vehicle is  $W/g$ .

The dynamic equilibrium equations are

$$\sum F_x = 0: \quad -F_I + \mu N_R = 0 \quad (a)$$

$$\sum F_y = 0: \quad W = N_R + N_F \quad (b)$$

$$\sum M_G = 0: \quad cN_R = bN_F + h\mu N_R \quad (c)$$

Moments are conveniently taken about  $G$  to eliminate  $W$  and  $a$  from the moment equation.

Using Eq. (a) together with the expression for  $F_I$  gives

$$N_R = \frac{Wa}{\mu g}$$

Applying this to Eq. (b) gives

$$N_F = W \left( 1 - \frac{a}{\mu g} \right)$$

Substitution of these expressions into Eq. (c) gives, after some rearrangement,

$$\frac{a}{g} \left( \frac{b+c}{\mu} - h \right) = b$$

or

$$A = \frac{a}{g} = \frac{\mu b}{b+c-\mu h}$$

where  $A$  is the required ratio of the acceleration to the gravitational acceleration. Substitution of the values of  $\mu$ ,  $b$ ,  $c$ , and  $h$  given in the problem statement results in

$$A = 0.457$$

That is, the maximum acceleration that can be achieved by the vehicle is 45.7% of the gravitational acceleration.

2. The free-body diagram for front-wheel drive is shown in Fig. 14.3.

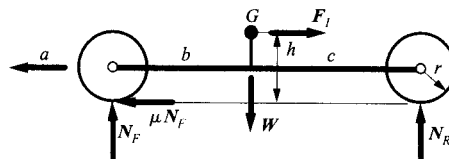


FIGURE 14.3 The free-body diagram when the vehicle is driven via the front wheels.

The dynamic equilibrium equations are

$$\sum F_x = 0: -F_f + \mu N_F = 0 \tag{d}$$

$$\sum F_y = 0: W = N_R + N_F \tag{e}$$

$$\sum M_G = 0: cN_R = bN_F + h\mu N_F \tag{f}$$

Substitution for  $F_f$  in Eq. (d) gives

$$N_F = \frac{Wa}{\mu g}$$

Substitution in Eq. (e) gives

$$N_R = W \left( 1 - \frac{a}{\mu g} \right)$$

Substitution of these values into Eq. (f) gives, after rearrangement,

$$\frac{a}{g} \left( \frac{b+c}{\mu} + h \right) = c$$

Hence

$$A = \frac{a}{g} = \frac{\mu c}{b+c+\mu h}$$

Substitution of the given values yields

$$A = 0.364$$

As can be seen, for the values given, the acceleration that can be achieved with front-wheel drive is significantly lower than with rear-wheel drive.

3. The free-body diagram for braking is shown in Fig. 14.4.

In this case the inertia force is directed forward. The dynamic equilibrium equations are, in this instance,

$$\sum F_x = 0: -F_f - \mu(N_R + N_F) = 0 \tag{g}$$

$$\sum F_y = 0: W = N_R + N_F \tag{h}$$

$$\sum M_G = 0: cN_R + h\mu(N_R + N_F) = bN_F \tag{i}$$

Substitution from Eq. (h) into Eq. (g), together with substitution for  $F_f$ , gives

$$\frac{Wa}{g} = \mu W$$

or  $A = \mu$ . For the values given,  $A = 0.8$ .

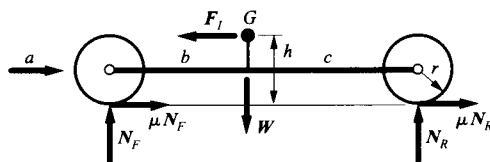


FIGURE 14.4 The free-body diagram during braking.



Substitution from Eq. (h) into Eq. (i) gives

$$N_F(b+c) = (c+h\mu)W$$

or

$$N_F = W \frac{c+h\mu}{b+c}$$

For the values given

$$N_F = 0.778 W \quad \text{and} \quad N_R = 0.222 W$$

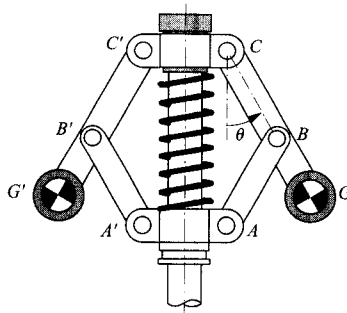
Therefore, 77.8% of the braking effort is at the front wheels, which is why the front brakes of automotive vehicles are usually much bigger than the rear brakes.

Notice also that, for this configuration, the deceleration available through optimal braking is considerably greater than the maximum possible acceleration.

### EXAMPLE 14.2 Flyball Governor

A flyball governor is arranged as shown in Fig. 14.5 to allow adjustment of the governed speed by adjusting the preload in the spring. As the weights swing outward under the influence of centrifugal force, the spring is compressed.

The governor operates a throttle valve to control the speed of an engine. The valve is fully closed when the angle  $\theta$  is  $75^\circ$ . Compute the speed at which the valve is closed if the effective centers of mass of the arms are in the locations  $G$  and  $G'$  shown and other inertias can be neglected. The weight of each arm is 0.25 lb. The adjusting nut is set so that the spring is at its natural or free length when  $\theta = 5^\circ$ . The stiffness of the spring is 20 lb/in. The lengths of the links are as indicated in the figure caption.



**FIGURE 14.5** The flywheel governor discussed in Example 14.2. The dimensions are  $AB = BC = A'B' = B'C' = 1.5$  in,  $CG = C'G' = 2.438$  in, and  $CC' = 1.25$  in.  $G$  and  $G'$  are the effective centers of mass of the arms.

### Solution

The radius of rotation of the center of mass of each arm is

$$r = 2.438 \sin 75^\circ + 0.625 = 2.979 \text{ in}$$

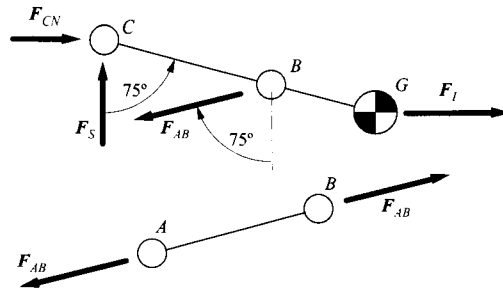
Hence the centrifugal acceleration of the point  $G$  is

$$a_G = r\omega^2 = (2.979/12)\omega^2 = 0.248 \omega^2$$

The magnitude of the inertia force is

$$F_I = ma_G (0.25/32.2) \times 0.248\omega^2 = 0.00193\omega^2$$

Since  $a_G$  is directed inward toward the center of rotation,  $F_I$  is directed outward as shown. Free-body diagrams of links  $AB$  and  $BC$  are shown in Fig. 14.6. Since  $AB$  is a two-force member, the forces at  $A$  and  $B$  are equal, opposite, and collinear. For link  $BC$ ,



**FIGURE 14.6** Free-body diagrams of links *AB* and *BC* used in the solution of Example 14.2.

$$\sum F_x = 0: F_{CN} + F_I - F_{AB} \sin 75^\circ = 0 \quad (\text{a})$$

$$\sum F_y = 0: F_S - F_{AB} \cos 75^\circ = 0 \quad (\text{b})$$

where  $F_S$  is half the force from the spring, and  $F_{CN}$  is the force at  $C$  normal to the vertical axis.

Taking moments about point  $C$  in the free-body diagram for link  $BC$ , we have

$$\sum M_C = 0: F_{AB} BC \sin 30^\circ - F_I CG \sin 15^\circ = 0 = F_{AB} 1.5 \sin 30^\circ - F_I 2.438 \sin 15^\circ \quad (\text{c})$$

The distance  $AC$  in this position is

$$AC = 2 \times 1.5 \cos 75^\circ = 0.776 \text{ in}$$

When the spring is at its natural length

$$AC = 2 \times 1.5 \cos 5^\circ = 2.989 \text{ in}$$

Hence the spring is compressed the distance

$$x = 2.989 - 0.776 = 2.212 \text{ in}$$

and the spring force for half of the governor is given by

$$2F_S = 20 \times 2.212 = 44.24 \text{ lb}$$

or

$$F_S = 22.12 \text{ lb}$$

Hence, from Eq. (b)

$$F_{AB} = F_S / \cos 75^\circ = 22.12 / \cos 75^\circ = 85.47 \text{ lb}$$

Using Eq. (c) we get

$$F_I = \frac{1.5 \sin 30^\circ}{2.438 \sin 15^\circ} F_{AB} = \frac{1.5 \sin 30^\circ}{2.438 \sin 15^\circ} 85.47 = 101.58 \text{ lb}$$

Therefore

$$\omega^2 = F_I / 0.00193 = 101.58 / 0.00193$$

or

$$\omega = 229.4 \text{ rad/s}$$

or

$$\omega = 2191 \text{ rpm}$$

This is the speed at which the governor will close the valve.

### 14.2.2 Conservation of Energy

Conservation of energy is useful in mechanism problems in which there is interchange between kinetic and potential energy. Most often the potential energy is either gravitational potential energy or strain energy. If the total energy in the system can be calculated in some position of the system and the system has mobility one, then the kinetic energy and hence the velocity can be calculated in any other position of the system, provided joint friction can be neglected. This type of calculation is usually much more efficient than pursuing the same result via dynamic equilibrium. Conservation of energy provides only information on the variables that determine energy components. Thus, although positions and velocities can be related in this way, the method will yield no information on accelerations.

Conservation of energy can often be used in association with conservation of momentum to solve problems in which energy is stored in a spring, a raised weight, or a flywheel and then rapidly released, as in punching and stamping machines, jackhammers, and similar types of mechanisms.

### 14.2.3 Conservation of Momentum

Conservation of momentum is particularly useful in mechanism problems that involve impacts or other short-period, impulsive events. The methodology is to compare the momentum of the system immediately before and immediately after the impulsive event. In problems involving one-dimensional motion, only conservation of linear momentum is required. In problems involving two- or three-dimensional rigid-body motion, conservation of angular momentum is also required.

The general methodology of problems involving conservation of energy and conservation of momentum can be studied in the following example.

#### **EXAMPLE 14.3** **Hydraulic** **Impactor**

A hydraulic impactor (jackhammer) uses a rotary hydraulic motor to turn the follower of a cylindrical cam, as shown in Fig. 14.7. The follower is mounted on the hammer *via* a sliding sleeve. The cam has a ramp, which causes the follower to compress a spring, and a step, which releases the follower and allows the spring to extend, accelerating the hammer. At the end of the stroke, the hammer strikes the impactor bit, driving it into the ground. If it is assumed that the impact between the hammer and the bit is perfectly elastic (no loss of energy), find the velocity and kinetic energy of the bit immediately after it is struck by the hammer. The bit weighs 20 lb, and the hammer weighs 17.5 lb. The spring has a rate of 2000 lb/in, and the cam lift is 2 in. At the end of the stroke, when the hammer strikes the bit, the spring is compressed 0.5 in. Also estimate the hydraulic power needed to drive the device if it delivers 5 strokes per second.

#### **Solution**

The critical position and velocity parameters for this problem are shown in Fig. 14.8. We first use conservation of energy to find the velocity of the hammer at the instant of impact.

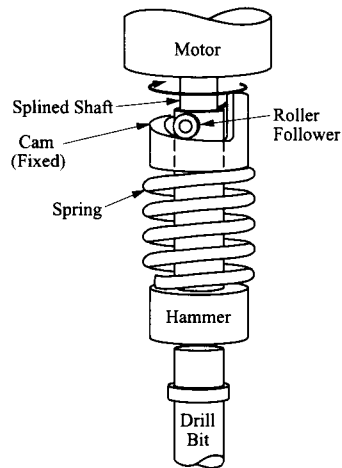


FIGURE 14.7 The drive mechanism of the hydraulic impactor discussed in Example 14.3.

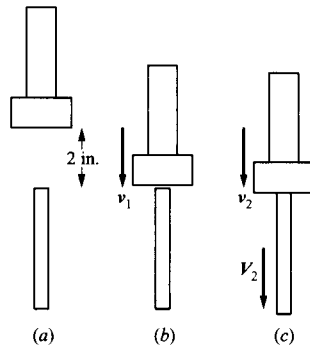


FIGURE 14.8 Three critical configurations of the system: (a) with the hammer fully raised and both hammer and bit at rest; (b) at the instant before impact with the hammer at velocity  $v_1$  and the bit at rest; and (c) at the instant after impact with both hammer and bit moving, the hammer at velocity  $v_2$  and the bit at velocity  $V_2$ .

When the hammer is in the fully raised position (Fig. 14.8a), the hammer and bit are at rest so kinetic energy is

$$K_0 = 0$$

The strain energy is

$$P_{0S} = \frac{1}{2}KS^2 = \frac{1}{2} \times 2000 \times 2.5^2 = 6250 \text{ in-lb} = 520.8 \text{ ft-lb}$$

Here 2.5 in is used because that is the total compression of the spring in this position. Note that the spring is compressed 0.5 in even when the cam follower is in its lowest position.

If the position at which the hammer strikes the bit is taken as the zero reference, the gravitational potential energy of the hammer is

$$P_{0G} = 17.5 \times 2/12 = 2.9 \text{ ft-lb}$$

Hence the total mechanical energy of the system when the hammer is fully raised is

$$U_0 = K_0 + P_{0S} + P_{0G} = 523.7 \text{ ft-lb}$$

Now consider the instant immediately before the impact of the hammer on the bit, which is illustrated by Fig. 14.8b.

If the velocity of the hammer is  $v_1$  the kinetic energy of the system is

$$K_1 = \frac{1}{2} \times \frac{17.5}{32.2} \times v_1^2 = 0.272v_1^2 \text{ ft-lb}$$

The strain energy is now

$$P_{1S} = \frac{1}{2} \times 2000 \times 0.5^2 = 250 \text{ in-lb} = 20.8 \text{ ft-lb}$$

and the gravitational potential energy is zero.

Therefore, the total mechanical energy is

$$U_1 = K_1 + P_{1S} = 0.272v_1^2 + 20.8 \text{ ft-lb}$$

Equating this expression to the system energy when the hammer is fully raised gives

$$U_1 = U_0 = 0.272v_1^2 + 20.8 = 523.7 \text{ ft-lb}$$

Hence, solving for  $v_1$ , we get

$$v_1 = 43.0 \text{ ft/s}$$

and

$$K_1 = 523.7 - 20.8 = 502.9 \text{ ft-lb}$$

We now use both conservation of momentum and conservation of energy to determine the velocities of hammer and bit immediately after the impact, which is the condition shown in Fig. 14.8c.

Let  $v_2$  be the velocity of the hammer immediately after impact, and let  $V_2$  be the velocity of the bit at that instant. Both are taken to be positive in the downward direction. The momentum of the system before impact is

$$g_1 = \frac{17.5}{32.2} \times 43.0 = 23.4 \text{ lb-s}$$

Immediately after impact, the momentum is

$$g_2 = \frac{20}{32.2} \times V_2 + \frac{17.5}{32.2} \times v_2$$

Equating  $g_1$  and  $g_2$  gives

$$23.4 = \frac{20}{32.2} \times V_2 + \frac{17.5}{32.2} \times v_2$$

or

$$V_2 + 0.875v_2 = 37.63 \tag{a}$$

The kinetic energy of the system immediately after the impact is

$$K_2 = \frac{1}{2} \times \frac{20}{32.2} V_2^2 + \frac{1}{2} \times \frac{17.5}{32.2} v_2^2$$

Since the impact is elastic,  $K_1$  and  $K_2$  can be equated:

$$502.9 = \frac{1}{2} \times \frac{20}{32.2} V_2^2 + \frac{1}{2} \times \frac{17.5}{32.2} v_2^2$$

or

$$1619 = V_2^2 + 0.875 v_2^2 \quad (b)$$

Substitution for  $V_2$  from Eq. (a) into Eq. (b) gives

$$1619 = (37.63 - 0.875 v_2)^2 + 0.875 v_2^2$$

Expansion and simplification of this equation give

$$1.641 v_2^2 - 65.85 v_2 - 203.0 = 0$$

Solution of this quadratic equation in  $v_2$  gives the following values:

$$v_2 = 43.0 \quad \text{and} \quad v_2 = -2.875 \text{ ft/s}$$

The first of these values is the velocity of the hammer before impact. That must be a solution because the values before impact give the same energy and momentum, but the second value is then the correct solution for the velocity of the hammer after impact. The negative value indicates that the hammer rebounds slightly in the upward direction.

Substitution back into Eq. (a) gives

$$V_2 = 37.63 - 0.875 \times (-2.875) = 40.1 \text{ ft/s}$$

The kinetic energy of the bit at this instant is

$$K_B = \frac{1}{2} \times \frac{20}{32.2} \times 40.1^2 = 499 \text{ ft-lb}$$

The strain energy put into the spring by each rotation of the cam is

$$P_{0S} - P_{1S} = 520.8 - 20.8 = 500 \text{ ft-lb}$$

The gravitational potential energy put in by raising the hammer is

$$P_{0G} = 2.9 \text{ ft-lb}$$

Hence the energy put in on each rotation of the cam is

$$u = 502.9 \text{ ft-lb}$$

If the cam rotates 5 times per second, the power put in is

$$P = 5 \times 502.9 = 2510 \text{ ft-lb/s} = 2510/550 = 4.57 \text{ hp}$$

This completes solution of the problem.

### 14.3 DYNAMIC EQUILIBRIUM OF SYSTEMS OF RIGID BODIES

Equation (14.3) is applicable for general spatial motion. The matrix  $I_G$  is a symmetric,  $3 \times 3$  matrix.

In the present work, we will restrict consideration to planar motion with one of the principal axes normal to the plane of motion. In this case Eq. (14.3) becomes

$$\Sigma M_G \cdot \boldsymbol{w} = I_G \boldsymbol{\alpha} \quad (14.6)$$

where  $I_G$  is a scalar quantity, being the moment of inertia of the body about an axis through the center of mass normal to the plane of motion,  $\boldsymbol{w}$  is a unit vector normal to the plane of motion, and  $\boldsymbol{\alpha}$  is the angular acceleration, taken to be positive in the  $\boldsymbol{w}$  direction. That is,

$$\boldsymbol{\alpha} = \alpha \boldsymbol{w} \quad (14.7)$$

We make this restriction because the vast majority of machine dynamics problems are planar motion problems. Solutions of problems involving general spatial motion follow the same lines as the examples studied in the following, but require use of the general forms of Euler's equation: Eq. (14.3) or Eq. (14.5).

If a body is in motion, the sum of the forces acting on it is equal to its mass multiplied by the acceleration of its center of mass; that is,

$$\Sigma \boldsymbol{F} = m \boldsymbol{a}_G \quad (14.8)$$

If we introduce a force  $\boldsymbol{F}_I$  such that

$$\boldsymbol{F}_I = -m \boldsymbol{a}_G \quad (14.9)$$

called the inertia force, which is applied on a line passing through the center of mass, and a couple,

$$M_I = -I_G \alpha \quad (14.10)$$

called the inertia torque, and treat these in the same way as any other external force and torque, then the dynamic equilibrium equations assume the same form as the static equilibrium equations:

$$\Sigma \boldsymbol{F} = 0 \quad (14.11)$$

$$\Sigma M_O = 0 \quad (14.12)$$

where  $O$  is any point in the plane about which moments are taken. Notice that, since all moment vectors are normal to the plane of motion, the moment equation may be treated as a scalar equation. The summation of the forces  $\Sigma \boldsymbol{F}$  now includes  $\boldsymbol{F}_I$ , and  $\Sigma M_O$  includes  $M_I$ . Note that the point of application of the inertia force is defined to be the center of mass and that the moment of inertia used in computing the inertia couple is that about the center of mass, whether or not the moments are taken about the center of mass.

The replacement of the  $-m \boldsymbol{a}_G$  term with the inertia force, and replacement of  $-I_G \alpha$  with the inertia torque, to convert the dynamic equilibrium equations into the same form as the static equilibrium equations is known as d'Alembert's principle. The general procedure for solving a dynamic equilibrium problem in machine dynamics is the following:

1. Solve the position, velocity and acceleration kinematics of the system using the procedures of Chapters 2–5 to obtain the accelerations of all bodies with significant mass and the angular accelerations of all bodies with significant inertia.
2. Compute the inertia force and couple acting on each body according to d'Alembert's principle.
3. Apply the inertia force and couple as an external force and torque to each member. The line of action of the inertia force passes through the center of mass of each member.
4. Draw a free-body diagram of each member including all external forces acting on that member and all reaction forces from other members to which it is connected.

5. Write three force and moment equilibrium equations for each member.
6. Solve the equations for the unknown forces.

It may be seen that the last three steps in the process are identical to the solution of a static equilibrium problem.

### EXAMPLE 14.4

#### Dynamic Force Analysis

The members of the mechanism of Example 2.4 and Fig. 2.16 have the following inertial properties: (See Fig. 14.9.) Find the driving torque that must be applied to the crank, member 2, to maintain the constant angular velocity of 60 rpm in the clockwise direction. Friction in all joints (including the prismatic joint) and the mass and moment of inertia of link 5 may be neglected. The mechanism moves in the horizontal plane.

$$\begin{aligned}
 AB &= 1.5 \text{ in, } FG_3 = 1.82 \text{ in, } DG_6 = 1.5 \text{ in} \\
 BF &= 2.75 \text{ in, } \lambda = 7.84^\circ \\
 CF &= 2.75 \text{ in, } m_3g = 0.5 \text{ lb, } k_3 = 0.87 \text{ in} \\
 BC &= 0.75 \text{ in, } m_4g = 1.0 \text{ lb} \\
 DC &= 2.25 \text{ in, } m_6g = 0.5 \text{ lb, } k_6 = 0.87 \text{ in} \\
 DE &= 3.0 \text{ in, } \omega_2 = 60 \text{ rpm CW, } \alpha_2 = 0
 \end{aligned}$$

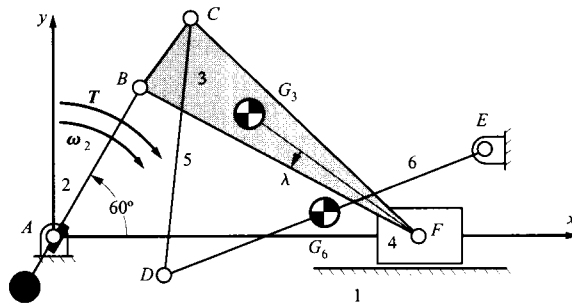


FIGURE 14.9 The mechanism for Example 14.4.

#### Solution

Since the geometry and velocity and acceleration are identical to those of Example 2.4, that solution can be used for parts 1 and 2 of the solution procedure, with one modification. It is necessary to find the accelerations of points  $G_3$  and  $G_6$ .

In both cases the acceleration image is used.  $G_6$  is at the midpoint of  $DE$ . Since point  $E$  is a fixed point, it maps into point  $o'$  on the acceleration polygon, and hence the image of  $\overline{DE}$  is  $\overline{d'o'}$ . Next  $g_6'$  is located at the midpoint of  $\overline{d'o'}$ , and the acceleration  $\mathbf{a}_{G_6}$  is the vector  $\overline{o'g_6'}$ .

Similarly, point  $g_3'$  can be located on the image  $b'c'f'$  of  $BCF$  by constructing  $\angle b'f'g_3'$  equal to  $\angle BFG_3 = \lambda$ , and making

$$\frac{f'g_3'}{b'f'} = \frac{FG_3}{BF}$$

The accelerations of these two points can now be scaled from the acceleration diagram:

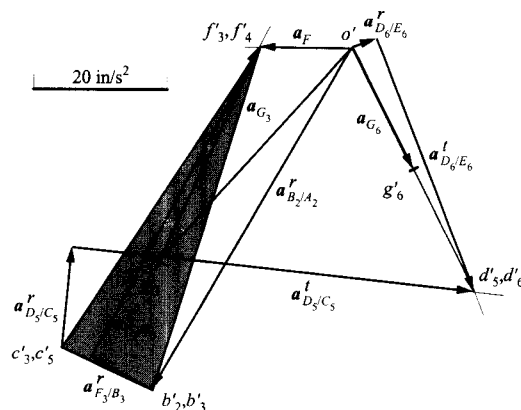
$$\mathbf{a}_{G_6} = 1.00 \times 20 = 20 \text{ in/s}^2 \text{ at } -63^\circ \text{ to the } x \text{ axis}$$

$$\mathbf{a}_{G_3} = 2.16 \times 20 = 43.2 \text{ in/s}^2 \text{ at } -132^\circ \text{ to the } x \text{ axis}$$



Scaling  $a'_{F/B}$  from Fig. 14.10 gives

$$\alpha_3 = \frac{a'_{F/B}}{BF} = \frac{2.63 \times 20}{2.75} = 19.1 \text{ rad/s}^2 \text{ CCW}$$



**FIGURE 14.10** The acceleration diagram of Fig. 2.17 modified to allow computation of the acceleration of points  $G_3$  and  $G_6$ . The acceleration image is used. It is necessary only to construct the positions of point  $g'_3$  such that  $\angle c'f'g'_3 = \lambda$  and  $f'g'_3/f'c' = FG_3/FC$  and of point  $g'_6$  at the midpoint of  $o'd'$ .

In addition, we need the angular acceleration information that was derived in Example 2.4:

$$\alpha_6 = 40/3.0 = 13.3 \text{ rad/s}^2 \text{ CCW}$$

$$a_F = 14.9 \text{ in/s}^2 \text{ (to the left)}$$

It may be noted that we have not attempted to find the acceleration of the center of mass of link 2, and in fact there is insufficient information to find it. This is because it is not needed as long as we are seeking only the torque,  $T$ , and not the reaction force at point A, and as long as the angular velocity of member 2 is constant.

Step 3 in the aforementioned procedure can now be addressed. The free-body diagrams for the mechanism are shown in Fig. 14.11.

The inertia force acting at  $G_3$  is calculated as follows:

$$F_{13} = -m_3 a_{G_3} = \frac{0.5}{32.2} \times \frac{43.2}{12} = 0.056 \text{ lb at } 48^\circ \text{ to the } x \text{ axis}$$

Notice that the direction of  $F_{13}$  is determined by simply adding  $180^\circ$  to the direction of  $a_{G_3}$ .

Similarly, the inertia force acting at  $G_6$  is calculated as

$$F_{16} = -m_3 a_{G_6} = \frac{0.5}{32.2} \times \frac{20.0}{12} = 0.026 \text{ lb at } 117^\circ \text{ to the } x \text{ axis}$$

The inertia force acting on the translating mass 4 is

$$F_{14} = -m_4 a_{G_4} = \frac{1.0}{32.2} \times \frac{13.9}{12} = 0.036 \text{ lb along the } x \text{ axis}$$

The inertia couple acting on member 3 is calculated as follows:

$$M_{13} = -I_3 \alpha_3 = -m_3 k_3^2 \alpha_3 = \frac{0.5}{32.2} \times \left( \frac{0.87}{12} \right)^2 \times 19.1 = 0.00156 \text{ ft-lb} = 0.0187 \text{ in-lb CW}$$

The inertia couple acting on member 6 is

$$M_{16} = -I_6 \alpha_6 = -m_6 k_6^2 \alpha_6 = \frac{0.5}{32.2} \times \left( \frac{0.87}{12} \right)^2 \times 13.3 = 0.00109 \text{ ft-lb} = 0.0130 \text{ in-lb CW}$$

Step 4 in the procedure is the drawing of free-body diagrams of all members. This is shown in Fig. 14.11.

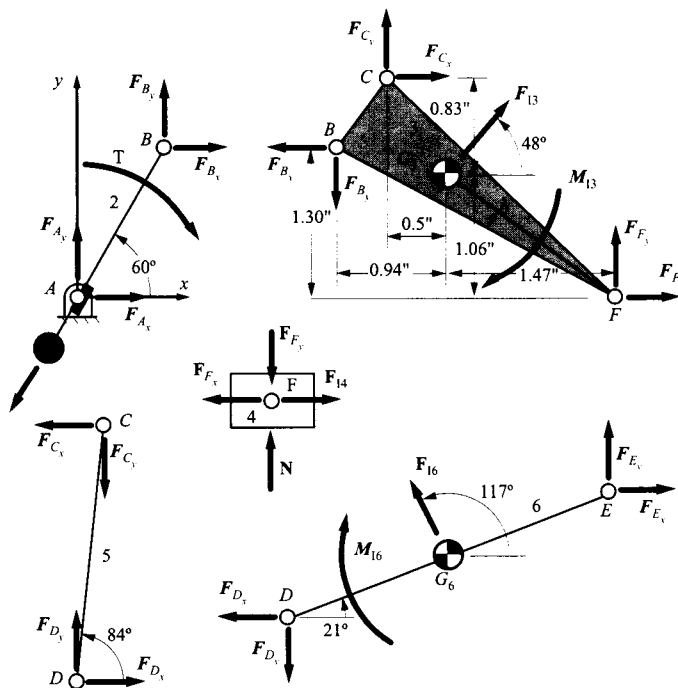


FIGURE 14.11 Free-body diagrams for Example 14.4.

Step 5 of the solution procedure is writing dynamic equilibrium equations for each member. Starting with member 2, we have

$$\Sigma M_A = 0: \quad T + F_{B_x} \times 1.5 \sin 60^\circ = F_{B_y} \times 1.5 \cos 60^\circ$$

Here we have chosen to take moments about point  $A$  because doing so eliminates the components of  $F_A$  and also  $F_{12}$ . Force equilibrium would, in this case, give two equations that could ultimately be solved for the components of  $F_A$ . Since we are not interested in  $F_A$ , they are not written out.

Moving to member 3, we have

$$\Sigma F_x = 0: \quad F_{C_x} + F_{F_x} + 0.056 \cos 48^\circ = F_{B_x}$$

$$\Sigma F_y = 0: \quad F_{C_y} + F_{F_y} + 0.056 \sin 48^\circ = F_{B_y}$$

$$\begin{aligned} \Sigma M_{G_3} = 0: \quad & F_{C_x} \times 0.83 + F_{C_y} \times 0.5 + 0.0187 = F_{B_x} \times 0.24 + F_{B_y} \times 0.94 \\ & + F_{F_x} \times 1.06 + F_{F_y} \times 1.47 \end{aligned}$$

Here the choice of the point about which to take moments makes little difference. Use of  $G_3$  slightly simplifies the equation since it eliminates  $F_{13}$ .

Continuing with member 4, we get

$$\Sigma F_x = 0: \quad 0.036 = F_{F_x}$$

$$\Sigma F_y = 0: \quad N = F_{F_y}$$

No moment equation is written because this member is restrained from rotation.

Member 5 is a two-force member because its mass and moment of inertia are neglected. This implies both that  $FC = FD$  and that both forces are aligned and opposed along the axis of the member. The alignment along the axis is required by the moment equation. Consequently,

$$\Sigma F_x = 0: \quad F_{C_x} + F_{D_x}$$

$$\Sigma F_y = 0: \quad F_{C_y} + F_{D_y}$$

$$\Sigma M_D = 0: \quad F_{C_x} \times 2.25 \cos 84^\circ = F_{C_y} \times 2.25 \sin 84^\circ$$

or

$$F_{C_y} + F_{C_x} \tan 84^\circ \quad \text{and} \quad F_{D_y} + F_{D_x} \tan 84^\circ$$

Finally, for member 6,

$$\Sigma M_E = 0: \quad 0.0130 + F_{D_x} \times 3 \sin 21^\circ + 0.026 \times 1.5 \sin 96^\circ = F_{D_y} \times 3 \cos 21^\circ$$

The force equilibrium equations would yield only expressions for the components of  $F_E$ . Since we are not interested in  $F_E$  and can eliminate it by taking moments about point E, the force equilibrium equations are not needed. Substitution of the previous relationship between  $F_{D_x}$  and  $F_{D_y}$  into this equation gives

$$0.0130 + F_{D_x} \times 3 \sin 21^\circ + 0.026 \times 1.5 \sin 96^\circ = F_{D_x} \tan 84^\circ \times 3 \cos 21^\circ$$

or

$$F_{C_x} = F_{D_x} = 0.0020 \text{ lb}$$

Then

$$F_{C_y} = F_{D_y} = 0.0020 \times \tan 84^\circ = 0.0193 \text{ lb}$$

Substitution of these values into the force equilibrium equations of member 3 gives

$$F_{B_x} = 0.0395 + F_{F_x} = 0.0395 + 0.036 = 0.0755$$

$$F_{B_y} = 0.0609 + F_{F_y}$$

Substitution into the rotation equations gives

$$\begin{aligned} 0.0300 &= 0.24F_{B_x} + 0.94F_{B_y} + 1.06F_{F_x} + 1.47F_{F_y} \\ &= 0.24 \times 0.0755 + 0.94F_{B_y} + 1.06 \times 0.036 + 1.47F_{F_y} \end{aligned}$$

or

$$0 = 0.0263 + 0.94F_{B_y} + 1.47F_{F_y}$$

Elimination of  $F_{F_y}$  gives

$$0 = 0.0263 + 0.94F_{B_y} + 1.47(F_{B_y} - 0.0609)$$

or

$$F_{B_x} = 0.0262 \text{ lb}$$

The values obtained for  $F_{B_x}$  and  $F_{B_y}$  can be substituted into the moment equation of member 2 to give

$$T + 0.0755 \times 1.5 \sin 60^\circ = 0.0262 \times 1.5 \cos 60^\circ$$

or

$$T = -0.078 \text{ in-lb}$$

Therefore, when passing through this position a torque of 0.078 in-lb in the counterclockwise direction is needed to prevent member 2 from accelerating and to maintain its constant speed of rotation.

## 14.4 FLYWHEELS

Flywheels are used to store energy and to smooth speed fluctuations during a machine cycle. They serve a function similar to that of a capacitor in an electric circuit or an accumulator in a hydraulic circuit. In a typical situation, a machine that needs to operate at near-constant speed must be matched to a load that produces significant torque fluctuations. For example, an electric motor that works best at near-constant speed may need to drive a punch press, or reciprocating compressor, that produces a strongly fluctuating load torque. Conversely, an internal combustion engine that produces strong torque fluctuations may be required to drive a load shaft at close to constant velocity.

Actually, a flywheel is usually an essential component of an internal combustion engine because the cycle includes strokes in which air is being compressed in the cylinder, so the engine is absorbing energy rather than producing it. The flywheel allows energy to be stored during the power stroke when the charge is burning and expanding and returned to the piston when it is compressing the charge. This is also a reason for the use of engines with multiple cylinders: The torque fluctuations for different cylinders can be evenly distributed over the engine cycle, reducing the output torque fluctuations and reducing the size of the requisite flywheel.

If the machine-induced energy fluctuations are known and the allowable speed fluctuation is specified, the requisite flywheel inertia is readily calculated. The coefficient of speed fluctuation,  $c_\delta$ , is defined as follows:

$$c_\delta = \frac{\omega_2 - \omega_1}{\omega} \quad (14.13)$$

where  $\omega_2$  is the maximum flywheel angular velocity,  $\omega_1$  is the minimum flywheel angular velocity, and  $\omega$  is the average flywheel velocity. The allowable fluctuation coefficient varies by application, from 0.05 or more for agricultural and mining machinery down to about 0.003 for alternating-current generators. Values appropriate to given applications may be found in machine design handbooks.

If the moment of inertia of the flywheel is  $I_w$ , the change in flywheel energy is

$$\Delta E = \frac{I_w}{2} (\omega_2^2 - \omega_1^2) \quad (14.14)$$

Although speed may fluctuate asymmetrically over the cycle, it is often adequate to approximate the average angular velocity as the mean of  $\omega_2$  and  $\omega_1$ :

$$\omega = \frac{\omega_2 + \omega_1}{2}$$

so

$$\omega_2^2 - \omega_1^2 = 2c_8\omega^2$$

and then

$$I_w = \frac{\Delta E}{c_8\omega^2} \quad (14.15)$$

can be used to estimate the required flywheel inertia.

The following example illustrates the way in which a flywheel can be sized for a particular application.

### EXAMPLE 14.5 Punch Press

#### Solution

A machine used to punch holes in metal plate is to be driven by an induction motor with a rated speed of 1700 rpm. The allowable drop in motor speed is 15%. The machine will be required to punch holes of diameter up to 1 in in steel plate up to 0.5-in thick with shear strength of 50,000 psi. The holes are to be punched at a rate of one every 2.5 s. Find the requisite motor power and flywheel inertia.

The maximum punch force is

$$F = \pi d t \tau$$

where  $\tau = 50,000$  psi is the shear strength of the material,  $d$  is the diameter of the hole, and  $t$  is the plate thickness. That is, the maximum punch force is simply the shear area multiplied by the shear strength. The force profile as the punch penetrates is irregular with the peak force occurring at a penetration distance of about 3/8 of the plate thickness. A typical profile is sketched in Fig. 14.12.

The area under the curve of punch force versus depth of penetration is the energy used in the punching operation. It can be measured experimentally, but

$$\Delta E = \frac{Ft}{2} \quad (14.16)$$

is a frequently used approximation. In the present instance

$$F = \pi \times 1.0 \times 0.5 \times 50,000 = 78,540 \text{ lb}$$

So

$$\Delta E = 78,540 \times 0.5 / 2 = 19,600 \text{ in-lb} = 1640 \text{ ft-lb}$$

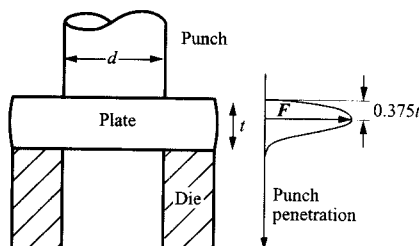
At a punching rate of once every 2.5 s the average power required is

$$P = 1640 / 2.5 = 654 \text{ ft-lb/s} = 1.19 \text{ hp}$$

This is the power for which the motor should be sized.

Now, if the rated motor speed is 1700 rpm we can assume that the maximum motor speed will be this value, so

$$\omega_2 = \frac{1700 \times 2\pi}{60} = 178 \text{ rad/s}$$



**FIGURE 14.12** Punch force as a function of depth of penetration. The peak force,  $F$ , occurs at a penetration depth of about  $0.375 t$ , where  $t$  is the plate thickness.

Also, we can assume that the motor speed quickly drops to its minimum value during the punch stroke and that it is then built back up approximately uniformly to the maximum value in the remainder of the cycle time. Therefore

$$\omega = \frac{\omega_1 + \omega_2}{2}$$

is an adequate approximation to the average motor speed,  $\omega$ .

Since the allowable motor speed variation is 15%,  $c_\delta = 0.15$  and so, applying Eq. (14.13), we have

$$0.15 = \frac{\omega_2 - \omega_1}{\omega} = \frac{2(\omega_2 - \omega_1)}{\omega_2 + \omega_1}$$

Substitution of  $\omega_2 = 178$  gives

$$0.075(178 + \omega_1) = 178 - \omega_1$$

or

$$\omega_1 = 153 \text{ rad/s}$$

Also, applying Eq. (14.14), we get

$$1640 = \frac{I_w}{2} (178^2 - 153^2)$$

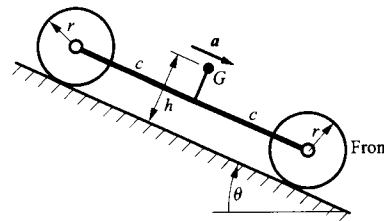
or

$$I_w = 0.396 \text{ ft-lb/s}^2$$

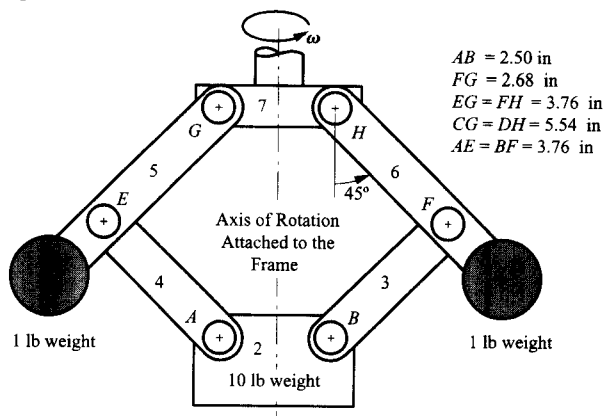
Sizing of a flywheel for an internal combustion engine starts with the pressure–volume chart of the engine's combustion cycle. Multiplication of the pressure by the piston area produces the piston force. A force analysis of the slider-crank mechanism of the engine with the piston force as input produces crankshaft torque as a function of crank angle. The flywheel is then sized to bring the speed fluctuations produced by the torque variation within acceptable limits. Although this process is beyond the scope of this book, it is fully explained in texts on the dynamics of reciprocating machinery.

## PROBLEMS

**14.1** The four-wheeled vehicle shown slides down a steep slope with its rear wheels locked (not moving relative to the body) and its front wheels rolling freely. If  $M$  is the mass of the vehicle,  $h$  is the normal distance from its center of mass  $G$  to the ground,  $r$  is the wheel radius, and  $2c$  is the distance between the axles, find the acceleration of the vehicle. The angle of the slope is  $\theta$ , and the coefficient of friction between the wheels and the ground is  $\mu$ . The mass and moment of inertia of each wheel about its axle may be neglected. What is the largest value for the angle  $\theta$  at which the vehicle will not slide?



14.2 The flyball governor shown is started from rest and accelerated slowly about the axis of rotation. At what speed of rotation will it be in the position shown? Friction may be neglected. Ignore the masses of the four links.

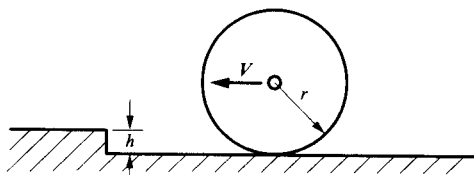


14.3 Solve Problem 14.2 assuming a coefficient of friction of 0.3 at each of the six pin joints. The diameter of each joint is 0.8 in.

14.4 A wheel, of mass  $m$  and radius  $r$ , rolls without slipping on a horizontal plane. It hits a step of height  $h$ . If the velocity of the center of the wheel before striking the step is  $V$ , directed as shown, find the following:

- (a) the magnitude and direction of the velocity of the center of the wheel immediately after the impact,
- (b) the minimum value of  $V$  for which the wheel surmounts the step, and
- (c) the impulse exerted on the wheel by the edge of the step at impact

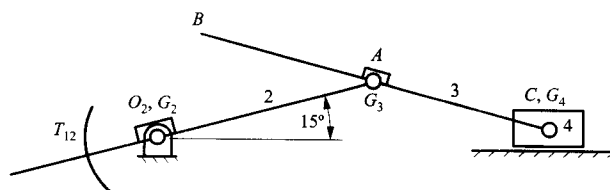
The impact may be considered to take place over a vanishingly small time interval. The wheel is assumed to remain in contact with the edge of the step after the impact. The wheel may be considered to have a moment of inertia about its center in the direction of rotation of  $I = mr^2$ .



14.5 In the mechanism shown, link 2 rotates at an angular velocity of 20 rad/s (CW) and angular acceleration of 140 rad/s<sup>2</sup> (CW). Find the torque that must be applied to link 2 to maintain equilibrium. Link 2 is balanced so that its center of mass is at the pivot  $O_2$ . The center of mass of link 3 is at  $A$ , and the mechanism moves in the horizontal plane. Friction may be neglected. Use the following values:

$$O_2A = CA = 100 \text{ mm}, \quad m_3 = 0.74 \text{ kg}, \quad m_4 = 0.32 \text{ kg}$$

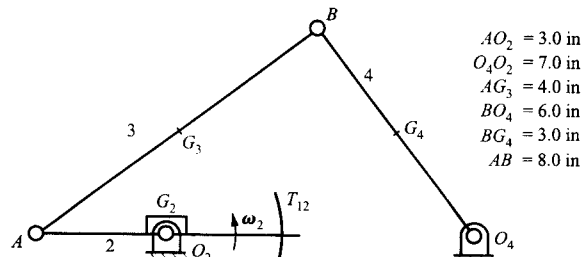
$$I_{G_3} = .00205 \text{ N-s}^2\text{-m}, \quad I_{G_4} = .0062 \text{ N-s}^2\text{-m}$$



14.6 Find the external torque ( $T_{12}$ ) that must be applied to link 2 of the mechanism illustrated to drive it at  $\omega_2 = 1800 \text{ rad/s}$  CCW and  $\alpha_2 = 0 \text{ rad/s}^2$ . Link 2 is in a horizontal position, and it is balanced so that its center of mass is at the pivot  $O_2$ . The mechanism moves in the horizontal plane, and friction may be neglected. Use the following values:

$$W_3 = 0.708 \text{ lb}, \quad I_{G_3} = 0.0154 \text{ lb-s}^2\text{-in}$$

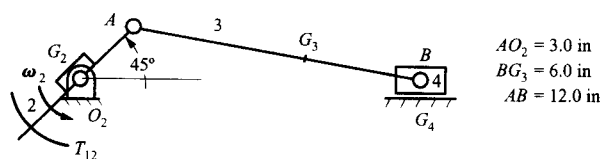
$$W_4 = 0.780 \text{ lb}, \quad I_{G_4} = 0.0112 \text{ lb-s}^2\text{-in}$$



14.7 Find the external torque ( $T_{12}$ ) that must be applied to link 2 of the mechanism illustrated in order to drive it at  $\omega_2 = 210 \text{ rad/s}$  CCW and  $\alpha_2 = 0 \text{ rad/s}^2$ . Link 2 is balanced so that its center of mass is at the pivot  $O_2$ . The mechanism moves in the horizontal plane and friction may be neglected. Use the following values:

$$W_3 = 3.4 \text{ lb}, \quad I_{G_3} = 0.1085 \text{ lb-s}^2\text{-in}$$

$$W_4 = 2.86 \text{ lb}$$

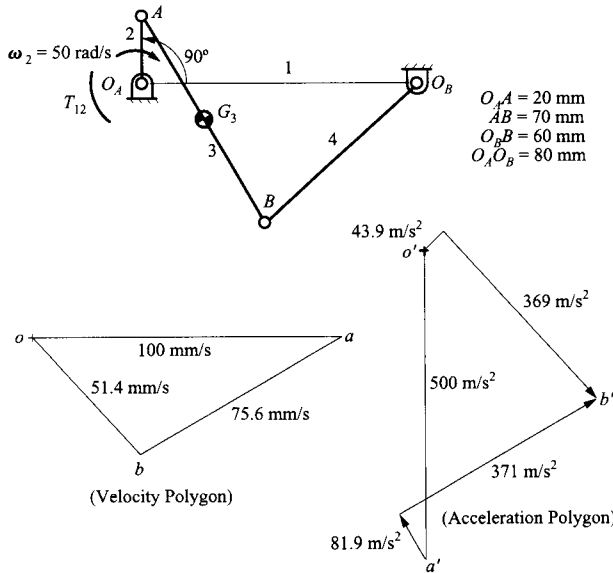


14.8 In the mechanism shown, the center of mass of link 3 is at  $G_3$ , which is located at the center of link 3. The mass of link 3 is 0.5 kg. Its moment of inertia about  $G_3$  is 0.0012 N-s<sup>2</sup>-m. The weights and moments of inertia of members 2 and 4 may be neglected. Link 2 is driven at a constant angular velocity of

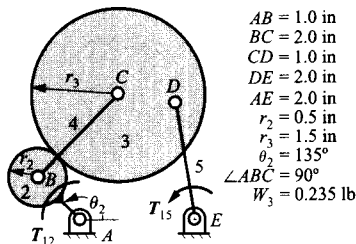
50 rad/s CW by the torque applied to link 2. The mechanism moves in the horizontal plane, and friction may be neglected.

(a) Find the magnitudes and directions of the inertia force and inertia torque acting on link 3.

(b) Find the magnitudes and directions of the forces exerted on link 3 by link 2 at *A* and by link 4 at *B*. You may use either a graphical solution or numerical solution of the dynamic equilibrium equations.



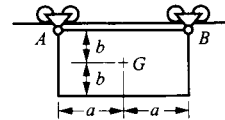
14.9 Link *AB* of the geared five-bar linkage shown drives CCW against a load torque  $T_{15} = 25 \text{ in}\cdot\text{lb}$ . If  $\omega_2 = 0.001 \text{ rpm}$  CW, find the driving torque  $T_{12}$ . The mechanism moves in the horizontal plane, and friction may be neglected. The gears 2 and 3 are represented by their pitch circles. Both gears turn on bearings supported by the tie link, 4. The weight of link 2 is small and can be neglected. Gear 3 is 0.2-in thick and may be treated as a solid disk.



14.10 A punch press similar to that of Example 14.5 is to punch holes of diameter up to 0.75 in through steel plate up to 0.375-in thick. The shear strength of the steel will range up to 60,000 psi. The rated speed of the motor is 1500 rpm, and a 10% drop in motor speed is allowable. If holes are to be punched at a maximum rate of 1 per second, find the requisite motor power and flywheel inertia.

14.11 A uniform rectangular plate is suspended from a rail by means of two bogies as shown. The plate is connected to the bogies by means of frictionless hinge joints at *A* and at *B*. At time  $t = 0$  the pin of joint *B* breaks, allowing the plate to swing downward. Write the equations of motion of the plate as it starts to move. Hence find its initial angular acceleration and the initial acceleration of point *A*.

You may assume that the rollers that support point *A* are frictionless and that they remain in contact with the rail. You may also assume that the angular displacement from the initial position is small. The moment of inertia of a uniform rectangular plate with sides  $2a$  and  $2b$  about an axis normal to its plane passing through its centroid is  $m(2a + 2b)/12$ , where  $m$  is the mass of the plate.





---

# SHAKING FORCES AND BALANCING

---

## 15.1 INTRODUCTION

---

Fast-moving machinery with rotating or reciprocating masses is a significant source of vibration excitation. A major theme in machine dynamics and machine design is seeking to minimize the fluctuating forces that such machinery applies to its environment via its mounts. Rapidly rotating masses such as those in electric motors and generators, steam and gas turbines, vehicle wheels, and many other situations can generate significant fluctuating forces with even tiny amounts of unbalance. Combinations of rotating and reciprocating masses are found in internal combustion engines, pumps, compressors, and many other types of machinery. They are strong generators of fluctuating forces, but those forces can be at least partially balanced by appropriately placed weights. It is necessary to discuss the procedures used for balancing in these somewhat diverse types of systems.

When any mechanism is operated at high speeds, two types of forces must be considered: externally applied forces and inertial forces. Inertial forces arise when the individual members are subjected to large accelerations. In general, the inertial force system acting on a given member can be represented as an inertia force acting on a line through the center of mass, together with an inertia torque, as was described in Section 14.2. The force is given by  $-ma$  and the couple by  $-I\alpha$  where  $m$  is the mass of the member,  $I$  is the mass moment of inertia about the center of mass,  $a$  is the linear acceleration of the center of mass, and  $\alpha$  is the angular acceleration of the member. In high-speed machinery, the inertial forces may be larger in magnitude than the external forces. Consequently, when the mechanism is designed, both types of forces must be taken into account.

In general, the external forces will be associated with the useful function that the mechanism is to perform and with driving the mechanism. There is often little that can be done to alter their magnitudes. In contrast, the inertial forces are due entirely to the mass and motion characteristics of the machine members. Therefore, prudent design practice dictates that the inertial forces be minimized. This can be done either by reducing the masses and moments of inertia of the moving members or by reducing the linear and angular accelerations. The masses may be reduced by using lighter materials and optimal geometries. For a given kinematic geometry, the angular accelerations cannot be reduced. However, the linear accelerations of the centers of mass can be reduced by moving the centers of mass toward points of zero acceleration. The way this is often done is to add mass in the form of balance weights to move the overall center of mass of a given member to a location of reduced acceleration.

## 15.2 SINGLE-PLANE (STATIC) BALANCING

In spite of all the care that may be taken in the design and manufacture of a rotating part, whether the part is completely machined, cast, or forged or is assembled from various parts as in the case of the armature of an electric motor, it is uncommon for it to run smoothly, particularly if the operating speed is high. Variations in dimensions due to machining, variations in inhomogeneity of the material, variations in the methods of assembly, and eccentricity of bearing surfaces all contribute to offsetting the center of mass from the axis of rotation.

The curve in Fig. 15.1 emphasizes the effect of a small amount of unbalance at high speeds. The curve shows the centrifugal force produced by an inch-ounce of unbalance at various angular speeds. (An inch-ounce is defined as 1 ounce of weight at 1 inch from the axis of rotation.) The centrifugal force due to 1 in-oz at 1000 rpm is 1.76 lb. At 10,000 rpm it is 176 lb. That is, it increases as the square of the speed. It is evident that the centrifugal force produced on a large rotor can be very large, even if the center of gravity is displaced only a small amount from the axis of rotation, and consequently large shaking forces will be produced on the structure. For example, consider the rotor of an aircraft gas turbine weighing 400 lb that operates at 16,000 rpm and suppose the center of mass is 0.001 in from the axis of rotation. The 6.4 in-oz of unbalance would cause a centrifugal force of

$$F = mR\omega^2 = \frac{400}{32.2} \cdot \frac{0.001}{12} \cdot \left( \frac{2\pi \cdot 16,000}{60} \right)^2 = 2924 \text{ lb}$$

Such a force could cause considerable damage to the machine. Since it is usually impossible to manufacture the rotor of a machine so that the center of gravity will lie within 0.001 in of the axis of rotation, the part must be balanced after manufacture, and the balancing is done experimentally.

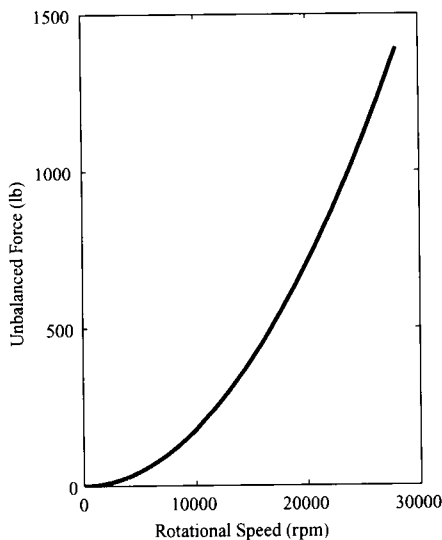


FIGURE 15.1 Effect of 1 in-oz of unbalance.

To illustrate the principles that are involved in balancing a rotating mass, we will first consider a rod rotating at a constant angular velocity  $\omega$  to which is attached a single concentrated mass of weight  $W$  at radius  $r$ . Let  $W_e$  be the weight (called the counterbalance weight) that must be added at some radius  $r_e$  to produce equilibrium as shown in Fig. 15.2. Static balance will be produced if the sum of the moments of the weights about the axis of rotation is zero. That is,

$$-Wr \cos \theta + W_e r_e \cos \theta = 0$$

or

$$W_e r_e = Wr \quad (15.1)$$

If the value of  $r_e$  is arbitrarily chosen, then the value of  $W_e$  can be found from Eq. (15.1). When the system is statically balanced, the shaft will not have any tendency to rotate in its bearings under the influence of gravity regardless of the position to which it is rotated. If the system is rotated with angular velocity  $\omega$ , the static balance condition also ensures that the sum of the inertia forces is zero, as illustrated in Fig. 15.2. That is,

$$\frac{W}{g} r \omega^2 - \frac{W_e}{g} r_e \omega^2 = 0$$

or

$$W_e r_e = Wr$$

which is identical to Eq. (15.1).

The simplest situation is a single rotor that can be regarded as rotating in a single plane, such as that just considered. This type of balancing is called static balancing because a static-type balance procedure in which the measurements are made on the rotor while it is stationary can be used. If the rotor cannot be regarded as spinning in a single plane, the balance procedure involves measurements while the rotor is spinning. This procedure is called dynamic balancing.

Of course, there are situations in which an eccentric mass is deliberately spun to produce a rotating force vector. Example 15.1 concerns an eccentric rotor used to excite vibratory motion of a screen used to sort material particles by size.

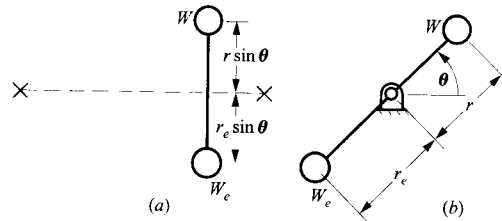
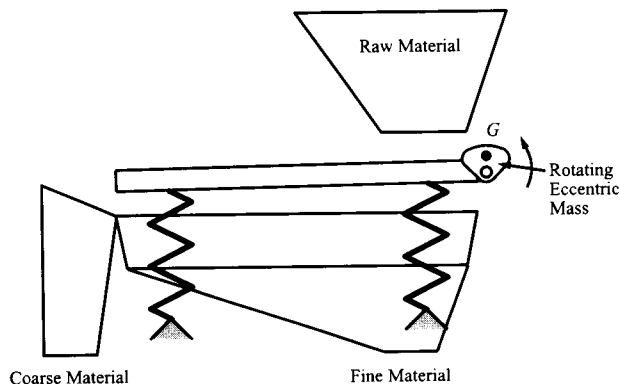


FIGURE 15.2 Single rotating mass.

### EXAMPLE 15.1 Eccentric Mass out of Balance

An eccentric mass is rotated on a shaft mounted on the frame of a vibrating screen used to sort iron ore into different sizes. The mass is shaped as a circular sector as shown in Fig. 15.3. The mass weighs 20 lb, and its mass center is 4 in from the shaft axis. If it is rotated at 600 rpm, what is the force that it exerts on the shaft and hence on the frame of the screen?



**FIGURE 15.3** The vibrating screen arrangement discussed in Example 15.1.  $G$  is the center of mass of the rotor.

### Solution

The exciting force here is simply the centrifugal force of the rotating mass. The angular velocity is

$$\omega = 600 \times 2\pi/60 = 62.83 \text{ rad/s}$$

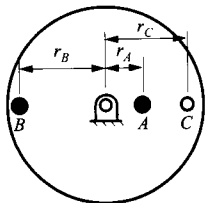
so the acceleration of the center of mass is

$$a = r\omega^2 = (4/12) \times 62.83^2 = 1316 \text{ ft/s}^2$$

Therefore, the magnitude of the rotating force is

$$F = ma = (20/32.2) \times 1316 = 817 \text{ lb}$$

The product of the mass of a rotor and the distance from its center of mass to the shaft axis is called the *unbalance*. An unbalance of a given magnitude may be removed by adding a mass  $180^\circ$  out of phase with it or by subtracting mass with the same unbalance in phase with it. Referring to Fig. 15.4, we see that if the mass of the rotor is  $m_A$  and is located at point  $A$ , then its unbalance is  $m_A r_A$ . If a balancing mass is to be placed at point  $B$  directly opposite point  $A$ , then its mass must be  $m_B$  such that  $m_B r_B = m_A r_A$ . Similarly, balance can also be achieved by *removing* mass  $m_C$  at point  $C$  on the same line with  $A$  and the shaft axis provided  $m_C r_C = m_A r_A$ .

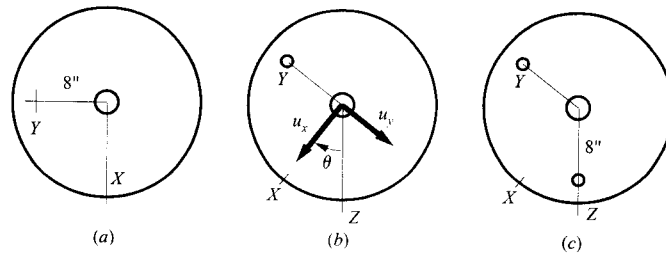


**FIGURE 15.4** A rotor with an eccentric mass with mass center at point  $A$ . The unbalance can be removed by placing a mass at point  $B$  or removing a mass at point  $C$ .

### EXAMPLE 15.2 Static Balancing

A factory producing gear sets statically balances spur gear wheels using the following procedure (Fig. 15.5):

The wheel is mounted on a spindle that turns in very low friction bearings. The wheel is allowed to turn freely under gravity until it comes to rest. The low point,  $X$ , is marked. A small, known mass,  $m_y$ , is next removed from the wheel at point  $Y$ , which is  $90^\circ$  clockwise from  $X$  and at a set radius,  $r_y$ . The wheel is then replaced on the spindle and comes to rest with point  $Z$  at its lowest point. A calculated mass,  $m_z$ , is then drilled out at a specified radius,  $r_z$ , on the radial line through  $Z$  to balance the wheel.



**FIGURE 15.5** The static balance procedure used in Example 15.2. Three stages in the process are shown from left to right.

If the mass drilled out of a given wheel at point  $Y$  weighs 0.1 lb at radius 8 in, and the angle,  $\theta$ , between the radial lines through  $X$  and  $Z$  is  $35^\circ$ , find the weight of the mass to be removed at  $Z$  if it is also drilled out at a radius of 8 in.

### Solution

Let the initial unbalance be  $u_x$ . The unbalance of the trial mass at point  $Y$  is

$$u_y = 0.1 \times 8 = 0.8 \text{ in-lb}$$

Now, when the wheel is in equilibrium after the trial mass is removed

$$u_x \sin \theta = u_y \cos \theta$$

Note that the unbalance is in the opposite direction to  $Y$  since mass was removed at  $Y$ , not added. Therefore

$$u_x = 0.8 \cot 35^\circ = 1.143 \text{ in-lb}$$

The total unbalance is then

$$u_z = u_x \cos \theta + u_y \sin \theta = 1.143 \cos 35^\circ + 0.8 \sin 35^\circ = 1.394 \text{ in-lb}$$

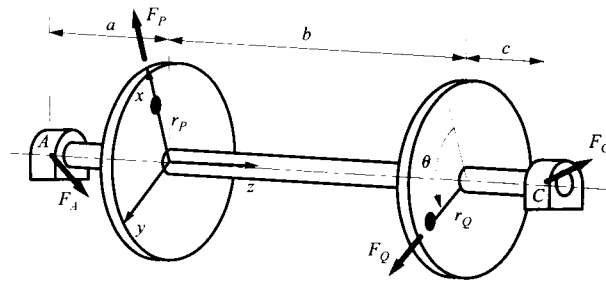
Hence the weight of the mass to be removed at  $Z$  is

$$m_z = 1.394/8 = 0.174 \text{ lb}$$

## 15.3 MULTIPLANE (DYNAMIC) BALANCING

If the inertial mass distribution of the rotor cannot be regarded as planar, fluctuating moments will be generated about axes normal to the axis of rotation in addition to the radial forces. Although the system may be statically balanced by eliminating the resultant radial forces, the shaking moments produced can still be potent sources of vibration excitation. Multiplane or dynamic balancing techniques allow elimination of both radial unbalance forces and moments.

To see how this works, consider the system shown in Fig. 15.6. The shaft shown has two rotors mounted on it, each with an unbalance. The shaft turns in two bearings, as shown. Let us first calculate the unbalance forces,  $F_A$  and  $F_C$ , exerted on the shaft by the bearings.



**FIGURE 15.6** A shaft with two rotors, both of which have unbalances. The left rotor plane is designated by  $P$  and the right by  $Q$ .

The unbalance of the left-hand rotor is

$$u_P = m_P r_P$$

where  $m_P$  is the mass of the left-hand rotor and  $r_P$  is the eccentricity of its center of mass. Hence, at a constant rotation speed  $\omega$ , the unbalance force magnitude is

$$F_P = u_P \omega^2$$

Similarly, at the right-hand rotor, the unbalance is

$$u_Q = m_Q r_Q$$

where  $m_Q$  is the mass of the right-hand rotor and  $r_Q$  is the eccentricity of its center of mass. Hence, the unbalance force magnitude is

$$F_Q = u_Q \omega^2$$

Using a reference frame fixed to the left-hand rotor as shown in Fig. 15.6 with the  $z$  axis along the shaft axis and the  $x$  axis aligned with the direction of the unbalance  $u_P$ , we can write the following force equilibrium equations:

$$\Sigma F_x = 0: F_P + F_Q \cos \theta + F_{A_x} + F_{C_x} = 0 \quad (15.2)$$

$$\Sigma F_y = 0: F_Q \sin \theta + F_{A_y} + F_{C_y} = 0 \quad (15.3)$$

It is convenient to take moments about  $A$  because then  $F_C$  is the only unknown force appearing in the equations. This gives

$$\Sigma M_A = 0: a\mathbf{k} \times F_P \mathbf{i} + (a+b)\mathbf{k} \times F_Q (\cos \theta \mathbf{i} + \sin \theta \mathbf{j}) + (a+b+c)\mathbf{k} \times (F_{C_x} \mathbf{i} + F_{C_y} \mathbf{j}) = 0$$

or

$$aF_P \mathbf{j} + (a+b)F_Q (\cos \theta \mathbf{j} - \sin \theta \mathbf{i}) + (a+b+c)(F_{C_x} \mathbf{j} - F_{C_y} \mathbf{i}) = 0$$

Separating the component equations then yields

$$-(a+b)F_Q \sin \theta - (a+b+c)F_{C_y} = 0 \quad (15.4)$$

$$aF_P + (a+b)F_Q \cos \theta + (a+b+c)F_{C_x} = 0 \quad (15.5)$$

We can solve for the components of  $F_C$  from Eqs. (15.4) and (15.5) and then solve for the components of  $F_A$  from Eqs. (15.2) and (15.3). From Eq. (15.4),

$$F_{C_y} = -\frac{(a+b)F_Q \sin \theta}{a+b+c}$$

and from Eq.(15.5),

$$F_{C_x} = -\frac{aF_P + (a+b)F_Q \cos \theta}{a+b+c}$$

From Eq.(15.2),

$$F_{A_x} = -F_P - F_Q \cos \theta - F_{C_x} = -F_P - F_Q \cos \theta + \frac{aF_P + (a+b)F_Q \cos \theta}{a+b+c}$$

or

$$F_{A_x} = -\frac{(b+c)F_P + cF_Q \cos \theta}{a+b+c}$$

From Eq. (15.3),

$$F_{A_y} = -F_Q \sin \theta - F_{C_y} = -F_Q \sin \theta + \frac{(a+b)F_Q \sin \theta}{a+b+c}$$

or

$$F_{A_y} = -\frac{cF_Q \sin \theta}{a+b+c}$$

Thus the forces applied to the bearings by the shaft are

$$\mathbf{F}_A^* = -\mathbf{F}_A = \frac{\{(b+c)F_P + cF_Q \cos \theta\}\mathbf{i} + cF_Q \sin \theta \mathbf{j}}{a+b+c}$$

and

$$\mathbf{F}_C^* = -\mathbf{F}_C = \frac{\{aF_P + (a+b)F_Q \cos \theta\}\mathbf{i} + (a+b)F_Q \sin \theta \mathbf{j}}{a+b+c}$$

These forces rotate with the shaft, so they fluctuate sinusoidally in any given direction.

If the system is statically balanced by adding a balance weight in the plane  $P$ , the required unbalance is

$$\mathbf{u} = -\mathbf{u}_P - \mathbf{u}_Q = -u_P \mathbf{i} - u_Q (\cos \theta \mathbf{i} + \sin \theta \mathbf{j})$$

Addition of an unbalance of this magnitude and direction in plane  $P$  adds a force

$$\mathbf{F} = \omega^2 \mathbf{u} = -\mathbf{F}_P - \mathbf{F}_Q$$

to the system. The dynamic equilibrium equations become

$$\Sigma F_x = 0: \quad -F_P - F_Q \cos \theta + F_P + F_Q \cos \theta + F_{A_x} + F_{C_x} = F_{A_x} + F_{C_x} = 0 \quad (15.6)$$

$$\Sigma F_y = 0: -F_Q \sin \theta + F_Q \sin \theta + F_{A_y} + F_{C_y} = F_{A_y} + F_{C_y} = 0 \quad (15.7)$$

Once again, taking moments about  $A$ , we get

$$\begin{aligned} \Sigma M_A = 0: & -ak \times \{F_P i + F_Q (\cos \theta i + \sin \theta j)\} + ak \times F_P i + (a+b)k \times F_Q (\cos \theta i + \sin \theta j) \\ & + (a+b+c)k \times (F_{C_x} i + F_{C_y} j) = 0 \end{aligned}$$

or

$$bF_Q (\cos \theta j - \sin \theta i) + (a+b+c)(F_{C_x} j - F_{C_y} i) = 0$$

Therefore

$$\begin{aligned} F_{C_x} &= -\frac{bF_Q \cos \theta}{a+b+c} \\ F_{C_y} &= -\frac{bF_Q \sin \theta}{a+b+c} \end{aligned}$$

and, from Eqs. (15.6) and (15.7),

$$\begin{aligned} F_{A_x} &= -F_{C_x} = \frac{bF_Q \cos \theta}{a+b+c} \\ F_{A_y} &= -F_{C_y} = \frac{bF_Q \sin \theta}{a+b+c} \end{aligned}$$

As may be seen, although the system is now statically balanced in that the resultant radial force is zero, the forces exerted on the bearings are not zero, and so a vibration excitation effect is still present. Since  $F_A = -F_C$ , the bearing forces form a couple with moment

$$\begin{aligned} M &= (a+b+c)k \times (F_{A_x} i + F_{A_y} j) = (a+b+c)(F_{A_x} j - F_{A_y} i) \\ &= (a+b+c)F_Q (\cos \theta j - \sin \theta i) \end{aligned}$$

This couple rotates with the shaft.

### EXAMPLE 15.3 Two-Plane Balance

A small gas turbine rotor carries four blade disks positioned in planes  $A$ ,  $B$ ,  $C$ , and  $D$  as shown in Fig. 15.7. The shaft turns in bearings in planes  $P$  and  $Q$ . Relative to the reference frame shown, the unbalances of the blade disks are, respectively,

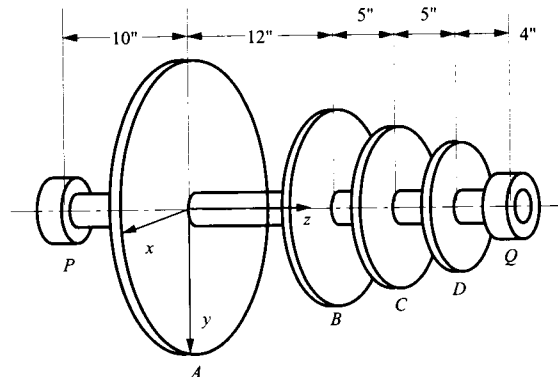


FIGURE 15.7 The turbine rotor whose balance is analyzed in Example 15.3.



$$u_A = 0.08 \text{ in-lb at } 0^\circ, \quad u_B = 0.03 \text{ in-lb at } 70^\circ, \quad u_C = 0.04 \text{ in-lb at } -115^\circ, \\ u_D = 0.03 \text{ in-lb at } 160^\circ$$

1. Compute the rotating radial forces that the rotor would apply to the bearings when spinning at the engine's normal operating speed of 15,000 rpm.
2. The rotor is to be balanced by removing material from disk *A* at radius 3.5 in and from disk *D* at radius 2.0 in. Calculate the mass that must be removed at each location and the angular position at which it must be removed.

**Solution**

1.  $\omega = 15,000 \times 2\pi/60 = 1571 \text{ rad/s}$ . Therefore, the unbalance forces at the respective blade disks are

$$F_A = \frac{0.08 \times 1571^2}{32.2 \times 12} = 511 \text{ lb } \angle 0^\circ$$

$$F_B = \frac{0.03 \times 1571^2}{32.2 \times 12} = 192 \text{ lb } \angle 70^\circ$$

$$F_C = \frac{0.04 \times 1571^2}{32.2 \times 12} = 255 \text{ lb } \angle -115^\circ$$

$$F_D = \frac{0.03 \times 1571^2}{32.2 \times 12} = 192 \text{ lb } \angle 160^\circ$$

Let  $F_P = F_{P_x}i + F_{P_y}j$  be the force exerted on the shaft by the bearing at *P*, and let  $F_Q = F_{Q_x}i + F_{Q_y}j$  be the force exerted on the shaft by the bearing at *Q*. The force equilibrium equations are:

$$\Sigma F_x = 0: \quad F_{P_x} + F_{Q_x} + F_A \cos 0^\circ + F_B \cos 70^\circ + F_C \cos(-115^\circ) + F_D \cos 160^\circ = 0$$

or

$$F_{P_x} + F_{Q_x} + 511 + 192 \cos 70^\circ + 255 \cos(-115^\circ) + 192 \cos 160^\circ = 0$$

giving

$$F_{P_x} + F_{Q_x} = -288 \text{ lb} \tag{15.8}$$

and

$$\Sigma F_y = 0: \quad F_{P_y} + F_{Q_y} + F_A \sin 0^\circ + F_B \sin 70^\circ + F_C \sin(-115^\circ) + F_D \sin 160^\circ = 0$$

or

$$F_{P_y} + F_{Q_y} + 192 \sin 70^\circ + 255 \sin(-115^\circ) + 192 \sin 160^\circ = 0$$

giving

$$F_{P_y} + F_{Q_y} = -15 \text{ lb} \tag{15.9}$$

Taking moments about *P*, we have

$$\Sigma M_P = 0:$$

$$10\mathbf{k} \times 511\mathbf{i} + 22\mathbf{k} \times (65.7\mathbf{i} + 180\mathbf{j}) + 27\mathbf{k} \times (-107.8\mathbf{i} - 231\mathbf{j}) + 32\mathbf{k} \times (-180\mathbf{i} + 65.7\mathbf{j}) \\ + 36\mathbf{k} \times (F_{Q_x}\mathbf{i} + F_{Q_y}\mathbf{j}) = 0$$

Therefore

$$F_{Q_y} = \frac{1}{36}(-3960 + 6237 - 2102) = 4.9 \text{ lb}$$

$$F_{Q_x} = -\frac{1}{36}(5110 + 1445 - 2911 - 5760) = 58.8 \text{ lb}$$

and substitution back into Eqs. (15.8) and (15.9) gives

$$F_{P_x} = -288 - 59 = -347 \text{ lb}$$

$$F_{P_y} = -15 - 5 = -20 \text{ lb}$$

Consequently, the magnitude and direction of the bearing force at  $P$  is

$$F_P = \sqrt{347^2 + 20^2} = 348 \text{ lb } \angle 183.3^\circ$$

Similarly, the bearing force at  $Q$  is

$$F_Q = \sqrt{4.9^2 + 58.8^2} = 59 \text{ lb } \angle 4.8^\circ$$

2. Since the unbalance force is simply the unbalance multiplied by  $\omega_2$  and has the same direction as the unbalance, it is convenient to simply work with the unbalances.  $u_A$  is the required unbalance to be added to disk  $A$ , and  $u_D$  is the unbalance to be added to disk  $D$ . If the rotor is fully dynamically balanced, the forces at the bearings  $P$  and  $Q$  are both zero. The  $x$  direction force equilibrium equation gives

$$u_{A_x} + 0.08 + 0.03 \cos 70^\circ + 0.04 \cos(-115^\circ) + 0.03 \cos 160^\circ + u_{D_x} = 0$$

The  $y$  direction equation is

$$u_{A_y} + 0 + 0.03 \sin 70^\circ + 0.04 \sin(-115^\circ) + 0.03 \sin 160^\circ + u_{D_y} = 0$$

These equations give

$$u_{A_x} + u_{D_x} = -0.0452 \text{ in-lb} \quad (15.10)$$

$$u_{A_y} + u_{D_y} = -0.0022 \text{ in-lb} \quad (15.11)$$

Since the bearing forces are zero, it is better to take moments about  $A$ , so only the components of  $u_D$  appear as unknowns in the moment equations. Hence

$$\begin{aligned} 12\mathbf{k} \times (0.03 \cos 70^\circ \mathbf{i} + 0.03 \sin 70^\circ \mathbf{j}) + 17\mathbf{k} \times (0.04 \cos(-115^\circ) \mathbf{i} + 0.04 \sin(-115^\circ) \mathbf{j}) \\ + 22\mathbf{k} \times ((0.03 \cos 160^\circ + u_{D_x}) \mathbf{i} + (0.03 \sin 160^\circ + u_{D_y}) \mathbf{j}) = 0 \end{aligned}$$

This reduces to

$$0.0523 - 22u_{D_x} = 0$$

$$-0.7845 + 22u_{D_y} = 0$$

or

$$u_{D_x} = 0.0357 \text{ in-lb}$$

$$u_{D_y} = 0.0024 \text{ in-lb}$$

so the magnitude of the required additional unbalance at disk  $D$  is

$$u_D = \sqrt{0.0357^2 + 0.0024^2} = 0.0358 \text{ in-lb}$$

and its direction is

$$\angle u_D = \tan^{-1}(0.0024/0.0357) = 3.8^\circ \text{ relative to the } x \text{ axis}$$

Substitution back into Eqs. (15.10) and (15.11) gives

$$u_{A_x} = -0.0452 - 0.0357 = -0.0809 \text{ in-lb}$$

$$u_{A_y} = -0.0022 - 0.0024 = -0.0046 \text{ in-lb}$$

so the magnitude of the required additional unbalance at disk  $A$  is

$$u_A = \sqrt{0.0809^2 + 0.0046^2} = 0.0810 \text{ in-lb}$$

and its direction is

$$\angle u_A = 180 + \tan^{-1}(0.0046/0.0809) = 183.3^\circ \text{ relative to the } x \text{ axis}$$

Now the unbalance at  $A$  is to be created by *removing* mass at the radius 3.5 in. The weight of the mass to be removed is

$$m_A = 0.0810/3.5 = 0.023 \text{ lb}$$

Since the material will be removed, it should be removed at the angle  $180^\circ + 183.3^\circ = 363.3^\circ$ , that is, at angle  $3.3^\circ$  to the  $x$  axis in the positive rotation direction about the  $z$  axis.

Similarly, at disk  $D$  the material is to be removed at the radius 2.0 in. The weight to be removed is

$$m_D = 0.0358/2.0 = 0.0179 \text{ lb}$$

and it must be removed at the angle  $180^\circ + 3.8^\circ = 183.8^\circ$  measured from the positive  $x$  axis direction.

## 15.4 BALANCING RECIPROCATING MASSES

A second major source of vibration excitation in machinery is the presence of masses that perform oscillatory motions. Of course, the classic case is the reciprocating piston mass in an internal combustion engine, or a reciprocating pump or compressor.

Although the motion of the reciprocating mass in one of these machines is not strictly harmonic, it is customary to treat it as being so for the purposes of trying to reduce the tendency of the machine to excite vibration. There are several reasons for making this approximation. One is that a simple harmonic oscillation is easy to model and conceptualize. Another is that the fundamental frequency of oscillation is really most important. If we imagine the oscillatory acceleration decomposed into Fourier components, there will be a large-amplitude fundamental with the period of the overall oscillation and a train of higher harmonics with much smaller amplitudes. Not only are these harmonics less effective in exciting vibration because of their smaller amplitudes, but also their frequencies are much higher than the fundamental. Because higher frequency vibrations are much more effectively damped out in most structures, the fundamental frequency tends to dominate the transmitted vibration.

Another approximation that is commonly used when dynamically modeling reciprocating machines is to model the mass of the connecting rod as two equivalent masses, one located on the crank pin axis and the other at the wrist pin axis. That is, the distributed mass of the connecting rod is split into a reciprocating point mass, at the wrist pin, and a pure

rotating point mass, at the crank pin. The reciprocating component then simply becomes a part of the piston mass, and the rotating component becomes a part of the mass of the crank pin.

This decomposition can be done to preserve the correct location of the center of mass of the connecting rod. However, the moment of inertia of the two mass elements about that center of mass will not be exactly the same as that of the connecting rod. The error introduced in this manner is minimal in most analyses.

### 15.4.1 Expression for Lumped Mass Distribution

To develop an expression for discretizing the distribution of the masses of the crank and connecting rod consider the slider-crank mechanism shown in Fig. 15.8. The crank is assumed to rotate with a constant angular velocity  $\omega$ . Points  $A$  and  $B$  are the crank pin and wrist pin, respectively, and  $G_2$  and  $G_3$  are the centers of mass of links 2 and 3, respectively. The sum of the weights of the crank and crank pin is  $m_2g$ , and the centrifugal force acts outward along line  $G_2A$  as shown in Fig. 15.8b. In Fig. 15.8c, the masses of the crank and crank pin have been replaced by a concentrated mass  $m_A$  located at  $A$  such that the centrifugal forces shown in Figs. 15.8b and 15.8c will be equal. Thus,

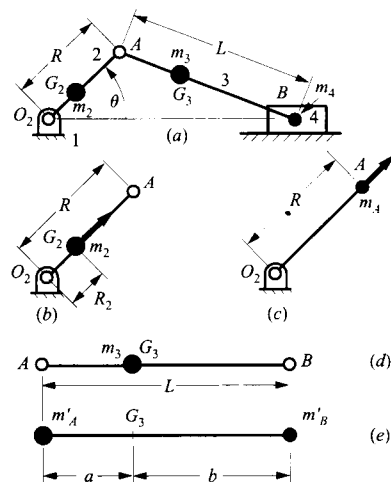
$$m_A R \omega^2 = m_2 R_2 \omega^2$$

or

$$m_A = \frac{R_2}{R} m_2 \quad (15.12)$$

Note that in Eq. (15.12) it is assumed that the center of mass of the crank and point  $A$  are on the same side of the rotation axis. If  $G_2$  is on the opposite side, the effective mass of the crank will be *negative*. This is because the inertial force due to  $G_2$  will be in the opposite direction from that due to a mass at  $A$ .

The connecting rod of mass  $m_3$  in Fig. 15.8d can be approximated by the system shown in Fig. 15.8e, which consists of the two concentrated weights  $m'_A$  and  $m'_B$  connected



**FIGURE 15.8** A slider-crank mechanism: replacement of connecting rod and crank pin inertias by approximately equivalent lumped masses located at points  $A$  and  $B$ .

by a weightless rod. For the center of mass of the substitute masses  $m'_A$  and  $m'_B$  to remain at  $G_3$

$$m'_B(a+b) = (m'_A + m'_B)a$$

or

$$m'_B = \frac{m_3 a}{a+b} = \frac{m_3 a}{L} \quad (15.13)$$

where  $m_3 = (m'_A + m'_B)$  is the mass of the connecting rod,  $b$  is the distance from the center of mass of the connecting rod to the center of the piston pin, and  $a$  is the distance from the center of mass of the connecting rod to the center of the crank pin. Similarly,

$$m'_A = \frac{m_3 b}{a+b} = \frac{m_3 b}{L} \quad (15.14)$$

The replacement system in Fig. 15.8e will have the same inertia forces as the actual connecting rod but its inertia torque will be somewhat different. The total equivalent masses at  $A$  and  $B$  can be represented by

$$\bar{m}_A = m'_A + m_A \quad (15.15)$$

and

$$\bar{m}_B = m'_B + m_4 \quad (15.16)$$

where  $m_4$  is the weight of the piston.

It should be noted that this replacement is an approximation. It almost always increases the effective moment of inertia of the connecting rod about its mass center. This is because the radius of gyration of the central bar portion of the member is actually relatively small:  $L/\sqrt{12}$  if the bar is uniform. Modeling it as lumped masses at its ends always increases the effective moment of inertia.

The shaking forces generated by the reciprocating and rotating masses of a reciprocating machine can now be estimated as in the following example.

#### EXAMPLE 15.4 Shaking Force Calculation

A single-cylinder reciprocating air compressor has a piston that weighs 2.5 lb and a connecting rod of length 12 in weighing 2.0 lb, with its center of mass 4 in from the center of the crank pin. The crank radius is 3 in with a counterbalance weight of 4.0 lb and center of mass 2 in on the reverse side of the crankshaft axis. Estimate the shaking force for a constant crank angular velocity of 300 rpm CW at 30° after top dead center.

#### Solution

Figure 15.9 shows the linkage geometry in the specified position, together with the corresponding velocity and acceleration diagrams.

The angular velocity of the crank (member 2) is

$$\omega_2 = 300 \times 2\pi/60 = 31.42 \text{ rad/s CW}$$

Hence the velocity of point  $A$  is

$$v_A = 0.25 \times 31.42 = 7.85 \text{ ft/s } \angle -30^\circ$$

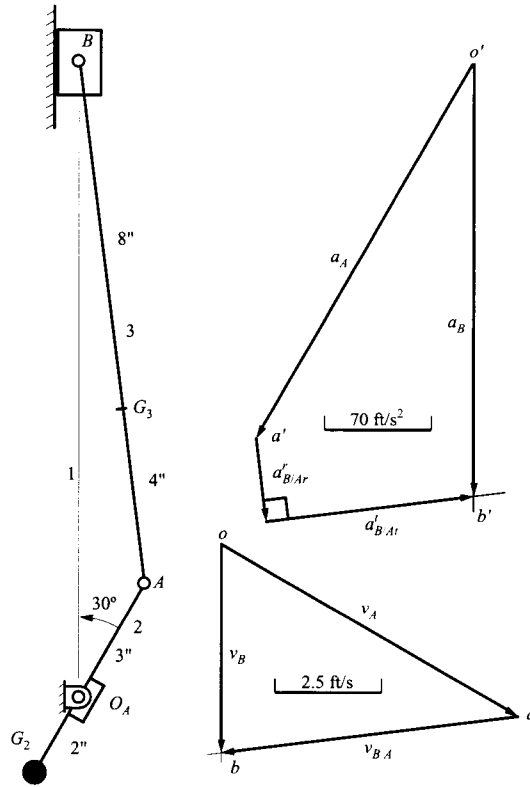


FIGURE 15.9 Position, velocity, and acceleration diagrams for the air compressor mechanism of Example 15.4.

which is plotted as  $\overline{oa}$  on the velocity diagram. The velocity of point  $B$  is given by  $\mathbf{v}_B = \mathbf{v}_A + \mathbf{v}_{B/A}$ . The directions of both  $\mathbf{v}_B$  and  $\mathbf{v}_{B/A}$  are known. Completion of the triangle by drawing  $\overline{ob}$  parallel to the slide and  $\overline{ab}$  normal to  $\overline{AB}$  gives

$$\mathbf{v}_{B/A} = \overline{ab} = 6.87 \text{ ft/s in the direction shown}$$

Hence, the angular velocity of the connecting rod, member 3, is

$$\omega_3 = \frac{ab}{AB} = \frac{6.87}{1.0} = 6.87 \text{ rad/s CCW}$$

Since the angular velocity of member 2 is constant

$$\mathbf{a}_A = \mathbf{a}_A^r = 0.25 \times 31.42^2 = 246.8 \text{ ft/s}^2 \angle -120^\circ$$

This is plotted on the acceleration diagram as  $\overline{o'a'}$ . The acceleration of  $B$  is given by  $\mathbf{a}_B = \mathbf{a}_A + \mathbf{a}_{B/A} = \mathbf{a}_A + \mathbf{a}_{B/A}^r + \mathbf{a}_{B/A}^t$ . The radial component of

$$\mathbf{a}_{B/A}^r = 1.0 \times 6.87^2 = 47.20 \text{ ft/s}^2 \text{ parallel to } \overline{BA}$$

can be calculated and plotted as shown in the figure. The direction of  $\mathbf{a}_{B/A}^t$  can now be plotted through the tip of this arrow. Its intersection with the direction of  $\mathbf{a}_B$ , parallel to the slide, gives the point  $b'$  and completes the polygon. Scaling from the diagram gives

$$\mathbf{a}_B = 248 \text{ ft/s}^2 \text{ (down)}$$

This is actually all the acceleration information needed to solve the problem, because the distributed mass of the connecting rod will be approximated by lumped masses at points  $A$  and  $B$ .

Applying Eqs. (15.13) and (15.14) gives the equivalent weights for the connecting rod:

$$m'_A = (8/12)2.0 = 1.333 \text{ lb}$$

$$m'_B = (4/12)2.0 = 0.667 \text{ lb}$$

Therefore, the total effective weight at point  $B$  is

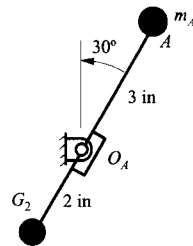
$$\bar{m}_B = 0.667 + 2.5 = 3.167 \text{ lb}$$

The reciprocating shaking force component is, therefore,

$$F_B = -\bar{m}_B a_B = 248 \times 3.167/32.2 = 24.4 \text{ lb (up)}$$

The rotating mass at  $A$  in Fig. 15.10 will be the sum of  $m'_A$  and the effective mass  $m_A$  of the crank referred to point  $A$ . Note that points  $A$  and  $G_2$  are on opposite sides of the rotation axis. Therefore, the effective mass of the crank alone will be negative. From Eq. (15.12) the effective mass  $m_A$  of the crank is given by

$$m_A = \frac{R_2}{R} m_2 = -\frac{2}{3} 4.0 = -2.666 \text{ lb}$$



**FIGURE 15.10** Effective mass distribution of the continuously rotating crank of Example 15.4. The mass  $m_A$  is the equivalent rotating mass of the connecting rod.

The total equivalent mass at  $A$  is given by Eq. (15.15) as

$$\bar{m}_A = m'_A + m_A = 1.333 - 2.666 = -1.333 \text{ lb}$$

Therefore, the center of gravity for  $M_A$  is on the same side of the rotation axis as  $G_2$ . Consequently, the inertia force due to the effective rotating mass is

$$F_A = \bar{m}_A R \omega^2 = \frac{-1.333(3)(31.42)^2}{12 \times 32.2} = -10.220 \angle 60^\circ = 10.220 \angle -120^\circ \text{ lb}$$

If the effective mass at  $A$  were positive, the direction of the inertial force would be opposite to the acceleration of point  $A$  or at an angle of  $60^\circ$  with the horizontal axis. In this system, the rotating masses contribute very little to the shaking force. The reciprocating masses are dominant in the generation of the shaking force.

### 15.4.2 Analytical Approach to Balancing a Slider-Crank Mechanism

As already discussed, the inertia of the connecting rod can be approximated by two concentrated masses, one at the crank pin and the other at the wrist pin. The slider-crank system then becomes a combination of a mass assumed to be rotating at constant angular velocity (the crank mass together with the equivalent mass at the crank pin from the connecting rod)

and a reciprocating mass (the piston and wrist pin mass, together with the equivalent mass from the connecting rod concentrated at the wrist pin). To a first approximation, the piston motion can be regarded as a simple harmonic motion. This is equivalent to replacing a Fourier series by its fundamental term; it is an approximation, but a useful one. The inertia force from the reciprocating mass is then a simple harmonic force acting along the cylinder axis. The inertia force from the rotating mass rotates with the crank. Its component along the cylinder axis is also harmonic, with the same period as the inertia force from the reciprocating mass. The rotating inertia force can be completely removed by counterweighting the crank so that the center of mass of the equivalent mass system is at the crankshaft axis. The inertia force of the reciprocating mass cannot be completely removed. However, it can be offset by increasing the mass of the counterweight on the crank so that the axial component of the crank inertia force opposes the inertia force from the reciprocating mass. This reduces the magnitude of the axial inertia force from the reciprocating mass, but at the cost of reintroducing a lateral shaking force from the counterweighted crank. A popular arrangement for single-cylinder engines is to use a crank counterweight that is large enough to halve the amplitude of the reciprocating inertia force. This results in a rotating inertia force of half the amplitude of the original reciprocating unbalance. The resultant inertia force rotates in the *opposite* direction to the crank. If one is willing to tolerate the extra complexity of arranging a counterrotating counterweight on the crankshaft axis, this remaining unbalance force can also be removed.

The *shaking force* is the *resultant of all the forces acting on the frame of a mechanism due to inertia forces only*. Thus, if the resultant of all the forces due to inertia effects acting on the frame is zero, there is no shaking force. There may, nevertheless, be a *shaking couple* present. Balancing a mechanism consists of eliminating the shaking force and shaking couple. In some instances we can accomplish both. We shall discover that in most mechanisms, by adding appropriate balancing weights, we can reduce the shaking force and shaking couple, but it is usually not practical to provide a means of completely eliminating them.

Since the slider-crank mechanism is so widely used in such machines as internal-combustion engines and compressors, considerable work has been done on the development of techniques for balancing these mechanisms. The approach to balance the slider-crank mechanism will use the approximate mass distribution developed in Section 15.4.1 along with an approximation for the acceleration of point B at the piston. An expression for the acceleration of the piston is developed in the following subsection.

**Approximate Expression for Piston Acceleration** If the crank moves with constant angular velocity  $\omega$ , the acceleration of any point on the crank is given by

$$a_c = r\omega^2 \quad (15.17)$$

where  $r$  is the distance from  $O_2$  to the point of interest. In Fig. 15.11, point  $A$  is the primary point of interest. If the lumped-mass model is used for the connecting rod, the only other point of interest is point  $B$  at the wrist pin. The acceleration of this point can be determined using Fig. 15.11. A local  $x, y$  coordinate system is located at point  $O_2$  as shown such that the  $x$  axis is along the line  $O_2B$ .

The position of the point  $B$  relative to  $O_2$ , the origin of the  $x$  and  $y$  coordinate axes, is represented by  $x$ . Link 2 is at an angle  $\theta$  from the  $x$  axis for the position shown. The connecting rod makes an angle of  $\phi$  with the  $x$  axis. The distance  $x$  may be represented by the sum of the projection of the crank and connecting rod on the  $x$  axis:

$$x = R \cos \theta + L \cos \phi \quad (15.18)$$



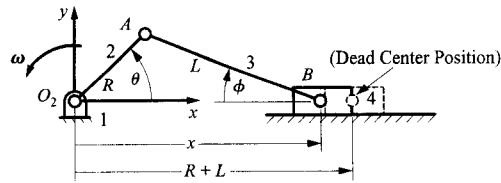


FIGURE 15.11 Slider-crank mechanism coordinate system.

It is desirable to represent  $x$  as a function of  $R$ ,  $L$ , and  $\theta$ . To do this,  $\phi$  may be eliminated by noting that the vertical projections of  $R$  and  $L$  are equal, or

$$R \sin \theta = L \sin \phi$$

or

$$\sin \phi = \left(\frac{R}{L}\right) \sin \theta \quad (15.19)$$

but

$$\cos \phi = \sqrt{1 - (\sin \phi)^2} \quad (15.20)$$

Therefore, substitution of Eq. (15.19) into Eq. (15.20) gives

$$\cos \phi = \sqrt{1 - \left[\left(\frac{R}{L}\right) \sin \theta\right]^2} \quad (15.21)$$

Substitute Eq. (15.21) into Eq.(15.18) to get

$$x = R \cos \theta + L \sqrt{1 - \left[\left(\frac{R}{L}\right) \sin \theta\right]^2} \quad (15.22)$$

Equation (15.22) is an exact expression for the location of the piston relative to the center of the crank bearing.

The expression for the velocity may be obtained by differentiating  $x$  with respect to  $t$ . Noting that  $d\theta/dt = \omega$ , we have for the velocity of the piston

$$v_B = \frac{dx}{dt} = -R\omega \left[ \sin \theta + \frac{R}{2L} \sin 2\theta \left/ \sqrt{1 - \left(\frac{R}{L} \sin \theta\right)^2} \right. \right] \quad (15.23)$$

The expression for the acceleration of the piston may be obtained by differentiating  $v$  with respect to  $t$  and remembering that  $\omega$ , the angular speed of the crank, is constant. Then,

$$a_B = \frac{dv_B}{dt} = -R\omega^2 \left[ \cos \theta + \frac{\frac{R}{L} \cos 2\theta \left\{ 1 - \left(\frac{R}{L}\right)^2 \right\} + \left(\frac{R}{L}\right)^3 \cos^4 \theta}{\left\{ 1 - \left(\frac{R}{L} \sin \theta\right)^2 \right\}^{3/2}} \right] \quad (15.24)$$

If the velocity or acceleration is negative, it is directed from the piston to the crank bearing. The angular velocity of the crank is positive if it is counterclockwise.

For most practical engines, the value of  $R/L$  will be less than  $1/4$  so that  $(R/L)^2$  will be small compared with 1. With this approximation, the expression for the acceleration can be simplified with little loss of accuracy to

$$a_B = -R\omega^2 \left[ \cos\theta + \frac{R}{L} \cos 2\theta \right] \quad (15.25)$$

The maximum error in these approximate expressions is around 0.5% of the maximum values for  $(R/L = 1/4)$ . Therefore, because of the form for the equations, the approximate expressions are sometimes used in analytical work. However, when a computer is used, the simplification is not necessary because it is only slightly more difficult to compute the exact value for the acceleration of the piston.

## 15.5 EXPRESSIONS FOR INERTIAL FORCES

We can represent the inertia forces as the vectors

$$f_A = -\bar{m}_A a_A = \bar{m}_A R\omega^2 \angle\theta \quad (15.26)$$

and

$$f_B = -\bar{m}_B a_B \cong \bar{m}_B R\omega^2 \left( \cos\theta + \frac{R}{L} \cos 2\theta \right) \angle 0^\circ \quad (15.27)$$

Therefore, in terms of  $x$  and  $y$  components, the total shaking force would be

$$f_S = f_A + f_B = R\omega^2 \left[ (\bar{m}_A + \bar{m}_B) \cos\theta + \bar{m}_B \left( \frac{R}{L} \right) \cos 2\theta \right] i + R\omega^2 (\bar{m}_A \sin\theta) j \quad (15.28)$$

If a counterbalance mass is added to the crank, the mass would be added to the side of the crank that is opposite A. As discussed in Section 15.2, this is equivalent to subtracting mass from the side of the crank where A is located. Regardless of whether we add or subtract mass, it is convenient to represent the “added” mass as an equivalent mass at A by using Eq. (15.12). If the counterbalance mass is  $m_{cb}$ , at a distant  $R_c$  from the crank axis, the equivalent mass  $\bar{m}_{cb}$  at point A would be

$$\bar{m}_{cb} = \frac{R_c}{R} m_{cb}$$

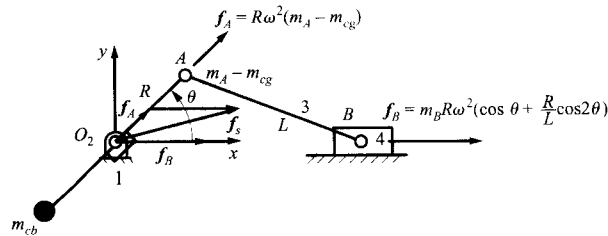
The total inertial force at point A would then be

$$f_A = (\bar{m}_A - \bar{m}_{cb}) R\omega^2 \angle\theta$$

and Eq. (15.28) can be rewritten as

$$f_S = f_A + f_B = R\omega^2 \left[ (\bar{m}_A + \bar{m}_B - \bar{m}_{cb}) \cos\theta + \bar{m}_B \left( \frac{R}{L} \right) \cos 2\theta \right] i + R\omega^2 (\bar{m}_A - \bar{m}_{cb}) \sin\theta j \quad (15.29)$$

The results are shown schematically in Fig. 15.12. Equation (15.29) can be easily programmed using MATLAB. This permits the user to compute the shaking force as a function of  $\theta$  and to determine the best choice of counterbalance weight to minimize the maximum value for the shaking force. The program *shake.m*, which is included on the disk with this book, performs the necessary calculations and plots the results.



**FIGURE 15.12** Equivalent slider-crank mechanism with inertial forces ( $\omega = \text{constant}$ ).

Notice that  $\bar{m}_{cb}$  appears in both components of  $f_s$ . The objective of the balancing procedure is to adjust  $\bar{m}_{cb}$  to reduce the magnitude of  $f_s$  that varies directly with  $\theta$  and in part with  $2\theta$ . It is customary to refer to the portion of the force occurring at the circular frequency  $\omega$  rad/s as the primary inertia force and the portion occurring at  $2\omega$  rad/s as the secondary inertia force. We note that the vertical component has only a primary part and that it therefore varies directly with the crankshaft speed. In contrast, the horizontal component, which is in the direction of the cylinder axis, has a primary part varying directly with the crankshaft speed and a secondary part that varies at twice the crankshaft speed.

Note also that the equations derived are in terms of mass. In general, we will measure directly the weights for the crank and connecting rod and not the mass. However, as used in the earlier examples, the mass can be conveniently determined from the weight by dividing the weight by the acceleration of gravity.

### EXAMPLE 15.5 Balancing a Slider-Crank Mechanism

The purpose of this example is to introduce the student to a numerical technique for balancing a model of a slider-crank mechanism and to give an example of the use of a computer program for balancing a slider-crank mechanism. The computer program *shake.m* will be used to determine the “optimum” counterbalance value for a slider-crank mechanism that might be used in a small engine.

The program computes the maximum value of the shaking force for a specified value of the counterbalance weight (assumed to be located at a distance equal to the crank radius). The program also computes the maximum shaking force value for no counterbalance weight and for the optimum counterbalance weight. The maximum value is found through a simple search over the crank angle range of  $0^\circ$  to  $360^\circ$ . Given the counterbalance weight  $W_{cb}$ , the program increments the crank angle  $\theta$  in  $1^\circ$  increments. The shaking force is computed at each of these  $\theta$  values, and the maximum value is selected.

For the analysis, assume that the following data have been recorded:

Piston	$W_4 = 20$ lb
Rod	$L = 14$ in
	$W'_A = 24.29$ lb
	$W'_B = 9.71$ lb
Crank	$R = 4.0$ in
	$W_A = 3.75$ lb
Rotation speed	1000 RPM
Gravity	$g = 386$ in/s <sup>2</sup>

Use the program *shake.m* given on the disk with this book to find the optimum counterbalance weight for the mechanism. Note that the weights of the crank and the connecting rod mentioned are already referred to the crank pin and the piston pin.

### Solution

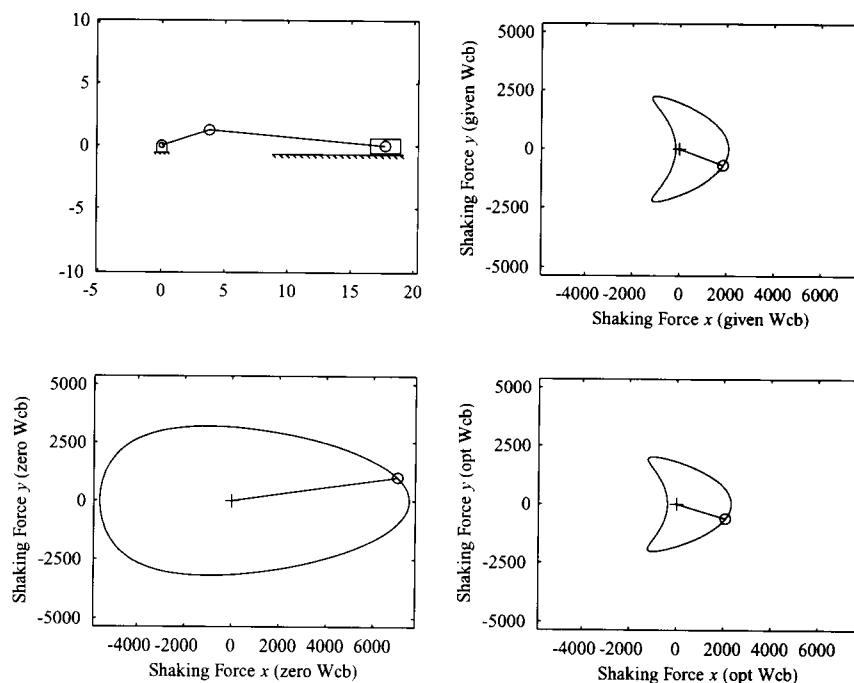
Begin the optimization with an initial value for the counterbalance mass as  $\bar{m}_{cb} = \bar{m}_A + 2\bar{m}_B/3$ . This value is often suggested as the optimum counterbalance mass. The counterbalance weight corresponding to this mass is

$$W_{cb} = (W_A + W'_A) + 2(W'_B + W_4) / 3 = (3.75 + 24.29) + 2(9.71 + 20) / 3 = 47.85 \text{ lb}$$

The program *shake.m* was run with three values for the counterbalance force. The first value was the given value (47.85 lb), the second value was no counterbalance force, and the third value was the optimum value (45.87 lb) determined by the program. The corresponding maximum shaking force values are given in Table 15.1. The program also plots the corresponding shaking force for each of the values of the counterbalance force. These are shown in Fig. 15.13. Notice that the shaking force can be reduced by almost 70% by the addition of the simple counterbalance weights.

**TABLE 15.1 Summary of Shaking Force Values for Example 15.5**

Counterbalance weight (lb)	Maximum shaking force (lb)	Crank angle
0	7527.4	0°
47.85	2495.4	98.18°
45.87	2313.7	258.18°



**FIGURE 15.13** Shaking force diagrams for Example 15.5. The top right diagram is for the given counterbalance weight. The bottom left diagram is for no counterbalance weight, and the bottom right diagram is for the optimum counterbalance weight.

## 15.6 BALANCING MULTICYLINDER MACHINES

The approximation of the connecting rod and crank pin masses used here is also routinely used when discussing multicylinder engine balancing. Because of these approximations and manufacturing variations, even a perfectly balanced multicylinder engine, pump, or compressor will generate some residual vibration. For this reason, vibration-isolating mounts are always necessary. In many situations it is necessary to trade off the complexity involved in achieving a higher level of balance against using a simpler scheme and relying on vibration mounts to further reduce the remaining vibration.

Balance is not the only constraint when selecting an automotive engine configuration. The firing sequence of the cylinders must be even, and engine designers try to optimize the firing sequence to minimize the elastic windup of the crankshaft. Two-stroke and diesel engines, which fire every piston stroke, require different crankshaft geometries and balance arrangements from four-stroke engines that fire every second piston stroke.

In multicylinder engines and compressors, the weight of the crankshaft and the part of the weight of the connecting rod that is concentrated at the crank pin can be counterbalanced exactly using the procedures discussed earlier. Therefore, only the balancing of the reciprocating weights will be considered here.

If we have  $n$  cylinders, the inertial force associated with each piston is in the direction of the piston travel and is given by

$$f_{B_i} = \bar{m}_{B_i} R_i \omega^2 \left[ \cos(\theta + \phi_i - \psi_i) + \frac{R_i}{L_i} \cos 2(\theta + \phi_i - \psi_i) \right], \quad i = 1, 2, \dots, n \quad (15.30)$$

where  $\bar{m}_{B_i}$ ,  $R_i$ ,  $L_i$ , and  $\psi_i$ , are the reciprocating mass, the crank radius, the connecting rod length, and the phase angle, respectively, for the  $i$ th cylinder. The angle  $\theta$  gives the position of the piston axis for cylinder 1 relative to the  $x$  axis, and each cylinder axis is oriented at an angle of  $\psi_i$  relative to the axis of cylinder 1. If the first crank starts in the direction of the  $x$  axis, the angle  $\theta$  is equal to the crank angular velocity multiplied by the time. In most engines and compressors,  $\bar{m}_{B_i}$ ,  $R_i$ , and  $L_i$ , will be the same for all cylinders. Therefore, the subscript  $i$  must be maintained for the angles  $\phi_i$  and  $\psi_i$  only. The phase angle  $\phi_i$  gives the angle from crank 1 to crank  $i$  as shown in Fig. 15.14. Both  $\phi_1 = 0$  and  $\psi_1 = 0$ , although both angles are usually included in the equations for symmetry.

The total shaking force will be the vector sum of the forces from all of the cylinders. For the analysis, the coordinate axes will be oriented as shown in Fig. 15.14. The  $z$  axis is along the rotation axis of the crankshaft, the  $x$  axis is in the direction of the piston travel of the first cylinder, and the  $y$  axis is defined such that a right-handed coordinate system results. Then, the  $x$  component of the shaking force from the  $i$ th cylinder is

$$f_{B_{x_i}} = f_{B_i} \cos \psi_i = \bar{m}_{B_i} R \omega^2 \left[ \cos(\theta + \phi_i - \psi_i) + \frac{R}{L} \cos 2(\theta + \phi_i - \psi_i) \right] \cos \psi_i \quad (15.31)$$

and the  $y$  component is

$$f_{B_{y_i}} = f_{B_i} \sin \psi_i = \bar{m}_{B_i} R \omega^2 \left[ \cos(\theta + \phi_i - \psi_i) + \frac{R}{L} \cos 2(\theta + \phi_i - \psi_i) \right] \sin \psi_i \quad (15.32)$$

The total inertial force vector due to the reciprocating masses is given by summing the vector contribution from each cylinder. It is convenient to sum the  $x$  and  $y$  components separately when doing this. The result is

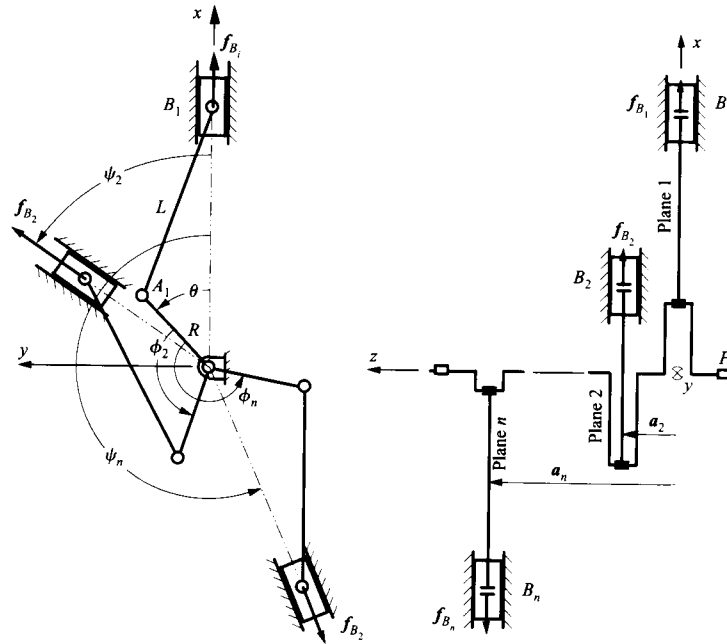


FIGURE 15.14 Schematic diagram of shaking forces in a multicylinder engine.

$$f_x = \bar{m}_B R \omega^2 \left[ \sum_{i=1}^n \cos(\theta + \phi_i - \psi_i) \cos \psi_i + \frac{R}{L} \sum_{i=1}^n \cos 2(\theta + \phi_i - \psi_i) \cos \psi_i \right] \quad (15.33)$$

and

$$f_y = \bar{m}_B R \omega^2 \left[ \sum_{i=1}^n \cos(\theta + \phi_i - \psi_i) \sin \psi_i + \frac{R}{L} \sum_{i=1}^n \cos 2(\theta + \phi_i - \psi_i) \sin \psi_i \right] \quad (15.34)$$

Equations (15.33) and (15.34) can be simplified using the following trigonometric identities:

$$\cos(\theta + \phi_i - \psi_i) = \cos \theta \cos(\phi_i - \psi_i) - \sin \theta \sin(\phi_i - \psi_i) \quad (15.35)$$

and

Then

$$\begin{aligned}
 f_x &= \bar{m}_B R \omega^2 \left[ \sum_{i=1}^n \cos(\theta + \phi_i - \psi_i) \cos \psi_i + \frac{R}{L} \sum_{i=1}^n \cos 2(\theta + \phi_i - \psi_i) \cos \psi_i \right] \\
 &= \bar{m}_B R \omega^2 \left[ \cos \theta \sum_{i=1}^n \cos(\phi_i - \psi_i) \cos \psi_i - \sin \theta \sum_{i=1}^n \sin(\phi_i - \psi_i) \cos \psi_i \right. \\
 &\quad \left. + \frac{R}{L} \cos 2\theta \sum_{i=1}^n \cos 2(\phi_i - \psi_i) \cos \psi_i - \frac{R}{L} \sin 2\theta \sum_{i=1}^n \sin 2(\phi_i - \psi_i) \cos \psi_i \right] \quad (15.37)
 \end{aligned}$$

and

$$\begin{aligned}
 f_y &= \bar{m}_B R \omega^2 \left[ \sum_{i=1}^n \cos(\theta + \phi_i - \psi_i) \sin \psi_i + \frac{R}{L} \sum_{i=1}^n \cos 2(\theta + \phi_i - \psi_i) \sin \psi_i \right] \\
 &= \bar{m}_B R \omega^2 \left[ \cos \theta \sum_{i=1}^n \cos(\phi_i - \psi_i) \sin \psi_i - \sin \theta \sum_{i=1}^n \sin(\phi_i - \psi_i) \sin \psi_i \right. \\
 &\quad \left. + \frac{R}{L} \cos 2\theta \sum_{i=1}^n \cos 2(\phi_i - \psi_i) \sin \psi_i - \frac{R}{L} \sin 2\theta \sum_{i=1}^n \sin 2(\phi_i - \psi_i) \sin \psi_i \right] \quad (15.38)
 \end{aligned}$$

To balance the forces, it is necessary for  $f_x$  and  $f_y$  to be zero. This can be achieved by making the resultant of the terms on the right-hand side of Eqs. (15.37) and (15.38) equal to zero. This occurs for all values of  $\theta$  when

$$\sum_{i=1}^n \cos(\phi_i - \psi_i) \cos \psi_i = 0 \quad (15.39)$$

$$\sum_{i=1}^n \cos(\phi_i - \psi_i) \sin \psi_i = 0 \quad (15.40)$$

$$\sum_{i=1}^n \sin(\phi_i - \psi_i) \sin \psi_i = 0 \quad (15.41)$$

$$\sum_{i=1}^n \sin(\phi_i - \psi_i) \cos \psi_i = 0 \quad (15.42)$$

$$\sum_{i=1}^n \cos 2(\phi_i - \psi_i) \cos \psi_i = 0 \quad (15.43)$$

$$\sum_{i=1}^n \cos 2(\phi_i - \psi_i) \sin \psi_i = 0 \quad (15.44)$$

$$\sum_{i=1}^n \sin 2(\phi_i - \psi_i) \sin \psi_i = 0 \quad (15.45)$$

and

$$\sum_{i=1}^n \sin 2(\phi_i - \psi_i) \cos \psi_i = 0 \quad (15.46)$$

Equations (15.39)–(15.42) are necessary to balance the primary shaking forces, and Eqs. (15.43)–(15.46) are necessary to balance the secondary shaking forces. In some crank

arrangements, it will be possible to satisfy all eight equations. In other cases, it may be possible to satisfy either Eqs. (15.39)–(15.42) or Eqs. (15.43)–(15.46). If there is a choice, it is generally more important to balance the primary shaking forces rather than the secondary shaking forces because the factor  $(R/L)$  will always be less than 1, making the primary shaking forces larger than the secondary shaking forces.

In most cases, the cylinders will be offset along the  $z$  axis. Therefore, the individual shaking forces will not be in a single plane, and there is a possibility of a shaking moment. The components of the shaking moment can be determined by summing moments about the  $x$  and  $y$  axes, which are in the plane of cylinder 1. This will give two components of the shaking moment. If  $a_i$  is the distance from the plane of cylinder 1 to the plane of cylinder  $i$  ( $a_i = 0$ ), the  $x$  component of the moment is given by

$$\begin{aligned}
 M_x = & - \sum_{i=1}^n f_{B_{y_i}} a_i = \\
 & \bar{m}_B R \omega^2 \left[ \cos \theta \sum_{i=1}^n a_i \cos(\phi_i - \psi_i) \sin \psi_i - \sin \theta \sum_{i=1}^n a_i \sin(\phi_i - \psi_i) \sin \psi_i \right. \\
 & \left. + \frac{R}{L} \cos 2\theta \sum_{i=1}^n a_i \cos 2(\phi_i - \psi_i) \sin \psi_i - \frac{R}{L} \sin 2\theta \sum_{i=1}^n a_i \sin 2(\phi_i - \psi_i) \sin \psi_i \right] \quad (15.47)
 \end{aligned}$$

and the  $y$  component is given by

$$\begin{aligned}
 M_y = & - \sum_{i=1}^n f_{B_{x_i}} a_i = \\
 & \bar{m}_B R \omega^2 \left[ \cos \theta \sum_{i=1}^n a_i \cos(\phi_i - \psi_i) \cos \psi_i - \sin \theta \sum_{i=1}^n a_i \sin(\phi_i - \psi_i) \cos \psi_i \right. \\
 & \left. + \frac{R}{L} \cos 2\theta \sum_{i=1}^n a_i \cos 2(\phi_i - \psi_i) \cos \psi_i - \frac{R}{L} \sin 2\theta \sum_{i=1}^n a_i \sin 2(\phi_i - \psi_i) \cos \psi_i \right] \quad (15.48)
 \end{aligned}$$

For dynamic balance, it is important to balance both the shaking force and the shaking moment. Both will cause undesirable vibrations at the engine base. To balance the shaking moment, we want the moment components in Eqs. (15.47) and (15.48) to be zero. This occurs when

$$\sum_{i=1}^n a_i \cos(\phi_i - \psi_i) \cos \psi_i = 0 \quad (15.49)$$

$$\sum_{i=1}^n a_i \cos(\phi_i - \psi_i) \sin \psi_i = 0 \quad (15.50)$$

$$\sum_{i=1}^n a_i \sin(\phi_i - \psi_i) \sin \psi_i = 0 \quad (15.51)$$

$$\sum_{i=1}^n a_i \sin(\phi_i - \psi_i) \cos \psi_i = 0 \quad (15.52)$$

$$\sum_{i=1}^n a_i \cos 2(\phi_i - \psi_i) \cos \psi_i = 0 \quad (15.53)$$



$$\sum_{i=1}^n a_i \cos 2(\phi_i - \psi_i) \sin \psi_i = 0 \quad (15.54)$$

$$\sum_{i=1}^n a_i \sin 2(\phi_i - \psi_i) \sin \psi_i = 0 \quad (15.55)$$

and

$$\sum_{i=1}^n a_i \sin 2(\phi_i - \psi_i) \cos \psi_i = 0 \quad (15.56)$$

As in the case of the shaking force, Eqs. (15.49)–(15.52) are necessary to balance the primary shaking moments, and Eqs. (15.53)–(15.56) are necessary to balance the secondary shaking moments.

Notice that it may be possible to reduce the shaking forces using counterweights even though Eqs. (15.39)–(15.46) and (15.49)–(15.56) are not satisfied. However, it is much more efficient if the shaking forces can be internally balanced by a careful design of the crank phase angles. Even in cases in which it is not possible to balance the shaking forces perfectly by satisfying all of the equations directly, if the equations are satisfied approximately, the shaking forces and moments will be reduced, and the sizes of any additional counterbalance weights will also be reduced.

To illustrate the use of the equations, we will investigate two examples. For a more extensive consideration of the topic, the reader is referred to the work by Holowenko.<sup>1</sup>

### 15.6.1 Balancing a Three-Cylinder In-Line Engine

Three-cylinder in-line engines are commonly used in small utility tractors. An example of this cylinder arrangement is shown in Fig. 15.15. Notice that  $\psi_i$  is zero for each cylinder, and the crank phase angles are distributed symmetrically about the crankshaft axis. Because  $\psi_i = 0$ ,  $\sin \psi_i = 0$  and  $\cos \psi_i = 1$ . Therefore, Eqs. (15.40), (15.41), (15.44), and (15.45) and

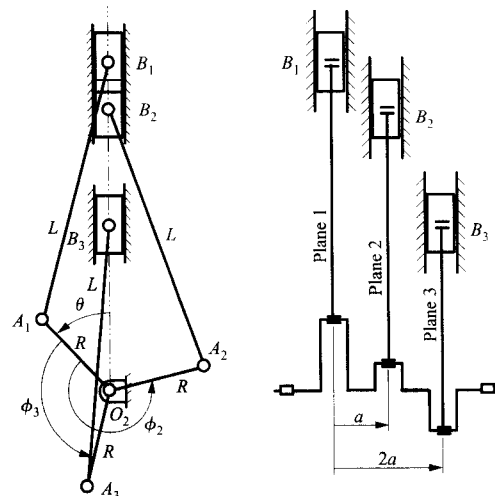


FIGURE 15.15 Schematic diagram of a three-cylinder in-line engine.

Eqs. (15.50), (15.51), (15.54), and (15.55) are satisfied identically. The left-hand sides of the remaining equations are given in the following:

$$\begin{aligned}\sum_{i=1}^3 \cos \phi_i &= 1 + \cos 240^\circ + \cos 120^\circ = 1 - \frac{1}{2} - \frac{1}{2} = 0 \\ \sum_{i=1}^3 \sin \phi_i &= 0 + \sin 240^\circ + \sin 120^\circ = 0 - \frac{\sqrt{3}}{2} + \frac{\sqrt{3}}{2} = 0 \\ \sum_{i=1}^3 \cos 2\phi_i &= 1 + \cos 480^\circ + \cos 240^\circ = 1 - \frac{1}{2} - \frac{1}{2} = 0 \\ \sum_{i=1}^3 \sin 2\phi_i &= 1 + \sin 480^\circ + \sin 240^\circ = 1 + \frac{\sqrt{3}}{2} - \frac{\sqrt{3}}{2} = 0 \\ \sum_{i=1}^3 a_i \cos \phi_i &= 0 + a \cos 240^\circ + 2a \cos 120^\circ = 0 - \frac{a}{2} - \frac{2a}{2} = -\frac{3a}{2} \\ \sum_{i=1}^3 a_i \sin \phi_i &= 0 + a \sin 240^\circ + 2a \sin 120^\circ = 0 - \frac{a\sqrt{3}}{2} + \frac{2a\sqrt{3}}{2} = \frac{a\sqrt{3}}{2} \\ \sum_{i=1}^3 a_i \cos 2\phi_i &= 0 + a \cos 480^\circ + 2a \cos 240^\circ = 0 - \frac{a}{2} - \frac{2a}{2} = -\frac{3a}{2} \\ \sum_{i=1}^3 a_i \sin 2\phi_i &= 0 + a \sin 480^\circ + 2a \sin 240^\circ = 0 + \frac{a\sqrt{3}}{2} - \frac{2a\sqrt{3}}{2} = -\frac{a\sqrt{3}}{2}\end{aligned}$$

In this engine, the shaking forces are balanced exactly, but the primary and secondary moments are not balanced. The moments form a shaking couple on the engine. The magnitude of the couple is given by Eq. (15.48) as

$$\begin{aligned}M &= \bar{m}_B R \omega^2 \left[ -\frac{3a}{2} \cos \theta - \frac{a\sqrt{3}}{2} \sin \theta - \frac{R}{L} \frac{3a}{2} \cos 2\theta + \frac{R}{L} \frac{a\sqrt{3}}{2} \sin 2\theta \right] \\ &= \frac{\bar{m}_B a R \omega^2}{2} \left[ -3 \cos \theta - \sqrt{3} \sin \theta - 3 \frac{R}{L} \cos 2\theta + \frac{R}{L} \sqrt{3} \sin 2\theta \right]\end{aligned}\quad (15.57)$$

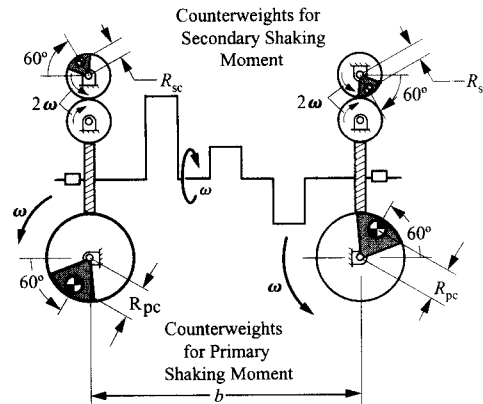
This equation can be simplified by the trigonometric relationship

$$p \cos \beta + q \sin \beta = \sqrt{p^2 + q^2} \sin(\beta + \gamma)\quad (15.58)$$

where  $\tan \gamma = p/q$ . Equation (15.57) can then be written as

$$M = \frac{\bar{m}_B a R \omega^2}{2} \left[ -2\sqrt{3} \sin(\theta + 60^\circ) - 2 \frac{R}{L} \sqrt{3} \sin(2\theta - 60^\circ) \right]\quad (15.59)$$

The first term is the primary shaking moment and the second term is the secondary shaking moment. The primary shaking moment can be balanced by counterweights that rotate at the engine speed but are out of phase with the first crank by positive  $60^\circ$ . The secondary shaking moment can be balanced by counterweights that rotate at two times the engine speed and are out of phase with the first crank by negative  $60^\circ$ . Figure 15.16 shows one balancing scheme for the shaking moments. The masses of the counterbalances for the primary and secondary moments are,<sup>1</sup> respectively,



**FIGURE 15.16** Arrangements to balance primary and secondary shaking moments. The counterbalance weights are shown for the position when  $\theta = 0$ .

speed and are out of phase with the first crank by negative  $60^\circ$ . Figure 15.16 shows one balancing scheme for the shaking moments. The masses of the counterbalances for the primary and secondary moments are,<sup>1</sup> respectively,

$$m_{\text{cb}_{\text{primary}}} = 2\sqrt{3}\bar{m}_B \frac{R}{R_{\text{pc}}} \frac{a}{b}$$

and

$$m_{\text{cb}_{\text{secondary}}} = \frac{3}{4}\bar{m}_B \frac{R}{R_{\text{sc}}} \frac{a}{b}$$

where  $R_{\text{pc}}$  is the radial location of the center of mass of the counterweights for the primary shaking moment,  $R_{\text{sc}}$  is the radial location of the center of mass of the counterweights for the secondary shaking moment, and  $b$  is the distance between the rotation axes of the counterweights. The counterweights for the primary shaking moment rotate at the same velocity as the crankshaft, and the counterweights for the secondary shaking moment rotate at twice the velocity of the crankshaft.

### 15.6.2 Balancing an Eight-Cylinder V Engine

Eight-cylinder V engines (V-8) are commonly used in high-performance automobiles. An example of this cylinder arrangement is shown in Fig. 15.17. The engine shown is assumed to have the cylinder banks oriented at  $90^\circ$  to each other. Cylinders 1 and 5, 2 and 6, 3 and 7, and 4 and 8 are symmetrically located relative to the vertical axis. Then  $\psi_i$  is  $90^\circ$  for cylinders 5, 6, 7, and 8 and  $0^\circ$  for cylinders 1, 2, 3, and 4. The phase angles are  $\phi_1 = \phi_5 = 0^\circ$ ,  $\phi_2 = \phi_6 = 90^\circ$ ,  $\phi_3 = \phi_7 = 270^\circ$ , and  $\phi_4 = \phi_8 = 180^\circ$ . Substitution of the known angles into Eqs. (15.39)–(15.46) and (15.53)–(15.56) show that the shaking-force equations and the secondary shaking moment equations are satisfied. However, the primary shaking moment equations are not satisfied. The left-hand sides of Eqs. (15.49)–(15.52) give

$$\sum_{i=1}^n a_i \cos(\phi_i - \psi_i) \cos \psi_i = -3a, \quad \sum_{i=1}^n a_i \cos(\phi_i - \psi_i) \sin \psi_i = -a$$

$$\sum_{i=1}^n a_i \sin(\phi_i - \psi_i) \sin \psi_i = 3a, \quad \sum_{i=1}^n a_i \sin(\phi_i - \psi_i) \sin \psi_i = -a$$

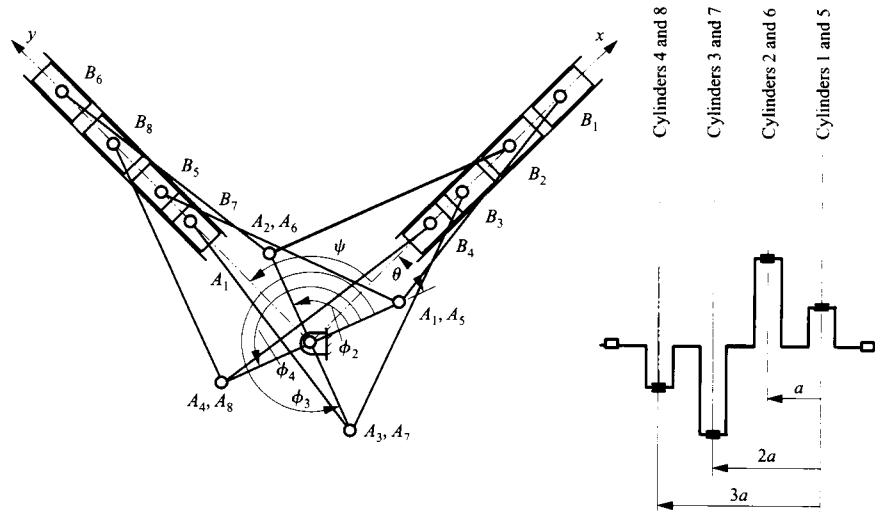


FIGURE 15.17 Eight-cylinder engine with 90° V.

The  $x$  component of the shaking moment is given by Eq. (15.47). Substitution of numbers into that equation gives

$$\begin{aligned}
 M_x = & -\bar{m}_B R \omega^2 \left[ \cos \theta \sum_{i=1}^n a_i \cos(\phi_i - \psi_i) \sin \psi_i - \sin \theta \sum_{i=1}^n a_i \sin(\phi_i - \psi_i) \sin \psi_i \right. \\
 & \left. + \frac{R}{L} \cos 2\theta \sum_{i=1}^n a_i \cos 2(\phi_i - \psi_i) \sin \psi_i - \frac{R}{L} \sin 2\theta \sum_{i=1}^n a_i \sin 2(\phi_i - \psi_i) \sin \psi_i \right] \\
 = & -\bar{m}_B R \omega^2 a [\cos \theta + 3 \sin \theta]
 \end{aligned}$$

or using Eq. (15.58) with the trigonometric identity  $\sin \theta = \cos(\theta - 90^\circ)$ , we have

$$M_x = \sqrt{10} \bar{m}_B R \omega^2 a \cos(\theta - 71.56^\circ) \tag{15.60}$$

The  $y$  component of the shaking force is given by Eq. (15.46). Substitution of numbers into that equation gives

$$\begin{aligned}
 M_x = & -\bar{m}_B R \omega^2 \left[ \cos \theta \sum_{i=1}^n a_i \cos(\phi_i - \psi_i) \cos \psi_i - \sin \theta \sum_{i=1}^n a_i \sin(\phi_i - \psi_i) \cos \psi_i \right. \\
 & \left. + \frac{R}{L} \cos 2\theta \sum_{i=1}^n a_i \cos 2(\phi_i - \psi_i) \cos \psi_i - \frac{R}{L} \sin 2\theta \sum_{i=1}^n a_i \sin 2(\phi_i - \psi_i) \cos \psi_i \right] \\
 = & -\bar{m}_B R \omega^2 a [-3 \cos \theta + \sin \theta]
 \end{aligned}$$

or using Eq. (15.58), we get

$$M_y = \sqrt{10} \bar{m}_B R \omega^2 a \sin(\theta - 71.56^\circ)$$

The  $x$  and  $y$  components of the shaking moment can be combined vectorially to form the vector

$$M = \sqrt{10\bar{m}_B}R\omega^2 a[\cos(\theta - 71.56^\circ)\mathbf{i} + \sin(\theta - 71.56^\circ)\mathbf{j}]$$

Therefore, the shaking moment is of constant magnitude and can be balanced by the couple formed by rotating counterweights. The magnitude of the couple must be equal to  $\sqrt{10\bar{m}_B}R\omega^2 a$ . A possible counterbalance arrangement for the crankshaft position corresponding to  $\theta = 0$  is given in Fig. 15.18.

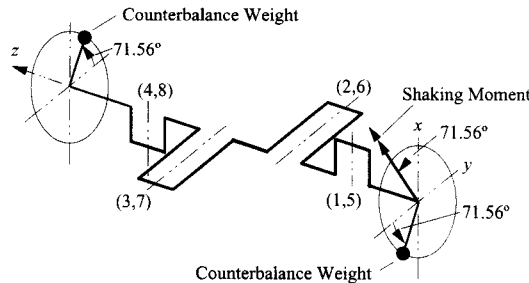


FIGURE 15.18 Rotating counterweights used to balance shaking forces in an eight-cylinder V engine.

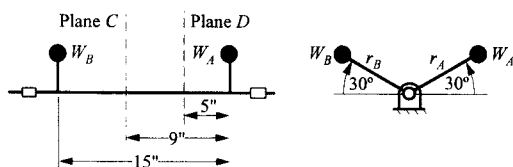
## REFERENCES

<sup>1</sup>Holowenko, A. R., *Dynamics of Machinery*, John Wiley & Sons, New York (1955).

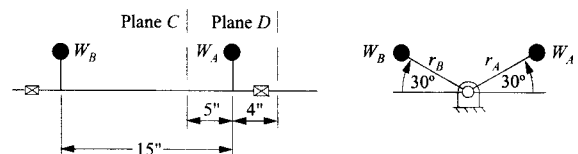
## PROBLEMS

### EXERCISE PROBLEMS ON ROTARY BALANCE

15.1 The figure shows a system with two weights,  $W_A$  and  $W_B$ , that have been found to balance a system of weights (not shown) on the shaft. The weights for  $W_A$  and  $W_B$  are 4 and 8 lb, respectively, and the radii,  $r_A$  and  $r_B$ , are both 6 in. Later, it is decided to replace  $W_A$  and  $W_B$  by weights  $W_C$  and  $W_D$ , where the planes for the two weights are as shown. What are the magnitudes and angular locations of  $W_C$  and  $W_D$  if the radius of the center of gravity for both links is 5 in?

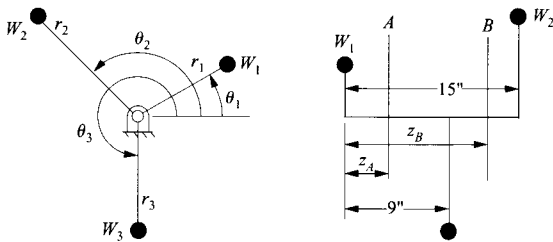


15.2 The figure shows a system with two weights,  $W_A$  and  $W_B$ , that have been found to balance a system of weights (not shown) on the shaft. The weights for  $W_A$  and  $W_B$  are 6 and 8 lb, respectively, and the radii,  $r_A$  and  $r_B$ , are both 5 in. It is decided to replace  $W_A$  and  $W_B$  by weights  $W_C$  and  $W_D$ , where the planes for the two weights are as shown. What are the magnitudes and angular locations of  $W_C$  and  $W_D$  if the radius of the center of gravity for both links is 6 in?



**15.3** Three rotating weights  $W_1$ ,  $W_2$ , and  $W_3$  are to be balanced by two weights  $W_A$  and  $W_B$  in planes  $A$  and  $B$ . Determine the magnitude and angular locations of the counterbalance weights necessary to balance the rotating weights. Use the following values:

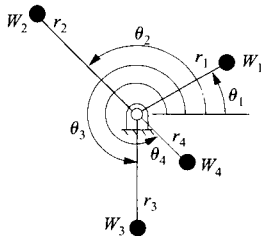
- $W_1 = 12 \text{ lb}$ ,  $r_1 = 2.5 \text{ in}$ ,  $\theta_1 = 30^\circ$ ,  $z_A = 4 \text{ in}$
- $W_2 = 9 \text{ lb}$ ,  $r_2 = 2.5 \text{ in}$ ,  $\theta_2 = 150^\circ$ ,  $z_B = 14 \text{ in}$
- $W_3 = 8 \text{ lb}$ ,  $r_3 = 2.5 \text{ in}$ ,  $\theta_3 = 270^\circ$
- $r_A = 2.5 \text{ in}$
- $r_B = 2.5 \text{ in}$



**15.4** Re-solve Problem 15.3 if  $z_A$  and  $z_B$  are 4.5 in and 12 in, respectively.

**15.5** Four weights,  $W_1$ ,  $W_2$ ,  $W_3$ , and  $W_4$ , are all rotating in a single plane. Determine the magnitude and angular location of the single weight necessary to balance the four rotating weights. Assume that the radius to the center of gravity of the balancing weight is 9 in. The shaft is rotating at 1800 rpm. Use the following values:

- $W_1 = 12 \text{ lb}$ ,  $r_1 = 9 \text{ in}$ ,  $\theta_1 = 30^\circ$
- $W_2 = 9 \text{ lb}$ ,  $r_2 = 12 \text{ in}$ ,  $\theta_2 = 135^\circ$
- $W_3 = 8 \text{ lb}$ ,  $r_3 = 10 \text{ in}$ ,  $\theta_3 = 270^\circ$
- $W_4 = 5 \text{ lb}$ ,  $r_4 = 8 \text{ in}$ ,  $\theta_4 = 315^\circ$

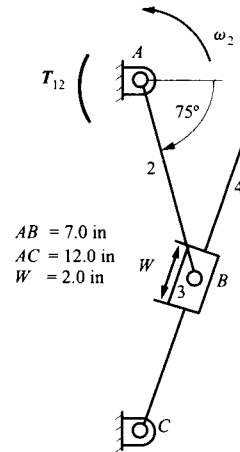


**15.6** Re-solve Problem 15.5 for the following set of data:

- $W_1 = 20 \text{ lb}$ ,  $r_1 = 4 \text{ in}$ ,  $\theta_1 = 45^\circ$
- $W_2 = 10 \text{ lb}$ ,  $r_2 = 12 \text{ in}$ ,  $\theta_2 = 135^\circ$
- $W_3 = 8 \text{ lb}$ ,  $r_3 = 12 \text{ in}$ ,  $\theta_3 = 180^\circ$
- $W_4 = 6 \text{ lb}$ ,  $r_4 = 10 \text{ in}$ ,  $\theta_4 = 270^\circ$

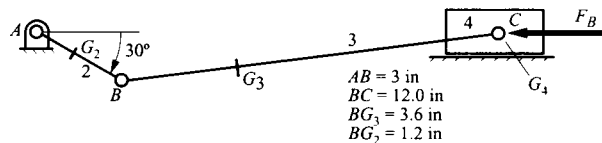
**PROBLEMS INVOLVING SHAKING FORCES**

**15.7** For the mechanism shown, determine the magnitude and location of the shaking force acting on the frame. Determine the location with respect to point  $A$ . Also find the magnitude of the reaction forces at point  $A$  and at point  $C$ . Assume that  $W_3 \gg W_2$  and  $W_4$ . Use  $W_3 = 2.0 \text{ lb}$ ,  $I_3 = 0.1 \text{ lb}\cdot\text{s}^2\text{-in}$ , and  $\omega_2 = 6.28 \text{ rad/s}$  CCW (constant).



**15.8** For the mechanism and data given, determine the shaking force and its location relative to point  $A$ . Draw the shaking force vector on the figure. The force  $F_B$  is 10 lb in the direction shown. For the moments of inertia of link 3, use  $g = 386 \text{ in/s}^2$  and  $I_G = m\ell^2/12$ .

- $\omega_2 = 160 \text{ rad/s}$  CCW,  $\alpha_2 = 0 \text{ rad/s}^2$ ,  $W_2 = 0.95 \text{ lb}$
- $I_{G_2} = 0.00369 \text{ lb}\cdot\text{s}^2\text{-in}$ ,  $W_3 = 3.5 \text{ lb}$ ,  $W_4 = 2.5 \text{ lb}$

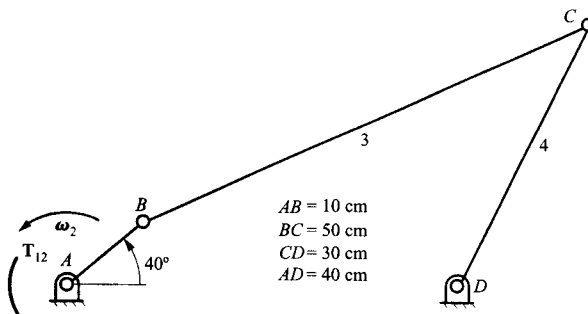


**15.9** For the mechanism shown, determine the magnitude and location of the shaking force acting on the frame. Determine the location with respect to point *A*. Draw the shaking force vector on the figure. Use the following values:

$$\omega_2 = 12 \text{ rad/s CCW}, \quad \alpha_2 = 0$$

$$W_2 = 0.5 \text{ N}, \quad W_3 = 2.5 \text{ N}, \quad W_4 = 1.5 \text{ N}$$

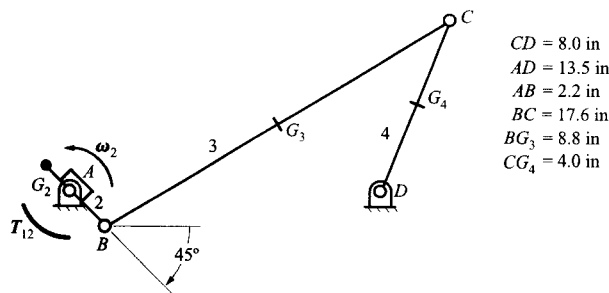
For the moments of inertia for the links, use  $g = 9.81 \text{ m/s}^2$  and  $I_G = m\ell^2/12$ .



**15.10** For the mechanism given, assume that  $\omega_2$  is 200 rad/s CCW (constant) and that link 2 is balanced so that its center of mass is located at the pivot at point *A*. Also assume that  $I_{G_2}$  is small enough to be neglected. For the data given, determine the shaking force and its location relative to point *A*. Draw the shaking force vector on the figure.

$$I_{G_3} = 0.0106 \text{ lb-s}^2\text{-in}, \quad W_3 = 2.65 \text{ lb}$$

$$I_{G_4} = 0.0531 \text{ lb-s}^2\text{-in}, \quad W_4 = 6.72 \text{ lb}$$



**15.11** A single-cylinder engine is mounted so that the crankshaft is horizontal as shown in Fig. 15.12. The engine is characterized by the following data:

Rotational speed 1200 rpm

Stroke 6 in

Length of connecting rod 12 in

Distance from crank pin to 4 in

center of gravity of connecting rod

Equivalent unbalanced 6 lb

weight of crank at a 3-in radius

Weight of piston 7 lb

Weight of connecting rod 15 lb

Determine the magnitude of the shaking force when the crank angle is 120° if there is no counterbalance weight. Then determine the shaking force at the crank location if a counterbalancing weight is added that is equal to  $\bar{m}_{cb} = \bar{m}_A + 2\bar{m}_B/3$ .

**15.12** Re-solve Problem 15.11 if the stroke is 4 in, the engine speed is 1800 rpm, and the equivalent unbalanced weight of the crank at a 2-in radius is 5 lb.

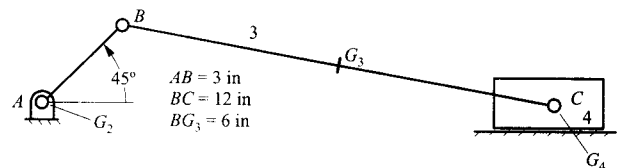
**15.13** For the mechanism and data given, determine the shaking force and its location relative to point *A*. The engine is mounted horizontal. Draw the shaking force vector on the figure.

$$\omega_2 = 210 \text{ rad/s CCW}, \quad \alpha_2 = \text{rad/s}^2 \text{ CCW}, \quad W_2 = 3.40 \text{ lb}$$

$$I_{G_3} = 0.1085 \text{ lb-s}^2\text{-in}, \quad W_3 = 3.40 \text{ lb}, \quad W_4 = 2.85 \text{ lb}$$

**EXERCISE PROBLEMS INVOLVING RECIPROCATING BALANCE**

**15.14** For the engine given in Problem 15.11, lump the weight of the connecting rod at the crank pin and piston pin and draw the polar shaking force diagram for the following three cases:



(a) No counterbalancing weights.

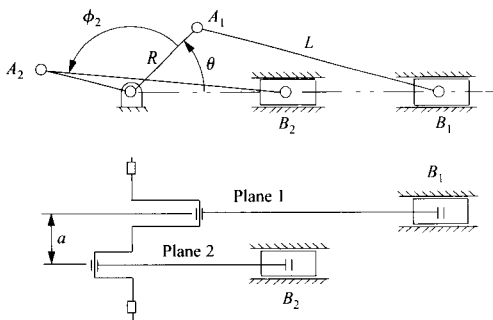
(b) A counterbalancing weight equal to the sum of the crank weight at the crank radius, the part of the connecting rod weight assumed to be concentrated at the crank pin, the weight of the piston, and the part of the connecting rod weight concentrated at the piston pin.

(c) A counterbalancing weight equal to the sum of the crank weight at the crank radius, the part of the connecting rod weight assumed to be concentrated at the crank pin, and half of the weight concentrated at the piston pin (weight of the piston and part of the connecting rod weight concentrated at the piston pin).

**15.15** For the engine given in Problem 15.11, lump the weight of the connecting rod at the crank pin and piston pin and locate the counterbalancing weight at the crank radius. Determine the optimum counter balancing weight which will give

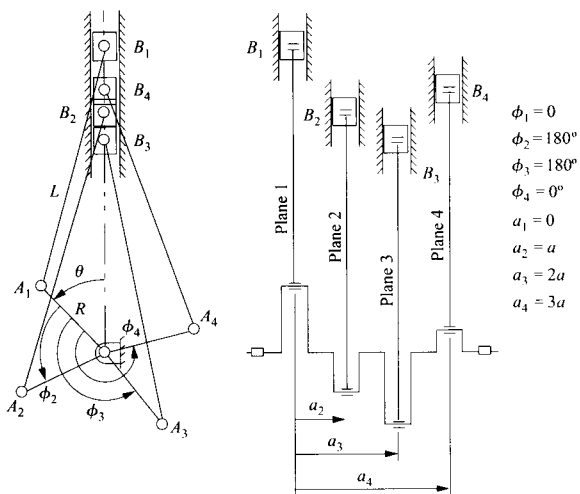
- (a) the smallest horizontal shaking force,
- (b) the smallest vertical shaking force.

**15.16** The two-cylinder engine shown has identical cranks, connecting rods, and pistons. The rotary masses are perfectly balanced. Derive an expression for the shaking forces and shaking moments using the symbols indicated if  $\phi_2 = 90^\circ$ . Are the primary or secondary shaking forces balanced? What about the primary and secondary shaking moments?



**15.17** Re-solve Problem 15.16 when  $\phi_2 = 180^\circ$ .

**15.18** The four-cylinder engine shown has identical cranks, connecting rods, and pistons. The rotary masses are perfectly balanced. Derive an expression for the shaking forces and shaking moments for the angles and offset values indicated. Are the primary or secondary shaking forces balanced? What about the primary and secondary shaking moments?



**15.19** Re-solve Problem 15.18 for the following values for the phase angles and offset distances:

$$\phi_1 = 0^\circ, \phi_2 = 90^\circ, \phi_3 = 270^\circ, \phi_4 = 180^\circ$$

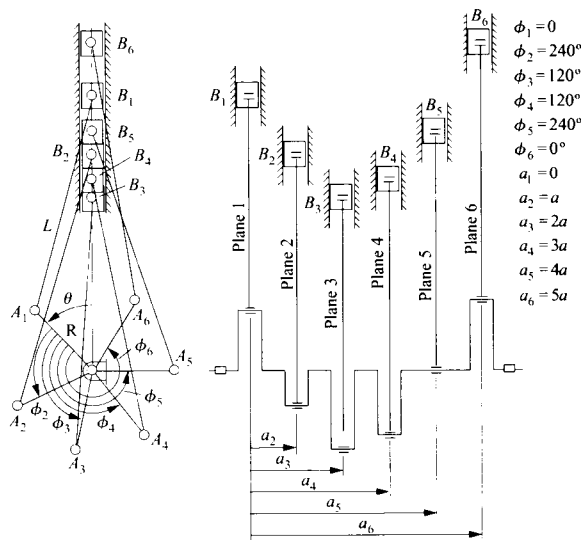
$$a_1 = 0, \quad a_2 = a, \quad a_3 = 2a, \quad a_4 = 3a$$

**15.20** Re-solve Problem 15.18 for the following values for the phase angles and offset distances:

$$\phi_1 = 0^\circ, \phi_2 = 180^\circ, \phi_3 = 90^\circ, \phi_4 = 270^\circ$$

$$a_1 = 0, \quad a_2 = a, \quad a_3 = 2a, \quad a_4 = 3a$$

**15.21** The six-cylinder engine shown has identical cranks, connecting rods, and pistons. The rotary masses are perfectly balanced. Derive an expression for the shaking forces and shaking moments for the angles and offset values indicated. Are the primary or secondary shaking forces balanced? What about the primary and secondary shaking moments?



**15.22** Re-solve Problem 15.21 for the following values for the phase angles and offset distances:

$$\phi_1 = 0^\circ, \quad \phi_2 = 120^\circ, \quad \phi_3 = 240^\circ,$$

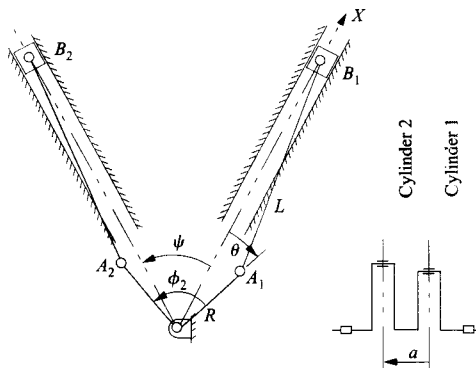
$$\phi_4 = 60^\circ, \quad \phi_5 = 300^\circ, \quad \phi_6 = 180^\circ$$

$$a_1 = 0, \quad a_2 = a, \quad a_3 = 2a,$$

$$a_4 = 3a, \quad a_5 = 4a, \quad a_6 = 5a$$

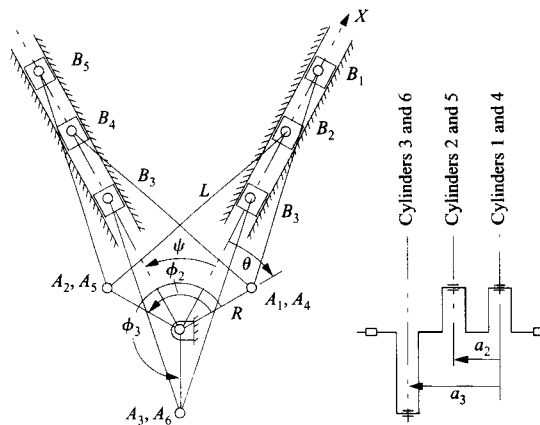


**15.23** The two-cylinder V engine shown has identical cranks, connecting rods, and pistons. The rotary masses are perfectly balanced. Derive an expression for the shaking forces and shaking moments for the angles and offset values indicated. The V angle is  $\psi = 60^\circ$ , and the phase angle is  $\phi_2 = 90^\circ$ . Are the primary or secondary shaking forces balanced? What about the primary and secondary shaking moments?



**15.24** Re-solve Problem 15.23 if  $\psi = 180^\circ$  and  $\phi_2 = 180^\circ$ .

**15.25** The six-cylinder V engine shown has identical cranks, connecting rods, and pistons. The rotary masses are perfectly balanced. Derive an expression for the shaking forces and shaking moments for the angles and offset values indicated. The V angle is  $\psi = 60^\circ$ , and the phase angles  $\phi_1$ ,  $\phi_2$ , and  $\phi_3$  are  $0^\circ$ ,  $120^\circ$ , and  $240^\circ$ , respectively. Are the primary or secondary shaking forces balanced? What about the primary and secondary shaking moments?



# INDEX

*Italicized page numbers reflect pages on which photographs appear.*

## A

- Acceleration, 2, 3
  - chain rule for, 102
  - Coriolis component of, *see* Coriolis term of coupler point, 186–187
  - in elliptic trammel mechanism, 224–228
  - equivalent linkages, 124–128
  - in four-bar linkages, 180–182
  - general coincident points, analysis using, 130–136
  - graphical analysis of, 31, 65–67, 79–84, 89–95, 96–144
  - higher pairs, mechanisms with, 244–248
  - in Oldham mechanism, 229–233
  - in planar linkage analysis, 174–175
  - points *P* and *Q* fixed to *B*, 104–105
  - quick-return mechanism, 107–111
  - of rigid body, 184–187
  - rolling contacts, 111–120
  - in RPRP mechanism, 216–218
  - in RRPP mechanism, 219–223
  - in slider-crank mechanism, 195–200, 207–211
  - in spatial mechanisms, 422–423, 426–428
  - special-case equations for, 104–106
- Acceleration image theorem, 79–84, 94–95
- Ackermann geometry, 349–350
- Actuation, 32–37, 48–53
- Actuators, 2
  - commutated motors, 50–51
  - controlled/servomotors, 52
  - definition, 48
  - electrical, 49–52
  - hydraulic, 53
  - noncommutated motors, 51–52
  - operational stability, 48–49
  - pneumatic, 53
  - solenoids, 52
  - speed control, 52
- Adaptive Suspension Vehicle, *I*, 335
- Addendum, 464–466
- Addendum circle, 464–465
- AGMA, 520, 524
- Air motors, 53
- Analysis techniques, 2
- Angular acceleration
  - chain rule for, 103–104
  - quick-return mechanism, 107–111

- rigid body, 185
- rolling contacts, 116–120
- velocity image theorem, 77
- Angular bevel gears, 521, 524, 524
- Angular velocity, 2, 61, 64
  - chain rule for, 102–103
  - friction drives, 459
  - general equations for, 99–100
  - and instant centers of velocity, 145, 163
  - inversion analysis of, 86–88
  - quick-return mechanism, 107–108
  - reference frames, 97
  - rigid body, 185
  - rolling contacts, 112, 118–120
  - slider-crank inversion, 209
  - velocity image theorem, 76–77
- Animation, 10
- Annular gears, 474–475
- Approximate straight-line mechanisms, 329–331, 332
  - Chebyshev straight-line mechanisms, 330, 331
  - Roberts straight-line mechanism, 330–331
  - Watt straight-line mechanism, 330
- Armature, 49
- Aronholdt. *See* Kennedy-Aronholdt theorem
- Assembly configurations, 270–271
- Automotive applications
  - acceleration/braking, dynamic force analysis of, 610–613
  - balancing of eight-cylinder V engine, 655–657
  - steering mechanisms, 349–353, 360–361
  - suspension mechanisms, 329, 349, 353–354
  - universal joints, 345–347
- Axial joints, 432–435. *See also* Cylindrical joints; Prismatic joints; Revolute joints
- Axial pitch, 497, 499, 504–505, 510, 514–516, 528–529
- Axodes, 151

## B

- Backhoe, 200
- Balancing, 629–661
  - exercises, 657–661
  - and expressions for inertial forces, 646–648
  - of multicylinder machines, 649–657
  - multiplane (dynamic), 633–639

- of reciprocating masses, 639–648, 659–661
  - single-plane (static), 630–633
  - Base pitch, 464–465
  - Bearings
    - ball bushings, 47
    - hydrodynamic, 44
    - hydrostatic, 44–45
    - lubrication of, 47
    - rolling-element bearings, 7, 45
    - solid contact bearings, 45
  - Bennett mechanism, 26–28
  - Bernoulli, Johann, 145
  - Bevel gears, 111, 517–527, 518
    - angular, 521, 524, 524
    - crown, 521–522, 522
    - exercises, 529
    - face gears, 522, 523
    - formulas for, 525
    - hypoid gears, 526–527, 527
    - loads with, 602–603
    - miter gears, 521, 523
    - nomenclature, 520–521
    - planetary gear trains with, 549–550
    - spiral, 525–526, 526
    - Tredgold's approximation for, 519–520
    - Zerol, 524
  - Binary links, 7–9
  - Blank fabrication, 475–476
  - Braking, dynamic force analysis of, 610–613
  - Branch, change of, 270–272
  - Brushes, motor, 50
  - Brushless direct current (DC) motor, 50
  - Bucket support linkages, 28–29
- ## C
- Cams, 9
    - contacts, *see* Cam contacts
    - design, *see* Cam design
    - graphical force analysis of, 571–573
    - harmonic, 373–375
    - linkages vs., 47–48, 362
    - lubrication of cam and follower pairs, 47
    - radius of curvature for, 393–395, 397
  - Cam contacts
    - analysis of mechanism with, 244–246
    - friction in, 579
    - graphical analysis of, 96, 111, 118–128, 141–142
    - instant centers of velocity of general cam-pair contact, 149–150

- Cam design, 362–420  
 cam-follower systems, 363–364  
 exercises, 417–420  
 follower-displacement functions, 366–380, 417–418  
 profile, *see* Profile cam design  
 synthesis of motion programs, use of, 364–366  
 and types of motion, 366
- Cardan joints. *See* Universal joints
- Center of mass, 608
- Centroides, 150–152, 152
- Chain rule, 101–104
- Chebyshev approximate straight-line mechanism, 330, 331
- Chebyshev linkage, 339–340
- Chebyshev polynomial, use for precision points of, 288–289
- Circle method, to find instant center, 155–156
- Circular pitch, 464–465
- Closed chains, 8
- Closed circuits, 8
- Closed-loop linkages  
 planar linkage analysis, 175–184  
 spatial linkage analysis, 445–448
- Closures, constraint, 19–21, 29
- CNC milling machines, 475, 487
- Cognate linkages, 318–320  
 of Chebyshev mechanism, 339–340  
 exercises, 327–328, 360  
 and pantographs, 333, 337–340
- Coincident points, general. *See* General coincident points
- Commutated motors, 50–51
- Complex number notation, 171, 248–251
- Compound gear trains, 534, 534–540  
 concentric gear trains, 537–540, 538  
 exercises, 554–556  
 velocity ratio for, 534–536
- Compound joints, 5–6
- Compound mechanisms  
 closure/loop equation approach for, 233–243  
 lubrication, 47  
 rotating-radius method to find velocity, 158–159
- Compound wound motor, 51
- Computer-aided design, 2, 10–11, 171, 258–259. *See also* MATLAB
- Concentric gear trains, 537–540, 538
- Connecting rods, balancing and, 639–641, 649
- Connectivity, 5–6, 11, 13, 23–24
- Conservation of energy, 590–597, 604–606, 615–618
- Conservation of momentum, 615–618
- Constant-velocity couplings, 347–349, 348
- Constant velocity ratio (spur gears), 458–461
- Constraint analysis, 11–23  
 and idle degrees of freedom, 23–25  
 and overconstrained linkages, 25–29  
 of spatial linkages, 18–23
- Contacts  
 cam, *see* Cam contacts  
 rolling, *see* Rolling contacts
- Contact ratio  
 parallel-shaft helical gears, 505–506  
 spur gears, 467–471
- Coordinate transformation operators, 171
- Coordination, problem of robotic, 428
- Coriolis term, 122  
 acceleration, component of, 96, 107, 109  
 position, function of, 131  
 velocities, function of, 101, 105, 127, 131, 132
- Couple  
 force and, 561  
 moment of, 560–561
- Coupler (definition), 32
- Coupler curves, 85  
 design of six-bar linkages using, 309–314  
 Hrones and Nelson coupler-curve atlas, 308  
 motion generation for parallel motion, 315–317
- Coupler-driven linkages, 37, 42–44
- Coupler point, velocity/acceleration analysis of, 186–187
- Cranks, 31–34. *See also* Slider-crank mechanisms  
 design, given circle or center points, 282  
 inversion, solution by, 84–85  
 synthesis of, with chosen fixed pivots, 266–268
- Crank-rocker linkages  
 actuation, 34, 36  
 centroides associated with instant center, 151  
 change of branch, 271  
 motion limits, 40  
 synthesis of, 294–308, 325–326  
 topological interference, 41–42
- Crossed helical gears, 498, 509–512
- Crown bevel gears, 521–522, 522
- Curvature  
 center of, 112–113, 114, 118, 122–125, 128–134, 136, 141–144, 148, 243–244, 246–248, 383, 387, 393–396, 404  
 radius of, 112, 116, 133, 148, 349, 351, 353, 363, 367, 381, 383, 393–395, 397–398, 402, 406, 408, 413, 415–416
- Cycloidal follower-displacement programs, 375–376
- Cycloidal tooth geometries, 461–462
- Cylindrical joints, 4, 5, 432
- D**
- D'Alembert's principle, 559, 619
- Dedendum, 464–466
- Dedendum circle, 464–465
- Degrees of freedom. *See also* Connectivity; Mobility  
 idle, 23–25  
 number of, 3, 5–6, 11, 13–15
- Design. *See also* Cam design; Planar linkage design; Profile cam design  
 analysis and synthesis, 2–3  
 historic perspective, 1–2  
 practical design considerations, 44–53
- Diametral pitch, 464–467
- Different mechanism, 17
- Differential gear train, 543, 543
- Digital control, actuator, 48
- Diophantine equation, 15, 18
- Direction of rotation (gear trains), 530–531
- Direct kinematics (serial chains), 428–438
- Double-cranks. *See* Drag-link mechanisms
- Double rocker linkages, 259–262, 321  
 analytical solution procedure, 261–262  
 drive failure, 271  
 graphical solution procedure, 260–261  
 type 1, 34, 37, 42–43, 330  
 type 2, 34, 36, 44, 331
- Drag-link mechanisms, 34, 37, 41–44  
 centroides associated with instant center, 151–152  
 change of branch, 271
- Drilling-mud pump, force analysis of, 576–578, 592–594
- Dual universal joints, 345–347
- Dynamic balancing, 633–639
- Dynamic equilibrium, 619–624
- Dynamic equilibrium equations, 609
- Dynamic force analysis, 559, 608–628  
 conservation of energy, 590–597, 615–618  
 conservation of momentum, 615–618  
 exercises, 626–628  
 flywheels, 624–626  
 particle kinetics, 610–618  
 rigid bodies, 619–624
- E**
- EDM (electron-discharge machining), 475
- Eight-cylinder V engine, 655–657
- Eight-link mechanism for parallel motion generation, 315–317
- Einstein, Albert, 31
- Electrical actuators, 49–52
- Electron-discharge machining (EDM), 475
- Elliptic trammels, 257–258  
 analytical equations for, 223–228  
 design of, 268–270
- End effector. *See* Hand, robot
- Energy, conservation of, 590–597, 604–606, 615–618
- Engineering vs. science, 2–3
- Engines  
 internal combustion, 187, 188, 639, 649–657  
 multicylinder, 649–657  
 single cylinder, 641–643

- Equations of motion, 609
- Equilibrium  
dynamic, 619–624  
static, 562
- Equivalence, kinematic, 5
- Equivalent linkages, analysis of cam contact using, 124–128
- Euler's equation, 608–609
- Exact straight-line mechanisms, 332–333
- Externally applied forces, 629
- F**
- Face gears, 522, 523
- Ferguson's paradox, 553–554
- Five-bar linkage, example of geared, 116
- Fixed links (frame), 8, 31, 32
- Fluctuating forces. *See* Shaking forces
- Flyball governor, dynamic force analysis of, 613–615
- Flywheels, 624–626
- Followers, cam. *See* Cams
- Foot-pump mechanism, 209, 209–211
- Force analysis. *See* Dynamic force analysis; Static force analysis
- Forces (definition), 560–561
- Formed cutters, gear, 475, 476
- Fouling, gear, 475
- Four-bar linkages, 257  
acceleration analysis of, 71–74, 180–182, 184  
analytical closure equations for, 171, 175–184  
analytical force analysis of, 573–575  
cognate linkages, *see* cognate linkages  
conservation of power, analysis using, 594–595  
equivalent linkages, 124  
function generation using, 285–287, 289–293, 324–325  
graphical analysis of, 67–74, 569–571  
Grashof's rules, 32–37, 58–59  
instant center, 151, 154–155  
mobility analysis of, 14, 16–18  
motion generation, 258, 263–266, 270, 272–274  
position analysis of, 67–69, 176–179, 182–184  
position synthesis of, 272–274  
spherical, 342–343, 360  
topological and physical limitations of, 40–41  
transmission angle in, 575–576  
velocity analysis of, 69–71, 176, 179–180, 182, 184
- Four-link mechanisms, 257. *See also* Elliptic trammels; Four-bar linkages; Oldham mechanism; Rapson Slide mechanism; Scotch Yoke mechanism; Slider-crank mechanisms
- Frames  
definition, 8, 32  
reference, *see* Reference frames
- Free-body diagrams, 562–565, 604
- Friction, 578–586  
in cam contact, 579  
and lubrication, 47, 128  
in revolute joints, 581–582  
in slider-crank mechanism, 583–586  
in slider joints, 579–581
- Friction drives, 458–459
- Front-end loader, 28, 28–29
- Function generation (planar linkages), 283–294
- G**
- Gears  
bevel, *see* Bevel gears  
conjugacy, 459  
helical, *see* Helical gears  
internal, 474–475  
lubrication of, 47  
manufacture of, 475–479, 476, 477, 479, 501, 501, 502  
spur, *see* Spur gears  
standards for, 465–467  
terminology, 464–465, 497–500  
worm, *see* Worm gears
- Gear loads, 597–603  
bevel gears, 602–603  
exercises, 607  
helical gears, 599–601  
spur gears, 597–599  
worm gears, 601–602
- Gear trains, 530–558  
compound, *see* Compound gear trains  
and direction of rotation, 530–531  
exercises, 554–558  
instant centers of velocity for, 163–164  
planetary, *see* Planetary gear trains  
simple, 531–533
- General coincident points, 105–106, 128–136  
acceleration analysis involving, 130–136  
exercises, 142–144  
momentarily coincident, 105  
velocity analysis involving, 130
- Geneva mechanisms, 354–359, 361
- Gimbals, 343
- Graphical analysis, 60–61  
of acceleration, *see* Acceleration  
of cam contact, *see* Cam contacts  
chain rule in, 101–104  
of crank-rocker linkages, 295–300  
exercises, 89–95, 136–144, 165–170  
force analysis, static, 565–573  
of four-bar linkages, *see* Four-bar linkages  
function generation, 293–300  
of general coincident points, 105–106, 128–136  
of instant centers of velocity, 145–170  
inversion, solution by, 84–88  
of pin-in-slot joint mechanism, 128, 132–136  
of position, 61  
of quick-return mechanism, 107–111  
and reference frames, 96–98  
rolling contact, linkages with, 96, 105–106, 111–120, 139–141  
rotating sliding joints, linkages with, 106–111, 136–139  
of six-bar linkages, 78–79, 81–83  
of slider-crank mechanisms, 74–76  
special case equations, 104–106  
of velocity, *see* Velocity
- Grashof linkages  
exercises, 58–59  
neutral, 37  
type 1 and type 2, 33–34, 37, 178, 339
- Grashof's rules, 32–37, 39–40, 58–59
- H**
- Hall effect sensors, 50
- Hand, robot, 428–429
- Harmonic follower-displacement programs, 373–375
- Helical gears, 111, 496, 496–512, 498  
crossed, 498, 509–512  
exercises, 528–529  
formulas for, 509–510, 512  
loads with, 599–601  
manufacture of, 501, 501, 502  
minimum tooth number with, 501–503  
with parallel shafts, *see* Parallel-shaft helical gears  
replacement of spur gears with, 507–509  
terminology, 497–500
- Herringbone gears, 496, 497
- Hertzian contact stresses, 459
- Higher pair joints, 3–6, 9, 47
- Higher pair mechanisms. *See also* Cam contacts; Gear trains; Pin-in-slot joints; Rolling contacts; Sliding joints/sliders  
closure equations for, 243–248  
degrees of freedom for, 15  
and instant centers of velocity, 145
- Hobbing, 478–479, 479, 501
- Hooke joints. *See* Universal joints
- Hrones and Nelson coupler-curve atlas, 308
- Hydraulic actuators, 53
- Hydraulic impactor, dynamic force analysis of, 615–618
- Hydraulic shaft puller, 189
- Hydrodynamic bearings, 44
- Hydrodynamic lubrication, 44
- Hydrostatic bearings, 44–45
- Hypoid gears, 526–527, 527

- I**
- Idle degrees of freedom, 23–25
  - Indexing mechanisms, 329, 354–359, 361
  - Induction motors, 51–52, 52
  - Inertia forces, 629, 633, 640–644, 646–648, 650
  - Inertia matrix, 609
  - Inertial reference frames, 31
  - Informal synthesis techniques, 3
  - In-plane forces, 586
  - Instantaneous screw axis (ISA), 151
  - Instant centers of velocity, 145–170
    - and centrodes, 150–152, 151, 152
    - circle diagram as strategy for finding, 155–156
    - of curved slider, 148
    - definition, 145–146
    - drafting programs, finding using, 164
    - exercises, 165–170
    - of gear mechanism, 163–164
    - of general cam-pair contact, 149–150
    - instantaneous, 146
    - and Kennedy-Aronholdt theorem, 153–155
    - location of, 147–148, 155–156, 164
    - permanent, 146
    - of prismatic joint, 148–149
    - proof of existence of, 146–147
    - for quick-return mechanisms, 160–163
    - at revolute joint, 148
    - of rolling contact pair, 149
    - rotating-radius method to find velocities, 156–159
    - of Stephenson-II six-bar linkage, 159–160
  - Interference
    - with spur gears, 479–482
    - topological, 40–44
  - Interference point, 479
  - Internal combustion engine, 187, 188, 639, 649–657
  - Inverse position kinematics (serial chains), 428, 438
  - Inverse velocity kinematics (serial chains), 438, 444–445
  - Inversion, 17, 30, 260, 293
    - analytical equation for slider-crank, 200–211
    - of RRPP mechanism, 228–233
    - solution by, 84–88
  - Inverters, 52
    - Involute function, 471–474
  - Involutes
    - bevel gears, *see* Bevel gears
    - helical gears, 496
    - spur gears, 461–463, 471–474, 487–493
    - worms, meshing of, 513
    - Involutometry, 471–474
- J**
- Joints, 1, 3, 7, 8, 96
    - Cardan, *see* Universal joints
    - constant velocity, 347–349, 348
    - compound, 5–6, 47
    - definition, 44
    - higher pair, 3–6, 9, 47
    - Hooke, *see* Universal joints
    - lower pair, 3–7, 448–452, *see also* Revolute joints
    - lubrication, 128
    - pin-in-slot, *see* Pin-in-slot joints
    - prismatic, *see* Prismatic joints
    - revolute, *see* Revolute joints
    - rolling contact, *see* Rolling contacts
    - sliding, *see* Sliding joints/sliders
    - solid contact, 45
    - spherical, 7
    - universal, *see* Universal joints
- K**
- Kennedy-Aronholdt theorem, 153–155
  - Kinematics (definition), 2
  - Kinematic equivalence, 5
  - Kinematic joints. *See* Joints
  - Kinetics, 3, 31, 608
  - KINSYN, 259
  - Kutzbach criterion, 18
- L**
- LEGOS Technics, 12
  - Lemniscate, 330
  - Leonardo da Vinci, 1
  - Level-luffing crane, 331, 332
  - Limits, motion, 31–32
  - LINCAGES, 259
  - Line of action, 465
  - Linkages
    - cams vs., 47–48, 362
    - coupler-driven, 37
    - definition, 8–9
    - drag-link, *see* Drag-link mechanisms
    - equivalent, 124–128
    - exercises, 54
    - transition, 37
  - Linkage analysis. *See* Planar linkage analysis; Spatial linkage analysis
  - Lower pair joints, 3–7, 448–452. *See also* Revolute joints
  - Lubrication of joints, 44–45, 47, 128
- M**
- Machine dynamics problems, 609
  - Magnets, permanent, 50, 51
  - Manipulators
    - acceleration analysis of, 426–428
    - direct rate kinematics of three-axis, 441–443
    - parallel, 452–454
    - velocity analysis of, 423–426
  - MATLAB
    - analytical linkage analysis, 178, 180, 181, 185, 194, 195, 207, 208, 212, 216
    - centrodes, 151
    - inertial forces, expressions for, 646
    - planar linkage design, 279, 281, 283, 291, 308, 311
    - profile cam design, 396, 406
  - Mechanisms
    - definition, 1, 8–9
    - design of, 1–3
    - idealized, 3
  - Meshing spur gears, 460
  - Miter gears, 523, 523
  - Mobility
    - computation of, 13–16
    - definition, 11, 13
    - examples, 14–16
    - in spatial mechanism (example), 19–22
  - Mobility equation
    - connectivity, determining, 23–24
    - uses of, 29
  - Module, 465
  - Moments, 560–561
  - Momentum, conservation of, 615–618
  - Motion
    - equations of, 609
    - types of, 366
  - Motion generation (cams), 364–376
    - follower-displacement programs, 366–380, 417–418
    - parabolic motion, 368–372
    - synthesis of motion programs, 364–366
    - and types of motion, 366
    - uniform motion, 367–368
  - Motion generation (planar linkages), 259
    - change of branch, 270–272
    - crank with chosen fixed pivots, 266–268
    - elliptic trammels, 268–270
    - and order problem, 270–272
    - for parallel motion using coupler curves, 315–317
    - rigid body guidance, 276–283, 321–324
    - slider cranks, 268–270, 274–275
    - three positions with selected moving pivots, 266, 272–274
    - two positions, 263–266
  - Motion limits, 31–32, 38–40
  - Motion platforms, 452–454
    - mechanisms actuated in parallel, 452
    - Stewart platform, 452–454
    - 3–2–1 platform, 454
  - Motors. *See* Actuators
  - Multicylinder machines
    - balancing, 649–657

- Multicylinder machines (*Continued*)  
 eight-cylinder V engine, 655–657  
 three-cylinder in-line engine, 653–655  
 Multiplane balancing, 633–639
- N**  
 Newton-Euler equations, 608  
 Newton's laws of motion, 31, 559, 562, 608  
 No-load speed, actuator, 49  
 Nonstandard gearing, 482–487  
 Normal pitch, 497–498, 503, 509, 528–529  
 Numerical control (NC) machining, 362
- O**  
 Oldham mechanism, 17. *See also* Elliptic trammels  
 analytical equations for, 228–233  
 use of, 257  
 Osculating circles, 113–114, 118, 124, 130, 148  
 Out-of-plane forces, 586–590, 606–607  
 Overconstraint, 25–29
- P**  
 Pantographs, 333–340  
 planar collinear, 334–336  
 and Roberts' theorem, 337–339  
 skew, 336–338  
 Parabolic motion (cams), 368–372  
 Parallel-shaft helical gears, 503–510  
 axial force, designing for, 509  
 center distance of, 504  
 contact ratio for, 505–506  
 minimum width for, 504  
 velocity ratio for, 504  
 Particle kinetics, 610–618  
 conservation of energy, 615–618  
 conservation of momentum, 615–618  
 with flyball governor, 613–615  
 with hydraulic impactor, 615–618  
 with vehicle acceleration/braking, 610–613  
 Path synthesis (planar linkage), 308–320, 326–327  
 four-bar cognate linkages, 318–320, 327–328  
 six-bar linkages, 309–314  
 Peaucellier linkage, 332–333  
 Ping-pong table linkage, 189  
 Pin-in-slot joints, 5, 200, 201  
 graphical analysis of, 106, 128, 132–136  
 instant centers used to analyze, 163–164  
 inversions, 30  
 kinematic analysis of mechanism with, 246–247  
 Pinion  
 interference, 479–481  
 internal gear, 474–475  
 and rack, *see* Rack and pinion  
 Piston mass, reciprocating, 639, 644–646
- Pitch circles, 464–465  
 Pitch cylinder, 460  
 Pitch diameter, 464–465  
 Pitch point, 464  
 Plagiographs, 333–340  
 Planar collinear pantographs, 334–336  
 Planar linkages, 7–9  
 exercises, 54–57  
 overconstrained, 27  
 visualization of, 9–10  
 Planar linkage analysis, 171–254  
 acceleration representation for, 174–175  
 for compound mechanisms, 233–243  
 for elliptic trammel, 223–228  
 exercises, 251–256  
 four-bar linkages, 175–184  
 graphical approach to, *see* Graphical analysis  
 for higher pair mechanisms, 243–248  
 for Oldham mechanism, 228–233  
 position representation for, 172  
 for rigid body, 184–187  
 for RPRP mechanisms, 211–218, 229–230  
 for RRPP mechanisms, 218–223  
 for slider-crank inversion, 200–211  
 for slider-crank mechanism, 187–200  
 special mechanisms, *see* Special mechanisms  
 vector vs. complex-number notations for, 171, 248–251  
 velocity equations/analysis, 97–98, 172–173, 179–180, 182, 194, 205–207, 209–211, 216–218  
 Planar linkage design, 257–328  
 crank-rocker linkages, 294–308, 325–326  
 double rockers, 259–262, 321  
 exercises, 321–328  
 function generation, 283–300, 324–325  
 motion generation, 259, 263–283  
 path synthesis, 308–320, 326–327  
 Planetary gear trains, 540–554, 541, 543  
 with bevel gears, 549–550  
 equation method for analysis of, 544–550  
 exercises, 556–558  
 nomenclature for, 542–543  
 in series, 547–548  
 tabular method for analysis of, 550–554  
 Plate cam with roller follower, graphical analysis of, 118–120  
 Pneumatic actuators, 53  
 Poles (rigid body guidance), 279–281  
 Polynomial follower-displacement programs, 376–380  
 Position  
 chain rule for, 102  
 describing, 2  
 Position analysis/equations, 219  
 for compound mechanisms, 237–243  
 for elliptic trammel mechanism, 224–228  
 for four-bar linkage, 176–179, 182–184  
 graphical analysis, 61  
 for Oldham mechanism, 228–232  
 planar linkage analysis, 172  
 for rigid body, 184–186  
 for RPRP mechanisms, 212–216  
 for RRPP mechanism, 219–221  
 serial chains, position kinematics for, 428–438  
 for slider-crank inversion, 202–206, 209  
 for slider-crank mechanism, 190–194, 196–199  
 Power, conservation of, 590–597, 604–606  
 Prime mover, 2, 48  
 Principal axes of inertia, 609  
 Prismatic joints, 4, 5, 7, 8, 432, 434  
 analytical linkage analysis, 211, 218  
 constraint analysis, 21  
 degrees of freedom for, 16–17  
 free-body diagrams, 562  
 instant centers of velocity of, 148–149  
 position analysis, 61  
 practical design considerations, 46–47  
 Profile cam design, 380–416  
 analytical determination, 391–416  
 graphical layout, 381–391  
 Punch press, dynamic force analysis of, 625–626  
 Pure rolling contact, 4–5
- Q**  
 Quaternary links, 8  
 Quick-return mechanisms  
 graphical analysis, 107–111  
 instant centers of velocity for, 160–163
- R**  
 Rack, 460  
 Cartesian coordinates of involute tooth generated with, 487–493  
 undercutting, 480–481  
 Rack and pinion, 480–481  
 helical gear, 497  
 spur gear, 460, 460  
 steering, 351–352  
 Radius of curvature (cam), 393–395, 397  
 Rapson slide, 258  
 Rational synthesis techniques, 2  
 Reciprocating masses, balancing, 639–643, 659–661  
 RECSYN, 259  
 Reference frames  
 fixed links and, 31, 32  
 multiple, 31, 96–98  
 principal, principal axes of inertia as, 609  
 Reuleaux, Franz, 3, 13  
 Reversing mechanisms (gear trains), 533

- Revolute joints, 4, 5, 7, 40, 432, 434  
   actuators, connecting to base of, 32  
   analytical linkage analysis, 175, 200, 211, 218  
   constraint analysis, 21  
   degrees of freedom for, 16–17  
   equivalent linkages, 124  
   free-body diagrams, 562, 565  
   friction in, 581–582  
   instant centers of velocity at, 148  
   lubrication, 44–45, 47  
   position analysis, 61  
   practical design considerations, 44–45  
   spherical linkages, 27
- Rigid bodies, 276–283  
   acceleration image theorem, 79–84, 94–95  
   analytical equations for, 184–187  
   center of circle, finding, 281  
   coordinate transformations, 276–278  
   and crank design, 282  
   dynamic equilibrium of systems of, 619–624  
   exercises, 321–324  
   image pole, 281  
   poles, finding, 279–281  
   and slider design, 282–283  
   velocity image theorem, 76–79, 94–95
- Robert's approximate straight-line mechanism, 330–331
- Robert's theorem, 318, 337–339
- Robotic mechanisms, 21–23, 428–429, 586–590
- Rockers, 32–34, 36, 41–43
- Rolling contacts, 5, 6, 45, 47  
   basic relationships, 112–118  
   closure equations for, 243, 247–248  
   example, 116–118  
   free-body diagrams, 563–564  
   graphical analysis of, 96, 105–106, 111–120, 139–141  
   instant centers of velocity of, 149  
   plate cam with roller follower, 118–120, 247–248  
   pure, 4–5, 47, 149  
   Rotating-radius method, 156–159
- Rotating sliding joints, graphical analysis of linkages with, 106–111, 136–139
- Rotor, 49, 50
- RPRP mechanisms, analytical equations for, 211–218  
   acceleration equations, 216–218  
   velocity equations, 216–218  
   when  $\theta_2$  is known, 212–213  
   when  $r_3$  is known, 215–216  
   when  $r_4$  is known, 213–215
- RRPP mechanisms  
   analytical equations for, 218–223  
   inversion of, 17, *see also* Elliptic trammels; Oldham mechanism
- Run away (actuator), 49, 51
- S**
- SCARA robot, 586–590
- Science vs. engineering, 2–3
- Scotch yoke mechanism, 17–18, 222–223, 257
- Serial chains, 421  
   direct position kinematics for, 428–438  
   direct velocity kinematics for, 438–444  
   inverse position kinematics for, 428, 438  
   inverse velocity kinematics for, 438, 444–445
- Series wound motor, 51
- Servomotors, 52
- Shaking forces, 629, 633, 639, 644, 646–657. *See also* Balancing calculation, 641–643  
   exercises, 658–659
- Shaping, gear, 477, 477, 479–480, 502
- Shunt wound motor, 50
- Simple gear trains, 531–533
- Single-plane balancing, 630–633
- Six-bar linkages  
   centrodes, 152, 152  
   design of, using coupler curves, 309–314  
   graphical analysis of, 78–79, 81–83, 116  
   inversion, solution by, 84  
   Stephenson, 16, 84, 159–160  
   Watt, 16, 39
- Skew pantographs, 336–338
- Sliders. *See* Sliding joints/sliders
- Slider-crank mechanisms, 257–258  
   analytical equations for, 187–200  
   balancing, 640–641, 643–648  
   conservation of power, analysis using, 592–594  
   with crank input, 196, 198–199  
   degrees of freedom for, 16  
   design of, 46, 268–270, 274–275  
   friction in, 583–586  
   graphical analysis of, 74–76  
   instant centers, circle method to find, 155–156  
   inversion, analytical equations for, 200–211  
   inversion example, 17, 30  
   motion limits for, 38–40  
   position synthesis of, 274–275  
   with slider input, 197, 199–200
- Sliding joints/sliders  
   analytical linkage analysis, 175, 200, 211  
   degrees of freedom for, 16  
   design of, 46–47, 282–283  
   equivalent linkages, 125–126  
   friction in, 579–581  
   graphical analysis of linkages with rotating, 96, 106–111, 128, 136–139  
   instant centers of velocity of curved, 148  
   jamming in, 46–47
- Sliding velocity (cam mechanism), 128
- Solenoids, 52
- Solution branches, 270–271
- Spatial linkages  
   exercises, 57–58  
   overconstrained, 26–27  
   visualization of, 10–11
- Spatial linkage analysis, 421–457  
   acceleration relationships, 422–423, 426–428  
   closed-loop linkages, 445–448  
   constraint analysis, 18–23  
   exercises, 455–457  
   lower pair joints, 448–452  
   motion platforms, 452–454  
   robotic mechanisms, 428–429  
   serial chains, 445  
   velocity relationships, 422–426
- Special mechanisms, 329–361. *See also* Special planar mechanisms  
   automotive steering/suspension mechanisms, 329, 349–354, 360–361  
   constant-velocity couplings, 347–349, 348  
   exercises, 360–361  
   four-bar linkages, 342–343, 360  
   gimbals, 343  
   indexing mechanisms, 329, 354–359  
   spherical linkages, 340–347  
   universal joints, 343–347
- Special planar mechanisms, 329–340  
   approximate straight-line mechanisms, 329–331, 332  
   exact straight-line mechanisms, 332–333  
   pantographs, 333–340
- Spherical joints, 7
- Spherical linkages, 340–347  
   four-bar linkages, 342–343, 360  
   gimbals, 343  
   overconstrained, 27–28  
   universal joints, 343–347
- Spiral bevel gears, 525–526, 526
- Spur gears, 111, 458–495  
   constant velocity ratio for, 459–461  
   contact ratio for, 467–471  
   exercises, 494–495, 528  
   formulas for, 485–486  
   helical gear replacement of, 507–509  
   interference/undercutting with, 479–483  
   internal gears, 474–475  
   involute tooth geometry, 461–463, 471–474, 487–493  
   loads with, 597–599  
   manufacture of, 475–480, 476, 477, 479  
   meshing, 460  
   nonstandard, 482–487  
   standards for, 465–467  
   terminology, 464–465
- Stall/stall torque (actuator), 49, 51
- Static balancing, 630–633
- Static equilibrium, 562
- Static force analysis, 559–607  
   analytical approach to, 573–578  
   characteristics of forces, 560–561

- Static force analysis (*Continued*)  
 and conservation of energy/power, 590–597, 604–606  
 constraint criterion, 20–21  
 couples, 560–561  
 equilibrium, static, 562  
 exercises, 604–607  
 free-body diagrams, use of, 562–565, 604  
 friction considerations in, 579–586  
 with gear loads, 597–603, 607  
 graphical approach to, 565–573  
 and in-plane/out-of-plane force systems, 586–590, 606–607  
 moments, 560–561  
 virtual work, 595–597
- Static machines, 559
- Stator, 49, 50
- Steering mechanisms, 329, 349–353, 360–361
- Stephenson six-bar linkages, 16, 84, 159–160
- Stepping motors, 52
- Stewart platform, 24–25, 452–454
- Straight-line mechanisms  
 approximate, 329–331  
 exact, 332–333
- Suspension, automotive, 329, 349, 353–354
- Synchronous motors, 50, 52
- Synthesis techniques, 2–3
- T**
- Ternary links, 7–8
- Three-axis manipulator, direct rate kinematics of, 441–443
- Three-cylinder in-line engine, 653–655
- 3–2–1 platform, 454
- Topological interference, 40–44
- Topology, 8
- Torque motors, 51
- Transition linkages, 37
- Transverse pitch, 497, 499, 508–509, 528
- Tredgold's approximation, 519–520
- Turning links, 32, 41
- U**
- Unbalance, 629–634
- Undercutting  
 with helical gears, 501–503  
 with spur gears, 479–483
- Uniform motion  
 cams, 367–368  
 gears, 458
- Universal joints, 6, 343–347  
 dual, 345–347  
 input-output relationship of, 446–448  
 properties of, 343–345
- V**
- Vector notation, 171, 248–251
- Velocity  
 angular, *see* Angular velocity  
 chain rule for, 102–103  
 of coupler point, 186–187  
 in elliptic trammel mechanism, 224–228  
 equivalent linkages, 124–128  
 in four-bar linkages, 179–180, 182, 184  
 friction drives, 459  
 general coincident points, analysis using, 130  
 general equations for, 98–100  
 graphical analysis of, 62–65, 76–79, 89–95, 98–144  
 higher pairs, mechanisms with, 244–248  
 instant centers of, *see* Instant centers of velocity  
 inversion analysis of, 86–88  
 in Oldham mechanism, 229–233  
 in planar linkage analysis, 172–173  
 quick-return mechanism, 107–111  
 and reference frame, 31  
 of rigid body, 184–186  
 rolling contacts, 111–120  
 in RPRP mechanism, 216–218  
 in RRPP mechanism, 219–223  
 serial chains, direct and inverse velocity problems, 438–445  
 in slider-crank inversion, 205–207, 209–211  
 in slider-crank mechanism, 194, 196–200, 198–200  
 sliding, in cam mechanism, 128  
 in spatial mechanisms, 422–426  
 special case equations for, 104–106  
 of two points fixed in a lamina, 104–105
- Velocity image theorem, 76–79
- Velocity polygons, planar, 62–65, 97–98
- Velocity ratio (compound gear trains), 534–536
- Vibration, 633, 639. *See also* Shaking forces
- Vice-grip pliers  
 free-body diagram, 564–565  
 graphical force analysis of, 567–569  
 virtual work, analysis using, 596–597
- Virtual link, 112, 114, 118–120, 124–126, 130–131
- Virtual work, 595–597
- Visualization, 9–11
- W**
- Walking toy, 201
- Watt, James, 2, 330
- Watt six-bar linkages, 16, 39
- Watt straight-line mechanism, 330
- Whole depth, 465–466
- Work, virtual, 595–597
- Worm gears, 513, 513–517  
 exercises, 529  
 formulas for, 516  
 geometry, 517  
 loads with, 601–602  
 nomenclature, 514–516  
 types of, 513–514
- Z**
- Zerol gears, 524